Essential

A Practical Handbook With DVD

Edited by

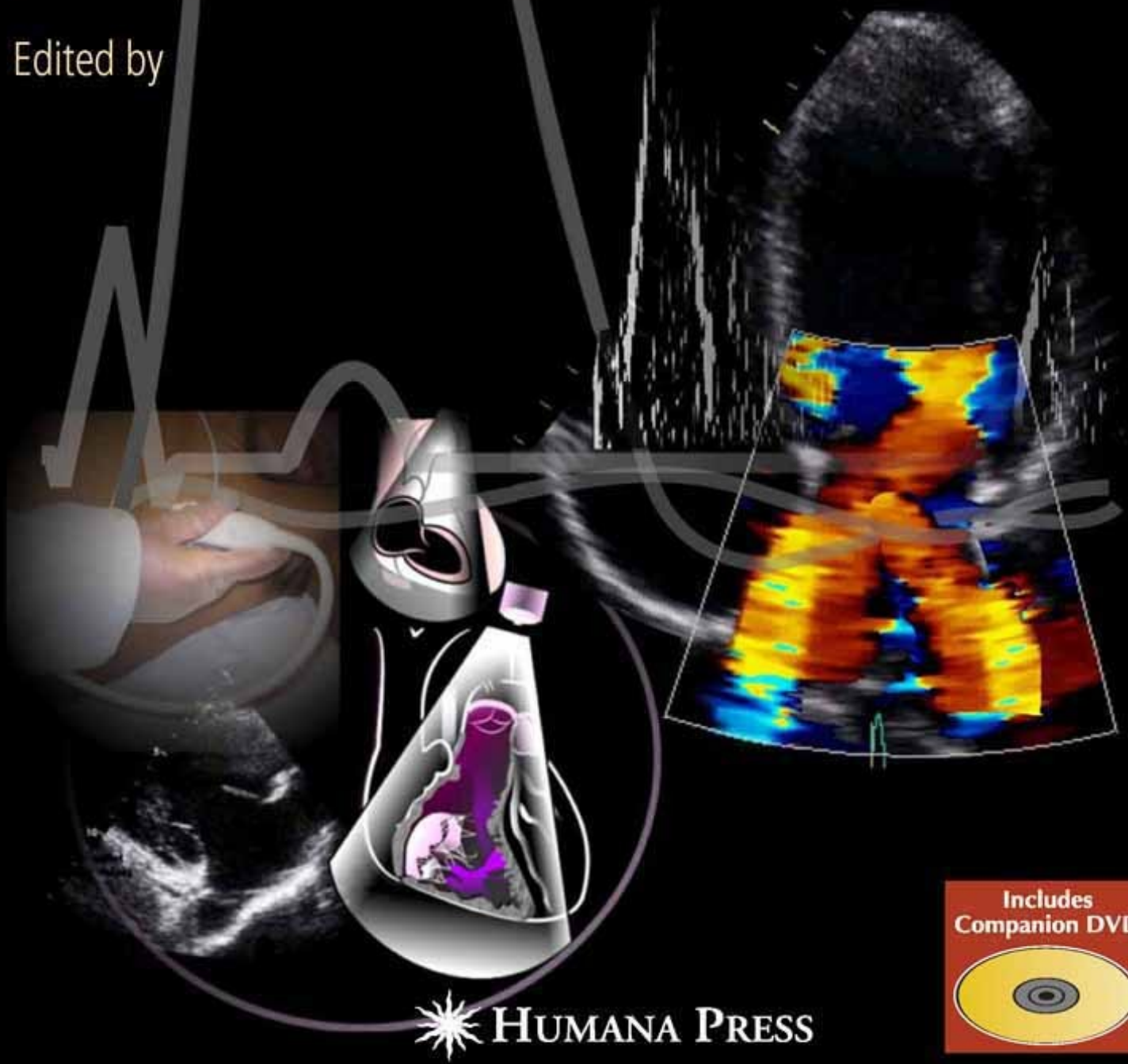

Includes Companion DVD

HUMANA PRESS

Essential Echocardiography

CONTEMPORARY CARDIOLOGY

CHRISTOPHER P. CANNON, MD
SERIES EDITOR
ANNEMARIE M. ARMANI, MD
EXECUTIVE EDITOR

Cardiovascular Magnetic Resonance Imaging, edited by *Raymond Y. Kwong, MD, 2007*
Essential Echocardiography: *A Practical Handbook With DVD,* edited by *Scott D. Solomon, MD, 2007*
Management of Acute Pulmonary Embolism, edited by *Stavros Konstantinides, MD, 2007*
Stem Cells and Myocardial Regeneration, edited by *Marc S. Penn, MD, PhD, 2007*
Handbook of Complex Percutaneous Carotid Intervention, edited by *Jacqueline Saw, MD, Jose Exaire, MD, David S. Lee, MD, Sanjay Yadav, MD, 2007*
Preventive Cardiology: *Insights Into the Prevention and Treatment of Cardiovascular Disease, Second Edition,* edited by *JoAnne Micale Foody, MD, 2006*
The Art and Science of Cardiac Physical Examination: *With Heart Sounds and Pulse Wave Forms on CD,* by *Narasimhan Ranganathan, MD, Vahe Sivaciyan, MD, and Franklin B. Saksena, MD, 2006*
Cardiovascular Biomarkers: *Pathophysiology and Disease Management,* edited by *David A. Morrow, MD, 2006*
Cardiovascular Disease in the Elderly, edited by *Gary Gerstenblith, MD, 2005*
Platelet Function: *Assessment, Diagnosis, and Treatment,* edited by *Martin Quinn, MB BCh BAO, PhD and Desmond Fitzgerald, MD, FRCPI, FESC, APP, 2005*
Diabetes and Cardiovascular Disease, Second Edition, edited by *Michael T. Johnstone, MD, CM, FRCP(C) and Aristidis Veves, MD, DSC, 2005*
Angiogenesis and Direct Myocardial Revascularization, edited by *Roger J. Laham, MD, and Donald S. Baim, MD, 2005*
Interventional Cardiology: *Percutaneous Noncoronary Intervention,* edited by *Howard C. Herrmann, MD, 2005*
Principles of Molecular Cardiology, edited by *Marschall S. Runge, MD and Cam Patterson, MD, 2005*
Heart Disease Diagnosis and Therapy: *A Practical Approach, Second Edition,* by *M. Gabriel Khan, MD, FRCP(LONDON), FRCP(C), FACP, FACC, 2005*
Cardiovascular Genomics, edited by *Mohan K. Raizada, PhD, Julian F. R. Paton, PhD, Michael J. Katovich, PhD, and Sergey Kasparov, MD, PhD, 2005*
Surgical Management of Congestive Heart Failure, edited by *James C. Fang, MD and Gregory S. Couper, MD, 2005*
Cardiopulmonary Resuscitation, edited by *Joseph P. Ornato, MD, FACP, FACC, FACEP and Mary Ann Peberdy, MD, FACC, 2005*
CT of the Heart: *Principles and Applications,* edited by *U. Joseph Schoepf, MD, 2005*
Coronary Disease in Women: *Evidence-Based Diagnosis and Treatment,* edited by *Leslee J. Shaw, PhD and Rita F. Redberg, MD, FACC, 2004*
Cardiac Transplantation: *The Columbia University Medical Center/New York-Presbyterian Hospital Manual,* edited by *Niloo M. Edwards, MD, Jonathan M. Chen, MD, and Pamela A. Mazzeo, 2004*
Heart Disease and Erectile Dysfunction, edited by *Robert A. Kloner, MD, PhD, 2004*
Complementary and Alternative Cardiovascular Medicine, edited by *Richard A. Stein, MD and Mehmet C. Oz, MD, 2004*
Nuclear Cardiology, The Basics: *How to Set Up and Maintain a Laboratory,* by *Frans J. Th. Wackers, MD, PhD, Wendy Bruni, BS, CNMT, and Barry L. Zaret, MD, 2004*
Minimally Invasive Cardiac Surgery, Second Edition, edited by *Daniel J. Goldstein, MD and Mehmet C. Oz, MD, 2004*
Cardiovascular Health Care Economics, edited by *William S. Weintraub, MD, 2003*
Platelet Glycoprotein IIb/IIIa Inhibitors in Cardiovascular Disease, Second Edition, edited by *A. Michael Lincoff, MD, 2003*
Heart Failure: *A Clinician's Guide to Ambulatory Diagnosis and Treatment,* edited by *Mariell L. Jessup, MD and Evan Loh, MD, 2003*
Management of Acute Coronary Syndromes, Second Edition, edited by *Christopher P. Cannon, MD 2003*
Aging, Heart Disease, and Its Management: *Facts and Controversies,* edited by *Niloo M. Edwards, MD, Mathew S. Maurer, MD, and Rachel B. Wellner, MPH, 2003*
Peripheral Arterial Disease: *Diagnosis and Treatment,* edited by *Jay D. Coffman, MD and Robert T. Eberhardt, MD, 2003*
Cardiac Repolarization: *Bridging Basic and Clinical Science,* edited by *Ihor Gussak, MD, PhD, Charles Antzelevitch, PhD, Stephen C. Hammill, MD, Win K. Shen, MD, and Preben Bjerregaard, MD, DMSC, 2003*
Primary Angioplasty in Acute Myocardial Infarction, edited by *James E. Tcheng, MD, 2002*
Management of Acute Coronary Syndromes, edited by *Christopher P. Cannon, MD, 2002*
Essentials of Bedside Cardiology, edited by *Jules Constant, MD, 2002*
Cardiogenic Shock, edited by *David Hasdai, MD, Peter B. Berger, MD, Alexander Battler, MD, David R. Holmes, Jr., MD, Penny Hodgson, MD, 2002*
Management of Cardiac Arrhythmias, edited by *Leonard I. Ganz, MD, 2001*
Diabetes and Cardiovascular Disease, edited by *Michael T. Johnstone, MD and Aristidis Veves, MD, DSC, 2001*
Vascular Disease and Injury: *Preclinical Research,* edited by *Daniel I. Simon, MD and Campbell Rogers, MD, 2000*
Nitric Oxide and the Cardiovascular System, edited by *Joseph Loscalzo, MD, PhD and Joseph A.Vita, MD, 2000*
Blood Pressure Monitoring in Cardiovascular Medicine and Therapeutics, edited by *William B. White, MD, 2001*
Annotated Atlas of Electrocardiography, edited by *Thomas M. Blake, 1998*

Essential Echocardiography

A Practical Handbook With DVD

Edited by

Scott D. Solomon, MD

Noninvasive Cardiac Laboratory, Brigham and Women's Hospital
Harvard Medical School, Boston, MA

With

Bernard Bulwer, MD

Medical Illustrator and Associate Editor
for Illustrations and Videos
Brigham and Women's Hospital, Harvard Medical School, Boston, MA

Foreword by

Peter Libby, MD

Chief, Cardiovascular Medicine, Brigham and Women's Hospital
Mallinckrodt Professor of Medicine
Harvard Medical School, Boston, MA

Humana Press
Totowa, New Jersey

999 Riverview Drive, Suite 208
Totowa, New Jersey 07512
www.humanapress.com

For additional copies, pricing for bulk purchases, and/or information about other Humana titles, contact Humana at the above address or at any of the following numbers: Tel.: 973-256-1699; Fax: 973-256-8341, E-mail: orders@humanapr.com; or visit our Website: http://humanapress.com

Production Editor: Melissa Caravella

Cover design by Patricia F. Cleary

Cover artwork by Bernard Bulwer, MD

This publication is printed on acid-free paper. ∞
ANSI Z39.48-1984 (American National Standards Institute) Permanence of Paper for Printed Library Materials.

Printed in the United States of America. 10 9 8 7 6 5 4 3 2 1

eISBN 1-59259-977-X

Library of Congress Cataloging-in-Publication Data

Essential echocardiography : a practical handbook with DVD / edited by Scott D. Solomon ; associate editor for illustrations and videos, Bernard Bulwer.
p. ; cm. -- (Contemporary cardiology)
Includes bibliographical references and index.
ISBN-13: 978-1-58829-322-0 (alk. paper)
ISBN-10: 1-58829-322-X (alk. paper)
1. Echocardiography. 2. Heart--Diseases--Diagnosis. I. Solomon, Scott D. II. Bulwer, Bernard E. III. Series: Contemporary cardiology (Totowa, N.J. : Unnumbered)
[DNLM: 1. Echocardiography--methods. WG 141.5.E2 E78 2006]
RC683.5.U5E87 2006
616.1'207543--dc22 2005037877

To the memory of my father,
Edwin Frederick Solomon

FOREWORD

Echocardiography occupies a pivotal position in contemporary cardiovascular medicine. The results of the echocardiographic examination have almost assumed a position alongside the vital signs and the electrocardiogram in the evaluation of the patient with or suspected of having cardiovascular disease. The ubiquity and utility of this examination have even given rise, among some medical trainees, to a mentality that seeks the results of the echocardiographic evaluation before seeing the patient!

Given its prominence in current practice, it is hard to conceive that the utility of echocardiography as other than an experimental curiosity really dates back only a few decades. Springing from the roots of sonar developed for marine surveillance, medical ultrasound assumed real utility in cardiology with the development of the M mode. The echocardiograms recorded using M mode required substantial special training for decipherment. The introduction of two-dimensional echocardiography rendered the arcana of wavy lines in the M mode virtually obsolete. The appreciation of cardiac anatomy using this modality was nearly intuitive. The interpretation of echocardiograms became accessible to a much broader population of practitioners.

Echocardiography results from a fusion of physics, engineering, anatomy, and physiology. The more recent introduction of Doppler techniques to the echocardiogram, the advent of transesophageal echocardiography, and the use of echo contrast illustrate the union of these disciplines in the service of cardiovascular diagnosis.

Essential Echocardiography: A Practical Handbook With DVD, lavishly illustrated and carefully selected, is a primer that illustrates the seamless coalescence of physics, instrumentation, hemodynamics, anatomy, and patho-physiology. Accurate but approachable, extensive but not exhaustive, this manual provides a practical but scholarly overview of the contemporary state of echocardiography. It should be useful to trainees, sonographers, and cardiologists who practice echo-cardiography as a daily pursuit.

The very quotidian acceptance of echocardiography, however, raises several concerns for the future of the specialty of cardiovascular medicine and the field of noninvasive imaging. We have entered an era in which laptop devices can provide strikingly useful echocardiographic images at the bedside. The advent of these small ultrasound machines obviates the need for wheeling a bulky instrument. This advance has also facilitated the broad dissemination of echo-cardiography. Can the introduction of palm-sized micro-ultrasound devices with penlight-sized transducers lag far behind the laptop ultrasound instruments? The increasing facility of acquisition of echocardiograms raises the important question of the qualifications of the acquirer and interpreter. Who should properly perform and interpret echocardio-graphic examinations? Should the handheld echocar-diograph become an extension of the physician's physical examination, taking its place beside the stetho-scope and sphygmomanometer? How much training and oversight would optimize the benefit to patients of such broad dissemination of echocardiography? Should the use of miniature echocardiography be restricted to cardiologists, to internists, or be disseminated to emergency physicians, anesthesiologists, surgeons, etc.? These impor-tant issues require resolution with the patient's interests paramount and academic and medical "turf" considerations subsidiary.

The ease of modern echocardiography presents another challenge. The availability and accurate infor-mation available from the echocardiogram has fostered an ingrained reliance on this noninvasive imaging modality, quite possibly to the detriment of skills in bedside physical diagnosis. Does echocardiography represent a threat to the traditional toolkit of the cardiovascular practitioner, careful observation with the physician's own senses, independent of micro-processors and electronic displays? Has the physical exam become antiquated, and have those who resist the reliance upon the echocardiogram instead of the physical examination become Luddites resisting inevitable and desirable progress? Will cardiovascular medicine lose its soul by forsaking the primacy of the physical examination, or will we enhance our ability to help patients through examination that, in the right hands, promises prompt and accurate evaluations?

The elements of echocardiography presented in this volume indirectly help us with both of those issues. First, whatever their specialty, training, or background, those who wish to add acquisition and/or interpretation of echocardiograms to their skill set can benefit remarkably from this clear and readable text. Second, by integrating echocardiography into the physiological tradition of cardiovascular medicine, Solomon and colleagues provide a firm foundation for those who wish to supplement the complete and careful physical examination by the aware practitioner with state-of-the-art information available from the latest technological advances in noninvasive diagnosis.

Peter Libby, ***MD***
Chief, Cardiovascular Medicine
Brigham and Women's Hospital
Mallinckrodt Professor of Medicine
Harvard Medical School, Boston, MA

PREFACE

In 2006, echocardiography remains the most commonly used cardiac imaging technique. Despite the existence of other methods to image the heart, such as nuclear imaging, angiography, cardiac magnetic resonance, and cardiac computed tomography, echocardiography continues to be the "bread and butter" imaging modality of cardiologists worldwide. Echocardiography has become so central to our care of patients precisely because it is almost universally available, can be performed in the outpatient setting or the intensive care unit, provides usable clinical information on the vast majority of patients, is relatively inexpensive, and has significant clinical and prognostic value.

The goal of *Essential Echocardiography: A Practical Handbook With DVD* is to teach echocardiography to anyone learning the discipline. Although most previous echocardiography books have been designed either for physicians—generally cardiologists—or cardiac sonographers, the basic principles of echocardiography are the same regardless of the learner. In the general practice of echocardiography, these distinctions blur. Indeed, sonographers are often the first to make an important diagnosis; conversely, in many institutions, physicians, not sonographers, perform echocardiographic scans. Written by a variety of experts with a commitment to the education and training of sonographers, students, and cardiology fellows, all the chapters in *Essential Echocardiography: A Practical Handbook With DVD* are designed to be basic enough for the introductory student, but offer enough substance to serve as a reference for the more advanced practitioner.

Echocardiography is the perfect marriage between anatomy and physiology, and an essential understanding of both is required of the echocardiographer. A substantial amount of this text is dedicated to the underlying physical and physiological principles. Yet echocardiography is primarily a visual discipline. The principles discussed in the text will be reinforced by the abundant echocardiographic images and dedicated illustrations demonstrating relevant cardiac anatomy and physiology. Our experience teaching echocardiography to fellows suggests that it can be difficult to learn a dynamic imaging modality such as echocardiography from static images. Thus, in addition to the large number of embedded images in the text, this book is uniquely accompanied by a DVD containing moving images illustrating virtually all of the major points in the chapters. The DVD will provide a unique learning tool for the introductory student, who is encouraged to view the DVD while reading the text, and a comprehensive visual encyclopedia for the more experienced learner.

Even as we embrace other emerging cardiac imaging technologies, advances in ultrasound technology in general and cardiac ultrasound in particular are leading to continued improvements in image quality and new techniques and applications of cardiac ultrasound. These advances will ensure that echocardiography will continue to remain the leading cardiac imaging modality for some time to come. *Essential Echocardiography: A Practical Handbook With DVD* will provide the physiological, anatomical, and diagnostic grounding all students of cardiac ultrasound need and provide a sound basis for a more general understanding of cardiac imaging.

Scott D. Solomon, MD

Contents

Contributors

David Aguilar, MD • *Baylor Heart Clinic, Baylor College of Medicine, Houston, TX*

Nagesh S. Anavekar, MD • *Clinical Pharmacology and Therapeutics, University of Melbourne, Austin Health, Melbourne, Australia*

Marcus Averbach, MD • *Cardiology Associates, St. Luke's Hospital, Bethlehem, PA*

Laura Benzaquen, MD • *Cardiovascular Division, Brigham and Women's Hospital, Harvard Medical School, Boston, MA*

Edmund A. Bermudez, MD, MPH • *Department of Cardiology, Lahey Clinic Medical Center, Burlington, MA; Assistant Professor of Medicine, Tufts University School of Medicine, Boston, MA*

Bernard E. Bulwer, MD, MSc • *Cardiovascular Division, Brigham and Women's Hospital, Boston, MA*

Ming Hui Chen, MD, MSc • *Cardiovascular Division, Children's Hospital, Harvard Medical School, Boston, MA*

Carolyn Y. Ho, MD • *Cardiovascular Genetics Center, Cardiovascular Division, Brigham and Women's Hospital, Harvard Medical School, Boston, MA*

Rajesh Janardhanan, MD, MRCP • *Echo Core Lab, Brigham and Women's Hospital, Boston, MA*

Michael J. Landzberg, MD • *Boston Adult Congenital Heart (BACH) and Pulmonary Hypertension Group, Children's Hospital Boston, Boston, MA; Cardiovascular Division, Brigham and Women's Hospital, Harvard Medical School, Boston, MA*

Dara Lee, MD • *Department of Cardiology, Albuquerque Veterans Affairs Medical Center Presbyterian Heart Group, Albuquerque, NM*

Leonard S. Lilly, MD • *Cardiovascular Division, Brigham and Women's Hospital, Harvard Medical School, Boston, MA*

Warren J. Manning, MD • *Cardiovascular Division, Beth Israel Deaconess Medical Center, Harvard Medical School, Boston, MA*

Robert J. Ostfeld, MD, MS • *Cardiovascular Division, Albert Einstein College of Medicine, Bronx, NY*

Ashvin N. Pande, MD • *Cardiovascular Division, Brigham and Women's Hospital, Harvard Medical School, Boston, MA*

Sharon C. Reimold, MD • *Clinical Cardiology, University of Texas Southwestern Medical Center, Dallas, TX*

Jose Rivero, MD • *Brigham and Women's Hospital, Harvard Medical School, Boston, MA*

Susan M. Sallach, MD • *Clinical Cardiology, University of Texas Southwestern Medical Center, Dallas, TX*

Faisal Shamshad, MD • *Mt. Sinai Medical Center, Miami, FL*

Stanton K. Shernan, MD • *Cardiac Anesthesia, Brigham and Women's Hospital, Harvard Medical School, Boston, MA*

Scott D. Solomon, MD • *Noninvasive Cardiac Laboratory, Brigham and Women's Hospital, Harvard Medical School, Boston, MA*

Jacqueline Suk Danik, MD, MPH • *Center for Cardiovascular Disease Prevention, Division of Preventive Medicine, Brigham and Women's Hospital and Cardiovascular Division, Boston VA Healthcare Center, Harvard Medical School, Boston, MA*

Justina C. Wu, MD, PhD • *Noninvasive Cardiac Laboratory, Brigham and Women's Hospital, Harvard Medical School, Boston, MA*

COMPANION DVD

The companion DVD-ROM contains a video playback application with more than 200 individual video clips corresponding to the chapters in this book. The application is compatible with most Mac and PC computers. You will need a computer with a DVD-ROM drive, as the DVD will not operate in a CD-ROM drive.

The individual video clips are cited in the text along with the figure to which they correspond by number. In addition, descriptive captions are provided in the DVD, and these will appear when you draw the cursor over the video selection listing.

PC Users

The application "Humana_EE.exe" should launch automatically on most Windows computers when the disc is inserted. If the application does not start after a few moments, simply double click the application "Humana_EE.exe" located on the root of the DVD-ROM.

Mac Users

OSX: Double click the application "Humana_EE OSX" after inserting the DVD-ROM. The Mac OSX operating system does not support an auto-start feature.

OS9: The application "Humana_EE" should launch automatically on Mac computers running OS 9.2 when the disc is inserted. If the application does not start after a few moments, simply double click the application "Humana_EE" located on the root of the DVD-ROM.

System Requirements

PC/WINDOWS

Intel Pentium II with 64 MB of available RAM running Windows 98, or

Intel Pentium III with 128 MB of available RAM running Windows 2000 or Windows XP.

APPLE MACINTOSH OS X

Power Macintosh G3 with 128 MB of available RAM running Mac OS X 10.1.5, 10.2.6 or higher.

APPLE MACINTOSH CLASSIC

Power Macintosh G3 with 64 MB of available RAM running System 9.2.

Illustrations

All llustrations appearing in the book are also included on the Companion DVD. The image files are organized into folders by chapter number and are viewable in most Web browsers. The number following "f" at the end of the file name identifies the corresponding figure in the text.

I Introduction

1 Echocardiographic Instrumentation and Principles of Doppler Echocardiography

Scott D. Solomon, MD

Contents

INTRODUCTION

Echocardiography has emerged as the principal tool for noninvasive assessment of the cardiovascular system. The basic principles of echocardiography, including the mechanical features of echocardiographic equipment, are no different from diagnostic ultrasound in general. Nevertheless, there are aspects of echocardiography that set it apart from general ultrasonography. Because the heart is a moving organ, and because echocardiography must additionally capture that movement, an understanding of echocardiography requires an understanding of both cardiac anatomy and physiology. This chapter reviews the basic principles of echocardiography and serves as a basis for understanding the specific disease processes discussed in the remainder of this text.

PRINCIPLES OF ULTRASOUND

Ultrasound is simply high-frequency sound well outside the range of human hearing. Sound frequency is measured in hertz (cycles per second); humans can hear sounds between 20 and 20,000 Hz. Ultrasound begins in the range of 1 million hertz (MHz). Ultrasound waves share the same characteristics of all sound waves (Fig. 1): frequency (*f*, number of cycles per second, and similar to the pitch of a note), wavelength (λ, the distance between sound waves), amplitude (equivalent to the loudness or magnitude of the sound waves), and propagation speed (*c*, the rate at which the sound waves travel through a particular medium). Ultrasound frequencies of 2.5–10 MHz are typically utilized for normal diagnostic work. Frequency and wavelength are inversely related, but this relationship is dependent on the propagation velocity (speed) of ultrasound. Sound waves traverse different media—water, tissue, air, bone—at different speeds.

The following equation defines the relationship between frequency, wavelength, and propagation velocity:

$$c = \lambda \cdot f$$

The speed of sound (at any frequency) through water and through most bodily tissues is roughly 1540 m/s. Hence, ultrasound waves with a frequency of 2.5 MHz will have a wavelength of 0.616 mm. This relationship is important because the resolution of ultrasound—the ability to discern small structures—is dependent on the wavelength; the shorter the wavelength, the higher the resolution. The resolution of ultrasound is about half of the wavelength. For a frequency of 2.5 MHz, this translates to a resolution of approx 0.3 mm.

Ultrasound Image Generation

Ultrasound machines emit sound waves from a transducer; these waves bounce off internal structures within the body and generate reflections that return back to the transducer. Because sound travels at essentially a constant

From: *Contemporary Cardiology: Essential Echocardiography: A Practical Handbook With DVD*
Edited by: S. D. Solomon © Humana Press, Totowa, NJ

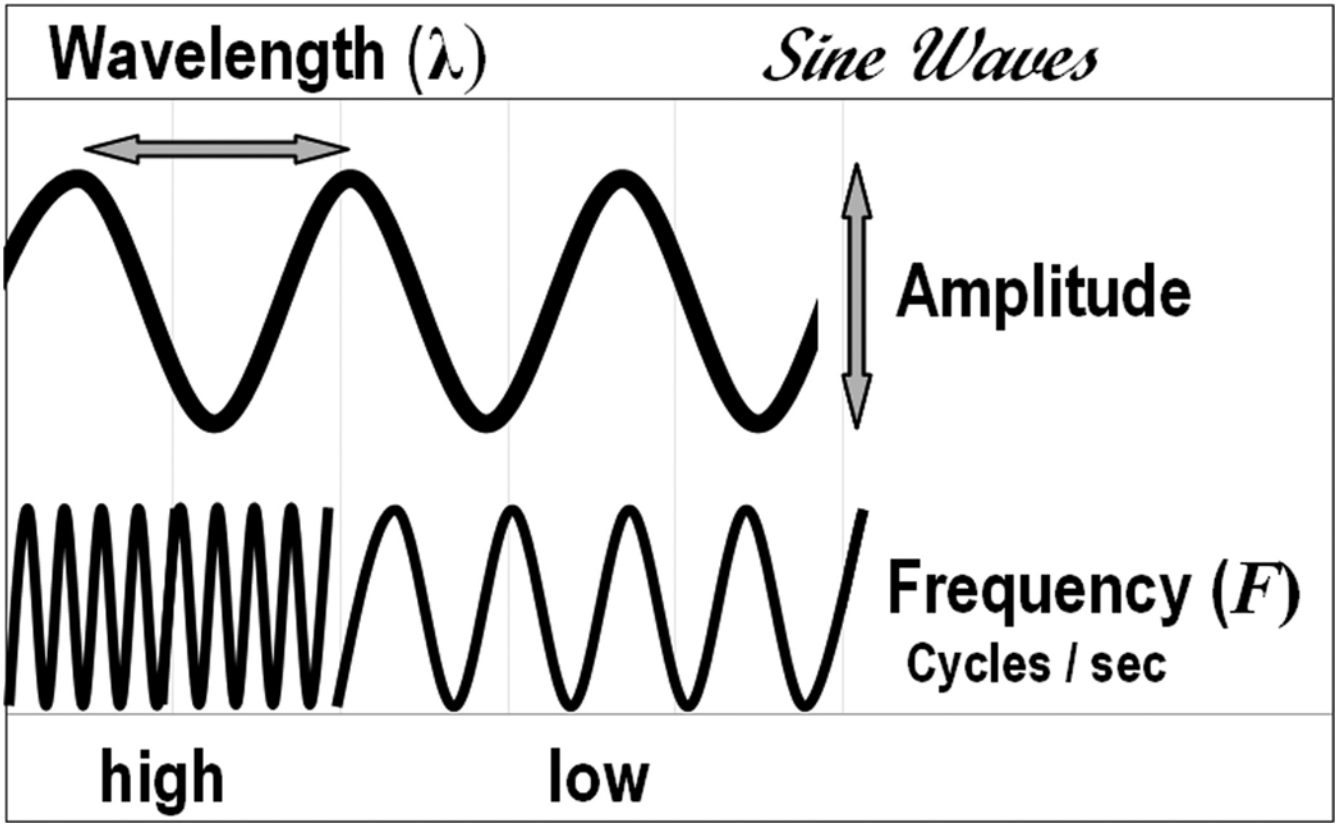

Fig. 1. Simple figure of a sine wave illustrating amplitude and wavelength. Frequency is inversely related to amplitude.

rate through tissue, the ultrasound machine can calculate the time required for the sound waves to make the round-trip between the transducer and the reflecting structure. From that transit time, the machine can calculate the depth within the body of the reflecting structure(s). This information can be used to generate a scanline in which reflecting structures are depicted on a screen along the scanline based on the distance from the transducer and the amplitude of the reflected waves. Early ultrasound machines utilized a single directional beam of ultrasound that was manually directed toward different reflecting structures; this technique is called "M-Mode" echocardiography and is still used today (Fig. 2). In M-Mode echocardiography, the resulting scanline is displayed along a moving paper sheet (or on a screen) so that time is recorded on the *x*-axis and distance from the transducer on the *y*-axis. The amplitude of the reflection is recorded as the intensity of an individual point along the scanline. M-mode echocardiography is utilized as part of the standard echocardiographic examination (*see* Chapters 2 and 3).

Modern ultrasound machines utilize multiple scanlines (up to 512) to generate a two-dimensional (2D) image (Fig. 3). Early 2D echocardiographic machines generated multiple scanlines by utilizing a mechanically rotating transducer. Modern equipment, however, use electronically steered phased array transducers to generate multiple scanlines (Fig. 4). Most ultrasound machines use between 128 and 512 phased array elements to generate pulses of ultrasound in an orderly sequence, with the result being similar to that which can be achieved with a mechanically rotating transducer, but with better spatial resolution.

For standard imaging, ultrasonic transducers emit sound waves in pulses rather than continuously. The frequency of these pulses, called the pulse repetition frequency (PRF), is designed to allow sound waves to reflect from structures within the body and return to the transducer before emitting another pulse. If the PRF were too fast, then the ultrasound machine would not be able to determine which pulse was returning and would, therefore, not be able to accurately determine the depth of the reflecting structure. The PRF is determined by the velocity of ultrasound and by the greatest depth that is being interrogated (the depth setting on the ultrasound machine). For example, as many as 7700 pulses

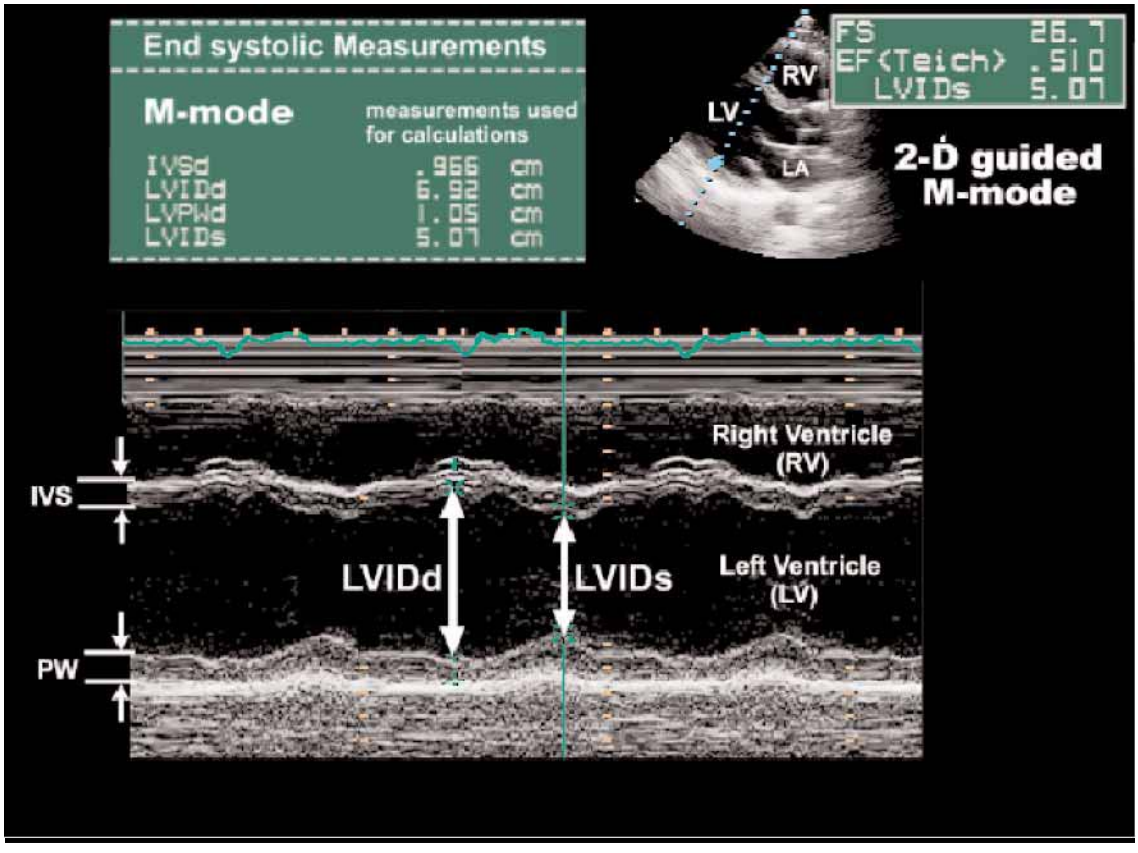

Fig. 2. M-mode echocardiogram. An M-mode image represents a single scan line on the *y*-axis with time on the *x*-axis. In this illustration, we can see the movement of the interventricular septum (IVS) and posterior wall during ventricular contraction. The small 2D image in the upper right-hand corner shows where the M-mode "slice" is made.

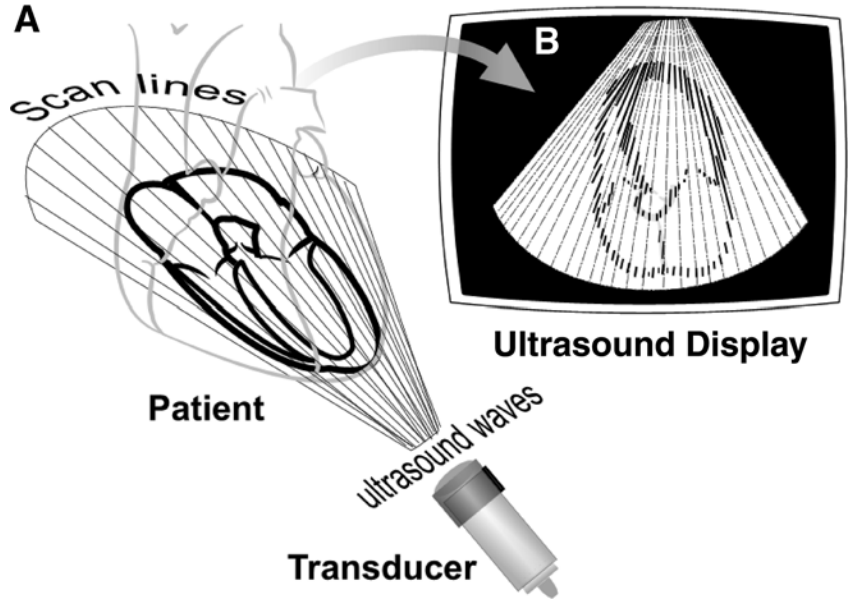

Fig. 3. How an ultrasound image is generated. (**A**) The phased array ultrasound transducer generates multiple scan lines. (**B**) Illustrates the resulting image on the screen. Although scanlines were visible in early ultrasound images, modern ultrasound equipment performs interpolation between scanlines to generate a smooth image without the appearance of scanlines.

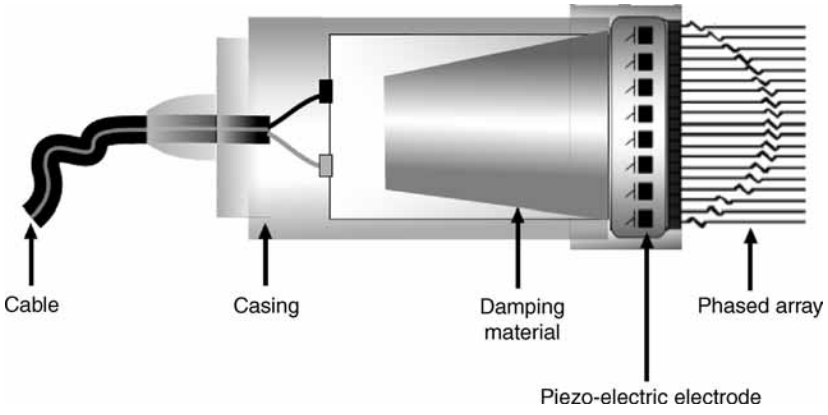

Fig. 4. Generation of scanlines with a phased-array transducer.

could make the return trip between the transducer and the edge of the 10-cm interrogation area.

Interaction of Ultrasound With Tissues

Ultrasonic images are produced because of the unique interaction of ultrasound with different tissues and fluids in the body. Reflections occur primarily at tissue interfaces (e.g., at the interface of blood and tissue). These reflections form the clearest boundaries on ultrasonic images and are termed specular reflections in which a significant proportion of the ultrasound energy is reflected back to the transducer. In contrast, reflections that occur from within relatively homogeneous tissues, such as myocardium, tend to be scattered in a variety of directions. These types of reflections are termed backscatter. Although some of the scattering ultrasound returns back to the transducer, the energy associated with these reflections is significantly lower than that emitted by the transducer. All sound waves are attenuated when they travel through tissue or fluid. Some tissues attenuate ultrasound to a greater extent than others. Finally, refraction occurs when ultrasound is reflected at an angle from the original ultrasound beam. All of these interactions with tissue are important in the ultimate image that is generated.

Although ultrasound can easily traverse through bodily fluids, including water and blood, as well as most soft tissues, ultrasound does not pass easily through bone or air. This limitation represents a major problem in cardiac imaging because the heart is surrounded by the thorax (bone) and the lungs (air). Ribs can cause significant artifacts. Air in the lungs can make imaging difficult. Indeed, patients with emphysema, who have overexpanded lungs, can be extremely challenging to image.

Ultrasound Resolution: Trade-Off With Penetration

Resolution, the ability to discern detail, in ultrasound images is dependent on the wavelength (inversely related to frequency) of the ultrasound. The limit of the resolution of ultrasound is approximately one-half of the wavelength. With a standard imaging frequency of 2.5 MHz, this translates to a wavelength of approximately one 0.6 mm, which suggests a resolution of 0.3 mm. Although resolution can be increased by increasing the frequency of the ultrasound used, higher frequency ultrasound is less able to penetrate through tissues. Therefore, although higher frequency ultrasound can be used for high-resolution imaging, its use will be limited because of decreased penetration. For this reason, high-frequency transducers only image well at short distances. Pediatric imaging, which requires less penetration, is often carried out at a frequency is of 5 MHz or higher. Because of decreased penetration, image quality can drop off dramatically when using higher frequencies in adults. In contrast, adults who have larger chest cavities will often require lower frequency probes. Indeed, 2.5–3 MHz resolution probes have become the standard for adult imaging.

Harmonic Imaging

Modern ultrasound machines tend to use two different imaging modes: fundamental imaging and harmonic imaging. In fundamental imaging, the ultrasound transducer listens for the returning ultrasound at the same frequency at which it was emitted. However, ultrasound can cause tissues to vibrate at frequencies that are multiples of the frequency of the original ultrasound pulse. The transducer can thus be set to listen at a frequency that is higher (by a multiple) than the original frequency. Harmonic imaging allows for improved

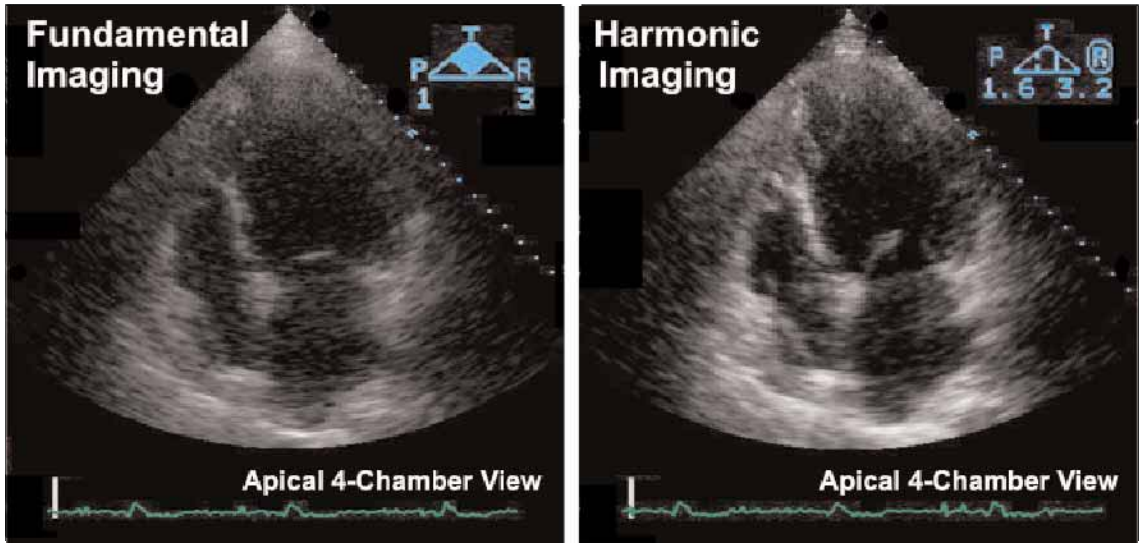

Fig. 5. Two side-by-side images from the same patient with fundamental imaging (left) and second harmonic imaging (right). Notice the improved endocardial resolution and ability to distinguish tissue from cavity utilizing harmonic imaging. (Please *see* companion DVD for corresponding video.)

resolution of tissue interfaces, in particular, the endocardial border. Harmonic imaging is an option on many modern ultrasound machines (Fig. 5; please *see* companion DVD for corresponding video). However, image quality is not always improved by harmonic imaging, and in some patients, fundamental imaging provides better overall image quality.

Obtaining Images and Image Quality

Echocardiography is dependent on the operator applying the transducer to the chest of the patient and obtaining images in real-time. The quality of the images, therefore, is dependent on the skill of the operator, as well as the body habitus of the patient. In addition, the ability to obtain the quality images can often be hampered by aspects of the patient's medical care that cannot be controlled, such as the patient being on a ventilator, or having bandages following surgery that interfere with scanning. Well-trained sonographers and echocardiographers learn to work around many of the inherent limitations imposed by the need to scan very sick patients. Obesity and chronic obstructive pulmonary disease are probably the two patient characteristics that affect image quality most.

Ultrasound Artifacts

Imaging artifacts suggesting the appearance of structures that are not actually present are common in ultrasonic imaging. Artifacts include both the apparent presence of structures that do not exist, or the obscuring of structures that do exist. Artifacts in the aorta and the left atrial appendage frequently pose important diagnostic and decision-making challenges (Chapters 16, 17, and 19). To identify artifacts, the experienced echocardiographer must understand the reasons for artifact appearance in ultrasonic images. Artifacts can be caused by many of the same problems that result in poor image quality, including body habitus and the location of ribs. Indeed, rib artifact remains one of the most prominent artifacts seen in echocardiographic studies (Fig. 6; please *see* companion DVD for corresponding video). Rib artifacts can often be distinguished from actual structures because the artifact will remain in one place relative to the transducer while the beating heart moves separately from the artifact. Often, however, a rib artifact will move with respiration owing to movement of the thorax with breathing. It is, therefore, sometimes necessary to distinguish respiratory movement from cardiac movement in order to distinguish artifacts from real structures.

Reverberation artifacts are caused by reflections that occur internally within the imaging region. Calcifications frequently cause ultrasound signals to "ping-pong" within the interrogated structure before returning to the transducer (Fig. 7). Not accounting for the internal reverberation, the ultrasound machine interprets the extra time for the ultrasound to return as an indication that the reflections occur at a further depth, resulting in a ghost reflection usually at a distance that is a multiple of the original reflection.

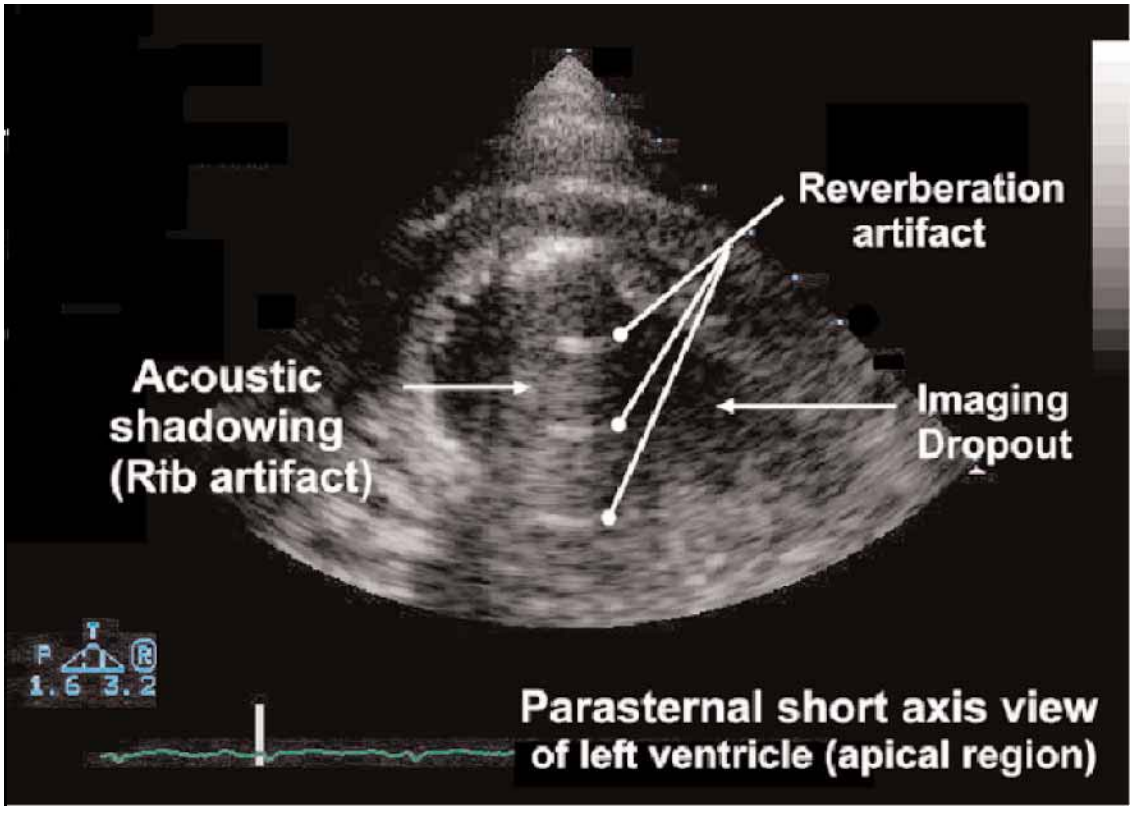

Fig. 6. Three types of artifacts are visible in this parastenal short axis at the mid ventricular level in a 50-yr-old patient with a left ventricular assist device. (Please *see* companion DVD for corresponding video.) Reverberation artifacts (multiple arrows) generated by the cannula of the device are seen along with acoustic shadowing from the ribs, and dropout owing to loss of lateral resolution.

Another type of artifact originates from the fact that ultrasound beams can be wider than the scanline representation on the image. Thus, an ultrasound beam may reflect from a structure slightly off the true axis of the beam, causing a loss in lateral resolution. Mirror image artifacts are frequently seen in the aorta on transesphageal echocardiography (Fig. 8; please *see* companion DVD for corresponding video).

PRINCIPLES OF DOPPLER ULTRASOUND

Doppler ultrasound relies on the Doppler principle to determine the velocity of moving fluids or tissues. The Doppler principle states that the frequency of a sound (or any wave) will shift (higher or lower) when it is emitted from, or reflected off, a moving object. This occurs because sound waves emitted from a moving source (or reflected off a moving source) are either compressed or expanded depending on the direction of the movement. This is the same principle responsible for the changing frequency of an ambulance siren as it travels toward or away from an observer (Fig. 9).

In diagnostic ultrasonography, waves are emitted from the transducer at a particular frequency and reflected off moving red blood cells within the heart or blood vessels. If the flow of blood is moving toward the transducer, the sound waves will be compressed (and the frequency of the returning ultrasound will be slightly higher than the emitted ultrasound). The opposite is true for blood flow moving away from the transducer (Fig. 9). The difference between the emitted frequency and the returning frequency is called the Doppler shift. Because the ultrasound machine emits sound at a particular known frequency, the difference between the original ultrasound frequency and the returning ultrasound frequency can be easily determined. This difference in frequency is directly related to the velocity of the structures reflecting the sound (the red blood cells) and, therefore, is related to the velocity of blood flow. This relationship is described by the following equation:

$$v = \frac{c(F_s - F_t)}{2F_t(Cos\,\theta)}$$

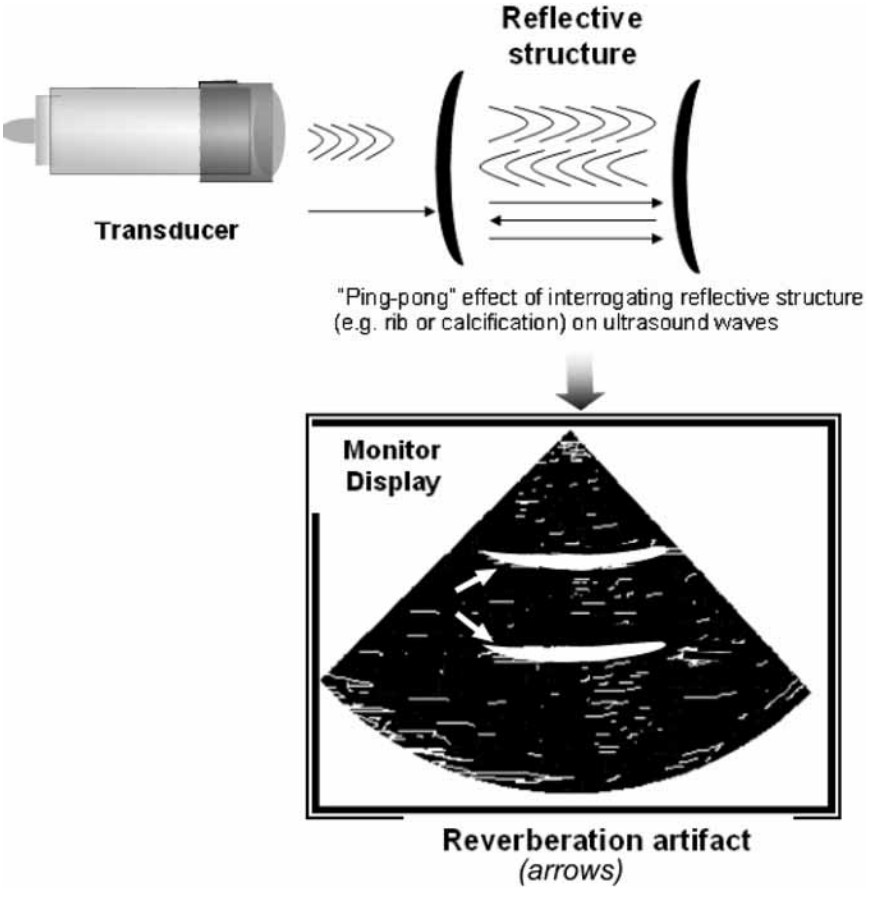

Fig. 7. Illustration of the generation of a reverberation artifact. In this case, a reflective structure, such as an area of calcification, causes an "internal" reverberation. The additional "back-and-forth" trip causes the machinery to place an artifactual distal to the original image, but spaced a multiple away from the original distance between the transducer and the reflective structure.

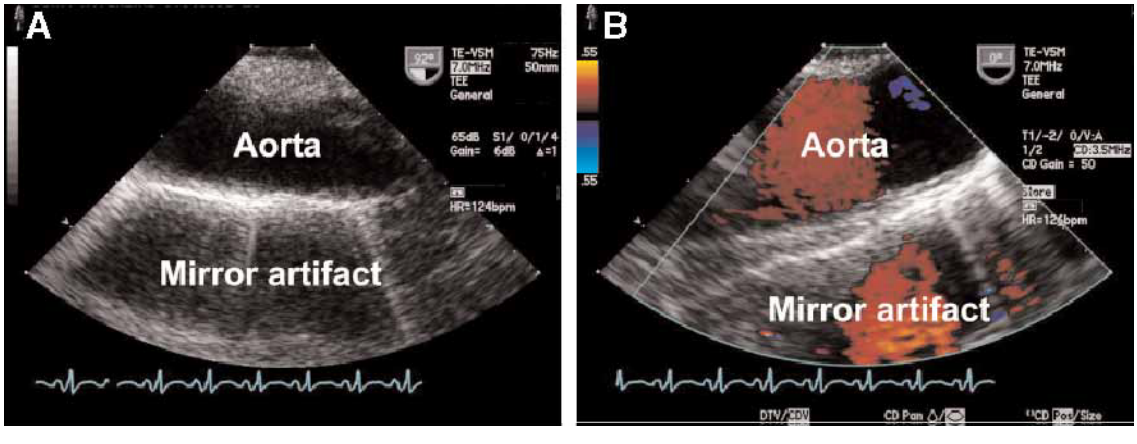

Fig. 8. Mirror artifacts are commonly seen in the aorta on transesphageal echocardiography as shown in these still frame images. (Please *see* companion DVD for corresponding video.)

where v = the velocity of blood flow, c = the propagation velocity of sound through the tissue (1540 m/s), F_s = the shifted (returned) ultrasound velocity, F_t = the original emitted ultrasound frequency, and θ = the angle of incidence between the ultrasound beam and the blood flow.

Pulsed- and Continuous-Wave Doppler

Two modes of Doppler ultrasound are typically employed in standard diagnostic ultrasonography—pulsed-wave (PW) Doppler and continuous-wave (CW) Doppler (Figs. 10 and 11). PW Doppler requires individual

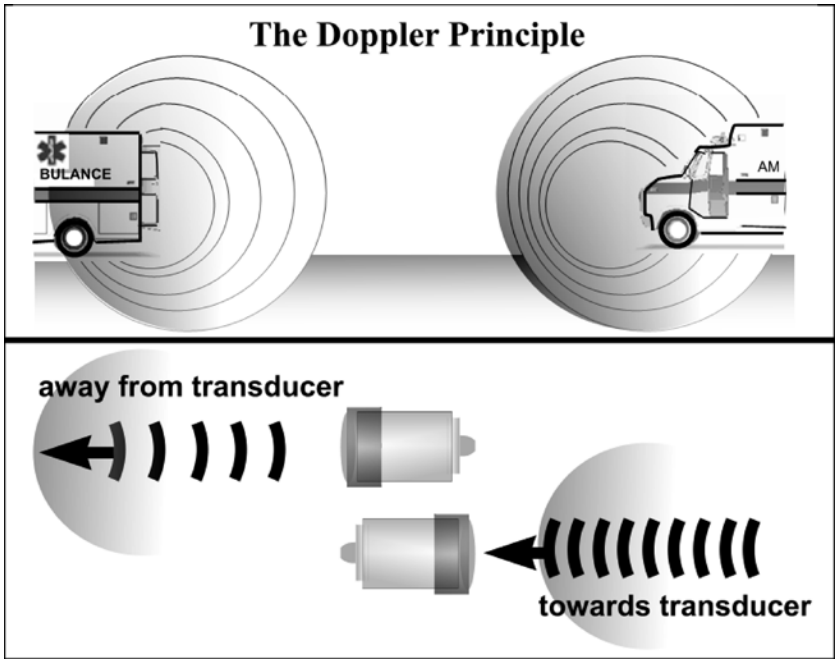

Fig. 9. The Doppler principle: when the sound emitting source (in the illustration, the ambulance), is moving toward the listener, the wavelength of the sound waves shorten (or the frequency increases); when the sound emitting source is moving away from the listener, the sound waves will lengthen (the frequency will decrease). Ultrasound emitted from the transducer bounces off moving red blood cells (Bottom), and returns to the transducer. The difference between the emitted frequency and the returning frequency is the Doppler shift.

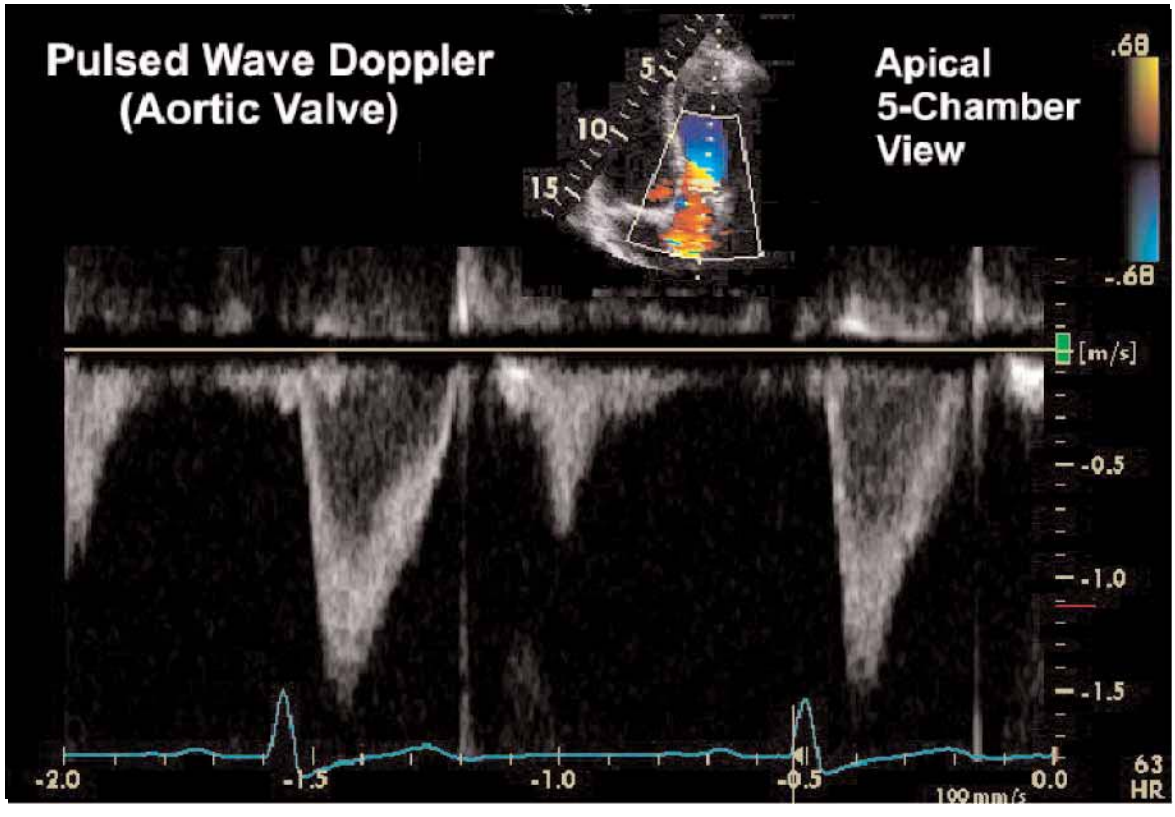

Fig. 10. Pulsed-wave Doppler interrogation at the level of the aortic valve.

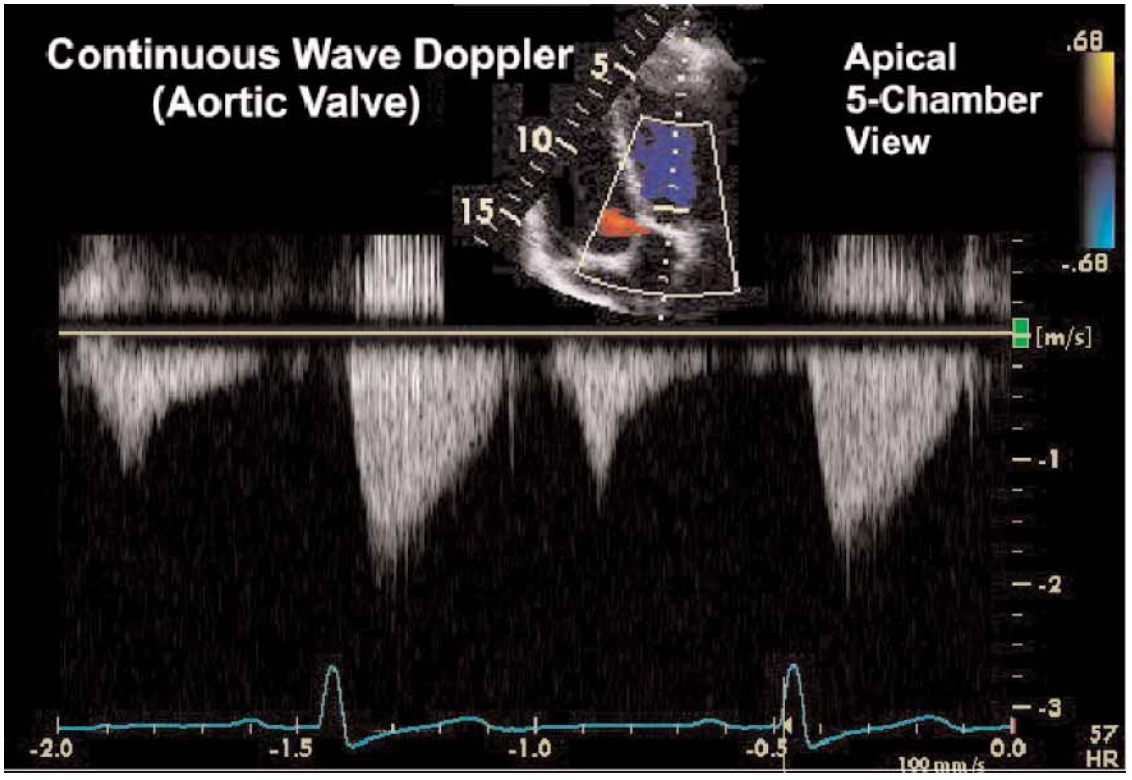

Fig. 11. Continuous-wave Doppler interrogation across the aortic valve.

pulses of ultrasound to be emitted and returned to the transducer. The rate at which these pulses are emitted is the PRF. It is important to understand the difference between the PRF and the frequency of the ultrasound wave itself. The ultrasound frequency is equivalent to the pitch of a note played on a piano, whereas the PRF represents the rate at which the note is repeated. Because pulses emitted from a transducer return to the transducer at the same rate at which they were emitted, the PRF essentially represents the sampling rate of the Doppler acquisition.

A cardinal principle of digital sampling in general states that the sampling rate must always be at least double the frequency of the waveform being sampled. This is true for digital audio recording as well as for ultrasound acquisition. For example, because humans can hear sounds up to 20,000 Hz, compact discs are recorded using a sampling rate of 44.1 kHz, ensuring the sampling of all frequencies. In Doppler ultrasound, we are sampling the frequency, not of the ultrasound itself, but of the Doppler shift, i.e., the frequency difference between the emitted and the received waveforms. This frequency, as previously discussed, is directly related to the velocity of blood flow. Hence, the sampling rate (or PRF) is a major determinant of the maximal Doppler shift that the ultrasound machine can accurately sample, and thus a major determinant of the maximal velocity that can be assessed (*see* Understanding Aliasing in Doppler; Figs. 12 and 13).

The point at which a waveform cannot be sampled unambiguously happens at a sampling rate of twice the highest frequency that needs to be sampled. This point is called the Nyquist limit, and is one-half the PRF. When the frequency of the Doppler shift (and hence the velocity of blood flow) is greater than twice the PRF, the waveform cannot be accurately sampled, and the velocity cannot be accurately assessed. The resultant image will demonstrate "aliasing." Aliasing occurs because the machine cannot figure out accurately the velocity or the direction of flow when the velocity exceeds the Nyquist limit. It is important to remember that the effective sampling rate is dependent on the PRF. What, then, limits the PRF? Because ultrasonic pulses must leave the transducer, reflect off moving blood cells, and return to the transducer, the PRF cannot be higher than the amount of time it takes for the ultrasound to make this round-trip. Thus, because the speed of sound is constant, the PRF is dependent on the depth of the region being interrogated. When using PW Doppler, we have the ability to select a particular

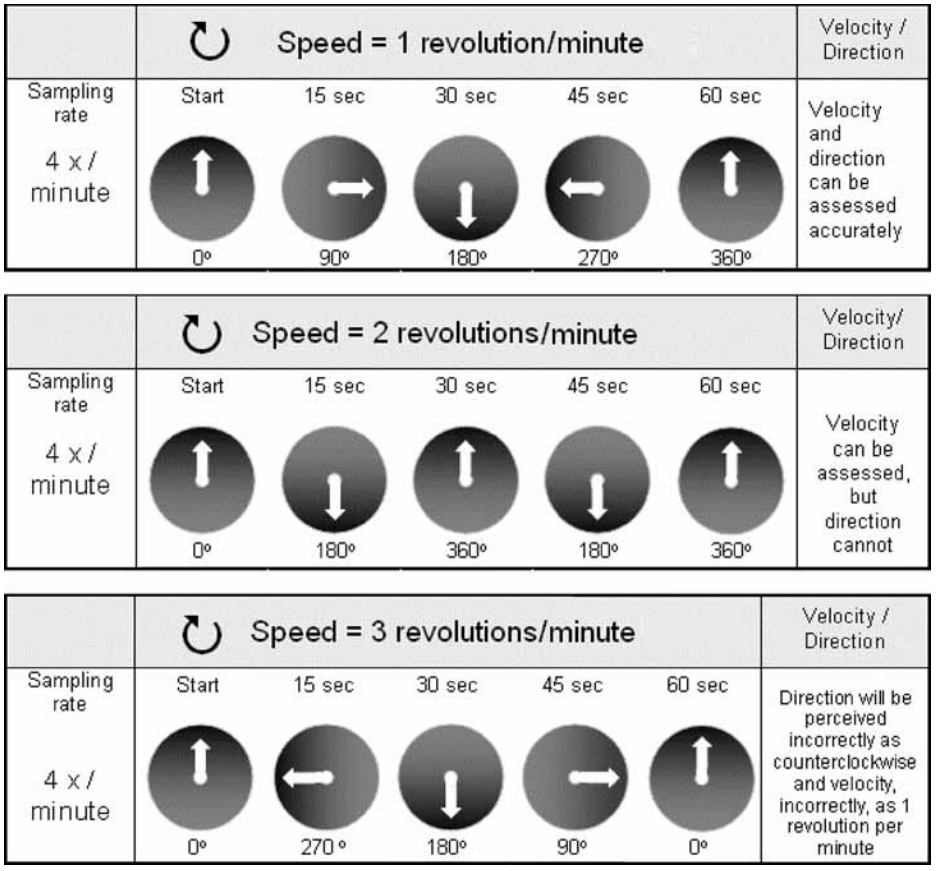

Fig. 12. Understanding aliasing: aliasing can best be understand by this simple example from sampling theory, the so-called "wagon-wheel" example, named after the wagon wheel illusion in old western motion pictures. Consider a rotating clock hand. In the top panel, the hand is rotating at one revolution per minute. If we were to "sample" the clock every 15 s (four times per minute) by snapping a picture, we would easily be able to "capture" the motion of the clock, we would see that the hand is rotating clockwise and would be able to discern the rate of rotation. If, however, we increased the rotational speed to two revolutions per minute, and maintained the same sampling rate, we would only "capture" the hand at the 12 o'clock and 6 o'clock positions. We could tell the rate of rotation, but would *not* be able to discern the direction. Finally, in the bottom panel, if the velocity of revolution increased to three revolutions per minute (still in the clockwise direction), with the same sampling rate, the perceived direction, based on the sampling, would be counterclockwise, and the perceived rate of rotation would be one revolution per minute.

location (depth) to be interrogated. On the ultrasound machine, this is accomplished by placing a cursor over a specific area on the 2D image (Fig. 10). What the ultrasound machine is actually doing is emitting a pulse, then waiting the exact amount of time it would take that pulse to travel to the cursor location and return to the transducer. In PW Doppler, the time between pulses cannot be less than that round-trip transit time and the PRF will be inversely related to that time. Figures 12 and 13 illustrate the aliasing principles in Doppler echocardiography.

Blood Flow Profiles in the Heart

Blood flowing through the heart and blood vessels can be either laminar or turbulent. Laminar flow occurs when the majority of flow is moving in the same direction and at similar velocities. Turbulent flow occurs when flow is disturbed, by a stenosis or in the setting of significant regurgitation. The type of flow can be discerned from the PW Doppler waveform. With laminar flow, the waveform will appear "hollow" because the majority of blood cells will be moving at similar velocities (and close to the maximal velocity). With turbulent or non-laminar flow, the velocities will cover a wider spectrum, with some blood cells moving very rapidly and some moving very quickly. Thus, the waveform will appear "filled" (Fig. 14).

Practical Aspects of PW Doppler

PW Doppler is used primarily to obtain velocity information for relatively low velocity flows at a specific

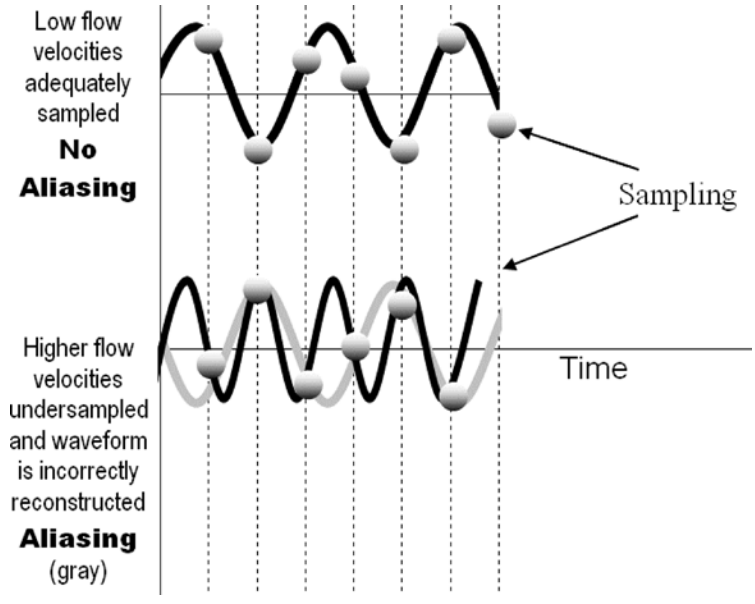

Fig. 13. The problem of aliasing occurs when sampling a sound wave as well as when the sampling frequency is less than twice the frequency of the wave that is being sampled. In the example, when the sampling rate is twice the frequency of the original wave (in black), it is possible to reconstruct the wave accurately. However, when the sampling frequency is less than twice the frequency of the wave, the wave is reconstructed incorrectly, as is shown in the bottom panel, where the reconstructed wave is shown in gray. In Doppler echocardiography, we are "sampling" the Doppler shift. The sampling rate is determined by the pulse repetition frequency (PRF). The Doppler shift is reflective of the velocity of the blood flow (by the Doppler equation). Thus, higher PRFs are able to discern higher velocities of blood flow.

location within the heart or blood vessels. Examples of Doppler assessments that are typically made with PW Doppler include assessing the left ventricular outflow tract velocity (except in conditions in which they outflow tract velocity is markedly elevated in which case CW Doppler would be needed), assessment of mitral inflow velocities, and assessment of pulmonary venous velocities. These are all relatively low velocity flows within the heart.

CW Doppler

Unlike PW Doppler, in which individual pulses are emitted and reflected back to the transducer, ultrasonic beeps, CW Doppler emits a continuous tone from the transducer. Reflections from this continuous ultrasound tone are then received by the transducer continuously as well (Fig. 11). Because the machinery is not waiting for a pulse to reflect and return, it is impossible for the ultrasound equipment to determine the location of the reflection. Nevertheless, moving blood cells will reflect the continuous ultrasound tone and this reflection will be subject to the Doppler shift as a function of the velocity of the blood flow (just as with pulsed Doppler). The advantage of CW Doppler is that because "sampling" is occurring continuously, the ability to detect particular frequencies is not subject to the Nyquist limit, and we can thus interrogate much higher velocities than is possible with PW Doppler. The disadvantage of CW Doppler, however, is that because we are *not* sampling, we cannot "gate" the returning ultrasound pulse and thus cannot listen for a reflection that is coming from a particular depth. Thus, CW Doppler tells us the maximal velocity along the line of the ultrasound beam. We cannot, however, determine the location of the maximal velocity. CW Doppler is particularly useful then for assessing high velocity blood flow, for example, the velocity across the aortic valve in aortic stenosis, or the velocity of tricuspid regurgitation.

Color Flow Doppler

Color flow Doppler imaging uses the same general technology as PW Doppler imaging. However, color flow Doppler samples multiple locations along a scan line simultaneously and determines the velocity of individual locations. These velocities are then "color encoded" utilizing a color map in which particular colors are used to represent particular velocities (Fig. 15). The color map is displayed on the ultrasound image so that the relationship between particular colors and velocities are visible. By convention, flow that is moving away from the transducer

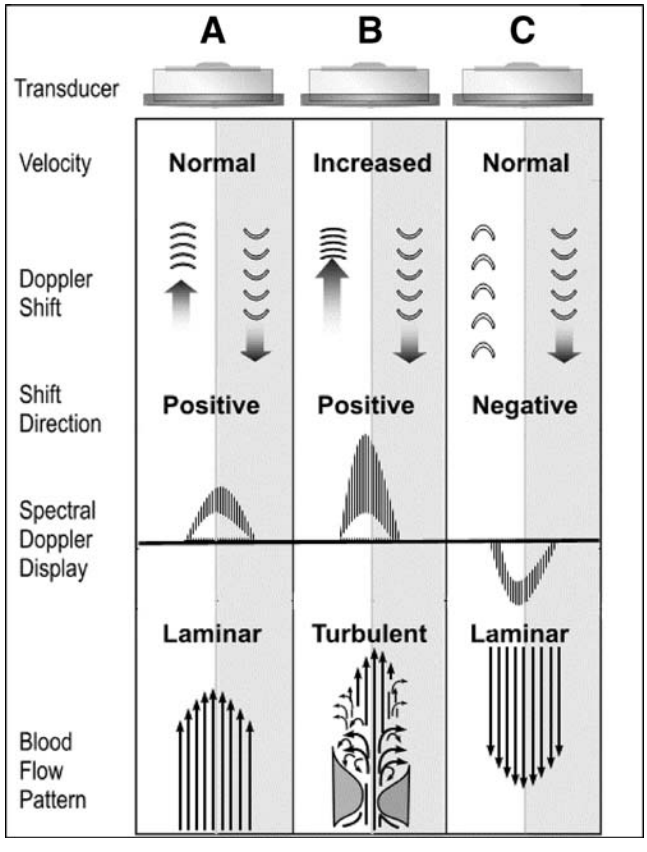

Fig. 14. Pulsed-wave Doppler profiles of (**A**) laminar and (**B**) turbulent flow. (**C**) Demonstrates flow away from the transducer. Notice that the flow profile of laminar flow is "hollow" indicating that the most of the blood cells are traveling at similar velocities. When flow is turbulent, there is a wider range of velocities, and the flow profile appears filled in.

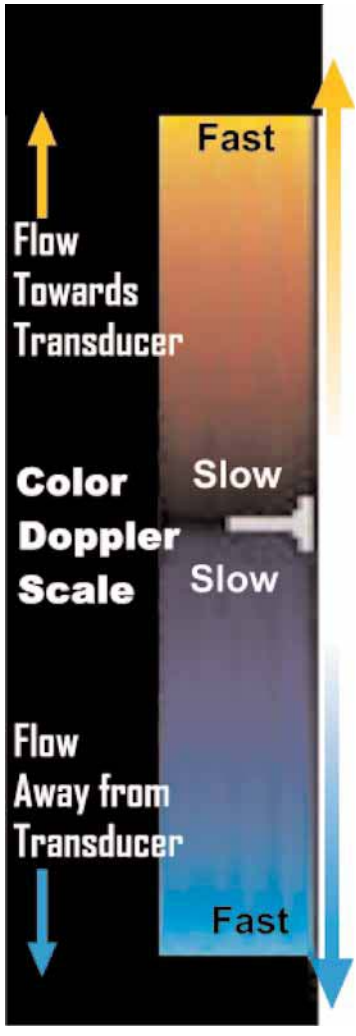

Fig. 15. Color Doppler scale depicting flow direction and relative velocities.

is encoded in blue, and flow that is moving toward the transducer is encoded in red (Fig. 16; please *see* companion DVD for corresponding video). Because color flow Doppler utilizes the same basic principles as PW Doppler, it is also subject to sampling issues and the problem of "aliasing." Doppler shift frequencies (and hence velocities) that are above the Nyquist limit are encoded as a "green mosaic." The Doppler information is superimposed on the 2D image, providing a very powerful visual assessment of blood movement in the heart. Because color flow Doppler displays velocity information on top of anatomical information, it is possible to visualize even very fast flows in the heart, although color flow Doppler does not allow accurate assessment of velocities beyond the Nyquist limit. As with standard pulsed Doppler, the PRF is an important setting in color flow Doppler, and can be adjusted by the operator. The PRF can be lowered or raised to decrease or increase the aliasing velocity.

From Velocity to Pressure: Measuring Gradients in the Heart

Doppler echocardiography measures the velocity of blood movement within the heart and blood vessels. From this velocity information, it is possible to estimate pressure gradients utilizing the Bernoulli equation. The Bernoulli principle states that the velocity of flow through a fixed orifice will be dependent on the pressure gradient across the orifice. Intuitively, this principle states that the higher the pressure gradient, the faster the blood flow. The full form of the Bernoulli equation is relatively complex:

$$p_1 - p_2 = 1/2\rho(v_2^2 - v_1^2) + \rho\int_1^2 \frac{dv}{dt}\vec{ds} + R(\vec{v})$$

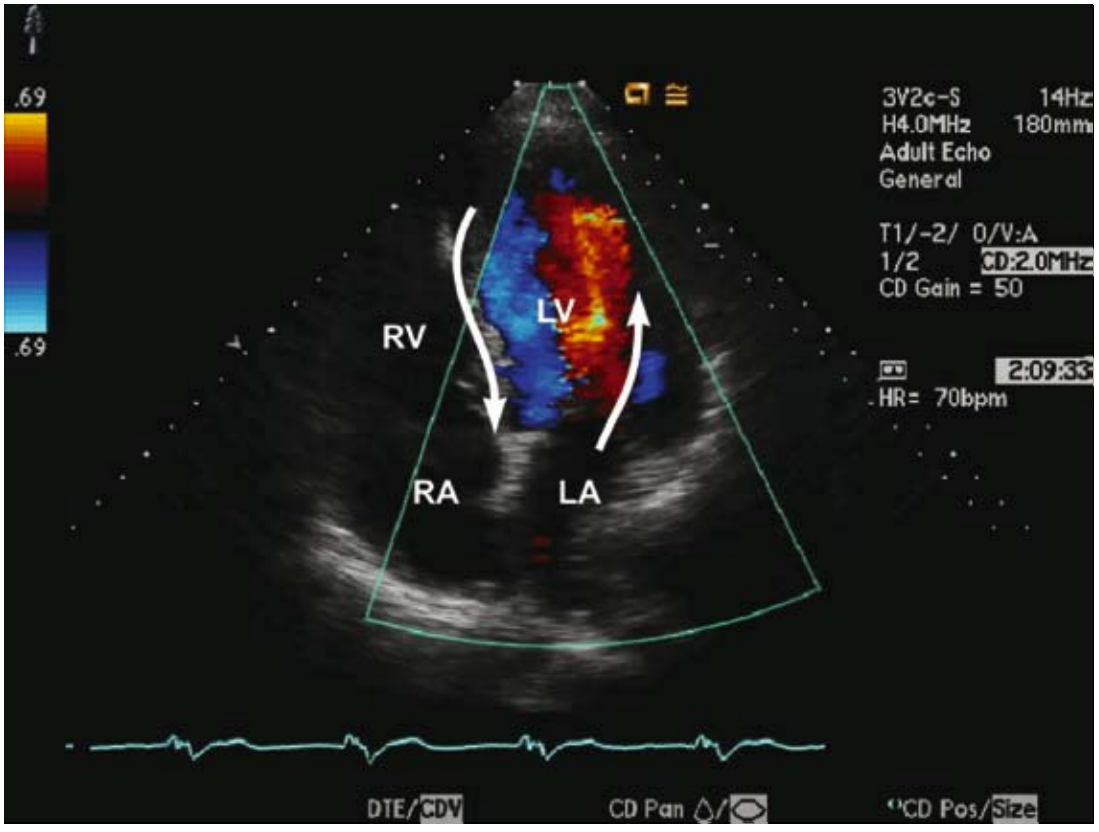

Fig. 16. Apical view with superimposed color Doppler showing flow direction during early systole. (Please *see* companion DVD for corresponding video.)

In general ultrasound use, the following simplification can be made:

$$P = 4(V_2^2 - V_1^2)$$

where p = pressure gradient, v_1^2 = proximal velocity, v_2^2 = distal velocity. With most velocities that are greater than 1 m/s, proximal velocities can often be ignored, leaving the following simplified modified Bernoulli equation: $P = 4V_2^2$. This equation is useful for translation of velocities to gradients in most clinical circumstances.

For example, a maximal CW velocity across a stenotic aortic valve of 4 m/s is equivalent to a pressure gradient of 64 mmHg across the valve. Likewise, a maximal CW velocity of tricuspid regurgitation of 3 m/s is equivalent to a systolic gradient between the right ventricular and the right atrium of 36 mmHg. It is important, however, to recognize clinical situations when the proximal flow velocities cannot be ignored. For example, if there is significant flow acceleration proximal to the aortic valve—as, for example, in the case of a patient with aortic stenosis and subaortic stenosis (caused by a membrane or by septal hypertrophy), it would be necessary to use the longer form of the Bernoulli equation, thus, taking into account the increased proximal flow velocities.

Doppler Cautions and Caveats

Doppler cannot measure pressure directly. Nor can Doppler measure "flow." Doppler measures the velocity of blood flow. For this reason, much of the information that we ultimately derive from Doppler measurements has to be inferred. For example, although we can measure the gradient between the right ventricle and the right atrium by looking at the tricuspid regurgitant velocity, to estimate pulmonary artery systolic pressures we need to make the following assumptions: first, we need to assume that there is no pressure gradient between the right ventricle and the pulmonary artery. Obviously, in patients with pulmonic stenosis, we would be unable to calculate the pulmonary systolic pressures from the tricuspid regurgitant velocity without taking into account the gradient across the pulmonic valve. In addition, because we know the gradient between the right ventricle and the right atrium, to calculate right ventricular systolic

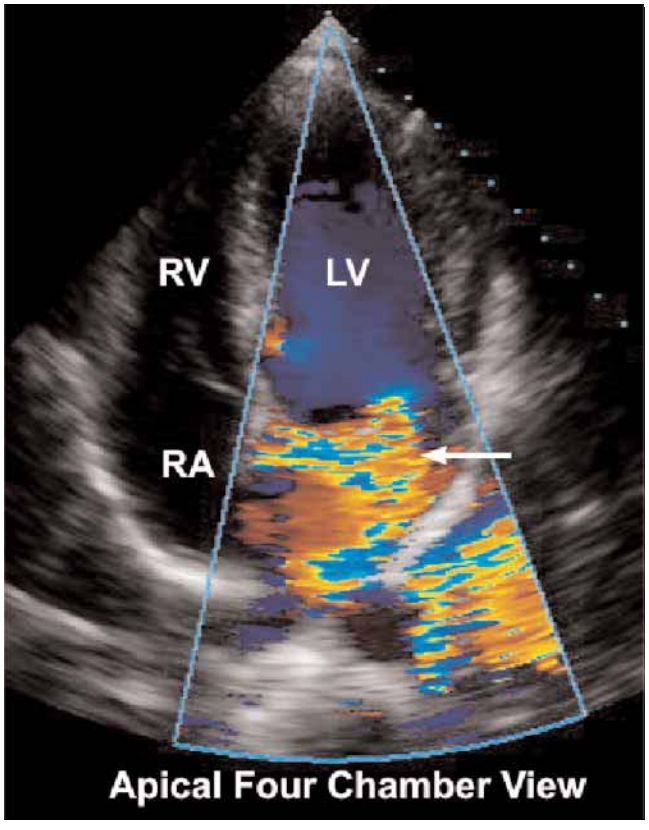

Fig. 17. Aliasing on color Doppler reflecting high velocity turbulent flow in a patient with severe mitral regurgitation. (Please *see* companion DVD for corresponding video.)

pressure we need to know the estimated right atrial pressure. Assessment of right atrial pressure is indirect at best with echocardiography. Although certain echocardiographic parameters, such as increased right atrial size and dilatation of the inferior vena cava, help us "guesstimate" right atrial pressure (*see* Chapter 18, Table 3), these are notoriously inaccurate, especially if pressures are high. By adding the gradient obtained from the tricuspid regurgitant velocity signal to our estimate of right atrial pressure we can obtain an estimate of right ventricular systolic pressure, which in turn should be equivalent to pulmonary artery systolic pressure.

Similarly, because echocardiography measures blood velocity, not blood flow, our estimate of the volumetric degree of regurgitation by echocardiography is limited. We cannot directly measure the volume traversing the aortic valve in, for example, aortic insufficiency. For this reason, Doppler is, in many ways, better for assessment of the severity of stenotic lesions than for assessment of the severity of regurgitant lesions.

Color flow Doppler utilizes the same concepts and technology as pulse wave Doppler and is, therefore, subject to the same limitations. The colors that we see in color flow Doppler are simply color encoded pixels that represent the velocity of blood flow at that particular spatial location. Colors that are pure red or blue in color flow Doppler represent velocities that are below the aliasing velocity of the Doppler signal (Fig. 16). Colors that appear to be yellow-green or mosaic, depending on the color map utilized, suggest high velocity (higher than the aliasing velocity) or turbulent flow (Fig. 17; please *see* companion DVD for corresponding video). The aliasing velocity, in centimeters per second, is usually listed on the scale present on the ultrasound image. Although we often estimate the volume of regurgitant lesions, including mitral and aortic regurgitation, from the color flow Doppler signal, we cannot do this directly because color flow Doppler provides limited assessment of the volumetric degree of regurgitation.

SUMMARY

The properties of ultrasound permit real-time generation of cardiac anatomical and hemodynamic data.

Improvements in transducer design and imaging modalities have led to improved image quality. The addition of Doppler ultrasound to 2D echocardiography provides reliable noninvasive determination of velocity shifts and pressure gradients within and across cardiac chambers. Echocardiographic data is influenced by limitations intrinsic to ultrasound and Doppler technology, patient characteristics, and operator skill.

SUGGESTED READING

Cape EG, Yoganathan AP. Principles and instrumentation for Doppler. In: Skorton DJ, Schelbert HR, Wolf GL, Brundage BH, eds. Marcus Cardiac Imaging. A Companion to Braunwald's Heart Disease, 2nd ed. Philadelphia: WB Saunders, 1996: 273–291.

Feigenbaum H. Echocardiography, Fourth ed. Lea and Febiger, Malvern, PA: 1986.

Geiser EA. Echocardiography: physics and instrumentation. In: Skorton DJ, Schelbert HR, Wolf GL, Brundage BH, eds. Marcus Cardiac Imaging. A Companion to Braunwald's Heart Disease, 2nd ed. Philadelphia: WB Saunders, 1996:273–291.

Seghal CM. Principles of ultrasonic imaging and Doppler ultrasound. In: St. John Sutton MG, Oldershaw PJ, Kotler MN, eds. Textbook of Echocardiography and Doppler in Adults and Children. Cambridge, MA: Blackwell Science, 1996:3–30.

Ultrasonography task force. Medical diagnostic ultrasound instrumentation and clinical interpretation. Report of the ultrasonography task force. Council on Scientific Affairs. JAMA 1991;265:1155–1159.

2 Introduction to Imaging

The Normal Examination

Dara Lee, MD and Scott D. Solomon, MD

CONTENTS

CASE PRESENTATION

A 30-yr-old pregnant woman is referred for an echocardiogram to evaluate a heart murmur. She has no significant medical problems and is in the third trimester of an uncomplicated pregnancy. The systolic murmur was noticed on a routine obstetrical examination; the patient has no complaints of dyspnea, chest discomfort, or palpitations. She walks daily without limiting cardiac or respiratory symptoms. She has no history of rheumatic fever and has never been told of a heart murmur in the past.

Findings

As expected, the study is entirely normal. The most likely cause of the patient's murmur is the increased intravascular volume expansion associated with third trimester pregnancy, which often leads to a benign "flow murmur." Such a murmur may be auscultated in other states of increased flow across a normal valve, such as fever or hyperthyroidism.

TWO-DIMENSIONAL, M-MODE, AND DOPPLER ECHOCARDIOGRAPHY

The basic principles of echocardiography, including the basics of physics and instrumentation are discussed in Chapter 1. This chapter is an introduction to the echocardiographic examination, and a detailed description follows in Chapter 3.

TWO-DIMENSIONAL ECHOCARDIOGRAPHY

Two-dimensional (2D) images form the basis of the echocardiographic study, providing structural and functional information as well as guiding the use of M-mode and Doppler techniques. The tomographic images described next constitute the 2D study. As discussed in Chapter 1, ultrasound waves generated from the ultrasound transducer travel to the heart and are then reflected back to the transducer. Returning ultrasound waves are analyzed for depth location (based on the time elapsed between signal emission and return), and density (denser structures will reflect a greater proportion of the ultrasound beam than less refractile objects). Figures 1 and 2 demonstrate a 2D image from the parasternal long-axis (please *see* companion DVD for corresponding video for Fig. 1).

From: *Contemporary Cardiology: Essential Echocardiography: A Practical Handbook With DVD*
Edited by: S. D. Solomon © Humana Press, Totowa, NJ

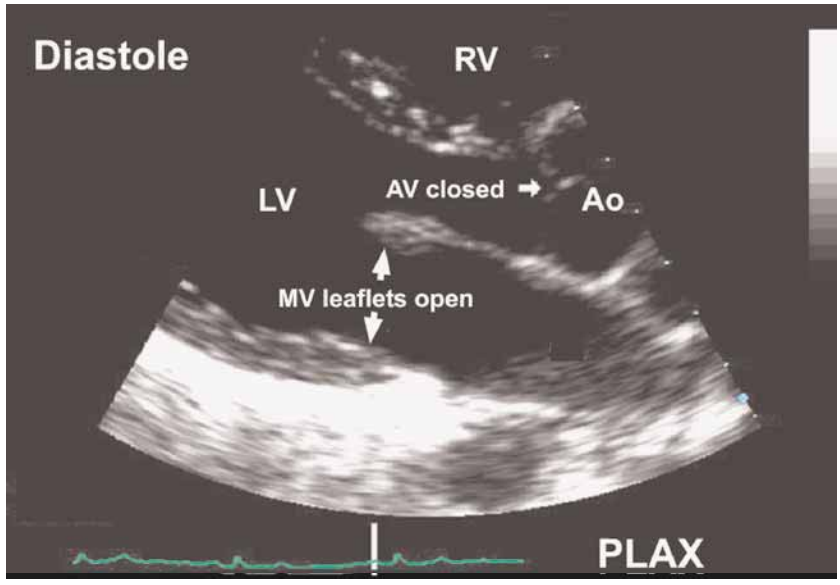

Fig. 1. Parasternal long-axis view (PLAX) demonstrating the following cardiac structures: RV, right ventricle; LV, left ventricle; AV, aortic valve; Ao, aorta; MV, mitral valve. This image is normal, as are all the images in this chapter. (Please *see* companion DVD for corresponding video.)

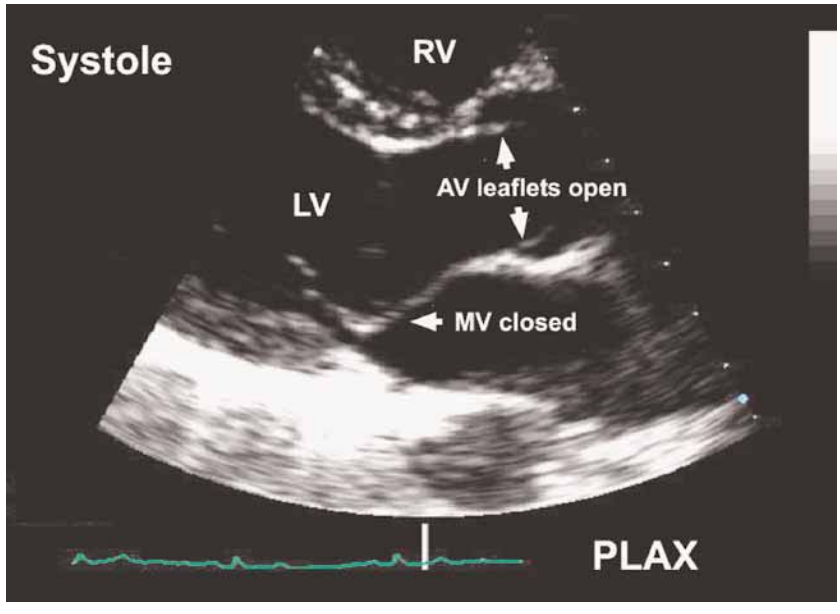

Fig. 2. Parasternal long-axis view at end systole demonstrating the following cardiac structures: RV, right ventricle; LV, left ventricle; AV, aortic valve; MV, mitral valve.

M-Mode Echocardiography

M-mode images (M stands for "motion") can be thought of as a one dimensional, or "ice-pick" image, recorded over time. Most M-mode images are recorded in the parasternal long-axis view previously described (still frame of M-mode in parasternal long-axis). The ultrasound beam is maneuvered to slice through the structure of interest, producing a high-resolution image of this slice over time. The high resolution of M-mode images, and the ability to correlate them with a simultaneously recorded electrocardiogram, makes M-mode the image of choice for many measurements. Figures 3 and 4 demonstrate M-mode views through the left ventricle (LV) and through the mitral valve (MV).

Doppler Echocardiography

Doppler echocardiography is used to measure blood flow; it can assess flow velocity, direction, and turbulence

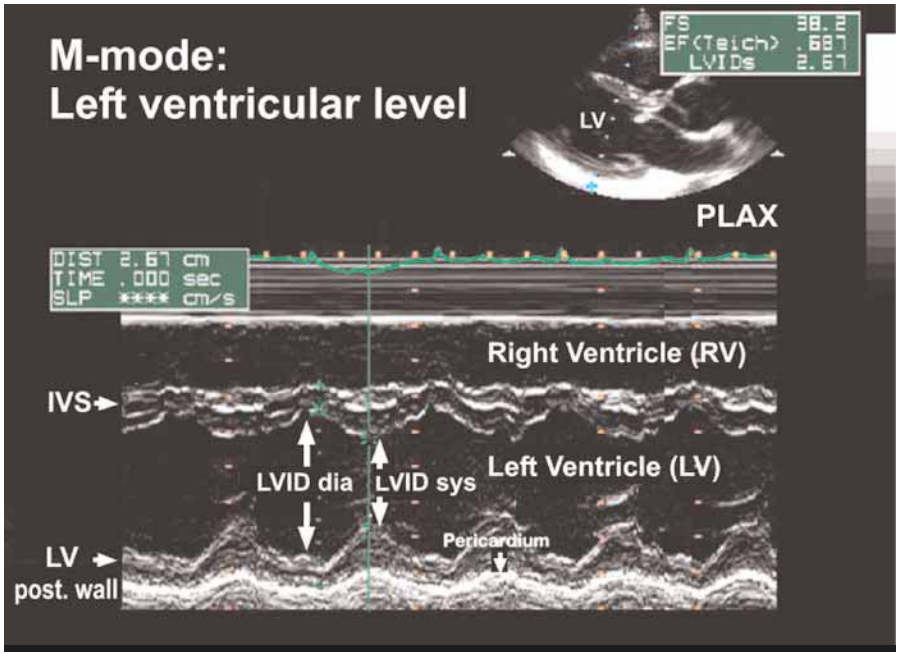

Fig. 3. M-mode through the left ventricle. From this view, measurements of left ventricular wall thickness, and end-diastolic and end-systolic diameter can be made. The electrocardiogram is useful for timing the cardiac cycle.

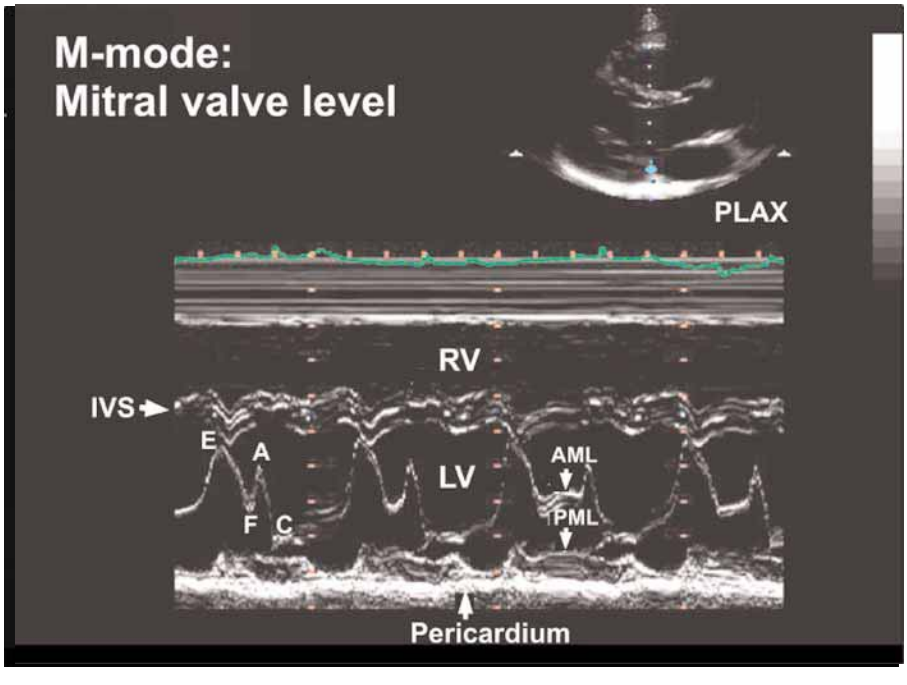

Fig. 4. M-mode through the mitral valve. From this measurement, the morphology of the mitral valve can be visualized. Note the typical M configuration of the mitral valve during early diastolic filling (E), and atrial filling (A). The anterior mitral leaflet (AML) and the posterior mitral leaflet (PML) are noted, as is the pericardium.

(*see* Chapter 1). Doppler is primarily used to assess blood flow velocity. Spectral Doppler (Fig. 5) shows waveforms that represent blood velocity, with time on the *x*-axis and velocity on the *y*-axis. *See* Chapter 1 for an explanation of the differences between pulsed- and continuous-wave Doppler.

Color Flow Doppler Echocardiography

Color flow Doppler depicts blood velocity data superimposed on the 2D image (Fig. 6; please *see* companion DVD for corresponding video). Nonturbulent flow that is below the Nyquist limit (*see* Chapter 1) and directed toward the transducer appears in red and nonturbulent

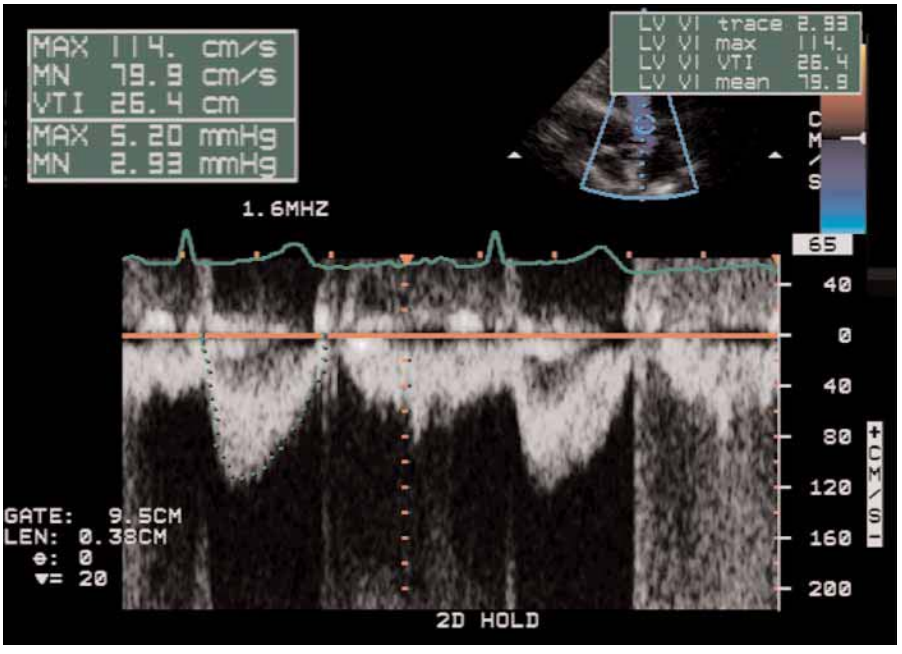

Fig. 5. Pulsed Doppler through the left ventricular outflow tract. The waveform demonstrates the velocity of blood (*y*-axis), with time on the *x*-axis. The electrocardiogram allows correlation with the cardiac cycle.

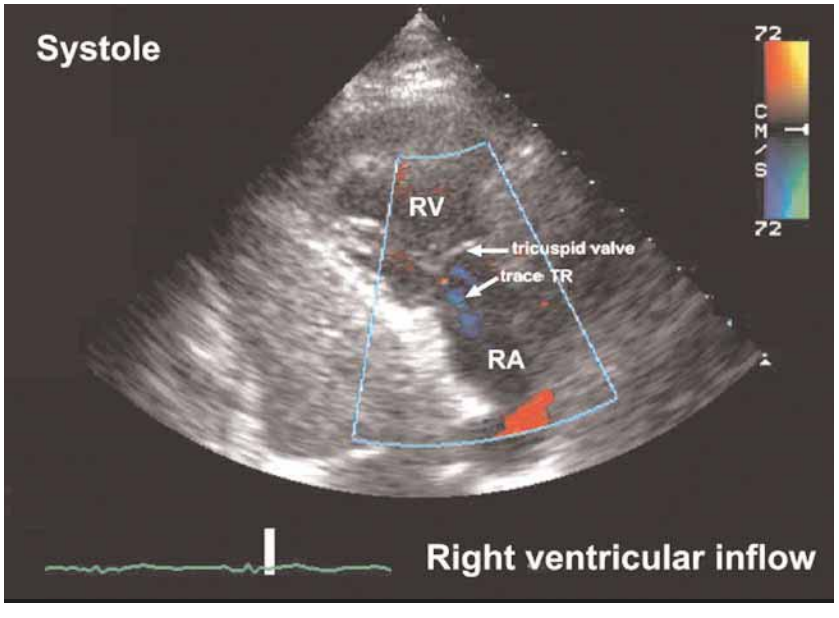

Fig. 6. Example of color flow Doppler demonstrating tricuspid regurgitation (a normal finding in this patient). Color flow Doppler is a form of pulsed-wave Doppler in which blood velocities are color encoded and superimposed on top of the two-dimensional image. The scale on the upper right hand side of the image shows the velocity associated with each color gradation as described in the text. (Please *see* companion DVD for corresponding video.)

flow below the Nyquist limit directed away from the transducer appears in blue. Perpendicular flow is not well visualized by Doppler images. Turbulent flow, and flow in which the velocities are faster than the Nyquist limit, is seen as a multi-color mosaic signal.

The Views

This patient's study, like most studies, is comprised of a standard set of views recommended by the American Society of Echocardiography. Multiple different viewing angles are needed to fully visualize all the cardiac

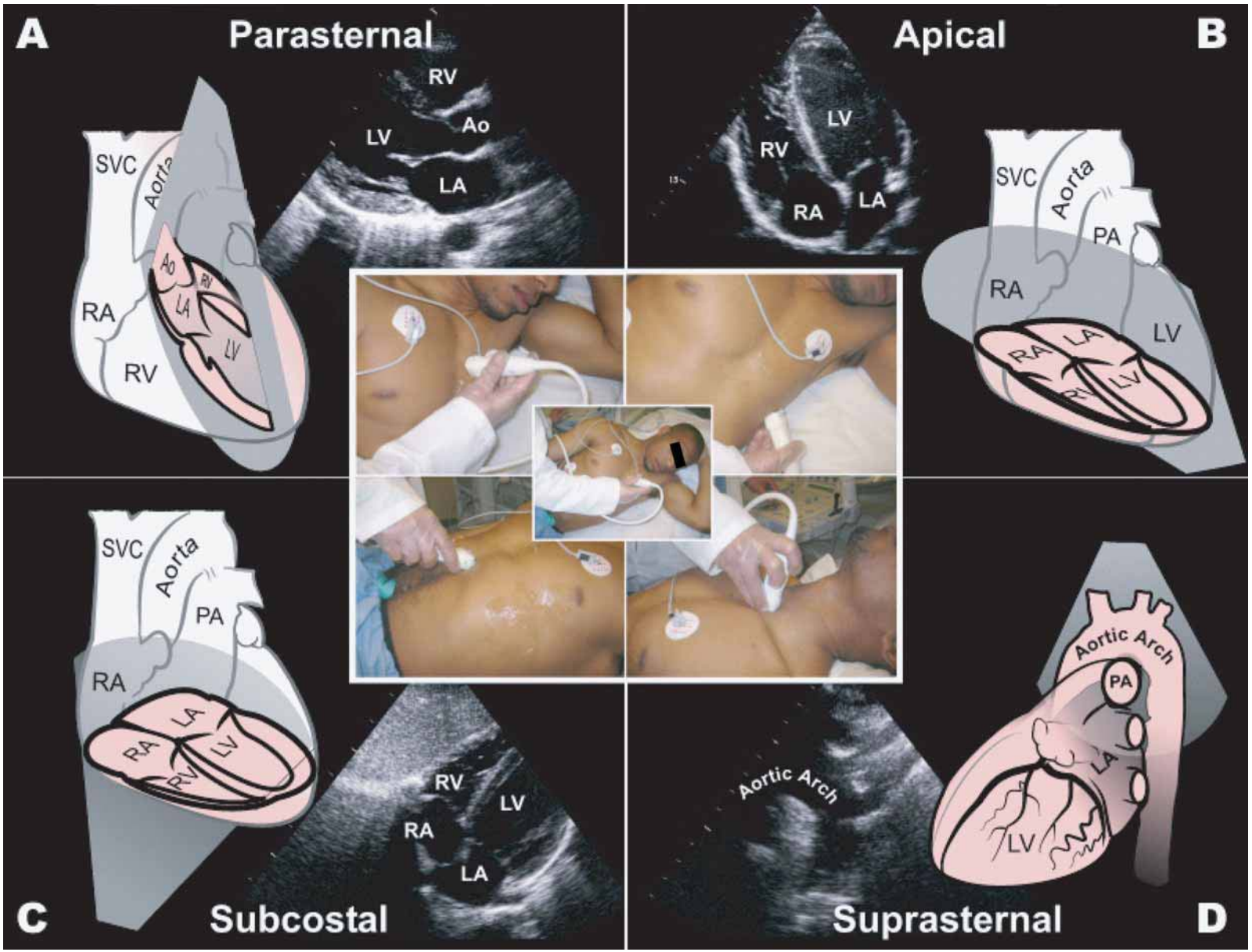

Fig. 7. Illustration showing transducer placement for each of the major echocardiographic views: **(A)** parasternal location for parasternal long and short-axis; **(B)** apical location for apical four-, two-chamber and long-axis views; **(C)** subcostal location for subcostal views; **(D)** suprasternal location for suprasternal notch view.

Table 1
Echocardiographic Views

View	*Patient/transducer position*	*Structures imaged*	*Doppler*
Left parasternal: long-axis view	Supine/third to fourth interspace	Overview of cardiac structures, chamber dimensions, and ventricular function. Most standard measurements, including LA, aortic root, LV diastolic and systolic dimensions. RV size and function measurements variable in this (and all) views.	Color flow Doppler looking for mitral regurgitation and aortic insufficiency.
Left parasternal: RV inflow	Same but tilt inferomedially, slight clockwise rotation	Long-axis view of RV, RA; good view for TV and regurgitant velocity.	Color flow Doppler looking for tricuspid regurgitation; spectral Doppler (CW) demonstrating tricuspid regurgitant velocity.
Left parasternal: short-axis view	Same but rotate perpendicular, tilt up and down to image from base to apex	Cross-section of LV to assess global and regional LV function from apex to base as transducer is tilted. Papillary muscles, MV in cross-section—good for planimetry of MV in mitral stenosis. At base, AV seen in cross-section; RVOT seen across top of image, PV to right of AV.	Color flow Doppler through the aortic valve for assessment of aortic insufficiency.
Apical: four and five chamber	Left lateral decub/point of maximal impulse. Anterior rotation produces five-chamber view.	All four chambers; ventricular septum, lateral wall of LV. Atrial septum, MV and TV with regurgitant jets and inflow velocity profiles. Inferior pulmonary veins seen as they enter LA. In five chamber view, aortic valve and root also seen, good view to assess for aortic regurgitation or stenosis.	Color flow Doppler looking for mitral regurgitation, aortic insufficiency, and tricuspid regurgitation; spectral Doppler (PW) of mitral inflow, outflow tract, and in suspected aortic stenosis, CW Doppler of aortic valve. CW Doppler for assessment of tricuspid regurgitant velocity.
Apical: two and three chamber	Same but with perpendicular rotation.	LV anterior and inferior walls, LA, MV and regurgitant jet. Three-chamber view brings aortic valve and root into view, and shifts to inferolateral and anteroseptal segments of LV.	Color flow Doppler for mitral regurgitation (two- and three-chamber views), and aortic insufficiency (three-chamber view).
Subcostal	Supine with hips and knees flexed/subxiphoid, at or slightly right of midline	Often best view in patients with hyperinflated lungs; long-axis similar to parasternal window but may provide better visualizaion of apex, RA and IVC, interatrial septum. Good view to look for PFO/ASD. Short-axis similar to parasternal. Abdominal aorta can be seen in this window.	Color flow Doppler of intra-atrial septum looking for evidence of atrial septal defect.

(Continued)

Table 1 ***(Continued)***

View	*Patient/transducer position*	*Structures imaged*	*Doppler*
Suprasternal	Supine with pillow under shoulders, head to left/suprasternal notch.	Ascending aorta, aortic arch, proximal brachiocephalic vessels, descending thoracic aorta, and right and main PAs (sometimes the left PA). Good position to measure transaortic velocity/gradient in aortic stenosis, assess for diastolic flow reversal in aortic regurgitation. Depending on image quality, may detect aortic aneurysm or dissection, postductal coarctation or patent ductus arteriosus; superior vena cava flow velocity profile.	PW or CW Doppler can be used to interrogate possible coarctation of the aorta.

CW, continuous wave; LA, left atrium; LV, left ventricle; MV, mitral valve; PA, pulmonary artery; PW, pulsed wave; RA, right atrium; RVOT, right ventricular outflow tract; TV, tricuspid valve.

structures, because each echo view provides only a 2D image of the 3D heart. There are four major transducer positions: the parasternal, apical, subcostal, and suprasternal notch positions (Fig. 7). From each transducer position, rotating and tilting the probe will produce several different tomographic images.

By convention, the echo images shown here and at most centers are presented in a triangular window, with the top of the triangle generally at the top of the screen (Fig. 1). Some labs, by convention, invert the triangle. The location of the transducer, relative to the image, is always at the top of the triangle; the structures closest to the top are therefore those closest to the transducer (and closest to the patient's skin). An electrocardiogram tracing is recorded simultaneously with the echo images, so that the phase of the cardiac cycle can be correlated to the mechanical activity of the heart; this is usually located at the bottom of the screen.

The proper positioning of the patient and the probe is described for each view. Transducer heads are marked with a notch, groove, or dot known as the "index;" this index is perpendicular to the imaging plane.

Keep in mind that the views and positions described next are those most frequently used in the majority of patients. However, certain anatomical variations or pathological conditions may require nonstandard views; deviating from the usual transducer positions may be necessary to obtain optimal images in these cases.

ECHOCARDIOGRAPHIC VIEWS

Table 1 describes each echocardiographic view, the patient and transducer position, and structures imaged in each view.

The Parasternal Position

For the parasternal views, the patient lies in the left lateral decubitus position with the left arm supporting the head. The transducer is generally placed just left of the sternum, in the second, third, or fourth intercostal space (Fig. 7). From here, both short- and long-axis views of the heart can be obtained.

Parasternal Long-Axis View (Fig. 1)

The index is pointed toward the patient's right shoulder, producing a longitudinal section through the LV. Remember that the image is displayed as if the transducer tip were at the top of the triangle; therefore, the structures at the top of the triangle are the most anterior (i.e., closest to the surface of the chest). The right ventricle (RV) lies anterior to the LV, so the chamber at the top of the triangle is the RV. (If there is a pericardial fluid collection or a prominent epicardial fat pad anterior to the RV, this will be seen above the RV in the parasternal long-axis view.) Below the RV is the LV; the anterior interventricular septum is uppermost, and the posterior LV wall is below, with the LV apex to the left. The ascending aorta is on the

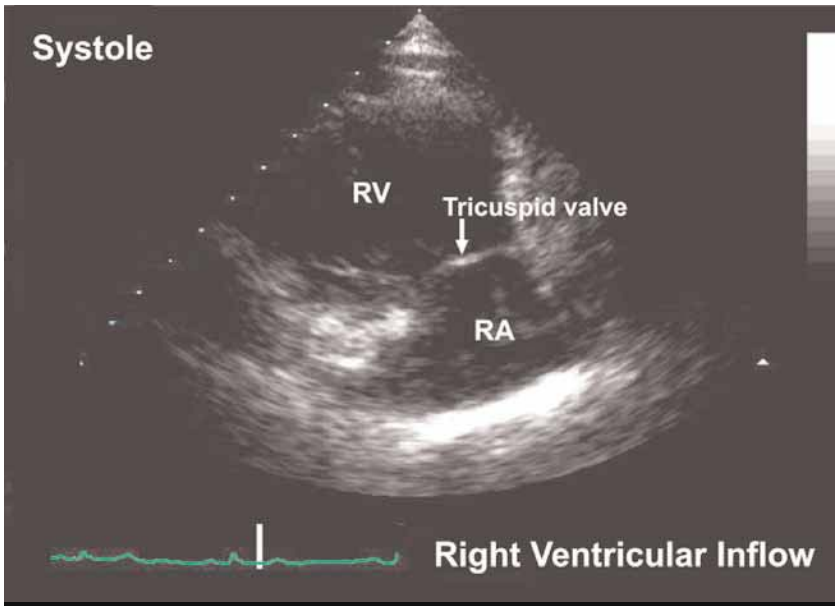

Fig. 8. Right ventricular inflow view. From this view, we can see a longitudinal view of the right ventricle (RV) and right atrium (RA). The RA is to the right and bottom (posterior) and the RV is above (anterior) and left. This view allows visualization of the tricuspid valve, as well as assessment of tricuspid regurgitation and measurement of tricuspid regurgitant velocity. (Please *see* companion DVD for corresponding video.)

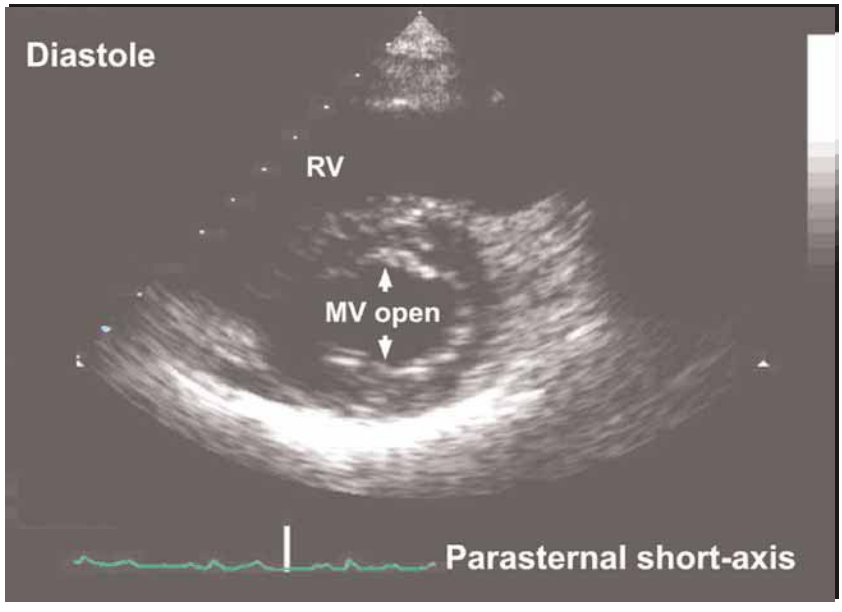

Fig. 9. Parasternal short-axis view, mitral position. This view represents a "breadloaf" slice through the heart at the level of the mitral valve. From this view, you can see the mitral valve in cross-section ("fishmouth" view) with anterior and posterior leaflets (arrows) indicating the wide open early diastolic position. (Please *see* companion DVD for corresponding video.)

right of the screen; moving leftward, the aortic valve (AV) (right coronary AV leaflet superiorly and noncoronary leaflet inferiorly) and LV outflow tract (LVOT) are next. The left atrium (LA) and MV are at the bottom of the screen. The MV chordal apparatus and papillary muscles are also seen in this view.

The parasternal long-axis view is an excellent overview image of the heart. It is generally the best window for measuring the aortic root and LA, LV chamber dimensions, and LV wall thickness. The mitral and aortic valves are well seen, and anterior structures, such as the RV and pericardial effusions,

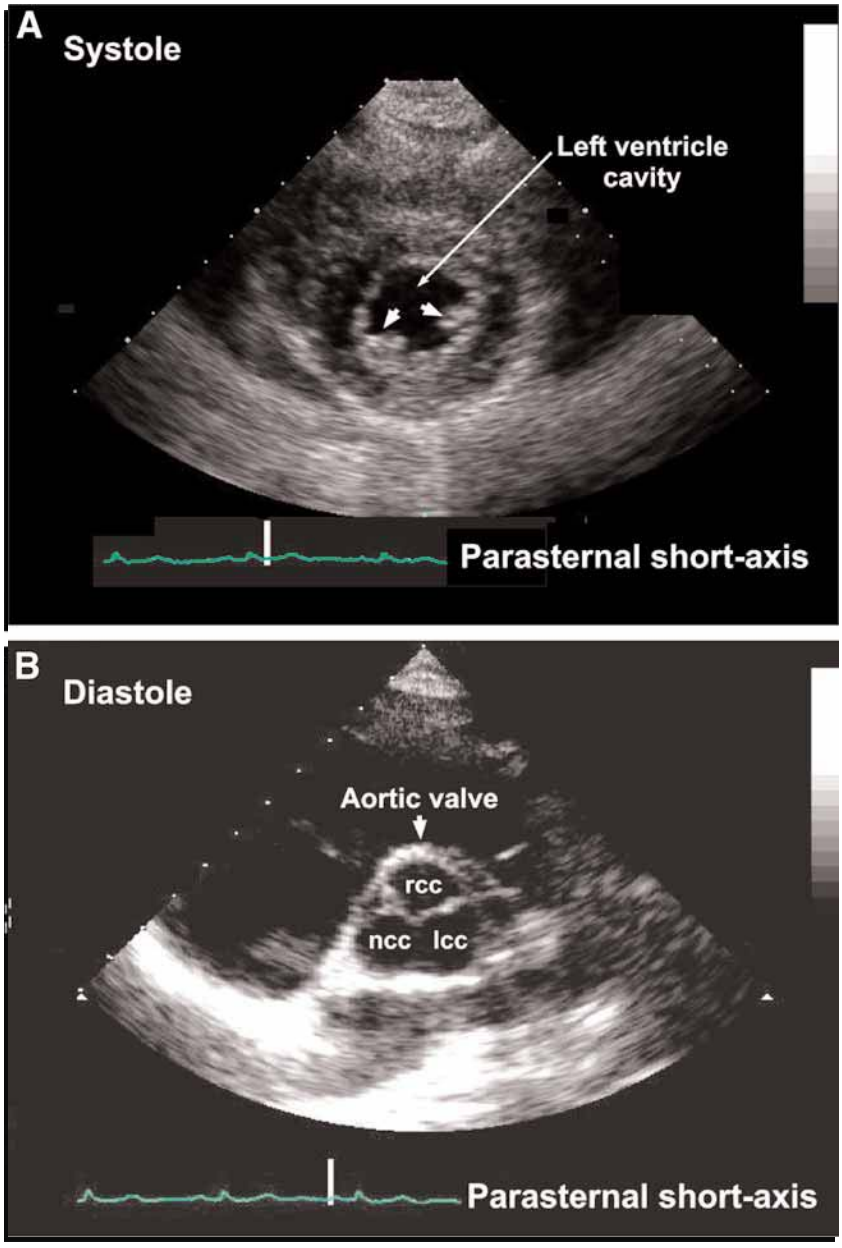

Fig. 10. (A) Parasternal short-axis view, papillary muscle level. This view is similar to the short-axis mitral position but more apical in the ventricle. The papillary muscles (PM) are visualized. This is an excellent view for assessing regional wall motion in the left ventricle. **(B)** Short axis through the aortic valve, visualized in the center of the screen, is comprised of three cusps, the right coronary cusp (RCC), the non-coronary cusp (NCC) and the left coronary cusp (LCC). Anterior to the aortic valve is the right ventricular outflow tract, with the tricuspid valve seen at 10 o'clock, and the pulmonic valve seen at approx 2 o'clock to 3 o'clock. The left atrium is immediately posterior to the aortic valve in this view. (Please *see* companion DVD for corresponding video.)

can be visualized as well. This view is generally used for measurement of the LVOT diameter (*see* Chapter 11). In addition, color flow Doppler in this view can reveal evidence of mitral regurgitation or aortic insufficiency. There is generally no need for using spectral Doppler in this view.

RV Inflow View

With inferomedial tilt of the transducer (still in the same parasternal position), a longitudinal view of the RV and right atrium (RA) can be obtained (Fig. 8; please *see* companion DVD for corresponding video). In this window, the RA is to the right and bottom (posterior) and the

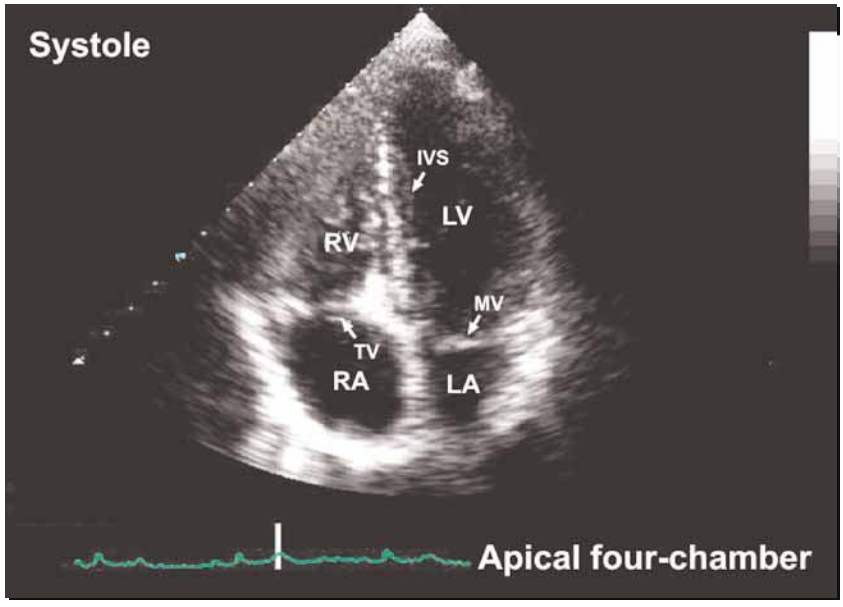

Fig. 11. Apical four-chamber view. From this view, the following structures are easily visualized: left ventricle (LV), right ventricle (RV), left atrium (LA), right atrium (RA), mitral valve (MV), and tricuspid valve (TV). Pulmonary veins (PV) can be visualized at the bottom of the left atrium. Note the prominent moderator band (MB), a normal structure, in the apical third of the right ventricle. (Please *see* companion DVD for corresponding video.)

RV is above (anterior) and left. This view allows visualization of the tricuspid valve, as well as assessment of tricuspid regurgitation by colorflow and measurement of tricuspid regurgitant velocity utilizing spectral continuous-wave Doppler.

Parasternal Short-Axis Views

Still in position at the left parasternal third or fourth intercostal space, the transducer is rotated 90° clockwise to obtain the short-axis views (Figs. 9 and 10; please *see* companion DVD for corresponding video). The index is now facing the patient's left shoulder. From this position, the LV is imaged in cross-section. Slices (as from a loaf of bread) can be obtained at three levels: the base, the midventricle, and the apex. The basal third of the heart is seen by angling the transducer superiorly and rightward; this view includes the MV leaflets and extends to the tips of the papillary muscles. Directing the transducer so that it is perpendicular to the chest wall visualizes the middle third of the LV; this view comprises the length of the papillary muscles, from their chordal attachments to their insertion in the LV. In this position, the RV is seen at the top (because it is anterior) and to the left of the screen. The LV should appear round in this view; if it appears oval, then the LV is being imaged obliquely. This is generally an excellent view for assessing global and regional LV contractility. The apical third of the LV can be seen with further inferior tilting of the probe.

When the transducer is moved even further up the torso or angulated slightly caudally, a cross-section through the aortic valve is obtained (Fig. 10B; please *see* companion DVD for corresponding video). Color flow Doppler in the short axis through the aortic valve can be useful for assessing aortic insufficiency.

Apical Position

With the patient still in the left lateral decubitus position, the probe is moved to the cardiac apex, just lateral and caudal to the point of maximal impulse. From this position, the transducer direction is varied to obtain the four-, five-, and two-chamber views of the heart: as a general rule, the apical position is superior to the parasternal for looking at mitral or aortic regurgitation, because the regurgitant jets tend to be more parallel to the color Doppler imaging beam.

Apical Four-Chamber View

From the apex, the transducer is angled superiorly toward the patient's right shoulder with the index pointing down (toward the patient's left flank) to obtain the four-chamber view; the imaging plane is perpendicular to the interventricular septum (Fig. 11; please *see* companion DVD for corresponding video). On the screen, the heart is

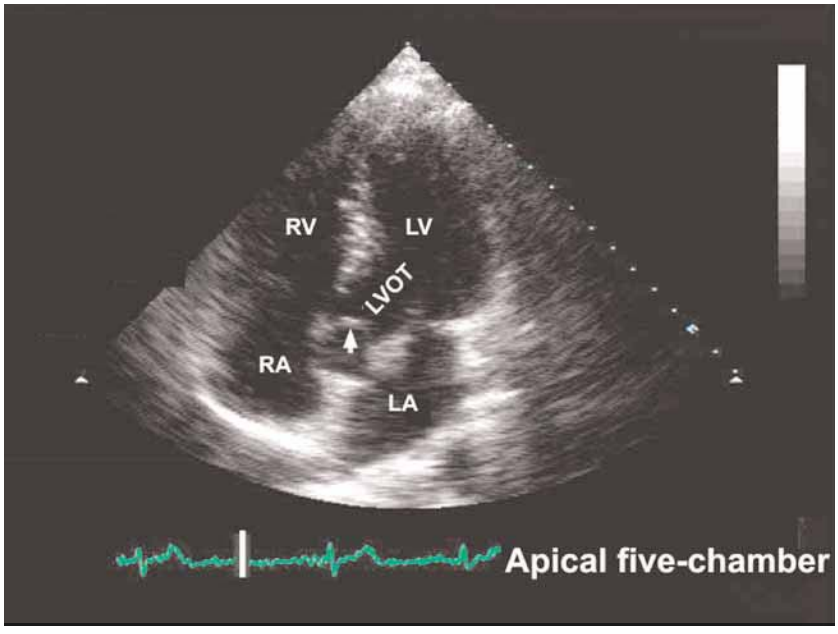

Fig. 12. Apical five-chamber view. Obtained by tilting the scan head 10–20° from the apical four-chamber view, this view allows for visualization of the aortic valve (arrow) and left ventricular outflow tract (LVOT). It is also the best view for obtaining Doppler flow through the aortic valve. (Please *see* companion DVD for corresponding video.)

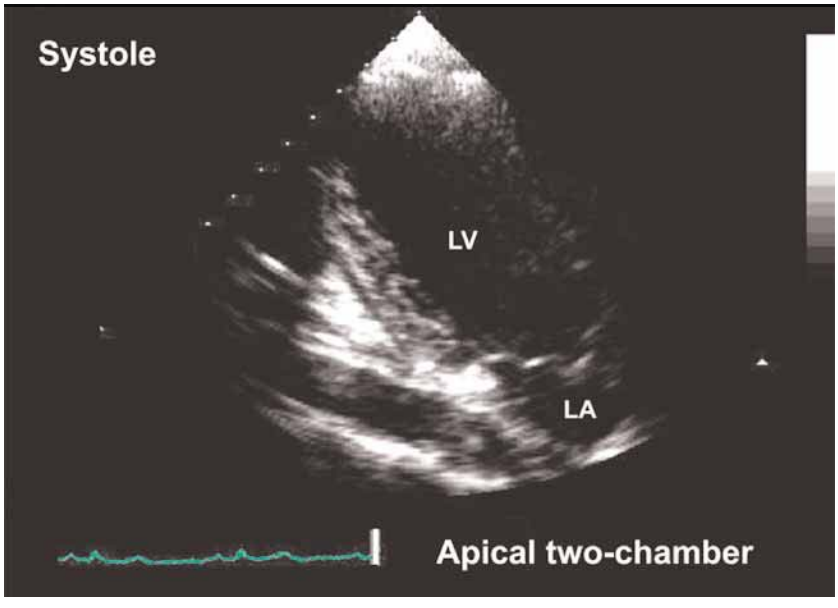

Fig. 13. Apical two-chamber view. Obtained by rotating the transducer 90° counterclockwise from the apical four-chamber view. This view shows the left ventricle (LV) and left atrium (LA), but the right-sided structures are no longer visible. This view is useful for visualizing regional wall motion of the anterior and inferior walls and is also the best angle from which to view the plane of mitral valve coaptation, useful in the diagnosis of mitral valve prolapse. (Please *see* companion DVD for corresponding video.)

displayed upside down, from the perspective of the apically placed transducer. The apex is the structure closest to the transducer and, therefore, it is at the top of the screen; the atria are at the bottom. The LV and LA are on the right and the RV and RA on the left, divided by the interventricular septum and interatrial septum. Notice that the inner surface of the RV is more heavily trabeculated than that of the LV, and that the RV apex does not reach the LV apex. In many patients, a prominent moderator band can be visualized in the RV; this is a normal

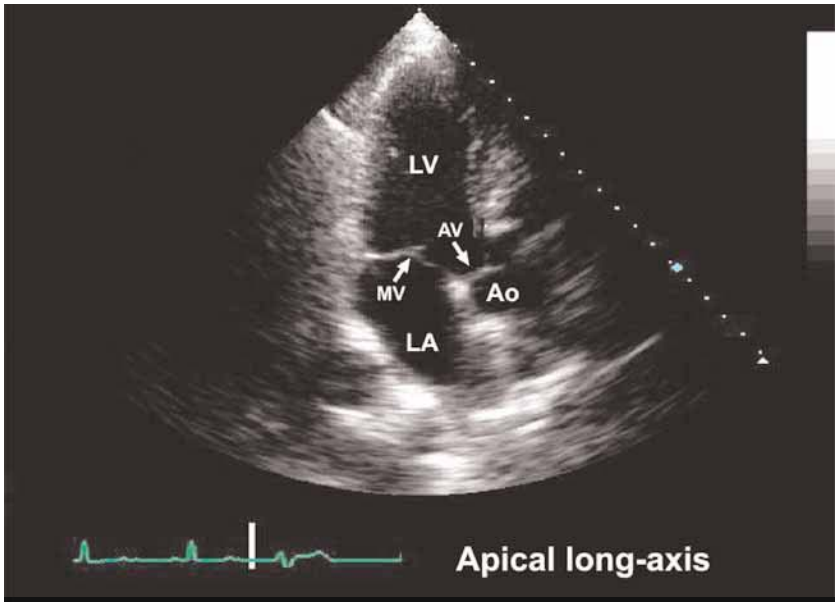

Fig. 14. Apical long-axis view. Obtained by further rotating the transducer another 45° counterclockwise from the apical two-chamber view. This view is almost identical to the parasternal long-axis, although the image is rotated 90° clockwise and the apex is well visualized. This view provides good images of the left ventricular posterior wall, interventricular septum, mitral valve, and aortic valve. (Please *see* companion DVD for corresponding video.)

finding. Also notice that the attachment of the septal leaflet of the tricuspid valve is approx 5–8 mm closer to the cardiac apex than the mitral attachment. These findings can be helpful in distinguishing the cardiac chambers. The apical four-chamber view is good for assessing ventricular function, particularly the motion of the interventricular septum and the lateral wall of the LV. The anterior RV wall and the AV valves are visualized in this view as well.

Color flow Doppler is used in this view to look for and assess possible mitral regurgitation, aortic insufficiency, and tricuspid regurgitation. The color flow sector should be positioned over the appropriate valve for proper visualization. In addition, color flow of the LVOT can alert the viewer of possible turbulence in this region that might be caused by subaortic stenosis owing to hypertrophic cardiomyopathy or a subaortic membrane.

Spectral Doppler is used to assess mitral inflow. The Doppler cursor is placed at the tips of the leaflets and the mitral inflow signal is assessed. Tricuspid regurgitant velocity can be assessed by continuous-wave Doppler through the tricuspid valve. The tricuspid regurgitant velocity is dependent on the gradient between the RV and the RA. Using the Bernoulli equation (*see* Chapter 1), the pulmonary systolic pressure can be estimated (in the absence of pulmonic stenosis) by adding the estimated gradient between the RV and the RA to an estimate of RA pressure (*see* Chapter 1).

Apical Five-Chamber View

Without changing the position or rotation of the transducer, tilting of the scan head 10–20° anteriorly reveals the five-chamber view, with the imaging plane now traversing the AV and LVOT (the "fifth chamber;" Fig. 12; please *see* companion DVD for corresponding video). This is often the best view for assessing the structure and function of the aortic valve. Doppler color flow mapping and Doppler pulsed-wave images obtained in this view are useful in determining the presence and severity of aortic regurgitant or stenotic lesions.

Apical Two-Chamber View (Fig. 13; Please *See* Companion DVD for Corresponding Video)

The anterior and inferior walls of the LV are not visualized in the four- and five-chamber views because the imaging plane does not traverse them; these can be seen by rotating the imaging plane 90° counterclockwise (so the index now points to the patient's left shoulder), producing the apical two-chamber view (the two chambers are the LA and LV). Regional wall motion of the anterior and inferior walls is seen in this view; it is also the best angle from

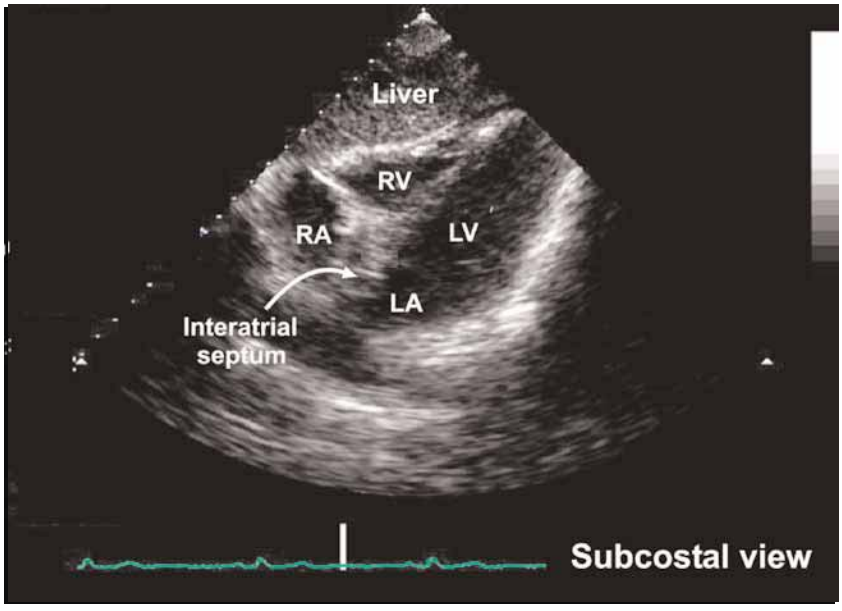

Fig. 15. Subcostal view, showing interatrial septum. The subcostal view demonstrates the right heart structures well. In addition, this view is useful for examination of the interatrial septum, and is used to help rule out atrial septal defects. This is also a useful view for asessing the hepatic veins and inferior vena cava (IVC). (Please *see* companion DVD for corresponding video.)

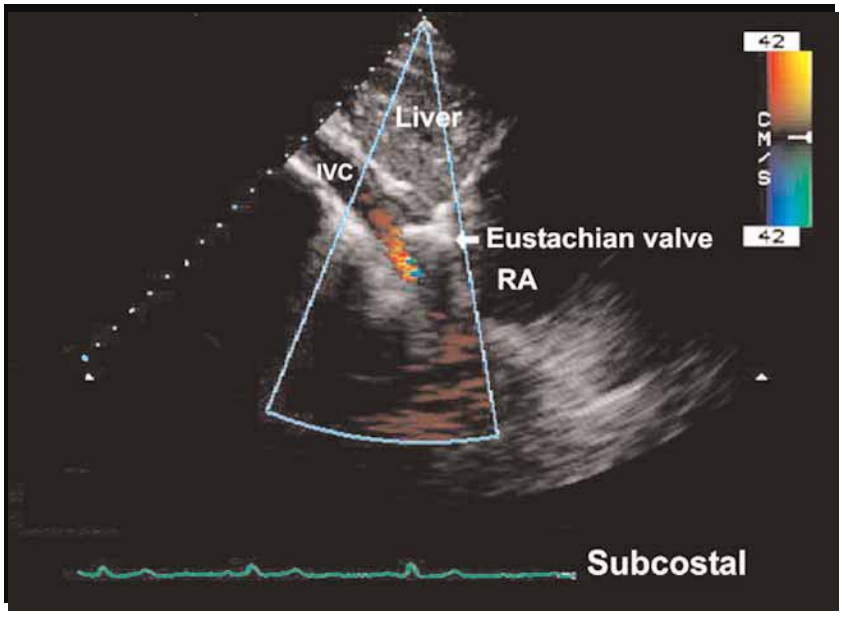

Fig. 16. Subcostal view showing hepatic veins and inferior vena cava (IVC). Elevated right atrium pressure may lead to IVC dilation and loss of the expected inspiratory collapse. (Please *see* companion DVD for corresponding video.)

which to view the plane of MV coaptation, useful in the diagnosis of MV prolapse. Color flow Doppler should be used in this view as well to visualize potential mitral regurgitation in the orthogonal plane to the four-chamber view.

Apical Long-Axis View

Further counterclockwise rotation of the transducer head produces the apical long-axis or three-chamber view (Fig. 14; please *see* companion DVD for corresponding video). This imaging plane is very similar to

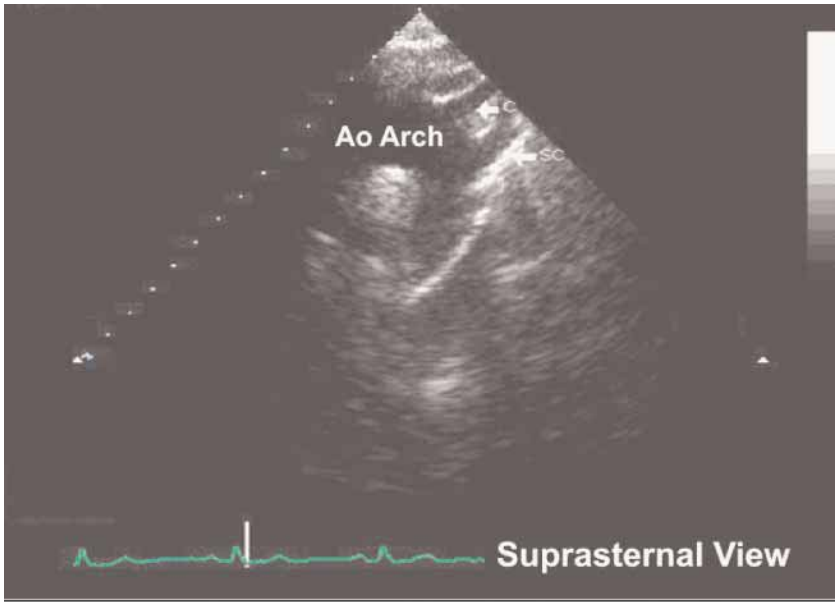

Fig. 17. Suprasternal view. The suprasternal transducer position allows visualization of the aortic arch and its major branches. The inominate artery arises from the ascending aorta (seen on the left of the screen); the left carotid and subclavian arteries arise from the left arch as it becomes the descending thoracic aorta. The right pulmonary artery (RPA) may be seen in cross-section beneath the aortic arch. (Please *see* companion DVD for corresponding video.)

the parasternal long-axis, and provides a good image of the LV posterior wall, interventricular septum, MV, and aortic valve. Color flow Doppler in this view can be useful to view potential aortic insufficiency.

Subcostal Position

For the subcostal views, the transducer is placed in the subxiphoid region, just to the right of center (Figs. 15 and 16; please *see* companion DVD for corresponding video). In this position, the ultrasound beam travels through the abdominal wall, part of the liver, and the diaphragm on its way to the heart. In some patients, such as those with emphysema, this may be the best imaging position (hyperinflated lungs obscure the parasternal windows, and flattened diaphragms optimize subcostal windows). However, in obese patients, subcostal windows may be difficult to obtain. For the subcostal views, the patient is placed in the supine position with knees flexed to relax the abdominal muscles. Deep inspiration with breath hold facilitates optimal imaging in this view.

From this position, a four-chamber view can be obtained by angulation of the transducer head toward the left shoulder, with the index facing the patient's left flank. In this image, the apex of the heart points up and to the right; the RA and RV are above the left heart chambers, adjacent to the liver. The right heart structures are well visualized in this view. The interatrial septum can be examined with color Doppler imaging for septal defects or patent foramen ovale. Rotating the transducer so the index points to the patient's head emphasizes the right heart structures as well as the hepatic veins and inferior vena cava (IVC). This is the optimal view for assessing the IVC, which can provide an indirect assessment of RA pressure; elevated RA pressure may lead to IVC dilation and loss of the expected inspiratory collapse. Clockwise rotation of the transducer produces a subcostal short-axis view of the LV and RV.

Color flow Doppler should be used to interrogate the interatrial septum for possible atrial septal defects, particularly secundum defects, which are best visualized in this view.

Suprasternal Position

The suprasternal transducer position allows visualization of the aortic arch and its major branches (Fig. 17; please *see* companion DVD for corresponding video). The transducer is placed in the suprasternal notch with the index toward the patient's head and the tip angled caudally; slight anterior or posterior tilting of the transducer maneuvers the imaging plane along the major axis of the aorta. The innominate artery arises from the ascending aorta (seen on the left of the screen); the left carotid and subclavian arteries arise from the left arch as it becomes the descending thoracic aorta. The right

pulmonary artery may be seen in cross-section beneath the aortic arch. Ninety degree rotation of the transducer head reveals the aortic arch in cross-section and the right pulmonary artery in longitudinal axis. This view can be useful in the diagnosis of some aortic diseases and congenital anomalies, including severe aortic insufficiency and aortic coarctation.

SUMMARY

A solid understanding of the normal echocardiogram is a necessary prerequisite to the identification of disease states. Watch this normal study several times, paying close attention to the valve structures and Doppler patterns in each window, the normal thickening of the myocardium, and the relative sizes of the various cardiac chambers. It may be useful to refer back to this study when abnormalities in subsequent chapters are encountered. The next chapter (Chapter 3) describes technical details of the standard echocardiographic examination in greater detail, and is designed to complement the overview presented in this chapter.

SUGGESTED READING

Jawad IA. Ultrasound in cardiology. In: Jawad IA, ed. A Practical Guide to Echocardiography and Cardiac Doppler Ultrasound, 2nd ed. Boston: Little, Brown, and Co, 1996:13–85.

Oh JK, Seward JB, Tajik AJ. Transthoracic echocardiography. In: Oh JK, Seward JB, Tajik AJ, eds. The Echo Manual, 2nd ed. Philadelphia: Lippincott-Raven, 1999:7–22.

Sehgal CM. Principles of Doppler imaging and ultrasound. In: St. John Sutton MG, Oldershaw PJ, Kotler MN, eds. Textbook of Echocardiography and Doppler in Adults and Children, 2nd ed. Cambridge: Blackwell Science, 1996:3–30.

St. John Sutton MG, Oldershaw PJ, Plappert TJ. Normal transthoracic Doppler echocardiographic examination. In: St. John Sutton MG, Oldershaw PJ, Kotler MN, eds. Textbook of Echocardiography and Doppler in Adults and Children, 2nd ed. Cambridge: Blackwell Science, 1996:31–66.

3 Protocol and Nomenclature in Transthoracic Echocardiography

Bernard E. Bulwer, MD, MSc and Jose Rivero, MD

Contents

EQUIPMENT BASICS

The transducer probe is the component that houses the piezoelectric crystals (*see* Chapter 1) and emits and receives the sound waves (Fig. 1).

The central processing unit receives raw data from the transducer, instrument controls, and the keyboard. It integrates and translates received data into visual images and calculations (on the display monitor). Some newer models are bundled with sophisticated software that permit postprocessing of acquired images and newer research tools.

Transducer and Doppler controls adjust the amplitude, frequency, and duration of the ultrasound waves emitted from the transducer probe. The details of instrument settings, e.g., power output, receiver gain, filters, sample volumes, velocity scale, sweep speed, and dynamic range, are outside the scope of this chapter, but are essential for optimal image acquisition and reporting. Some equipment models routinely display these on acquired images.

The ultrasound display allows visualization of images, calculations, and reports. Storage devices may be analog or digital. Digital images require much

From: *Contemporary Cardiology: Essential Echocardiography: A Practical Handbook With DVD*
Edited by: S. D. Solomon © Humana Press, Totowa, NJ

Fig. 1. Adult transthoracic echocardiography transducers generally range between 2 and 7 mmHz, with lower frequency transducers—2.5 and 3 mmHz—being the most commonly used. Higher frequency transducers are routinely used in pediatric echocardiography and transesophageal echocardiography. They provide increased resolution, but decreased penetration. The dedicated Doppler transducer (bottom right) is a nonimaging probe. These are standard components on modern echocardiography machines.

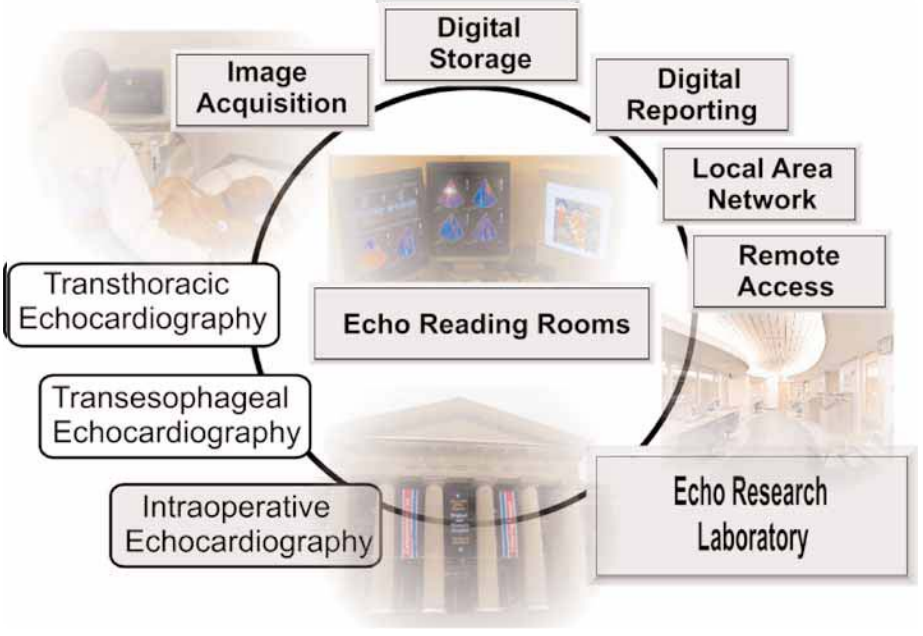

Fig. 2. Panorama of echocardiography services at a university teaching hospital. Guidelines on echocardiography laboratory standards and training are available at the American Society of Echocardiography website (www.asecho.org).

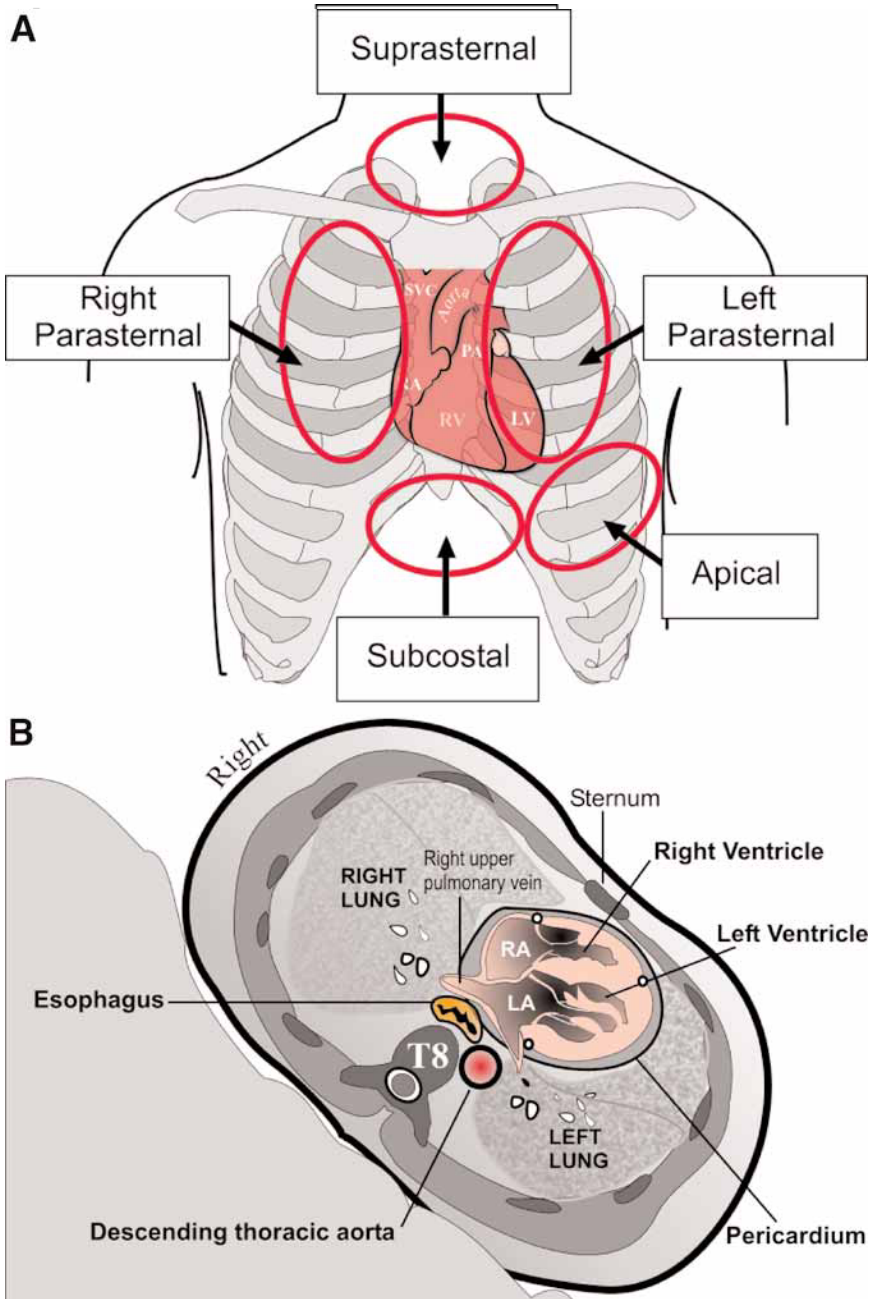

Fig. 3. (**A**) Standard transducer positions. (**B**) Cross-sectional cardiac topography.

memory. Hard disks, CDs, DVDs, central digital storage, and imaging work stations are parts of a modern digital echocardiography service (Fig. 2).

STANDARD TRANSDUCER POSITIONS

The standard echocardiographic images are acquired by transducer maneuvers within four standard anatomical positions—left parasternal (or simply parasternal), left apical, subcostal, and suprasternal (Fig. 3).

Individual patient and clinical characteristics often require the use of additional or non-standard windows, e.g., in congenital heart disease and post-chest surgery patients.

TRANSDUCER SCAN PLANE AND INDEX MARK

The ultrasound scan plane fans out from the piezoelectric electrodes housed in the transducer tip as shown (Fig. 4, left).

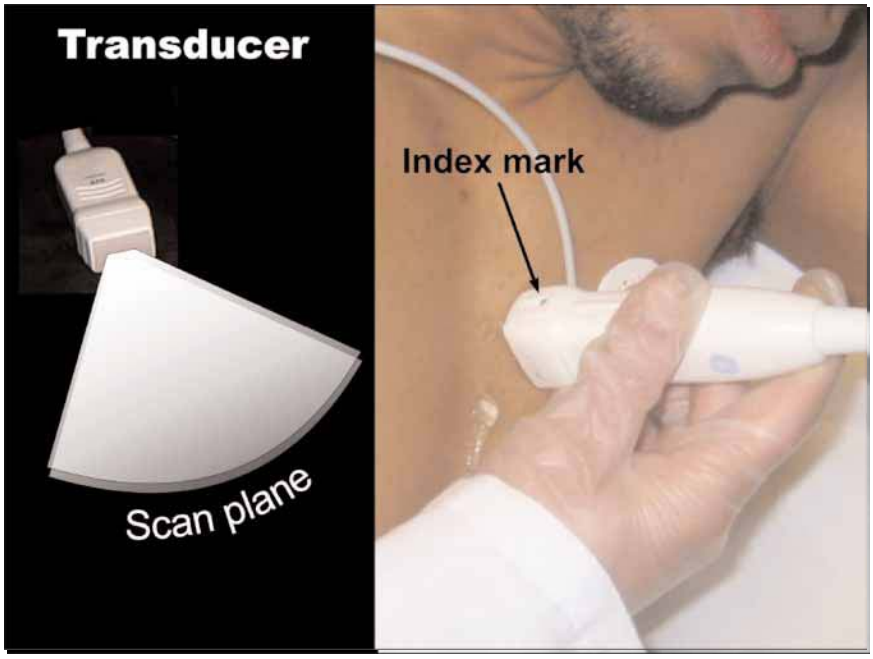

Fig. 4. Transducer scan plane and index mark.

Note the position of the index mark—a constant guide to transducer positions during the examination (Fig. 4, right). This model and others are designed with a palpable ridge.

By convention, the index mark indicates the part of the image plane that appears on the right side of the image display.

TWO-DIMENSIONAL ECHOCARDIOGRAPHIC IMAGING PLANES

Three orthogonal planes that transect the long and short axes of the heart are the reference standards during the two-dimensional (2D) echocardiographic examination.

Two parameters—transducer position (Fig. 3) and imaging plane (Fig. 5)—are used to define images in 2D echocardiography.

TRANSDUCER MANEUVERS

Three major transducer movements are described—tilting, angling, and rotating are shown in Figs. 6–8.

The aim of these movements is to acquire the best possible image of the area of interest.

Transducer movements are fluid and a skilled sonographer maneuvers the transducer to capture the desired images (Fig. 9).

EXAMINATION PROTOCOL

Following equipment and patient preparation, the examination begins at the left parasternal window, followed by apical, subcostal, and suprasternal views (Fig. 3).

At each window, a standard images and measurements are obtained as outlined in Table 1. The still frames in the protocol described below are from normal individuals.

Depending on the indication, the examination can be extended according to the clinical indication (Chapter 4). Additional imaging and analyses are conducted and discussed in the chapters that follow.

Following image acquisition, the formal echocardiography report follows. This is usually performed by attending cardiologists.

PARASTERNAL VIEWS

From the left parasternal position, the parasternal long-axis (PLAX) views, the right ventricle (RV) inflow and outflow views, and parasternal short-axis (PSAX) views are obtained.

Unless stated otherwise, parasternal views refer to the left parasternal position.

PLAX VIEW

With the index mark at approx the 10 o'clock position (Fig. 10) indicating a scan plane as shown in Figs. 11

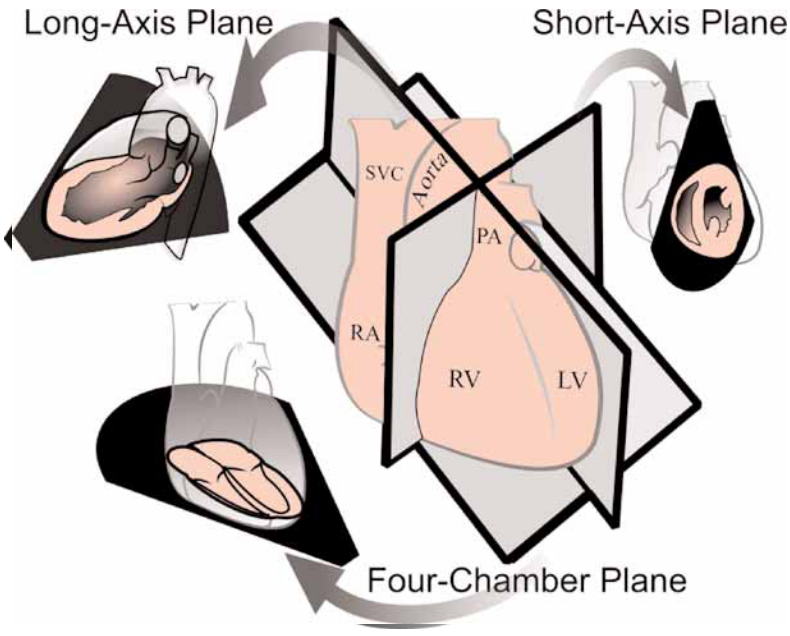

Fig. 5. Imaging planes: 2D transthoracic echocardiography.

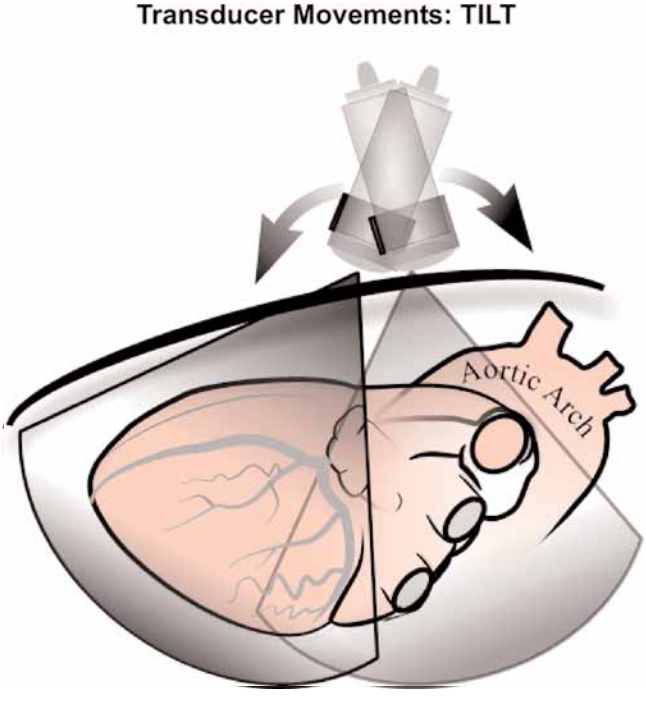

Fig. 6. Transducer movements: TILT.

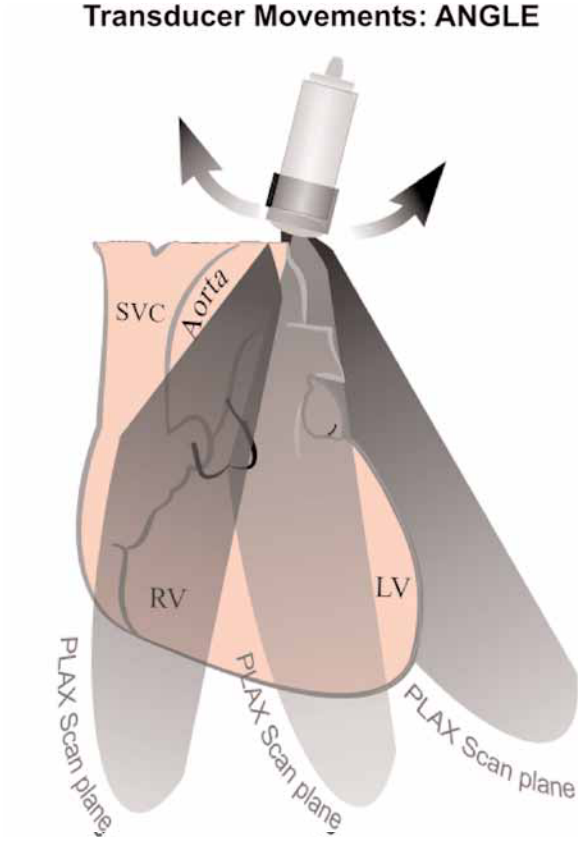

Fig. 7. Transducer movements: ANGLE.

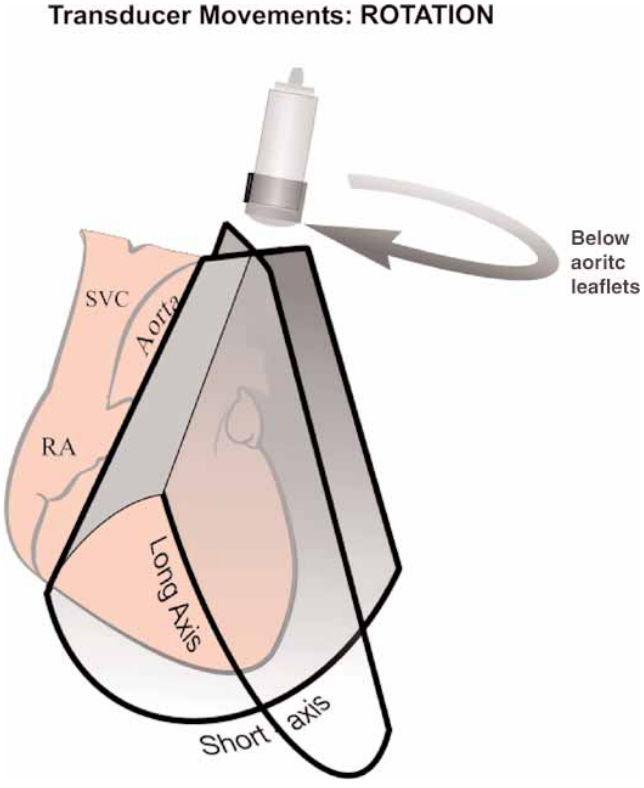

Fig. 8. Transducer movements: ROTATION.

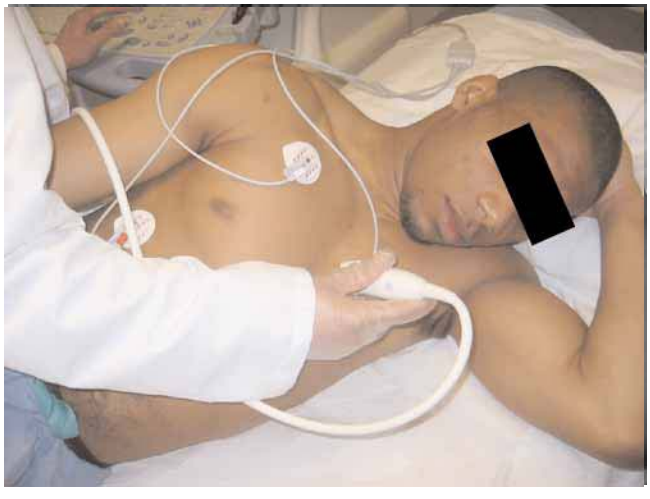

Fig. 9. Examination model (sonographer) in the left lateral position with attached electrocardiogram leads and transducer in the left parasternal position. Transducer gel is routinely used. It eliminates the air pocket—a poor conductor of ultrasound—between the transducer and the chest wall.

Table 1
2D Transthoracic Echocardiogram Examination Protocol[a]

1. Parasternal long axis—depth 20–24 cm
2. Parasternal long axis—depth 15–16 cm
   a. M-mode MV/AV, aortic root/LA, LV
   b. Measure aortic root (end systole; 2D or M-mode)
   c. Suspected aortic stenosis measure LVOT 1 cm below aortic leaflets (end systole; 2D)
   d. Measure LA (end of diastole; 2D or M-mode)
   e. Measure IVS in diastole/LV internal diameter/posterior wall thickness (2D or M-mode)
   f. Measure LV internal diameter in systole (2-D or M-mode)
   g. Zoom on MV/AV
   h. Color Doppler on MV/AV for regurgitation
3. RV inflow—depth 20 cm, then 15–16 cm
   a. Zoom on TV
   b. Color Doppler TV for TR
   c. CW TR for max velocity
4. Parasternal short axis
   a. 2D AV level; zoom on AV, color for AI width
   b. Color Doppler TV for TR, CW TR for velocity
   c. Color Doppler PV for PI (PW and CW)
   d. 2D image of PA bifurcation, PW from RVOT to bifurcation (look for PDA)
   e. 2D MV level (color Doppler optional)
   f. 2D papillary level
   g. 2D apical level
5. Apical four chamber —depth 20–24 cm
6. Apical four chamber—depth 15–16 cm
   a. Decrease depth to visualize apex
   b. Color Doppler MV for MR
   c. PW pulmonary veins
   d. PW mitral inflow (tips of leaflets in LV) for velocity, E:a ratio
   e. CW MV
   f. PW tissue Doppler at level of mitral annulus (lateral and septal), scale 20:20
   g. Visualize RV, color TV
   h. CW if TR present
7. Apical five chamber
   a. Visualize AV
   b. Color Doppler AV for AI
   c. PW along septum from apex for valve
   d. Aortic stenosis PW 1 cm below AV; freeze and trace TV1
   e. Aortic stenosis CW through AV; freeze and trace for TV2
   f. Afib trace five beats in a row
8. Apical two chamber
   a. Color Doppler for MR

(Continued)

Table 1 *(Continued)*

9. Apical three chamber
a. Color Doppler MV/AV regurgitation
10. Subcostal four chamber
a. Color Doppler atrial septum for ASD
b. Color Doppler RV for TR
c. Visualize IVC; color Doppler, measure IVC, and PW hepatic vein
11. Suprasternal notch—depth 24 cm, decrease if necessary
a. Color Doppler and PW descending aorta

[a]Additional views, measurements, and modalities are performed based on the clinical context, the information requested, and findings encountered during the examination.

2D, two dimensional; MV, mitral valve; AV, atrioventricular; LVOT, left ventricular outflow tract; LA, left atrium; IVS, interventricular septum; LV, left ventricle; TV, tricuspid valve; TR, tricuspid regurgitation; CW, continuous wave; AI, aortic insufficiency; PV, pulmonary vein; PI, pulmonic insufficiency; PW, pulsed wave; PA, pulmonary artery; RVOT, right ventricular outflow tract; PDA, patent ductus arteriosus; MR, mitral regurgitation; ASD, atrial septal defect.

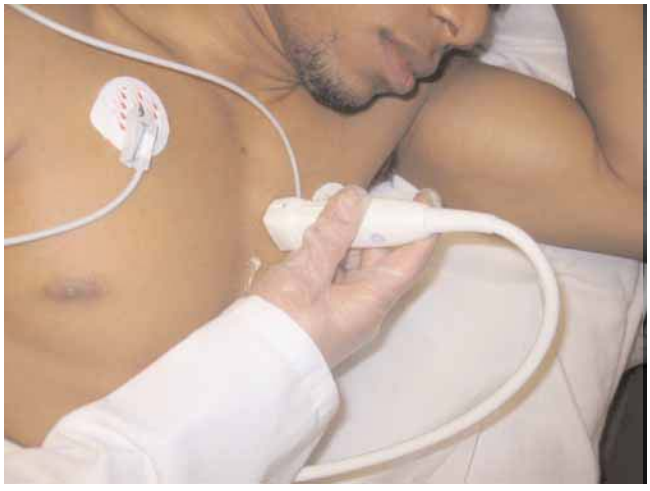

Fig. 10. Patient and transducer positioning: parasternal long-axis views (PLAX).

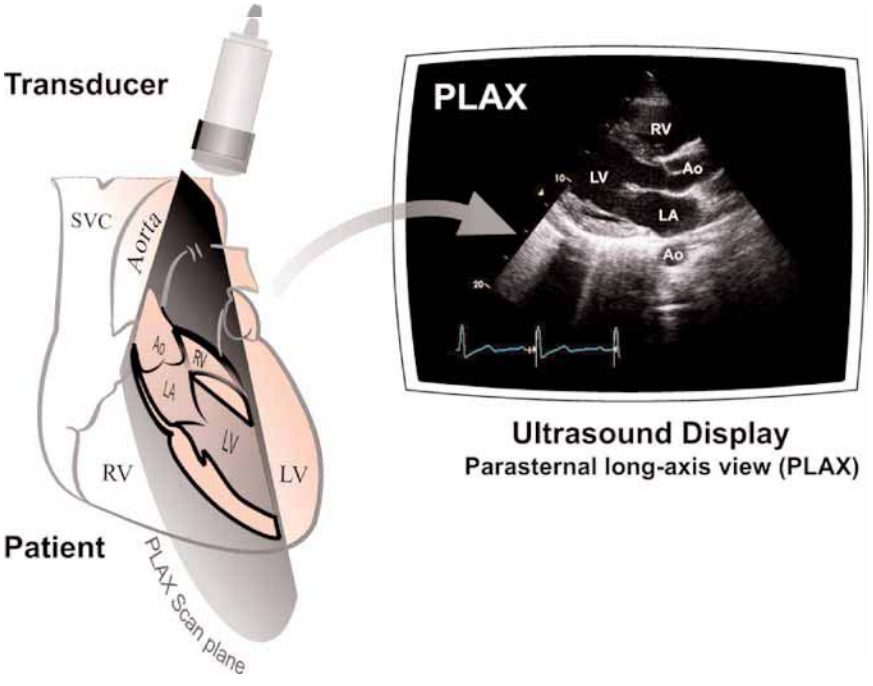

Fig. 11. Parasternal long-axis (PLAX) (depth 20–24 cm). (*See* companion DVD.)

and 12, and at a depth of 20–24 cm to visualize extracardiac structures, e.g., descending thoracic aorta or possible pleural effusion, cine images are optimized (adjust gain, depth, and sector width) and then acquired. Depth is then decreased to 15–16 cm for closer views of cardiac structures (area of interest).

At each position during the examination, the desired standard views (areas of interest) are optimized and acquired. When a particular frame or measurement is desired, the freeze function is used, measurements are taken and/or annotated accordingly.

M-mode sweep through the aortic valve, mitral valve (MV), and just distal to the tips of the mitral leaflets and standard measurements are obtained.

Color flow Doppler is applied to the region(s) of interest and images are acquired (Figs. 13–16).

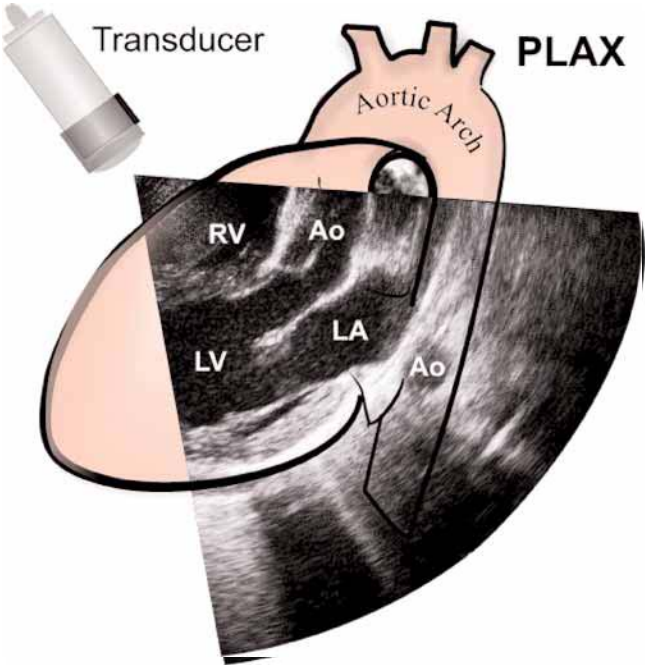

Fig. 12. Parasternal long-axis (depth 15–16 cm, PLAX). (*See* companion DVD.)

RV INFLOW

With the transducer in the standard PLAX position the transducer is slightly angled inferomedially (Fig. 17) until the RV inflow view (Figs. 18–20) comes into view. Images are then optimized and acquired at depths of approx 20 and 15–16 cm.

The tricuspid valve is evaluated (by zoom or decrease depth), color Doppler is applied (Fig. 21A) and followed by continuous-wave (CW) Doppler interrogation of flow across the tricuspid valve (Fig. 21B).

RV OUTFLOW

The sonographer may opt to image the RV outflow by angling supero-laterally with the transducer scan plane transecting the pulmonary artery (PA) as shown in (Fig. 21C) followed by Doppler evaluation (Fig. 21D).

This view provides good visualization of the pulmonary valves and the bifurcation of the main PA trunk into the right and left PAs (right pulmonary artery, left pulmonary artery; "trunk and trousers" view).

PSAX VIEW

With the transducer in the initial left PLAX position and with the aortic valve in focus, the transducer is then

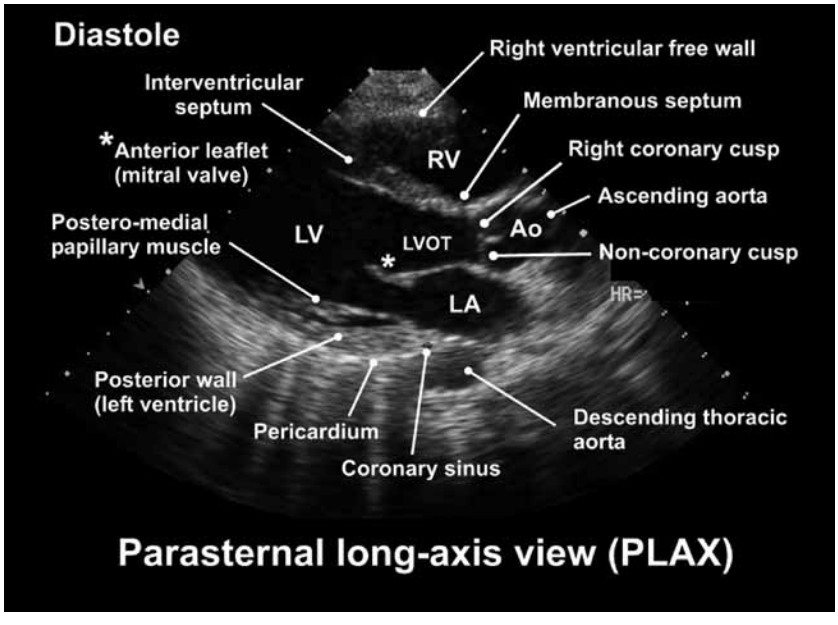

Fig. 13. Annotated parasternal long-axis view (PLAX) (depth 15–16 cm). Ao, aortic root; LA, left atrium; LV, left ventricle; RA, right atrium; RV, right ventricle.

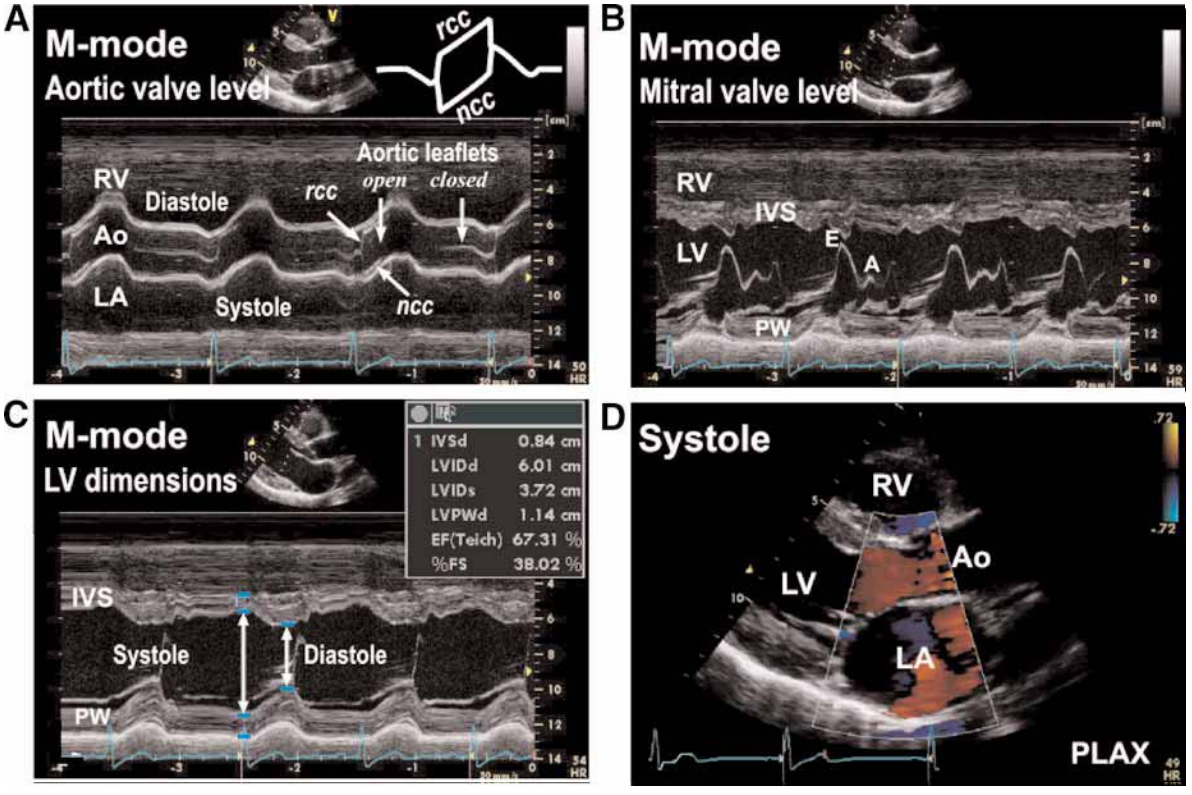

Fig. 14. Parasternal long-axis (PLAX) measurements. Ao, aortic root; LA, left atrium; IVS, interventricular septum; LV, left ventricle; ncc, noncoronary aortic cusp; PW, posterior wall; RA, right atrium; rcc, right coronary aortic cusp; RV, right ventricle. M-Mode sweeps through the aortic valve, mitral valve, and upper left ventricular levels (**A**–**C**) reveals structures as shown. (**A**) Note the systolic anterior movement of the aortic root during systole. Atrial volumes and hence measured 2D left atrial dimensions are maximal during systole. Aortic valve leaflets may appear faint on M-mode in young patients with normal aortic valve leaflets (cusps). Note the thin diastolic closure line and the normal box-like opening and closing profile of the normal aortic cusps (sketch). (**C**) Shows M-mode recording done just distal to the tips of the mitral leaflets. This is the standard M-mode image from which to measure left ventricular dimensions. At end-diastole, the ventricular septal diameter (septal thickness, IVSd), the maximal left ventricular internal diameter (LVIDd), the left ventricular posterior wall diameter (thickness, LVPWd) are measured. At end-systole, the left ventricular internal diameter (LVIDs) is measured. The upper limit of normal for maximal wall thickness is 1.1 and 5.5 cm for maximal LVIDd in the "average" adult. (**D**) Color flow Doppler is applied to the region of interest to identify regurgitant or stenotic jets across the aortic and mitral valves. Flow across a ventricular septal defect in the membranous septum (Fig. 13) is best visualized in the PLAX view. An end-systolic frame is shown in **A**. (*See* companion DVD.)

rotated clockwise to approximately the 12 o'clock position (Fig. 22) or until the short-axis view of aortic valve ("inverted Mercedes Benz sign") is visualized (Figs. 23 and 24).

The aortic valve is then zoomed (decrease depth) and interrogated by color Doppler (Fig. 25A,B) to evaluate possible aortic insufficiency (Fig. 26).

The region of interest then moves to the tricuspid valve. Color Doppler is applied across the valve followed by CW Doppler assessment (Fig. 25C,D). Peak tricuspid regurgitation velocity measured 2.5 m/s.

Next is the evaluation of the pulmonary valve for pulmonary regurgitation using color flow Doppler, pulsed-wave (PW) Doppler and CW Doppler.

Imaging of the PA bifurcation, and PW interrogation from the right ventricular outflow tract to the bifurcation can be performed when looking for a patent ductus arteriosus.

Slight transducer movements (or angling) toward the cardiac apex permits the acquisition of a series of PSAX at the level of the MV, the papillary muscles, and the apex (Figs. 27–30).

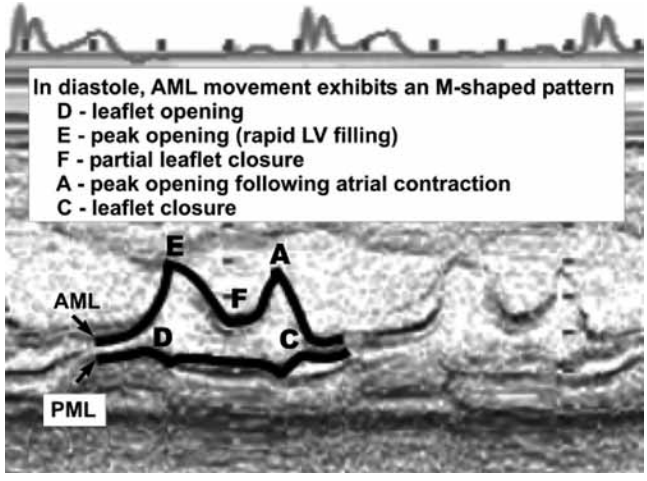

Fig. 15. M-Mode: mitral valve leaflets. Normal ranges for these dimensions are shown in the EF slope reflects the speed of anterior mitral leaflet (AML) closure. This pattern is significantly altered in mitral stenosis, becoming box-like. Posterior mitral leaflet (PML) movement essentially mirrors that of the anterior leaflet.

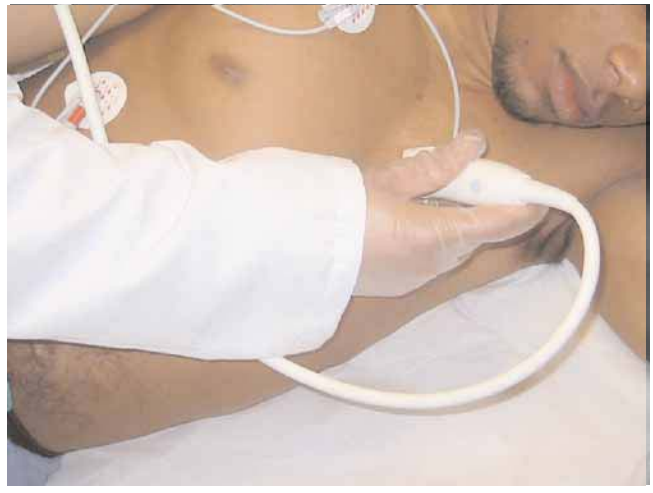

Fig. 17. Patient and transducer positioning: right ventricular inflow view.

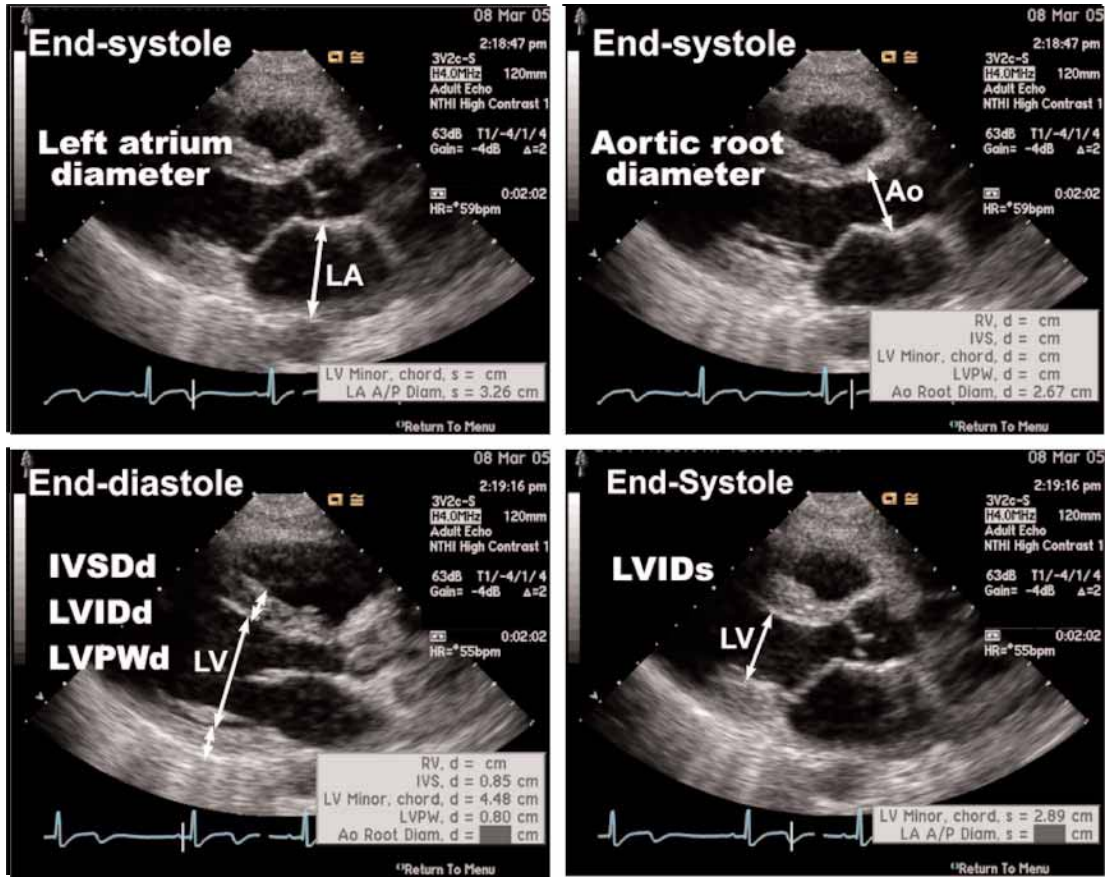

Fig. 16. Left ventricular M-mode dimensions. M-mode delivers superior image resolution compared to 2D, but variations in cardiac topography and morphology frequently leads to off-axis measurements. Some newer instrument models are equipped with software for postprocessing (measuring M-mode from selected 2D images) to overcome this frequent pitfall. However, it is logistically simpler to obtain 2D measurements—"leading edge to leading edge"—during image acquisition as shown.

APICAL FOUR-CHAMBER VIEW

The examination proceeds to the apical position, with the index mark at approx 3 o'clock position (Fig. 31). The apical four-chamber view is then visualized and optimized, initially at a depth 20–24 cm, and then 15–16 cm for better visualization of cardiac structures (Figs. 32–34).

Depth is then further decreased to visualize the left ventricular apex (Fig. 35A). This is important when looking for apical thrombus.

Next come color flow Doppler (Fig. 35B) assessment of the MV for regurgitation followed by PW Doppler to the pulmonary vein , usually the right upper pulmonary vein (Fig. 35C,D).

Mitral inflow (left ventricular inflow) is assessed by PW at the level of the tips of the mitral leaflets (Fig. 36A) to assess velocities and the E/A ratio. This is followed by CW Doppler across the MV.

Tissue Doppler imaging (or Doppler tissue imaging) at the mitral annulus (lateral and septal Fig. 36B) with the velocity scale set at 20:20 (Fig. 36C,D) is then performed.

RV function is evaluated by systolic function assessment (*see* Chapter 4) color Doppler and CW across the tricuspid valve to assess tricuspid regurgitation (Fig. 37).

APICAL FIVE-CHAMBER VIEW

Superior angulation of the tranducer toward to aortic valve level brings the aortic root into view (Figs. 38–40).

The aortic valve is visualized and color Doppler applied to assess aortic insufficiency.

Color flow Doppler application reveals flow along the interventricular septum, the left ventricular outflow tract and the aortic outflow (Fig. 40B).

PW Doppler interrogation along the interventricular septum from the apex to the valve can detect intracavitary gradients including dynamic left ventricular outflow tract obstruction (Fig. 40C). CW Doppler across the aortic valve detects peak transaortic gradients (Fig. 40D).

In suspected or existing aortic stenosis (*see* Chapter 11) the following measurements should be performed: PW measurement is acquired at 1 cm below the aortic valve. The "freeze" function is applied and the spectral Doppler envelope is traced to quantify the velocity time integral (TVI or VTI). CW Doppler across the aortic valve is then performed and its TVI measured. From these, the aortic valve area can be calculated using continuity equation.

APICAL TWO-CHAMBER VIEW

Counter-clockwise rotation of the transducer as shown in Figs. 41–43 permits visualization of the apical two-chamber view.

This view permits the best visualization of the inferoposterior ventricular wall.

Color flow Doppler is applied to assess for mitral regurgitation and additional measurements, e.g., tissue Doppler can be performed (Fig. 43).

APICAL THREE-CHAMBER VIEW

Further anti-clockwise rotation of the transducer (with the index mark pointing toward the right shoulder (Fig. 44) permits visualization of the apical three-chamber view (Figs. 45–47).

Color Doppler application (Fig. 48) can reveal aortic and mitral regurgitation.

SUBCOSTAL VIEWS

Proper patient positioning for subcostal imaging are shown in Fig. 49A,B.

The knee-flexed position relaxes the upper abdominal muscles and breath holding at end-inspiration moves the heart closer to the transducer thereby improving visualization (Figs. 50 and 51).

Several views are obtainable from the subcostal position, but the subcostal four-chamber view is recommended in the standard examination.

Tricuspid and mitral regurgitation are well visualized on color flow Doppler, and the interatrial septum is then evaluated for a patent foramen ovale or an atrial septal defect (Fig. 52).

Anti-clockwise rotation of the transducer permits visualization and pulsed Doppler examination of the IVC, the intrahepatic veins, and the upper abdominal aorta (Fig. 53).

SUPRASTERNAL VIEWS

With the patient supine and the neck extended the standard transthoracic examination concludes with the suprasternal examination (Figs. 54 and 55).

This includes the application of color Doppler and pulsed Doppler to the descending thoracic aorta (Fig. 56). Coarctation of the aorta can be visualized in this view.

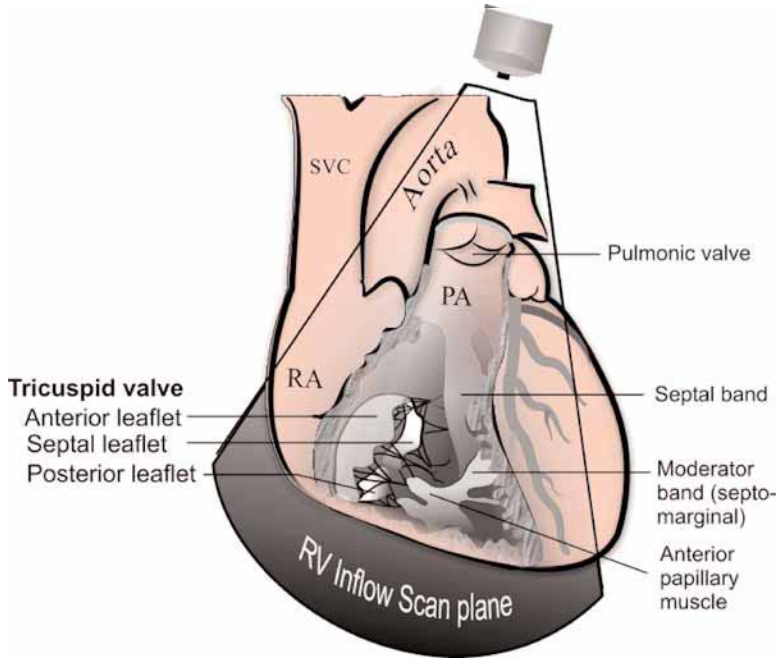

Fig. 18. Anatomical sketch: right ventricle inflow scan plane.

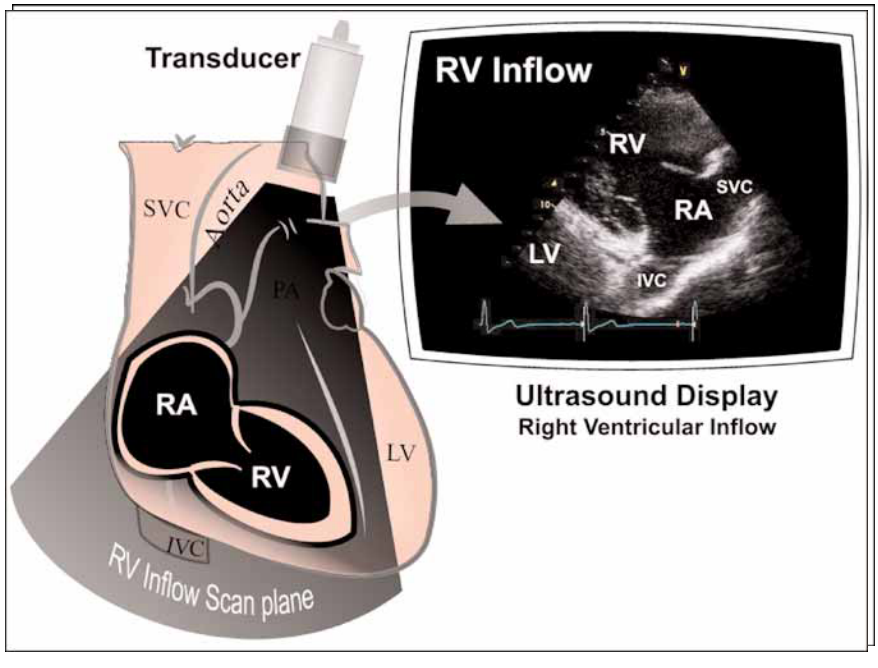

Fig. 19. Right ventricular inflow scan plane and two-dimensional image. (*See* companion DVD.)

EXAMINATION REPORT

The examination report follows recommendations outlined by the America Society of Echocardiography.

The standard report format includes patient demographic data, echocardiographic evaluation—comprising semi-quantitative and quantitative measures, Doppler assessment, and wall scoring (Figs. 57–59).

SUMMARY

Optimal image acquisition in 2D echocardiography is the foundation for accurate assessment and interpretation.

Familiarity with the normal transthoracic examination serves as the basis for interpreting abnormality.

Additional components and applications of 2D transthoracic echocardiography are addressed in the chapters that follow.

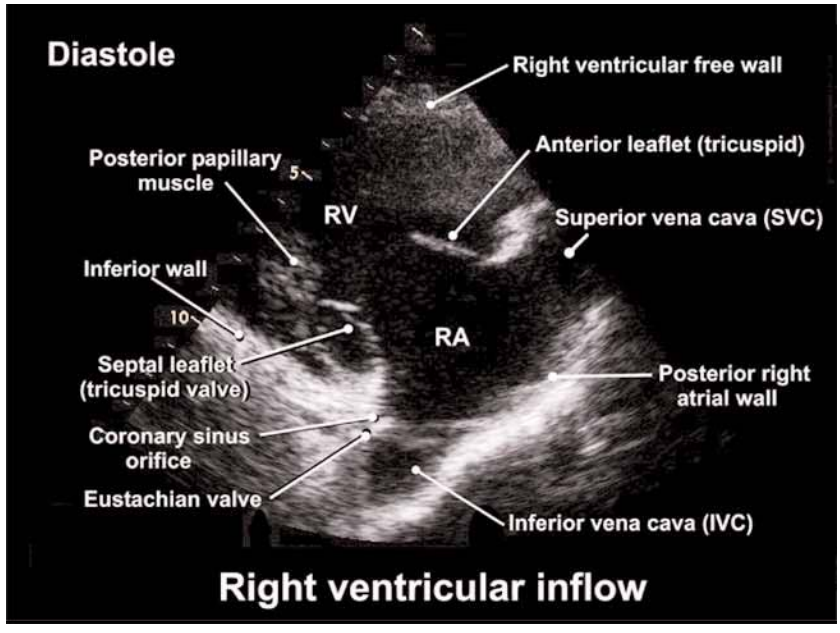

Fig. 20. Annotated right ventricular inflow view.

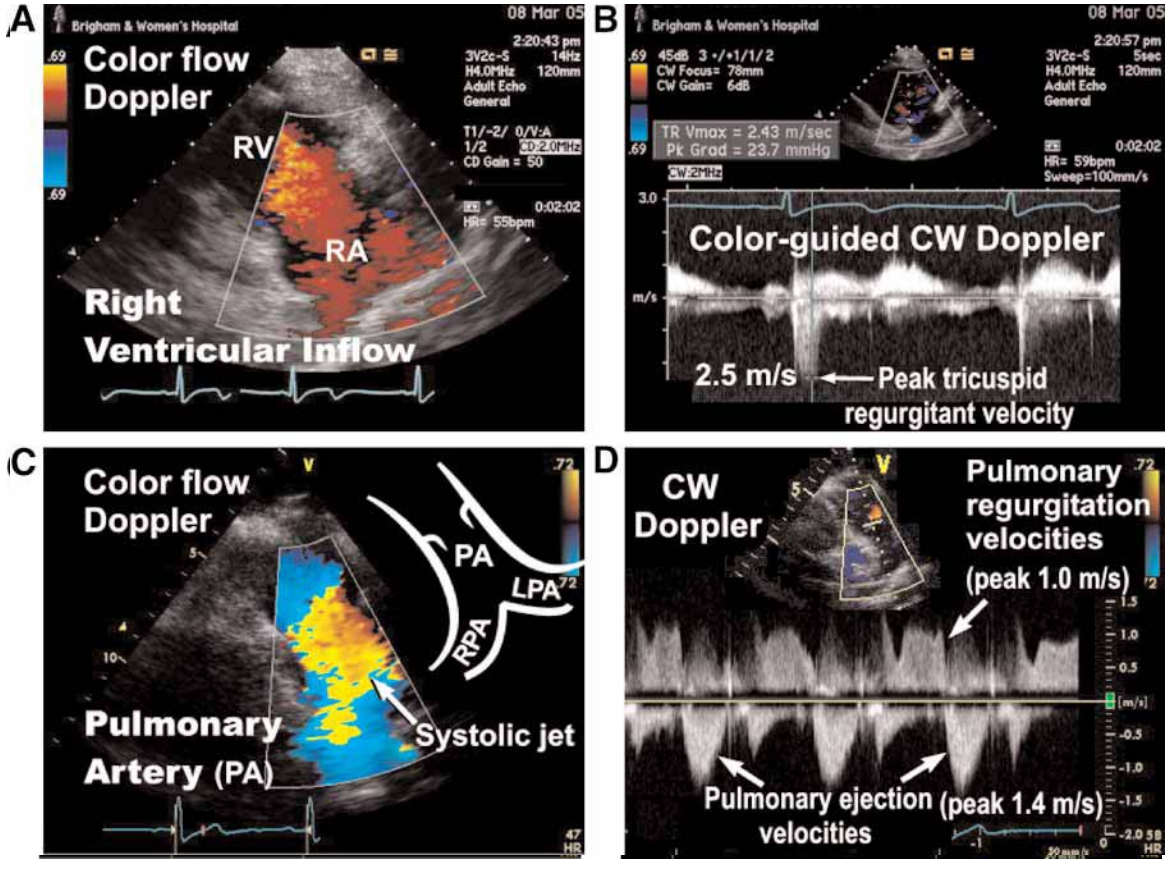

Fig. 21. Right ventricular (RV) inflow and outflow. Color Doppler still frame of the RV ventricular inflow (**A**) at end systole. Color Doppler should guide Doppler examination across the tricuspid valve. Mild tricuspid regurgitation—a finding in normal individuals—was detected on color Doppler. The resulting spectral Doppler profile shows peak tricuspid regurgitant velocity measuring 2.5 m/s (**B**). Color Doppler applied across the right ventricular outflow tract/pulmonary artery (**C**) shows peak ejection velocities of 1.4 m/s on continuous-wave (CW) spectral Doppler (**D**) with mild pulmonary regurgitant velocities of 1.0 m/s. (A,C, *see* companion DVD.)

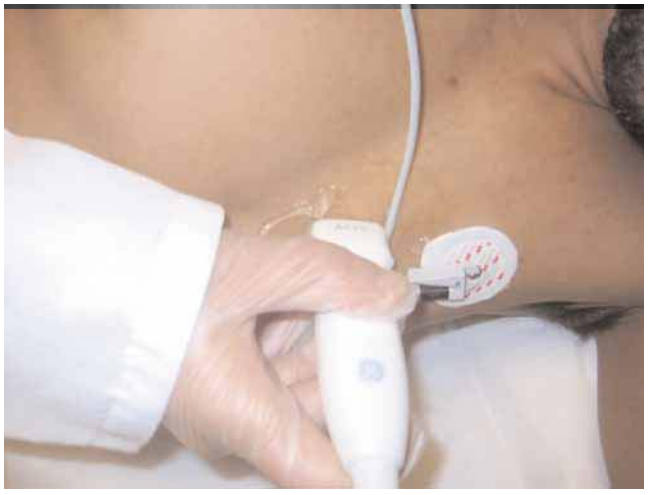

Fig. 22. Patient and transducer positioning: parasternal short-axis view (PSAX).

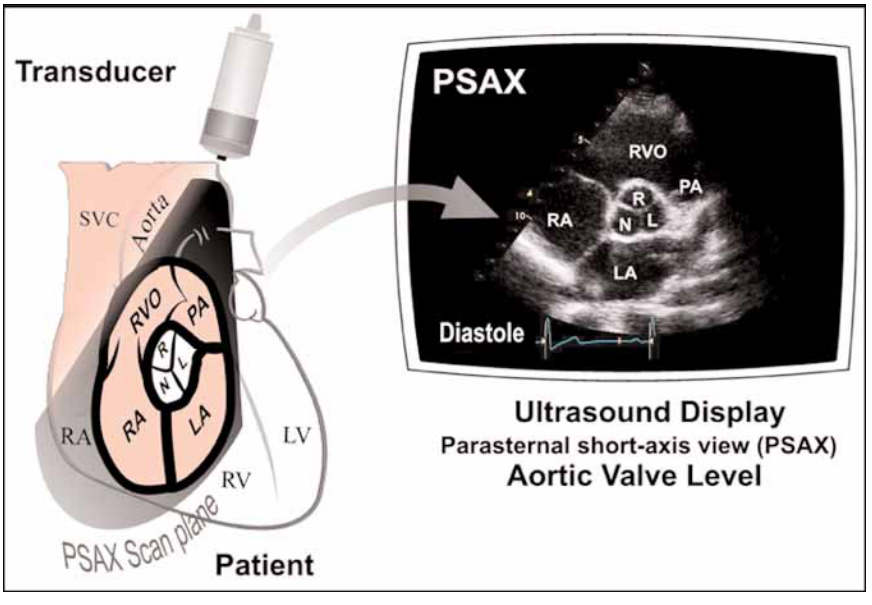

Fig. 23. Parasternal short axis-view: aortic valve level (PSAX). (*See* companion DVD.)

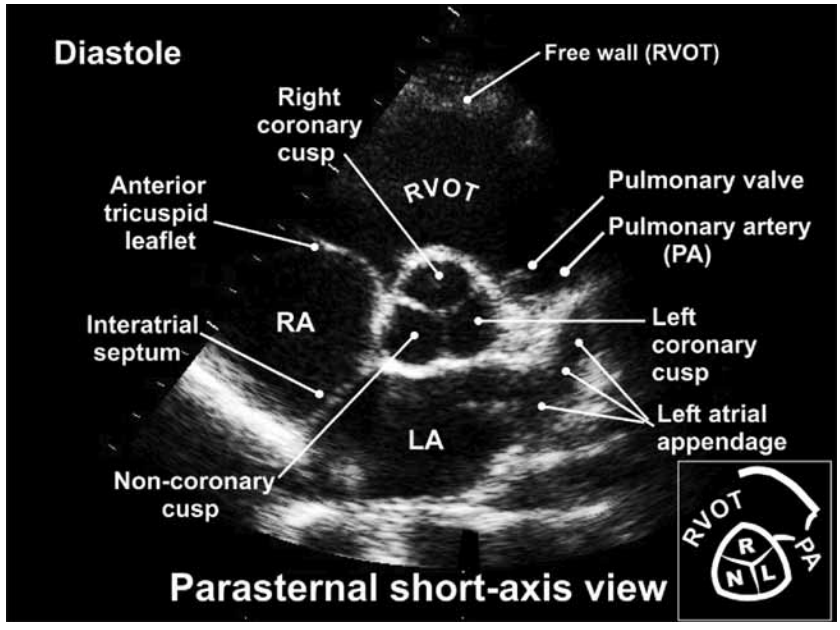

Fig. 24. Annotated parasternal short-axis view: aortic valve level (PSAX).

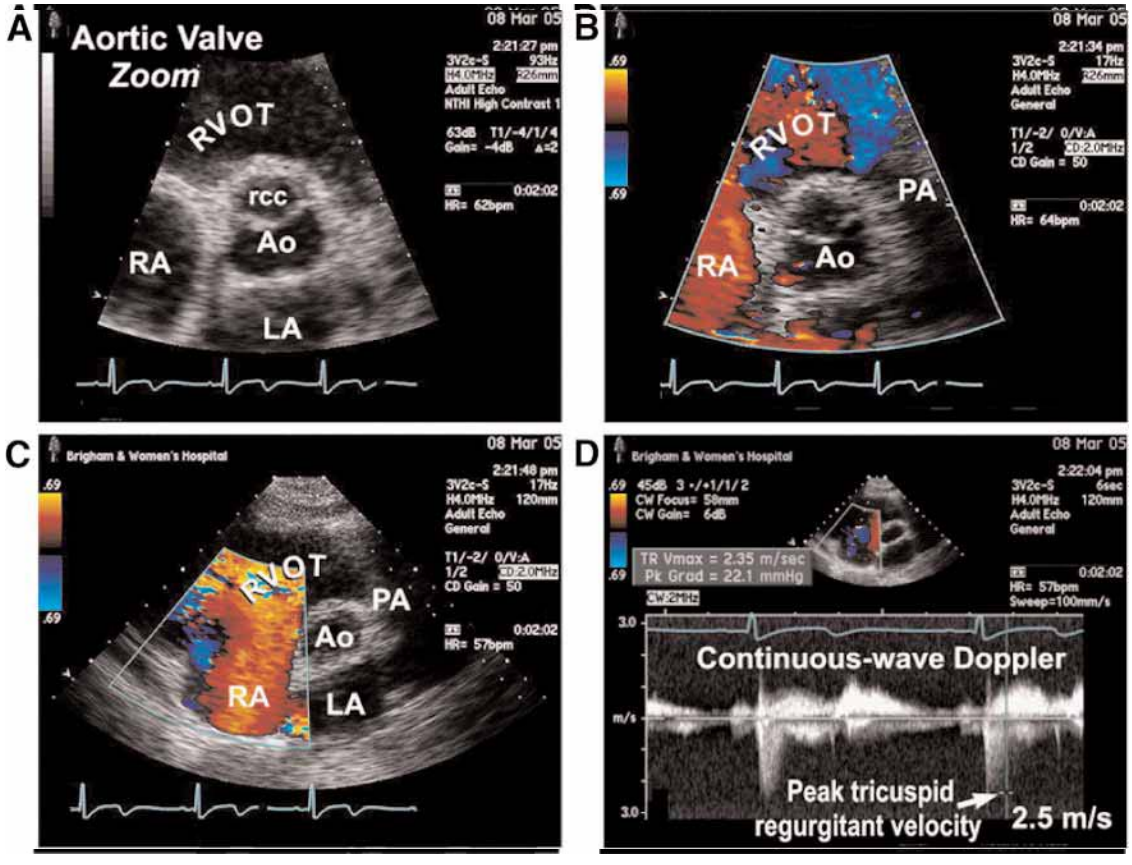

Fig. 25. Parasternal short-axis (PSAX): aortic valve level. (A,B, *see* companion DVD.)

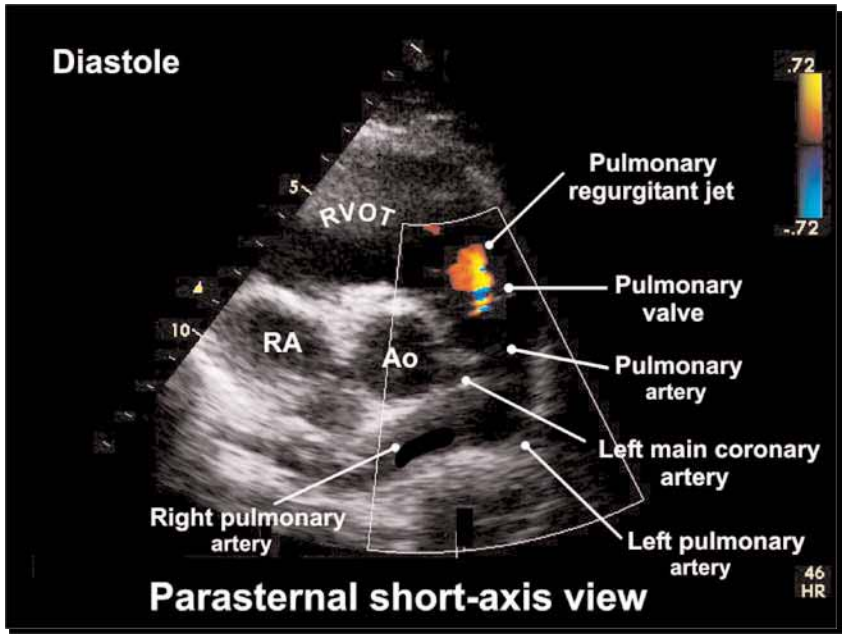

Fig. 26. Annotated parasternal short-axis view: pulmonary artery view (PSAX). (Level just superior to still frame shown in Fig. 24; *see* companion DVD.)

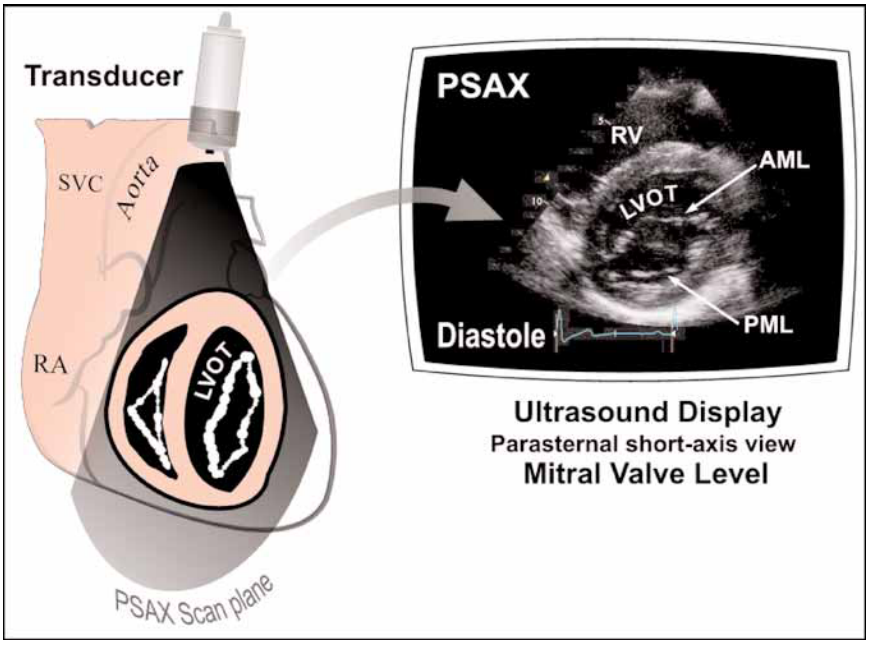

Fig. 27. Parasternal short axis view: mitral valve level (PSAX). (*See* companion DVD.)

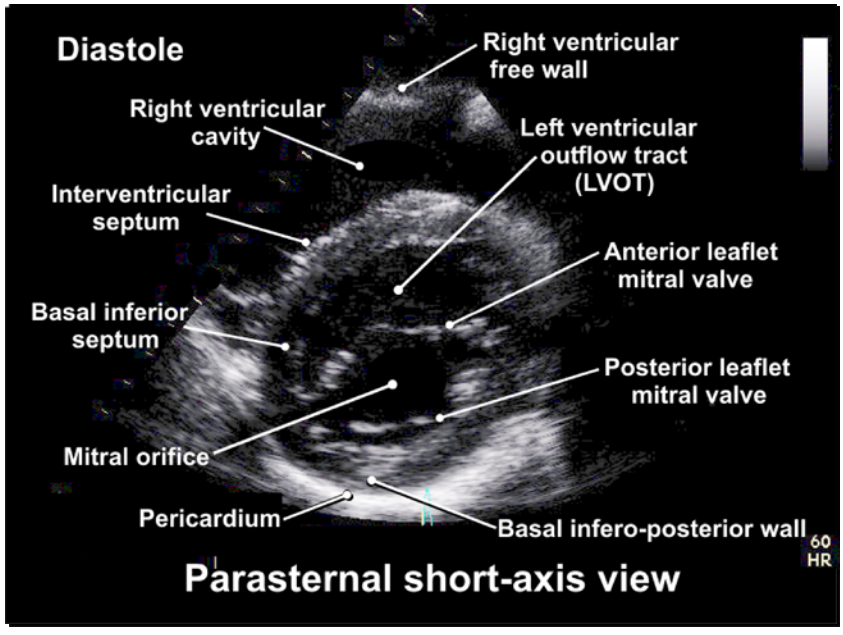

Fig. 28. Annotated parasternal short-axis view: mitral valve level (PSAX).

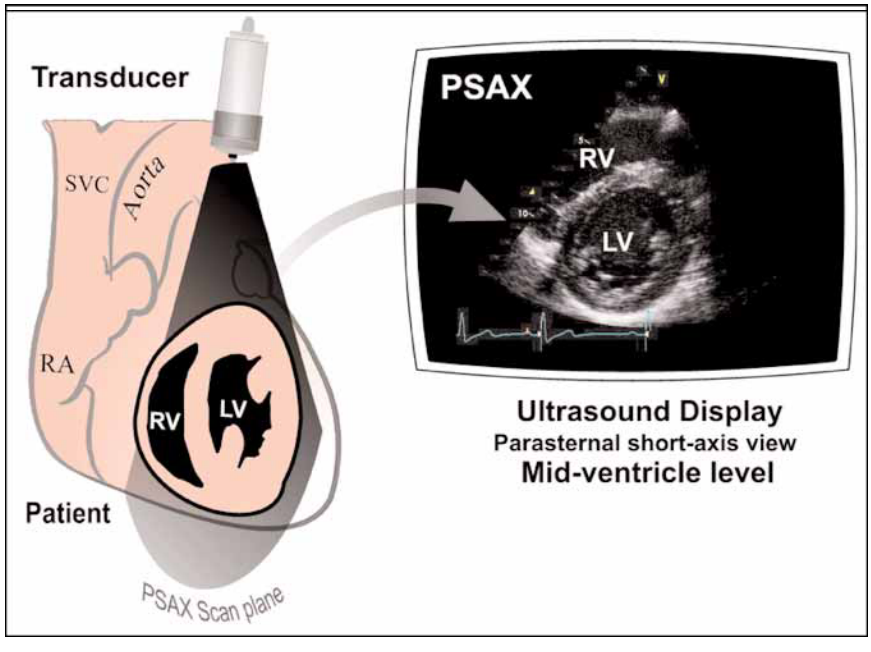

Fig. 29. Parasternal short axis (PSAX) view: midventricle/papillary muscle level. (*See* companion DVD.)

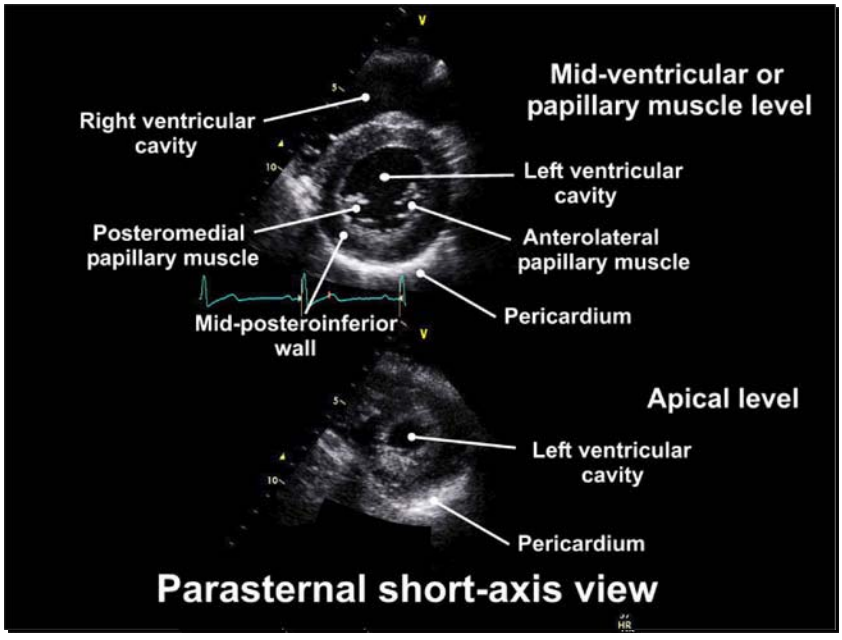

Fig. 30. Annotated parasternal short axis (PSAX) view: midleft ventricle level and apex (PSAX). (*See* companion DVD.)

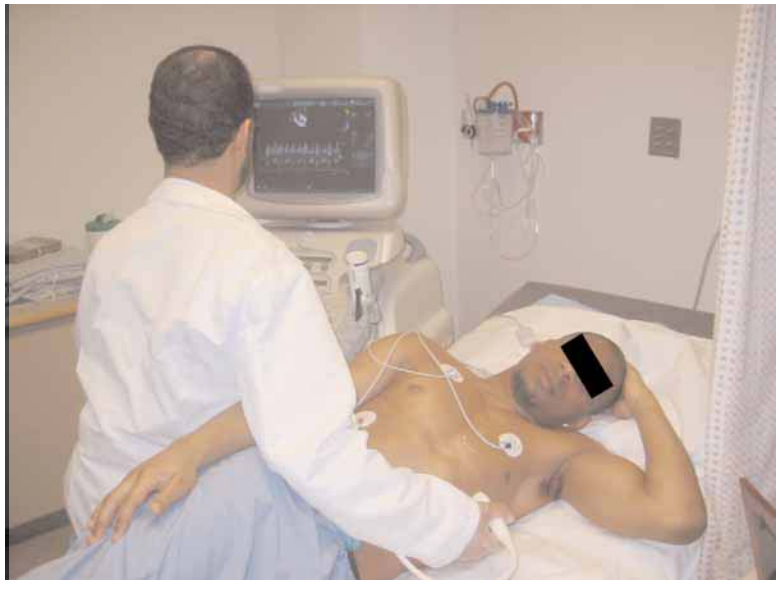

Fig. 31. Patient and transducer positioning: apical location.

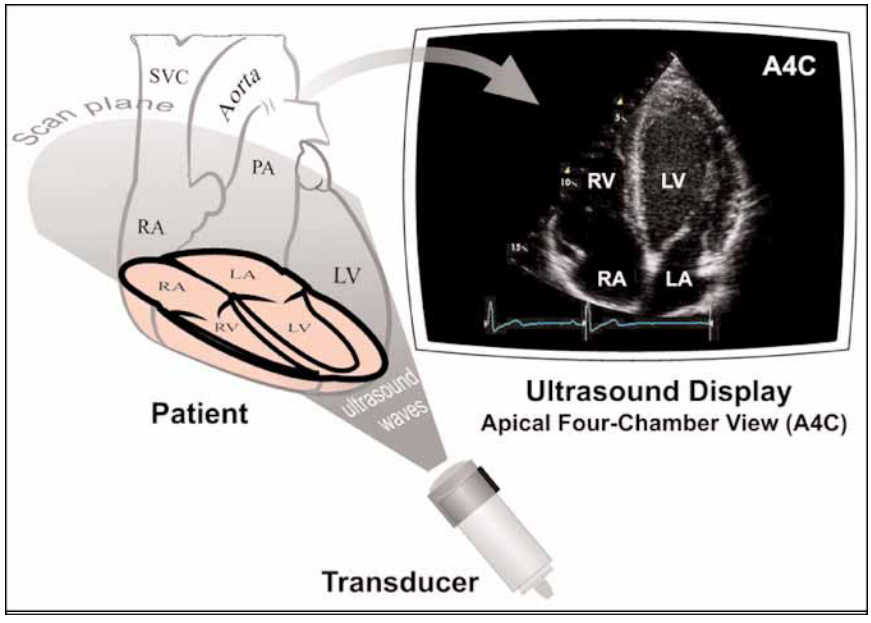

Fig. 32. Apical four-chamber (A4C) views. (*See* companion DVD.)

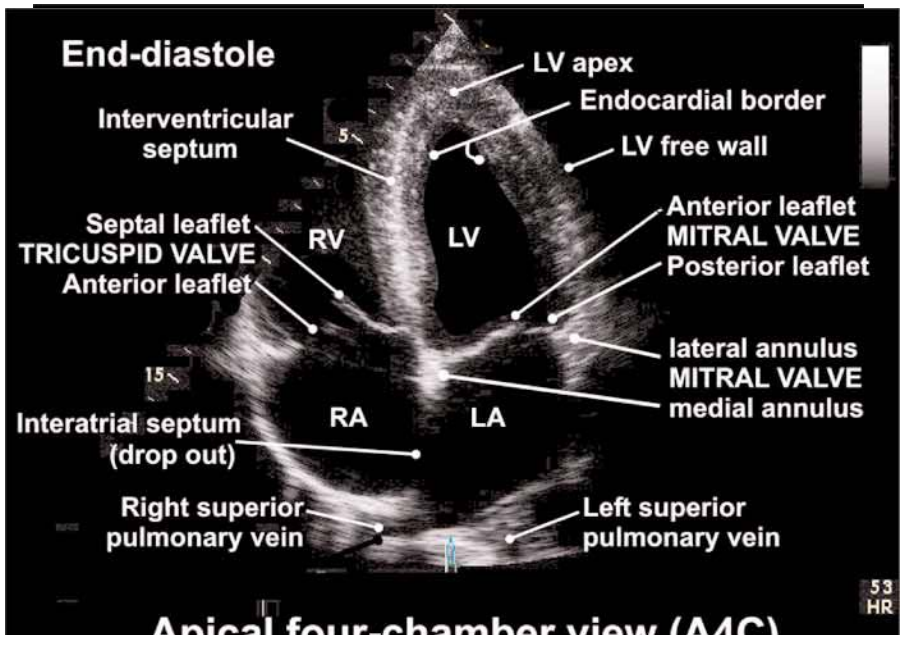

Fig. 33. Annotated apical four-chamber view (A4C).

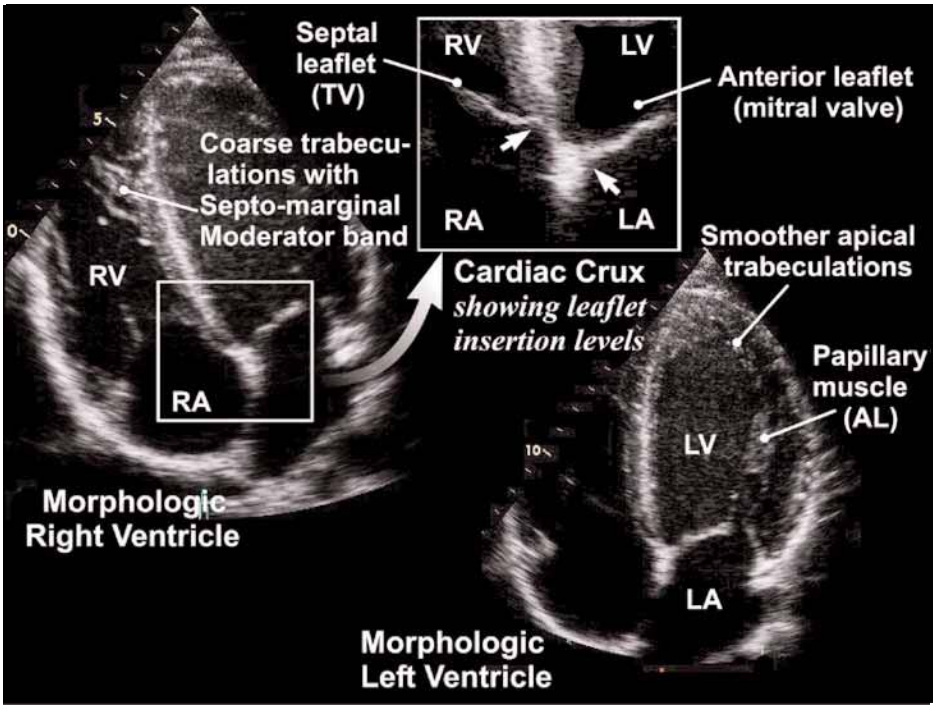

Fig. 34. Defining morphological left and right ventricles on two-dimensional (2D) echocardiography (A4C). The confluence of the interventricular and interatrial septa and the septal insertions of the tricuspid and mitral valve leaflets constitute the internal cardiac crux (cross). The normal cross-like configuration on 2D echocardiography is not symmetrical. The septal leaflet of the tricuspid valve is inserted more apically, i.e., toward the cardiac apex. This relationship becomes important in evaluating certain congenital heart lesions, e.g., atrioventricular canal defects. Another distinguishing echocardiographic feature of the morphological right ventricle is its coarser trabeculated endocardial surface (including the moderator band), the presence of a tricuspid valve, and the absence of two distinct papillary muscles. These characteristics are important in segmental sequential analysis of congenital heart disease. (*See* companion DVD.)

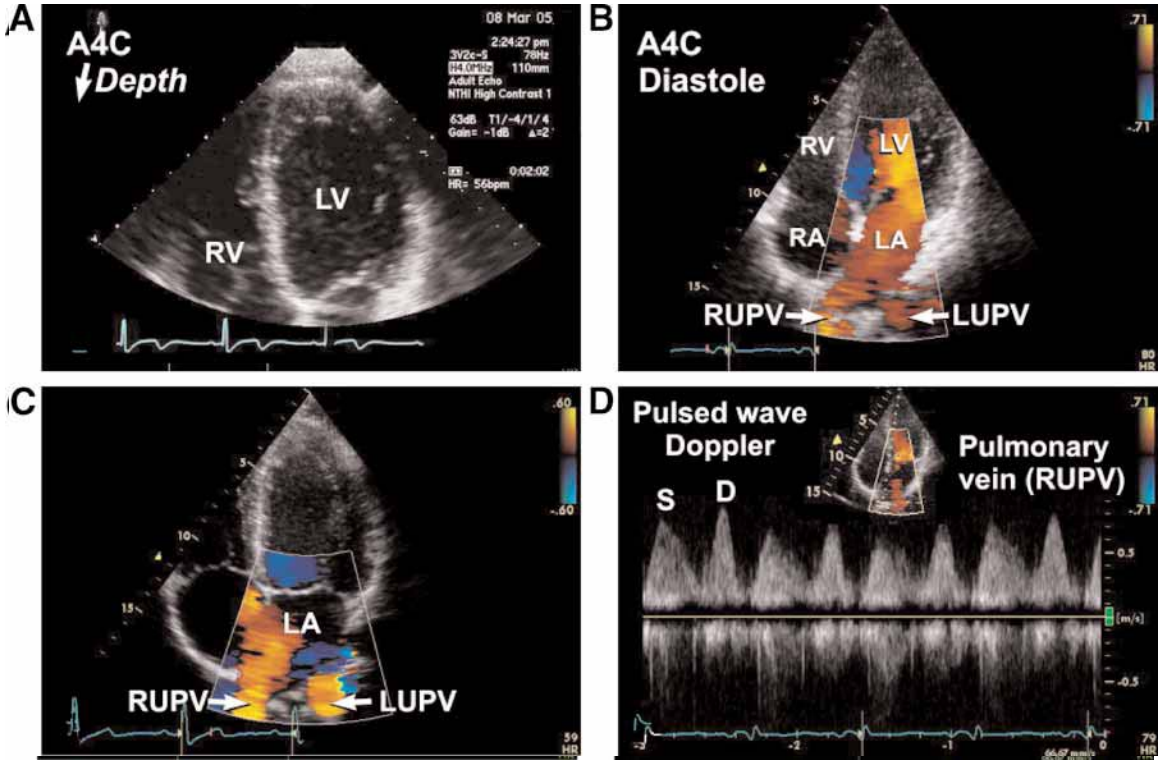

Fig. 35. Apical four-chamber view (A4C). Zooming on (reduce depth) the left ventricle (**A**) provides better definition of the left ventricular endocardium and apex. Further improved definition can be achieved by use of a higher frequency transducer and/or contrast agent. Diastolic A4C frame with superimposed color flow Doppler (**B**) shows flow extending from the right and left upper pulmonary veins through the mitral valve toward the left ventricle. Pulmonary vein flow (**C**) is phasic, with normal systolic (S) and diastolic (D) peaks (**D**). This pattern varies with age and disease states, e.g., diastolic heart failure and restrictive cardiomyopathy. (*See* companion DVD.)

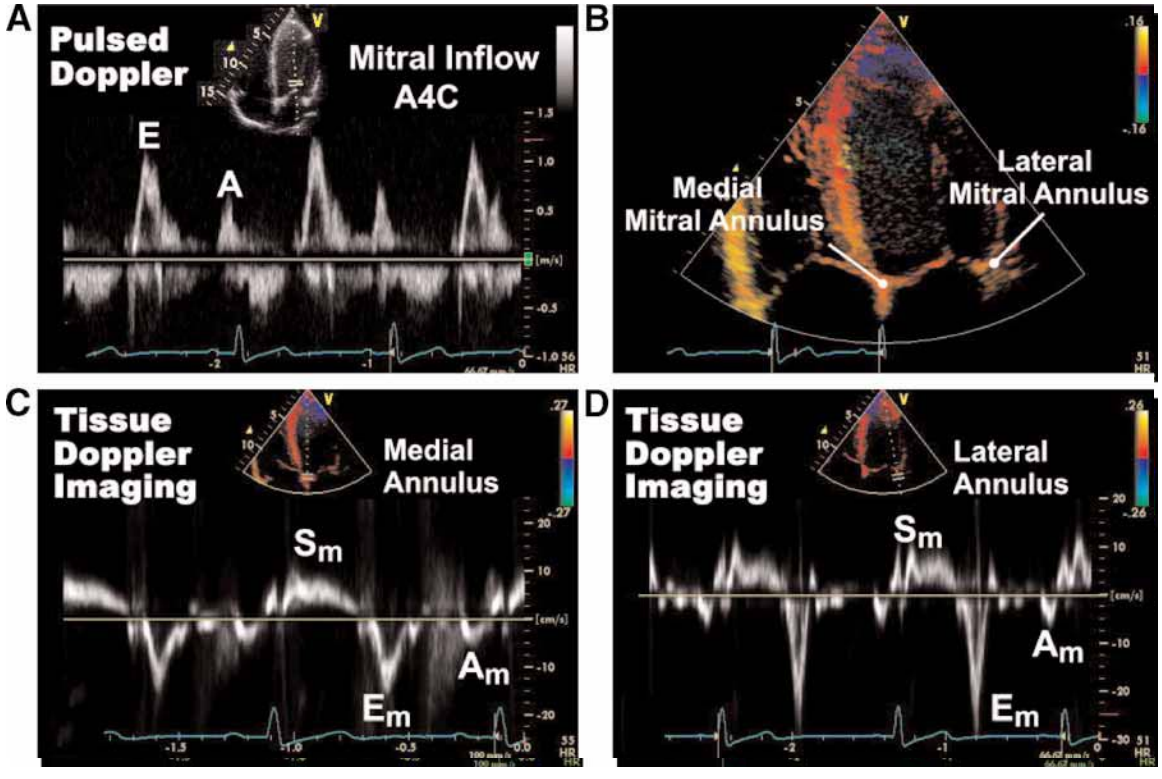

Fig. 36. Apical four-chamber view (A4C). Pulsed Doppler evaluation of normal mitral inflow shows early rapid filling (E) velocities and lower A velocities owing to atrial contraction **(A)**. The normal E:a ratio is >1. Loss of A velocities is seen in atrial fibrillation. Clear identification of mitral annulus **(B)** is necessary for optimal tissue Doppler imaging (TDI or DTI). Mitral annular movement assessed on TDI normally shows three waveforms **(C**,**D)**: systolic velocities toward the apex (S_m) and diastolic velocities (E_m and A_m) away from the apex. These lower velocities normally exceed 8–10 cm/s. The lateral annulus is the preferred site. (A,B, *see* companion DVD.)

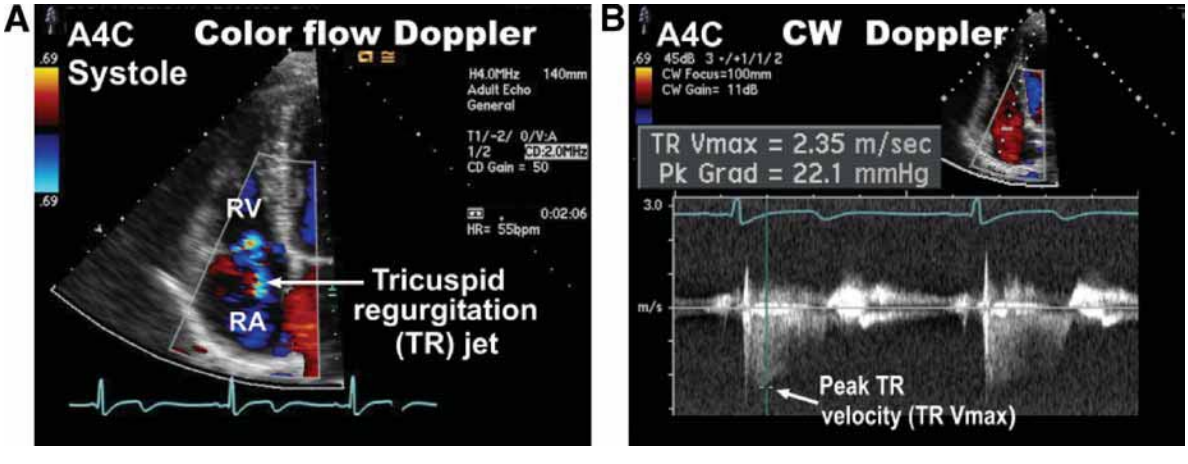

Fig. 37. Apical four-chamber view (A4C). (A, *see* companion DVD.)

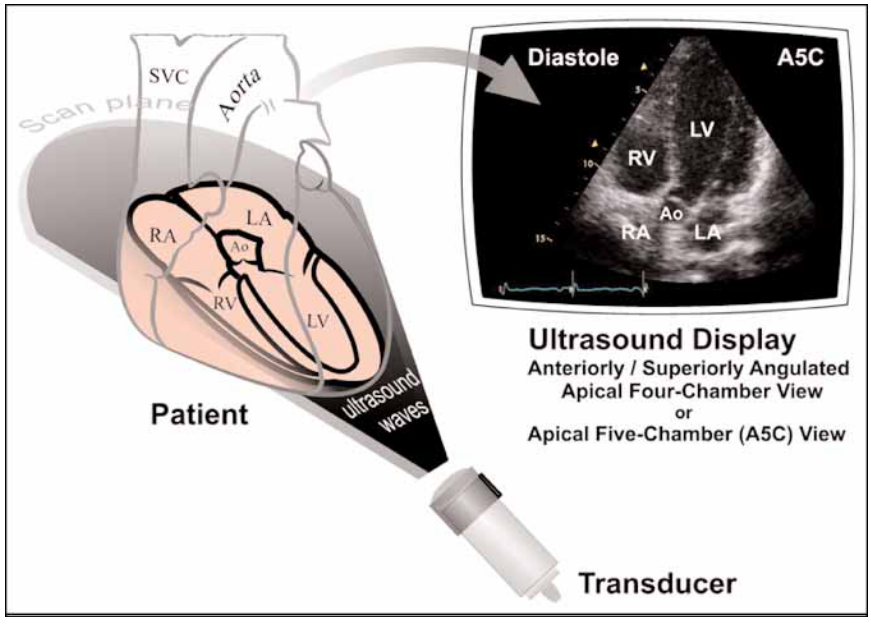

Fig. 38. Apical four-chamber view (anterior/superior tilt)—also known as apical five-chamber (A5C) view. (*See* companion DVD.)

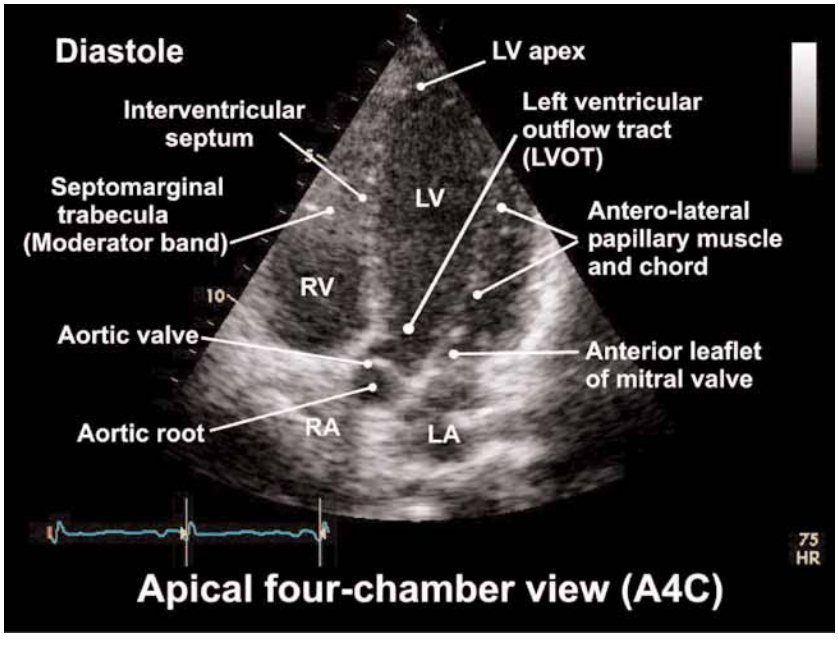

Fig. 39. Annotated apical five-chamber (A5C) view.

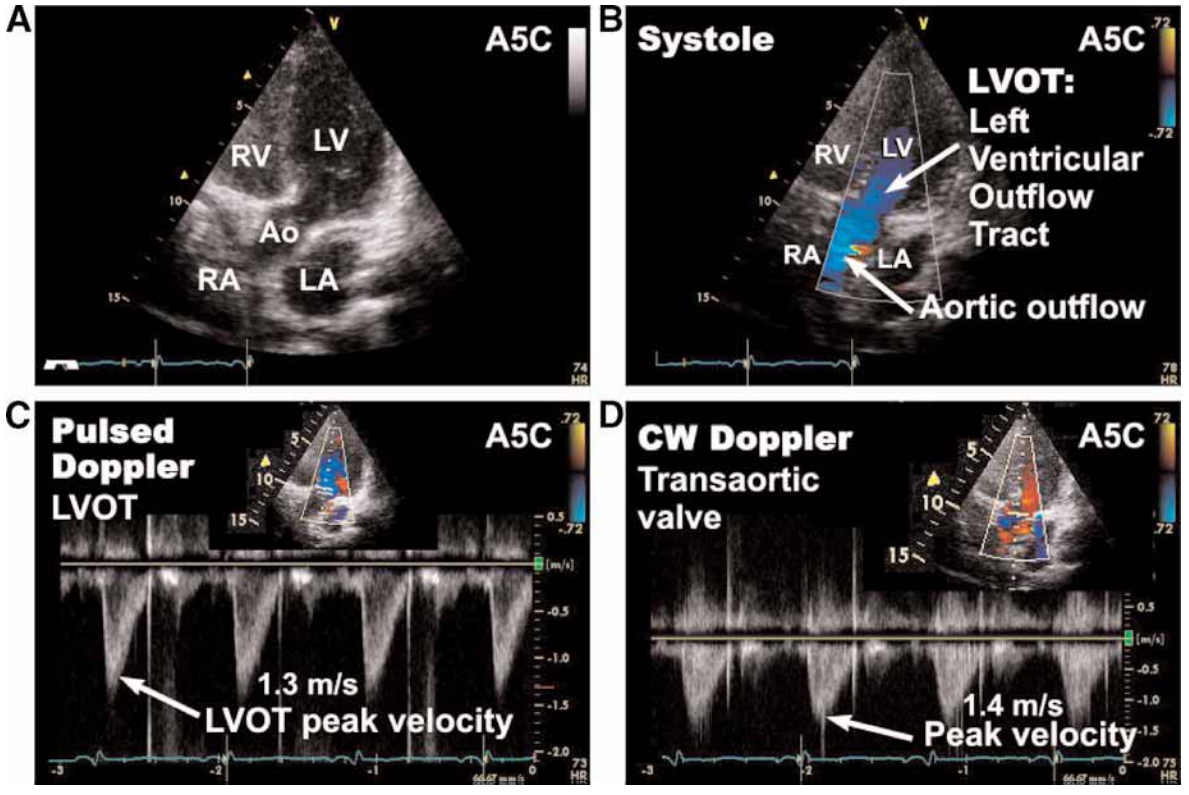

Fig. 40. Apical five-chamber view (A5C).

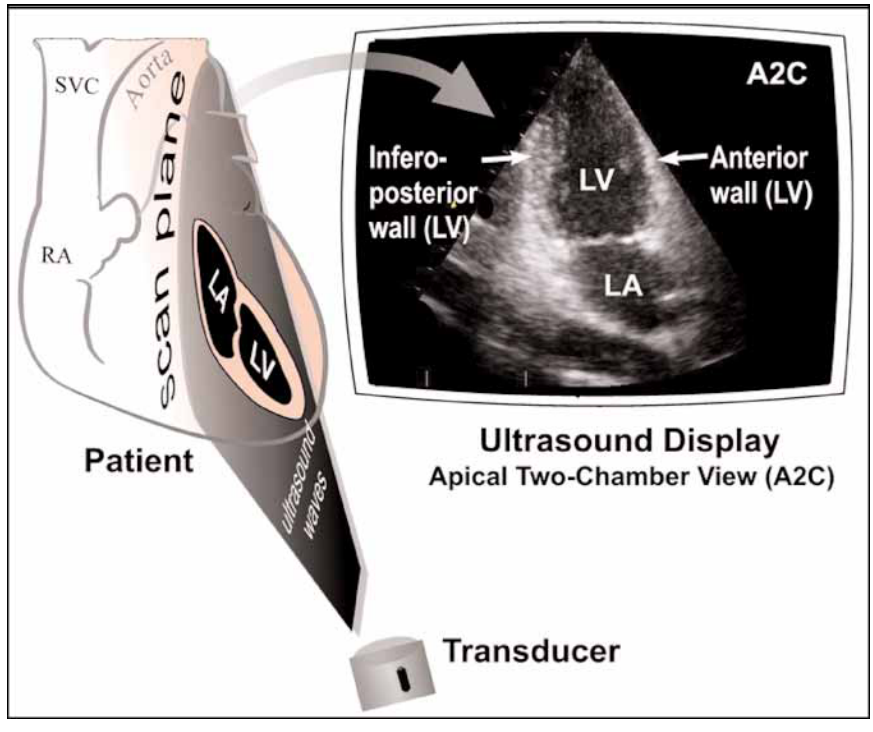

Fig. 41. Apical long-axis or apical two-chamber (A2C) view. (*See* companion DVD.)

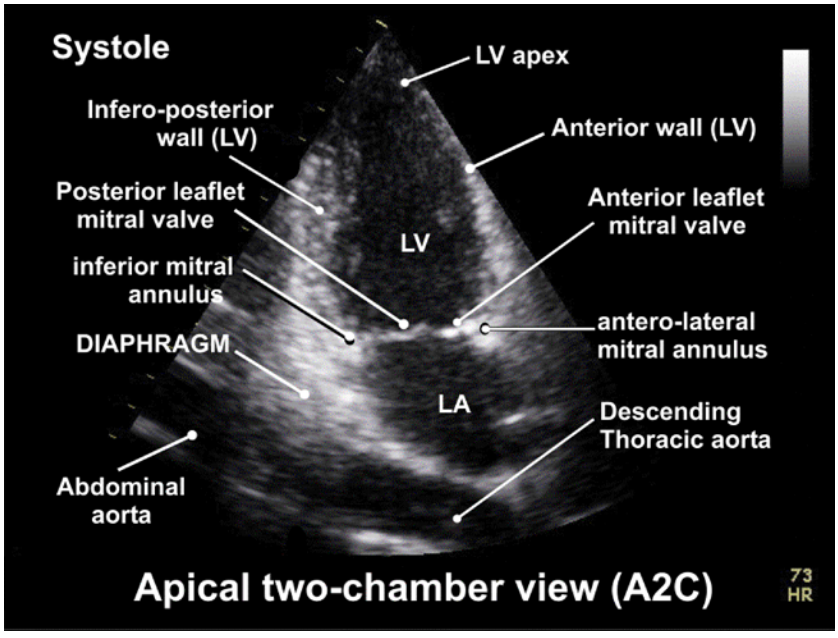

Fig. 42. Annotated apical two-chamber view (A2C).

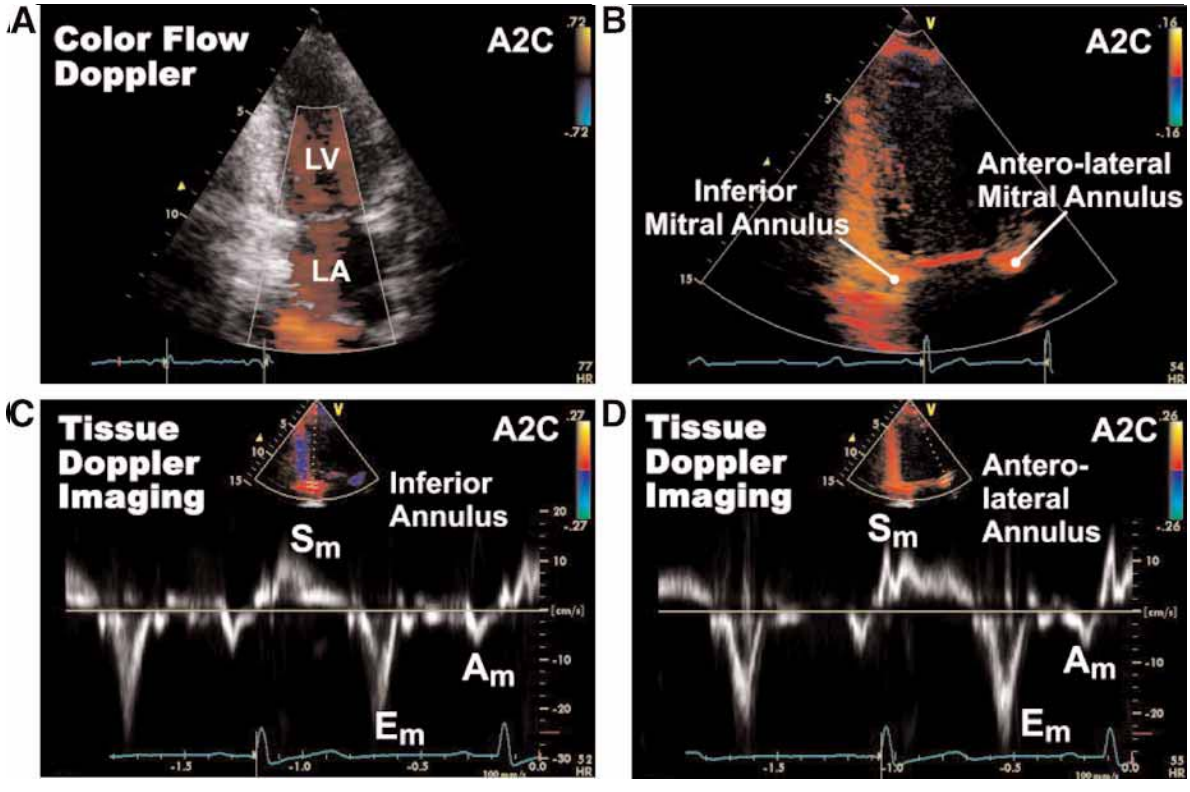

Fig. 43. Apical long-axis or apical two-chamber (A2C) view. (A,B, *see* companion DVD.)

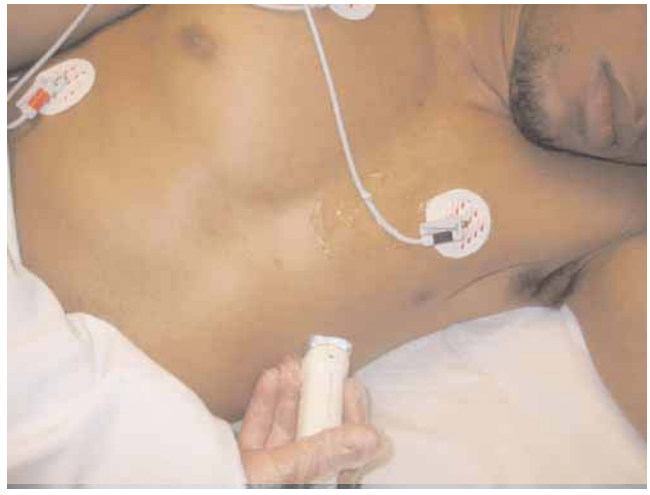

Fig. 44. Patient and transducer positioning: apical long-axis (apical three-chamber [A3C] view).

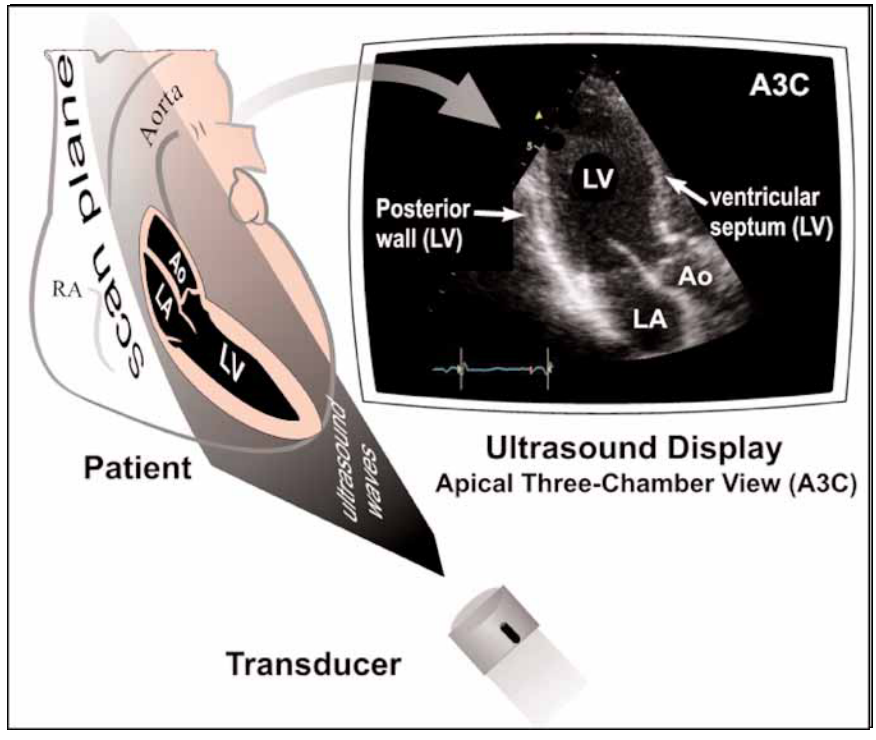

Fig. 45. Apical long-axis or apical three-chamber (AC3) view. (*See* companion DVD.)

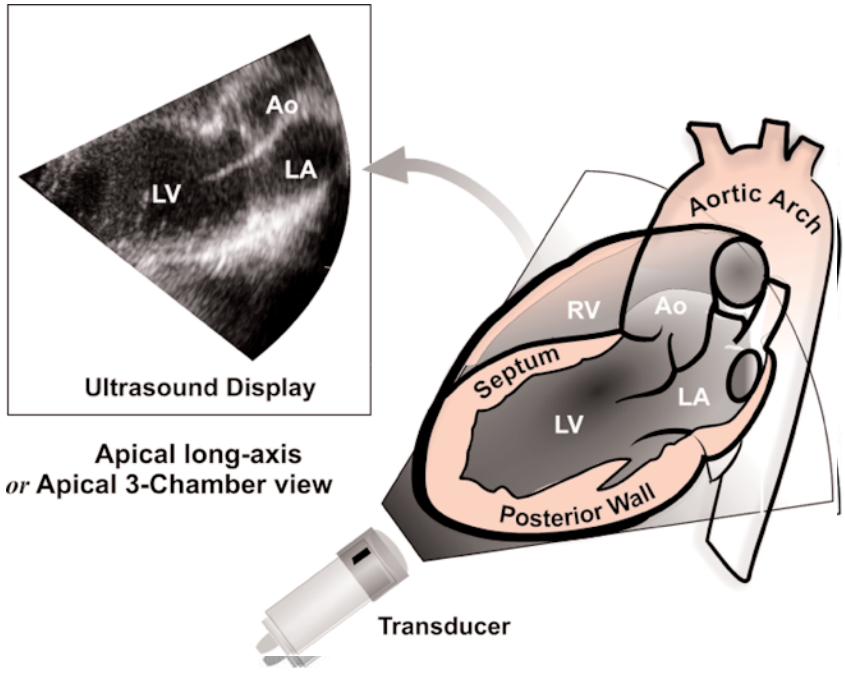

Fig. 46. Apical long-axis or apical three-chamber (AC3) view. (*See* companion DVD.)

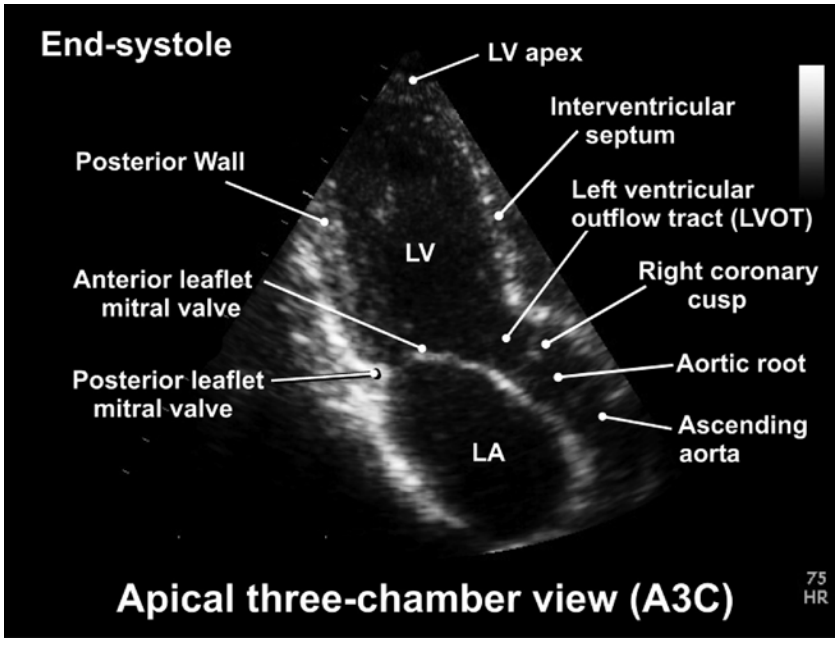

Fig. 47. Annotated apical three-chamber view (A3C). (*See* companion DVD.)

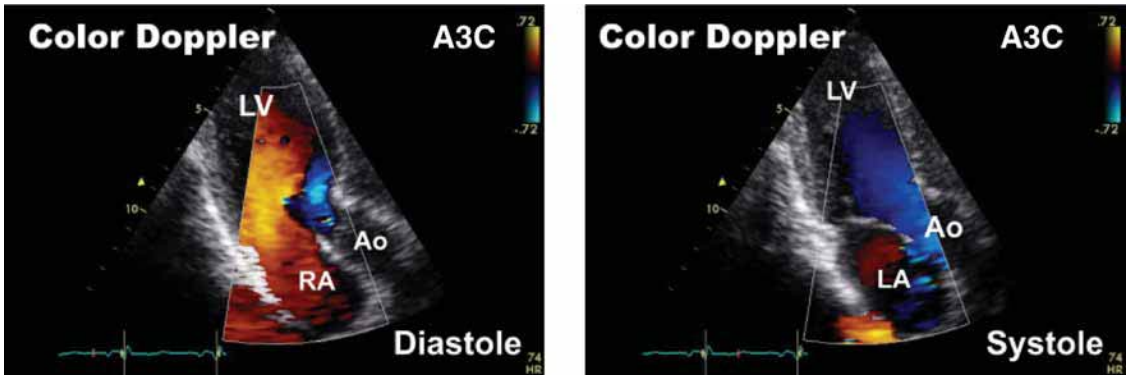

Fig. 48. Apical long-axis or apical three-chamber (A3C) view. (*See* companion DVD.)

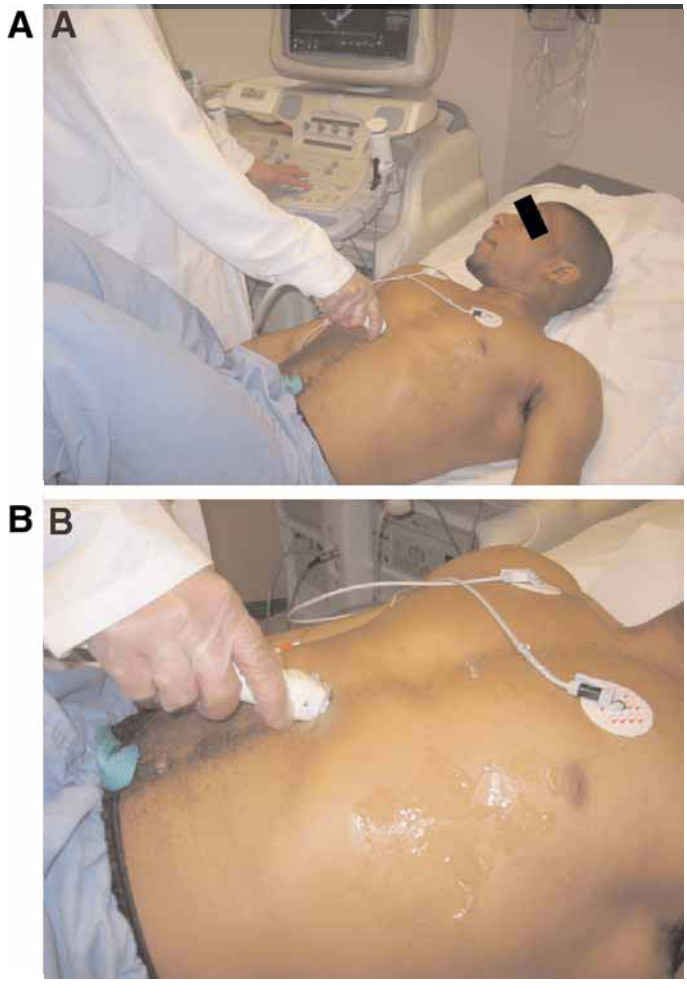

Fig. 49. (**A**) Patient and transducer positioning: subcostal location. (**B**) Patient and transducer positioning: subcostal location.

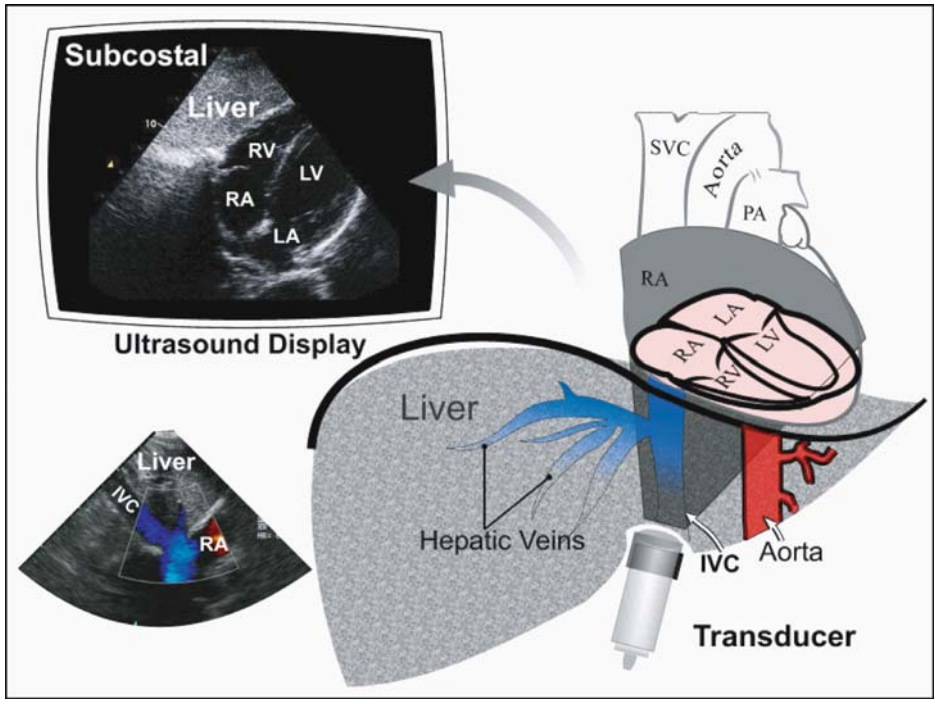

Fig. 50. Subcostal four-chamber view. (*See* companion DVD.)

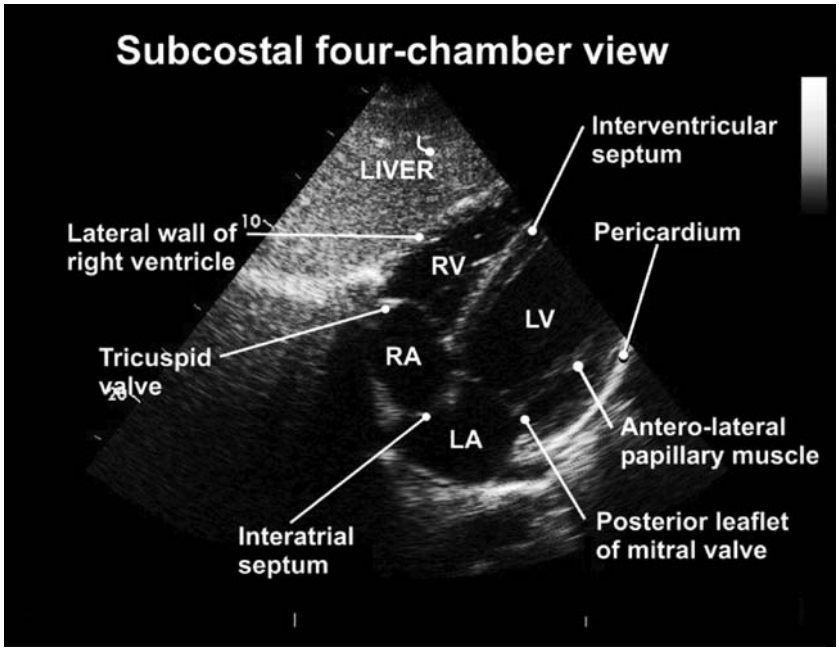

Fig. 51. Annotated subcostal view.

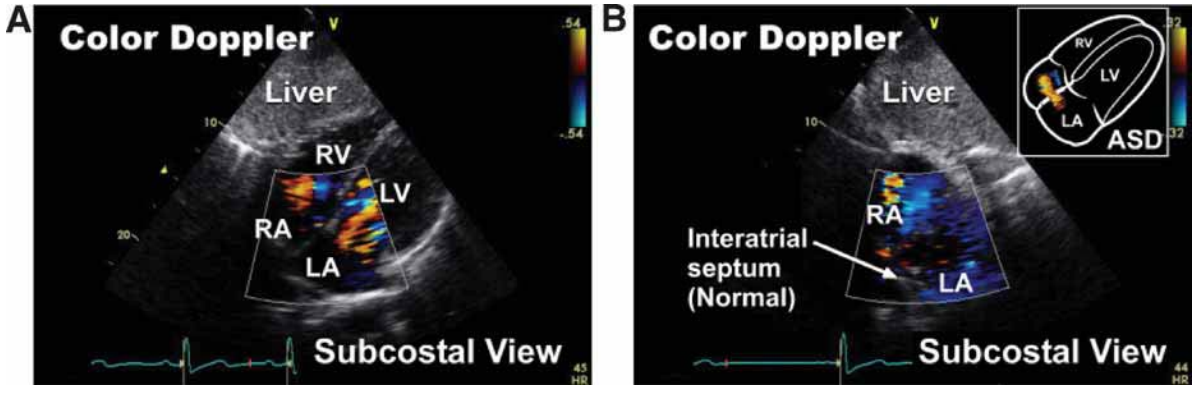

Fig. 52. Subcostal views (evaluate tricuspid regurgitation and atrial septal defect. (*See* companion DVD.)

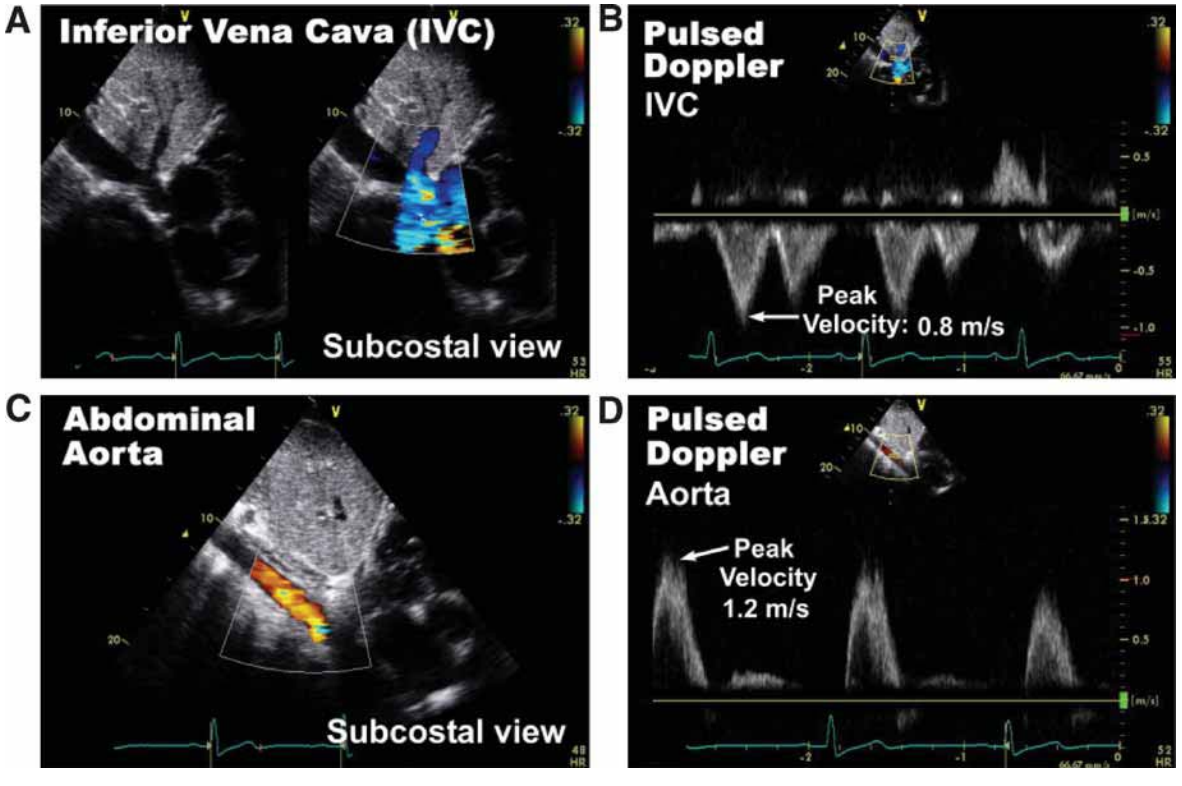

Fig. 53. Subcostal views (inferior vena cava and aorta). (A,C, *see* companion DVD.)

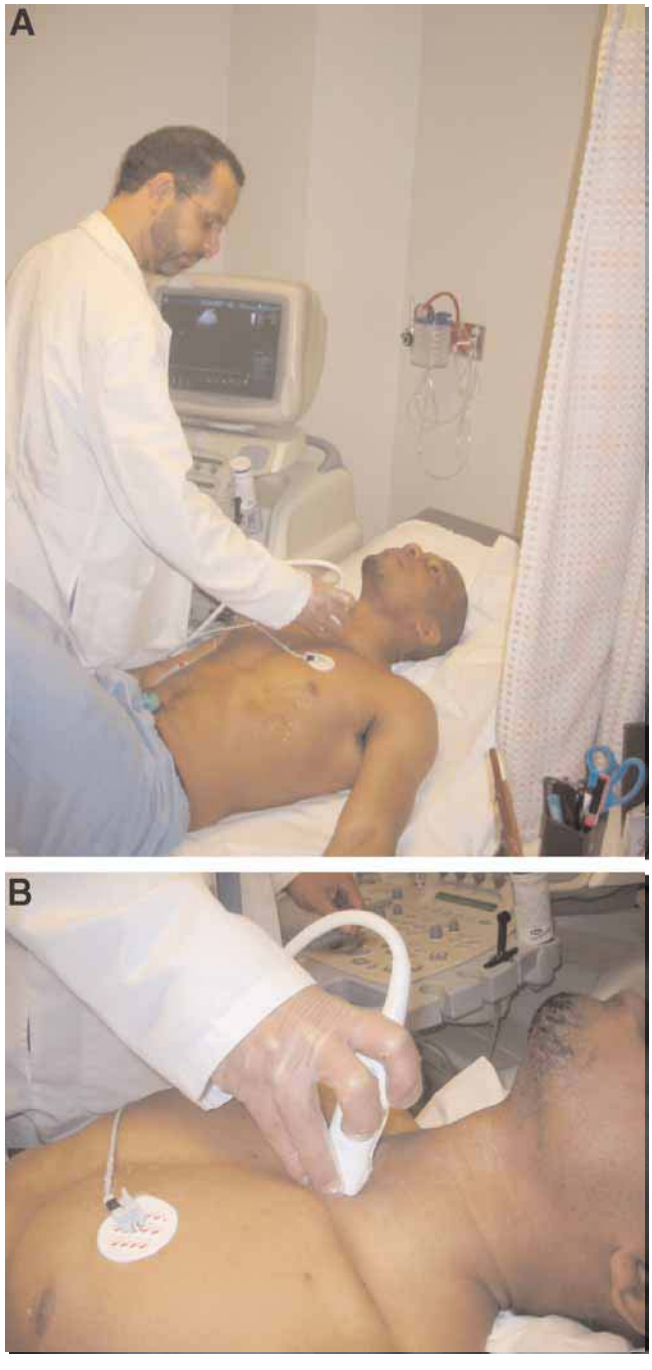

Fig. 54. (**A**) Patient and transducer positioning. Suprasternal location. (**B**) Patient and transducer positioning: suprasternal location.

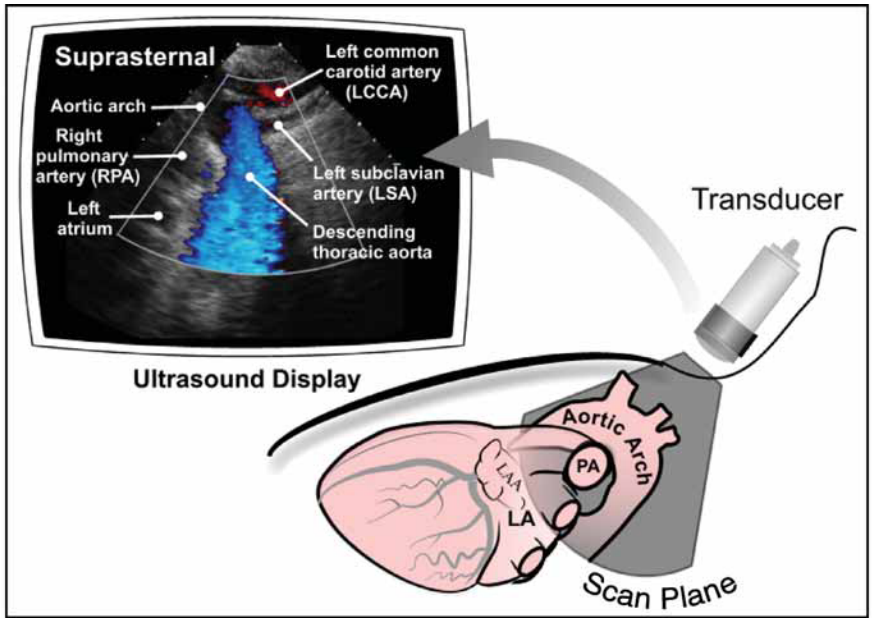

Fig. 55. Suprasternal long-axis view. (*See* companion DVD.)

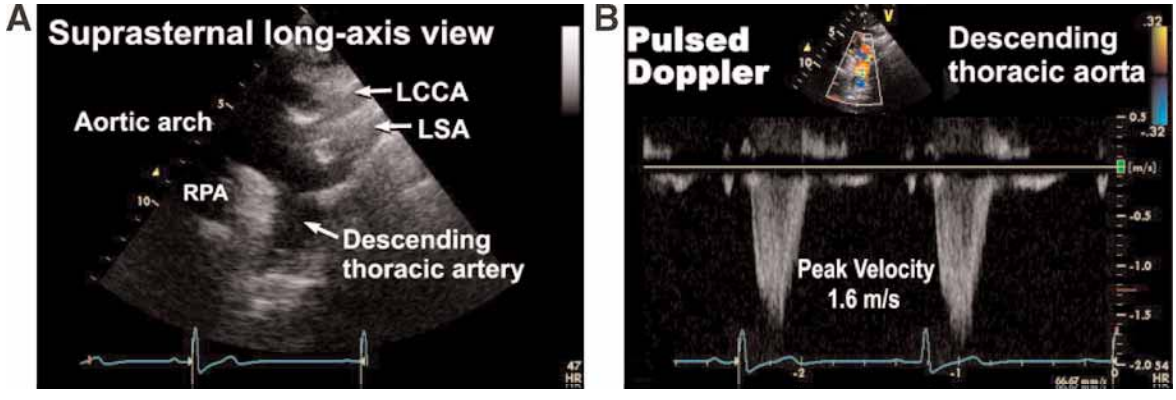

Fig. 56. Suprasternal long-axis view.

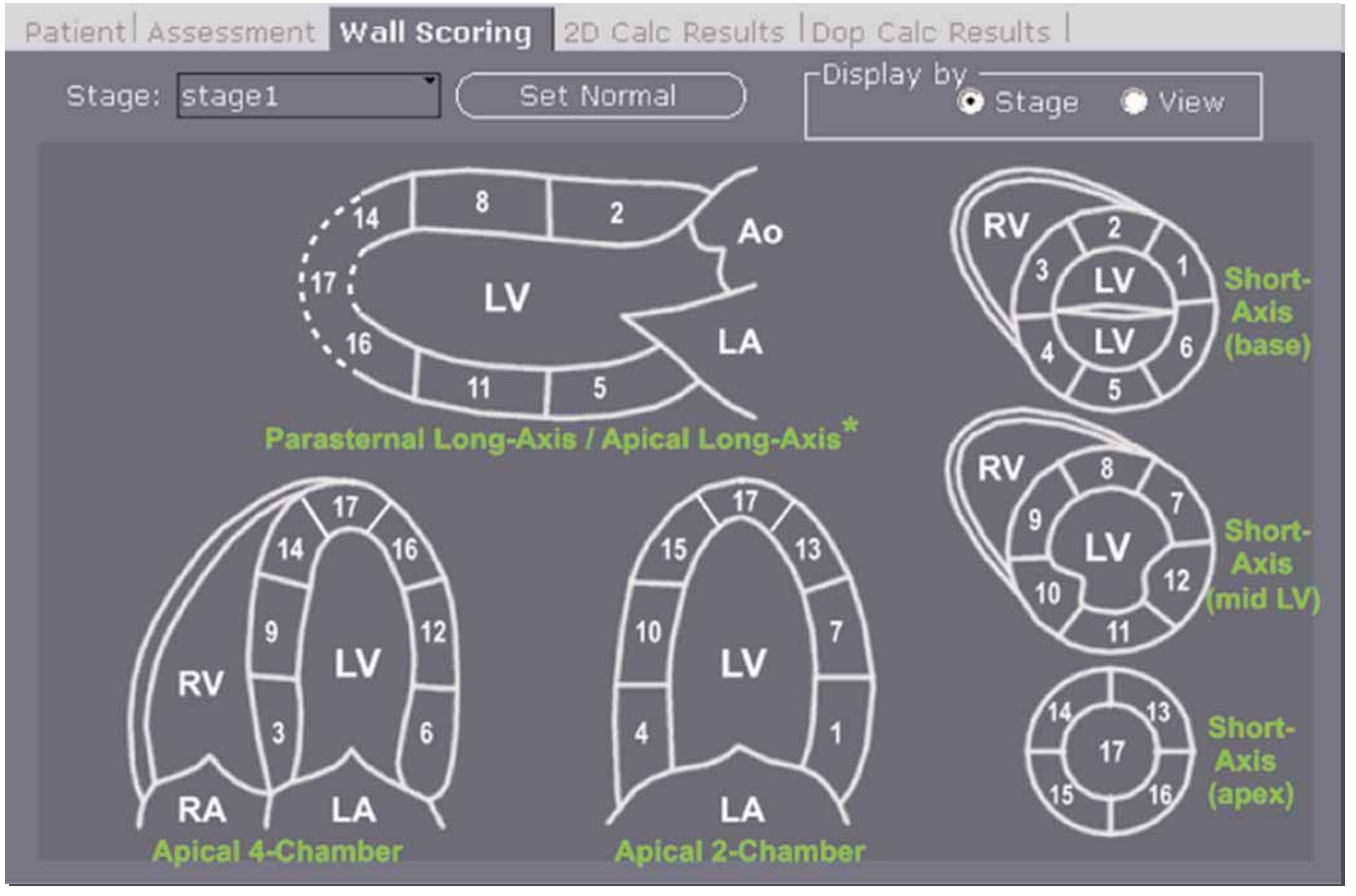

Fig. 57. Wall scoring.

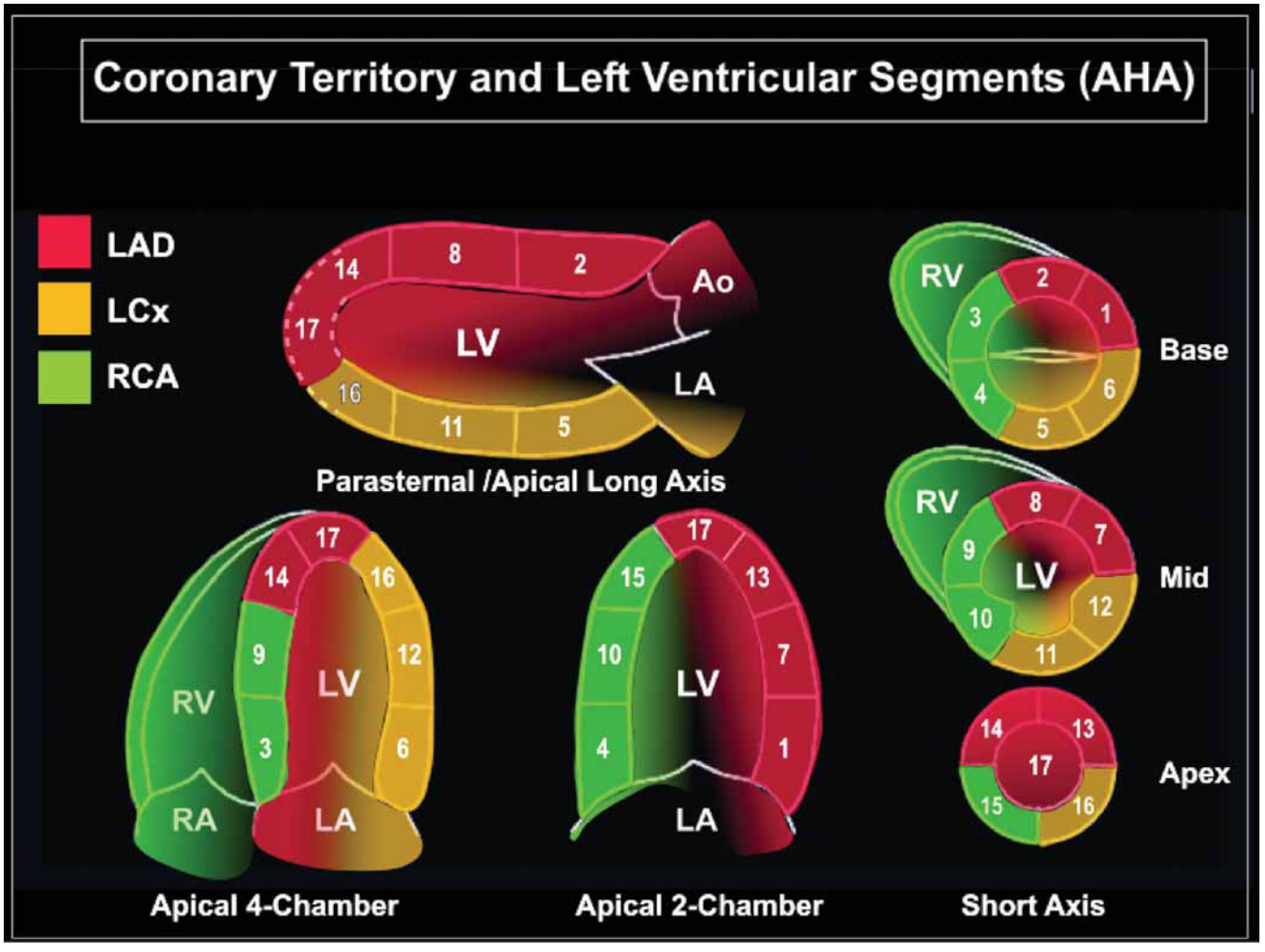

Fig. 58. Coronary artery territories.

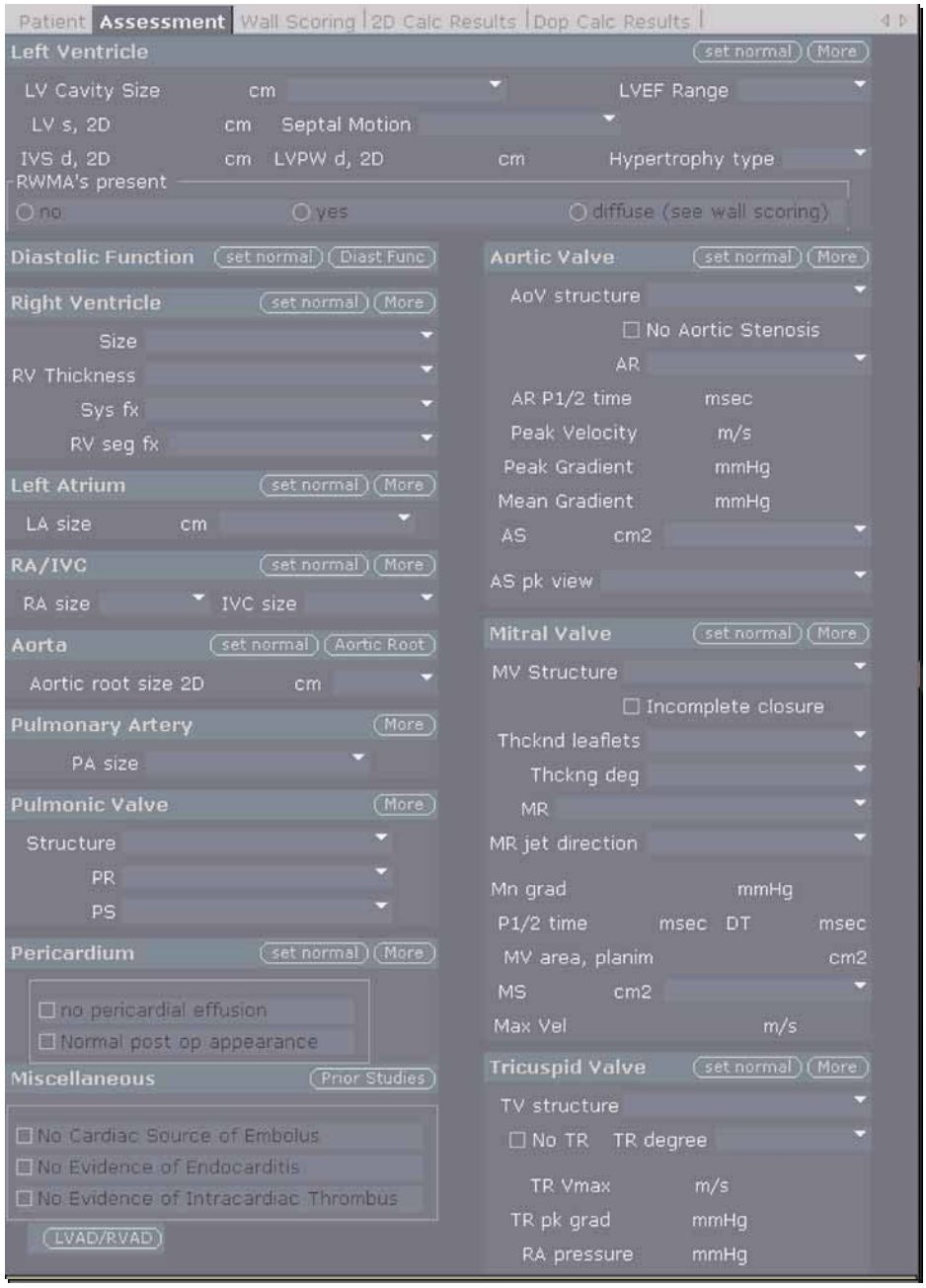

Fig. 59. Examination report.

4 Clinical Utility of Echocardiography

Bernard E. Bulwer, MD, MSc, Faisal Shamshad, MD, and Scott D. Solomon, MD

Contents

SCOPE OF ECHOCARDIOGRAPHY

Cardiac ultrasonography has evolved considerably since the first M-mode recording of ventricular wall movement in 1953 (Table 1 A,B). Reasoned application of this technology can improve patient care, optimize outcomes, and streamline costs in cardiovascular practice.

Cardiac ultrasonography has both practical and technical advantages over other cardiovascular imaging techniques (Table 2). Doppler echocardiographic assessment of cardiovascular structure, function, and hemodynamics is a reliable noninvasive tool to localize and quantify the severity of cardiovascular disorders in a cost-effective and noninvasive manner.

EVIDENCE-BASED USE OF ECHOCARDIOGRAPHY

Given its great clinical utility, widespread availability, and comparative advantages, the temptation exists to request echocardiography as "routine." Such tendencies should be discouraged, because echocardiography, although less costly than other imaging techniques, still adds to the burden of health care costs. Furthermore, incidental findings of no clinical significance in otherwise normal individuals can create unnecessary alarm and additional expensive testing.

Echocardiography, therefore, is no substitute for a careful history and cardiovascular examination. Requests

From: *Contemporary Cardiology: Essential Echocardiography: A Practical Handbook With DVD*
Edited by: S. D. Solomon © Humana Press, Totowa, NJ

Table 1A
Modalities and Applications of Cardiac Ultrasonography

Transthoracic Echocardiography			
Modality		*Application*	*Utility/assessment*
Two-dimensional (2D) echocardiography		Structure	• Chamber size • Wall thickness • LV mass • Valve structure, morphology, integrity • Masses (tumor, clot, vegetation) in cardiac chambers • Pericardial effusion • Congenital heart disease (children and adults)
		Function	• Global systolic function • Regional wall motion
M-mode echocardiography	M-mode (standard)	Structure	• Chamber size • Wall thickness • LV mass • SAM • Mitral valve prolapse • Pericardial effusion
		Function	• Pericardial tamponade • Dyssynchrony and cardiac resynchronization therapy
	M-mode (with color Doppler)	Function	• Diastolic function (flow propagation velocity) • Aortic regurgitation severity
Doppler echocardiography	Spectral Doppler: PW, CW	Function	• Velocities and gradients (peak, mean) • Valvular stenosis and regurgitation severity • Prosthetic valve evaluation • Pericardial tamponade (respirophasic changes) • Constrictive pericarditis vs. restrictive cardiomyopathy • Congenital heart disease (shunts, obstructive lesions, conduits, baffles) • MPI (Tei index)
	Color flow Doppler (multigated PW)	Function	• Intracardiac shunts[a] • Valvular stenosis and regurgitation severity • Prothetic valve evaluation • Congenital heart disease (shunts, obstructive lesions, conduits, baffles)
	TDI (or DTI)	Function	• Ventricular diastolic and systolic function
	Tissue velocity imaging, Doppler strain imaging, strain quantification, left ventricular torsion	Function	• Dyssynchrony and resynchronization therapy • Diastolic function
Stress echocardiography	Exercise, pharmacological, pacing	Functional	• Diagnosis, risk stratification, and prognosis in coronary artery disease
Contrast echocardiography	Right-sided contrast studies (agitated saline)	Structural	• Right-to-left shunts • PFO • Persistent left superior vena cava

(Continued)

Table 1A *(Continued)*

Transthoracic Echocardiography			
Modality		*Application*	*Utility/assessment*
	Left-sided contrast studies (micro bubbles)	Structural	• LVO, endocardial definition (± stress echocardiography) • Enhancement of Doppler signals
		Functional	• MCE—perfusion imaging: stenosis severity
Three-dimensional (3D) echocardiography		Structure Function	• Cardiac dimensions, volumes, mass • Left and right ventricular quantification, flow dynamics, mechanics, perfusion • Dyssynchrony and cardiac resynchronization therapy

CW, continuous wave; DTI, Doppler tissue imaging; LV, left ventricle; LVO, left ventricular opacification; MCE, myocardial contrast echocardiography; MPI, myocardial performance index; PFO, patent foramen ovale; PW, pulsed wave; TDI, tissue Doppler imaging; SAM, systolic anterior motion.

Table 1B
Modalities and Applications of Cardiac Ultrasonography

TEE	• Improved visualization when TTE is limited • Masses (tumor, clot, vegetation) in cardiac chambers • Infective endocarditis • Diseases of the large vessels (aorta, pulmonary arteries, and pulmonary veins) • Prosthetic valve evaluation • Intra-operative echocardiography • Congenital heart disease (children and adults): shunts, obstructive lesions, conduits, baffles
Intracardiac ultrasonography	• Monitoring invasive procedures, e.g., percutaneous shunt closures, catheter ablation, coronary flow reserve assessment, valvuloplasty
IVUS	• Plaque burden in coronary artery disease • Guide to percutaneous coronary intervention • Perioperative cardiovascular evaluation

IVUS, intravascular ultrasonography; TEE, transesophageal echocardiography; TTE, transthoracic echocardiography.

Table 2
Practical Advantages of Echocardiography Over Other Noninvasive Cardiac Imaging Modalities (e.g., Cardiac CT, Cardiac MRI)

Good diagnostic performance
Excellent clinical utility
Widely available
Portable (in-hospital and point-of-care testing)
Immediate results
Safe
Lower cost
Minimal patient discomfort
No radiation (compare CT, angiography, and so on)
No special breath-holding (compare MRI)

CT, computed tomography; MRI, magnetic resonance imaging.

should underscore the clinical context, the questions that need to be answered, and how the results would impact further management (Table 3).

This chapter incorporates the 2003 joint guidelines issued by the American College of Cardiology (ACC), the American Heart Association (AHA), the American Society of Echocardiography (ASE), and others.

It is within this broad context that the evidence for echocardiography (two-dimensional, M-mode, Doppler, and transesophageal echocardiography) was evaluated by the ACC/AHA/ASE task force. They employed a three-class system to limit the use of echocardiography to situations in which the incremental information provided can benefit patient management. Follow-up

Table 3
Determination of Utility for Echocardiography

1. How will it affect the referring physician's diagnosis (impact on diagnostic and prognostic thinking)?
2. Does it then influence patient management (therapeutic impact)?
3. Now does the test compare with other modalities.

or serial studies are generally indicated only when there is a change in clinical status, and when the information thereby provided can improve patient care.

AHA/ACC Classification

Class I: Evidence and/or general agreement of benefit.
Class IIa: Weight of evidence in favor.
Class IIb: Evidence not well established.
Class III: No evidence of its utility.

Newer and rapidly evolving echocardiographic modalities and techniques (Table 1A,B), e.g., three-dimensional, tissue Doppler, myocardial contrast imaging, intracardiac, and intravascular ultrasound were not addressed in the ACC/AHA/ASE guidelines and are not covered in this chapter.

Because echocardiographic techniques are heavily operator-dependent, the guidelines also highlighted the need for appropriate training and competence in echocardiography. This is especially relevant as techniques and their applications evolve.

ECHOCARDIOGRAPHY IN CLINICAL PRACTICE: GENERAL CONSIDERATIONS

A careful history and physical examination remains the cornerstone of sound medical management. Echocardiography assists in the diagnosis and management of patients who exhibit symptoms and signs suggestive of heart disease, as well as those with existing cardiovascular disease. Common requests for echocardiography include patients with murmurs, chest pain, dyspnea, palpitations, syncope, or an abnormal electrocardiogram (ECG) (Tables 4–6).

An abnormal finding on echocardiography may be incidental to the clinical question. Therefore, discussions between the referral and the echocardiography teams are encouraged. This ensures that appropriate emphasis is given to answer the clinical question. Although echocardiographic screening of the general population and athletes with a normal cardiovascular history is not recommended, conditions exist where such screening is advisable (Table 7).

Echocardiography in Acute Chest Pain and Myocardial Ischemia

Chest pain may be cardiac or noncardiac in origin. Echocardiography, although useful, should not interfere with the management of patients with myocardial infarction. It adds little to the diagnosis if ECG and cardiac enzymes are already clearly diagnostic for acute myocardial infarction (Table 8). When doubt exists, e.g., nondiagnostic ECG changes, or when other causes of chest pain are entertained, transthoracic echocardiography can be of value. New regional wall motion abnormalities appearing in previously normal ventricular segments support the diagnosis of acute myocardial ischemia and may precede changes in the ECG. Likewise, other findings may argue against acute coronary syndrome, including pericardial effusion (as might be seen in pericarditis), and right ventricular enlargement (as might be seen in pulmonary embolism). Although new regional wall motion abnormalities can be highly suggestive of acute ischemia or infarction, this diagnosis can be considerably more challenging in patients with prior history of myocardial infarction or abnormal regional wall motion.

Following myocardial infarction, echocardiography can have substantial value (Chapter 7). Early and late post-myocardial infarction complications, e.g., ventricular septal defect or papillary muscle rupture can be diagnosed with echocardiography. In the postinfarction period, echocardiography can assist with the diagnosis, risk assessment, and prognosis (Table 8).

In chronic myocardial ischemia, echocardiography can provide added information on disease severity and risk stratification that impacts further clinical management (Tables 8 and 9; Chapter 8). Where indicated, exercise or pharmacological stress echocardiography are useful adjuncts in assessing global and regional systolic function as well as myocardial contractile reserve.

PULMONARY EMBOLISM

Although less sensitive and specific than ventilation-perfusion scans and pulmonary angiography in acute

Table 4
Common Clinical Signs, Symptoms, or Conditions for Which Echocardiography Is Indicated

Clinical symptom or sign	*Possible echocardiographic findings*	*Indications for echocardiography*
	Clinical signs	
Systolic murmur	Aortic sclerosis Aortic stenosis Subaortic stenosis Mitral regurgitation Tricuspid regurgitation Pulmonic stenosis Atrial septal defect	Indicated in patients with cardiac symptoms or ECG abnormalities Not indicated when the murmur is clearly identified as innocent or benign by an experienced clinician
Diastolic murmur	Aortic regurgitation Mitral stenosis Atrial septal defect	Indicated for the diagnosis of all diastolic murmurs Not indicated for repeat studies when a definitive diagnosis has previously been made and signs/symptoms have not changed
Continuous murmur	Patent ductus arteriosus	Indicated for all continuous murmurs except when previously diagnosed without change in symptoms or signs
Thrill	Ventricular septal defect	Indicated for evaluation of thrill except when previously diagnosed without change in symptoms or signs
Mid-systolic click	Mitral valve prolapse	Indicated when the diagnosis of prolapse has not previously been made
Third heart sound	Left ventricular dysfunction	Indicated for the diagnosis of a new third heart sound in patients not known to have left ventricular dysfunction
Dyspnea	Left ventricular dysfunction Valvular heart disease Right ventricular enlargement Right ventricular dysfunction	Indicated for dyspnea in the presence of clinical signs/symptoms of heart disease Not indicated when dyspnea is attributable to a noncardiac cause
Cyanosis	Atrial septal defect with Eisenmenger's physiology Unsuspected congenital heart disease	Indicated for patients with cyanosis not otherwise explained
Cardiomegaly on chest radiograph	Pericardial effusion Cardiomyopathy Left ventricular hypertrophy Congenital heart disease	Indicated for patients with undiagnosed cardiomegaly detected on chest radiography
	Clinical symptoms	
Syncope	Aortic stenosis Left ventricular dysfunction (predisposes patients to arrhythmia)	Indicated for evaluation of possible aortic stenosis in patients with undiagnosed systolic murmur and syncope Not indicate in patients with neurocardiogenic or Vaso-vagal syncope
Chest pain	Regional wall motion abnormalities Right ventricular enlargement and dysfunction Pericardial effusion	Indicated in patients with ECG abnormalities and no previous history of infarction Indicated for the diagnosis of myocardial infarction when standard diagnostic methods are not definitive Indicated for ECG abnormalities suggestive of pericarditis
	Conditions	
Supraventricular tachycardia	Atrial septal defect (common with WPW syndrome) Epstein's anomaly Atrial enlargement	Indicated in patients undergoing electrophysiological study or ablation or in patients being considered for anti-arrhythmic therapy May not be indicated in young patients who have no other symptoms or signs and whose arrhythmia breaks easily

(Continued)

Table 4 *(Continued)*

Clinical symptom or sign	*Possible echocardiographic findings*	*Indications for echocardiography*
Atrial fibrillation or flutter	Left atrial enlargement Mitral stenosis Mitral regurgitation Left ventricular dysfunction/hypertrophy Pericardial abnormalities	Indicated in patients with new atrial fibrillation or flutter who have not had a recent echocardiogram

ECG, electrocardiogram; WPW, Wolff-Parkinson-White.

Reproduced from Solomon SD. Principles of echocardiography. In: Braunwald E, Goldman L, eds. Primary Cardiology, 2nd ed. Philadelphia, Saunders-Elsevier, 2003.

Table 5
Clinical Utility of Echocardiography

	Two dimensional	*Doppler*	*Color flow Doppler*	*CW Doppler*	*TEE*	*Stress*
Pericardial disease	1	2	3	4	4	N/A
Valvular heart disease						
Murmur	1	1	1	3	4	N/A
Mitral stenosis	1	1	1	—	3	3
Mitral regurgitation	1	1	1	—	3	N/A
Aortic stenosis/regurgitation	1	1	1	—	3	3
Prosthetic heart valve dysfunction	1	1	1	—	2	N/A
CAD						
Chest pain syndrome	1	3	3	4	4	1
Rule out CAD	1	3	3	4	4	1
Diagnose acute MI	1	3	3	4	4	N/A
Complications of MI						
Aneurysm	1	3	3	4	4	N/A
Thrombus	1	3	3	4	4	N/A
VSD/papillary muscle rupture	1	1	1	3	2	N/A
Assess LV function	1	1	2	4	4	3
Congenital heart disease	1	1	1	3	3	3
Atrial septal defect	1	1	1	2	2	4
Cardiomyopathy						
Dilated	1	1	1	3	4	3
Hypertrophic	1	1	1	3	4	3
Endocarditis	1	1	1	4	2	N/A
Pulmonary hypertension						
Known	1	1	1	2	3	3
Occult	1	1	1	2	3	2
Congestive heart failure	1	1	1	4	4	3

(Continued)

Table 5 ***(Continued)***

	Two dimensional	*Doppler*	*Color flow Doppler*	*CW Doppler*	*TEE*	*Stress*
Stroke/source of embolus	1	2	2	1	2	N/A
Aortic dissection	2	2	1	4	1	N/A
Dyspnea evaluation	1	1	1	1	4	1

1, indicated and essential; 2, often required—may add, informative; 3, necessary in select instances for specific question; 4, rarely necessary.

CW, continuous wave; TEE, transesophageal echocardiography; CAD, coronary artery disease; LV, left ventricle; MI, myocardial infarction; VSD, ventricular septal defect; N/A, not applicable.

Reproduced with permission from Armstrong WF. Echocardiography. In: Humes HD, ed. Kelly's Textbook of Internal Medicine, 4th ed. Philadelphia, Lippincott-Raven, 2000.

Table 6
Electrocardiographic Abnormalities Suggestive of Heart Disease in Asymptomatic Patients

ECG abnormality	*Possible echocardiographic finding*
Pathological Q-waves	Regional wall motion abnormalities consistent with previous infarction
Right bundle branch block, RSR′ pattern	Atrial septal defect
Left bundle branch block	Regional wall motion abnormality consistent with infarction
Atrial flutter	Pericardial effusion
Atrial fibrillation	Mitral valve abnormalities
	Left atrial dilatation
Delta wave (Wolff-Parkinson-White syndrome)	Atrial septal defect
	Ebstein's anomaly
ST-segment elevation	Acute myocardial infarction Ventricular aneurysm Acute pericarditis
Low-voltage ECG	Amyloid and infiltrative cardiomyopathies
Electrical alternans	Pericardial effusion
LVH criteria on ECG	Left Ventricular Hypertrophy Hypertrophic cardiomyopathy

ECG, electrocardiogram; LVH, left ventricular hypertrophy.

Modified from Solomon SD. Principles of Echocardiography. In: Braunwald E, Goldman L, eds. Primary Cardiology, 2nd ed. Philadelphia, Saunders-Elsevier, 2003.

pulmonary embolism, echocardiography has value in detecting right ventricular enlargement and dysfunction that result from the acute increase in pulmonary vascular resistance and right ventricular afterload. Echocardiography is also helpful in distinguishing pulmonary embolism from other causes of acute chest pain, e.g., acute myocardial infarction, acute pericarditis, or cardiac tamponade. Direct visualization of a large pulmonary saddle embolus in the pulmonary arteries or the right heart chambers is detectable, although seen only occasionally (Table 8; Chapter 18).

DISEASES OF THE GREAT VESSELS

Transesophageal echocardiography is the preferred modality if acute aortic dissection is suspected as it is more sensitive than the transthoracic examination. (Table 8; Chapter 20). Aortic dissection involving the ascending aorta may be accompanied by pericardial

Table 7
Clinical Conditions in Which Screening Echocardiography is Indicated in Asymptomatic Patients

Suspected condition	*Clinical indications for screening*	*Echocardiographic findings*
Hypertrophic cardiomyopathy	Patients with a first degree-family relative with hypertrophic cardiomyopathy or sudden death at a young age	Unexplained ventricular hypertrophy Systolic anterior motion of the mitral valve
	Patients with unexplained left ventricular hypertrophy on an electrocardiogram	Left ventricular outflow tract obstruction
Marfan syndrome	Patients with a first-degree relative with Marfan syndrome	Aortic root dilatation
	Patients with the classic findings of Marfan syndrome	Myxomatous degeneration of the mitral and tricuspid valves
Familial dilated cardiomyopathy	Patients with more than one first-degree relative with a history of cardiomyopathy	Left ventricular dilatation or dysfunction Mitral regurgitation
Patient's undergoing potential cardiotoxic therapy (chemotherapy)	Baseline echocardiogram to assess ventricular function Before additional cycles of chemotherapy	Reduced left ventricular function after chemotherapy

Modified from Solomon SD. Principles of Echocardiography. In: Braunwald E, Goldman L, eds. Primary Cardiology, 2nd ed. Philadelphia, Saunders-Elsevier, 2003.

Table 8
Echocardiography in Chest Pain and Coronary Artery Disease

	Class I indications (ACC/AHA/ASE, 2003)
Echocardiography useful in: myocardial ischemia/infarction, aortic dissection, valvular heart disease especially aortic stenosis, mitral valve prolapse, pericarditis, hypertrophic cardiomyopathy, and pulmonary embolism.	
Chest pain	Chest pain with suspected acute myocardial ischemia, when baseline ECG and lab biomarkers are nondiagnostic (I)
	Chest pain in suspected aortic dissection (I)
	Chest pain and clinical evidence of valvular, pericardial, or primary myocardial disease (I)
	Chest pain, hemodynamic instability unresponsive to simple therapeutic measures (I)
Acute myocardial ischemic syndromes	**Diagnosis**
	Echocardiography during or within minutes of chest pain (I)
	Diagnosis of suspected acute ischemia or infarction not evident by standard means (I)
	Measurement of baseline LV function (I)
	Evaluation of patients with inferior MI and clinical evidence suggesting possible RV infarction (I)
	Assessment of mechanical complications and mural thrombus[a] (I)
	Risk assessment, prognosis, and assessment of therapy
	Assessment of infarct size and/or extent of jeopardized myocardium (I)
	In-hospital assessment of ventricular function when the results are used as a guide to therapy (I)
	In-hospital or early post-discharge assessment of the presence/extent of inducible ischemia whenever baseline abnormalities are expected to compromise ECG interpretation[b] (I)
	Assessment of myocardial viability when required to define potential efficacy of revascularization[c] (I)
Aortic dissection other aortic diseases	To diagnose, localize, and assessment of the extent (I)
	Follow-up of aortic dissection, especially when complicated or progression is suspected (I)
	Aortic aneurysm[d] (I)
	Aortic intramural hematoma (I)
	Aortic rupture (I)

(Continued)

Table 8 *(Continued)*

	Class I indications (ACC/AHA/ASE, 2003)
	Degenerative or traumatic aortic disease with clinical atheroembolism(I)
	Aortic root dilatation in Marfan syndrome or other connective tissue syndromes[d] (I)
	First-degree relative of a patient with Marfan syndrome or other connective tissue disorder for which TEE is recommended[d] (I)
Acute pulmonary embolism	For distinguishing cardiac vs noncardiac etiology of dyspnea in patients in whom clinical and laboratory clues are ambiguous[e] (I)
	Follow-up of pulmonary artery pressures in patients with pulmonary hypertension in response to treatment (I)
	Lung disease with clinical suspicion of cardiac involvement or suspected cor pulmonale (I)
	Suspected pulmonary hypertension (I)
Pericardial disease	Suspected pericardial disease, including effusion, constriction, or effusive-constrictive process (I)
	Suspected bleeding into the pericardial space, e.g., trauma, perforation (I)
	Follow-up studies to evaluate recurrence of effusion or to diagnose early constriction.
	Repeat studies directed to answer a specific clinical question (I)
	Pericardial friction rub in the setting of acute MI, and accompanied by persistent pain, hypotension, and nausea (I)
Chronic ischemic heart disease	**Diagnosis**
	Diagnosis of myocardial ischemia in symptomatic individuals[e] (I)
	Exercise echocardiography for diagnosis of myocardial ischemia in selected patients (whose ECG assessment is less reliable owing to digoxin, LVH with >1 mm ST depression at rest on baseline ECG, pre-excitation syndrome (Wolff-Parkinson-White), complete LBBB, with intermediate pretest likelihood of CAD (I)
	Assessment of global ventricular function at rest (I)
	Assessment of myocardial viability (hibernating myocardium) for planning revascularization[f] (I)
	Assessment of functional significance of coronary lesions (if not already known) in planning percutaneous transluminal coronary artery angioplasty[e] (I)
	Diagnosis, Risk Stratification, Clinical Management
	Prognosis of myocardial ischemia in selected patients (whose ECG assessment is less reliable) with the following ECG abnormalities: pre-excitation syndrome (Wolff-Parkinson-White), electronically paced ventricular rhythm, >1 mm ST depression at rest, complete LBBB[e] (IIa)
	Detection of coronary arteriopathy in patients postcardiac transplantation (IIa)
	Detection of myocardial ischemia in women with an intermediate pretest likelihood of CAD[e] (IIa)
Interventions in coronary artery disease	Assessment of LV function when needed to guide institution and modification of drug therapy in patients with known or suspected LV dysfunction (I)
	Assessment for restenosis after revascularization in patients with atypical recurrent symptoms[b] (I)
	Assessment for restenosis after revascularization in patients with typical recurrent symptoms[b] (IIa)
	Assessment of LV function in patients with previous myocardial infarction when needed to guide possible placement of ICD in patients with known or suspected LV dysfunction (IIa)

[a]TEE is indicated when TEE studies are not diagnostic.

[b]Exercise or pharmacological stress echocardiogram.

[c]Dobutamine stress echocardiogram.

[d]TTE should be the first choice in these situations, and TEE should only be used if examination is incomplete or additional information is needed.

[e]Exercise or pharmacological stress echocardiogram.

[f]Dobutamine stress echocardiogram.

CAD, coronary artery disease; ECG, electrocardiogram; ICD, implantable cardioverter-defibrillator; LBBB, left bundle branch block; LVH, left ventricular hypertrophy; MI, myocardial infarction; RV, right ventricle; TEE, transesophageal echocardiography; TTE, transthoracic echocardiography.

Table 9
Stress Echocardiography: Utility and Indications

	Protocol	*Utility*	*Indications/comments*
Exercise stress echocardiography	Treadmill, bicycle (supine or upright)	Diagnostic	Patients with abnormal baseline ECG or limited exercise tolerance • Nonspecific ST-T-wave changes • Left bundle branch block • Left ventricular hypertrophy • Digoxin therapy • Wolff-Parkinson-White syndrome
		Prognostic	• Chronic coronary artery disease • Post-myocardial Infarction
		Risk stratification	• In heart failure: contractile reserve, mitral valve function, right ventricular function • Perioperative evaluation for noncardiac surgery
Pharmacological stress echocardiography	Sympathomimetic amines, e.g., dobutamine, dobutamine (+ atropine) —agent of choice (US)	As for exercise stress echocardiography (in patients unable to exercise)	• Indications as for exercise stress echocardiography (when patients unable to exercise) • Myocardial viability assessment (for biphasic response) • Contractile reserve in patients with heart failure and low-gradient aortic stenosis
	Vasodilators, e.g., dipyridamole, adenosine	As for exercise stress echocardiography (in patients unable to exercise)	Less sensitivity than with sympathomimetic amines (use mainly outside the US)
	Other; ergonovine–ergometrine, enoximone		Diagnostic evaluation of vasospastic coronary artery disease
Pacing stress echocardiograpy	Atrial Transesophageal atrial pacing	Diagnostic	Patients with known or suspected coronary artery disease
Stress echocardiography with Doppler		Low gradient aortic stenosis (with left ventricular dysfunction)	Assessment of contractile reserve (Dobutamine stress)
		Heart failure; assessment of systolic/diastolic dysfunction	Mitral regurgitation and Transmitral Doppler indices using exercise or pharmacological protocols

effusion, cardiac tamponade, or new onset aortic regurgitation. These, along with a proximal dissection flap, can be rapidly sought on a limited transthoracic study while awaiting an emergent transesophageal echocardiography examination or contrast CT sean.

Echocardiography in Pericardial Disease

The normal pericardium is best assessed by imaging techniques other than echocardiography, but in pathological states, e.g., acute pericarditis, pericardial effusion or tamponade, echocardiography is of

Table 10
Dyspnea, Edema, and Diseases of the Heart Muscle

	Class I indications (ACC/AHA/AS/E, 2003)
Dyspnea, edema, and cardiomyopathy (CM)	Assessment of LV size and function in patients with suspected CM or clinical heart failure[a] (I) Edema with clinical signs of elevated CVP when a potential cardiac etiology is suspected or when CVP cannot be reliably estimated and high clinical suspicion of heart disease[a] (I) Dyspnea with clinical signs of heart disease[a] (I) Unexplained hypotension, especially in the ICU[a] (I) Exposure to cardiac toxins, to guide additional or increased dose (I) Re-evaluation of LV function in patients with established CM with documented change in clinical status or as guide to medical therapy (I) Suspicion of HCM based on abnormal physical exam, ECG, or family history (I) Intraprocedural contrast echocardiographic assessment of myocardial infarct zone during septal alcohol ablation in HCM (I)
Hypertension	Assessment of resting LV function, hypertrophy, or concentric remodeling when important in clinical decision making (1) Detection and assessment of functional significance of concomitant CAD by stress echocardiography (I) Follow-up assessment of LV size and function in patients with LV dysfunction when there has been a documented change in clinical status or to guide medical therapy (I)

[a]TEE when TTE not diagnostic.

CAD, coronary artery disease; CM, cardiomyopathy; CVP, central venous pressure; HCM, hypertrophic cardiomyopathy; ICU, intensive care unit; TEE, transesophageal echocardiography.

diagnostic valve, and can serve as a guide to management (Table 8; Chapter 10). Echocardiography is the most efficient method to assess the size and hemodynamic consequences of pericardial effusion.

ECHOCARDIOGRAPHY IN DYSPNEA, VENTRICULAR DYSFUNCTION, AND HEART FAILURE

In patients with suspected heart failure, echocardiography is useful in evaluating global and regional ventricular function. In patients with heart failure, post-myocardial infarction, and cardiomyopathy, quantitative and semi-quantitative indices of ventricular function (e.g., chamber dimensions, ejection fraction, and cardiac output) are of important diagnostic and prognostic value (Table 10; Chapters 5, 6, and 9).

CARDIAC MURMURS AND VALVULAR HEART DISEASE

The medical history, physical examination, and cardiac auscultation are fundamental to proper assessment of murmurs and valvular heart disease, but echocardiography plays an invaluable role (Table 11; Chapters 11–15).

Patients with systolic murmurs need echocardiographic evaluation when cardio-respiratory symptoms are present. Asymptomatic patients benefit only when there is a reasonably high probability of underlying structural heart disease. All diastolic and continuous murmurs should be further evaluated by echocardiography, but systolic murmurs deemed innocent by an experienced clinical examiner do not warrant echocardiography. Serial follow-up of patients is indicated when there is a change in clinical status.

Echocardiography is needed in patients with valvular heart disease to confirm the diagnosis, assess the severity, and influence clinical management (Table 11). Such patients also benefit from additional echocardiography when there is a subsequent change in symptoms and signs, including pregnancy. Echocardiography is justified in severe valvular heart disease even when such patients are asymptomatic. The timing and follow-up of interventions in patients with valvular heart disease, including prosthetic valves, can be guided by the parameters obtained by echocardiography.

Table 11
Echocardiography in Cardiac Murmurs and Valvular Heart Disease

	Class I indications (ACC/AHA/ASE, 2003)
Cardiac murmur on auscultation	
No symptoms	Diastolic or continuous (I) Holosystolic or late systolic (1) Grade 3 or midsystolic (I) Abnormal physical findings, ECG, CXR (IIa)
Symptoms	Symptoms/signs of heart failure, MI, syncope (I) Symptoms/signs consistent with infective endocarditis (1) and thromboembolism (I)
Valvular heart disease (VHD)	
Both valvular stenoses (VS) and regurgitation (VR)	Diagnosis (I) Assessment of hemodynamic severity (I) Assessment of LV and RV size, function, and hemodynamics (I) Re-evaluation of patients with known VS or VR with changing symptoms or signs (I) Assessment of hemodynamic severity and ventricular compensation in patients with known VS or VR in pregnancy (I) Re-evaluation of asymptomatic patients with severe VS or VR (I)
Valvular stenoses (VS)	Assessment of hemodyamic significance of mild to moderate VS by Doppler echocardiography (IIa) Re-evaluation of patients with mild to moderate AS with LV dysfunction or hypertrophy, even if asymptomatic (IIa)
Valvular regurgitation (VR)	Re-evaluation of asymptomatic patients with mild to moderate VR with ventricular dilatation (I) Assessing the impact of medical therapy on VR severity and ventricular compensation and function when it might change medical management (I) Assessment of valvular morphology and regurgitation in patients with h/o anorectic drug use or agent associated with VHD, who are asymptomatic, have cardiac murmurs, or inadequate auscultation (I)
Mitral valve prolapse	Diagnosis Assessment of hemodynamic severity, leaflet morphology, and/or ventricular compensation in patients with physical signs of MVP, e.g., systolic click, murmur (I)
Interventions in valvular heart disease and prosthetic valves	Assessment of timing of valvular intervention based on ventricular compensation, function, and/or severity of primary and secondary lesions (I) Selection of alternative therapies for MV disease, e.g., balloon valvuloplasty, operative valve repair, valve replacement[a] (I) Use of echocardiography (especially TEE) to guide performance of intervention techniques and surgery (e.g., balloon valvotomy and valve repair) for valvular disease (I) Post-intervention baseline studies for valve function (early) and ventricular remodeling (late) (I) Re-evaluation of patients with valve replacement with changing clinical signs and symptoms; suspected prosthetic dysfunction (stenosis, regurgitation) or thrombosis[a] (I)

[a]TEE adds incremental value over TTE.

AR, aortic regurgitation; AS, aortic stenosis; CXR, chest X-ray; LV, left ventricle; MR, mitral regurgitation; MS; mitral stenosis; RV, right ventricle; TEE, transesophageal echocardiography; TTE, transthoracic echocardiography.

INFECTIVE ENDOCARDITIS

Although the diagnosis of infective endocarditis should be made clinically, the Duke classification includes positive echocardiographic findings as one of its major diagnostic criteria. Detection and characterization of vegetations and perivalvular structures is made possible by echocardiography (Table 12; Chapter 15). Such findings have important prognostic value.

Table 12
Echocardiography in Infective Endocarditic

Class I indications (ACC/AHA/ASE, 2003)	
Both native and prosthetic valves	Detection and characterization of valvular lesions, their hemodynamic severity, and /or ventricular compensation[a] (I) Detection of associated abnormalities (e.g., abcesses, shunts)[a] (I) Re-evaluation in complex endocarditis, e.g., virulent organism, severe hemodynamic lesion, aortic valve involvement, persistent fever or bacteremia, clinical change, or symptomatic deterioration (I)
Native valves	Detection of vegetations and characterizations of lesions in patients with congenital HD suspected of having infective endocarditis (I) Evaluation of patients with high clinical suspicion of culture-negative endocarditis[a] (I) If TTE is equivocal, TEE evaluation of bacteremia especially *Staphylococcus* bacteremia or fungemia without a known source (I) Evaluation of persistent non-*Staphylococcus* bacteremia without a known source[a] (IIa) Risk stratification in established endocarditis[a] (IIa)
Prosthetic valves	Evaluation of suspected endocarditis and negative cultures[a] (I) Evaluation of bacteremia without known source[a] (I) Evaluation of persistent fever without evidence of bacteremia or new murmur[a] (IIa)

[a]TEE adds incremental value over TTE.
TEE, transesophageal echocardiography; TTE, transthoracic echocardiography.

Table 13
Echocardiography in Syncope, Palpitations, and Arrhythmias

Class I indications (ACC/AHA/ASE, 2003)

Syncope

Anatomical cardiac differential diagnosis includes: aortic dissection, aortic stenosis, atrial myxoma, cardiac tamponade, hypertrophic cardiomyopathy, mitral stenosis, myocardial ischemia/infarction, pulmonary embolism, pulmonary hypertension

Syncope in a patient with clinically suspected heart disease (I)

Peri-exertional syncope (I)

Palpitations and Arrhythmias

Stuctural heart disease leading to, or associated with arrhythmias include: congenital heart disease; acquired diseases of the coronary arteries, myocardium, pericardium, or valves

Arrythmias with clinical suspicion of structural heart disease (I)

Arrythmia in a patient with family history of a genetically transmitted cardiac lesion associated with arrhythmias e.g., tuberous sclerosis, rhabdomyoma (I)

Evaluation of patients as a component of the workup before electrophysiological ablative procedures (I)

Arrhythmia requiring treatment (IIa)

TEE or intracardiac ultrasound guidance of radiofrequency ablative procedures (IIa)

Precardioversion

Patients requiring urgent (not emergent) cardioversion for whom extended precardioversion anticoagulation is not desirable[a] (I)

Patients with prior cardioembolic events thought to be related intra-atrial thrombus[a] (I)

Patients for whom anticoagulation is contraindicated and for whom a decision about cardioversion will be influenced by TEE results[a] (I)

Patients for whom intra-atrial thrombus has been demonstrated in previous TEE[a] (I)

Evaluation of patients for whom a decision concerning cardioversion will be impacted by knowledge of prognostic factors (such as LV function or coexistent mitral valve disease) (I)

Patients with atrial fibrillation of <48 h duration and other heart disease (TEE only)[a] (IIa)

[a]TEE when TTE not diagnostic.
TEE, transesophageal echocardiography; LV, left ventricle.

Table 14
Cardiac Masses, Tumors, and Vascular Occlusive Events

Class I indications (ACC/AHA/ASE, 2003)
Cardiac masses and tumors
Suspect in the context of the clinical presentation, e.g., patients with:
1. Extensive anterior MI
2. Atrial fibrillation
3. One or more embolic peripheral or neurological events
4. Suggestive auscultatory findings, e.g., tumor plop
5. Hemodynamic findings suggesting intermittent obstruction to intracardiac flow
Evaluation of clinical syndromes and events suggestive of underlying cardiac mass (I)
Evaluation of underlying cardiac disease known to predispose to mass formation for whom a therapeutic decision regarding surgery or anticoagulation will depend on the results of echocardiography (I)
Follow-up or surveillance studies after surgical removal or with masses known to have a likelihood of recurrence (i.e., myxoma) (I)
Patients with known primary malignancies when echocardiographic surveillance for cardiac involvement is part of the disease staging process (I)
Neurological and vascular occlusive events
Patients (any age) with abrupt occlusions of a major peripheral or visceral artery (I)
Younger patients (typically <45 yr) with neurological events without evidence of cerebrovascular disease or other obvious cause (I)
Older patients (typically >45 yr) with neurological events with no evidence of cerebrovascular disease or other obvious cause (I)
Patients for whom a clinical therapeutic decision (e.g., anticoagulation) will depend on the echocardiography results (I)

Table 15
Adult Patients With Congenital Heart Disease (CHD)

Class I indications (ACC/AHA/ASE, 2003)
Two main groups:
1. CHD compatible surviving to adult life without surgery or interventional catheterization
2. CHD compatible surviving to adult life after surgery or interventional catheterization
General rule: all patients with CHD must be followed indefinitely
Essential: knowledge of anatomy, clinical issues, treatments, expected residua for each patient
Patients with clinically suspected CHD, as evidenced by signs and symptoms such as murmur, cyanosis, unexplained arterial desaturation, and an abnormal ECG or radiograph suggesting CHD (I)
Patients with known CHD when there is a change in clinical findings on follow-up (I)
Patients with known CHD when there is uncertainty as to the original diagnosis or when the precise nature of the structural abnormalities or hemodynamics is unclear (I)
Periodic echocardiograms in patients with known CHD lesions and for whom ventricular function and atrioventricular valve regurgitation must be followed, e.g., patients with a functional single ventricle after Fontan procedure, transposition of the great arteries after Mustard procedure. L-transposition and ventricular inversion, and palliative shunts (1)
Patients with known CHD for whom the following pulmonary artery pressure is important, e.g., with hemodynamically important, moderate, or large VSD, single ventricle, or any of the above with an additional risk factor for pulmonary HTN (I)
Periodic echocardiography in patients with repaired (or palliated) CHD with the following: change in clinical condition or clinical suspicion of residual defects, obstruction of conduits and baffles, LV or RV function that must be followed, or when there is a possibility of hemodynamic progression or a history of pulmonary HTN (I)
To direct interventional procedures: catheter valvotomy, radiofrequency ablation, and interventions in the presence of complex cardiac anatomy (I)
Identification of the site of origin and initial course of coronary arteries (TEE may be indicated in some patients) (I)

CHD, congenital heart disease; HTN, hypertension; TEE, transesophageal echocardiography.

Table 16
The Critically Ill and Injured Patient

Class I indications (ACC/AHA/ASE, 2003)
The critically ill patient
Special considerations in the critically ill patient in the emergency or critical care units. Recommendations vary according to the clinical scenario and among institutions. Critically ill patients have highly differing clinical circumstances. Clinical presentation of, e.g., chest pain or shock may be atypical. Detectable conditions by echocardiography include: acute MI and complications, cardiac tamponade, aortic dissection, complications of prothestic valves, source of embolism.
The hemodynamically unstable patient (I)
Suspected aortic dissection (1)
Transesophageal echocardiography (TEE) most valuable and provides the most definitive diagnosis in:
Suspected aortic dissection (I)
The hemodynamically unstable patient with sub-optimal transthoracic echocardiography (TTE) images (I)
The hemodynamically unstable patient on a ventilator (I)
Major trauma or postoperative patient (unable to be positioned for TTE) (I)
Suspected aortic injury (I)
Other conditions in which TEE is superior (I)
The critically injured patient
Special considerations in the critically injured patient in the emergency or critical care units. Recommendations vary among institutions and the clinical scenario—critically injured patients have highly differing clinical circumstances.
Serious blunt or penetrating chest trauma (suspected pericardial effusion or tamponade) (I)
Mechanically ventilated multiple-trauma patient or chest trauma patient (I)
Suspected pre-existing valvular or myocardial disease in the trauma patient (I)
The hemodynamically unstable multiple-injury patient without obvious chest trauma, but with a mechanism of injury suggesting potential cardiac or aortic injury (deceleration or crush) (I)
Widened mediastinum, post-injury suspected aortic injury (I)
Potential catheter guide wire, guide wire, pacer electrode, or pericardiocentesis (I)

Table 17
Intra-Operative Echocardiography

Class I indications (ACC/AHA/ASE, 2003)
Utility in mitral valve repair, valve replacement, ischemic heart disease, minimally invasive cardiac surgery, air embolization, aortic atheromatous disease
Evaluation of acute, persistent, and life-threatening hemodynamic disturbances in which ventricular function and its determinants are uncertain and have not responded to treatment (I)
Surgical repair of valve lesions, hypertrophic obstructive cardiomyopathy (HCM), and aortic dissection with possible aortic valve involvement (I)
Evaluation of complex valve replacements requiring homografts or coronary reimplantation, such as the Ross procedure (I)
Surgical repair of most congenital heart lesions that require cardiopulmonary bypass (CPB) (I)
Surgical intervention for endocarditis when preoperative testing was inadequate or extension to perivalvular tissue is suspected (I)
Placement of intracardiac devices and monitoring of their position during port access and other cardiac surgical interventions (I)
Evaluation of pericardial window procedures in patients with posterior or loculated pericardial effusions (I)

Echocardiography in Syncope, Palpitations, and Arrhythmias

Syncope can be secondary to underlying structural heart disease, such as congenital heart disease or aortic stenosis. When underlying structural heart disease is suspected, echocardiography is warranted (Table 13). Echocardiography is a useful adjunct in patients with arrhythmias scheduled for ablative procedures and electrical cardioversion (Table 13; Chapter 16). Echocardiography is rarely of benefit in patients with isolated palpitations.

Cardiac Masses, Tumors, and Vascular Occlusive Events

Echocardiography is useful for detecting cardiac masses and tumors, including thrombi. When symptoms and signs are suggestive, e.g., embolic events or neurological symptoms, echocardiography can be useful (Table 14; Chapters 17 and 19). However, if the findings do nothing to aid management, as in the terminally ill patient, there is no justifiable clinical role for echocardiography.

Echocardiography in Adult Congenital Heart Disease

Echocardiography plays an invaluable role in the management of adult congenital heart disease. Doppler echocardiography has largely obviated the need for invasive pre-operative assessment of shunts and gradients in this patient population (Table 15; Chapter 21 and 22).

Echocardiography in the Critically Ill or Injured Patient

Despite the logistical challenges of performing echocardiography in these settings, the critically ill and the critically injured patient can greatly benefit from echocardiographic evaluation of mechanical causes of hemodynamic instability and possible cardiac injury (Table 16). The subcostal transthoracic examination or the transesophageal route may be the only available windows. The latter is the examination of choice when aortic injury or dissection is suspected.

Transesophageal Echocardiography and Intra-Operative Echocardiography

The basics of the transephageal examination are presented in Chapter 23. Intra-operative echocardiography is now a standard during cardiac surgical procedures, especially for valvular pathology and complex cardiac surgical intervention (Table 17).

SUGGESTED READING

Cheitlin MD, Armstrong WF, Aurigemma GP, et al. American College of Cardiology; American Heart Association; American Society of Echocardiography. ACC/AHA/ASE 2003 guideline update for the clinical application of echocardiography: summary article: a report of the American College of Cardiology/American Heart Association Task Force on Practice Guidelines (ACC/AHA/ASE Committee to Update the 1997 Guidelines for the Clinical Application of Echocardiography). Circulation 2003;108: 1146–1162.

Eagle KA, Berger PB, Calkins H, et al. ACC/AHA guideline update for perioperative cardiovascular evaluation for noncardiac surgery update: a report of the American College of Cardiology/American Heart Association Task Force on Practice Guidelines (Committee to Update the 1996 Guidelines on Perioperative Cardiovascular Evaluation for Noncardiac Surgery). Available at: http://www.acc.org/clinical/guidelines/perio/update/periupdate_index.htm. Accessed June 12, 2002.

Fryback DG, Thornbury JR. The efficacy of diagnostic imaging. Med Decis Making 1991;11:88–94.

Mintz GS, Nissen SE, Anderson WD, et al. American College of Cardiology clinical expert consensus document on standards for acquisition, measurement and reporting of intravascular ultrasound studies (IVUS): a report of the American College of Cardiology Task Force on Clinical Expert Consensus Documents. J Am Coll Cardiol 2001; 37:1478–1492.

Quinones MA, Douglas PS, Foster E, et al. American College of Cardiology; American Heart Association; American College of Physicians; American Society of Internal Medicine Task Force on Clinical Competence. American College of Cardiology/American Heart Association clinical competence statement on echocardiography: a report of the American College of Cardiology/American Heart Association/American College of Physicians—American Society of Internal Medicine Task Force on Clinical Competence. Circulation 2003;107:1068–1089.

Smith SC, Jr, Dove JT, Jacobs AK, et al. ACC/AHA guidelines of percutaneous coronary interventions (revision of the 1993 PTCA guidelines: executive summary: a report of the American College of Cardiology/American Heart Association Task Force on Practice Guidelines (Committee to Revise the 1993 Guidelines for Percutaneous Transluminal Coronary Angioplasty). J Am Coll Cardiol 2001;37: 2215–2239.

Solomon SD. Principles of echocardiography. In: Braunwald E, Goldman L., eds. Primary Cardiology, 2nd ed. Philadelphia: Saunders-Elsevier, 2003.

II Diseases of the Myocardium and Pericardium

5 Echocardiographic Assessment of Ventricular Systolic Function

Bernard E. Bulwer, MD, MSc, Scott D. Solomon, MD, Rajesh Janardhanan, MD, MRCP

Contents

CASE PRESENTATION

A 72-yr-old Caucasian male with a history of coronary artery disease and congestive heart failure was relatively well until he began experiencing orthopnea, paroxysmal noctural dyspnea, and acute deterioration 2 d before admission.

Past medical history: he suffered a myocardial infarct 6 mo earlier and underwent cardiac

From: *Contemporary Cardiology: Essential Echocardiography: A Practical Handbook With DVD*
Edited by: S. D. Solomon © Humana Press, Totowa, NJ

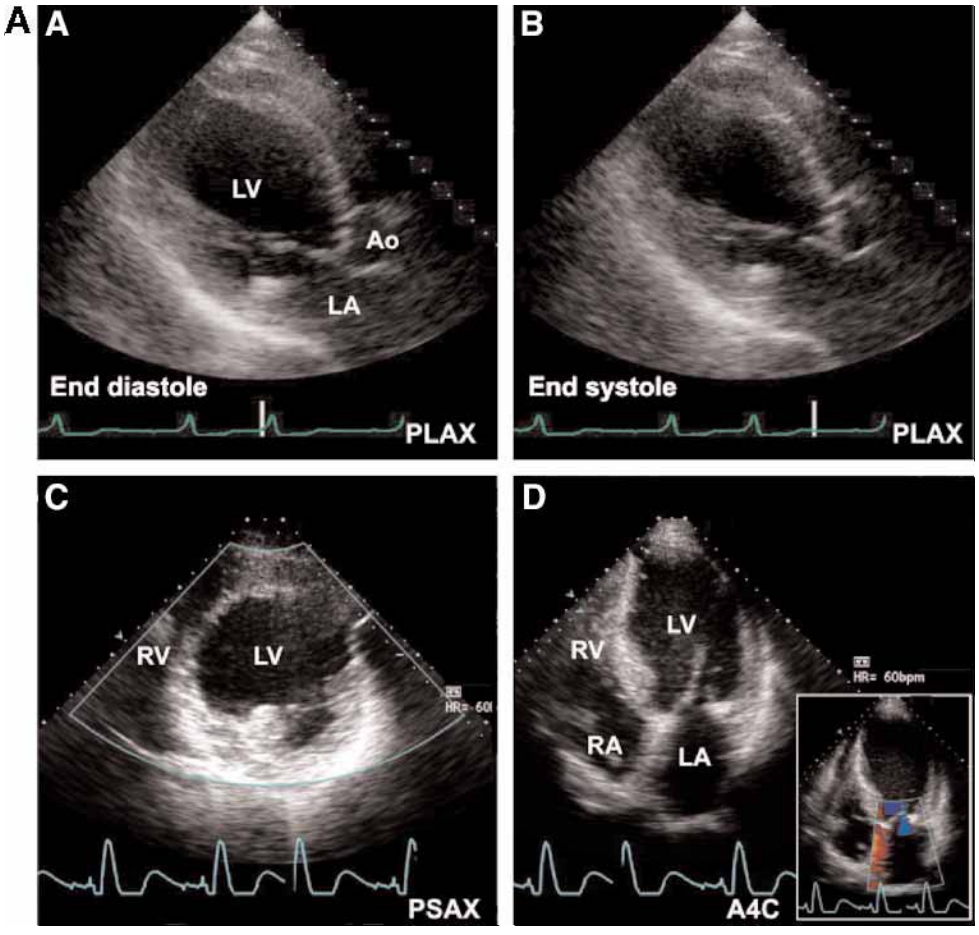

Fig. 1. *(Continued)*

catheterization and coronary angiography, which revealed significant three-vessel disease. Two years previously, he underwent placement of an implantable cardioverter defibrillator with biventricular pacing following episodes of ventricular tachycardia. His additional medical problems included hypertension, dyslipidemia, chronic obstructive pulmonary disease, and chronic renal impairment.

On physical examination, he was tachypneic (respiratory rate >40 breaths/min) with a regular pulse of 62 bpm, and blood pressure measuring 180/90 mmHg. His oxygen saturation on pulse oximetry was 93% on room air. He was afebrile and acyanotic. His jugular venous pressure was elevated and inspiratory crackles were heard halfway up both lung fields posteriorly. His chest X-ray showed signs of pulmonary edema with enlarged cardiac silhouette. Echocardiographic assessment of left ventricular function revealed a moderately dilated left ventricle (LV) with severely reduced global systolic function with regional variation. Select images from his echocardiogram are shown in Fig. 1A–D (please *see* companion DVD for corresponding video).

A major clinical application of echocardiography is the assessment of ventricular systolic function. This is a fundamental part of the standard echocardiographic examination, but is especially important in patients with heart failure and post-myocardial infarction (Fig. 2). Two-dimensional (2D) and Doppler echocardiography plays important roles in the diagnosis, management, and risk stratification of patients with systolic dysfunction.

Common causes of LV dysfunction in industrialized countries are listed in Table 1. Precipitating factors

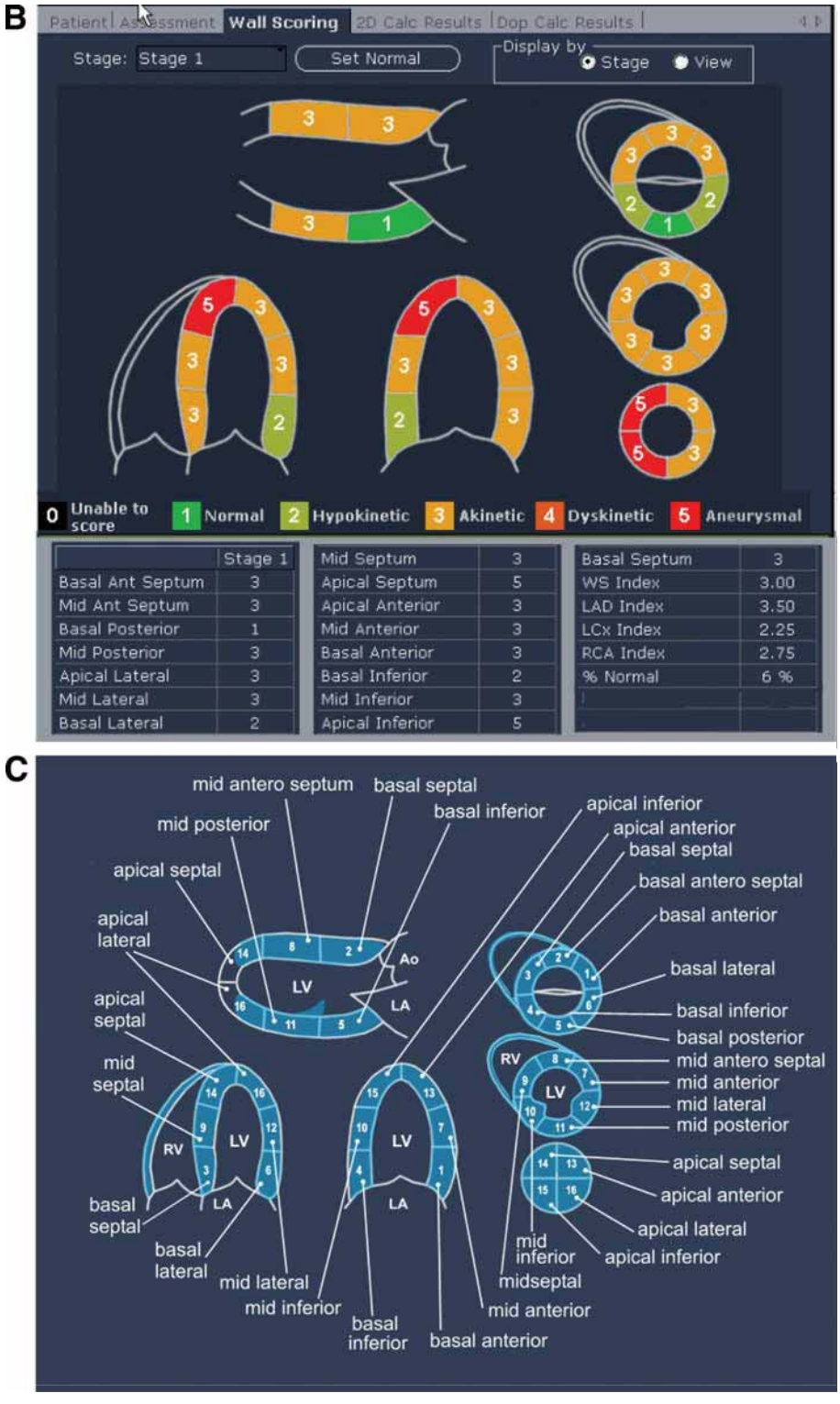

Fig. 1. *(Continued)*

(Table 2) should always be sought and the examination should be interpreted within this wider context (Table 3). This chapter discusses echocardiographic assessment of systolic function.

ECHOCARDIOGRAPHIC ASSESSMENT OF LV SIZE

Assessment of LV size is one of the most important components of quantitation of ventricular function.

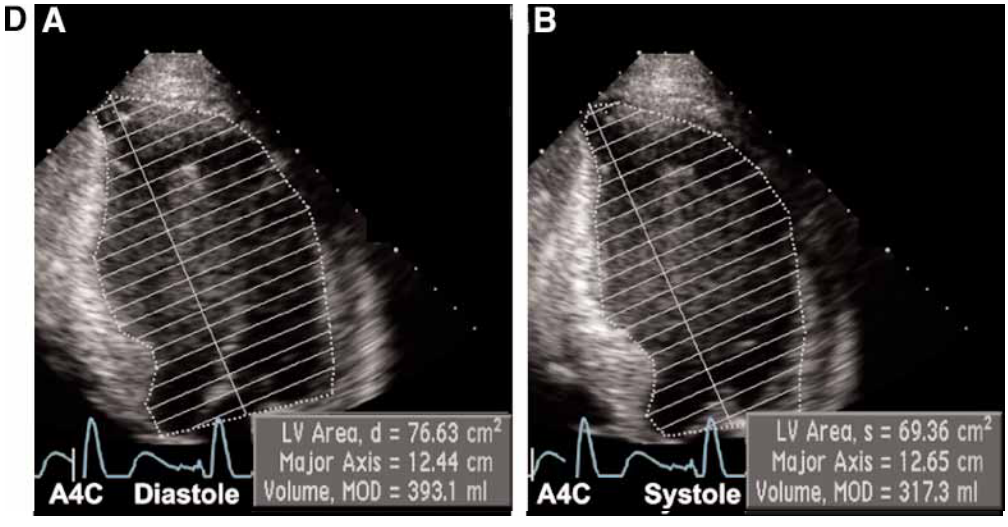

Fig. 1. **(A)** A 72-yr-old man with history of coronary artery disease and heart failure. The left ventricular ejection fraction measured 15%. The apical septal and apical inferior segments were aneurysmal. The entire anterior wall, mid- and distal lateral walls, anterior septal, midposterior segment, midseptal segments, midinferior segment, and basal septal segments were akinetic. The basal lateral and basal inferior segments were hypokinetic. The basal inferior segment contracts and thicken normally. Right ventricular size was not enlarged and right ventricular systolic function was preserved. **(B)** Computerized record of regional wall motion scores. Computerized record of left ventricular wall motion of patient in **A** with wall motion score index (WI) of 3.1 (normal = 1) (please *see* **C**). **(C)** Left ventricular segmental nomenclature. Left ventricular segmental nomenclature according to the American Heart Association/American Society of Echocardiography recommendations (*see* Fig. 10A,B). **(D)** Left ventricular volumes calculated by the biplane method of discs. The recommended method of quantifying left ventricular ejection fraction employs volumetric calculations using two orthogonal biplanes according to the method of discs, (*see* Fig. 14). (Please *see* companion DVD for corresponding video.)

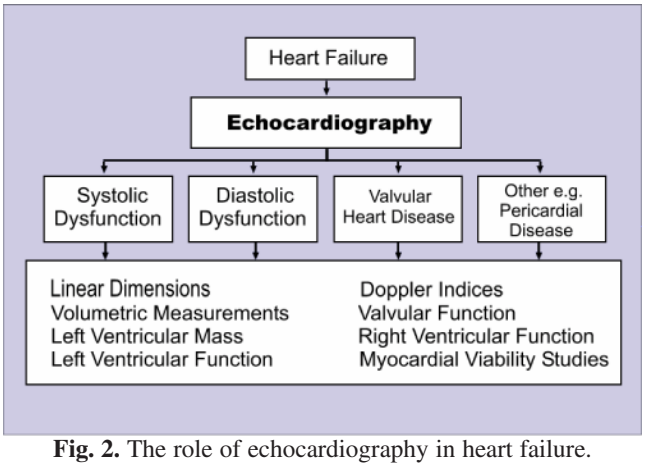

Fig. 2. The role of echocardiography in heart failure.

Qualitative and quantitative data derived from echocardiography, e.g., LV dimensions and wall thickness, can influence patient management and serve as potent predictors of outcomes (Table 4). In patients with chronic stable coronary artery disease, there is a consistent relationship between heart size and outcomes. As heart size increases, so does mortality. The same applies to patients without heart failure. Data from the Framingham Heart Study showed that even in patients without a history of heart failure or myocardial infarction, LV size (by M-mode echocardiography) was an important predictor of subsequent risk of heart failure.

Table 1
Common Underlying Causes of Ventricular Dysfunction

- Ischemic heart disease (~75% in industrialized countries)
- Cardiomyopathies
- Pressure overload states
  - Hypertensive heart disease
  - Valvular heart disease: aortic stenosis
- Volume overload states
  - Valvular heart disease: aortic incompetence, mitral regurgitation
  - Ventricular septal defect
- Rapid ventricular rate states
  - Sustained ventricular tachycardias (e.g., atrial fibrillation with rapid ventricular response)
- Congenital heart disease

LV DIMENSIONS BY M-MODE

The oldest and still widely used method for linear measurements of LV size is M-mode echocardiography. It is simple, reproducible, accurate (when properly applied), and provides excellent endocardial border definition (owing to high frame rate). The American Society of Echocardiography (ASE) recommends measurement of LV dimensions with the M-mode line perpendicular to

Table 2
Common Precipitants of Heart Failure

- Therapeutic noncompliance
- Arrhythmias
- Acute ischemia, including myocardial infarction
- Systemic or cardiac infection, e.g., myocarditis
- Physical, environmental, and emotional stress
- Pulmonary embolism
- High output states, e.g., anemia, thyrotoxicosis, pregnancy
- Drugs and toxins, including nonsteroidal anti-inflammatory drugs, ethanol

Table 3
Pathophysiological Mechanisms in Heart Failure

Structural abnormalities	Cellular/cardiac myocyte abnormalities: necrosis, fibrosis, hypertrophy, excitation–contraction coupling Left ventricular remodeling: dilatation, increased sphericity, aneursymal dilatation Coronary artery abnormalities: stenosis, endothelial inflammation
Functional abnormalities	Mitral regurgitation Myocardial "stunning" or hibernation Arrhythmias
Neuro-hormonal influences	Renin-angiotensin-aldosterone system Sympathetic nervous system Others
Comorbidities	Age, coronary artery disease, diabetes, hypertension, renal dysfunction, metabolic syndrome, anemia

Table modified from Jessup M, Brozena S. Heart failure. N Engl J Med 2003;348:2007–2018.

the long axis of the heart and immediately distal to the tips of the mitral valve leaflets in the parasternal long-axis view (Fig. 3).

Measurements are taken at end-diastole (d)—defined as the beginning of the QRS complex—but preferably using the at the widest LV cavity diameter, and at end-systole (s)—using the narrowest LV cavity diameter. The leading-edge convention of the ASE is the recommended method of measurement. The diastolic measurements obtained are the interventricular septal wall thickness, the LV internal diameter at end diastole (LVIDd) and posterior wall thickness. In systole, the LV systolic diameter (LVIDs) is measured (Fig. 3). Calculations of other indices of LV systolic function, e.g., LV ejection fraction (EF), volumes, and mass can then be performed (Table 4).

Table 4
M-Mode Parameters Used to Assess Left Ventricular Systolic Function

LVID (LVIDs < 3.7 cm; LVIDd < 5.6 cm are normal)
Left ventricular WT Percent change in WT = (WTs – WTd/WTs)
Left ventricular volume Prolate ellipse calculation: volume= $\pi/3$ $(LVIDd)^3$ Teichholz formula: volume = [7/(2.4 + LVIDd)] $(LVIDd)^3$
Ejection fraction (EDV – ESV)/EDV
Fractional shortening (FS) (%) = (LVIDd – LVIDs)/LVIDd
Mitral valve E point—septal separation (normal > 7 mm)
Left ventricular mass $(Mass_{LV}) = 0.8 \times [1.04\ (IVS + PWT + LVIDd)^3 - LVIDd^3] + 0.6$ g

LVIDs, left ventricular internal diameter at end systole; LVIDd, left ventricular internal diameter at end diastole; WT, wall thickness; WTs, wall thickness at end systole; WTd, wall thickness at end diastole; EDV, end diastolic volume; ESV, end systolic volume; IVS, septal wall thickness, PWT, posterior wall thickness.

LIMITATIONS OF M-MODE MEASUREMENTS

A common pitfall of M-mode measurements is the nonperpendicular alignment of the M-mode line in relation to the long axis of the LV. This leads to overestimation of ventricular dimensions. Two-dimensional (2D)-guided M-mode measurements can aid proper alignment thereby minimizing error.

Another challenge is to accurately identify the endocardial and epicardial borders and avoid confusion with contiguous structures, e.g., chordae, trabeculations near the posterior wall, and false-tendons. The endocardial border is distinguished from ventricular trabeculations and chordae by its appearance as a continuous line of reflection throughout the cardiac cycle. The latter structures appear intermittently. The epicardium lies just anterior to the highly echo-reflective parietal pericardium (*see* Chapter 3, Figs. 13 and 14).

A major drawback of M-mode measurements is that these are valid only when LV geometry is normal. When LV geometry is abnormal, as in aneurysmal remodeling or in the presence of regional wall motion abnormality following myocardial infarction, M-mode measurements of heart size may be misleading. An exponential relationship exists between ventricular diameters and ventricular volumes. M-mode parameters, and indeed all other parameters of LV systolic function, are dependent on ventricular loading conditions.

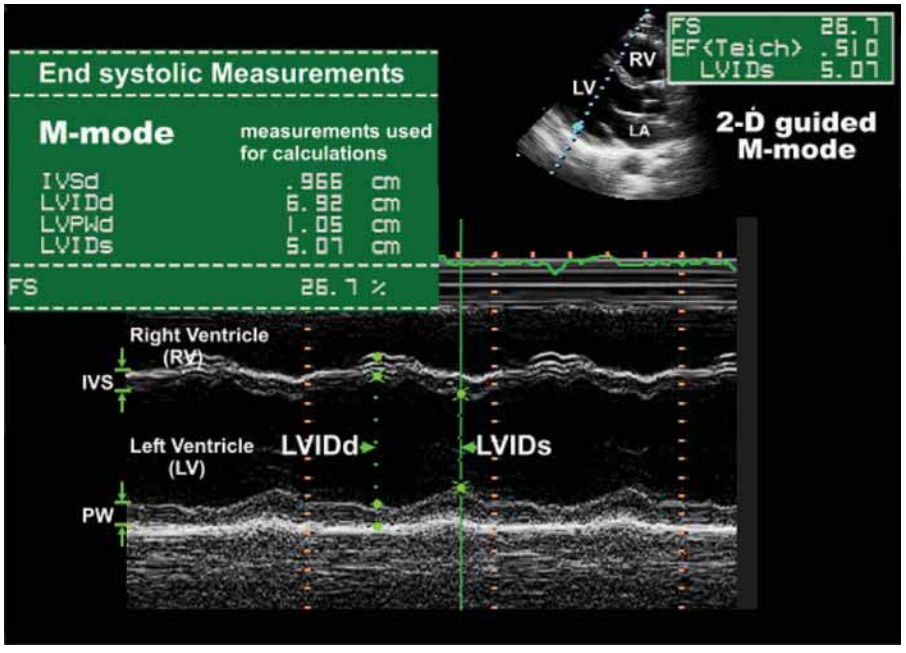

Fig. 3. Two-dimensional-guided M-mode measurements and derived indices. M-mode is simple, reproducible, and accurate when ventricular geometry is normal. It provides good endocardial resolution. The ejection fraction (EF, Teich) is an automated calculation based on the Teichholz method (*see* Table 4).

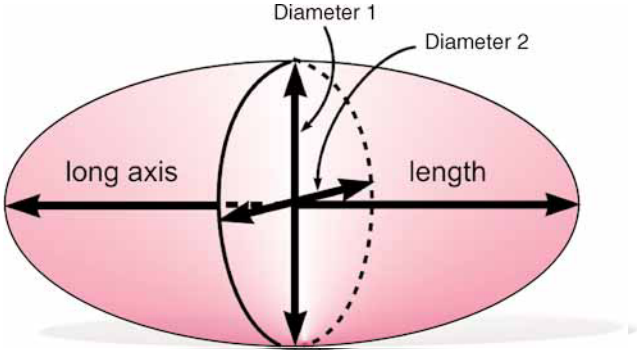

Fig. 4. Prolate ellipsoid. One geometric model used to calculate left ventricular volumes from on M-mode measurements assumes an elliposoid shape for the left ventricle. This model uses diameters (D) and length to calculate areas and volumes. A hemi-ellipsoid model is preferred in left ventricular volumetric and mass quantification using two-dimensional echocardiography (Figs. 13 and 15).

LV VOLUMES AND EF BY M-MODE

Estimates of LV volumes and EF by M-mode rely on geometrical assumptions of LV morphology. The simplest formula cubes the LVIDd. Another calculates volume using the formula for a prolate ellipsoid (Fig. 4). These measures become even more inaccurate when applied to dilated ventricles. The Teichholz method (Table 4) is commonly used to calculate ventricular volumes from M-mode measurements (from which EF can be calculated). However, this method is only recommended when ventricular geometry is relatively normal (*see* Chapter 3, Fig. 14D). Specifically, in patients with myocardial infarction involving the apex, M-mode measurements, which are obtained at the base of the heart, will underestimate ventricular size and overestimate ventricular function.

LV PARAMETERS BY 2D ECHOCARDIOGRAPHY

2D echocardiography is the primary modality used for qualitative and quantitative assessment of ventricular systolic performance (Table 5). In postmyocardial infarction and heart failure patients, 2D echo has great utility in their management and risk stratification. An inverse relationship exists between cardiovascular morbidity, mortality, and LV systolic function—specifically LVEF. EF, however, is not the only predictor of survival in patients with advanced heart failure.

LIMITATIONS OF 2D ASSESSMENT OF LV SYSTOLIC FUNCTION

2D echocardiography is not a true tomographic technique (like cardiac computed tomography or cardiac magnetic resonance imaging). Off-axis measurements,

Table 5
Two-Dimensional Parameters in Left Ventricular Function

Qualitative/semi-quantitative parameters	*Quantitative parameters*
• Global function: ventricular wall motion and thickening	Left ventricular wall dimensions: Wall thickness Internal diameters: LVIDd, LVIDs
• RWM assessment	MWFS: from linear measures of diastolic and systolic cavity sizes and wall thickenesses:
• Visual estimation of ejection fraction	Inner shell = ([LVIDd + SWTd/2 + PWTd/2]^3 – LVIDd^3 + LVIDs^3) $^{1/3}$ – LVIDs $\text{MWFS} = \frac{([\text{LVIDd} + \text{SWTd}/2 + \text{PWTd}/2] - [\text{LVIDs} + \text{inner shell}])}{(\text{LVIDd} + \text{SWTd}/2 + \text{PWTD}/2) \times 100\%}$
• Longitudinal ventricular shortening	Left ventricular quantification Biplane method of discs (modified Simpson's rule) Multiple diameter method Others based on assumptions for left ventricular geometry, e.g., cylinder-hemiellipse, biplane ellipsoid, hemisphere-cylinder, bullet, models
• Mitral annular motion	Left ventricular ejection fraction (%) = [(EDV – ESV)/EDV] × 100% Left ventricular mass (Mass_{LV}) = 0.8 × [1.04 (LVIDd + PWTd + SWTd)^3 – (LVIDd)^3] + 0.6 g Left ventricular wall stress (σ) Meridional wall stress Circumferential

Table modified from Recommendations for Chamber Quantification. American Society of Echocardiography, 2005.
RWM, regional wall motion; LVIDd, left ventricular internal diameter at end diastole; LVIDs, left ventricular internal diameter at end systole; MWFS, mid-wall fractional shortening; SWTd, septal wall thickness; PWTd, posterior wall thickness; EDV, end diastolic volume; ESV, end systolic volume; FS, fractional shortening.

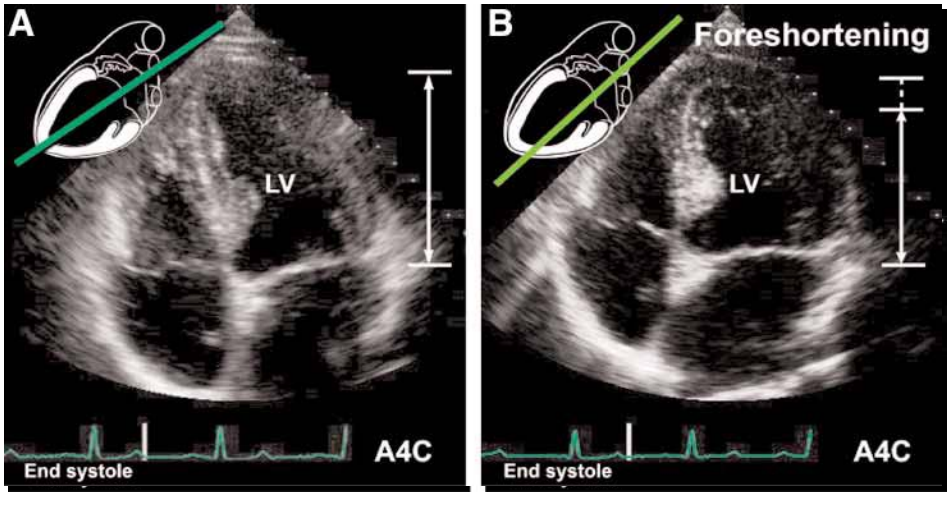

Fig. 5. Left ventricular foreshortening. Foreshortening (shown right) occurs when the imaging plane does not transect the center of left ventricular apex (left). It is a common source of error in left ventricular quantification in two-dimensional echocardiography. (Please *see* companion DVD for corresponding video.)

e.g., foreshortening, easily occur (Fig. 5; please *see* companion DVD for corresponding video). Distortions of LV geometry seen in patients with ischemic heart disease pose challenges to 2D assessment (Figs. 1A,B and 6).

QUALITATIVE AND SEMI-QUANTITATIVE MEASURES OF LV SYSTOLIC FUNCTION

Making linear measurements of cardiac chamber dimensions by 2D echo follows the principles outlined

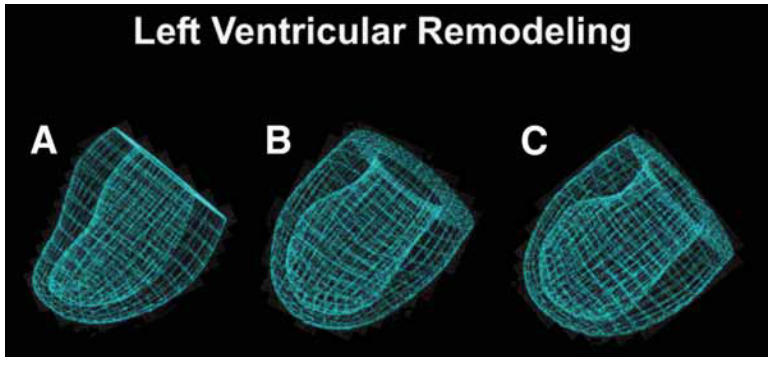

Fig. 6. Three-dimensional (3D) images showing gross distortion of left ventricular geometry post-myocardial infarction. 3D representation of progressive remodeling of the left ventricle in a patient with a large anterior-apical myocardial infarction. Note the progressive distortion of the ventricular geometry with time **(A–C)**.

using M-mode described earlier (*see also* Chapter 3, Fig. 16). "Eyeball" estimates of LVEF are routinely used in clinical practice, but interobserver variability is high, and should be "calibrated" by quantitative measurements.

Accurate assessment of ventricular wall movements during the cardiac cycle is dependent on image quality. Optimal image acquisition is influenced by patient characteristics, operator skill, and instrument settings. Proper patient positioning helps to optimize imaging of parasternal and apical views (Chapter 3, Fig. 9). Images are best acquired at end-expiration or during quiet respiration.

Failure to accurately visualize the endocardial border introduces uncertainty into 2D measurements. To minimize this, techniques to improve endocardial border definition, e.g., harmonic imaging, B-color imaging, LV opacification with contrast agents, and Doppler based techniques are often employed (Figs. 7 A,B and 8; please *see* companion DVD for corresponding video).

QUALITATIVE GRADES OF LV SYSTOLIC FUNCTION

Normal ventricular walls thicken during systole—a manifestation of myocardial fiber shortening—as both ventricles contract. Ventricular systolic contraction is accompanied by a reduction in ventricular cavity size and can be qualitatively assessed as normal, reduced, or hyperdynamic (Fig. 9). Normally, 60–70% of ventricular end-diastolic volume is ejected during each cardiac cycle.

Reduction of LV systolic function can be estimated to the nearest 5 or 10% by an experienced observer. EF of 55% or more is generally considered normal. EF between 40 and 55% is considered mildly reduced; EF between 30 and 40% is considered moderately reduced; EF less than 30% is considered severely reduced. Global reduction of systolic function is frequently accompanied by regional variation.

When the EF exceeds 70%, it is considered to be "hyperdynamic." EFs exceeding 75% manifest as near obliteration of ventricular cavity when viewed from the parasternal or apical windows. This can be seen in hypovolemia or in patients with hypertrophic cardiomyopathy.

Estimations of EF by experienced sonographers correlates well with other quantitative measures of EF. It is, therefore, a practical first step in qualified hands.

GRADING REGIONAL WALL MOTION

Regional LV wall motion assessment generally employs the 16-segment model recommended by the ASE (1989), or the more recent 17-segment model (which adds an additional region for the apex). Ventricular segment scores are assigned based on two qualitative measures of ventricular wall behavior during systole: (1) wall movement (contraction) and (2) wall thickening. Graded scores of contractility of the individual segments range from a normal score of 1 to the worst score of 5 (Figs. 1B and 10A; please *see* companion DVD for corresponding video for Fig. 8). The myocardium of a dysfunctional segment thickens less, or becomes thinner, during systole.

A segment that shows noticeable reduction in contractility is *hypokinetic* and assigned a score of 2. A segment that barely moves or thickens during systole is *akinetic* (score = 3). *Dyskinetic* myocardium moves paradoxically during systole (score = 4). *Aneurysmal* myocardium remains deformed during diastole. The integrated wall motion score is the sum of the scores divided by the number of scored segments. A wall score index of 1 indicates normality. Larger scores reflect more severe degrees of systolic dysfunction (Fig. 1B; please *see* companion DVD for corresponding video).

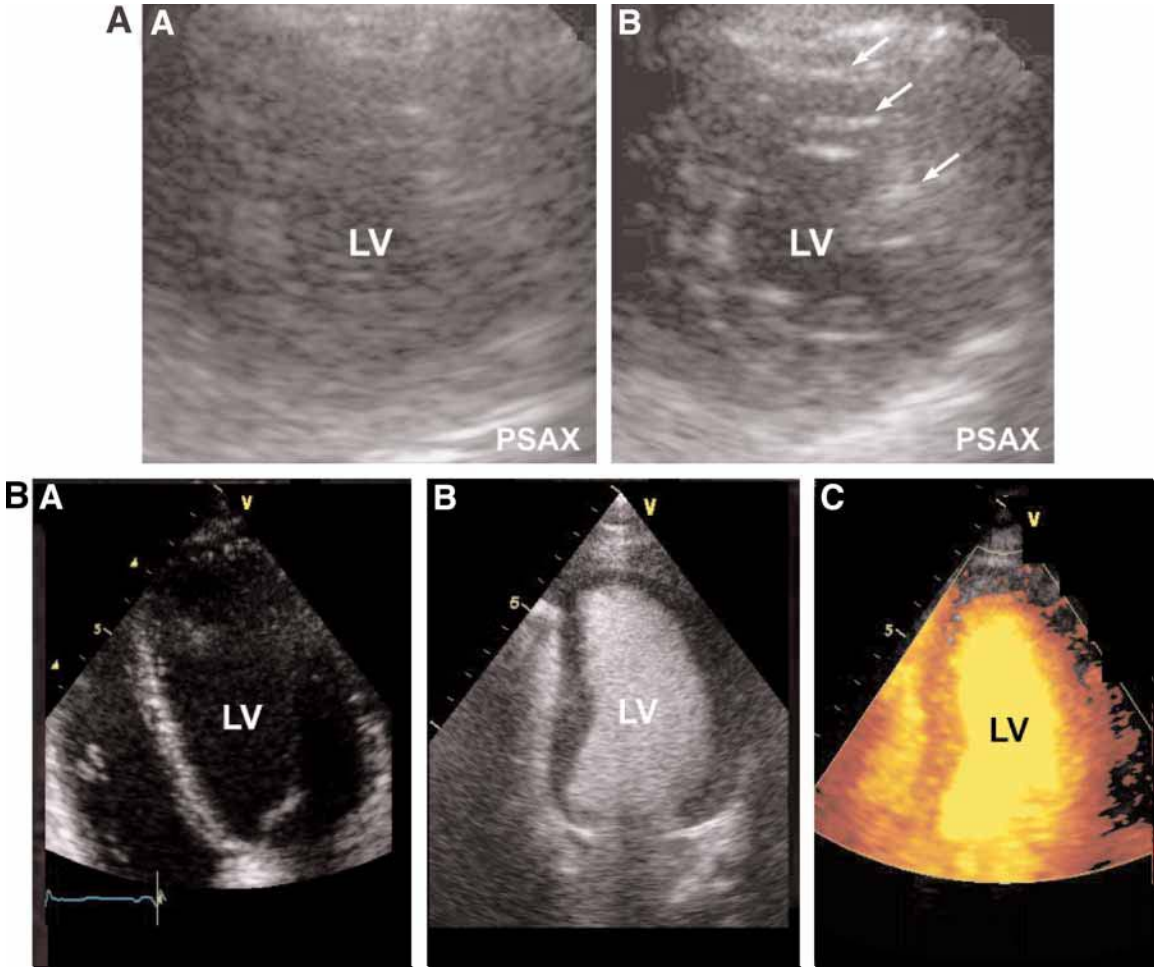

Fig. 7. (**A**) Tissue harmonic imaging. Even with suboptimal imaging (**left panel**, parasternal short axis view of the left ventricle) tissue harmonic imaging markedly improves endocardial definition. Note reverberation artefacts (arrows) arising from ribs. (**B**) Left ventricular opacification/endocardial border definition. Contrasts methods assist in delineating the endocardial border. Left ventricular opacification using microspheres (e.g., Optison® or Definity®) are popular (compare **left** and **middle panels**). Another myocardial contrast imaging technique is shown in **right panel**. (Please *see* companion DVD for corresponding video.)

In an effort to standardize nomenclature of myocardial segments across other cardiac imaging specialties, the American Heart Association (2002) issued a unifying 17-segment model (Fig. 10B). Using this model, LV segments 1–6 are at the base (mitral valve level), segments 7–12 are in the middle (papillary muscle level), segments 13–16 occupy the apical region, and segment 17 represents the very tip of the apex. The latter does not encroach into the ventricular cavity. The segmental numerical model can be matched to the more practical anatomical descriptive terminology as shown in Fig.10B.

The segmental numerical model nomenclature also corresponds well with coronary artery distribution (*see* Chapter 3, Fig. 58; Chapter 7, Figs. 3–6). From this, various indices of coronary artery territory involvement, e.g., left anterior descending artery, may be derived.

LIMITATIONS OF REGIONAL WALL MOTION ASSESSMENT

Regional wall motion assessment is heavily influenced by image quality. Endocardial border definition deteriorates when still frames are acquired from digital video files. The audio/video interleaved (AVI) and the digital imaging and communications in medicine (DICOM) video format are the two most popular. Digital videos consist of multiple still frames in rapid succession, usually in the order of 30–60 frames per second. When the video is stopped, and a single still frame is selected, image quality characteristically degrades, including endocardial border definition.

Angulation of the transducer during acquisition of short-axis views may misrepresent true segmental

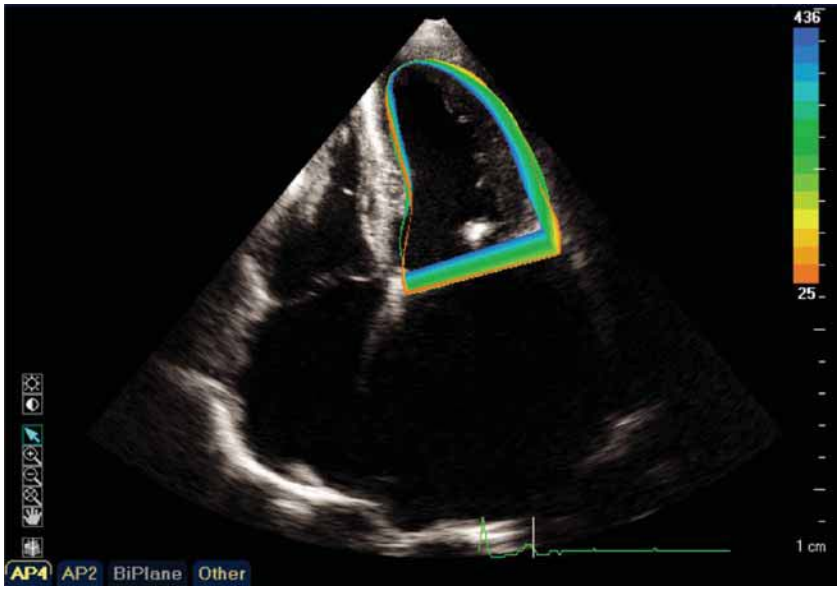

Fig. 8. Dynamic endocardial border analysis. Dynamic left ventricular endocardial border analysis is shown in this patient with mitral stenosis (and a severely dilated left atrium). (Please *see* companion DVD for corresponding video.)

anatomy and is avoided by using the recommended technique (Fig. 11). Translational and rotational movements of the heart during the cardiac cycle cannot be avoided, but can be minimized by acquiring images during end-expiration. Care should be taken to avoid triggering the Valsalva maneuver.

Restricted septal movement can be mistaken for septal hypokinesis or akinesis. Apparent hypokinesis of the septum can be seen following any surgery that breaches the pericardium. Closer observation of the septum will often show normal systolic thickening in the absence of true ischemic injury.

Paradoxical septal motion in the presence of otherwise normal septal myocardium is seen in right ventricle (RV) pressure and volume overload states (Chapters 18 and 21), pericardial effusion and constrictive pericarditis (Chapter 10), or with certain arrhythmias, e.g., left bundle branch block.

QUANTITATIVE MEASURES OF LV SYSTOLIC FUNCTION

Comparisons of LV end-diastolic and end-systolic dimensions form the basis of quantitative estimates of LV function, e.g., fractional shortening and EF (Fig. 12, Table 6). Fractional shortening—the percentage change in the LV minor axis in a symmetrically contracting ventricle—can be derived using the formula:

$$\text{Fractional Shortening (FS)}(\%) = (\text{LVIDd} - \text{LVIDs})/\text{LVIDd} \times 100\%$$

$$\text{FS} = 25\% - 45\% \text{ (normal range)}$$

Volumetric estimates of LV volumes by 2D echocardiography are based on three geometric methods that combine measurements of LV dimensions and area to calculate volume (Table 6; Fig. 13A). These are:

1. Prolate ellipsoid method.
2. Hemi-ellipsoid (bullet) method.
3. Biplane method of discs (modified Simpson's rule).

The prolate ellipsoid method assumes a prolate ellipsoid systolic and diastolic LV geometry). Area-length or length-diameter methods can be used. The single-plane and biplane area-length methods are shown in Fig. 13B,C.

The combined geometric model—of a hemisphere and an ellipsoid (hemi-ellipsoid)—provides a better estimate of LV volume (Fig. 13D), but the biplane method of discs (modified Simpson's rule) is recommended by the ASE and the European Association of Echocardiography. This method does not assume a predetermined geometry of the LV, but instead defines the LV geometry following manual tracing of the acquired LV cavity borders. The LV volume is then quantified by assuming the LV cavity is a stack of elliptical discs whose volumes are quantified and summated (Fig. 14).

Two orthogonal views—apical four-chamber and apical two-chamber—and manual tracing of endocardial borders manually traced at end systole and end-diastole are needed. Automated software divides the LV into a stack of discs oriented perpendicular to the long axis of the ventricle, and summates their individual volumes (Fig. 14).

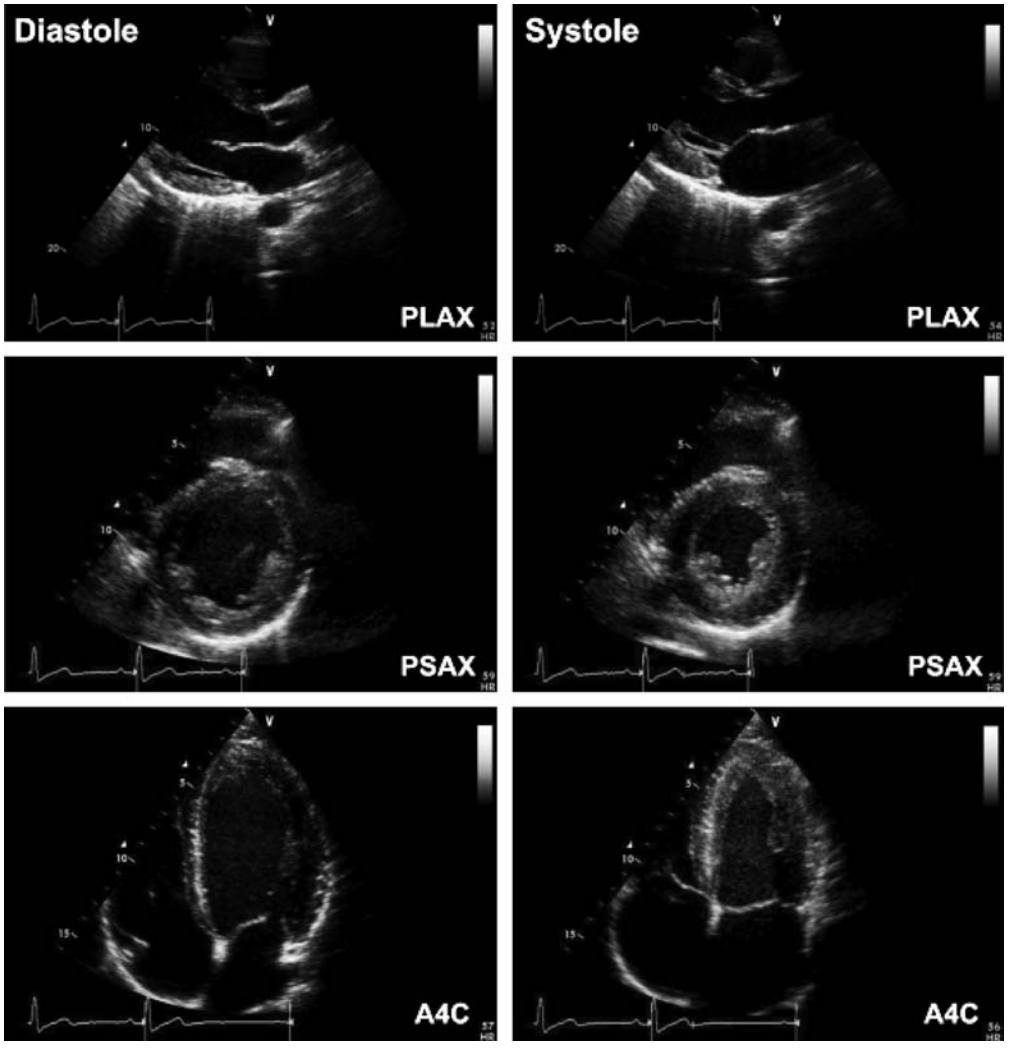

Fig. 9. Normal systolic function. Knowledge of normal left ventricle systolic function is essential for interpreting abnormalities.

From the end-diastolic frame, the end-diastolic volume is calculated. From the end-systolic frame, the end-systolic volume is calculated. The stroke volume (SV) is then:

$$SV = EDV - ESV \text{ (mL)}$$

The EF is therefore:

$$EF = \frac{EDV - ESV}{EDV} \times 100\%$$

Cardiac output (CO) is product of the EF and the heart rate (HR):

$$CO = EF \times HR$$

The advantage of the modified Simpson's method over other volumetric methods listed in Table 5 is that it makes no assumptions about ventricular geometry. Nevertheless, considerable sonographer experience is required as images must be optimized and endocardial borders accurately identified and traced according to convention. Poor endocardial border definition, foreshortened views, and improper technique can compromise this technique.

LVEF shows high correlation, but less striking agreement, with radionuclide ventriculography and contrast cine-angiography. Even quantitative measures of LVEF can be inaccurate owing to limitations inherent in quantification formulae, as well as those of cardiac ultrasonography itself. Interobserver-variability remains a vexing issue in 2D echocardiography.

LIMITATIONS OF VOLUMETRIC MEASURES (EF) OF LV SYSTOLIC FUNCTION

Overwhelming evidence from landmark clinical trials in heart failure and postmyocardial patients have demonstrated the proven value of LVEF assessment on patient management and prognosis. Nevertheless,

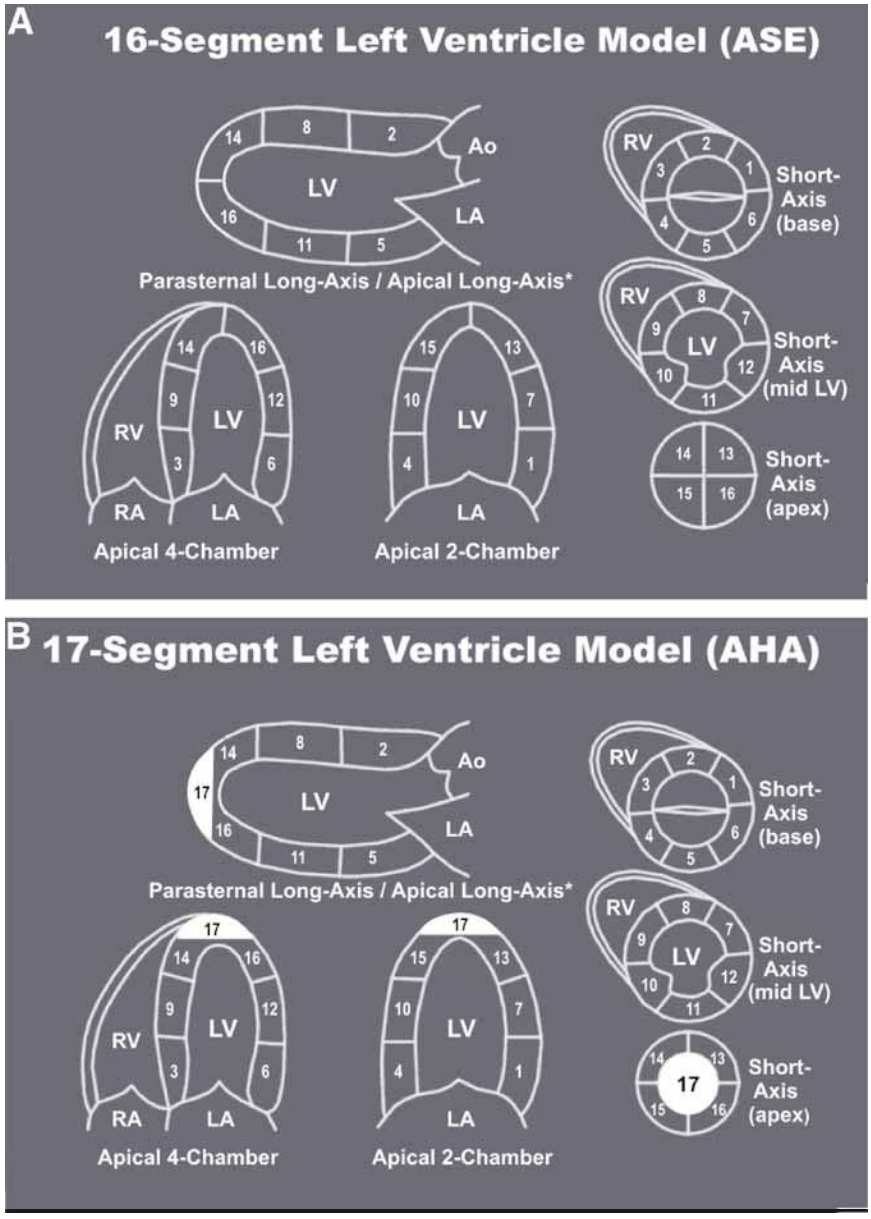

Fig. 10. The American Society of Echocardiography (ASE) issued a 16-segment left ventricle model for wall motion assessment. The American Heart Association's (AHA) 17-segment model has an additional apical segment "cap" added to harmonize left ventricular segment nomenclature with nuclear cardiology and cardiac magnetic resonance imaging. **(A)** A 16-segment model of left ventricular segments (ASE). **(B)** A 17-segment model of left ventricular segments (AHA).

LVEF is not the sole or a complete measure of LV function. Diastolic and other measures of ventricular function are needed because nearly 40% of patients with clinical heart failure have persevered systolic function (normal LVEF). Furthermore, systolic function can be abnormal even in the presence of normal LVEF.

Quantification of LV volumes by 2D echocardiography faces significant technical and clinical limitations. As 2D echocardiography is not a true tomographic technique, LV foreshortening and off-axis views remain a challenge. The LVEF may be normal in patients with acute myocardial infarction, as hypokinesis or akinesis in the affected myocardial territory may be compensated by hyperkinesis in the unaffected segments. The same LVEF in a patient with mitral regurgitation has a different clinical and prognostic implication than in a patient with aortic stenosis.

Therefore, the tendency by many clinicians to request an echocardiographic study for "LVEF only" or

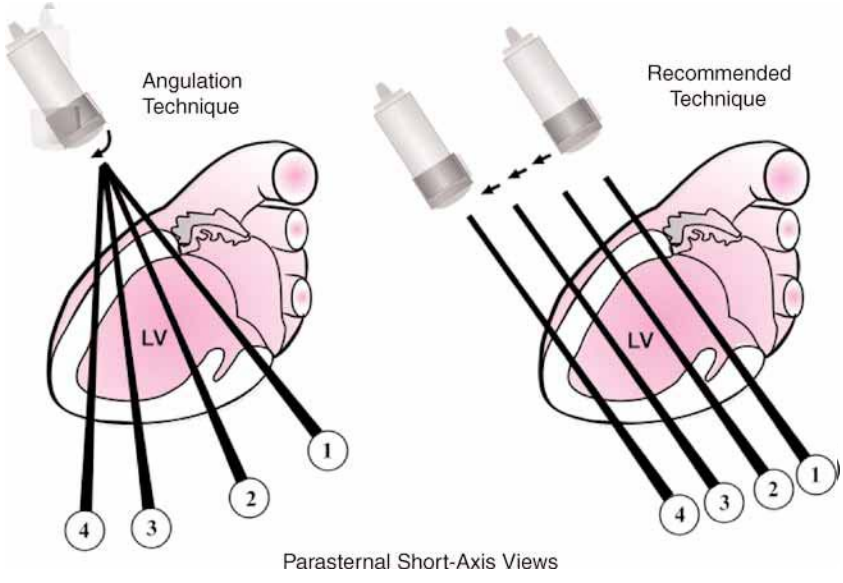

Fig. 11. Angulated vs orthogonal parasternal short-axis imaging of the left ventricle (LV). The angulation technique (left) may acquire short-axis views of the LV segments tangentially, thereby influencing the accuracy of regional wall motion assessment. Images are best acquired at planes orthogonal to the long axis of the left ventricle as shown (right).

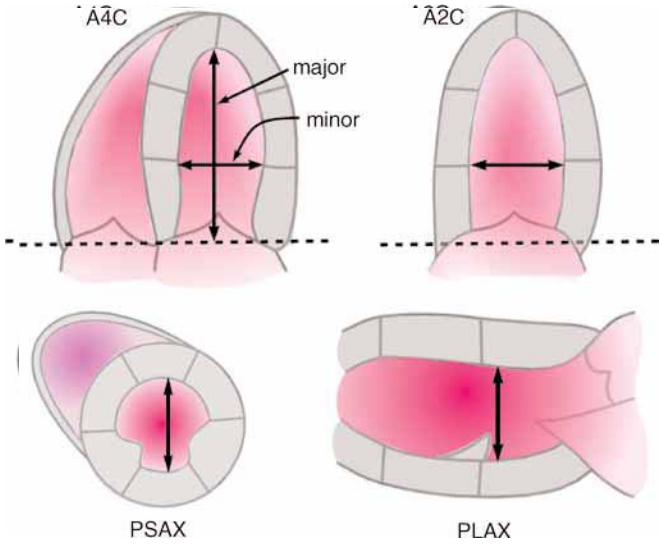

Fig. 12. Left ventricular cavity dimensions.

to equate the LVEF as "the sole measure" of LV function should tempered with other parameters of function.

LV MASS

A clear relationship exists between LV mass and outcomes in cardiovascular disease, especially in hypertension. LV mass is calculated using the formula listed in Table 5 and is based on an area-length method or that for a cylinder hemi-ellipsoid model (Fig. 13). Such measurements of LV mass, whether by M-mode or 2D, essentially subtract ventricular cavity volume from the total ventricular volume to obtain the "shell" or myocardial volume (Fig. 15). This value

Table 6
Cardiac Measurements by Two-Dimensional Echocardiography

Window	*Normal range (cm) (mean – SD)*	*Index adjusted for BSA (cm/m²)*
PLAX	PLAX	PLAX
LVIDd	3.5 – 6.0	2.3 – 3.1
LVIDs	2.1 – 4.0	1.4 – 2.1
Fractional shortening	25 – 46	—
PSAX (papillary muscle level)	PSAX (papillary muscle level)	PSAX (papillary muscle level)
LVIDd	3.5 – 5.8	2.2 – 3.1
LVIDs	2.2 – 4.0	1.4 – 2.2
Fractional shortening	25 – 43	
A4C	A4C	A4C
LVIDd major	6.9 – 10.3	4.1 – 5.7
LVIDd minor	3.3 – 6.1	2.2 – 3.1
LVIDs minor	1.9 – 3.7	1.3 – 2.0
Fractional shortening	27 – 50	

BSA, body suface area; PLAX, parasternal long-axis ; LVIDd, left ventricular internal diameter at end diastole; LVIDs, left ventricular internal diameter at end systole; PSAX, parasternal short-axis; A4C, apical four chamber.

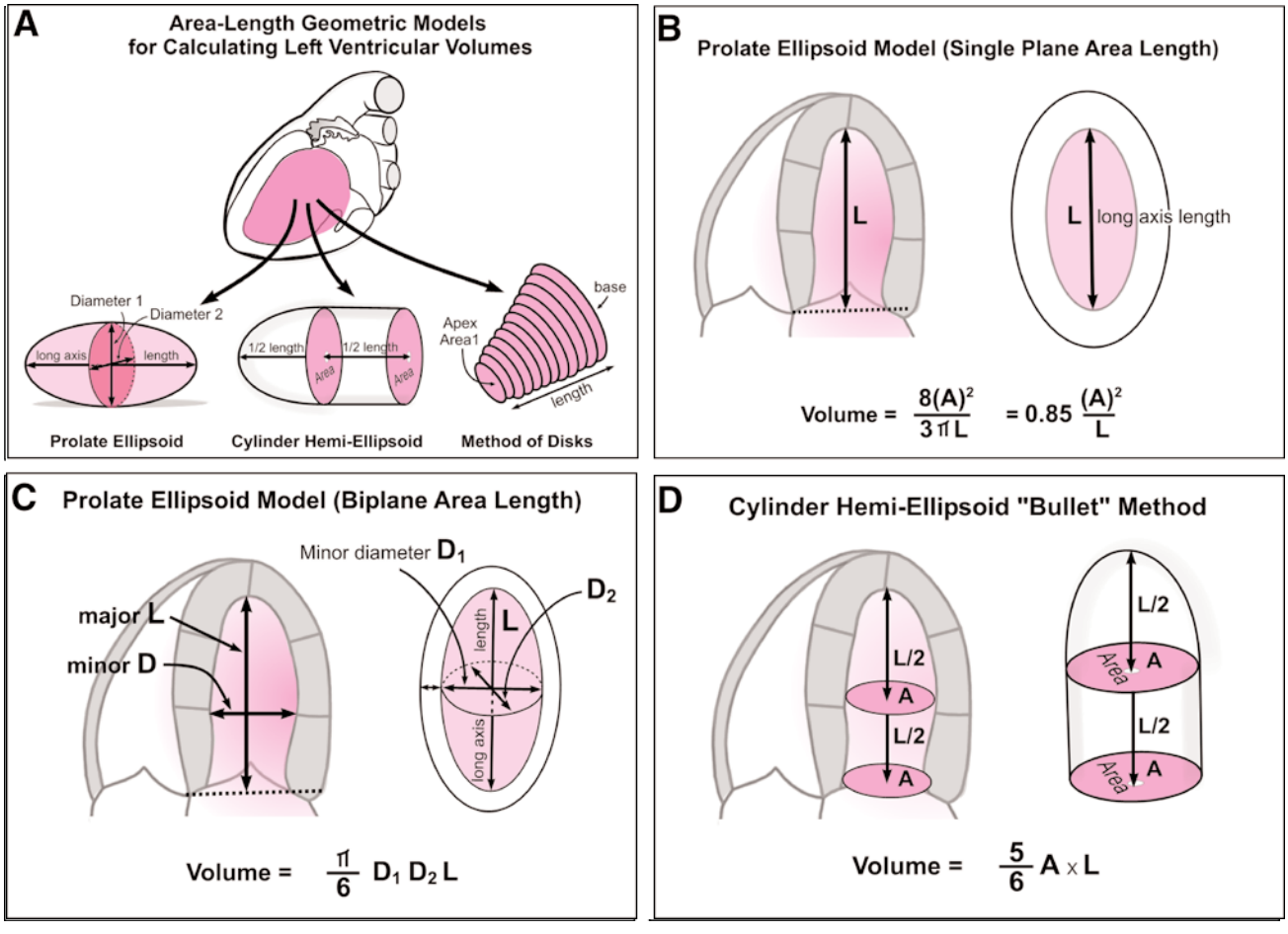

Fig. 13. Geometric models to estimate left ventricle (LV) volumes by two-dimensional echocardiography use short-axis area multiplied by long-axis length. Comparison of volumes at end-systole and end-diastole can be a measure of LV systolic function.

multiplied by the density of the myocardium gives the LV mass.

$$\text{Left ventricular mass } (\text{Mass}_{LV}) = 0.8 \times [1.04\ (\text{IVS} + \text{PWT} + \text{LVIDd})^3 - \text{LVIDd}^3] + 0.6 \text{ g}$$

Accurate measures are crucial, as errors will be cubed.

3D Echocardiography

3D echocardiography will likely replace current echocardiographic methods of calculating ventricular mass and volumes in the near future (Figs. 16A–D; please *see* companion DVD for corresponding video). The limitations and assumptions of 2D and M-mode echocardiography are overcome by both real-time and off-line reconstructive 3D echocardiography. Modern 3D equipment uses planar array transducer technology to obtain a pyramidal "volume" of data. This makes 3D echocardiography less dependent on the sonographer imaging the correct plane.

ASSESSMENT OF MYOCARDIAL VIABILITY

Dobutamine echocardiography can provide additional information on the LV contractile reserve. This has value in predicting recovery of function following coronary revascularization procedures. Assessment of myocardial viability is also important in heart failure patients.

The important clinical question that frequently confronts the cardiology team is whether coronary revascularization procedures will benefit a particular patient with LV dysfunction. To answer this, we need to help predict the probability of improvement following the proposed revascularization procedure. Nuclear techniques assess myocardial perfusion, but not contractile reserve. A biphasic response on dobutamine stress echocardiography, however, can be a good predictor of improvement in patients scheduled to undergo coronary revascularization procedures (Fig. 17; *see* companion DVD for corresponding video; *see also* Chapter 8).

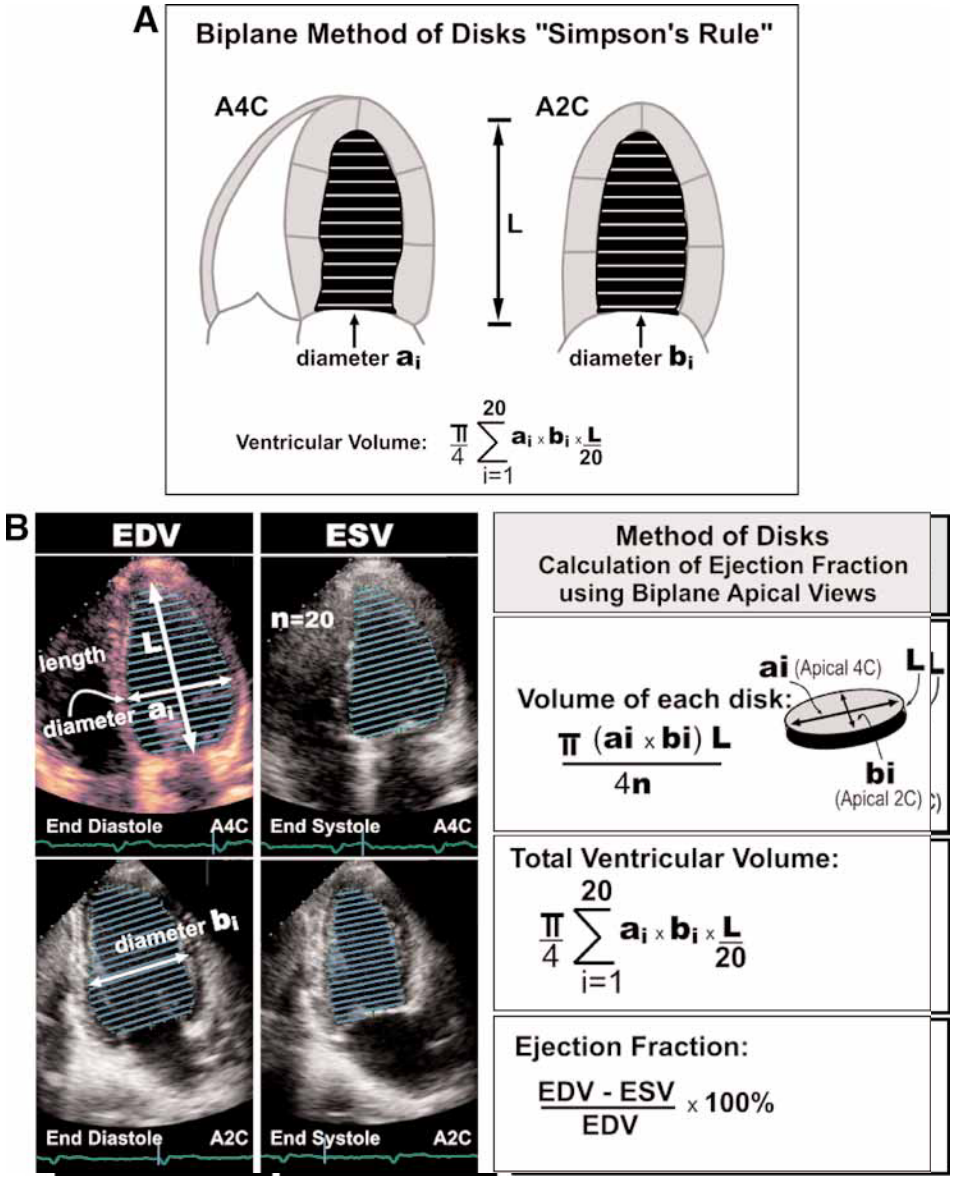

Fig. 14. (A,B) Modified Simpson's method. The American Society of Echocardiography recommends the modified Simpson's method (biplane method of discs) for calculating left ventricular volumes and ejection fraction. Manual tracing of ventricular endocardium at end-systole and end-diastole from two orthogonal planes, and summation of the volumes of discs derived, serve as the basis of this calculation.

DOPPLER ASSESSMENT OF VENTRICULAR SYSTOLIC FUNCTION

Doppler assessment provides complementary and alternative indices of ventricular systolic function (Table 7). Traditional Doppler indices are used to calculate SV and CO. SV is calculated from the equation: *volume = area × velocity time integral*; where *area* is the cross-sectional area of ventricular outflow or inflow tract of interest; *velocity time integral* corresponds to the velocity time integral across the same. CO is then calculated according to the equation:

$$CO = SV \times HR$$

Cardiac index calculated by dividing CO by body surface area.

Doppler indices have the advantage in being independent of geometric assumptions used in M-mode and 2D-based calculation of volumes. The most accurate and reproducible Doppler method for calculating SVs uses the left LV outflow tract (LVOT) diameter and the velocity

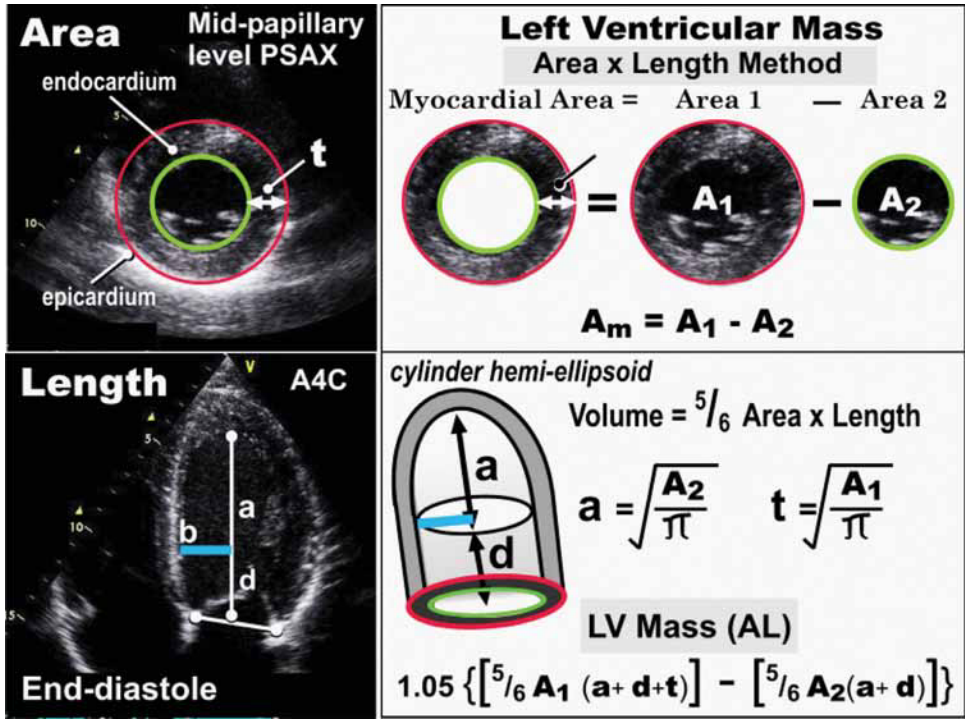

Fig. 15. Left ventricular mass. The area-length method for using a cylinder hemi-ellipsoid of the left ventricle (LV) is the recommended equation for measuring LV mass. It is a simple formula with easily obtainable measurements. End-diastolic measurements using parasternal short-axis (PSAX) and apical four-chamber at the mid- or high-papillary muscle levels are made and inserted into the equation as shown. The sum of a + d is the end-diastolic LV cavity length; b = minor axis radius; t = wall thickness; A_1= total planimetered PSAX area at the mid- or high-papillary muscle level; A_2 = LV cavity planimetered PSAX area.

time integral across the LVOT by pulsed Doppler examination (Fig.18A; *see also* "Continuity Equation" in Chapter 11) LVOT geometry most closely approximates a circle compared with the ellipsoid mitral annulus (Fig. 18B), and is logistically easier to measure than the pulmonary artery diameter (Figs. 18C). Tricuspid annular geometry is complex, and is almost never used to calculate SVs.

Continuous-wave Doppler of the mitral regurgitant jet can reveal clues about LV performance by assessing changes in LV pressure over time (dP/dT). The pressure is measured at two points (at ~1 m/s and 3 m/s after the onset of the mitral regurgitation) and the Bernoulli equation ($dP = 4v^2$) applied. Normal dP/dT is greater than 1200 mmHg/s.

OTHER DOPPLER MEASURES OF VENTRICULAR SYSTOLIC FUNCTION

Tissue Doppler imaging is a useful tool in ventricular diastolic function assessment, but also shows promise in assessing systolic function (Fig. 19). Doppler interrogation of the mitral annulus can provide a measurable index of annular movement and velocity, and the information derived can be extrapolated to assess ventricular function. A good relationship exists between tissue Doppler assessment of myocardial contraction velocity and LVEF.

Tissue velocity imaging employs color codes to reflect ventricular longitudinal shortening using the scheme: red—for movement toward the transducer, and blue—movement away from transducer (Fig. 20; please *see* companion DVD for corresponding video). It is based on the rationale that most of the cardiac muscle fibers are oriented longitudinally. A direct relationship exists between pulsed-wave tissue velocity imaging and ventricular systolic function.

EF is not a load-independent measure of contractility. Load is important when considering contractility and this is not normally accounted for in traditional measures. Newer less load-dependent methods, e.g., Doppler strain imaging, are being investigated. Strain—a dimensionless quantity, measures deformation produced by the application of stress. It represents the percentage change in myocardial fiber length from its original or unstressed dimension (Fig. 21A–C). Comparisons of Doppler velocities at interrogation points along the myocardium are used to measure LV strain.

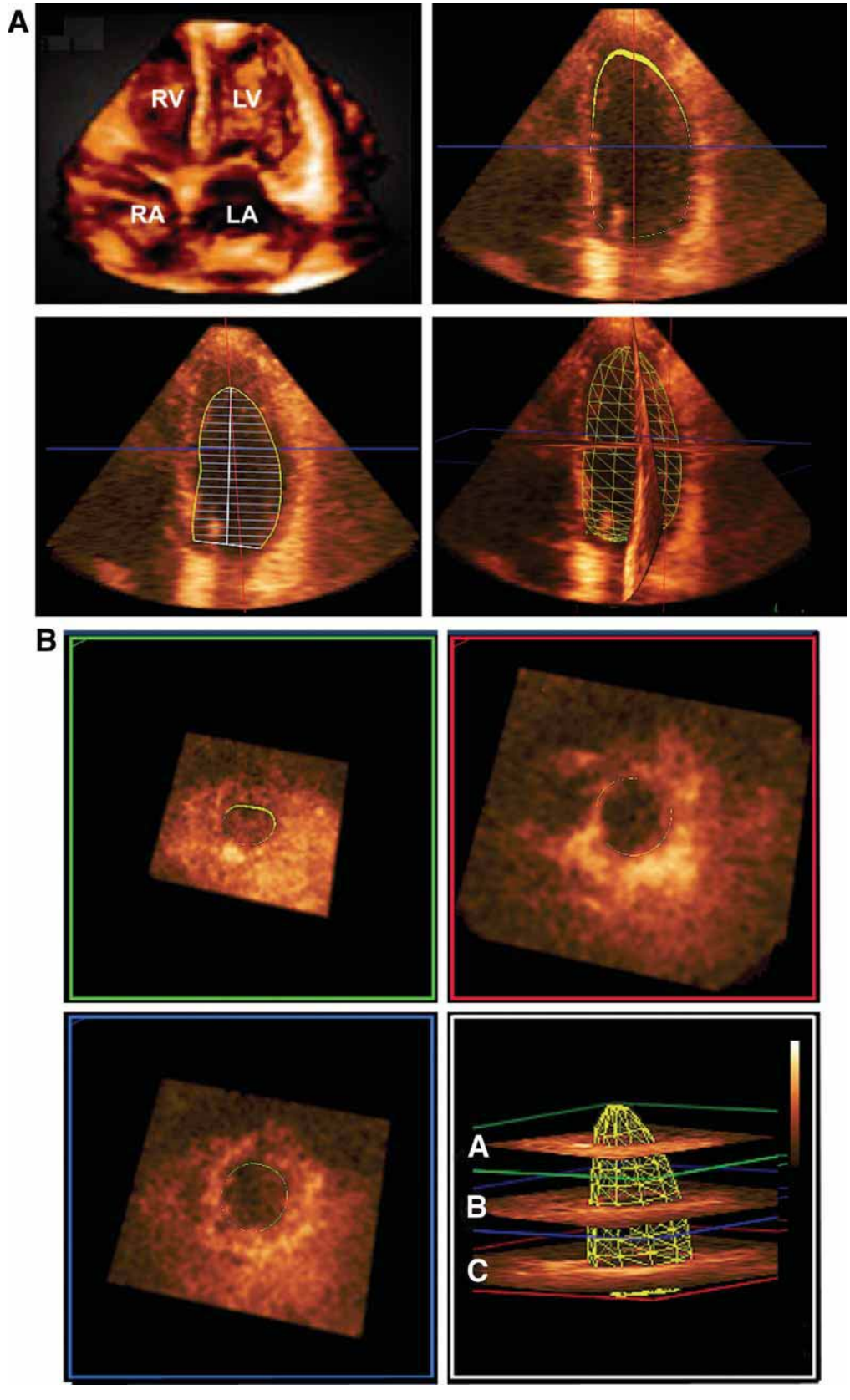

Fig. 16. *(Continued)*

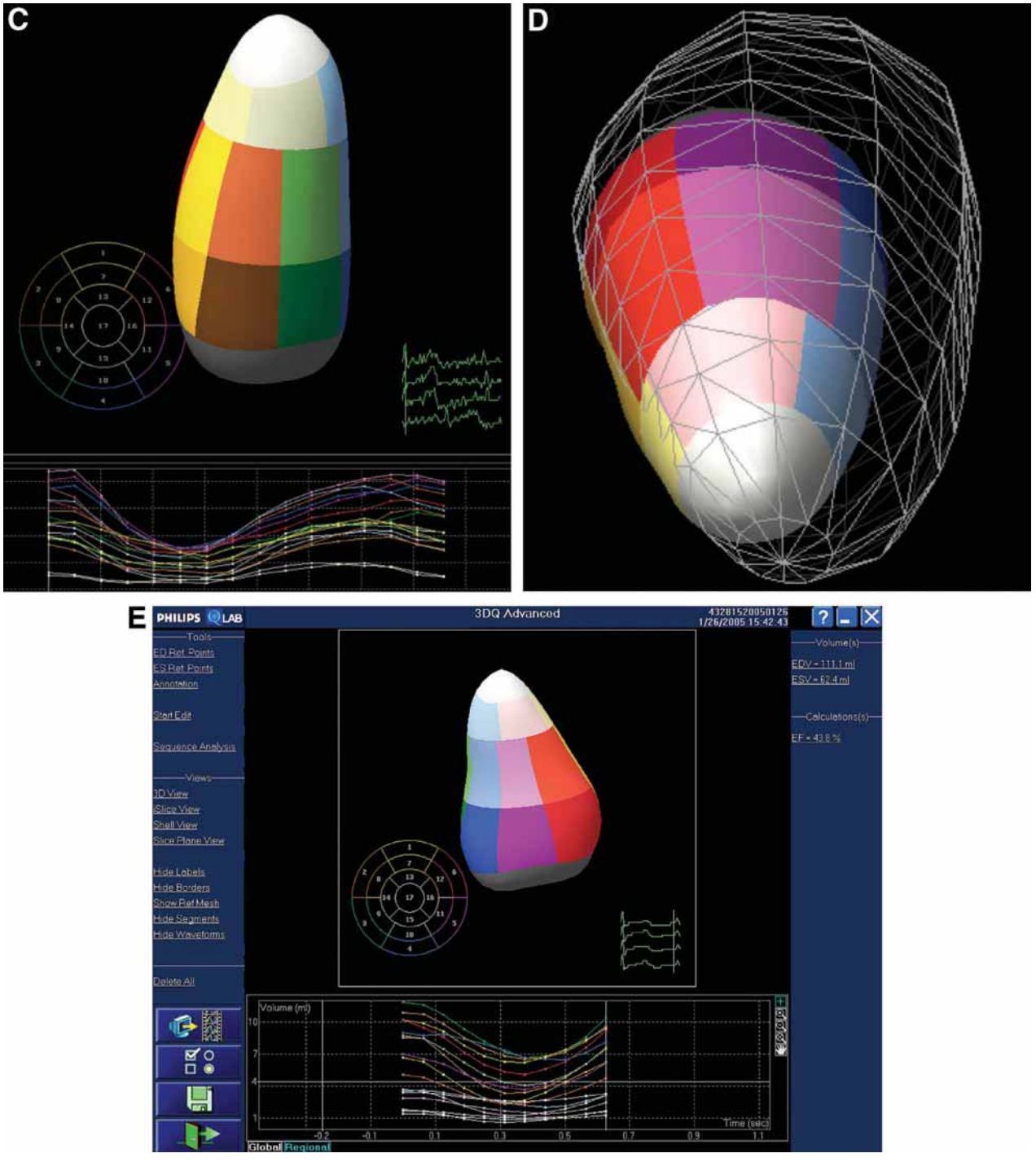

Fig. 16. Left ventricle (LV) quantification by three-dimensional (3D) echo. **(A)** Apical full-volume cropped 3D image. **(B)** Semi-automatic border detection with multiplanar reconstruction (MPR) in 3D echocardiography. **(C)** A 17-segment 3D volumetric data for left ventricular segmental analysis. 3D echocardiography overcomes several limitations of 2D echocardiography in quantification of systolic function including: endocardial border definition, foreshortening, off-axis views, and translational motion. It is slated to supercede 2D echocardiography in the assessment of LV function, mass, and volumetric assessments. 3D echo is especially valuable in right ventricular assessment and quantification, with utility comparable to that of cardiac magnetic resonance imaging. **(D)** LV systolic frame with diastolic reference mesh. **(E)** Systolic frame in patient with cardiomyopathy and asynchrony. (Please *see* companion DVD for corresponding video.)

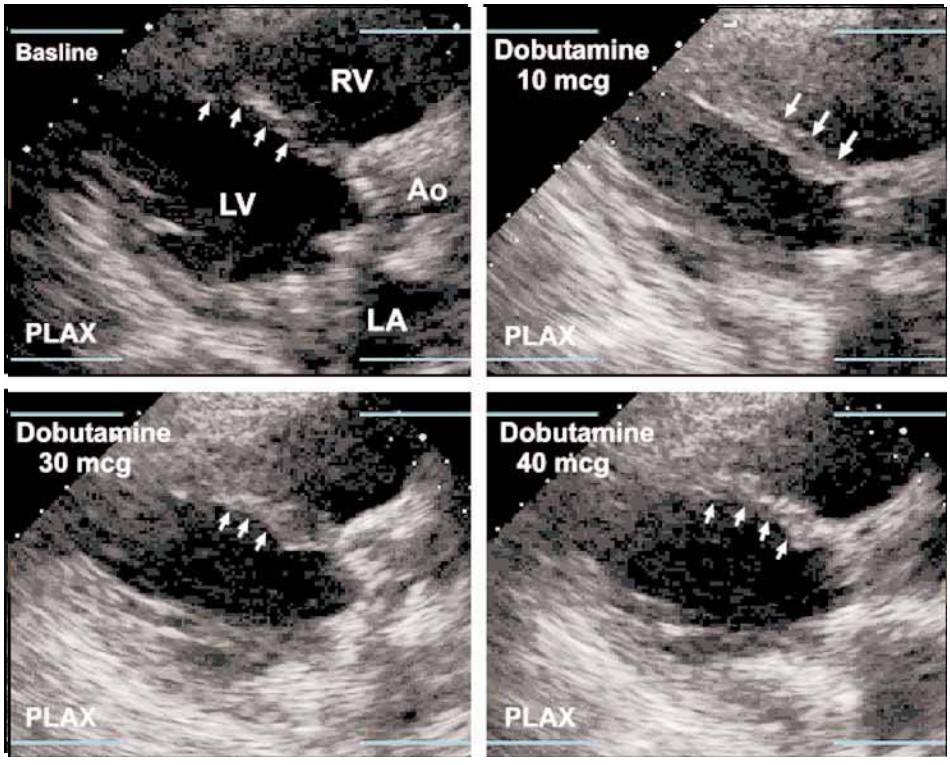

Fig. 17. Dobutamine stress echocardiogram: biphasic response. A biphasic response on dobutamine stress echocardiography may be a candidate for coronary artery revascularization procedures. This patient shows augmentation of a previously poorly functioning region on low dose dobutamine (10 μg), but demonstrates ischemia (decreased contractility) at higher doses. At baseline, this region of the heart (arrows) are hypokinetic—contractility improves at the 5 μg infusion rate, is maintained at 10 μg, worsens at 40 μg. This represents an ischemic region that augmented at low doses that can benefit from revascularization. (Please *see* companion DVD for corresponding video.)

Table 7
Doppler Indices of Left Ventricular Systolic Function

Traditional Doppler indices	*Newer Doppler indices*
$SV = VTI \times CSA = VTI \times \pi r^2$ $= VTI \times \pi D^2/4 = 0.785\ D^2 \times VTI$	TDI/DTI
Measurement sites: LVOT Left ventricular inflow (mitral valve) Pulmonary artery	
$CO = SV \times HR$ CI = CO/body surface area	TVI for left ventricular dyssynchrony
CW Doppler in mitral regurgitation: dP/dt = 32/time (mmHg/s)	Doppler strain imaging: strain and strain rate
Velocity/acceleration times, e.g., aortic flow/velocity acceleration, aortic ejection time	Left ventricular torsion by TDI

SV, stroke volume; VTI, velocity time integral; CSA, cross-sectional area; D, diameter; TDI, tissue Doppler imaging; DTI, Doppler tissue imaging; LVOT, left ventricular outflow; CO, cardiac output; HR, heart rate; CI, cardiac index; TVI, tissue velocity imaging; CW, continuous wave; dP/dT, rate of ventricular pressure rise.

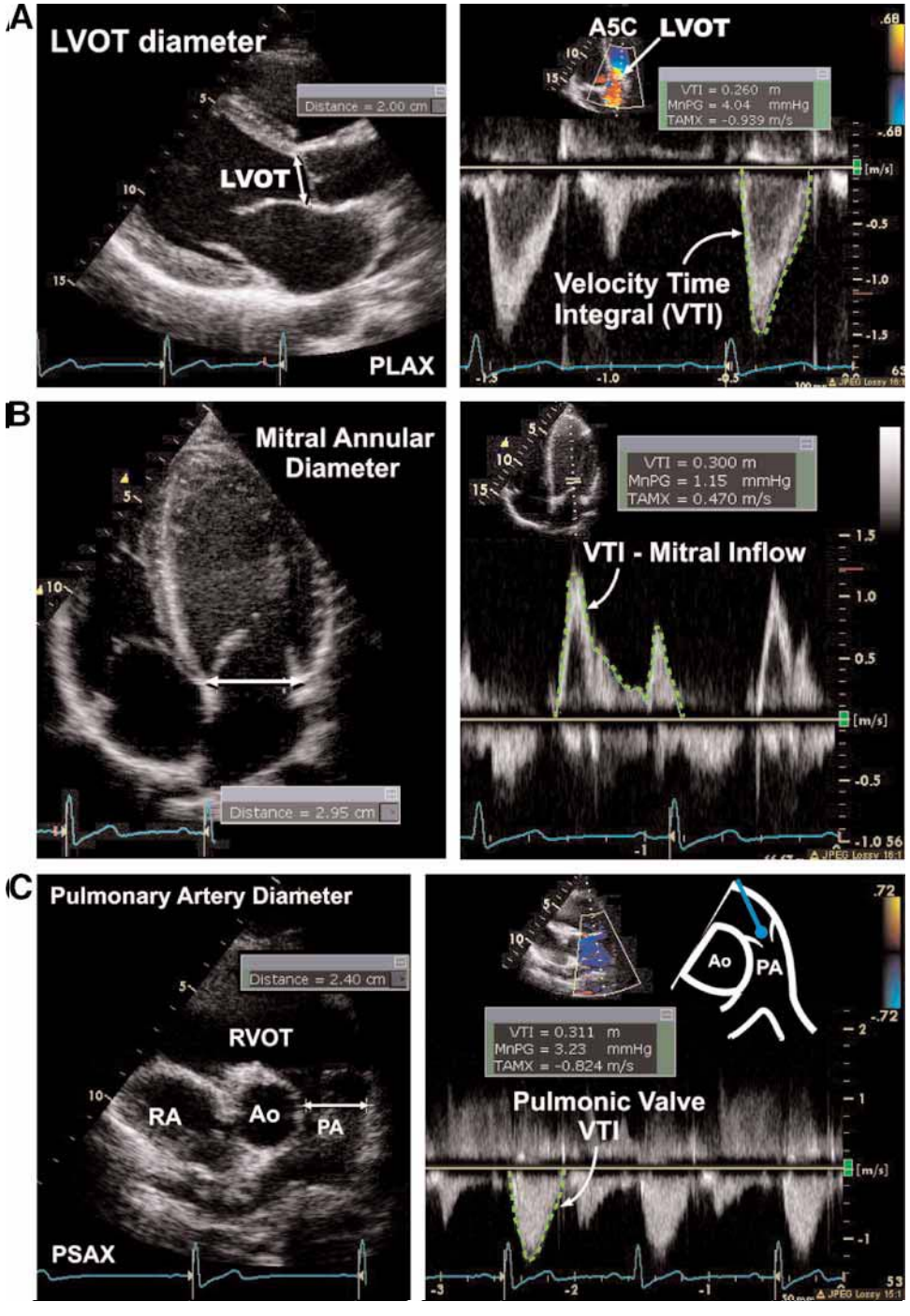

Fig. 18. **(A)** Stroke volume by Doppler (LVOT). **(B)** Stroke volume by Doppler (mitral inflow). **(C)** Stroke volume by Doppler (pulmonary artery).

MYOCARDIAL PERFORMANCE INDEX (TEI INDEX)

The myocardial performance index (MPI) is a Doppler-derived integrated measure of ventricular systolic and diastolic function.

It has been the subject of much interest since its inception in 1995, and has been well received for its ability to assess both LV and RV function in a variety of patients—heart failure, cardiomyopathy, coronary heart disease, heart transplantation, and in prospective clinical trials. It is reproducible, easy to measure and can predict morbidity and mortality in patients with cardiomyopathy and heart failure.

When applied to the LV, it is the sum of the isovolumic contraction and relaxation times (ICT + IRT) divided by

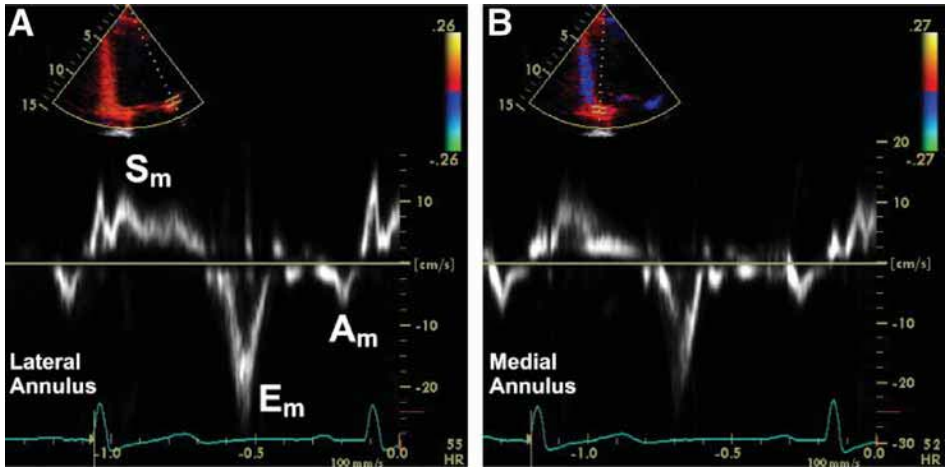

Fig. 19. Tissue Doppler imaging (TDI). Tissue Doppler assesses myocardial velocities during the cardiac cycle. Doppler shift measured at the lateral **(A)** and septal annulus **(B)** are shown. Systolic shifts (S_m) are upward (positive). Shifts away from the transducer (E_m and A_m), reflecting early and late diastolic velocities, are downward (negative).

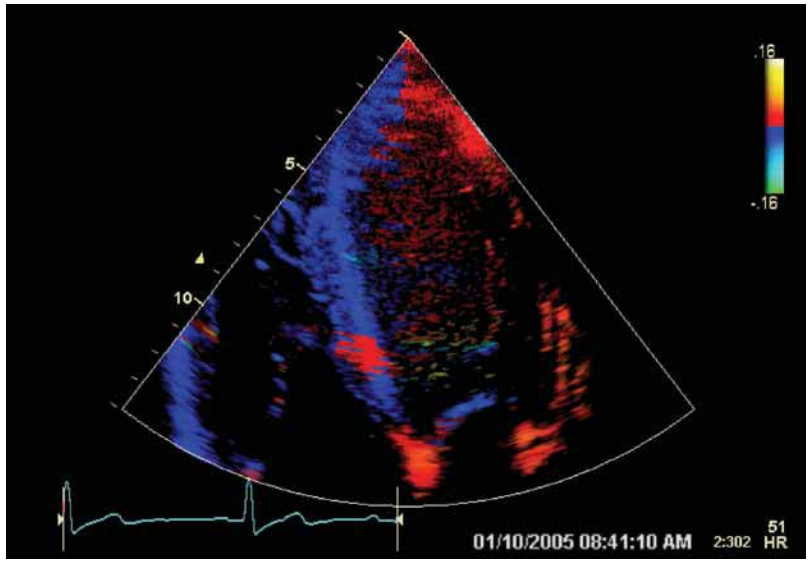

Fig. 20. Tissue velocity imaging (TVI). Differential tissue velocities by color Doppler can detect differential contractility of left ventricle (LV) segments—and color coded as shown. This reflects LV dyssynchrony and impaired LV systolic function. (Please *see* companion DVD for corresponding video.)

the ejection time. These measurements are obtained by Doppler assessment of both LV inflow and outflow and using the formula (Fig. 22):

$$\text{Left Ventricular MPI} = \frac{(\text{ICT} + \text{IRT})}{\text{ET}}$$

The MPI has its limitations. It is not a load-independent measure, and one of its components, the IRT, is less discriminatory in patients with worsening diastolic dysfunction. Therefore, despite its utility, it should complement (not substitute) established measures of LV function, e.g., ventricular volumes and EF.

ASSESSMENT OF RV FUNCTION IN HEART FAILURE AND POSTMYOCARDIAL INFARCTION

In patients with heart failure, RV dysfunction is associated with increased mortality. RV dysfunction is an important predictor of risk and heart failure following myocardial infarction.

MORPHOLOGICAL CONSIDERATIONS

The RV exhibits a far more complex geometry than that of the LV. It is thin walled (<0.5 cm) and assumes

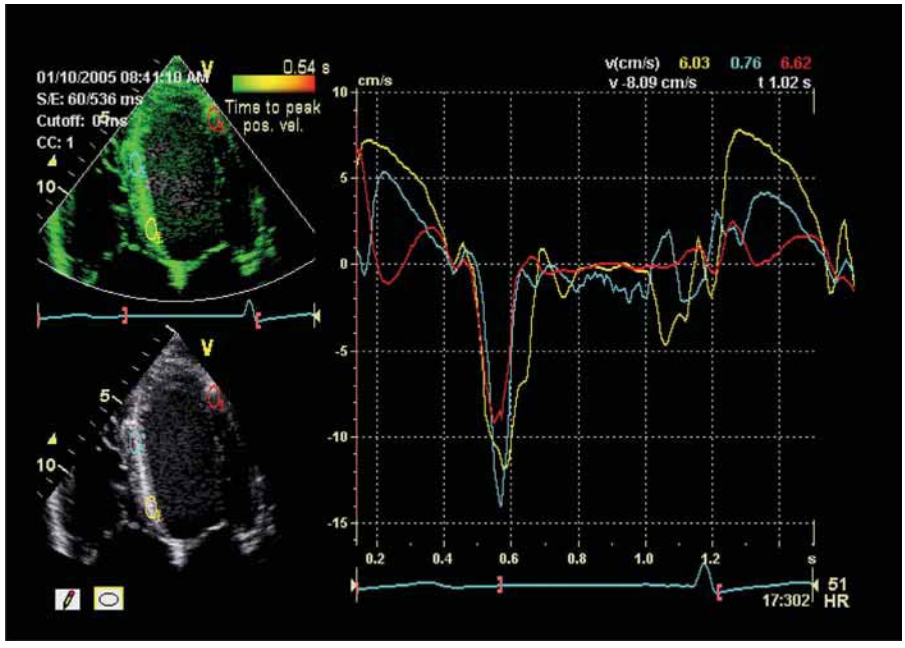

Fig. 21. Doppler strain imaging. Doppler strain imaging showing normal synchronous tissue Doppler tracings of three interrogated myocardial segments are shown.

a flattened pear-shaped appearance folded over the LV (Fig. 23). Such geometry makes it especially difficult to assess by 2D techniques. Most volumetric methods of RV assessment are complex and not well validated, especially in diseased states—when RV geometry is becomes even more complex (Chapter 18).

RV CHAMBER DIMENSIONS

Like the LV, the RV should be assessed using multiple windows. The subcostal window provides the best visualization of the RV free wall. RV size, wall thickness, and systolic function should be recorded, and systolic function described as normal or reduced to varying degrees. RV enlargement can be estimated using the "rule of thirds" in the parasternal long-axis view, or by comparing its size relative to that of the LV in the apical four-chamber view. The RV diameter does not normally exceed one-third the total ventricular width in the apical four-chamber view (Fig. 24; Tables 8 and 9).

Attempts to quantify RV volumes and systolic function by echocardiography include indices like tricuspid annular motion, tricuspid fractional shortening, and RV fractional area change (RVFAC). Tricuspid annular motion refers to the distance the tricuspid annulus moves in the antero-posterior direction. Tricuspid fractional shortening is an assessment

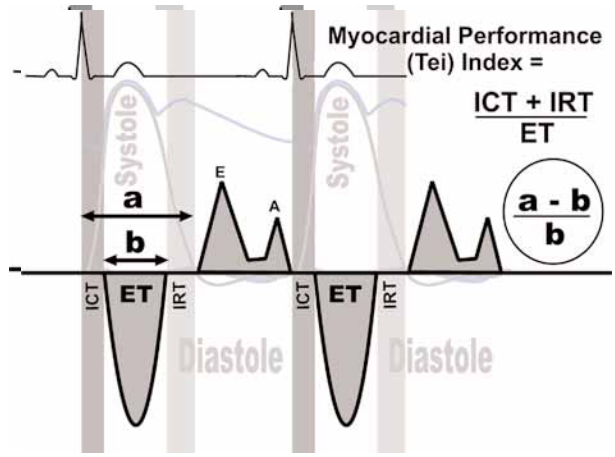

Fig. 22. Myocardial infarction (Tei) index.

of the difference between the maximal and minimal distance between the tricuspid annuli during the cardiac cycle. RVFAC is assessed by measuring RV areas in the apical four-chamber view and comparing the relative change between diastolic and systole. When all three approaches are compared to cardiac magnetic resonance imaging (MRI), the best correlation is seen with RVFAC measurements. RV MPI has also proven a useful measure of RV function. Standards for RV volumetric assessment, however, are yet to be established.

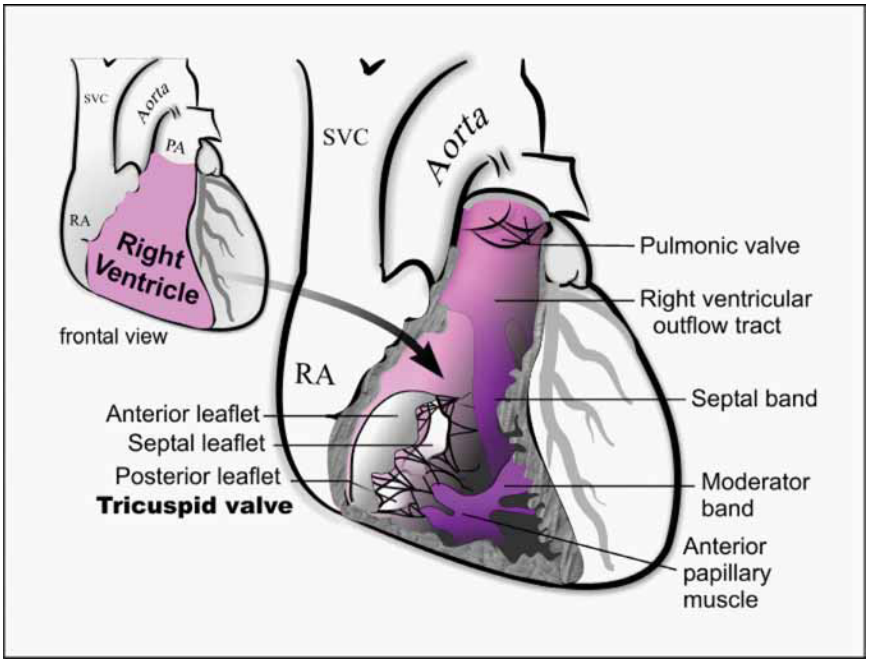

Fig. 23. Right ventricular morphology.

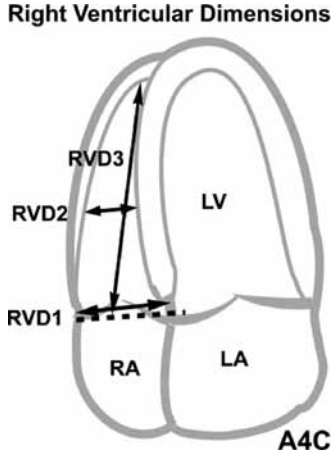

Fig. 24. Right ventricle dimensions (cm). (Please *see* companion DVD for corresponding video.)

ECHOCARDIOGRAPHY TO DETERMINE ETIOLOGY OF SYSTOLIC DYSFUNCTION

Echocardiography can be of use in determining the etiology of systolic dysfunction (Table 1). Patients with ischemic heart disease almost always have discrete regional wall motion abnormalities—most often secondary to prior myocardial infarction. In contrast, global systolic dysfunction, without regional variation, is more suggestive of nonischemic cardiomyopathy. Severe regurgitant valvular heart disease, such as mitral and aortic regurgitation, can lead to a dilated LV with reduced systolic function. Pressure overload conditions, such as aortic stenosis, severe hypertension, or coarctation, usually lead to hypertrophy, although ventricular dilatation and dysfunction can occur late in the course of disease. Various forms of congenital heart disease can lead to systolic dysfunction and can usually be identified on echocardiography. Infiltrative diseases such as amyloidosis can cause severe LV dysfunction and can usually be identified by pathognomonic echocardiographic features. In the case of amyloid, severe LV hypertrophy, "speckled" appearing myocardium, atrial dilatation, nonspecific valve thickening and pericardial effusions are common. Occasionally, hypertrophic cardiomyopathy can ultimately lead to ventricular dilatation and dysfunction (so-called "burnt-out" hypertrophic cardiomyopathy).

USE OF CONTRAST AGENTS IN ECHOCARDIOGRAPHY

As early as the late 1960s, it was noted that intravascular injection of almost any solution resulted in a contrast effect detectable by echocardiography. Contrast microbubbles are used nowadays to complement the imaging process in ultrasound. The advances in imaging modalities in the modern ultrasound systems in tandem with the development of newer agents has made contrast imaging more effective and applicable in daily clinical practice.

Table 8
Reference Limits and Partition Values of Right Ventricular Size

	Reference range	*Mildly abnormal*	*Moderately abnormal*	*Severely abnormal*
RV Dimensions				
Basal right ventricular diameter (RVD1) (cm)	2.0–2.8	2.9–3.3	3.4–3.8	≥3.9
Mid right ventricular diameter (RVD2) (cm)	2.7–3.3	3.4–3.7	3.8–4.1	≥4.2
Base-to-apex length (RVD3) (cm)	7.1–7.9	8.0–8.5	8.6–9.1	≥9.2

Table modified from Recommendations for Chamber Quantification. American Society of Echocardiography (ASE), 2005.

Table 9
Reference Limits and Partition Values of Right Ventricular Size and Function as Measured in the Apical Four-Chamber View

	Reference range	*Mildly abnormal*	*Moderately abnormal*	*Severely abnormal*
Right ventricular diastolic area (cm^2)	11–28	29–32	33–37	≥38
Right ventricular systolic area (cm^2)	7.5–16	17–19	20–22	≥23
Right ventricular fractional area change (%)	32–60	25–31	18–24	≤17

Table modified from Recommendations for Chamber Quantification. American Society of Echocardiography (ASE), 2005.

Contrast Agents

Contrast agents are encapsulated bubbles of gas smaller than the red blood cells and, therefore, capable of circulating freely within the body. The use of contrast dates back to 1968 when Gramiak and Shah first used injected saline to enhance the signals from the blood pool. This was followed years later by encapsulated air bubbles, and more recently by the use of encapsulated low solubility gas bubbles (such as perfluorocarbons). These newer agents are capable of passing through the pulmonary circulation without destruction.

Contrast agents approved for use in the United States to improve LV opacification (LVO) in technically difficult echocardiograms include Optison®, an octafluoropropane within albumin microspheres, Definity™, an octafluoropropane in a phospholipid shell, and Imavist®, a perfluorohexane and other perfluorocarbon gases encapsulated within a surfactant shell. In Europe, Sonovue™, which contains sulfur hexafluoride in a phospholipid shell, is widely used.

The ideal contrast agent should be a nontoxic, easily injectable intravenously (as a bolus or infusion) and should remain stable during cardiac and pulmonary passage for the duration of the ultrasound examination. The agent should have strong echogenic interaction in response to incident ultrasound waves.

Preparation and Administration of the Contrast Agent

The ASE recommends that cardiac sonographers take the appropriate steps to become trained in the preparation and administration of contrast agents. The sonographer is often the first person to recognize the need for contrast, but the physician is ultimately responsible for prescribing its use, which should be done on a case-by-case basis.

Venous access and appropriate instrument settings should be performed prior to preparation of the contrast agent. Each agent has a different method of preparation and administration. Each manufacturer's separate instructions should therefore be followed. The choice between bolus vs continuous infusion depends on the indication for the study and the type of information required. Bolus administration is easier to perform and is sufficient for LVO and Doppler enhancement. However, continuous infusion may be required for myocardial perfusion studies and quantitative analysis. A registered nurse or physician usually administers the injection or infusion of the contrast agent while the sonographer acquires the images.

Ultrasound and Contrast

The mechanical index (MI) represents the normalized energy to which a target (such a bubble) is exposed in an ultrasound field. It gives an estimate of the peak negative pressure to which tissue is exposed. In simple terms, the MI is the intensity of the transmitted ultrasound beam. It varies with the depth in the image. In most of the ultrasound systems, the MI ranges from 0.1 to 2.0. In the absence of attenuation, the MI is maximal at the focus of the ultrasound beam.

Gas bubbles are very effective scatterers of ultrasound waves within the diagnostic frequency range compared to solids. The degree of scattering increases as the MI is increased. Echo signals from microbubbles contain harmonics, which can be detected. Bubble destruction at high MI emits a strong harmonic echo.

There are three main patterns of scattering produced by microbubbles, depending on the peak pressure of the incident sound field. At a peak pressure of less than 100 kPa (MI < 0.1), bubbles produce "linear" oscillations resulting in backscatter enhancement. During this low MI imaging, bubbles act as simple, but powerful, echo enhancers. This is the principle utilized for enhancing spectral Doppler such as in pulmonary venous flow signals. At a peak pressure of 100 kPa to 1 MPa (MI 0.1–1.0), there is "nonlinear" oscillation resulting in harmonic backscatter. This principle is utilized in harmonic B-mode LVO and real-time perfusion imaging. At a peak pressure of more than 1 MPa (MI > 1.0), there is bubble disruption resulting in transient harmonic echoes. This is the principle utilized in power Doppler imaging.

Contrast Imaging Modes

Conventional grayscale imaging results in linear backscatter, and, hence, is useful for enhancement of the LV cavity, providing better endocardial definition (*see* Fig. 7B). The concept of "harmonic imaging" emerged from the observation that "nonlinear" oscillations of the microbubbles results in the generation of "second harmonics." Therefore, imaging can be improved by preferential detection of these "second harmonics" that emanate directly from the microbubbles themselves rather than the tissue. In harmonic B mode imaging, the transmitted frequency typically lies between 1.5 and 3 MHz and the received frequency between 3 and 6 MHz to enable detection of these bubble harmonics.

"Contrast-Specific" Imaging Modalities

Although harmonic imaging improves visualization of bubble harmonics, it imposes some fundamental limitations in bandwidth and hence fails to completely suppress the tissue harmonics. Detection of bubbles in myocardial capillaries (i.e., perfusion), therefore, would require tedious off-line background subtraction to suppress the echoes produced by the tissue. To overcome this, "contrast specific" methods are required for assessment of myocardial perfusion by enhancing contrast harmonics while suppressing tissue harmonics.

Examples of such modalities are:

1. Pulse inversion: high MI technique. By sending two pulses (one inverted) in rapid succession toward the tissue, summation occurs and results in a strong harmonic signal that is exclusively from the microbubbles. However, wall motion artifacts could still attenuate image quality.
2. Harmonic power Doppler: intermittent imaging (high MI technique). The strong, transient echoes produced by bubble destruction provide a highly sensitive method of imaging the microbubbles. The disadvantage is that wall motion (which produces a Doppler shift), is also detected and this potentially interferes with image quality.
3. Low power "real-time" contrast imaging (power pulse inversion/power modulation/coherent imaging): this is a nondestructive, continuous real-time imaging (low MI) technique. In this mode, sequences of more than two pulses are transmitted in alternating phase. Although the sensitivity may be slightly lower than the high power technique, this method allows wall motion information to be available without the need for bubble disruption. This method is much easier to use and avoids many artifacts that occur with high power harmonic imaging. The echoes from the bubbles are well separated from those of tissues, thereby providing better characterization of "real-time" myocardial perfusion.

Clinical Uses of Contrast Echocardiography

LV Opacification

One of the most common clinical indications for echocardiography is in the assessment of regional and global LV function. This should be accurate and reproducible. A pre-requisite for reliable assessment of LV function is accurate visualization of the endocardium. In up to 20% of resting studies, endocardial border definition is suboptimal—defined as the inability to visualize at least two myocardial segments of the LV. The advent of tissue harmonic imaging has significantly improved endocardial definition compared to fundamental imaging.

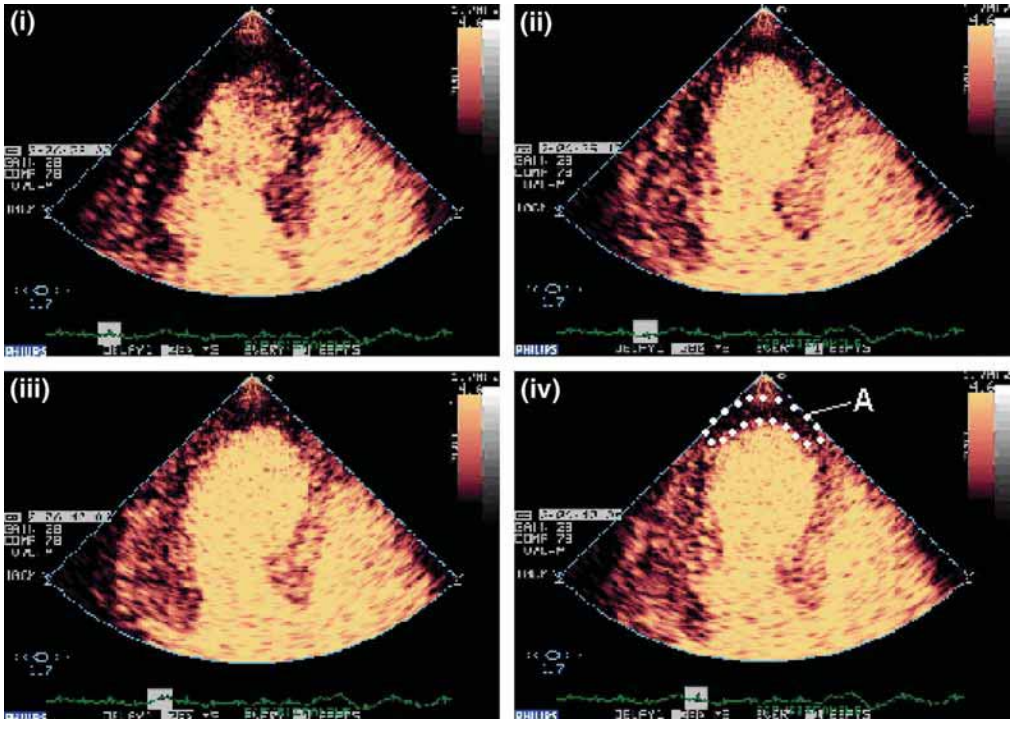

Fig. 25. Frame (i) is immediately following a high power ultrasound flash that destroys the microbubbles within the myocardium. Frames (ii) to (iv) show replenishment of microbubbles in the septum and lateral walls within two heartbeats. A clear apical perfusion defect **(A)** that persists is demonstrated. (Reproduced with permission from R Janardhanan, et al. Myocardial contrast echocardiography: a new tool for assessment of myocardial perfusion. Ind Heart J 2005;57:210–216.)

Nevertheless, 5–10% of studies employing tissue harmonics imaging are still suboptimal.

The primary clinical use of contrast echocardiography is for LVO (Chapter 5, Fig. 7B; Chapter 8, Figs. 8 and 10). By injecting microbubbles that traverse the pulmonary circulation, the LV can be opacified and endocardial definition significantly improved. Studies using contrast-enhanced LVO have shown excellent correlation with MRI in the determination of LV volumes and EF. Currently, this use is the only Food and Drug Administration-approved indication for echocardiographic contrast agents.

Many studies have shown the incremental value of using contrast agents to improve image quality, the percentage of wall segments visualized, and the confidence of interpretation of resting and stress echocardiography images (Chapter 8, Figs. 8 and 10). Contrast agents in stress echocardiography should be used whenever resting image quality is suboptimal.

Contrast agents can assist in the identification of LV thrombi. Approximately 15–45% of echocardiographic studies may fail to identify a LV thrombus. Fundamental imaging from the apical windows may fail to detect apical LV thrombi owing to near-field artifacts. The use of contrast agents permits almost 90% of initially non-diagnostic images to become diagnostic.

Enhancement of Doppler Flow Signals

The accuracy of spectral Doppler velocity measurements depends on obtaining a clear envelope of the Doppler signal. The quality of Doppler recordings, e.g., tricuspid regurgitation velocity, pulmonary venous signals, and so on, can be augmented by using contrast agents. Contrast agents may also be useful in the detection of suspected intracardiac and intrapulmonary shunts.

Echocardiographic Contrast Agents vs Saline Contrast. Echocardiographic contrast agents that traverse the pulmonary circulation differ from agitated saline contrast used for detecting intracardiac shunts. Saline bubbles do not traverse the pulmonary circulation, except when an arterio-venous malformation is present. Because they do not traverse the pulmonary circulation, agitated saline contrast provide no LVO under normal conditions. Echocardiographic contrast agents that traverse the pulmonary circulation should not be used to diagnose intracardiac shunts.

Myocardial Perfusion Imaging

Myocardial contrast echocardiography (MCE) can accurately assess both myocardial blood volume and microbubble velocity (both of which determine myocardial blood flow). Although not yet licensed for this indication, MCE shows great potential as a clinical tool to evaluate myocardial perfusion.

MCE may be superior to techniques like sestamibi SPECT in the detection of myocardial perfusion. This is most likely explained by the superior temporal and spatial resolution of MCE over SPECT. Furthermore, MCE can be performed at the bedside and does not involve ionizing radiations.

MCE detects contrast bubbles at the capillary level within the myocardium and hence, is marker of capillary integrity. This is the principle behind the use of MCE in patients post-MI in the detection of myocardial viability (Fig. 25).

Safety Considerations. Current contrast agents have an excellent safety profile, and complications are rare. Allergic reactions have been occasionally reported. However, in patients with intracardiac or intrapulmonary right-to-left shunts, the potential for adverse events are slightly greater. There are conflicting reports of increased frequency of premature ventricular complexes especially with high MI-triggered imaging. However, this has not been shown in larger studies.

SUGGESTED READING

2001 Heart and stroke statistical update. Dallas: American Heart Association, 2000.

Amico AF, Lichtenberg GS, Reisner SA, Stone CK, Schwartz RG, Meltzer RS. Superiority of visual versus computerized echocardiographic estimation of radionuclide left ventricular ejection fraction. Am Heart J 1989;118:1259–1265.

Bax JJ, Marwick TH, Molhoek SG, et al. Left ventricular dyssynchrony predicts benefit of cardiac resynchronization therapy in patients with end-stage heart failure before pacemaker implantation. Am J Cardiol 2003;92:1238–1240.

Becher H, Burns PN. Handbook of Contrast Echocardiography: LV function and Myocardial Perfusion. Frankfurt: Springer-Verlag, 2000.

Birnbaum Y, Luo H, Nagai T, et al. Noninvasive in vivo clot dissolution without a thrombolytic drug: recanalization of thrombosed iliofemoral arteries by transcutaneous ultrasound combined with intravenous infusion of microbubbles. Circulation 1998;97:130–134.

Boersma E, Poldermans D, Bax JJ, et al. DECREASE Study Group (Dutch Echocardiographic Cardiac Risk Evaluation Applying Stress Echocardiogrpahy). Predictors of cardiac events after major vascular surgery: role of clinical characteristics, dobutamine echocardiography, and beta-blocker therapy. JAMA 2001;285:1865–1873.

Bommer WJ, Shah PM, Allen H, et al. The safety of contrast echocardiography: report of the Committee on Contrast Echocardiography for the American Society of Echocardiography. J Am Coll Cardiol 1984;3:6–13.

Cerqueira MD, Weissman NJ, Dilsizian V, et al. Standardized myocardial segmentation and nomenclature for tomographic imaging of the heart: a statement for healthcare professionals from the Cardiac Imaging Committee of the Council on Clinical Cardiology of the American Heart Association. Circulation 2002;105:539–542.

Cho GY, Park WJ, Han SW, Choi SH, Doo YC, Oh DJ, Lee Y. Myocardial systolic synchrony measured by Doppler tissue imaging as a role of predictor of left ventricular ejection fraction improvement in severe congestive heart failure. J Am Soc Echocardiogr 2004;17:1245–1250.

Dargie HJ. Effect of carvedilol on outcome after myocardial infarction in patients with left-ventricular dysfunction: the CAPRICORN randomised trial. Lancet 2001;357:1385–1390.

Devereux RB, Alonso DR, Lutas EM, et al. Echocardiographic assessment of left ventricular hypertrophy: comparison to necropsy findings. Am J Cardiol 1986;57:450–458.

Devereux RB, Roman MJ, Palmieri V, et al. Left ventricular wall stresses and wall stress-mass-heart rate products in hypertensive patients with electrocardiographic left ventricular hypertrophy: the LIFE study. Losartan Intervention For Endpoint reduction in hypertension. J Hypertens 2000;18:1129–1138.

Devereux RB, Wachtell K, Gerdts E, et al. Prognostic significance of left ventricular mass change during treatment of hypertension. JAMA 2004;292:2350–2356.

Dickstein K, Kjekshus J; OPTIMAAL Steering Committee of the OPTIMAAL Study Group. Effects of losartan and captopril on mortality and morbidity in high-risk patients after acute myocardial infarction: the OPTIMAAL randomised trial. Optimal Trial in Myocardial Infarction with Angiotensin II Antagonist Losartan. Lancet 2002;360:752–860.

Effect of ramipril on mortality and morbidity of survivors of acute myocardialinfarction with clinical evidence of heart failure. The Acute Infarction Ramipril Efficacy (AIRE) Study Investigators. Lancet 1993;342:821–828.

Gallik DM, Obermueller SD, Swarna US, et al. Simultaneous assessment of myocardial perfusion and left ventricular function during transient coronary occlusion. J Am Coll Cardiol 1995;25:1529–1538.

Gillebert TC, Van de Veire N, De Buyzere ML, De Sutter J. Time intervals and global cardiac function. Use and limitations. Eur Heart J 2004;25:2185–2186.

Givertz MM, Colucci WS, Braunwald E. Clinical aspects of heart failure; pulmonary edema, high-output failure. In: Brauwald's heart disease: a textbook of cardiovascular medicine, 7th ed. Zipes DP, Libby P, Bonow RO, Braunwald E (eds). Philadelphia: Elsevier Saunders 2005;539–568.

Gopal AS, Shen Z, Sapin PM, et al. Assessment of cardiac function by three-dimensional echocardiography compared with conventional noninvasive methods. Circulation 1995;92:842–853.

Hammermeister KE. Survival in patients with coronary disease. Circulation 1979;60:1427.

Janardhanan R, Dwivedi G, Hayat S, Senior R. Myocardial contrast echocardiography: a new tool for the assessment of myocardial perfusion. Ind Heart J 2005;57:210–216.

Janardhanan R, Moon JCC, Pennell DJ, Senior R. Myocardial contrast echocardiography accurately reflects transmurality of myocardial necrosis and predicts contractile reserve after acute myocardial infarction. Am Heart J 2005;149:355–362.

Janardhanan R, Senior R. Accuracy of dipyridamole myocardial contrast echocardiography for the detection of residual stenosis of the infarct related artery and multivessel disease early after acute myocardial infarction. J Am Coll Cardiol 2004;43: 2247–2252.

Janardhanan R, Swinburn JMA, Greaves K, Senior R. Usefulness of myocardial contrast echocardiography using low-power continuous imaging early after acute myocardial infarction to predict late functional ventricular recovery. Am J Cardiol 2003;92:493–497.

Jessup M, Brozena S. Heart failure. N Engl J Med 2003;348: 2007–2018.

Kaul S. Myocardial contrast echocardiography: 15 years of research and development. Circulation 1997;96:3745–3760.

Khand A, Gemmel I, Clark AL, Cleland JG. Is the prognosis of heart failure improving? J Am Coll Cardiol 2000;36:2284–2286.

Kober L, Torp-Pedersen C, Carlsen JE, et al. A clinical trial of the angiotensin-converting-enzyme inhibitor trandolapril in patients with left ventricular dysfunction after myocardial infarction. Trandolapril Cardiac Evaluation (TRACE) Study Group. N Engl J Med 1995;333:1670–1676.

Konstam MA. Progress in heart failure management? Lessons from the real world. Circulation 2000;102:1076–1078.

Kotler MN, Segal BL, Mintz G, Parry WR. Pitfalls and limitations of M-mode echocardiography. Am Heart J 1977;94:227–249.

Massie B. Heart failure: pathophysiology and diagnosis. In: Cecil textbook of medicine, 22nd ed.

McMurray J, Ostergren J, Pfeffer M, et al.; CHARM committees and investigators. Clinical features and contemporary management of patients with low and preserved ejection fraction heart failure: baseline characteristics of patients in the Candesartan in Heart failure-Assessment of Reduction in Mortality and morbidity (CHARM) programme. Eur J Heart Fail 2003;5:261–270.

McMurray JJ, Ostergren J, Swedberg Km et al.; CHARM Investigators and Committees. Effects of candesartan in patients with chronic heart failure and reduced left-ventricular systolic function taking angiotensin-converting-enzyme inhibitors: the CHARM-Added trial. Lancet 2003;362:767–771.

Mueller X, Stauffer JC, Jaussi A, Goy JJ, Kappenberger L. Subjective visual echocardiographic estimate of left ventricular ejection fraction as an alternative to conventional echocardiographic methods: comparison with contrast angiography. Clin Cardiol.1991;14:898–902.

Mulvagh SL, DeMaria AN, Feinstein SB, et al. Contrast echocardiography: current and future applications. J Am Soc Echocardiogr 2000;13:331–342.

Naik MM, Diamond GA, Pai T, Soffer A, Siegel RJ. Correspondence of left ventricular ejection fraction determinations from two-dimensional echocardiography, radionuclide angiography and contrast cineangiography. J Am Coll Cardiol 1995;25:937–942.

Palmieri V, Bella JN, Arnett DK, et al. Impact of type II diabetes on left ventricular geometry and function: the Hypertension Genetic Epidemiology Network (HyperGEN) Study. Circulation 2001;103:102–107.

Pitt B, Remme W, Zannad F, et al. Eplerenone Post-Acute Myocardial Infarction Heart Failure Efficacy and Survival Study Investigators. Eplerenone, a selective aldosterone blocker, in patients with left ventricular dysfunction after myocardial infarction. N Engl J Med 2003;348:1309–1321.

Rasmussen S, Corya BC, Phillips JF, Black MJ. Unreliability of M-mode left ventricular dimensions for calculating stroke volume and cardiac output in patients without heart disease. Chest 1982; 81:614–619.

Roberto M. Lang et al. Recommendations for Chamber Quantification. A report from the American Society of Echocardiography's Nomenclature and Standards Committee and the Task Force on Chamber Quantification, developed in conjunction with the American College of Cardiology Echocardiography Committee, the American Heart Association, and the European Association of Echocardiography, a branch of the European Society of Cardiology, 2005 (in press).

Roman MJ, Pickering TG, Schwartz JE, Pini R, Devereux RB. The association of carotid atherosclerosis and left ventricular hypertrophy. J Am Coll Cardiol 1995;25:83–90.

Sahn DJ, DeMaria A, Kisslo J, Weyman A. Recommendations regarding quantitation in M-mode echocardiography: results of a survey of echocardiographic measurements. Circulation 1978;58: 1072–1083.

Sahn DJ, DeMaria A, Kisslo J, Weyman A. Recommendations regarding quantitation in M-mode echocardiography: results of a survey of echocardiographic measurements. Circulation. 1978; 58:1072–1083.

Schiller NB, Acquatella H, Ports TA, et al. Left ventricular volume from paired biplane two-dimensional echocardiography. Circulation 1979;60:547–555.

Schiller NB, Shah PM, Crawford M, et al. Recommendations for quantitation of the left ventricle by two-dimensional echocardiography. J Am Soc Echocardiogr 1989;2:358–367.

Schiller NB, Shah PM, Crawford M, et al. Recommendations for quantitation of the left ventricle by two-dimensional echocardiography. American Society of Echocardiography Committee on Standards, Subcommittee on Quantitation of Two-Dimensional Echocardiograms. J Am Soc Echocardiogr 1989;2:358–367.

Schnittger I, Gordon EP, Fitzgerald PJ, Popp RL. Standardized intracardiac measurements of two-dimensional echocardiography. J Am Coll Cardiol 1983;2:934–938.

Senior R, Soman P, Khattar RS, et al. Improved endocardial visualization with second harmonic imaging compared with fundamental two-dimensional echocardiographic imaging. Am Heart J 1999;138:163–168.

Shiina A, Tajik AJ, Smith HC, Lengyel M, Seward JB. Prognostic significance of regional wall motion abnormality in patients with prior myocardial infarction: a prospective correlative study of two-dimensional echocardiography and angiography. Mayo Clin Proc 1986;61:254–262.

Shohet RV, Chen S, Zhou YT, et al. Echocardiographic destruction of albumin microbubbles directs gene delivery to the myocardium. Circulation 2000;101:2554–2556.

St. John Sutton M, Pfeffer MA, Moye L, et al. Cardiovascular death and left ventricular remodeling two years after myocardial infarction: baseline predictors and impact of long-term use of captopril: information from the Survival and Ventricular Enlargement (SAVE) trial. Circulation 199718;96: 3294–3299.

Stevenson WG, Stevenson LW, Middlekauff HR, et al. Improving survival for patients with atrial fibrillation and advanced heart failure. J Am Coll Cardiol 1996;28:1458–1463.

Stevenson WG, Stevenson LW, Middlekauff HR, et al. Improving survival for patients with advanced heart failure: a study of 737 consecutive patients. J Am Coll Cardiol 1995;26:1417–1423.

Sugishita Y, Iida K, Ohtsuka S, Yamaguchi I. Ventricular wall stress revisited. A keystone of cardiology. Jpn Heart J 1994;35: 577–587.

Tei C, Ling LH, Hodge DO, et al. New index of combined systolic and diastolic myocardial performance: a simple and reproducible

measure of cardiac function—a study in normals and dilated cardiomyopathy. J Cardiol 1995;26:357–366.

Teichholz LE, Kreulen T, Herman MV, Gorlin R. Problems in echocardiographic volume determinations: echocardiographic-angiographic correlations in the presence of absence of asynergy. Am J Cardiol 1976;37:7–11.

Thanigaraj S, Schechtman KB, Perez JE. Improved echocardiographic delineation of left ventricular thrombus with the use of intravenous second generation contrast image enhancement. J Am Soc Echocardiogr 1999;12:1022–1026.

The SOLVD Investigators. Effect of enalapril on mortality and the development of heart failure in asymptomatic patients with reduced left ventricular ejection fractions. N Engl J Med 1992;327: 685–691.

The SOLVD Investigators. Effect of enalapril on survival in patients with reduced left ventricular ejection fractions and congestive heart failure. N Engl J Med 1991;325:293–302.

Timperley J, Mitchell ARJ, Becher H. Contrast echocardiography in left ventricular opacification. Heart 2003;89:1394–1397.

Vasan RS, Larson MG, Benjamin EJ, Evans JC, Levy D. Left ventricular dilatation and the risk of congestive heart failure in people without myocardial infarction. N Engl J Med 1997;336: 1350–1355.

Verdecchia P, Schillaci G, Borgioni C, et al. Prognostic significance of serial changes in left ventricular mass in essential hypertension. Circulation 1998;97:48–54.

Waggoner AD, Ehler D, Adams D, et al. Guidelines for the cardiac sonographer in the performance of contrast echocardiography: Recommendations of the American Society of Echocardiography Council on Cardiac Sonography. J Am Soc Echocardiogr 2001; 4:417–420.

Wei K, Jayaweera AR, Firoozan S, et al. Quantification of myocardial blood flow with ultrasound-induced destruction of microbubbles administered as a constant venous infusion. Circulation 1998; 97:473–483.

Zornoff LA, Skali H, Pfeffer MA, et al. SAVE Investigators. Right ventricular dysfunction and risk of heart failure and mortality after myocardial infarction. J Am Coll Cardiol 2002;39:1450–1455.

6 Echocardiographic Assessment of Diastolic Function

Carolyn Y. Ho, MD

CONTENTS

CASE PRESENTATION

A 63-yr-old female presents to her primary care physician complaining of increased exertional dyspnea. Her exercise tolerance has been slowly declining for the past several months and she occasionally notes orthopnea and paroxysmal nocturnal dyspnea. She has had no anginal symptoms. Her past medical history is notable for hypertension, diabetes, and obesity. Physical examination is notable for poorly controlled blood pressure, elevation of central venous pressures, a fourth heart sound and murmur compatible with mitral regurgitation, and mild lower extremity edema. Echocardiography shows concentric left ventricular hypertrophy and vigorous systolic function without segmental wall motion abnormalities. There is mild mitral regurgitation and moderate left atrial enlargement.

PHYSIOLOGY OF DIASTOLE

Diastole is the portion of the cardiac cycle that spans from isovolumic ventricular relaxation to the completion of antegrade mitral flow. There are four distinct phases of diastole (Fig. 1): (1) isovolumetric ventricular relaxation: an active, adenosine triphosphate (ATP)-requiring process that occurs from end-systole until left ventricular pressure falls below left arterial pressure leading to mitral valve (MV) opening; (2) rapid early ventricular filling: blood flows from left atrium (LA) into the left ventricle (LV) during continued, active, then passive LV relaxation; (3) diastasis: active ventricular relaxation is completed and near equilibration of LA and LV pressures occurs with resultant slow LA filling from pulmonary venous (PV) flow; and (4) atrial systole: increased transmitral pressure gradient from atrial contraction results in acceleration of blood flow from LA to LV.

Normal diastolic function is dependent on rapid ventricular relaxation and a compliant chamber. The normal ventricle relaxes quite vigorously leading to rapid pressure decline early in diastole. This contributes to a suction effect that draws blood from the LA into the LV despite relatively low LA pressures. This process is energy-dependent, fueled by the hydrolysis of ATP to release actin and myosin cross-bridges. As such,

From: *Contemporary Cardiology: Essential Echocardiography: A Practical Handbook With DVD*
Edited by: S. D. Solomon © Humana Press, Totowa, NJ

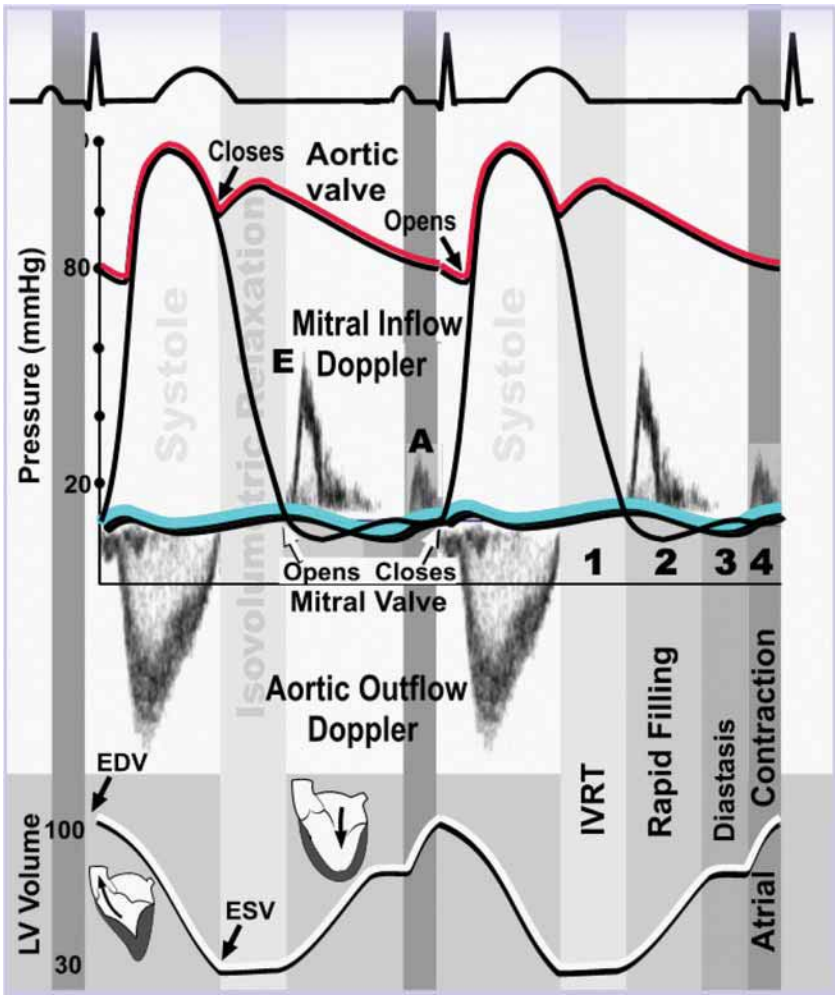

Fig. 1. Cardiac cycle: with spectral doppler relationships. (**A**) Intracardiac pressures and volumes recorded throughout the cardiac cycle shown with spectral Doppler and volumetric relationships. A, atrial filling; E, rapid early filling; EDV, end-diastolic volume; ESV, end-systolic volume; IVRT, isovolumetric relaxation time.

diastolic function is vulnerable to disease states that may compromise energy production, such as myocardial ischemia. Experimental studies have demonstrated that diastolic function is more sensitive to ischemia than systolic function, with diastolic abnormalities being manifested earlier than systolic function after blood supply is compromised.

Ventricular stiffness or compliance is another critical determinant of proper diastolic function. The normal ventricle is relatively compliant so that small changes in volume are accompanied by proportionally small changes in pressure. Many factors contribute to ventricular stiffness, including intrinsic distensibility and elasticity, wall thickness, cavity dimensions, and pericardial constraint (Table 1). If compliance decreases, there will be an exaggerated rise in pressure in response to increased volume.

Table 1
Factors Influencing Left Ventricular Filling

Left ventricular compliance
Intrinsic distensibility and elasticity
LV cavity dimensions
Rate of relaxation
Left atrial compliance
Left atrial pressure
Valvular regurgitation: Aortic (AR); Mitral (MR)
Pericardial restraint

The atria act as reservoir, conduit, and pump during the cardiac cycle, therefore, processes that disrupt normal

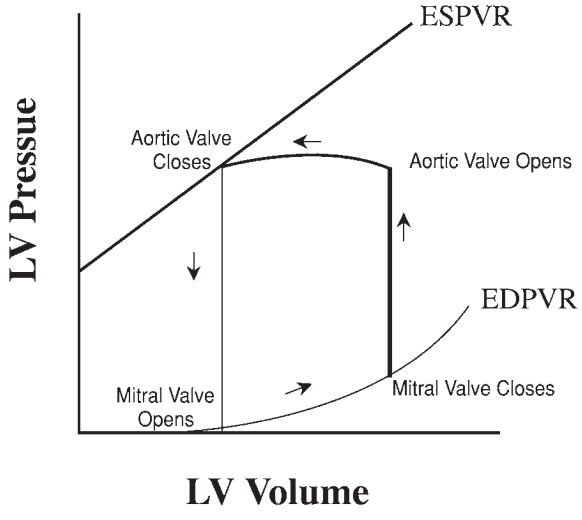

Fig. 2. Normal pressure-volume loop. (**A**) Ventricular filling. (**B**) Isovolumetric contraction. (**C**) Systolic ejection. (**D**) Isovolumetric relaxation. EDPVR: end-diastolic pressure-volume relationship; ESPVR: end-systolic pressure-volume relationship.

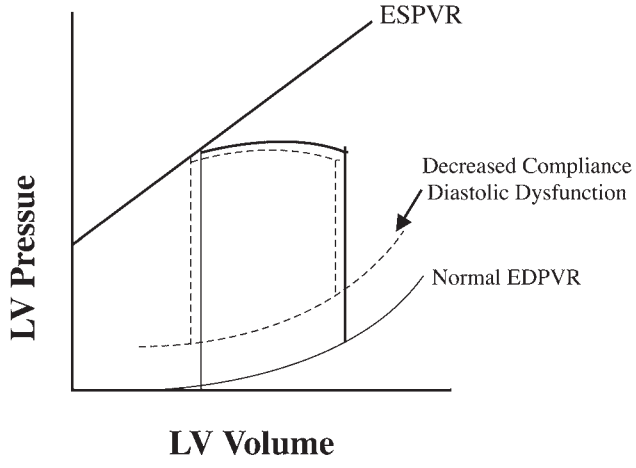

Fig. 3. Pressure-volume loop in diastolic dysfunction. The EDPVR in a patient with diastolic dysfunction (shown with dotted line) is shifted upwards and to the left—for any given volume, the diastolic filling pressure acquired to achieve that volume is higher.

atrial function may also contribute to diastolic dysfunction. In young, healthy subjects, atrial contraction contributes approx 20% of ventricular filling. This proportion increases slightly with aging but typically does not exceed 50% of ventricular filling.

DIASTOLIC DYSFUNCTION

Congestive heart failure is a major public health problem in the United States. Approximately 500,000 new cases are diagnosed annually and it is the most common discharge diagnosis in hospitalized patients. In the majority of cases, heart failure is a result of a combination of systolic and diastolic abnormalities, but in approximately one-third of patients, heart failure symptoms are primarily caused by diastolic dysfunction, as LV systolic function is relatively preserved.

The pathophysiological basis of diastolic dysfunction is that adequate filling of the ventricles, and, therefore, adequate cardiac output, occurs at the expense of abnormal elevation of intracardiac filling pressures. In some instances, intracardiac filling pressures may be normal at rest, but rise precipitously with exercise. This altered pressure–volume relationship (Figs. 2 and 3) can result in symptoms of pulmonary congestion, such as shortness of breath or exercise intolerance. Table 2 lists different causes of diastolic dysfunction as well as conditions that may mimic it.

Table 2
Conditions That Cause or Mimic Diastolic Dysfunction

Conditions associated with diastolic dysfunction
Hypertension
Ischemic heart disease
Hypertrophic cardiomyopathy
Restrictive cardiomyopathy
Constrictive pericarditis and cardiac tamponade
Dilated cardiomyopathy
Cardiac transplant rejection
Conditions that mimic diastolic dysfunction
Pulmonary disease
Deconditioning
Anemia
Thyroid disease
Valvular heart disease
Congenital heart disease

STANDARD ECHOCARDIOGRAPHIC ASSESSMENT OF DIASTOLIC FUNCTION

Doppler Interrogation of Flow

Traditionally, evaluation of spectral Doppler patterns of mitral inflow has been used to assess LV diastolic function. This approach assumes that transmitral flow velocity is an accurate surrogate for volumetric flow. However, transmitral velocities reflect the *pressure*

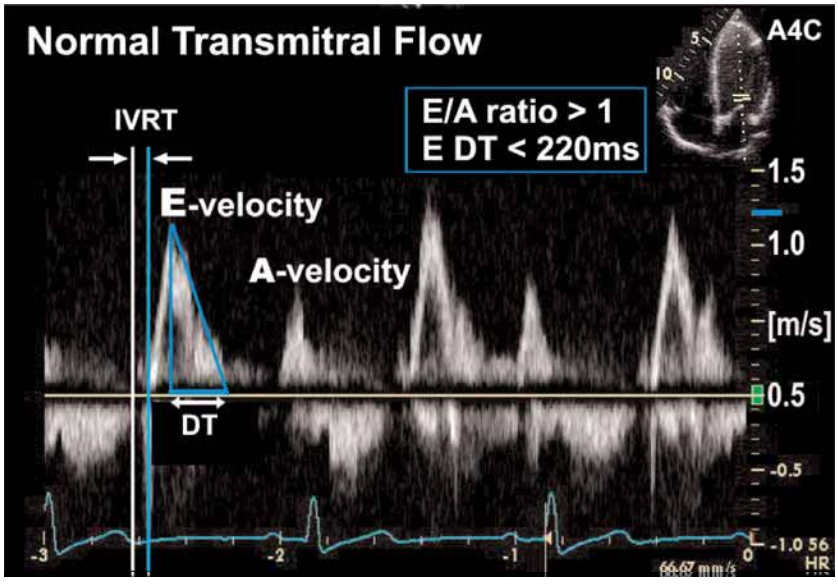

Fig. 4. Normal transmitral flow pattern. Pulse wave Doppler profile of normal transmitral flow during diastole sampled at the tip of the mitral leaflets using the apical four-chamber view. Note the early (E) and atrial (A) velocities representing early and late filling. DT, deceleration time.

gradient between the LA and LV, rather than actual flow. Furthermore, this parameter is highly dependent on loading conditions, heart rate and rhythm, atrial contractile function, and age, thereby limiting its ability to accurately describe diastolic function. Despite these limitations, because transmitral Doppler flow is easy to acquire and well described, characterization of these waveforms remains the basis for categorizing patterns of diastolic function.

TRANSMITRAL DOPPLER PROFILES

Figure 4 shows a normal transmitral flow pattern. There are two major components of normal transmitral flow: the rapid early filling phase, designated the E-wave, and filling associated with atrial contraction, designated the A-wave. Normal transmitral flow is characterized by an E:A ratio slightly greater than one and relatively brisk (150–220 ms) E-wave deceleration, defined as the time from the peak of the E-wave to the end of early mitral flow. The atrial contribution to ventricular filling typically does not exceed 20%.

Technical Issues in Measuring MV Inflow

Normal flow is directed toward the mid- to distal posterolateral wall (approx 20° lateral to the apex); this lateral direction becomes more exaggerated with LV dilation (*see* Fig. 5).

1. Position the sample volume at the tips of the leaflets. Recordings obtained from the mitral annulus, between the body of the leaflets or apical to the leaflet tips have lower peak E-velocities. E-wave deceleration time is lengthened when the sample volume is too apically placed and shortened when the sample volume is too close to the mitral annulus.
2. Orient the image such that the transducer beam is parallel to flow (color flow Doppler may be used to optimize beam placement).
3. Sample volume size should be 1–2 mm; pulse wave Doppler should be used.
4. The velocity scale should be adjusted according to the peak velocity recorded (normal range of 60–130 cm/s); velocity filters should be minimized to record middiastolic flow and eliminate wall motion artifacts, sweep speed 50–100 mm/s.
5. Record several cardiac cycles during breath holding at the end of expiration.

Classification of Mitral Inflow Patterns

General classification of diastolic function is based predominantly on the pattern of mitral inflow as determined by the relative heights of the E- and A-waves (E:A ratio), their peak velocities, and the rate of deceleration of the E-wave. Acceleration of flow across the MV (reflected predominantly in peak E-wave velocity) is influenced primarily by the transmitral pressure gradient. This pressure gradient is directly related to LA pressure and inversely related to ventricular relaxation (as LA pressure rises, or LV relaxation declines, peak

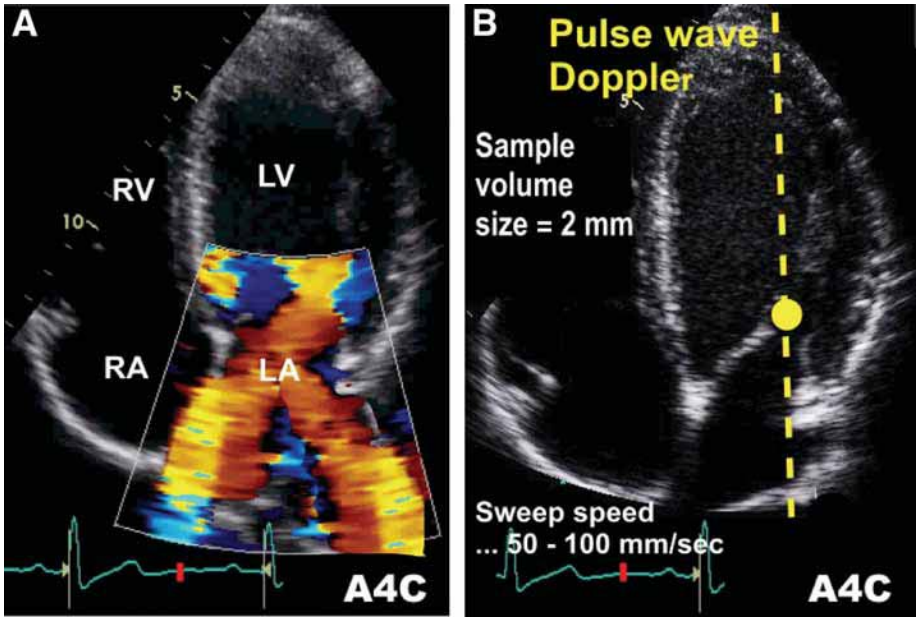

Fig. 5. Measuring mitral valve inflow (*see* Technical Issues in Measuring MV Inflow section for explanation).

E-wave velocities tend to increase). Deceleration of mitral inflow is directly related to MV area and inversely related to ventricular compliance (as MV area or compliance decrease, E-wave deceleration time increases). Mitral inflow patterns are highly modulated by filling pressures and loading conditions, particularly LV preload. A rise in LA pressure is associated with an increase in peak E-wave velocity. Conversely, decreased LA pressure can be associated with a decrease in peak E-wave velocity as well as E-wave deceleration time, independently of the intrinsic relaxation properties of the LV. This dependence limits the clinical applicability of using MV inflow patterns to predict filling pressures and diastolic function (Fig. 6).

ABNORMAL MITRAL INFLOW PATTERNS

Impaired Relaxation

The Doppler pattern of impaired relaxation (Fig. 7) is characterized by E- to A-wave reversal (peak A-wave velocity > peak E-wave velocity, or E:A < 1) and prolongation of E-wave deceleration time more than 220 ms. This pattern may be seen more commonly in elderly patients and is not necessarily accompanied by pathophysiological changes, but it generally suggests early abnormalities of diastolic function if detected in patients less than 60 yr old. This pattern occurs because as LV relaxation becomes impaired or LV compliance decreases and LA pressure has not become abnormally elevated, there is greater impedance to blood flow from

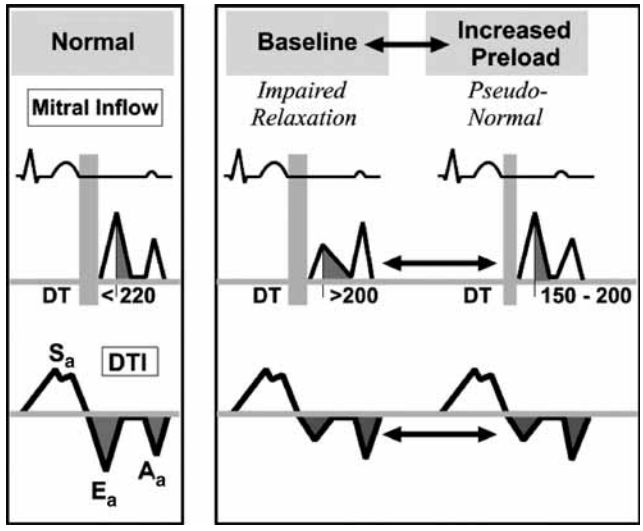

Fig. 6. Limitation of transmitral Doppler profile. Transmitral Doppler profiles showing normal and mild diastolic dysfunction profiles. The limitation of relying on transmitral flow patterns alone for the assessment of diastolic function is that a normal E:A-wave ratio can occur in patients with impaired relaxation and elevated filling pressure (right column). This ambiguity in the relationship of E:A ratio and the severity of diastolic dysfunction mandates the incorporation of other echocardiographic parameters to arrive at an accurate assessment of diastolic function. Doppler tissue imaging profiles are less influenced by loading conditions. Impaired relaxation and increased preload states of diastolic dysfunction are both associated with reduced E_a velocities.

LA to LV, manifested as a diminution in peak E-wave velocity and a slowing of deceleration. Given the slowing

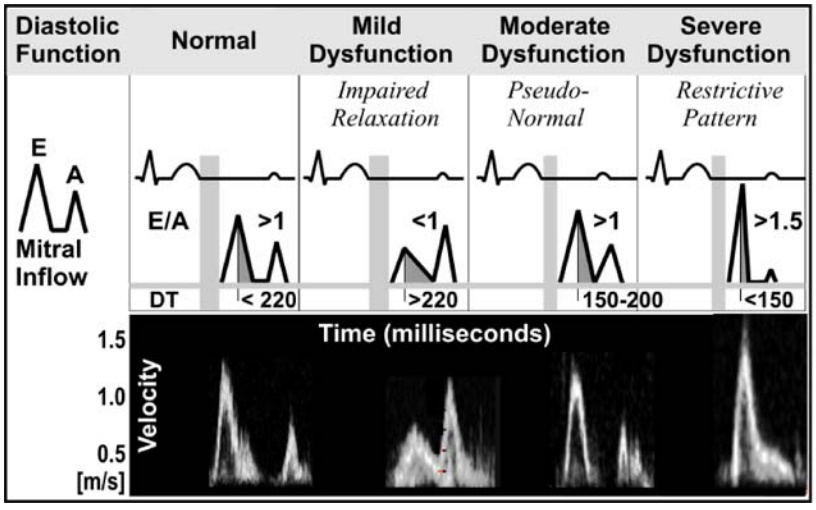

Fig. 7. Transmitral Doppler flow patterns. Transmitral Doppler flow patterns showing normal filling, impaired relaxation (A-wave > E-wave), pseudonormal filling and restrictive filling (E-wave > A-wave; increased E-wave velocity and shortened E-wave deceleration time). These patterns form the basis of grading diastolic function from mild to severe (grade 1–4).

Table 3
Stages of Diastolic Dysfunction

	Normal (young)	*Normal (adult)*	*Delayed relaxation grade 1*	*Pseudonormal filling grade 2*	*Restrictive filling grades 3–4*
E:A	>1	>1	<1	1–2	>2
EDT (ms)	<220	<220	>220	150–200	<150
IVRT (ms)	<100	<100	>100	60–100	<60
Pulm vein S/D	<1	≥1	≥1	<1	<1
Pulm vein AR (cm/s)	<35	<35	<35	>35[a]	≥25[a]
E_a (cm/s), lateral mitral annulus	>12	>8–10	<8	<8	<8
LV relaxation	Normal	Normal	↓	↓	↓
LV filling pressure	Normal	Normal	↑	↑	↑

Table modified from Garcia MJ, Thomas JD, Klein AL. New Doppler echocardiographic applications for the study of diastolic function. J Am Coll Cardio 1998;32:865–875.

[a]Unless atrial mechanical failure present.

AR, pulmonary venous peak atrial contraction reversal velocity; EDT, early left ventricular filling deceleration time; IVRT, isovolumic relaxation time; S/D, systolic-to-diastolic pulmonary venous flow ratio.

of early LV filling and the greater contribution by atrial contraction, patients with this pattern of MV inflow often are poorly tolerant of tachycardia (decreased diastolic filling period) and atrial fibrillation (loss of atrial kick). This pattern has been designated as grade 1 diastolic dysfunction. The grades of diastolic dysfunction are summarized in Table 3.

Pseudonormal MV Inflow

If elevated intracardiac filling pressures are superimposed upon impaired LV relaxation, the Doppler pattern of mitral inflow can again appear normal, with an E:A ratio greater than 1 and decreased E-wave deceleration time (Fig. 7). This occurs because increased LA pressure re-establishes a higher gradient between the LA and the LV, providing a larger pressure head to drive LV filling in early diastole. The result is a higher peak E-wave velocity and more rapid filling (decreased E-wave deceleration time). The fact that this apparently normal pattern occurs in the presence of impaired LV relaxation and elevation of left-sided filling pressures underlies the problem with using mitral inflow

profiles as the sole measure of diastolic function (Fig. 6). This pattern has been designated as grade 2 diastolic dysfunction.

Restrictive Mitral Inflow

With further progression of diastolic dysfunction and rise in filling pressures, LV filling can become restrictive with an increase in peak E-velocity (owing to a higher transmitral gradient resulting from increased LA pressures), marked shortening of the E-wave deceleration time (owing to rapid equilibration of LA and LV diastolic pressures in the noncompliant LV), and a diminutive A-wave (owing, in part, to high LV diastolic pressures and coexistent atrial systolic dysfunction). The result is a tall, thin E-wave and small A-wave with the bulk of LV filling occurring over a very brief period of time in early diastole (Fig. 7). This pattern has been designated as grade 3 diastolic dysfunction (if the pattern is reversible) or grade 4 (if the pattern is irreversible; *see* next section). The development of restrictive mitral inflow can be an ominous sign in patients with heart failure. A cohort of patients with advanced heart failure who showed an irreversibly restrictive pattern had a worse prognosis and increased mortality as compared to patients who did not have this pattern.

Altering MV Inflow Patterns

Because MV inflow, particularly the E-wave, is highly dependent on loading conditions, maneuvers that alter preload can alter patterns of mitral inflow. In addition to demonstrating the underlying pathophysiology, performing these maneuvers simultaneously with echocardiography may assist in discriminating between normal and pseudonormal filling. Decreasing LV preload (nitroglycerin administration, diuresis) is associated with a decrease in peak E-wave velocity and E-wave deceleration time. Thus, the underlying impairment of LV relaxation may be unmasked by this maneuver, with the caveat that even individuals with normal LV relaxation may appear to have an impaired relaxation pattern with excessive volume depletion. If a patient has a restrictive pattern of MV inflow, decreasing preload may cause a transition to a pseudonormal pattern. If this can be accomplished, it is associated with a better prognosis than an irreversibly restrictive pattern.

Increasing LV preload (intravenous fluid bolus, passive leg raising) increases peak E-wave velocity and decreases E-wave deceleration time. Thus, a patient with an impaired relaxation pattern at baseline may develop a pseudonormal pattern; a patient with a pseudonormal pattern may appear restrictive.

PV DOPPLER FLOW PATTERNS

Evaluation of PV flow provides further information about LV diastolic function and can be used to more accurately interpret mitral filling patterns. There are typically three components of PV flow (Fig. 8): (1) S-wave, during ventricular systole. Forward flow from the pulmonary veins to the LA is driven by atrial relaxation and apical descent of the mitral annulus during ventricular systole. There may be two components to the S-wave; (2) D-wave, during ventricular diastole. Diastolic flow is largely passive and follows mitral inflow from LA to LV; (3) Ar-wave, atrial reversal as the force of atrial contraction forces a small amount of blood retrograde from the LA to the pulmonary veins.

As with mitral inflow, the pattern of PV flow varies with age. In children and young adults, the typical pattern is S < D-wave. During adulthood, S > D is the normal pattern (Fig. 8). Impaired LV relaxation may be perceived as increased atrial afterload and lead to decreased LA compliance and impaired atrial relaxation. This is reflected by blunting of the PV S-wave such that it is lower than the D-wave. Decreased LV compliance may also lead to an increase in the peak velocity and duration of the atrial reversal wave, as blood flows preferentially into the pulmonary veins rather than into the noncompliant LV. Thus, integration of PV flow patterns may assist with the proper interpretation of mitral flow patterns in the assessment of diastolic function (Fig. 9). If a normal-appearing MV inflow pattern is accompanied by a PV pattern with S < D and/or an increased A_r-wave, it may be more correctly interpreted as pseudonormalized (Table 3).

Technical Issues in Measuring PV Flow

1. Obtain an apical four-chamber view with slight anterior angulation (Fig. 10). Color flow Doppler may be used to help localize PV flow.
2. In pulse wave Doppler mode, a 2- to 3-mm sample volume is placed 1–2 cm into the pulmonary vein. Typically the right upper pulmonary vein is most optimally aligned with the transducer beam in this view, but all may be sampled to obtain the best spectral pattern.
3. The velocity filter setting should be as low as possible. If the Doppler signal is weak or incomplete, a 4- to 5-mm sample volume, higher Doppler gain or supine positioning of the patient may be helpful.

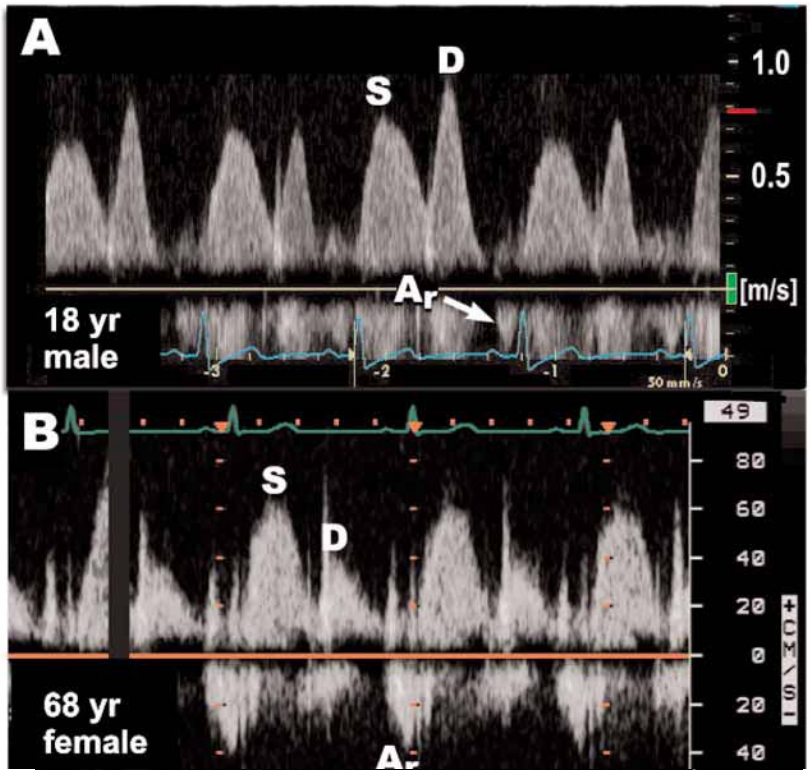

Fig. 8. Normal pulmonary venous flow patterns. Doppler patterns of pulmonary venous flow in a normal 18-yr-old male (**A**) and a normal 68-yr-old female. Note the typical S < D pattern in children and young adults and the typical S > D pattern in older adulthood.

ISOVOLUMIC RELAXATION TIME

The isovolumic relaxation time (IVRT) of the LV is the time interval between aortic valve closure to MV opening and the start of transmitral flow. This is influenced by the rate of LV relaxation and LA pressure. Excessive prolongation of IVRT (>100 ms) is associated with impaired relaxation, whereas abnormal shortening of IVRT (<60 ms) is associated with elevation of LA pressure. This time interval is typically measured from Doppler recordings, which display the transient of aortic valve closure and the spectral pattern of mitral inflow.

Technical Issues in Recording IVRT

1. From an apical view using PW Doppler, position a 3- to 4-mm sample volume near the mitral leaflet tips to display mitral inflow. The transducer beam is then angulated toward the LV outflow tract until the transient of aortic valve closure appears above and below the baseline. IVRT is measured as the time interval between the aortic valve transient and the onset of mitral inflow (Fig. 11).
2. If the results are suboptimal, CW Doppler can be used with similar positioning, to simultaneously record aortic and mitral flow. IVRT is measured as the time between the cessation of aortic flow and the onset of mitral flow.

ADVANCEMENTS IN THE ASSESSMENT OF DIASTOLIC FUNCTION

Doppler Tissue Imaging

Doppler tissue imaging (DTI), also known as tissue Doppler imaging (TDI), enables the measurement of the high amplitude, low velocity signals of myocardial motion, rather than blood flow velocities as with standard Doppler interrogation. This is accomplished by bypassing the high pass filter (to pick up strong signal reflections from the myocardium) and using low gain amplification (to eliminate weaker blood flow signals) (Fig. 12; *see* companion DVD for corresponding video). The main advantage of DTI information is that it is less load-dependant than standard Doppler. The assessment of early myocardial relaxation velocities provides an additional window on LV diastolic function

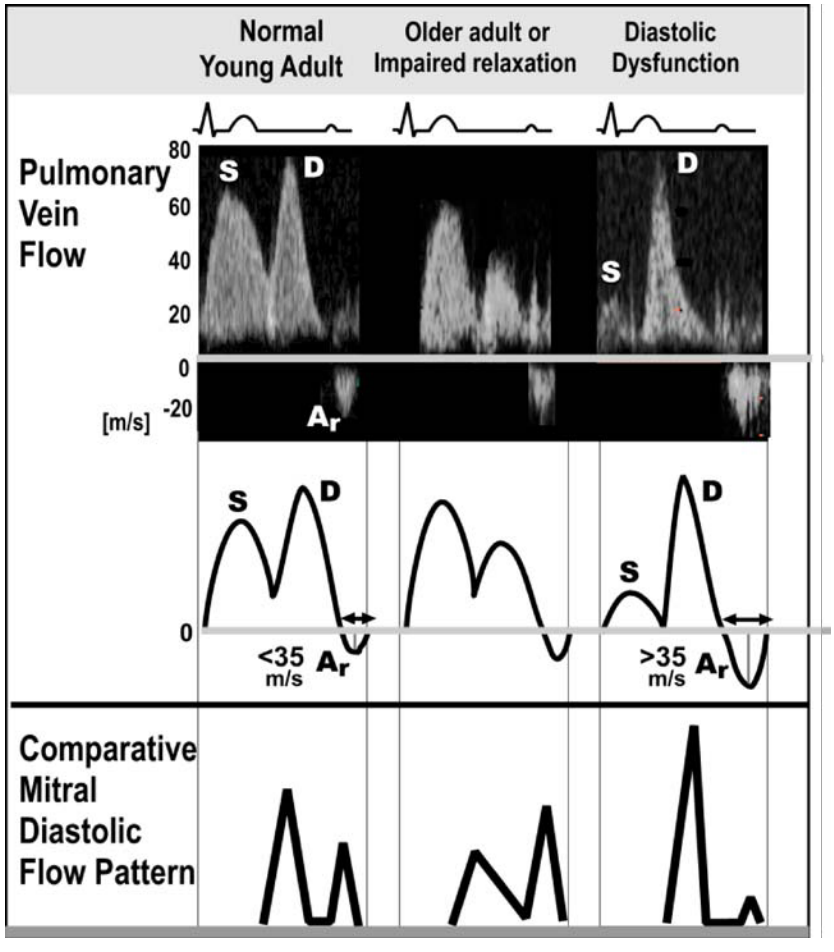

Fig. 9. Pulmonary venous flow: normal vs dysfunction. Doppler patterns of pulmonary venous flow. Abnormal pulmonary venous flow is characterized by blunting of the systolic wave and increased atrial reversal velocity and/or duration. S, systolic flow; D, diastolic flow; A_r, atrial reversal.

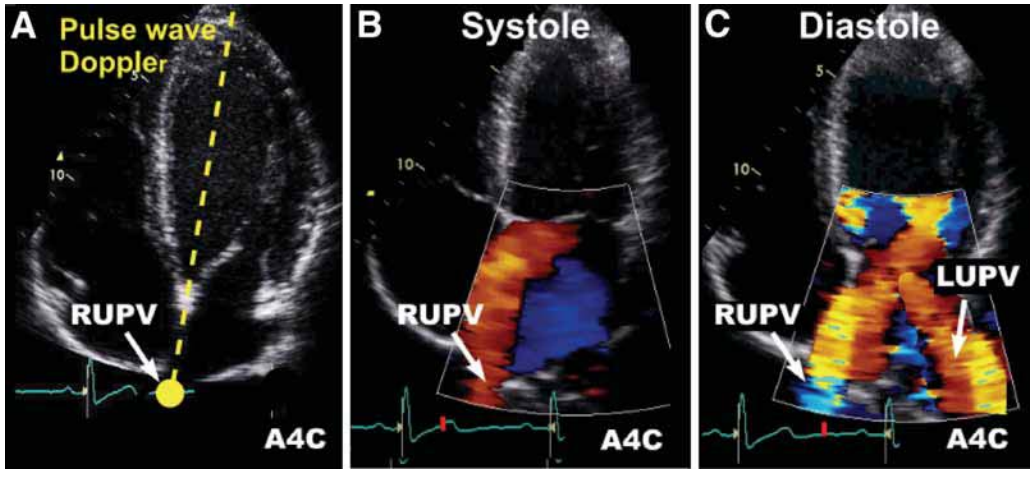

Fig. 10. Measuring pulmonary venous flow (*see* Technical Issues in Measuring PV Flow section for explanation).

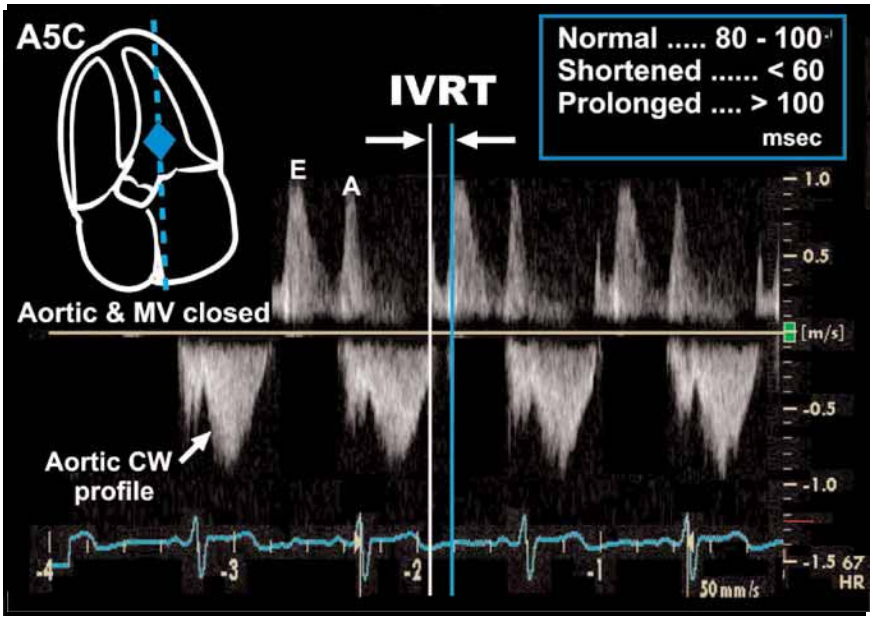

Fig. 11. Recording isovolumic relaxation time (IVRT) (*see* Technical Issues in Recording IVRT section for explanation).

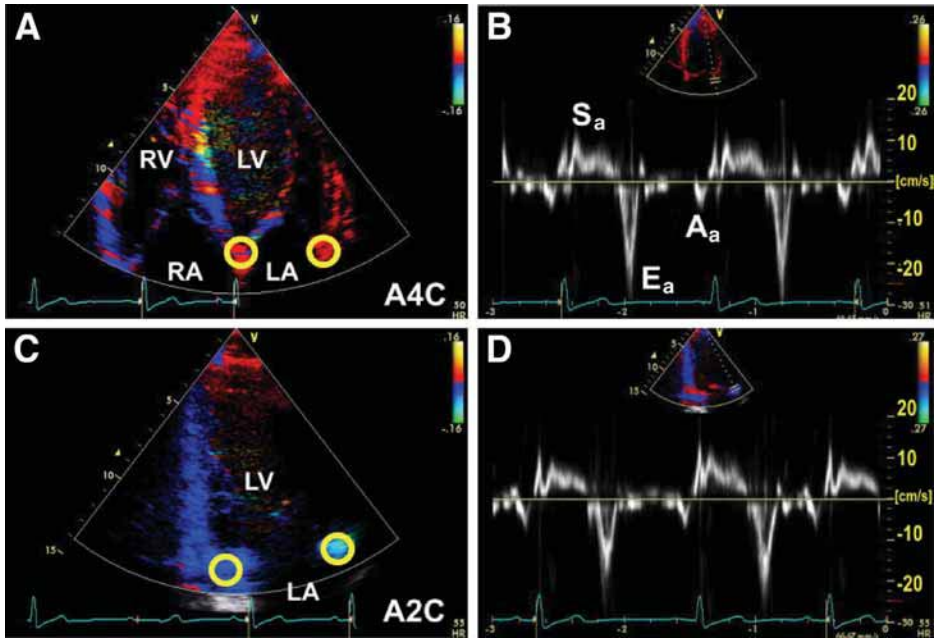

Fig. 12. Doppler tissue imaging technique (see Technical Issues in Performing Doppler Tissue Imaging section for explanation). (Please *see* companion DVD for corresponding video.)

in a manner complementary to evaluation of mitral inflow and PV flow patterns (Table 3).

Spectral waveforms from pulse wave tissue Doppler are used to measure peak myocardial velocities. The apical views allow the most favorable alignment of the transducer beam to the longitudinal motion of the heart. The sample volume is typically placed in the ventricular myocardium immediately adjacent to the mitral annulus to minimize contamination from the translational and rotational motion of the heart and to maximize the longitudinal excursion of the annulus as it descends toward the apex in systole and ascends away from the

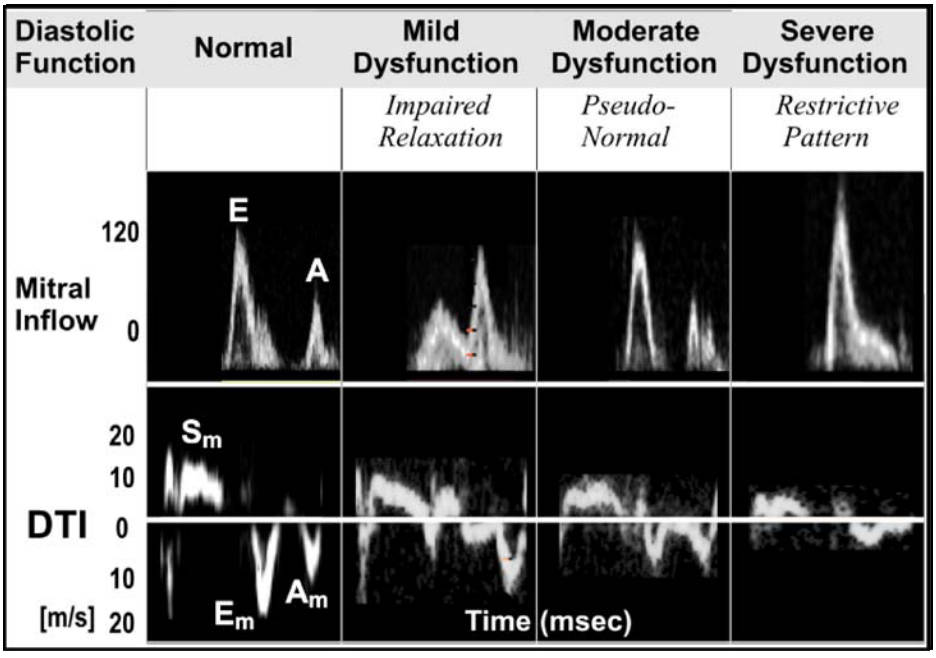

Fig. 13. Integrating mitral inflow Doppler and Doppler tissue imaging. Pulsed wave tissue Doppler imaging spectral waveforms with simultaneous standard Doppler mitral valve inflow. In the normal heart, there is brisk early myocardial relaxation. With impaired relaxation, there is marked slowing of the early myocardial relaxation velocity. S_a, systolic myocardial tissue Doppler velocity; E_a, early myocardial relaxation velocity; A_a, myocardial velocity associated with atrial contraction.

apex in diastole. Thus, a cardiac cycle is represented by three waveforms (Fig. 12): (1) S_a, systolic myocardial velocity above the baseline; (2) E_a, early diastolic myocardial relaxation velocity below the baseline; (3) A_a, myocardial velocity associated with atrial contracation, below the baseline. The subscripts "a" for annulus or "m" for myo- cardial (E_a or E_m) or the superscript "prime" (E′) are used to differentiate tissue Doppler velocities from the corresponding standard Doppler blood flow velocities.

The peak E_a velocity is used in the analysis of LV diastolic function. This can be measured from any aspect of the mitral annulus (lateral, septal, inferior, or anterior from the apical four- and two-chamber views, respectively), however the lateral and septal velocities are most commonly employed. Owing to intrinsic differences in myocardial fiber orientation, septal E_a velocities tend to be slightly lower than lateral E_a velocities. E_a reflects the velocity of early myocardial relaxation as the mitral annulus ascends from the apex toward the base in association with early rapid LV filling (E-wave). DTI has been validated against invasive measures of LV filling and has been found to correlate relatively well with tau, the time constant of isovolumic relaxation. E_a is also somewhat more robust than mitral inflow patterns under different loading conditions. Reduction in lateral E_a velocity less than 8–10 cm/sec is an indication of impaired LV relaxation (Table 3). In contrast to standard mitral flow inflow patterns, E_a velocities tend to remain consistently reduced through all phases of diastolic dysfunction (Fig. 13).

Technical Issues in Performing Doppler Tissue Imaging

1. From the apical views, decrease the image depth to focus on the LV and mitral annular region (Fig. 12).
2. Adjust the image to orient the transducer beam as parallel to the motion of the wall as possible.
3. Using the color tissue Doppler mode, place the sample volume on the ventricular side of the annulus in a position where the myocardium stays within the sample volume for a maximum amount of the cardiac cycle.
4. Use a sample volume of 3–6 mm. A smaller size may be required if LV systolic function is poor (the spectral pattern will appear unfocused). Try to optimize frame rate.
5. Switch to pulse wave DTI and record during a held breath at the end of expiration.

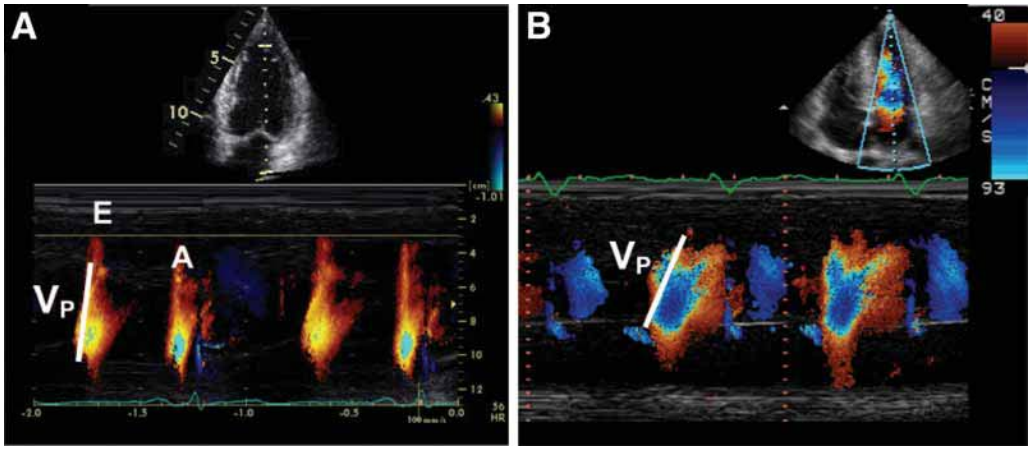

Fig. 14. Color M-mode flow propagation velocity. Color M-mode propagation velocities in a patient with normal (left) and abnormal (right) diastolic function. Vp, color M-mode color flow propagation velocity (normal Vp [cm/s] > 45; diastolic dysfunction < 45).

Novel Uses of DTI

In addition to assessing diastolic function, E_a velocities can be used to estimate LV filling pressures, to discriminate between constrictive pericarditis and restrictive cardiomyopathy, and to differentiate athlete's heart from hypertrophic cardiomyopathy (HCM).

Estimation of LV Filling Pressures

Several investigators have performed simultaneous cardiac catheterization and echocardiographic studies to estimate LV filling pressures using the ratio of the mitral inflow E-wave and the tissue Doppler E_a-wave. Different regression formulas have been proposed to calculate either LV end diastolic pressure (LVEDP) or pulmonary capillary wedge pressure. Perhaps more practical than specific regression formulae is the correlation with the ratio of E/E_a alone.

E/E_a more than 10–15 correlates with an elevated LVEDP (>12 mmHg).

E/E_a less than 8 correlates with a normal LVEDP.

Differentiation Between Constrictive and Restrictive Physiology

With both constrictive pericarditis and restrictive cardiomyopathy, there is abnormal LV filling. With constrictive physiology, extrinsic factors (pericardial constraint) impede normal filling of the LV. In the case of restrictive cardiomyopathy, abnormal filling is secondary to factors intrinsic to the myocardium that cause impaired relaxation and decreased compliance. E_a velocities with constrictive pericarditis in the absence of coexistant myocardial pathology are typically normal. In contrast, E_a velocities in restrictive cardiomyopathy are typically reduced (*see* Chapter 9, Fig. 13).

Differentiation of Athletes' Hearts From HCM

Approximately 2% of elite athletes may have an increased LV wall thickness, raising the potential diagnosis of HCM. It can be clinically challenging to discriminate the physiologic hypertrophy that results from intense athletic conditioning from pathological hypertrophy. Recent studies incorporating measurement of E_a velocities may be helpful in making this differentiation. Athletes typically have brisk E_a velocities, reflective of a highly compliant LV, whereas individuals with HCM typically have reduced E_a velocities owing to decreased LV compliance and impaired LV relaxation (*see* Chapter 9, Table 14).

Color M-Mode

Color M-mode Doppler imaging from the apical four-chamber window is an alternative method to relate mitral inflow to LV relaxation, again in a less load-dependent manner than standard transmitral Doppler. The velocity of propagation of flow (Vp) from the LV base toward the apex is measured in early diastole. The slope of this flow signal is thought to represent the LV intraventricular gradient, influenced by active recoil (suction forces) and relaxation. This is accomplished by measuring the slope of the leading edge of flow (the transition from black to color) or an isovelocity line (e.g., the first aliasing velocity line). Normal Vp exceeds 55 cm per second. Vp less than 45 cm per second is thought to indicate impaired relaxation. In real practice, precise measurement of Vp has proven challenging, thus the most common application of this technology is as a qualitative measure of diastolic function. If the Vp slope appears nearly upright by visual estimate, this is an

indication of preserved diastolic function. If the Vp slope appears quite blunted, this indicates impaired diastolic function (Fig. 14).

COMPREHENSIVE ECHOCARDIOGRAPHIC ASSESSMENT OF DIASTOLIC FUNCTION

Accurate assessment of diastolic function requires the assessment of multiple parameters. By integrating information gleaned from mitral inflow patterns, PV flow, and TDI, as well as looking for surrogate evidence of decreased LV compliance, such as left ventricular hypertrophy or LA enlargement, the overall state of LV diastolic function may be best evaluated (Table 3).

Diastolic Function Assessment Algorithm

1. Assess overall LV and RV systolic function from two-dimensional images. "Yes" answers increase the likelihood of diastolic dysfunction.
   a. Are chamber sizes normal?
      i. Is LA enlargement seen?
      ii. Is LVH present?
      iii. Is LV systolic function abnormal?
   b. Standard Doppler interrogation of mitral inflow and PV flow.
      i. If mitral inflow appears normal, integrate the above information and assess the PV flow pattern to differentiate from a pseudonormal pattern.
   c. DTI to measure E_a.
   d. Color M-mode of mitral inflow with qualitative assessment of Vp.
   e. If further investigation is required, consider:
      i. Assessment of mitral filling patterns in response to alterations in loading conditions (administration of sublingual nitroglycerin to decrease preload or passive leg raising to increase preload).
      ii. Response to exercise.
      iii. Estimation of LV filling pressures using E/E_a.
      iv. Measurement of IVRT.

SUGGESTED READING

Appleton CP, Hatle LK, Popp RL. Relation of transmitral flow velocity patterns to left ventricular diastolic function: new insights from a combined hemodynamic and Doppler echocardiographic study. J Am Coll Cardiol 1988;12:426–440.

Appleton CP, Jensen JL, Hatle LK, Oh JK. Doppler evaluation of left and right ventricular diastolic function: a technical guide for obtaining optimal flow velocity recordings. J Am Soc Echocardiogr 1997;10:271–292.

Cardim N, Oliveira AG, Longo S, et al. Doppler tissue imaging: regional myocardial function in hypertrophic cardiomyopathy and in athlete's heart. J Am Soc Echocardiogr 2003;16: 223–232.

Cohen GI, Pietrolungo JF, Thomas JD, Klein AL. A practical guide to assessment of ventricular diastolic function using Doppler echocardiography. J Am Coll Cardiol 1996;27:1753–1760.

Drazner MH, Hamilton MA, Fonarow G, Creaser J, Flavell C, Stevenson LW. Relationship between right and left-sided filling pressures in 1000 patients with advanced heart failure. J Heart Lung Transplant 1999;18:1126–1132.

Farias CA, Rodriguez L, Garcia MJ, Sun JP, Klein AL, Thomas JD. Assessment of diastolic function by tissue Doppler echocardiography: comparison with standard transmitral and pulmonary venous flow. J Am Soc Echocardiogr 1999; 12:609–617.

Garcia MJ, Rodriguez L, Ares M, Griffin BP, Thomas JD, Klein AL. Differentiation of constrictive pericarditis from restrictive cardiomyopathy: assessment of left ventricular diastolic velocities in longitudinal axis by Doppler tissue imaging. J Am Coll Cardiol 1996;27:108–114.

Garcia MJ, Thomas JD, Klein AL. New Doppler echocardiographic applications for the study of diastolic function. J Am Coll Cardiol 1998;32:865–875.

Giannuzzi P, Imparato A, Temporelli PL, et al. Doppler-derived mitral deceleration time of early filling as a strong predictor of pulmonary capillary wedge pressure in postinfarction patients with left ventricular systolic dysfunction. J Am Coll Cardiol 1994;23:1630–1637.

Nagueh SF, Middleton KJ, Kopelen HA, Zoghbi WA, Quinones MA. Doppler tissue imaging: a noninvasive technique for evaluation of left ventricular relaxation and estimation of filling pressures. J Am Coll Cardiol 1997;30:1527–1533.

Nagueh SF, Lakkis NM, Middleton KJ, Spencer WH, 3rd, Zoghbi WA, Quinones MA. Doppler estimation of left ventricular filling pressures in patients with hypertrophic cardiomyopathy. Circulation 1999;99:254–261.

Nishimura RA, Tajik AJ. Evaluation of diastolic filling of left ventricle in health and disease: Doppler echocardiography is the clinician's Rosetta Stone. J Am Coll Cardiol 1997;30:8–18.

Pinamonti B, Zecchin M, Di Lenarda A, Gregori D, Sinagra G, Camerini F. Persistence of restrictive left ventricular filling pattern in dilated cardiomyopathy: an ominous prognostic sign. J Am Coll Cardiol 1997;29:604–612.

Rakowski H, Appleton C, Chan KL, et al. Canadian consensus recommendations for the measurement and reporting of diastolic dysfunction by echocardiography: from the Investigators of Consensus on Diastolic Dysfunction by Echocardiography. J Am Soc Echocardiogr 1996;9:736–760.

Sohn DW, Chai IH, Lee DJ, et al. Assessment of mitral annulus velocity by Doppler tissue imaging in the evaluation of left ventricular diastolic function. J Am Coll Cardiol 1997;30: 474–480.

Yamada H, Oki T, Mishiro Y, Tabata T, et al. Effect of aging on diastolic left ventricular myocardial velocities measured by pulsed tissue Doppler imaging in healthy subjects. J Am Soc Echocardiogr 1999;12:574–581.

Yamamoto K, Nishimura RA, Chaliki HP, Appleton CP, Holmes DR, Jr., Redfield MM. Determination of left ventricular filling pressure by Doppler echocardiography in patients with coronary artery disease: critical role of left ventricular systolic function. J Am Coll Cardiol 1997;30: 1819–1826.

7 Echocardiography in Myocardial Infarction

Justina C. Wu, MD, PhD

Contents

CASE PRESENTATION

An 80-yr-old male with a history of hypertension who presented with acute onset of chest pain associated with mild shortness of breath and palpitations, lasting a total of 20 min by the time he was transported to the hospital. On physical exam he appeared uncomfortable, diaphoretic, tachycardic, and with a blood pressure of 90/60 mmHg. Lungs were clear to auscultation, and a cardiac exam revealed an S3 without murmurs or rub. His electrocardiogram (ECG) displayed 5-mm ST elevations in leads V1-5 with lesser elevations in the inferior leads, and the initial chest X-ray showed clear lungs. Cardiac enzymes were sent, and the patient started on aspirin and heparin in addition to lytic therapy with Retavase®.

The patient was ultimately transferred to a tertiary care institution for cardiac catheterization. He became chest pain-free en route, but catheterization showed a tight proximal left anterior descending (LAD) stenosis, which was balloon-angioplastied and stented. However, only partial flow was noted at the end of the procedure. Left ventriculogram was not done because of an elevated creatinine level, and instead a transthoracic echocardiography (TTE) was performed.

Figure 1A,B (please *see* companion DVD for corresponding video) shows the typical immediate sequelae of an acute anteroseptal myocardial infarction (MI). Note: (1) left ventricular hypertrophy, as indicated by wall thicknesses of more than 11 mm in diastole, indicative of long-standing hypertension; (2) normal sized left ventricle (LV) (end-diastolic diameter <5.6 cm at the base in parasternal long axis), but decreased shortening fraction (increased end-systolic diameter >4.0 cm); (3) absence of myocardial thickening in systole (akinesis) of the anterior and anteroseptal wall from midventricle to apex. In an ongoing untreated MI involving only one coronary artery territory, the other territories with preserved coronary blood supply will often be hyperdynamic.

From: *Contemporary Cardiology: Essential Echocardiography: A Practical Handbook With DVD*
Edited by: S. D. Solomon © Humana Press, Totowa, NJ

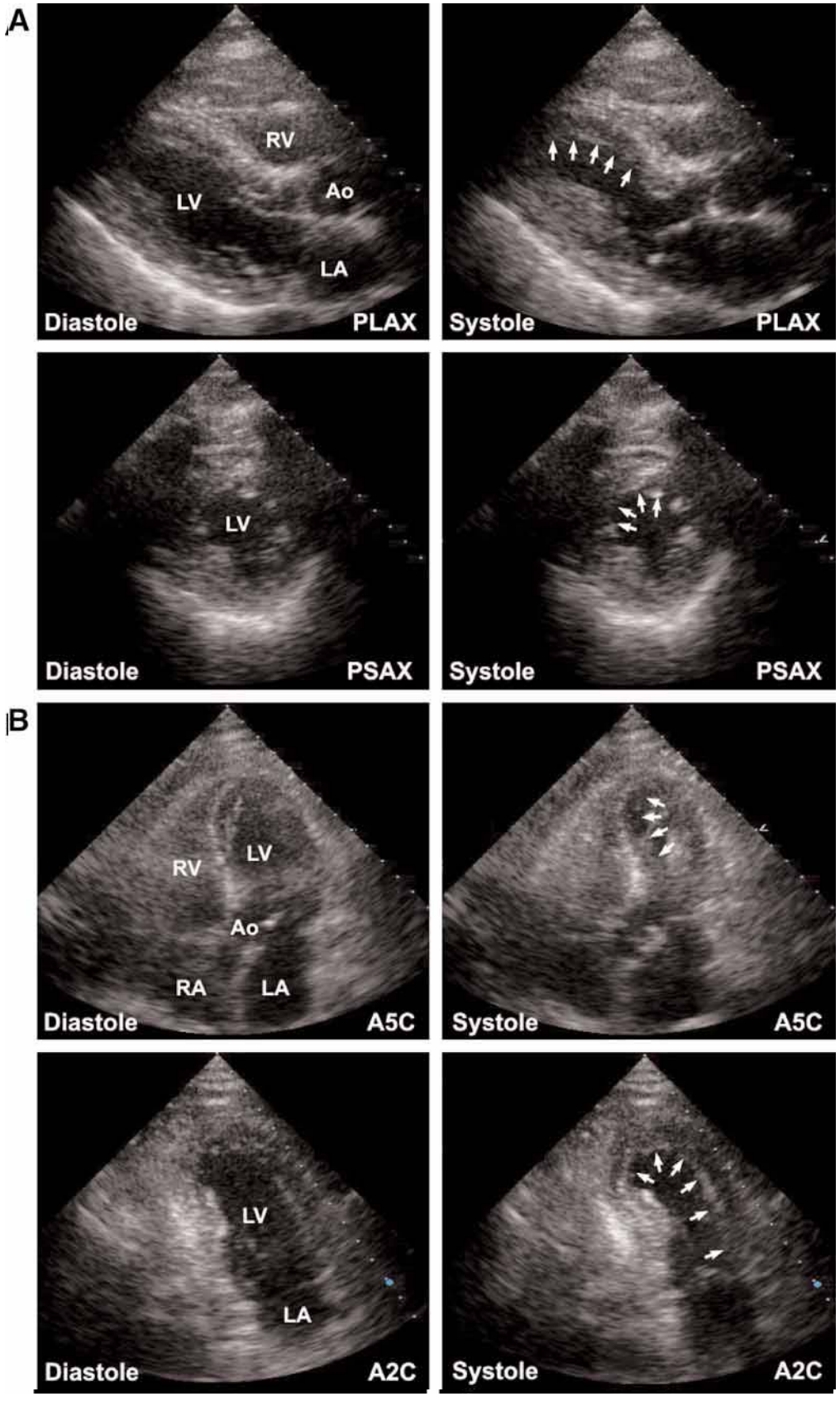

Fig. 1. Case presentation: 80-yr-old male with hypertension and acute-onset chest pain. Parasternal long-axis (PLAX) and short-axis (PSAX) images from an 80-yr-old male with acute-onset chest pains. Note marked antero-septal hypokinesis (arrows) of left

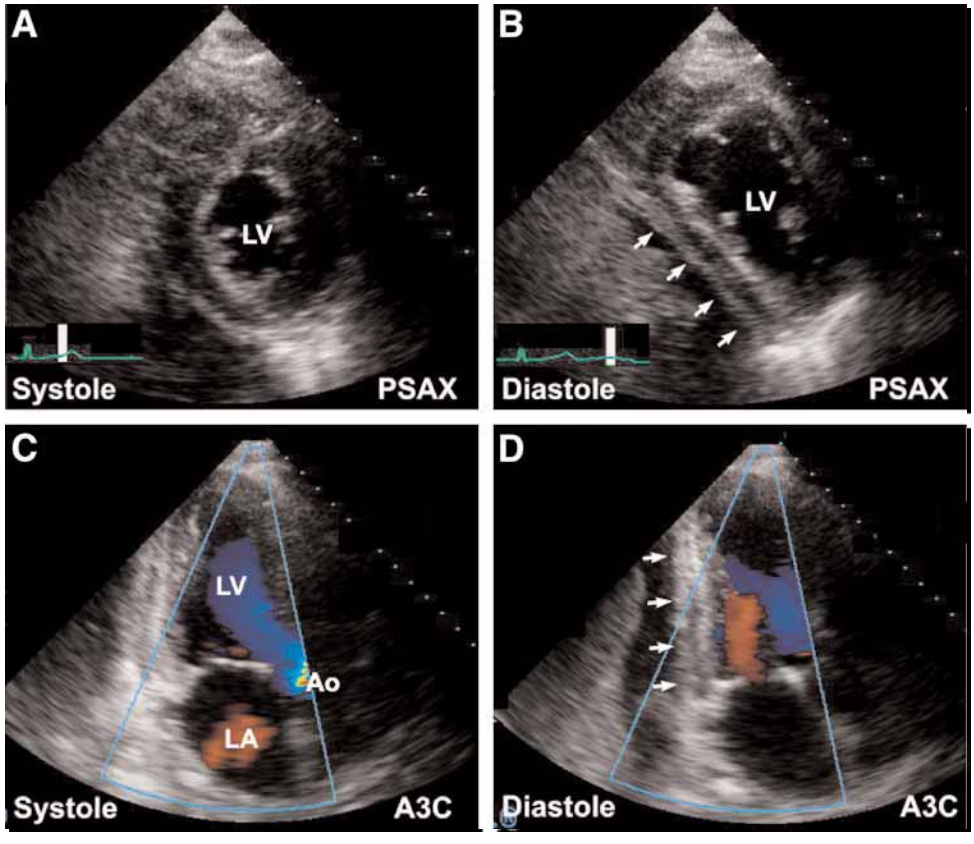

Fig. 2. Pseudo-dyskinesis in 54-yr-old male with end-stage liver disease. Left ventricular walls in this 54-yr-old male with end-stage cirrhosis owing to chronic alcohol use and hepatitis C virus infection was normal during diastole (**A–C**). Apparent hypokinesis/dyskinesis in the postero-inferior walls (**B**,**D**, arrows) was a result of external pressure from tense ascites secondary to his end-stage liver disease. (Please *see* companion DVD for corresponding video.)

ECHOCARDIOGRAPHIC FINDINGS IN ACUTE MI

Wall Motion Abnormalities

Among the earliest detectable changes in myocardial ischemia or an acute MI are regional LV and potentially also right ventricular wall motion abnormalities. The LV can be divided into 17 anatomic segments, which can be viewed as a composite from the standard echocardiographic views, and have standardized nomenclature as recommended by the American Heart Association (AHA) (*see* Chapter 5, Figs. 1 and 10). Normal wall motion (normally kinetic segments) is seen as wall thickening, caused by the contraction of individual myocardial fibers; on echocardiography, this is seen as the radial distance between the epi- and endocardial borders, which increases by at least 10–20% during systole. Abnormal wall motion owing to insufficient blood supply to the myocardium may be graded as hypokinetic (thickening, but less than normal), akinetic (no thickening), and dyskinetic or aneurysmal (no thickening, with outward movement of the segment during systole, owing to increased intraventricular pressure on a scarred and noncontractile area of myocardial fibrosis). In general, myocardium that is transmurally infarcted tends to have more severe dysfunction, with akinetic or dyskinetic motion.

It is important to carefully distinguish between wall thickening, as opposed to just epicardial or endocardial border movement during systole. Pitfalls in diagnosing wall motion abnormalities abound: these include both false-positives owing to poor visualization of the endocardium (the artifact of echo "dropout"), superior angulation of the probe such that the membranous, nonmuscular portion of the upper interventricular septum is misinterpreted as an infarct, extracardiac compression of the inferior wall by ascites or abdominal contents ("pseudodyskinesis," *see* Fig. 2; please *see* companion DVD for corresponding video), and para-

Fig. 1. *(Continued)* ventricular regions supplied by the left anterior descending coronary artery during systole. Compare these regions to the segments and coronary artery territories depicted in Figs. 3–5. (Please *see* companion DVD for corresponding video.)

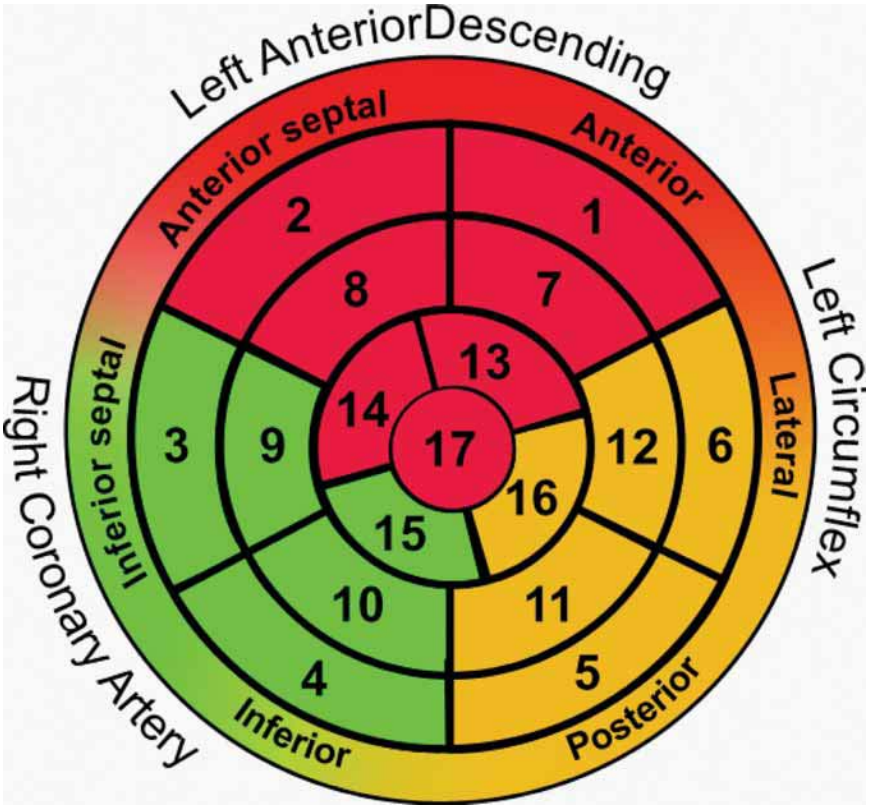

Fig. 3. "Bull's eye" left ventricular segmentation (American Heart Association [AHA]) with corresponding coronary artery territories. "Bull's eye" left ventricular segmentation (AHA nomenclature) with corresponding coronary artery supply. There are six basal segments (1–6), beginning with the antero-basal segment, and numbering in an anti-clockwise direction The next six middle segments (7–12) follow the same pattern, followed by the next four apical segments, and the last segment (17) occupying the tip. Compare this to the anatomical schema shown in Figs. 4 and 5.

doxical or dissynchronous septal motion owing to bundle branch blocks or postsurgical states. False-negatives, i.e., missing a wall motion abnormality that is present, can also occur owing to poor image quality or off-axis imaging. In some cases, the injection of an intravenous contrast agent can help delineate endocardial borders.

The main epicardial coronary arteries supply distinct territories that should be individually evaluated during the ultrasound exam. In general, the LV can be divided into anterior, inferior, septal, and lateral quadrants. At the basal and midventricular levels, the septal and lateral walls are further subdivided into anterior and inferior sections. (Many cardiologists refer to the basal-most and more lateral portion of the inferior wall as the "posterior" wall.) Each wall is further divided along the long-axis into basal, mid, and apical thirds, with the distal apex designated as a separate segment, giving a total of 17 wall segments under the AHA scheme (Fig. 3; Chapter 5, Figs. 1 and 10).

Coronary Artery Territories

The majority of the blood supply to the heart is from the left main coronary artery, which normally arises from the left coronary cusp and divides into the LAD artery and left circumflex (LCx) (*see* Fig. 4). The LAD supplies most of the anterior ventricular wall (proceeding from base to apex, segments 1, 7, 13 [Fig. 5], and its septal branches also supply the anterior two-thirds of the septum [segments 2, 8, 14]). In addition, diagonal branches of the LAD supply the anterolateral wall (segments 6, 12). Large LADs can occasionally "wrap around" the apex of the heart and supply the distalmost portion of the inferior wall (segments 15, 17). The LCx runs in the atrioventricular groove and its branches (obtuse marginals) supply the inferolateral and lateral wall (segments 5, 11, 16). The right coronary artery (RCA) arises from the right coronary cusp, and supplies blood to the inferior one-third of the septum and the inferior wall (segments 3, 9, 14). It also supplies the right ventricle (RV) as well.

In an acute MI, a blockage in the coronary artery owing to a ruptured plaque and intraluminal thrombus causes partial or complete occlusion of the arterial lumen. This in turn reduces blood flow to the supplied segments, reduces contraction (and relaxation) of

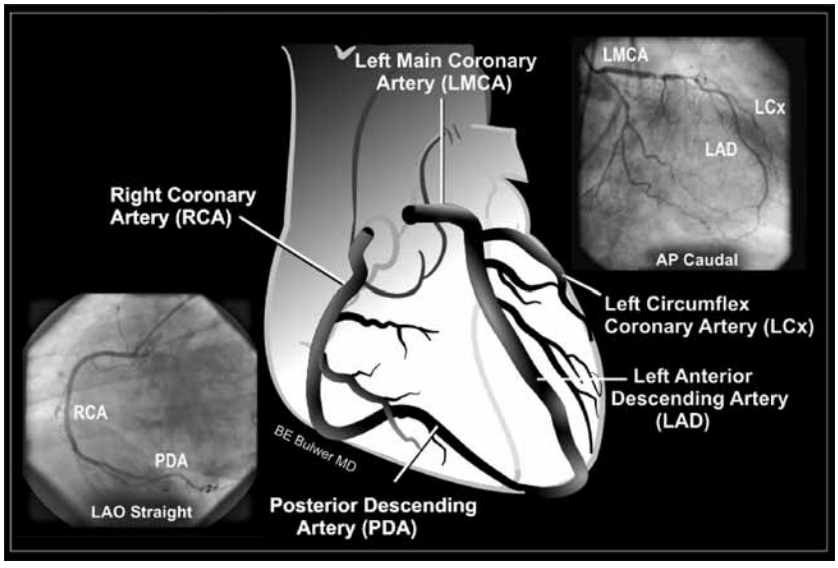

Fig. 4. Coronary blood supply. Anatomical sketch depicting coronary blood supply. Still frames of right and left coronary angiograms appear as inserts. These main epicardial arteries give rise to intramural branches that further subdivide into subepicardial and subendocardial arterioles and capillary plexuses. In the normal heart, anastomotic branches and networks connect the major coronary arteries. These serve as the framework for collateral circulation development following total or near-total occlusion of a major epicardial artery.

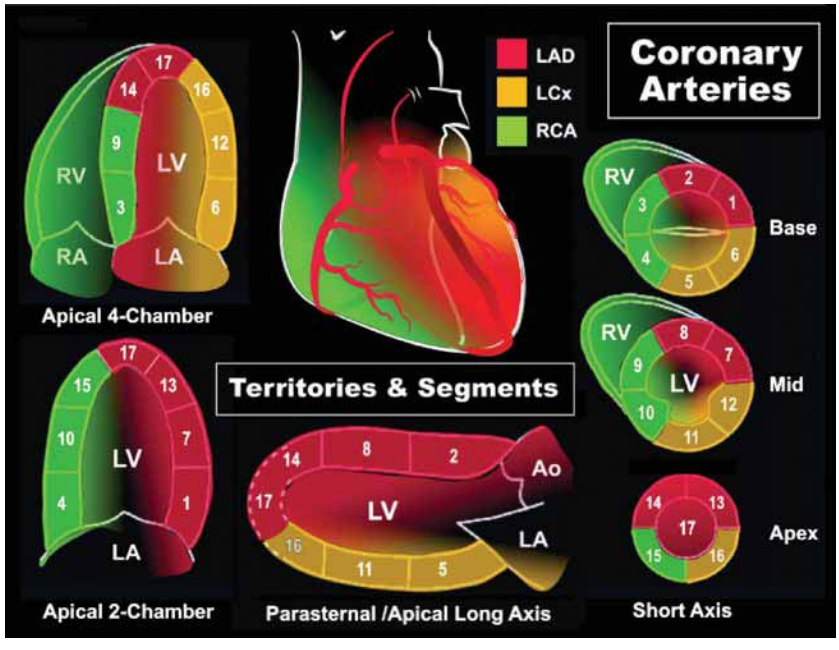

Fig. 5. Coronary artery territories and segments. Anatomical left ventricular segments used in reporting regional wall motion (American Heart Association classification) and their corresponding blood supply. Significant overlap and congenital variations in coronary blood supply can occur.

individual myocytes, and thereby causes a wall motion abnormality in the respective segment. At least a 70% reduction in cross-sectional diameter is required before the stenosis becomes hemodynamically significant. A proximal lesion will tend to affect more territory, i.e., basal to apical segments, whereas a more distal blockage will affect only more apical segments. An acute left main coronary artery occlusion can be lethal, as it supplies an extensive territory, and only the inferior septum and inferior wall would be spared. A lesion in the

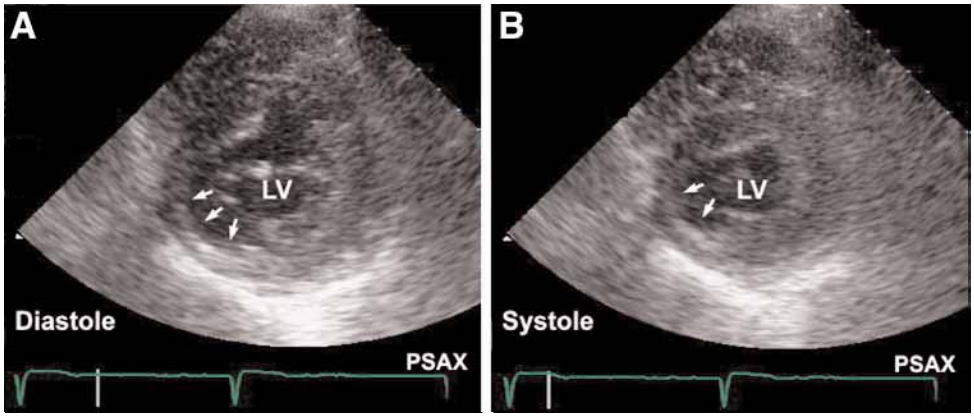

Fig. 6. An 89-yr-old male with multiple malignancies and pre-existing coronary artery disease. This 89-yr-old male with three-vessel disease and multiple malignancies presented with chest pains and dyspnea. Diastolic images show infero-postero basal hypokinesis that were less apparent during systole. Collateral circulation develops in response to significant ischemia, and make a significant contribution to blood flow and improved ventricular function.

Table 1
Utility of Echocardiography in Detecting Complications of Myocardial Infarction

Early complications
Regional wall motion abnormalities
Infarct expansion
Right ventricular infarction
Pericardial effusion
Mitral regurgitation
Papillary muscle rupture
Ventricular septal defect
Ventricular free wall rupture ± pseudoaneurysm
Late complications
Ischemic cardiomyopathy ± mitral regurgitation
Intracavitary thrombus, esp. ventricular
Left ventricular aneurysm
Pericardial effusion

proximal RCA can additionally cause RV dysfunction and infarction, which can contribute to hypotension during an inferior MI. When the RV is infarcted, RV dilation, RV segmental wall motion abnormalities, and tricuspid regurgitation may be seen on echocardiography.

The presence of previously existing coronary artery disease can modify the wall motion abnormalities seen during an acute MI. Small collateral vessels from other unobstructed coronary arteries can develop and perfuse the peripheral territory of affected vessels, thus diminishing the dysfunctional territory (Fig. 6).

A wall motion score index has been developed as a scale for quantitating the extent and severity of LV systolic function. The system uses a 14 or 16 segment division of the LV (similar to the AHA system previously detailed), and assigns a number to each wall segment from 0–5 (0, hyperkinetic; 1, normal; 2, hypokinetic; 3, akinetic; 4, dyskinetic; 5, aneurysmal [*see* Chapter 5, Fig. 1B]). The wall motion score index score is equal to the sum of these numbers/number of segments visualized, such that a normokinetic ventricle should have a score of 1.0. This score has prognostic value, as a higher score is correlated with morbidity and mortality following MI.

The Role of Echo in Evaluating Chest Pain

Echocardiography is often called into use during episodes of chest pain to determine whether ischemia is the cause of the chest pain, as opposed to a noncardiac cause. Echocardiography—specifically transthoracic studies—can play a crucial role in acute MI. This is especially true for detecting early and late complications of MI (Table 1). Wall motion abnormalities are pathognomic of ischemia or early infarct, and have been shown to precede ECG changes and chest pain. However, it should be kept in mind that smaller (subendocardial) coronary arteries can cause more subtle or more localized wall motion abnormalities, and thus the sensitivity of echocardiography for subendocardial ischemia is reduced. However, in the absence of visualized wall motion abnormalities, other causes of chest pain should be considered. Although noncardiac chest pain is frequently the case, other etiologies such as aortic or coronary artery dissection, pericarditis, myocarditis, and endocarditis should be considered in the differential diagnosis.

INDICATIONS FOR TRANSTHORACIC ECHOCARDIOGRAPHY DURING AND AFTER MI

When is an echocardiogram of clinical utility in the setting of an acute MI? Simply stated, TTE is appropriate when (1) the diagnosis is unclear, (2) complications of MI are suspected, and (3) the results add information that may be used to risk-stratify a patient and guide future therapy.

In the uncomplicated acute MI, symptoms are the direct result of ongoing ischemia, which causes chest pain, as well as systolic and diastolic dysfunction. The segmental myocardial dysfunction can be extensive enough to cause a drop in cardiac output, leading to left-sided (and occasionally right-sided) heart failure. In this situation, the diagnosis is clear from a focused history, physical, and ECG, and the first priority should be to stabilize the patient with medical therapy, then proceed as soon as possible to primary revascularization strategies, i.e., thrombolysis and/or angioplasty. Obtaining an echocardiogram in the setting of an uncomplicated MI would only delay appropriate therapy.

However, if the patient had persistent or recurrent chest pain, ECG changes, hypotension, a new murmur, congestive heart failure, stroke, or a late tachyarrhythmia, an echocardiogram would be crucial to rule out serious post-MI complications in the acute and chronic setting (discussed in the remainder of this chapter).

In this patient's case, a TTE was ordered after the angioplasty to evaluate LV ejection fraction (EF), because a left ventriculogram was not performed during his catheterization. Of note, an echocardiogram is not automatically indicated in all postinfarct patients for risk stratification; if there is already enough clinical information from the patient's history, physical, and available data (e.g., ventriculogram) to estimate postinfarct cardiac function and guide therapy, echocardiography may be redundant. For instance, 93–98% of patients with interpretable EKGs, no history of Q-wave MI or congestive heart failure, and an index MI that is not a Q-wave or anterior infarction will have LVEFs more than 40% (Krumholz et al. and Silver et al.). However, this clinical predictor of EF has only been applied to elderly (≥65 yr old) patients, and certain conditions (presentation >6 h after the onset of chest pain, a history of coronary artery bypass surgery, and diabetes mellitus) invalidate the rule.

Subacute Complications

Echocardiography is useful for detecting negative sequelae in the first 1–3 wk after MI. Many of these complications are associated with more extensive Q-wave or transmural infarcts, and their cumulative incidence appears to be decreasing in the current era of reperfusion by angioplasty or thrombolysis. Nevertheless, when they occur, they are often heralded by abrupt clinical decline (hypotension and flash pulmonary edema, i.e., cardiogenic shock), and echocardiography can be the key to a swift diagnosis.

Acute Severe Mitral Regurgitation

Acute severe mitral regurgitation (MR) is caused by infarct and subsequent rupture of the chordae tendinae (Fig. 7), a papillary muscle (Fig. 8; please *see* companion DVD for corresponding video), or a muscle head.

Clinically a new harsh holosystolic murmur may be appreciated, although if the patient is extremely hypotensive and in cardiac shock, one may not be appreciated. Because the anterolateral papillary muscle receives dual blood supply from both the LAD (diagonals) and LCx, it is far less likely to rupture than the posteromedial papillary muscle, which is supplied mainly by the RCA (posterior descending artery) alone. Hence, papillary muscle rupture is seen more frequently with inferior infarcts, and more frequently involves the posterior leaflet (although there is crossover between chordae from individual papillary muscles and the corresponding leaflet). It is more common to see one head, or tip, of a papillary muscle disrupted, rather than the entire muscle trunk.

By two-dimensional (2D) echocardiography, one will see a flail (or partially flail) leaflet corresponding to the ruptured supporting muscle and chordae, which prolapses into the left atrium during systole. A triangular or pyramidal mobile echodensity, which represents the head of the papillary muscle, attached to the tip of the flail leaflet is pathognomic. Color Doppler will usually show severe MR, which can be extremely eccentrically directed away from the defective leaflet. Thus, anterior flail mitral leaflets will cause the visualized MR color jet to be directed posterior and laterally; posterior flail leaflets cause an eccentric anteroseptally directed jet of MR.

Severe MR can also occur in the absence of rupture of the mitral apparatus. The mechanism involves incomplete closure of the valve, and is thought to be a result of papillary muscle dysfunction (particularly with occlusion of the LCx artery),

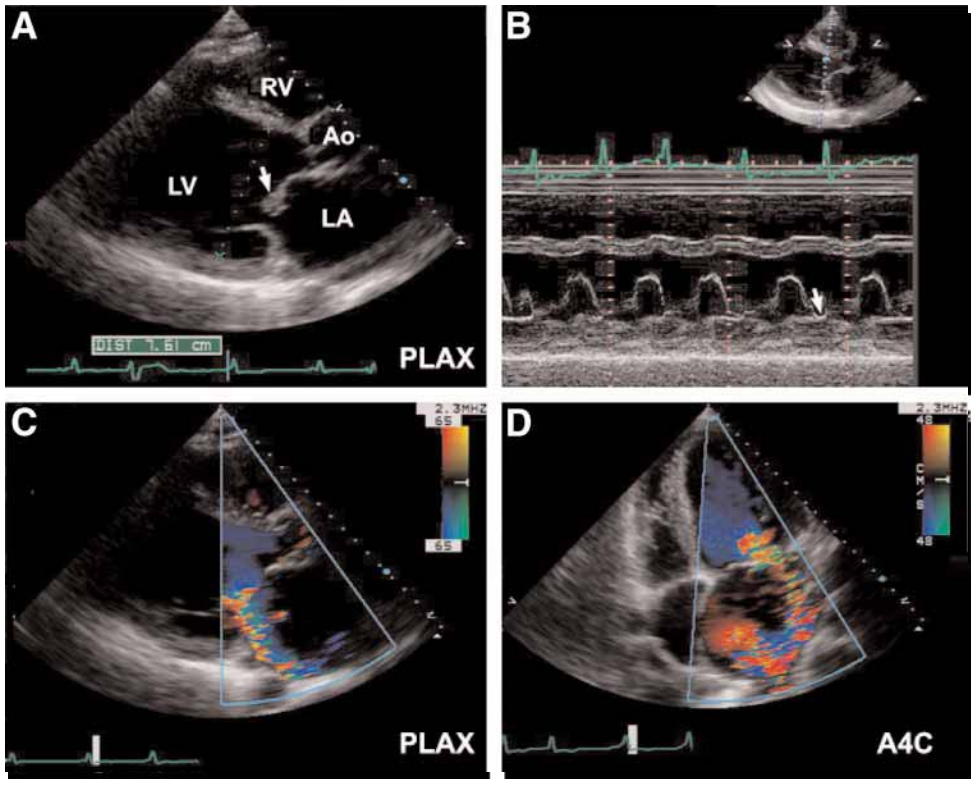

Fig. 7. Flail anterior mitral valve leaflet in a 53-yr-old male with dilated cardiomyopathy. This 53-yr-old male with dilated cardiomyopathy, mitral regurgitation, and atrial fibrillation developed partial flail of anterior mitral valve leaflet (**A**, arrow in parasternal long-axis [PLAX] view; **B**, M-mode view). Note the severe mitral regurgitation with a posteriorly directed jet (**C**,**D**).

termed "ischemic MR" and/or lateral displacement of the papillary muscles by LV dilatation (*see* "Chronic Implications" section).

Pitfalls in detecting severe MR: this eccentricity of MR jet, particularly the "wall-hugging" jets can be severe enough to cause the diagnosis to be missed entirely on echocardiography. (1) Eccentric wall jets may escape the scan plane, and when they are seen by color Doppler jet area, are usually underestimated in volume by at least 40%. Other pitfalls which can cause severe MR to be undetected on echo include: (2) "wide-open" MR with a completely incompetent valve and very high left atrial pressures, in which there is less pressure gradient and flow turbulence between the left atrium and ventricle; (3) a failing LV that is unable to generate much driving pressure for forward or backward cardiac output; (4) very transient MR in a tachycardic patient; and (5) inappropriately high- or low-gain settings. It cannot be emphasized enough that when a strong clinical suspicion for acute MR or other subacute complications for MI exists, the absence of such a finding on TTE even after diligent scanning does *not* rule out the complication. In such cases, the decision tree should rapidly progress to either a TEE for confirmatory diagnosis if the patient can be stabilized, or else directly to the operating room for exploratory surgery.

Ventricular Septal Defect

Ventricular septal defect (VSD) owing to rupture once complicated 0.5–3% of acute MIs, before the widespread use of thrombolytic therapy. The risk of developing VSD was highest in patients who were female, hypertensive, 60 yr or older, and without a previous history of angina or MI (Birnbaum). The latter risk factor is presumed to be a result of the absence of collateral flow preserving infracted segments. However, a more recent analysis of the Global Utilization of Streptokinase and Tissue Plasminogen Activator for Occluded Coronary Arteries (GUSTO-I) trial has revealed that the incidence of VSD after reperfusion therapy has declined to 0.2–0.3% in patients receiving thrombolysis, far lower than previous (Crenshaw). Infarctions of large territories, involving the RV, or those caused by total occlusion of the culprit vessel were more likely to develop VSD.

In the unreperfused patient, ruptures were rare early in the course of MI. When they did occur within the first 24 h, they are thought to be owing to large intramural hemotomas that dissect directly through a

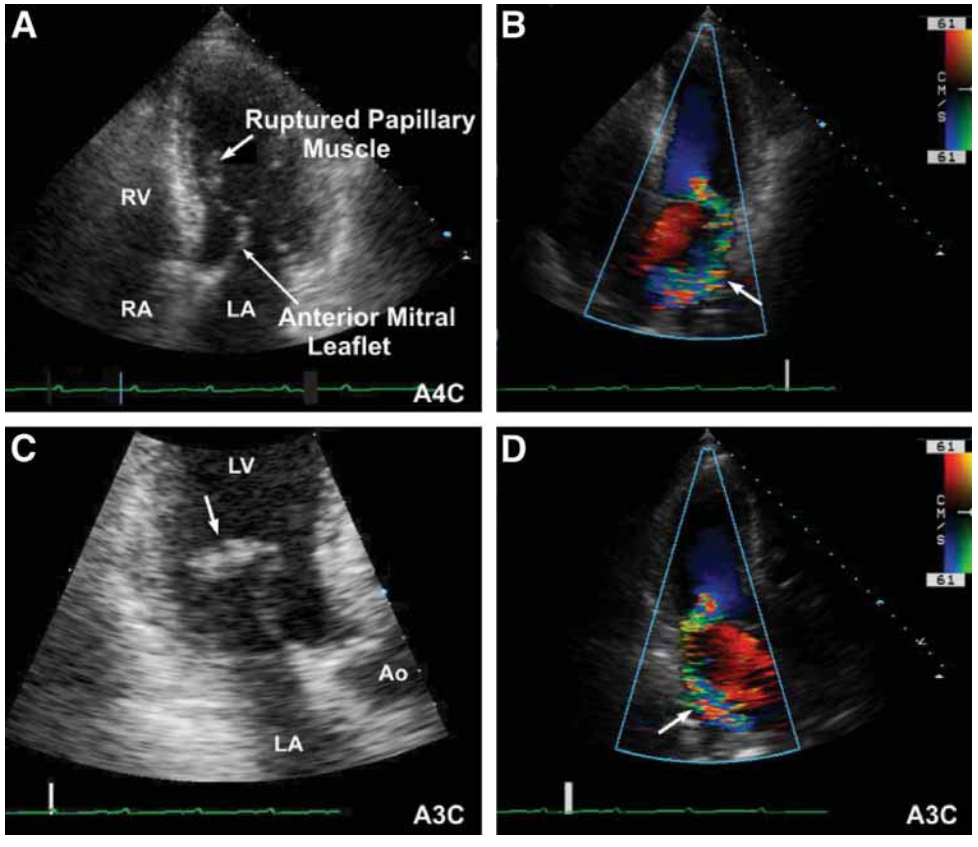

Fig. 8. Ruptured papillary muscle in a 74-yr-old male post-myocardial infarction. This 74-yr-old male presented with severe dyspnea and mitral regurgitation post-myocardial infarction. Echocardiographic images revealed avulsed papillary muscle and chordae attached to anterior mitral leaflet that prolapsed intermittently into the left atrium (apical four-chamber and apical three-chamber [A3C] views, **A**,**C**). Severe mitral regurgitation with a posteriorly directed jet was seen (**B**,**D**). At surgery for emergency mitral valve replacement, two-thirds of the posterolateral papillary muscle was totally detached. (Please *see* companion DVD for corresponding video.)

large infarcted area. VSDs are more common 3–5 d after the acute MI, when the pathogenesis involves necrosis and thinning of the septum, with tissue disintegration hastened by the release of lytic enzymes from inflammatory cells. Interestingly, although the use of thrombolytics reduces the size of the infarct and risk of septal rupture, the onset of septal rupture in thrombolysed patients appears to be earlier (median time from onset of MI to rupture was 1 d in GUSTO-I trial and 16 h in the Should We Emergently Revascularize Occluded Coronaries in Cardiogenic Shock (SHOCK) trial, perhaps because of more intramyocardial hemorrhage.

Although 2D echo alone has limited sensitivity detecting VSDs, the addition of color Doppler increases the sensitivity and specificity of TTE for detecting VSD to almost 100%. On echocardiogram, the VSD may be seen as a discrete discontinuity or echo "dropout" in the muscular portion of the interventricular septum (Fig. 9A). Because of the asymmetry of most defects, it is important to inspect the septum from multiple windows when a VSD is suspected. The actual orifice size may range from millimeters or up to several centimeters in maximal dimension, and often expands during systole compared to diastole. Color flow Doppler will demonstrate turbulence and left-to-right flow through the VSD, because LV pressures are higher than RV pressures continuously throughout the cardiac cycle (Fig. 9B; please *see* companion DVD for corresponding video). Injecting agitated saline intravenously ("bubble study") can occasionally help define left-to-right flow by showing a negative contrast effect in the RV emanating from the VSD orifice. Morphologically, septal ruptures can be described as a simple perforation (i.e., direct defect through both sides of the septum at the same level), or more complex, with irregular serpiginous tracts entering and exiting the septum at different levels. Anterior VSDs are usually simple and located toward the apex (as in the ensuing case

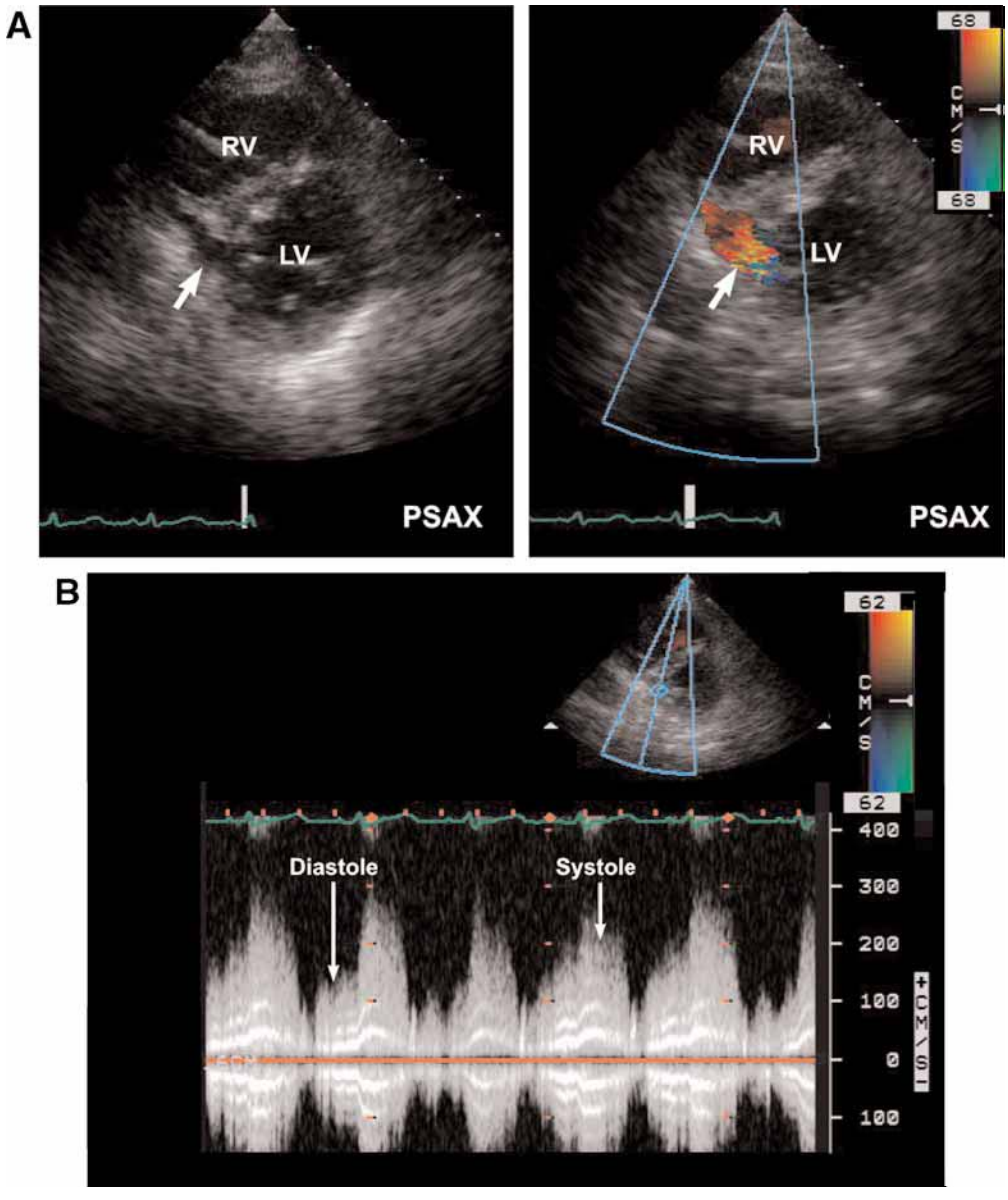

Fig. 9. (**A**) Postmyocardial infarction ventricular septal defect in a 72-yr-old male. This 72-yr-old male with a 1-wk history of chest pains and inferior myocardial infarction showed a breach in the mid-to-basal infero-septal segments on two-dimensional echocardiography (**left panel**, arrow). Color Doppler revealed a left-to-right shunt consistent with a ventricular septal defect. This was confirmed on ventriculography. Angiography revealed 100% right coronary artery occlusion. (**B**) Continuous-wave (CW) Doppler examination of postmyocardial infarction ventricular septal defect. CW Doppler of the ventricular septal defect showed a high-velocity left-to-right (3.0 m/s) flow with limited low-velocity flow (1.4 m/s) in the opposite direction during diastole. (Please *see* companion DVD for corresponding video.)

vignette), whereas inferior infarctions often involve the adjacent basal septum and are more likely to be complex.

Echocardiography of a patient with VSD should define the location, type (simple or complex), and size of the defect if possible. Additional useful information includes an estimate of the degree of left-to-right shunting (by the combined 2D and Doppler technique of estimating Qp and Qs), the pressure gradient across the septum (from which RV systolic pressure [RVSP] can be calculated using the formula RVSP = systolic BP – 4[VSD velocity]^2, or RVSP = right atrial pressure + 4[TR velocity]^2), and RV function. In severe VSDs, there may be associated rupture of papillary muscles or even free wall rupture (*see* "Free Wall Rupture" section).

Clinically, a significant VSD will be heralded by the patient experiencing chest pain, dyspnea, and potentially

cardiogenic shock. The shunting of blood across the VSD may be appreciated on physical exam as a harsh loud holosystolic murmur at the left sternal border and a palpable thrill. As the LV fails, systemic vascular resistance increases (to maintain blood pressure), and right-sided pressures increase, the amount of left-to-right shunting will decrease and biventricular failure ensues. Mortality of VSD is high, approx 24% in the first day and reaching up to 82% at 2 mo in medically treated patients, and, thus, operative repair (or in some cases, potentially closure with a percutaneous septal occluding device) should be initiated as soon as possible.

CASE PRESENTATION (CONTINUED)

Two days later, the patient developed recurrent chest pain. An ECG showed sinus tachycardia and persistent ST elevations. Echocardiogram showed akinetic aneurysmal apex and paradoxical septal motion. Post-MI VSD at the apical septum with L-R shunt flow, measuring 1.5–1.7 cm. The gradient across the gradient was 49 mmHg. The LV was hyperdynamic at the base and midventricle and the RV was dilated and diffusely hypokinetic. An emergent intra-aortic balloon pump was placed and the patient underwent surgical repair with a pericardial patch. Repeat TTE showed patch material and no residual shunting.

Pseudoaneurysm

A pseudoaneurysm is thought to be secondary to a subacute ventricular perforation that is locally contained. Pathologically, all three layers of the heart are disrupted, such that blood from the LV courses through endocardium and myocardial wall into the pericardial space (Fig. 10A,B; please *see* companion DVD for corresponding video). Local containment of the extruded blood by adherent parietal pericardium and scar tissue forms a globular echo-free space adjacent to and continuous with the LV internal chamber. Because of the local containment adjacent to the ventricle, this space appears similar to a ventricular aneurysm (Fig. 10C,D).

The distinction between these two entities is vitally important: a pseudoaneurysm is a surgical emergency because of risk of impending rupture, whereas a true aneurysm is less likely to rupture and can often be observed. A key difference is that there is no myocardium in the wall of a pseudoanuerysm. Both entities may contain associated formed thrombus. In general, echo characteristics associated with a pseudoaneurysm include:

1. A narrow neck (an orifice:pseudoaneurysm body diameter <0.5).
2. An abrupt or ragged interruption in the LV wall, indicating a through-and-through discontinuity of all layers of the heart, as opposed to the gradual tapering and thinning of the myocardial layer seen in a true aneurysm. (This criteria is better for anterior than inferior aneurysms.)
3. Color or pulse-waved Doppler showing bidirectional blood flow and increased turbulence within the neck of the aneurysm.
4. If the patient is stable enough and the diagnosis is unclear from standard echocardiography, the injection of intravenous echo-opaque contrast agents such as Optison or Definity may help define a pseudoaneurysm, by delineating the myocardial tear and extravasating into the pericardial space.

The most frequent presentation of pseudoaneurysm is chest pain and congestive heart failure, although patients may also present with syncope, vagal symptoms, or nonspecific symptoms (Frances et al.). Sudden cardiac death occurs in a small percentage. However, in a completely contained rupture, more than 10% of patients are entirely asymptomatic. Persistent ST-segment elevations occur in 20% of patients with pseudoaneurysms, and it is possible that recurrent ischemia or reinfarction may contribute to its pathogenesis. Pseudoaneurysms appear about twofold more common after inferior MIs, as opposed to anterior MIs, but have been seen arising from lateral and apical walls as well. The mortality is high owing to late rupture, and operative treatment should be undertaken urgently.

Free Wall Rupture

Free wall rupture is one of the most feared complications of MI, owing to its sudden onset and lethality. Unlike pseudoaneurysm, in a free wall rupture blood flows freely into the pericardium and thorax, causing cardiogenic shock and tamponade. It is seen 2–8 d after MI, with risk factors similar to those for VSDs: patients with Q-wave MI or their first MI are at highest risk. Female gender, advanced age, and hypertension increase the risk, as does delayed recognition of the MI or continued physical activity. Acute chest pain, agitation, and cardiogenic shock occur abruptly and 90% of cases are fatal.

Echocardiograms of acute free wall ruptures are rare, owing to the rapid lethality of this complication.

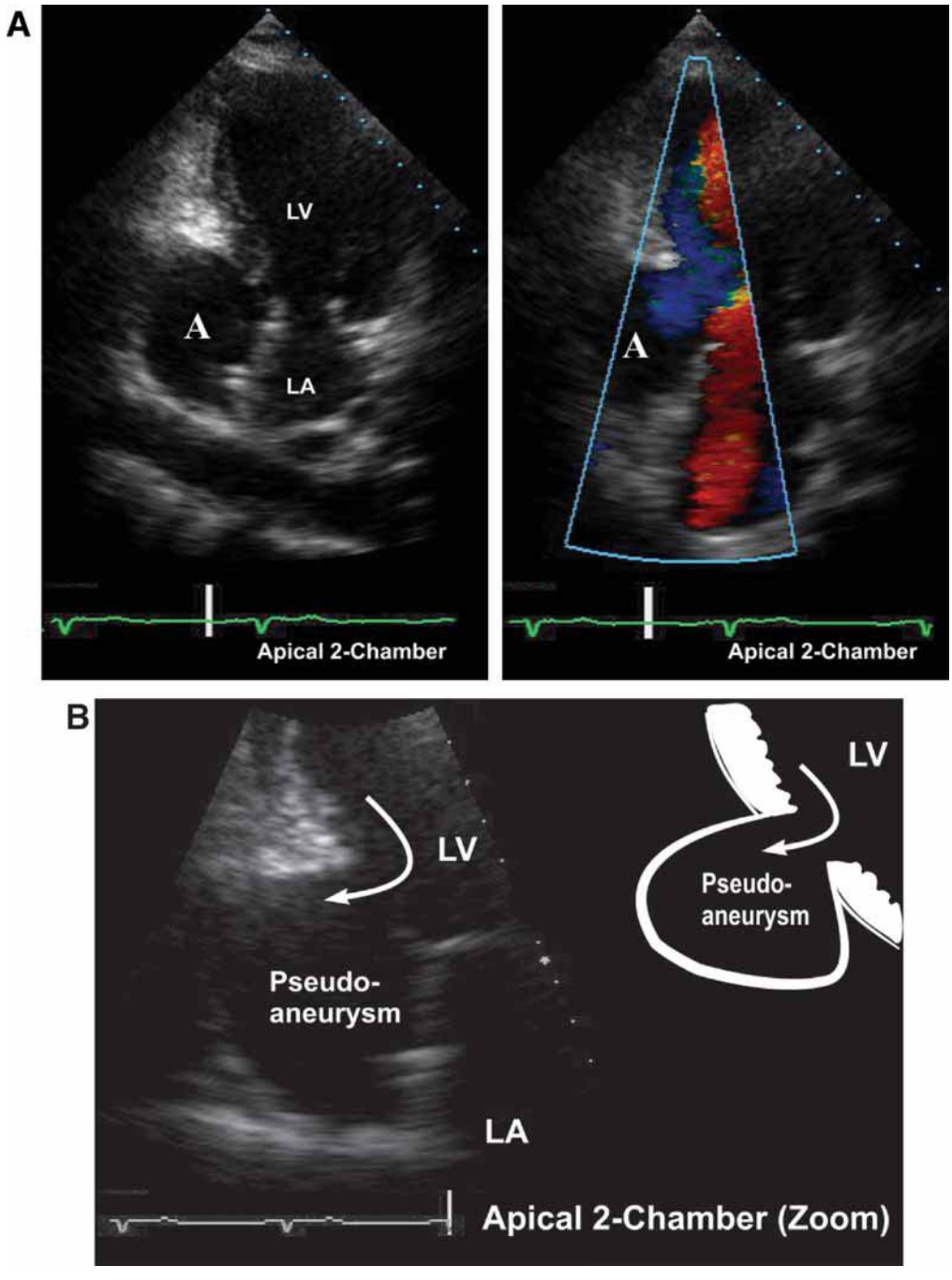

Fig. 10. *(Continued)*

However, if captured, the findings on TTE (or TEE) may include a pre-existing pseudoaneurysm (now ruptured), discontinuity or marked thinning and akinesis of the involved wall at the terminal territory of the culprit occluded vessel, a pericardial effusion (occasionally with thrombus in the pericardial sac), and low velocity color Doppler flow into the pericardium. Prompt surgery is the only treatment for this complication.

Left Ventricular Thrombus

Left ventricular thrombus is a relatively common complication of MI. It has been found in 20–60% of cases in postmortem series before the thrombolytic era. More recent Gruppo Italiano per lo Studio della Streptochinasi nell'Infarto Miocardico (GISSI)-3 study data shows an overall incidence of 5.1% in thrombolysed patients, and patients with anterior infarcts, large

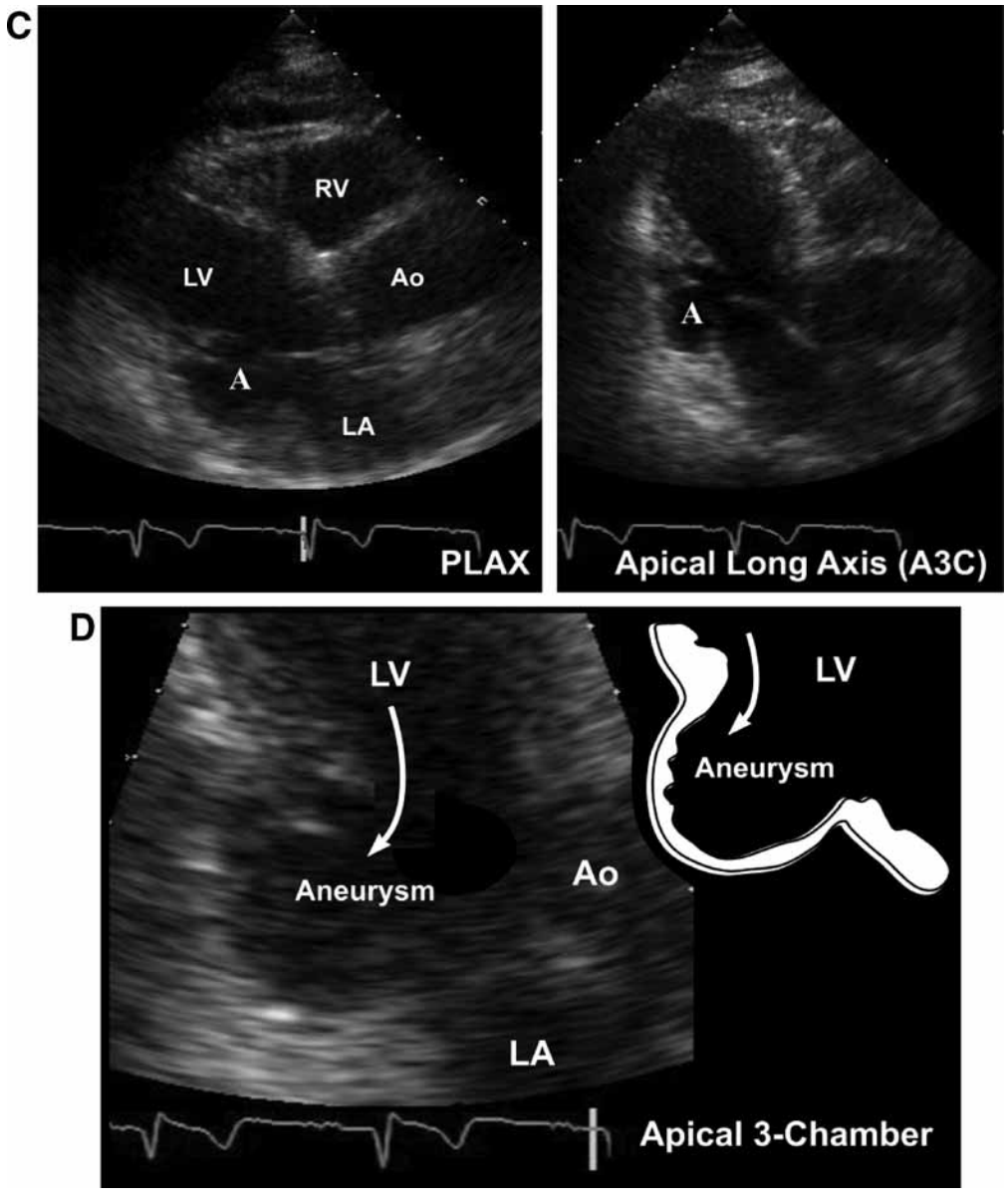

Fig. 10. (**A**) Pseudo-aneurysm (postmyocardial infarction [post-MI]). This 64-yr-old woman suffered an inferior MI and required implantable cardioverter defibrillator placement. Her apical two-chamber images show a narrow-necked cavity (**left panel**) that communicated with the left ventricular cavity. No intracavitary thrombus was seen. Surgical removal confirmed it was a pseudo-aneurysm. (**B**) Pseudo-aneurysm: anatomy. A post-MI pseudoaneurysm of the left ventricular wall is essentially a contained ruptured of the ventricular wall that is not lined by myocardium. (**C**) 77-yr-old female with history of previous MI and of ventricular aneurysm. Her parasternal long-axis (PLAX) and apical long axis images show aneurysmal remodeling of the basal infero-posterior wall. No intracavitary thrombus was seen. (**D**) Anatomy: true aneurysm. In a true ventricular aneurysm, the entire wall of the aneurysm is still lined by endocardium/myocardium. (Please *see* companion DVD for corresponding video.)

dysfunctional territories, or LVEF less than 40% are at the highest risk. Anticoagulation is usually indicated to prevent systemic embolization.

Transthoracic echocardiography has a sensitivity of nearly 95% and specificity of 90% for LV thrombi. (TEE is less sensitive, and therefore an inappropriate test for detecting LV thrombi; this is because of difficulty visualizing the apex, which is more distant from the TEE probe, particularly in patients with large dilated ventricles.) Thrombi are usually detected between 4 and 14 d after the infarct, and typically appear as discrete, echogenic, homogenous speckled masses lying adjacent

to an akinetic or dyskinetic segment of endocardium. The individual characteristics of thrombi vary widely; many appear fixed and adherent to the endocardial wall ("mural thrombi") with smooth laminar surfaces, but they may also be rounded or pyramidal, have independently mobile portions and protruding filaments, or be pedunculated. Those that are mobile or protruding are at particularly high risk of embolization, and adjacent hyperkinetic myocardial segments also increase embolic potential. Older or well-organized thrombi are often observed to include more echo-bright elements.

With anticoagulation, LV thrombi have been observed to resolve in 47% of patients by 1 yr and 76% by 2 yr of follow-up, although they are less likely to resolve in those patient with apical dyskinesis.

Pericardial Complications: Infarct-Related Acute Pericarditis, Tamponade

Less severe complications of MI frequently involve the pericardium. Early or acute pericarditis, as defined by a pericardial friction rub with or without chest discomfort and/or ECG changes typical of pericarditis, is estimated to occur in 5–20% of patients with MI, with the lower incidence in patients who have smaller infarcts or those who are thrombolysed. The rub is generally transient and lasts 3 d or less. A pericardal effusion occurs in up to one-third of cases—similar to the other complications of MI, larger infarctions or concurrent RV infarctions appear to be risk factors. The effusions are usually asymptomatic, small in size, and only rarely cause tamponade. However, the effusions may take weeks to months to resolve, and patients with significant effusions appear to have higher morbidity and mortality.

Post-MI pericarditis, or Dressler's syndrome, may occur as a late complication of MI (and cardiac surgery) weeks to months after the acute event. It is characterized by pleuritic chest pain, a pericardial rub, fever, and elevated leukocyte count.Echocardiography of the pericardium may show a thickened pericardium and/or pericardial effusion, often with associated "shaggy" echodensities, which represent fibrin, and inflammatory material within the pericardium adherent to the visceral or parietal pericardium. Adjacent "sympathetic" pleural effusions may be present as well. The incidence of post-MI pericarditis was estimated in up to 3–4% of infarcts before the thrombolysis era, but appears to have declined enormously in reperfused patients.

Chronic Implications

Heart Failure: Decline in Systolic and Diastolic Function

Echocardiography is a useful tool for risk assessment and determining prognosis in the weeks to months after an MI. The EF is the most frequently used index of clinical heart failure, and both EF and infarct size have been shown to be a strong predictors of survival post-MI (*see* Chapter 5). Emerging indications for automatic implantable cardioversion defibrillator placement post-MI include an EF of 30% or less, with or without ventricular tachyarrhythmias.

Diastolic dysfunction (*see* Chapter 6) is also abnormal both early and late in the course of MI, and quantitative measures of LV relaxation or restriction can have prognostic and therapeutic implications as well.

Dilation and Remodeling: Heart Failure

Although an infarct causes immediate local myocardial dysfunction in the necrosed segments, further adjacent and even distal territories may be negatively affected and become functionally abnormal in the few months following an acute infarct. This process has been termed cardiac remodeling, or infarct expansion (*see* Chapter 5, Fig. 6). On cardiac ultrasound, this is manifested by enlargement of the hypokinetic or akinetic zones, which are still viable, as well as overall dilatation of the LV chamber. The ventricle often takes on a more spherical shape, with an aneurysmal apex. Pathologically, LV hypertrophy is usually present as measured by overall LV mass, but because the overall internal chamber size has increased, the measured wall thicknesses on echocardiography may remain within normal limits. Angiotensin-converting enzyme inhibitors have been shown to limit the process of remodeling after MI.

Aneurysm (and Thrombus)

Injured myocardial segments may become scarred, and if extensive enough can "balloon out" to form aneurysmal segments (Fig. 11; please *see* companion DVD for corresponding video). These appear as thinned, highly echogenic areas of scarred myocardium, which are in continuity with the adjacent viable myocardium, have wide necks, and appear to bulge from the LV cavity in systole. *See* "Pseudoaneurysm" and "Free Wall Rupture" sections for the distinction between aneurysms and pseudoaneurysms; these can be difficult to discriminate, and in some cases may require surgical/pathological determination. Although they can

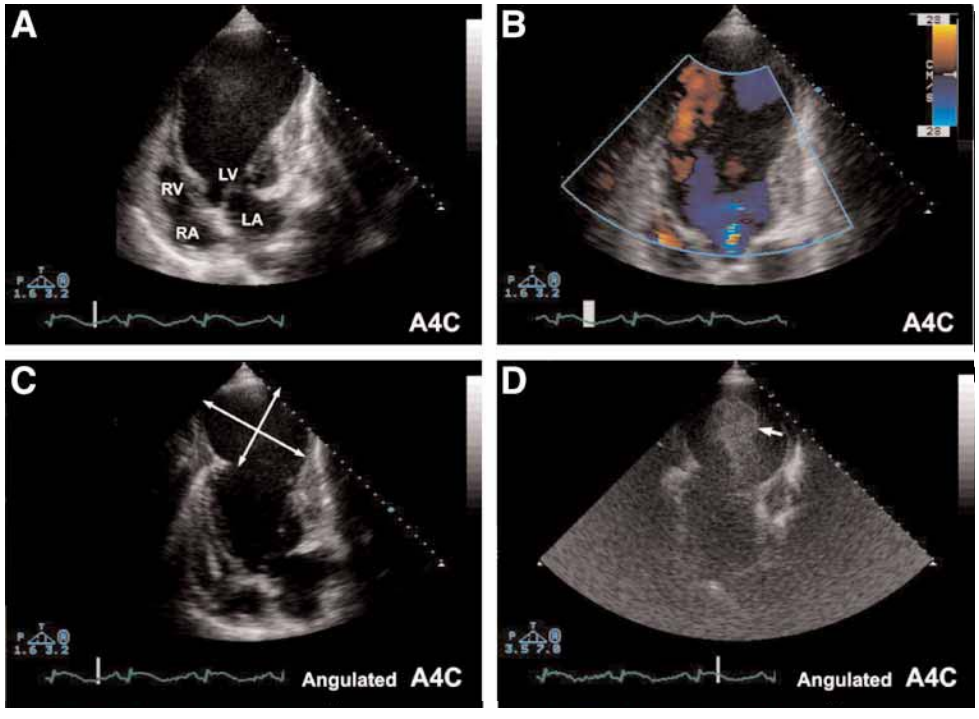

Fig. 11. A 74-yr-old male with a 2-mo history of myocardial infarction (MI) and congestive heart failure. This 74-yr-old man with a history of MI 2 mo earlier presented with wide-complex tachycardia requiring implantable cardioverter defibrillator placement. Echocardiography revealed large left ventricular aneurysm measuring approx 9 × 9 cm in two dimensions. Ejection fraction was estimated at 10% (**A**,**C**). Moderate mitral regurgitation was seen by color Doppler. (**B**) No left ventricular thrombus was observed. Higher frequency echocardiogram revealed the presence of spontaneous echocontrast in the aneurysmal segment (**D**). (Please *see* companion DVD for corresponding video.)

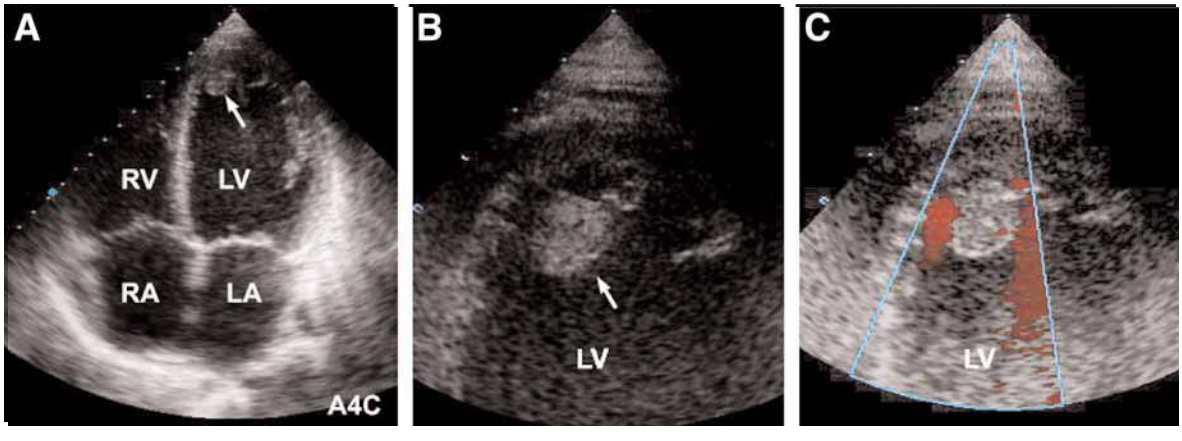

Fig. 12. A 40-yr-old male with left ventricular thrombus. Apical four-chamber image shows moderately directed left ventricle with global hypokinesis and estimated ejection fraction of 25%. An echodensity was observed in the apical region (**A**, arrow), which, on higher frequency and color Doppler imaging, showed appearances consistent with a thrombus. (Please *see* companion DVD for corresponding video.)

arise from anywhere in the LV, the majority involve the apex. Many (from 34 to 77%) of these aneurysms are associated with indwelling mural thrombi, with comprises a stroke risk (*see* Fig. 12; please *see* companion DVD for corresponding video; *see also* "Free Wall Rupture" section). Finally, because the scar comprising the aneurysm cannot conduct electrical impulses, it can form the substrate for ventricular tachycardias.

Mitral Regurgitation (Without Flail Leaflet)

Mild or greater degrees of MR often accompany remodeling post-MI, and increasing severity is associated with increased cardiovascular mortality. In the absence of a flail leaflet owing to rupture of a papillary muscle or chordae, the MR appears to be caused by incomplete valve closure, which in turn is because of displacement of the papillary muscles, with the laterally displaced chordae tethering the leaflets open. On echocardiogram, the anterior leaflet appears elongated and both leaflet tips are angulated toward the lateral apex. The mitral leaflet tips appear not to coapt fully at end-diastole, and a clear jet of color flow Doppler originating at or just proximal to the central orifice can be seen. Whether interventions such as mitral annuloplasties or LV aneurysectomies, which decrease the amount of MR, actually decrease cardiac morbidity or mortality remains to be seen.

In summary, echocardiography serves as a diagnostic and prognostic tool to guide therapeutic intervention in both the acute myocardial infarct as well as the aftermath. It should be used judiciously to answer specific questions in a given clinical scenario, and an appropriately high suspicion for the development of acute or chronic complications should be borne in mind.

SUGGESTED READING

Birnbaum Y, Fishbein MC, Blanche C, Siegel RJ. Ventricular septal rupture after acute myocardial infarction. N Engl J Med 2002;347:1426–1432.

Cerqueira MD, Weissman NJ, Dilsizian V, et al. Standardized myocardial segmentation and nomenclature for tomographic imaging of the heart. Circulation 2002;105:539–542.

Chiarella F, Santoro E, Domenicucci S, Maggioni A, Vecchio C. Predischarge two-dimensional echocardiographic evaluation of left ventricular thrombosis after acute myocardial infarction in the GISSI-3 study. Am J Cardiol 1998;81:822–827.

Crenshaw BS, Granger CB, Birnbaum Y, et al. Risk factors, angiographic patterns, and outcomes in patients with ventricular septal defects complicating acute myocardial infarction. Circulation 2000;101:27–32.

Edwards BS, Edwards WD, Edwards JE. Ventricular septal rupture complicating acute myocardial infarction: identification of simple and complex types in 53 autopsied hearts. Am J Cardiol 1984;54:1201–1205.

Figueras J, Cortadellas J, Soler-Soler J. Comparison of ventricular septal and left ventricular free wall rupture in acute myocardial infarction. Am J Cardiol 1998;81:495–497.

Fortin DF, Sheikh KH, Kisslo J. The utility of echocardiography in the diagnostic strategy of postinfarction ventricular septal rupture: a comparison of two-dimensional echocardiography versus Doppler color flow imaging. Am Heart J 1991;121:25–32.

Frances C, Romero A, Grady D. Left ventricular pseudoaneurysm. J Am Coll Cardiol 1998;32:557–561.

Gillam LD, Hogan RD, Foale RA, et al. A comparison of quantitative echocardiographic methods for delineating infarct-induced abnormal wall motion. Circulation 1984;70:113–122.

Haugland JM, Asinger RW, Mikell FL, Elsperger J, Hodges M. Embolic potential of left ventricular thrombi detected by two-dimensional echocardiography. Circulation 1984;70:588–598.

Krumholz HM, Howes CJ, Murillo JE, Vaccarino LV, Radford MJ, Ellerbeck EF. Validation of a clinical prediction rule for left ventricular ejection fraction after myocardial infarction in patients > or = 65 years old. Am J Cardiol 1997;80:11–15.

Lamas GA, Mitchell GF, Flaker GC, et al. Clinical significance of mitral regurgitation after acute myocardial infarction. Survival and Ventricular Enlargement Investigators. Circulation 1997; 96:827–833.

Meltzer RS, Visser CA, Fuster V. Intracardiac thrombi and systemic embolization. Ann Intern Med 1986;104:689–698.

Menon V, Webb JG, Hillis LD, et al. Outcome and profile of ventricular septal rupture with cardiogenic shock after myocardial infarction: a report from the SHOCK Trial Registry. J Am Coll Cardiol 2000;36;1110–1116.

Moss AJ, Zareba W, Hall WJ, et al; Multicenter Automatic Defibrillator Implantation Trial II Investigators. Prophylactic implantation of a defibrillator in patients with mycardial infarction and reduced ejection fraction. N Engl J Med 2002;346:877–883.

Nijland F, Kamp O, Karreman AJ, van Eenige MJ, Visser CA. Prognostic impications of restrictive left ventricular filler in myocardial infarction: a serial Doppler echocardiographic study. J Am Coll Cardiol 1997;30:1618–1624.

Nishimura RA, Reeder GS, Miller FA, Jr, et al. Prognostic value of predischarge 2-dimensional echocardiogram after acute myocardial infarction. Am J Cardio 1984;53:429–432.

Shahar A, Hod H, Barabash GM, Kaplinsky E, Motro M. Disappearance of a syndrome: Dressler's syndrome in the era of thrombolysis. Cardiology 1994;85:255–258.

Silver MT, Rose GA, Paul SD, O'Donnell CJ, O'Gara PT, Eagle KA. A clinical rule to predict preserved left ventricular ejection fraction in patients after myocardial infarction. Ann Intern Med 1994;121:750–756.

Siu SCB, Weyman AE. Coronary artery disease: clinical manifestations and complications. In: Weyman AE (ed.); Principles and Practice of Echocardiography, 2nd ed. Philadelphia: Lea and Febiger, 1994:656–686.

Smyllie JH, Sutherland GR, Geuskens R, Dawkins K, Conway N, Roelandt JR. Doppler color flow mapping in the diagnosis of ventricular septal rupture and acute mitral regurgitation after myocardial infarction. J Am Coll Cardiol 1990;5:1449–1455.

Stratton JR, Lighty GW, Jr, Pearlman AS, Ritchie JL. Detection of left ventricular thrombus by two-dimensional echocardiography: sensitivity, specificity, and causes of uncertainty. Circulation 1982;66:156–166.

Stratton JR, Resnick AD. Increased embolic risk in patients with left ventricular thrombi. Circulation 1987;75:1004–1011.

Tofler GH, Muller JE, Stone PH, et al. Pericarditis in acute myocardial infarction: Characterization and clinical significance. Am Heart J 1989;117:86–92.

Visser CA, Kan G, Meltzer RS, Dunning AJ, Roelandt J. Embolic potential of left ventricular thrombus after myocardial infarction: a two dimensional echocardiographic study of 119 patients. J Am Coll Cardiol 1985;5:1276–1280.

Waggoner AD, Williams GA, Gaffron D, Schwarze M. Potential utility of left heart contrast agents in diagnosis of myocardial rupture by 2-dimensional echocardiography. J Am Soc of Echocardiogr 1999;12:272–274.

Welin L, Vedin A, Wilhelmsson C. Characteristics, prevalence, and prognosis of postmyocardial infarction syndrome. Br Heart J 1983;50:140–145.

8 Stress Echocardiography

Indications, Protocols, and Interpretation

Edmund A. Bermudez, MD, MPH
and Ming Hui Chen, MD, MMSc

Contents

INTRODUCTION

Stress echocardiography is a common diagnostic procedure used in the evaluation of coronary artery disease. In fact, stress echocardiography is now a widely accepted test utilized for the diagnosis, prognostication, and risk stratification of ischemic heart disease (Fig. 1). Imaging is most often coupled with treadmill stress, however, it can be easily coupled with pharmacological stress, bicycle exercise, or pacing. In skilled hands, stress echocardiography is safe, versatile, and accurate, providing important information on segmental wall motion and overall ventricular function.

The interpretation of echocardiographic images is based on changes in regional myocardial thickening with stress. In the setting of significant coronary artery disease, regional myocardial thickening will decrease as a result of oxygen supply–demand mismatch. The area supplied by the stenosed coronary artery will, therefore, display a change in contraction, enabling the identification and extent of underlying coronary ischemic disease. In the absence of hemodynamically significant coronary stenoses, an increase in systolic wall thickening should be observed in all coronary territories with a decrease in the size of the left ventricular cavity. Therefore, localization and burden of ischemic heart disease can be routinely assessed.

INDICATIONS

Stress echocardiography is indicated in the diagnosis of coronary artery disease in those with an intermediate likelihood of coronary artery disease and an abnormal electrocardiogram (Fig. 1, Table 1). Those individuals with left bundle branch block, Wolff-Parkinson-White syndrome, left ventricular hypertrophy, digoxin use, or more than 1 mm ST segment depression on electrocardiogram should undergo imaging with stress as interpretation of ST segments are an unreliable marker of ischemia in these settings. If the patient is able to exercise, treadmill stress, or bicycle stress (supine or upright) should be performed. When this is not feasible, dobutamine stress may be used. In the United States, vasodilator stress is an uncommon modality for stress echocardiography.

In peri-operative evaluations for noncardiac surgery, stress echocardiography can aid in risk stratification. According to the American College of Cardiology/American Heart Association guidelines, stress echocardiography is indicated when there are intermediate predictors of cardiovascular risk with low functional capacity or when a high-risk surgical procedure is planned. When high-risk results are obtained (extensive inducible wall motion abnormalities) from this testing, coronary angiography is usually warranted. However,

From: *Contemporary Cardiology: Essential Echocardiography: A Practical Handbook With DVD*
Edited by: S. D. Solomon © Humana Press, Totowa, NJ

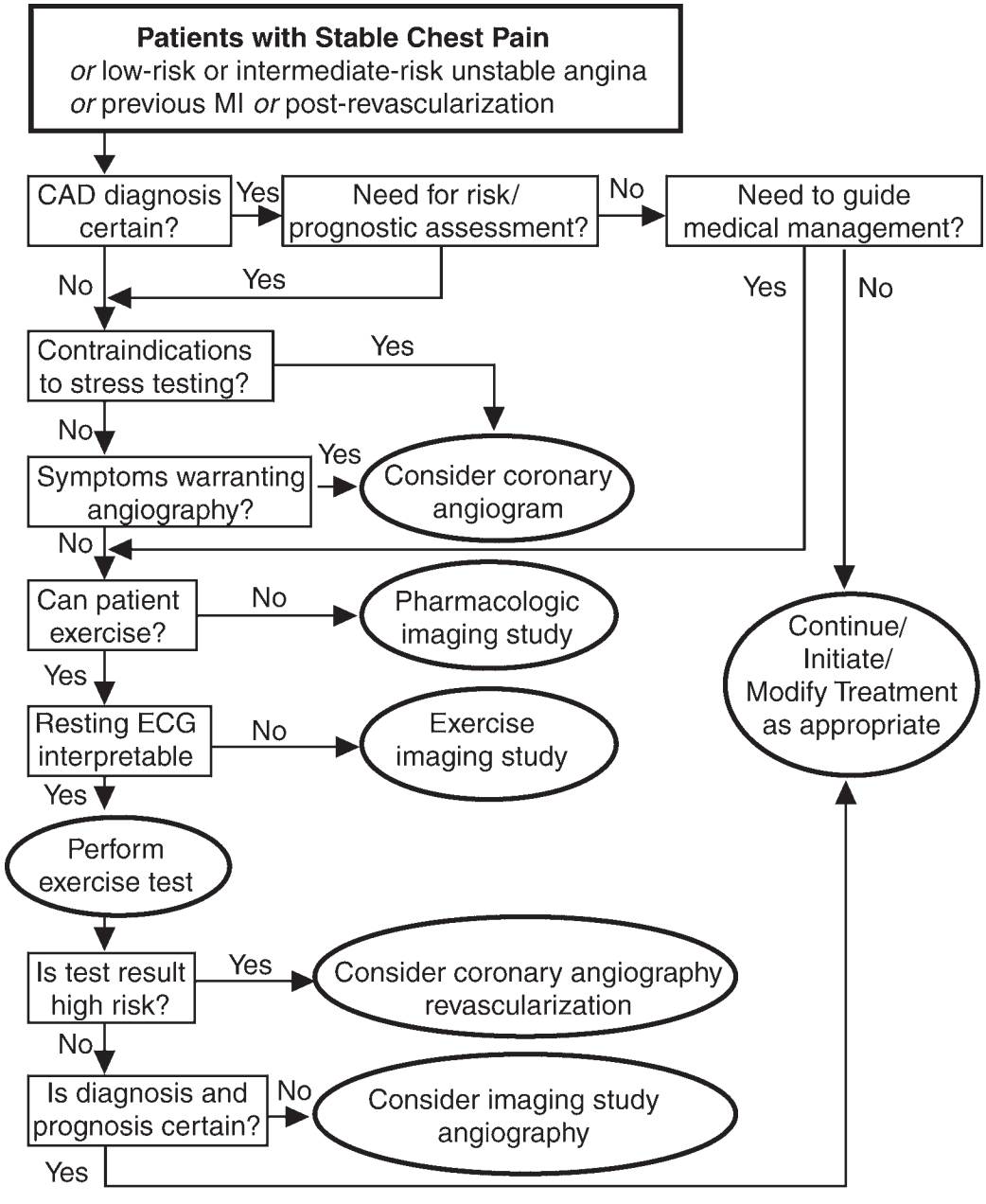

Fig. 1. American College of Cardiology/American Heart Association (ACC/AHA) guideline update on stress testing. (Modified from ACC/AHA Exercise Testing Guidelines: http://www.acc.org/clinical/guidelines/exercise/fig1.htm.)

when no wall motion abnormalities can be induced with adequate stress, surgery can usually be performed at relatively low risk for perioperative events.

Stress echocardiography can be used for prognostic purposes in those with chronic coronary artery disease and in post-myocardial infarction. As in risk stratification, the extent and severity of ischemia as evidenced by inducible wall motion abnormalities is a main determinant of prognosis, as well as overall left ventricular function. Among individuals with known or suspected coronary disease, a normal stress echocardiogram portends a more benign prognosis compared to those with abnormal stress echocardiography results. In addition, the presence of viability with dobutamine echocardiography (biphasic response) in those with coronary artery disease can identify those in whom revascularization and functional recovery is more likely (*see* Chapter 5, Fig. 17).

Finally, stress echocardiography can be utilized with Doppler to evaluate valvular function. In those individuals

Table 1
Overview of Qualitative Reporting of Left Ventricular Wall Motion Abnormalities During Stress Echocardiography

Wall motion/endocardial thickening at baseline	*Wall motion/endocardial thickening at peak stress*	*Interpretation*
Normal	Hyperdynamic	Normal
Normal	Hypokinetic-akinetic	Ischemic
Hypokinetic	Worsening hypokinesis	Ischemic
Akinetic (± wall thinning)	Akinetic-dyskinetic	Infarcted
Hypokinetic/akinetic	Augmentation with lower dose of dobutamine; deterioration with high dose (biphasic response)	Viability with ischemia

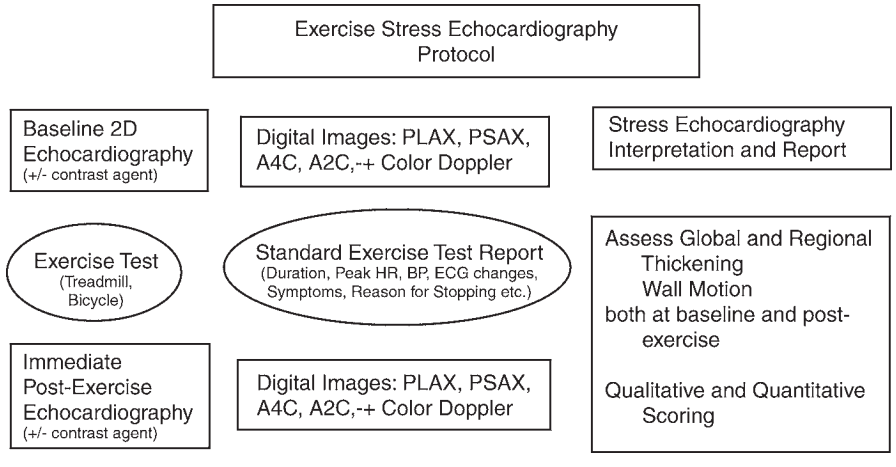

Fig. 2. Exercise stress echocardiography protocol.

with small, calculated aortic valve areas, low ejection fractions, and low transaortic gradients, stress echocardiography can be used to increase cardiac output and further define the severity of aortic stenosis by calculating changes in aortic valve area with stress. In a similar fashion, mitral stenosis can be evaluated and pulmonary systolic pressures calculated after or at peak stress. Therefore, in situations where the severity of stenotic valve lesions is questioned, stress echocardiography may provide important information to guide management decisions.

STRESS PROTOCOLS

Exercise Echocardiography (Fig. 2)

Standardized images are acquired before the initiation of exercise and immediately after exercise. Two parasternal views (parasternal long axis and parasternal short axis) and two apical views (apical four-chamber and apical two-chamber) are used to assess endocardial wall motion (Fig. 3; please *see* companion DVD for corresponding video). A common practice is to hold atrioventricular nodal blocking agents prior to testing, as the attainment of at least 85% of predicted maximal heart rate is desirable. It is important that the acquisition of images occurs immediately postexercise when using the treadmill machine. If images are acquired late after exercise, the heart rate may decrease substantially, giving time for any peak wall motion abnormalities to subside and, therefore, go undetected. The use of a supine bicycle machine may improve the timing of image acquisition, as images can be acquired at almost any time point during exercise and give true peak stress imaging. It is, therefore, believed that supine bicycle imaging may improve the sensitivity of testing over treadmill exercise.

Pharmacological Stress Echocardiography (Fig. 4)

Pharmacological stress echocardiography is utilized when patients are unable to exercise maximally. In the diagnosis of the coronary artery disease, stress to maximal

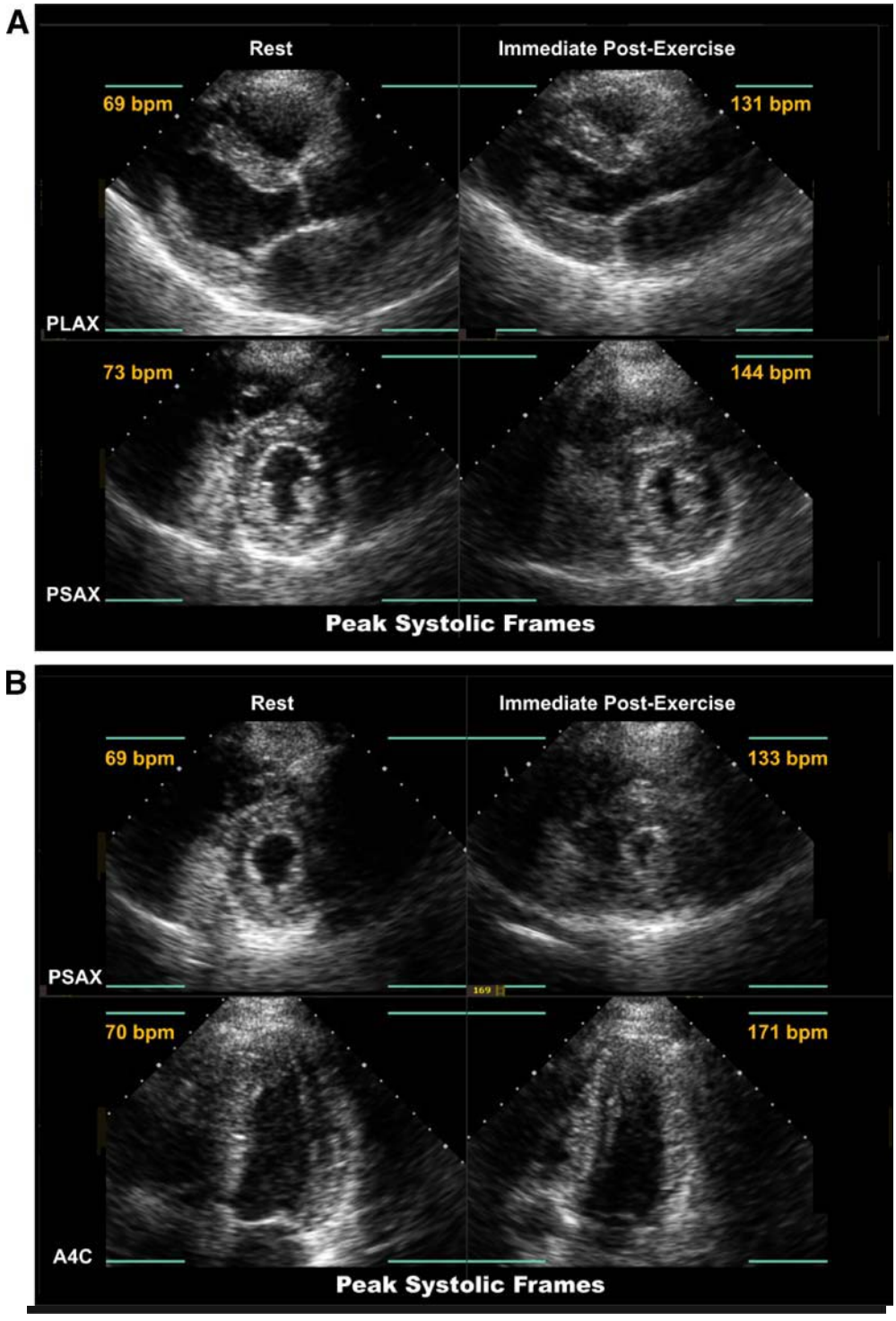

Fig. 3. This 45-yr-old man with a history of hypertension and new right bundle branch block exercised for 12 min on a standard Bruce protocol, stopping secondary to fatigue. Heart rate and blood pressure at peak exercise was 179 bpm and 168/78 mmHg, respectively. There was 1-mm ST segment depression in lead III, becoming upsloping in V4–V6. Baseline left ventricular dimensions were within normal limits with estimated ejection fraction of 60–65%. No regional wall motion abnormalities were present. Immediate postexercise imaging showed appropriate decrease in left ventricular chamber size with augmented contractility of all ventricular (**A,B**). (Please *see* companion DVD for corresponding video.)

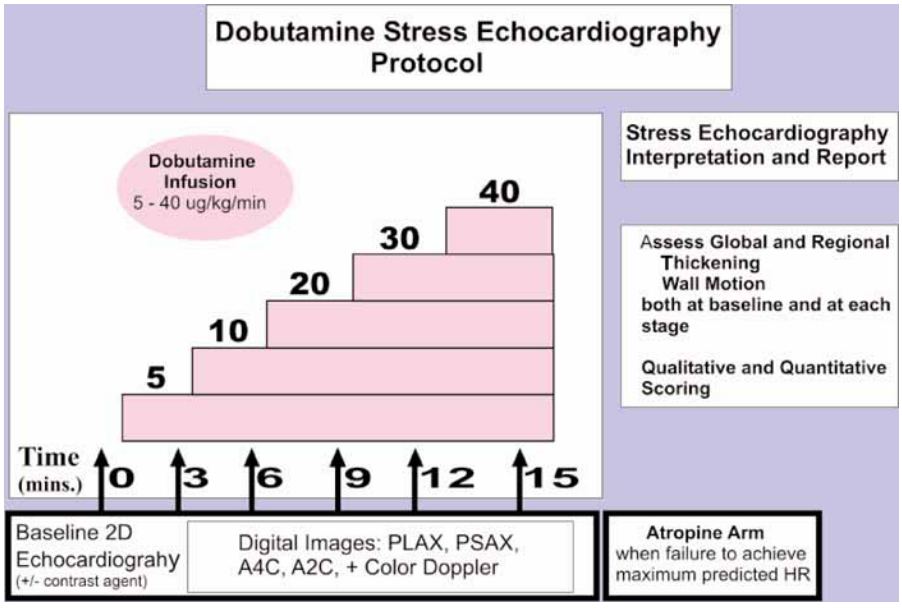

Fig. 4. Dobutamine stress echocardiography protocol.

levels is an important component in the evaluation. However, in regard to viability testing, dobutamine echocardiography is primarily utilized over exercise stress in the identification, localization, and extent of viable myocardium.

Dobutamine is the most commonly utilized pharmacological agent that is combined with echocardiography for the assessment of coronary artery disease. This cardiac inotrope provides stress through β1 receptor stimulation and increasing myocardial oxygen consumption. Typically, dobutamine is infused in 3–5 min stages starting at low doses (5 μg/kg/min) and increased until the maximal predicted heart rate is achieved or peak infusion levels are reached (40 μg/kg/min) (Figs. 4 and 5). Additional intravenous injections of atropine may be used to augment the heart rate in some individuals whom higher heart rates are needed. At peak levels, it is not uncommon to observe a drop in systolic blood pressure, owing to the mild vasodilatory effects of dobutamine. In contrast to exercise stress, this drop is not specific for severe coronary ischemia.

Echocardiographic images are obtained in the same views as treadmill testing, i.e., the parasternal long, parasternal short, apical four-, and apical two-chamber views. Images are acquired at rest before infusion, low dose infusion (5 or 10 μg/kg/min), peak infusion, and postinfusion. Images are displayed in quad-screen format (the four views mentioned previously on one screen) for each stage and routinely digitized for interpretation (Fig. 5; please *see* companion DVD for corresponding video). This protocol is often augmented when resting wall motion abnormalities are seen on the echocardiographic images. In this case, images are often acquired at both low dose levels (5 and 10 μg/kg/min) to capture any changes in wall motion with low-dose infusion.

Vasodilator and Pacing Stress

As in nuclear stress testing, vasodilator stress has been used in combination with echocardiography. The agents typically used are dipyridamole or adenosine, both of which cause coronary vasodilation and perfusion mismatch with subsequent ischemia when significant stenoses are present. This approach has not been routinely applied in the United States, however, has been more extensively used in Europe.

Pacing can be used when exercise and pharmacological means are not feasible because of contraindications. Pacing is more favorably achieved via the atrium, as ventricular pacing may cause differential wall contraction and theoretically pacing induced wall motion abnormalities. Atrial pacing can be accomplished through esophageal pacing leads. This modality has not gained wide use, because it appears more invasive than pharmacological stress and may cause discomfort in some patients. Nonetheless, this modality offers an alternative

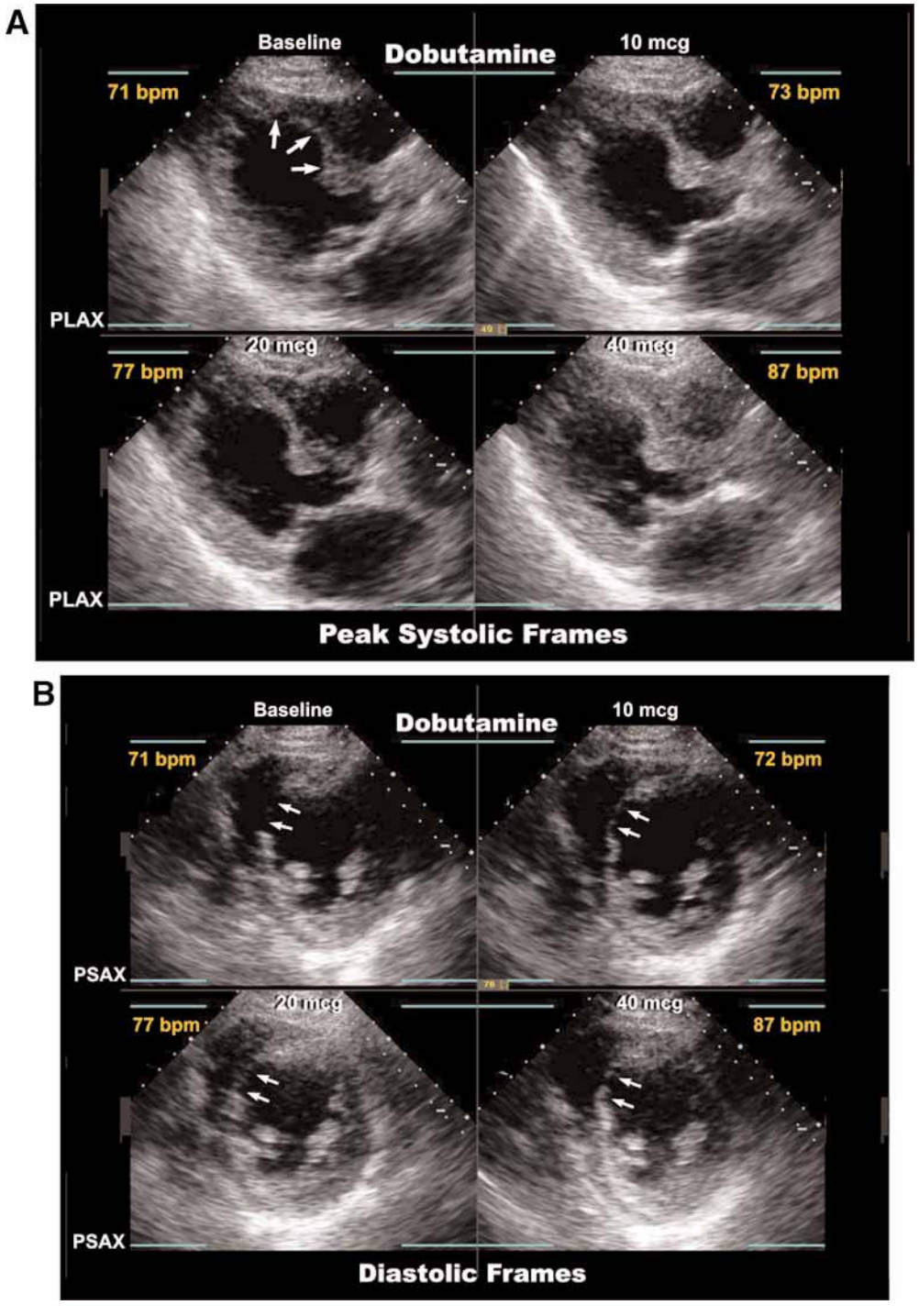

Fig. 5. (*See* legend facing page)

to pharmacological measures, and ensures the ability to achieve maximal heart rates.

INTERPRETATION

The myocardium is divided into 16 segments (*see* Chapter 5, Fig. 10A) corresponding to different coronary territories: left anterior descending distribution, right coronary artery distribution, and left circumflex distribution. In general, the anterior, septal, and apical segments are supplied by the left anterior descending, lateral, and basal posterior segments by the left circumflex, and the inferior and posterior segments by the right

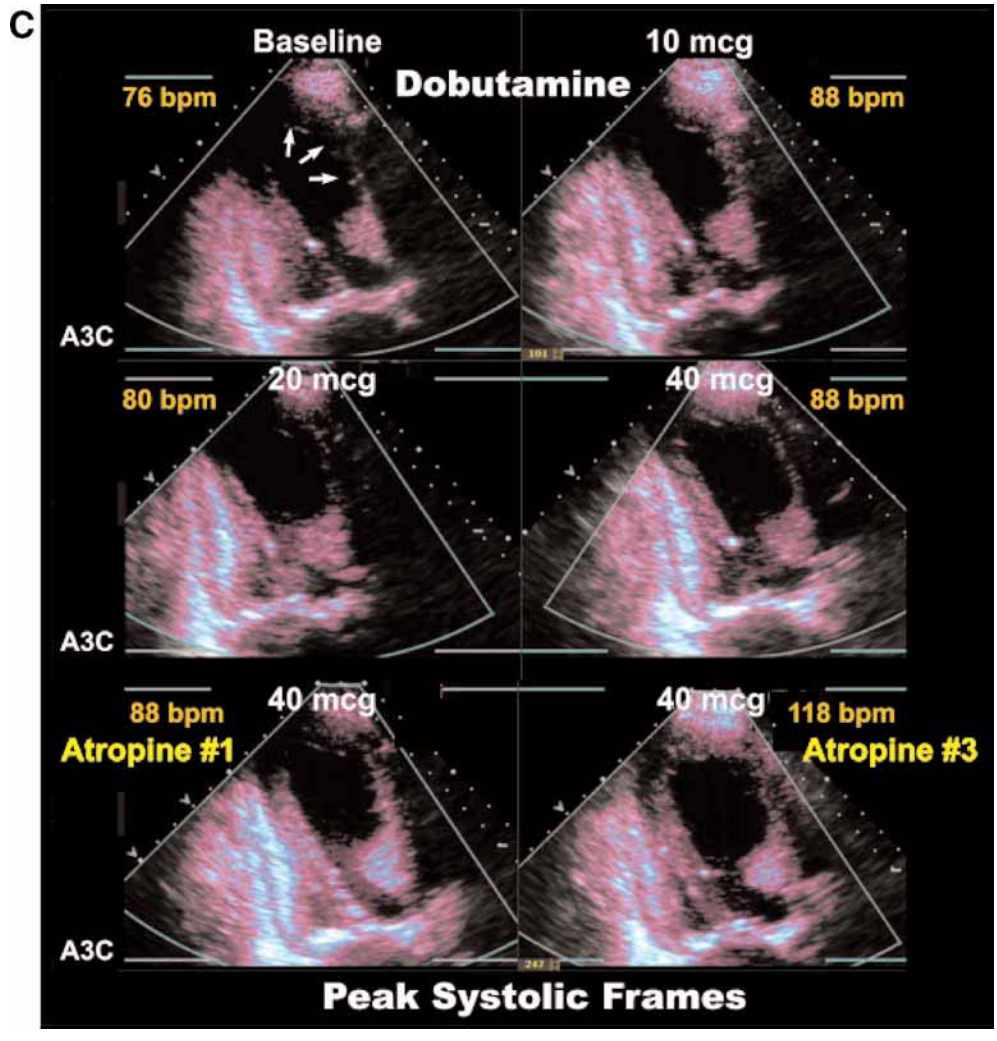

Fig. 5. A 64-yr-old female with coronary artery disease and aortic valve disease underwent dobutamine stress echocardiography. Graded doses of dobutamine were infused in 3 min stages to a peak dose of 40 μg/kg/min. Atropine (0.4 mg × 3) was given to achieve heart rate targets. Maximal heart rate achieved was 118 bpm (74% of predicted heart rate) and blood pressure was 110/82 mmHg. Patient had no symptoms. Baseline electrocardiogram showed normal sinus rhythm with ST abnormalities suggestive of a digitalis effect. Baseline echocardiogram showed dialated ventricular cavity size with estimated ejection fraction (EF) of 40–45% with akinesis and thinning of the basal-to-midanteroseptal and anterior wall. Images at peak infusion showed no increase in global systolic function (estimated EF 40%). The akinetic anteroseptal and anterior segments became progressively dyskinetic during the infusion—consistent with a transmural infarct/scarring. In addition, the inferior wall, mildly hypokinetic at baseline, becomes akinetic at the high dose of dobutamine. Overall study was consistent with a large anterior and anteroseptal infarct with no significant peri-infarct ischemia. Sensitivity was limited because target heart rate was not achieved. (Please *see* companion DVD for corresponding video.)

coronary artery (*see* Chapter 7, Figs. 3–5). However, there can be considerable overlap in perfusion territories and depends on coronary dominance, which should be taken into consideration when interpreting segments that may belong to more than one coronary distribution. More recently, a 17-segment model has been developed that takes into account the true apex (*see* Chapter 5, Fig. 10B). This model has neither been routinely used, nor made a significant change in interpretation of stress echocardiographic images to date.

First, each myocardial segment is assessed for systolic thickening at rest and overall ventricular function. Areas of prior infarction are identified by thinned segments of hypokinesia or akinesia. Thickening is the primary measure of regional function, not myocardial motion itself. Second, the myocardial segments are examined at peak stress or post stress. Normal myocardial segments should sufficiently thicken to a greater extent with stress. The stress images are then analyzed in addition to the size of the left ventricular cavity,

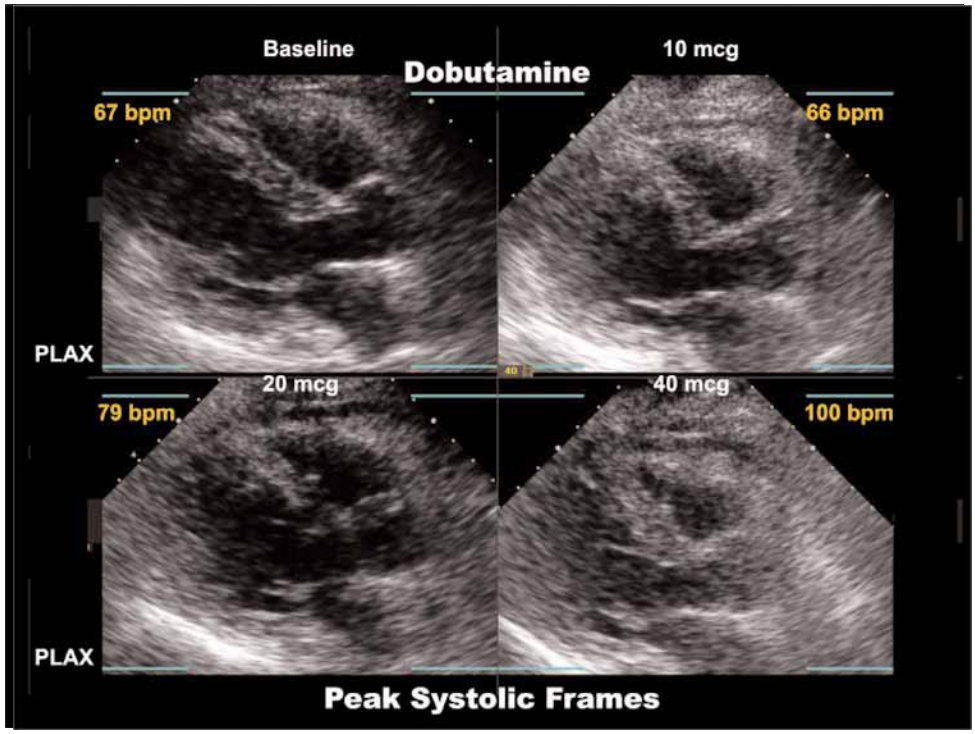

Fig. 6. A 72-yr-old female patient underwent dobutamine infusion with atropine to achieve targeted heart rate. Baseline echocardiographic images showed borderline left ventricular hypertrophy with preserved systolic function. Minimal septal hypokinesis was noted. With increasing doses of dobutamine, augmentation of all segments accompanied by decrease in left ventricular cavity size up to a heart rate of 110 bpm. However, at heart rates more than 115 bpm, left ventricular dilatation accompanied by hypokinesis of the postero-inferior walls from base to apex was observed. These findings were consistent with ischemia in the right coronary/left circumflex artery territory. The septal wall that appeared mildly hypokinetic at baseline augmented during stress testing, suggesting no ischemia in this territory.

which should become smaller with augmentation of ejection fraction. When a myocardial segment thickens less with stress, hypokinesia or akinesia is present and signifies stress-induced ischemia (Fig. 6). Dyskinesia is defined by the presence of outward movement of the myocardium in systole in an area of akinesis (Fig. 5; please *see* companion DVD for corresponding video). If an abnormal area at rest does not change with stress, this result is likely secondary to infarcted or scarred myocardium. The thought is that the greater the supply–demand mismatch, the greater will be the deficit during systolic thickening. Areas surrounding zones of ischemia may display decreased thickening, or so-called tethering. Overall, the territories corresponding to areas of decreased thickening define the coronary distribution and extent of ischemia (Fig. 7; please *see* companion DVD for corresponding video).

A qualitative or quantitative approach to interpretation can be used. Qualitatively, each myocardial segment is observed at rest and with stress and an appreciation for single or multivessel ischemia can be assessed. However, quantitative schemes have been developed in order to gain a more objective, standardized interpretation for stress echocardiograms. In this light, each of the 16 myocardial segments is given a score: 1 for normal segments; 2 for hypokinetic segments; 3 for areas of akinesis; 4 for dyskinetic areas; 5 for aneurysmal segments (*see* Chapter 5, Fig. 1B). Areas that are unable to be visualized adequately are not scored. An overall index for wall motion is then calculated by summing all of the wall scores and then dividing by the number of segments analyzed. This can be done for the rest images and also for the stress images.

When dobutamine is used for the assessment of myocardial viability, the changes in myocardial thickening are assessed at rest, low dose, and peak images (*see* Chapter 5, Fig. 17). Viable myocardium that is more likely to recover function with revascularization is typical when a biphasic response is observed: hypokinesis at rest, improvement with low-dose dobutamine and worsening with high-dose dobutamine. This is the most specific

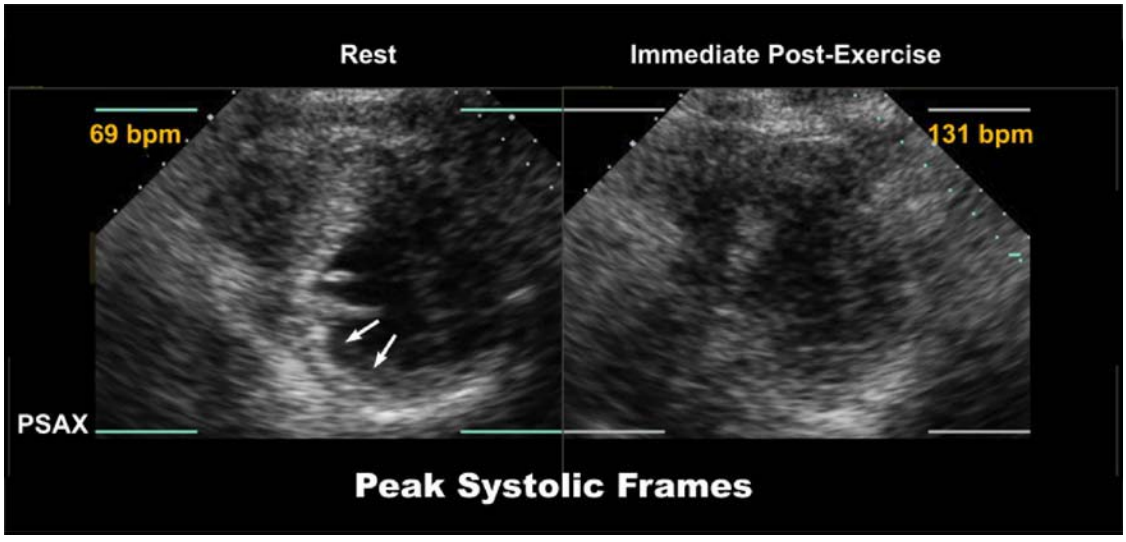

Fig. 7. A 58-yr-old man with a history of aortic insufficiency stopped 1 min 50 s into a standard Bruce protocol. Baseline echocardiogram showed hypokinesis of the basal inferior segment. Despite suboptimal test, peak systolic images showed modest increase in overall systolic function with estimated ejection fraction of 65–70%. All left ventricular segments, including the basal inferior segment, showed augmented contractility, with no inducible wall motion abnormalities. This finding indicates viable nonischemic myocardium with non-flow limiting coronary artery stenosis. (Please *see* companion DVD for corresponding video.)

response for recovery of function following surgical revascularization. A uniphasic response is seen when an area of hypokinesis improves continuously with dobutamine infusion and also indicates myocardial viability but this area appears to be less likely to recover full function after revascularization. The definition of ischemia is the same as with exercise modalities, i.e., worsening of wall thickening with stress infusion of dobutamine.

The range of left ventricular wall motion characteristics seen during stress echocardiography and their interpretation are summarized in Table 1.

PITFALLS

Stress echocardiography has its advantages and disadvantages (Table 2). Several caveats should be taken into account during interpretation. False-positive stress echocardiograms can result from a number of issues. First, a hypertensive response has been associated with a higher likelihood of wall motion abnormalities with stress in the setting of nonobstructive coronary artery disease. A hypertensive response has been defined as a systolic blood pressure over 220 mmHg for men and systolic blood pressure higher than 190 mmHg for women or as an increase in diastolic blood pressure higher than 10 mmHg with exercise or diastolic blood pressure higher than 90 mmHg during exercise. The exact mechanisms for this phenomenon are unclear but may be a result of abnormal loading conditions that eventually lead to subendocardial ischemia at the microvascular level.

Left bundle branch block may be a cause for false-positive readings (Fig. 8; please *see* companion DVD for corresponding video). With left bundle branch block, septal motion may be abnormal with systole as a result of the interventricular conduction delay. In this setting, one should again focus on thickening of the myocardium in the septal area and not on the septal motion. False-positive results may be related to increased heart rates in this setting. Therefore, one might speculate that vasodilator stress may be more specific in this setting, as has been the case with adenosine nuclear perfusion imaging.

Finally, interpretation of echocardiographic images can be difficult in certain patients. These patients may be obese individuals in whom inadequate penetration of the ultrasound beam results in poor endocardial resolution. Myocardial diseases, e.g., myocarditis can affect systolic performance and regional wall motion. Stress testing in this setting (for evaluation of chest pain) should be interpreted with caution (Fig. 9). Further, patients with chronic obstructive lung disease and hyperinflated lungs may impede the quality of echocardiographic images. In situations where endocardial border definition may be tenuous, the addition of intravenous echocontrast agents may help to better delineate

Table 2
Advantages/Disadvantages of Stress Echocardiography

Advantages
Sensitivity and specificity comparable to exercise nuclear imaging
Utility in diagnosis, prognosis, and risk-stratification
Assessment of multiple parameters: systolic function, valvular function, and ischemia
Widely available
Portability
Relatively inexpensive
No radiation
No need for iodinated contrast agents
Disadvantages
Highly dependent on sonographer and interpreter skills
Difficult acoustic windows can limit imaging. Echocontrast agents may be necessary

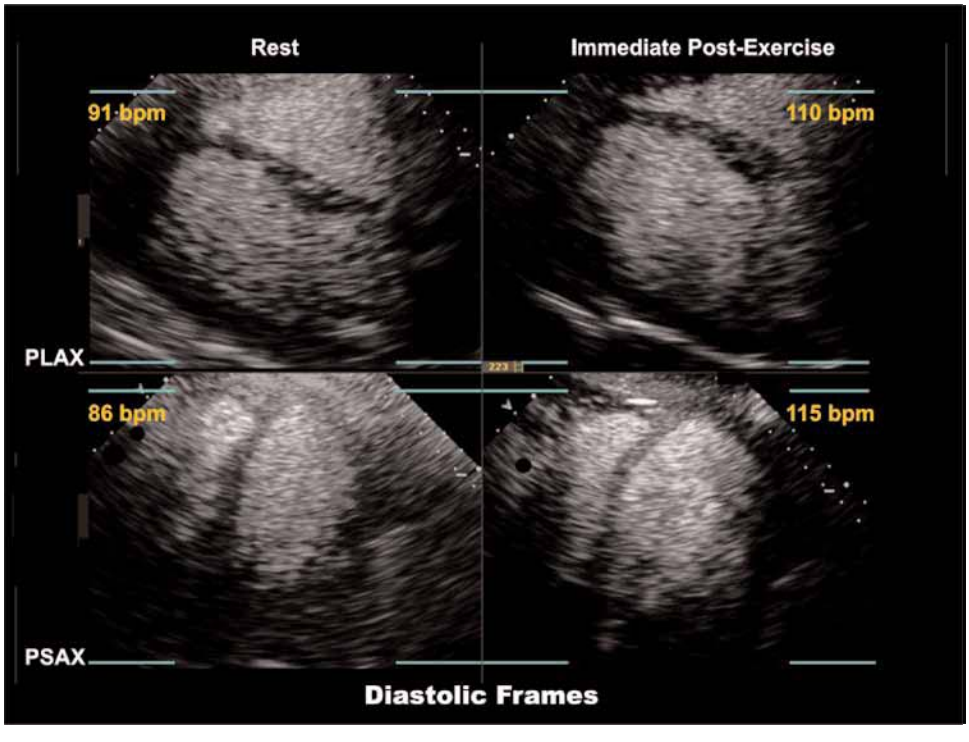

Fig. 8. A 62-yr-old man with baseline left bundle branch block (LBBB) exercised for 3 min, achieving peak heart rate of 115 bpm and peak blood pressure of 110/60 mmHg. Definity® (perflutren lipid microspheres) contrast agent was administered to improve endocardial border definition. Baseline images revealed moderately impaired left ventricular systolic function with abnormal septal motion (likely related to his LBBB) and hypokinesis of the mid- and distal septum. Postexercise images showed no increased contractility and worsening of septal hypokinesis. Findings are consistent with ischemia in the mid- and distal anterior septum—areas supplied by the left anterior descending coronary artery (*see* Chapter 7, Figs. 3–5; *see also* companion DVD for corresponding video).

regional endocardial thickening (Figs. 8 and 10; please *see* companion DVD for corresponding video for Fig. 8). This procedure should be routinely employed should any question arise regarding image resolution on rest imaging. Ideally, if one should use contrast, it should be used for each set of images (rest and stress) so as to compare similar images with one another.

Acquisition of images post-treadmill exercise demands extensive experience in obtaining quality images for

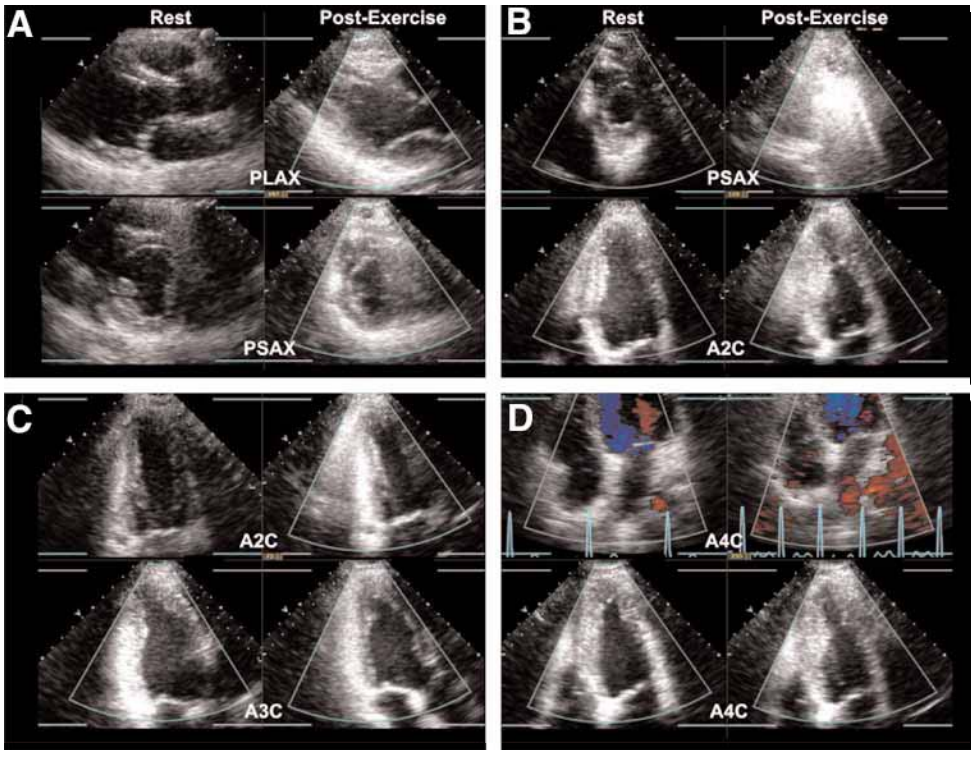

Fig. 9. A 35-yr-old woman with recent onset chest pain and dyspnea exercised for 13 min on the Bruce protocol, stopping owing to fatigue. At rest (heart rate 60 bpm), basal inferior wall hypokinesis with preserved function of the remaining left ventricular segments were present. Immediate postexercise images obtained between heart rates 136–180 bpm showed abnormal septal motion with augmented contractility of the remaining segments. The differential diagnosis included postmyocarditis or a cardiomyopathy with possible exercise-induced septal ischemia at achieved workload. Clinical correlation and/or further evaluation with another investigative modality was recommended.

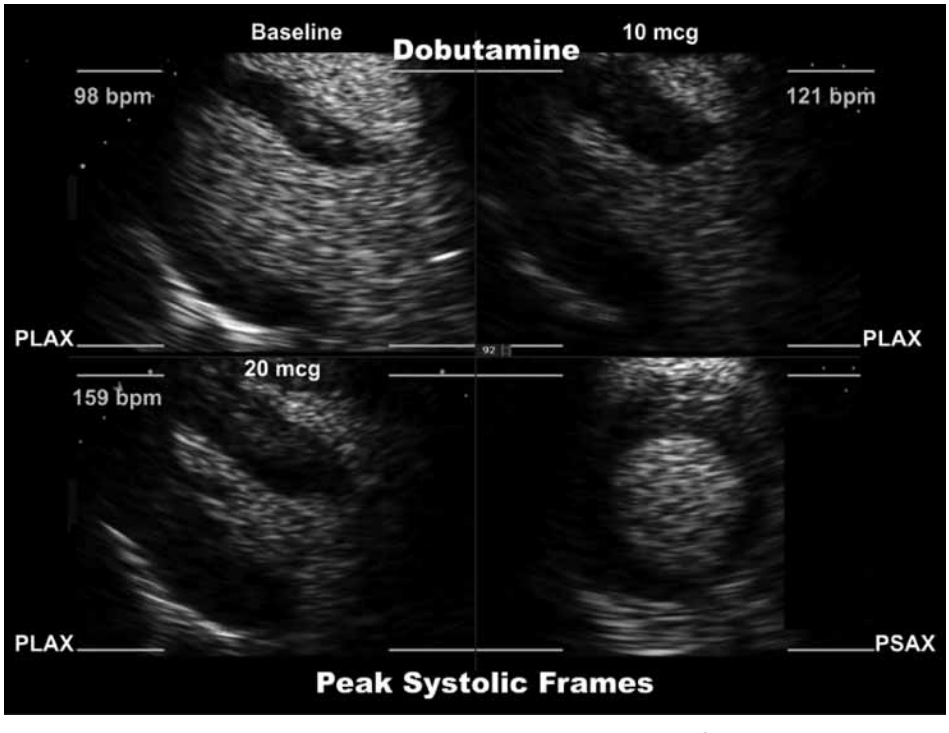

Fig. 10. A 47-yr-old male status postheart transplant. Myocardial contrast agent (Definity®, perflutren lipid micropsheres) was used to improve endocardial definition both at baseline and during image acquisition. Dobutamine was infused up to a peak dose of 20 μg/kg/min. The target heart rate of 160 bpm was achieved. Peak blood pressure was 180/87 mmHg. Echocardiographic parameters were normal at baseline, and dobutamine stress echocardiography images revealed normal recruitment of systolic function with no evidence of ischemia.

interpretation. Correct image orientation is essential to accurate diagnoses. In turn, accurate interpretation and diagnosis depends chiefly on experience of the sonographer in acquiring images and on the expertise of the physician interpreting them. Therefore, it is essential that the interpreting physician have a complete understanding of resting transthoracic principles prior to gaining experience with stress echocardiography.

In summary, stress echocardiography is a routine diagnostic procedure for the initial assessment of coronary artery disease, the follow up of patients with known coronary artery disease, and for management decisions regarding revascularization in patients with chronic coronary disease. It is a powerful tool in the assessment of regional and overall myocardial function in skilled hands. As its use broadens, new applications are emerging, such as the assessment of valvular disease and contrast myocardial perfusion, continuing to expand this already versatile modality.

SUGGESTED READING

Cerqueira MD, Weissman NJ, Dilsizian V, et al. Standardized myocardial segmentation and nomenclature for tomographic imaging of the heart. Circulation 2002;105:539–542.

Eagle KA, Brundage BH, Chaitman BR. Guidelines for perioperative cardiovascular evaluation for noncardiac surgery. J Am Coll Cardiol 1996;27:910–948.

Gibbons RJ, Chatterjee K, Daley J, et al. ACC/AHA/ACP-ASIM guidelines for the management of patients with chronic stable angina: executive summary and recommendations. Circulation 1999;99:2829–2848.

Jong-Won H, Juracan EM, Mahoney DW, et al. Hypertensive response to exercise: a potential cause for new wall motion abnormality in the absence of coronary artery disease. J Am Coll Cardiol 2002;39:323–327.

Shan K, Nagueh SF, Zoghbi WA. Assessment of myocardial viability with stress echocardiography. Cardiol Clin 1999;17:539–553.

9 Cardiomyopathies

Bernard E. Bulwer, MD, MSc and Scott D. Solomon, MD

Contents

DEFINITION

Cardiomyopathies are a varied group of heart diseases that are characterized by abnormalities of the heart muscle. Although these generally exclude those secondary to coronary artery disease, hypertension, congenital, valvular, or pericardial pathology, this definition has loosened, and terms such as "ischemic cardiomyopathy" or "hypertensive cardiomyopathy" have become popular (Fig. 1).

Cardiomyopathy is traditionally divided into three functional categories: dilated, hypertrophic, and restrictive (Fig. 2, Table 1). Echocardiography, in conjunction with the clinical presentation, serves as the basis for this categorization. Evaluation of cardiac structure and function by two-dimensional (2D), M-mode, and Doppler can help in the diagnosis, management, and prognosis in patients with cardiomyopathy. The various cardiomyopathies may share features in their presentation and echocardiographic characteristics.

DILATED CARDIOMYOPATHY

CASE PRESENTATION

A 56-yr-old male presented to the emergency department following worsening episodes of shortness of breath, orthopnea, and paroxysmal nocturnal dyspnea. His history of dyspnea began 7 yr ago and at that time he was started on an angiotensin-coverting enzyme inhibitor, furosemide, and digoxin. Investigations revealed no clear cause of his cardiomyopathy, but he admitted a 20-yr history of excess alcohol intake. An echocardiogram done at that time reported an ejection fraction of less than 20%. Cardiac catheterization was normal except for a 30% stenosis of the midleft anterior descending artery.

At the time of presentation, his medications included captopril, lasix, digoxin, potassium chloride, aspirin, multivitamins, and unspecified dietary supplements. He had no known drug allergies. His family history was significant for coronary heart disease. He smoked more than two packs of cigarettes daily for more than 20 yr, and averaged almost a quart of alcoholic beverages of various descriptions. He admitted no intravenous drug use, but occasionally used cocaine.

On examination, he was afebrile, pulse rate 119 bpm, blood pressure 112/71 mmHg, respiratory rate 18 breaths/min, and oxygen saturation measured 94% on room air. Significant cardiorespiratory findings included an elevated jugular venous pressure of 12.0 cm, basilar crackles up to the lower third of both lung fields, and a laterally displaced apex beat. He was in sinus rhythm with occasional premature ventricular contractions. Normal S1, a split S2, and a palpable S3 gallop were noted, but no murmurs. Bilateral pitting edema of both lower extremities

From: *Contemporary Cardiology: Essential Echocardiography: A Practical Handbook With DVD*
Edited by: S. D. Solomon © Humana Press, Totowa, NJ

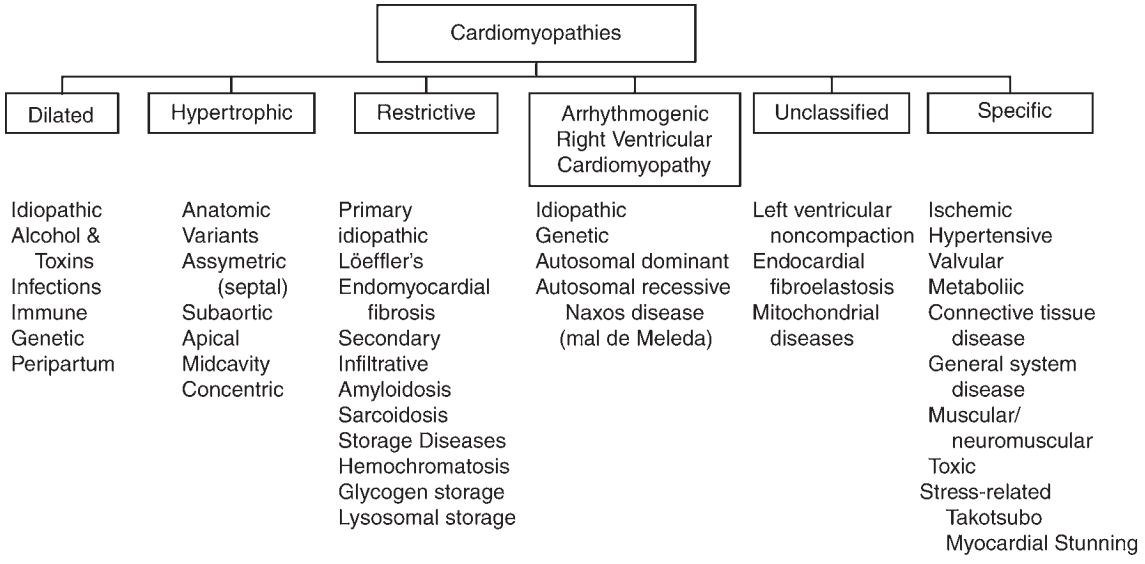

Fig. 1. Cardiomyopathies: classification.

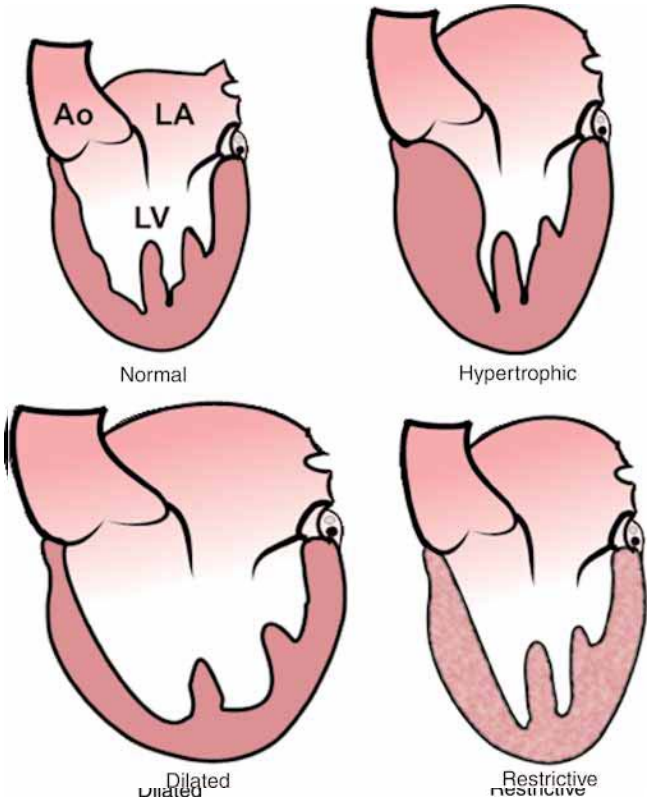

Fig. 2. Cardiomyopathies: three major functional types. Two-dimensional and Doppler echocardiography play central roles in the identification of the three major functional types of the cardiomyopathies. Major distinguishing features of these classes are listed in Table 1. Ao, aorta; LA, left atrium; LV, left ventricle.

was present and all peripheral pulses were palpable, although of reduced volume. Sinus tachycardia at 112 bpm, frequent premature ventricular contractions and 1.0 mm ST depression in V6, left axis deviation, left atrial enlargement, poor R-wave progression and lateral ST/T-wave abnormalities were all noted on his electrocardiogram (ECG).

Echocardiography revealed a dilated cardiomyopathy. Some of his images are shown in Figs. 3 and 4 (please *see* companion DVD for corresponding video).

Table 1
Cardiomyopathies: Three Major Functional Types

	Dilated cardiomyopathy	*Hypertrophic cardiomyopathy*	*Restrictive cardiomyopathy*
Clinical presentation and frequency	Dyspnea on exertion; congestive heart failure	Often asymptomatic; syncope; sudden death; genetic mutation (~1 in 500)	Progressive dyspnea, right-sided heart failure; features of underlying disorder
Cardiac chamber dimensions	Dilated cardiac chambers, esp. the left ventricle; dilated atria; right sided chambers can be dilated as well	Reduced left ventricular cavity size; dilated atria	Reduced ventricular cavity size; dilated atria—marked; dilated right sided chambers
Wall dimensions	Normal, mildly increased, or decreased	Asymmetric septal hypertrophy most common; other variants seen (Fig. 8)	Usually increased, and may involve all cardiac chambers
Systolic indices and ejection fraction (normal >55%)	Reduced systolic function; decreased EF, <30%	Normal or increased systolic function; dynamic LVOT obstruction and intracavitary gradients	Normal systolic function in early phases; reduced with advanced disease
Diastolic function	Impaired; may reflect volume overload	Impaired; asynchronous relaxation	Impaired with progressive restrictive physiology
Valvular function: MR; TR	MR secondary to annular dilation and apical tethering; TR frequent	MR with SAM of mitral leaflets	MR and TR frequent

Table modified from Warner Stevenson L. Diseases of the myocardium. In: Cecil Textbook of Medicine, 22nd ed. Goldman L, Ausiello D., eds., Saunders, Philadelphia: 2004:441–454.

EF, ejection fraction; LVOT, left ventricular outflow tract; MR, mitral regurgitation; SAM, systolic anterior motion; TR, tricuspid regurgitation.

Dilated cardiomyopathy is characterized by a dilated poorly functional left ventricle. The echocardiographic appearance of dilated cardiomyopathy can be remarkably similar despite the multiple etiologies (Table 2). Although regional wall motion abnormalities can be extremely suggestive of an ischemic etiology, some patients with nonischemic cardiomyopathy have regional dysfunction.

Dilated cardiac chambers characterize advanced stages of a dilated cardiomyopathy, predominantly the left ventricle, associated with accompanying systolic dysfunction. All indices of ventricular systolic function—left ventricular volumes, ejection fraction, stroke volume, cardiac output, and others—are generally reduced (Table 3; *see* also Chapter 4, Tables 4–7). Nevertheless, some patients may demonstrate minimal dilatation with significant ventricular dysfunction.

Wall thickness in dilated cardiomyopathy is usually within normal limits, but may be increased or decreased. Overall cardiac mass is invariably increased (Fig. 5). Dilated cardiomyopathy often leads to dilated mitral annulus, papillary muscle displacement resulting in poor mitral leaflet coaptation, both of which contribute to functional mitral regurgitation. These are best visualized using parasternal and apical windows. (Fig. 6; please *see* companion DVD for corresponding video; *see also* Chapter 14, Figs. 5 and 6). Dilated cardiomyopathy may present with relative sparing of regional wall function, especially of the basal and inferior walls (Fig. 3; please *see* companion DVD for corresponding video), or with multiple regional wall motion abnormalities, although, if nonischemic in etiology, not usually in a coronary distribution. Distinguishing between ischemic and nonischemic etiology by echocardiography can be challenging.

A dilated akinetic-hypokinetic left ventricular chamber increases the risk of intracardiac thrombus, which is more prone to form in areas of relative stasis. The majority of thrombi that form are mural; therefore, careful examination of the ventricular walls, using techniques to improve visualization of spontaneous echocontrast or thrombus (such as using a high-frequency transducer or myocardial contrast agents) should be employed. Intracavitary thrombi are more common in the left ventricular apex (*see* Chapter 7, Figs. 11 and 12).

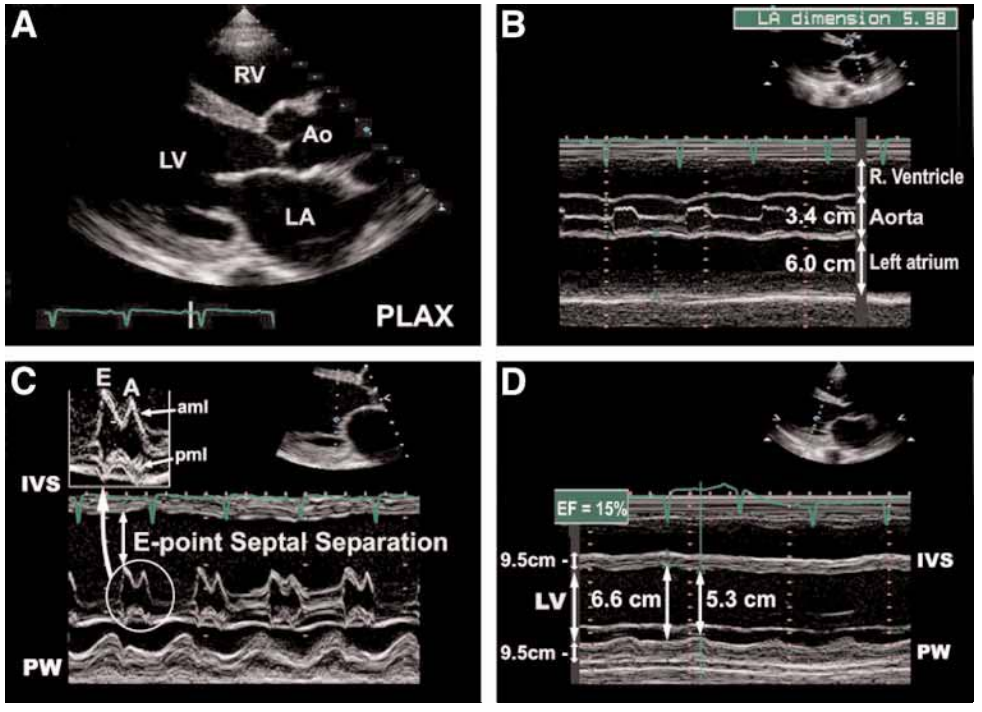

Fig. 3. Dilated cardiomyopathy. Left ventricular, left atrial, and right ventricular dilatation are seen in the parasternal long-axis view **(A)**. Wall thicknesses were within normal limits. Severe hypokinesis with akinetic segments, poor wall thickening are seen. Reduced systolic function leads to poor aortic valve opening, premature closure secondary to reduced stroke volume, and reduced anterior motion of aortic root during systole **(B)**. M-mode at the mitral valve level shows increased E-point septal separation. Note poor mitral valve closure, the akinetic septum, and the relatively preserved postero-basal segment **(C)**. M-mode more just distal to the mitral leaflets **(D)** shows dilated ventricular chambers with minimal excursion of the ventricular walls, little difference between systole and diastole, and calculated ejection fraction of 15% (Teichholz method, *see* Chapter 4). (Please *see* companion DVD for corresponding video.)

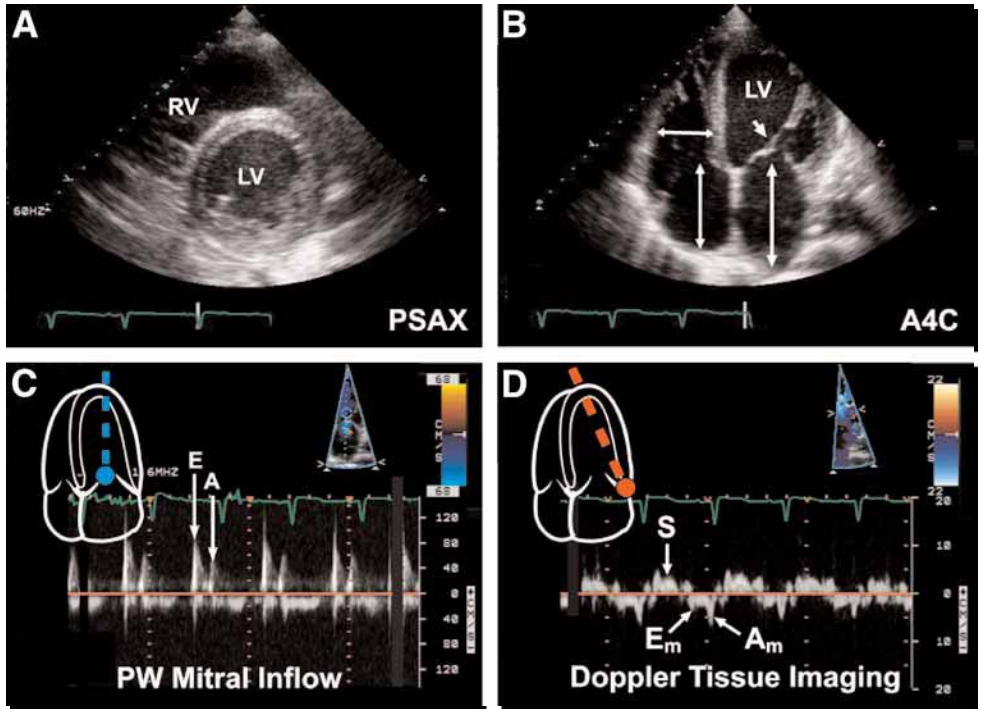

Fig. 4.

Table 2
Causes of a Dilated Cardiomyopathy on Echocardiography

Idiopathic (most common)
Ischemic
Valvular heart disease
Chronic hypertension
Tachyarrythmias (including SVTs, VTs)
Toxins (alcohol, anthracycline, e.g., daunorubicin)
Infections (HIV and viral, bacterial, parasitic, including Chagas)
Metabolic
Systemic and connective tissue disease
Other

SVT, supraventricular tachycardia; VT, ventricular tachycardia.

Table 3
Dilated Cardiomyopathy: Echocardiographic Findings

Modality	*Description*
Two-dimensional findings	Dilated left ventricle[a] (sine qua non)
	Dilated right ventricle[a] (frequent)
	Dilated atria (frequent)
	Low left ventricle ejection fraction[a]
	Low right ventricle ejection fraction[a] reduced indices of systolic function (*see* Chapter 4)
	Normal wall thickness, sometimes decreased or increased
	Sometimes spontaneous echo contrast ± intracavitary thrombus
M-Mode	Dilated cardiac chambers
	increased E-point septal separation
Doppler findings	Diastolic dysfunction[a]—initial impaired relaxation ± later restrictive pattern (*see* Chapter 5);
	mitral regurgitation (functional): secondary to apical tethering ("tenting") leading to restricted leaflet closure, annular dilatation, and papillary muscle displacement

[a]Association with adverse outcomes.

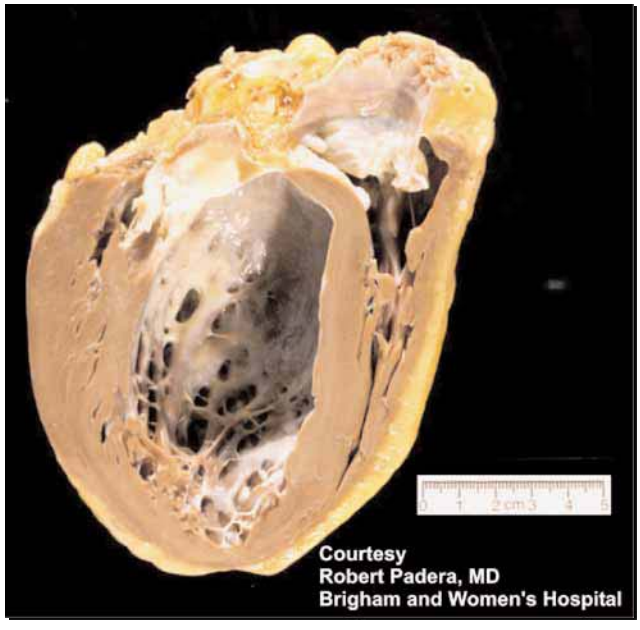

Fig. 5. Dilated cardiomyopathy: explanted heart. Gross explanted heart specimen (minus atria) from 56-yr-old male with end-stage dilated cardiomyopathy who received a heart transplant. Note the marked increase in total heart mass (heart weighed 780 g; normal < 360 g). Bilateral atrial enlargement was present, but portions of both atrium remained within transplant recipient. No intracavitary thrombus was seen.

Additional Parameters

Evaluation of right heart function, including the presence of right-sided chamber dilatation, tricuspid regurgitation, and pulmonary artery pressures, should be assessed in patients with cardiomyopathy, and can have prognostic importance (*see* Chapter 4). High tricuspid regurgitation velocities have been associated with worse outcomes.

Patients with dilated cardiomyopathy frequently exhibit some degree of diastolic dysfunction. Diastolic dysfunction almost always accompanies systolic dysfunction. A very rapid mitral deceleration time (DT) is indicative of so-called restrictive physiology, which can be seen on pulse-wave Doppler evaluation of mitral inflow. A "restrictive" Doppler pattern has been associated with worse prognosis in patients with heart failure (Fig. 7). Mitral DT less than approx 140 ms is associated with poor prognosis.

Fig. 4. *(Opposite page)* Dilated cardiomyopathy. Parasternal short-axis views at the papillary muscle level shows dilated cardiac chambers. Note the thinned septal regions **(A)**. Apical four-chamber view **(B)** shows four-chamber dilatation and apical tethering (tenting) of mitral valve leaflets—factors contributing to mitral regurgitation. Mitral inflow pulse Doppler velocity profile appears normal **(C)**, but when integrated with the reduced velocities and reversed pattern seen on Doppler tissue imaging **(D)**, should be interpreted as "pseudonormal"—both evidence of diastolic dysfunction. (Please *see* companion DVD for corresponding video.)

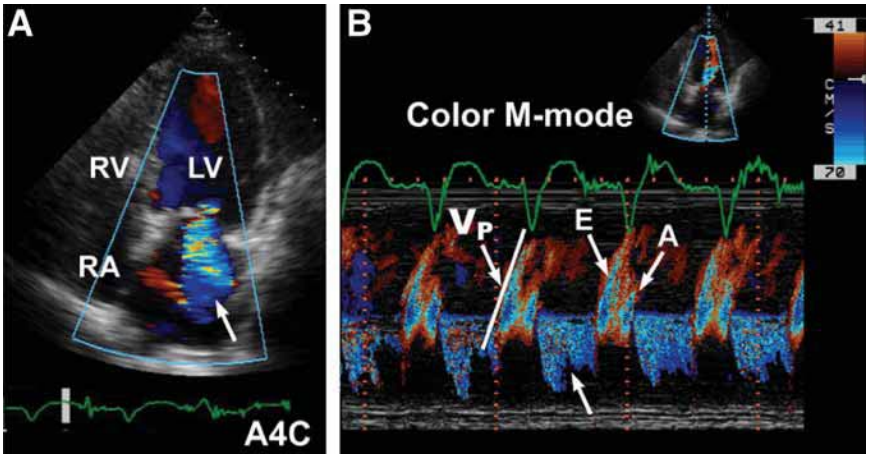

Fig. 6. Dilated cardiomyopathy: Mitral regurgitation. Mitral annular dilatation, lateral papillary muscle displacement, and apical tethering prevent normal leaflet coaptation. The result is typically mitral regurgitation (MR) with a centrally directed jet. Worsening MR heralds a worse prognosis. Color M-mode Doppler across the mitral valve (apical four-chamber view) during diastole provides a spatio-temporal display of blood velocities across the vertical interrogation line. This parameter may be less affected by loading conditions. The slope of this flow signal—flow propagation velocity (Vp)—is the slope of the first aliasing velocity measured on the E wave. Normal Vp is > 55 cm/s. Vp < 45cm/s may indicate impaired relaxation. (Please *see* companion DVD for corresponding video.)

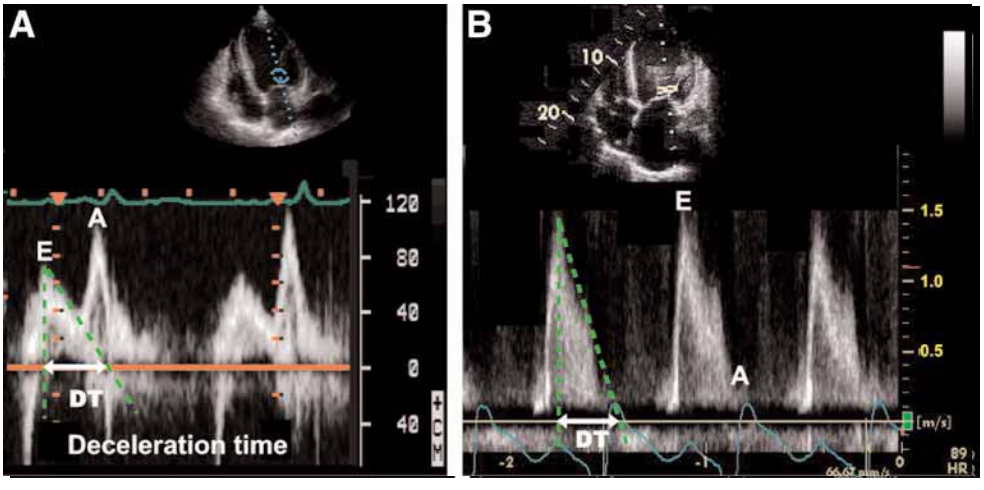

Fig. 7. Mitral inflow profiles showing evidence of diastolic dysfunction in dilated cardiomyopathy. The mitral inflow pulse Doppler profile in dilated cardiomyopathy often shows an impaired relaxation pattern **(A)** with prolonged deceleration time (DT > 200 ms) and reversal of the normal E:a ratio during the early stages. Later worsening of diastolic dysfunction is accompanied by a compensatory increase in left atrial filling pressures (driving pressure) results in early rapid filling of the left ventricle (a tall, thin E-wave) in the setting of a dilated left atrium. The marked fall in the A-wave velocity reflects atrial systolic dysfunction owing to a poorly compliant left ventricle.

RESTRICTIVE AND INFILTRATIVE CARDIOMYOPATHY

CASE PRESENTATION

A 76-yr-old male was admitted for investigation and management of decompensated heart failure. He presented earlier with a 3-mo history of progressive shortness of breath on exertion, paroxysmal nocturnal dyspnea, and ankle swelling. He denied any chest pain or palpitations. He gave no history of coronary artery disease. Both his previous coronary angiogram done in 1999 and a nuclear study in 2002 were reported as normal. His past medical history also includes aortic valve replacement in 5 yr earlier, paroxysmal atrial fibrillation, chronic obstructive pulmonary disease, essential thrombocytopenia, hypertension, and bilateral carpal tunnel syndrome. Significant investigations include an elevated brain natriuretic peptide levels, mild cardiomegaly on chest X-ray, and bilateral pleural effusions. His ECG

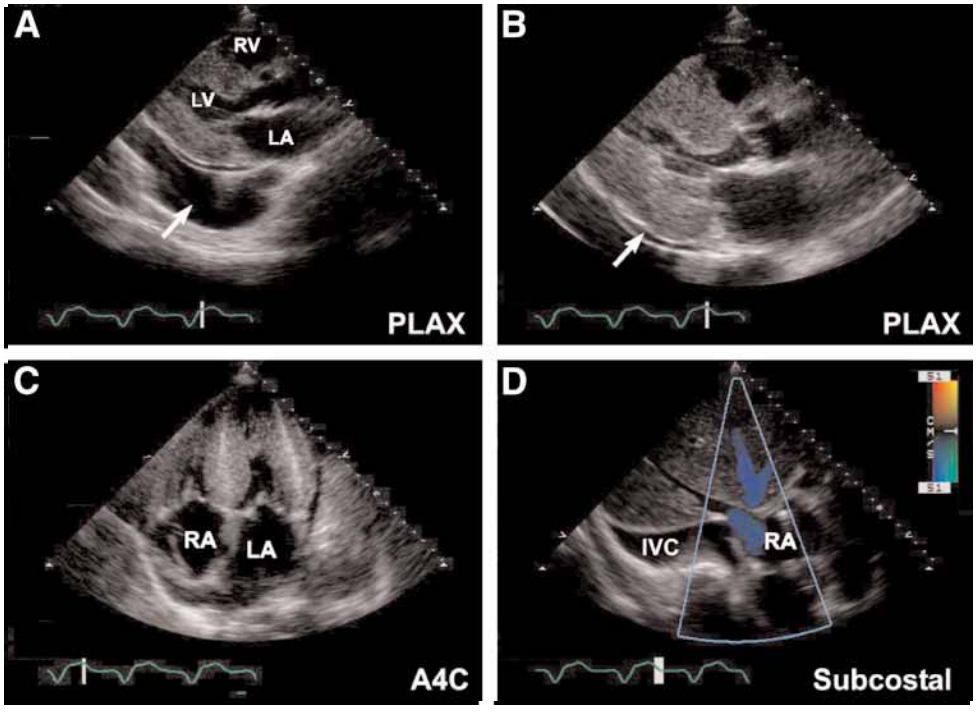

Fig. 8. Restrictive cardiomypathy: amyloid heart disease. Concentric left ventricular hypertrophy with reduction in left ventricular cavity size, dilated left atrium, left-sided pleural effusion (arrow, **A**), and smaller pericardial effusion (arrow, **B**) are features consistent with cardiac amyloidosis. Note thickened right ventricular wall and interatrial septum with moderate increase in right ventricular cavity size. A distinctive, but not specific sign of cardiac amyloidosis is the "ground-glass" or "sparkling" appearance of the myocardium **(A–C)**. Right heart failure with increased right sided pressures are evident in this patient. Note the markedly dilated inferior vena cava (IVC, **D**). (Please *see* companion DVD for corresponding video.)

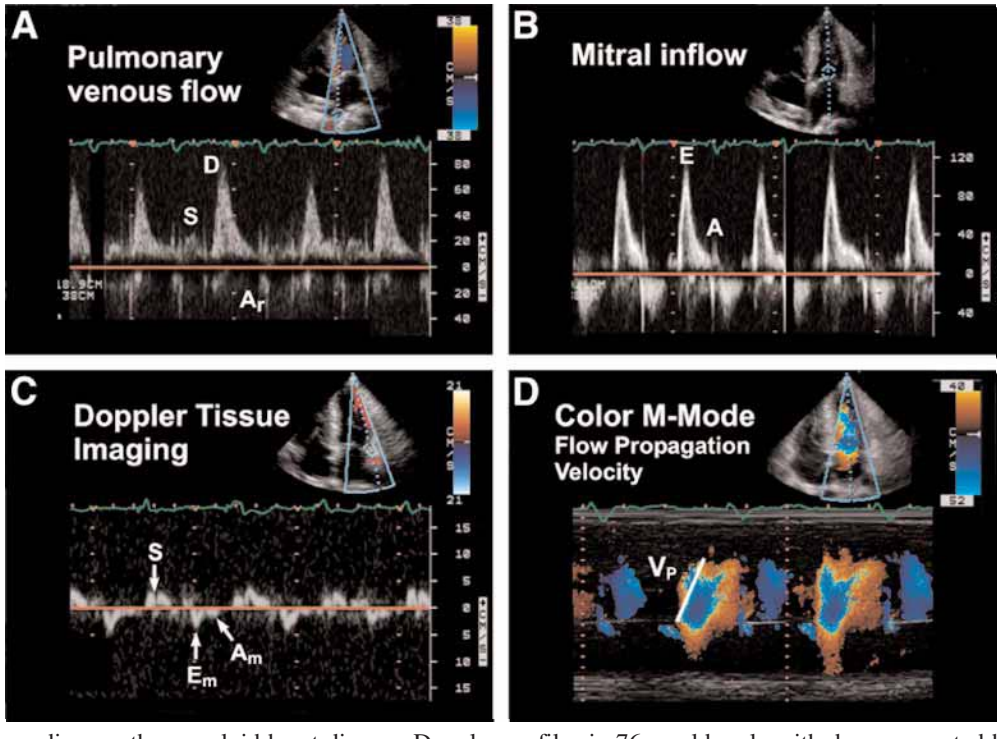

Fig. 9. Restrictive cardiomypathy: amyloid heart disease. Doppler profiles in 76-yr-old male with decompensated heart failure and amyloid cardiomyopathy shows classic Doppler findings in restrictive cardiomyopathy **(A)**. Right upper pulmonary venous flow with reduced systolic:diastolic flow ratio **(B)**. Mitral inflow profile with increased E:a ratio < 2 **(C)**. Markedly reduced velocities on Doppler tissue imaging **(D)**. Blunted Vp slope on color flow propagation velocity M-mode.

Table 4
Restrictive Cardiomyopathy

Common Causes of Restrictive Cardiomyopathy	
Primary	Idiopathic
	Hypereosinophilic syndrome (Löeffler endocarditis)
	Endomyocardial fibrosis
Secondary	Infiltrative disease: amyloidosis (primary, secondary), sarcoidosis
	Post-radiation, carcinoid syndrome
	Storage diseases, hemochromatosis, glycogen storage diseases
	Diabetes mellitus (most common)

Table 5
Cardiomyopathies With Diastolic Dysfunction

Restrictive cardiomyopathy
Dilated cardiomyopathy
Hypertrophic cardiomyopathy
Hypertensive cardiomyopathy
Ischemic cardiomyopathy

was notable for low-voltage QRS complexes and left bundle branch block.

Echocardiographic study showed preserved left ventricular ejection fraction and echocardiogenic speckling suggestive of cardiac amyloid. His pulmonary artery pressure on echocardiography was estimated at 50 mmHg plus right atrial pressure. Selected still frames are shown in Figs. 8 and 9 (please *see* companion DVD for corresponding video for Fig. 8).

The restrictive cardiomyopathies are characterized by diastolic dysfunction because of poor ventricular compliance (reduced chamber distensibility). The underlying restrictive or infiltrative processes (Table 4), despite the specific etiology, typically lead to progressive biventricular stiffness and elevated filling (diastolic) pressures, manifesting clinically as exertional dysnea and right heart failure. Yet it is important to recognize that diastolic dysfunction is not specific to restrictive cardiomyopathy, and frequently accompanies other cardiomyopathies that are not primarily restrictive (Table 5).

The diagnosis of restrictive cardiomyopathy is primarily clinical, but 2D and Doppler echocardiography play supportive/confirmatory roles (Table 6). Left ventricular cavity size is characteristically preserved, but wall

Table 6
A Summary of Echocardiographic Findings in Restrictive Cardiomyopathies

Modality	*Findings*
Two-dimensional findings	Normal ventricular volumes, preserved systolic function, marked biatrial enlargement
Doppler findings	Limited (<20%) variation in inflow velocities with respiration (compared with constrictive pericarditis)
Mitral inflow	Reduced isovolumic relaxation time (<70 m/s)
	Increased E velocity (>1 m/s)
	Reduced deceleration time (<160 ms)
	Reduced A velocity (<0.5 m/s)
	Reduced A wave duration
	Increased E:a ratio (>2)
Pulmonary vein	Reduced systolic flow
	Increased diastolic flow
	Reduced systolic:diastolic flow ratio
	Increased peak atrial reversal velocity and duration
Doppler tissue imaging	Reduced Em velocity (lateral annulus), <8–10 cm/s
Color M-mode (flow propagation velocity; Vp)	Quantitative: *V*p < 45 cm/s (quantitative) (normal >55 cm/s)
	visual estimate: blunted Vp slope (normal ~90°, upright)

thicknesses may be normal, increased, or even decreased. In amyloid heart disease, the prototype restrictive cardiomyopathy, concentric left ventricular thickening is typical and systolic function preserved (until the advanced stages). The pattern of myocardial wall thickening (involving the right ventricle and interatrial septum) are clues to the diagnosis (Table 7). Right ventricular dilatation frequently occurs and biatrial enlargement is almost always present. In addition, a small pericardial effusion and nonspecific valvular thickening are common. A "ground-glass" or "sparkling" appearance of ventricular myocardium is distinctive, but nonspecific for amyloid. However, when combined with other echocardiographic findings, it is highly suggestive of amyloid.

A helpful confirmatory parameter in cardiac amyloid is assessment of the voltage-to-mass ratio. Amyloid infiltration of the myocardium increases ventricular mass (Fig. 10) while reducing QRS voltage. This finding may be characteristic of amyloid and

Table 7
Echocardiographic Findings in Amyloid Heart Disease

Modality	*Description*
Two-dimensional/ M-mode findings	Left ventricular hypertrophy (with low QRS voltages or pseudoinfarct pattern on electrocardiogram), diminution of left ventricular cavity size, right ventricular hypertrophy, distinctive "ground-glass or sparkling" appearance of myocardium (nonspecific), thickened inter-atrial septum and valve leaflets, biatrial enlargement, echocardiographic signs of right heart failure, multi-valvular regurgitation; small to moderate pericardial effusion, LV function usually preserved until advanced stages
Doppler findings	Diastolic dysfunction (commonest and earliest abnormality), restrictive cardiomyopathy Doppler profile

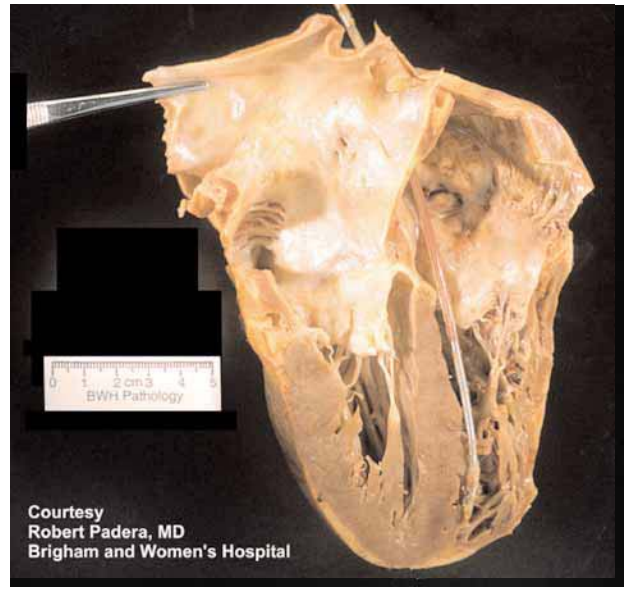

Fig. 10. Restrictive cardiomyopathy: amyloid heart disease. Gross heart specimen from a 66-yr-old man patient with systemic amyloidosis who died from congestive heart failure. Heart weighed 650 g (adjusted normal <350 g). Note thickened left ventricle with reduced cavity size, dilated atria, and intracardiac device. Biatrial enlargement reflects the consequences of impaired ventricular filling—a characteristic of restrictive cardiomyopathies.

other infiltrative disease, and distinguish it from other causes of increased wall thickness, such as hypertensive hypertrophy or hypertrophic cardiomyopathy.

Doppler profiles found in restrictive cardiomyopathy (Table 6) reveal abnormal diastolic filling patterns (*see also* Chapter 6). Reduced ventricular compliance (increasing ventricular stiffness) requires greater filling pressures, i.e., elevated ventricular end-diastolic pressures and markedly increased atrial pressures.

In the early stages, an impaired relaxation pattern predominates (Fig. 7A). Early rapid filling is slowed (decreased peak E velocity with prolonged DT) and increased atrial filling (kick) is required to compensate. E:a reversal or E:a ratio less than 1 and DT greater than 200 m/s defines the condition. Over time, increased early rapid filling is restored as higher filling pressures generated by a now dilated/thickened atria compensate and manifests as a "pseudonormalized" pattern. Repeat recordings during stage 2 of the Valsalva maneuver can unmask pseudonormalization—this acutely reduces filling pressures and reveals the underlying impaired relaxation. Pulmonary venous flow patterns provide supportive evidence. As the pathological processes ensue, a restrictive pattern becomes established (Fig. 9). The tall steep E-wave reflects higher transmitral gradients with very rapid equilibration during early diastole. Deteriorating atrial function frequently leads to atrial fibrillation (absent A-wave) or a markedly diminished A-wave (E:a ratio >1 and DT <150 ms). The most reliable diastolic abnormality by echocardiography is reduced myocardial relaxation velocities. Patients with advanced restrictive heart disease, such as amyloid, can have lateral mitral annular diastolic velocities of 5 cm/s or less (*see* Chapter 6).

The more common etiologies for restrictive cardiomyopathy are: (1) cardiac amyloid, which is the most common cause in the industrialized world; (2) hypereosinophilic syndrome and endomyocardial fibrosis, common in parts of Latin America, Asia, and Africa; (3) carcinoid heart disease (*see* Chapter 19); (4) Sarcoidosis (sarcoid granulomata primarily affect the reticulo-endothelial system, the lungs, and skin, but cardiac involvement occurs). Right heart failure may be a sequel to pulmonary fibrosis, but sarcoid granulomatous infiltration of the heart can lead to a restrictive cardiomyopathy as well as impaired systolic function and conduction disturbances (Fig. 11).

Restrictive cardiomyopathy can resemble, and can be difficult to distinguish from, constrictive pericarditis. Preservation of systolic function and abnormal diastolic filling patterns are seen in both. However, a thickened pericardium and respirophasic variation in inflow velocities are indicative of constrictive pericarditis (Fig. 12). In addition, mitral annular diastolic relaxation velocities are typically normal in patients with constrictive

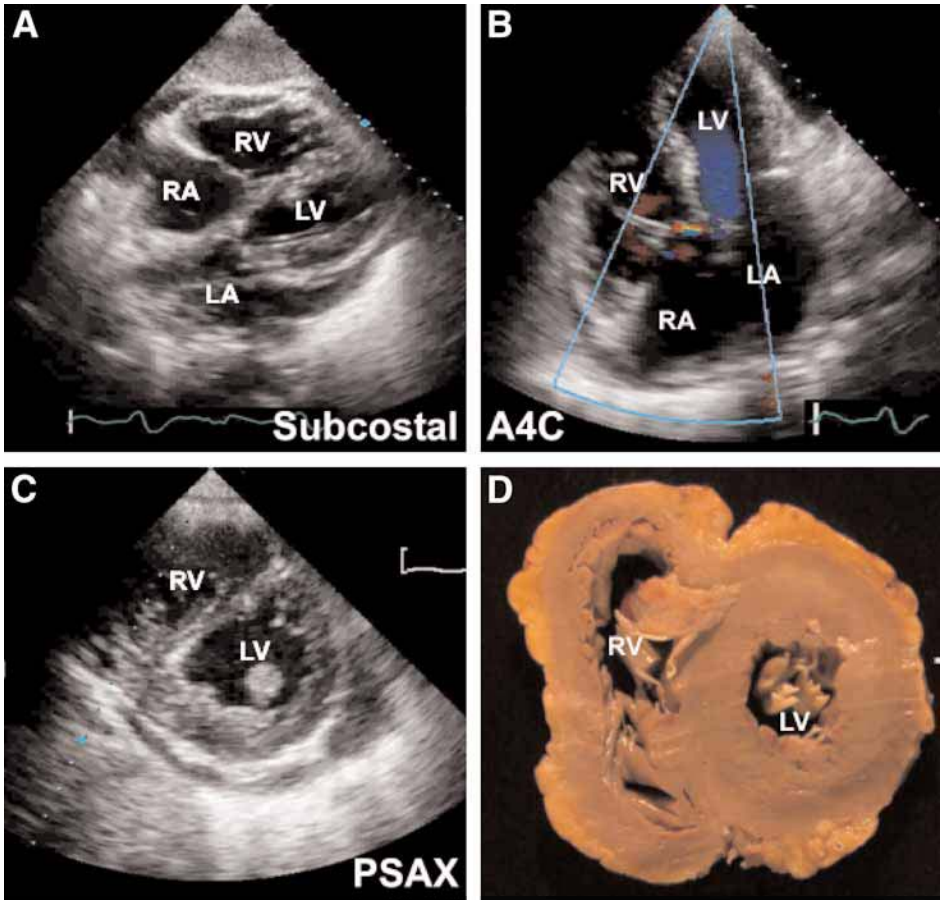

Fig. 11. Restrictive cardiomypathy: cardiac sarcoid. Echocardiographic images and a gross heart specimen from a 58-yr-old female who succumbed to complications related to severe pulmonary sarcoid, pulmonary fibrosis, and bronchiectasis are shown. In addition to Doppler indices consistent with a restrictive cardiomyopathy, biatrial enlargement and right ventricular hypertrophy secondary to pulmonary hypertension were seen **(A–D)**.

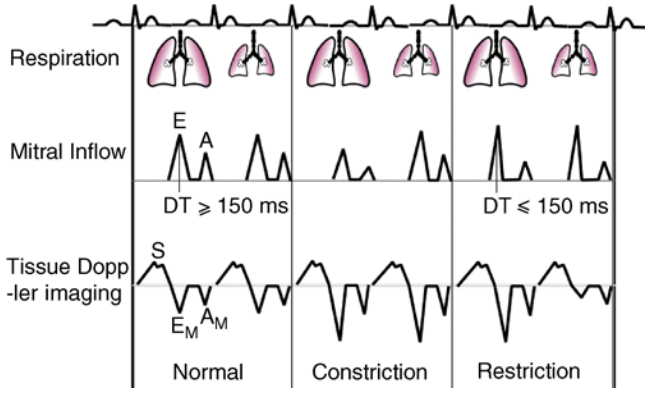

Fig. 12. Doppler indices: constrictive pericarditis vs restrictive cardiomyopathy. Simplified schema integrating Doppler profiles of mitral inflow, Doppler tissue imaging, and respirophasic changes to distinguish constrictive pericarditis from restrictive cardiomyopathy. Other Doppler profiles of tricuspid valve flow (Chapter 10, Fig. 12), pulmonary venous flow, and hepatic venous flow, should be integrated to improve assessment. However, the basis of the distinction remain the clinical presentation, two-dimensional echocardiographic findings, and computed tomography /magnetic resonance imaging.

physiology, whereas quite abnormal in patients with restrictive disease.

Clinically silent diastolic and systolic dysfunction eventually occurs in most patients with diabetes mellitus, even in well-controlled individuals. Diabetic cardiomyopathy is increasingly recognized as perhaps the most prevalent type of restrictive cardiomyopathy.

HYPERTROPHIC CARDIOMYOPATHY

CASE PRESENTATION

A 27-yr-old Caucasian male presented with episodes of palpitations. He gave no history of prescription drug or illicit drug use or smoking and led a physically active lifestyle. Family history was significant for hypertrophic cardiomyopathy. Physical examination was completely normal, including cardiac examination at rest and during Valsalva maneuver. His ECG showed normal sinus

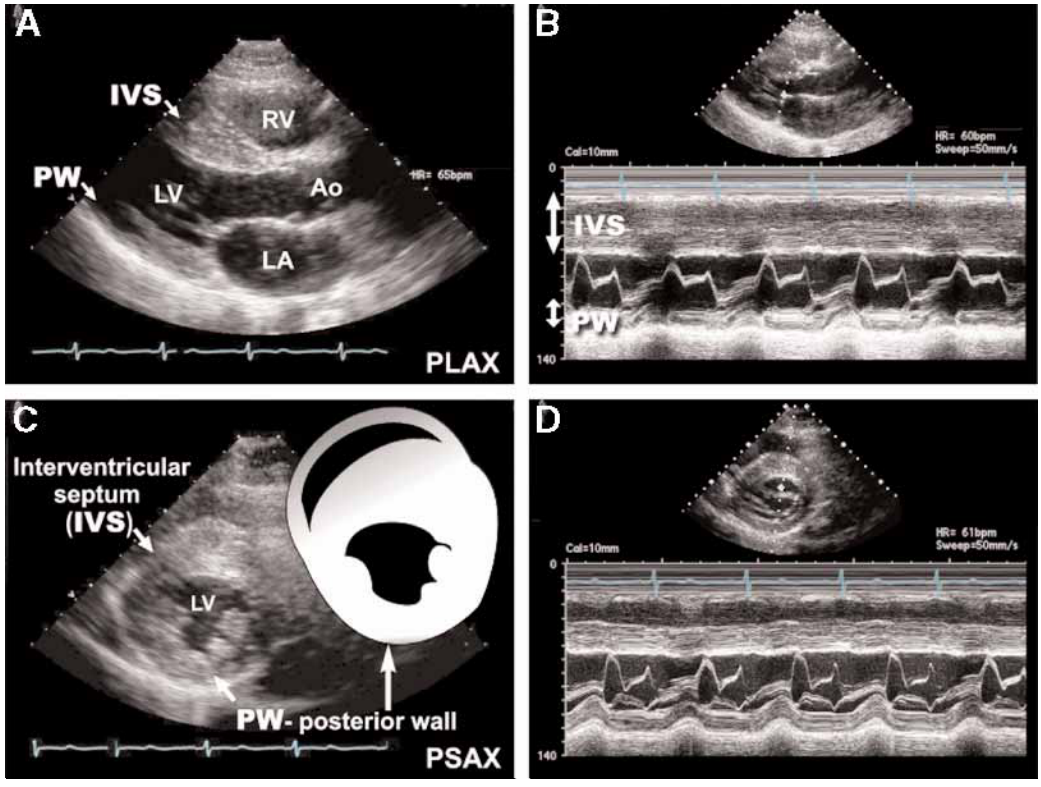

Fig. 13. Case presentation: hypertrophic cardiomyopathy. Thickened interventricular septum (IVS) measuring 20 cm, normal posterior wall thickness, and normal chamber sizes are seen on parasternal long-axis (PLAX) view **(A)**. M-mode at the mitral valve level shows the hypertrophied septum with E-point septal contact **(B)**. Parasternal short-axis view confirms assymetric hypertrophy **(C)**, which most often spares the basal posterior wall as shown on this M-mode through the short-axis view at the mitral level **(D)**. (Please *see* companion DVD for corresponding video.)

rhythm, heart rate of 67 bpm, normal intervals, and normal axis. Right ventricular conduction delay, left ventricular hypertrophy (LVH), and repolarization abnormalities were present.

On echocardiography, his left ventricular size was normal with normal left ventricular function and ejection fraction 70–75% (Figs. 13 and 14, please *see* companion DVD for corresponding video). No regional wall motion abnormalities were present but marked septal hypertrophy with maximal wall thickness of 24 mm (proximal-midseptum) was noted. Only minor systolic anterior motion (SAM) of the mitral chords was seen. No significant intracavitary gradient was detected either at rest or with the Valsalva maneuver. Reversed curvature of the interventricular septum was seen. The aortic root and leaflets were normal but trace aortic regurgitation was present. The right ventricle, tricuspid valve, and both atria were normal in size and function. The inferior vena cava and the pericardium were normal.

Hypertrophic cardiomyopathy is typically defined as unexplained ventricular hypertrophy, and can be generally diagnosed in a patient with hypertrophy not associated with hypertension or other obvious causes, such as aortic stenosis. The majority of cases of hypertrophic cardiomyopathy are caused by sarcomeric genetic mutations, although many specific gene mutations have been identified. Approximately 50% of cases are autosomal dominant.

Hypertrophic cardiomyopathy exhibits great heterogeneity both in morphological appearance and clinical presentation. Most patients with hypertrophic cardiomyopathy present clinically between ages 20 and 40 yr. Presentation later in life is generally associated with less severe forms of the disease.

Echocardiography has great utility in hypertrophic cardiomyopathy (Table 8). It helps establish the diagnosis in symptomatic patients, and exclude secondary causes of ventricular hypertrophy. It is an essential screening tool in identifying and monitoring relatives of affected patients. 2D, M-mode, and stress echocardiography are indispensable for

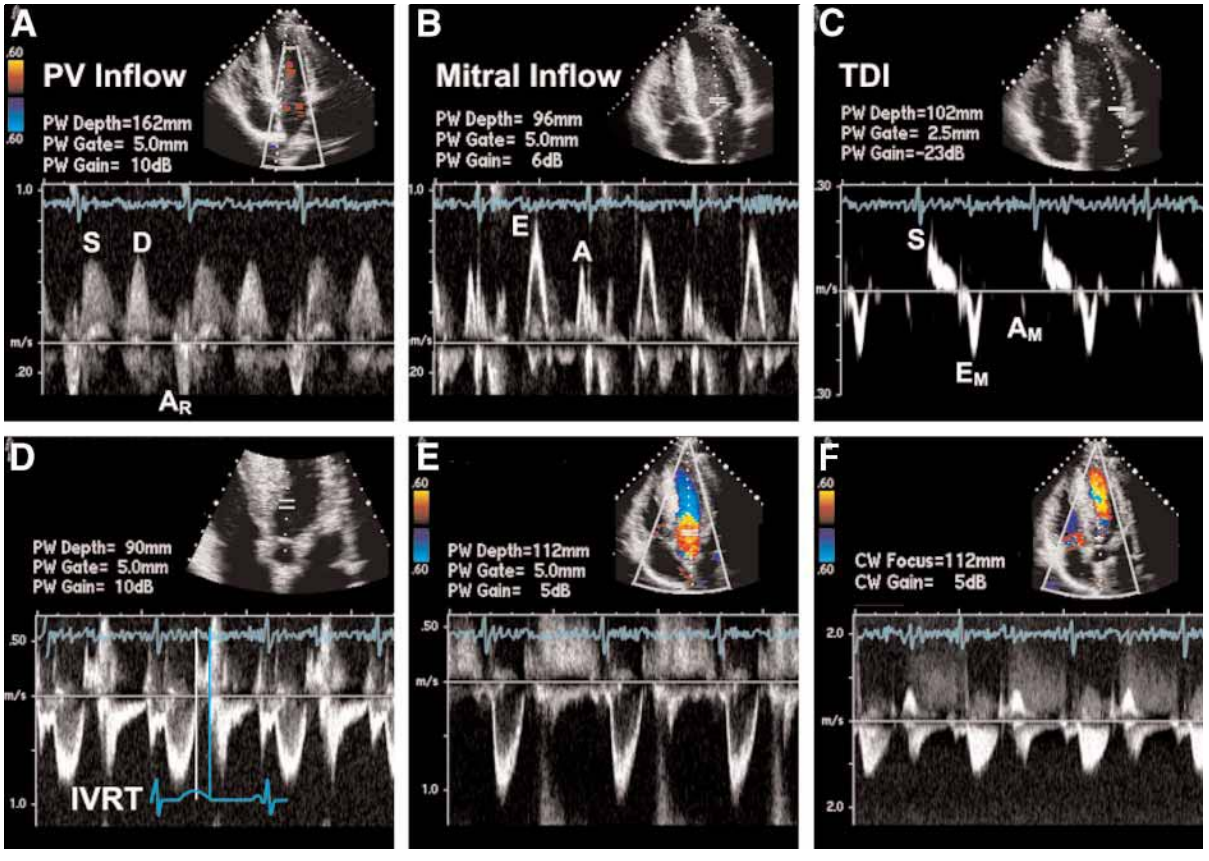

Fig. 14. Case presentation: hypertrophic cardiomyopathy. Spectral Doppler profiles of patient in our case presentation shows normal Doppler profiles in the evaluation of pulmonary venous flow, mitral inflow, and Doppler tissue imaging at the lateral mitral annulus **(A–C)**. Pulse Doppler interrogation along the septum using apical windows showed no stepwise increase in gradient **(D**,**E)**. Continuous-wave Doppler evaluation confirmed the same **(E)**.

Table 8
Utility of Echocardiography in Hypertrophic Cardiomyopathy

1.	Definitive diagnosis; excludes secondary causes, e.g., aortic stenosis
2.	Screening tool for first-degree and other relatives
3.	Assessment of morphological variants—and distribution and magnitude of left ventricular outflow tract gradients
4.	Assessment of mitral regurgitation severity (when present)
5.	Evaluation of diastolic function
6.	Patient selection for intervention procedures e.g., septal ablation or surgical myotomy-myectomy (stress echocardiography and other maneuvers)
7.	Myocardial contrast echocardiography: improves success rate of septal ablation and reduce need for permanent pacing
8.	Monitoring and follow-up postmedical or surgical intervention

detecting dynamic outflow tract obstruction and its various components, as well as in the assessment of provocative maneuvers. Intraprocedural myocardial contrast echocardiography can improve the success rates of septal ablation procedures for hypertrophic cardiomyopathy.

Echocardiographic Findings

Echocardiographic features of the most common variant—assymetric septal hypertrophy—includes marked hypertrophy along the length of the entire interventricular septum, often at the expense of the left ventricular cavity and normal or increased ventricular systolic function. Often, the septal-to-posterior wall thickness ratio is greater than 1.3, although it is also not uncommon to find relatively concentric hypertrophy. Reversed curvature of the interventricular septum is a typical finding in hypertrophic cardiomyopathy. Typically, hypertrophy extends down the majority of the length of the septum and is distinct from upper septal disproportionate thickening common in hypertensive hypertrophy of the elderly.

A typical feature of the enlarged interventricular septum is its impact on the Doppler profile of the left ventricular outflow tract (LVOT). This “dagger-shaped” spectral Doppler pattern reflects late-peaking systolic flow through

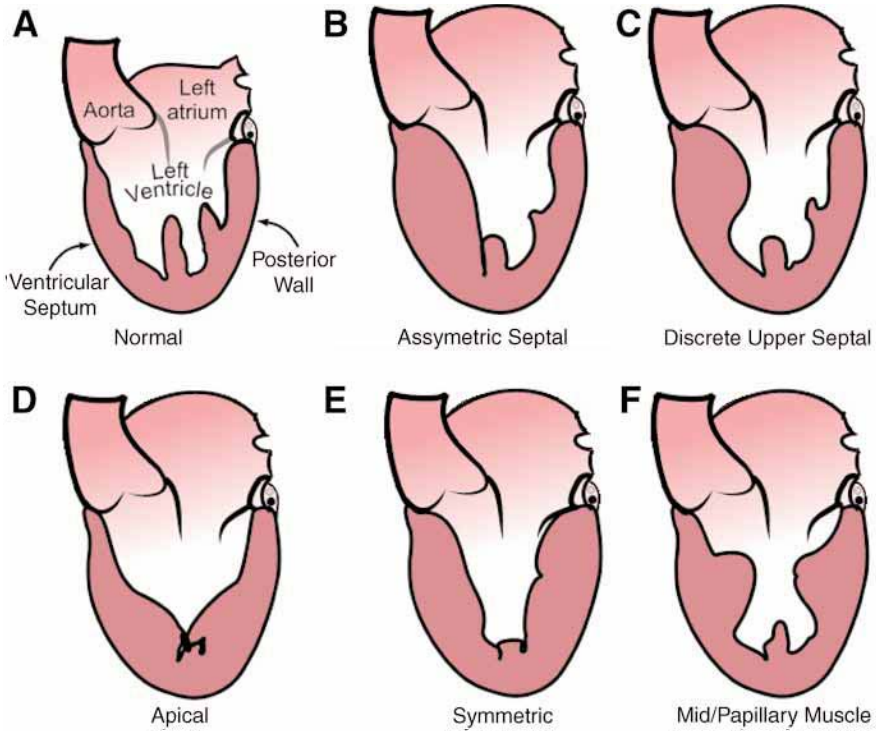

Fig. 15. Hypertrophic cardiomyopathy: variants. Hypertrophic cardiomyopathy morphology exhibits heterogeneity. The most common variant is assymetric septal hypertrophy involving the entire septum **(B)**. Discrete upper septal hypertrophy displays a sigmoid-shaped septum **(C)**. It is not the same as discrete/disproportionate upper septal thickening (DUST) or "septal knuckle" often seen in the elderly. The apical variant of hypertrophic cardiomyopathy **(D)** was first described in Japan, but occurs globally. The left ventricular chamber assumes an "ace of spades" configuration and is best seen in the apical 4-chamber view. It must be differentiated from left ventricular noncompaction. The concentric pattern of hypertrophic cardiomyopathy **(E)** occurs, exhibiting symmetrical thickening of the entire left ventricular wall. Concentric left ventricular hypertrophy with pressure overload states can be confused with this variant. Hypertrophied papillary muscles or midventricular hypertrophic cardiomyopathy is an uncommon variant. It may be associated with midcavity obstruction.

the LVOT (Fig. 15). Echocardiographic features found in hypertrophic cardiomyopathy are summarized in Table 9 and Figs. 16 and 17.

LVOT Obstruction and SAM of the Mitral Valve

Marked narrowing of the LVOT is seen or inducible in about one-fourth of patients. The result is dynamic LVOT obstruction (Fig. 18; please *see* companion DVD for corresponding video). This involves more than obstruction caused by the hypertrophied septum. SAM of the anterior mitral valve leaflet and abnormalties of the entire mitral valve complex commonly occur (Table 10). Enlarged elongated mitral leaflets and abnormalities of the subvalvular apparatus—papillary muscles and chordal attachments—all participate in the septal anterior motion and outflow tract obstruction. A posteriorly directed mitral regurgitant jet typically accompanies SAM.

SAM of the mitral valve (Figs. 18 and 19; please *see* companion DVD for corresponding video) is not pathognomonic of hypertrophic cardiomyopathy; it occurs in

Table 9
Echocardiographic Findings in Hypertrophic Cardiomyopathy

Modality	*Description*
Two-dimensional findings	• Asymmetric; isolated septal hypertrophy (commonest variant), although concentric hypertrophy also common
	• Septal: Posterior wall thickness ratio >1.3 elongated mitral leaflets—coaptation point along the body, not the tips of leaflets (Figs. 18 and 19)
M-mode	• SAM of mitral valve; midsystolic notching/fluttering of the aortic valve
Doppler findings	• Dynamic LVOT obstruction; "dagger-shaped" CW profile; mitral regurgitant (accompanying SAM) with posteriorly directed jet; relaxation abnormality/ diastolic dysfunction

LVOT, left ventricular outflow tract; CW, continuous wave; SAM, systolic anterior motion.

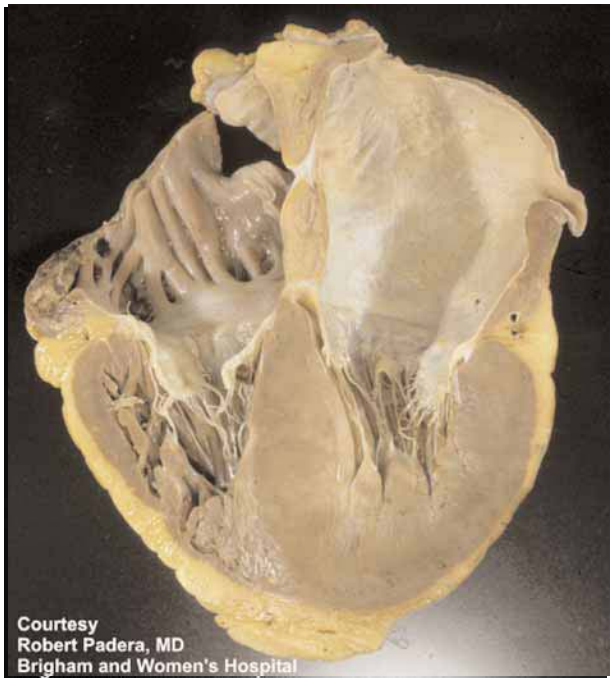

Fig. 16. Hypertrophic cardiomyopathy: concentric variant. Hypertrophic cardiomyopathy of the concentric variety in a 38-yr-old male who succumbed to surgical complications unrelated to his cardiomyopathy. Note the massive hypertrophy confined to the left ventricle and marked dilatation of his left atrial chamber.

Table 10
Factors Contributing to Dynamic Left Ventricular Outflow Trait Obstruction

1.	Septal hypertrophy
2.	Systolic anterior motion of mitral valve leaflets
3.	Systolic anterior displacement of entire mitral valve complex (including papillary muscles)
4.	Redundant mitral valve leaflets
5.	Hydrodynamic drag forces (Venturi effect)

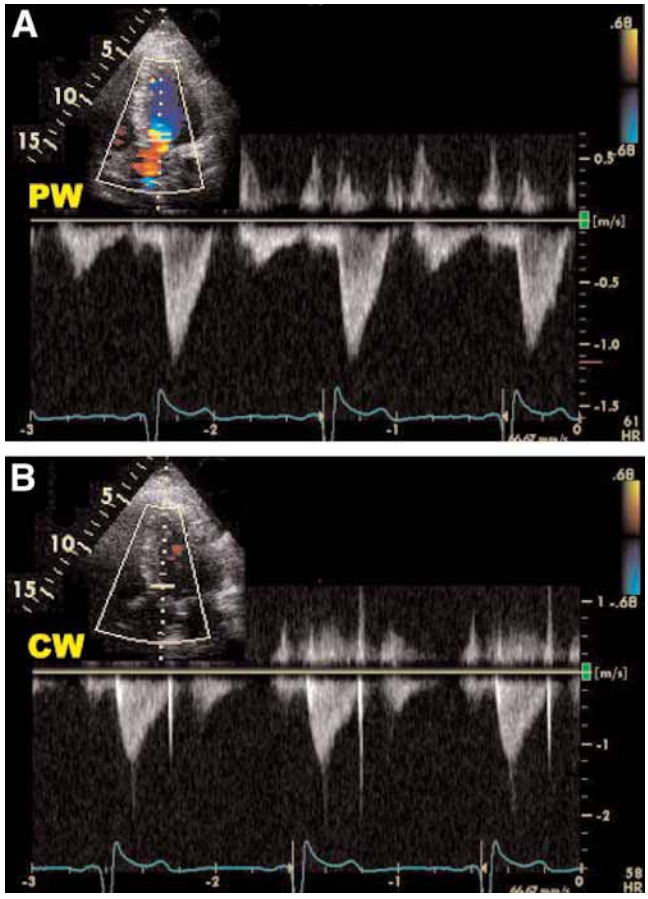

Fig. 17. Hypertrophic cardiomyopathy. Spectral Doppler profile of characteristic "dagger-shaped" flow distal to the hypertrophied septum. This reflects late peaking maximal velocities—a manifestation of some obstruction to systolic flow.

secondary hypertrophic cardiomyopathies and hypercontractile states (Table 11). The time of onset and the duration of SAM are best appreciated on M-mode echocardiography. Both such measurements are related to the severity of LVOT obstruction (Fig. 20).

A midsystolic drop in LVOT velocities—a reflection of impedance to flow within the aorta—typically manifests as midsystolic notching and fluttering of the aortic valve leaflets on M-mode ("lobster claw abnormality," Fig. 21). Dynamic outflow obstruction may be absent at rest, but provoked by maneuvers that reduce preload (e.g., Valsalva maneuver or amyl nitrite inhalation (Table 12; Fig. 22); or increased by maneuvers that increase preload, such as simple leg lifting.

Dynamic outflow obstruction is best appreciated on continuous-wave Doppler. Interrogation of velocities across the LVOT produces a characteristic late-peaking Doppler profile. Using the simplified Bernoulli equation, peak velocities can be converted into pressure gradients across the LVOT. Exercise provokes increased LVOT gradients and exercise stress echocardiography may provide better correlation between symptoms and disease severity compared to amyl nitrite inhalation (Table 12, Fig. 23A).

A similar pattern of dynamic outflow tract obstruction can be seen in midcavity obstruction owing to variant hypertrophic cardiomyopathy (Fig. 23B). The discrete or disproportionate upper septal hypertrophy ("DUST") commonly seen in elderly individuals bears

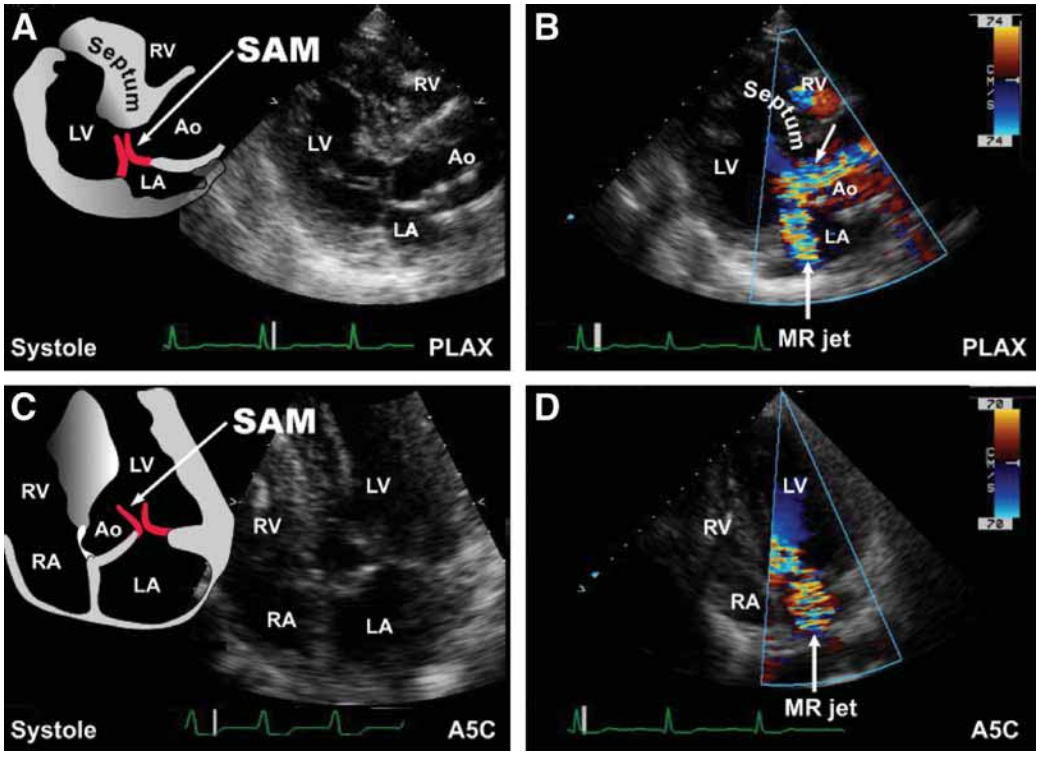

Fig. 18. Dynamic left ventricular outflow tract obstruction. Dynamic left ventricular outflow tract obstruction with systolic anterior motion of the mitral valve leaflets (SAM) are shown in this parasternal long-axis (PLAX) view **(A)**. Suboptimal mitral leaflet coaptation accompanies SAM and is typically accompanied by a posteriorly directed mitral regurgitant jet. Note the turbulence created in within the left ventricular outflow tract (arrow, **B**). Apical five-chamber (A5C) views of the same features above are shown **(D)**. (Please *see* companion DVD for corresponding video.)

no clear etiological relationship to hypertrophic cardiomyopathy. Nevertheless, the prominent septal "knuckle" found in DUST may cause dynamic outflow tract obstruction (Fig. 24).

Mitral Regurgitation in Hypertrophic Cardiomyopathy

A posteriorly directed jet of mitral regurgitation typically accompanies SAM of the mitral valve for reasons explained previously (Figs. 18 and 19). It temporally follows the onset of LVOT obstruction and care should be taken not to confuse its Doppler velocity profile with that of LVOT obstruction. The peak gradients, timing, and configuration of the spectral Doppler profile help to differentiate between the two.

Diastolic Dysfunction in Hypertrophic Cardiomyopathy

Diastolic filling of the left ventricle is impaired in about 80% of individuals with hypertrophic cardiomyopathy, and can even be observed in asymptomatic patients without overt hypertrophy but who are genetically affected. No clear relationship exists between the severity of hypertrophy and the severity of diastolic dysfunction. Asynchronous myocardial relaxation of the hypertrophied muscle can lead to complex patterns of intracavitary flow during diastole.

Echocardiography in Septal Ablation and Myectomy-Myotomy

Echocardiography plays a central role in identifying clinically significant LVOT obstruction that requires intervention, i.e., septal ablation or myectomy-myotomy of the hypertrophied muscle. Intraprocedural echocardiography with myocardial contrast imaging has become routine during alcohol septal ablation (Fig. 25).

The septal perforating branch of the left anterior descending coronary artery that supplies the hypertrophied septum (where it contacts the anterior mitral leaflet) is cannulated via a percutaneous transluminal approach and myocardial contrast agent then injected. Intraprocedural echocardiography is essential to guide and monitor the procedure and dehydrated alcohol is

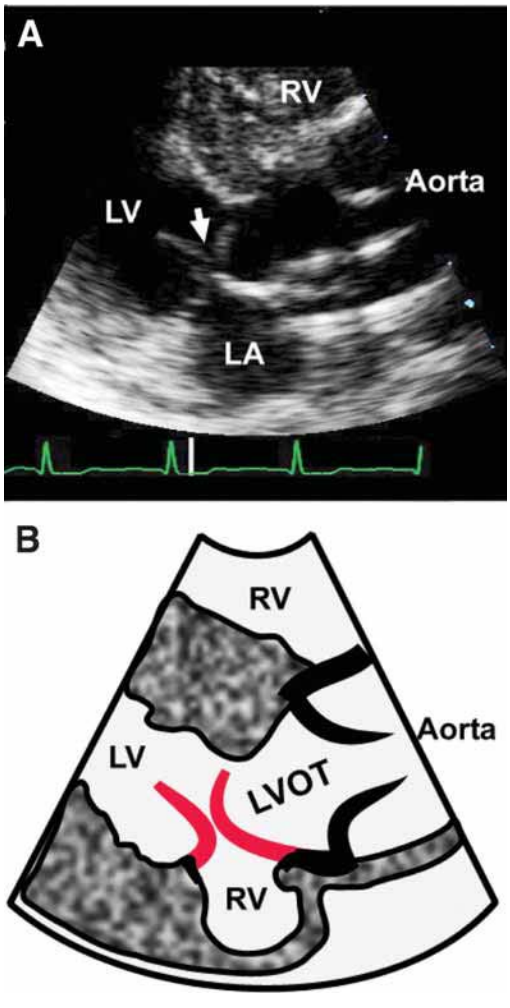

Fig. 19. Systolic anterior motion of the mitral valve (SAM). SAM of the mitral valve dynamically obstructs normal left ventricular outflow (LVOT). Note the anterior movement of both mitral leaflets (and supporting mitral structures) and the incomplete coaptation at a point halfway the body of the elongated mitral leaflets. These result in the characteristic posteriorly directed jet of mitral regurgitation (Fig. 18). (Please *see* companion DVD for corresponding video.)

Table 11
Systolic Anterior Motion

Hypertrophic cardiomyopathy
Left ventricular hypertrophy
Infiltrative cardiomyopathies with septal involvement
Hypercontractile states
Mechanical causes
Others

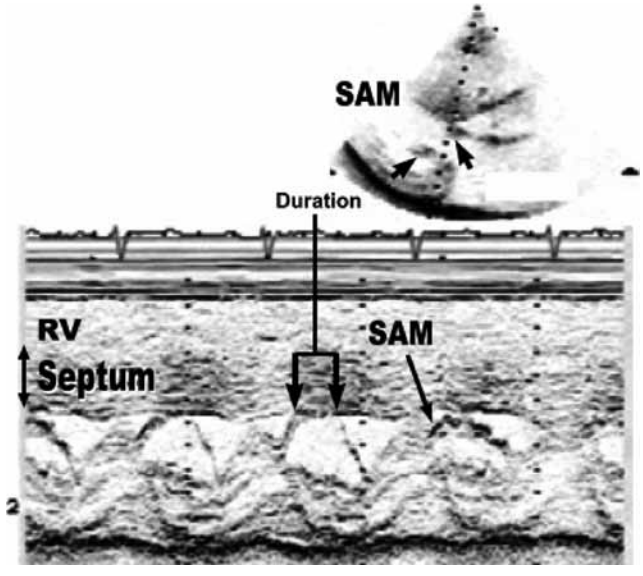

Fig. 20. Systolic anterior motion of the mitral valve (SAM). M-mode at the mitral valve level can reveal the timing and duration of the SAM of the mitral valve leaflets. A linear relationship exists between the time of onset and duration of SAM, and the severity of the dynamic left ventricular outflow tract (LVOT) obstruction (Pollick C. Circ 1984:69, 47). Note that systolic anterior displacement involves not just the anterior mitral leaflet, but also the chordae and papillary muscles—giving appearance of "crowding" during systole on M-mode (arrow labeled SAM).

injected when the site of maximal obstruction is identified. Improved success rates and fewer complications occur when myocardial contrast echocardiography is employed.

Intra-operative transeophageal echocardiography is routinely employed during surgical myectomy-myotomy of the hypertrophied septum.

Apical Variant of Hypertrophic Cardiomyopathy

A peculiar variant of hypertrophic cardiomyopathy that accounts for near 25% of cases in Japan and 40% in parts of China (but <5% of cases in the United States) is characterized by "giant" negative T-waves on ECG (Fig. 26) and "spade-like" geometry of the left ventricular cavity at end-diastole on 2D echocardiography. It runs a more benign course and presents later than other variants, but unfamiliarity with its ECG findings and echocardiographic features, including complex mitral filling patterns (Figs. 27 and 28) can lead to injudicious management.

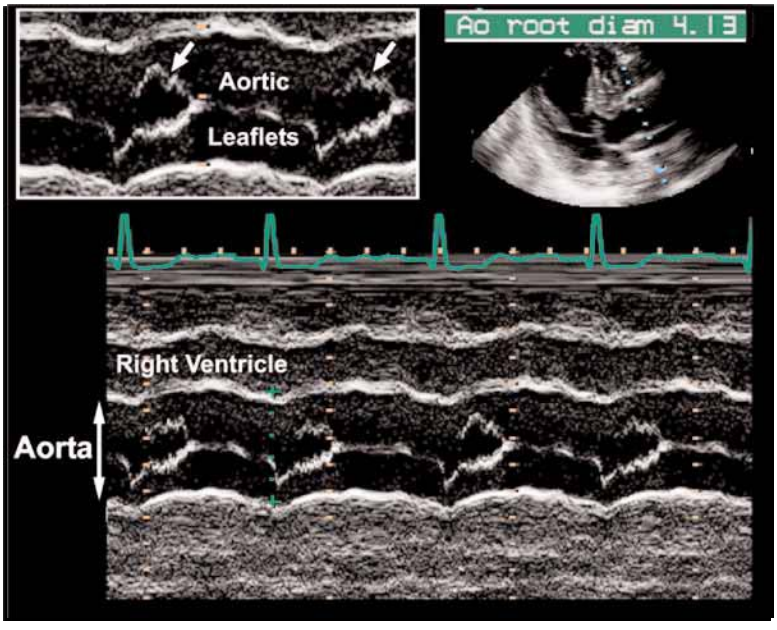

Fig. 21. Midsystolic aortic valve notch/flutter. M-mode through the aortic root at the aortic valve level. In this elderly woman, a septal "knuckle" shows the impact of dynamic left ventricular outflow tract obstruction on aortic valve behavior. Midsystolic notching and fluttering are common—a reflection of turbulence and dynamic nature of the obstruction—the so-called "lobster claw" abnormality.

Table 12
Physiological States, Maneuvers, and Interventions That Influence LVOT Gradient in Hypertrophic Cardiomyopathy

	Preload	*Afterload*	*Contractility*
Valsalva (strain phase)	decrease	decrease	–
Standing	decrease	–	–
Leg raising	decrease	–	–
Exercise	increase	increase	increase
Isometric handgrip	–	increase	–
Tachycardia	decrease	–	increase
Hypovolemia	decrease	decrease	increase
Amyl nitrite inhalation	decrease	decrease	increase
IVCS; general anaesthesia	– or decrease	–	decrease

Conditions that decrease preload, lower afterload, and increase contractility generally increase LVOT gradient (and the systolic murmur)

Table modified from Wynne J, Braunwald E. The Cardiomyopathies. In: Braunwald's heart disease—a Textbook of Cardiovascular Medicine, Zipes DP, Libby P, Bonow RO, Braunwald E eds., Elsevier Saunders. Philadelphia, 2005.

IVCS, intravenous conscious sedation; LVOT, left ventricular outflow tract.

Athelete's Heart or Hypertrophic Cardiomyopathy?

Sudden cardiac death in the young, specifically in the athletic population, poses clinical, echocardiographic (and medico-legal) challenges. Hypertrophic cardiomyopathy is the most common cause of death in athletes. Current data indicate that hypertrophic cardiomyopathy is responsible for up to one-third of such deaths.

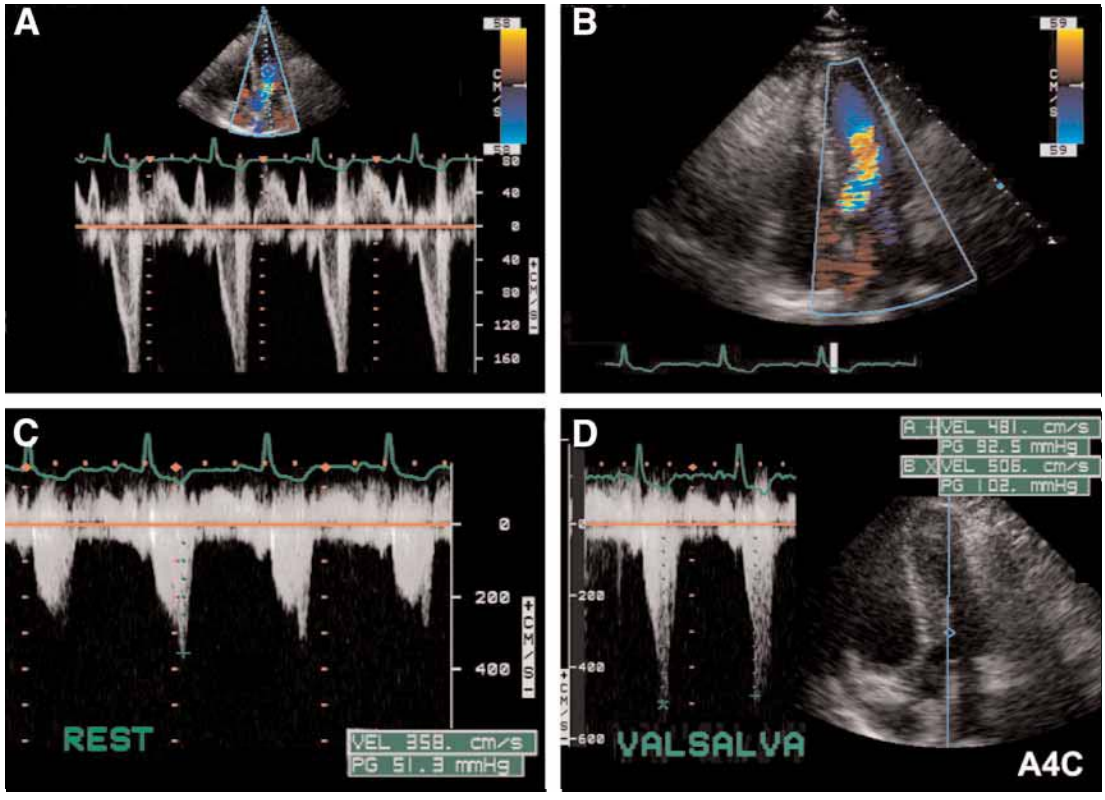

Fig. 22. Valsalva maneuver and hypertrophic cardiomyopathy. Gradients across the left ventricular outflow tract obstruction are influenced by conditions affecting preload (Table 11). **A**,**B** show velocities at rest on pulse Doppler with accelerated flow evident on color flow Doppler. In this patient, peak gradients averaged 50 mmHg, but exceeded 100 mmHg during the strain phase of the Valsalva maneuver. This was associated with chest pain he was referred for septal ablation.

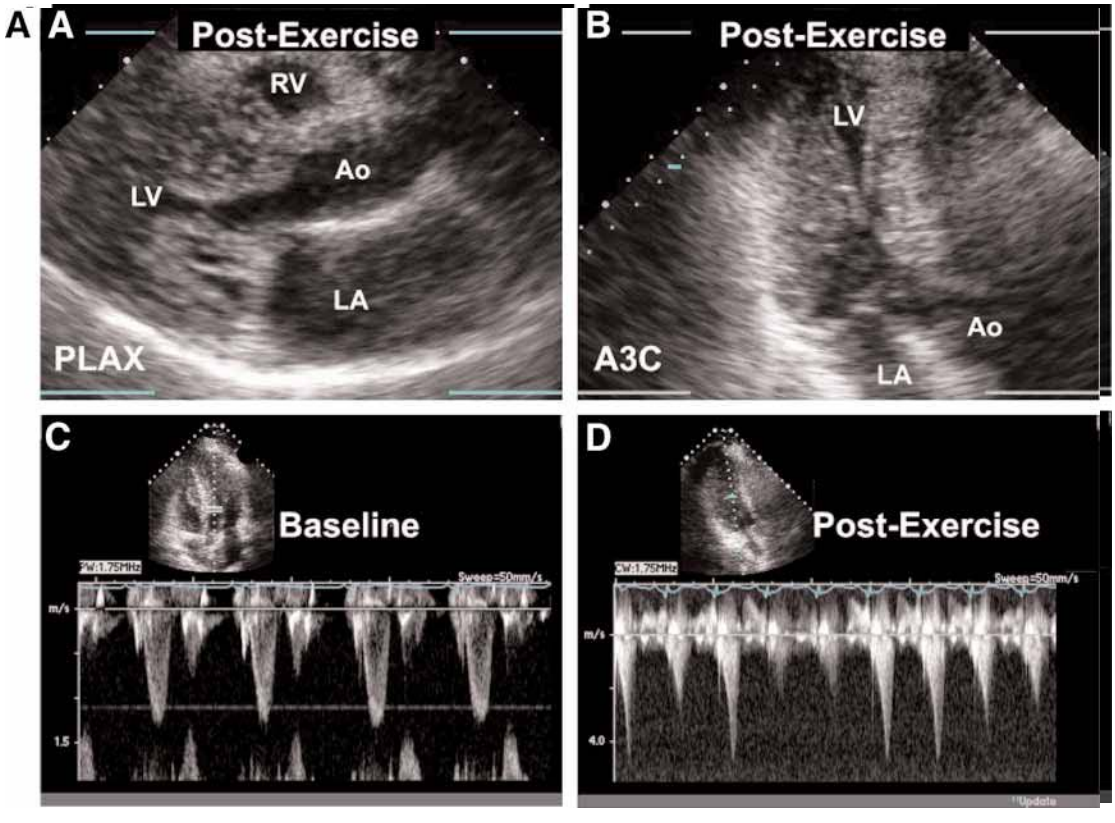

Fig. 23. *(Continued)*

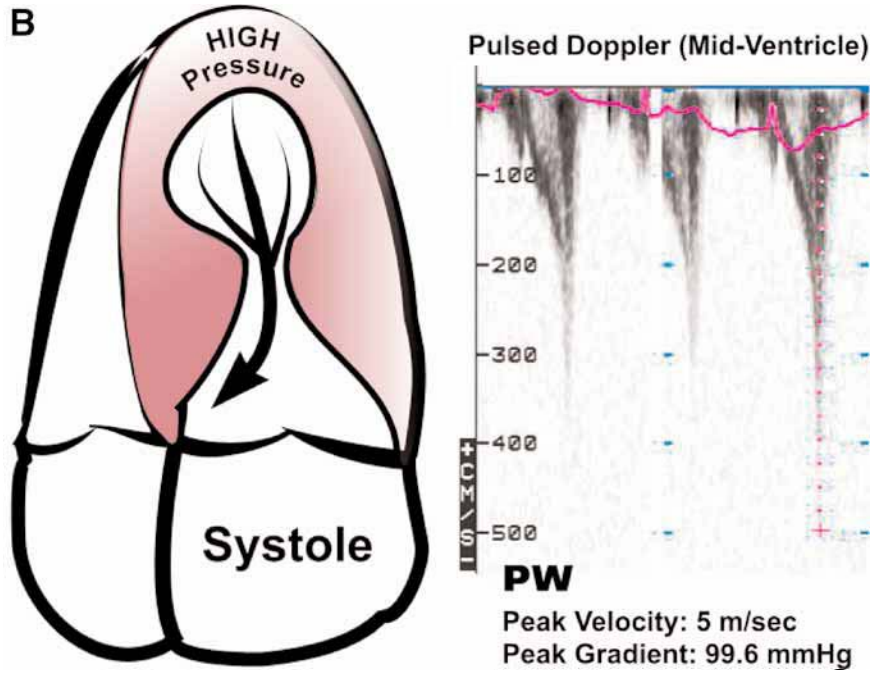

Fig. 23. (A) Exercise stress testing in hypertrophic cardiomyopathy. Stress testing in hypertrophic cardiomyopathy can provide information on gradients that correlate with patient symptoms and serve as a guide to the timing and efficacy of interventions. Systolic frames postexercise show marked ventricular outflow obstruction **(top panels)** Baseline pulse Doppler (PW) shows shows normal aortic outflow velocities **(bottom left panel)**, which markedly accelerate, exceeding 5 m/s **(bottom right panel)**. **(B)** Dynamic midcavity obstruction. Sketch depicting late-peaking Doppler velocity envelope in midcavity obstruction in hypertrophic cardiomyopathy involving primarily the midleft ventricular segments and papillary muscles (*see also* Fig. 27A).

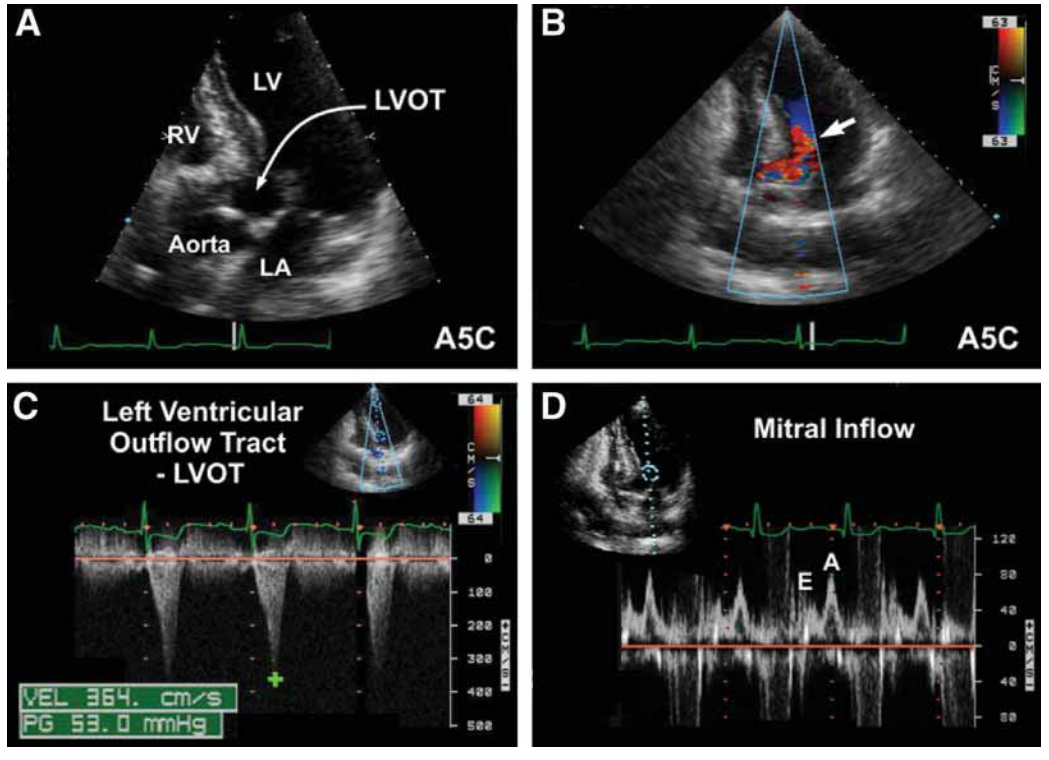

Fig. 24. DUST: discrete/disproportionate upper septal hypertrophy in the elderly. Disproportionate upper septal hypertrophy is commonly seen in othewise normal elderly individuals. Note the relationship of the septal "knuckle" to the left ventricular outflow tract **(A)** with flow acceleration on color flow Doppler **(B)**. Spectral Doppler envelope shows late-peaking velocities **(C)**. The impaired relaxation pattern (E:a ratio < 1) occurs in normal aging **(D)**.

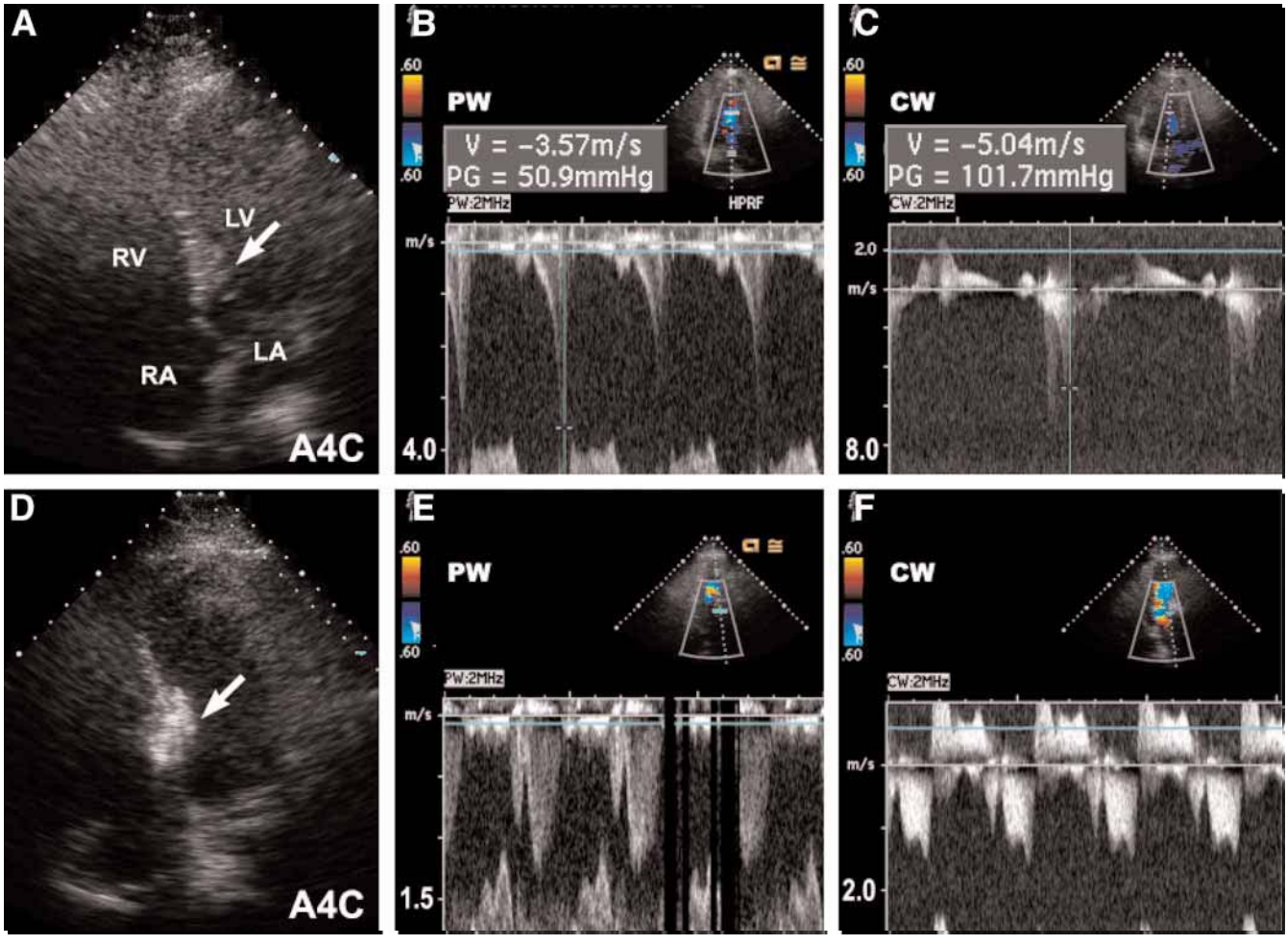

Fig. 25. Septal ablation: intraprocedural echocardiography. Images from the same patient in Fig. 23 are obtained pre- and postseptal ablation. At baseline **(A)** in the cardiac catheterization suite, resting gradient was 50 mm **(B)** increasing to 100 mmHg with Valsalva **(C)**. Cannulation of the septal artery supplying the offending septal region followed by slow infusion of dehydrated alcohol to ablate the same. Echocardiographic staining of the injected septal region is evident **(D)**. Immediately postprocedure, the resting gradient fell remarkably at baseline **(E)** and during Valsalva **(E)**. Repeat echocardiography done 2 wk later showed continued echocardiographic and clinical improvement.

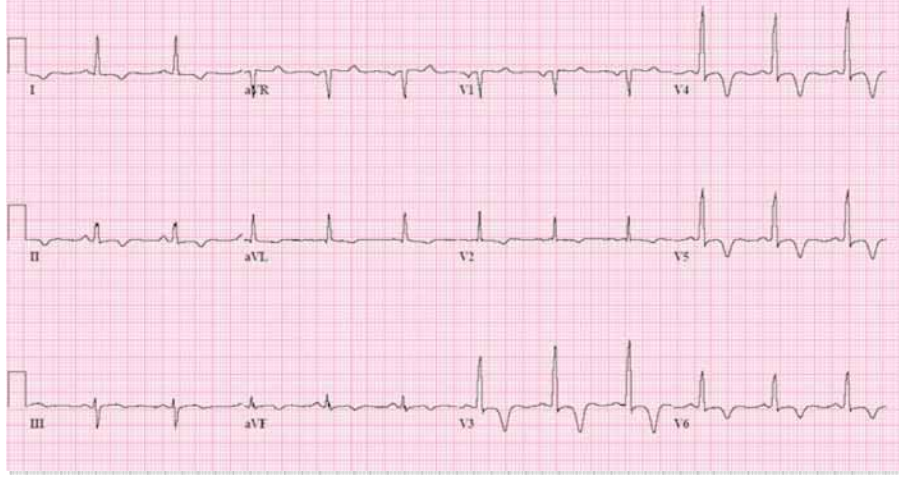

Fig. 26.

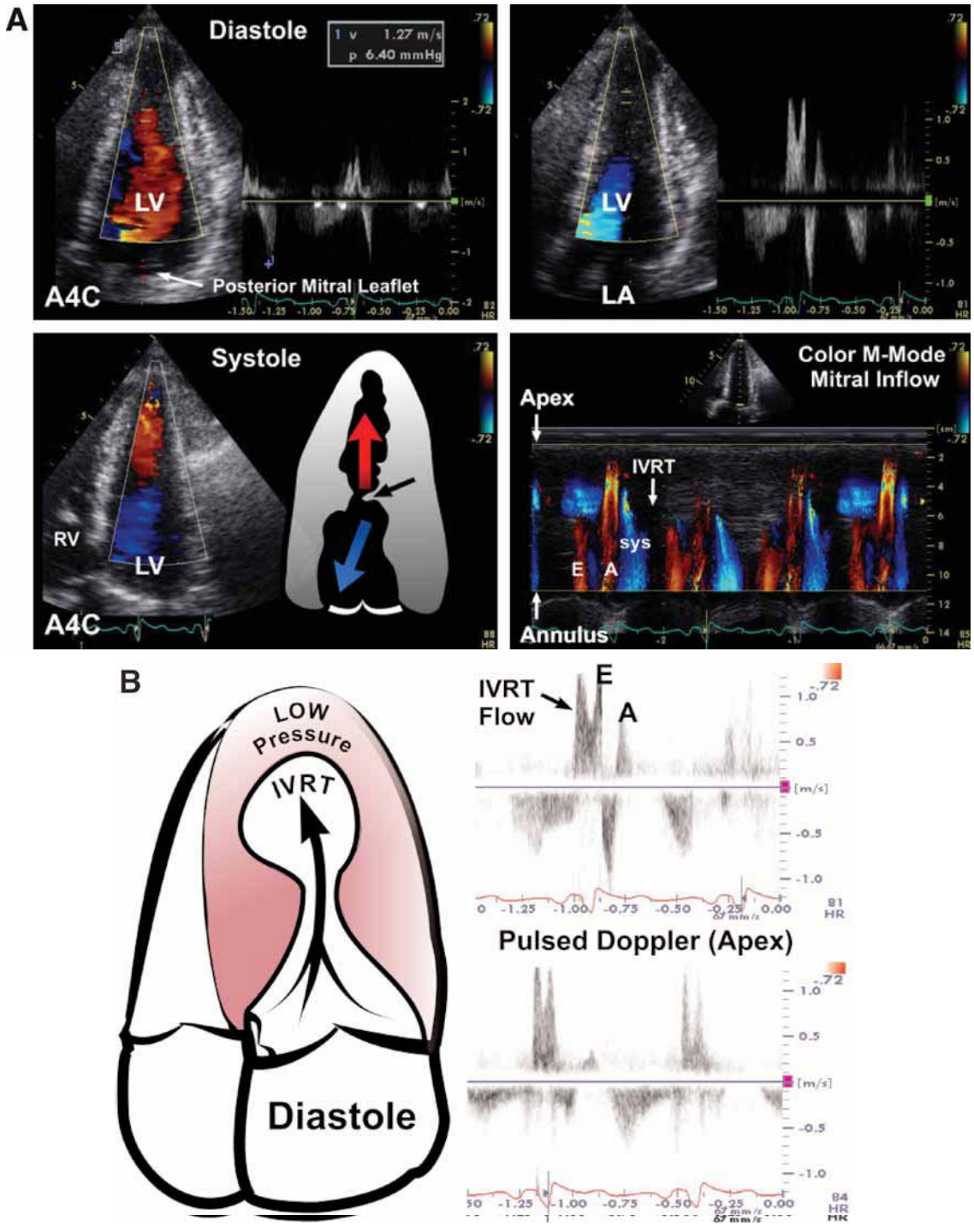

Fig. 27. Intracavitary isovolumetric relaxation time (IVRT) flow. **(A)** Asynchronous relaxation of the hypertrophied ventricle is common in hypertrophic cardiomyopathy. Early relaxation of the apical anterior segments can create low (suction) pressure regions within the left ventricular cavity during the IVRT. This resulted in a complex pattern of flow that appeared triphasic **(top panels; B)**. Systolic midcavity obstruction can result in bidirectional flow as shown on color flow Doppler **(bottom left panel)**. Color M-mode of mitral inflow pattern in this patient shows an irregular filling pattern **(bottom right panel)**. **(B)** Sketch depicting the intracavity IVRT flow patterns on spectral Doppler discussed in Fig. 26A.

Fig. 26. *(Opposite page)* A 12-lead electrocardiogram in a 65-yr-old male with coronary artery disease, hyperlipidemia, and type 2 diabetes. A 12-lead electrocardiogram in this patient with apical variant hypertrophic cardiomyopathy shows normal sinus rhythm, left atrial enlargement, increased QRS voltage, and deep T-wave inversion in the precordial leads.

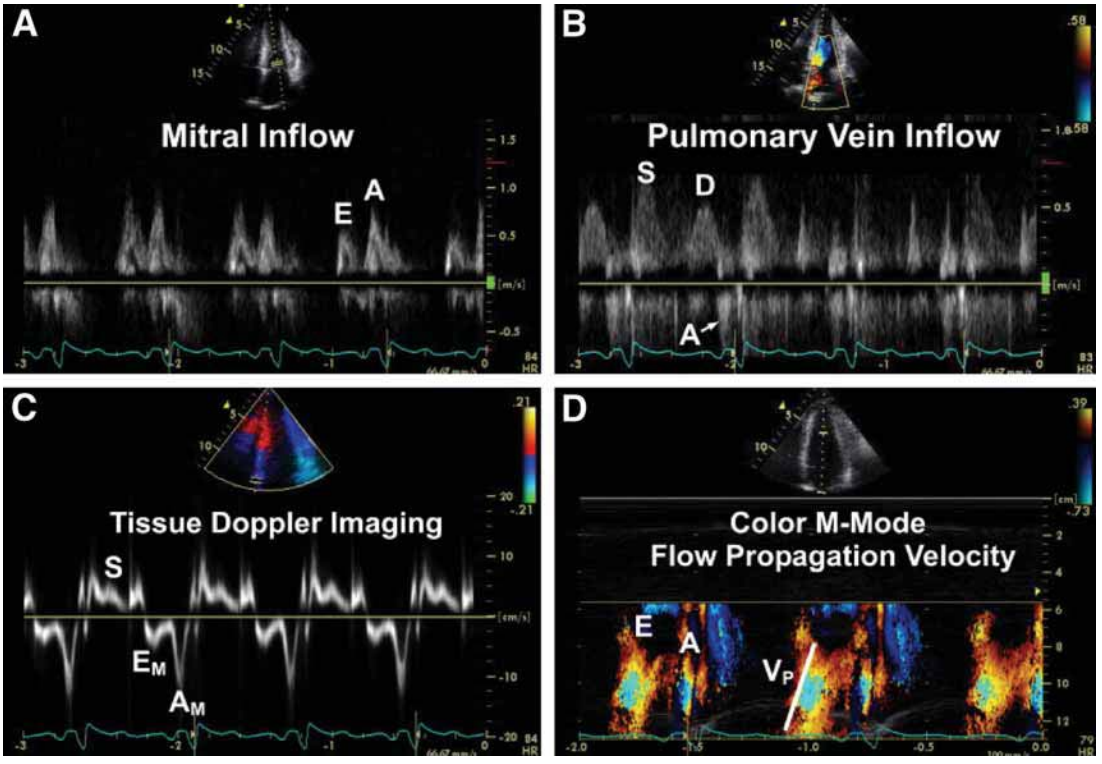

Fig. 28. Doppler indices of diastolic function in apical hypertrophic cardiomyopathy. Mitral inflow Doppler velocity profile in 65-yr-old male suggests mild left ventricular relaxation abnormality **(A)** with relatively normal pulmonary venous flow Doppler **(B)**. Relatively low velocities are seen on Doppler tissue imaging with reversal of the normal E_m: A_m ratio **(C)** and blunted Vp slope on color flow propagation velocity M-mode **(D)**.

The most challenging scenario occurs when the hallmark features of hypertrophic cardiomyopathies are absent, and when left ventricular wall thickness lies within the "gray zone" of 13–15 mm. Echocardiography within the clinical context is central to making the distinction. The distinction can have significant implications for further patient management (Table 13).

HYPERTENSIVE CARDIOMYOPATHY

CASE PRESENTATION

A 34-yr-old male Haitian immigrant with no reported past medical history suddenly reported feeling unwell while playing with sister's children. He vomited, fell to floor unresponsive, and was taken to hospital where his blood pressure measured 320/220 mmHg. Head computed tomography showed scan showed subarachoid hemorrhage.

Appropriated management was instituted, but his blood pressure proved extremely difficult to control. He was extubated, but expired 10 d following admission. His echocardiography images and videos appear in Figs. 29–31.

Hypertension is the most prevalent cardiovascular disease, and hypertensive heart disease including LVH is far more prevalent than the other cardiomyopathies combined. LVH is a strong independent risk factor for cardiovascular morbidity and mortality in population studies, in primary and secondary hypertension, and in patients with heart disease. Echocardiographically derived LVH is a better measure (more sensitive) and a stronger predictor of outcomes than electrocardiographic LVH.

A summary of echocardiographic findings in hypertensive cardiomyopathy is shown in Table 14. Echocardiographic findings in hypertension generally present less dramatically than in our case presentation, but concentric LVH remains the hallmark echocardiographic finding. This manifests as increased left ventricular wall thickness with no increase in cavity size. Remodeling can occur in response to ischemic injury or heart failure.

Table 13
Parameters for Differentiating Athelete's Heart Vs Hypertrophic Cardiomyopathy Within "Gray Zone"

"Gray zone" of LV wall thickness 13–15 mm	*Athlete's heart*	*Hypertrophic cardiomyopathy*
Clinical presentation	Asymptomatic; ECG signs of LVH often present	Most asymptomatic; but also syncope, tachyrrhythmias, dynamic murmur, sudden death, family history, gene mutations; ECG often shows bizarre patterns
LV cavity	LV cavity > 55 mm	LV cavity < 45 mm
Pattern of hypertrophy	Physiology concentric LVH; may regress with deconditioning	Asymmetric septal hypertrophy and other variants (Fig. 13)
Systolic function and EF	Increased EF; hyperdynamic systolic function; bradycardia	Normal or increased EF; normal systolic function
Diastolic function; E_m velocities	Normal highly compliant LV; brisk E_m velocities	Impaired diastolic indices with reduced E_m velocities
Left atrial size	Normal	Enlarged

EF, ejection fraction; ECG, electrocardiogram; LV, left ventricular; LVH, left ventricular hypertrophy.

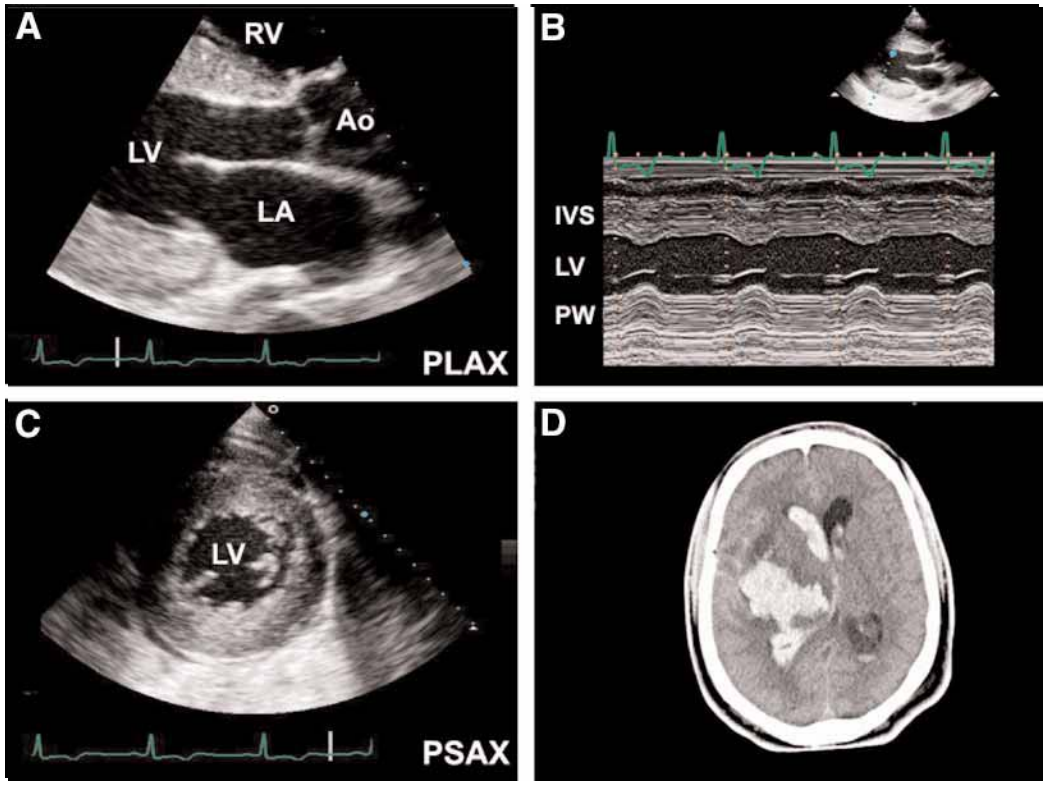

Fig. 29. Case presentation: hypertensive cardiomyopathy. These images are from a 33-yr-old Haitian immigrant who was perfectly "well" until he vomited and fell to the floor unresponsive. Admission blood pressure was 300/150 mmHg show severe concentric left ventricular hypertrophy on two-dimensional and M-mode. Computed tomography scan showed a large right frontoparietal acute hemorrhage with subarachnoid and intraventricular extension.

Standards for the echocardiographic diagnosis of LVH on echocardiography compare left ventricular mass to body surface area (left ventricular mass index ≥134 g/m^2 [men] and ≥110 g/ m^2 [women]), or height (≥163 g/m for men and ≥121 g/m for women). Left ventricular mass calculations are based on geometric assumptions of the left ventricle (*see* Chapter 5, Table 5 and Fig. 13). 3D echocardiography

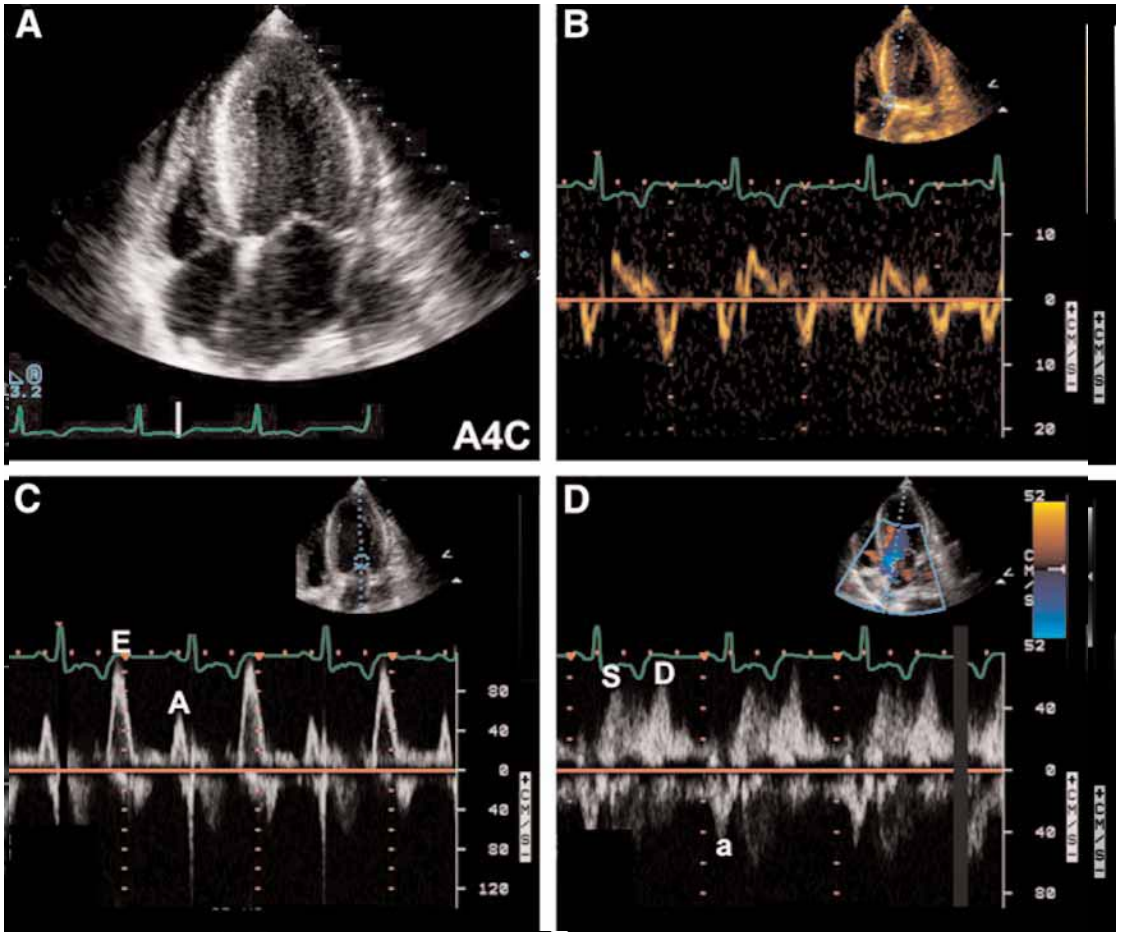

Fig. 30. Case presentation: hypertensive cardiomyopathy. Apical four-chamber view shows isolated marked concentric left ventricular hypertrophy with left atrial dilatation **(A)**. Doppler tissue imaging, mitral inflow patterns, and right upper pulmonary venous flow Doppler showed evidence of impaired diastolic function **(B–D)**.

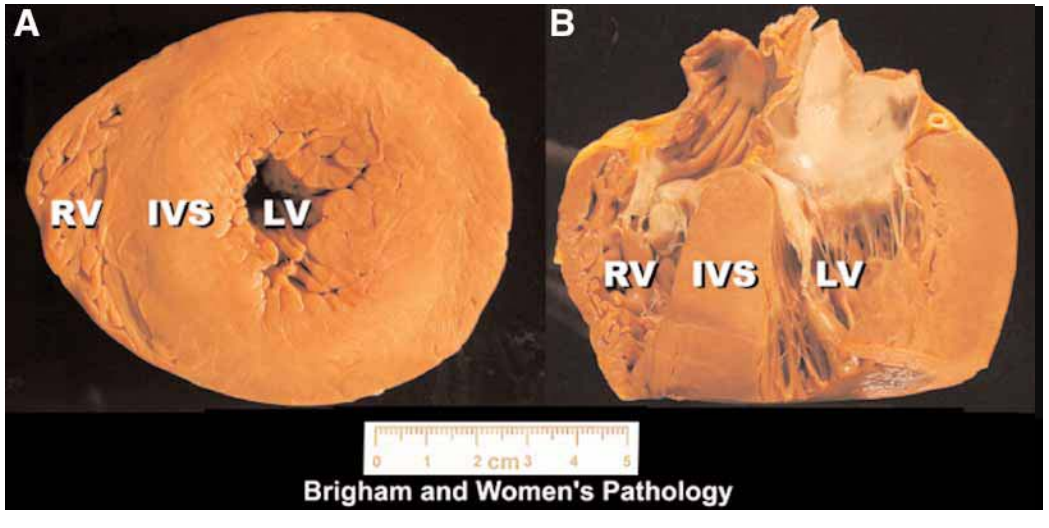

Fig. 31. Case presentation: hypertensive cardiomyopathy. Gross heart specimen showed cardiomegaly (740 g, normal < 360 g) with severe concentric cardiomyopathy). A small left ventricular papillary muscle infarct and pericardial effusion measuring 100 mL were present.

Table 14
Hypertensive Cardiomyopathy: Echocardiographic Findings: A Summary

Modality	*Description*
Two-dimensional findings	• Concentric left ventricular hypertrophy (↑LV mass); normal or hyperdynamic systolic function (if no co-existent coronary artery disease); aortic root dilatation (elderly); aortic valve sclerosis (elderly); mitral annular calcification (elderly); increased left atrial size + atrial fibrillation
M-mode	• Concentric left ventricular hypertrophy; systolic anterior motion (with severe hypertrophy)
Doppler findings	• Relaxation abnormality/diastolic dysfunction

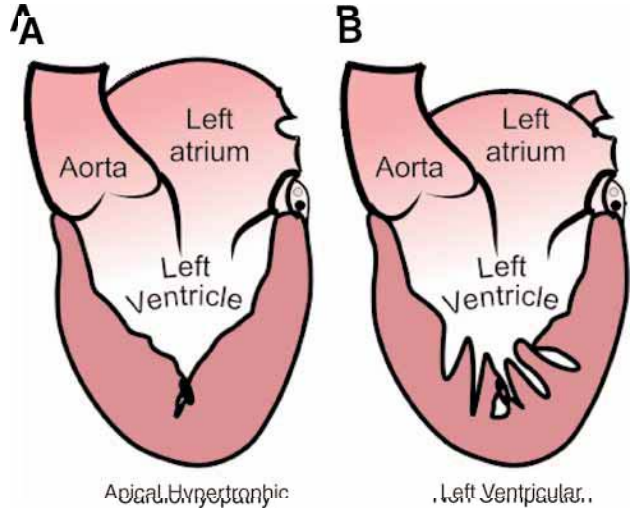

Fig. 32. Apical hypertrophic cardiomyopathy vs left ventricular (LV) noncompaction. The apical variant of hypertrophic cardiomyopathy should not be confused with LV noncompaction. The latter exhibits a spongiform appearance-reflecting deep trabeculations within the endocardium.

can provide more accurate estimates of left ventricular mass and LVH.

Patterns of hypertrophy other than concentric LVH can occur in hypertension and the extent and geometric appearance is related to the duration, the severity, and the nature of the hemodynamic load. Diastolic dysfunction is seen in LVH owing to hypertension, but the earliest echocardiographic signs in hypertension (without LVH) are lower E/A ratios and longer isovolumic relaxation times. Hypertension commonly co-exists with diabetes, and both conditions cause diastolic dysfunction, even when the diagnosis is subclinical.

MISCELLANEOUS CARDIOMYOPATHY

Left Ventricular Noncompaction

Left ventricular noncompaction is a rare unclassified cardiomyopathy with markedly prominent apical trabeculae with deep intertrabecular recesses (Fig. 32). These are best visualized on color flow Doppler of the left ventricle using apical windows. The trabeculations have a spongy appearance on short axis views and should not be confused with intracavitary thrombi. (Fig. 33; please *see* companion DVD for corresponding video). Left ventricular noncompaction may present in childhood or later adulthood. The prognosis is generally poor. Associated intracavitary thrombi and embolic complications have been reported in the setting of systolic dysfunction.

Stress-Related Cardiomyopathies

There is renewed interest in a peculiar form of dilated cardiomyopathy initially described in Japan and named "*takotsubo*" (Japanese for octopus trap—Fig. 34) for its echocardiographic appearance (Fig. 35; please *see* companion DVD for corresponding video). It occurs in stressful states and predominantly affects women. Stress or stress-related cardiomyopathies include those named "transient myocardial stunning owing to sudden emotional stress" and "acute reversible cardiomyopathy provoked by stress." These are helpful clinical terminologies, but transient apical ballooning best describes the morphological and temporal presentation.

Stress cardiomyopathies mimic acute myocardial infarction and acute coronary syndromes, but a constellation of features help to draw the distinction (Table 15). Echocardiographic features in the acute phase show marked apical hypokinesis-akinesis with compensatory hyperkinesis of the basal left ventricular segments, resulting in a balloon-like apex during systole Recovery of normal function within 4 wk of presentation is typical. A not-too-dissimilar picture occurs in some patients with proven myocardial infarction who recover normal ventricular function on serial echocardiographic examination.

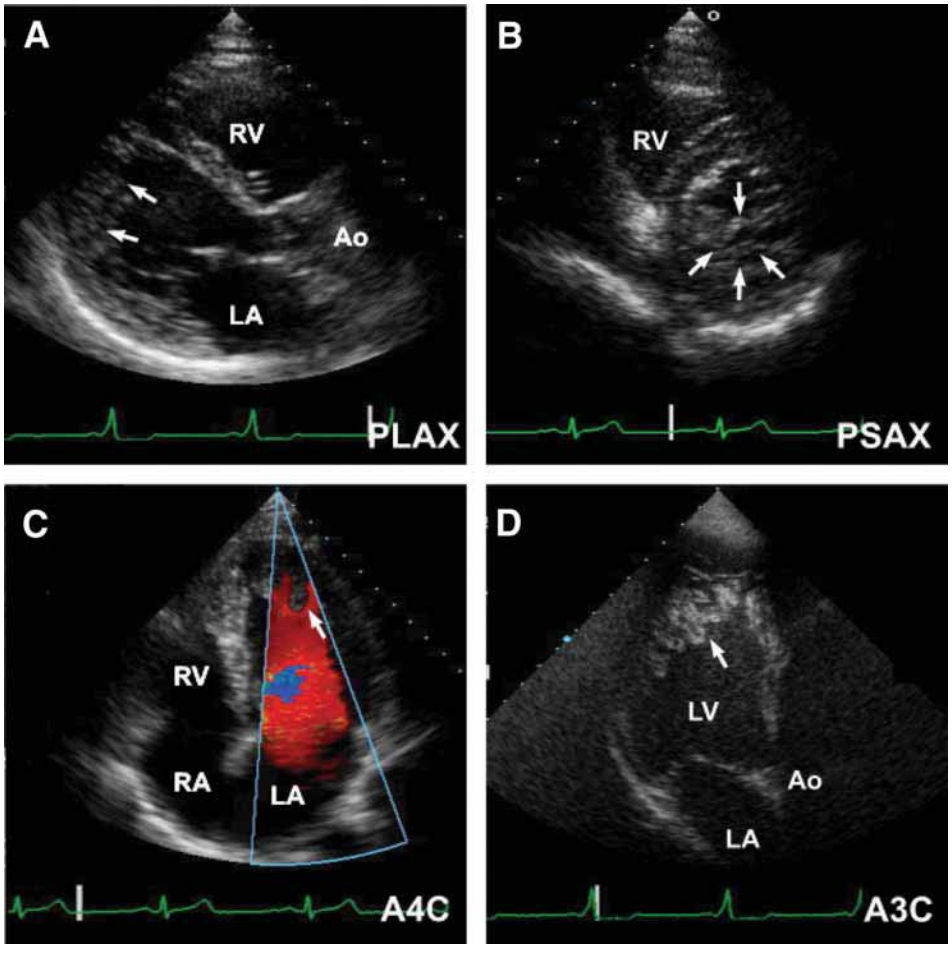

Fig. 33. Left ventricular noncompaction. Parasternal long-axis images from a 41-yr-old female whose initial presentation was heart failure in pregnancy shows evidence of systolic impairment (noncompaction) that results from exuberant apical trabeculations (arrows, **A**). Parasternal short-axis view shows a similar appearance (arrows, **B**). Color Doppler application to the left ventricular region reveals deep intertrabecular recesses within the markedly thickened endocardium **(C)**. Apical long axis view shows the localized distribution of the pathology vis-à-vis apical and mid-inferior regions of the left ventricle **(D)**. (Please *see* companion DVD for corresponding video.)

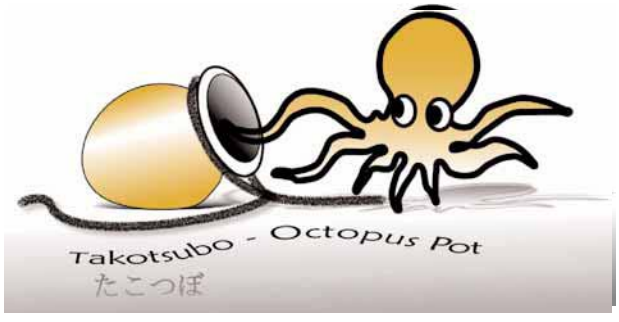

Fig. 34. Transient apical ballooning: Takotsubo.

Arrhythmogenic Right Ventricular Cardiomyopathy (Dysplasia)

Arrhythmogenic right ventricular cardiomyopathy (dysplasia) ARVD/ARVC is a rare cardiomyopathy characterized by progressive fibro-fatty replacement of right ventricular myocytes. It is diagnosed on the basis of the clinical presentation, the ECG, noninvasive imaging (Table 16) and magnetic resonance imaging,

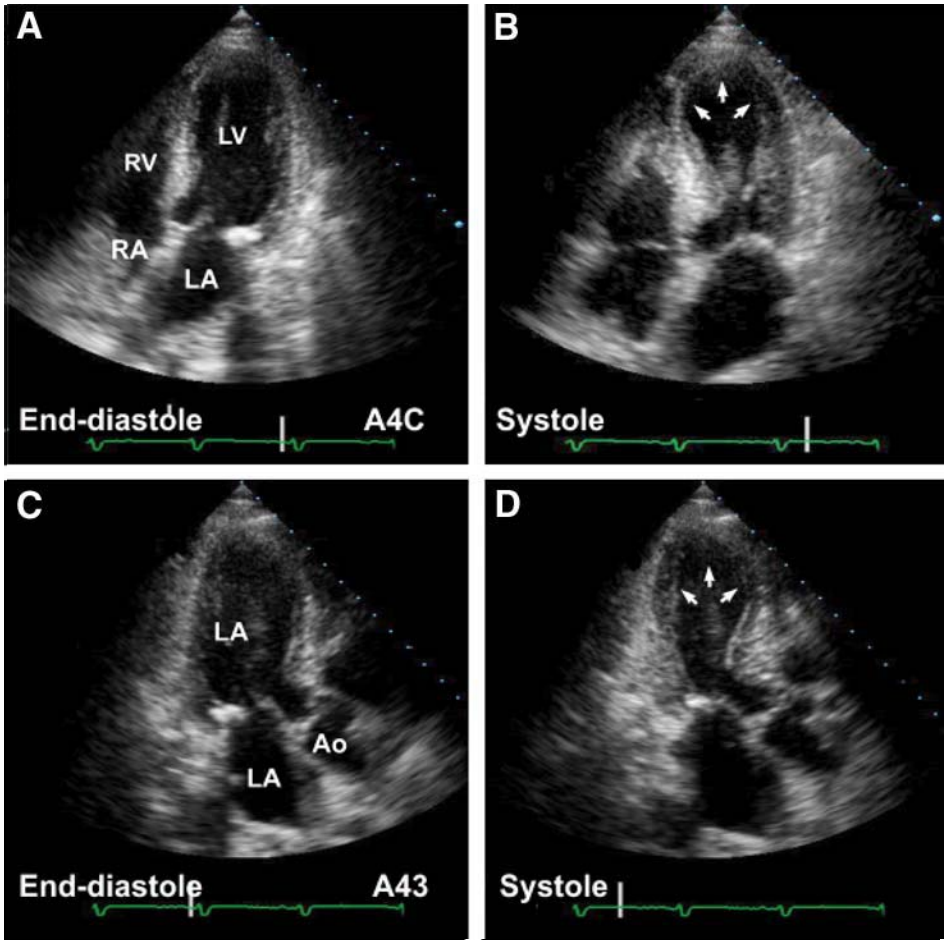

Fig. 35. Transient myocardial stunning: stress-related Takotsubo: transient left apical ballooning. Apical four-chamber views in this 62-yr-old female who presented with chest pains show akinetic apical segments, markedly hypokinetic mid-ventricular segments, with preserved basal segments—a pattern not consistent with coronary artery anatomy. Work-up for acute myocardial infarct—enzymes, electrocardiogram, and cardiac catheterization—were nondiagnostic. Follow-up echocardiogram 6 wk later showed normal cardiac function. (Please *see* companion DVD for corresponding video.)

Table 15
Stress-Related Cardiomyopathies: Echocardiographic Findings: A Summary

Modality	*Findings*
Two-dimensional findings	• Apical akinesis or dyskinesis ("apical ballooning"); moderate-to-severe dysfunction at midventricular level; preserved basal systolic function; overall severe left ventricular dysfunction (median ejection fraction ~20%); rapid resolution of ventricular dysfunction at 2–4 wk
Other	• Female preponderance; emotional stress (exaggerated sympathetic stimulation); elevated plasma catecholamines (↑2–3X values seen in myocardial infarction); electrocardiogram changes (QT, T-wave); minor elevation in cardiac enzymes (e.g., troponin I); normal coronary arteries/no fixed stenoses (angiography)

and histological examination of right ventricular biopsies (Fig. 36 [please *see* companion DVD for corresponding video] and Table 16). Some cases exhibit strong familial (autosomal dominant mode of inheritance) and is more common in males and in young adulthood. It is a cause of sudden cardiac death in athletes.

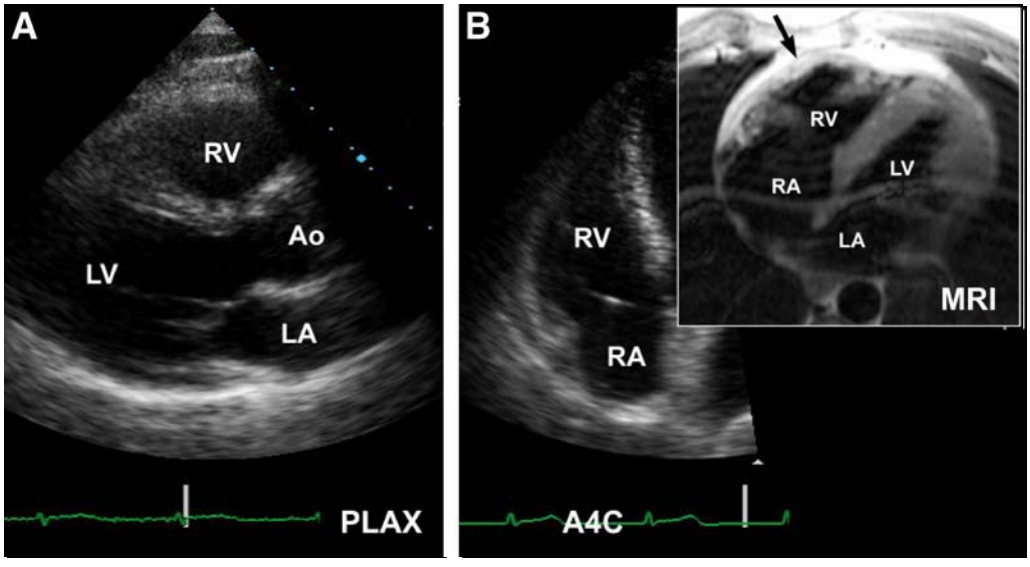

Fig. 36. Transthoracic echocardiography in this 37-yr-old male who presented with recurrent episodes of tachycardia were normal except for moderate right ventricular dilatation with decreased right ventricular function **(A,B)**. Magnetic resonance imaging (MRI) scan (using fat saturation mode, **B**, insert) showed moderate right ventricle dilatation, decreased right ventricular systolic function, dyskinesis of the basal free wall of the right ventricle, and a highlighted area indicating fatty replacement (arrow). MRI image courtesy Raymond Kwong, MD, Brigham and Women's Hospital. (Please *see* companion DVD for corresponding video.)

Table 16
Arrhythmogenic Right Ventricular Cardiomyopathy: Summary of Echocardiographic Findings

Modality	*Description*
Two-dimensional findings	Right ventricle dilatation; right ventricular free wall hypokinesis
Doppler findings	Tricuspid regurgitation and increased right heart pressures (with right heart failure)
Comment	Magnetic resonance imaging, can present with ventricular tachycardia with left bundle branch block contour, right axis deviation, T-wave abnormalities or supraventricular arrhythmias

SUGGESTED READING

Devereux RB. Is the electrocardiogram still useful for detection of left ventricular hypertrophy? Circulation 1990;81:1144–1146.

Faber L, Ziemssen P, Seggewiss H. Targeting percutaneous transluminal septal ablation for hypertrophic obstructive cardiomyopathy by intraprocedural echocardiographic monitoring. J Am Soc Echocardiogr 2000;13:1074–1079.

Falk RH, Plenn JF, Deering T, et al. Sensitivity and specificity of echocardiographic features of cardiac amyloidosis. Am J Cardiol 1987;59:418–422.

Ho HH, Lee KL, Lau CP, Ts, HF. Clinical characteristics of and long-term outcome in Chinese patients with hypertrophic cardiomyopathy. Am J Med 2004;116:19–23.

Klein AL, Hatle LK, Burstow DJ, et al. Comprehensive Doppler assessment of right ventricular diastolic function in cardiac amyloidosis. J Am Coll Cardiol 1990;15:99–108.

Klues HG, Maron BJ, Dollar AL, Roberts WC. Diversity of structural mitral valve alterations in hypertrophic cardiomyopathy. Circulation 1992;85:1651–1660.

Kushwaha SS, Fallon JT, Fuster V. Restrictive cardiomyopathy. N Engl J Med 1997;336:267–276.

Leenen FH. Increased risk attributed to left ventricular hypertrophy in hypertension. Curr Opin Cardiol 1996;11:464–470.

Liebson PR, Grandits G, Prineas R, et al. Echocardiographic correlates of left ventricular structure among 844 mildly hypertensive men and women in the Treatment of Mild Hypertension Study (TOMHS). Circulation 1993;87: 476–486.

Mason JW. Classification of cardiomyopathies. In: Fuster V, Wayne Alexander R, O'Rourke RA, eds. Hurst's The Heart Manual of Cardiology, 11th ed. New York: McGraw-Hill, 2004: 1883–1888.

Mathew V, Olson LJ, Gertz MA, Hayes DL. Symptomatic conduction system disease in cardiac amyloidosis. Am J Cardiol 1997;80:1491, 1492.

Pinamonti B, Di Lenarda A, Sinagra G, Camerini F. Restrictive left ventricular filling MFVP in dilated cardiomyopathy assessed by Doppler echocardiography: clinical, echocardiographic and hemodynamic correlations and prognostic implications. Heart Muscle Disease Study Group. J Am Coll Cardiol 1993;22:808–815.

Poirier P, Bogaty P, Garneau C, Marois L, Dumesnil JG. Diastolic dysfunction in normotensive men with well-controlled type 2 diabetes: importance of maneuvers in echocardiographic screening for preclinical diabetic cardiomyopathy. Diabetes Care 2001;24:5–10.

Pollick C, Rakowski H, Wigle ED. Muscular subaortic stenosis: the quantitative relationship between systolic anterior motion and the pressure gradient. Circulation 1984;69:43–49.

Reisinger J, Dubrey SW, Lavalley M, Skinner M, Falk RH. Electrophysiologic abnormalities in AL (primary) amyloidosis with cardiac involvement. J Am Coll Cardiol 1997;30:1046–1051.

Richardson P, McKenna W, Bristow M, et al. Report of the 1995 World Health Organization/International Society and Federation of Cardiology Task Force on the Definition and Classification of the cardiomyopathies. Circulation 1996;93:841, 842.

Rihal CS, Nishimura RA, Hatle LK, Bailey KR, Tajik AJ. Systolic and diastolic dysfunction in patients with clinical diagnosis of dilated cardiomyopathy. Relation to symptoms and prognosis. Circulation 1994;90:2772–2779.

Sharkey SW, Lesser JR, Zenovich AG, et al. Acute and reversible cardiomyopathy provoked by stress in women from the United States. Circulation 2005;111:472–479.

Simons M, Isner JM. Assessment of relative sensitivities of noninvasive tests for cardiac amyloidosis in documented cardiac amyloidosis. Am J Cardiol 1992;69:425–427.

Siqueira-Filho AG, Cunha CLP, Tajik AJ, et al. M-mode and two-dimensional echocardiographic features in cardiac amyloidosis. Circulation 1981;63:188–196.

Stevenson LW. Diseases of the myocardium. In: Goldman L, Ausiello D, eds. Textbook of Medicine, 22nd ed. Philadelphia: Saunders, 2004:441–454.

Tsuchihashi K, Ueshima K, Uchida T, et al. Transient left ventricular apical ballooning without coronary artery stenosis: a novel heart syndrome mimicking acute myocardial infarction. Angina Pectoris-Myocardial Infarction Investigations in Japan. J Am Coll Cardiol 2001;38:11–18.

Wittstein IS, Thiemann DR, Lima JA, et al. Neurohumoral features of myocardial stunning due to sudden emotional stress. N Engl J Med 2005;352:539–548.

Wynne J, Braunwald E. The cardiomyopathies. In: Zipes DP, Libby P, Bonow RO, Braunwald E, eds. Braunwald's Heart Disease—A Textbook of Cardiovascular medicine. Philadelphia: Elsevier Saunders, 2005.

Yazaki Y, Isobe M, Hiramitsu S, et al. Comparison of clinical features and prognosis of cardiac sarcoidosis and idiopathic dilated cardiomyopathy. Am J Cardiol 1998;82: 537–540.

Zabalgoitia M, Ismaeil MF, Anderson L, Maklady FA. Prevalence of diastolic dysfunction in normotensive, asymptomatic patients with well-controlled type 2 diabetes mellitus. Am J Cardiol 2001;87:320–323.

10 Pericardial Disease

Ashvin N. Pande, MD and Leonard S. Lilly, MD

CONTENTS

CASE PRESENTATION

A 59-yr-old woman presents with a history of diabetes mellitus, hypertension, and end-stage renal disease. She presented with several weeks of fevers, sweats, fatigue, and progressive exertional dyspnea. On initial evaluation, she was mildly short of breath. Vital signs were: temperature, 100.2°F; pulse, 108; blood pressure, 98/60. Physical examination was notable for bibasilar rales, jugular venous pressure (JVP) of 10 cm H_2O, and mild peripheral edema. Chest X-ray showed cardiomegaly, clear lung parenchyma, and small bilateral pleural effusions. She was admitted for further evaluation. The following morning, she underwent peritoneal dialysis, after which she developed worsening dyspnea and transient hypotension. Electrocardiogram (ECG) at that time revealed sinus tachycardia and electrical alternans. An urgent echocardiogram was performed (Fig. 1; please *see* companion DVD for corresponding video).

INTRODUCTION

This chapter reviews key topics in pericardial disease and their characteristic echocardiographic features. Echocardiography serves a vital role in the diagnosis and evaluation of pericardial disease, which is often difficult to recognize by bedside examination alone.

ANATOMY

The pericardium consists of two layers that surround the heart and proximal portions of the great vessels. The inner layer, the visceral pericardium, is a thin serosal membrane formed by a single layer of mesothelial cells. This layer reflects back on itself to line the outer layer, the parietal pericardium—a thick, fibrous structure providing mechanical support to the heart by means of ligamentous links to the sternum, diaphragm, and vertebrae. The parietal and visceral pericardium form a closed space circumscribing the heart, with finger-like projections leading to blind pockets around the great vessels. Reflections of the pericardium at the pulmonary veins and at the aorta and pulmonary trunk result in the oblique and transverse sinuses, respectively (Fig. 2A,B).

A few anatomical descriptions are notable regarding the complexity of pericardial anatomy. First, because of the nature of pericardial reflections around the systemic and pulmonary vessels, the pericardium blankets the anterior and medial aspects of the right atrium, whereas the pericardial space terminates around the vena cavae superiorly and posteriorly. The pericardial space reaches lateral to the left atrium and to the pericardial reflections around

From: *Contemporary Cardiology: Essential Echocardiography: A Practical Handbook With DVD*
Edited by: S. D. Solomon © Humana Press, Totowa, NJ

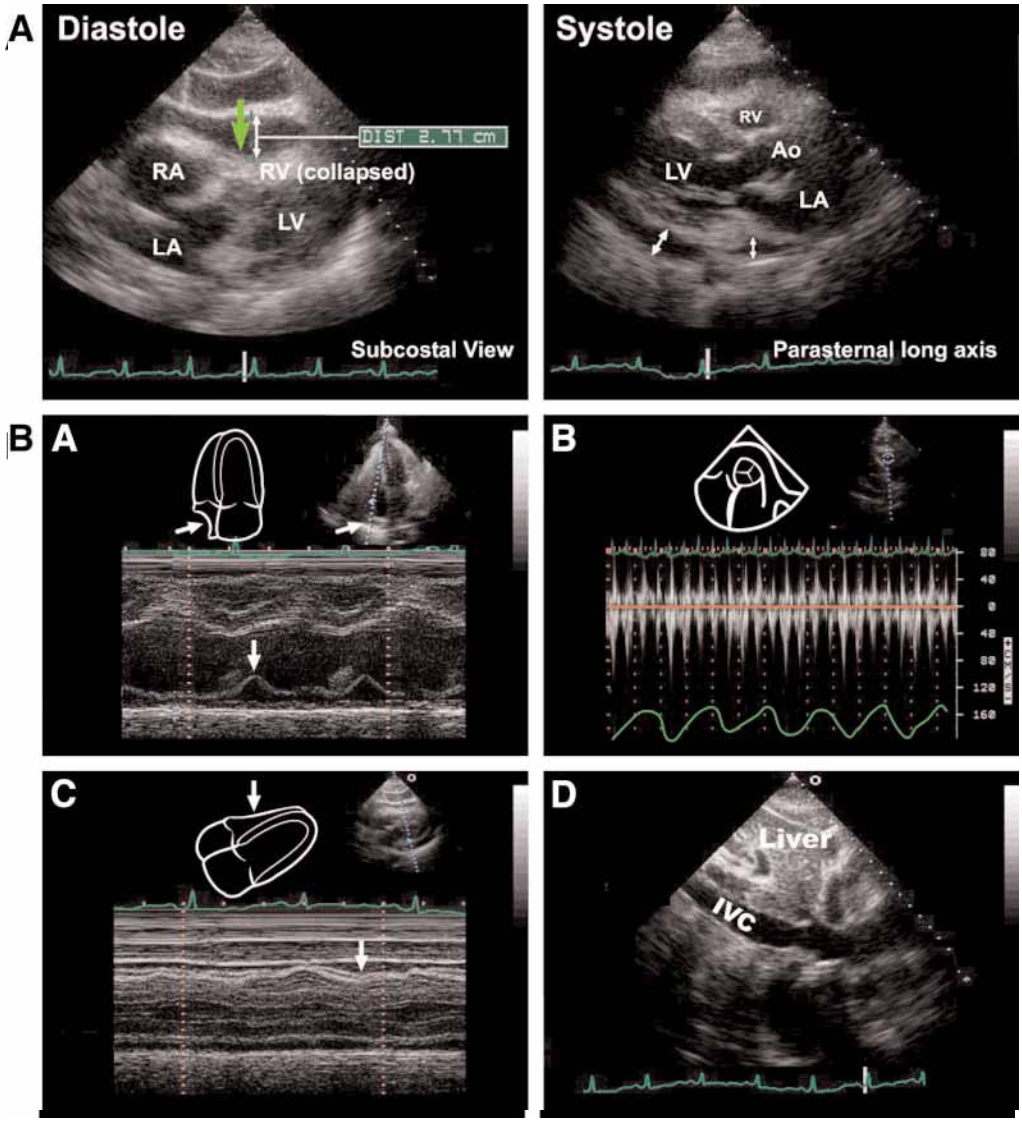

Fig. 1. Case vignette: 59-yr-old female with fever, fatigue, and progressive exertional dyspnea. **(A)** Subcostal and parasternal long-axis views showing right ventricular diastolic collapse (green arrow) in the midst of a relatively large pericardial effusion. Right ventricular diastolic collapse is a highly specific (90–100%) finding in cardiac tamponade. **(B)** M-Mode echocardiography **(top left panel)** of the same patient in **A** shows right atrial inversion or systolic collapse (arrows). Exaggerated respirophasic changes in right ventricular outflow pattern is shown on pulsed wave Doppler examination of the right ventricular outflow tract **(top right panel)**. M-mode through right ventricle on subcostal views confirms right ventricular diastolic collapse (arrows, **bottom left panel**). Inferior vena cava plethora with loss of normal respirophasic movements—an indication of increased right atrial pressures—was present **(bottom right panel)**. (Please *see* companion DVD for corresponding video.)

the tethering pulmonary veins. Therefore, the common locations where pericardial fluid can collect are medially, laterally, and apically, whereas superior and posterior extension is necessarily limited by pericardial reflections.

Epicardial fat is a common anatomic and echocardiographic finding, often present on the anterior aspect of the cardiac surface. It is more common in older patients with obesity or diabetes. It is occasionally detected posteriorly where it can be particularly difficult to distinguish from pericardial effusion as discussed next (Fig. 3; please *see* companion DVD for corresponding video).

A small amount (15–35 mL) of pericardial fluid separates the two layers and serves a physiological lubricating function. The fluid consists of a plasma ultrafiltrate generated by the mesothelial lining of the pericardium and is drained by the thoracic lymphatic system. This small amount of pericardial fluid may be visualized by echocardiography under normal conditions,

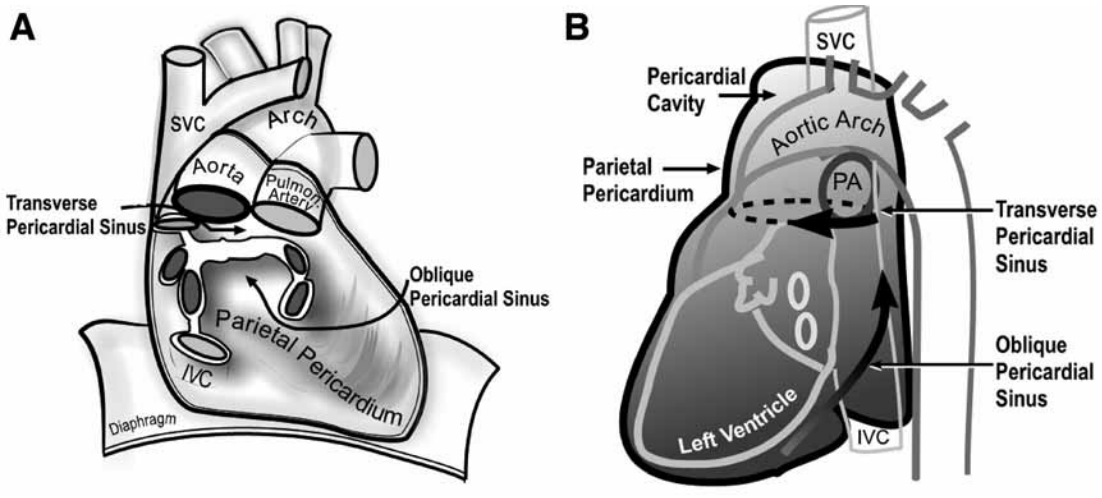

Fig. 2. Pericardium: anatomical relationships. The pericardium completely invests the heart and proximal portions of the great vessels and consists of two separate layers—the thin visceral pericardium (epicardium) and a thicker fibrous parietal pericardium. (**A**) Posterior view. The inferior parietal pericardium is adherent to the central tendon of the diaphragm. Most of the lateral and posterior parietal pericardium is in contact, but not adherent to the parietal pleura. A portion of the anterior parietal pericardium lies immediately posterior to the sternum and related fascia. (**B**) Lateral view. The transverse pericardial sinus lies between the arterial and venous poles of the heart. The oblique pericardial sinus is a blind recess running between the pulmonary veins and the inferior vena cava.

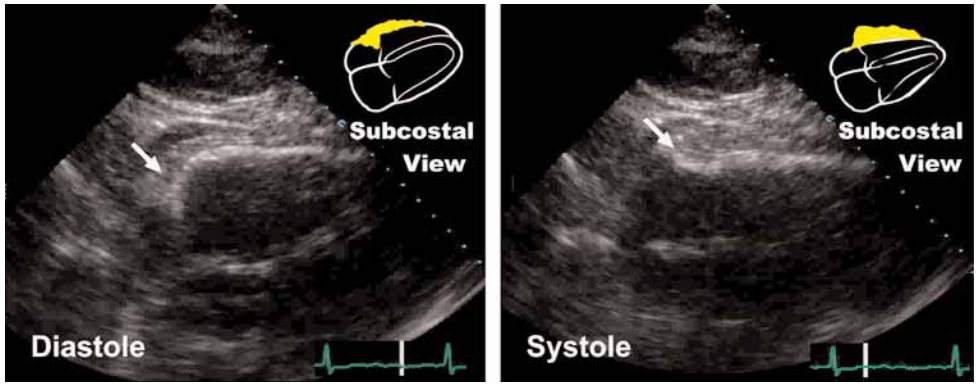

Fig. 3. Pericardial fat pad. Subcostal views show a prominent pericardial fat pad (becoming more prominent during systole). It is more common in obese and older adults. (Please *see* companion DVD for corresponding video.)

usually posterior to the left ventricle (LV) near the atrioventricular groove.

Echocardiographically, the pericardium is visualized as a thin, echo-dense structure surrounding the heart, most evident at the posterior cardiac interface (Fig. 4). The pericardium can usually be visualized in all standard echocardiographic windows such that diffuse pericardial pathology can be observed in most views. Localized pericardial disease, such as loculated fluid collections or hematomas, may require more focused examinations. In patients with pericardial fluid or infiltration, the pericardium appears more prominent and distinction between the parietal and visceral layers is often more evident. In general, the evaluation of pericardial thickness by transthoracic echocardiography is less accurate than by other imaging modalities, such as computerized tomography or magnetic resonance imaging.

PHYSIOLOGY

The normal physiological functions of the pericardium are of some debate, given the relatively benign consequences of its absence, either surgically or congenitally. Nevertheless, one obvious mechanical function is to allow the heart to beat in a minimal friction environment. Another function may be one of passive restraint of the structures contained by the pericardium. Specifically, the fibrous parietal pericardium likely

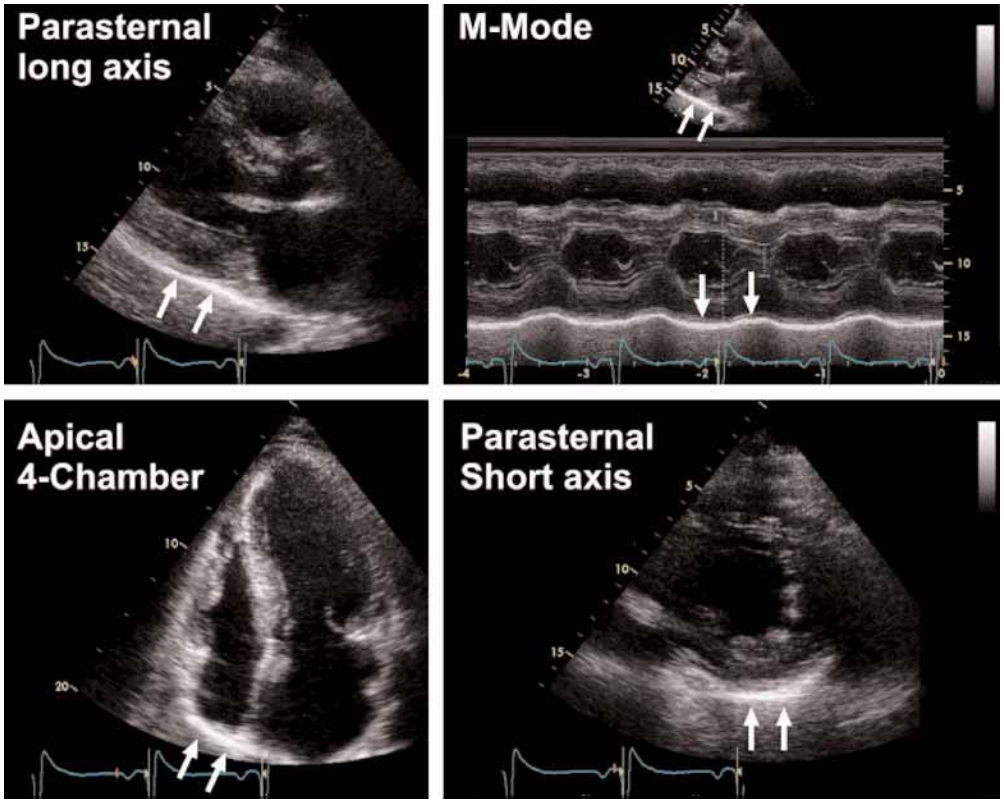

Fig. 4. Normal pericardium. The normal pericardium appears as a hyperechoic linear structure surrounding the heart. Increased echoreflectivity occurs at the interface between cardiac tissue and the air-filled lungs (*see* arrows). Normal pericardial thickness is less than 3 mm (best assessed by transesophageal echocardiography), but its appearance on transthoracic echocardiography is influenced by image quality and instrument settings.

contributes to resting diastolic pressures within the heart and it may also limit acute cavity dilation. Although these effects may be modest in normal individuals, in states of pericardial pathology they can have a profound impact on the heart's hemodynamic performance. Of particular import is that the relative stiffness of the parietal pericardium causes the intrapericardial pressure to rise rapidly with an acute increase in volume. Conversely, a chronic, slow accumulation of pericardial fluid is better tolerated because pericardial stretching with augmented compliance can gradually increase over time.

The mechanical restraint of the pericardium contributes to *ventricular interdependence*: the LV and right ventricle (RV) share a common wall in the interventricular septum and are surrounded by the relatively noncompliant pericardium. Therefore, the volume in one ventricle can influence the diastolic pressure and filling characteristics of the opposite chamber. This physiology is accentuated in states of pericardial pathology (Table 1), as described in "Chronic Constrictive Pericarditis" and "Pericardial Effusions and Compressive Syndromes" sections.

ACQUIRED PERICARDIAL DISEASE

Acute Pericarditis

Pericarditis is the most common affliction of the pericardium and reflects inflammation that can result from a broad variety of local and systemic disorders. Most causes can be assigned to one of six categories: infectious, "idiopathic," metabolic, collagen vascular/autoimmune disease, postinjury, and neoplastic.

Viral infections and "idiopathic" are the most common categories of pericarditis accounting for 40–80% of cases in hospitalized patients. Although idiopathic pericarditis is a diagnosis of exclusion, most such cases are likely viral in origin.

Microbiological agents that can infect the pericardium include viruses, bacteria, fungi, and parasites. The most commonly involved viruses include cocksackievirus, echovirus, and adenovirus, although pericardial involvement can occur with virtually any viral infection. Pericardial effusions occur in 15–40% of patients with AIDS. These are mostly classified as idiopathic,

Table 1
Spectrum of Acquired Pericardial Diseases

Acute pericarditis
Infectious[a]
Idiopathic[a]
Metabolic, e.g., uremia, myxedema
Collagen vascular/autoimmune disease
Trauma—direct or indirect, e.g., surgery, postmyocardial infarction, radiation
Neoplastic—primary or secondary
Drugs, e.g., procainamide, hydralazine, methysergide
Other associations, e.g., pancreatitis
Chronic pericarditis ± constrictive pericarditis
Idiopathic[a]
After cardiac surgery/pericardial injury[a]
Infectious, e.g., tuberculosis, viral, pyogenic
Postviral or purulent pericarditis
Neoplastic
Mediastinal radiation
Uremia (dialysis)
Collagen vascular disease
Pericardial effusions and compressive syndromes

[a]Most common causes.

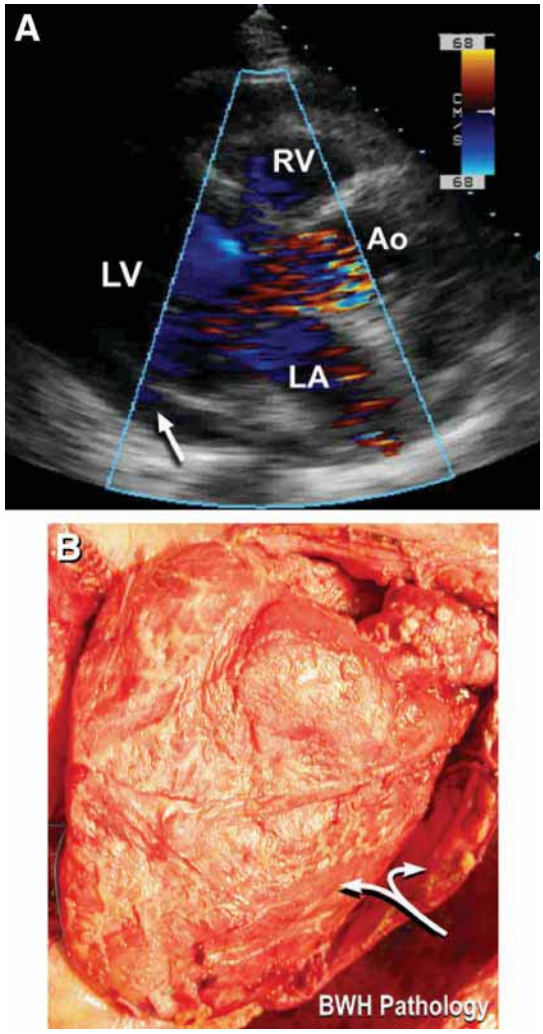

Fig. 5. Acute bacterial pericarditis. This 42-yr-old woman with a 2-wk history of chills, fever and pleuritic chest pains developed fulminant septicemia *(Staphylococcus aureus)*, endocarditis with new-onset aortic regurgitation, and multisystem failure. Her parasternal long axis image **(A)** showed a pericardial effusion (arrow), but no echocardiographic evidence of tamponade. Examination of the pericardium revealed a deep red pericardium with fibrinoid deposits on both visceral and parietal layers **(B)**.

although a variety of viral, bacterial, and fungal pathogens have been isolated.

Bacteria are now a rare cause of pericarditis. In the preantibiotic era, such purulent pericarditis occurred as a complication of pulmonary or pleural infections with extension to the pericardium, mostly owing to *Streptococcus pneumoniae* or *Staphyloccocus aureus* (Fig. 5). Antibiotics have markedly reduced the incidence of complicated pulmonary infections, and the incidence of purulent pericarditis has fallen accordingly. The demographic of patients with purulent pericarditis has also shifted from otherwise healthy individuals with pulmonary infections to older patients with systemic comorbid conditions. Other implicated agents include gram-negative bacilli, meningococci, legionella, and, in children, *Haemophilus influenzae*.

Mycobacterial infections involving the pericardium were, at one time, a common cause of chronic pericardial effusions and constrictive pericarditis. However, the advent of effective anti-tuberculous therapy has resulted in less than 1% of patients with pulmonary tuberculosis (TB) developing acute or chronic pericarditis. TB pericarditis is typically a result of extension from contiguous sites, such as the lung, spine, or mediastinal/hilar nodes, or via hematogenous seeding. Although rare in industrialized societies, in Africa and Asia TB pericarditis remains one of the most common causes of pericardial effusion. Establishing the diagnosis can be difficult, even after pericardiocentesis, as analysis of pericardial fluid rarely detects acid-fast bacilli, and cultures are negative for TB in nearly 50% of cases. An elevated level of the enzyme adenosine deaminase in the pericardial fluid is highly suggestive of this diagnosis. Antibiotic therapy is the same as that for pulmonary TB; the addition of

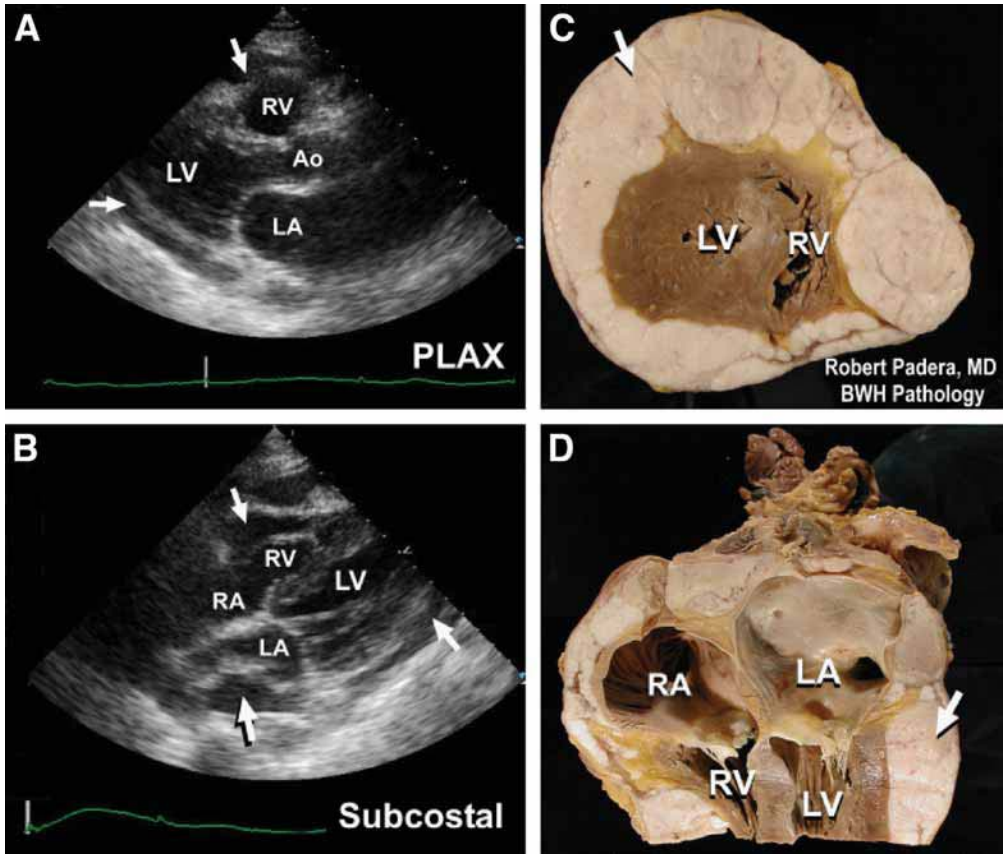

Fig. 6. Primary malignant mesothelioma of the pericardium. This 68-yr-old female with a history of gastric cancer, stroke, myocardial infarction, and heart failure presented with chest pains and heart block. She underwent echocardiography that showed a near-circumferential echolucency (arrows, **A**,**B**) that mimicked a pericardial effusion with fibrinoid echodensities. Pathological examination diagnosed a primary malignant mesothelioma of the pericardium—a rare finding (arrows, **C**,**D**). (Please *see* companion DVD for corresponding video.)

corticosteroid treatment has been shown to improve outcomes and reduce the need for surgical pericardiectomy.

Fungal pericarditis is rare. Typically, pericardial involvement occurs as a consequence of systemic fungal infections, such as disseminated histoplasmosis or coccidiomycosis. In the case of histoplasmosis, up to 6% of patients with disseminated disease are found to have pericardial involvement. In some cases this represents a sterile inflammatory response to adjacent infection in mediastinal nodes, whereas in others direct infection may occur. Pericardial infection from *Candida*, *Aspergillus*, cryptococcus usually arises only in debilitated and immunocompromised patients. Localized fungal infection of the pericardium is rare and is usually a complication of cardiac and/or mediastinal surgery.

Autoimmune disorders, including systemic lupus erythematosus, rheumatoid arthritis, and scleroderma may cause acute pericarditis as the first manifestation of the systemic illness. Acute rheumatic fever can involve the pericardium as part of a pancarditis. Certain drugs may cause pericarditis and/or pericardial effusion either by inducing a lupus-like syndrome (e.g., hydralazine or procainamide), or by nonlupus, unknown mechanisms (e.g., minoxidil, anthracycline antitumor agents).

Uremic pericarditis occurs in up to one-third of patients with chronic renal failure and those on chronic hemodialysis. A pericardial friction rub is often heard on auscultation, but of note, pain is frequently absent. Management usually involves nonsteroidal anti-inflammatory drugs and more aggressive dialysis.

Pericardial inflammation after cardiac injury can occur in a variety of settings, including postmyocardial infarction, postcardiac surgery, or as a result of penetrating or blunt trauma to the heart. The mechanism of this syndrome may be a hypersensitivity reaction owing to myocardial antigens released by the primary injury.

Neoplastic pericarditis results from advancement of malignancy into the pericardium, either by direct extension from adjacent structures or from hematogenous or

Table 2
Pericardial Disease: Echocardiographic Findings

Acute pericarditis[a]
Normal
Pericardial effusion
Findings related to contributing factors, e.g., valvular involvement or vegetations in endocarditis/sepsis
Chronic pericarditis
Pericardial thickening ± calcification
Pericardial effusion ± increased echogenicities (fibrinous), strands (adhesions)
Abnormal septal motion: septal "bounce" diastolic "checking," septal "shudder"
Cardiac Tamponade[b]
Pericardial effusion
Right atrial inversion/compression
Right ventricular diastolic compression/collapse
Respiro-phasic changes in right and left ventricular volumes (2D)
Exaggerated respiro-phasic variation on Doppler examination of transvalvular flow:
Reciprocal changes in right vs left heart signs owing to ventricular interdependence
Right-sided changes: TV[c], IVC, PV: ↑ during inspiration; ↓ during expiration;
Left-sided changes: MV[c], AV: ↓ during inspiration; ↑ during expiration
IVC: plethora/loss of normal respirophasic movement

[a]Acute pericarditis is a clinical diagnosis.
[b]Cardiac tamponade is a clinical diagnosis.
[c]MV and TV are better indicators.
PV, pulmonic valve; IVC, inferior vena cava; TV, tricuspid valve; MV, mitral valve; AV, aortic valve.

lymphatic spread. The most common malignancies involving the pericardium are carcinomas of the lung and breast and lymphomas. Pericardial malignancies, although rare, are notoriously difficult to detect on echocardiography (Fig. 6; please *see* companion DVD for corresponding video). Clinical manifestations include chest discomfort, atrial arrythmias, and at its extreme, cardiac tamponade.

Echocardiographic findings in pericarditis depend on the nature and the tempo of the inflammatory process (Table 2). In some patients, the echocardiogram may be entirely normal. In others, a pericardial effusion may be present. Fibrinous stranding may be evident and provides evidence of an ongoing inflammatory process. Increased echogenicity within the pericardial space may raise suspicion for intrapericardial blood, thrombus, or malignancy (Fig. 7).

Over time, persistent inflammation results in increased pericardial thickness and stiffness. Thickening is manifest as increased echogenicity of the pericardial layers. The hemodynamic significance of pericardial effusions, when present, should be carefully assessed (*see* "Pericardial Effusions and Compressive Syndromes" section), particularly if clinical features suggest a process of acute onset and rapid course.

Chronic Constrictive Pericarditis

Chronic constrictive pericarditis results from the initial or repeated healing of pericardial inflammation, with granulation and scar tissue formation leading to fibrosis and obliteration of the pericardial space. This results in a firm, fibrous, noncompliant encasement around the heart and impairment of ventricular filling during diastole.

Historically, the most common cause of chronic pericarditis with constriction was tuberculous pericarditis. In developing nations, this remains a potential etiology. In the United States, however, this diagnosis is now rare; more likely causes include past episodes of viral or purulent pericarditis, postcardiac injury/surgery, neoplastic pericarditis, mediastinal radiation, chronic uremia, or repeated pericarditis owing to collagen vascular disease.

The physiological consequences of pericardial constriction relate to impaired late diastolic filling of the ventricles. Early diastolic filling is rapid owing to the associated elevated atrial pressures and the absence of impedance to flow into the ventricles during that phase. However, there is a precipitous cessation of ventricular filling in mid- to late diastole as ventricular expansion is prevented by the physical limits imposed by the constricting pericardium. The atrial pressure tracings of patients with constrictive pericarditis show unimpaired early diastolic filling, reflected by a rapid "y" descent. In ventricular pressure tracings, the "dip-and-plateau" configuration reflects the rapid "dip" of early diastole, and the "plateau" of late diastole as the stiffened pericardium limits further filling (Fig. 8).

The clinical presentation of constrictive pericarditis is usually subtle and gradual. Patients may describe weakness, fatigue, lassitude, and anorexia, reflective of chronic illness, as well as exertional dyspnea and peripheral edema. Physical findings reflect the consequences of chronically elevated heart pressures, particularly on the right side of the circulation: jugular venous distention (sometimes with the classic Kussmaul sign—an

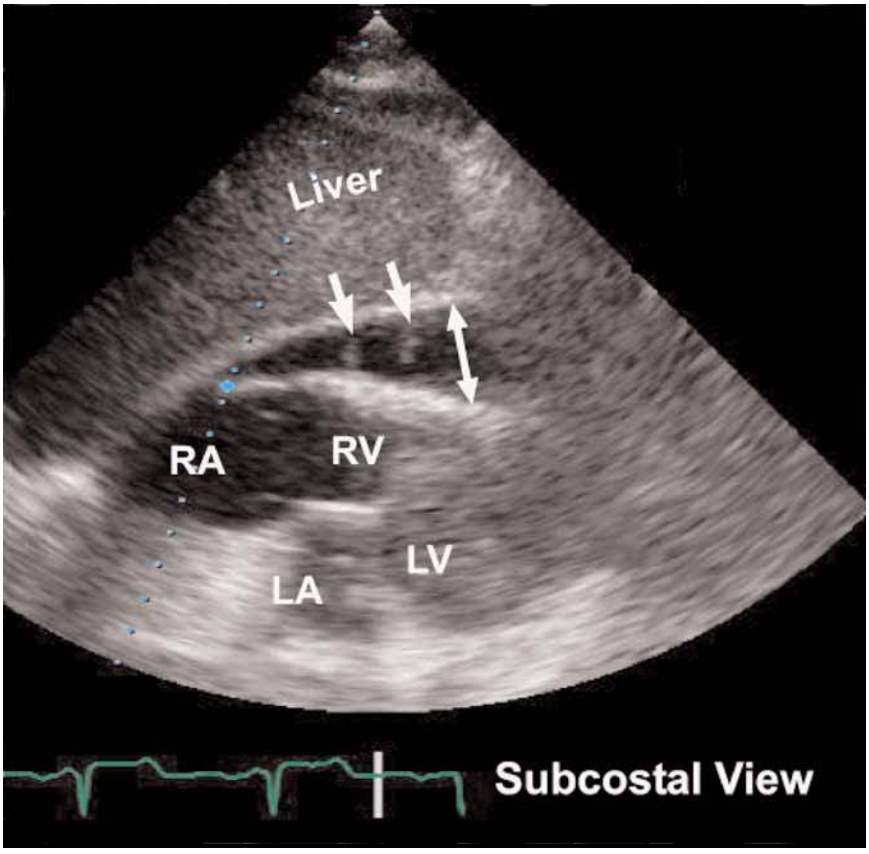

Fig. 7. Increased echogenicity within pericardial space. Subcostal view showing mobile echodensities (arrow) within the pericardial effusion (double arrow). The differential diagnosis includes hemopericardium, suppurative infection, and malignancy.

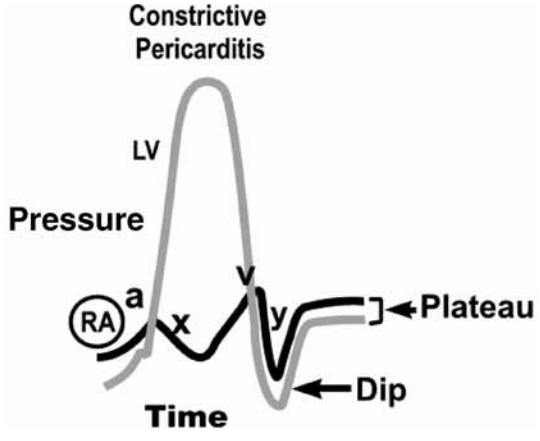

Fig. 8. Pressure tracings in constrictive pericarditis (*see* "Chronic Constrictive Pericarditis" section). a, a wave; LA, left atrium; LV, left ventricle; RA, right atrium; v, v-wave; x, x descent; y, y descent.

abnormal rise in jugular venous pressure upon inspiration), hepatomegaly, ascites and peripheral edema. Occasionally, a pericardial knock can be auscultated as a low-pitched early diastolic sound. The ECG often reveals diffuse T-wave flattening. Atrial fibrillation is common.

Certain echocardiographic findings are consistent with the diagnosis of constrictive pericarditis (Table 2). Typically, ventricular chamber sizes and wall thicknesses are normal. Imaging may reveal a thickened pericardium (Fig. 9), although this is an insensitive finding (computed tomography and magnetic resonance imaging are often more useful in delineating abnormal pericardial thickness). Often, the inferior vena cava (IVC) and hepatic veins are dilated, owing to an elevated right atrial pressure. M-mode recordings may reveal multiple linear and parallel echoes posterior to the LV representing the thickened pericardium. More helpful is the finding of impaired outward movement of the posterior LV wall during mid- to late diastole, reflecting the filling limit of the stiffened pericardium (Fig. 10). This finding, known as posterior wall "flattening," is relatively sensitive, present in 85% of patients with constrictive pericarditis, but is nonspecific as up to 20% of normal individuals also demonstrate this pattern. Other echocardiographic features in constrictive pericarditis include paradoxical motion of the interventricular septum (septal "bounce") and premature opening of the pulmonic valve in diastole,

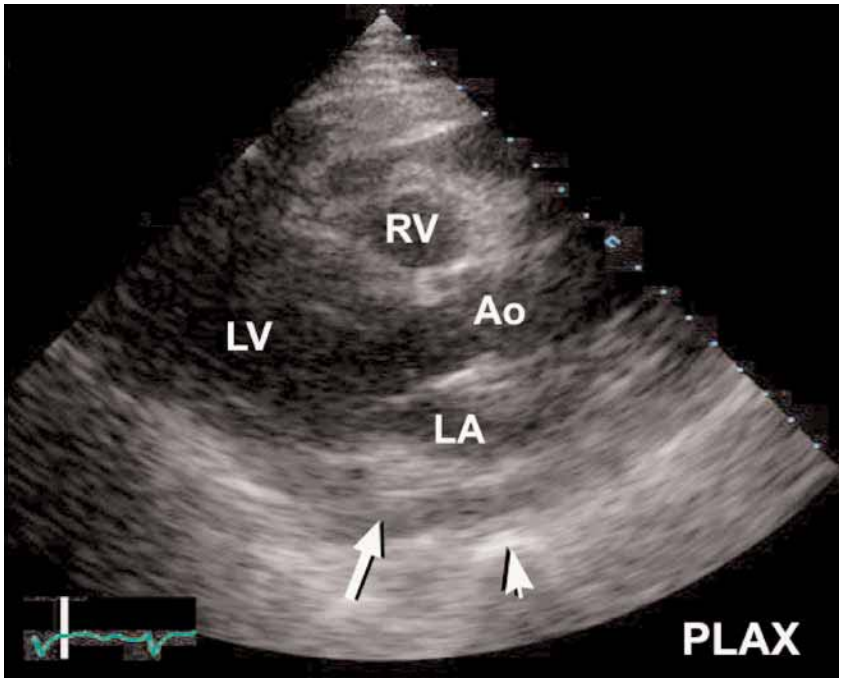

Fig. 9. Constrictive pericarditis. Parasternal long-axis (PLAX) view showing loculated pericardial effusion (arrow) and pericardial thickening with increased calcification (arrowhead).

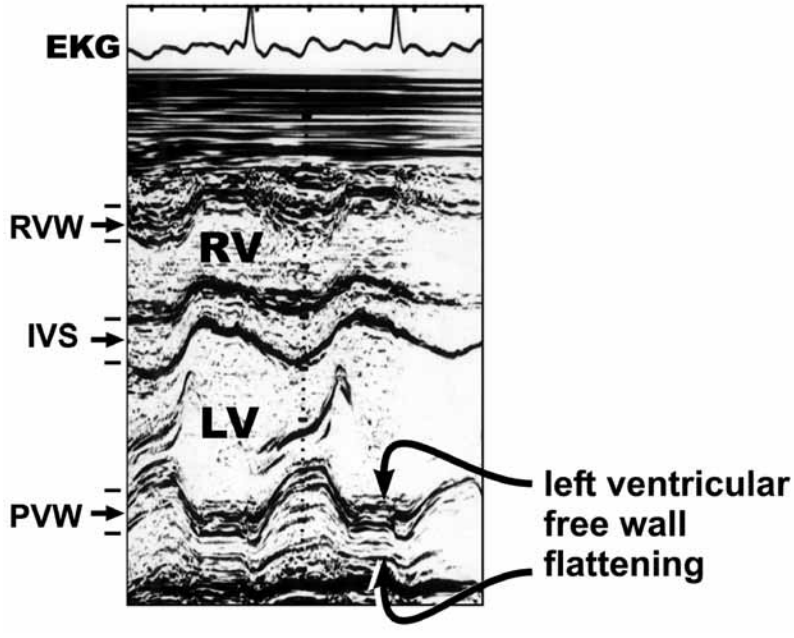

Fig. 10. Constrictive pericarditis. M-Mode echocardiogram showing posterior wall diastolic flattening—a characteristic finding in constrictive pericarditis.

especially with inspiration (Fig. 11; please *see* companion DVD for corresponding video). Commonly, the normal respiratory variation of the diameter of the IVC is blunted.

Doppler evaluation provides further evidence of constrictive physiology. Pulsed Doppler interrogation of hepatic vein flow shows an accentuated A-wave. Pulsed Doppler of transmitral diastolic inflow shows

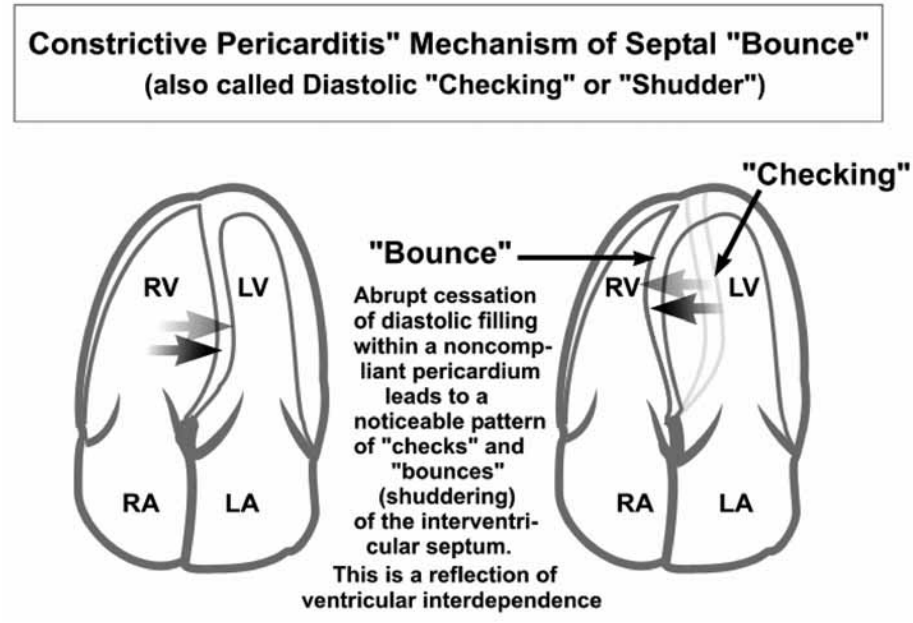

Fig. 11. Mechanism of septal "bounce"/diastolic "checking"/ "shuddering" in constrictive pericarditis. Signs of ventricular interdependence are manifest in constrictive pericarditis. During inspiration, right heart filling proceeds at the expense of left ventricular filling (seen on spectral Doppler pattern)—shifting the interventricular septum to the left. This is followed by an abrupt cessation of diastolic filling (diastolic "checking") corresponding to a third heart sound or pericardial "knock." During expiration, increased left heart filling occurs at the expense of the right ventricle with reciprocal movement in the interventricular septum. (Please *see* companion DVD for corresponding video.)

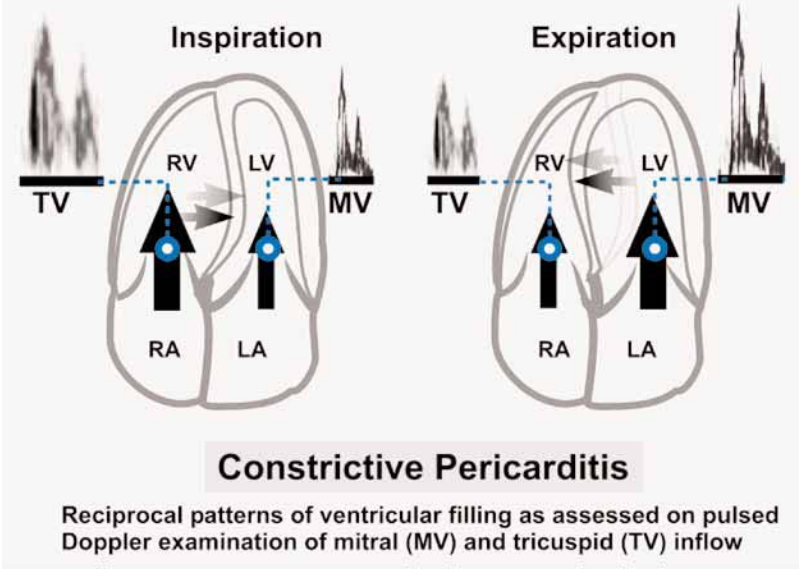

Fig. 12. Constrictive pericarditis. Sketch depicting exaggerated patterns of ventricular filling in inspiration and expiration in constrictive pericarditis. In inspiration, an exaggerated increase in right ventricular (tricuspid valve [TV]) inflow velocities occurs at the expense of left ventricular (mitral valve [MV]) inflow as manifest on pulsed Doppler tracings. During expiration, reciprocal changes occur. Similar respirophasic variations on pulsed Doppler can be seen in pulmonary embolism, right ventricular infarction, and chronic obstructive pulmonary disease.

an increased E velocity with a shortened deceleration time and a reduced A-wave velocity, owing to impaired late diastolic filling. Marked respiratory variation may be noted in early diastolic right and left ventricular filling, with a more than 25% increase of transtricuspid valve flow and more than 25% decrease of transmitral valve flow during inspiration (Fig. 12; *see* Chapter 9, Fig. 12).

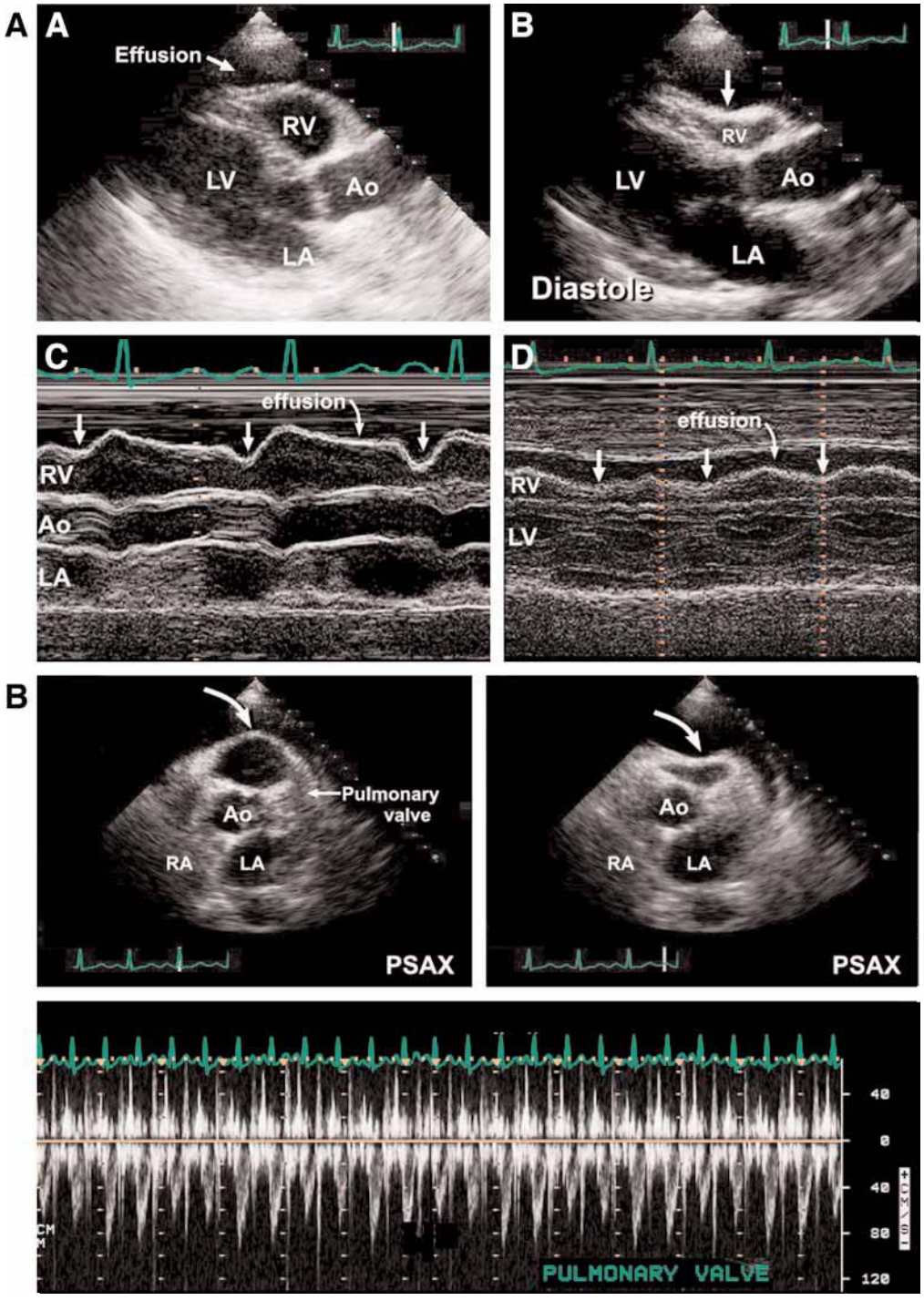

Fig. 13. (*See* legend, next page)

Pericardial Effusions and Compressive Syndromes

Pericardial effusions develop as a response to injury of the pericardium. The clinical presentation of the effusion may vary depending on the etiology, but as intrapericardial pressure rises, cardiac chamber compression can occur with the development of the clinical syndrome of cardiac tamponade. The variability of cardiac compression from a pericardial effusion depends not only on the overall volume of effusion but also on the rate at which the fluid has accumulated. A very gradually developing pericardial effusion, as may be seen in chronic hypothyroidism, may enlarge to more than a liter in volume without evidence of cardiac compression, as the pericardium stretches over time. Conversely, acute

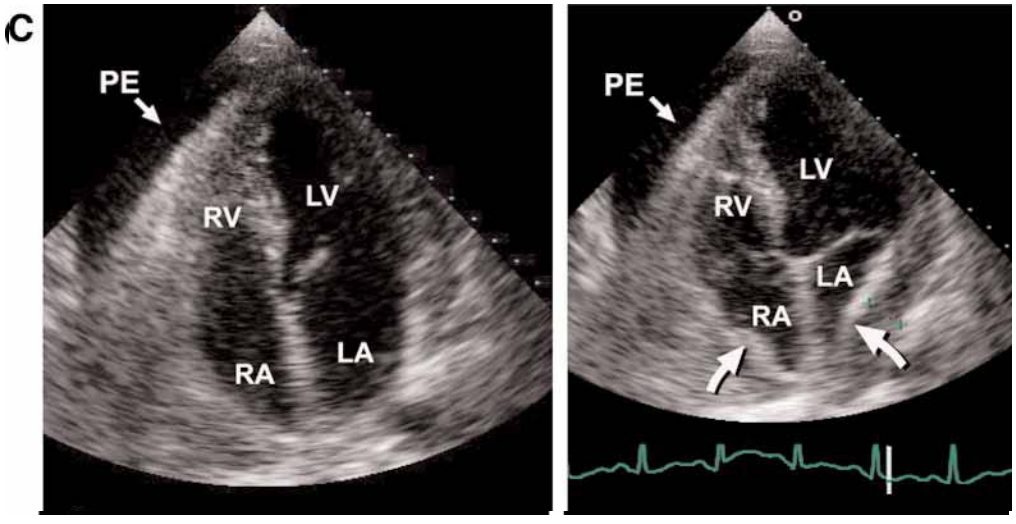

Fig. 13. Pericardial tamponade. **(A)** Two-dimensional parasternal long axis views **(top panels)**, and M-mode taken from parasternal long axis **(bottom left panel)** and subcostal **(bottom right panel)** positions in a patient with cardiac tamponade. The arrows in the top right and bottom left panels indicate RV collapse. **(B)** Systolic and diastolic parasternal short axis views (PSAX) showing diastolic compression of right ventricular outflow tract. Respirophasic variation in flow across pulmonary valve on pulsed Doppler examination is shown **(bottom panel)**. **(C)** Apical four-chamber views showing both right and left atrial inversion (collapse, curved arrows) during systole. Right atrial systolic collapse is a sensitive finding in pericardial tamponade, but left atrial systolic collapse is less commonly seen. (Please *see* companion DVD for corresponding video.)

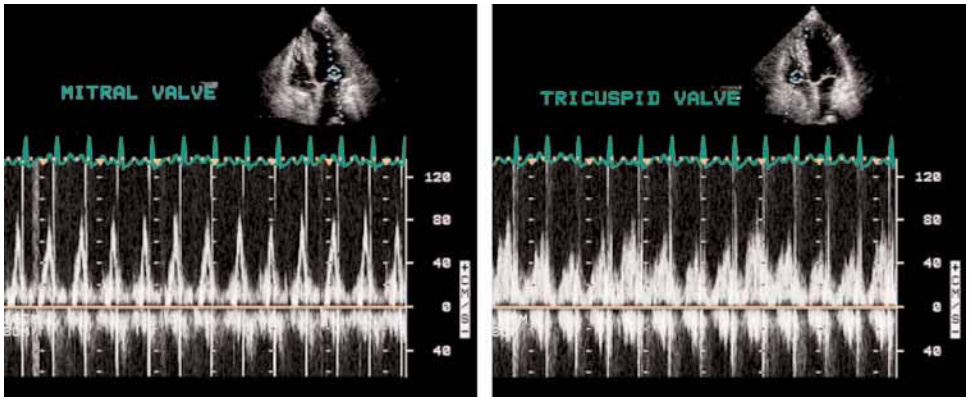

Fig. 14. Cardiac tamponade: ventricular filling. Minor respirophasic variation in left ventricular filling (mitral valve inflow Doppler) was seen in the patient featured in Fig. 13A–D was seen, but right ventricular filling (tricuspid valve inflow) showed marked respirophasic changes.

hemorrhage into the pericardium could cause clinical tamponade with less than 100 cc of fluid accumulation.

The pathophysiology of pericardial tamponade relates to the elevation of intrapericardial pressure and the consequent compression of the cardiac chambers (Fig. 13A–C; please *see* companion DVD for corresponding video). As the intrapericardial pressure rises, there is a progressive increase, and eventually equalization of diastolic pressures of all four cardiac chambers. This leads to impairment of venous return and filling of the ventricles during diastole (Fig. 14). In distinction to pericardial constriction, impairment of ventricular filling in tamponade occurs throughout diastole, including the early phase. This is reflected by a blunted "y" descent on the atrial pressure tracings. The impairment of ventricular filling leads to elevated systemic and pulmonary venous pressures and reduced stroke volume and cardiac output. Pulsus paradoxus results when the inspiratory increase in venous return to the heart expands the RV and, because of ventricular interdependence, reduces LV filling such that LV stroke volume subsequently falls.

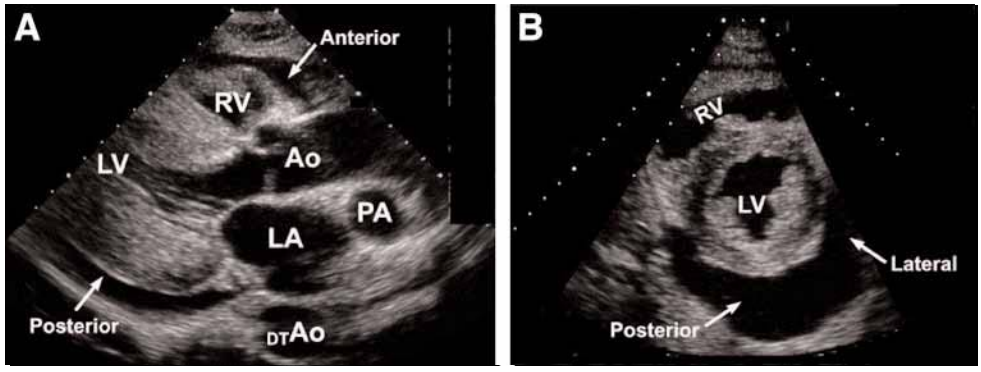

Fig. 15. Pericardial effusion: anatomical relationships. Images from two different patients showing anatomical relationships of anterior and posterior pericardial effusions (parasternal long axis view, **A**) and postero-lateral effusion (parasternal short axis view, **B**). Note the presence of marked left ventricular hypertrophy in **A**. Standard abbreviations apply; also PA, pulmonary artery, DTAo, descending thoracic aorta. (Please *see* companion DVD for corresponding video.)

The etiologies of pericardial effusions are largely the same as those that cause acute pericarditis (Table 1). Large effusions are most commonly seen in malignancies, tuberculous pericarditis, myxedema, uremia, and connective tissue diseases. One important cause of a pericardial effusion unrelated to pericarditis is hemopericardium, e.g., owing to perforation of a cardiac chamber as may occur after chest trauma, or iatrogenically during a cardiac catheterization procedure.

The clinical manifestations of a pericardial effusion may include the sharp, pleuritic chest pain of pericarditis, dyspnea, cough, or a dragging or heavy sensation in the chest. In the case of tamponade, the presentation may be more dramatic, including more pronounced dyspnea, hypotension, and/or shock.

Physical findings related to pericardial effusion are variable. Jugular venous distention is evident when the effusion is compressive such that there is elevation of right-sided filling pressures. The cardiac exam may be notable for a faint apical impulse, soft or muffled heart sounds, and if tamponade is present, hypotension and tachycardia. The classic sign of cardiac tamponade, pulsus paradoxus (>10 mmHg fall in systolic blood pressure with inspiration) is suggestive of tamponade in the appropriate clinical setting, although it can also be detected in other forms of intrathoracic pathology. Laboratory studies that suggest the presence of a pericardial effusion include an enlarged, globular heart on chest radiography, and low voltage and/or electrical alternans on the ECG.

Echocardiographic imaging for evaluation of pericardial fluid is very sensitive and relies on the visualization of an echolucent space between the pericardial layers (Fig. 15; please *see* companion DVD for corresponding video). Volumes as little as 15–50 mL of fluid can be detected. On two-dimensional (2D) imaging, an echo-free space superior to the right atrium in the apical four-chamber view is the most sensitive finding.

Table 3
Pericardial Effusion:
Echocardiographic Differential Diagnosis

Pericardial fat pad
Pleural effusion
Pericardial cyst
Primary mesothelioma of the pericardium (rare)

Actual characteristics of pericardial fluid can be difficult to determine echocardiographically. Findings such as increased echogenicity of the fluid may suggest the nature and composition of the fluid but the correlative power of such findings is unreliable.

Other conditions can mimic the presence of a pericardial effusion (Fig. 3, Table 3). As previously described, epicardial fat is a common finding, usually located on the anterior surface of the heart, although it may also be observed posteriorly where it can be confused with an effusion. Distinguishing features include the more granular echogenic appearance of fat compared to effusion. Left-sided pleural fluid may also be confused with pericardial effusion, but the descending aorta provides a useful landmark in distinguishing the two (Fig. 16). In the parasternal long-axis view, *pleural* fluid extends posterior to the descending aorta, whereas *pericardial* fluid is usually limited anterior to it. Visualization of atelectatic lung tissue adjacent to pleural fluid is also helpful (Fig. 7; *see* Chapter 19).

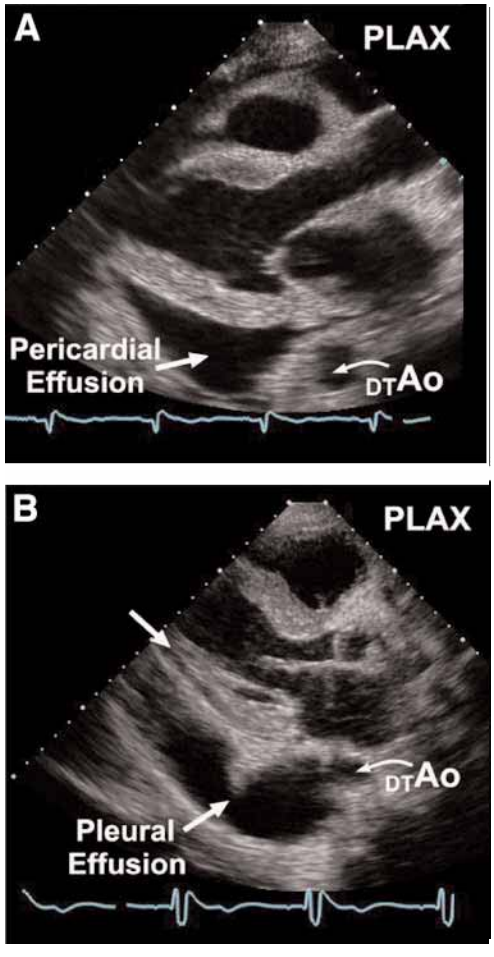

Fig. 16. (A) Pericardial vs (**B**) pleural effusion. Parasternal long axis views showing the anatomical relationships of pericardial vs pleural effusions (arrows) and their relationship to the descending thoracic aorta (DTAo). Note the small pericardial effusion (arrow at upper left) in **B**.

Confusion between pericardial fluid and ascites can occur in the subcostal view, which can be resolved by defining the diaphragmatic border.

Quantitation of pericardial fluid by echocardiography is imprecise, although estimates can be made imaging in multiple planes. Small effusions (100–200 mL) are generally observed only posteriorly in the supine patient, and the echolucent space between the parietal and visceral percardium is generally less than 0.5 cm. Moderate effusions (200–500 mL) separate the pericardial layers by 0.5–2 cm in diameter, and are usually seen circumferentially. Large effusions (greater than 500 mL) extend more than 2 cm in diameter and almost always surround the heart. A swinging motion of the heart during the cardiac cycle may be seen, with electrical alternans as the ECG correlate (Fig. 17).

Loculated pericardial effusions require more careful echocardiographic inspection to identify and characterize. These typically occur in the setting of previous pericardial or cardiac surgery, severe or chronic inflammation, or neoplastic disease, all of which create adhesions and closed spaces within the pericardial sac (Fig. 18; please *see* companion DVD for corresponding video). Localized fluid collections, which cause compression of only a single cardiac chamber, may create severe hemodynamic embarrassment without classic features of cardiac tamponade (Fig. 19). A specific form of loculated pericardial fluid collection is a pericardial hematoma that can form after cardiac surgery or cardiac laceration. After cardiac surgery, such hematomas are usually located anterior and lateral to the right atrium, and may have a variable echocardiographic appearance, ranging from an echolucent collection to a highly echogenic mass. They are prone to cause cardiac compression, particularly of pliable chambers such as the atria, and it is important to distinguish them from intra-atrial thrombi (Fig. 20).

Once a pericardial effusion has been identified, it is important to assess its hemodynamic significance, i.e., to evaluate for the echocardiographic features of cardiac tamponade. It is important to emphasize that the diagnosis of cardiac tamponade is a clinical one, associated with elevated venous pressures, hypotension, and tachycardia, supported by appropriate imaging and laboratory findings.

There are several features on 2D echocardiography that suggest a hemodynamically significant pericardial effusion (Table 2). Most sensitive is cyclical compression, inversion, or collapse of the right atrium. This is first observed in late ventricular diastole and persists into early ventricular systole; the sensitivity of this sign for tamponade is between 90 and 100%. The specificity of this sign for tamponade is lower, ranging between 60 and 80%, but can be improved if the right atrial inversion time index is used. This is a quantitative measure of the amount of time in the cardiac cycle the right atrium is compressed or inverted as a fraction of the total cardiac cycle. If the right atrial inversion time index is more than 0.34, this sign has higher sensitivity and specificity for hemodynamically significant tamponade. Left atrial compression or inversion is less sensitive but more

Fig. 18. *(Opposite page)* Adhesions in chronic pericarditis. Images of chronic pericarditis showing effusions with adhesion strands bridging visceral and parietal pericardium (arrows) from three different patients **(A–C)**. (Please *see* companion DVD for corresponding video.)

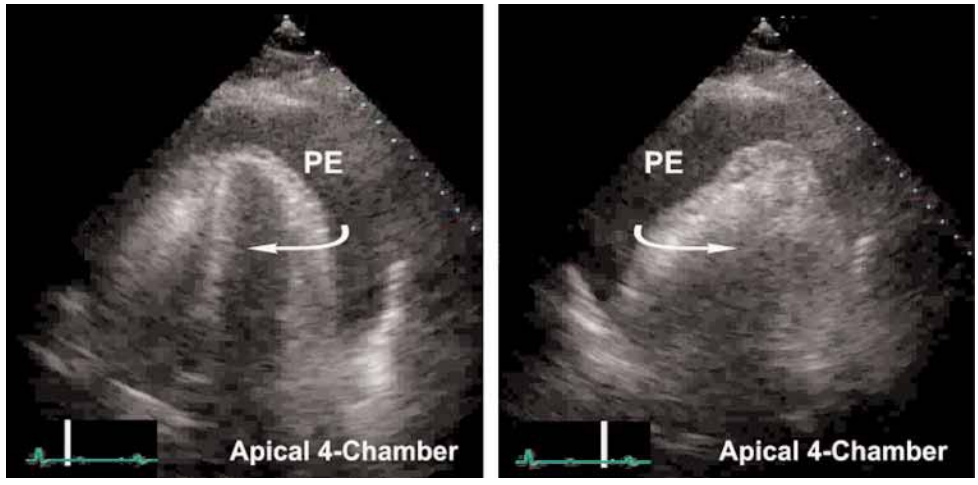

Fig. 17. Large pericardial effusion with "mechanical alternans." These apical four-chamber views demonstrate the swinging motion (curved arrows) of the heart within a large pericardial effusion (PE). This "mechanical alternans" corresponds to electrical alternans on the electrocardiogram.

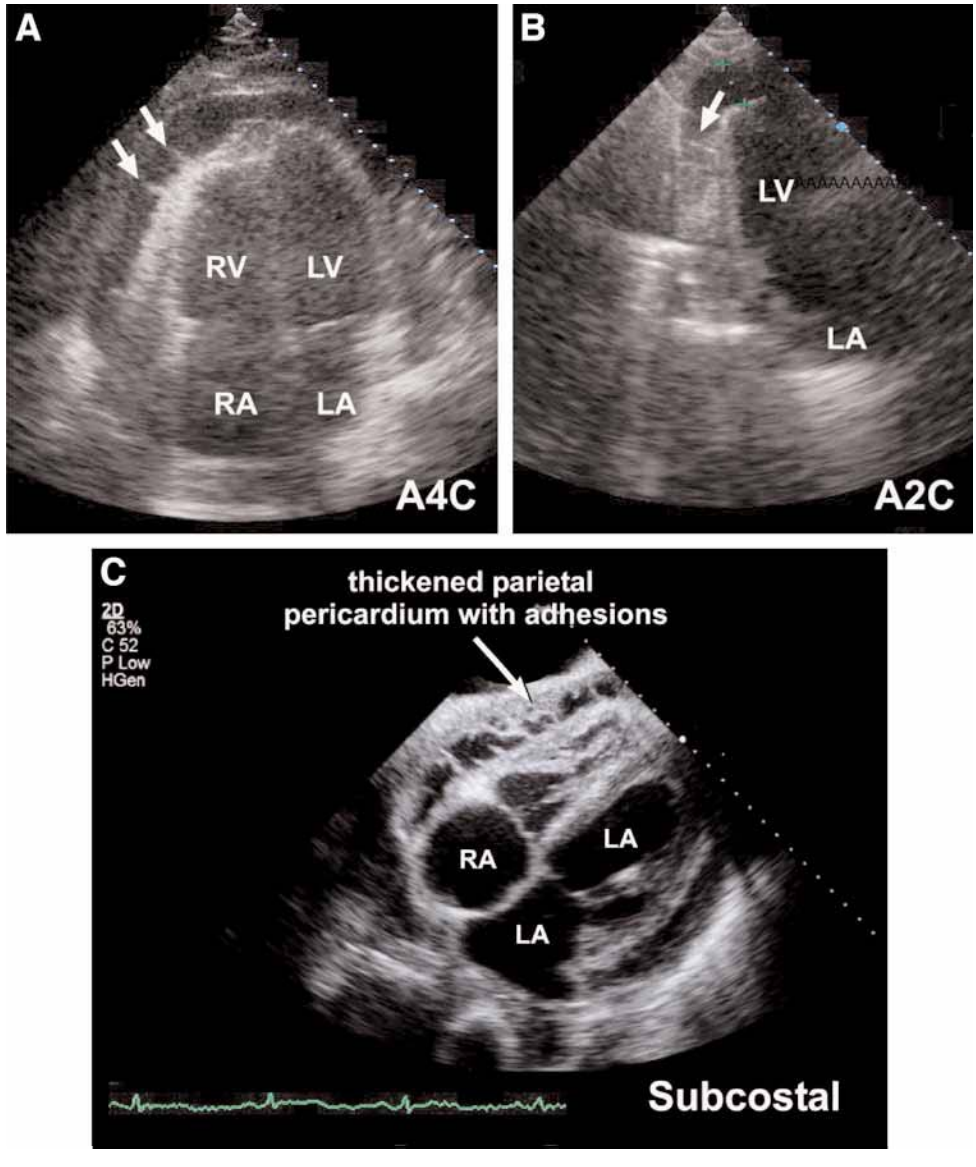

Fig. 18.

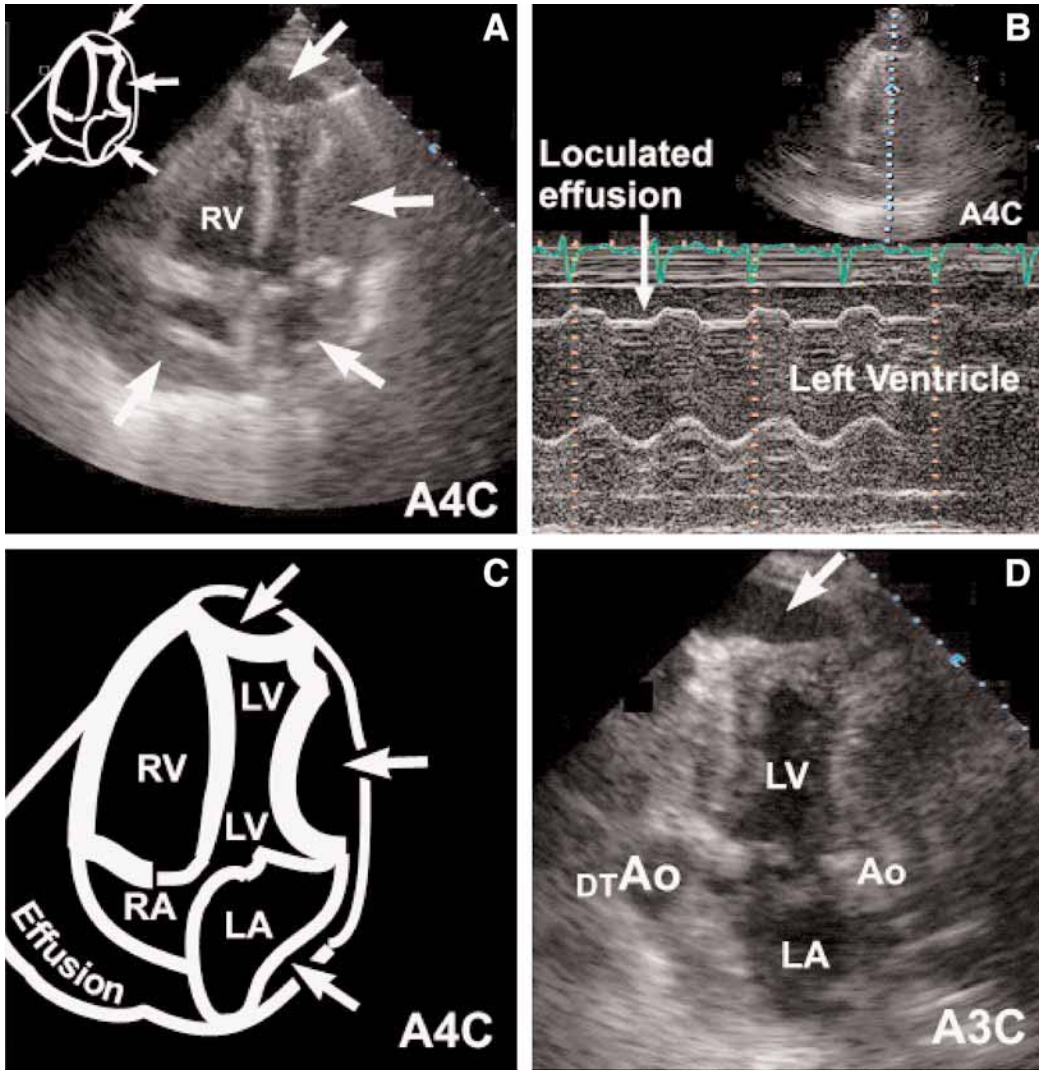

Fig. 19. Localized pericardial effusion with cardiac compression. This patient who underwent a previous pericardial window creation for malignant effusions presented with hypotension. An apical four-chamber view **(A)** reveals multiple, loculated fluid collection at the ventricular apex, lateral to the left ventricle (LV), posterior to the left atrium, and adjacent to the right atrium (*see* arrows). **(B)** M-mode echocardiography through the LV apex shows a region of loculated effusion (*see* arrow). **(C)** A schematic highlights the anatomical relationships of the loculated pockets of fluid. **(D)** An apical three-chamber view shows another view of the apical effusion.

specific, in that normal left atrial pressure tends to be higher than right atrial pressure.

A more specific sign of cardiac tamponade is the echocardiographic finding of RV diastolic collapse, compression, or inversion. These patterns are visualized as persistent posterior or inward motion of the RV free wall during diastole, representing elevation of intrapericardial pressure above RV diastolic pressure. The parasternal or subcostal long-axis views are best for visualizing this effect. The sensitivity of this finding is less than that of right atrial collapse (approx 60–80%), but the specificity is high (between 90 and 100%). Several clinical factors may affect the sensitivity and specificity of RV collapse including intravascular volume depletion, the presence of pulmonary hypertension and RV hypertrophy. The degree and duration of the compression correspond to the severity of the hemodynamic effect.

IVC plethora, or dilation of the inferior vena cava without respirophasic changes in flow or IVC size (<50% reduction in diameter during inspiration on 2D subcostal view), indicative of elevated right-heart pressures, is also a sensitive sign of cardiac tamponade (Fig. 21). However, right-heart pressures may be high for any number of

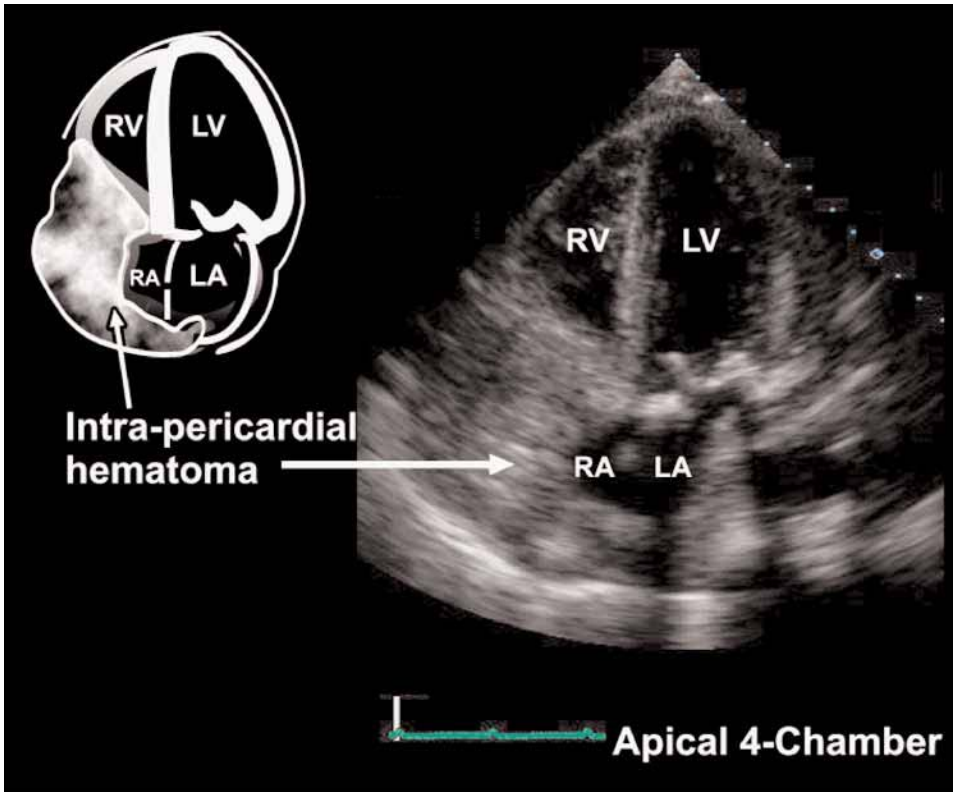

Fig. 20. Intra-pericardial hematoma. Apical four-chamber view showing large opacity, apparently within right atrial cavity, which was confirmed to be an intrapericardial hematoma.

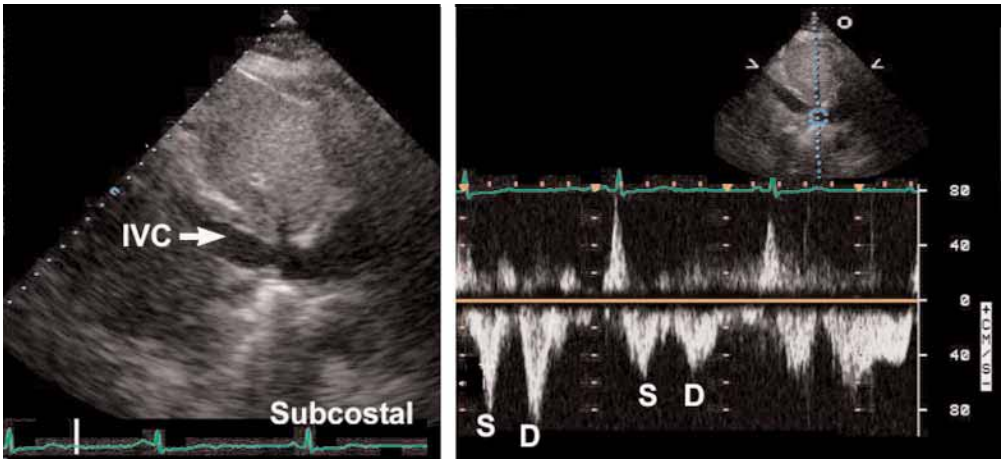

Fig. 21. Inferior vena cava. Loss of normal respirophasic variation of the inferior vena cava diameter (<50% decrease during inspiration) is a reflection of significantly increased right atrial pressures. S, systole; D, diastole.

reasons, including right-sided heart failure, pulmonary hypertension, constrictive pericarditis, or tricuspid valve disease. Thus, specificity of this finding for tamponade is low, between 20 and 40%.

Doppler examination of right and left ventricular inflow patterns are helpful in confirming tamponade physiology. These findings underscore the physiological concept of ventricular interdependence, as reflected by the accentuation of the normal reciprocal patterns in mitral and tricuspid flow patterns during respiration. Normally with inspiration, RV early diastolic filling increases while left ventricular filling decreases, and these changes are seen as small changes in pulsed Doppler inflow velocities across the tricuspid and mitral

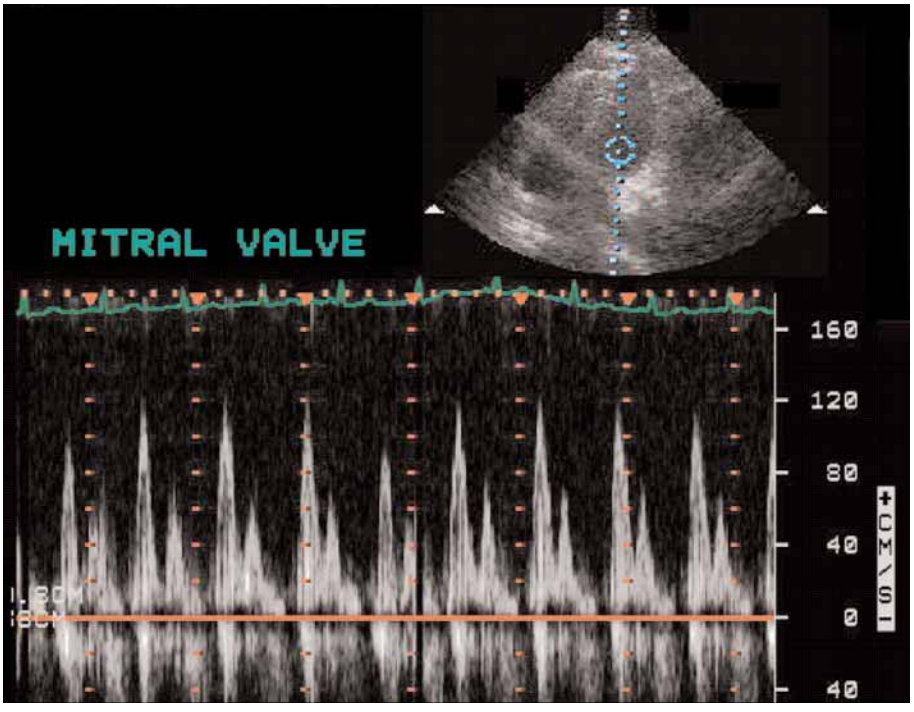

Fig. 22. Mitral inflow. Pulsed wave Doppler of mitral valve inflow showing exaggerated respirophasic pattern of left ventricular filling. This may be observed in the presence of cardiac tamponade.

valves, respectively. With cardiac tamponade, there is exaggeration of these physiological changes. Specifically, an increased respiratory variation of diastolic filling of the tricuspid or mitral inflows (i.e., >25%) is suggestive of tamponade physiology (Fig. 22).

CONCLUSION OF CASE PRESENTATION

Based on the echocardiographic findings and clinical impression of cardiac tamponade, the patient was taken urgently to the cardiac catheterization laboratory, where right-heart catheterization confirmed tamponade physiology with elevation and equalization of pericardial and intracardiac diastolic pressures. She underwent pericardiocentesis without complication. Clinical and cytological evaluation for TB and malignancy were unrevealing, and the diagnosis of uremic pericarditis was made. There has been no recurrence with a more aggressive dialysis regime.

SUGGESTED READING

Benoff LJ, Schweitzer P. Radiation therapy-induced cardiac injury. American Heart J 1995;129:1193–1196.

Chen Y, Brennessel D, Walters J, et al. Human immunodeficiency virus-associated pericardial effusion: report of 40 cases and review of the literature. Am Heart J 1999;137:516–521.

Hurrell DG, Nishimura RA, Higano ST, et al. Value of dynamic respiratory changes in left and right ventricular pressures for the diagnosis of constrictive pericarditis. Circulation 1996;93: 2007–2013.

Ling L, Oh J, Schaff HV, et al. Constrictive pericarditis in the modern era: evolving clinical spectrum and impact on outcome after pericardiectomy. Circulation 1999;100:1380–1386.

Oh JK, Hatle LK, Seward JB, et al. Diagnostic role of Doppler echocardiography in constrictive pericarditis. J Am Coll Cardiol. 1994;23:154–162.

Pepi M, Muratori M, Barbier P, et al. Pericardial effusion after cardiac surgery: incidence, site, size and haemodynamic consequences. Br Heart J 1994;72:327–331.

Sagrista-Sauleda J, Angel J, Permanyer-Miralda G, et al. Long-term follow-up of idiopathic chronic pericardial effusion. New England J Med 1999;341:2054–2059.

Shabetai R. The Pericardium. New York: Grune and Stratton, 1981.

Spodick DH. The Pericardium: A Comprehensive Textbook. New York: Marcel Dekker, 1997.

11 Echocardiographic Assessment of Aortic Stenosis

Edmund A. Bermudez, MD, MPH

Contents

INTRODUCTION

Transthoracic echocardiography has largely replaced cardiac catheterization as the primary modality for the hemodynamic assessment of valvular heart disease. A comprehensive evaluation of valve structure, function, and hemodynamics is possible through a carefully performed transthoracic study. In the case of aortic stenosis, echocardiography is used to define the initial severity of disease, etiology, and monitor its progression through serial follow up studies. Evaluation of aortic stenosis would be incomplete without a comprehensive examination of overall left ventricular function and estimation of pulmonary artery pressures. Transthoracic echocardiography, therefore, can provide important information about the initial diagnosis, management, and follow-up of adult patients with native aortic valve stenosis.

ETIOLOGY

When considering the etiology of aortic stenosis, it is important to consider the age and the demographics of the patient (Fig. 1). Rheumatic valvular disease, once the most common form of aortic stenosis, is less common today in developed countries. Commissural fusion is a hallmark of this disease and often presents with concomitant mitral stenosis (Fig. 2; please *see* companion DVD for corresponding video). Less commonly, the commissures may fuse eccentrically, producing a de facto bicuspid valve. In this case, differentiation from a congenitally bicuspid valve can be difficult.

Calcific degeneration is currently the most common form of aortic stenosis in the developed world. It generally presents later in adult life and is sometimes called senile calcific degeneration (Fig. 3). Commissural fusion can occur, but is not a hallmark of this disease process. Calcification is visualized as "echo bright" reflectivity of the valve leaflets and the aortic root.

Congenital bicuspid aortic valves may calcify and thicken over time, eventually producing stenotic lesions that present earlier than other common causes of adult aortic valvular stenosis (Fig. 1). When observed in the parasternal short-axis view, bicuspid aortic valves exhibit either a vertical or a horizontal commissural orientation in the parasternal short-axis view. In the vertical orientation, commissures are in the anterior and posterior position with a right and left cusp. In the horizontal orientation, commissures are in the right and left positions, with anterior and posterior cusps. Raphes are commonly seen in both of these orientations (Fig. 4).

From: *Contemporary Cardiology: Essential Echocardiography: A Practical Handbook With DVD*
Edited by: S. D. Solomon © Humana Press, Totowa, NJ

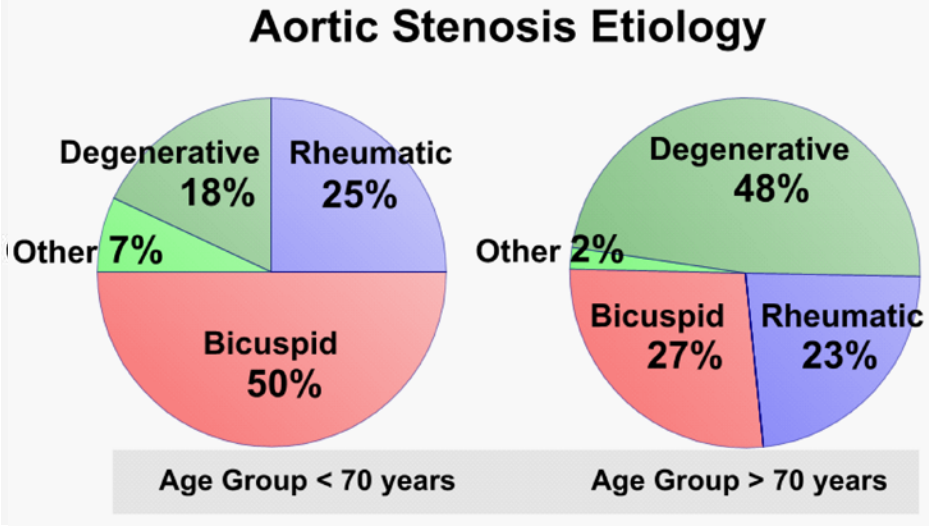

Fig. 1. The etiology of aortic stenosis by age group. (Reproduced with permission from Passik CS, Ackermann DM, Pluth JR, Edwards WD. Temporal changes in the causes of aortic stenosis: a surgical pathologic study of 646 cases. Mayo Clin Proc 1987;62:119–123.)

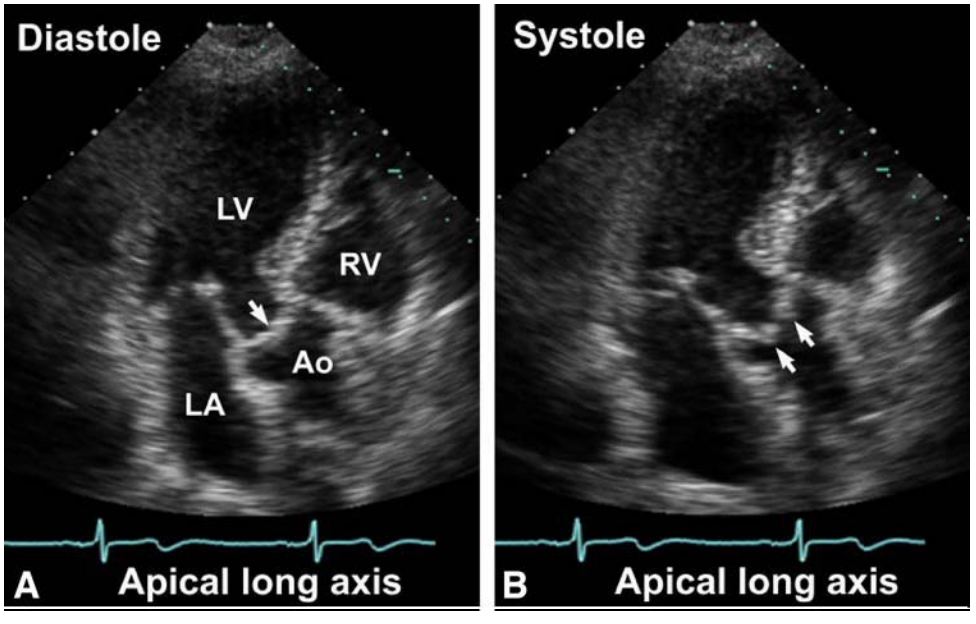

Fig. 2. (*See* legend, facing page)

The appearance of the valve in systole is characteristic of this etiology, and has been referred to as a fish-mouth appearance, rather than the triangular appearance of normal valves (Fig. 5; please *see* companion DVD for corresponding video).

TWO-DIMENSIONAL ASSESSMENT

Important morphological information can be gained from initial two-dimensional (2D) views of the aortic valve. Leaflet restriction in the setting of adequate cardiac output is the hallmark of aortic stenosis, which can be readily discerned in the parasternal long-axis view. Failure of aortic leaflets to open fully with ventricular ejection often signifies some degree of aortic stenosis (Fig. 6; please *see* companion DVD for corresponding video). Eccentric valve opening visualized in the parasternal long views is a further clue to the presence of a bicuspid aortic valve. Stenotic aortic valves are generally thickened or calcified. This is easily seen on either 2D or M-mode assessment of the valve (Fig. 7).

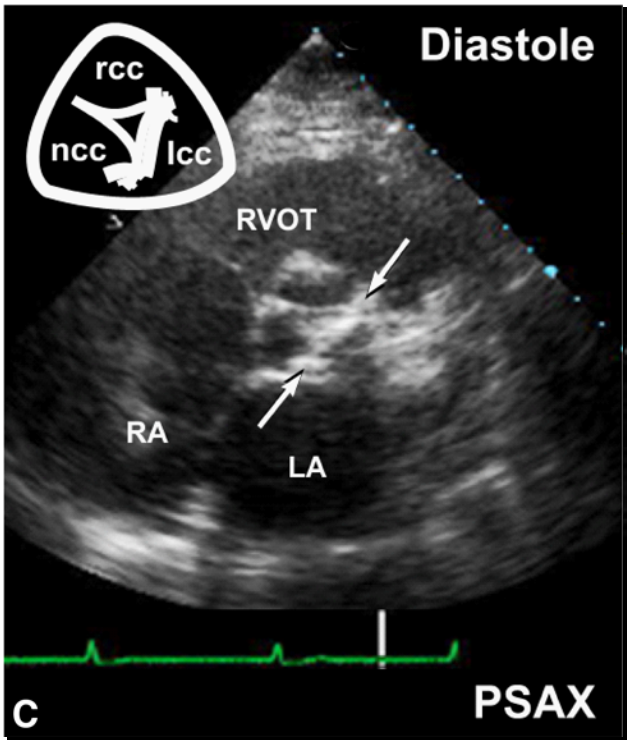

Fig. 2. (**A–C**) Aortic stenosis showing thickened valve leaflets. (**C**) Commissural fusion (arrows) is a hallmark feature of rheumatic valvular heart disease. (Please *see* companion DVD for corresponding video.)

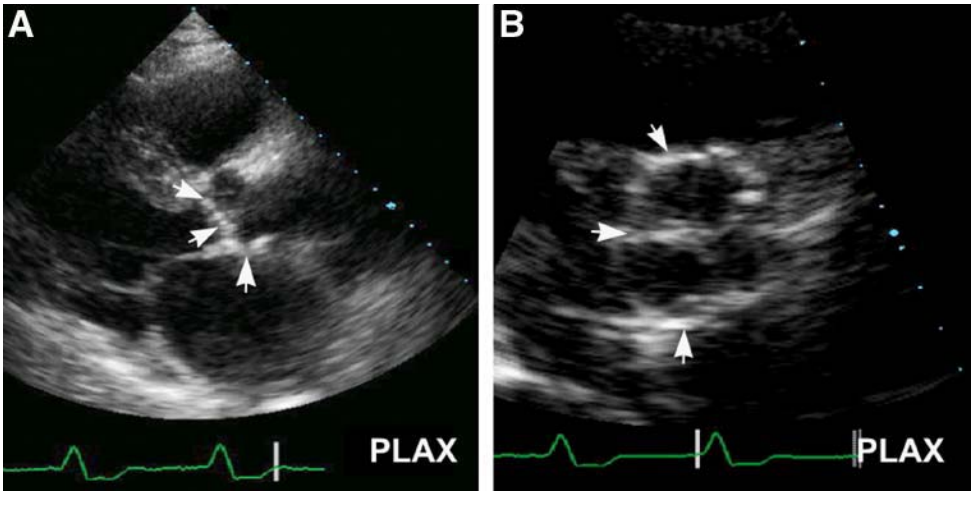

Fig. 3. Calcific ("senile") degeneration of aortic valve showing "echo-bright" reflection (arrows).

Therefore, the 2D characteristics of the aortic valve can provide important clues to the etiology of aortic stenosis (Table 1).

DOPPLER ASSESSMENT

Doppler measurements across the aortic valve are essential to the determination of the severity of aortic stenosis. As the aortic valve narrows, the velocity of blood flow across the valve will generally increase. This velocity is dependent on the pressure gradient across the valve. Continuous-wave (CW) Doppler measurements across the aortic valve should be performed where the ultrasound beam is most parallel to the flow of blood across the valve. Therefore, measurements are best

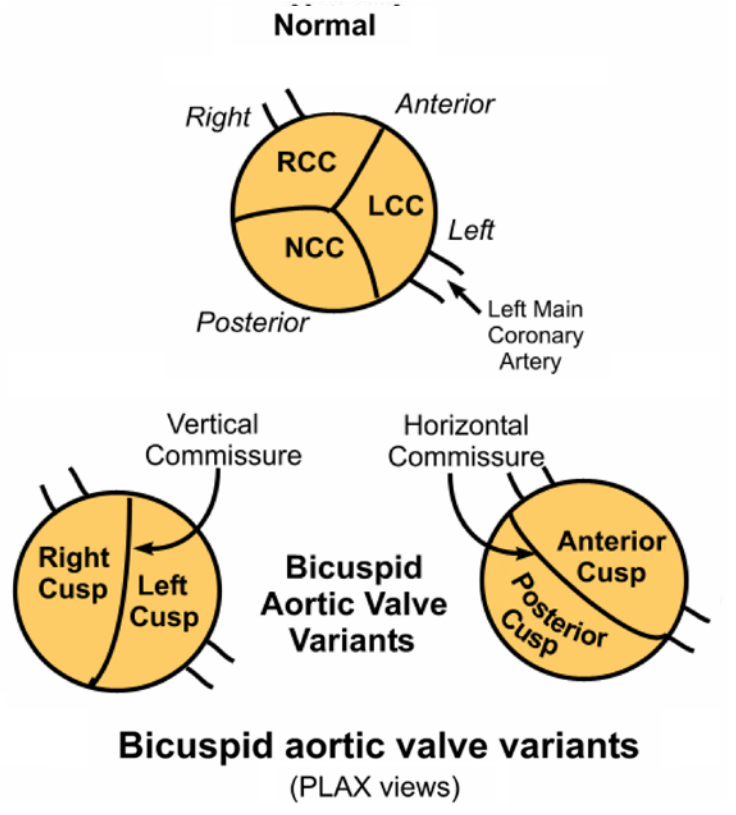

Fig. 4. Sketch showing bicuspid aortic valve variants with different commissural orientations (parasternal short-axis views [PLAX]).

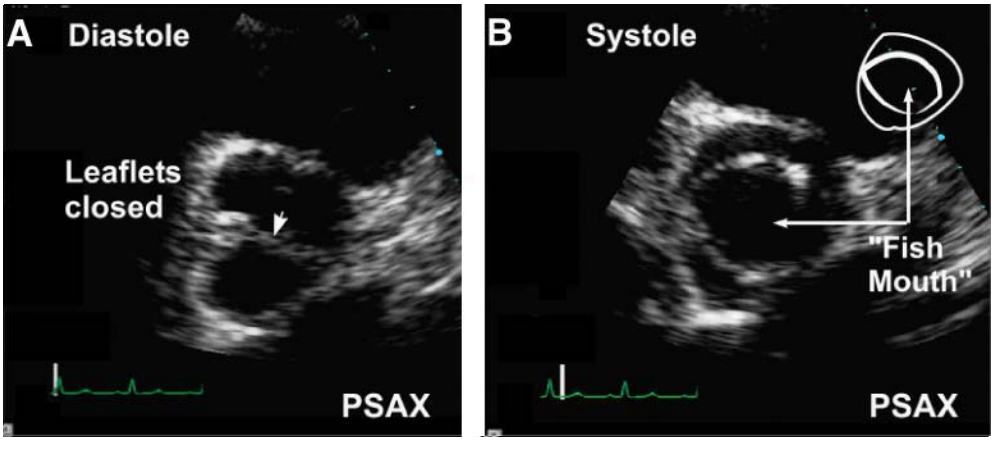

Fig. 5. (*See* legend, facing page)

acquired in the apical five-chamber, right parasternal long axis, or suprasternal views to obtain the highest velocities across the valve. The maximum velocity obtained is highly dependent on accurate transducer positioning, and will be underestimated when Doppler beam angle deviates from that of blood flowing through the stenotic valve (Fig. 8). A nonimaging probe can be used if inadequate envelopes are found with the duplex imaging transducer.

The calculation of transvalvular pressure gradients is based upon the Bernoulli principle. The modified Bernoulli principle relates the transaortic pressure gradient to the square of the maximal velocity found on CW Doppler: $P = 4V^2$, and is used when the velocity of blood proximal to the stenosis is negligible. In significant aortic stenosis, high gradients across the aortic valve can be seen. The relationship is accurate

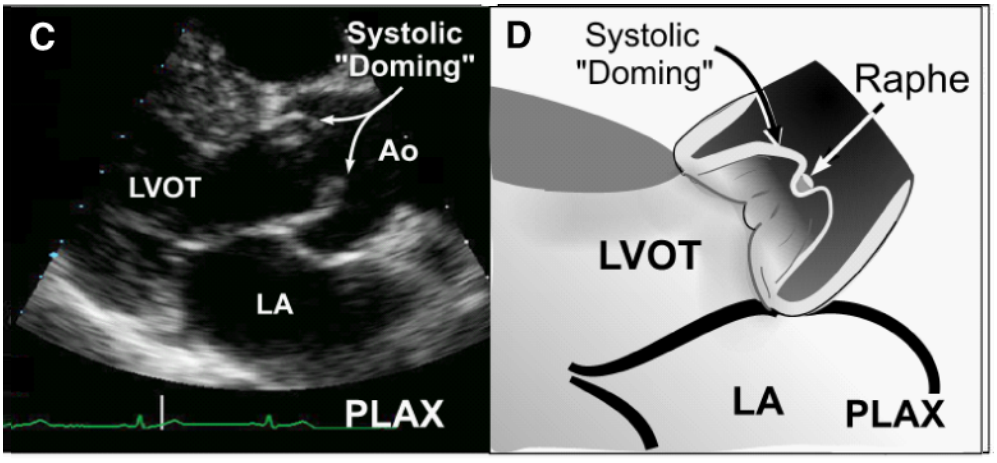

Fig. 5. Bicuspid aortic valve during diastole (**A**) and systole (**B**) in parasternal short-axis (PSAX) view. Note horizontal commissure (arrow) in diastole and "fish mouth" appearance during systole. (**C**,**D**) Systolic doming of bicuspid aortic valve during systole (parasternal long-axis view [PLAX]). (Please *see* companion DVD for corresponding video.)

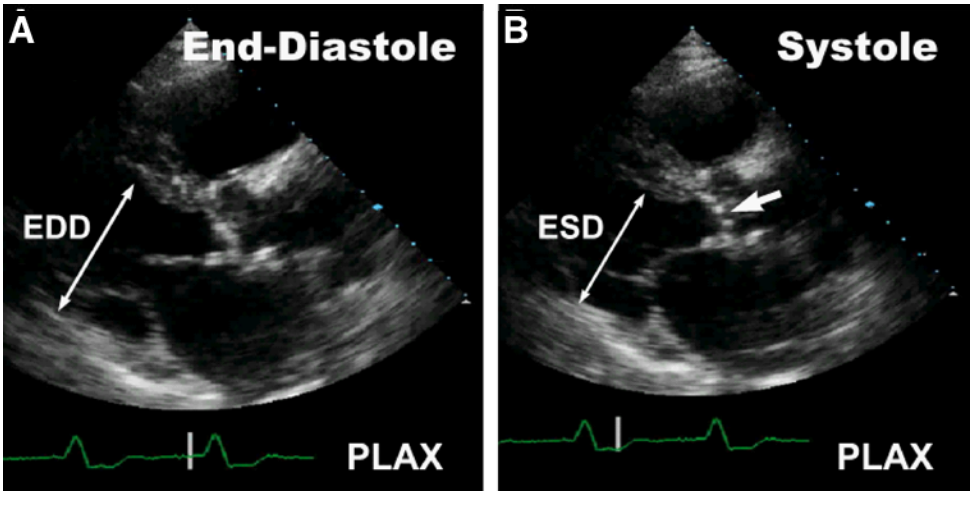

Fig. 6. Aortic stenosis showing restricted leaflet opening (arrow) during systole (parasternal long-axis view [PLAX]). Left ventricular ejection fraction was reduced, hence "low stroke volume-low gradient" aortic stenosis. (Please *see* companion DVD for corresponding video.)

when the velocity proximal to the stenosis is less than 1.5 m/s. Should the velocity in the left ventricular outflow tract (LVOT) exceed 1.5 m/s, then the long version of the Bernoulli equation should be used to calculate the transaortic gradient. Therefore:

$$\text{Transaortic pressure gradient} = 4\,(V_{max}^{\,2} - V_{LVOT}^{\,2})$$
$$\text{when } V_{LVOT} \geq 1.5 \text{ m/sec}$$

In most cases, the modified Bernoulli equation is an accurate and simple measure of the peak instantaneous transaortic pressure gradient.

Peak transaortic gradient measured by Doppler should be differentiated from the peak-to-peak gradient obtained at cardiac catheterization. Hemodynamically, the peak-to-peak gradient measures the difference between the peak left ventricular pressure and the peak aortic pressure—which are not measured simultaneously. Therefore, peak-to-peak gradients are not physiological, and no Doppler measurement exactly corresponds to this measurement in the catheterization laboratory. However, mean gradients across the aortic valve are similar when measured by Doppler and by cardiac catheterization.

The Doppler derived mean gradient is the average gradient over the systolic ejection period. This is usually calculated by tracing the CW envelope obtained across the aortic valve, and the numerical values are automatically calculated by the machine's software

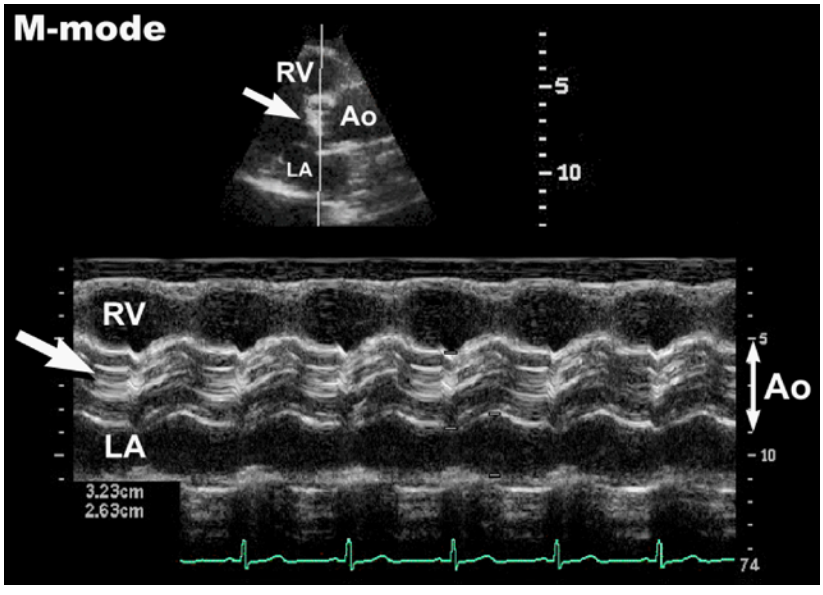

Fig. 7. M-mode through aortic valve showing characteristic thickening of valve leaflets in aortic stenosis (compare Chapter 3, Fig. 14A).

Table 1
Two-Dimensional Characteristics of Classic Aortic Stenosis According to Disease Etiology

	Calcific degenerative	*Rheumatic*	*Bicuspid*
Eccentric closure line in the parasternal long-axis	No	No	Yes
Leaflet doming in systole	No	Yes	Yes
Commissural fusion	No	Yes	No
Associated aortic coarctation	No	No	Yes
Fish-mouth appearance of valve in systole	No	No	Yes

package (Fig. 9). It is important to ensure that it is actually the aortic envelope that is traced, as a mitral or tricuspid regurgitant jet may mimic an aortic stenotic envelope (Fig. 10).

CALCULATION OF AORTIC VALVE AREA

The calculation of aortic valve area (AVA) is based on the continuity equation (Fig. 11). This equation relates the flow proximal to the stenosis and flow through the valve.

$$\text{Area}_{\text{LVOT}} \times V_{\text{LVOT}} = \text{AVA} \times V_{\text{max}}$$

Where the AVA is the aortic valve area and V_{max} is the maximal velocity obtained by CW Doppler. V_{LVOT} is the velocity in the LVOT obtained by pulse wave Doppler usually in the apical five-chamber view. Area_{LVOT} is the area of the LVOT and is calculated by multiplying π by the square of the radius of the LVOT. The equation thus becomes:

$$\text{AVA} = \pi(\text{radius of LVOT})^2 \times V_{\text{LVOT}}/V_{\text{max}}$$

Therefore, the AVA can be easily calculated using velocities. Alternatively, the velocity time integral (VTI) can also be used instead of velocities to obtain the AVA.

ASSESSMENT OF STENOSIS SEVERITY

The normal aortic valve orifice area in adults ranges from 2 to 4 cm^2. In general terms, severe stenosis is not seen with an AVA of more than 1.0 cm^2. According to American College of Cardiology/American Heart Association guidelines, severe aortic stenosis is seen when the AVA is less than 1 cm^2 (Table 2). Transvalvular gradients should not be ignored when assessing severity of aortic stenosis. Overall, when the mean transvalvular gradient exceeds 50 mmHg, severe stenosis is usually present.

Alternative methods of assessing aortic stenosis severity exist (Table 3). The Doppler Velocity index or Dimensionless index is a measure of the ratio of the LVOT velocity to the AV velocity using CW Doppler

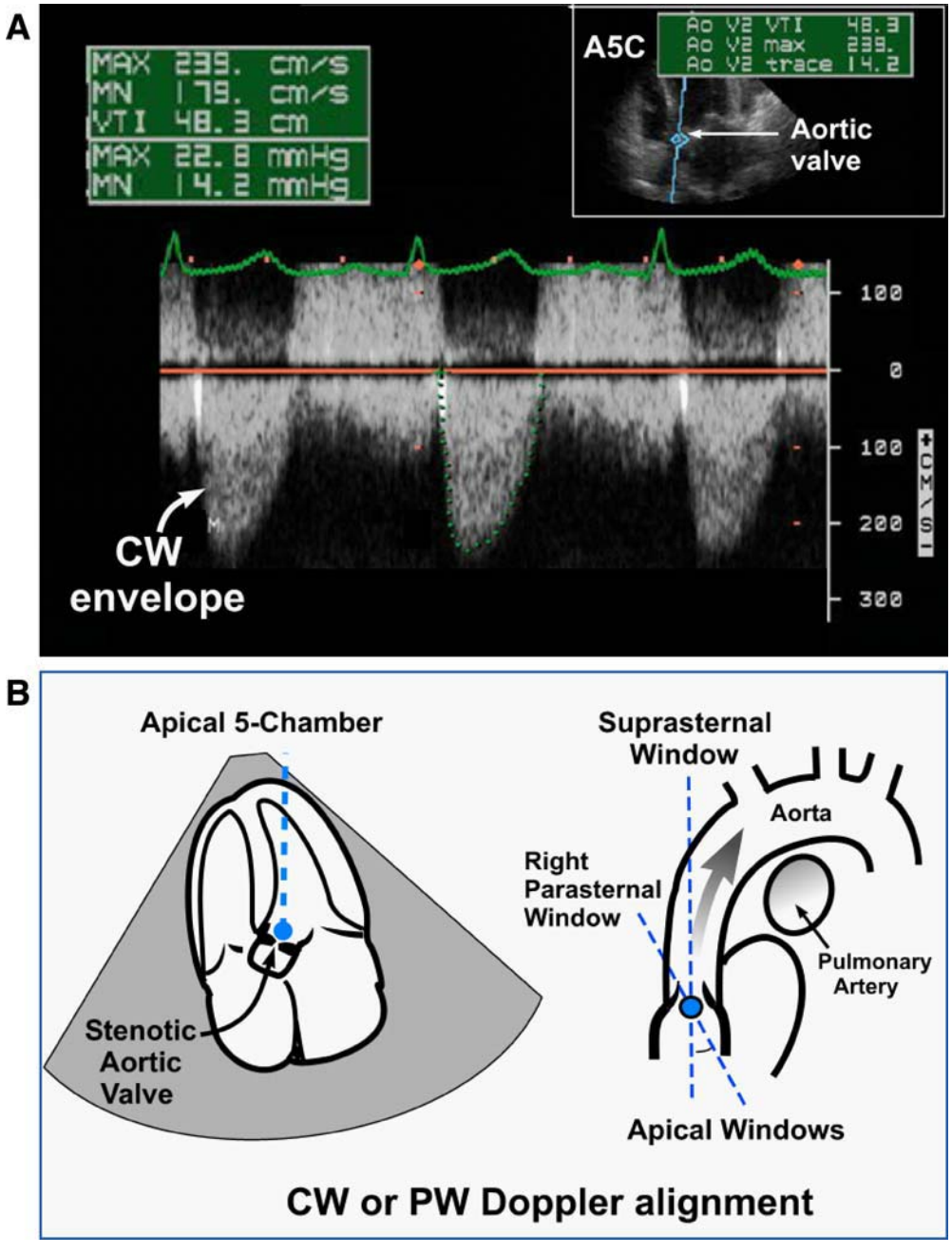

Fig. 8. (**A**) Continuous-wave (CW) Doppler of maximum velocity across stenotic aortic valve. (**B**) Optimal Doppler alignment for assessment of peak velocities in aortic stenosis.

across the aortic valve (Fig.12). It is normally higher than 0.28 but decreases with significant aortic stenosis. An index of less than 0.25 generally correlates with severe aortic stenosis. VTI may be used instead of velocities. In addition, because peak transvalvular gradients are linearly correlated with mean gradients, a peak gradient greater than 4.5 m/s is also indicative of severe stenosis.

Therefore, a combination of methods may be used to assess aortic stenosis severity. Nonetheless, symptoms are the major guide to therapeutic decisions, and no single measurement is used to guide referral for surgical intervention. Thus, echocardiographic measurements of severe stenosis in conjunction with the wider clinical picture are the benchmarks for referral for aortic valve replacement.

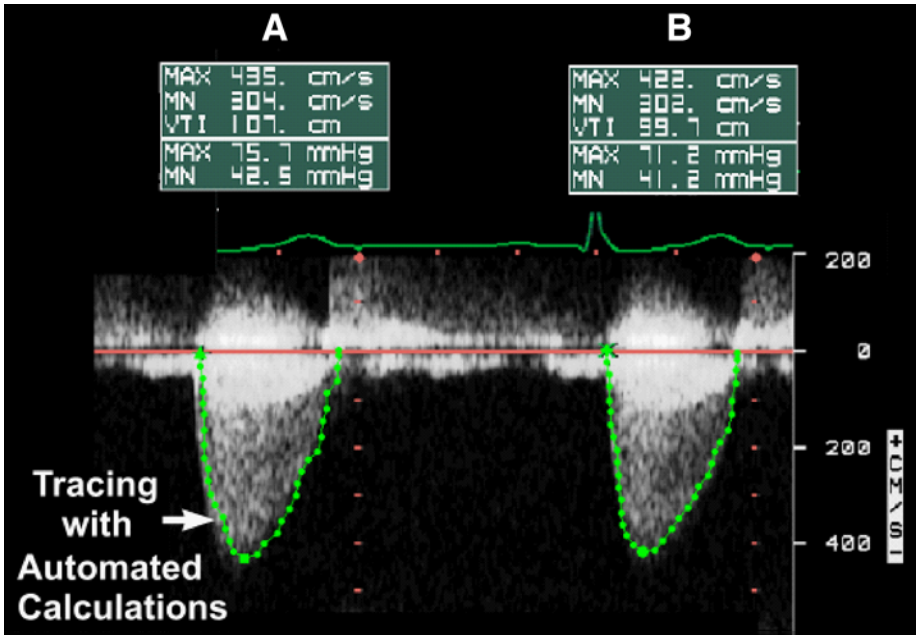

Fig. 9. Calculation of trans-aortic gradients by continuous-wave Doppler.

LOW-GRADIENT AORTIC STENOSIS

In some situations, patients present with severe aortic stenosis (calculated AVA <1.0 cm^2) and low transvalvular gradients (<30 mmHg). These patients have low ejection fractions and low cardiac output (Fig. 6). In this situation, the calculated AVA may be small secondary to the low flow state, and should be interpreted with caution. These patients may benefit from further testing to differentiate true severe aortic stenosis from apparent severe aortic stenosis owing to a functionally stenotic valve because of the low output state. Dobutamine echocardiography can help to differentiate these two conditions. With the infusion of low-dose dobutamine, stroke volume increases and the calculated AVA increases in those with functionally stenotic valves. However, in those with true severe aortic stenosis, the calculated AVA remains unchanged. Low-dose dobutamine challenge therefore can assess the "contractile reserve"—a predictor of which patients are more likely to benefit from aortic valve replacement.

Even patients with critical stenoses (valve area <0.75 cm^2), low gradients (<30 mmHg), and low ejection fraction (<35%) may benefit from aortic valve replacement if they exhibit contractile reserve. Those who do not exhibit augmentation in cardiac output are problematic and prognosis is generally poor. The quantitative assessment of severity with low-dose dobutamine challenge should follow the same guidelines as in other situations (AVA, transvalvular gradients, and dimensionless index).

Although planimetry may be used to measure the orifice area by transesophageal echocardiography, it is not commonly implemented in clinical scenarios, as transvalvular gradients and AVA can be easily applied in most situations.

PITFALLS

The accurate assessment of aortic stenosis severity is contingent on factors related to the subject, image acquisition and analysis, and the interpretation of the data (Table 4). Potential pitfalls related to the patient cannot be helped, but the importance of a meticulous transthoracic examination by a skilled operator cannot be overstated. It is essential to acquire the maximum velocity using multiple windows to avoid underestimation of the peak velocity measurement and hence overestimation of AVA (Fig. 8). In addition, because the LVOT radius is squared in the continuity equation, careful measurement of this parameter is crucial for accurate calculations.

The modified Bernoulli equation ($P = 4V^2$) should not be used when the velocity proximal to the stenosis (V_{LVOT}) is greater than 1.5 cm^2. The long version of the Bernoulli equation should be used to calculate a more

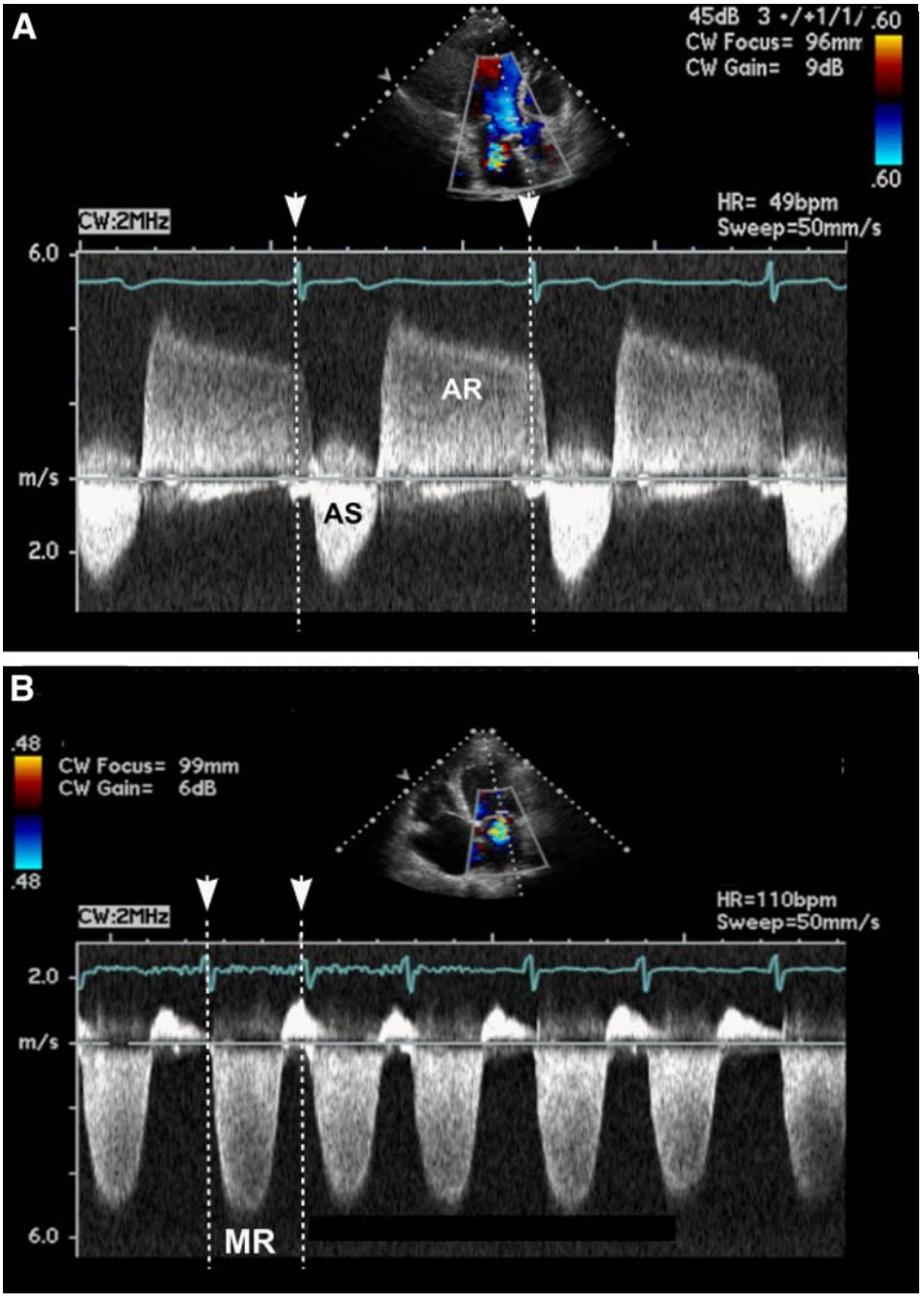

Fig. 10. Distinguishing aortic stenosis from mitral regurgitation on Doppler examination. Both jets both occur in systole and appear as downward spectral velocity shifts when recorded from the apex. The onset of ventricular systole and mitral regurgitation occurs prior to aortic valve opening. In addition, mitral regurgitation is longer in duration.

accurate peak transaortic gradient. In this situation, the proximal velocity cannot be ignored, as the modified Bernoulli is based on a negligible value for the proximal velocity.

It is essential to acquire adequate transaortic envelopes via CW Doppler. The aortic envelope must be distinguished from that of mitral regurgitation and tricuspid regurgitation. These envelopes are generally longer in duration as valve regurgitation usually encompasses isovolumetric contraction and relaxation. In addition, inspection of diastole often shows the presence of an aortic regurgitation signal that is not seen with mitral

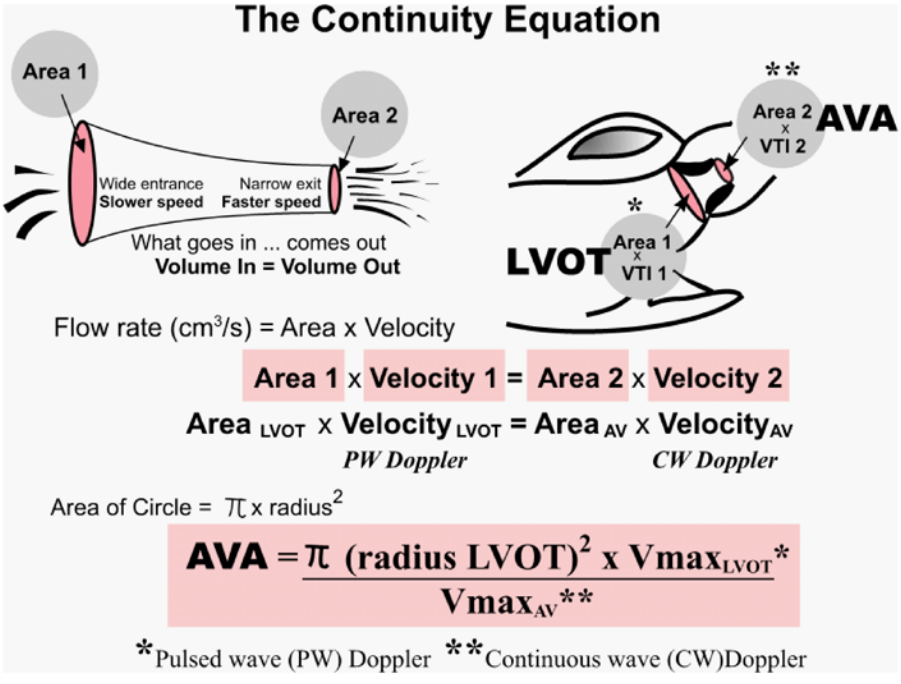

Fig. 11. The continuity equation and assumptions for measuring aortic valve area (AVA) in aortic stenosis.

Table 2
Severity of Aortic Stenosis by Valve Area

Severity	*Calculated valve area*
Mild	>1.5 cm^2
Moderate	1–1.5 cm^2
Severe	<1 cm^2

regurgitation. Mitral regurgitant velocities generally exceed 4–5 m/s, and usually exceed the transaortic velocity when found in the same patient.

A subaortic membrane should be considered when high velocities are observed on CW Doppler in the setting of normal aortic valve leaflet excursion on 2D examination. Local flow acceleration during color flow Doppler examination can often be seen in the LVOT even when no membrane is seen on transthoracic imaging (Fig. 13; please *see* companion DVD for corresponding video). In this situation, transesophageal echocardiography may confirm the presence of a subaortic membrane. Early systolic closure of the aortic valve leaflets on M-mode imaging may be seen in this condition.

A complete assessment of aortic stenosis incorporates other aspects of the transthoracic echocardiogram, as well as other factors that predict progression in individual patients. Aortic insufficiency frequently accompanies aortic stenosis and should be taken into account when considering surgery. The degree of left ventricular hypertrophy and LV function reflects the hemodynamic impact of the stenosis. Pulmonary hypertension in the presence of severe aortic stenosis may be an ominous sign. The presence of a bicuspid aortic valve should always prompt a search for coarctation of the aorta, because there is an established association between the two conditions.

CONCLUSION

Transthoracic echocardiography is the standard for evaluation of aortic stensosis severity. If a careful examination is performed, cardiac catheterization is rarely needed for confirmation. Many institutions only employ cardiac catheterization merely to assess coronary arteries' status prior to aortic valve replacement. Transthoracic echocardiography remains a comprehensive tool in the initial diagnosis, follow up, and management of patients with aortic valvular disease.

Table 3
Echocardiographic Quantitation Parameters to Assess Aortic Stenosis Severity

Components	*Measurement*	*Acquisition site*	*Echo modality*	*Utility*
Continuity equation	LVOT diameter, LVOT VTI, AV VTI mean gradient	PLAX, A5C, A3C, A5C, A3C, SSN, right PLAX	2D, pulsed Doppler, CW Doppler	Accurate, reproducible, flow-dependent
Doppler velocity index (dimensionless index)	Peak LVOT, Peak AV	A5C, A3C, right PLAX, SSN	CW or pulsed Doppler	Useful in patients with AF, PVCs, and prosthetic valves
Doppler pressure gradients	Doppler maximum gradient, Doppler mean gradient	A5C, A3C, right PLAX, SSN	CW Doppler	
Maximum aortic jet velocity	Maximum velocity	A5C, A3C, right PLAX, SSN	CW Doppler	
Planimetry	2D planimetry	Midesophageal views	TEE	Planimetry by TEE, when transthoracic study suboptimal

A3C, apical three-chamber view; A5C, apical five-chamber view; AF, atrial fibrillation; CW, continuous wave; 2D, two-dimensional; LVOT, left ventricular outflow tract; PLAX, parasternal long axis; SSN-suprasternal notch; TEE, transesophageal echocardiography; VTI, velocity time integral; PVC, premature ventricular contraction.

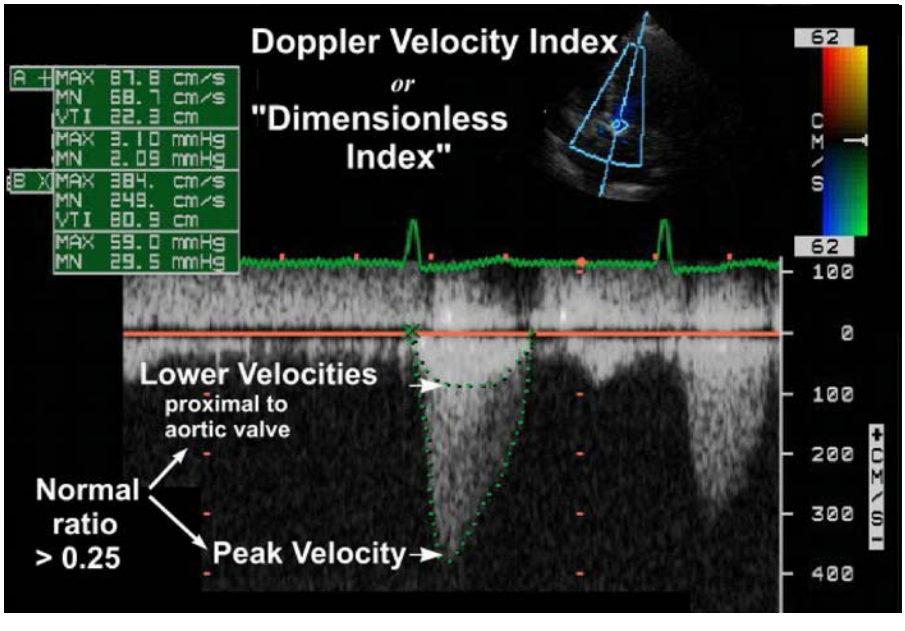

Fig. 12. The Doppler velocity index or dimensionless index by CW Doppler across aortic valve. The continuous-wave Doppler envelope shows a peak velocity of 3.8 m/s across aortic valve. The velocity proximal to the valve (depicted by the bright lower velocities highlighted by the arrow) reached 87 cm/s. The ratio of the latter to the former is less than 0.25. This Doppler velocity index, also known as dimensionless index, is normally more than 0.25, but decreases with significant valve stenosis.

Table 4
Pitfalls in the Echocardiographic Assessment of Aortic Stenosis

Pitfalls related to subject	Body habitus and anatomy
	General status: postoperative, acute illness, chest disorders—chronic obstructive pulmonary disease, and so on.
	Physiology: rate, rhythm
Pitfalls related to image acquisition	Operator skill and experience
	Mistaking MR or TR for AS
	Pitfalls re: continuity equation acquisition
	Underestimation of AVA if highest VTI or velocity not recorded
	Difficulty measuring LVOT diameter, e.g., heavy calcification
	Subaortic obstruction leading to difficulty measuring LVOT or VTI
	Inaccurate PW sampling—leading to over or under-estimation
	If patient not in sinus rhythm: 8–10 quality beats needed to accurately assess parameters, otherwise use CW, and measure Doppler velocity (dimensionless) index
Pitfalls related to analysis and interpretation	Inter- and intra-observer error in assessment
	Learning curve
Pitfalls related to method of assessment	Flow dependence: affects most methods, especially the continuity equation
	Low-dose dobutamine challenge may be needed to assess contractile reserve

AF, atrial fibrillation; AS, aortic stenosis; AVA, aortic valve area; CW, continuous wave Doppler; LVOT, left ventricular outflow tract; MR, mitral regurgitation; PVC, premature ventricular contraction; PW, pulsed wave; TR, tricuspid regurgitation; VTI, velocity time integral.

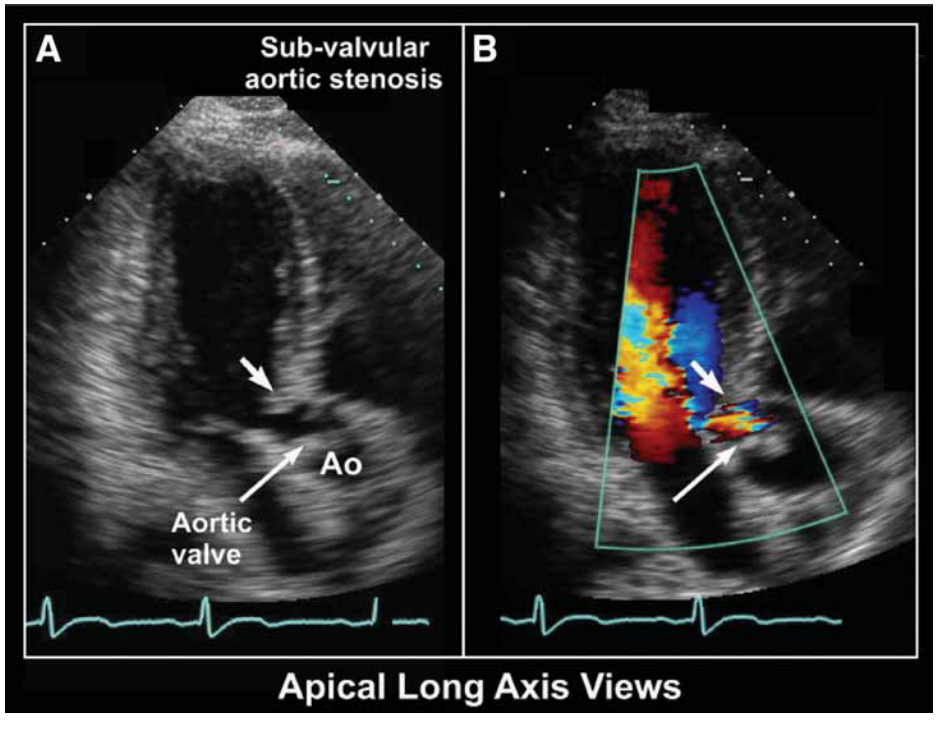

Fig. 13. Subvalvular aortic stenosis (arrows) with fixed membrane seen in apical long-axis view (**A**). (Please *see* companion DVD for corresponding video.)

SUGGESTED READING

Bonow RO, Carabello B, de Leon AC, Jr, et al. Guidelines for the management of patients with valvular heart disease: executive summary. A report of the American College of Cardiology/American Heart Association Task Force on Practice Guidelines (Committee on Management of Patients with Valvular Heart Disease). Circulation 1998;98: 1949–1984.

Currie PJ, Seward JB, Reeder GS, et al. Continuous-wave Doppler echocardiographic assessment of severity of calcific aortic stenosis: a simultaneous Doppler-catheter correlative study in 100 adult patients. Circulation 1985; 71:1162–1169.

deFilippi CR, Willett DL, Brickner ME, et al. Usefulness of dobutamine echocardiography in distinguishing severe from nonsevere valvular aortic stenosis in patients with depressed left ventricular function and low transvalvular gradients. Am J Cardiol 1995;75:191–194.

Oh J, Seward J, Tajik A. The Echo Manual, 2nd ed. Rochester: Lippincott Williams and Wilkins, 1999.

Oh JK, Taliercio CP, Holmes DR, Jr, et al. Prediction of the severity of aortic stenosis by Doppler aortic valve area determination: prospective Doppler-catheterization correlation in 100 patients. J Am Coll Cardiol 1988;11:1227–1234.

Pereira JJ, Lauer MS, Bashir M, et al. Survival after aortic valve replacement for severe aortic stenosis with low transvalvular gradients and severe left ventricular dysfunction. J Am Coll Cardiol 2002;39:1356–1363.

Skjaerpe T, Hegrenaes L, Hatle L. Noninvasive estimation of valve area in patients with aortic stenosis by Doppler ultrasound and two-dimensional echocardiography. Circulation 1985;72:810–818.

Weyman A. Principles and Practice of Echocardiography, 2nd ed. Philadelphia: Lea and Fibiger, 1994.

12 Echocardiographic Evaluation of Aortic Regurgitation

Susan M. Sallach, MD and Sharon C. Reimold, MD

Contents

INTRODUCTION

Aortic regurgitation occurs when a fraction of the blood ejected from the left ventricle into the aorta during systole flows back into the left ventricle during diastole. The onset may be acute or chronic depending on etiology, and can be categorized as mild, moderate, or severe (Table 1). This backflow of blood results in both volume and pressure overload of the left ventricle leading to increased left ventricular work. Volume overload can, over time, lead to left ventricular dilation and hypertrophy. Although many patients with aortic regurgitation remain asymptomatic for many years, significant aortic regurgitation can eventually lead to congestive heart failure. Echocardiography plays a valuable role in the assessment and management of patients with underlying aortic regurgitation.

ECHOCARDIOGRAPHIC ASSESSMENT IN PATIENTS WITH AORTIC REGURGITATION

Echocardiographic assessment of patients with aortic regurgitation involves assessment of valve morphology, the aortic root, the degree of aortic regurgitation, and assessment of ventricular size and function.

ASSESSMENT OF AORTIC VALVE MORPHOLOGY

To evaluate the patient with aortic regurgitation, it is important to first investigate the morphology of the aortic valve and adjacent structures (including the aortic root) followed by an assessment of the impact of aortic regurgitation on left ventricular geometry and function. Doppler measurements provide semiquantitative and quantitative assessment of the degree of severity of aortic regurgitation. Both transthoracic and transesophageal echocardiography may be used to evaluate and quantitate the severity of valvular dysfunction.

ANATOMY OF AORTIC VALVE

The aortic valve is trileaflet in most people. In individuals with trileaflet aortic valves, the mechanism of aortic regurgitation may be secondary to abnormalities of the aortic sinuses, annulus, leaflets and/or the geometrical relationship between the aortic valve and the left ventricular outflow tract (Figs. 1 and 2). For example, patients with Marfan syndrome may have dilated aortic sinuses and aortic annulus resulting in malcoaptation of the aortic leaflets and central aortic regurgitation, but otherwise normal aortic valve leaflets (Fig. 3; please *see* companion DVD for corresponding video). Patients with endocarditis

From: *Contemporary Cardiology: Essential Echocardiography: A Practical Handbook With DVD*
Edited by: S. D. Solomon © Humana Press, Totowa, NJ

Table 1
Etiology of Aortic Regurgitation

Diseases involving the aortic cusps (leaflets)

- Senile calcific degeneration
- Bicuspid aortic valves
- Rheumatic valvular heart disease
- Endocarditis

Diseases involving the aortic root

- Hypertension
- Bicuspid aortic valve complex
- Collagen disorders, e.g., Marfan and Ehlers Danlos syndromes
- Aortic dissection (Type A)
- Trauma
- Aortitis (vasculitic, infectious)
- Ventricular septal defect

may have a normal aortic annulus and aortic sinuses, but destruction of valve leaflets can ensue, leading to aortic valvular dysfunction (Fig. 4; please *see* companion DVD for corresponding video). In those patients with degenerative aortic valve disease, combined abnormalities of the annulus, sinuses, and leaflets may provide the anatomic basis for aortic regurgitation (annulo-aortic ectasia). Patients with congenital heart disease such as a ventricular septal defect (especially the membranous and perimembranous varieties) may have an anatomically abnormal relationship between the left ventricular outflow tract and aortic valve leading to aortic regurgitation (Fig. 1).

A small proportion (1–2%) of the total adult population has bicuspid aortic valves (Fig. 5; please *see* companion DVD for corresponding video). These valves often lead to stenosis, regurgitation, or both, owing to abnormal leaflet architecture and coaptation. Bicuspid aortic valves are associated with dilatation of the aortic sinuses. Patients with aortic dilatation owing to hypertension often develop aortic regurgitation, usually with a central regurgitant jet. In addition, some human lymphocyte antigen (HLA) types (e.g., HLA B27) are associated with an increased risk of root dilatation leading to aortic insufficiency.

ECHOCARDIOGRAPHIC EVALUATION OF AORTIC VALVE MORPHOLOGY

The parasternal long-axis view is used to measure the left ventricular outflow tract, aortic annulus, and aortic sinuses. Leaflet thickening and prolapse can be visualized from this imaging window. A congenitally abnormal valve should be strongly suspected whenever markedly eccentric leaflet coaptation is seen in parasternal views. Color jet width (*see* "Doppler Echocardiographic Evaluation of the Patient With Aortic Regurgitation" section) is also measured in this view. Parasternal short-axis images are the optimal views for identifying leaflet morphology (tricuspid vs bicuspid or quadricuspid). Vegetations may appear as masses attached to the valve leaflets that may prolapse into the left ventricular outflow tract. Endocarditis can cause valve leaflets to perforate, becoming evident as color flow abnormalities that indicate leaflet perforation. In patients with aortic regurgitation, the dimensions of the aortic annulus, aortic sinuses and sinotubular junction should be recorded, and the presence or absence of valve thickening and other congenital abnormalities should be noted.

IMPACT OF AORTIC REGURGITATION ON THE LEFT VENTRICLE

Over time, aortic regurgitation can lead to progressive left ventricular dilation and eccentric left ventricular hypertrophy. Left ventricular dilation is influenced by the degree and duration of regurgitation. In chronic regurgitation, therefore, it is uncommon for a patient with severe aortic regurgitation to have normal left ventricular chamber dimensions. Most patients with significant aortic regurgitation develop left ventricular dilation prior to developing left ventricular systolic dysfunction. The extent of left ventricular dilation predicts the need for subsequent aortic valve replacement. Women with aortic regurgitation tend to have smaller ventricles for the same degree of aortic regurgitation compared to men. For this reason, chamber dimensions should be indexed to body surface area. Left ventricular size and function can predict outcomes and/or need for surgery (e.g., an end-diastolic diameter of 80 mm and an end-systolic diameter >50 mm). An indexed end-systolic diameter (>25 mm/m^2) is a useful cutoff in both men and women. A left ventricular ejection fraction less than 55% and changes in ejection fraction on exertion are also predictors of outcomes in aortic regurgitation.

Careful measurements of left ventricular end-diastolic and end-systolic dimensions as well as ejection fraction, therefore, are important components of evaluating patients with aortic regurgitation (Fig. 6A,B). These dimensions are typically measured from the parasternal long-axis view, from which the ejection fraction may can be calculated, or alternatively from volumes obtained using apical windows (*see* Chapter 4).

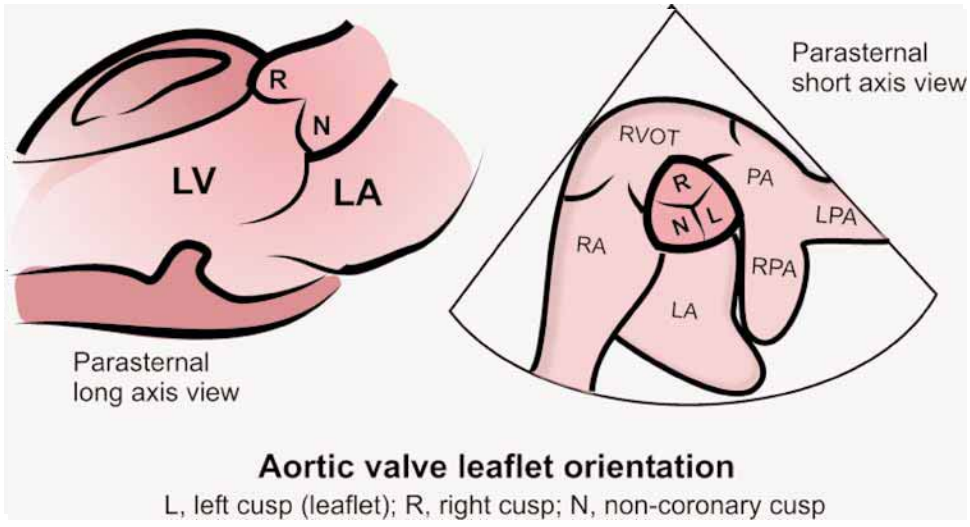

Fig. 1. Anatomical relationships of aortic valve and leaflets on two-dimensional echocardiography.

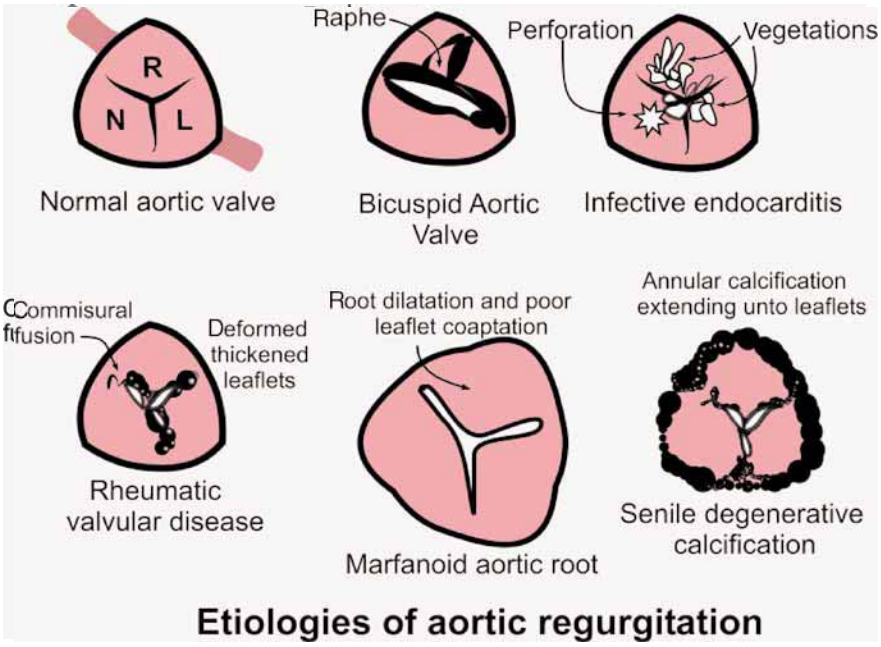

Fig. 2. Sketch illustrating various etiologies of aortic regurgitation.

Aortic regurgitant flow leads to rapid increase in left ventricular diastolic pressure. When this exceeds left atrial pressure, the mitral valve closes. Premature closure of the mitral valve and other echocardiographic signs of left ventricular overload may be evident (Fig. 7).

Because aortic regurgitation hemodynamically overloads the left ventricle, it leads to an absolute increase in left ventricle ejection fraction. Patients whose ejection fraction falls below 55% have depressed left ventricular systolic function. This may be partly reversible if aortic valve replacement is undertaken within 6 mo of the development of systolic dysfunction. For this reason assessment of systolic function is an important component of the echocardiographic examination in aortic regurgitation.

DOPPLER ECHOCARDIOGRAPHIC EVALUATION OF THE PATIENT WITH AORTIC REGURGITATION

Color flow Doppler imaging provides a semiquantitative method to evaluate the severity of aortic regurgitation. The regurgitant jet can be visualized by color flow

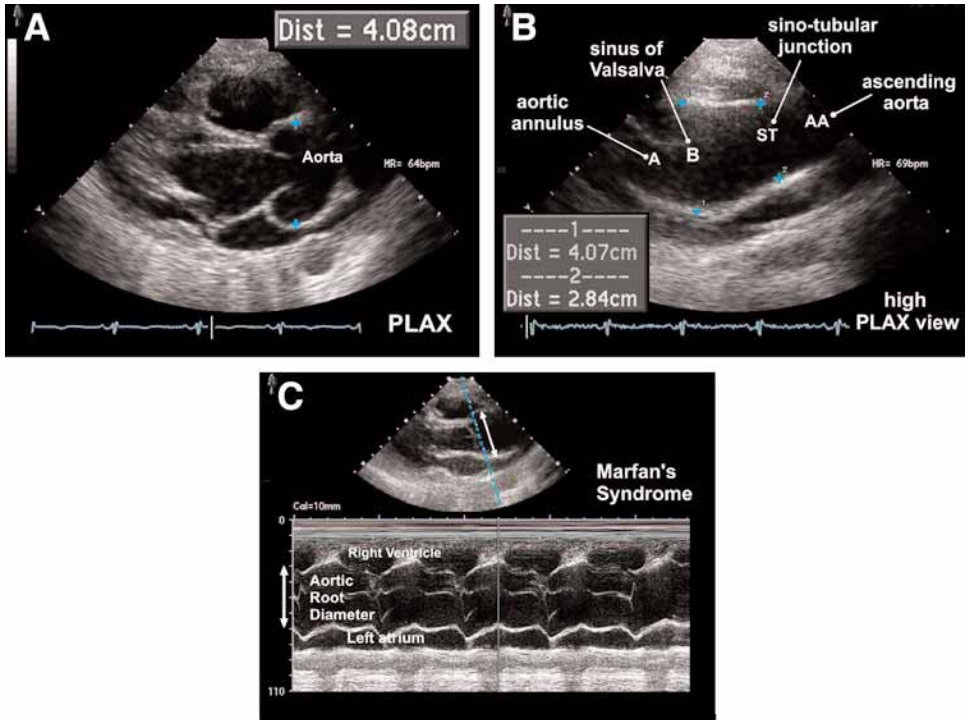

Fig. 3. Aortic regurgitation secondary to aortic root dilatation in a 26-yr-old female with Marfan syndrome. Annular dilatation can lead to inadequate central coaptation of valve leaflets and aortic regurgitation. (Please *see* companion DVD for corresponding video.)

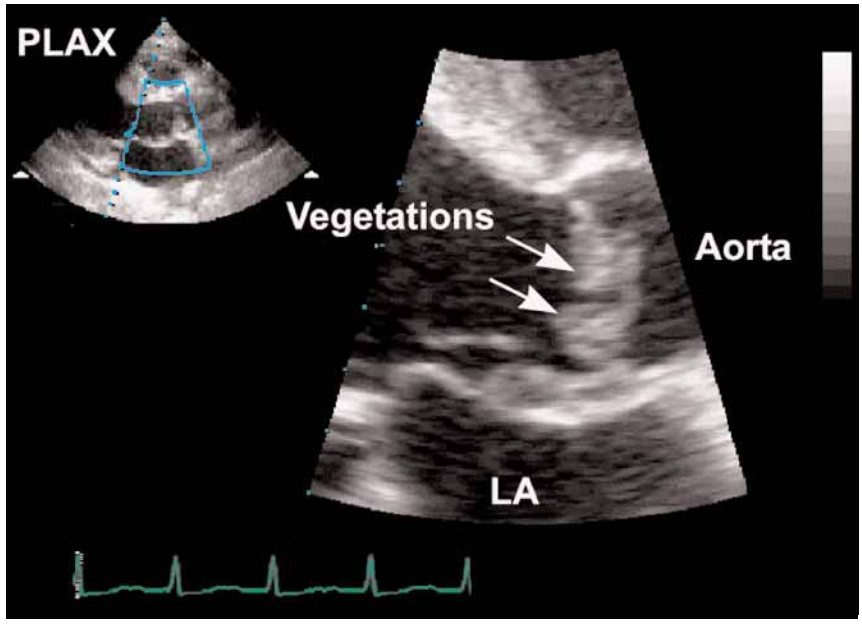

Fig. 4. Endocarditis of aortic valve leaflets showing vegetations. Endocarditis may lead to leaflet destruction as seen in this view. (Please *see* companion DVD for corresponding video.)

imaging in multiple views. Color flow Doppler in the parasternal long axis view provides an estimate of the size of the regurgitant orifice (Fig. 8). The color jet diameter (or width) is measured in diastole immediately below (within 1 cm) the aortic valve. In patients with aortic regurgitation because of trileaflet aortic valves this jet width is proportional to the size of the aortic valve defect. If the orifice is irregular, as in bicuspid aortic valve disease, the color jet

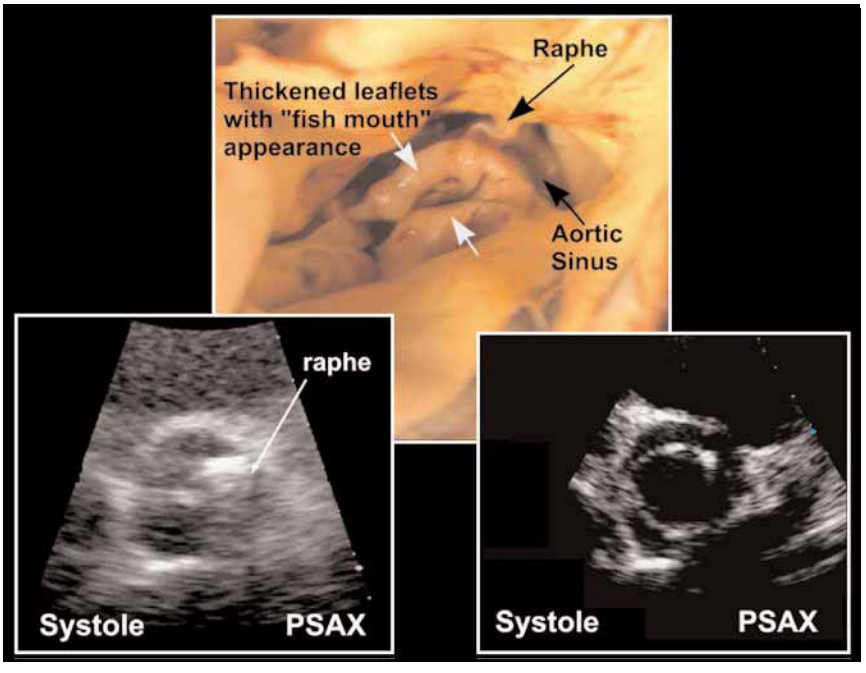

Fig. 5. Bicuspid aortic valves may have a visible raphe—the fusion ridge of two aortic leaflets. The aortic orifice often exhibits an ovoid or "fish mouth" appearance during systole. PSAX, parasternal short axis view. (Please *see* companion DVD for corresponding video.)

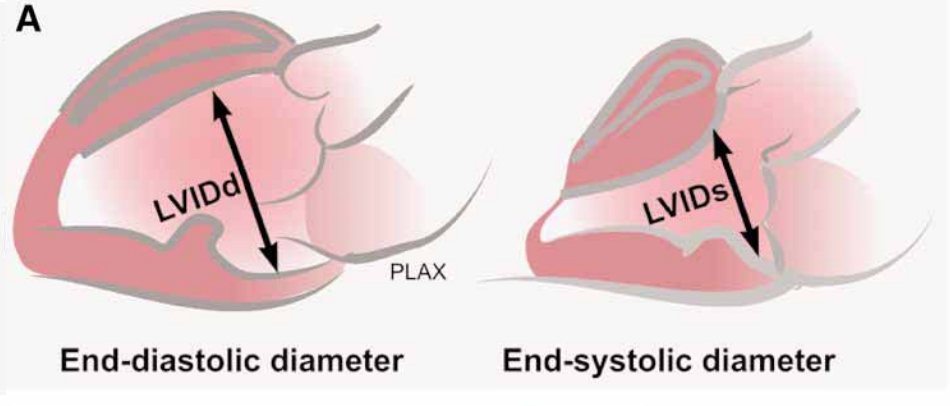

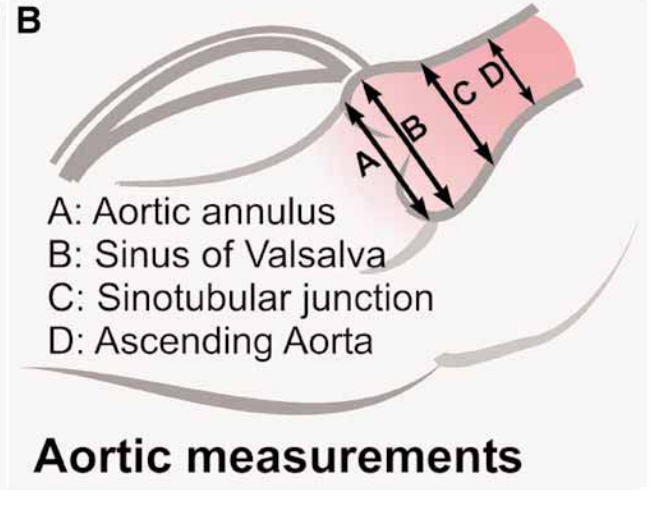

Aortic dimensions

Aortic diameters are proportional to body size and generally increase with aging

Parasternal long axis view measurements	Range (cm)
Aortic annular diameter	1.4–2.6
Sinus of Valsalva	2.1–3.5
Sinotubular junction	1.7–3.4
Ascending aorta	2.1–3.4

Cardiac Ultrasound Laboratory, Massachusetts General Hospital

Fig. 6. (A) Left ventricle dimensions (parasternal long-axis [PLAX] measurements). **(B)** Dimensions of the aorta (PLAX measurements).

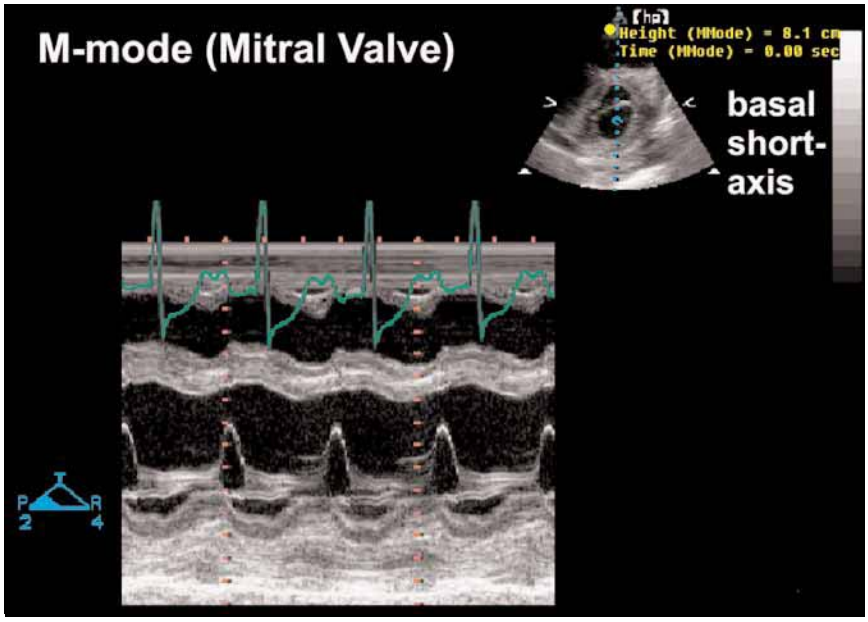

Fig. 7. M-mode showing premature diastolic closure of the mitral valve—a reflection of the hemodynamic impact of aortic regurgitation on the left ventricle. Other M-mode signs include anterior mitral valve leaflet fluttering (and less commonly, septal diastolic fluttering).

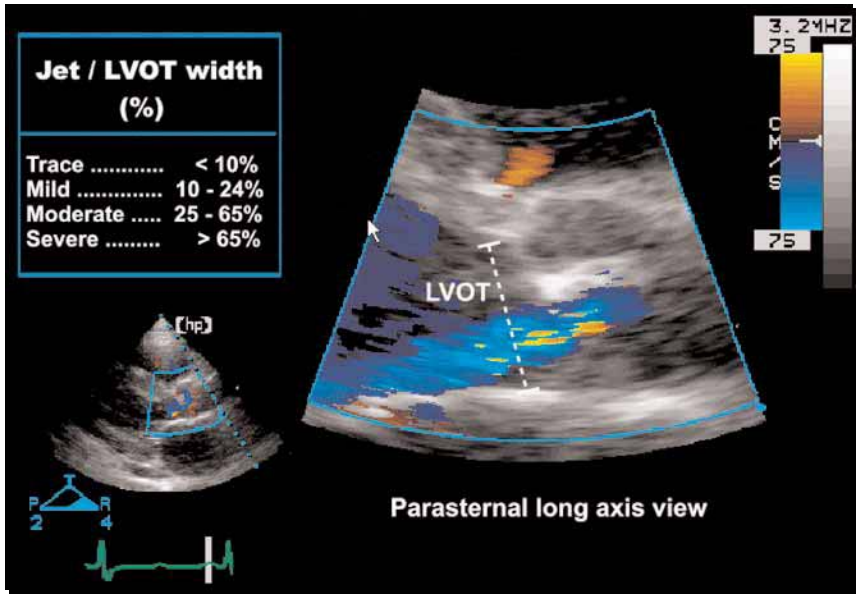

Fig. 8. Ratio of the aortic jet width (diameter) to left ventricular outflow tract (LVOT) diameter. The diameter of the color jet is measured immediately beneath the aortic valve is a semi-quantitative index of aortic regurgitation severity.

width *is not related* to the degree of regurgitation. The ratio of jet diameter to left ventricular outflow tract diameter can be calculated (Fig. 9). This ratio can provide a semi-quantitative estimate of the degree of regurgitation: less than 10%, trace; 10–24%, mild; 25–65%, moderate; and greater than 65%, severe.

Measurement of the vena contracta—the regurgitant jet as it traverses the aortic orifice or the effective regurgitant area—can also be used to estimate aortic regurgitant severity. Using a Nyquist limit of 50–60 cm/s, a vena contracta width of less than 0.3 cm correlates with mild aortic regurgitation. A vena contracta width of 0.3–0.6 cm is

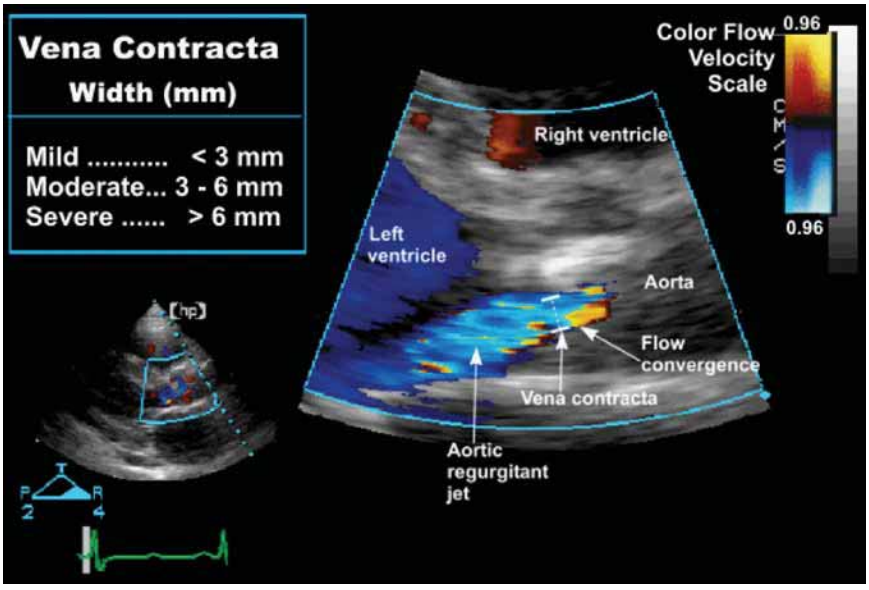

Fig. 9. Semi-quantitative assessment of aortic regurgitation severity by the vena contracta width. Note the three components of the aortic regurgitant flow: the flow convergence—above the orifice, the vena contracta—through the orifice, and the regurgitant jet—below the orifice.

consistent with moderate aortic regurgitation, whereas a vena contracta width greater than 0.6 cm indicates severe aortic regurgitation (Fig. 9).

Visualization of the color jet of aortic regurgitation on the parasternal short-axis view is another method for quantitation of the severity of regurgitation (Fig. 10A). The regurgitant color jet area can be measured and compared to that of the left ventricular outflow tract with the result expressed as a percentage (Fig. 10B). Using this simplified area ratio method, patients with mild aortic regurgitation have ratios of less than 5%. Severe aortic regurgitation occurs when ratios exceed 60%, with a broad range between 5 and 60% indicative of moderate aortic regurgitation.

The color jet disturbance of aortic regurgitation is also easily visualized from the apical windows (Fig. 11A; please *see* companion DVD for corresponding video). The color jet length and area, however, are less proportional (in these views) to the degree of regurgitation and are more influenced by the aortic to left ventricular diastolic pressure gradient as well as interactions between the regurgitant jet and the outflow tract walls (Fig. 11B, please *see* companion DVD for corresponding video). The color jet width is occasionally measured from this view but the parasternal projection provides better axial resolution.

QUANTITATIVE MEASURES OF AORTIC REGURGITATION

Continuous-wave Doppler of the aortic regurgitant jet reflects the pressure difference between the aorta and the left ventricle during diastole. The continuous-wave Doppler signal is best measured from the apical windows. For eccentric jets, better signals may be obtained from the second right intercostal window. The denser the spectral envelope, the more severe is the regurgitation (Fig. 12). The rate of deceleration of the continuous-wave Doppler signal is both a function of the degree of regurgitation and the ventricular end-diastolic pressure (Fig. 13). As the degree of regurgitation increases, the aortic diastolic pressure decreases and the left ventricular end-diastolic pressure increases. This leads to a rapid drop-off in pressure (as well as velocity) across the valves—corresponding to the familiar clinical signs of a widened pulse pressure. A pressure half-time of less than 200 ms is consistent with severe aortic regurgitation. Moderate aortic regurgitation equates to a pressure half-time of 200–500 ms, whereas mild regurgitation is indicated by a pressure half-time exceeding 500 ms (Fig. 14). Overall, pressure half-times are more accurate measures of acuity of aortic regurgitation than volumetric measures of aortic regurgitation, as pressure-half time is influenced by chamber compliance in addition to chamber

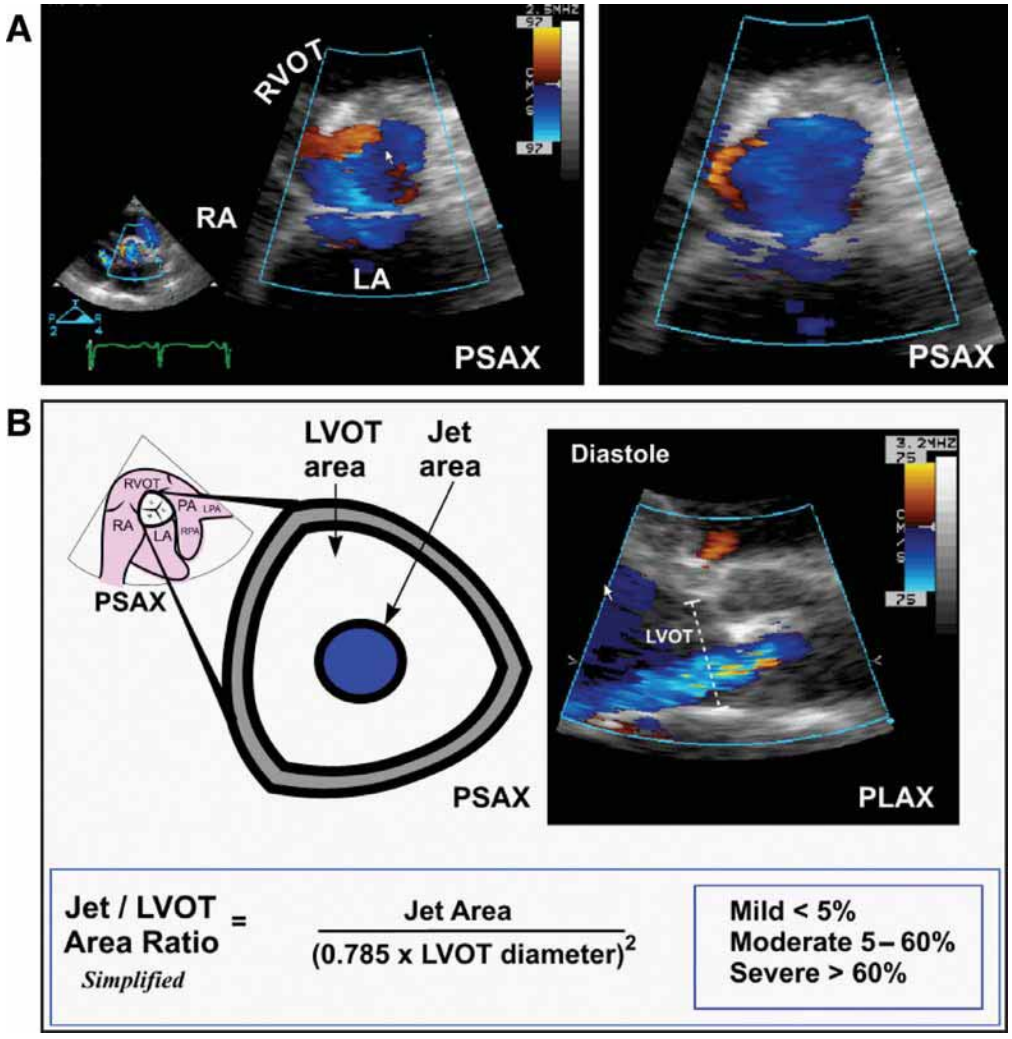

Fig. 10. (A) The color jet area measured from the parasternal short-axis view (PSAX) is proportional to the regurgitation orifice area. In these images, color from the aortic regurgitation (blue) is seen centrally, but varies throughout diastole owing to a changing orifice area (please *see* the companion CD for the video). **(B)** Semi-quantitative assessment of aortic regurgitation severity by color flow Doppler assessment (simplified jet/left ventricular outflow tract [LVOT] area ratio) using PSAX.

pressures. Accurate measurement of pressure half-time is also dependent on obtaining a well-visualized signal from the regurgitant jet. Patients with small volumes of regurgitation or poor windows may have incomplete spectra making measurement of this measurement difficult.

Calculation of regurgitant volume and regurgitant fraction provides a better quantization of the severity of valve insufficiency (Fig. 15). The regurgitant volume is equal to flow out the aortic valve (aortic stroke volume) minus flow through the mitral valve (mitral stroke volume). Calculation of regurgitant volume requires measurement of the left ventricular outflow tract and mitral annular diameters, as well as velocity time integrals (VTI) of flow through the left ventricular outflow tract and the mitral annulus. Aortic flow is equal to pi (π) multiplied by the square of the radius of the left ventricular outflow multiplied by the VTI of aortic flow. Mitral flow is calculated as π multiplied by the square of the radius of the mitral annular diameter multiplied by the VTI of mitral flow. Mild aortic regurgitation is considered when the regurgitant fraction is less than 30 mL/beat, moderate–between 30 and 60 mL/beat, and severe regurgitation—in excess of 60 mL/beat.

The regurgitant fraction is equal to the regurgitant volume divided by the total stroke volume. The total stroke volume is equivalent to flow out the aortic valve

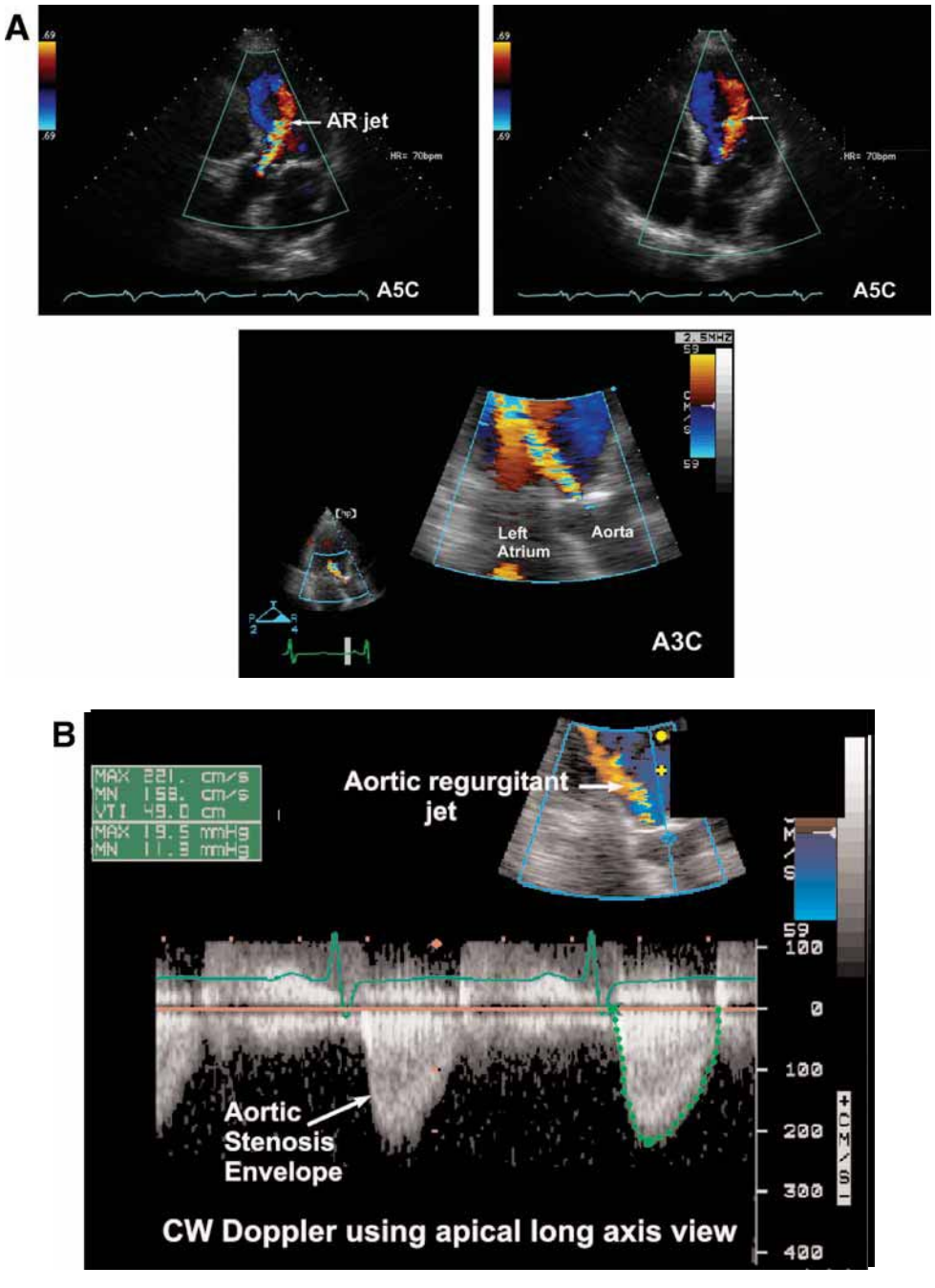

Fig. 11. (**A**) From the apical windows, the aortic regurgitation jet appears as a diastolic color flow disturbance in the left ventricular outflow tract. Jet length and jet area are influenced by the aortic driving pressure (aorta-to-left ventricular pressure) and are therefore less reliable indicators of disease severity. Measuring jet width from the apical projections is possible, but generally less reliable than parasternal measurements. (**B**) Continuous-wave (CW) Doppler assessment of flow across the aortic valve in a patient with aortic regurgitation. Many patients have mixed aortic valve disease. Increased transvalvular systolic velocities may represent stenosis. (Please *see* companion DVD for corresponding video.)

as previously defined. Regurgitant fractions of less than 30% are consistent with mild regurgitation, 30–50% with moderate regurgitation, and more than 50% with severe regurgitation.

The regurgitant orifice area may be calculated as the regurgitant volume multiplied by the VTI of the continuous-wave Doppler jet (Fig. 16). This parameter represents the average size of the defect in the aortic valve during

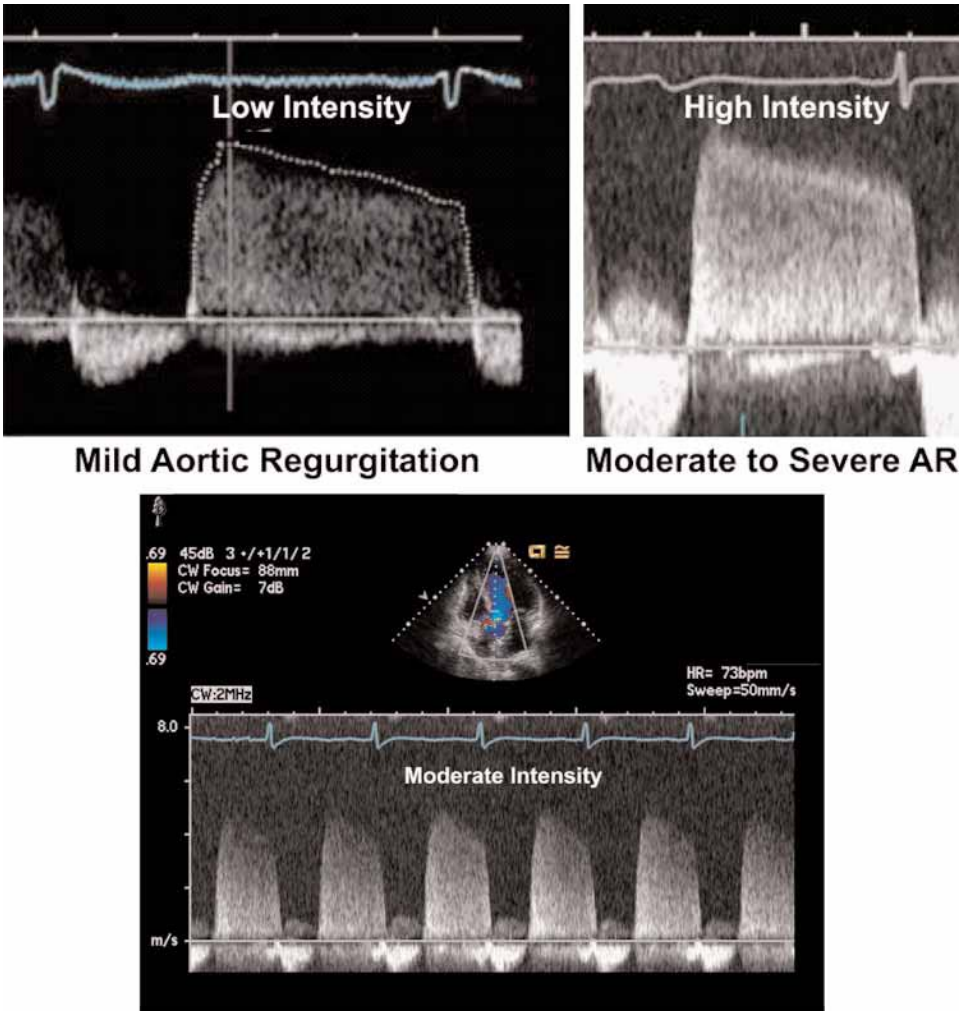

Fig. 12. Signal intensities in aortic regurgitation severity.

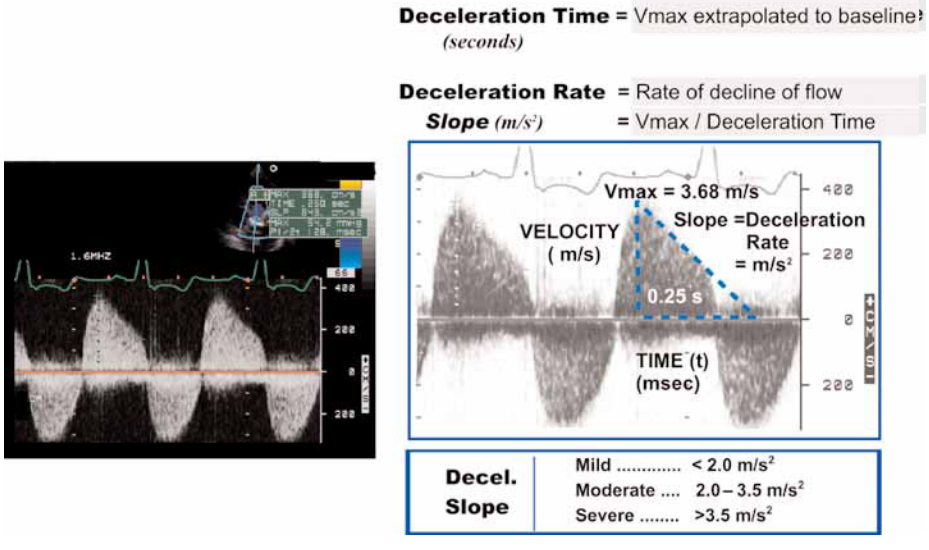

Fig. 13. Deceleration rate. The rate of deceleration of the continuous-wave Doppler signal reflects both the degree of regurgitation and the ventricular end-diastolic pressure.

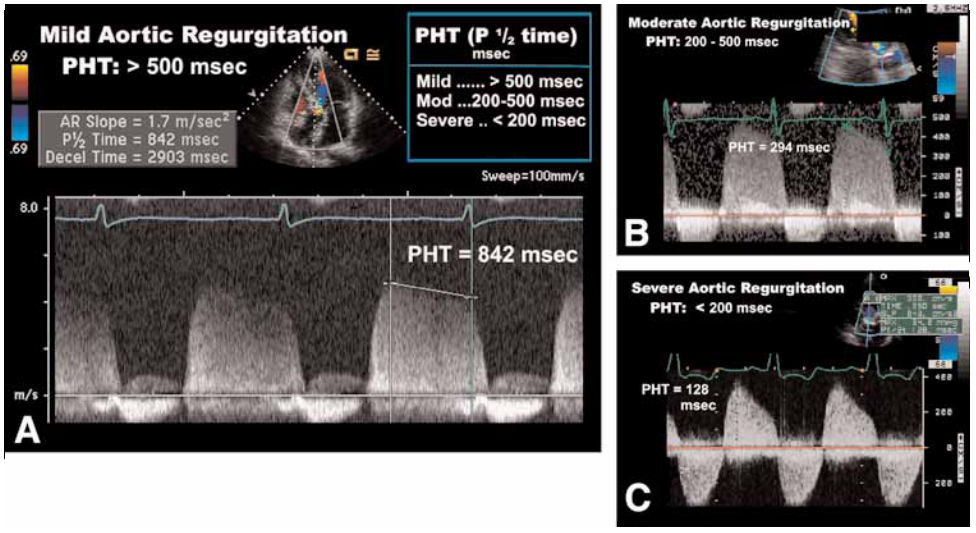

Fig. 14. Pressure half times (PHT or P 1/2 t). The pressure half time is the time it takes for peak pressure (mmHg) to drop to half its initial value. As the degree of regurgitation increases, the aortic diastolic pressure decreases and the left ventricular end-diastolic pressure increases. This leads to a rapid drop-off in pressure (as well as velocity) across the aortic valve. The more severe the aortic regurgitation, the greater the slope and the shorter the PHT.

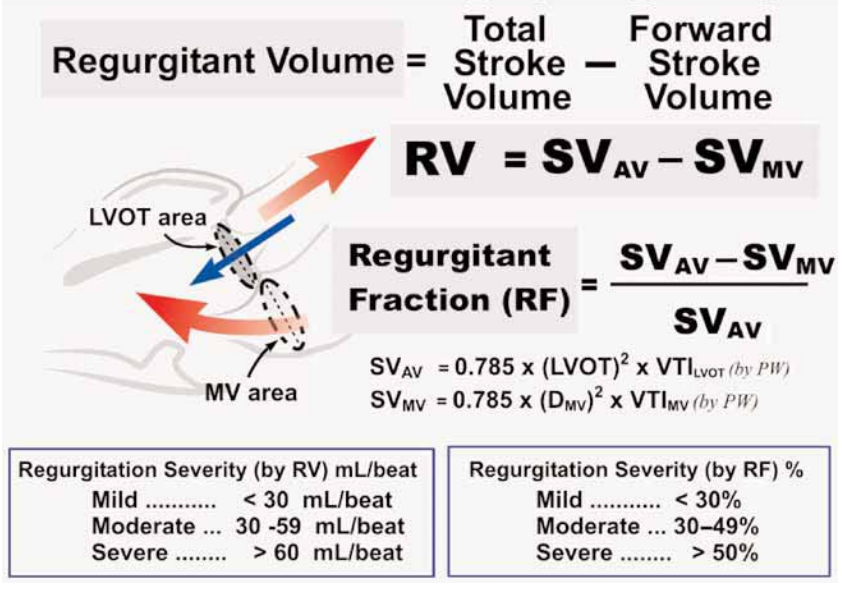

Fig. 15. Aortic regurgitant volume and fraction.

diastole and is proportional to regurgitant severity. Grading of aortic regurgitation severity using the regurgitant orifice area is as follows: mild, less than 0.10 cm^2; moderate, between 0.10 and 0.30 cm^2; and severe, more than 0.30 cm^2.

Calculation of the regurgitant volume, fraction, and orifice area is dependent on careful measurement of several variables. Errors in any one of these variables will lead to further errors in the calculations. Experienced laboratories should be able to perform these measurements and calculations accurately with careful attention to detail.

Aortic regurgitation can lead to diastolic flow reversal in the aorta (Fig. 17). With milder degrees of regurgitation, there is brief reversal of flow early in diastole. As the degree of regurgitation increases, flow reversal

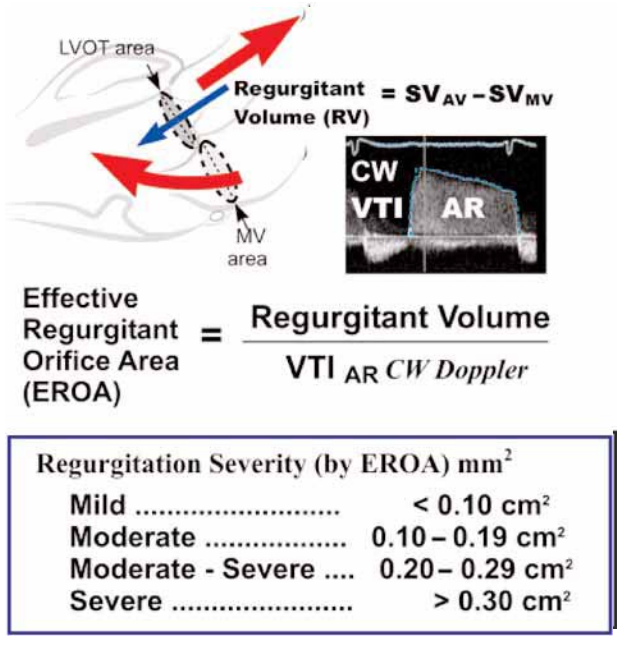

Fig. 16. The regurgitant orifice area or EROA represents the average size of the defect in the aortic valve during diastole and is proportional to regurgitant severity. The regurgitant volume across the aortic valve may be calculated as the difference between the LVOT volume and the transmitral volume, assuming there is no significant mitral regurgitation (*see* Fig. 15).

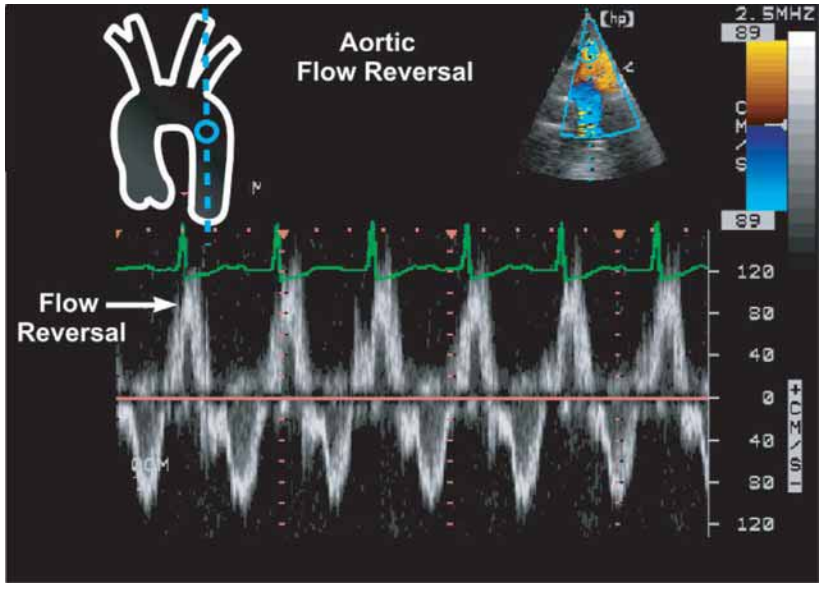

Fig. 17. Aortic flow reversal. Diastolic flow reversal can be seen in significant aortic regurgitation by Doppler interrogation of flow in the aortic arch and descending thoracic aorta. In this pulsed wave Doppler envelope, the regurgitant flow velocities almost equal those of systolic forward flow—a feature indicative of severe aortic regurgitation.

becomes sustained throughout diastole at velocities exceeding 20 cm/s. Criteria for flow reversal have been established in the distal aortic arch. Significant sustained reversal in the abdominal aorta is also a sensitive sign of severe aortic regurgitation.

Individuals with severe aortic regurgitation may exhibit altered mitral flow patterns. Because aortic regurgitation results in elevated diastolic left ventricular pressures and mitral inflow ceases early in diastole, this can lead to shortened mitral deceleration times. For this reason, the

Table 2
Assessment of Aortic Regurgitation Severity by Doppler Echocardiography: A Summary or Semi-Quantitative Methods

Classification of aortic regurgitation severity				
	Aortic regurgitation			
Variable	*Mild*	*Mild-moderate*	*Moderate-severe*	*Severe*
Jet/LVOT width	<25%	25–44%	45–64%	≥65%
Vena contracta width (mm)	<3	3–5.9	3–5.9	≥6
Regurgitant volume (mL/beat)	<30	30–44	45–59	≥60
Regurgitant fraction	<30%	30–39%	40–49%	≥50%
Effective regurgitant orifice area (mm^2)	<10	10–19	20–29	≥30
Pressure half time (P 1/2 t) (ms)	>500	350–500	200–350	<200
Deceleration rate (slope) (m/s^2)	<2	2–3	2–3.5	≥3.5

LVOT, left ventricular outflow tract.

Table 3A
Echocardiographic Findings of Aortic Regurgitation and Relationship to Disease Severity

Parameters	*Best TTE view*	*Literature evidence for grading with selected references*
Two-dimensional/M-mode		
LA dilatation	PLAX, A4C, A5C, A3C	
Premature MV closure	PLAX/PSAX	
AMVL fluttering or reverse doming	PLAX/PSAX M-mode	
Increased E-point septal separation (between AMVL and septum)	PLAX M-mode	
LV dilatation/function	A4C, A5C, A3C	Sensitive for chronicity
Aortic annular dilatation	PLAX, PSAX	
Diastolic AV opening/sagging	PLAX/PSAX M-mode, A5C, A3C	Simple, if present, AI is usually severe
Flow propagation velocity	PLAX	Onbasili 2002
Aortic root dilatation	A3C, R-PLAX, suprasternal	

A4C, apical four-chamber; A3C, apical three-chamber; A5C, apical five-chamber; AI, aortic regurgitation; AMVL, anterior mitral valve leaflet; LA, left atrium; MV, mitral valve; PLAX, parasternal long-axis; PSAX, parasternal short-axis; TTE, transthoracic echocardiography.

Table 3B
Echocardiographic Findings of Aortic Regurgitation and Relationship to Disease Severity

Parameters	*Best TTE view*	*Literature evidence for grading with selected references*
Color flow imaging		
Semi-quantitative		
LV filling/dilation/jet direction	PLAX, A5C, A3C, A4C	
RJA	PSAX	c/w angiographic severity (Perry 1987, Spain 1989, Enrique-Sarano 1993)

(Continued)

Table 3B *(Continued)*

Parameters	*Best TTE view*	*Literature evidence for grading with selected references*
Jet length	A5C, A3C	Poor (Grayburn 1986)
Jet width	PLAX	Poor c/w angiography (Perry 1987, Cape 1991)
Jet width/LVOT height	PLAX	Comparable with angiography (Perry 1987, Tribouilloy 1992)
Jet density	PLAX, PSAX	
Descending/abdominal Ao diastolic flow reversal by color	R-PLAX, supra-sternal, sub-costal	
Quantitative		
AV area (planimetry)	PSAX	Ozkan 2002
Vena contracta	PLAX, A3C, A5C, PSAX	Better than jet width and area in parasternal projections (Tribouilloy 2000), parasternal short-axis doesn't underestimate multiple/ irregular jets (Taylor 1990)
Proximal isovelocity surface area	PLAX, A3C, A5C, R-PLAX	Accurate quantitation (Recusani 1991, Utsunomiya 1991, Vandervoort 1993, Giesler 1993, Chen 1993, Tribouilloy 1998)

Table 3C
Echocardiographic Findings of Aortic Regurgitation and Relationship to Disease Severity

Parameters	*Best TTE view*	*Literature evidence for grading with selected references*
CW Doppler		
Retrograde CW jet density	A3C, A5C	Poor discernment between moderate and severe AI, good for distinguishing trace or mild AI from more severe disease
CW jet velocity	A3C, A5C	Jenni 1989
PHT of retrograde CW jet (diastolic jet deceleration)	A3C, A5C	Affected by LVEDP (Teague 1986, Masuyama 1986, Padial 1997) and AI chronicity (Griffin 1991)
Descending/abdominal aortic diastolic flow reversal, reverse VTI, reverse:forward VTI's	R-PLAX, supra-sternal, sub-costal	Severity proportional to increased duration and velocity of reversal (Boughner 1975) (Touche 1985) (Tribouilloy 1991)
Rate of LV isovolumic pressure rise and fall from AI regurgitant velocity	A3C, A5C, R-PLAX	Pai 1998
PW Doppler		
PW antegrade, VTI	A3C, A5C	Rokey 1986, Enriquez-Sarano 1993
Mitral inflow DT of E velocity	A4C, A3C, A5C	
Descending/abdominal aortic diastolic flow reversal, reverse VTI, reverse:forward VTI's	R-PLAX, supra-sternal, l sub-costa	Reimold 1996, also as per CW Doppler measurement

A4C, apical four-chamber; A3C, apical three-chamber; A5C, apical five-chamber; AI, aortic regurgitation; CW, continuous wave; DT, deceleration time; LV, left ventricle; PLAX, parasternal long-axis; PSAX, parasternal short-axis; R-PLAX, right parasternal; VTI, velocity time integral.

Table 3D
Echocardiographic Findings of Aortic Regurgitation and Relationship to Disease Severity

Parameters	*Best TTE view*	*Literature evidence for grading with selected references*
Calculations		
Jet width: LVOT width	PLAX, PSAX	Willems 1997
Jet CSA:LVOT CSA	PLAX, PSAX	Willems 1997
Regurgitant volume and fraction	PLAX and A3C, A5C	Ascah 1985 (AV+MV), Kitabatake 1985 (AV+PV), Rokey 1986 (AV+MV)
EROA	PLAX and A3C, A5C	Enriquez-Sarano 1993, 1994
Jet Momentum	PLAX and A3C, A5C	Not widely used, Cape 1989

MV, mitral valve; PLAX, parasternal long-axis; PSAX, parasternal short-axis; AV, aortic valve; A5C, apical five-chamber view; A3C, apical three-chamber view; A4C, apical four-chamber view; LVOT, left ventricular outflow tract; TTE, transthoracic echocardiography; CSA, cross-sectional area; EROA, effective regurgitant orifice area.

assessment of mitral valve area in a patient with mitral stenosis can be overestimated in patients with aortic insufficiency.

Common semi-quantitative methods using Doppler chocardiography for grading aortic regurgitant severity are shown in Table 2. A summary of various echocardiographic parameters used to assess aortic regurgitation are listed in Table 3A–D.

SUGGESTED READING

Ascah KJ, Stewart WJ, Jiang L, et al. A Doppler-two-dimensional echocardiographic method for quantitation of mitral regurgitation. Circulation 1985;72:377–383.

Boughner DR. Assessment of aortic insufficiency by transcutaneous Doppler ultrasound. Circulation 1975;52:874–879.

Cape EG, Skoufis EG, Weyman AE, Yoganathan AP, Levine RA. A new method for noninvasive quantification of valvular regurgitation based on conservation of momentum. In vitro validation. Circulation 1989;79:1343–1353.

Cape EG, Yoganathan AP, Weyman AE, Levine RA. Adjacent solid boundaries alter the size of regurgitant jets of Doppler color flow maps. J Am Coll Cardiol 1991;17:1094–1102.

Chen C, Koschyk D, Brockhoff C, et al. Noninvasive estimation of regurgitant flow rate and volume in patients with mitral regurgitation by Doppler color mapping of accelerating flow field. J Am Coll Cardiol 1993;21:374–383.

Enriquez-Sarano M, Bailey KR, Seward JB, Tajik AJ, Krohn MJ, Mays JM. Quantitative Doppler assessment of valvular regurgitation. Circulation 1993;87:841–848.

Enriquez-Sarano M, Seward JB, Bailey KR, Tajik AF. Effective regurgitant orifice area: a noninvasive Doppler development of an old hemodynamic concept. J Am Coll Cardiol 1994;23:443–451.

Giesler M, Grossmann G, Schmidt A, et al. Color Doppler echocardiographic determination of mitral regurgitant flow from the proximal velocity profile of the flow convergence region. Am J Cardiol 1993;71:217–224.

Grayburn PA, Smith MD, Handshoe R, Friedman BJ, DeMaria AN. Detection of aortic insufficiency by standard echocardiography, pulsed Doppler echocardiography, and auscultation: a comparison of accuracies. Ann Intern Med 1986;104:599–605.

Griffin BP, Flachskampf FA, Siu S, Weyman AE, Thomas JD. The effects of regurgitant orifice size, chamber compliance, and systemic vascular resistance on aortic regurgitant velocity slope and pressure half-time. Am Heart J 1991;122:1049–1056.

Jenni R, Ritter M, Eberli F, Grimm J, Krayenbuehl HP. Quantification of mitral regurgitation with amplitude-weighted mean velocity from continuous wave Doppler spectra. Circulation 1989;79:1294–1299.

Kitabatake A, Ito H, Inoue M, et al. A new approach to noninvasive evaluation of aortic regurgitant fraction by two-dimensional Doppler echocardiography. Circulation 1985;72:523–529.

Masuyama T, Kodama K, Kitabatake A, et al. Noninvasive evaluation of aortic regurgitation by continuous wave Doppler echocardiography. Circulation 1986;73:460–466.

Onbasili OA, Tekten T, Ceyhan C, Ercan E, Mutlu B. A new echocardiographic method for the assessment of the severity of aortic regurgitation: color M-mode flow propagation velocity. J Am Soc Echo 2002;15:1453–1460.

Özkan M, Özdemir N, Kaymaz C, Kirma C, Deligönül U. Measurement of aortic valve anatomic regurgitant area using transesophageal echocardiography: implications for the quantitation of aortic regurgitation. J Am Soc Echo 2002;2:1170–1174.

Padial LR, Oliver A, Vivaldi M, et al. Doppler echocardiographic assessment of progression of aortic regurgitation. Am J Cardiol 1997;80:306–314.

Pai RG, Stoletniy LN. Rates of left ventricular isovolumic pressure rise and fall from the aortic regurgitation velocity signal: description of the method and validation in human beings. J Am Soc Echo 1998;11:631–637.

Perry GJ, Helmcke F, Nanda NC, Byard C, Soto B. Evaluation of aortic insufficiency by Doppler color flow mapping. J Am Coll Cardiol 1987;9:952–959.

Recusani F, Bargiggia GS, Yoganathan AP, et al. A new method for quantification of regurgitant flow rate using color Doppler flow imaging of the flow convergence region proximal to

a discrete orifice. An in vitro study. Circulation 1991;83: 594–604.

Reimold SC, Maier SE, Aggarwal K, et al. Aortic flow velocity patterns in chronic aortic regurgitation: implications for Doppler echocardiography. J Am Soc Echo 1996;9:675–683.

Rokey R, Sterling LL, Zoghbi WA, et al. Determination of regurgitant fraction in isolated mitral or aortic regurgitation by pulsed Doppler two-dimensional echocardiography. J Am Coll Cardiol 1986;7:1273–1278.

Spain M, Smith M, Grayburn PA, et al. Quantitative assessment of mitral regurgitation by Doppler color flow imaging: angiographic and hemodynamic correlations. J Am Coll Cardiol 1989;13:585–590.

Taylor AL, Eichhorn EJ, Brickner ME, Eberhart RC, Grayburn PA. Aortic valve morphology: an important in vitro determinant of proximal regurgitant jet width by Doppler color flow mapping. J Am Coll Cardiol 1990;16:405–412.

Teague SM, Heinsimer JA, Anderson JL, et al. Quantification of aortic regurgitation utilizing continuous wave Doppler ultrasound. J Am Coll Cardiol 1986;8:592–599.

Touche T, Prasquier R, Nitenberg A, de Zuttere D, Gourgon R. Assessment and follow-up of patients with aortic regurgitation by an updated Doppler echocardiographic measurement of the regurgitant fraction in the aortic arch. Circulation 1985;72:819–824.

Tribouilloy C, Avinee P, Shen WF, Rey JL, Slama M, Lesbre JP. nd Diastolic flow velocity just beneath the aortic isthmus assessed by pulsed Doppler echocardiography: a new predictor of the aortic regurgitant fraction. Br Heart J 1991;65:37–40.

Tribouilloy C, Shen WF, Quere JP, et al. Assessment of severity of mitral regurgitation by measuring regurgitant jet width at its origin with transesophageal Doppler color flow imaging. Circulation 1992;85:1248–1253.

Tribouilloy CM, Enriquez-Sarano M, Bailey KR, Seward JB, Tajik AJ. Assessment of severity of aortic regurgitation using the width of the vena contracta: a clinical color Doppler imaging study. Circulation 2000;102:558–564.

Tribouilloy CM, Enriquez-Sarano M, Fett SL, Bailey KR, Seward JB, Tajik AJ. Application of the proximal flow convergence method to calculate the effective regurgitant orifice area in aortic regurgitation. J Am Coll Cardiol 1998;32: 1032–1039.

Utsunomiya T, Ogawa T, Tang HA, et al. Doppler color flow mapping of the proximal isovelocity surface area: a new method for measuring volume flow rate across a narrowed orifice. J Am Soc Echocardiogr 1991;4:338–348.

Vandervoort PM, Thoreau DH, Rivera JM, Levine RA, Weyman AE, Thomas JD. Automated flow rate calculations based on digital analysis of flow convergence proximal to regurgitant orifices. J Am Coll Cardiol 1993;22:535–541.

Willems TP, Steyerberg EW, van Herwerden LA, et al. Reproducibility of color Doppler flow quantification of aortic regurgitation Journal of the American Society of Echocardiography. J Am Soc Echo 1997;10:899–903.

13 Mitral Stenosis

Robert J. Ostfeld, MD, MS

CONTENTS

CASE PRESENTATION

A 55-yr-old woman presents with a chief complaint of dyspnea on exertion. Her past medical history is significant for gastro-esophageal reflux disease and rheumatic fever. She has no known history of valvular disease. Her only medication use is an occasional antacid. She has not seen a physician in approx 10 yr. Over the past year, she began to experience gradually increasing dyspnea on exertion, and she now becomes short of breath after walking up 7–10 steps. She denies shortness of breath at rest. She also denies chest pain, chest pressure, palpitations, claudication, and syncope. She reports the new onset of two-pillow orthopnea that began 6–8 mo ago. And, she denies paroxsysmal nocturnal dyspnea. Physical exam reveals a well-developed, well-nourished female in no acute distress. Her blood pressure is 116/75 mmHg. Her heart rate is 82 bpm and regular. Her complexion appears ruddy. Carotid pulses are normal and there are no carotid bruits. Her jugular venous pressure measures 9 cm of water with no V-waves. Cardiac exam reveals a diminished first heart sound with a normal second heart sound. An opening snap approx 70 ms after the second heart sound is audible along with a grade 2/4 diastolic rumble with presystolic augmentation at the apex. Her point of maximal impulse is 0.5 cm lateral to the midclavicular line. Her lungs are clear to auscultation and the rest of her exam is within normal limits. Her electrocardiogram demonstrates normal sinus rhythm with an enlarged left atrium (LA). There are no Q-waves or ST changes. Her chest X-ray has clear lung fields. No double density sign is appreciated.

Mitral stenosis was suspected and an echocardiogram (ECHO) was requested and confirmed the presence of mitral stenosis (Fig. 1; please *see* companion DVD for corresponding video). Her valve area was calculated as 0.9 cm^2 by pressure half-time ($P_{1/2}$ or PHT) and 0.95 cm^2 by planimetry. The mean gradient across her mitral valve (MV) was 10 mmHg. Her LA was enlarged and her pulmonary artery systolic pressure (PASP) was elevated. She had mild (1+) regurgitation. Her MV score was eight. Transesophageal ECHO revealed no LA or LA appendage thrombus and she underwent uncomplicated percutaneous mitral valvuloplasty (PMV). She was asymptomatic on her follow-up visit.

INTRODUCTION

Mitral stenosis occurs when thickened MV leaflets and chordae restrict blood flow from the LA to the left ventricle (LV) during diastole. Ultimately, hemodynamic changes within the LA may lead to an increased

From: *Contemporary Cardiology: Essential Echocardiography: A Practical Handbook With DVD*
Edited by: S. D. Solomon © Humana Press, Totowa, NJ

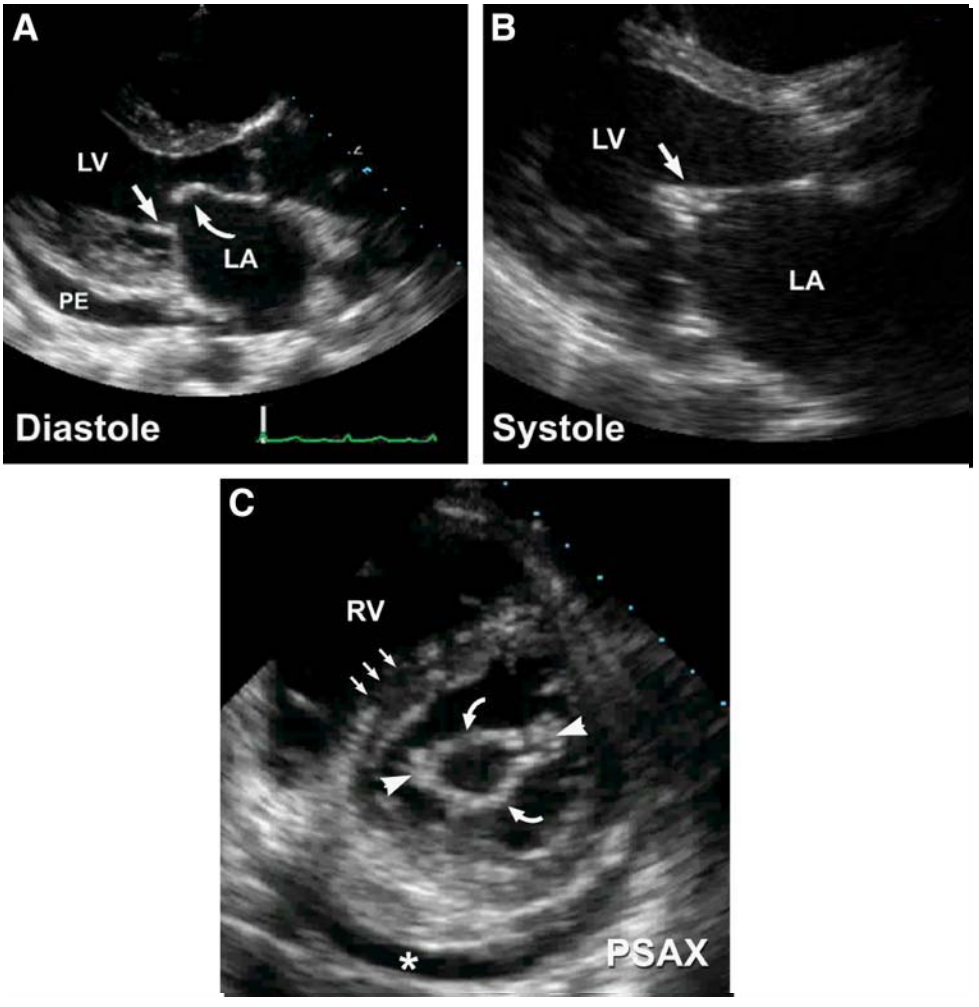

Fig. 1. Echocardiographic features of rheumatic mitral stenosis. **(A)** Diastolic doming of the thickened anterior mitral valve leaflet ("hockey stick" appearance, curved arrow) is indicative of restricted anterior leaflet motion. Note the thickened subvalvular structures, including the chordae (arrow). Note also the posterior pericardial effusion (PE). **(B)** A systolic frame showing thickened mitral valve leaflets. **(C)** Commissural fusion (arrowheads) and bilateral leaflet thickening (curved arrows) resulting in "fish mouth" appearance of the mitral valve leaflets during diastole (parasternal short-axis [PSAX] views). Dilated right ventricle (RV) with flattened interventricular "D-shaped" septum throughout the cardiac cycle (triple arrows) is indicative of right ventricular pressure and volume overload. A small posterior pericardial effusion (*) is present. (Please *see* companion DVD for corresponding video.)

pulmonary capillary wedge pressure, an elevated pulmonary vascular resistance and right heart chamber dysfunction. The patient's shortness of breath was likely related to an increase in her pulmonary capillary wedge pressure during exertion. An increased heart rate with activity gave her LA less time to empty and pressure would then "back-up," possibly leading to pulmonary edema and shortness of breath. Rheumatic heart disease, although now far less common in the industrialized world, remains the most common cause of mitral stenosis (Table 1).

Echocardiography has an important role in the diagnosis and assessment of mitral stenosis (Table 2).

Key aspects of the echocardiographic evaluation of mitral stenosis include the assessment of:

1. Valve and supporting structure morphology.
2. LA morphology, pulmonary arterial pressure, and right heart function.
3. Pressure gradients across the MV.
4. MV area.

VALVE AND SUPPORTING STRUCTURE MORPHOLOGY

The morphology of the MV and its supporting structures provides diagnostic and therapeutic insights.

Table 1
Etiology of Mitral Stenosis

Acquired
• Rheumatic heart disease (vast majority of cases)
• Calcific mitral stenosis
• Hypereosinophilia
• Cafergot toxicity
• SLE, malignant sarcoid, mucopolysaccharidosis
• Active infective endocarditis, Whipple's disease
Congenital
• Parachute mitral valve complex
• Shone's anomaly: parachute mitral valve with supra-valvar mitral ring, sub-valvular aortic stenosis and coarctation of the aorta

Table 2
Echocardiographic Features of Rheumatic Mitral Stenosis

• Thickened/calcified mitral leaflets
• Diastolic doming with "hockey stick" deformity of anterior leaflet
• Parallel anterior motion of both mitral valve leaflets
• Thickened/calcified subvalvular apparatus
• Decreased EF slope on M-mode
• Left atrial dilatation
• Atrial fibrillation with loss of A-waves on spectral Doppler
• Spontaneous echocontrast and left atrial thrombus (best observed by transesophageal echocardiography)
• Mitral regurgitation
• Signs of increased right-sided pressure and volume overload secondary to pulmonary hypertension—sequelae of chronic significant mitral stenosis—e.g., right ventricle hypertrophy, tricuspid regurgitation, dilatation of right heart chambers

For example, fused leaflet tips and a "hockey stick" appearance of the anterior mitral leaflet implicate rheumatic fever (Figs. 1A and 2; please *see* companion DVD for corresponding video for Fig. 1), whereas marked mitral annular echodensities implicate mitral annular calcification.

Therapeutically, when mechanical treatment options are being considered, the morphology of the MV and its supporting structures influences the choice between MV replacement and PMV. Grossly, a thin mobile noncalcified MV without subvalvular thickening is amenable to PMV. Whereas, a thickened, nonmobile, calcified MV with subvalvular thickening is not a good PMV candidate. The MV score, which is derived from the morphology of the MV and its supporting structures, helps to more objectively guide this decision by predicting the outcome after PMV (Table 3). Overall, as the MV score increases, the potential for procedural success decreases. A valve score of less than eight is associated with a good outcome. However, the decision regarding which mechanical option to utilize is a highly individualized one (Fig. 3C–E; please *see* companion DVD for corresponding video).

Two factors whose presence weigh strongly against (if not preclude) proceeding with PMV are co-existent LA thrombus and moderate to severe mitral regurgitation. First, a LA thrombus may become dislodged and embolize during PMV. Consequently, anticoagulation before PMV or surgical correction *in lieu* of PMV may be considered. Frequently, a transesophageal ECHO is necessary to evaluate fully for the presence of LA and LA appendage thrombus, as the standard transthoracic ECHO lacks sensitivity for this finding (Fig. 3A,B; please *see* companion DVD for corresponding video). Secondly, mitral regurgitation may be increased by PMV. Hence, coexistent moderate to severe mitral regurgitation may render PMV undesirable.

LA MORPHOLOGY, PULMONARY ARTERIAL PRESSURE, AND RIGHT HEART FUNCTION

Mitral stenosis may impact "proximal" cardiac chambers and blood vessels, such as the LA, pulmonary vasculature and right ventricle (Fig. 3; please *see* companion DVD for corresponding video). For example, elevated LA pressure may lead to LA enlargement, as noted in the above patient's ECG. This enlargement may predispose the patient to atrial fibrillation and its pathological sequelae, such as thromboembolism.

Elevated LA pressure is also transmitted back to the pulmonary vasculature. Although initially reversible, these elevated pressures may become largely fixed as the pulmonary vasculature remodels, and permanent pulmonary hypertension can ensue.

PASP is estimated by summing (1) the pressure gradient between the pulmonary artery and right atrium, as derived from the modified Bernoulli equation, $4V^2$, where V is the tricuspid regurgitant jet velocity (assuming no pulmonary stenosis) and (2) the estimated right atrial pressure (RAP). In other words, $PASP = 4V^2 + RAP$. With

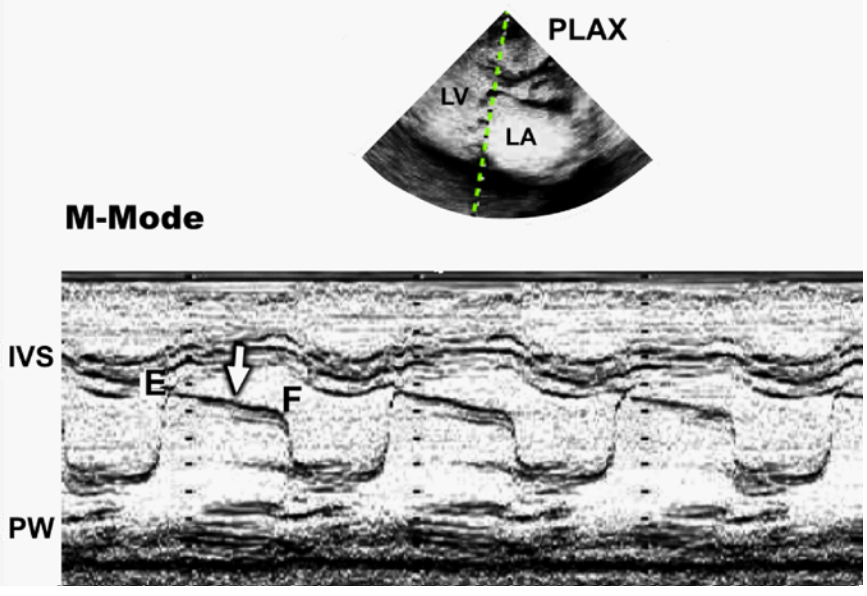

Fig. 2. M-mode echocardiogram in mitral stenosis. The M-mode echocardiogram in rheumatic mitral stenosis typically shows prolongation of the ejection fraction slope (arrow). Note the "hockey stick" appearance of the anterior leaflet of the mitral valve in the parasternal long axis (PLAX) still-frame image.

Table 3
Mitral Valve Scoring Criteria for Predicting Outcome of Balloon Valvuloplasty

Grade	*Leaflet mobility*	*Subvalvular thickening*	*Valve leaflet thickening*	*Calcification*
1	Highly mobile valve; restriction affects leaflet tips only	Minimal thickening immediately below mitral leaflets	Near normal leaflet thickness (4–5 mm)	Single echo-bright area
2	Middle and basal portions of leaflet show normal mobility	Thickened chordae ≤ one-third chordal length	Normal midleaflets, but marked marginal thickening (5–8 mm)	Scattered area of echo-brightnesss, but confined to leaflet margins
3	Valve moves forward in diastole, but mainly from the base	Thickened chordae ≤ two-thirds chordal length	Entire leaflet thickened (5–8 mm)	Scattered area of echo-brightnesss, now involving leaflet midportions
4	No or minimal forward movements of leaflets in diastole	Thickened chordae involving entire length extending to papillary muscles	Gross thickening of entire leaflet (>8–10 mm)	Extensive echo-brightness throughout most of leaflets

Scoring system derived from description of the above four parameters with a score of 1 for near-normal and 4 for the extensive involvement. An echocardiographic score of 8 or less, predicts better outcome of percutaneous mitral valvuloplasty. (Table modified from Wilkins GT, Weyman AE, Abascal VM, Block PC, Palacios IF. Percutaneous balloon dilation of the mitral valve: An analysis of echocardiographic variables related to outcome and the mechanism of dilation. Br Heart J 1988;60:299–308.)

long-standing pulmonary hypertension, changes in the right ventricle may occur (e.g., hypertrophy, enlargement, decrement in function, and shifting of the interventricular septum toward the LV as right-sided pressures approach or exceed left-sided pressures) (Fig. 4; *see also* Chapter 18).

Pressure Gradients

As the MV orifice becomes increasingly stenotic, higher-pressure gradients are necessary to "move" blood from the LA to the LV. These gradients can be measured and used as a means to estimate the hemodynamic significance of mitral stenosis.

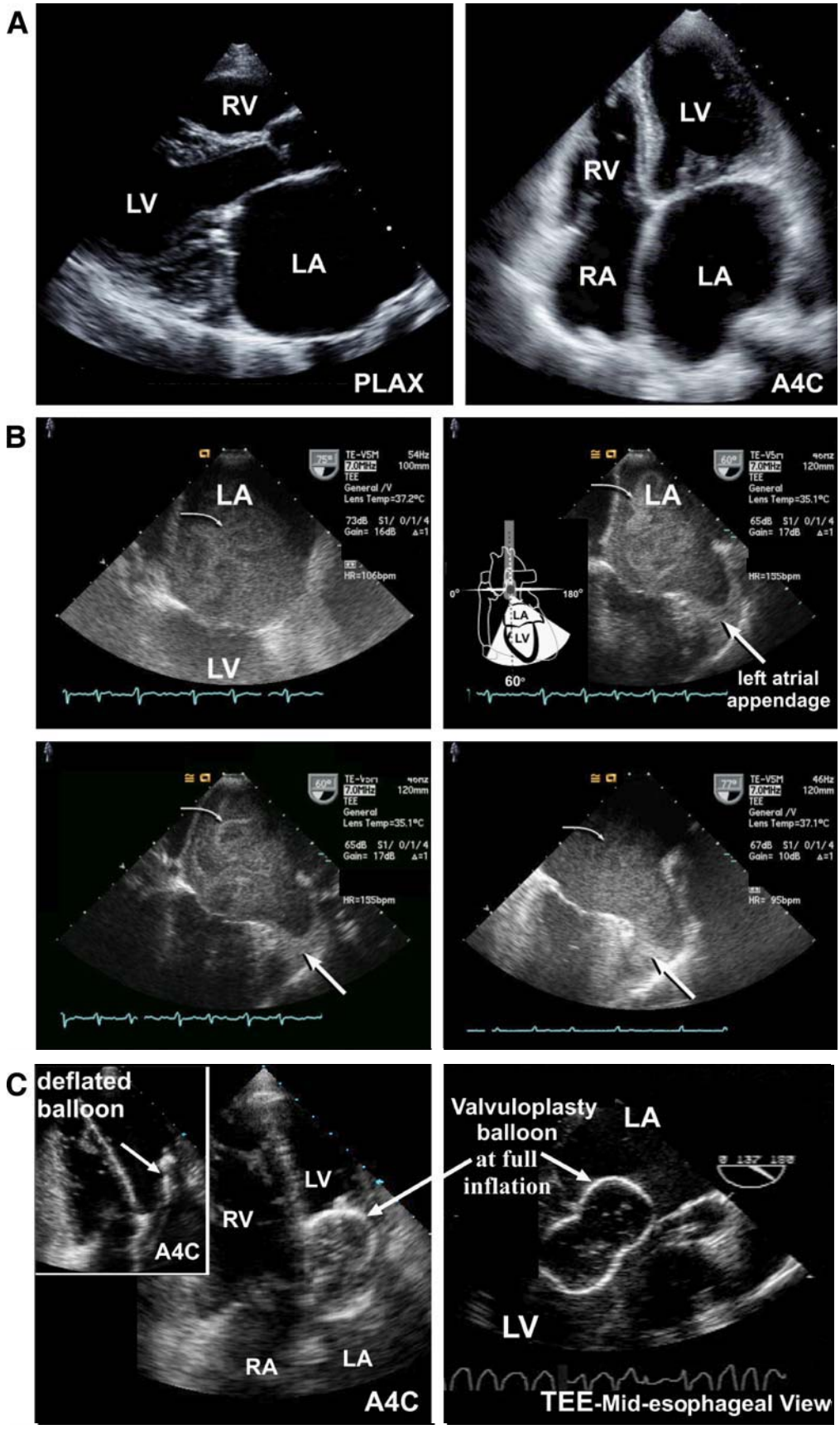

Fig. 3. (*See* legend, next page)

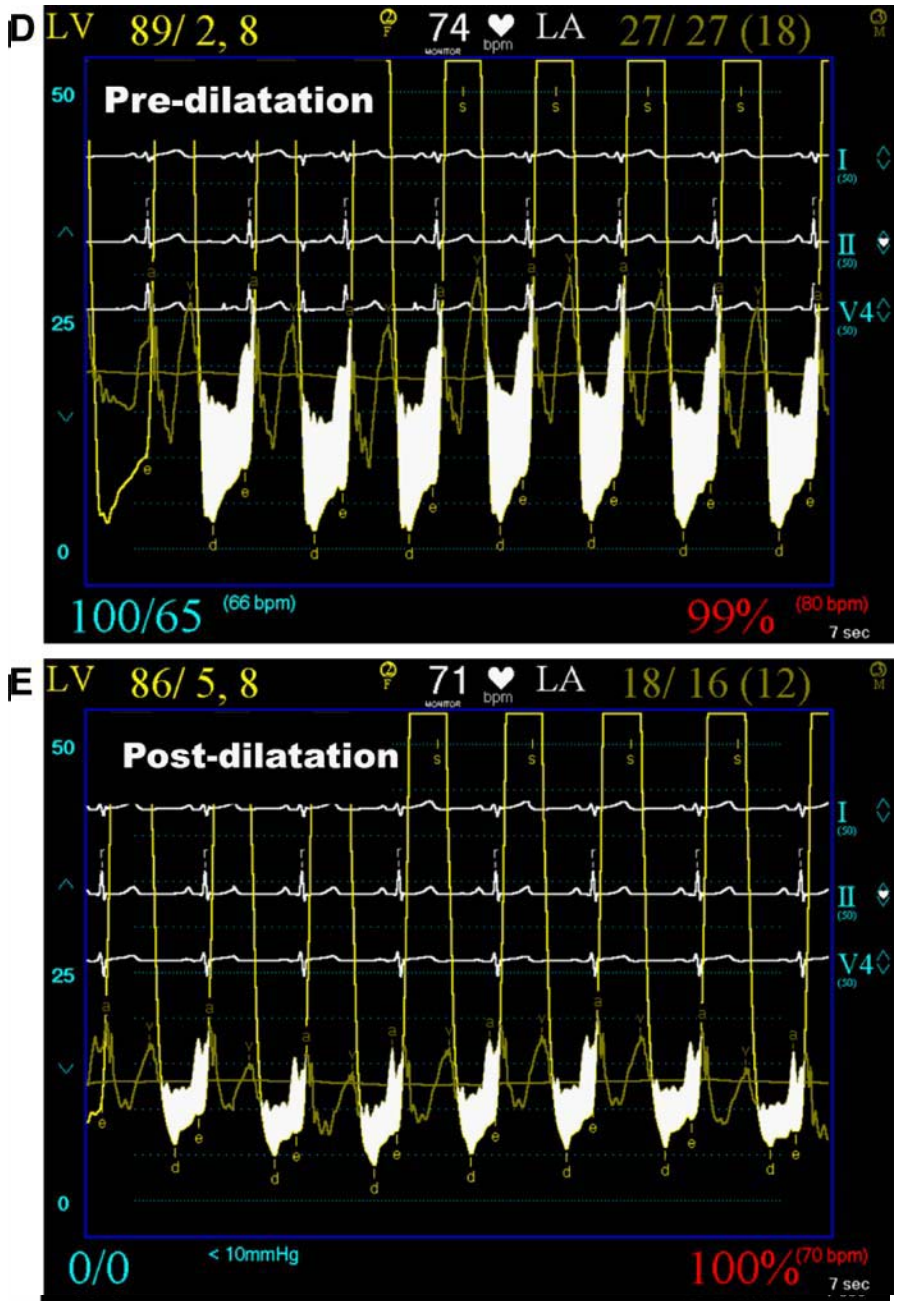

Fig. 3. **(A)** Echocardiographic features of rheumatic mitral stenosis in a 42-yr-old Haitian female with atrial fibrillation and multiple embolic episodes. Chronically increased left atrial pressures in mitral stenosis leads to left atrial dilatation (Fig. 3A) and atrial fibrillation. These predispose to thrombus formation. Note the left atrial enlargement in parasternal long axis (PLAX) and apical four-chamber (A4C) views. The right atrium was also enlarged. **(B)** Spontaneous echocontrast (curved arrows) was not visible on transthoracic examination in the patient **(A)**, but was visualized as "swirling smoke" within the left atrium and left atrial appendage on transesophageal echocardiography **(B)**. Note the clot in the left atrial appendage (straight arrow). **(C)** Transthoracic and Transesophageal views during percutaneous mitral balloon valvuloplasty for mitral stenosis. **(D,E)** Simultaneous left ventricular and pulmonary capillary wedge pressure tracings pre- and postpercutaneous balloon valvuloplasy in a patient with mitral stenosis. The pressure gradient across the stenotic valve decreased immediately post mitral balloon valvuloplasty. (Please *see* companion DVD for corresponding video.)

Pressure gradients across the MV are determined by placing the continuous-wave (CW) Doppler-probe across the MV orifice. The Doppler interrogation should be performed parallel to the direction of blood flow, in order to avoid underestimating the gradient.

The measurements that are reported most frequently are the peak and mean gradients (Figs. 5 and 6). Of the

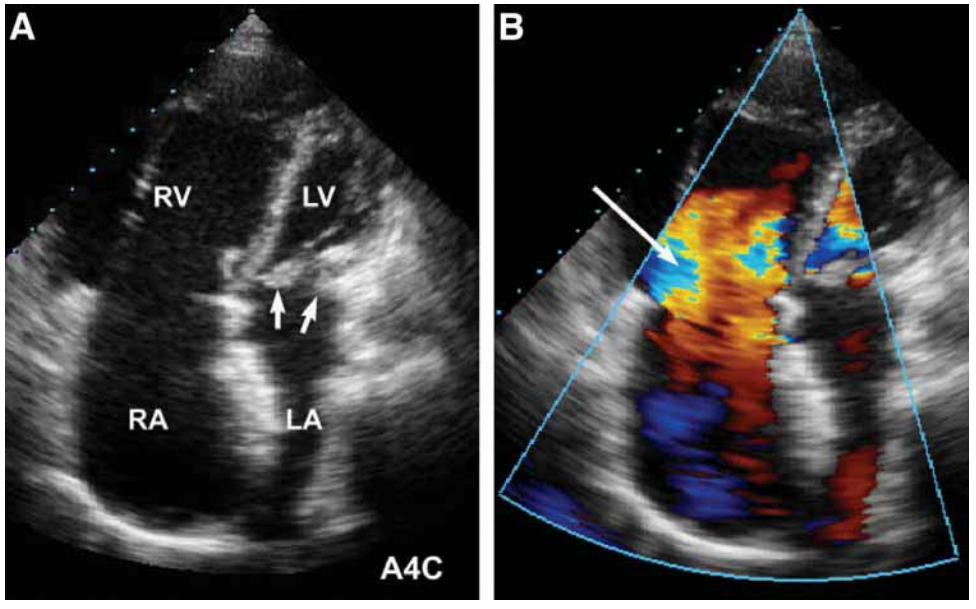

Fig. 4. Apical four-chamber views of severe longstanding mitral stenosis in a 44-yr-old Vietnamese female. **(A)** Note marked thickening and calcification of mitral valve leaflets (arrows) and subvalvular apparatus accompanied by marked distortion in left heart chamber architecture. **(B)** This patient had severe pulmonary hypertension with grossly dilated right heart chambers and severe tricuspid regurgitation (arrow).

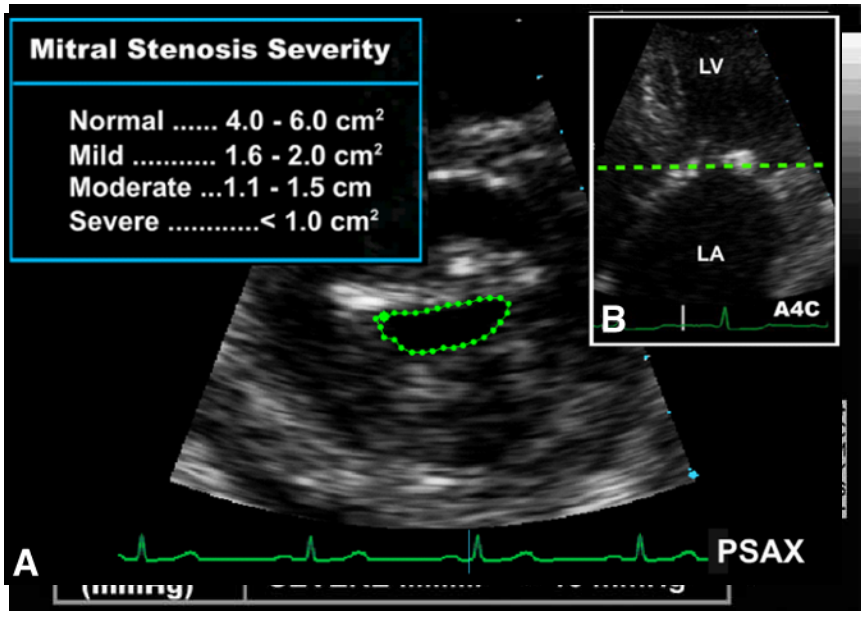

Fig. 5. Measurement of pressure gradients in mitral stenosis. Tracing the continuous-wave Doppler velocity time integral (VTI) envelope across stenotic mitral valve gives maximum and mean pressure gradients.

two gradients, the mean gradient is most frequently used clinically. The peak gradient can be calculated from the modified Bernoulli equation: $P = 4V^2$, where V is the peak velocity as measured by CW Doppler. The mean gradient is calculated from the time velocity integral across the MV as measured by CW Doppler. Although there are no absolute pressure gradient cutoffs demarcating the severity of stenosis, some general categories for the mean gradient are as follows:

Mean gradient
0–5 mmHg (mild stenosis)
5–10 mmHg (moderate stenosis)
>10 mmHg (severe stenosis)

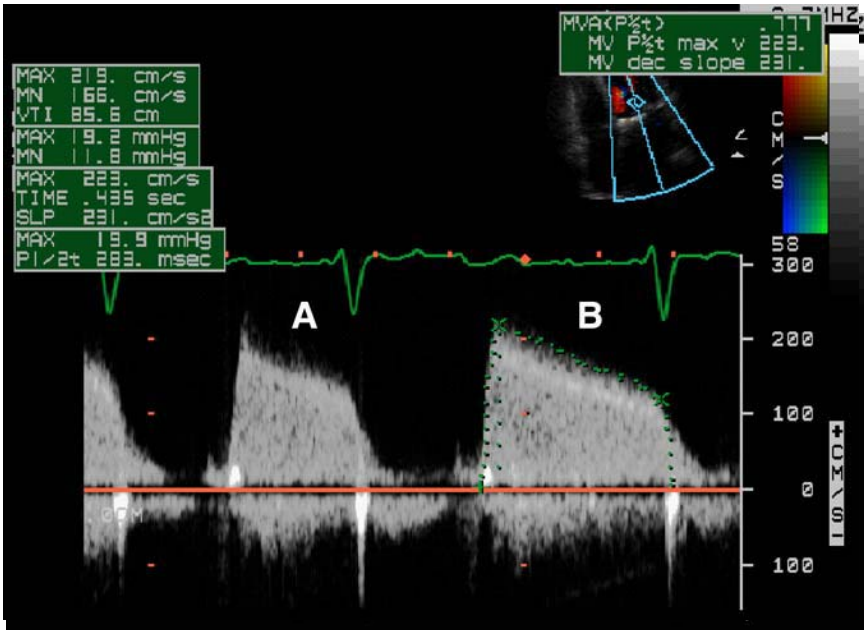

Fig. 6. Mean pressure gradient. Continuous-wave Doppler patterns in a patient with severe mitral stenosis. Atrial fibrillation is present and is reflected in marked variation in the tracings as shown in **A** and **B** (mean gradient approx 12 mmHg). In such patients, gradients should be averaged over 5–10 cardiac cycles. Mitral valve area calculated by the pressure half-time method (Figs. 8 and 9) was ~0.8 cm^2.

Table 4
Mean Pressure Gradient: Pitfalls

- Flow-rate dependent, e.g., affected by volume depletion or anemia
- Low cardiac output states and bradycardia may lead to low mean pressure gradient calculations in the presence of severe mitral stenosis
- Heart rate dependent, e.g., affected by exercise
- Atrial fibrillation: need to average over 5 to 10 cardiac cycles
- Doppler beam alignment dependent, especially with eccentric jets

A key caveat: pressure gradients are influenced by *both* the MV area, as previously discussed, *and* the amount of blood flow across the valve, as an increase in flow will yield a higher gradient for a given valve area. Therefore, using pressure gradients alone to estimate the severity of stenosis can be problematic. For example, it is possible to observe markedly elevated gradients with mild to moderate mitral stenosis in the setting of high flow (e.g., anemia) and to observe lower gradients with severe stenosis in the setting of low flow (although the latter example is more commonly an issue with aortic stenosis than with mitral stenosis) (Table 4).

Table 5
Mitral Valve Area: Quantification

- Two-dimensional planimetry
- Mean pressure gradient
- Pressure half-time
- Continuity equation
- Proximal isovelocity surface area

ASSESSMENT OF MITRAL VALVE AREA

There are a number of ways to determine the MV area (Table 5).

Planimetry

The orifice of the MV can be well visualized in the parasternal short-axis view. Consequently, direct measurement of the orifice area via planimetry is possible (Fig. 7). There is reasonable correlation between this echocardiographic technique and the mitral valve area determined at both the time of surgery and during cardiac catheterization. When assessing the MV in this way, it is necessary for the sonographer to slowly scan up and down in the plane of the MV in order to identify the smallest orifice. Otherwise, it is possible to overestimate the valve area. In addition, the imaging plane

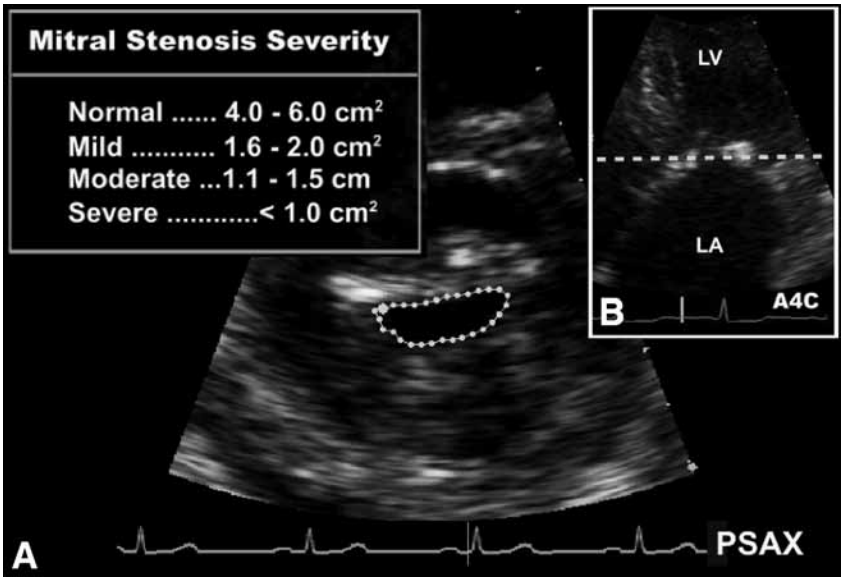

Fig. 7. Mitral valve area by two-dimensional planimetry.

should run parallel to the valve orifice, as off-axis views will likely lead to an overestimation of the true valve area (Table 6). Also, image acquisition should occur early in diastole, as the valve orifice is maximally dilated at that time.

Pressure Half-Time ($P_{1/2}$)

The $P_{1/2}$ is the time it takes for the pressure gradient across the MV to decrease by half (Fig. 8). The valve area is calculated using the equation, MVA = 220/$P_{1/2}$ where MVA = MV area and $P_{1/2}$ = pressure half-time (Figs. 9 and 10). This method correlates well with the invasive measurement of MVA. The concept behind the $P_{1/2}$ method is as follows: the LV fills when blood from the LA crosses the MV during diastole. As the MV orifice area decreases, blood flow from the LA to the LV becomes increasingly compromised, and the time required for blood to flow from LA to LV becomes longer. This decreasing valve area is reflected in the length of time required for the pressure gradient across the MV to fall during diastole. The smaller the valve orifice, the longer it takes for the pressure gradient to decrease.

In short, MV area is inversely related to the pressure half-time by the formula MVA = 220/$P_{1/2}$. It is important to remember that what is measured is the time it takes for the *pressure* to reach one-half of the original pressure. Pressure and velocity are related by the Bernoulli equation (pressure = 4 × velocity^2).

Table 6
Two-Dimensional Planimetry: Pitfalls

- Poor image quality
- Gross distortion of leaflet anatomy
- Improper tomographic plane
- Inadequate two-dimensional gain settings
- Heavy annular and leaflet calcification
- Postmitral commissurotomy

There are a number of important caveats (Table 7) to consider when assessing MV area by $P_{1/2}$:

1. Atrial fibrillation. Although the $P_{1/2}$ is largely independent of heart rate, if the heart rate for any given cycle is markedly elevated, a clear image of the pressure gradient fall may not be visible. Therefore, during atrial fibrillation it may be necessary to evaluate many beats (most labs assess at least 5 and often up to 10 beats).
2. Aortic regurgitation or other conditions that increase left ventricular end-diastolic pressure. Aortic regurgitation can shorten the time it takes for the LV to fill during diastole, as the LV is filled with blood from *both* the LA and the aorta. Therefore, the $P_{1/2}$ time may be "artificially" decreased leading to an overestimation of the MV area. This overestimation typically becomes clinically relevant in the setting of moderate to severe aortic regurgitation. In other

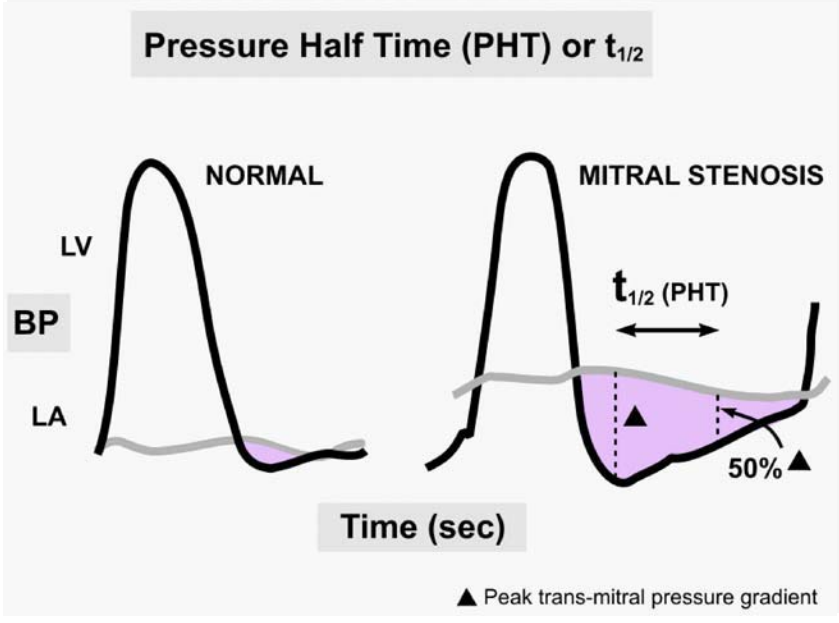

Fig. 8. PHT measures how quickly the peak pressure across the mitral valve drops by half. Does the peak transmitral gradient drop quickly or does it take a longer time? The longer the PHT, the worse the stenosis.

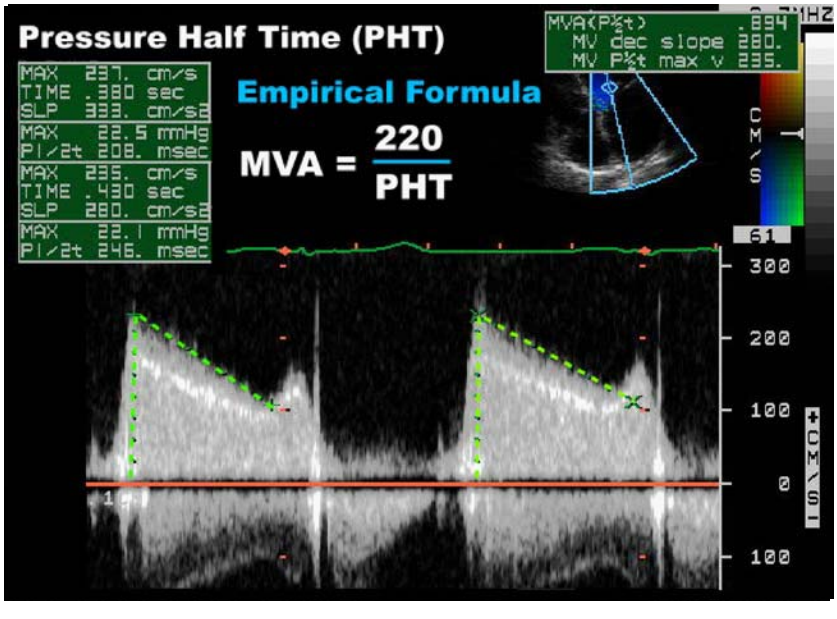

Fig. 9. The PHT is a reflection of the rate at which left atrial and ventricular pressures equilbrate during diastole. Mitral valve area is calculated as 220 divided by the PHT.

conditions in which left ventricular end-diastolic pressure is elevated, such as restrictive cardiomyopathy or ischemic heart disease, the rate of equilibration between LA and LV is increased, and the estimation of MV area by $P_{1/2}$ can also be falsely increased.

3. Post PMV. A key assumption for this equation is that the $P_{1/2}$ measurement is largely independent of LA and left ventricular compliance. After PMV, this assumption is not valid for approx 72 h as the chambers re-equilibrate. Therefore, during that time following mitral valvuloplasty, the $P_{1/2}$ method is not considered valid.

Continuity Equation

The MV orifice area can be determined by the continuity principle (Fig. 11). According to this principle,

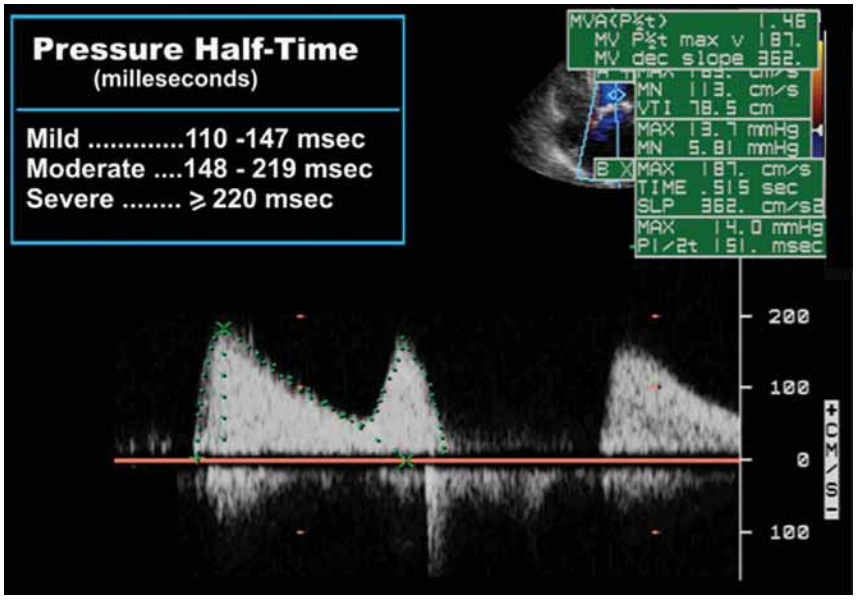

Fig. 10. Pressure half-time (PHT). Mitral stenosis can then be categorized as mild, moderate, or severe as shown. The PHT in this patient measured 187 ms—indicating moderate mitral stenosis.

Table 7
Pressure Half-Time Method: Pitfalls and Caveats

- Flow-rate dependent, e.g., affected by volume depletion or anemia
- Heart rate dependent, e.g., affected by exercise
- Atrial fibrillation: need to average over 5 to 10 cardiac cycles
- Doppler beam alignment dependent, especially with eccentric jets
- Measure $P_{1/2}$ from slope with longer duration whenever deceleration slopes differ
- $P_{1/2}$ can be prolonged (i.e., increased) in nonmitral stenotic states, e.g., diastolic dysfunction, but low E peak velocities may accompany the latter
- $P_{1/2}$ method is unreliable in patients with severe aortic regurgitation or immediately post-balloon valvuloplasty
- Atrial septal defects, immediate post-mitral valvotomy, and a noncompliant left atrium shorten $P_{1/2}$. This leads to overestimation of MVA
- Changes that prolong $P_{1/2}$, e.g., a chronically dilated and overcompliant left atrium leads to underestimation of MVA.

MVA, mitral valve area; $P_{1/2}$, pressure half-time.

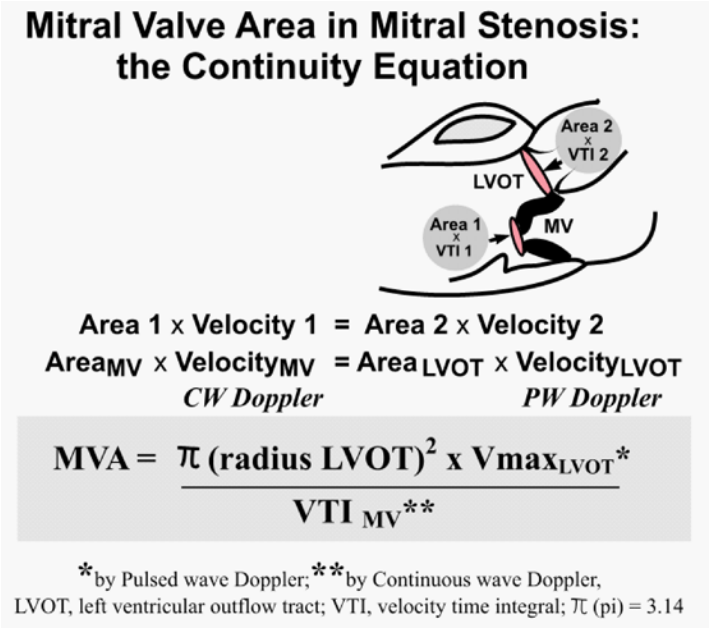

Fig. 11. Continuity equation in mitral stenosis.

flow at any point along a tube is constant (i.e., flow [Q] = $VTI_1 \cdot A_1 = VTI_2 \cdot A_2$, where VTI = velocity time integral at point$_x$ and A = area at point$_x$). Therefore, if we know the flow at another point in the "tube" (or heart), e.g., the left ventricular outflow track (LVOT), and we know the velocity time integral across the MV as measured by CW Doppler, we can solve for the MV area. Specifically, $Q = VTI_{LVOT} \cdot Area_{LVOT} = VTI_{MV} \cdot Area_{MV}$. Or, $Area_{MV} = A_{LVOT} \cdot VTI_{LVOT}/VTI_{MV}$. This method correlates well with the invasive assessment of MVA.

One key limitation of this method is that if there is regurgitation through the MV or the comparison point (e.g., aortic or pulmonic outflow tract), flow will not be the same at those two points (Table 8). Therefore, the estimation of the MV area may not be accurate.

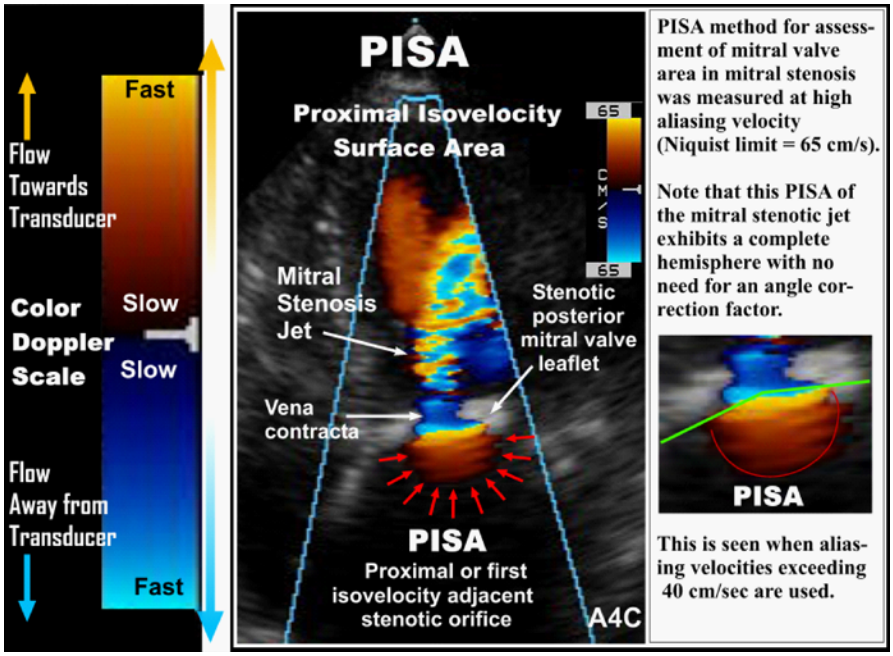

Fig. 12. Proximal isovelocity surface area (PISA) principle in mitral stenosis. Narrow sector scan of mitral stenotic jet using color flow Doppler in the apical four-chamber (A4C) view. The flow convergence zone exhibits a hemisphere of isovelocity (proximal isovelocity). The PISA principle stipulates that unobstructed flow convergence equates to concentric acceleration—the presence of concentric rings of flow acceleration that results when flow accelerates across the stenotic mitral valve. (Please *see* companion DVD for corresponding video.)

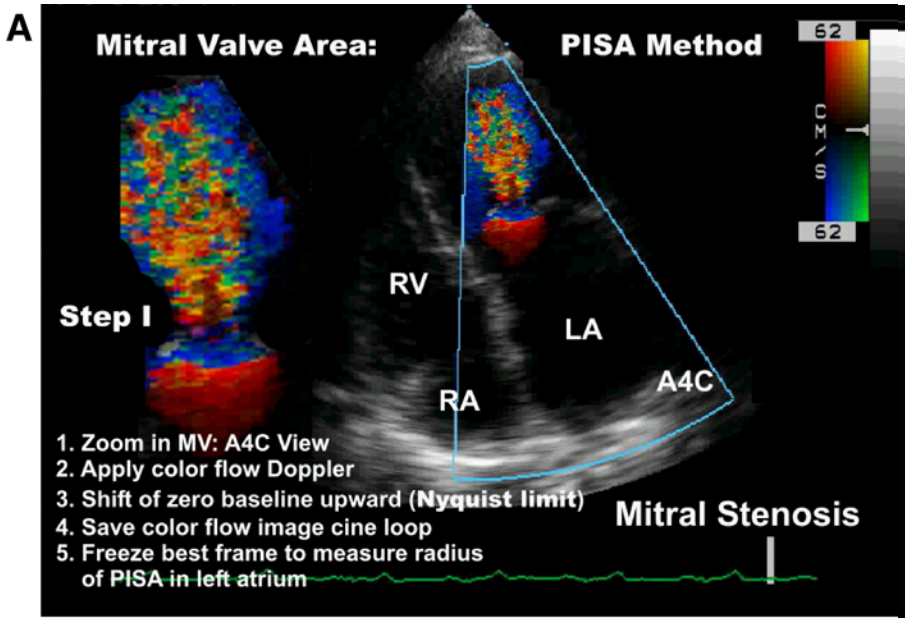

Fig. 13. Proximal isovelocity surface area (PISA) method in mitral stenosis: steps 1–5 *(Continued)*.

Proximal Isovelocity Surface Area

An extension of the continuity principle is to use the proximal isovelocity surface area to calculate the MVA. Here, the point of "comparison" is changed from the aortic or pulmonic outflow tracts, for example, to the point proximal to the MV in the LA where color Doppler flow aliases in the shape of a hemisphere (Figs. 12 and 13; please *see* companion DVD for corresponding video

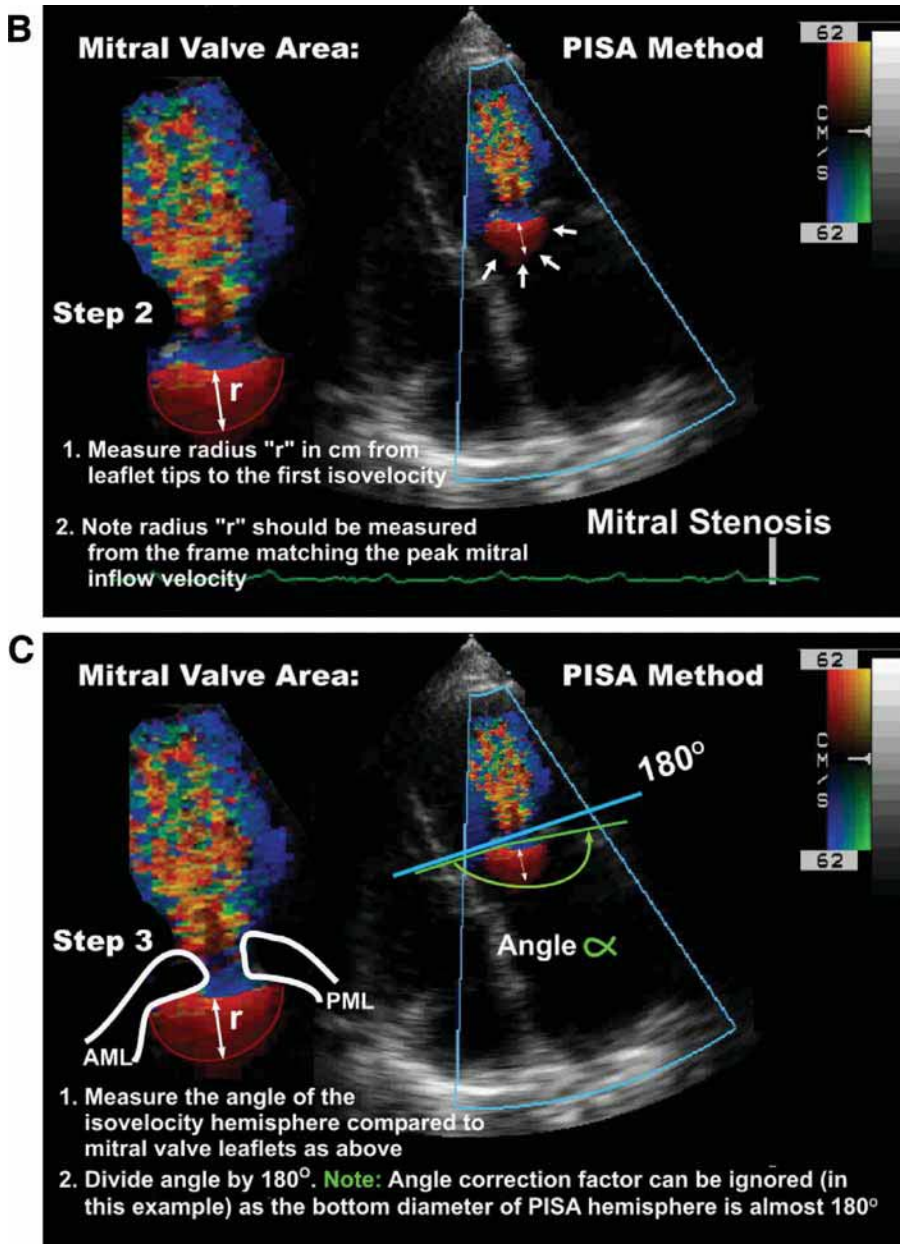

Fig. 13. *(Continued)*

Table 8
Continuity Equation in Mitral Stenosis: Pitfalls

- Atrial fibrillation: need to average over 5 to 10 cardiac cycles
- Doppler beam alignment dependent, especially with eccentric jets
- Lack of continuity of flow

for Fig. 12). The area at that point is calculated with the equation for the area of a hemisphere, $2\pi r^2$, where r is the distance from the point where the color Doppler flow aliases to the orifice of the MV. The velocity at the point where the color Doppler flow aliases is the nyquist limit on the color Doppler setting. Hence, we have the area and velocity at another point that we may use to solve for the MVA in the continuity equation. (MVA = $2\pi r^2 \cdot$ aliasing velocity/velocity$_{MV}$). (Note: an angle correction term may need to be added to this equation in order to account for the influence of the two MV leaflets on the area of the sphere [*see* Figs. 12 and 13; please *see* companion DVD for corresponding video for Fig. 12].)

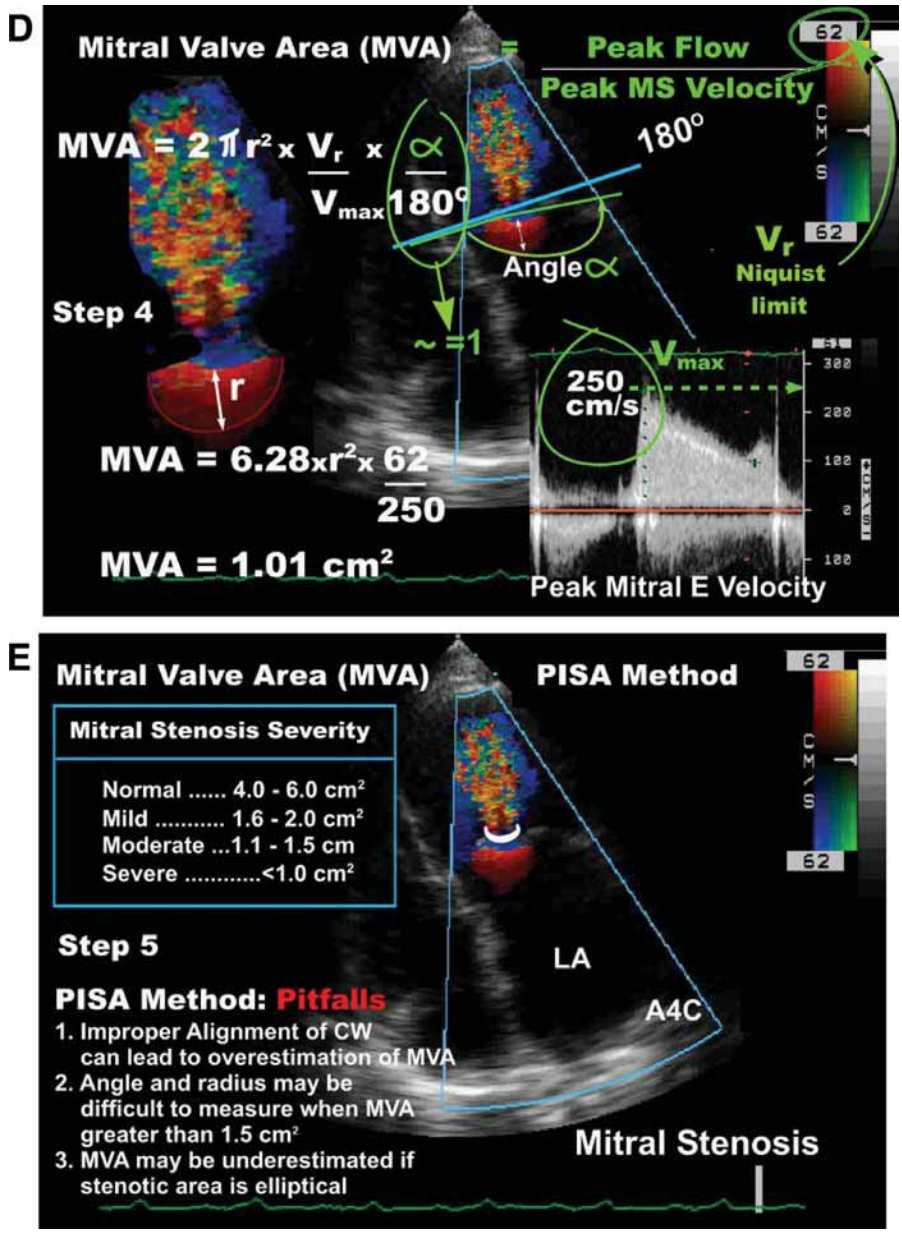

Fig. 13.

One benefit of this method is that, in theory, the measurement of MVA is not affected by coexistent mitral regurgitation as flow across the MV orifice and flow across the aliasing point in the LA will not be significantly different in the presence of mitral regurgitation. However, the proximal isovelocity surface area method is technically challenging and it is not commonly used in many laboratories when evaluating mitral stenosis.

CONCLUSION

In summary, the echocardiographic assessment of mitral stenosis provides insight into etiology, quantifies hemodynamics, grades severity, reveals "upstream" sequelae, and assists in choosing therapeutic options.

ACKNOWLEDGMENT

The author would like to thank the Massachusetts General Hospital echocardiography laboratory for their generous contribution of echocardiographic images for this chapter.

SUGGESTED READING

Braunwald E, Zipes DP, Libby P. Heart Disease. A Textbook of Cardiovascular Medicine. Philadelphia: WB Saunders, 2001.

Mohan JC, Pater AR, Passey R, et al. Is the mitral valve area flow-dependent in mitral stenosis? A dobuatmine stress echocardiography study. J Am Coll Cardiol 2002;40: 1809–1815.

Oh JK, Seward JB, Tajik AJ. The Echo Manual. Philadelphia: Lippincott Williams and Wilkins, 1999:103–132.

Otto CM. Textbook of Clinical Echocardiography. Philadelphia: WB Saunders, 2000:229–264.

Weyman AE. Principles and Practice of Echocardiography. Philadelphia: Lippincott Wilkind and Williams, 1994.

Wilkins GT, Weyman AE, Abascal VM, Block PC, Palacios IF. Percutaneous balloon dilation of the mitral valve: an analysis of echocardiographic variables related to outcome and the mechanism of dilation. Br Heart J 1988;60: 299–308.

14 Mitral Regurgitation

Jacqueline Suk Danik, MD, MPH and Bernard E. Bulwer, MD, MSc

Contents

INTRODUCTION

Mitral regurgitation (MR) is one of the most common acquired valvular heart diseases seen in the adult echocardiography practice. Its onset may be acute or chronic, and the etiology can stem from any process that disturbs the architecture of the mitral valve apparatus (Table 1; Figs. 1 and 2).

Echocardiography has several important roles in MR, including:

1. Evaluation of the etiology of MR.
2. Grading the severity of MR.
3. Assessment of its impact on overall cardiac function, especially left ventricular (LV) function.
4. Guidance for further management, including timing of surgical intervention.

Transthoracic echocardiography (TTE) is the modality of choice for evaluation and follow-up of MR and global cardiac function, but transesophageal echocardiography (TEE) plays an important role when differences exist between clinical assessment and TTE findings, or when mitral valve surgery is needed (Table 2).

ASSESSMENT OF MR ETIOLOGY AND MECHANISMS

The structure of the entire mitral valve apparatus which include the mitral leaflets, chordal attachments, annulus, papillary muscles, and the supporting ventricular walls affect overall function. Defining the etiology of MR is important as it can influence management and prognosis of such patients. Diseases that are primarily structural in origin can be managed differently from individuals with functional MR.

The cases that follow were chosen to highlight several common etiologies of MR. The most common causes of MR in North America include degenerative disease, ischemia, and functional MR.

CASE PRESENTATION 1: TRACE MITRAL REGURGITATION

A 26-yr-old woman was referred for TTE following clinical detection of a faint systolic murmur. She was completely asymptomatic and had no significant medical history (Fig. 2A).

From: *Contemporary Cardiology: Essential Echocardiography: A Practical Handbook With DVD*
Edited by: S. D. Solomon © Humana Press, Totowa, NJ

Table 1
Causes of MR

Mechanism	*Diagnosis*
Acute MR	
Structural	Ruptured chordae tendinae
	Ischemic papillary muscle dysfunction and/or rupture
Infectious	Bacterial endocarditis (both normal and prosthetic heart valves)
Chronic MR	
Degenerative/structural	Myxomatous degeneration of leaflets (mitral valve prolapse)
	Chordal rupture with flail leaflet
	Papillary muscle dysfunction and/or rupture with flail leaflet
	Paravalvular leak following prosthetic valve replacement
	Mitral annular calcification
	Collagen disorders, for example, Marfan syndrome and Ehlers Danlos syndrome
Ischemic and functional	Dilated cardiomyopathy with mitral annular dilatation and apical tethering
Infectious	Bacterial endocarditis (of both normal and prosthetic heart valves)
Inflammatory	Rheumatic heart disease
	Connective tissue disorders, for example, systemic lupus erythematosus, scleroderma

Table 2
Major Indications for Echocardiography in MR

- Diagnosis and evaluation of the etiology/mechanism of MR
- Asessment of hemodynamic severity, including impact on ventricular size, function, and hemodynamics
- Initial assessment and re-evaluation of asymptomatic and symptomatic patients with MR
- Assessment of effects of medical and surgical therapies in MR, including mitral valve repair or replacement
- TEE for pre-operative, intra-operative, and post-operative evaluation of patients with MR

The images show trace (trivial) MR. There is a centrally directed jet confined to an area just distal to the mitral leaflet closure line, seen in multiple windows. It is of short duration and low velocity and may simply represent volume displacement when the mitral leaflets close. This can be seen in up to 80% of normal adults increases in prevalence with age and has little pathological significance.

CASE PRESENTATION 2: MITRAL VALVE PROLAPSE

The second case is a 33-yr-old woman with a midsystolic click and an end-systolic murmur (Figs. 3–7; please *see* companion DVD for corresponding video for Figs. 3–6).

These images show classic mitral valve prolapse (MVP), one of the most common cardiac valvular abnormalities, which has been reported in 1–3% of North American populations. This particular example demonstrates prolapse of both anterior and posterior leaflets past the mitral annular plane. The leaflets are thickened (>5 mm) and there is concomitant severe regurgitation.

Classic MVP exists when there is exaggerated (>2 mm) superior displacement ("buckling" or "hammocking") of thickened mitral leaflets (>5 mm thick in diastole) beyond the plane of the mitral annulus during late systole. One of the most common reasons for MVP is fibromyxomatous degeneration of the mitral valve, which can lead to leaflet prolapse, chordal rupture, or partial flail of a segment of one or both leaflets. Strict echocardiographic features of MVP are shown in (Table 3). The parasternal long-axis and the apical long-axis views are the best views for the optimal assessment of MVP, and Figs. 4 and 5 (please *see* companion DVD for corresponding video) are classic examples of MVP. Of note, the normal saddle-shaped profile of the mitral valve leafleats may be exaggerated when viewed from the apical four-chamber window, resulting in overdiagnosis of MVP or "echocardiographic heart disease."

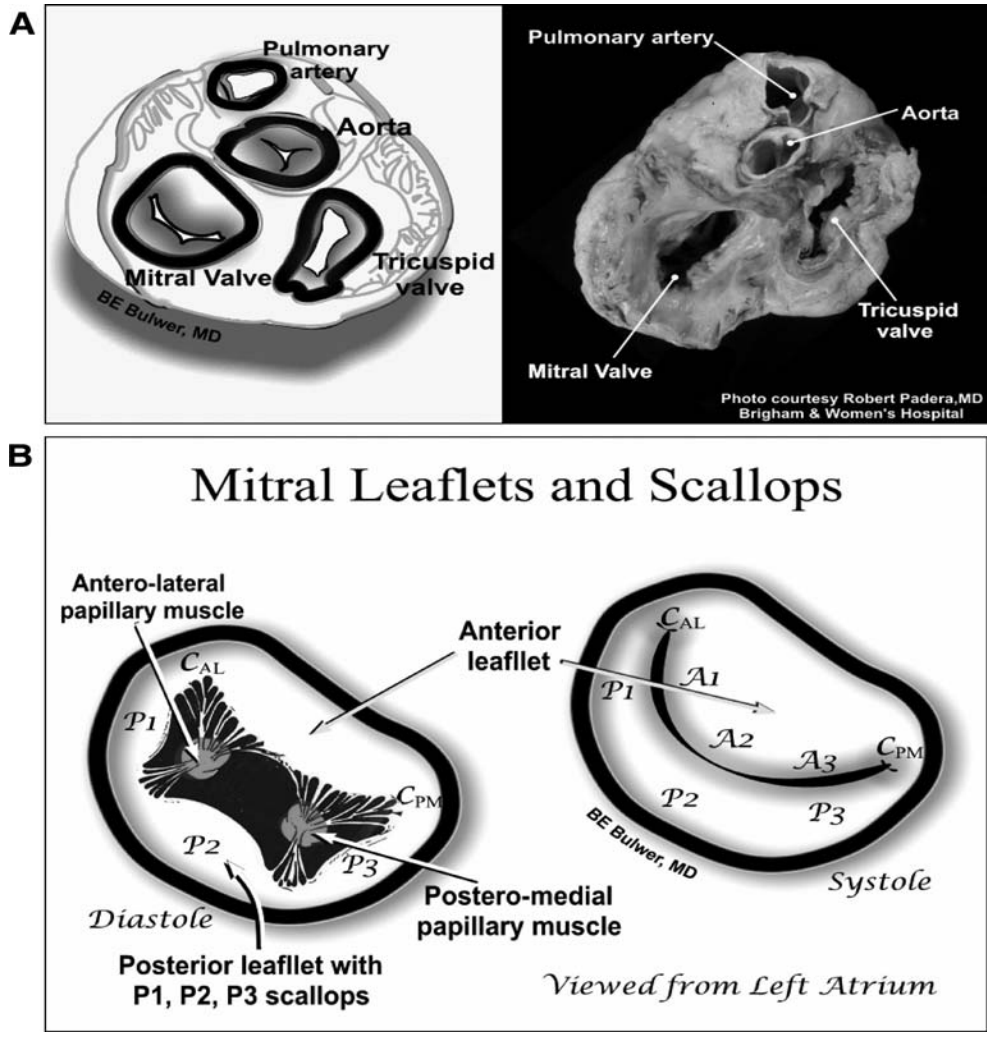

Fig. 1. (A) Mitral valve topography: base of heart view. **(B)** Anterior and posterior mitral valve leaflets and scallops.

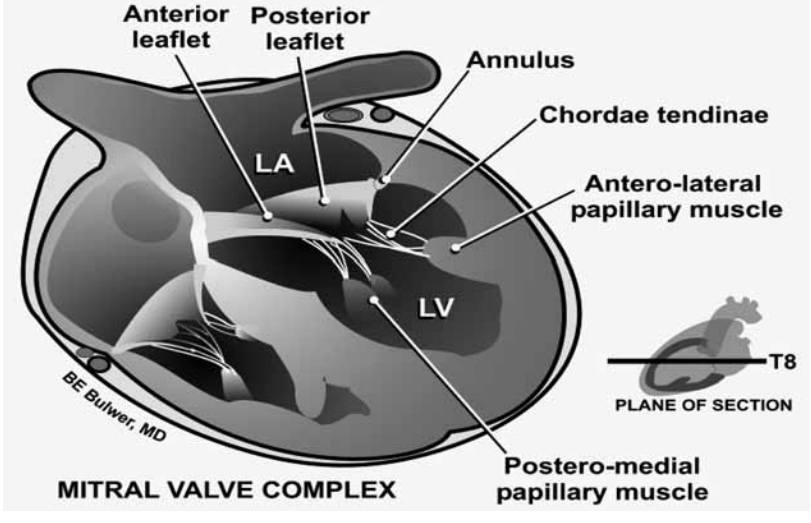

Fig. 2. Illustrations showing mitral valve leaflets, scallops (Carpentier nomenclature) and supporting structures. The mitral valve complex includes the mitral annulus, valve leaflets, chordae tendinae (primary, secondary, and tertiary), and their papillary muscle origins, as well as the supporting left ventricle, left atrium, and the aortic root.

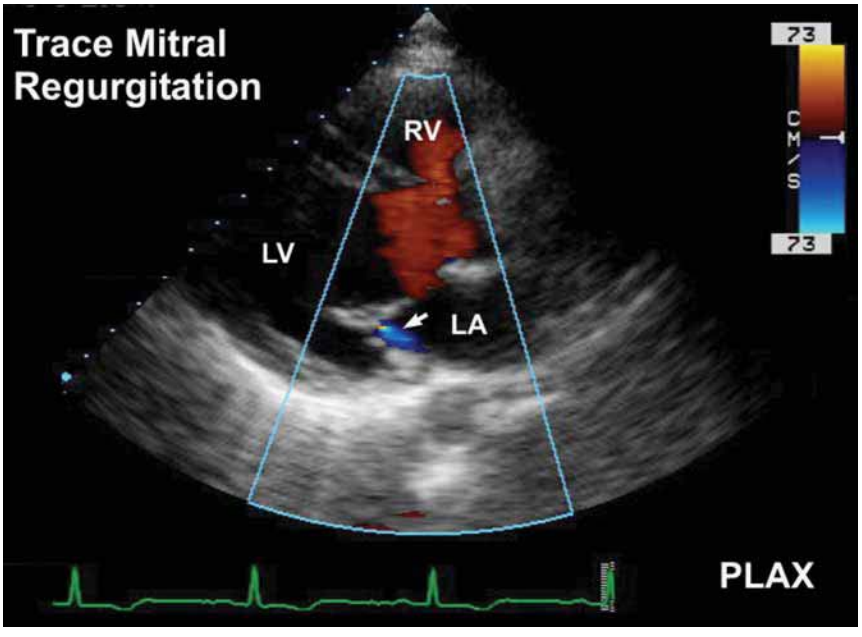

Fig. 3. Parasternal long-axis (PLAX) view showing trace mitral regurgitation (arrow). It is also termed "mitral regurgitation closing volume"—indicating mere volume displacement during leaflet closure. (Please *see* companion DVD for corresponding video.)

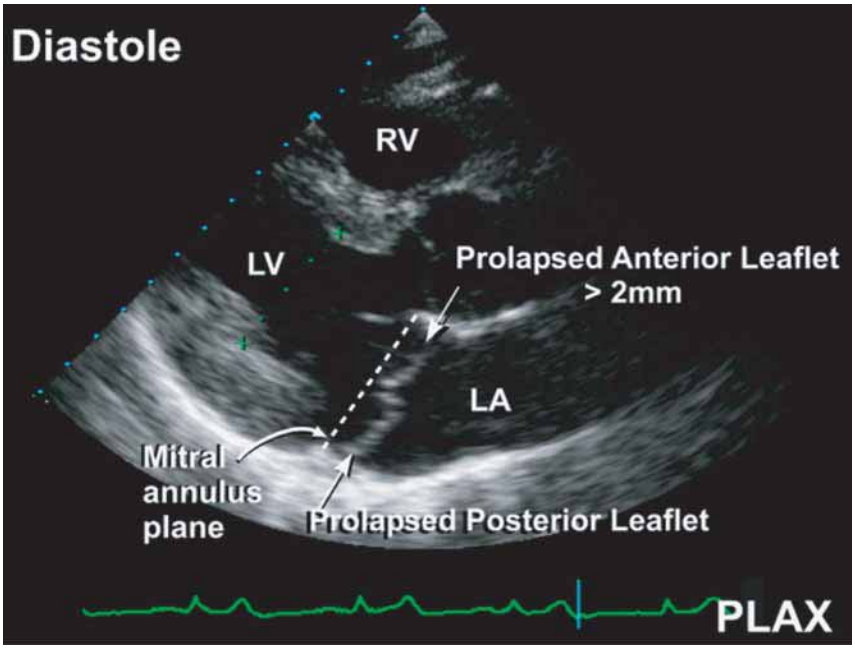

Fig. 4. Systolic frame of the parasternal long-axis (PLAX) shows significant prolapse (>2 mm) of both mitral valve leaflets above the mitral annular plane. (Please *see* companion DVD for corresponding video.)

Caveats about detection of mitral valve leaflets include mistaking myxomatous or floppy valves for vegetations or masses (*see* Chapter 19, Fig. 11). MR may be absent at rest, but can be precipitated by exercise in some patients with MVP, so exercise stress echocardiography may be useful for diagnosis.

Although echocardiography is useful in defining MVP, the MVP syndrome includes associated clinical features and auscultatory findings. Furthermore, the pathology underlying the primary MVP may also affect other intracardiac valves, and assessment for concomitant prolapse of the tricuspid, pulmonary,

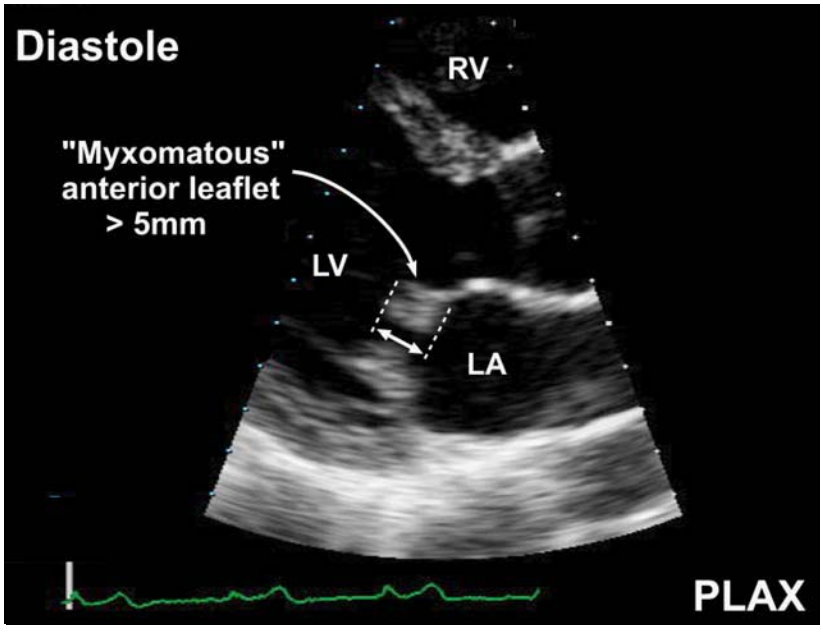

Fig. 5. During diastole, the myxomatous leaflets can be measured. Thickened leaflets more than 5 mm support the diagnosis of classic MVP. (Please *see* companion DVD for corresponding video.)

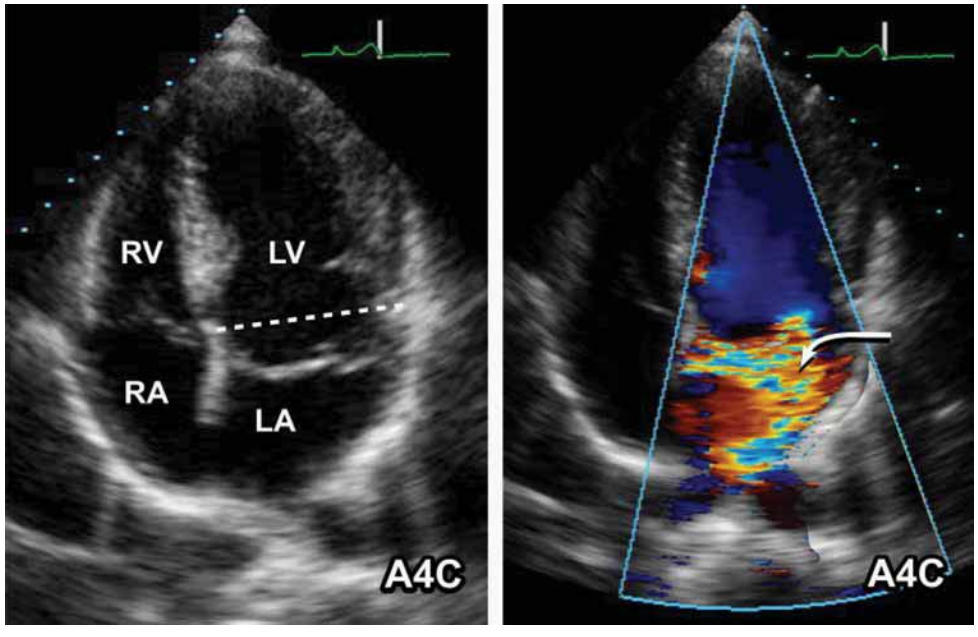

Fig. 6. Bileaflet prolapse is easily visualized in the apical four-chamber (A4C) view. However, the mitral valve profile is normally exaggerated in this view—and may lead to overdiagnosis of mitral valve prolapse (left panel). Severe mitral regurgitation was present (right panel). (Please *see* companion DVD for corresponding video.)

and aortic valves should be performed during the echocardiographic examination.

Important potential sequelae of MVP include progressive MR, potentially from progressive leaflet malcoaptation, disintegration of chordal integrity over time, and infective endocarditis.

CASE PRESENTATION 3: POST-MI MITRAL REGURGITATION

This 66-yr-old male with myocardial infarction (MI) 1 yr previously presented with congestive cardiac failure.

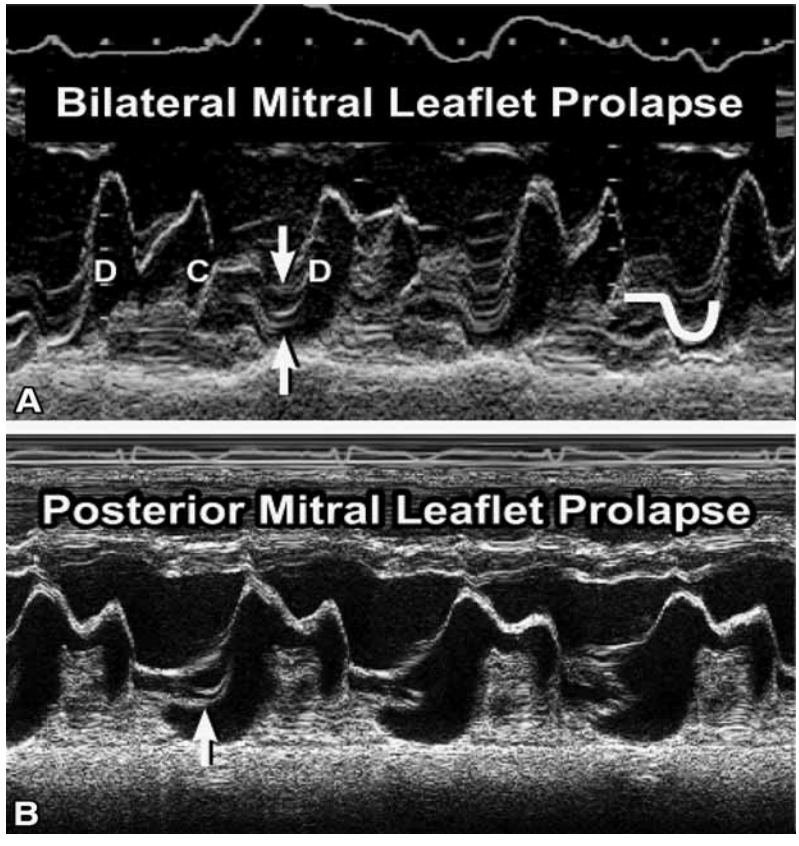

Fig. 7. M-mode echocardiogram of patient (Figs. 4–6) with classic mitral valve prolapse. **(A)** Both thickened valve leaflets show posterior displacement of the C, D segment during mid- to late systole. **(B)** Only the posterior leaflet is affected.

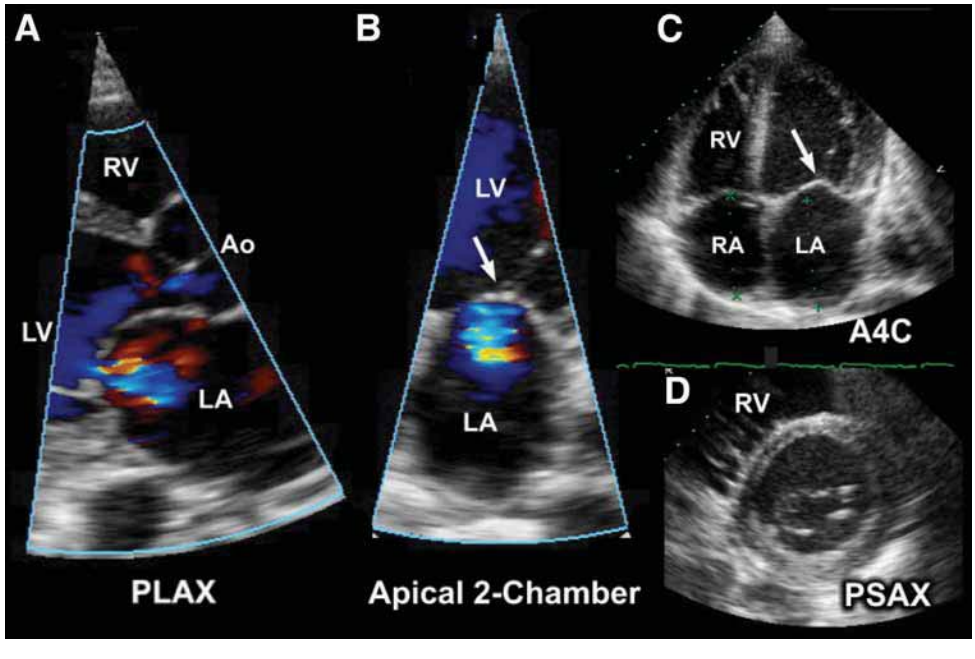

Fig. 8. Mitral regurgitation in dilated ischemic cardiomyopathy. This results in apical tethering ("tenting") of mitral valve leaflets during ventricular systole **(A–C)**, impaired leaflet coaptation, and mitral regurgitation **(B)**. "Tenting" is best seen in **C** and **D** (arrows). This term describes closure of the mitral valve well within the left ventricular cavity rather than at the level of the mitral annular plane **(C)**. Valve leaflet morphology is normal, but left ventricular dilation **(D)** leads to lateral displacement of papillary muscles (*see* Fig. 5). This causes leaflet malcoaptation that is typically symmetric **(C)**, and the jet of ischemic mitral regurgitation is centrally directed **(A**,**B)**.

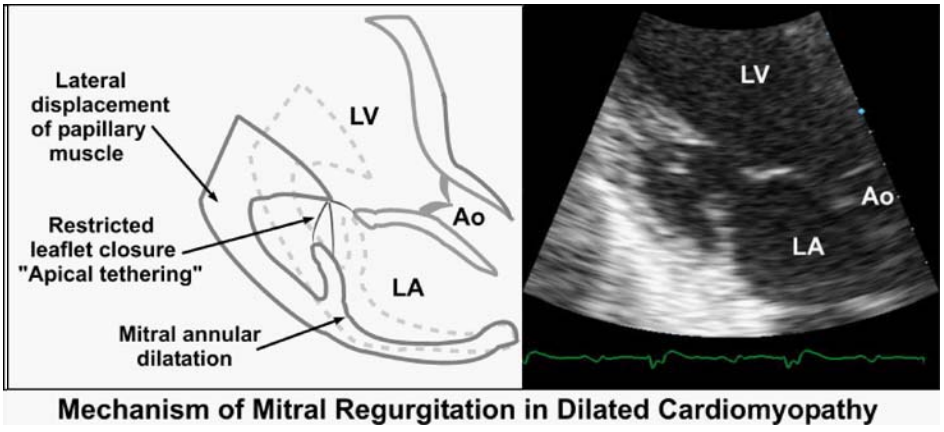

Fig. 9. The mechanism of mitral regurgitation in dilated ischemic cardiomyopathy. The three major contributors as shown prevent normal leaflet coaptation and functional mitral regurgitation. The mitral leaflets are morphologically normal.

Table 3
Echocardiographic Features of MVP

- Superior displacement of both[a] mitral valve leaflets (≥ 2 mm[a] above mitral annulus) with coaptation point at or above the mitral annular plane.
- Diffuse leaflet thickening (>5 mm[a]) in diastole ("myxomatous" appearance)
- Mitral annular dilatation
- Redundant mitral valve leaflets
- Chordal rupture with leaflet flail (partial)
- Mitral regurgitation
- Characteristic M-mode findings (Fig. 4A)

[a]Strict criteria for classical MVP or "floppy mitral valve."

The images (Figs. 8 and 9) show MR that result from left ventricular remodeling and dilatation. Such changes to LV geometry significantly change the spatial relationships between mitral leaflets, papillary muscles, and chordae tendinae. In this example, lateral displacement of the papillary muscles and chordae lead to poor leaflet coaptation and MR from LA dilatation. The resulting MR is centrally directed.

CASE PRESENTATION 4: FLAIL MITRAL LEAFLET

A 44-yr-old man complained of increasing shortness of breath and was found to have a murmur consistent with MR (Fig. 10; please *see* companion DVD for corresponding video).

These echocardiographic images illustrate how complete or partial flail of one or both mitral leaflets can lead to moderate to severe MR. Partial leaflet flail most commonly involves the posterior leaflet and is usually secondary to chordal rupture. The resultant MR may be severe, and the jet is typically directed anteriorly. Conversely, an anterior leaflet flail usually results in a posteriorly directed jet of regurgitation (*see* Chapter 7, Fig. 7).

Papillary muscle rupture in the setting of acute MI can present with acute severe regurgitation within the first 5 days post-MI. It more commonly involves dehiscence of the tip or a head of the muscle, and less commonly, complete transection (Fig. 11; please *see* companion DVD for corresponding video). In particular, the posteromedial papillary muscle is more susceptible to injury during infarction as its blood supply is derived almost solely from the posterior descending branch of the right coronary artery. The antero-lateral papillary muscle and those of the right ventricle have a dual blood supplies.

Different degrees of MR may result from ischemic dysfunction of the papillary muscles and supporting ventricular wall. This is seen in approx 30% of patients with coronary artery disease being considered for cardiac surgery.

Another example of disruption of mitral valve architecture is seen with degenerative mitral valve disease. For example, with mitral annular calcification, which can be seen with older patients, the excursion of the mitral leaflets can be limited, affecting leaflet coaptation. This also results in MR.

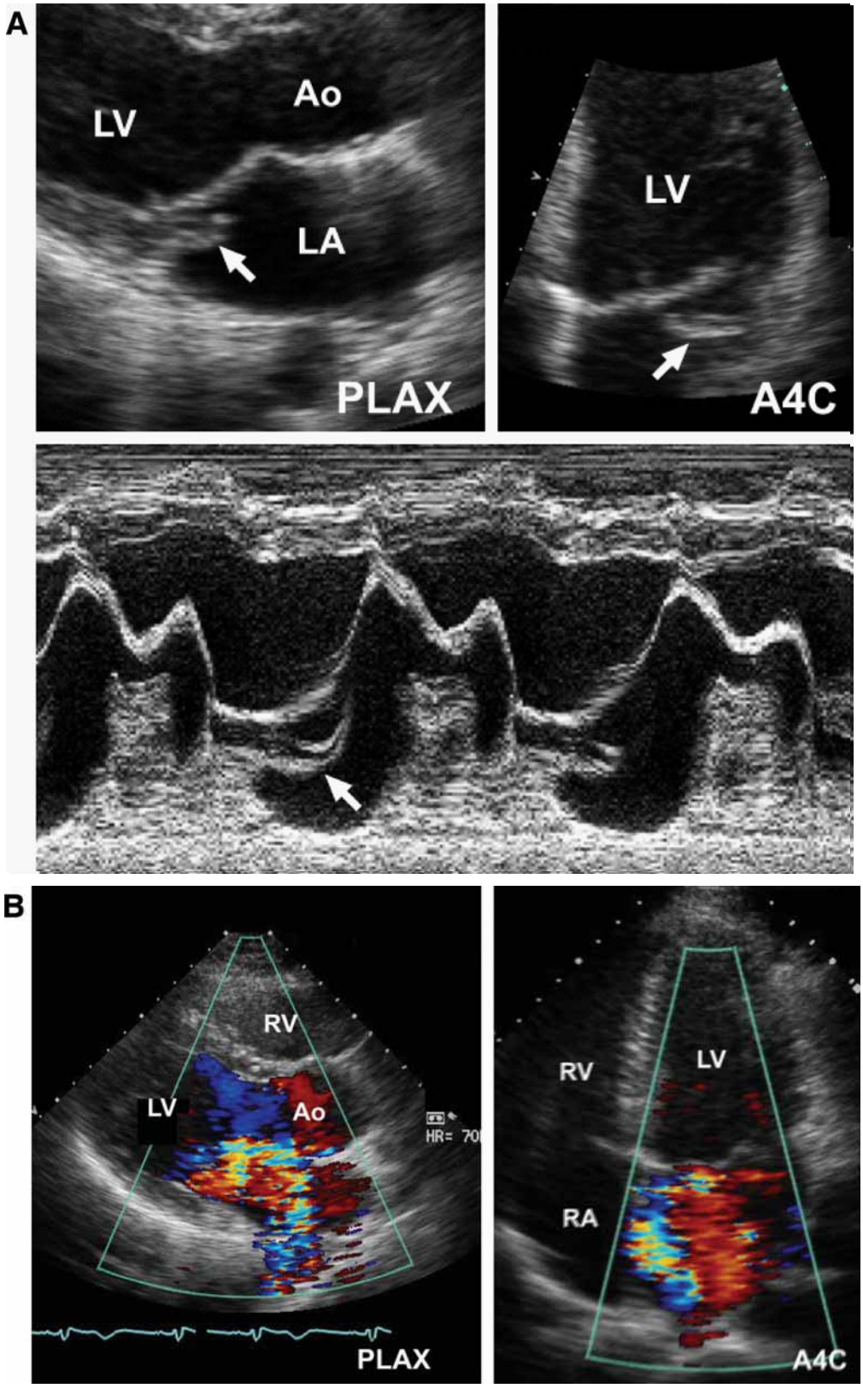

Fig. 10. (A) Parasternal long-axis view (PLAX) and apical four-chamber view (A4C) showing a partial flail of posterior mitral valve leaflet. Note that tip of leaflet points toward the left ventricle indicating that flail is incomplete **(top panels)**. Marked turbulence with this valvulopathy are seen on color flow Doppler examination. Note that the mitral regurgitant jet is anteriorly directed. M-mode examination shows that flail affected the posterior leaflet only. (Please *see* companion DVD for corresponding video.)

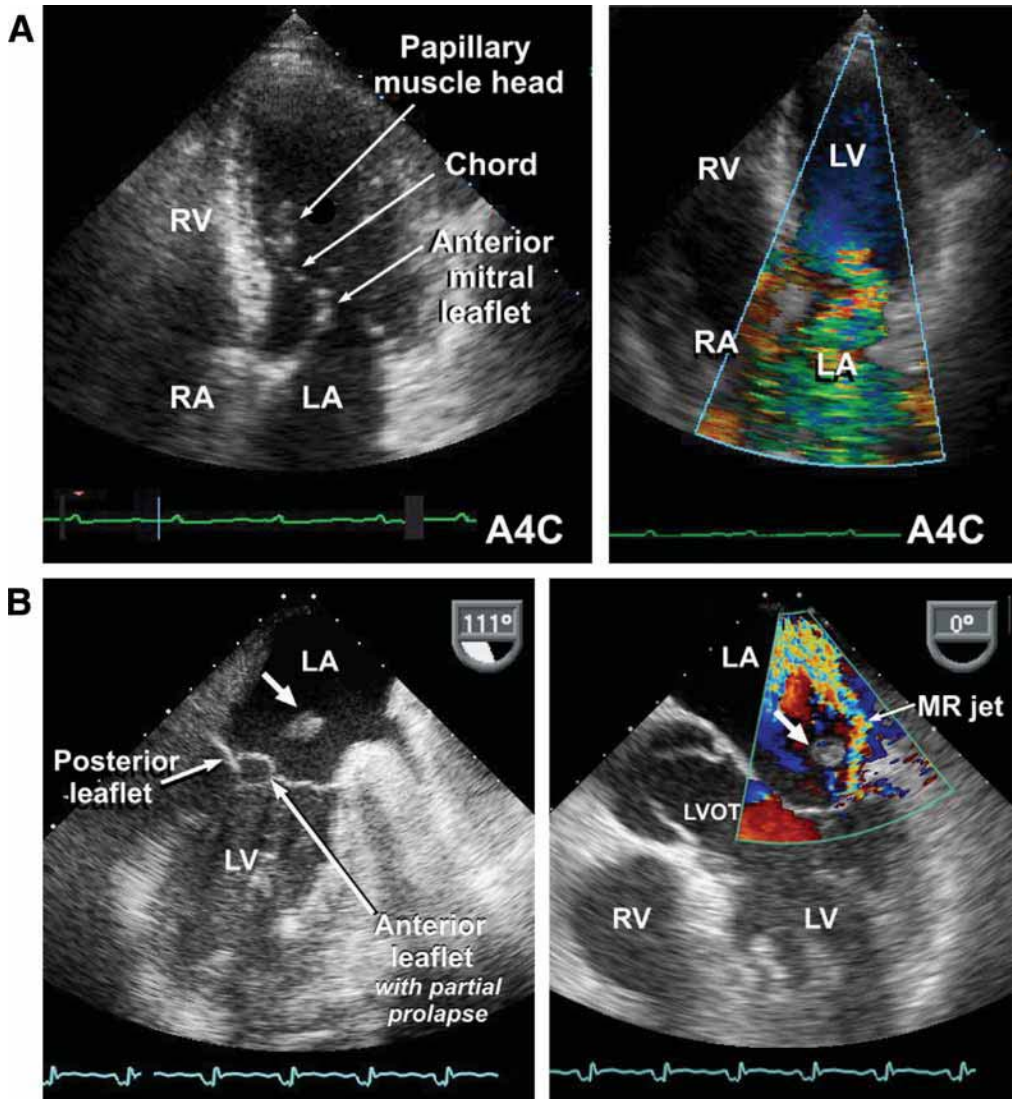

Fig. 11. Ruptured papillary muscle. **(A)** Transthoracic images a patient 5 d post-MI showed a mobile linear echodensity that ping-ponged between left atrium and left ventricle with each cardiac cycle (left panel). Attached at its end was the avulsed tip (head) of the posterior-medial papillary muscle. Right panel showed large postero-laterally directed MR jet as seen in from the apical four-chamber view. **(B)** Mid-esophageal views from patient showed the mobile tip of the dehisced papillary muscle (arrow in both panels) within the left atrium. Note the partial flail of the anterior mitral valve leaflet (left panel) with the resultant postero-laterally directed MR jet. (Please *see* companion DVD for corresponding video.)

CASE PRESENTATION 5: RHEUMATIC MITRAL REGURGITATION

A 39-yr-old female with known history of rheumatic heart disease and worsening shortness of breath was referred for an echocardiogram prior to consideration for percutaneous mitral balloon valvuloplasty.

Rheumatic heart disease is the major underlying cause of mitral stenosis. The postinflammatory

Table 4
Indicators for Poor Prognosis in MR

1.	Symptoms of heart failure
2.	Left ventricular ejection fraction (LVEF) < 50% with symptoms
3.	Acute-onset MR
4.	Acute flail of mitral valve leaflets
5.	Significant MR accompanying acute myocardial infarction

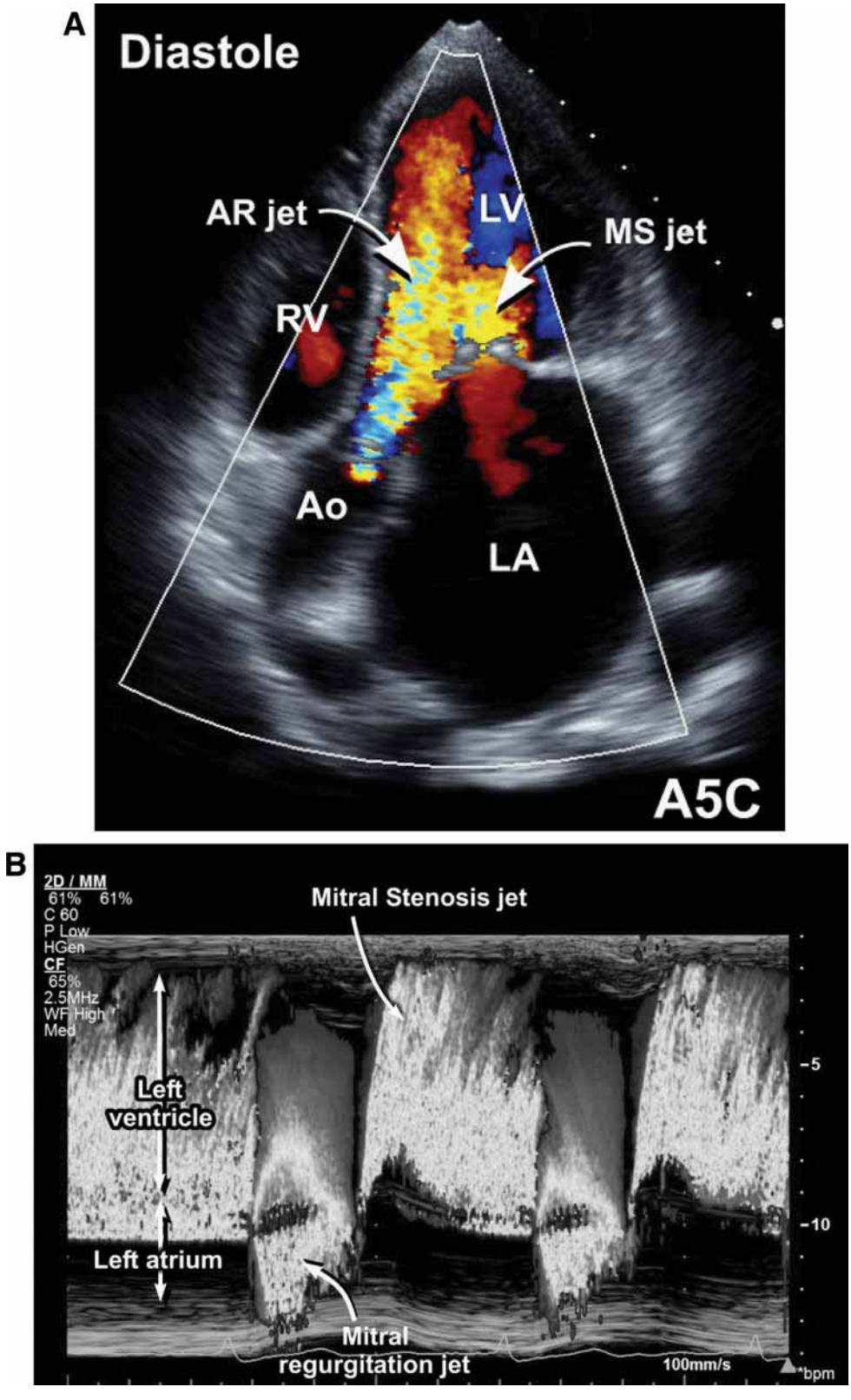

Fig. 12. (A) Mitral regurgitation in the setting of rheumatic heart disease is the result of structural distortion, thickening, and restricted leaflet motion. Mitral stenosis (MS) and aortic regurgitation (AR) were also present in this patient. **(B)** This color M-mode through the left atrium and ventricle in the same patient shows mixed mitral stenosis-mitral regurgitation jets.

Table 5
Grading MR Severity: Recommended Parameters

	Mild	*Moderate*	*Severe*
Structural parameters			
Left atrial size	N	N or Dilated	Usually D
Left ventricular size	N	N or Dilated	Usually D
Mitral leaflets and supporting complex	N or Abnormal	N or abnormal	Abnormal/Flail leaflet/Ruptured papillary muscle
Doppler parameters			
Color jet area (Niquist limit 50–60 cm/s)	Small, central jet (usually <4 cm^2 or <20% of left atrium area)	Variable Variable	Large central jet (usually >10 cm^2 or >40% left atrium area) or variable size wall-impinging jet swirling in left atrium
Mitral E- point velocity – PW	A-wave dominant	Variable	E-wave dominant (E usually >1.2 m/)
Jet density – CW	Incomplete or faint	Dense	Dense
Jet contour – CW	parabolic	Usually parabolic	Early peaking-triangular
Pulmonary vein flow – PW	Systolic dominance	Systolic blunting	Systolic flow reversal
Quantitative parameters			
Vena contracta width (cm)	<0.3 cm	0.3–0.69 cm	≥0.7 cm
Regurgitant volume (mL/beat)	<30	30–59	≥60 mL/beat
Regurgitant fraction (%)	<30%	30–49%	≥50%
EROA (effective regurgitant area orifice)	<0.2 cm^2	0.2–0.29 0.3–0.39 cm^2	≥0.4 cm^2

Modified from ASE, American Society of Echocardiography Report (2003)—ASE/ACC/AHA/ESC Guidelines. *See* ref. *3*.

fibrosis and thickening of leaflets and chordae that lead to mitral stenosis also prevent normal mitral leaflet coaptation during systole. Combined mitral stenosis-MR is the result. (Fig. 12; *see* Chapter 13, Table 3).

ASSESSMENT OF MR SEVERITY

A comprehensive assessment of a patient with MR should pay special attention to ventricular performance, with emphasis on the parameters of LA systolic function (*see* Chapter 5).

In addition to defining etiological and anatomic mechanisms of MR, assessment of MR severity and its hemodynamic impact on risk stratification and timing of intervention (Table 4).

The American Society of Echocardiography guidelines for the classification of grades of MR severity are shown in Table 5. Although the recommendation to grade MR severity is mild, moderate and severe, distinguishing mild from moderate and moderate from severe can be challenging. Thus, several qualititative and quantitive measures have been proposed, although limitations of each should be noted during their use; the most popular methods in use will be further delineated in this chapter. For example, most of the Doppler-based parameters apply only to isolated MR, and not to mixed valvular lesions, or MR secondary to LV dysfunction. Quantitative assessment of MR using these methods may involve relatively complex calculations,

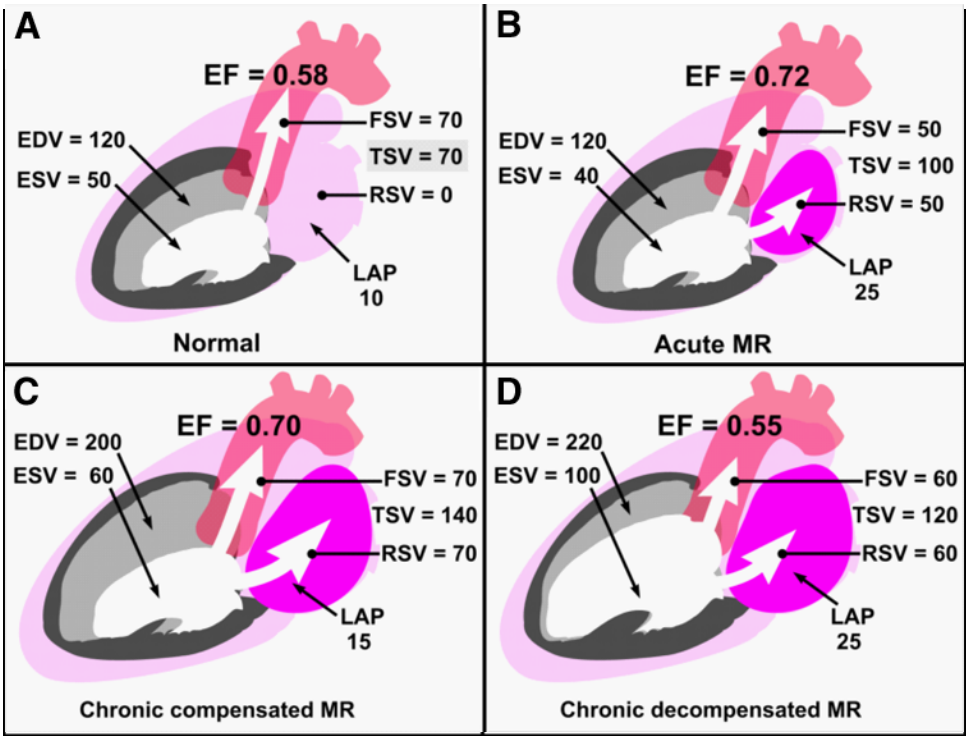

Fig. 13. Mitral regurgitation and the left ventricle: three phases of dysfunction. (Modified from Carabello BA. Progress in mitral and aortic regurgitation. Curr Probl Cardiol 2003;28:553.)

Table 6
Recommended Echocardiography Follow-up in Chronic Asymptomatic MR

MR severity	*LV size*	*LVEF*	*Frequency of follow-up*
Mild MR	ESD normal	Normal EF	5 yr
Moderate MR	ESD normal	Normal EF	1–2 yr
Moderate MR	ESD > 40 mm	<65%	1 yr
Severe MR	ESD normal	Normal EF	1 yr
Severe MR	ESD > 40 mm	<65%	6 mo

Adapted from: Otto CM. Evaluation and management of chronic asymptomatic mitral regurgitation. N Engl. J Med 2001;345:740–746.

and small errors in measurement easily lead to large errors in calculation. Therefore, they should be applied in the context of the patient, without reliance on a single measure.

TWO-DIMENSIONAL ECHOCARDIOGRAPHIC PARAMETERS FOR GRADING MR SEVERITY

LV Performance

Indices of LV systolic function—left ventricular end-systolic and end-diastolic dimensions, ejection fraction, wall thickness, and fractional shortening—are the most important echocardiographic barometers of the hemodynamic effects of MR on global cardiac function (*see* Chapter 5 for LV quantification).

Three major phases of MR on and their impact on LV performance are summarized in Fig. 13.

1. Acute MR phase.
2. Chronic compensated MR.
3. Chronic decompensated MR.

LV end-systolic dimensions (Fig. 14) and LV ejection fraction (LVEF) reflect the heart's ability to adapt, and therefore influences the frequency of clinical follow-up, timing of surgical intervention, and outcomes following

Table 7
Echocardiographic Signs and Surgical Considerations in MR

Variables	*Measures*	*Comment*
Clinical symptoms	Symptomatic vs Asymptomatic	Presence of symptoms favors earlier intervention
LVEF	<50 mm	Sign of decompensation
ESD (LVIDs)	<50–55 mm	Sign of decompensation
EDD (LVIDd)	>70 mm	Sign of decompensation
Surgical considerations	Repair vs Replacement	Earlier interventions with valve-sparing surgery favored

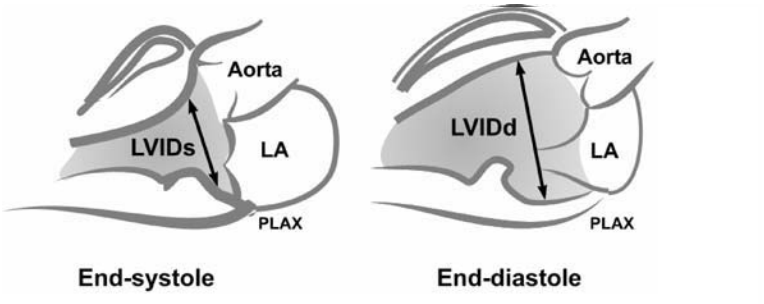

Left ventricular dimensions*		
LV Internal Diameters (PLAX)	**Normal Range (cm) (mean ± SD)**	**Index adjusted for body surface area (cm/m²)**
End-diastole: EDD or LVIDd	3.5 – 6.0	2.3 – 3.1
End-systole: ESD or LVIDs	2.1 – 4.0	1.4 – 2.1

*Values from cardiac ultrasound laboratory, Massachusetts General Hospitall

Fig. 14. Left ventricle dimensions in mitral regurgitation. Values from cardiac ultrasound laboratory, Massachusetts General Hospital.

mitral valve surgery (Tables 6 and 7). In chronic compensated MR, cardiac output is maintained via an increase in the LVEF, and such patients typically have LVEFs greater than 65%. LV hypertrophy is not a feature of isolated MR as the regurgitant chamber—the left atrium (LA)—usually adapts and dilates to accommodate increases in preload (end-diastolic volume [EDV]; Fig. 13C). Even in the acute setting, LV contractility and LVEF increase in response to an increase in preload (Fig. 13B). However, LV contractility can decrease silently and irreversibly in chronic MR. For this reason, increasingly earlier surgical interventions for less severe degrees of MR are being recommended (Fig. 13D).

LA Size

The LA will dilate in response to chronic volume and pressure overload. Its dimensions may help to assess MR severity and chronicity (Figs. 15 and 16). Acute-onset severe MR, as occurs with papillary muscle rupture, does not cause LA dilatation. The excess regurgitant blood entering the small noncompliant atrium causes acute increase in LA pressures and can precipitate acute pulmonary hypertension and right heart pressure overload. Increased LA pressures and systolic flow into reversal pulmonary veins may be the only echocardiographic findings that document the severity of acute-onset MR. LA size may predict the onset of atrial fibrillation, but is otherwise of little prognostic value in MR itself, in the absence of heart failure. Measurements should be adjusted for age and body surface area.

DOPPLER METHODS FOR GRADING MR SEVERITY

Color Flow Doppler Parameters

Color flow Doppler imaging is perhaps the most intuitive of all measures, is useful for detecting the jet origin, direction, and spatial relationships and has excellent sensitivity and specificity. Each of the three components

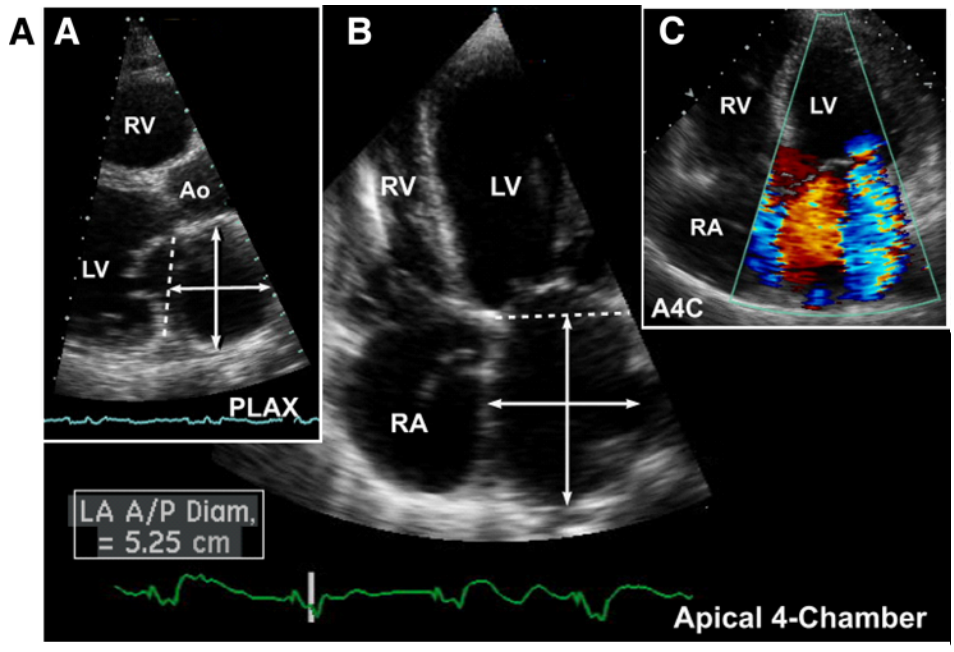

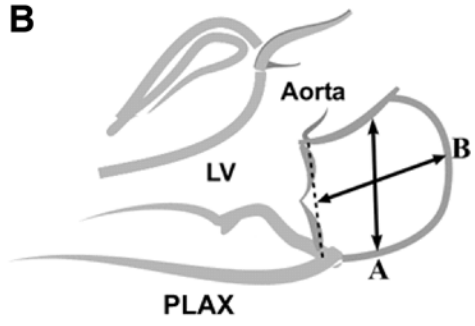

Parasternal Long Axis (PLAX) View (End-Systole)	
A (mid-cavity) Antero-posterior	4.8 ± 0.8
B (mid-cavity)	3.0 ± 0.3

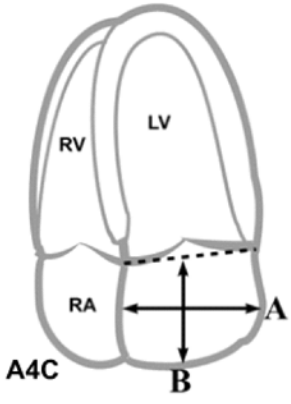

Apical 4-Chamber View (End-Systole)	
A (mid-cavity) Antero-posterior	4.0 ± 0.6
B (mid-cavity)	3.8 ± 0.4

Fig. 15. **(A)** Measuring left atrial size. **(B)** Left atrial measurements. Values from cardiac ultrasound laboratory, Massachusetts General Hospital.

of the MR jet—flow convergence zone, vena contracta, and jet profile—can provide a semiquantitative or quantitative measure of MR severity (Fig. 17).

MR jets are best assessed using multiple windows to obtain a three-dimensional (3D) perspective. Qualitative estimates of MR jets are categorized on a scale of 0–4: grade 0 = none or trace MR, grade 1 = mild MR through to grade 4 = severe MR (Fig. 18). The notation 1+, 2+, and so on, to denote increasing grades of MR severity is also popular (Table 8).

Color Jet Area

The same color jet profiles can be measured within the LA. Color jet areas are influenced by jet velocity, momentum, and direction. Mild MR jets cover less than 20% of total LA area (or a maximal jet area < 4.0 cm^2),

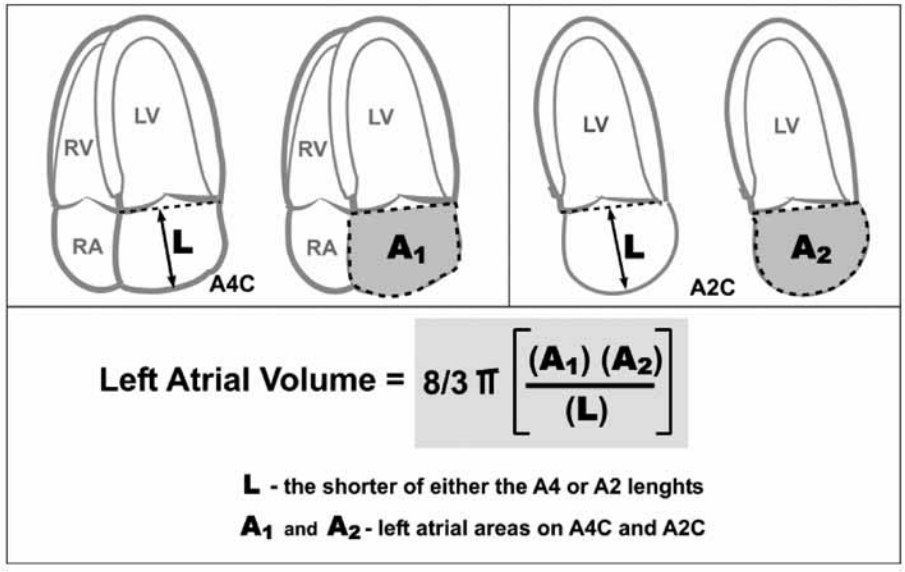

Fig. 16. Left atrial volume. (Reproduced with permission from Roberto M. Lang et al. Recommendations for chamber quantification. A report from the American Society of Echocardiography's Nomenclature and Standards Committee and the Task Force on Chamber Quantification American Society of Echocardiography, 2005.)

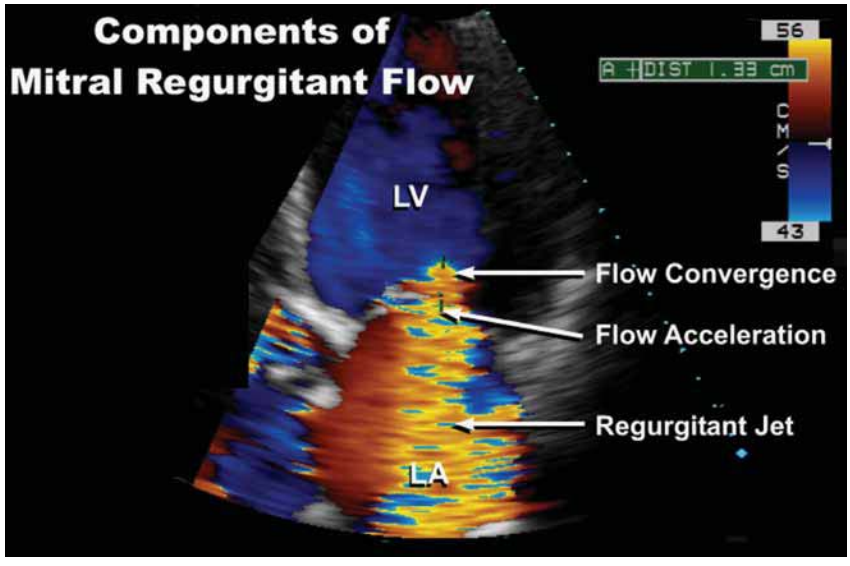

Fig. 17. Mitral regurgitation: color jet profile.

Table 8
Eyeball Estimation of Color Jet Area in MR

Advantages	*Disadvantages*
1. Ease of use	1. Can be unreliable for estimation of regurgitation severity
2. Good screening test for mild versus severe regurgitation	2. Not good at distinguishing moderate MR from mild or severe MR
3. Evaluate in at least 2 views (PLAX, A4C, A3, or A2C)	3. Influenced by transducer frequency and other instrument settings, especially pulse repetition frequency and color gain
4. Best "estimate" using scale of 1+ (mild) to 4+ (severe)	4. Size of color jet may be misleading, especially with eccentric jets

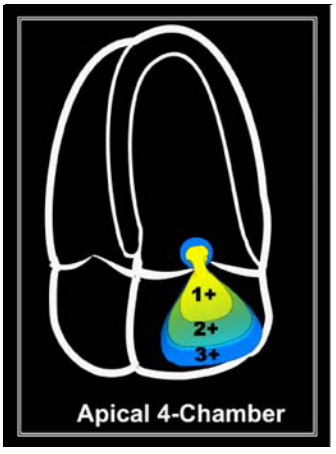

Eyeball Grading of Color Jet Profiles in Mitral Regurgitaion	
Mild	1+
Moderate	2+
Moderate-to-Severe	3+
Severe	4+

Fig. 18. Schema illustration of jet profile of mitral regurgitation as viewed from the apical four-chamber window. Color Doppler mapping allows visualization of the spatial distribution of blood flow within the heart by displaying the blood flow velocities in terms of ranges of color. Visual estimation of the jet profile is a simple method of estimating mitral regurgitation severity. Color Doppler mapping, however, is very sensitive to instrument settings, hemodynamic status, regurgitant orifice geometry (affects jet eccentricity), and atrial dynamics—e.g., wall constraint, wall impingement, and the presence of secondary flow.

with severe MR jets more than 40% of total LA area (or a maximal jet area > 10 cm^2). At least two orthogonal views should be used with the Nyquist limit set at 50–60 cm/s (Fig. 19; please *see* companion DVD for corresponding video).

Larger color jet areas indicate more severe MR when the jet is centrally directed, but can be misleading with eccentrically directed jets. Hugging or entrainment (Coanda effect) of the eccentric jet to the LA wall results in smaller jet areas even when MR is severe. A thorough evaluation of eccentrically directed jets should include evaluation for etiologies, such as a flail leaflet, prolapse or perforation. Severe MR with eccentrically directed jets sometimes exhibit a "wrap around" effect in the LA (Fig. 20).

In acute MR, even centrally directed jets may be misleadingly small. A small nondilated atrium in the setting of acute regurgitation constrains the regurgitant jet momentum and hence the visible color jet area.

Vena Contracta Width

The vena contracta is the narrow neck of the MR jet as it traverses the regurgitant orifice (Fig. 21). The vena contracta measured from the parasternal long-axis view is best optimized by using a narrow sector scan, optimal color gain, and Nyquist limit between 40–70 cm/s. The vena contracta appears as the well-defined light blue or light yellow high-velocity core on the red-blue color Doppler scale. This portion of the regurgitant jet, unlike the flow convergence zone and the distal turbulent jet profile, most closely mirrors that of the actual regurgitant orifice. It is, therefore, a more reliable marker of MR severity with significant advantages over other methods provided that the recommended technique is used (Table 9).

A single vena contracta width (VCW) measurement, however, is a 2D snapshot across an elongate regurgitant orifice area that extends to a variable degree along the crescenticleaflet coaptation line (Fig. 1B). A closer approximation of the actual regurgitant orifice area is best obtained by scanning through multiple planes and selecting the greatest VCW. Such considerations are better appreciated and measured on 3D echocardiography. Averaging VCW measurements over at least three beats and using two orthogonal planes is recommended. A VCW less than 0.3 cm indicates mild MR; a VCW more than 0.7 cm indicates severe regurgitation (Fig. 21; Table 5).

The effective regurgitant orifice area (EROA)—a marker of MR severity that is less affected by loading conditions—can be calculated from the VCW using the formula:

$$\text{EROA} = \pi(\text{VCW}/2)^2$$

Good agreement exists between this EROA formula and other validated measures of MR severity. VCW measurements are not valid for assessing MR severity with multiple MR jets (Fig. 22).

Proximal Flow Convergence and Proximal Isovelocity Surface Area

According to fluid dynamics, fluids within an enclosure stream symmetrically toward a narrowed outlet or orifice in near concentric isovelocity zones. This is akin to water being drained from a kitchen sink, or when water from a lake flows into a narrowed estuary (Fig. 23). The same principle applies when blood in the LV stream converges toward a narrowed (stenosed or regurgitant) orifice. This method can be used for estimating the area of the regurgitant orifice—which is hard to measure directly because actual regurgitant orifice is dynamic, functional, and 3D. As regurgitant blood converges toward the regurgitant orifice at the proximal convergence zone, the size and velocity of the innermost shell or hemisphere can be measured (Fig. 24).

Furthermore, according to the continuity principle (*see* Chapter 11, Fig. 11), the amount of fluid that passes through the regurgitant orifice is the same

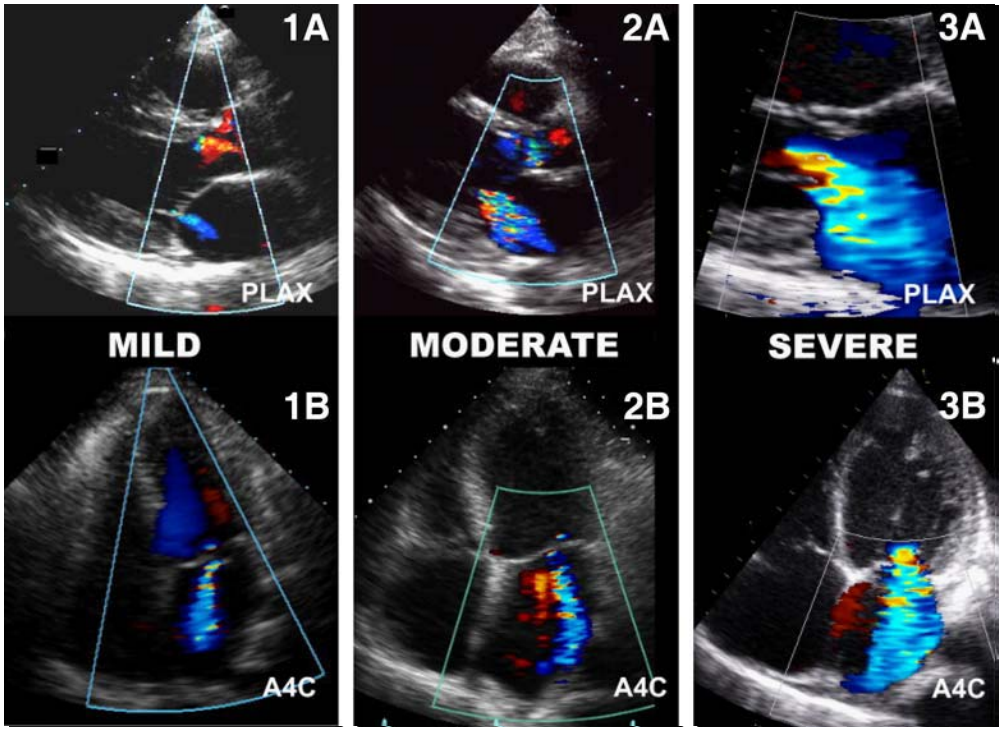

Fig. 19. Color flow jet areas. (Please *see* companion DVD for corresponding video.)

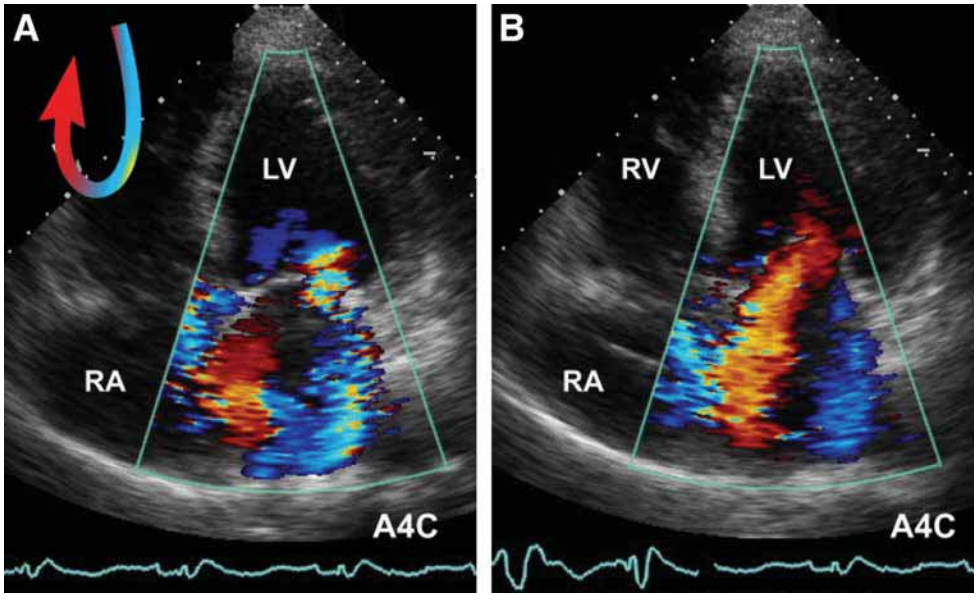

Fig. 20. Severe mitral regurgitation showing left atrial "wrap-around."

amount that flows in the regurgitant jet (the law of conservation of mass). Therefore, total flow at the proximal isovelocity surface area (PISA) will equal total flow in the distal MR jet.

The apical four-chamber view is recommended for optimal visualization of the MR jet PISA measurement. The area of interest is optimized by lowering imaging depth and lowering the Nyquist limit (on the color Doppler scale) to approx 40 cm/s. The velocity at which the blue-red color shift occurs identifies the PISA shell. The PISA radius (r) is then measured and multiplied by the PISA velocity, i.e., the aliasing velocity

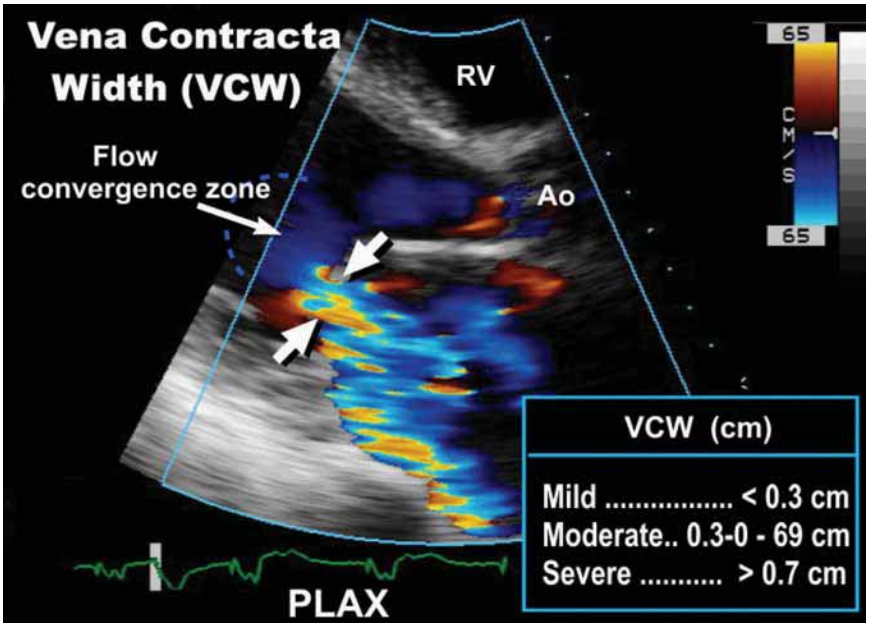

Fig. 21. Vena contracta width measurement.

Table 9
Vena Contracta Width Measurements in MR

Advantages	*Disadvantages*
1. Relatively quick and easy to assesses using standard windows	1. Not good at distinguishing mild from moderate MR or moderate from severe MR
2. Good for extremes of MR (mild and severe MR)	2. Small values; small measurement errors are multiplied
3. Assesses basic size of defect	3. True cross-sectional area may be difficult to obtain—use two apical diameteres
4. Relatively independent of flow rate, driving pressure, or entrainment (Coanda effect)	4. VCW measurement—a single temporal measurement
5. Not influenced by the presence of another regurgitant leak, for example, aortic regurgitation	5. Overestimates true regurgitant orifice area—a problem of resolution
6. No need for correction for convergence angle as with proximal isovelocity suface area measurement	6. Not valid for multiple MR jets

MR, mitral regurgitation.

(Nyquist limit)—V_{ALIAS}—to give the regurgitant flow rate (Fig. 24). If the base of the PISA hemisphere is not horizontal, it should be corrected to 180°.

$$\text{Reguritant flow rate} = 2\pi r^2 \times V_{ALIAS}\ (\text{mL/s})$$

From this, the EROA can be quantified using the continuity principle equation (Figs. 25 and 26; *see* Chapter 11, Fig. 11) for flow rate: $\text{Area}_1 \times \text{Velocity}_1 = \text{Area}_2 \times \text{Velocity}_2$; and V_{MAX} is the peak velocity of the MR jet on CW Doppler:

$$\text{EROA} = 2\pi r^2 \times V_{ALIAS}/V_{MAX}$$

Regurgitant volume and the regurgitant fraction can then be calculated (Fig. 27).

The PISA method can also be assessed by transesophageal echocardiography when indicated (Fig. 28).

The PISA method makes several assumptions (Table 10)—many of which are violated in the clinical setting. 3D echocardiography may ultimately assist in overcoming some of these limitations.

Other Doppler Methods

Systolic Flow Reversal in the Pulmonary Veins

The presence and the degree of reversal of blood flow from the LA into the pulmonary veins can indicate the hemodynamic impact of the MR jet. Visualization of flow reversal into one or more pulmonary veins on

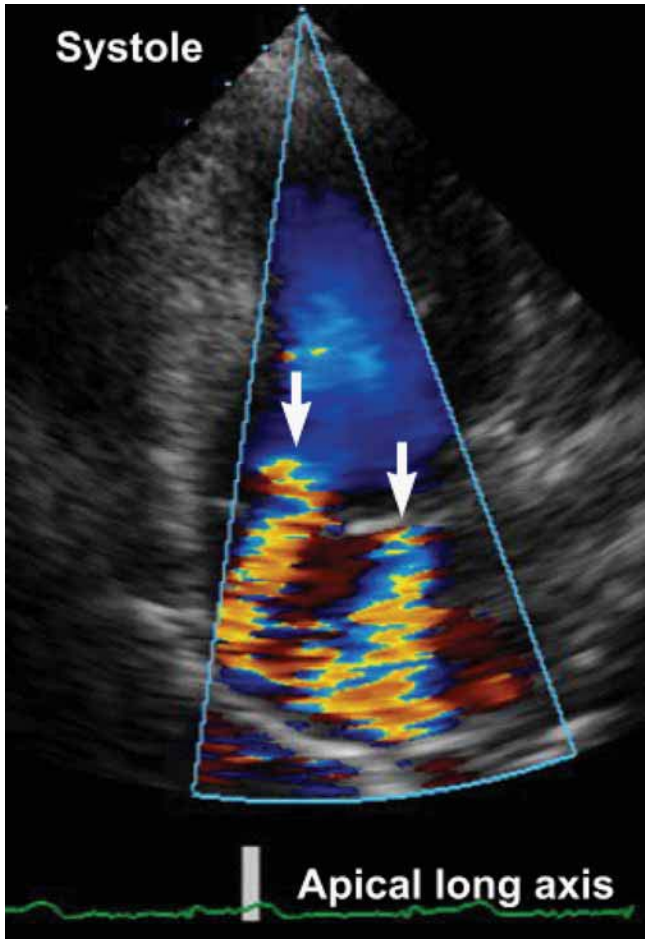

Fig. 22. Narrow sector scan (color flow Doppler) showing two separate mitral regurgitant (MR) jets viewed from the apical long axis view. This was confirmed when viewed from multiple windows. When assessing multiple MR jets, each jet should be analyzed and reported separately. Vena contract widths (VCW) measurements are invalid when multiple MR jets are present.

color flow Doppler, or more reliably—pulsed Doppler evidence of flow reversal into the pulmonary veins are measures of MR severity (Fig. 29). In normal individuals, a positive systolic *(S)* wave followed by a smaller positive diastolic *(D)* wave is seen, but with moderate or severe MR, blunting or reversal of this pattern may be seen (*see* Chapter 6). Systolic flow reversal may be indicative of severe MR even if the color jet area suggests milder disease.

Atrial fibrillation and elevated LA pressures from any cause can blunt forward systolic pulmonary vein flow. Blunting of pulmonary forward flow may lack specificity, but is nonetheless a useful parameter that provides information independent from color Doppler methods used to assess MR severity.

Mitral E-Point Velocity

The progressive increase in trans-mitral flow that occurs with increasing MR severity can be detected as higher flow velocities during early diastolic filling. A dominant E-wave more than 1.2 m/s may indicate more severe MR, providing there is no concomitant mitral stenosis (Fig. 30).

Continuous-Wave Jet Intensity and Morphology

Peak MR jet velocities by continuous-wave (CW) Doppler typically range between 4 and 6 m/s—a reflection of the systolic pressure gradient between LV and LA. If the blood pressure at the time of the study is low, the peak velocities and gradients will also be low. Peak MR jet velocities alone, therefore, are not reliable measures of MR severity.

The signal intensity (jet density) of the CW envelope of the MR jet can be a guide to MR severity, but this should be assessed relative to the density of antegrade flow signal (mitral inflow). A dense mitral regurgitant signal with a full envelope of equal in intensity to the antegrade flow signal indicates more severe regurgitation than a faint signal (Fig. 31).

The CW Doppler envelope may show blunting or notching of the CW envelope. This results from the rapid surge in LA pressures in severe MR—the atrial V-wave (Fig. 32). This may reflect an LA that has not yet dilated and show discordance with color Doppler severity.

LV Systolic Performance

The rate of rise of LV systolic pressure over time (dP/dT) may be a useful index of the LV systolic function in MR (Fig. 33). In patients with preserved systolic function, the MR jet velocity shows a rapidly early in systole. A lower dP/dT can unmask patients with declining systolic function, and therefore serve as a guide to more aggressive intervention, especially when supported by other indicators of severity.

Integrating Indices of Severity

Integrated scores have been devised to improve the diagnostic validity of parameters of MR severity. The MR index is a composite score comprising six echocardiographic parameters—jet length, PISA, CW jet density, pulmonary artery systolic pressure, pulsed wave Doppler, pulmonary vein flow pattern, and LA size. Such scores provide a better overall assessment of MR

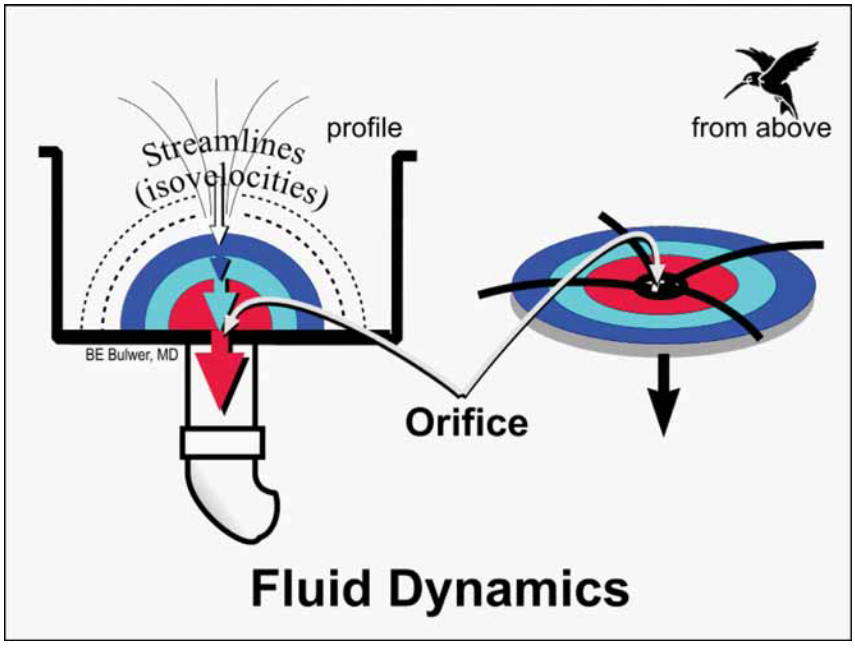

Fig. 23. The proximal isovelocity surface area method. Fluids within a confined space accelerate toward an outlet or orifice in concentric isovelocities. A familiar example of this occurs when water is released from a kitchen sink.

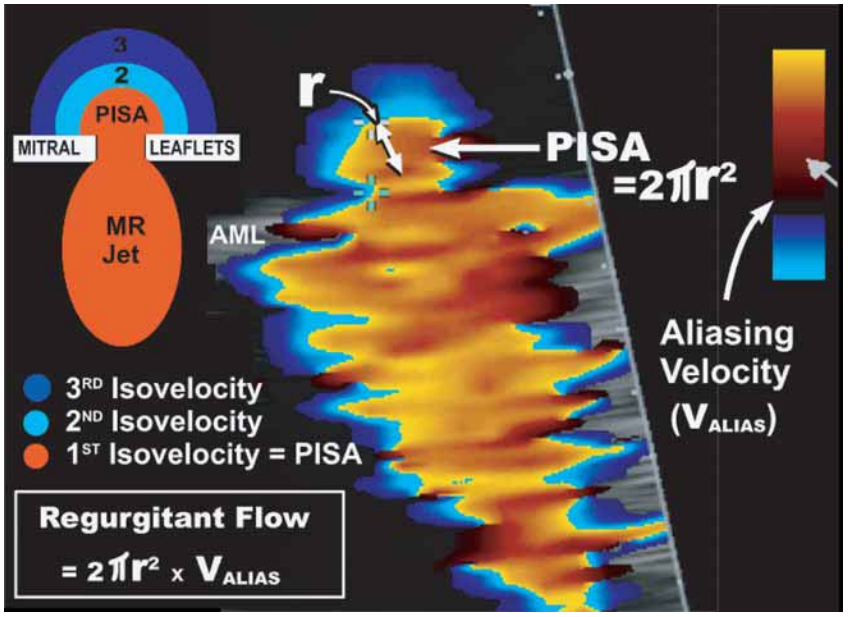

Fig. 24. Proximal isovelocity surface area (PISA).

severity itself, but should be further integrated with global cardiac function and the patient's clinical status. Newer methods of assessing MR severity show promise, e.g., 3D echocardiography and power Doppler imaging, but are not yet routinely used in clinical practice (Fig. 34; please *see* companion DVD for corresponding video).

SURGICAL CONSIDERATIONS IN MR

Anatomical Mechanisms of MR

Precise determination of the mechanism of MR results is necessary for successful reconstructive surgery of the mitral valve. Thus, the Carpentier's functional classification is often used (Fig. 35).

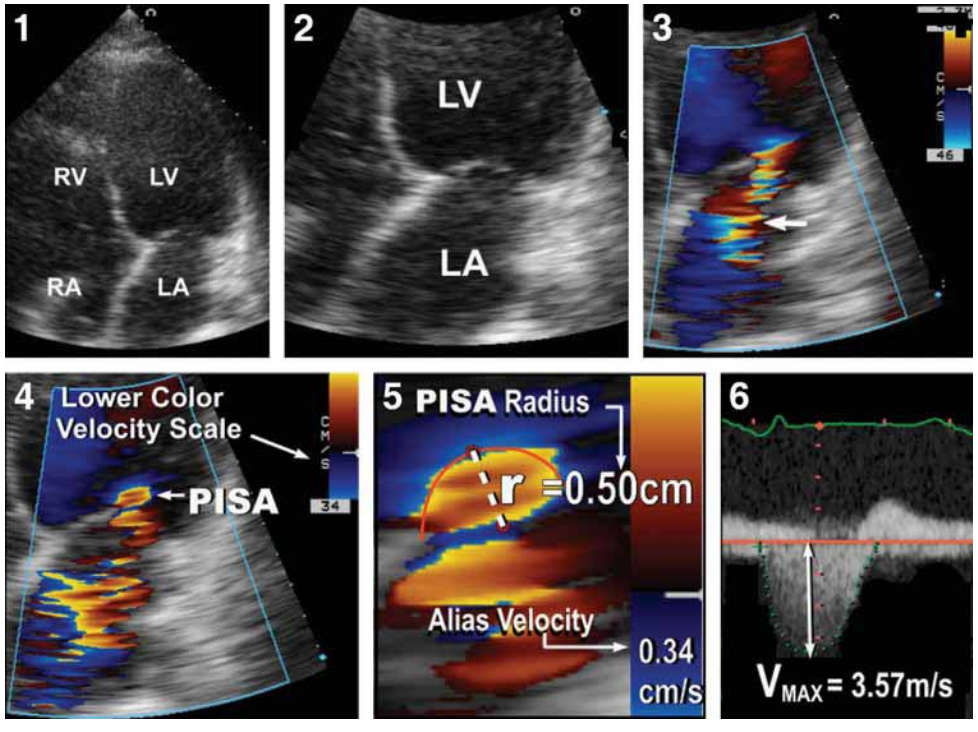

Fig. 25. Mitral regurgitation severity: proximal isovelocity surface area (PISA) method. Step 1: select the best apical four-chamber view (A4C) to indentify the region of interest—the regurgitant mitral valve (panel 1). Step 2: lower imaging depth, then zoom (panel 2). Step 3: apply color Doppler, then narrow color sector scan (panel 3). Step 4: shift color flow baseline on color Doppler scale downward (to lower Nyquist limit) to approx 40 cm/s. This optimizes the aliasing velocities enables the PISA hemispheric zone bigger and more measurable (panel 4). Step 5: record the Nyquist limit on the color Doppler Scale. This is the aliasing velocity of the PISA. Scroll through cine loop and optimize largest PISA (mid-systole) and measure radius (panel 5). Step 6: obtain the maximum velocity across the mitral regurgitation jet using continuous-wave Doppler (panel 6). (Please *see* companion DVD for corresponding video.)

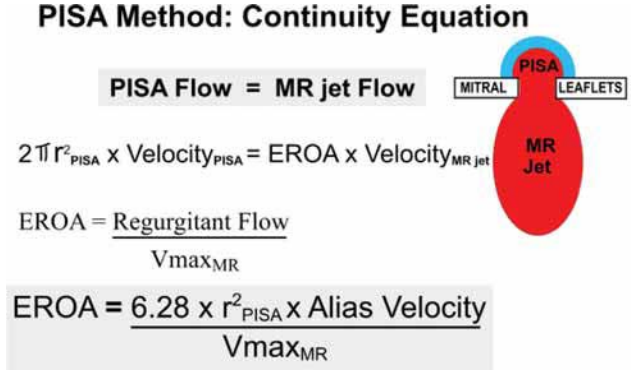

Fig. 26. Proximal isovelocity surface area (PISA) method: calculation of effective regurgitant orifice area (EROA) by the continuity equation. The PISA method is used to calculate the EROA according to the principle of conservation of mass. The continuity equation is used to calculate the EROA from the variables measured in Fig. 25.

Carpentier's Functional Approach to Mitral Regurgitation

The Carpentier functional classification of MR is based on the opening and closing motions of both leaflets. Normal mitral leaflet coaptation requires coordination of many structures including a normal-sized LV and a chordal apparatus that is not calcified and is well tethered to the mitral leaflets that coapt well (Fig. 35).

Functional Classification: Type I

MR that occurs despite normal leaflet motion is termed type I MR. This can be owing to annular dilatation seen

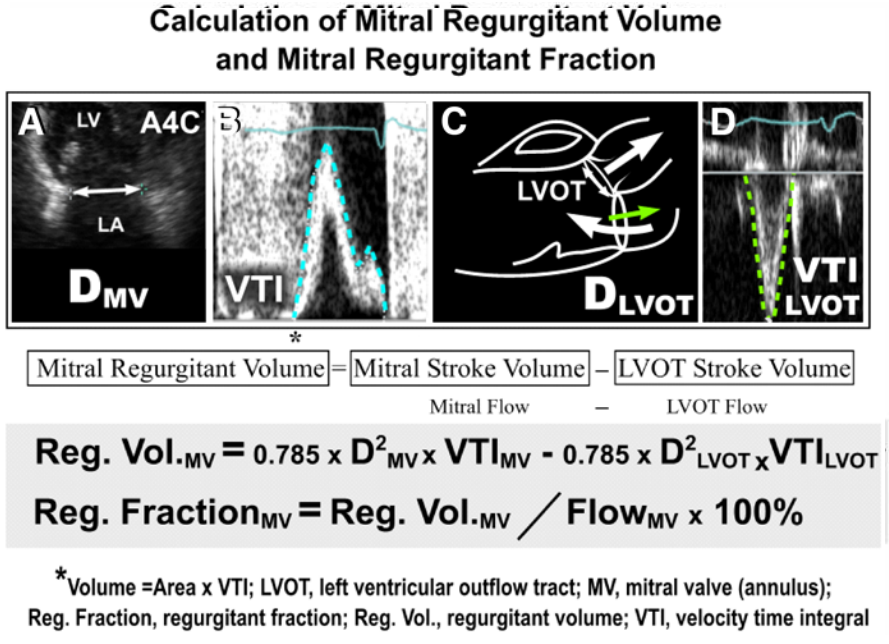

Fig. 27. Regurgitant volume and regurgitant fraction.

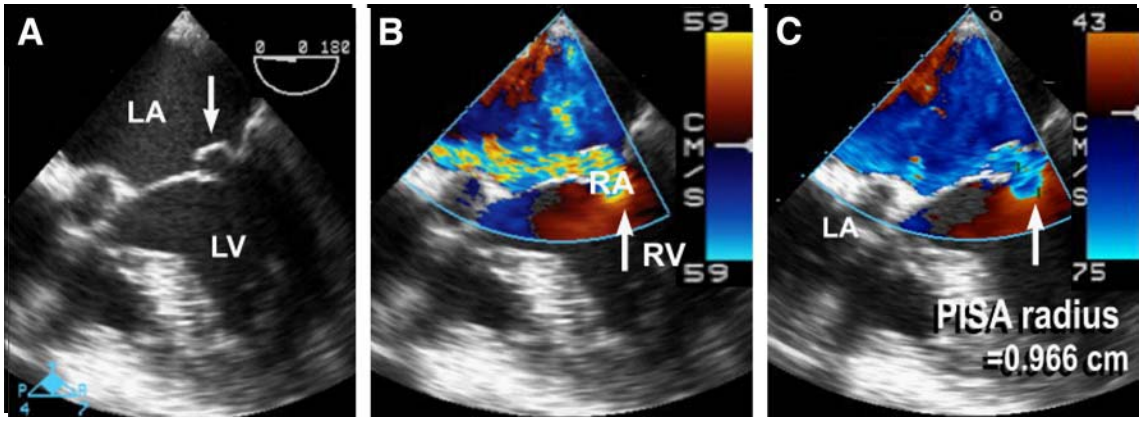

Fig. 28. (A) Transesophageal echocardiography (TEE) midesophageal view at omniplane 0° showing partial flail of posterior mitral valve leaflet. **(B)** Color Doppler imaging shows severe mitral regurgitation with proximal convergence zone with an anteriorly directed jet. Color Doppler scale set at 59 cm/s. **(C)** Color Doppler scale is then shifted upward (on TEE) to 43 cm/s showing clearly defined proximal isovelocity surface area (PISA) measuring 0.966 cm, consistent with severe mitral regurgitation.

Table 10
PISA Assumptions and Pitfalls

- Accurate measurements (subject to error, errors are squared, interobserver variability)
- Unconstrained flow (constrainment exists)
- Circular point-like orifice (regurgitant orifice irregular, often "smiley" shaped)
- Flat regurgitant orifice (actual orifice not flat)
- PISA is a hemisphere (PISA is more a hemi-ellipse)
- Constant orifice (PISA calculation is an instantaneous measurement, but PISA—like the cardiac cycle—is dynamic)
- PISA method not suitable for eccentric jets, or concomitant mitral stenosis

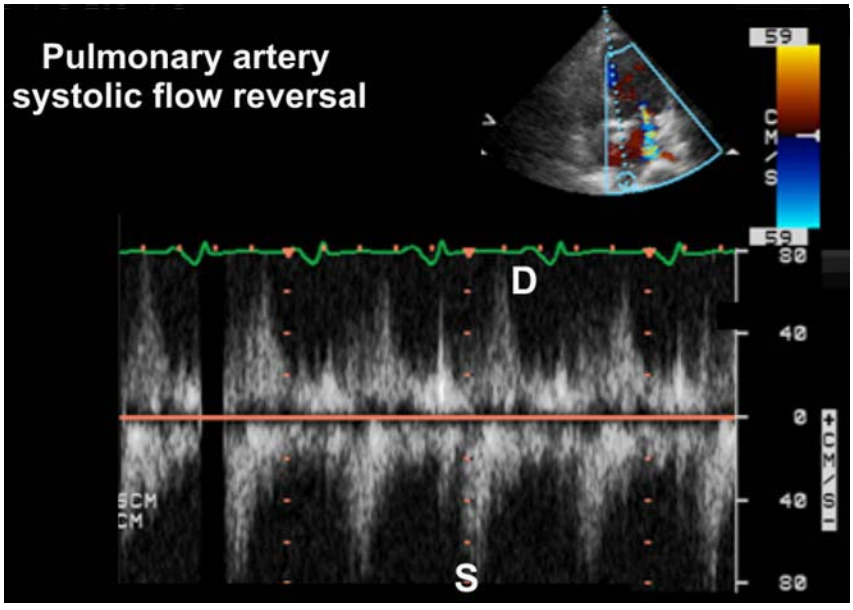

Fig. 29. Pulmonary vein systolic flow reversal. Pulsed Doppler examination right upper pulmonary vein flow in severe mitral regurgitation shows reversal of pulmonary vein systolic flow, as depicted by the negative S-wave.

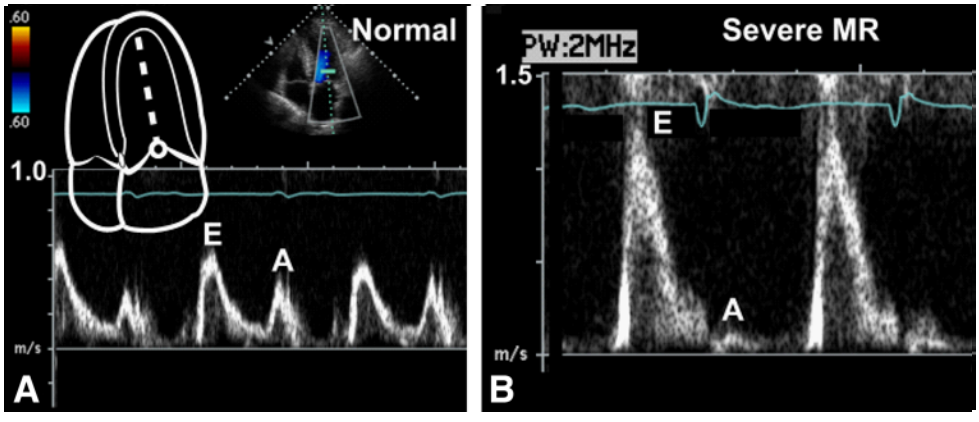

Fig. 30. Mitral E-point velocity. **(A)** Pulsed Doppler of normal mitral inflow characteristically shows an early diastolic E-wave followed by the atrial A wave. **(B)** In severe mitral regurgitation (MR), marked E-wave dominance is seen (>1.2 m/s), reflecting a marked increased in early diastolic flow—typical of severe MR.

in cardiomyopathy. With cardiomyopathy, the annulus becomes dilated and the exoskeleton of the LV becomes stretched. Despite preserved leaflet motion, the leaflets are unable to coapt because of the incompetent architecture of the LV and annulus. This often results in a central jet of MR (Figs. 8 and 9). Another etiology of MR despite preserved leaflet motion is leaflet perforation, as a sequelae of endocarditis.

Functional Classification: Type II

Type II regurgitation refers to MR that occurs because of leaflet prolapse. This may be owing to simple elongation of the leaflets, with prolapse into the left atrium. This may be owing to chordal rupture or papillary muscle rupture. An example of chordal rupture is shown in Fig. 35.

Functional Classification: Type IIIa Restricted Leaflet Motion

Valvular and subvalvular thickening can restrict mitral leaflet motion. Mitral annular calcification and thickening of the subvalvular apparatus are seen with increasing age, or as the sequelae of rheumatic heart disease. The resulting poor coaptation results in MR.

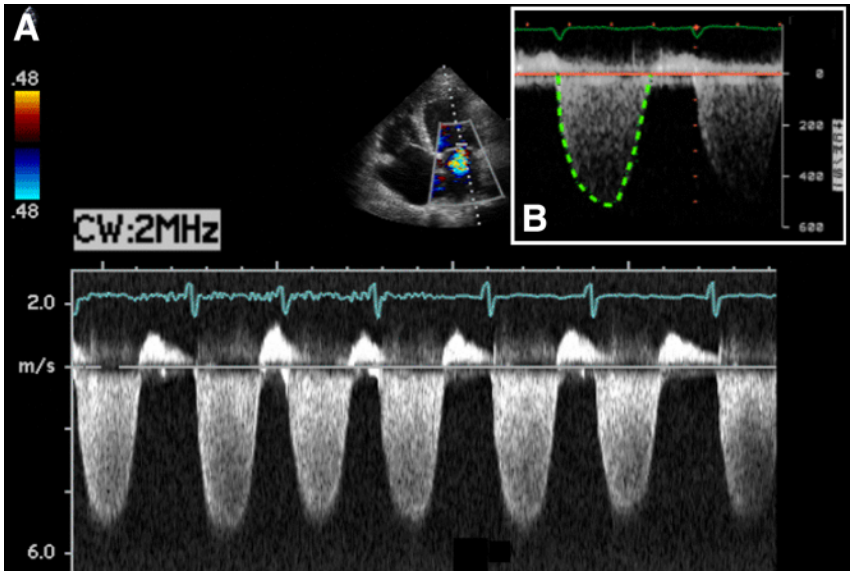

Fig. 31. Continuous-wave (CW) Doppler intensity. CW Doppler envelopes showing a higher intensity signal in moderate-to-severe regurgitation (**A**) compared to mild mitral regurgitation (**B**). Compare these densities to the antegrade (mitral inflow) signals above the baseline.

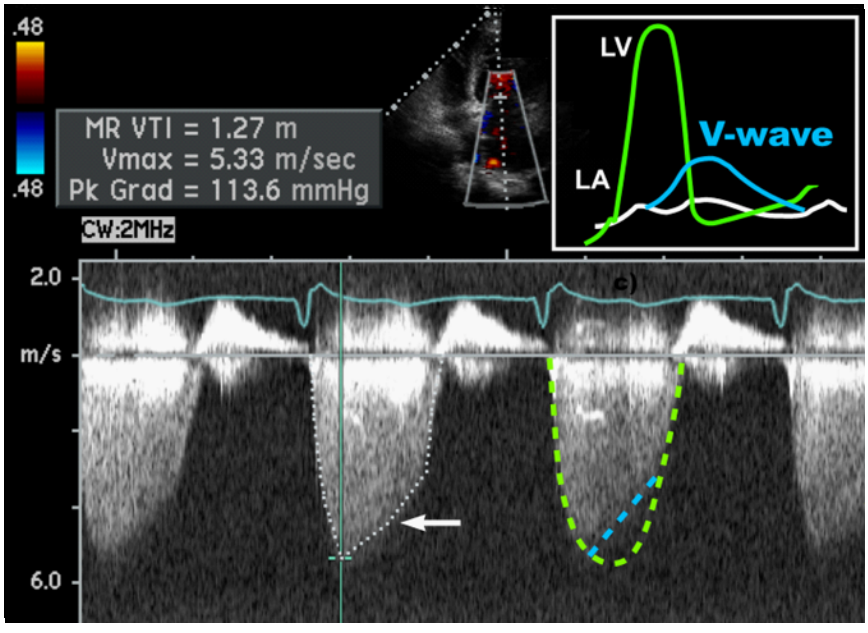

Fig. 32. Continuous-wave (CW) Jet with V-wave. Notching of the CW envelope can occur in severe mitral regurgitation, a reflection of the large atrial V-wave (insert). Left ventricular systolic performance (dP/dT).

Fig. 35 shows an example of such thickening of the valvular and subvalvular apparatus.

Functional Classification: Type IIIb Restricted Leaflet Motion

When leaflet motion is restricted, with displacement of the papillary muscles, this is referred to as type IIIb MR. The most common culprit is a dilated cardiomyopathy, where enlargement of LV chambers are accompanied by elongation of the papillary muscles and displacement of such muscles to the apex, relative to the mitral valve leaflets. Figure 35 shows such a schema and still frame of an enlarged LV and downwardly displaced papillary muscles. The resulting mitral valve incompetence often results in a centrally directed jet of MR.

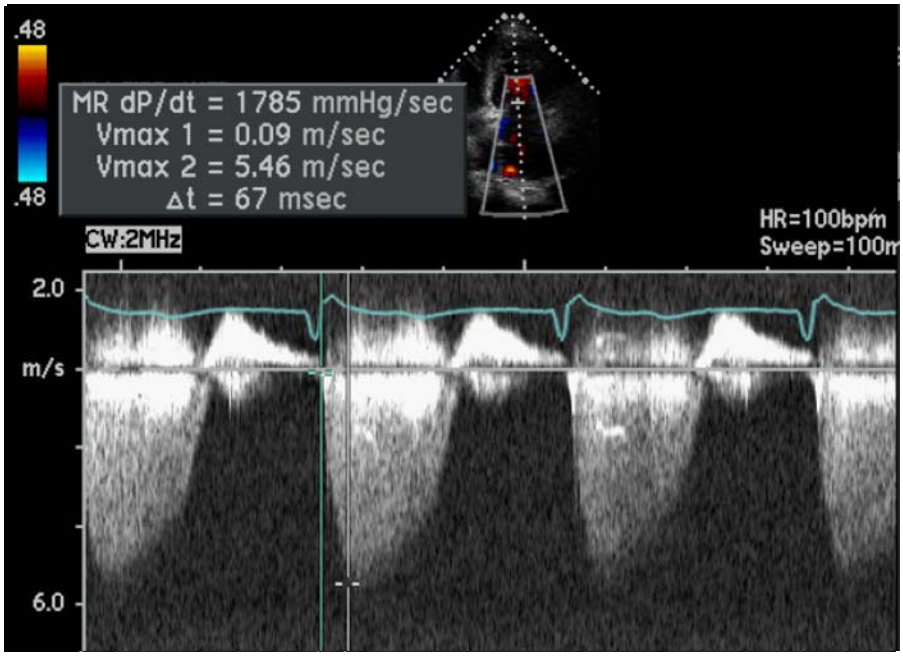

Fig. 33. Left ventricular systolic performance (dP/dT). During isovolumetric contraction, the rate of rise of left ventricular pressure (dP/dT) is a useful index of ventricular contractility. It may predict postoperative left ventricle function in patients with severe mitral regurgitation.

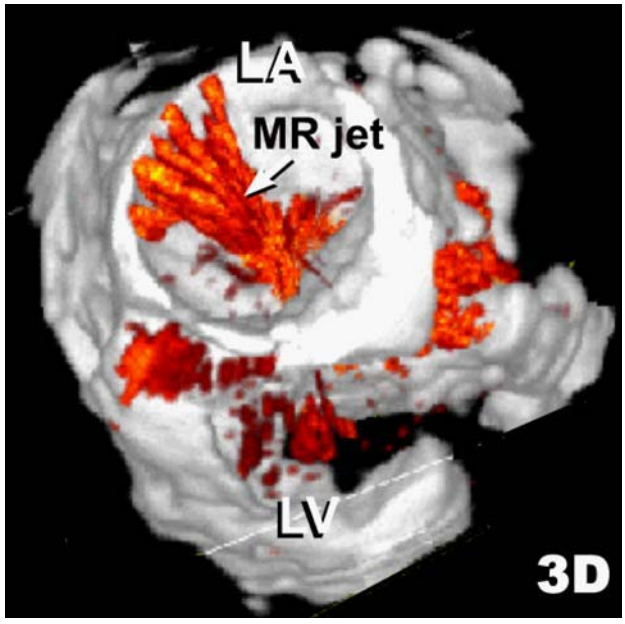

Fig. 34. Three-dimensional image acquisition of eccentric mitral regurgitant jet on transesophageal echocardiography. (Image courtesy of Michael D'Ambra, MD, Cardiothoracic Anesthesia, Brigham and Women's Hospital.) (Please *see* companion DVD for corresponding video.)

Valve Analysis

In patients with severe MR who are referred for surgical repair, it is important to delineate the anatomy of the anterior and posterior leaflets. During surgery, valve exposure is often performed by dissection of the interatrial groove, and left atriotomy; in difficult cases, a transseptal approach through the right atrium into the LA is taken. The valve is visualized looking down from the left atrium toward the LV during surgery, as shown in Figs. 1 and 2. Because this is the visual field in which any surgical repair will take place, it is helpful for the surgeon to map out mitral valve pathology from this view (Fig. 36). Looking down from the LA toward the LV, there are three scallops to each mitral valve leaflet. For orientation, one notes that the anterior leaflet faces the aorta. A commonly used nomenclature divides the anterior leaflet into A1, A2, A3 and the posterior leaflet into P1, P2, P3, with the numbering beginning at the anterolateral commissure and progressing toward the posteromedial commissure (Fig. 1B).

A great advance in mitral valve mapping has been the use of multiplanar TEE—both before referring patients to surgery and intra-operatively (*see* Chapter 23).

CASE PRESENTATION 6: POST-MITRAL VALVE SURGERY

This 84-yr-old woman presented with heart failure 14 yr after coronary artery bypass surgery and mitral valve replacement with a porcine bioprosthesis (Fig. 37; please *see* companion DVD for corresponding video).

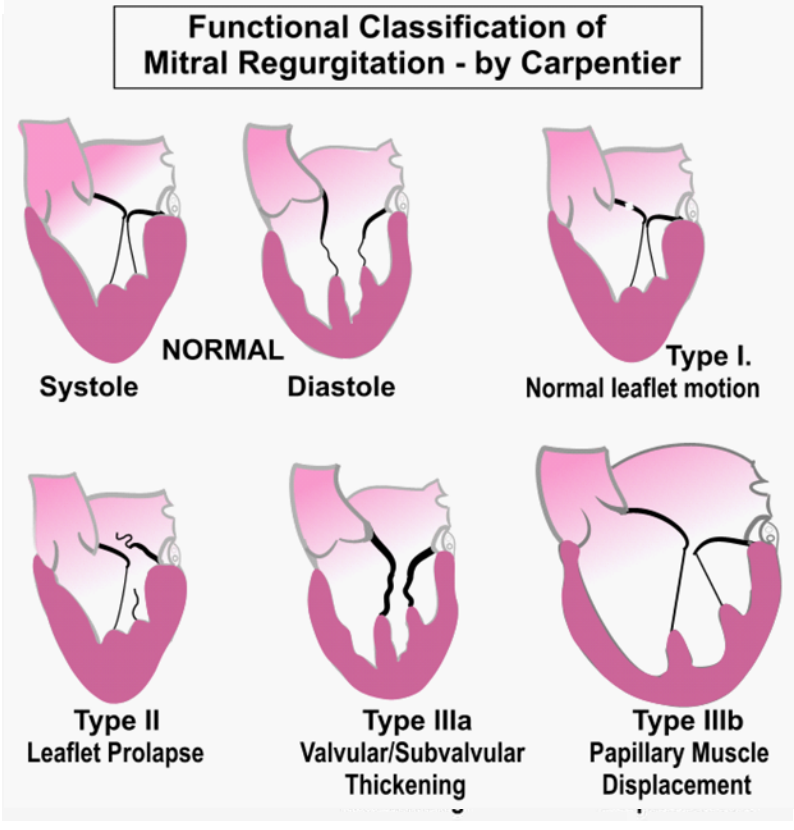

Fig. 35. Functional classification of mitral regurgitation (by Carpentier). (Figure courtesy of Dr. David Adams, Mount Sinai Medical Center, New York, NY.)

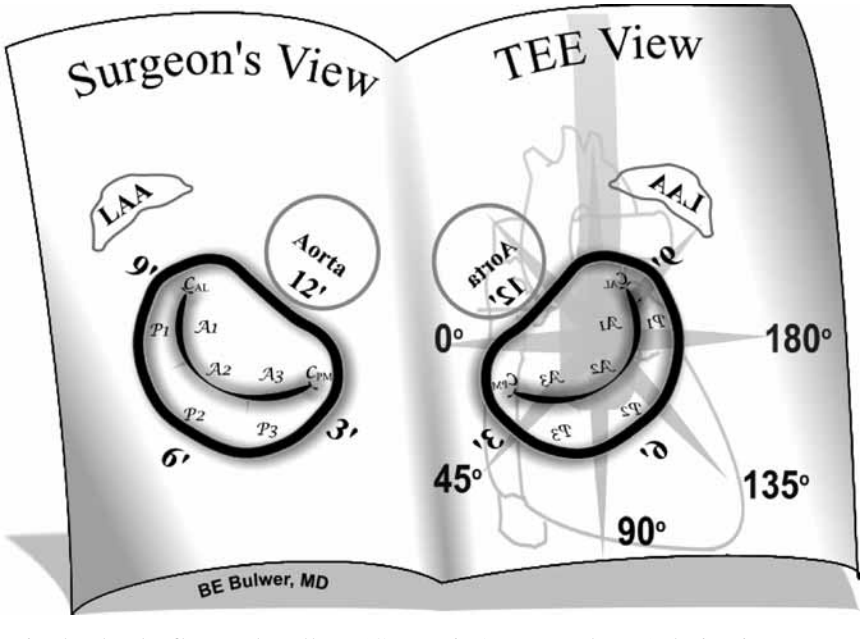

Fig. 36. Orientation of mitral valve leaflets and scallops (Carpentier's nomenclature) during intra-operative (TEE) echocardiography. The aorta is assigned the 12 o'clock position, the commissures—at the 3 o'clock and 9 o'clock positions as shown. The left atrial appendage (LAA) at the 9 o'clock/antero-lateral commissure position. The TEE operator's view is the mirror-image of the surgeon's view.

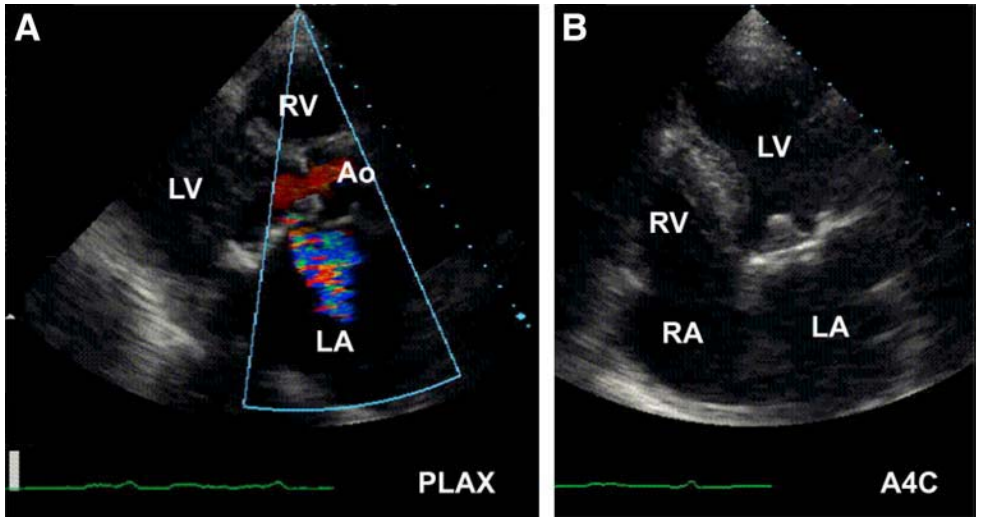

Fig. 37. A 84-yr-old woman after coronary artery bypass grafting and 14 yr status after porcine mitral valve replacement with congestive heart failure. (Please *see* companion DVD for corresponding video.)

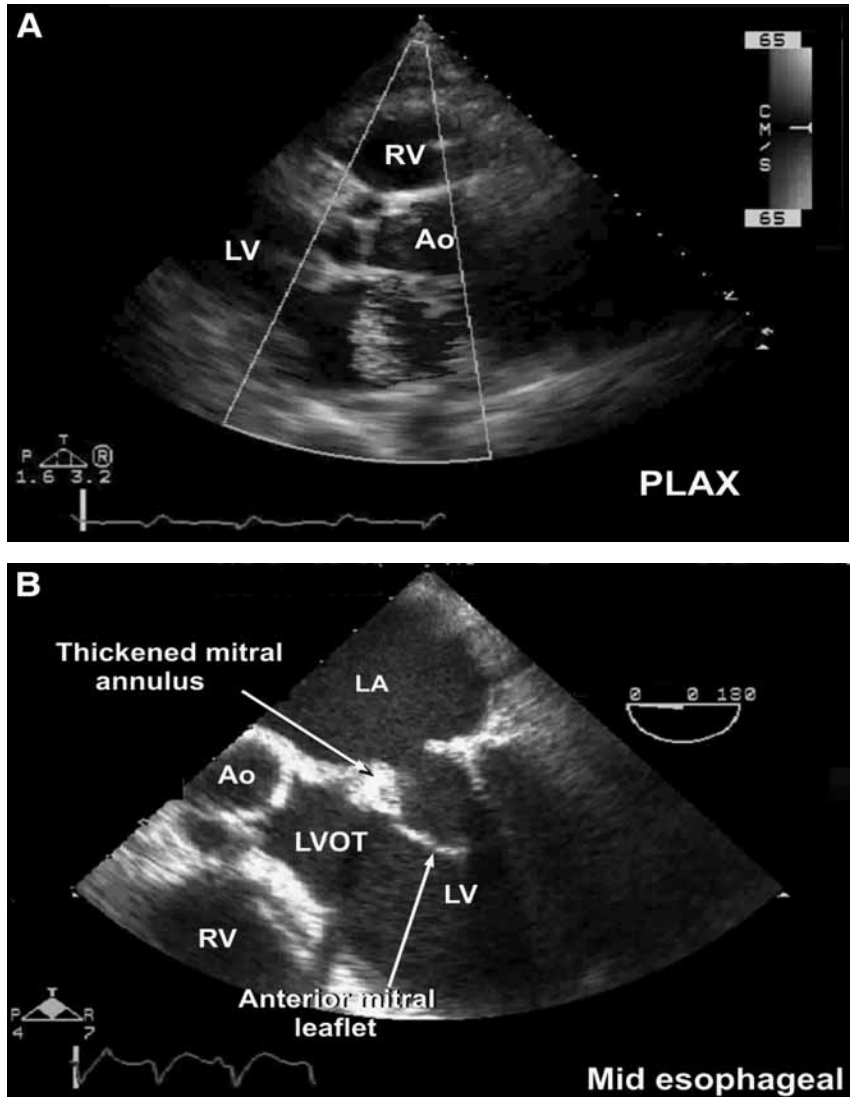

Fig. 38. A 72-yr-old man 2 wk after coronary artery bypass graft mitral valve repair, left ventricle aneurysm resection.

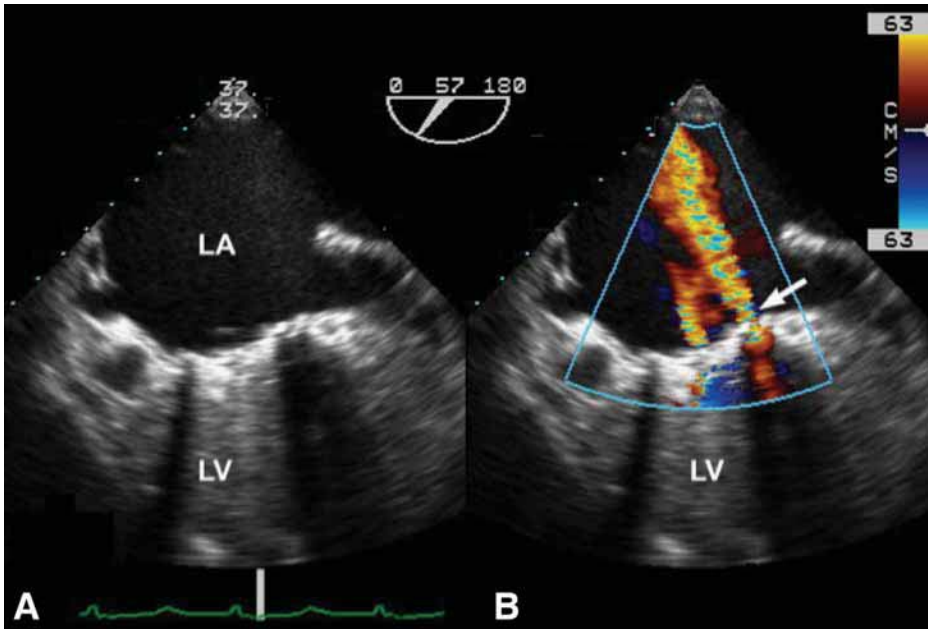

Fig. 39. Prosthetic mitral valve: paravalvular leak. Prosthetic mitral valve dysfunction leading to prosthetic mitral regurgitation can occur secondary to thrombus formation or pannus ingrowth that can interfere with normal valve closure. This is most often seen with mechanical valves compared to bioprosthetic valves. The most common type of regurgitation following mitral valve replacement is owing to a paravalvular leak which occurs outside the sewing ring. The nature and severity of the paravalular regurgitation can be detected on transthoracic echocardiography, but transesophageal echocardiography is necessary to map the extent of the dehiscence, which may be crescent-shaped and guide surgical repair. (Please *see* companion DVD for corresponding video.)

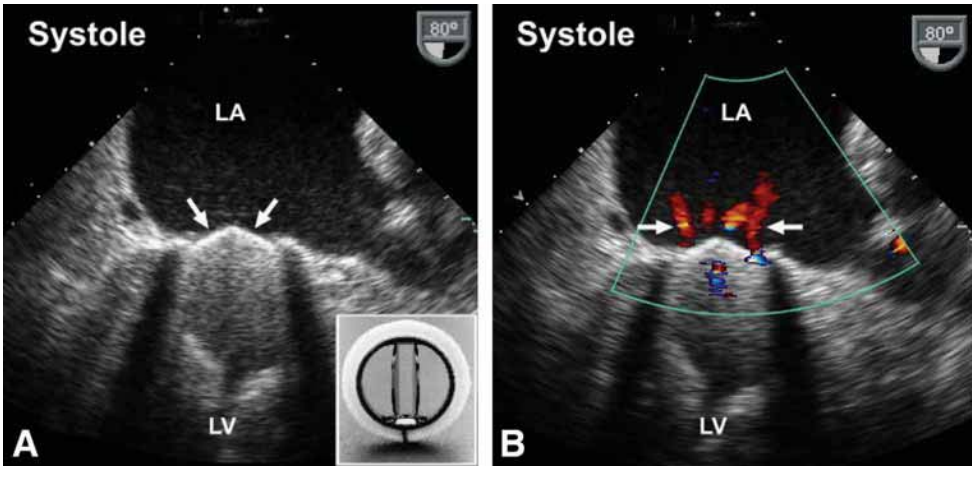

Fig. 40. Prosthetic mitral valve: normal signature regurgitation. Midesophageal two-chamber view showing St. Jude bileaflet prosthesis during systole at omniplane 80°. Normal leaflet appearance in closed position (arrows, **A**) with normal acoustic shadow pattern and reverbertion seen within left ventricular cavity. St. Jude valve with leaflets in open position is show in insert **A**. The two tiny jets of mitral regurgitation (arrows, **B**) seen at in this midesophageal two-chamber view are "signature MR" of normal functioning St. Jude mitral valve prosthesis. Other prosthetic valves have their own normal signature mitral regurgitations. They do not indicate prosthetic valve dysfunction.

These images illustrate a common complication after mitral valve surgery. Transthoracic images and subsequent transesophageal images confirm moderate to severe MR because of a paravalvular leak and dehiscence of a bioprothetic valve. Color flow doppler now illustrate that some of the regurgitation occurs outside of the struts of the porcine mitral valve. Superimposed on a central jet of MR is the regurgitant jet resulting from a paravalvular leak with dehiscence.

CASE PRESENTATION 7: MITRAL REGURGITATION ENDOCARDITIS

This 72-yr-old man had coronary artery bypass surgery, mitral valve repair and LV aneurysm resection. Fourteen days after surgery, he was still in the intensive care unit with signs of heart failure and low-grade temperatures, despite no evidence of bacteremia (Fig. 38).

Transthoracic images demonstrate a mitral regurgitant jet that appears to originate from outside the ring annulus. Transesophageal images reveal a thick mass on the anterior mitral leaflet. When this patient was brought back to the operating room, the sutures were noted to be incompetent. No vegetations were seen. The ring, coiled and loosened from its original points of attachment, resulted in a mass-like appearance on the anterior mitral valve leaflet, and MR.

CASE PRESENTATION 8: STATUS-POST MITRAL VALVE REPLACEMENT

This 56-yr-old man had mitral valve replacement 1 yr earlier, but was discovered to have a new MR murmur (Fig. 39; please *see* companion DVD for corresponding video).

Mitral valve mapping has an important application in the evaluation of prosthetic valves. Mapping of the regurgitant jet on TEE revealed a crescent-shaped dehiscence. Prosthetic valves normally demonstrate a small jet(s) that are characteristic of each model (Fig. 40). Such "signature" regurgitations are clinically insignificant.

SUGGESTED READING

Aklog L, Filsoufi F, Flores KQ, et al. Does coronary artery bypass grafting alone correct moderate ischemic mitral regurgitation? Circulation 2001;104:I68–I75.

Ballester M, Jajoo J, Rees S, Rickards A, McDonald L. The mechanism of mitral regurgitation in dilated left ventricle. Clin Cardiol 1983;6:333–338.

Bonow RO, Carabello B, de LA Jr, et al. Guidelines for the management of patients with valvular heart disease: executive summary; areport of the American College of Cardiology/ American Heart Association Task Force on Practice Guidelines (Committee on Management of Patients with Valvular Heart Disease). Circulation 1998;98:1949–1984.

Cape EG, Skoufis EG, Weyman AE, Yoganathan AP, Levine RA. A new method for noninvasive quantification of valvular regurgitation based on conservation of momentum: in vitro validation. Circulation 1989;79:1343–1353.

Cape EG, Yoganathan AP, Levine RA. Increased heart rate can cause underestimation of regurgitant jet size by Doppler color flow mapping. J Am Coll Cardiol 1993;21:1029–1037.

Cape EG, Yoganathan AP, Weyman AE, Levine RA. Adjacent solid boundaries alter the size of regurgitant jets on Doppler color flow maps. J Am Coll Cardiol 1991;17:1094–1102.

Carabello BA, Crawford FA Jr. Valvular heart disease. N Engl J Med 1997;337:32–41.

Carabello BA. Progress in mitral and aortic regurgitation. Curr Probl Cardiol 2003;28:553.

Chen C, Rodriguez L, Lethor JP, et al. Continuous wave Doppler echocardiography for noninvasive assessment of left ventricular dP/dt and relaxation time constant from mitral regurgitant spectra in patients. J Am Coll Cardiol 1994;23:970– 976.

Chen C, Thomas JD, Anconina J, et al. Impact of impinging wall jet on color Doppler quantification of mitral regurgitation. Circulation 1991;84:712–720.

Dujardin KS, Enriquez-Sarano M, Bailey KR, Nishimura RA, Seward JB, Tajik AJ. Grading of mitral regurgitation by quantitative Doppler echocardiography: calibration by left ventricular angiography in routine clinical practice. Circulation 1997;96: 3409–3415.

Enriquez-Sarano M, Avierinos J-F, Messika-Zeitoun D, et al. Quantitative determinants of the outcome of asymptomatic mitral regurgitation. N Engl J Med 2005;352:875–883.

Enriquez-Sarano M, Bailey KR, Seward JB, Tajik AJ, Krohn MJ, Mays JM. Quantitative Doppler assessment of valvular regurgitation. Circulation 1993;87:841–848.

Enriquez-Sarano M, Seward JB, Bailey KR, Tajik AJ. Effective regurgitant orifice area: a noninvasive Doppler development of an old hemodynamic concept. J Am Coll Cardiol 1994;23:443–451.

Enriquez-Sarano M, Tajik AJ, Bailey KR, Seward JB. Color flow imaging compared with quantitative Doppler assessment of severity of mitral regurgitation: influence of eccentricity of jet and mechanism of regurgitation. J Am Coll Cardiol 1993; 21:1211–1229.

Foster GP, Isselbacher EM, Rose GA, Torchiana DF, Akins CW, Picard MH. Accurate localization of mitral regurgitant defects using multiplane transesophageal echocardiography. Ann Thorac Surg 1998;65:1025–1031.

Freed LA, Levy D, Levine RA, et al. Prevalence and clinical outcome of mitral-valve prolapse.N Engl J Med 1999;341:1–7.

Freeman WK, Schaff HV, Khandheria BK, et al. Intraoperative evaluation of mitral valve regurgitation and repair by transesophageal echocardiography: incidence and significance of systolic anterior motion. J Am Coll Cardiol 1992; 20:599.

Haffajee CI. Chronic mitral regurgitation. In: Dalen JE, Alpert JS, eds. Valvular Heart Disease. 2nd ed. Boston: Little, Brown, and Co, 1987:112.

Hall SA, Brickner ME, Willett DL, Irani WN, Afridi I, Grayburn PA. Assessment of mitral regurgitation severity by Doppler color flow mapping of the vena contracta. Circulation 1997;95:636–642.

Heinle SK, Hall SA, Brickner ME, Willett DL, Grayburn PA. Comparison of vena contracta width by multiplane transesophageal echocardiography with quantitative Doppler assessment of mitral regurgitation. Am J Cardiol 1998;81: 175–179.

Helmcke F, Nanda NC, Hsiung MC, et al. Color Doppler assessment of mitral regurgitation with orthogonal planes. Circulation 1987;75:175–183.

Jutzy KR, Al-Zaibag M. Acute mitral and aortic valve regurgitation. In: Al-Zaibag M, Duran CMG, eds. Valvular Heart Disease. New York: Marcel Dekker, 1994:342–382.

Lamas GA, Mitchell GF, Flaker GC, et al. Clinical significance of mitral regurgitation after acute myocardial infarction. Survival and Ventricular Enlargement Investigators. Circulation 1997;96:827–833.

Lambert AS, Miller JP, Merrick SH, et al. Improved evaluation of the location and mechanism of mitral valve regurgitation with a systematic transesophageal echocardiography examination. Anesth Analg 1999;88:1205–1212.

Lester SJ, Ryan EW, Schiller NB, Foster E. Best method in clinical practice and in research studies to determine left atrial size. Am J Cardiol 1999;84:829–832.

McQuillan BM, Weyman AE. Severe mitral regurgitation secondary to partial papillary muscle rupture following myocardial infarction. Rev Cardiovasc Med 2000;1:57–60.

Mele D, Schwammenthal E, Torp H, et al. A semiautomated objective technique for applying the proximal isovelocity surface area method to quantitate mitral regurgitation: clinical studies with the digital flow map. Am Heart J 2001;141: 653–660.

Mele D, Vandervoort P, Palacios I, et al. Proximal jet size by Doppler color flow mapping predicts severity of mitral regurgitation: clinical studies. Circulation 1995;91:746–754.

Otto CM. Mitral Regurgitation. In: Otto CM, ed. Valvular HeartDdisease, 2nd ed. Philadelphia: Saunders, 2004:336–367.

Playford D, Weyman AE. Mitral valve prolapse: time for a fresh look. Rev Cardiovasc Med 2001;2:73–81.

Rokey R, Sterling LL, Zoghbi WA, et al. Determination of regurgitant fraction in isolated mitral or aortic regurgitation by pulsed Doppler two-dimensional echocardiography. J Am Coll Cardiol 1986;7:1273–1278.

Rossi A, Cicoira M, Golia G, Anselmi M, Zardini P. Mitral regurgitation and left ventricular diastolic dysfunction similarly affect mitral and pulmonary vein flow Doppler parameters: the advantage of end-diastolic markers. J Am Soc Echocardiogr 2001;14:562–568.

Sahn DJ. Instrumentation and physical factors related to visualization of stenotic and regurgitant jets by Doppler color flow mapping. J Am Coll Cardiol 1988;12:1354–1365.

Saiki Y, Kasegawa H, Kawase M, et al. Intraoperative TEE during mitral valve repair: does it predict early and late postoperative mitral valve dysfunction? Ann Thorac Surg 1998;66:1277.

Schiller NB, Shah PM, Crawford M, et al. Recommendations for quantitation of the left ventricle by two-dimensional echocardiography: American Society of Echocardiography Committee on Standards, Subcommittee on Quantitation of Two-Dimensional Echocardiograms. J Am Soc Echocardiogr 1989;2:358–367.

Schiller NB, Foster E, Redberg RF. Transesophageal echocardiography in the evaluation of mitral regurgitation. The twenty-four signs of severe mitral regurgitation. Cardiol Clin 1993;11:399.

Schwammenthal E, Chen C, Benning F, Block M, Breithardt G, Levine RA. Dynamics of mitral regurgitant flow and orifice area: physiological application of the proximal flow convergence method; clinical data and experimental testing. Circulation 1994;90:307–322.

Schwammenthal E, Chen C, Giesler M, et al. New method for accurate calculation of regurgitant flow rate based on analysis of Doppler color flow maps of the proximal flow field: validation in a canine model of mitral regurgitation with initial application in patients. J Am Coll Cardiol 1996;27: 161–172.

Stewart WJ, Currie PJ, Salcedo EE, et al. Intraoperative Doppler color flow mapping for decision-making in valve repair for mitral regurgitation: technique and results in 100 patients. Circulation 1990;81:556–566.

Stewart WJ, Salcedo EE, Cosgrove DM. The value of echocardiography in mitral valve repair. Cleve Clin J Med 1991;58:177–183.

Thomas JD, Liu CM, Flachskampf FA, O'Shea JP, Davidoff R, Weyman AE. Quantification of jet flow by momentum analysis: an in vitro color Doppler flow study. Circulation 1990;81:247–259.

Thomas L, Foster E, Hoffman JI, Schiller NB. The Mitral Regurgitation Index: an echocardiographic guide to severity. J Am Coll Cardiol 1999;33:2016–2022.

Thomas L, Foster E, Schiller NB. Peak mitral inflow velocity predicts mitral regurgitation severity. J Am Coll Cardiol 1998;31:174–179.

Tribouilloy C, Shen WF, Quere JP, et al. Assessment of severity of mitral regurgitation by measuring regurgitant jet width at its origin with transesophageal Doppler color flow imaging. Circulation 1992;85:1248–1253.

Wang Y, Gutman JM, Heilbron D, Wahr D, Schiller NB. Atrial volume in a normal adult population by two-dimensional echocardiography. Chest 1984;86:595–601.

Yoshida K, Yoshikawa J, Shakudo M, et al. Color Doppler evaluation of valvular regurgitation in normal subjects. Circulation 1988;78:840–847.

Zoghbi WA, Enriquez-Sarano M, Foster E, et al. American Society of Echocardiography. Recommendations for evaluation of the severity of native valvular regurgitation with two-dimensional and Doppler echocardiography. J Am Soc Echocardiogr 2003; 16:777–802.

15 Infective Endocarditis

Nagesh S. Anavekar, MD, Marcus Averbach, MD, and Bernard E. Bulwer, MD, MSc

Contents

CASE PRESENTATION 1

Clinical History

A 43-yr-old female with a past history of obesity, hypertension, and smoking was admitted with acute inferior myocardial infarction and underwent cardiac catheterization and balloon angioplasty with intracoronary stenting for blockage to her right coronary artery.

Over the following week she experienced pleuritic chest pains that went largely ignored until chills and fever ensued. She was admitted 10 d later with a working diagnosis of pericarditis. Blood cultures were positive for *Staphyloccus aureus*. Shortly after admission, she developed acute respiratory distress, severe metabolic acidosis, rapid atrial fibrillation followed by acute heart block, coagulopathy, and anuria.

Echocardiography

Emergency transthoracic echocardiogram revealed a circumferential pericardial effusion (but no tamponade) and new onset severe aortic insufficiency. No valvular vegetations were seen (Fig. 1). Transesophageal echocardiography (TEE) was requested but she was immediately whisked to the operating room for emergency surgery. The working diagnosis was aortic valve endocarditis complicated by a paravalvular abscess with involvement of her cardiac conduction system.

Surgical Findings

Inspection of the aortic valve at surgery revealed partial destruction and prolapse of the right and noncoronary cusps along with a contained rupture of the aortic root owing to an abscess cavity. The abscess had eroded into the interventricular septum causing complete heart block and a ventricular septal defect. Aortic valve replacement with a homograft valve, aortic root replacement, and repair of the ventricular septal defect using a pericardial patch were carried out. The patient never fully recovered, and she expired 2 d later. Autopsy confirmed the surgeon's findings (Fig. 2). Fibrinous pericarditis, cardiomegaly, and a friable thrombus on the adventitial aspect of the homograft were also noted.

From: *Contemporary Cardiology: Essential Echocardiography: A Practical Handbook With DVD*
Edited by: S. D. Solomon © Humana Press, Totowa, NJ

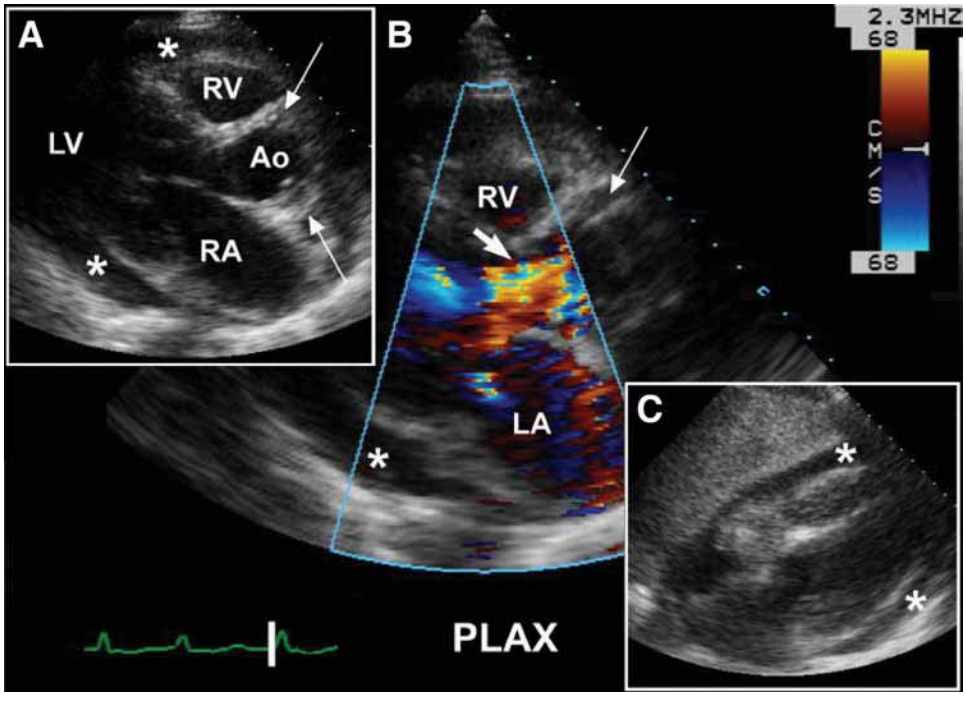

Fig. 1. A 43-yr-old woman admitted with fever, septicemia, and pleuritic chest pain. The peri-aortic soft tissues (fine arrows) appear thickened. The aortic leaflets were barely visible on parasternal long axis (PLAX) views, but wide-open aortic regurgitation (arrow) was noted on Color flow Doppler **(A**,**B)**. PLAX views showed a circumferential pericardial effusion (asterisks).

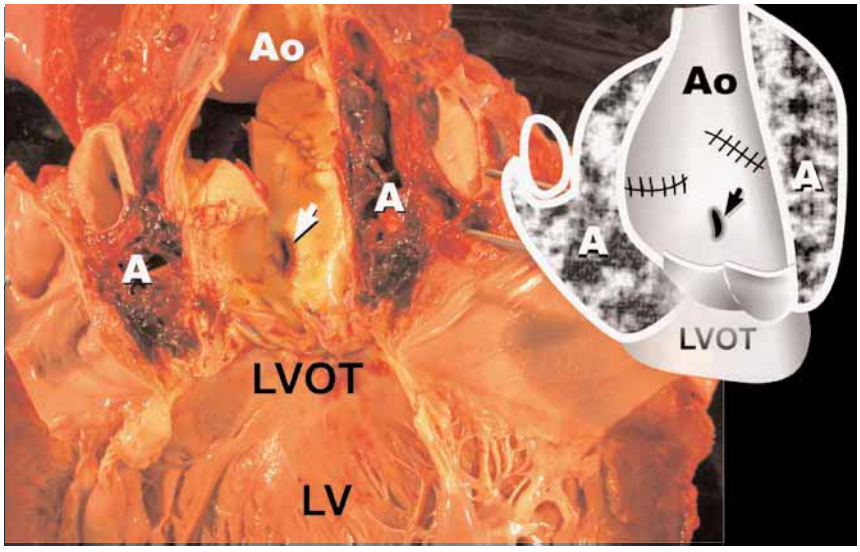

Fig. 2. Infective endocarditis: peri-aortic abscess. *See* Case 1 for description.

INTRODUCTION

Infective endocarditis (IE) is a microbial infection of the endothelial lining of the heart, most commonly involving the valves. Infection may also occur at the site of a septal defect, chordae tendinae, or mural endocardium. The diagnosis of IE is made on the basis of a combination of clinical, echocardiographic and pathological features using the modified Duke criteria (Table 1). Echocardiography features prominently in the diagnosis and follow-up of IE.

Damage to the endothelial surface of the valves or mural endocardium facilitates spontaneous platelet-fibrin deposition, giving rise to nonbacterial thrombotic

Table 1A
Modified Duke Criteria for the Diagnosis of Infective Endocarditis

Major criteria

Blood cultures positive for infective endocarditis

Positive blood cultures for typical organisms

IE isolated from two separate blood cultures:

Viridans streptococci, *Streptococcus bovis, Staphylococcus aureus*

HACEK group, Enterococci (in the absence of a primary focus)

Persistently positive blood cultures: recovery of microorganisms consistent with IE isolated from:

≥2 positive blood cultures >12 h apart

≥3 positive cultures of blood, the 1st and the last sample >1 h apart

Single blood culture for *Coxiella burnetii*

Antiphase I IgG antibody titer of >1:800

Evidence of endocardial involvement

Positive Echocardiogram for IE (transesphageal echocardiography recommended for prosthetic valve, possible infective endocarditis by clinical criteria, or complicated IE [i.e., a paravalvular abscess])

Oscillating intracardiac mass (vegetation) on the valve or supporting structures in the path of regurgitant jets or on implanted material in the absence of an alternative anatomic explanation

Abscess

New partial dehiscence of a valvular prosthesis

New valvular regurgitation (worsening or changing pre-existing murmur not sufficient)

HACEK, *Haemophilus* species (*H. aprophilus* and *H. paraaphrophilus*), *Actinobacillus actinoinycetemcomitans*, *Cardiobacterium hominis*, *Eikenella corrodens*, and *Kingella kingae*.

Table 1B
Modified Duke Criteria for the Diagnosis of Infective Endocarditis

Minor criteria

- Predisposing heart disease or injection drug use
- Temperature of >38°C (100.4°F)
- Vascular phenomenon:
  - Major arterial emboli
  - Septic pulmonary infarcts
  - Mycotic aneurysm
  - Intracranial or conjunctival hemorrhage
  - Janeway's lesions
- Immunological phenomenon:
  - Glomerulonephritis
  - Osler's nodes
  - Roth's spots
  - Rheumatoid factor
- Microbiological evidence: a positive blood culture that does not meet a major criterion (as previously noted) or serological evidence of active infection with an organism consistent with IE

Definite endocarditis: two major criteria or one major and three minor criteria or five minor criteria.
Possible endocarditis: one major plus one minor, or three minor criteria.

Table 2
Infective Endocarditis: Predisposing Cardiac Lesions

Higher risk	*Intermediate risk*	*Low or no increased risk*
• Prosthetic valves	• Mitral valve prolapse with regurgitation	• Cardiac pacemakers
• Previous endocarditis	• Mitral stenosis	• MVP with no regurgitation
• Aortic valve disease	• Tricuspid valve disease	• Cardiac lesions—post surgical correction
• Mitral regurgitation	• Pulmonary valve disease	• Tricuspid regurgitation with normal valves
• Combined mitral regurgitation and stenosis	• Assymetrical septal hypertrophy	• Atrial septal defect, secundum variety
• Congenital heart disease, especially cyanotic congenital heart disease, patent ductus arteriosus, ventricular septal defect, coarctation of the aorta	• Intracardiac lines (in right atrium) • Intracardiac implants (nonvalvular) • Degenerative valvular disease in the elderly	

Adapted from Fuster V, Alexander RW, O'Rourke RA. Hurst's: The Heart, 11th ed. New York: McGraw Hill, 2004.

endocarditis. These sites are susceptible to microbial seeding during episodes of bacteremia culminating in the characteristic "vegetation" that consists of an amorphous mass of platelets, fibrin, inflammatory cells, and microorganisms. Factors contributing to endocardial injury and the genesis of nonbacterial thrombotic endocarditis include: a high-velocity jet impacting the endothelium, flow from a high- to low-pressure chamber, and high-velocity flow across a narrow orifice. This explains the increased risk of endocarditis in certain patients (e.g., those with pre-existing valvular lesions or intracardiac prosthetic devices) as well as the common sites of vegetations (i.e., atrial surface of mitral valve, ventricular surface of aortic valve). However, in approx 30% of reported cases, no predisposing cause can be found. The incidence of this disease is relatively uncommon, approx 4.2 per 100,000 patient-years. With the advent and increased use of various intracardiac devices, the number of reported cases of infectious endocarditis is expected to rise. Cardiac lesions predisposing to IE are listed in Table 2.

If IE is not detected and managed in a timely manner, it can lead to devastating outcomes. Prompt recognition of IE requires a high index of clinical suspicion. The diagnosis must be considered and aggressively investigated when individuals with fever also present with bacteremia, predisposing cardiac lesions, prosthetic valves, other intracardiac devices, evidence of an active endo-cardial process, or embolic phenomena. The following cases exhibit diverse presentations and differential diagnoses of IE.

CASE PRESENTATION 2

An 86-yr-old female was admitted with ascending cholangitis, but developed streptococcal meningitis shortly thereafter. Subsequent transthoracic echocardiography (TTE) findings were suggestive of endocarditis. Patient developed acute renal failure, sepsis, and later demised. Her images appear in Figs. 3–5 (please *see* companion DVD for corresponding video for Fig. 3). Compare these to the findings shown in Figs. 6 and 7.

CASE PRESENTATION 3

A 72-yr-old man with end-stage renal disease and an atrioventricular fistula for hemodialysis presented to hospital with an infected graft and Methicillin-resistant *Staphylococcus aureus* bacteremia. He complained of increasing shortness of breath and orthopnea. Images from his transesophageal echocardiogram are shown in Fig. 8 (please *see* companion DVD for corresponding video).

CASE PRESENTATION 4

A 40-yr-old man with a history of daily heroin abuse presented with sudden onset of left lower extremity pain, intermittent blindness, delayed clotting to a small cut to his hand, and a fever recorded at 103.9°F. He recently tested positive for hepatitis C and HIV. At the time of examination, he was noted to have a grade 2/6 holosystolic crescendo-decrescendo

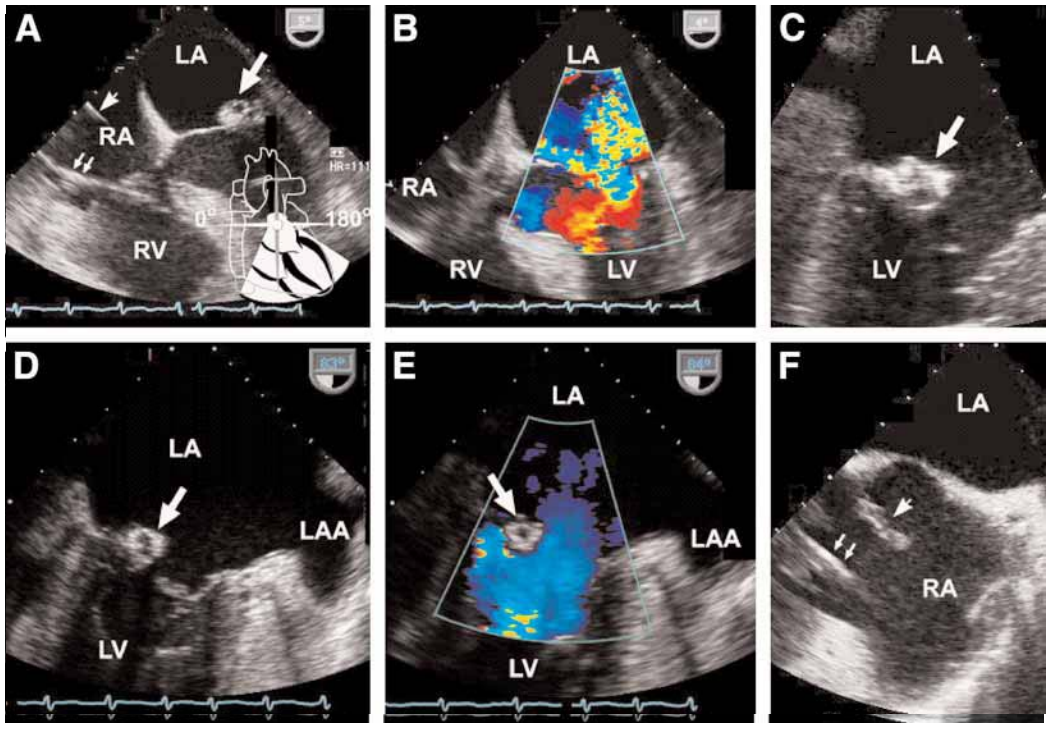

Fig. 3. An 86-yr-old woman with generalized sepsis. Transesophageal echocardiogram shows a well-circumscribed echodensity attached to atrial surface of the posterior mitral valve leaflet (white arrow; also seen in **A**,**C**–**E**). Color flow Doppler revealed new onset moderate-to-severe mitral regurgitation **(B)**. Note the linear echodensity (pacer wire) in the right heart chambers **(A,F)**. An undulating cuvilinear echodensity (arrow head; **A**,**E**) was seen in the right atrium and was thought to be clot or vegetation attached to the pacer wire (twin arrows; **A**,**F**), or even possibly Chiari's network. (Please *see* companion DVD for corresponding video.)

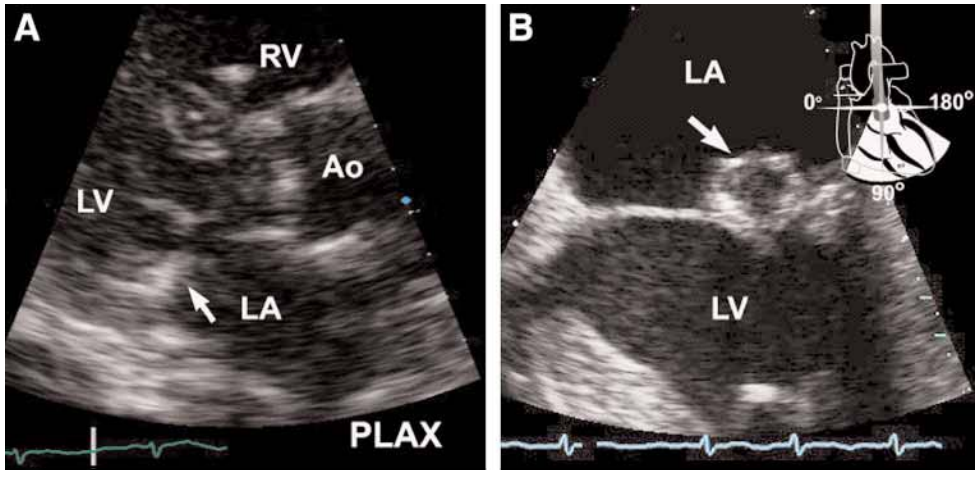

Fig. 4. An 86-yr-old woman with generalized sepsis. Parasternal long-axis still frame (suboptimal quality) show an echodense lesion near the posterior mitral valve annulus, the most common site for mitral annular calcification. On transesophageal echocardiography, a circumferential opacity with a central echolucent region was seen (*see* Fig. 5).

murmur heard best at the right lower sternal border. No peripheral stigmata of endocarditis was present. His initial electrocardiogram (ECG) showed sinus rhythm, right bundle branch block, and left anterior fascicular block. His echocardiographic images appear in Fig. 9.

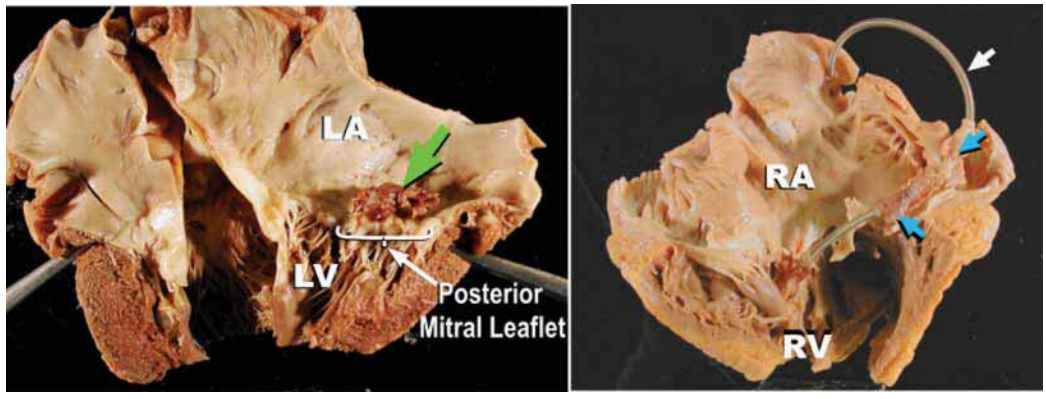

Fig. 5. An 86-yr-old woman with generalized sepsis. A large vegetation attached to the atrial surface of the posterior mitral valve leaflet is shown (left panel). A flesh-colored mass was adherent to the pacerwire. On histology, it proved to be organized thrombi with superimposed infection. (Pathology specimens courtesy of Robert Padera, MD, Brigham and Women's Hospital.)

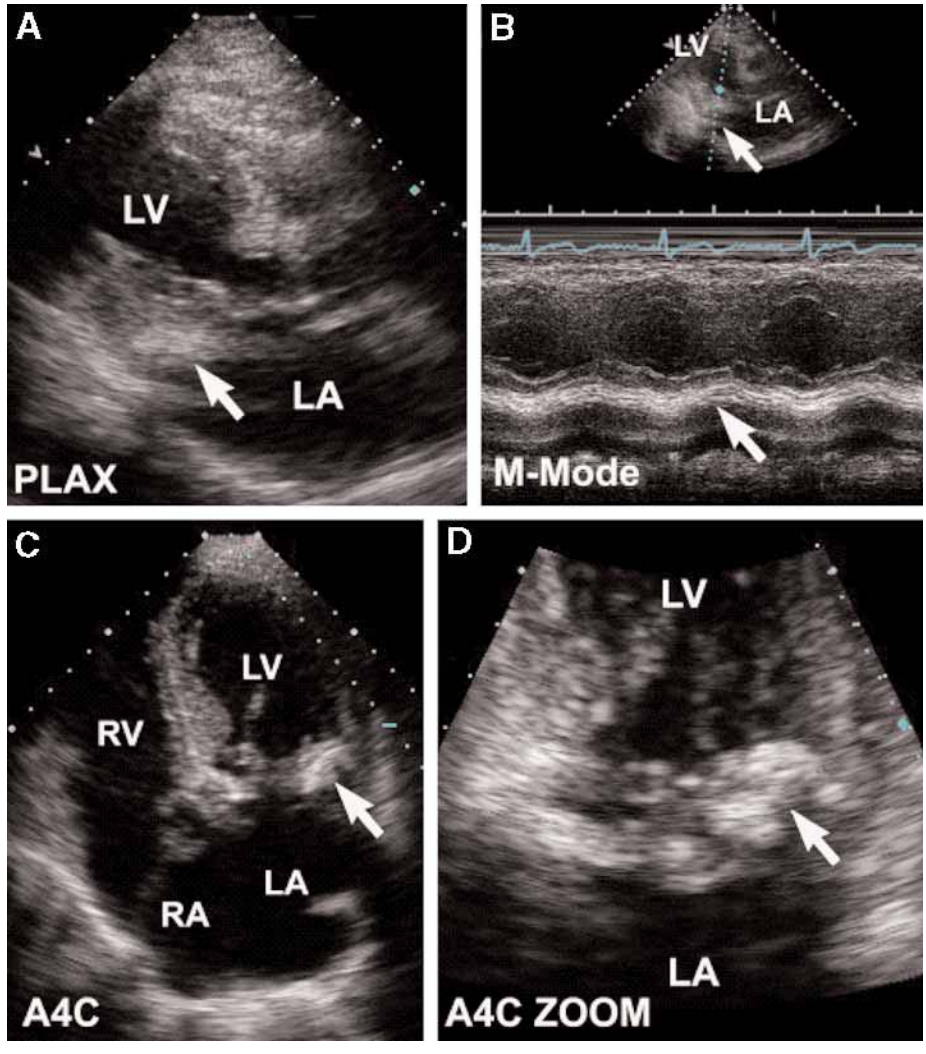

Fig. 6. Images from an 83-yr old woman with aortic and mitral regurgitation showed heavy calcification of the posterior mitral valve annulus with leaflet encroachment (white arrows). No fever or other symptoms that suggested infective endocarditis were present. Mitral annular calcification results from degenerative changes that become more prevalent with aging. M-mode through thickened mitral annulus shows echo-bright region that moves concordantly with cardiac chambers during the cardiac cycle **(B)**.

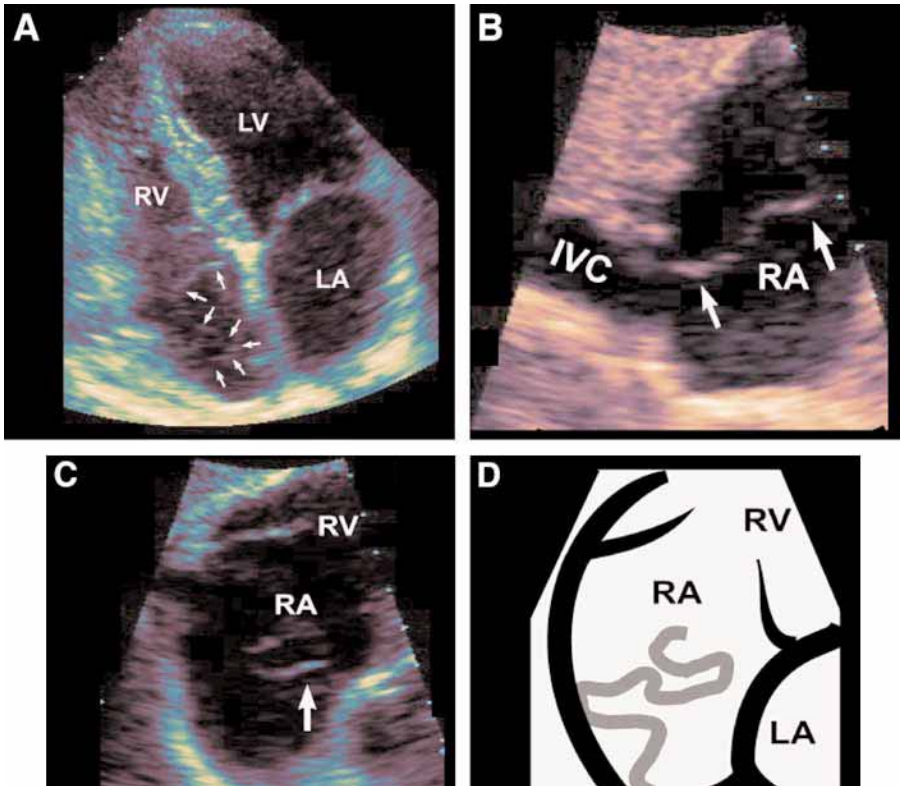

Fig. 7. Apical four-chamber view **(A)** and subcostal views **(B,C)** of Chiari's network. It is anatomically related to the Eustachian valve, a remnant of the embryonic right valve of the sinus venosus. It is a common finding in newborn. Transesophageal echocardiography and autopsy studies in adults indicate a prevalence of approx 2%. An undulating Chiari's network should trigger a closer examination of the inferior vena cava/right atrial junction (**B**, subcostal view) and the interatrial septum **(C)** for a patent foramen ovale or an atrial septal aneurysm.

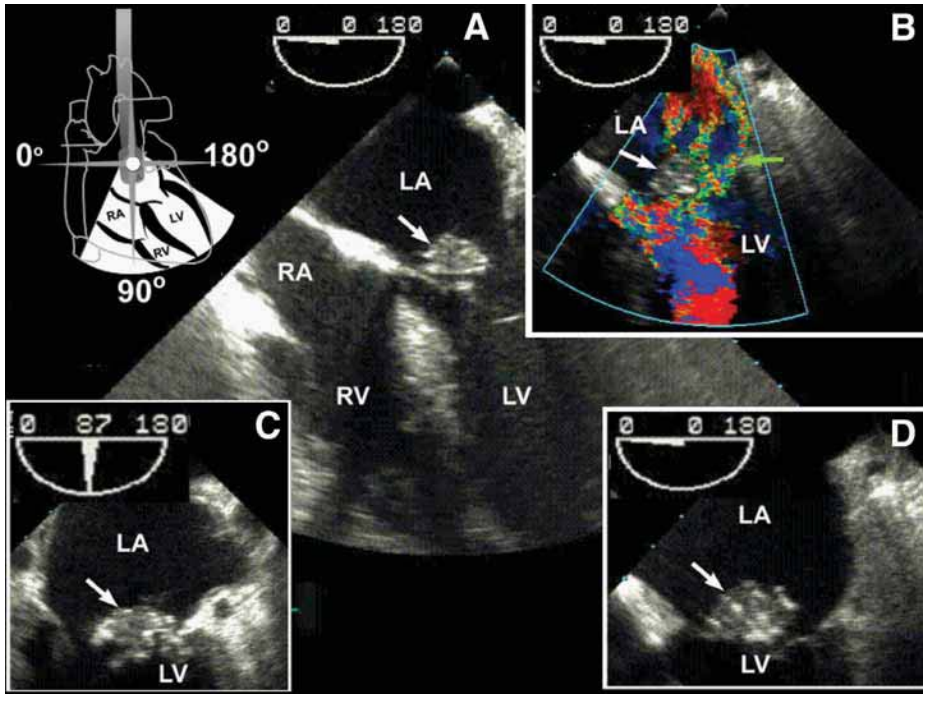

Fig. 8. A 72-yr-old man with Methicillin-resistant *Staphylococcus aureus* bacteremia. Transthoracic images in this patient were suboptimal, therefore a transesophageal echocardiograpahy was performed for persistent bacteremia. A 1.5 × 1.5 cm vegetation (white arrow) is visible on the atrial side of the anterior leaflet of the mitral valve **(A,C,D)**. Color flow Doppler showed mitral regurgitation along with a second color jet (green arrow) that entered the left atrium through a perforation in the posterior mitral leaflet. (Please *see* companion DVD for corresponding video.)

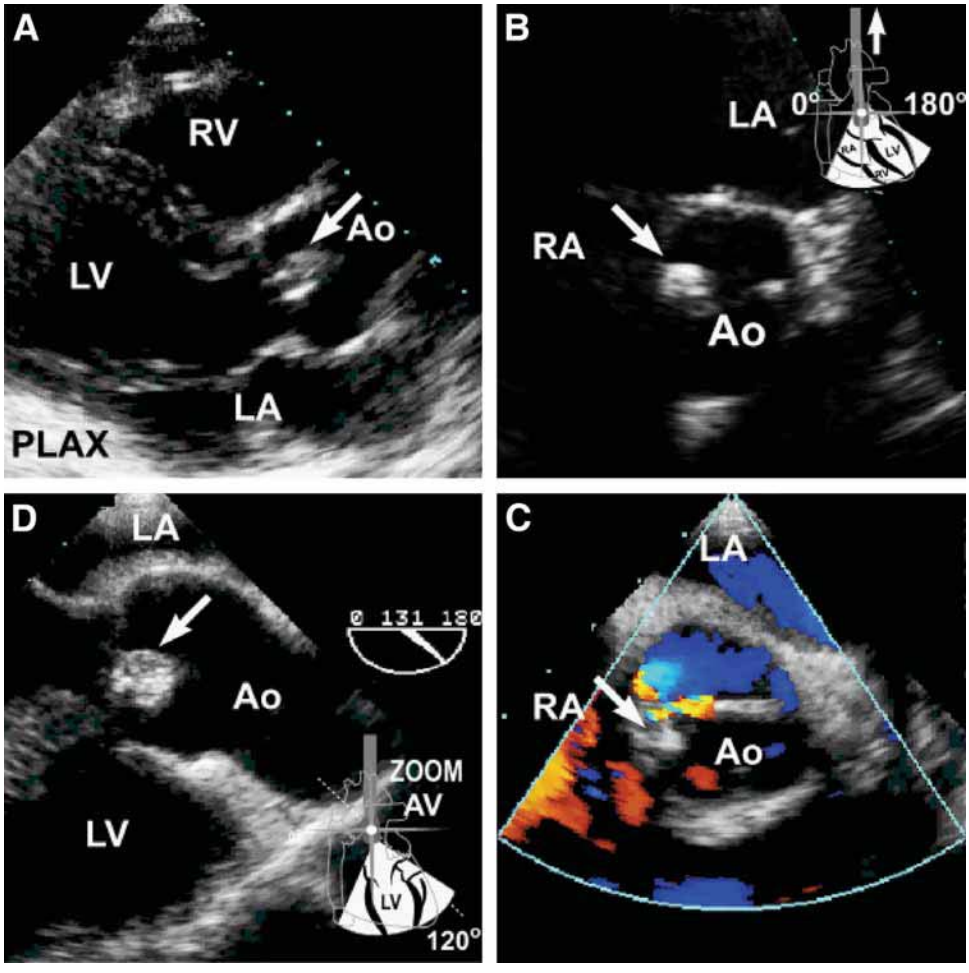

Fig. 9. A 40-yr-old heroin user presenting with leg pain, visual disturbances, fever, and a murmur. Transthoracic still frames showing a vegetation on the tip of an aortic valve cusp (arrow, **A**). This was believed responsible for patient's extracardiac complications. No tricuspid vegetations were observed. Transesophageal images revealed a circumscribed vegetation (arrows, **C**,**D**). Mild aortic regurgitation was seen on Color Doppler examination **(D)**.

CASE PRESENTATION 5

A 49-yr-old woman with a history of rheumatoid arthritis and intermittent steroid therapy presented with mental status changes, acute renal failure, and blood cultures positive for methicillin-sensitive *S. aureus*. Investigations were highly suggestive of multiple septic emboli to her brain and the kidneys. Her echocardiographic images are shown in Fig. 10; please *see* companion DVD for corresponding video.

CASE PRESENTATION 6

The images in Fig. 11 belong to a 72-yr-old man who underwent left ventricular aneurysm resection and repair, coronary artery bypass surgery, and mitral valve repair. Fourteen days postsurgery, he was still in the intensive care unit with signs of heart failure and low-grade temperatures, but no bacteremia.

CASE PRESENTATION 7

A 39-yr-old female with a history of congenital heart block treated with dual chamber permanent pacemaker at age 19 presented with fever and malaise. Blood cultures grew methicillin-sensitive *S. aureus*. Pacemaker was removed under general anesthesia and pus was noted in the pacemaker pocket and along the leads. Chest computed tomography has showed evidence of septic emboli to pulmonary vasculature. Her ECG showed runs of ventricular tachycardia and prolonged QT interval. Images from her echocardiogram appear in Fig. 12.

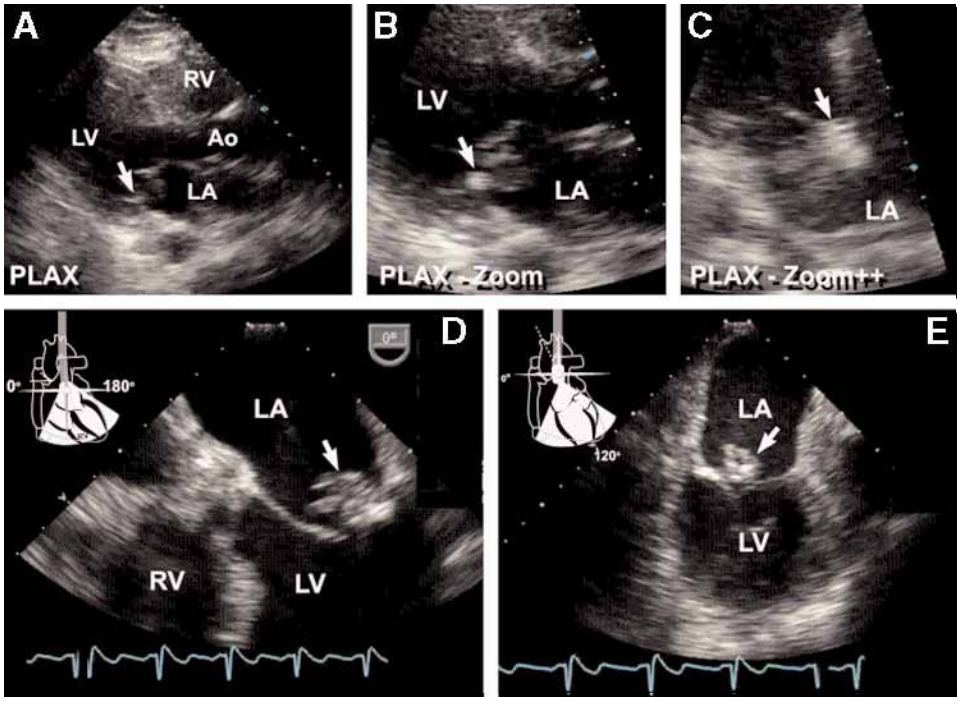

Fig. 10. A 49-yr-old woman with Methicillin-resistant *Staphylococcus aureus* bacteremia. Initial transthoracic images were technically limited **(A–C)** but suggested a vegetation on the posterior leaflet of the mitral valve. Transesophageal imaging revealed a well-defined mass on the posterior leaflet that intermittently prolapsed into the left ventricle **(D,E)**. This was the most likely cause of the patient's multiple embolic events. Her condition required surgical intervention. (Please *see* companion DVD for corresponding video.)

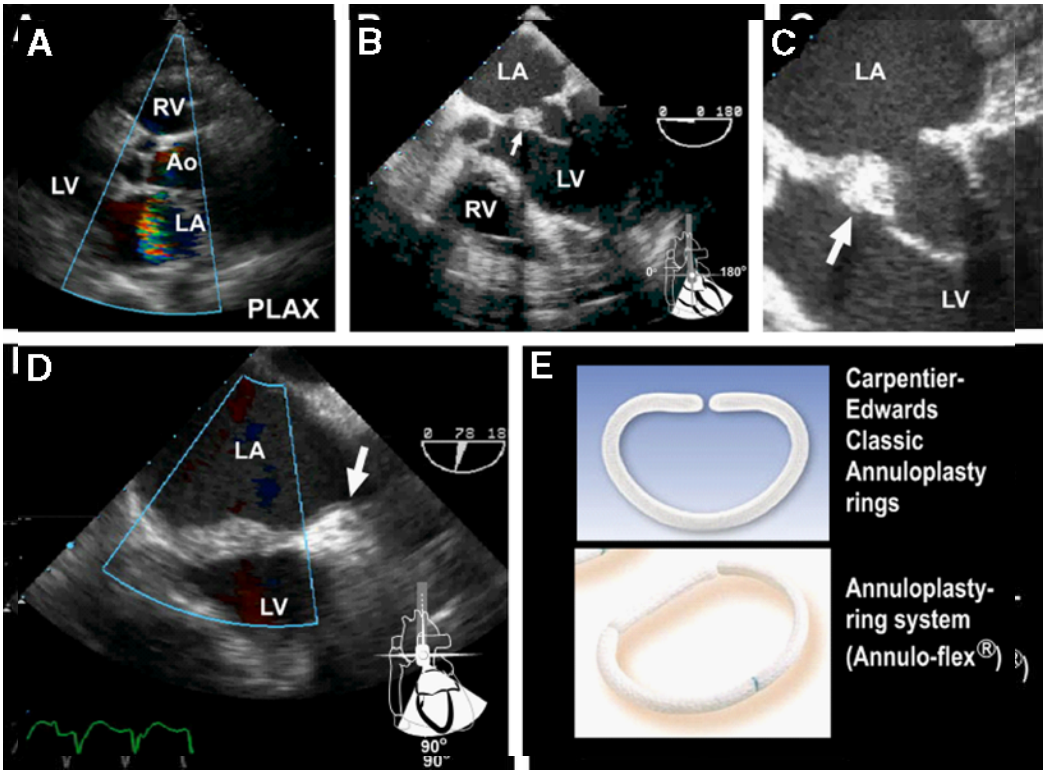

Fig. 11. A 74-yr-old man presenting 2 wk following coronary artery bypass graft, mitral valve repair, and left ventricular aneurysm resection. Transthoracic echocardiogram revealed a mitral regurgitant jet that originated from outside the mitral ring annulus **(A)**. Transesophageal echocardiography showed a thickened mass on the anterior mitral leaflet **(B–D)**. At surgery, the mass consisted of a partially loosened mitral annular ring. No vegetations were seen. **(D)** Shows two commonly used models of annuloplasty rings.

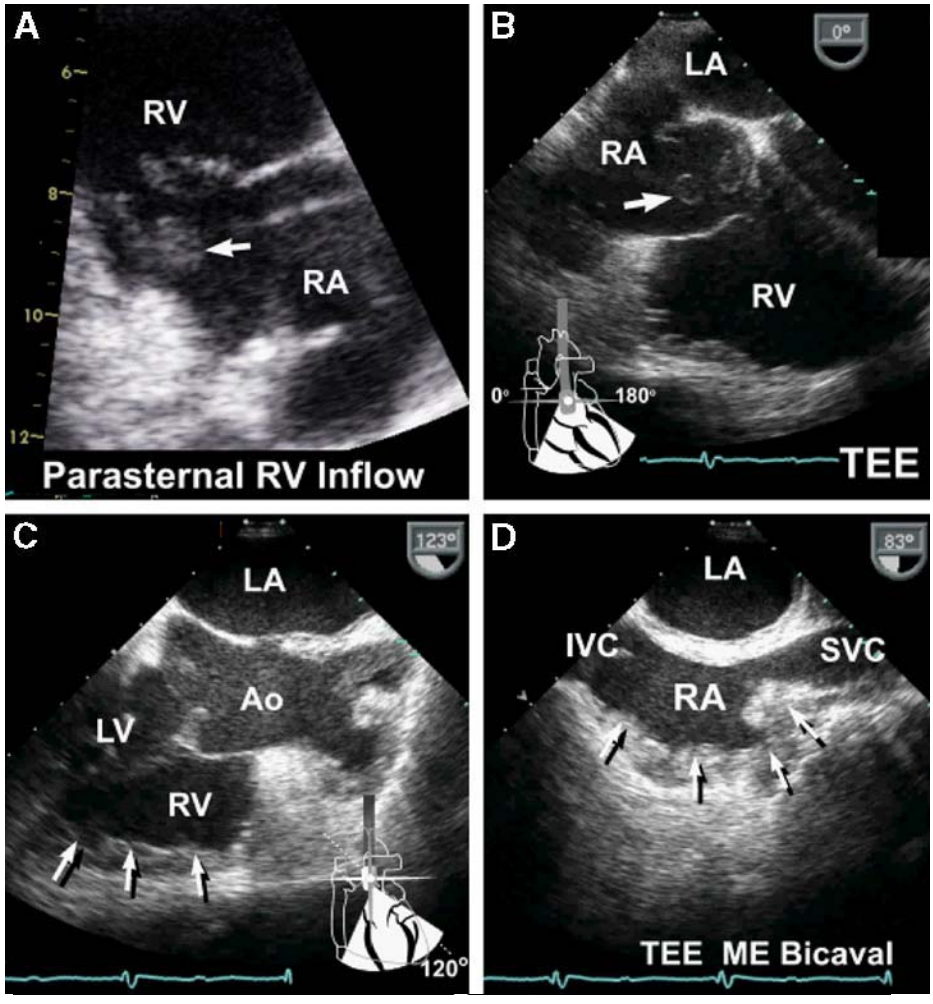

Fig. 12. A 39-yr-old female with permanent pacemaker for congenital heart block presenting with fever and malaise. Parasternal right ventricular inflow view showed a vegetation attached to the septal leaflet of the tricuspid valve that ping-ponged between right atrium and ventricle (arrow, **A**). Subsequent transesphageal echocardiography revealed multiple echodensities (mural vegetations) that studded the right ventricle, right atrium, and superior vena cava (arrows, **B**–**D**).

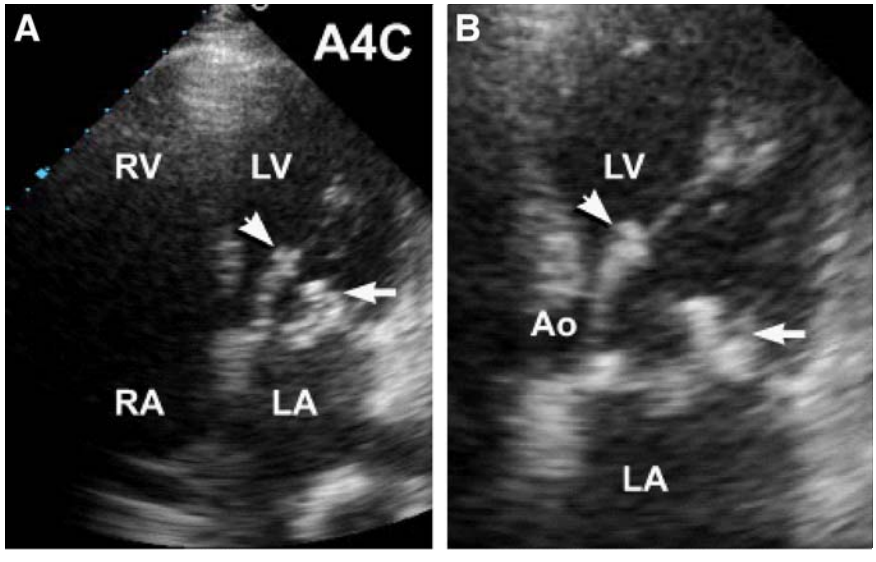

Fig. 13. *(Continued)*

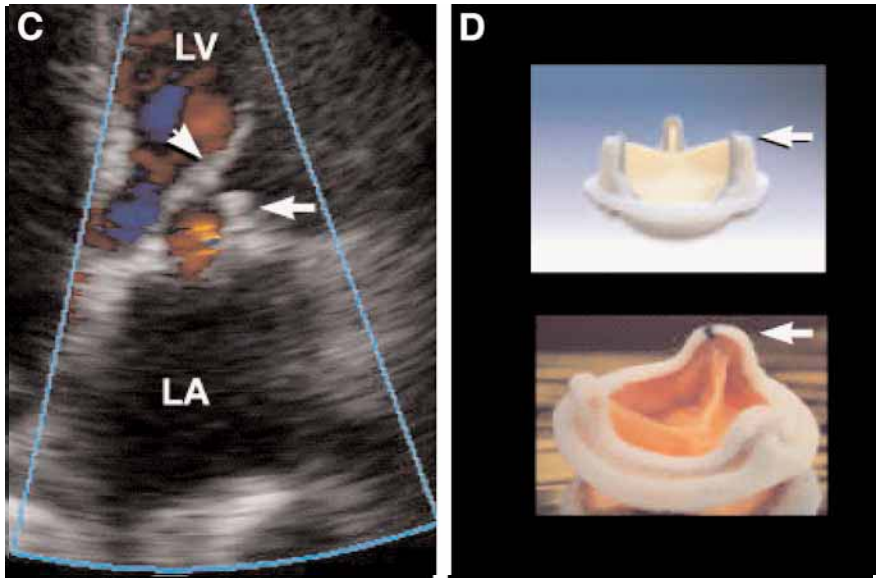

Fig. 13. A 58-yr-old male with previous mitral valve replacement presenting with increasing shortness of breath and suspected endocarditis. The struts of the bioprosthetic (tissue) valve (white arrows; **A**–**D**) can be visualized on echocardiography. This patient's anterior mitral leaflet was not excised (arrowhead), and caused dynamic obstruction of left ventricular outflow obstruction (arrowhead, **A**–**C**). The offending leaflet was excised. Histology reported mxyomatous degeneration and chronic inflammatory changes, but no evidence of infection. Bioprosthetic valves (**D**). (Please *see* companion DVD for corresponding video.)

CASE PRESENTATION 8

A 58-yr-old male underwent mitral valve replacement with a tissue valve prosthesis several years earlier, but now presented with increasing shortness of breath and suspected endocarditis. His echocardiogram images are shown in Fig. 13 (please *see* companion DVD for corresponding video).

ROLE OF ECHOCARDIOGRAPHY IN IE

Echocardiography features prominently in the diagnosis and the management of endocarditis, including the following roles:

1. Assists in diagnosis.
2. Detects or documents predisposing lesions.
3. Evaluation of complications.
4. Follow-up and response to therapy.
5. Guide to surgical intervention.

The American College of Cardiology and the American Heart Association Task Force issued its recommendations for echocardiography in IE for both native and prosthetic valves (*see* Chapter 4; Table 12).

The sensitivity of two-dimensional echocardiography for detecting vegetations is highly dependent on the size, location, and echocardiographic windows. TEE has a greater diagnostic yield over the transthoracic approach. TTE is unable to resolve vegetations less than 2 mm in diameter and is poor in evaluating prosthetic valves owing to acoustic shadowing. Overall, the sensitivity for detecting vegetations using transthoracic and TEE is 65–80% and 95%, respectively.

As the sensitivity of TTE for IE is relatively low, the absence of vegetations on TTE does not exclude the diagnosis of IE. Where clinical suspicion remains high, several limitations may mask or hinder TTE interpretation. These include: prosthetic valves, calcification, and sclerosis. Given the diagnostic advantages of TEE over TTE, many advocate that TEE be used routinely in all patients with suspected IE. This, however, is not a cost effective strategy, and TEE is not without risk.

Overall, TEE is the imaging modality of choice in patients with prosthetic valves or intracardiac devices. Deteriorating clinical status including referral for possible surgery may mandate an emergency TEE. Other indications for an emergent TEE examination include:

1. Rapidly worsening clinical status of a patient with known or suspected IE.
   a. Progressive conduction disturbances on ECG suggestive of aortic root involvement (Fig. 14A,B).
   b. Overwhelming sepsis despite appropriate antibiotic therapy.

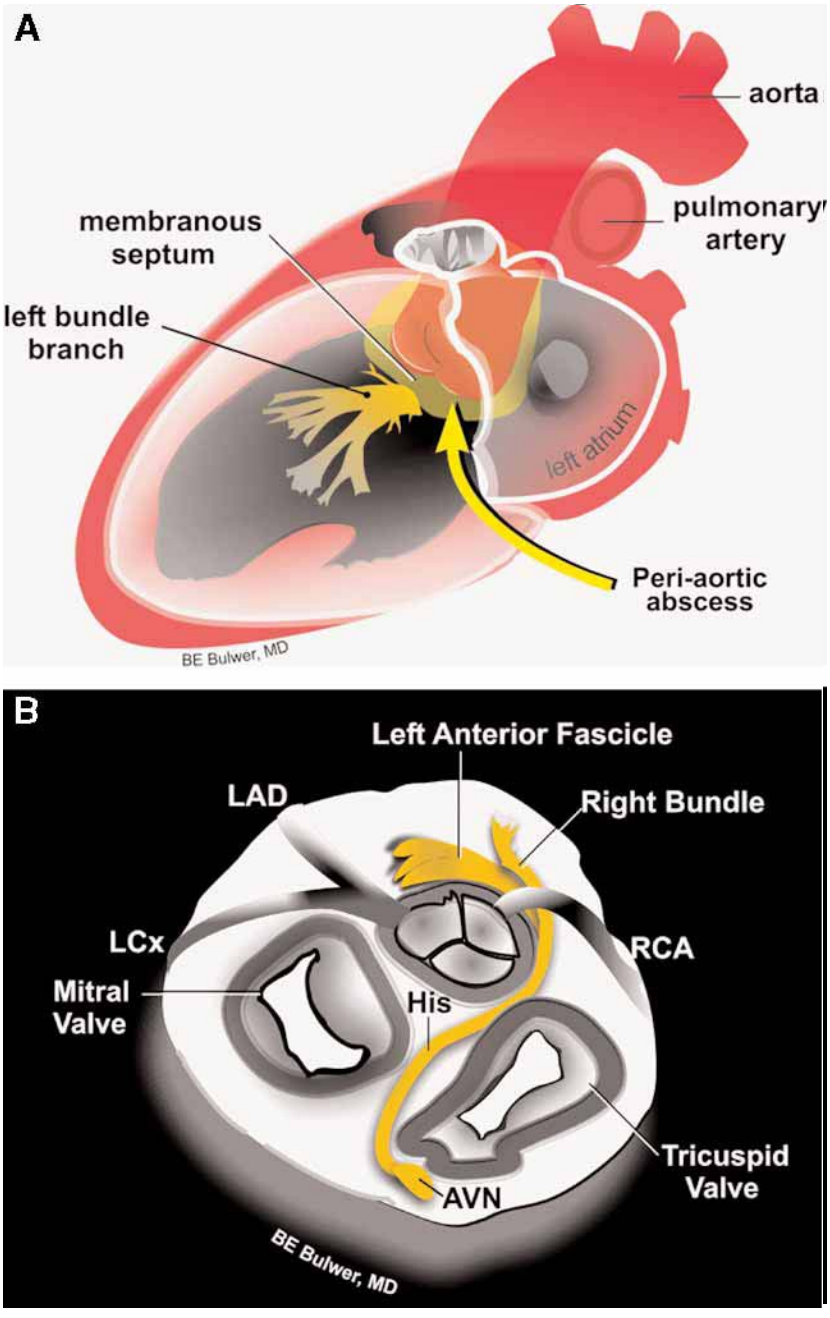

Fig. 14. Sketches showing relationship of the cardiac conduction system (left bundle branch) to a potential peri-aortic abscess (lateral and basal views). Conduction system involvement requires emergent TEE evaluation and possible surgical intervention.

2. Severe heart failure possibly related to acute valve dysfunction.
3. Embolic phenomena.

Choice of echocardiographic modality in evaluating suspected endocarditis in native valves is influenced by the likelihood of the diagnosis based on the clinical scenario and cost considerations. One recommendation based on a cost-effectiveness analysis is summarized below:

Pre-examination likelihood	
IE	*Echocardiographic approach*
<2%	Treat bacteremia; no echocardiography needed
2–4%	Obtain TTE
>5%	Proceed directly to TEE

It must be emphasized that echocardiography cannot distinguish between infective and noninfective or acute and chronic vegetations, or the causative organism. For these reasons, echocardiography alone should not be relied on to provide a definite diagnosis of IE.

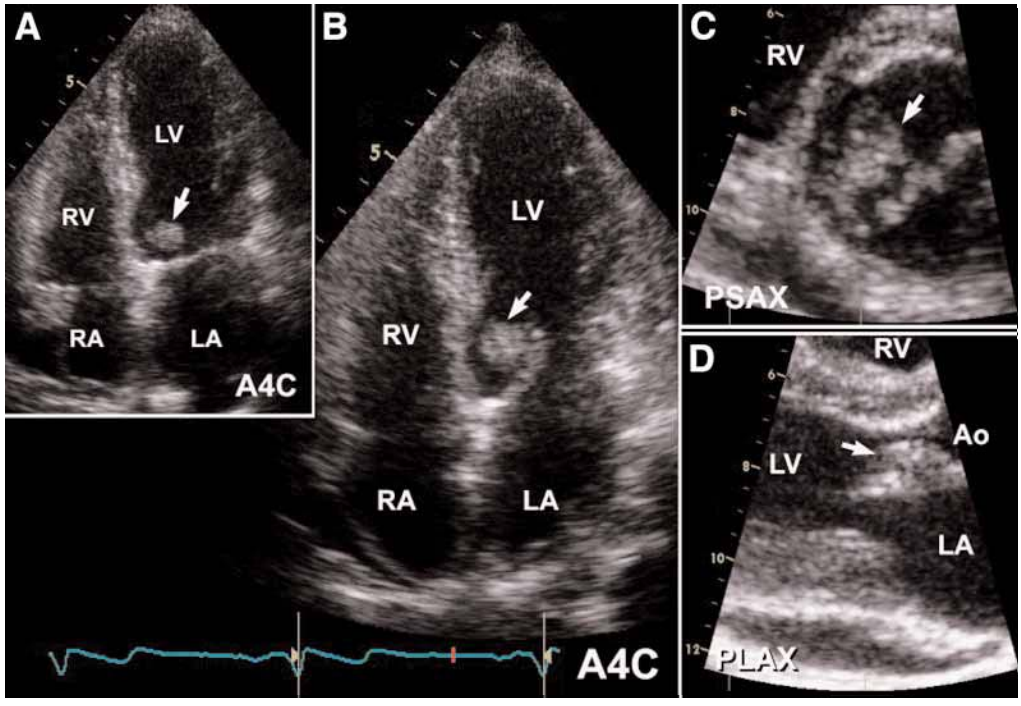

Fig. 15. These images are from a 76-yr-old woman with suspected endocarditis. The mobile vegetation (single arrows) was anterior to the anterior mitral valve leaflet. (Please *see* companion DVD for corresponding video.)

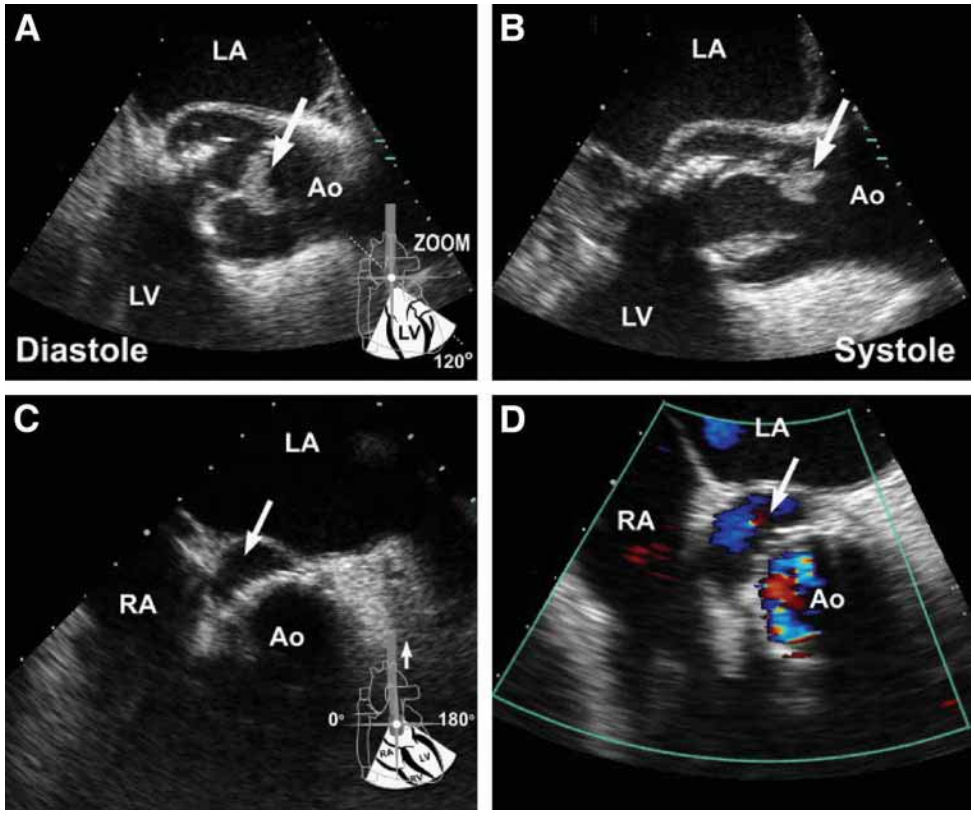

Fig. 16. These images from a 64-yr-old male with active endocarditis show verrucous vegetations (arrows, **A**,**B**). Note the peri-valvular echolucent foci indicative of an aortic root abscess (arrows; **C**,**D**). (Please *see* companion DVD for corresponding video.)

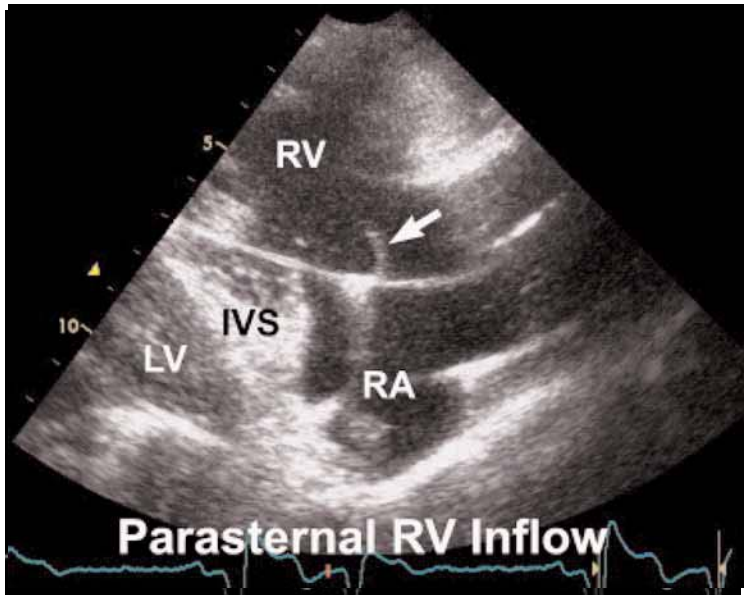

Fig. 17. This undulating vegetation (arrow) attached to the pacer wire was an incidental finding in an otherwise normal patient.

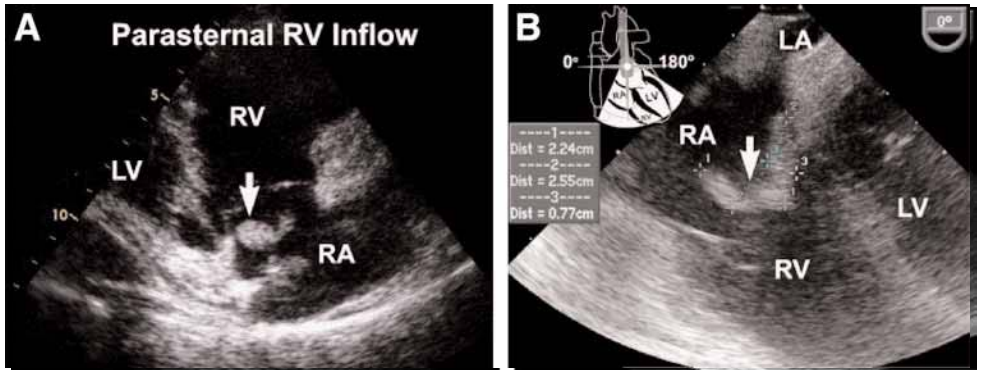

Fig. 18. These relatively large and highly mobile vegetations were visualized in the right heart chambers on both transthoracic (**A**) and transesophageal echocardiography (**B**). The patient's infected pacemaker was removed. (Please *see* companion DVD for corresponding video.)

Echocardiographic Characteristics

When both clinical presentation and blood culture evidence exist, typical echocardiographic features supporting IE include: (1) an oscillating intracardiac mass localized to a valve or intracardiac device, (2) intracardiac abscesses, (3) new partial dehiscence of a prosthetic valve, or (4) new or worsening valvular regurgitation.

Vegetations often appear as mobile echogenic masses attached to the valve, endocardial surface, or prosthetic materials within the heart and can present in a variety of shapes and sizes (Figs. 15–18; please *see* companion DVD for corresponding video for Figs. 15, 16, and 18). They frequently exhibit high frequency flutter or oscillations, with right-sided vegetations generally larger than left-sided ones. However, none of these features are pathognomonic for IE as they may exist separately or in conjunction with noninfectious causes. Correlation with clinical and microbial parameters is always warranted. Several differential diagnoses should be considered when confronted with mobile echogenic intracardiac masses (Table 3). In the absence of vegetations, new-onset valvular dysfunction on color flow Doppler interrogation may suggest IE.

COMPLICATIONS

The complications of IE result from the local destructive effects of vegetations, their propensity to embolize, and epiphenomena (Table 4). The presence

Table 3
Cardiac Vegetations in Infective Endocarditis vs Nonvegetation Masses

Characteristics	*Cardiac vegetations*	*Nonvegetative masses*
Location	Usually on valve suface facing path of blood flow (upstream)	Usually downstream surface of valve
Motion	Relatively independent of cardiac or valvular components; often oscillate or prolapse	Often concordant with other cardiac or valvular components
Morphology	Irregular morphology, sometimes lobulated or filiform	Morphology characteristic of underlying pathology
Echocardiographic texture	Same reflectivity as myocardium	Often shows increased calcification or reflectivity
Accompanying features	Cardiac and extracardiac manifestations of infective endocarditis (Table 5)	Usually absent

Table 4
Infective Endocarditis: Complications

- Cardiac
  - Leaflet perforation
  - Valvular incompetence leading to heart failure
  - Perivalvular abscess
  - Atrioventricular valves: chordal rupture, leaflet perforation
  - Extension leading to aneurysm/pseudoaneurysm, fistula, or invasion of cardiac conducting system (Fig. 14A,B)
  - Coronary artery emboli leading to acute myocardial infarction
  - Pericarditis
- Extracardiac
  - Emboli: stroke, mycotic aneurysms, infarctions of renal, splenic, and pulmonary bed, osteomyelitis, septic arthritis, metastatic abscesses, gangrene
  - Immunological: glomerulonephritis, Roth spots, Janeway lesions

and characteristics of vegetations seem to affect the prognosis and clinical course of patients. The frequency of complications seems to increase with greater mobility, extent, number, consistency, and increasing size of vegetations on repeat examinations. Always look for associated cardiac structural abnormalities in individuals with suspected or confirmed IE (Table 2). When present, these should be followed-up by serial examinations as these can guide decision making, including the need and timing of surgery. Echocardiographic regression or disappearance of vegetations is not a sign of cure in IE.

Echocardiographic Features Suggesting the Need for Surgical Intervention

Whenever, possible surgical intervention for IE should be avoided owing to the high associated morbidity and risk of prosthetic valve infection. The decision to proceed to surgery is not clear cut, and should be tailored to each clinical state, aided by certain echocardiographic features.

Echocardiographic features portending adverse outcomes with need for surgical intervention include:

1. Prosthetic valve endocarditis.
2. Worsening native valvular regurgitation despite treatment (Fig. 19).
3. Sinus of Valsalva aneurysm.
4. Large vegetations (>10 mm).
   a. With embolic phenomena.
   b. Causing valvular obstruction.
   c. Fungal endocarditis.
5. Aortic root and septal abscesses.

SUMMARY

Echocardiography can, in conjuction with positive blood cultures, help establish the diagnosis of IE (Table 1). It is also important in assessing complications and guiding further management and follow-up of patients with this condition. Both transthoracic and transesophagel echocardiography play important roles—each with its own advantages and disadavantages. Echocardiographic findings, however, must always be

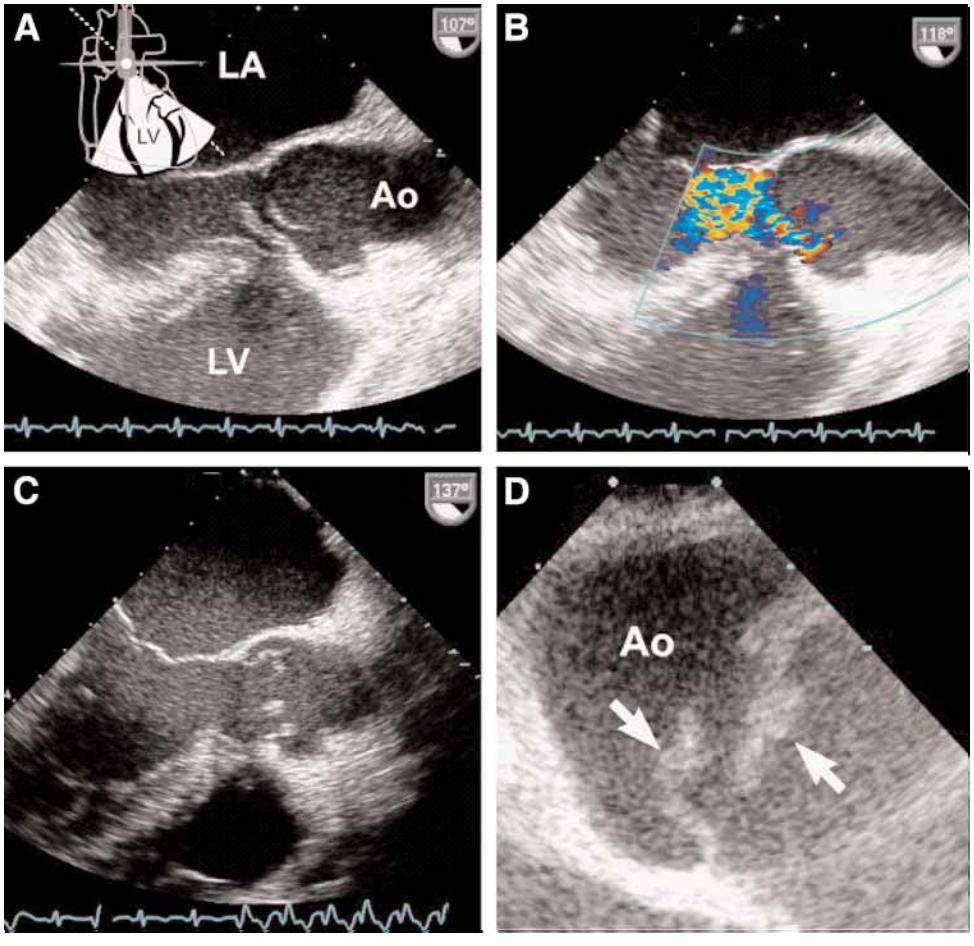

Fig. 19. A 38-yr-old male with acute bacterial endocarditis requiring aortic root replacement surgery. This gravely ill 38-yr-old male suffered marked destruction of his aortic valve leaflets secondary to infective endocarditis **(A–D)**. This led to severe aortic incompetence **(B)** and cardiac conduction disturbances. He underwent emergency aortic root and valve replacement surgery. The infection extended down to the membranous ventricular septum causing a ventricular septal defect (*see* Fig. 14 A,B).

interpreted within the clinical context and in close collaboration with the entire management team.

SUGGESTED READING

Baumgartner FJ, Omari BO, Robertson JM, Nelson RJ, Pandya A, Milliken JC. Annular abscesses in surgical endocarditis: anatomic, clinical, and operative features. Ann Thorac Surg 2000;70:442–447.

Blumberg EA, Karalis DA, Chandrasekaran K, et al. Endocarditis-associated paravalvular abscesses: do clinical parameters predict the presence of abscess? Chest 1995;107: 898–903.

Bonow RO, Carabello B, de Leon AC, Jr, et al. Guidelines for the management of patients with valvular heart disease: executive summary: a report of the American College of Cardiology/American Heart Association Task Force on Practice Guidelines (Committee on Management of Patients with Valvular Heart Disease). Circulation 1998;98: 1949–1984.

Brauwald E. Heart Disease: A Textbook of Cardiovascular Medicine, 6th ed. Philadelphia: WB Saunders, 2001.

Cheitlin MD, Alpert JS, Armstrong WF, et al. ACC/AHA guidelines for the clinical application of echocardiography: executive summary: a report of the American College of Cardiology/American Heart Association Task Force on Practice Guidelines (Committee on Clinical Application of Echocardiography): developed in collaboration with the American Society of Echocardiography. J Am Coll Cardiol 1997;29: 862–879.

Choussat R, Thomas D, Isnard R, et al. Perivalvular abscesses associated with endocarditis: clinical features and prognostic factors of overall survival in a series of 233 cases: Perivalvular Abscesses French Multicentre Study. Eur Heart J 1999;20: 232–241.

Daniel WG, Mugge A, Grote J, et al. Comparison of transthoracic and transesophageal echocardiography for detection of abnormalities of prosthetic and bioprosthetic valves in the mitral and aortic positions. Am J Cardiol 1993;71:210–215.

De Castro S, Cartoni D, d'Amati G, et al. Diagnostic accuracy of transthoracic and multiplane transesophageal echocardiography for valvular perforation in acute infective endocarditis: correlation with anatomic findings. Clin Infect Dis 2000;30:825–826.

Dodds GA, Sexton DJ, Durack DT, Bashore TM, Corey GR, Kisslo J. Negative predictive value of the Duke criteria for infective endocarditis. Am J Cardiol 1996;77:403–407.

Durack DT, Lukes AS, Bright DK. New criteria for diagnosis of infective endocarditis: utilization of specific echocardiographic findings. Duke Endocarditis Service. Am J Med 1994; 96:200–209.

Fox CS, Vasan RS, Parise H, et al. Framingham Heart Study. Mitral annular calcification predicts cardiovascular morbidity and mortality: the Framingham Heart Study. Circulation 2003; 107:1492–1496.

Fuster V, Alexander RW, O'Rourke RA. Hurst's: The Heart, 11th ed. New York: McGraw Hill, 2004.

Heidenreich PA, Masoudi FA, Maini B, et al. Echocardiography in patients with suspected endocarditis: a cost-effective analysis. Am J Med 1999;107:198–208.

Knosalla C, Weng Y, Yankah AC, et al. Surgical treatment of active infective aortic valve endocarditis with associated periannular abscess—11 year results. Eur Heart J 2000;21: 490–497.

Kuruppu JC, Corretti M, Mackowiak P, Roghmann MC. Overuse of transthoracic echocardiography in the diagnosis of native valve endocarditis. Arch Intern Med 2002;162:1715–1720.

Lindner JR, Case RA, Dent JM, Abbott RD, Scheld WM, Kaul S. Diagnostic value of echocardiography in suspected endocarditis: an evaluation based on the pretest probability of disease. Circulation 1996;93:730–736.

Lowry RW, Zoghbi WA, Baker WB, Wray RA, Quinones MA. Clinical impact of transesophageal echocardiography in the diagnosis and management of infective endocarditis. Am J Cardiol 1994;73:1089–1091.

Mylonakis E, Calderwood SB. Infective endocarditis in adults. N Engl J Med. 2001;345:1318–1330.

Roldan CA, Shively BK, Crawford MH. Valve excrescences: prevalence, evolution and risk for cardioembolism. J Am Coll Cardiol 1997;30:1308–1314.

Schneider B, Hofmann T, Justen MH, Meinertz T. Chiari's network: normal anatomic variant or risk factor for arterial embolic events? J Am Coll Cardiol 1995;26:203–210.

Schuchlenz HW, Saurer G, Weihs W, Rehak P. Persisting eustachian valve in adults: relation to patent foramen ovale and cerebrovascular events. J Am Soc Echocardiogr 2004;17: 231–233.

Shively BK, Gurule FT, Roldan CA, Leggett JH, Schiller NB. Diagnostic value of transesophageal compared with transthoracic echocardiography in infective endocarditis. J Am Coll Cardiol 1991;18:391–397.

Werner GS, Schulz R, Fuchs JB, et al. Infective endocarditis in the elderly in the era of transesophageal echocardiography: clinical features and prognosis compared with younger patients. Am J Med 1996;100:90–97.

III Miscellaneous Topics in Echocardiography

16 Role of Echocardiography in the Management of Atrial Fibrillation

Warren J. Manning, MD

CONTENTS

CASE PRESENTATION

J.R. is an 83-yr-old Caucasian man with a long history of hypertension treated with diuretics and an angiotensin converting enzyme inhibitor. One week before presentation, he noted the onset of increasing fatigue and occasional palpitations when walking briskly to his office. He has been able to continue working full-time in his optometric office, but for the past 2 d, has noted new pedal edema. Last night, he had an episode of paroxysmal nocturnal dyspnea. At presentation to his internist, he is found to be in mild respiratory distress with a respiratory rate of 18/min. Blood pressure is 164/86 mmHg bilaterally, heart rate 120 bpm, irregularly irregular. There is mild jugular venous distension. Carotids are brisk without bruits. Lung exam demonstrates bibasilar rales. His point of maximal impulse is in the fifth intercostal space, anterior axillary line. There is a normal S1, S2 with II/VI holosystolic murmur best heard at the apex in the left lateral decubitus position with no diastolic murmurs. Distal pulses are full. There is 1+ bilateral pitting edema. Resting electrocardiogram demonstrates atrial fibrillation (AF) with an average ventricular response of 110/min. He is referred to the emergency department and admitted for rate control, treatment of congestive heart failure, anticoagulation, and consideration of cardioversion. An echocardiographic examination is requested.

INTRODUCTION

The presentation of J.R. is typical of patients with their first episode of AF. AF is the most common sustained arrhythmia and is characterized by a loss of organized atrial electrical and mechanical activity. The associated loss of the atrial systolic contribution to left ventricular filling leads to reduced ventricular filling and depressed cardiac output with resultant symptoms of dyspnea and fatigue. In addition, atrial stasis predisposes to the formation of atrial thrombi, most commonly in the left atrial

From: *Contemporary Cardiology: Essential Echocardiography: A Practical Handbook With DVD*
Edited by: S. D. Solomon © Humana Press, Totowa, NJ

Table 1
Transthoracic Echocardiographic Findings in AF

Finding	*Significance*
Left atrial enlargement	More common in patients with atrial fibrillation (AF). Progressive dilation is associated with sustained atrial fibrillation.
Left ventricular hypertrophy	Patients with hypertension and LVH are at increased risk of AF.
Mitral valve disease	Mitral stenosis and mitral regurgitation are common causes of left atrial enlargement, which predisposes to AF.
Left atrial spontaneous contrast, "smoke"	Spontaneous contrast, or "smoke," is common in conditions of stasis and can be seen in patients with AF. Spontaneous contrast is caused by aggregation of red cells. The higher the transducer frequency, the greater the likelihood of seeing "smoke."
Pericardial effusion	Patients with pericarditis are prone to atrial arrhythmias.

appendage (LAA), and subsequent migration and clinical stroke or peripheral thromboembolism. AF is thought to be responsible for 10% of all clinical strokes and 50% of all cardiac sources of embolism. Rheumatic valvular AF is associated with an 18-fold increase in clinical thromboembolism, but even non-rheumatic AF is associated with a sixfold increase. Residual left atrial thrombi are seen in almost 50% of patients presenting with a stroke in the setting of newly recognized AF.

ROLE OF TRANSTHORACIC ECHOCARDIOGRAPHY

Transthoracic echocardiography (TTE) can be helpful in the management of AF by (1) identifying pathological conditions that may predispose to AF, and (2) identifying conditions that may increase the risk of thromboembolism (Table 1). For patients who present with their initial episode of AF, a search is usually made to determine the most likely "associated" systemic condition. The most common associated conditions include a history of systemic hypertension or coronary artery disease. Also to be considered are mitral valve disease (especially rheumatic mitral stenosis), pneumonia/sepsis, clinical or subclinical thyrotoxicosis (especially in the elderly), pericarditis, pulmonary embolism, pharmaceuticals (e.g., aminophylline), and excess caffeine or alchohol ingestion (Table 2). Patients are often referred for a TTE to investigate for occult mitral stenosis, to assess the severity of mitral regurgitation (with consideration of mitral valve surgery if it is severe), for assessment of left atrial size (but TTE is *not* sufficient for assessment/exclusion of atrial thrombi), for the presence of a pericardial effusion (although the absence of an effusion does not exclude the clinical diagnosis of pericarditis), and for assessment of left ventricular systolic function. Information regarding left ventricular systolic function is frequently helpful for guiding the choice of ventricular rate controlling agent with β-blockers used for patients with preserved systolic function and digoxin/diltiazem or a combination for patients with depressed left ventricular systolic function. Very rarely, AF may present as a manifestation of pulmonary embolism (severe right ventricular enlargement with free wall hypokinesis) or aortic stenosis. For patients who present with recurrent AF, repeated TTE studies are generally not fruitful (unless there has been a change in presentation).

Table 2
Atrial Fibrillation: Associated Conditions

Conditions associated with atrial fibrillation
- Older age
- Hypertension
- Coronary artery disease
- Valvular heart disease (especially mitral stenosis)
- Pulmonary disease, including pulmonary embolism
- Hyperthyroidism (clinical and subclinical)
- Sepsis including pericarditis
- Postcardiac surgery (especially valvular surgery)
- Drugs, including ethanol

CARDIOVERSION FOR AF: THE ROLE OF ECHOCARDIOGRAPHY

Among patients with persistent AF, cardioversion to sinus rhythm is often performed to relieve symptoms

and improve cardiac output, but should not be performed to specifically reduce the risk of thromboembolism. Current data from both the Atrial Fibrillation Follow-up Investigation of Rhythm Management and Rate Control and Rhythm Control studies suggest cardioversion itself does not reduce the need for chronic warfarin to prevent clinical thromboembolism. Unfortunately, both electrical and pharmacological cardioversion may be associated with clinical thromboembolism, most often occurring during the first 10 days following conversion. For patients with hemodynamic instability, emergent direct current cardioversion is often performed. For hemodynamically stable patients with persistent AF for 2 days or more, there is a 6% risk of cardioversion-related clinical thromboembolism if cardioversion is not preceded by several weeks of therapeutic (international normalization ratio [INR] 2.0–3.0) warfarin. The use of 3–4 wk of therapeutic warfarin before cardioversion results in an 80% reduction in clinical thromboembolic risk, to approx 1%.

CONVENTIONAL APPROACH TO CARDIOVERSION OF ATRIAL FIBRILLATION

Although no prospective, randomized studies have been performed to determine the optimal INR or duration of precardioversion warfarin, historical data suggested 3–4 wk of warfarin (INR 2.0–3.0) before elective cardioversion is sufficient. The use of this "conservative" strategy comes at the "cost" of a delay in cardioversion for the vast majority of patients who could otherwise undergo early and safe cardioversion. This 1-mo delay exposes the patient to prolonged precardioversion warfarin therapy (with associated risk of hemorrhagic complications) and prolongs the period of AF before cardioversion. It has been estimated that up to a quarter of patients receiving warfarin in preparation for cardioversion do *not* undergo the initially scheduled cardioversion because of hemorrhagic complications and/or a transient subtherapeutic INR. For patients with hemorrhagic complications, the clinician is faced with the difficult choice of reducing the intensity of anticoagulation, often to a subtherapeutic range (with the patient remaining in AF). For the patient with a transient subtherapeutic INR, the dose of warfarin is increased, and the "1-mo clock" must be restarted. Finally, the use of 1 mo of precardioversion warfarin serves to prolong the duration of AF before cardioversion, and thus adversely impacts the rate of recovery of atrial mechanical function and long-term maintenance of sinus rhythm. The impact on atrial function and long-term maintenance of sinus rhythm appears to be most relevant for those presenting with AF of only several weeks duration.

ANATOMICAL AND FUNCTIONAL CONSIDERATIONS IN TRANSESOPHAGEAL ECHOCARDIOGRAPHY: THE LAA

Understanding LAA anatomy is essential for interpretation of transesophageal echocardiography (TEE) findings. Its morphology is complex and highly variable. The LAA receives more attention than the right appendage in AF as it is (by far) the preferred site for thrombus formation. Its anatomical configuration—the narrow neck and multiple ridges—may promote thrombus formation in pathological states.

Topographical Relationships and External Anatomy

The LAA is an irregularly-shaped tubular expansion arising from the antero-lateral corner of left atrium (Fig. 1). Its external surface appears lobulated and forms part of the cardiac silhouette on chest radiographs. Antero-medial to the LAA lies the root of the pulmonary artery. Inferiorly, it sits above the short left main coronary artery as it bifurcates into the left anterior descending and left circumflex vessels, and the great cardiac vein, which flows into the coronary sinus. Laterally, the LAA is covered by parietal pericardium that abuts the adjacent pleura and lung.

Internal Morphology

The luminal surface of the LAA exhibits a varied array of ridges formed by the pectinate muscles (comb-like arrangement of cardiac muscle fibers) that line its floor and lateral walls (Fig. 2). The pectinate muscles commence distal to its distinct neck or waist that delineates it from the rest of the smooth-walled left atrium. Their appearance on TEE (Fig. 3A; please *see* companion DVD for corresponding video) must be appreciated and distinguished from artifact and thrombi (Fig. 3B–D [please *see* companion DVD for corresponding video] and Table 3). Familiarity with normal LAA morphology on TEE is perhaps the best way to distinguish between artifact, pectinate muscles, and thrombi.

The maximal internal length of the LAA is measured along a curvilinear line reflecting its curved tubular anatomy, but additional lobes and appendage orientation are commonly seen on TEE (Fig. 4). Necropsy resin casts have shown LAA dimensions to range from a 16 mm to 51 mm along its curvilinear length, and 5 to 40 mm

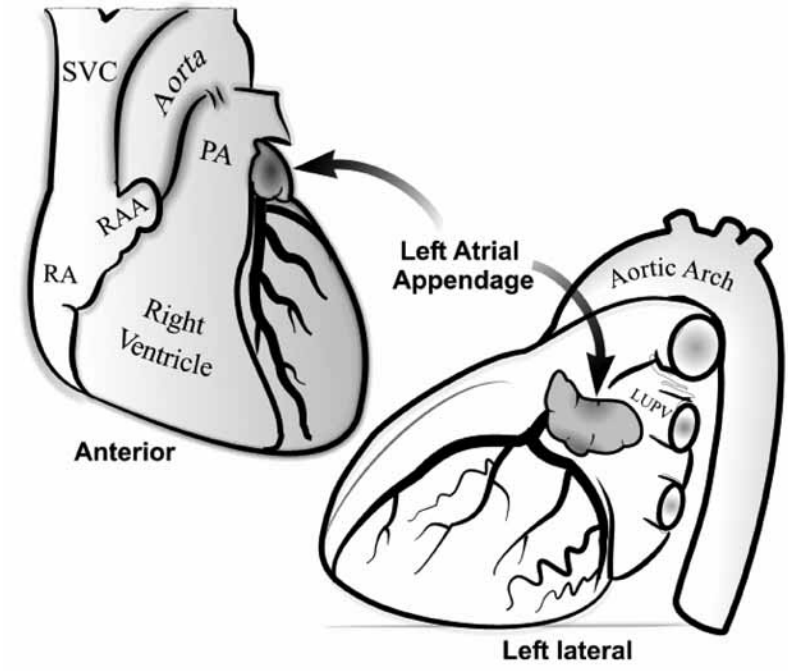

Fig. 1. Frontal and left lateral views of the heart showing the left atrial appendage.

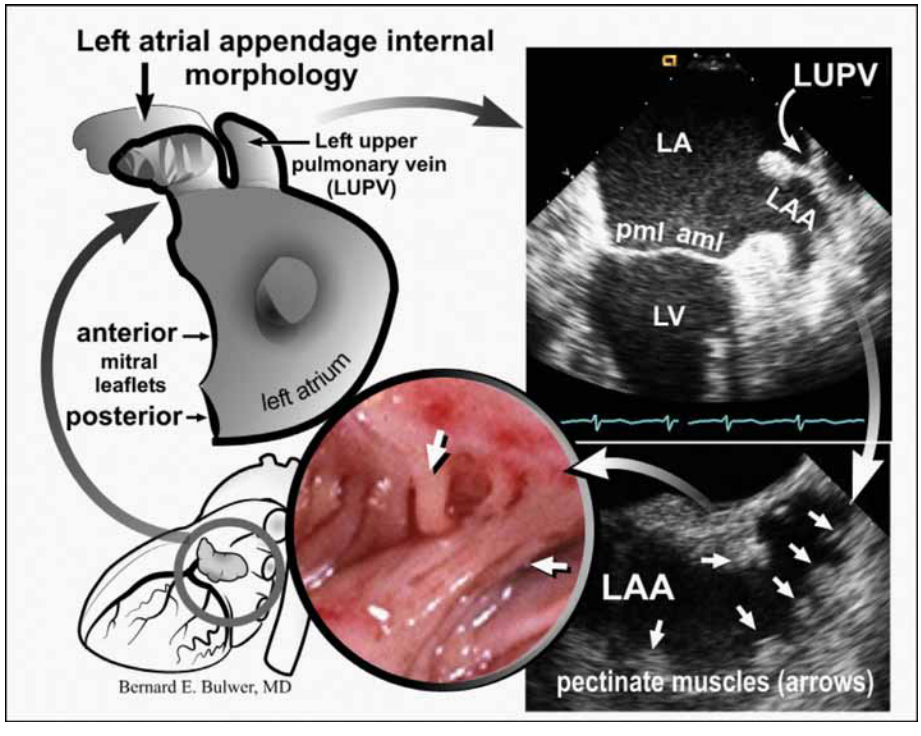

Fig. 2. Composite images showing the internal morphology of the left atrial appendage and pectinate muscles on transesphageal echocardiography.

in diameter measured at its neck. The area of the appendage measured on two-dimensional TEE in a small series of 117 patients averaged 3.7 cm.

NORMAL LAA HEMODYNAMICS

Our understanding of LAA function—apart from producing atrial naturetic peptide (indicating a role in

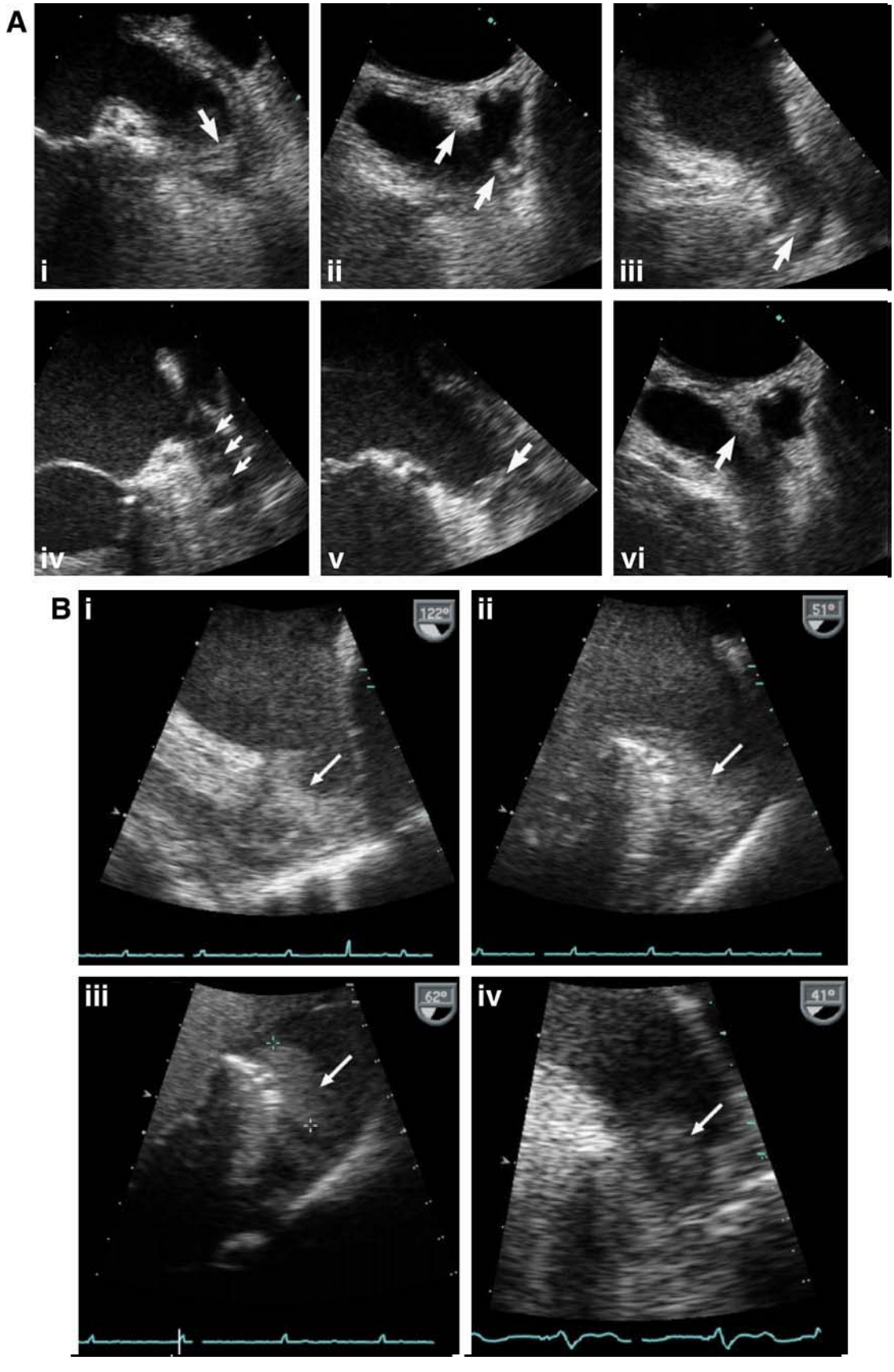

Fig. 3. (*See* legend, next page)

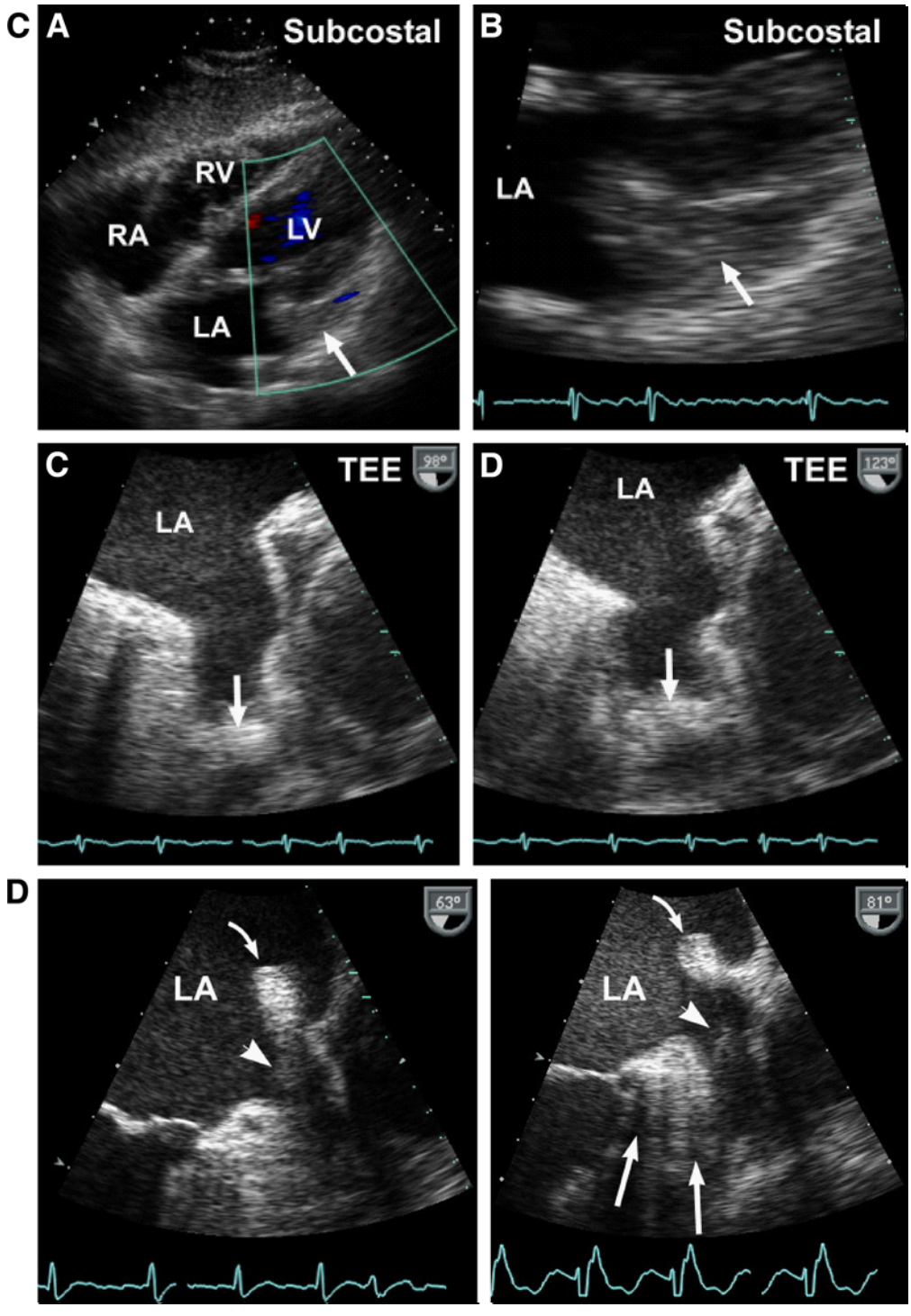

Fig. 3. (A) Images showing pectinate muscle morphology on transesphageal echocardiography (TEE). Note their identical echo-reflectivity pattern compared the left atrial appendage (LAA) wall. **(B)** Views of LAA containing thrombi in patients with atrial fibrillation (AF). Note the presence of spontaneous echocontrast. **(C)** Views of LAA containing thrombi (arrows) in a patient with AF, visualized in both subcostal view **(top panels)** and on TEE **(bottom panels)**. Spontaneous echo contrast was also seen in **bottom panels**. **(D)** The fold of tissue separating the LAA from the left upper pulmonary vein—the so-called "warfarin ridge" (curved arrows)—owing to false-positive diagnosis of thrombi within the LAA. (Please *see* companion DVD for corresponding video.)

Table 3
TEE Imaging of Left Atrial Appendage: Thrombi vs Artifacts and Anatomical Structures

Index	*Thrombi*	*Artifact*	*Pectinate muscles*
Location	Often at tip of LAA and always confined to LAA lumen (*see* Fig. 3B)	Acoustic shadowing near "warfarin ridge" or anatomical fold separating LAA and LUPV; reverberations are common, but are ×2 object distance from transducer (*see* Fig. 3C)	Confined to the body of the LAA (*see* Figs. 2 and 3A)
Motion with respect to LAA and heart movement	Relatively independent	Fully concordant	Fully concordant
Echoreflectivity pattern compared to LAA walls	Different	Reflectance artifacts Acoustic shadowing Reverberations	Identical
Anatomical morphology	Varied	Consistent with object or structure giving rise to artifact	Follows normal muscle anatomical orientation
Left atrial spontaneous echo contrast	Often present	No relationship	No relationship

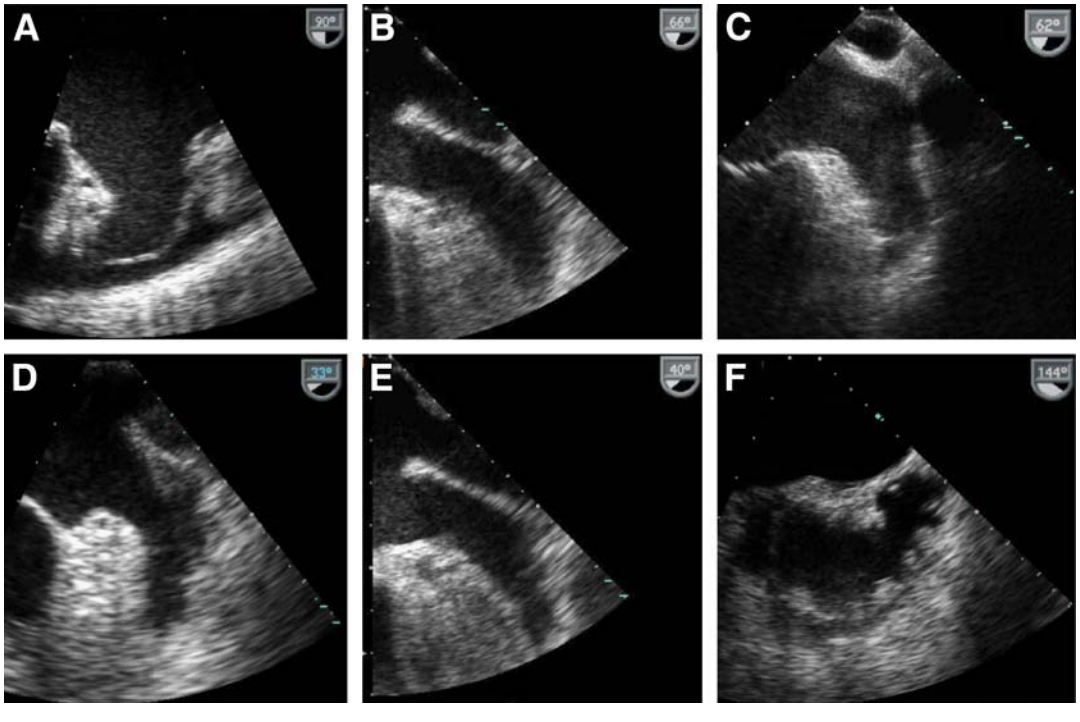

Fig. 4. The varied appearance of normal left atrial appearances on transesphageal echocardiography. Normal left atrial appendage morphology can be broadly described as unilobe, bilobed, or multilobed. Note the small pericardial effusion in **A**.

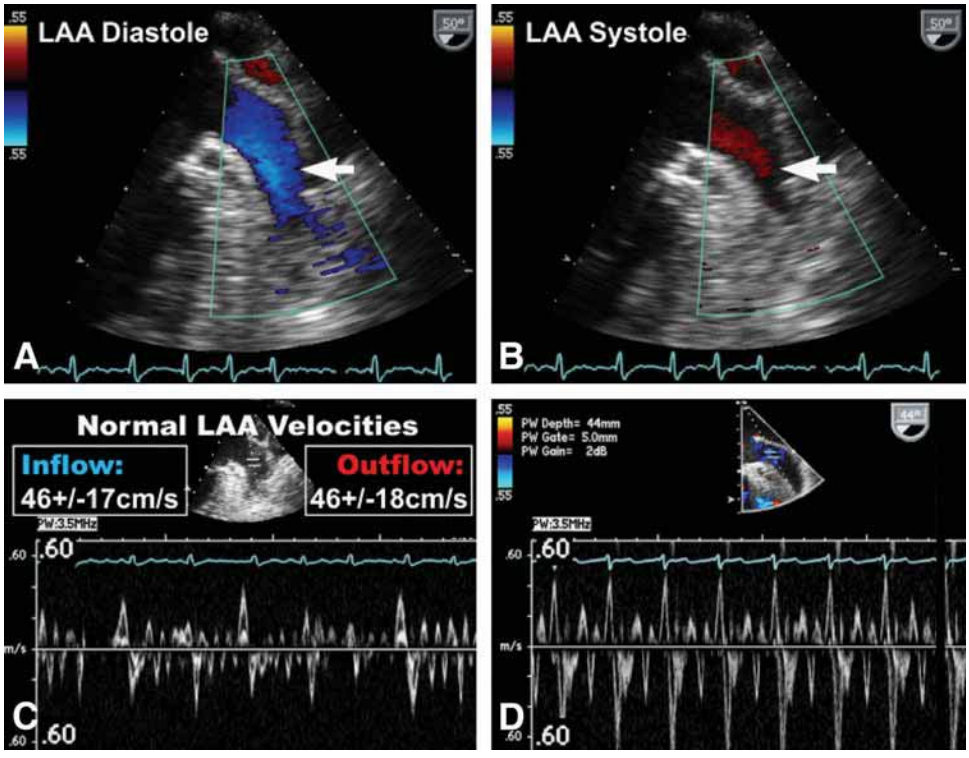

Fig. 5. Color flow Doppler and pulsed wave Doppler examination of the normal left atrial appendage. The normal appendage actively contracts in most individuals as seen on TEE **(A**,**B)** or at surgery. This contributes to the complex quadriphasic pattern seen on pulsed Doppler examination.

Table 4
Transesophageal Echocardiographic Findings in Atrial Fibrillation

Finding	*Significance*
Spontaneous contrast in left atrium or left atrial appendage	Spontaneous echo contrast is thought to increase the risk of thromboembolism.
Left atrial appendage thrombus	The most common location of occult thrombus in patients with AF. Thrombus must be distinguished from pectinate muscles that traverse the atrial appendage.
Attenuated left atrial appendage flow velocities	Flow velocities less that 20 cm/s in and out of the LAA is suggestive of stagnant flow.
Right atrial appendage thrombus	Not visualized by transthoracic echocardiography, thrombus can be present in right atrial appendage.

cardiovascular hemodynamics) and an expansion chamber for the left atrium—is incomplete.

Blood flow into and out of the LAA exhibits a complex quadriphasic pattern on spectral Doppler echocardiography (Fig. 5). This pattern reflects left atrial hemodynamics as well as contraction and relaxation patterns of the LAA itself. Normal inflow and outflow LAA velocities in healthy adults are 46 ± 17 cm/s and 46 ± 18 cm/s, respectively. Patterns of flow categorized as type I (sinus rhythm), type II (flutter), type III (fibrillatory), type IV (absent) have been described. Normal right artrial appendage ejection velocity is 40 ± 16 cm/s.

EXAMINATION OF THE LAA BY TEE: CONSIDERATIONS

Transesphageal echocardiography, systematically conducted, is an excellent tool for complete visualization of the LAA. It has a high sensitivity for detecting LAA thrombi (Table 4), but this is observer dependent.

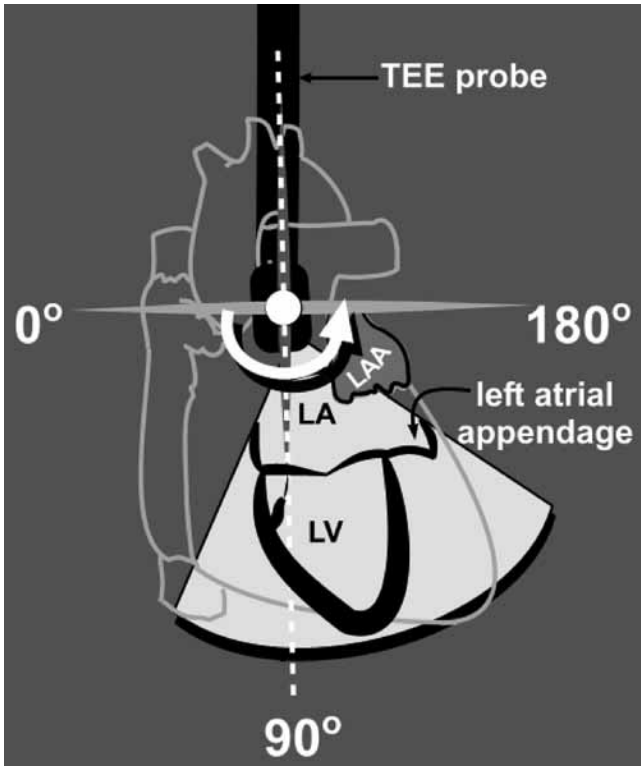

Fig. 6. A systematic examination of the complex left atrial appendage is imperative to "rule out" thrombus. A recommended schema is shown (*see* Chapter 23).

TEE evaluation of the left atrial appendage involves omni rotation from 0 through 180°, with additional counterclockwise (to the left) rotation of the entire probe between 60 and 90°, and again between 110 and 130° (Fig. 6; *see* Chapter 23). These serve as a guide, with the final positioning guided by optimal visualization of examined structure during each individual study.

TEE-FACILITATED EARLY CARDIOVERSION

LAA thrombi are associated with spontaneous echocardiographic contrast (Figs. 3B and 7; please *see* companion DVD for corresponding video for Fig. 3) and more depressed (<0.2 m/s) LAA ejection velocities (Fig. 8 [please *see* companion DVD for corresponding video], compare to Fig. 5). Although less than 10% of thrombi are seen in the right atrial appendage, this area is nearly impossible to see from TTE approaches, but well investigated by TEE (Fig. 9). Thus, TEE offers the opportunity to exclude atrial thrombi, and therefore facilitate early and safe cardioversion. The strategy we have advocated (Fig. 10) is for the patient to be therapeutically anticoagulated with unfractionated heparin (partial thromboplastin time ≥2X control) or warfarin (INR ≥ 2.0) at the time of TEE and extending for at least 1 mo after cardioversion. The use of systemic

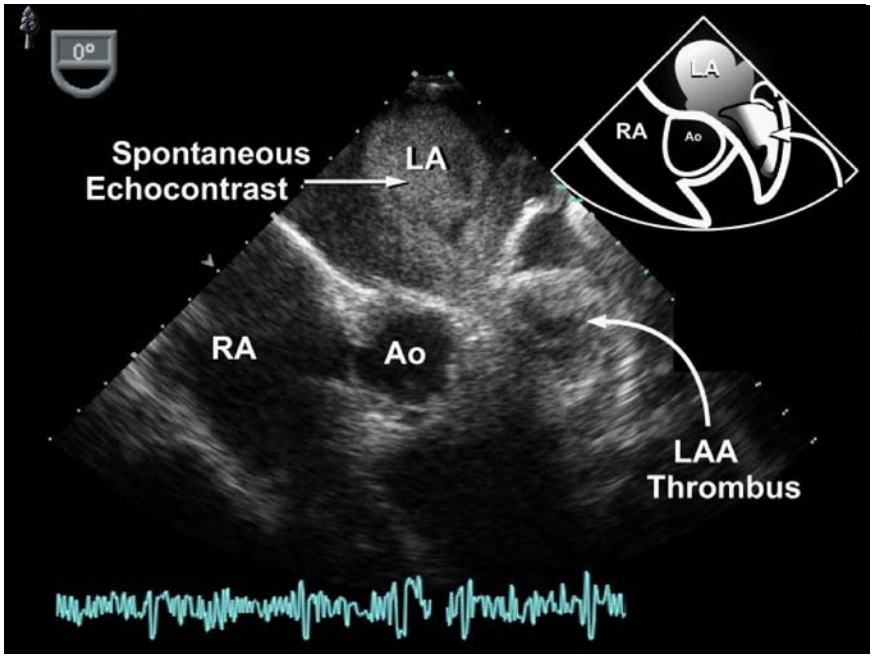

Fig. 7. Spontaneous echocontrast (smoke-like swirling) is visible within the left atrium and appendage during transesophageal echocardiography. It is a reflection of sluggish blood flow and rouleaux formation (*see* Chapter 13, Fig. 3). It is associated with thrombus formation (curved arrow) and embolic complications.

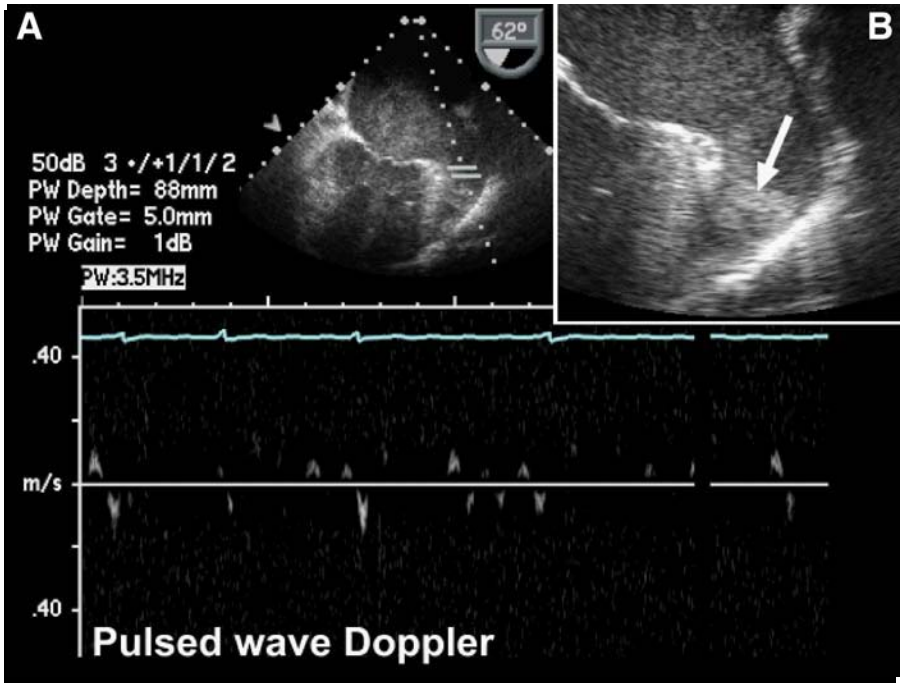

Fig. 8. Pulsed wave Doppler interrogation of left atrial appendage flow is a standard part of the transesphageal echocardiography examination of the appendage. Flow below 0.2 m/s is suggests stagnation (arrow) as seen in this patient with atrial fibrillation and left atrial thrombus (compare to Fig. 5). (Please *see* companion DVD for corresponding video.)

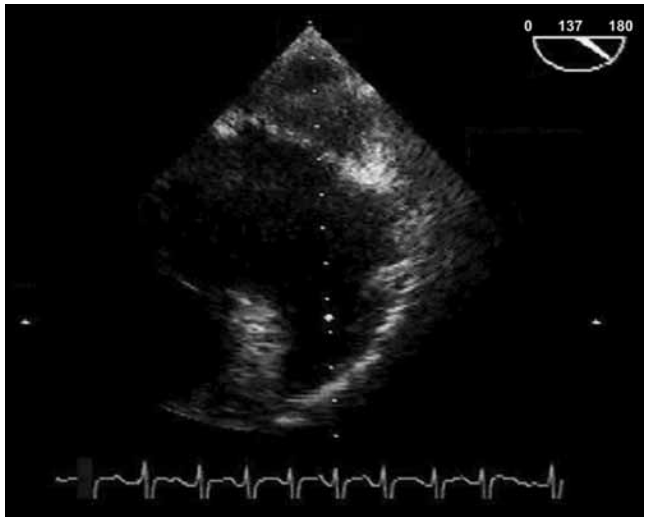

Fig. 9. Midesophageal view of right atrial appendage at omniplane 137°. Less than 10% of all atrial thrombi occur on the right. Note the broader neck of the right appendage compared to the left.

anticoagulation in this manner is intended to minimize the formation of microthrombi, and to prevent thrombi from forming during the postcardioversion period. It has been demonstrated that during the immediate postcardioversion period, electrical, pharmacological, and even spontaneous conversion to sinus rhythm is associated with relatively depressed atrial appendage mechanical function. The peri-cardioversion period, therefore, appears to be one in which a patient is at somewhat increased risk for new thrombus formation and physicians should be especially vigilant regarding therapeutic anticoagulation.

At least four prospective studies have examined the safety of a TEE-guided approach to early cardioversion of AF of 2 days or longer duration. These studies demonstrate that 12% of patients will have TEE evidence of atrial thrombi. This apparent discrepancy between the 12% prevalence of atrial thrombus on TEE and the 6% historical rate of clinical thromboembolism for nonanticoagulated patients is likely explained by (1) the imperfect specificity of TEE; (2) the likelihood that not all thrombi migrate after cardioversion; and (3) not all thrombus migration is associated with clinical thromboembolism. TEE evidence for atrial thrombus is associated with spontaneous echo contrast, prior thromboembolism, and left ventricular systolic dysfunction.

Using the anticoagulation strategy described in Fig. 10, and based on almost 2000 prospectively studied patients, clinical thromboembolism has been reported in less than 0.5% of patients following a "negative" TEE for atrial

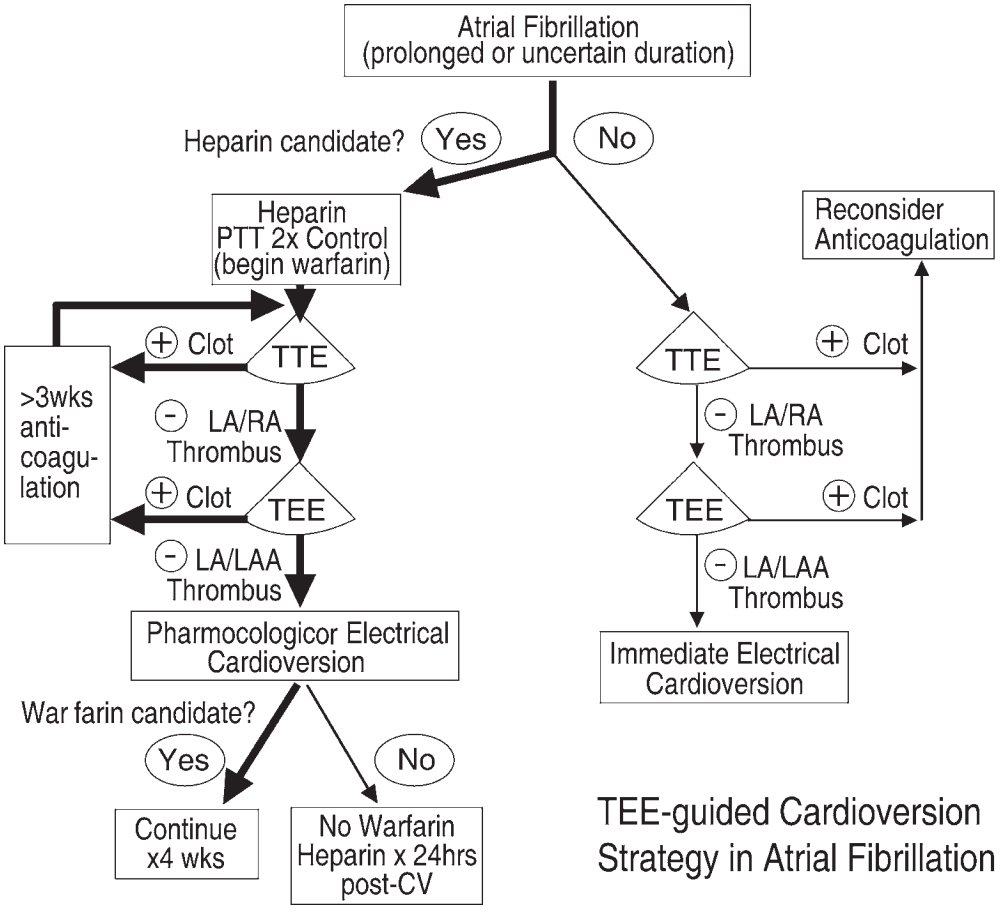

Fig. 10. Transesophageal echocardiography-guided cardioversion strategy in atrial fibrillation. Management of patients presenting with atrial fibrillation of unknown or more than 2 d duration. Patients with a thrombus on the initial transesphageal echocardiography (TEE) should received 1 mo of warfarin followed by a TEE to document complete thrombus resolution before elective cardioversion. (From Seto TB et al. Cost-effectiveness of transesophageal echocardiography guided cardioversion for hospitalized patients with atrial fibrillation. J Am Cardiol 1997;29:122–130.

thrombus. The largest reported series is the multicenter 1222 patient Assessment of Cardioversion Using Transesophageal Echocardiography trial in which patients were randomized to a conservative approach of 1 mo of warfarin or the TEE-facilitated approach. This study confirmed the "equivalence" of the expedited TEE and the conventional approaches. Optimal patients for TEE expedited cardioversion likely include those with a relatively brief (<1 mo) duration of AF, or those with an increased risk of hemorrhagic complications. Assuming expeditious performance of TEE and cardioversion, thereby not prolonging the initial hospitalization, the TEE approach has been shown to be cost effective for inpatients and for enhancing long-term maintenance of sinus rhythm. At our Center, TEE-facilitated cardioversion is offered for nearly all inpatients. For outpatients, TEE is only generally offered to those patients at increased risk for a warfarin complication or those who are highly symptomatic. Other sites equally offer the TEE strategy to inpatients and outpatients.

MANAGEMENT OF PATIENTS WITH TEE EVIDENCE OF THROMBUS

The optimal treatment for patients who have TEE evidence of atrial thrombi has not been identified. Despite therapeutic heparin or warfarin and avoidance of cardioversion, these patients remain at increased risk for adverse events. As illustrated in Fig. 10, we believe it is most prudent to perform a follow-up TEE (after ≥4 wk of warfarin) to document *complete thrombus resolution* before elective cardioversion. If residual thrombus is present, we do *not* advise cardioversion, although this area is controversial.

TEE Facilitated Cardioversion Without Anticoagulation

In the *absence* of the anticoagulation strategy outlined in Fig. 10, several centers have reported clinical thromboembolism following a "negative TEE" for atrial thrombus. The mechanism of these adverse events is unknown and may be related to thrombi not visualized by TEE or to thrombi that form during the pericardioversion period. Because of these reports, we strongly encourage the use of systemic anticoagulation at the time of TEE and extending to 1 mo after cardioversion. For the patient with nonvalvular AF in whom warfarin is contraindicated, we offer the option of full-dose heparin anticoagulation (partial thromboplastin time 50–70 s) at the time of TEE and extending to at least 24 h after cardioversion. Although unproven, this approach is likely to be preferred to "blind" cardioversion.

SUGGESTED READING

Al-Saady NM, Obel OA, Camm AJ. Left atrial appendage: structure, function, and role in thromboembolism. Heart 1999;82: 547–554.

Berger M, Schweitzer P. Timing of thromboembolic events after electrical cardioversion of atrial fibrillation or flutter: a retrospective analysis. Am J Cardiol 1998;82:1545–1547.

Black IW, Fatkin D, Sagar KB, et al. Exclusion of atrial thrombus by transesophageal echocardiography does not preclude embolism after cardioversion of atrial fibrillation: a multicenter study. Circulation 1994;89:2509–2513.

Bollmann A, Binias KH, Grothues F, Schwerdtfeger A, Klein HU. Left atrial appendage function and pulmonary venous flow in patients with nonrheumatic atrial fibrillation and their relation to spontaneous echo contrast. Echocardiography 2002;19: 37–43.

Chan SK, Kannam JP, Douglas PS, Manning WJ. Multiplane transesophageal echocardiographic assessment of left atrial appendage anatomy and function. Am J Cardiol 1995;76: 528–530.

Ernst G, Stollberger C, Abzieher F, et al. Morphology of the left atrial appendage. Anat Rec 1995;242:553–561.

Gallagher MM, Hennessy BJ, Edvardsson N, et al. Embolic complications of direct current cardioversion of atrial arrhythmias: Association with low intensity of anticoagulation at the time of cardioversion. J Am Coll Cardiol 2002;40: 926–933.

Garcia-Fernandez MA, San Roman D, Torrecilla E, et al. Transesophageal echocardiographic detection of atrial wall aneurysm as a result of abnormal attachment of mitral prosthesis. Am Heart J 1992;124:1650–1652.

Jue J, Winslow T, Fazio G, Redberg RF, Foster E, Schiller NB. Pulsed Doppler characterization of left atrial appendage flow. J Am Soc Echocardiogr 1993;6:237–244.

Kaymaz C, Ozdemir N, Kirma C, Sismanoglu M, Daglar B, Ozkan M. Location, size and morphological characteristics of left atrial thrombi as assessed by echocardiography in patients with rheumatic mitral valve disease. Eur J Echocardiogr 2001;2: 270–276.

Klein AL, Grimm RA, Black IW, et al. ACUTE Investigators. Cardioversion guided by transesophageal echocardiography: the ACUTE pilot study. A randomized, controlled trial. Ann Intern Med 1997;126:200–209.

Klein AL, Grimm RA, Murray RD, Apperson-Hansen C, et al. ACUTE Investigators. Use of transesophageal echocardiography to guide cardioversion in patients with atrial fibrillation. N Engl J Med 2001;344:1411–1420.

Maltagliati A, Pepi M, Tamborini G, et al. Usefulness of multiplane transesophageal echocardiography in the recognition of artefacts and normal anatomical variants that may mimic left atrial thrombi in patients with atrial fibrillation. Ital Heart J 2003;4:797–802.

Manning WJ, Silverman DI, Gordon SPF, Krumholz HM, Douglas PS. Cardioversion from atrial fibrillation without prolonged anticoagulation with use of transesophageal echocardiography to exclude the presence of atrial thrombi. N Eng J Med 1 993;328:750–756.

Manning WJ, Silverman DI, Katz SE, et al. Impaired left atrial mechanical function after cardioversion: relationship to the duration of atrial fibrillation. J Am Coll Cardiol 1994;23: 1535–1540.

Manning WJ, Silverman DI, Waksmonski CA, Oettgen P, Douglas PS. Prevalence of residual left atrial thrombi among patients presenting with thromboembolism and newly recognized atrial fibrillation. Arch Int Med 1995;155:2193–2197.

Manning WJ, Weintraub RM, Waksmonski CA, et al. Accuracy of transesophageal echocardiography for identifying left atrial thrombi: a prospective, intraoperative study. Ann Int Med 1995;123:817–822.

Mugge A, Kuhn H, Nikutta P, Grote J, Lopez JA, Daniel WG. Assessment of left atrial appendage function by biplane transesophageal echocardiography in patients with nonrheumatic atrial fibrillation: identification of a subgroup of patients at increased embolic risk. J Am Coll Cardiol 1994;23:599–607.

Omran H, Jung W, Rabahieh R, et al. Imaging of thrombi and assessment of left atrial appendage function: a prospective study comparing transthoracic and transoesophageal echocardiography. Heart 1999;81:192–198.

Orsinelli DA, Pearson AC. Usefulness of multiplane transesophageal echocardiography in differentiating left atrial appendage thrombus from pectinate muscles. Am Heart J 1996;131:622–623.

Seto TB, Taira DA, Tsevat J, Manning WJ. Cost-effectiveness of transesophageal echocardiography-guided cardioversion for hospitalized patients with atrial fibrillation. J Am Coll Cardiol 1997;29:122–130.

Silverman DI, Manning WJ. Current perspective: role of echocardiography in patients undergoing elective cardioversion of atrial fibrillation. Circulation 1998;98:479–486.

Stoddard MF, Dawkins P, Prince CR, Longaker RA. Transesophageal echocardiographic guidance of cardioversion in patients with atrial fibrillation. Am Heart J 1995;129: 1204–1215.

Subramaniam B, Riley MF, Panzica PJ, Manning WJ. Transesophageal echocardiographic assessment of right atrial appendage anatomy and function: comparison with the left atrial appendage and implications for local thrombus formation. J Am Soc Echocardiogr 2006 (in press).

The Atrial Fibrillation Follow-up Investigation of Rhythm Management (AFFIRM) Investigators. A comparison of rate

control and rhythm control in patients with atrial fibrillation. N Engl J Med 2002;347:1825–1833.

Van Gelder IC, Hagens VE, Bosker HA, et al. A comparison of rate control and rhythm control in patients with recurrent persistent atrial fibrillation. N Engl J Med 2002;347:1834–1840.

Veinot JP, Harrity PJ, Gentile F, et al. Anatomy of the normal left atrial appendage: a quantitative study of age-related changes in 500 autopsy hearts: implications for echocardiographic examination. Circulation 1997;96:3112–3115.

Weigner MJ, Thomas LR, Patel U, et al. Early cardioversion of atrial fibrillation facilitated by tranesophageal echocardiography: Short-term safety and impact on maintenance of sinus rhythm at 1 year. Am J Cardiol 2001;110: 694–702.

17 Cardiac Source of Embolus

Justina C. Wu, MD, PhD

Contents

CASE VIGNETTE 1, ELDERLY PATIENT

A 75-yr-old female with a history of hyperlipidemia, smoking, and hypertension awoke with acute right arm and leg numbness and right facial weakness that lasted for 30 h before she presented to the emergency room. She had no history of chest pain, shortness of breath, or other symptoms. She was evaluated by the neurology service, who felt she had suffered an embolic stroke. Subsequent carotid imaging revealed a 95% stenosis of her left internal carotid artery. Before planned carotid endarterectomy, an echocardiogram was ordered (Fig. 1).

This parasternal long axis view shows a prominent ridge of highly echodense material and a thickening of the anterior aspect of the ascending aortic root extending from the sinuses of Valsalva into the ascending aorta. This represents a prominent atherosclerotic plaque, and is a frequent location for such abnormalities in patients with peripheral vascular disease. Although it may not represent the culprit source of atheroemboli in stroke, it is a sign of widespread atheromatous burden, which in this case has also involved the culprit internal carotid artery.

An embolus is an intravascular mass, which usually comprises a thrombus, atheromatous, or cellular matter that has entered the circulation and causes symptoms by lodging in end arteries and interrupting blood flow to the organs. Emboli from the venous system can enter the right side of the heart and cause pulmonary emboli, whereas those originating from the left side of the heart and great arteries can cause infarcts in the brain, kidneys, intestines, and skin. Although small strokes and transient ischemic attacks (TIAs) are often caused by atheromatous debris from the aorta or major cerebral arteries, an embolus large enough to occlude multiple major peripheral or visceral arteries is more likely to originate from the heart. A paradoxical embolus is a systemic infarct in which the source of the embolus is thought to be from the venous system, which has bypassed the pulmonary circulation by means of an intracardiac shunt, and crossed into the arterial circulation.

Epidemiology of Cardiac Source of Embolus in Elderly Patients

Brain infarcts, or strokes, are the most frequent embolic disease, particularly in the elderly. A TIA is a temporary loss of blood flow to a region of the brain, which does not have the lasting clinical sequelae of a stroke but which represents a passing embolic event that has spontaneously resolved. The workup of a patient with a TIA or stroke and the potential role of echocardiography must be focused with respect to the type of stroke, patient's age, the likelihood of associated cardiovascular disease, and potential treatment options.

Embolic strokes are usually suggested by sudden onset of symptoms in the middle or anterior cerebral artery territories, or multiple events in peripheral territories. These

From: *Contemporary Cardiology: Essential Echocardiography: A Practical Handbook With DVD*
Edited by: S. D. Solomon © Humana Press, Totowa, NJ

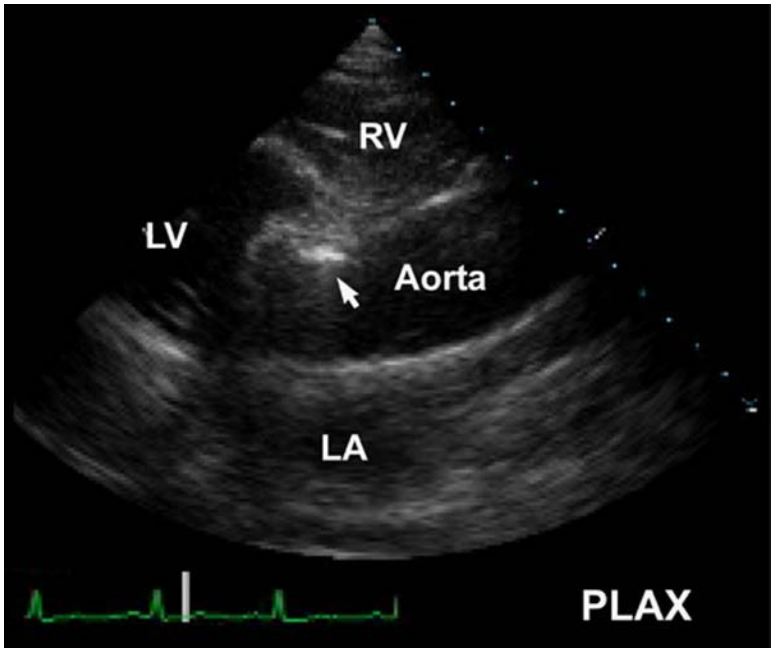

Fig. 1. A 75-yr-old female with cardiovascular risk factors and acute neurological deficits. High parasternal long-axis view showing calcified atherosclerotic plaque.

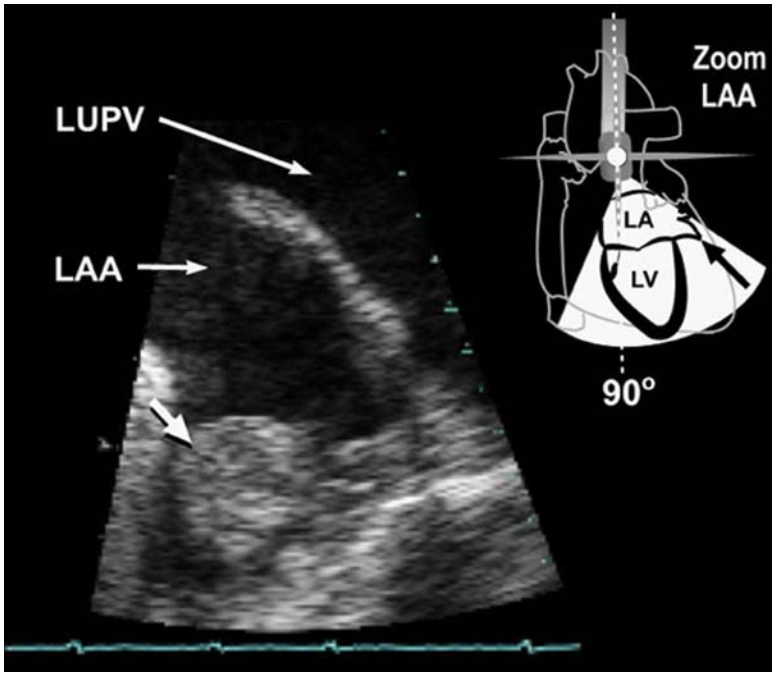

Fig. 2. Midesophageal zoomed image of the left atrial appendage (LAA) at omni 90° showing well-defined thrombus in a patient with atrial fibrillation.

should be distinguished from lacunar or hemorrhagic strokes, which are secondary to intrinsic cerebrovascular disease and/or hypertension. In elderly patients (>55 yr old), atherosclerosis of the great arteries and internal carotid arteries are thought to account for 20–60% of embolic strokes. These patients often have coexisting cardioaortic disease and internal carotid artery disease, rendering it difficult to identify which vessel is the culprit source of embolus in many cases. Atrial fibrillation with associated thrombus forming in the left atrial appendage (Fig. 2) is also one of the most frequent causes of embolic stroke. Younger patients (<55 yrs old) with embolic strokes are less likely to have significant atheromatous disease, and more likely to have cardiogenic sources of

Table 1
Potential Cardiovascular Etiologies of Stroke

A. From great arteries
Internal carotid artery atheroma
Aortic root and ascending aortic atheroma
Arterial dissection
Vasculitis
B. Cardioembolic
Atrial fibrillation, rheumatic heart disease → atrial thrombus
Left ventricular dysfunction → ventricular thrombus
Mitral stenosis, prolapse, mitral annular calcification
Endocarditis → valvular vegetations; marantic endocarditis
Tumors: myxoma, papillary fibroelastoma, fibrin strands
Mitral valve and aortic valve prostheses, particularly mechanical → thromboemboli
Intracardiac shunts:
Patent foramen ovale and/or atrial septal aneurysm
Atrial septal defect
Ventricular septal defect
Hematologic hypercoagulable state: activated protein C resistance/Factor V
Leiden mutation, anticardiolipin antibody, Lupus anticoagulant, prothrombin mutation

embolus or hypercoagulable states. Approximately 40% of strokes are of undetermined origin ("cryptogenic"), of which up to half have been associated with various cardiac abnormalities, which are detectable by echocardiography.

Other systemic emboli—those targeting the eye, kidney, spleen, or skin—are usually the result of vegetation or thrombus shed from an abnormal or prosthetic cardiac valve, or the result of atheromatous debris dislodged by intra-arterial catheter procedures.

A pulmonary embolus is the result of a deep venous thrombosis, which has broken free and traveled to the lung bed. Risk factors for venous stasis, the diagnosis, treatment, and echocardiographic findings of pulmonary embolism are discussed in Chapter 18.

Etiology

Potential cardiovascular etiologies of stroke are listed in Table 1. Transthoracic echocardiography (TTE) can detect the majority of the potential cardioembolic causes of systemic emboli. The prevalence of cardiac abnormalities predisposing to emboli differ according to the age of the patient.

In older patients, significant findings may include the following: atheroma may be seen as irregular thickening of the aortic wall in the aortic root, ascending aorta, arch, and descending abdominal aorta. Calcified plaques tend to appear very jagged and echobright, and associated thrombus can appear as tethered but mobile elements. Plaques that are more than 4 mm in thickness, or which contain mobile or protruding elements, are associated with a higher risk of stroke. Atheroma are better visualized on transesophageal echocardiography (TEE) (Fig. 3A,C; please *see* companion DVD for corresponding video). When coronary artery bypass surgery is contemplated in patients with significant aortic root disease, TEE or epiaortic scanning routinely assists in guiding bypass pump cannula placement, to decrease the risk of causing a stroke by dislodging plaque in the punctured area. The presence of atrial fibrillation, particularly in the presence of rheumatic heart disease, increases the risk of atrial thrombus formation. Atrial thrombi often occur in association with spontaneous echo contrast, which is thought to represent increased fibrin and red blood cells in the early stages of coagulation. Although TTE often does not fully visualize the left atrial appendage, thrombi may occasionally be seen in the body of the left or right atrium. Figure 4 is a parasternal short-axis view of a thrombus within the left atrial appendage (*see* Chapter 16). The presence of a dyskinetic or aneurysmal area of left ventricle in a patient with a history of myocardial infarction should always prompt evaluation for an associated intramural thrombus (*see* Chapter 7), which can vary greatly in shape and mobility.

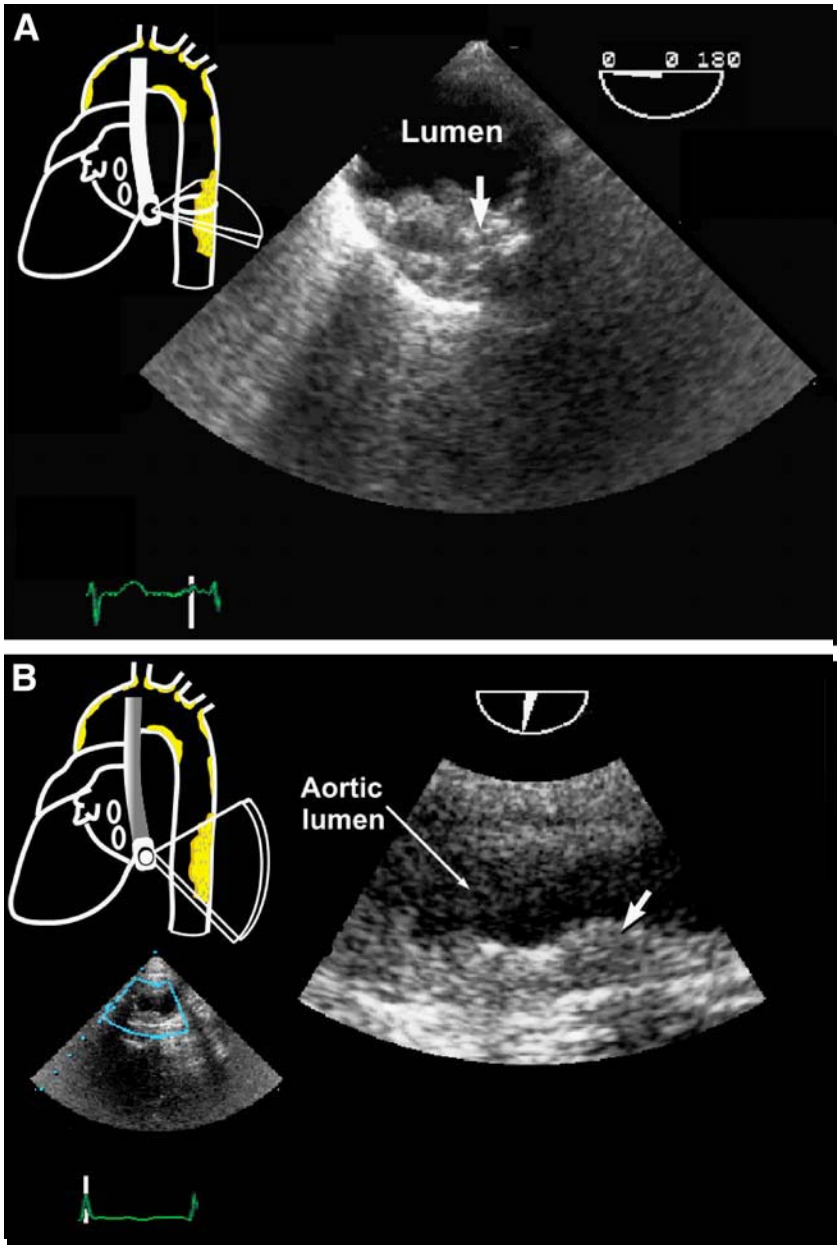

Fig. 3. (*See* legend, facing page)

Mitral stenosis, stranding, and mitral annular calcification have all been suggested to be associated with risk of embolus, although there are often confounding risk factors. Mitral valve prolapse was historically implicated as a risk factor, but this appears to be an artifact of overdiagnosis of mitral valve prolapse in this population, rather than comprising a true etiological substrate. Bacterial vegetations (Fig. 5; please *see* companion DVD for corresponding video) are more likely to occur on abnormal native valves, such as bicuspid aortic or myxomatous mitral valves. Prosthetic valve thrombus or vegetation may be detected as independently mobile echodensities, predominantly located on the low-pressure side of the valve. On mechanical prosthetic valves, the masses may not be clearly visualized because of acoustic shadowing by the prosthesis, but if one or more discs appear immobile or an unusually high transvalvular gradient is detected by Doppler, suspicion for obstruction remains high and a TEE should be performed. Marantic endocarditis is a disease associated with cancer, inflammatory, and hypercoagulable states, and is caused by continuous formation of fibrin and thrombus on the valves, which then break off into the bloodstream. Other findings commonly found in elderly

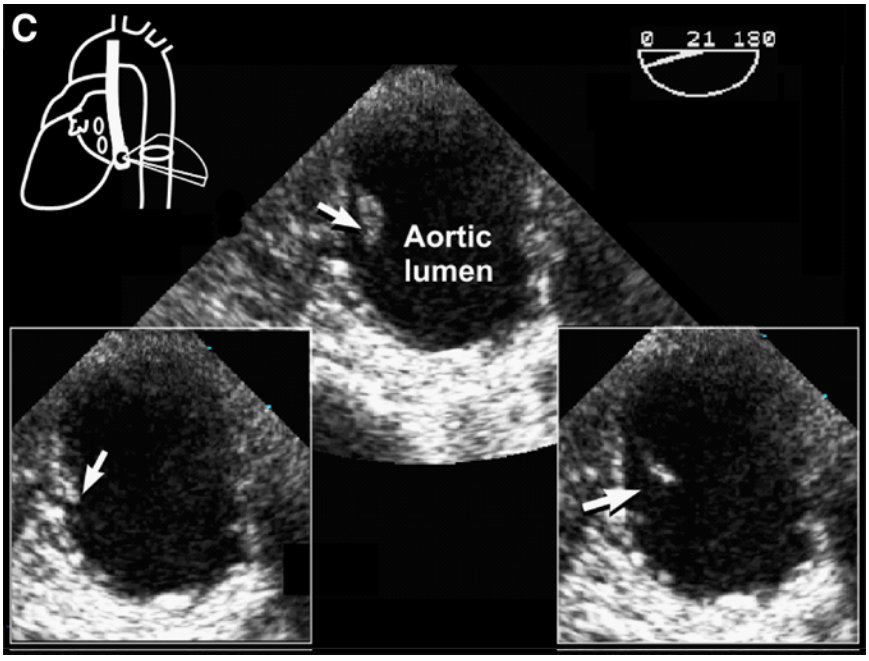

Fig. 3. (A) Transesophageal short-axis view of the descending thoraci aorta showing large calcified atheromatous plaque. **(B)** Transesophageal long-axis view of the desecending thoraci aorta (same patient in **A**) showing the longitudinal extent of the large calcified atheroma. **(C)** Serial short-axis transesohageal echocardiographic images of the aorta showing mobile element of atheromatous plaque. (Please *see* companion DVD for corresponding video.)

patients that may increase the risk of stroke include aortic sclerosis (irregular tissue thickening of the aortic valve leaflet edges), Lambl's excrescences (fibrin-containing strands found on the leaflet edges and occasionally in the left ventricle outflow tract), and papillary fibroelastomas (*see* Chapter 19). More rarely, echocardiography can discern aortic dissections with the intimal flap extending cranially to occlude a carotid artery. Subcostal views of the inferior vena cava infrequently detect previously unsuspected deep venous thrombi.

CASE VIGNETTE 2, YOUNGER PATIENT

A 25-yr old active male presented with a "grayed-out" section of his left upper visual field 1 d after returning home from a long intercontinental flight. He had no prior medical history, and recalled no recent headache, fevers, chest pain, shortness of breath, palpitations, weakness or pain in his extremities, or other neurological problems. A head magnetic resonance imaging (MRI) showed a subacute right occipital infarct, without evidence of acute bleeding. He was treated with intravenous heparin, and a TTE was obtained. Although the interatrial septum looked normal, and no shunting was detected by color Doppler, an injection of intravenous agitated saline ("bubble study") showed right-to-left interatrial shunting within five cardiac cycles. This is indicative of a patent foramen ovale (PFO) (Fig. 6; please *see* companion DVD for corresponding video). Note that the patient was asked to "sniff," a quick inhalation that transiently increases right atrial pressure to increase sensitivity for right-to-left shunting.

Epidemiology of Cardiac Source of Embolus in Younger Patients

The epidemiology of cardiogenic emboli in younger patients is different from that of older subjects. Those with abnormal native valves, such as myxomatous or prolapsed mitral valve or bicuspid aortic valves are susceptible to endocarditis and resultant vegetation, which can embolize. Vegetations, which are more than 10 mm are at the highest risk for causing embolic complications. Among intracardiac tumors, myxomas are also more often found in younger patients owing to embolization (*see* Chapter 19).

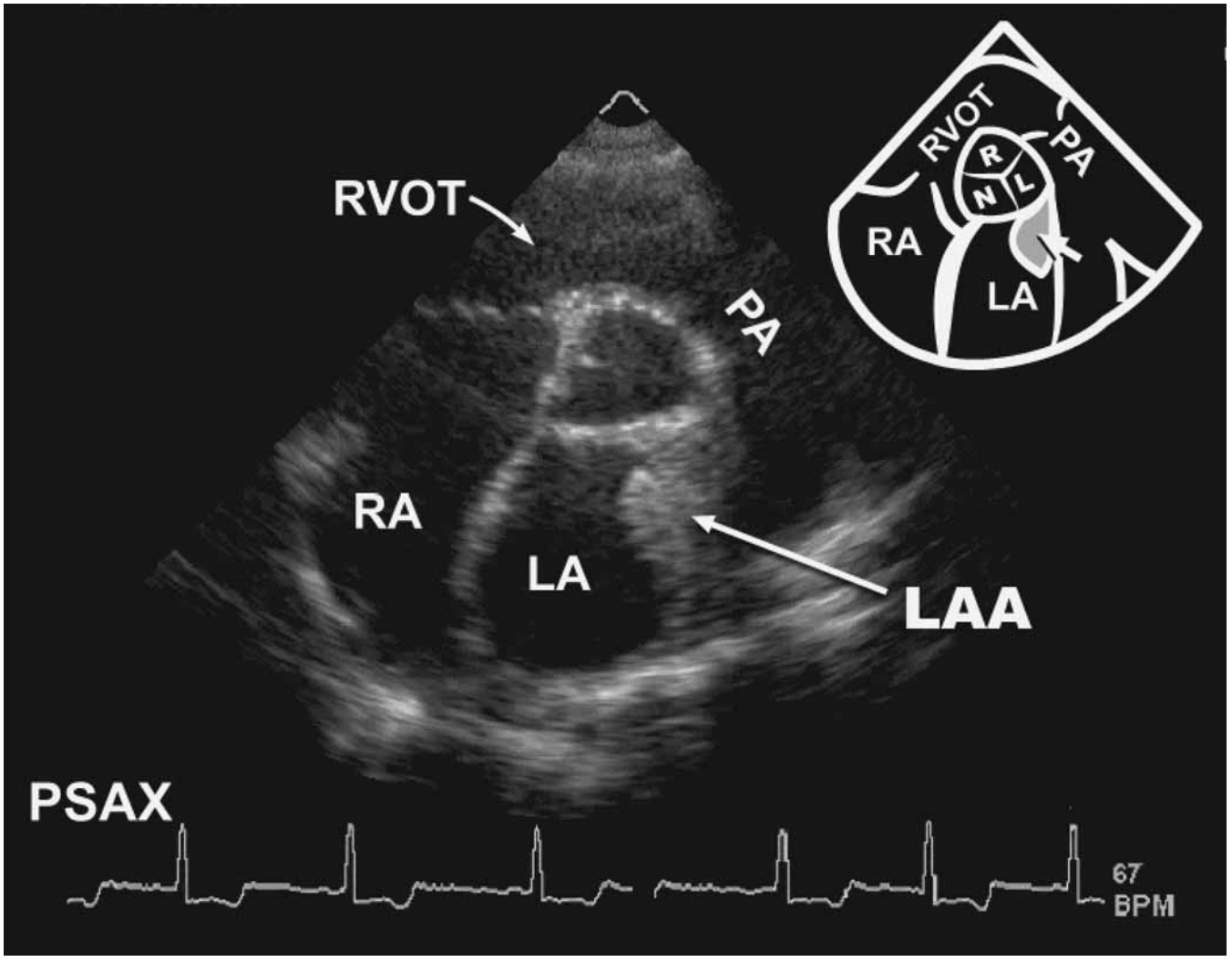

Fig. 4. Parasternal short-axis view showing clot in left atrial (LA) appendage.

Paradoxical embolus is a well-known risk of congenital heart disease with intracardiac shunting, as in the case of atrial septal defects or ventricular septal defects. The presence of a dilated right atrium and/or right ventricle in the absence of other causes should prompt a diligent search for intracardiac shunting by both two-dimensional imaging and Color Doppler (Fig. 7; please *see* companion DVD for corresponding video).

PFO is a condition in which the ostium primum arises from the left atrial side and spans the fossa ovalis, but does not fuse completely with the apposing ostium secundum. PFO is essentially a normal variant, occurring in 25–30% of the population. Under conditions in which right atrial pressure exceeds left atrial pressure, the PFO can allow right-to-left intracardiac flow to occur (similar to a trap door or flap). The potential channel of the PFO is typically not visible on two-dimensional echocardiography, although increased mobility of the septum in the fossa ovalis area can be a clue to the presence of one. A careful color Doppler scan of a sector zoomed in on the interatrial septum, particularly in the subcostal window, can occasionally detect flow across the PFO as a narrow red jet of transient left-to-right flow (Fig. 8). Flow is typically greatest in late systole and early diastole.

Care should be taken to avoid false positives caused by eccentric tricuspid regurgitant jets or swirling caval flow. A "bubble study," or injection of intravenous saline that has been agitated with air to produce echo contrast, is an echocardiographic method used to detect PFO. Because the bubbles produced by agitation within a syringe are relatively large and usually filtered by the pulmonary bed, the appearance of echogenic bubbles in the left side of the heart immediately (within six beats of opacifying the

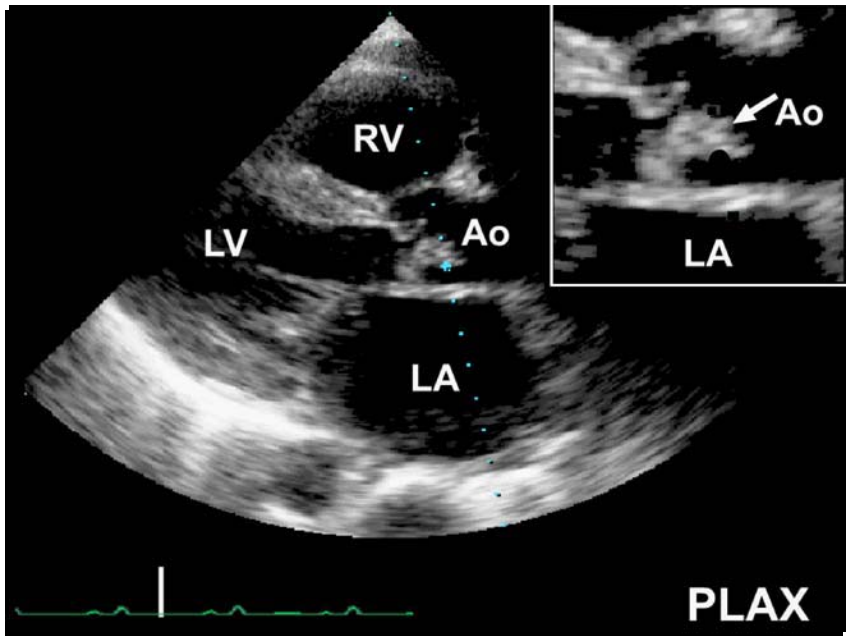

Fig. 5. Parasternal long-axis views (PLAX) showing verrucous bacterial vegetation affecting the aortic valve—especially the non-coronary cusp. (Please *see* companion DVD for corresponding video.)

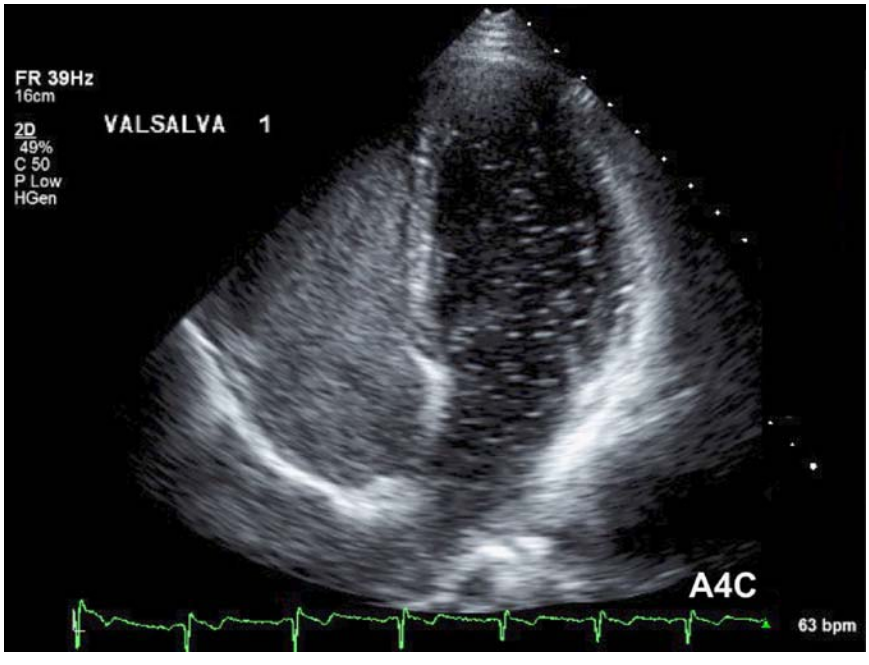

Fig. 6. Agitated saline contrast (bubble study) showing adequate right heart opacification in this apical four-chamber view. Note the right-to-left shunt (bubbles in the left heart chambers) via a patent foramen ovale (arrow). The Valsalva maneuver (sniff test) transiently increase right-sided pressures—thereby increasing the sensitivity of the "bubble study." (Please *see* companion DVD for corresponding video.)

right atrium) is indicative of right-to-left shunting (Fig. 6; please *see* companion DVD for corresponding video). Because left atrial pressure is usually higher than right atrial pressure, manuevers, which transiently increase right atrial pressure such as the Valsalva maneuver, coughing or sniffing, abdominal compression, or raising the legs can increase the sensitivity of a bubble study for detecting PFO. PFOs can allow paradoxical emboli from

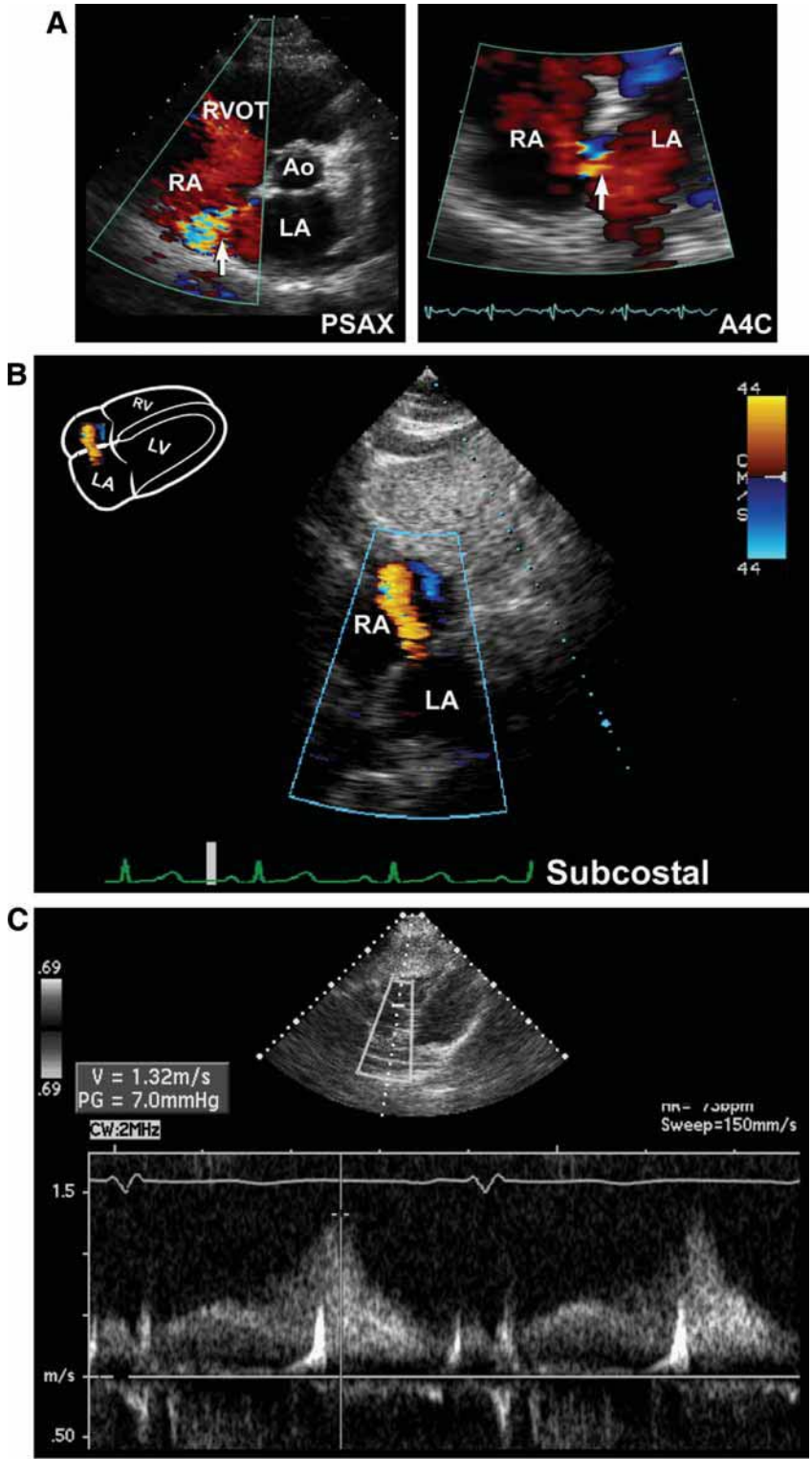

Fig. 7. (A) Parasternal short-axis (PSAX) and apical four-chamber views (A4C) show flow acceleration and left-to-right shunt across this secundum atrial septal defect on color Doppler examination. **(B)** Color flow Doppler applied to the interatrial septum from the subcostal window shows left-to-right shunt across interatrial septum. This view provides a better alignment for Doppler evaluation of shunt flow. **(C)** Continuous-wave Doppler examination of the atrial septal defect. Peak velocity of the left-to-right shunt across the defect was 1.3 m/s corresponding to peak gradient of 7.0 mmHg. (Please *see* companion DVD for corresponding video.)

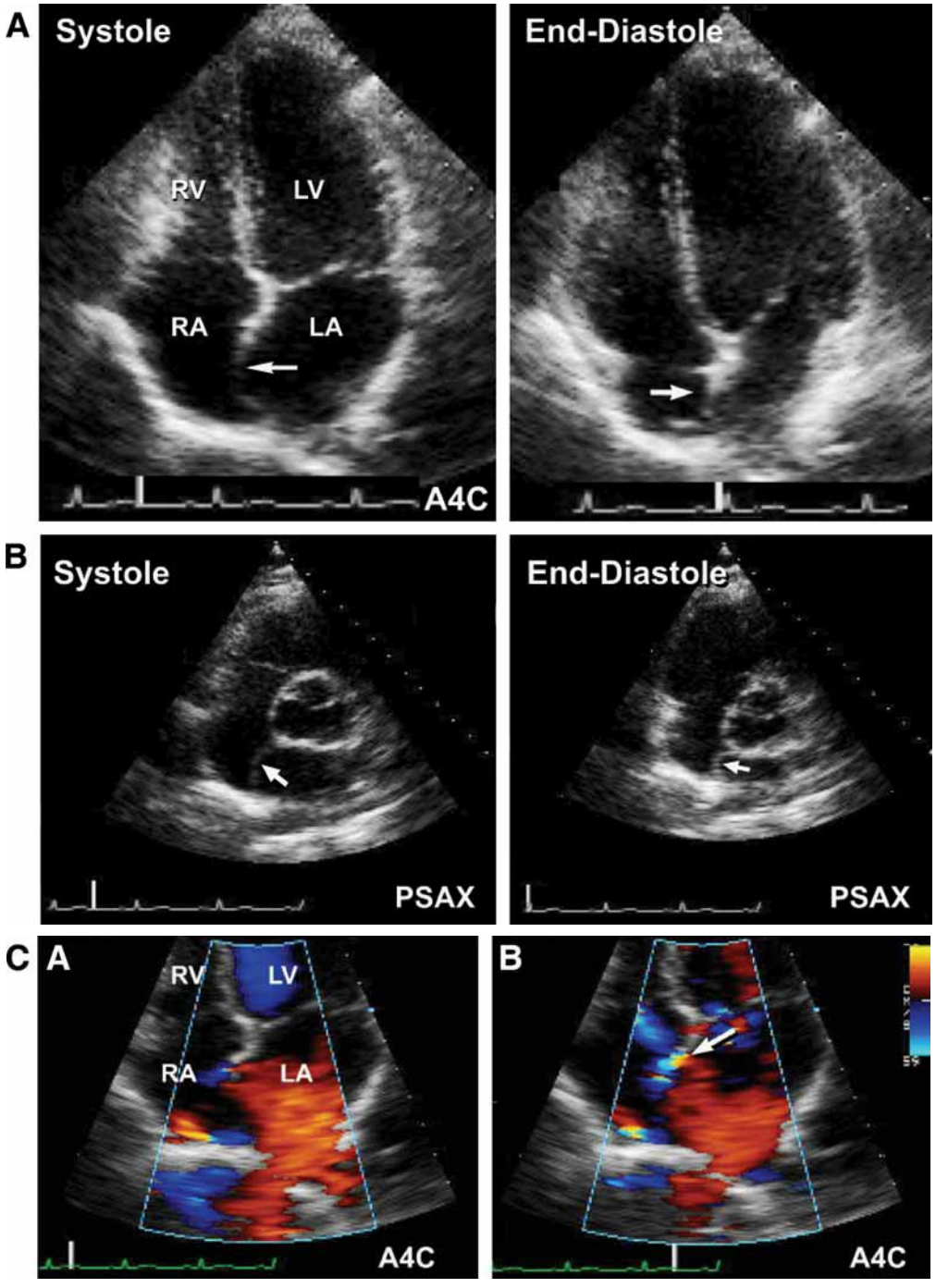

Fig. 8. (A) Apical four-chamber frames showing hypermobile interatrial septum. **(B)** Parasternal short axis views showing hypermobile interatrial septum. **(C)** Color flow Doppler interrogation of hypermobile interatrial septum in **A** and **B** revealed transient left-to-right shunt (arrow) via a patent foramen ovale.

the venous system to lodge in the systemic arteries, although the actual passage of a thromboembolus through a PFO is only rarely captured on echocardiographic views (Fig. 9; please *see* companion DVD for corresponding video). The incidence of PFO appears to be higher in patients with ischemic stroke, exceeding threefold higher in patients younger than 55 yr old.

An atrial septal aneurysm (ASA) is an excessively redundant hypermobile area of the interatrial septum, which can be seen on echocardiogram (Figs. 10 and 11;

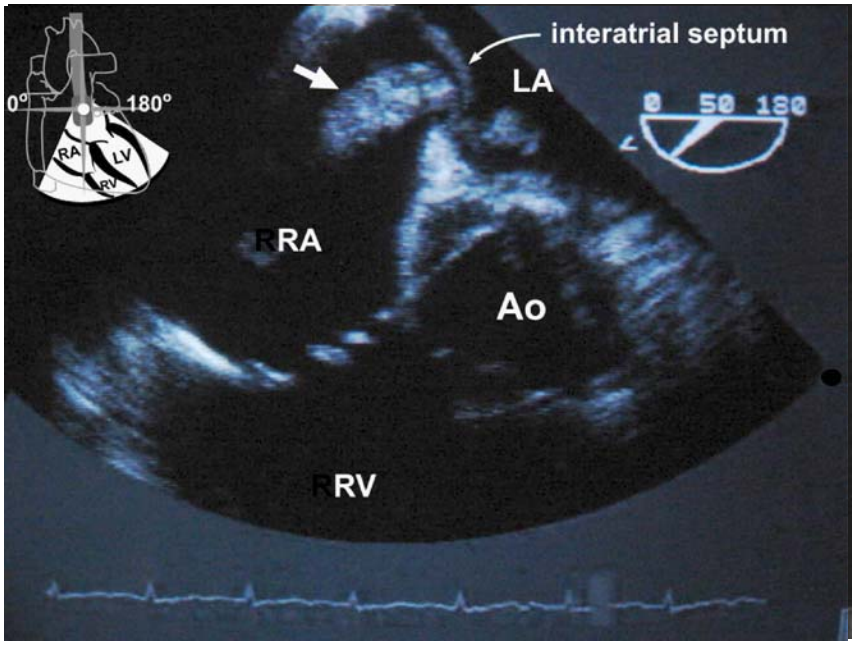

Fig. 9. Serial transesophageal echocardiographic images showing thromboembolus "in transit" (arrow) through a patent foramen ovale. (Please *see* companion DVD for corresponding video.)

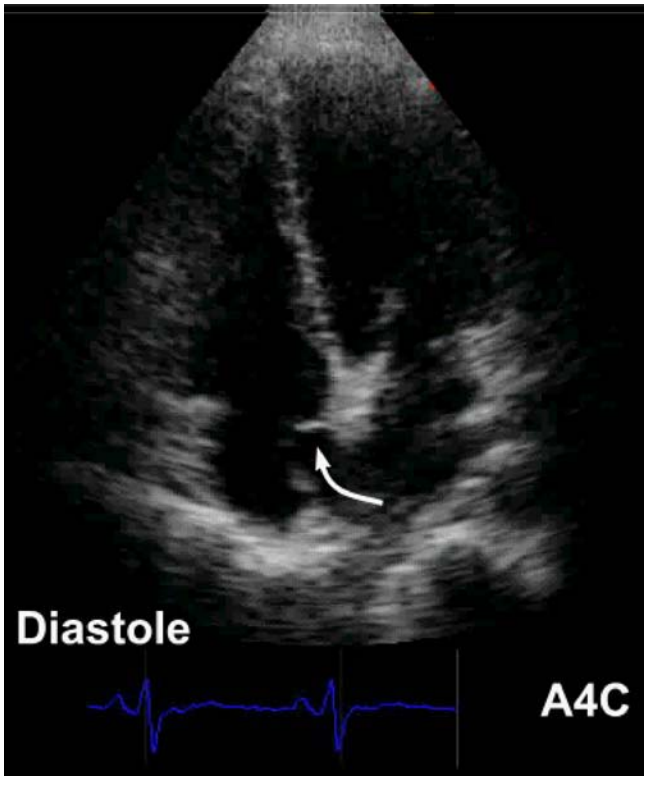

Fig. 10. Apical four-chamber view (A4C) showing interatrial septal aneurysm. (Please *see* companion DVD for corresponding video.)

please *see* companion DVD for corresponding video for Fig. 10). It is very frequently associated with PFO, and typically involves the area of the fossa ovalis, but can extend to include the surrounding limbic areas or even the entire interatrial septum. The criteria for the diagnosis of ASA vary, but it is generally accepted that maximal excursion of the interatrial septum more than 10 mm from centerline defines an ASA. Localized

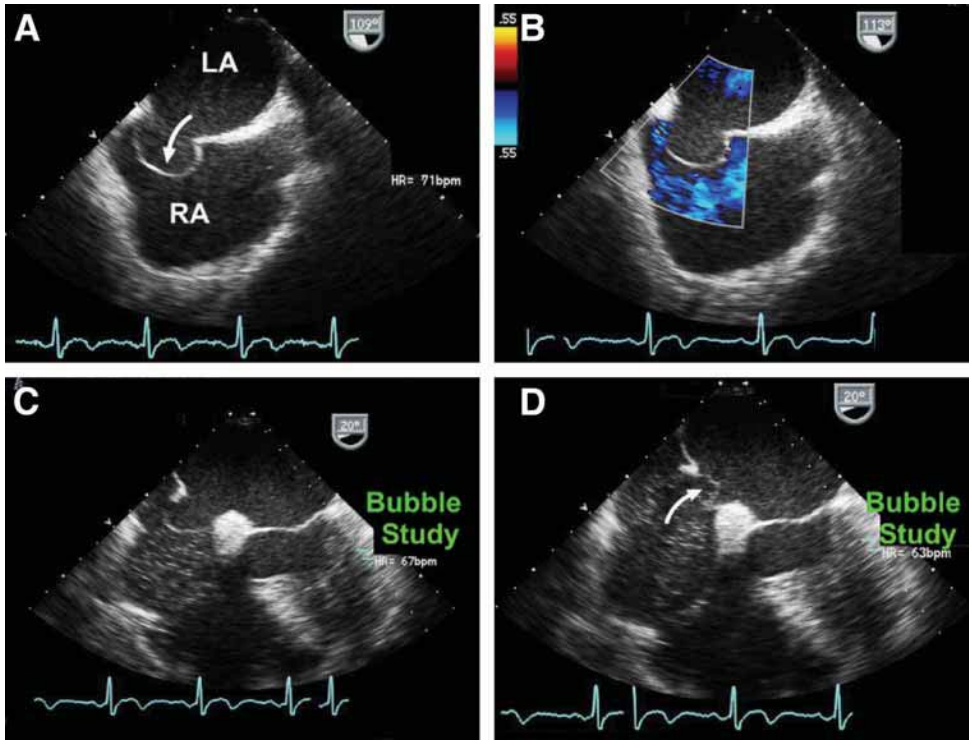

Fig. 11. Transesophageal echocardiographic images showing atrial septal aneurysm **(A–D)**. Color flow Doppler interrogation of interatrial septum **(B)** and agitated saline contrast "bubble" study **(C,D)** revealed no shunt. The aneurysmal wall inverted intermittently during the cardiac cycle (**D**, arrow).

thrombi have been found on an anecdotal basis nestled within ASAs, and ASAs are associated three- to sixfold higher in patients with ischemic stroke, again with the highest incidence in the younger population.

The incidence of both a PFO and an ASA is markedly increased in patients with embolic stroke, more than 15-fold in one meta-analysis. The data is compelling for a causal connection between these two entities, and theories to explain the causality include paradoxical embolus from venous sources, direct embolus from thrombus formed within the aneurysm, and formation of atrial thrombus as an indirect result of atrial arrhythmia.

Currently the treatment of young patients with interatrial septal abnormalities and an ischemic event is still controversial. Patients younger than 55 yr of age with a PFO alone appear not to be at higher risk of stroke than the general population. However, the presence of both PFO and ASA appears to confer a higher risk of a recurrent ischemic event, despite treatment with aspirin. A large amount of right-to-left shunting may also confer increased risk of paradoxical emboli. Options for therapy and secondary risk prevention at this point include aspirin, plus additional anticoagulation and/or closure of the PFO by surgery or transcatheter devices (Fig. 12; please *see* companion DVD for corresponding video).

CASE VIGNETTE 2 CONTINUED

A neck MRI/magnetic angiogram study (MRA) and hypercoagulability work-up in the patient was negative. A TEE showed a normal interatrial septum with a PFO, but no atrial septal aneurysm was detected. He was treated with aspirin, and is considering either Coumadin or percutaneous PFO closure in the future is further neurological events occur.

Suggested Work-Up for Source of Embolus

The utility and yield of echocardiography in searching for a presumed cardiac source of embolus will vary with patient's age and comorbidities. Echocardiography is more likely to be useful in younger patients, or those with known predisposing cardiac conditions. In contrast, the workup of most elderly patients with a stroke should start with an imaging modality of the internal carotid arteries (either carotid duplex ultrasound, angiographic computed tomography study, or MRI/MRA).

When is TEE indicated in the workup of stroke? If there is a high suspicion of cardiac source of embolus,

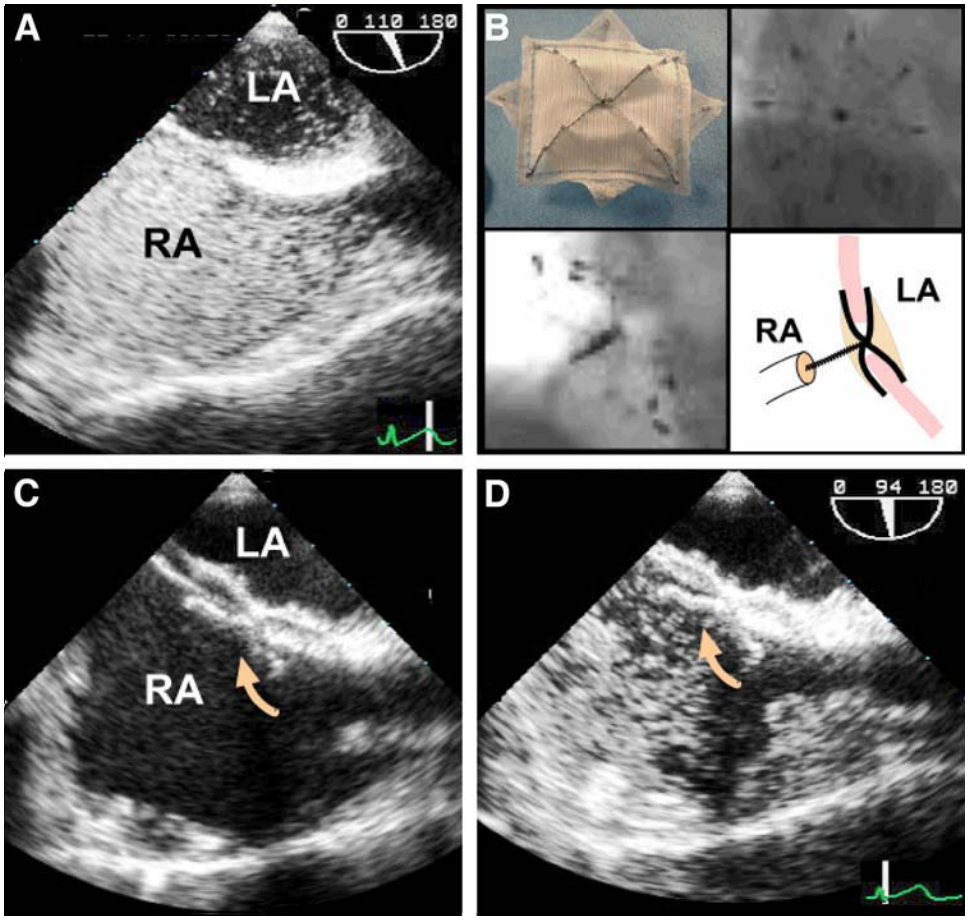

Fig. 12. Transesophageal echocardiography and agitated saline contrast ("bubble") study showing shunting of bubbles from right atrium (RA) to left atrium (LA) via patent foramen ovale (PFO) **(A)**. **(B)** Shows one popular model of transcatheter closure devices (CardioSEAL®), its appearance during cardiac catherization, and a sketch of its final deployment and anatomical relationship to the interatrial septum. The deployed closure device **(C)** followed by a repeat "bubble" study confirmed successful closure of the PFO—note the absence of bubbles in the left atrium **(D)**. (Please *see* companion DVD for corresponding video.)

and the TTE yields insufficient information to rule out a cardiac source, a TEE is indicated, provided that the results would impact therapy. The sensitivity of TEE has been shown to be superior for left atrial appendage thrombus (nearly 100 vs 39–63% for TTE), ascending aortic atheroma, and vegetations (88–100% sensitivity vs 44–60% for TTE). TEE is better able to evaluate prosthetic valves, particularly mitral valves, which often cause much acoustic shadowing artifact on transthoracic studies. TEE is also more sensitive (89 vs <50% for TTE using contrast) and 100% specific for detecting interatrial septal abnormalities. However, it is only moderately better (11 vs 4% for TTE) for detecting intracardiac masses, and there is no incremental yield in finding intracardiac masses (including thrombi) in patients without cardiovascular disease and a negative TTE.

Class I (definitely proven to be of benefit) American College of Cardiology/American Heart Association guidelines for clinical application of echocardiography in neurological disease include:

1. Patients of any age with abrupt occlusion of a major peripheral or visceral artery.
2. Younger patients (<45 yr) with cerebrovascular events.
3. Older patients (>45 yr) with neurological events, without evidence of cerebrovascular disease or other obvious causes.
4. Patients for whom a clinical therapeutic decision (e.g., anticoagulation) will depend on the results of the echocardiogram.

Class III (definitely proven to be unbeneficial) indications are: patients for whom the result of the echocardiogram will not impact the approach to diagnosis or therapy.

SUGGESTED READING

Amarenco P, Cohen A, Tzourio C, et al. Atherosclerotic disease of the aortic arch and the risk of ischemic stroke. N Engl J Med 1994;331:1474–1479.

Beattie JR, Cohen DJ, Manning WJ, Douglas PS. Role of routine transthoracic echocardiography in evaluation and management of stroke. J Int Med 1998;243:281–291.

Brickner ME. Cardioembolic stroke. Am J Med 1996;100: 465–474.

Cerebral Embolism Task Force. Cardiogenic brain embolism. The second report of the Cerebral Embolism Task Force. Arch Neurol 1989;46:727–743.

Cheitlin MD, Alpert JS, Armstrong WF, et al. ACC/AHA Guidelines for the Clinical Application of Echocardiography. A report of the American College of Cardiology/ American Heart Association Task Force on Practice Guidelines (Committee on Clinical Application of Echocardiography). Developed in collaboration with the American Society of Echocardiography. Circulation 1997;95:1686–1744.

Kistler JP, Ropper AH, Heros RC. Therapy of ischemic cerebral vascular disease due to atherothrombosis. N Engl J Med 1984;311: 27–34;100–105.

O'Brien PJ, Thiemann DR, McNamara RL, et al. Usefulness of transesophageal echocardiography in predicting mortality and morbidity in stroke patients without clinically known cardiac sources of embolus. Am J Card 1998;81:1144–1151.

Overell JR, Bone I, Lees KR. Interatrial septal abnormalities and stroke: a meta-analysis of case-control studies. Neurology 2000;55:1172–1179.

The French Study of Aortic Plaques in Stroke Group. Atherosclerotic disease of the aortic arch as a risk factor for recurrent ischemic stroke. New Engl J Med 1996;334:1216–1221.

The Stroke Prevention in Atrial Fibrillation Investigators Committee on Echocardiography. Transesophageal echocardiographic correlates of thromboembolism in high-risk patients with nonvalvular atrial fibrillation. Ann Intern Med 1998;128:639–647.

18 Echocardiography in Pulmonary Embolism and Secondary Pulmonary Hypertension

David Aguilar, MD and Bernard E. Bulwer, MD, MSc

Contents

CASE PRESENTATION

A 66-yr-old female, initially admitted to hospital with anorexia, malaise, weakness, shortness of breath, developed urosepsis and acute renal failure. Appropriate treatment, including transient dialysis, was started and her renal function improved. One week later, she complained of bilateral leg weakness and lower extremity swelling that was followed 2 d later by acute dyspnea. She reported no chest pains or hemoptysis.

On examination she was tachypneic (respiratory rate >28/min), tachycardic (heart rate 110 bpm). Significant findings included bilateral leg swelling with tenderness on deep palpation. Distal pulses in both lower extremities were normal. Jugular venous pressure was 13 cm. Heart sounds were normal and no murmurs were heard. Crackles were heard bilaterally in basal lung fields.

Initial echocardiogram showed sinus tachycardia with no signs of acute ischemia. Q-waves were seen in the inferior leads, but no S1Q3T3 pattern observed. Platelet count fell during admission, dropping from 118 K/dL to 18 K/dL and the diagnosis or heparin-induced thrombocytopenia entertained; platelet factor four (PF4) antibodies were requested. Plasma D-dimer enzyme-linked immunosorbent assay test (ELISA) and serum troponin I levels were both mildly elevated. Arterial blood gases were reported at the lower limits of normal.

Transthoracic echocardiography (TTE) showed preserved left ventricular function with estimated ejection fraction of 60%. Marked right ventricular dilation with lateral wall hypokinesis with apical sparing was noted. No right ventricular hypertrophy was apparent. Mild tricuspid regurgitation (TR) was present with peak velocity measuring approx 3.1 m/s and pulmonary artery systolic pressure (PASP) measuring 39 mmHg + right atrial pressure (RAP). A relatively mobile echo-dense structure was seen at the bifurcation of the main pulmonary artery (Figs. 1 and 2; please *see* companion DVD for corresponding video). Ventilation-perfusion scan confirmed the diagnosis. Bilateral deep vein thrombosis was diagnosed by venous ultrasonography of the lower extremities.

From: *Contemporary Cardiology: Essential Echocardiography: A Practical Handbook With DVD*
Edited by: S. D. Solomon © Humana Press, Totowa, NJ

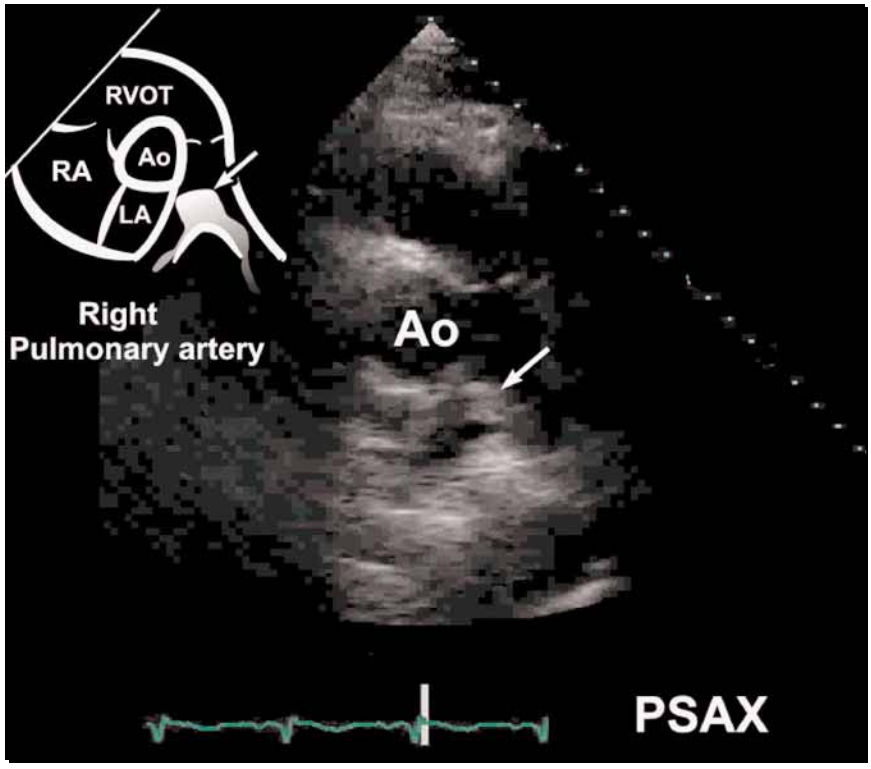

Fig. 1. Parasternal short axis (PSAX) view at the aortic valve level shows the right ventricular outflow tract (RVOT), main pulmonary artery, and right and left pulmonary artery. An echo-dense structure is seen in at the bifurcation of the main pulmonary artery, consistent with a pulmonary saddle embolus (arrow). (Please *see* companion DVD for corresponding video.)

Acute pulmonary embolism (PE) is a common problem with high morbidity and a 30-d mortality rate of 15–20%. Because of the scope and severity of the problem, the accurate diagnosis and management of acute PE is crucial. Echocardiography has increasing applications in the diagnosis, the risk assessment, and the management of PE. As a first-line tool, echocardiography allows for the preliminary differentiation of major life-threatening cardiovascular complications. Additionally, bedside echocardiography affords the opportunity to establish a prompt diagnosis and to identify patients with high-risk features, thus identifying a subset of patients that may benefit from more aggressive therapy, such as thrombolytic therapy. The use of echocardiography in the evaluation and management of PE is increasingly common as demonstrated in two recent registries, in which approx 50–75% of patients with PE underwent echocardiography.

Pathophysiology

Thrombi can form anywhere within the venous system and travel to the lungs to form a pulmonary embolus. Most typically, thrombi form within the deep veins of the legs and then travel through the venous system to the pulmonary circulation. When lodged in the pulmonary circulation, often at the bifurcation of the pulmonary arteries or within the proximal branches of the pulmonary arterioles, the effect of a PE is an acute increase in pulmonary vascular resistance. This increase in pulmonary vascular resistance is responsible for many of the echocardiographic findings seen in patients with acute severe PE. It is important to recognize that pulmonary pressure does not rise acutely in the setting of acute PE, just pulmonary resistance. Because the normal right ventricle (RV) is accustomed to relatively low pulmonary pressures, the maximal systolic right ventricular pressure is generally around 25 mmHg. A previously normal RV cannot acutely handle the increased load associated with a marked increase in pulmonary resistance. Pressure in the pulmonary artery, therefore, does not rise despite acute increase in pulmonary resistance.

ECHOCARDIOGRAPHIC FINDINGS SUPPORTING THE DIAGNOSIS OF PE

Echocardiography is normal in about 50% of unselected patients with acute PE, but it can provide direct

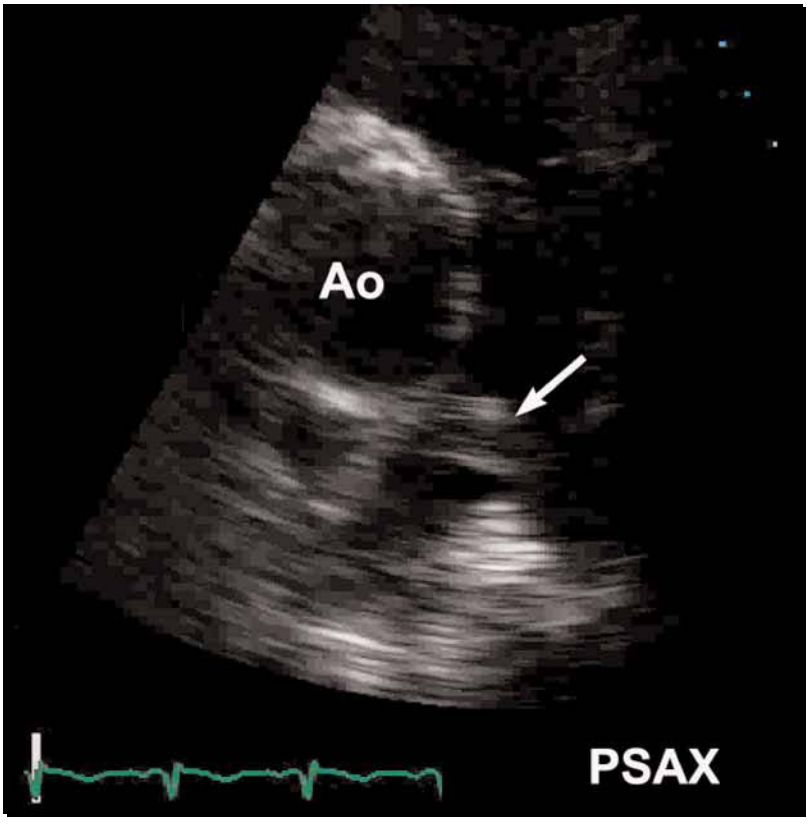

Fig. 2. A higher magnification of the parasternal short axis view at the aortic valve level of the patient with the pulmonary saddle embolus (arrow) described in Fig. 1. (Please *see* companion DVD for corresponding video.)

and indirect evidence of the diagnosis in patients with pulmonary embolus (Table 1).

Thrombi can be visualized within the venous system from the inferior vena cava, through the right atrium, the RV, the right ventricular outflow tract, and the pulmonary arteries until just distal to the pulmonary bifurcation. The direct visualization of thrombus in the pulmonary artery confirms the presence of a PE, but this finding is not usually seen on TTE. If a thrombus is visualized by TTE, it is usually limited to the right heart, the main pulmonary artery, or the bifurcation of the right and left pulmonary arteries (Figs. 1 and 2; please *see* companion DVD for corresponding video). Using TTE in the International Cooperative Pulmonary Embolism Registry (ICOPER) registry, intracardiac thrombi was visualized in approx 4% of patients with acute PE. In patients with a massive pulmonary embolus, the frequency of intracardiac thrombus may be increased. When intracardiac thrombus is visualized, it is most commonly visualized in the right atrium and often appears worm-like, although a small percentage is described as spherical in appearance. The differential

Table 1
Echocardiographic Signs of Pulmonary Embolism

Two-dimensional echo
Direct visualization of thrombus in the right heart or pulmonary artery
Right ventricular hypokinesis
Right ventricular enlargement
Reduced left ventricular size
McConnell's sign
Flattening of the intraventricular septum or paradoxical septal motion
Dilated pulmonary artery
Dilated right atrium
Distension of the inferior vena cava with loss of normal respiratory variation
Doppler
Increased peak velocity of tricuspid valve insufficiency
Shortened pulmonary ejection acceleration time (<80 ms)

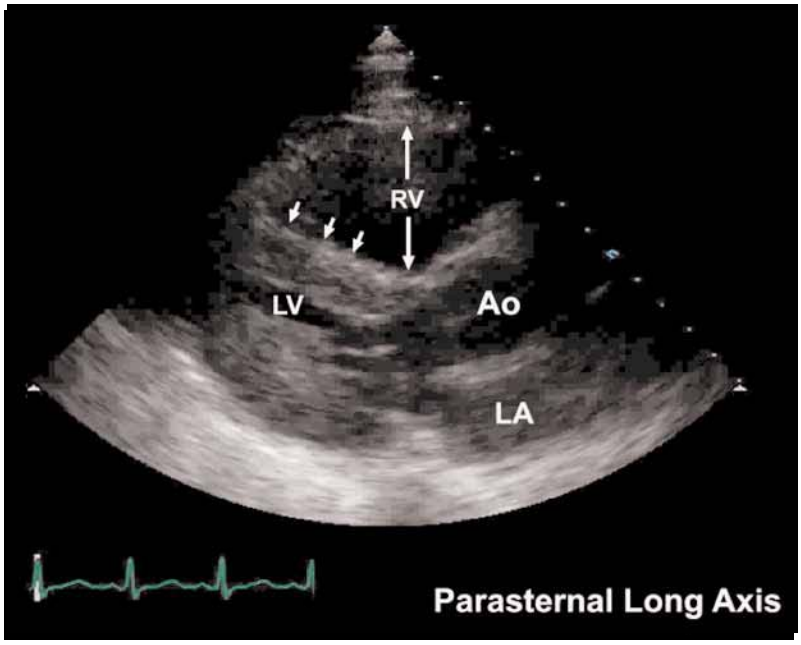

Fig. 3. Parasternal long axis view of a patient with acute pulmonary embolism demonstrates an enlarged, hypokinetic right ventricle (RV) with leftward displacement of the intraventricular septum (arrows). Left ventricular (LV) systolic function appears small, underfilled, and hyperdynamic. These are findings of severe RV dysfunction in the setting of acute pulmonary embolism.

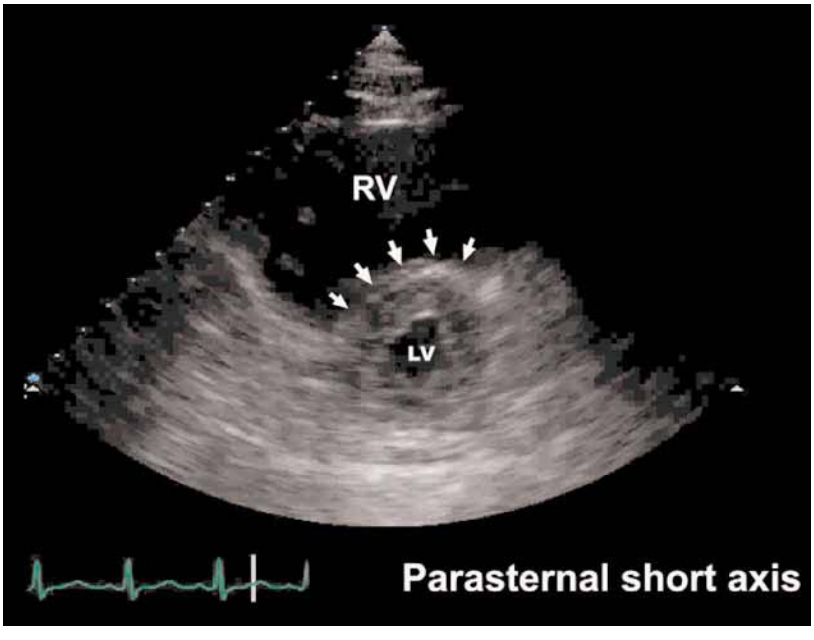

Fig. 4. Parasternal short-axis view of the left ventricle from patient in Fig. 3 demonstrates a severely enlarged right ventricle with intraventricular septal flattening (arrows) in systole and diastole, suggestive of both volume and pressure overload of the right ventricle (RV). The left ventricle (LV) appears small and hyperdynamic.

diagnosis for thrombus in the right heart includes congenital structures, such as a Chiari network or eustachian valve, or acquired structures, such as cardiac tumors or vegetations (*see* Chapter 19).

As direct visualization of the thrombus is unusual, one must rely on visualization of indirect manifestations of an acute PE on the heart. The RV normally faces little resistance as it empties into the low-pressure

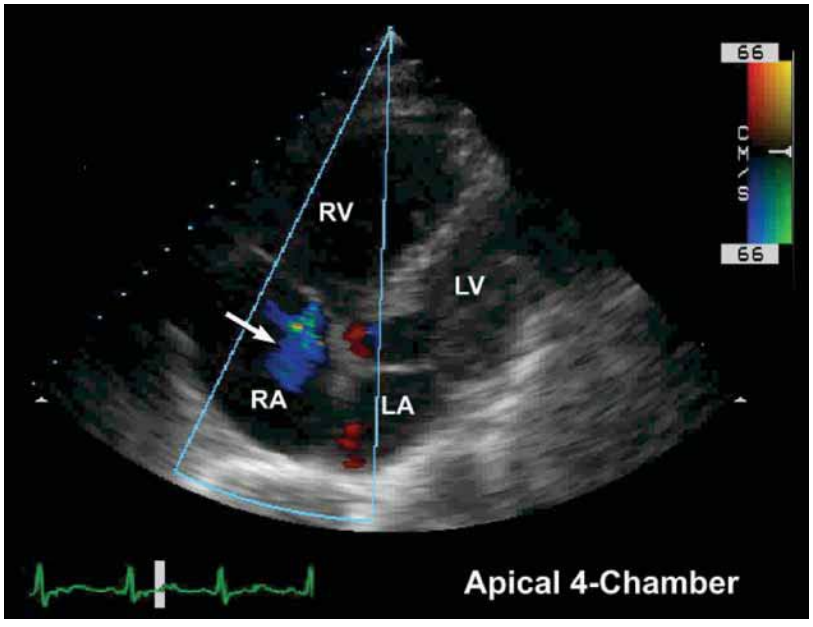

Fig. 5. Apical four-chamber view from patient in Figs. 3 and 4 demonstrates an enlarged and severely hypokinetic right ventricle (RV) with moderate tricuspid regurgitation (arrow). (Please *see* companion DVD for corresponding video.)

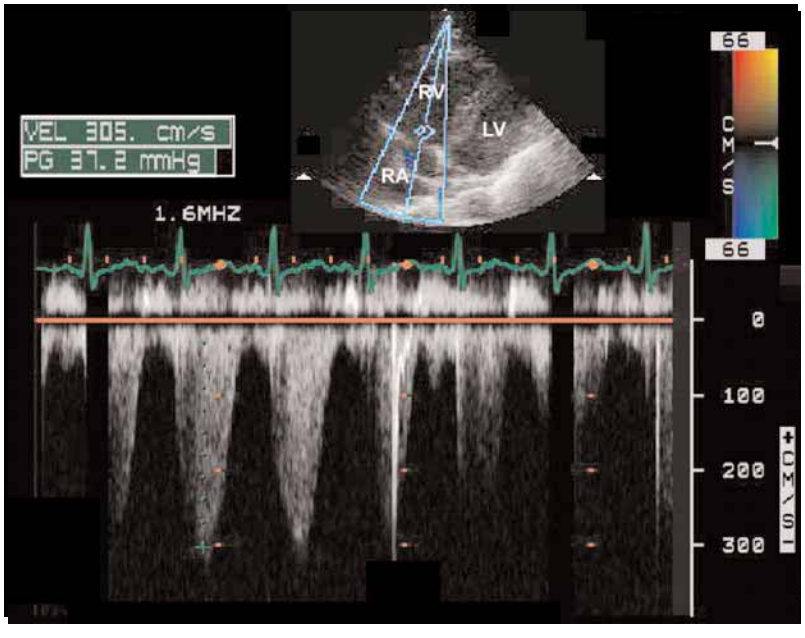

Fig. 6. Continuous-wave Doppler from the same patient in Figs. 3–5 demonstrates mild elevation of peak tricuspid velocity regurgitant velocity (3.0 m/s), which corresponds to a pulmonary artery systolic pressure of 37 mmHg plus right atrial pressure.

system of the normal pulmonary vasculature. When faced with acute obstruction to outflow, as occurs in acute PE, right ventricular function may not be able to compensate and the RV begins to fail as evidenced by enlargement and hypokinesis (Figs. 3–6; please *see* companion DVD for corresponding video for Fig. 5). The degree of dysfunction relates to the size and severity of the PE. The RV is often dilated with a right ventricular end-diastolic diameter in the parasternal long-axis view of more than 27 mm. The apical four-chamber view may also demonstrate right ventricular enlargement as evidenced by a right ventricular to left ventricular end-diastolic diameter ratio greater than the normal ratio of 0.6. In addition to right ventricular hypokinesis and enlargement, the intraventricular septum

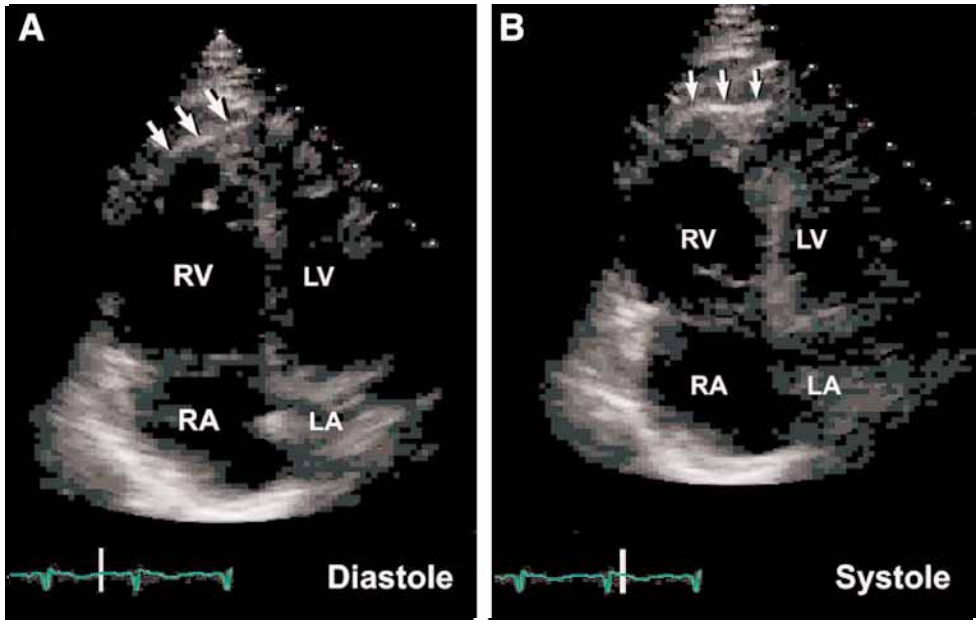

Fig. 7. Apical four-chamber demonstrates a characteristic regional right ventricular dysfunction (McConnell's sign) characterized by a severely hypokinetic free wall of the right ventricle, but a "spared" right ventricular apex. Note the markedly dilated right ventricular cavity. (Please *see* companion DVD for corresponding video.)

may be flattened or show leftward displacement as a result of the volume and/or pressure overload of the RV. Additionally, paradoxical septal motion may be visualized. Because of septal displacement, the left ventricular cavity size is often diminished and there may be Doppler evidence of impairment of diastolic left ventricular filling.

In addition to global dysfunction, a characteristic two-dimensional echocardiographic finding of regional right ventricular dysfunction has been described in patients with acute PE. This abnormality is characterized by the presence of normal or hyperdynamic wall motion of the right ventricular apex despite moderate or severe right ventricular free-wall hypokinesis (McConnell sign) (Fig. 7; please *see* companion DVD for corresponding video). This sign appears quite specific for the diagnosis of acute PE (specificity 94%), and, thus, may be useful to distinguish between right ventricular dysfunction owing to other cause such as pulmonary hypertension (Fig. 8).

In addition to echocardiographic abnormalities of the RV, other indirect echocardiographic manifestations are visualized. The right atria and the inferior vena cava may be dilated, with diminished normal respiratory variation of the inferior vena cava suggesting elevated right-sided pressures. The peak TR velocity may be mildly increased (>2.7 m/s) as a result of increased PASP, although the peak TR velocity often does not increase acutely to a significant degree, as the normal RV is unable to generate significantly elevated pressures. The pulmonary ejection acceleration time, measured in the right ventricular outflow tract, may be shortened (<80 m/s).

In general, the sensitivity of TTE for the diagnosis of an acute pulmonary embolus has been estimated to be between 50 and 60% with a specificity of 80–90%. Overall, approx 40–50% of patients with acute PE have echocardiographic evidence of right ventricular hypokinesis. In those with massive PE, echocardiographic evidence of PE may be seen in up to 80% of patients. Because of this finding, TTE is often helpful in the differential diagnosis of the hemodynamically compromised individual, but the diminished overall sensitivity of TTE for the diagnosis of PE limits the utility of echocardiography as a screening tool for all patients with this suspected disorder.

Several studies have suggested that transesophageal echocardiography (TEE) may have increased sensitivity over TTE in the detection of a pulmonary embolus (Fig. 9; please *see* companion DVD for corresponding video). Using TEE, the main pulmonary artery and the right pulmonary artery are better visualized, but visualization of the left pulmonary artery, as a result of the interposition of the left main pulmonary bronchus, and visualization of the distal pulmonary vasculature is limited. In patients with a clinical suspicion of PE and right

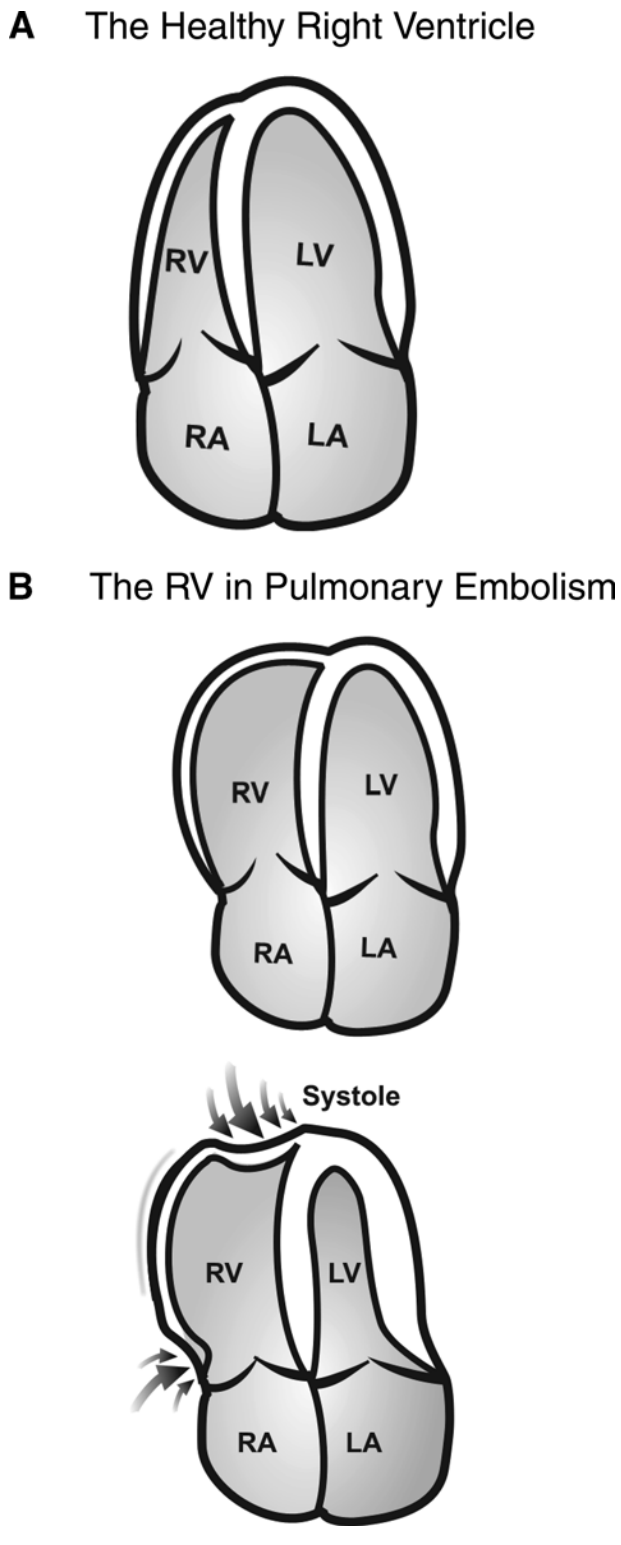

Fig. 8. Effects of pulmonary embolus on the right ventricle. The normal right ventricle (RV; **A**) is accustomed to low pulmonary resistance. Normal right ventricular pressures are low and compliance is high, with small changes in pressure resulting in large changes in volume. Unlike the left ventricle (LV), the normal RV does a poor job at acutely responding to sudden increases in afterload. Pulmonary embolism (PE) results in an increase in pulmonary vascular resistance. A previously normal RV is unable to acutely accommodate this additional load. The RV dilates **(B)** but cannot acutely increase pressure. Depending on the size of the PE, this can result in mild right ventricular strain or frank right ventricular failure.

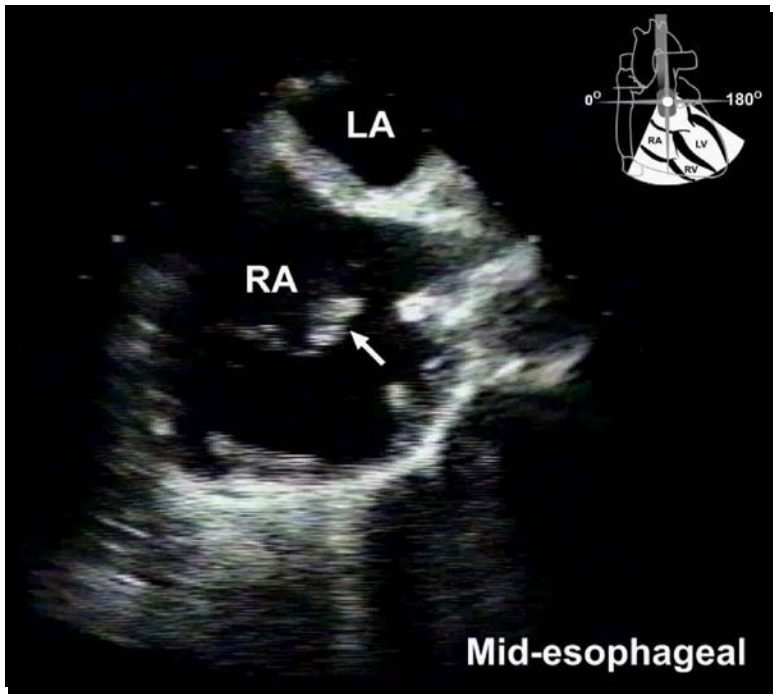

Fig. 9. Images of the right atrium on the midesophageal transesophageal echocardiography views demonstrate a mobile, worm-like thrombus (arrows). (Please *see* companion DVD for corresponding video.)

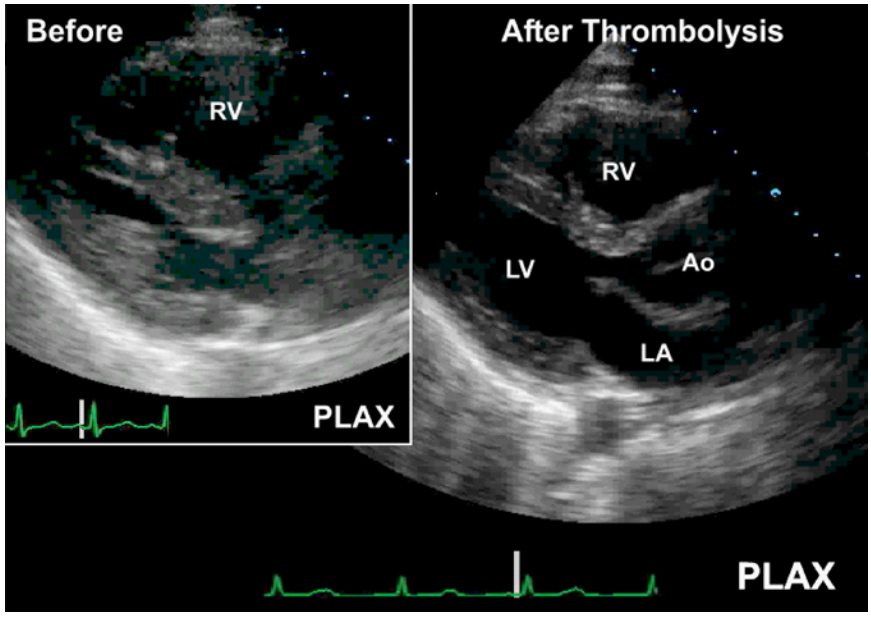

Fig. 10. Parasternal long-axis (PLAX) views of the same patient (Figs. 3–6) 1 d following thrombolysis shows improvement—although still impaired—of right ventricular function.

ventricular overload by TTE, the sensitivity of TEE was 80% with a specificity of 97%. Because of the inability of TEE to visualize the distal vasculature, the diagnostic accuracy in patients without evidence of right ventricular overload remains unclear. Despite its limitations, transesophageal allows for the investigation of patients who may be hemodynamically unstable and cannot have other tests such as computed tomography scan, nuclear perfusion studies, or pulmonary angiography, although it may be of limited value in acutely ill patients.

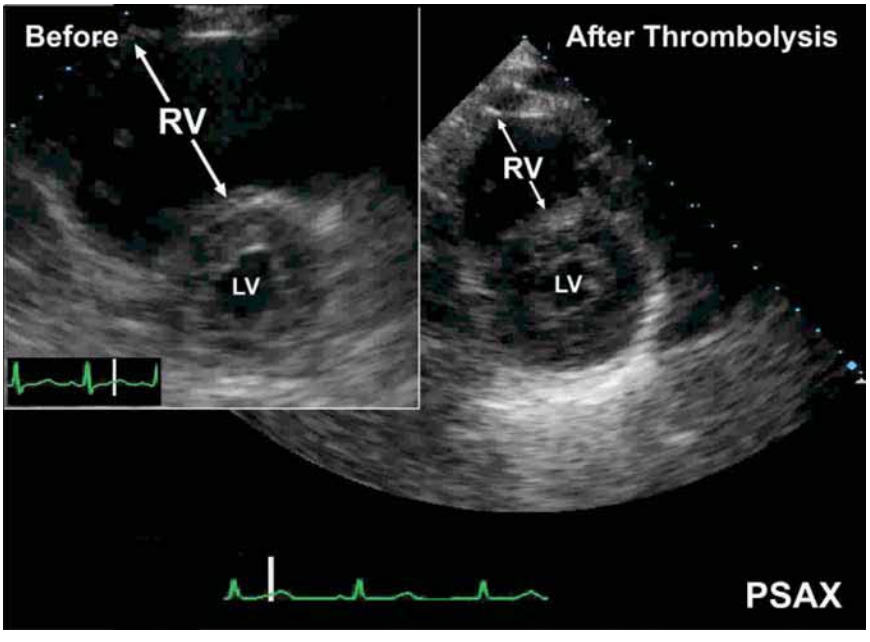

Fig. 11. Parasternal short-axis (PSAX) views of the same patient as in Fig. 9.

With chronic PE many of the previously described echocardiographic findings may be seen. Additionally, right ventricular hypertrophy and more significantly increased PASPs may also be seen as the RV adapts to chronic PE.

RISK ASSESSMENT AND MANAGEMENT

Echocardiography is a valuable prognostic tool in patients with acute PE. Multiple studies have demonstrated that right ventricular dysfunction demonstrated by echocardiography is associated with adverse clinical outcomes. In the ICOPER study, the presence of right ventricular hypokinesis on the baseline echocardiogram was associated with higher mortality at both 2 wk and 3 mo. In a multivariate model, the presence of right ventricular hypokinesis doubled the risk of death at 30 d.

A PASP of more than 50 mmHg at the time of diagnosis of acute PE is also associated with an adverse outcome. Additionally, the presence of a patent foramen ovale in patients with a PE and echocardiographic evidence of acute right ventricular pressure overload and/or pulmonary hypertension is an adverse predictor and identifies another high-risk subset. Finally, the presence of intracardiac thrombi in patients with PE identifies a high-risk group.

Table 2
Pulmonary Arterial Hypertension: Clinical Classification

Pulmonary arterial hypertension (primary and secondary):
• Primary idiopathic pulmonary hypertension (plexogenic pulmonary arteriopathy)
• Secondary to connective tissue diseases, congenital heart disease (e.g. left-to-right shunts: atrial septal defect, ventricular septal defect, patent ductus arteriosus), drugs/toxins, portal hypertension, HIV, other direct inflammatory disorders
Pulmonary venous hypertension:
• Left-sided atrial and ventricular heart disease (e.g., chronic left ventricle dysfunction)
• Left-sided valvular heart disease (e.g., mitral stenosis)
• Pulmonary vein obstruction: congenital or acquired
Pulmonary hypertension associated with pulmonary disorders and hypoxemia:
• Chronic obstructive pulmonary disease, interstitial lung disease, chronic alveolar hypoventilation, chronic high-altitude exposure
Pulmonary hypertension secondary to thrombotic and/or embolic disease

Modified from Rich S, ed. Primary pulmonary hypertension: Executive summary from World Symposium—Primary Pulmonary Hypertension, 1998. Available from the World Health Organization at www.int/ncd/cvd/pph.html.

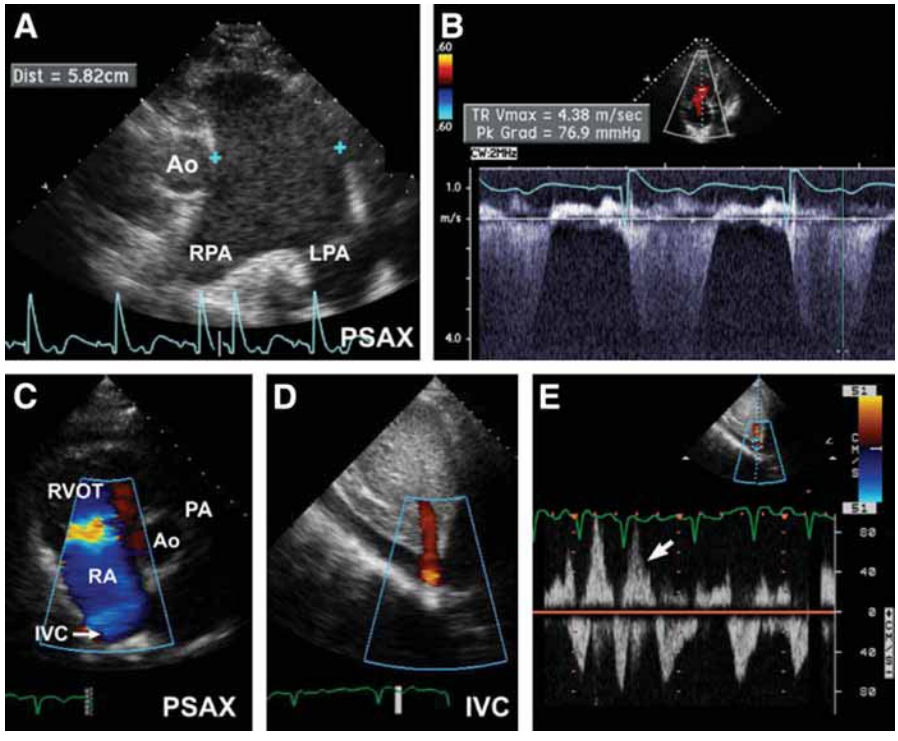

Fig. 12. Parasternal short-axis view (PSAX) showing markedly dilated pulmonary artery (diameter = 5.82 cm) in this 52-yr-old female with chronic pulmonary hypertension and chronic cor pulmonale **(A)**. Continuous-wave Doppler of the tricuspid regurgitant (TR) jet in pulmonary hypertension and chronic cor pulmonale corresponds to pulmonary artery systolic pressure of 77 mmHg plus right atrial pressure **(B)**. Large TR jet fills right ventricle (RV) and enters inferior vena cava (IVC)—(color flow Doppler, PSAX view, **C**). Note flow reversal is also evident in the dilated intrahepatic veins on Color Doppler **(D)**. This was confirmed on pulsed wave Doppler (arrow, **E**).

Table 3
Estimation of Right Atrial Pressures by Echocardiography

	Parameters of right atrial hypertension[a]		
	IVC measurements (cm)	*Inferior vena cava respirophasic movments (inspiratory collapse)*	*Corresponding right atrial pressures (mmHg)*
Normal	1.5–2.5	Complete collapse	5–10
Mild	>1.5	<50% collapse	10–15
Moderate	>2.5	<50% collapse	15–20
Severe	>2.5 (with dilated intrahepatic veins)	No collapse	>20

[a]Based on inferior vena cava measurements using subcostal window.

These adverse echocardiographic markers may identify a subset of individuals who may benefit from the use of more aggressive therapy in the management of PE, including thrombolytic therapy or pulmonary embolectomy. After thrombolysis for acute PE, right ventricular function has been demonstrated to improve echocardiographically (Figs. 10 and 11).

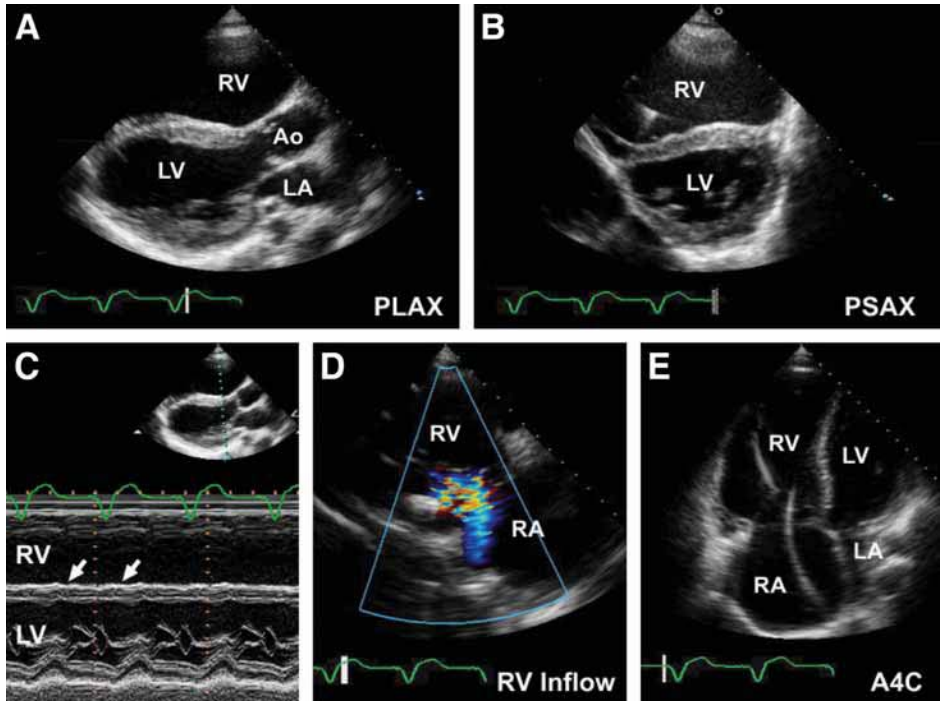

Fig. 13. Parasternal short-axis view (PSAX) showing grossly dilated right ventricle a patient with chronic pulmonary hypertension and chronic cor pulmonale **(A)** with septal flattening D-shaped septum on parasternal long-axis view parasternal long-axis (PLAX) **(B)**. Right ventricular (RV) pressure and volume overload with persistent septal flattening throughout the cardiac cycle is seen on M-mode echocardiography **(C)**. RV hypertrophy is also present. Marked right heart dilatation is seen in right ventricular inflow and apical four-chamber views **(D,E)**. Note the linear echodensities indicative of a dual-chamber pacemaker in **E**.

CHRONIC THROMBOEMBOLIC PULMONARY HYPERTENSION AND OTHER PULMONARY HYPERTENSION

Chronic pulmonary hypertension occurs in about 5% of patients within 2 yr following the first PE. The pulmonary vascular tree is a unique high flow, low pressure system (normal systolic/diastolic pressures 25/10 mmHg; mean 15 mmHg), but a number of pathological states, including PE, can trigger a vicious cycle of structural changes within the pulmonary vasculature, resulting in chronic pulmonary hypertension.

Chronic or recurrent PE can progressively obstruct the pulmonary vasculature, leading to clinical features of chronic pulmonary hypertension accompanied by signs of chronic cor pulmonale. Chronic thromboembolic pulmonary hypertension is present when the systolic and mean pulmonary artery pressures exceed 40 and 25 mmHg, respectively. Pulmonary hypertension of various etiologies (Table 2) can be categorized as mild, moderate, or severe based on PASPs measuring 40–45 mmHg, 46–60 mmHg, or more than 60 mmHg, respectively.

Pulmonary hypertension is most reliably quantified by spectral Doppler measurements of PASP and RAP—both routine measurements on TTE—provided pulmonary stenosis is absent (Fig. 12 and Table 3). These pressures should be interpreted within the context of the clinical presentation and other echocardiographic findings. On echocardiography, the hallmark of established pulmonary hypertension and cor pulmonale are signs of chronic right heart pressure overload (Figs. 13 and 14). Possible findings on TTE are summarized in Table 4. TEE provides better visualization of emboli with the pulmonary artery and atria (Fig. 9; please *see* companion DVD for corresponding video).

The PASP is measured using the simplified Bernoulli equation applied to peak TR velocity by continuous-wave Doppler. To this value, RAP should be added to complete the calculation (Table 3):

$$PASP = 4(TV)^2 + RAP$$

TR is present in most normal individuals, but the velocity rarely exceeds 2.5 m/s. Higher TR velocities may indicate pathology. The most common TR velocities

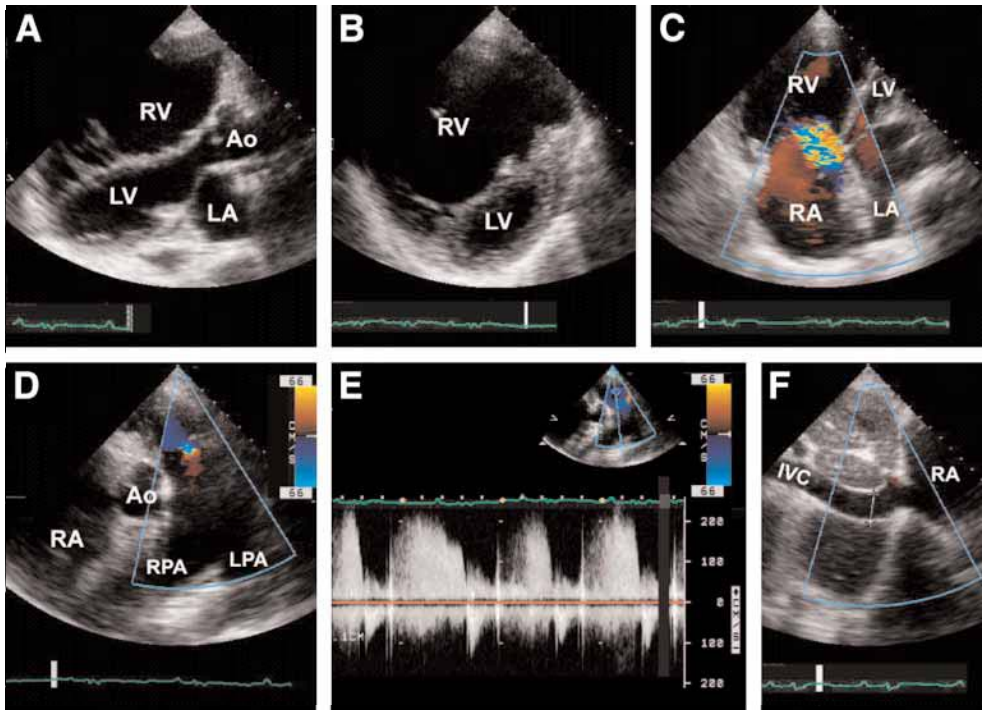

Fig. 14. Images depicting several features of chronic severe pulmonary hypertension and cor pulmonale (Table 4) are shown. Note the massively dilated right ventricle in parasternal views accompanied by tricuspid regurgitation **(C)** and pulmonary regurgitation **(D)**. Spectral Doppler interrogation across the pulmonic valve confirms marked pulmonary regurgitation exceeding 2 m/s **(E)**. Markedly dilated inferior vena cava (IVC) with complete loss of respirophasic variation was present **(F)**.

Table 4
Echocardiographic Findings in Pulmonary Hypertension and Chronic Cor Pulmonale

Two-dimensional echocardiography

- Right ventricular dilatation
- Right ventricular hypertrophy
- Right ventricular dysfunction/hypokinesis
- Signs of right ventricular pressure and volume overload:
  D-shaped septum (throughout cardiac cycle)
  Paradoxical septal motion
- Right atrial dilatation
- Dilated inferior vena cava
- Loss of normal inferior vena cava respirophasic movements

Doppler echocardiography

- Reversal of flow: tricuspid valve by color flow Doppler parameters, e.g., increased jet area, proximal isovelocity surface area, vena contracta width
- Reversal of flow: pulmonary valve by pressure half-time and jet length
- Reversal of flow: inferior vena cava and hepatic veins

seen in acute PE range between 2.5 and 3.0 m/s, rarely exceeding 3.5 m/s because the previously normal RV cannot generate higher pressures. This contrasts with pressures generated by the hypertrophied RV seen in acute-on-chronic or in recurrent PE and in the setting of chronic pulmonary hypertension, where TR velocities typically exceed 3.5 m/s.

TR velocity is a reflection of the pressure difference between the right atrium and RV, whereas continuous-wave Doppler intensity indicates severity. Therefore a high TR velocity (alone) does not equate to severe TR. TR severity can be assessed using the same Doppler parameters used to assess mitral regurgitant severity (*see* Chapter 14; e.g., jet areas, vena contracta width, and proximal isovelocity surface area, in conjuction with other echocardiographic parameters in Tables 3 and 4).

The most common pitfall in measuring PASP is failure to obtain the maximum TR velocity. To minimize this, multiple windows (parasternals, apical, and subcostal) and optimal Doppler alignment are necessary. Other Doppler measurements, e.g., acceleration times measured at the pulmonary valve, the TR velocity/velocity time integral ratio, and the pulmonary artery diastolic pressure, may be used.

SUGGESTED READING

Fedullo PF, Auger WR, Kerr KM, Rubin LJ. Chronic thromboembolic pulmonary hypertension. N Engl J Med 2001;345: 1465–1472.

Goldhaber SZ, Visani L, De Rosa M. Acute pulmonary embolism: clinical outcomes in the International Cooperative Pulmonary Embolism Registry (ICOPER). Lancet 1999; 353:1386–1389.

Goldhaber SZ. Echocardiography in the management of pulmonary embolism. Ann Intern Med 2002;136:691–700.

Goldhaber SZ. Pulmonary embolism. In: Zipes DP, Libby P, Bonow RO, Braunwald E, eds. Braunwald's Heart Disease: A Textbook of Cardiovascular Medicine, 7th ed. Philadelphia; Saunders, 2005;1781–1806.

Kedia A, Roldan CA. Pulmonary hypertension and cor-pulmonale. In: Roldan CA, ed. The Ultimate Echo Guide. Philadelphia: Lippincott Williams and Wilkins, 2005:71–84.

Leibowitz D. Role of echocardiography in the diagnosis and treatment of acute pulmonary thromboembolism. J Am Soc Echocardiogr 2001;14:921–926.

Miniati M, Monti S, Pratali L, et al. Value of transthoracic echocardiography in the diagnosis of pulmonary embolism: results of a prospective study in unselected patients. Am J Med 2001;110:528–535.

Nass N, McConnell MV, Goldhaber SZ, Chyu S, Solomon SD. Recovery of regional right ventricular function after thrombolysis for pulmonary embolism. Am J Cardiol 1999; 83:804–806.

Pengo V, Lensing AW, Prins MH, et al. Thromboembolic Pulmonary Hypertension Study Group. Incidence of chronic thromboembolic pulmonary hypertension after pulmonary embolism. N Engl J Med 2004;350:2257–2264.

Pruszczyk P, Torbicki A, Kuch-Wocial A, Szulc M, Pacho R. Diagnostic value of transoesophageal echocardiography in suspected haemodynamically significant pulmonary embolism. Heart 2001;85:628–634.

Ribeiro A, Lindmarker P, Johnsson H, Juhlin-Dannfelt A, Jorfeldt L. Pulmonary embolism: one-year follow-up with echocardiography Doppler and five-year survival analysis. Circulation 1999;99:1325–1330.

Ribeiro A. The role of echocardiography Doppler in pulmonary embolism. Echocardiography 1998;15:769–778.

19 Cardiac Masses and Tumors

Justina C. Wu, MD, PhD

Contents

CASE PRESENTATION

A 32-yr-old female presented with a 1-mo history of fatigue, intermittent fevers, and dyspnea on exertion. One day before her doctor's appointment, she noted transient monocular blindness that resolved within 1 h. On physical exam, she had both a holosystolic apical and late diastolic positional rumble, diminished S1, and an end-diastolic "plopping" sound heard in late systole. She was sent for an echocardiogram to rule out cardiac source of embolus (Fig. 1; please *see* companion DVD for corresponding video). She subsequently underwent cardiac surgery and a left atrial tumor was excised and confirmed to be a myxoma on pathological examination.

DIFFERENTIAL DIAGNOSIS OF A MASS: NON-NEOPLASTIC STRUCTURES

Masses in or around the heart are most often incidental findings on echocardiography. Less frequently, a tumor involving the heart causes direct symptoms that lead the clinician to suspect a cardiac abnormality.

True intracardiac or extracardiac masses need to be distinguished from the entities in the following section.

Normal Structures/Variants Simulating Tumors

Intracardiac

In the right atrium, the Eustachian valve (also known as the valve of the inferior vena cava [IVC]) is a ridge of tissue that extends from the entry of the IVC to the interatrial septum. In fetal life, this valve directs blood

From: *Contemporary Cardiology: Essential Echocardiography: A Practical Handbook With DVD*
Edited by: S. D. Solomon © Humana Press, Totowa, NJ

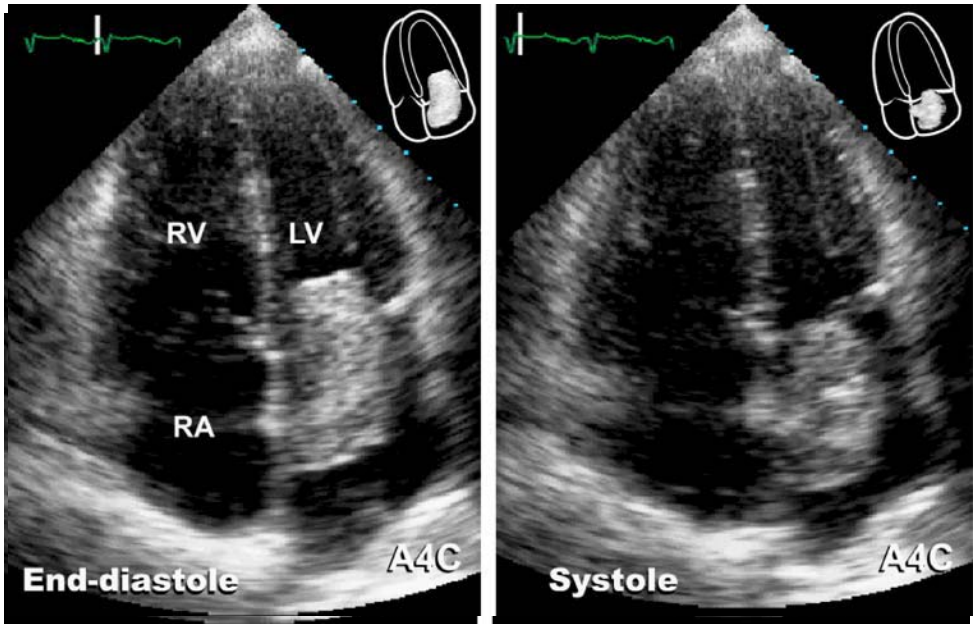

Fig. 1. This large atrial myxoma caused functional mitral stenosis and constitutional symptoms. They are usually solitary, mobile masses that are heterogenously hyperechoic. They arise most commonly from the interatrial septum and have a predilection for the left atrium. (Please *see* companion DVD for corresponding video.)

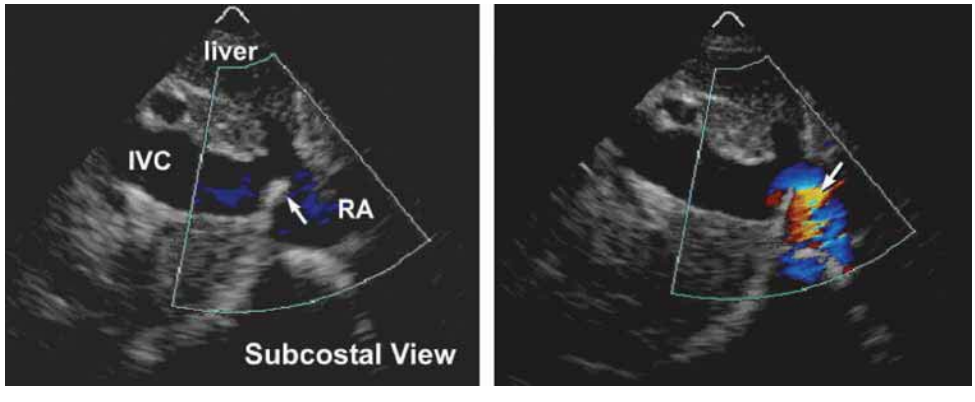

Fig. 2. Subcostal images showing Eustachian valve (left, arrow) with directed flow on color Doppler examination (right). (Please *see* companion DVD for corresponding video.)

to the fossa ovalis. It can remain prominent in adults, where it appears as a transverse linear echo running approximately parallel to the tricuspid annulus across the posterior right atrium in right ventricular inflow views, or in subcostal views (Figs. 2 and 3; please *see* companion DVD for corresponding video for Fig. 2). The Chiari network is similarly an embryonic remnant of the sinus venosus, which extends from and is continuous with the Eustachian valve. It persists in 2–3% of normal adults (confirmed by autopsy), and appears on ultrasound as a lacy weblike or fenestrated membranous echogenic mass with a characteristic chaotic, undulating motion independent from that of the tricuspid valve and right heart (Fig. 4). On parasternal long- or short-axis views, bulging of the interatrial septum into the right atrium, owing to an interatrial septal aneurysm or left atrial volume overload, can be mistaken for a "tumor" when the scanning plane cuts tangentially across the septum. Careful inspection of both atria from all windows should clarify this misdiagnosis.

Annular calcification, particularly of the mitral apparatus, and fat deposition, often seen around the tricuspid annulus and interatrial septum (interatrial septal lipomatous hypertrophy, Fig. 5; please *see* companion DVD for corresponding video), can also simulate intracardiac masses. Calcific deposits tend to be very

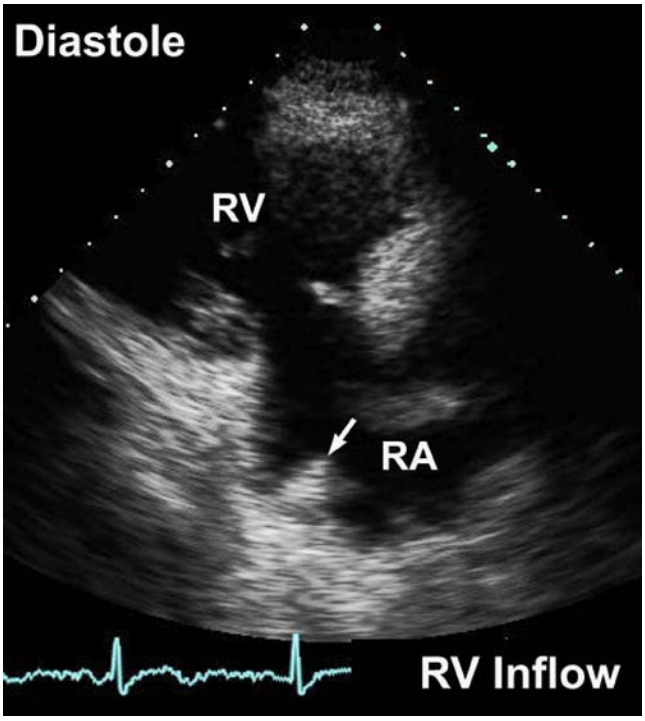

Fig. 3. When present, the Eustachian valve (arrow) can be well visualized in the right ventricular inflow view (*see* Chapter 3, Fig. 20). This patient's tricuspid valves were thickened and immobile owing to the carcinoid syndrome.

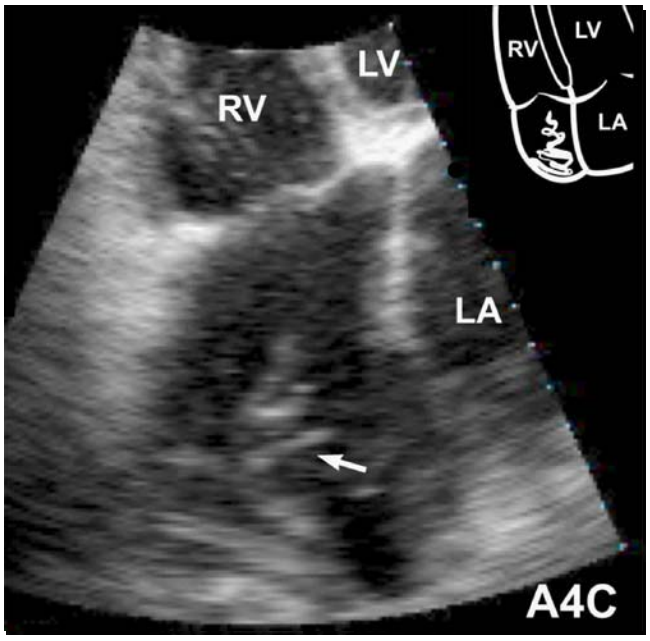

Fig. 4. Chiari's network usually appears as a highly mobile undulating echogenic mass arising in the right atrio–inferior vena caval junction. The presence of this embryonic remnant should trigger closer examination of the interatrial septum for aneurysm or patent foramen ovale.

echobright and irregular, whereas fat usually appears as a less echodense, homogenous mass with smoother edges. Myxomatous mitral valves, when severely thickened, have been mistaken for tumors. Within the left atrial appendage, pectinate muscles appear as small multiple pyramidal structures with their bases continuous with the myocardial wall. Unlike masses and thrombi, the pectinate muscles are not independently mobile from appendage contractions. Small short linear echodensities known as "Lambl's excrescences" are often noted at the tips of the aortic valve leaflets, on both the left ventricular outflow tract and aortic side, as well as on the mitral apparatus in patients older than 50 yr old. Pathological studies have revealed these to be long fibrin strands, although the larger and more developed strands may contain cellular elements of papillary fibroelastoma.

Within the left ventricle, prominent left ventricle trabeculations, false tendons (Fig. 6), aberrant muscle bands or bridges, and subaortic membranes should be distinguished from tumors. Delineation of the origins and insertions of these structures, a cylindrical or linear morphology, and the presence of thickening during systole can aid in the differential diagnosis. Within the right ventricle, the moderator band can appear quite thick, but its location extending from the apical free wall to the midseptum is characteristic.

Extracardiac

An epicardial fat pad usually appears as a discrete "soft" or deformable mildly granular echogenic mass lying adjacent to pericardium, typically anterior to the right heart and/or adjacent to the atrioventricular groove. A useful clue for distinguishing pericardial fat is the identification of the echolucent cylindrical lumen of the coronary artery running within it. However, epicardial fat pads may be distributed anywhere around the heart. They tend to increase in size with age or in patients with longstanding steroid use.

Pleural effusions and ascites are occasionally confused with pericardial effusions. Proper identification should avoid the occasional misdiagnosis of echogenic collapsed lung segments, fibrin, or thrombus within the pleural or abdominal cavities, which can appear similar to tumor masses (Fig. 7).

Thrombus

Thrombi can form in the left atrial body and appendage, particularly in patients with atrial fibrillation, mitral stenosis, or hypercoagulable states (Fig. 8).

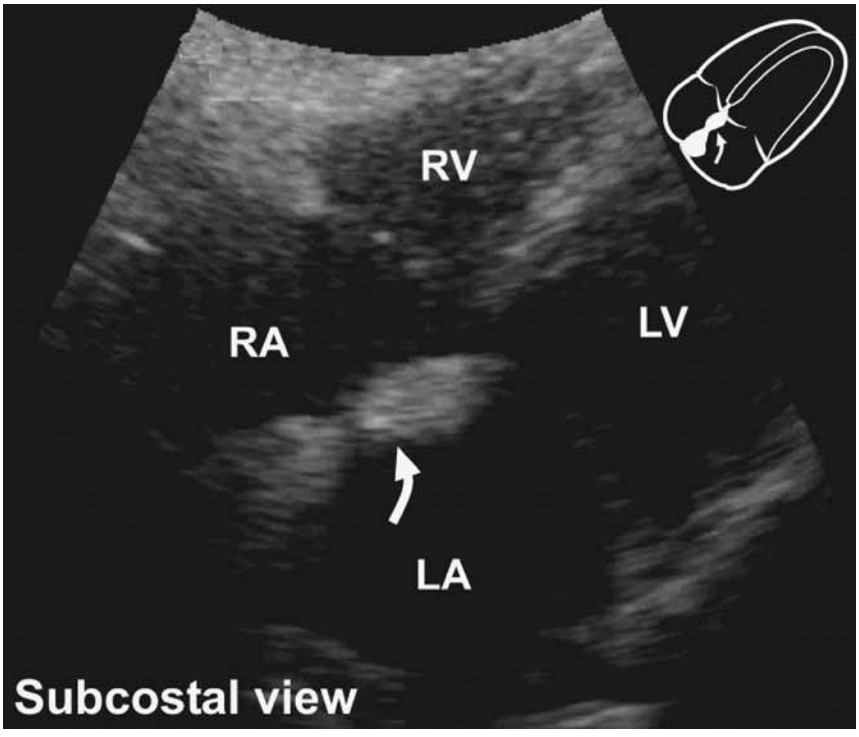

Fig. 5. Lipomatous hypertrophy (arrow) of the interatrial septum. (Please *see* companion DVD for corresponding video.)

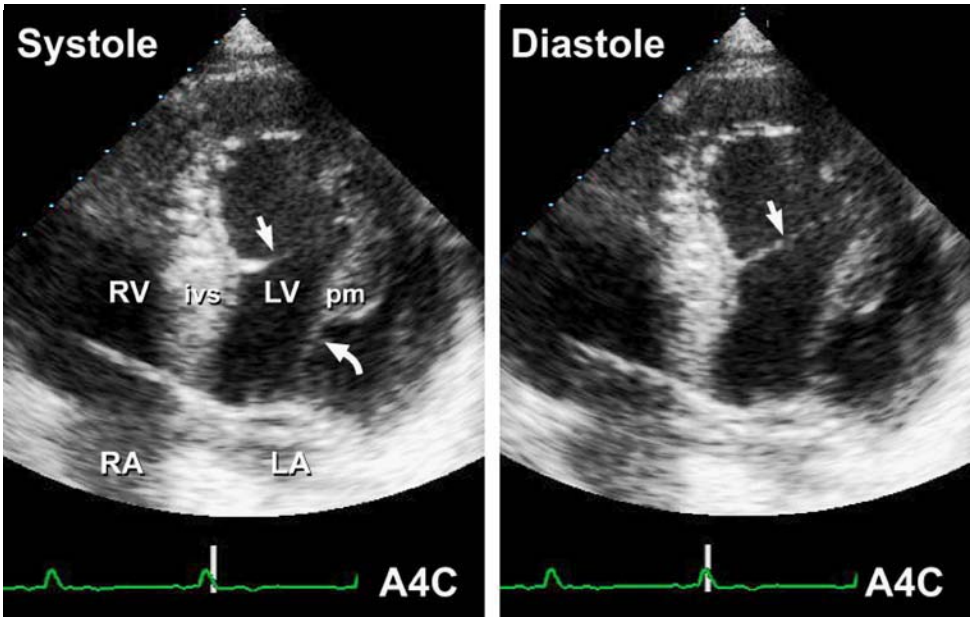

Fig. 6. A false tendon (straight arrow) appears as a mobile string (a few millimeters in width) that bowstrings the ventricular cavity. Note the attachments to the interventricular septum (ivs) and the base of the papillary muscle (pm). Note the appearance of the true tendon—chorda tendinae (curved arrow).

The thrombi vary tremendously in size, shape, and appearance. The differentiation of a thrombus from a tumor may be difficult if predisposing factors for thrombus are not present (Figs. 9 and 10; please *see* companion DVD for corresponding video for Fig. 9). In cases of trauma or mediastinal surgery, coagulated blood and fibrin may appear in the pericardial and pleural space as gelatinous or coalescing echogenic masses.

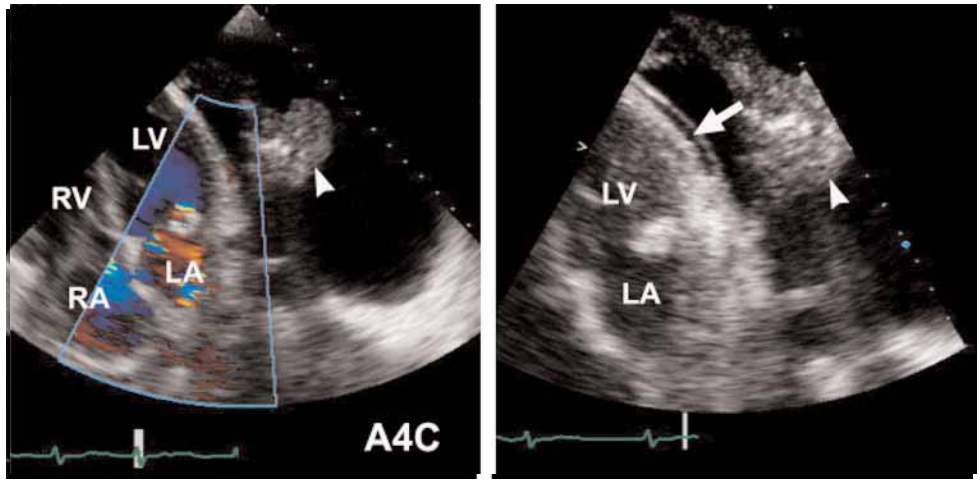

Fig. 7. Apical four-chamber (A4C) views from an 86-yr-old woman with generalized sepsis and endocarditis show a large left-sided pleural effusion with atelectatic lung segments (arrowheads). A pleural effusion should be distinguished from a pericardial effusion (arrow) by viewing from multiple views, and noting their relationships to regional anatomic structures, such as the aorta and the coronary sinus.

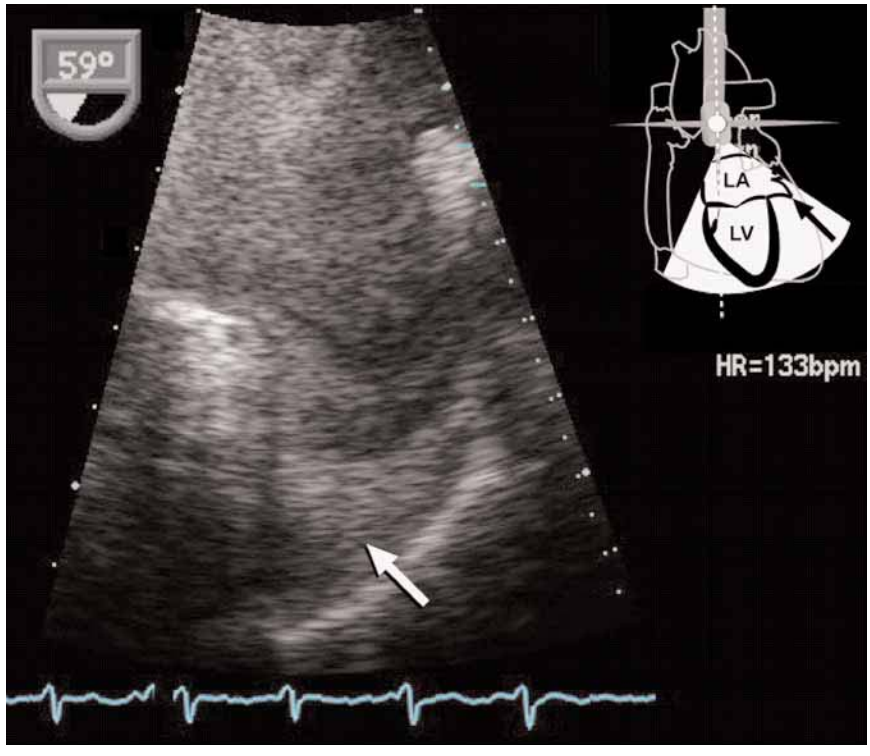

Fig. 8. Midesophageal image of the left atrial appendage (ominplane 59°) showing a left atrial thrombus (arrow) and spontaneous echocontrast within the left atrium (LA). Thrombi need to be distinguished from artifacts and the pectinate muscles that line the walls of the left atrial appendage. Spontaneous echocontrast frequently coexists with thrombus, as in the LA of this patient with mitral stenosis and atrial fibrillation.

Vegetation

Discrete mobile masses that are attached to valves are more likely to be vegetations, especially if clinical and laboratory signs of endocarditis are present, and symptoms of valvular regurgitation are of recent onset. Myxomatous mitral valves should also be distinguished from vegetation and tumors (Fig. 11).

Artifact

Artifacts resembling an echogenic mass can be caused by reflections from the pericardium, valves, and

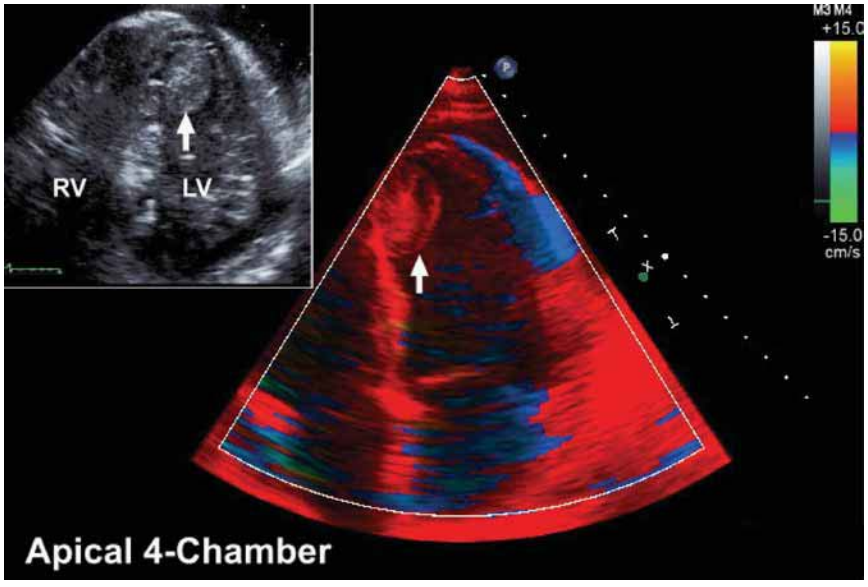

Fig. 9. These images are from a 63-yr-old man with coronary artery disease and lung cancer. Multiple echodensities (intracardiac thrombi) were observed in right and left heart chambers. Smaller thrombi had embolized to his coronary arteries resulting in multiple infarcts. (Please *see* companion DVD for corresponding video.)

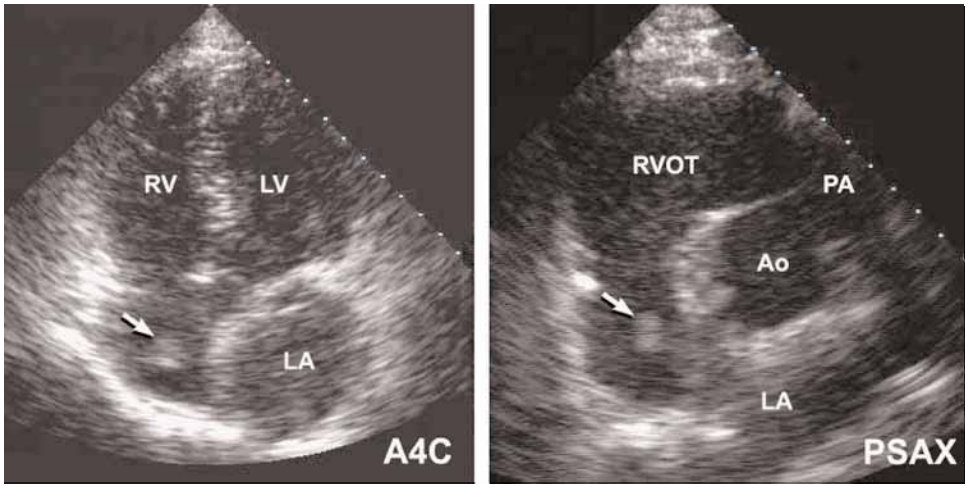

Fig. 10. These images are from a 51-yr-old male with end-stage liver disease, hepatitis C infection, ascites, and peritoneum-to-inferior vena cava (Denver) shunts. A thrombus was seen in his right atrium in addition to a patent foramen ovale.

foreign objects (e.g., catheters, pacemaker wires). Because of the way echo images are processed, artifacts often appear either halfway or whole multiples of distance from the reflecting object to the transducer, and do *not* move independently of heart motion. A useful way to distinguish an artifact is to examine the blood flow around the putative mass with color Doppler, which should respect the borders of a true mass but will appear to pass through an artifact (Fig. 12). On transesophageal echocardiography, the normal tissue infolding between the left atrial appendage and left upper pulmonary vein can cause an acoustic artifact which has occasionally been mistaken for a thrombus, hence the nickname "warfarin ridge" (Fig. 13).

In difficult cases, transesophageal echocardiography or even transcatheter biopsy may be called on to clarify the origins and nature of intracardiac masses.

TUMORS INVOLVING THE HEART AND PERICARDIUM

Primary Tumors

Primary tumors arising in the heart are rare, and only 25% of these are malignant. Ninety percent or more are

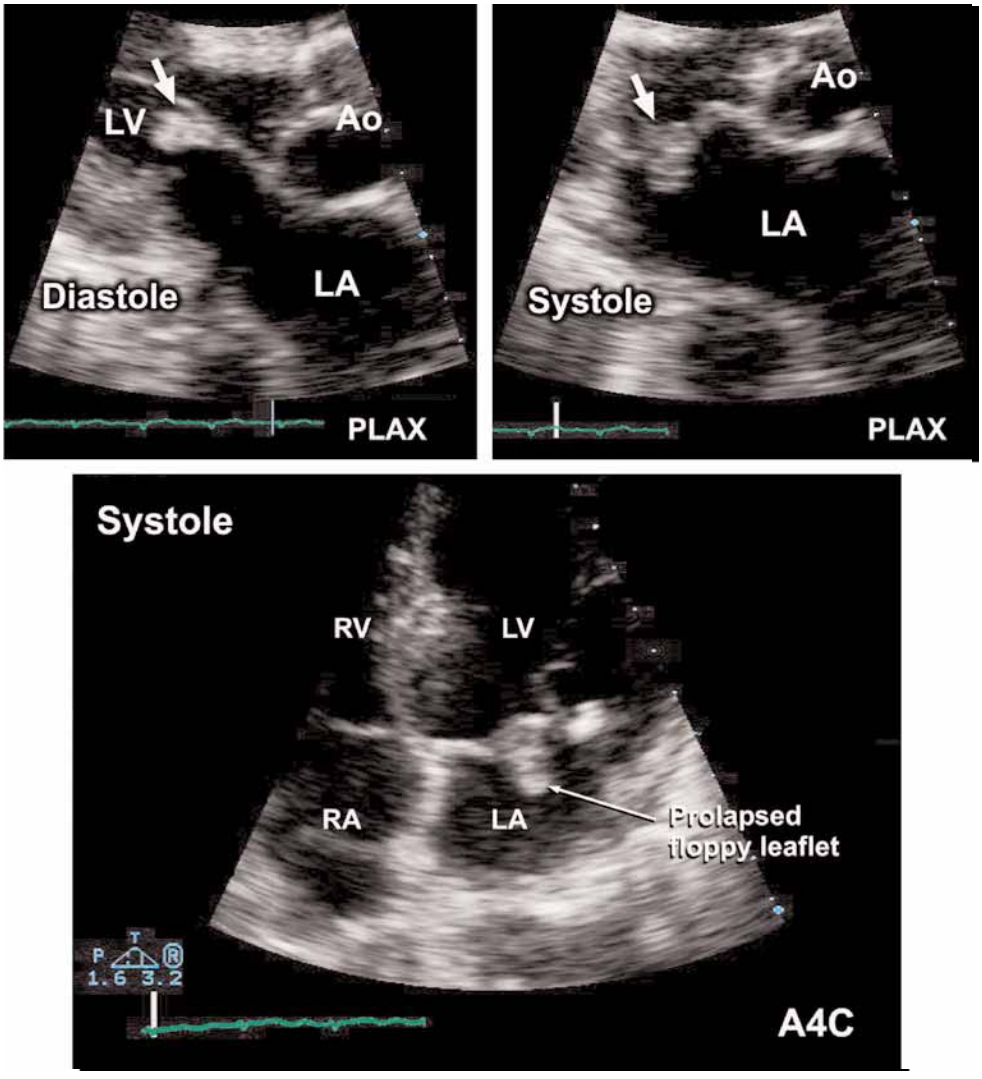

Fig. 11. These images show a floppy "myxomatous" anterior mitral valve leaflet that prolapsed into the left atrium during systole, which can create a tumor-like appearance. Marked mitral regurgitation was present.

detected incidentally, but some may cause symptoms by embolization or obstruction of cardiac inflow or output. In general, atrial tumors are more often intracavitary, whereas ventricular tumors are more frequently intramural (i.e., involving the myocardial layer).

From most common to least common, a brief description of these tumors follows. Table 1 summarizes neoplastic and non-neoplastic masses that may be seen on echocardiography.

In adults, cardiac myxoma is the most common cardiac tumor, accounting for 20–50% of all cases (Figs. 1 and 14; please *see* companion DVD for corresponding video for Fig. 1). There may be a female predominance, and familial syndromes with myxoma as a phenotypic trait (e.g., Carney syndrome) exist. Approximately 75% of myxomas occur in the left atrium, with the remainder largely arising within the right atrium. Cases arising from the ventricles and IVC, as well as multiple myxomas within the same atrium have also been described. The typical atrial myxoma arises from the interatrial septum near the fossa ovalis, and is often anchored via a stalk-like pedicle. Size can range from less than 1 cm to an extent that virtually fills the entire atrium. The echocardiographic appearance is typically either a compact, rounded, or ovoid mass, or, alternatively, a polypoid, papillary, friable mass. The echodensity may be homogenous or finely speckled. Myxoma can cause valvular obstruction (i.e., a functional stenosis) or may prolapse and cause regurgitation of the mitral or tricuspid valves leading to heart failure. In addition, systemic or pulmonic embolization can occur, as well as constitutional symptoms. Complete surgical excision is usually the cure.

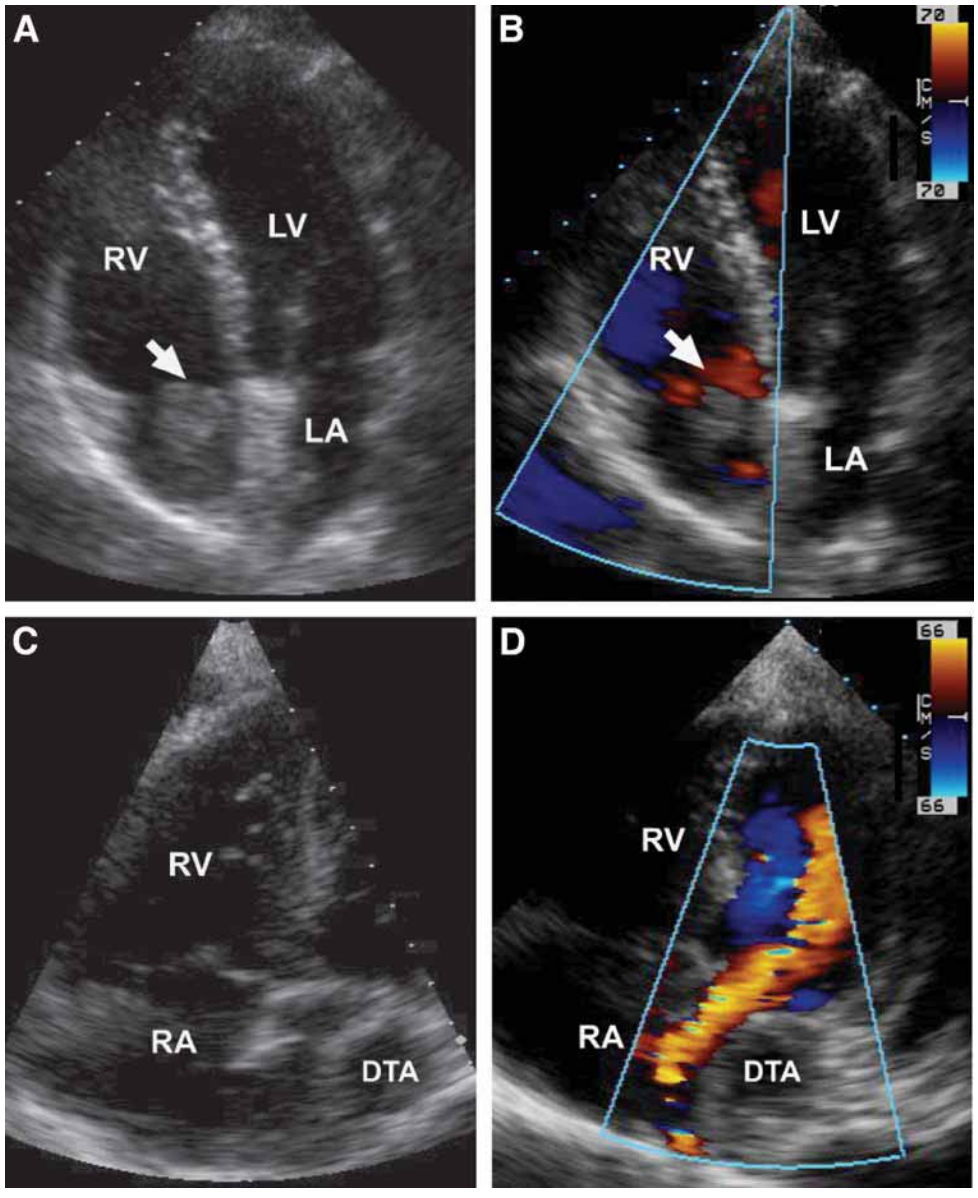

Fig. 12. Color Doppler interrogation of the right atrial mass (arrow, **A,B**) in confirmed its intracardiac location. Compare this to color Doppler interrogation of the left atrium that shows extracardiac compression by the descending thoracic aorta (DTA; **C,D**).

Papillary fibroelastomas are the next most common benign tumors, and consist primarily of dense connective tissue elements. These are found most frequently in elderly patients, and usually appear to arise from the valvular endocardium on either side of the heart. They manifest as small (<0.2–1.0 cm) mobile pedunculated echo masses which can be variably filamentous, frond-like, or oval in shape. They are characteristically attached to valve leaflets, with a predisposition mainly for the aortic valve (where they can arise from either surface), or secondly for the atrial side of mitral valves. Less frequently, they are attached to the mitral chordae or papillary muscles, or tricuspid or pulmonic valves. Because of their mobility, they are thought to be shed rather easily into the bloodstream and may cause embolic symptoms. Figure 15 shows an elongated thread-like papillary fibroelastoma on the LV outflow tract aspect of the aortic valve (please *see* companion DVD for corresponding video).

Cardiac lipomas are benign tumors that have been described throughout the heart, typically in a subepicardial or subendocardial location. Rarely, they can arise within the myocardium or from the leaflets. They often appear more echodense and fixed than myxomas, and are often clinically silent (Fig. 16;

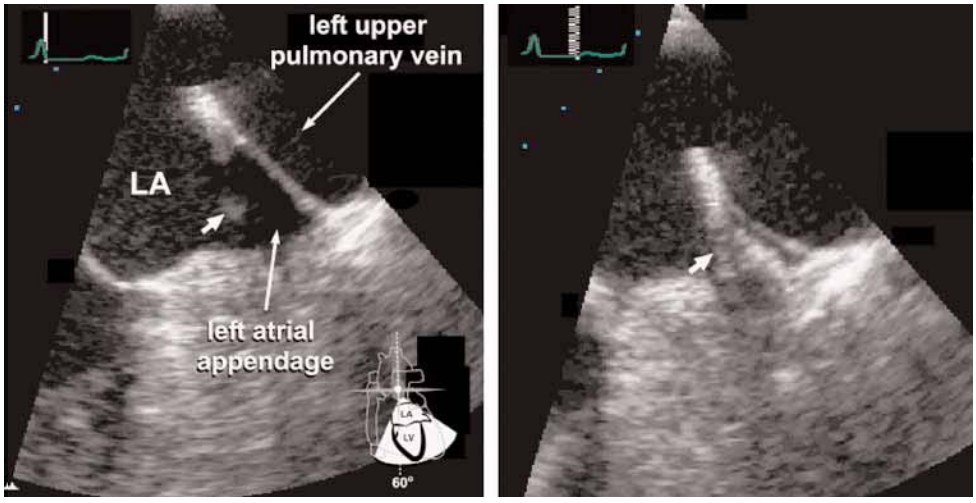

Fig. 13. "Warfarin ridge" artifact occurs owing to acoustic shadowing (short arrows) from the hyperechoic ridge or fold of tissue separating the left atrial appendage from the left upper pulmonary vein.

Table 1
Cardiac Masses

Non-neoplastic

- Thrombus (intracavitary)[a]
- Thrombus within ventricular aneurysm or pseudo-aneurysm
- Lipomatous hypertrophy of the interatrial septum
- Anatomic variants (e.g., Chiari's network, prominent crista terminalis, or pulmonary vein orifice)
- Valvular vegetation
- Ruptured papillary muscle
- Rheumatoid nodule
- Extracardiac structures and organs (e.g., fat in the atrioventricular groove)

Neoplastic

Primary cardiac tumors		*Secondary cardiac tumors*[b]	
More common	*Less common/rare*	*More common*	*Less common*
Myxoma[c]	Fibroma	Bronchogenic carcinoma	Musculoskeletal
Lipoma	Rhabdomyoma	Breast	Cervical
Papillary fibroelastoma	Lymphoma	Stomach	Renal angiomyolipoma
	Plasma cell granuloma	Colon	Germ cell tumor (e.g., testicular teratoma)
	Sarcoma	Lymphomas	Embryonal cell carcinoma
	Hemangiopericytoma	Leukemia	Choriocarcinomas
	Angioma	Hepatocellular carcinoma	Thyroid
	Atrioventricular nodal tumors	Renal cell carcinoma	
	Paragangliomas	Carcinoid tumor	
	Intracardiac pheochromocytoma		
	Primary cardiac sarcomas		

[a]Thrombi are the most common intracardiac mass.
[b]Myxomas are the most common benign cardiac tumors (~50%).
[c]Secondary cardiac tumors are 20–30 times more common than primary cardiac tumors.

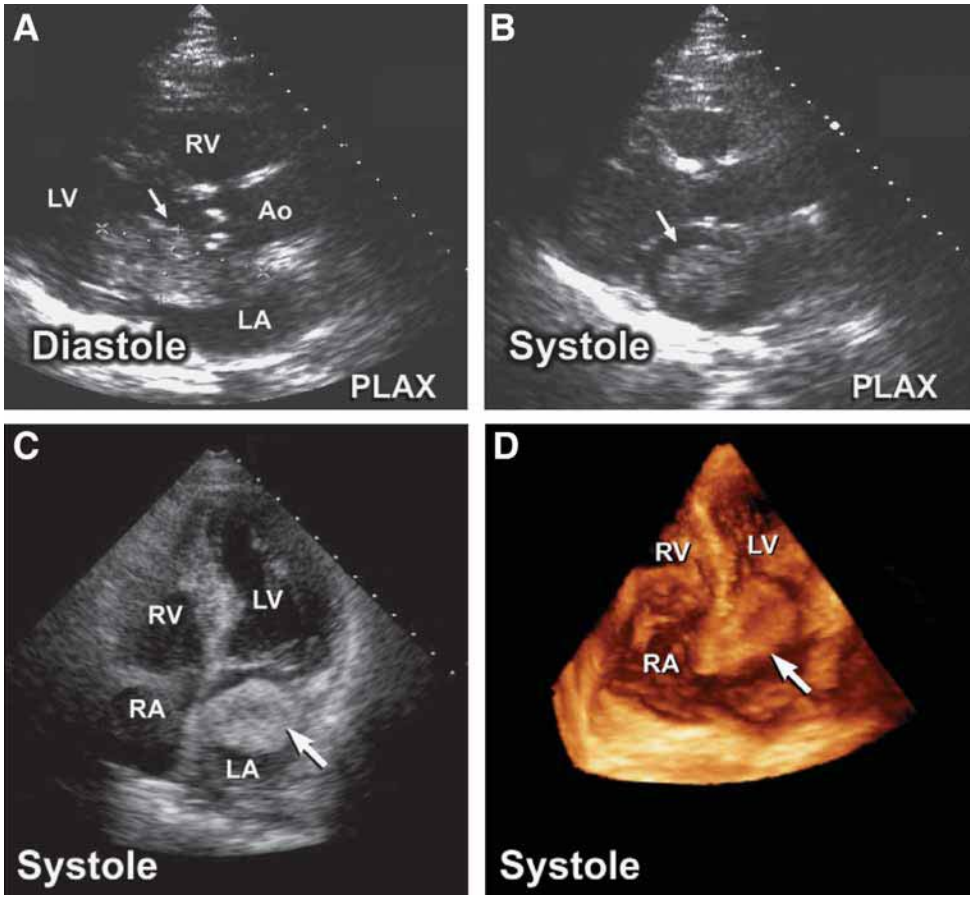

Fig. 14. Parasternal long axis images (PLAX) show a large atrial myxoma (arrow) with characteristic heterogeneous echogenicity. It occupies much of the left atrium and prolapses during diastole (**A,B**). Systolic still frames showing apical four-chamber view of a left atrial myxoma (arrow) and its appearance on three-dimensional echocardiography (**C,D**).

please *see* companion DVD for corresponding video). It is important to distinguish this entity from lipomatous hypertrophy, which is an accumulation of excess fat in the interatrial septum, sparing the fossa ovalis, giving a characteristic "dumbbell" shape to this structure (Fig. 5; please *see* companion DVD for corresponding video). Lipomatous interatrial septal hypertrophy is considered a normal variant of no real clinical significance, although it can become very prominent in some individuals.

Pericardial cysts are benign fluid-filled tumors of the parietal pericardium, which are occasionally detected on chest X-ray and usually occur at the cardiophrenic borders.

In the pediatric population, rhabdomyomas are the most common primary cardiac tumor. These tumors are rare after adolescence, and may regress in childhood. Most frequently involve the ventricle and ventricular cavity, and are often associated with tuberous sclerosis. An aid to diagnosis lies in the fact that 90% are multiple. Less common primary tumors, found predominantly in infants and children, include fibromas (rare tumors that typically occur within the septal myocardium), hemangiomas, and cysts.

Approximately one-fourth of primary cardiac tumors are malignant sarcomas. The various subtypes (angiosarcomas, rhabdomyosarcomas, lymphosarcomas) have been reported at all ages. Angiosarcomas tend to occur in the right heart, and rhabdomyosarcomas can arise in more than one area of the heart. However, there are no clear distinguishing echocardiographic features; all share common characteristics of rapid invasive growth and metastasis, with frequent extension to the pericardium and a poor prognosis.

Secondary Tumors

Tumors that are metastatic to the heart are 20–40 times more common than primary tumors. Almost any type of cancer, with the exception of brain tumors, can spread to the heart and pericardium. However, because of their high

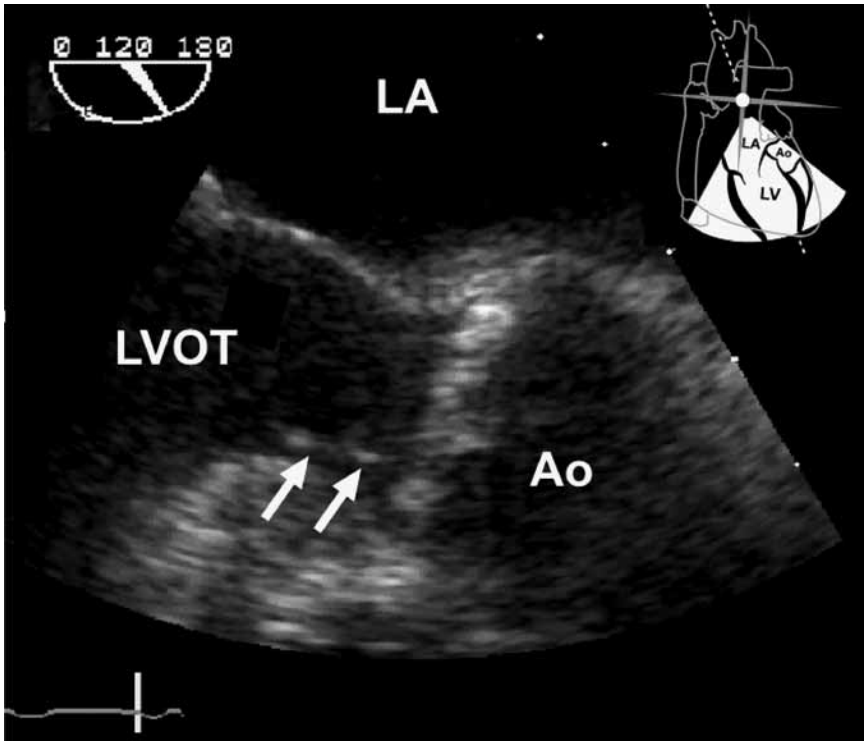

Fig. 15. Papillary fibroelastomas are generally small nonvegetative masses arising from cardiac valves or adjacent endocardium, most commonly the aortic valve. They sometimes resemble Lambl's excrescences, but they have a narrower base and have the potential to embolize. (Please *see* companion DVD for corresponding video.)

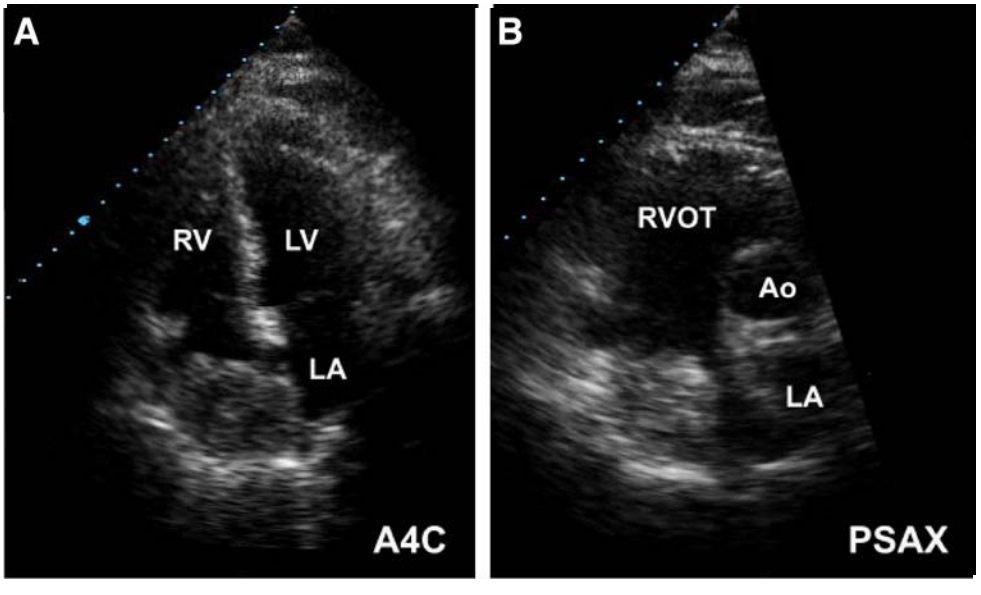

Fig. 16. *(Continued)*

prevalence, carcinomas arising from the breast and lung are the most common. Malignancies that are at high risk for metastasizing to the heart are melanoma (up to 64% of cases) and the leukemias and lymphomas (up to 46% have been observed to metastasize to the heart). Figure 17 is an example of a right atrial mass that was subsequently found to be melanoma, which presumably spread via the bloodstream, because there was no evidence of direct

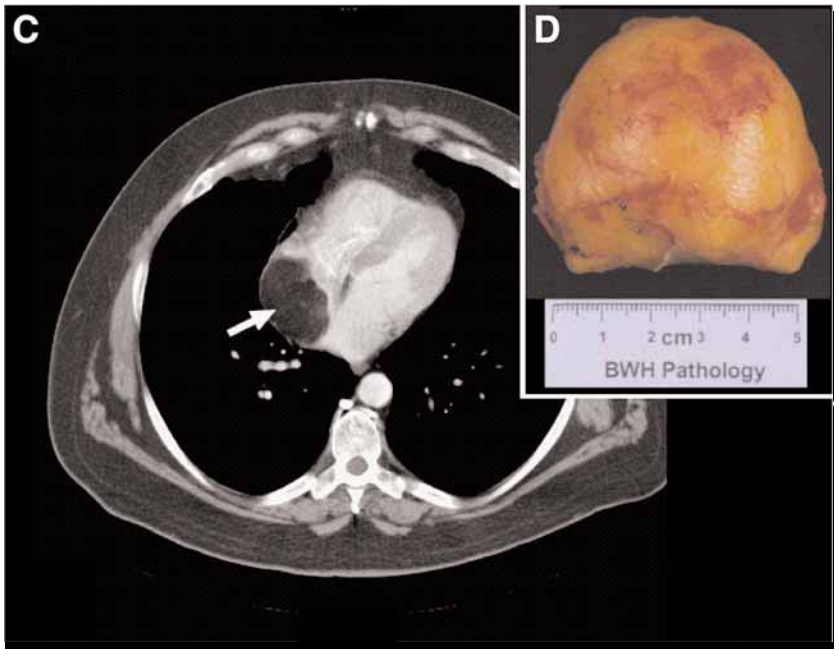

Fig. 16. These images are from a 63-yr-old man who presented with 1-wk history of lightheadedness, nausea, vomiting, and diaphoresis. A large right atrial mass was noted on echocardiography (**A** and **B**) that was further delineated by contrast computed tomography **(C)** before surgical removal. Gross examination revealed characteristic features of a lipoma **(D)**. (Please *see* companion DVD for corresponding video.)

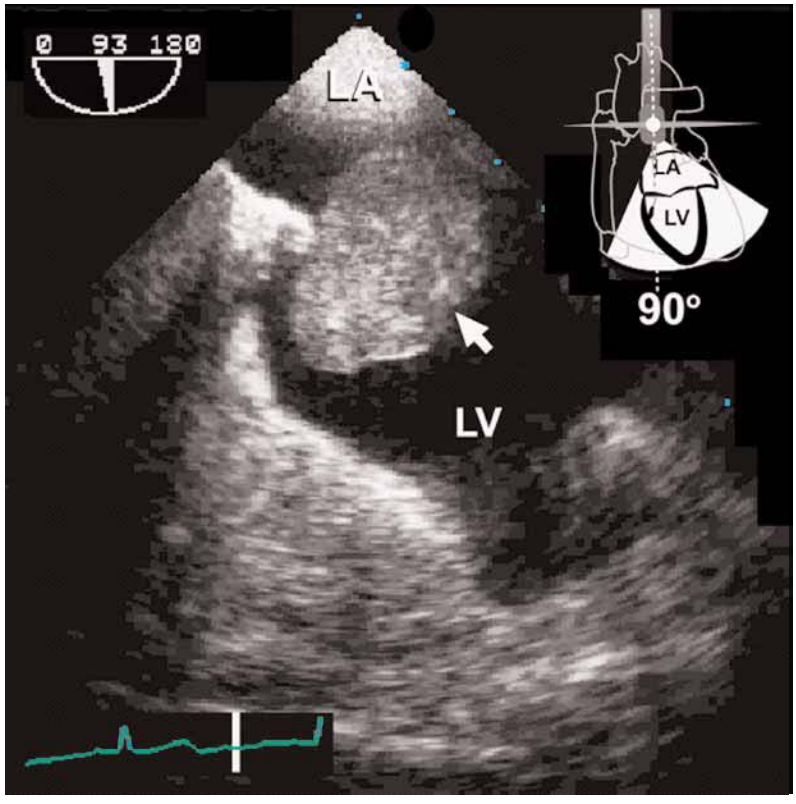

Fig. 17. Transesophageal echocardiography revealed a large mass attached to the posterior mitral valve leaflet. Histological examination revealed that it was a melanoma, arising from an extracardiac primary. (Please *see* companion DVD for corresponding video.)

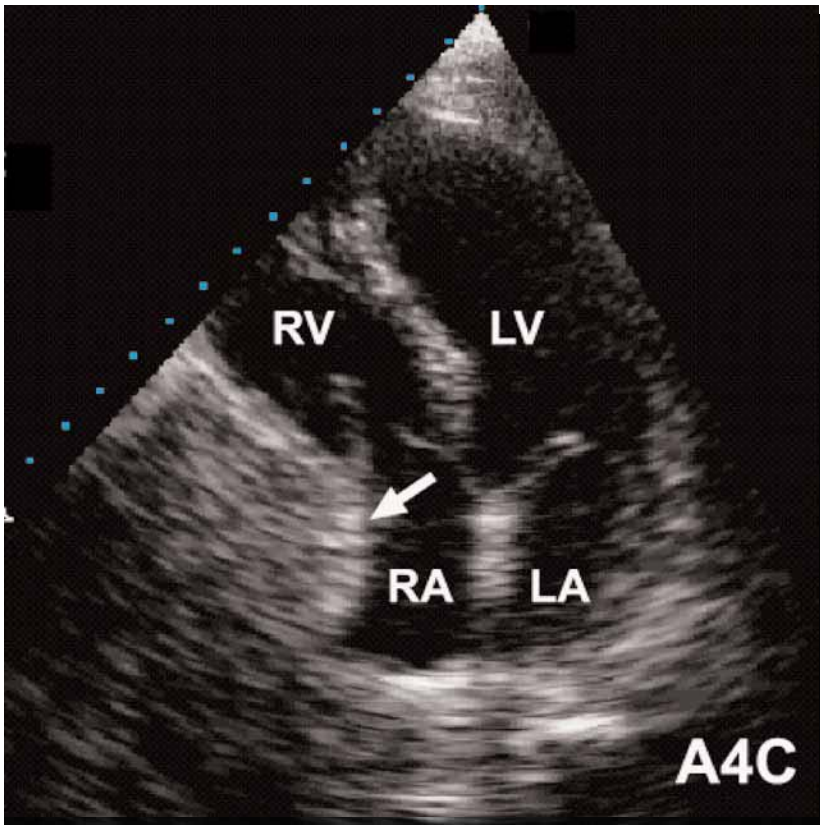

Fig. 18. Apical four-chamber (A4C) view showing compression of the right heart chambers from a large pleural mesothelioma. (Please *see* companion DVD for corresponding video.)

pericardial or myocardial invasion (please *see* companion DVD for corresponding video).

Metastatic spread frequently occurs by either direct extension to the pericardium, or via lymphangitic or hematogenous spread. Renal cell carcinoma, Wilms' tumor, and hepatocellular carcinoma can invade the right atrium by encroaching up the IVC, and bronchogenic neoplasms can enter the left atrium via the pulmonary veins. The involvement of pericardium or invasion of the tumor from either the cardiac free walls (as opposed to septum) or contiguous great vessels may be a clue to the secondary nature of these tumors. Clinical symptoms from secondary metastases are often the result of associated pericardial effusion and, less frequently, to embolization or mass effect on the myocardium (*see* next section).

EFFECTS OF CANCER ON THE HEART

Mass Effect: Extracardiac Compression or Intracavitary Obstruction

Even tumors that do not directly involve the heart and pericardium can occasionally be seen by echocardiography. Anterior mediastinal masses (cysts, thymomas, teratomas, lymphomas) can compress the right ventricular outflow tract, whereas posterior masses (sarcomas) or pleural tumors can compress the left atrium and ventricle. Figure 18 is an example of a pleural mesothelioma impinging on the right atrium and right ventricular inflow tract (please *see* companion DVD for corresponding video). Infiltrative growth of a tumor can cause obstruction to cardiac inflow or outflow, as in the superior vena cava syndrome. If the tumor invades onto a valve, prolapse of the involved leaflets and associated regurgitation ensues (the cause of the myxoma tumor "plop" in the Case Vignette).

Direct Infiltration of the Myocardium

Direct infiltration of the myocardium can lead to segmental wall motion abnormalities or restrictive disease, causing congestive heart failure. Less frequently, conduction disturbances have been described when malignant tissue invades the area of the atrioventricular node or septum, which contains the conduction system.

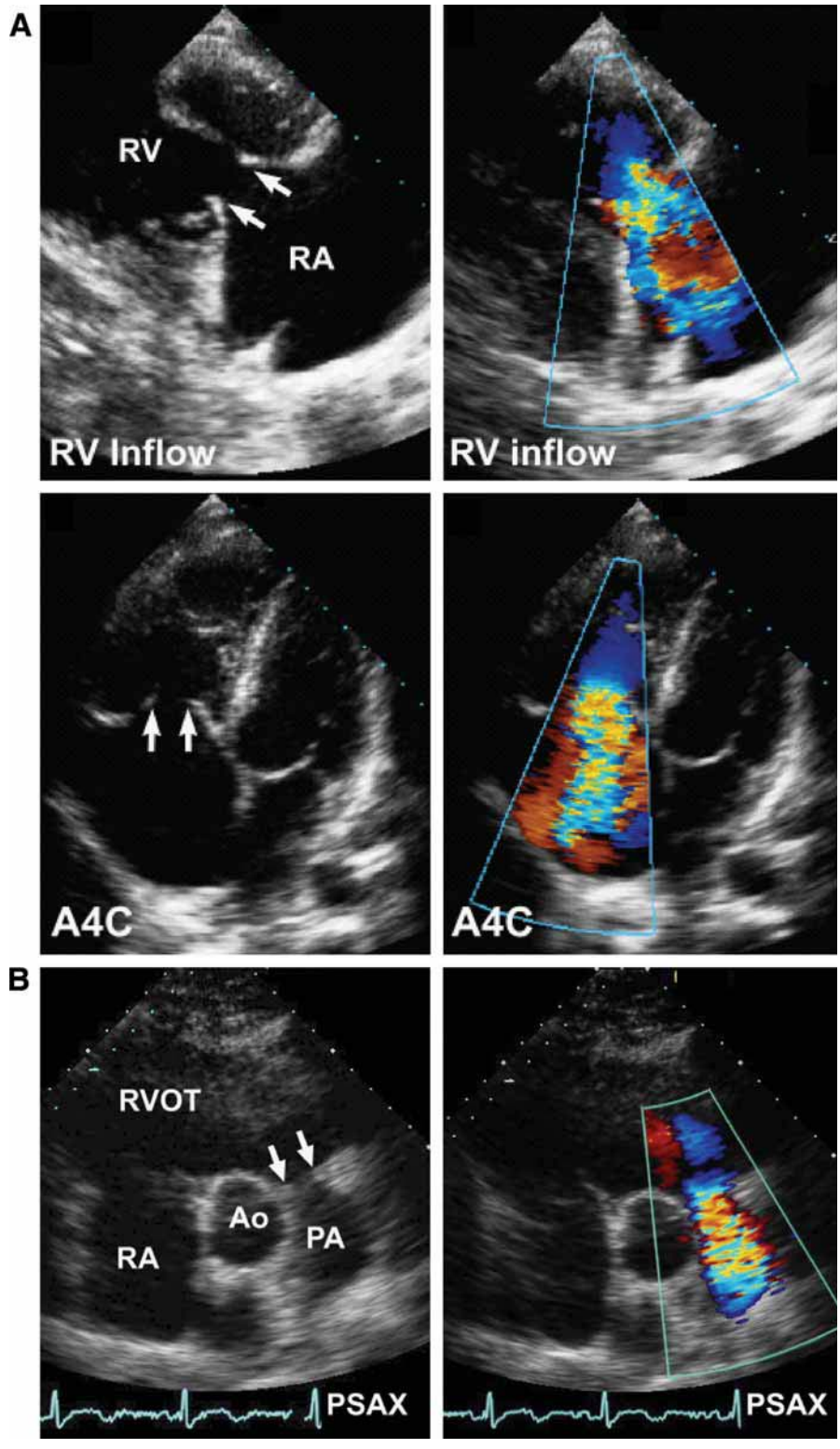

Fig. 19. (A) Transthoracic echocardiography showing the classic findings in carcinoid heart disease. Right ventricular inflow and apical four-chamber (A4C) views show the characteristic immobility of the tricuspid valve leaflets (arrows). Wide-open tricuspid regurgitation is seen in the upper- and bottom-right panels. **(B)** The pulmonic valve cusps of the patient with the carcinoid syndrome **(A)**, were thickened, retracted, and fixed with a stenotic pulmonary valve orifice (left panel, parasternal short-axis view). Color flow Doppler evaluation shows flow acceleration and turbulence across the stenotic pulmonary valve. (Please *see* companion DVD for corresponding video.)

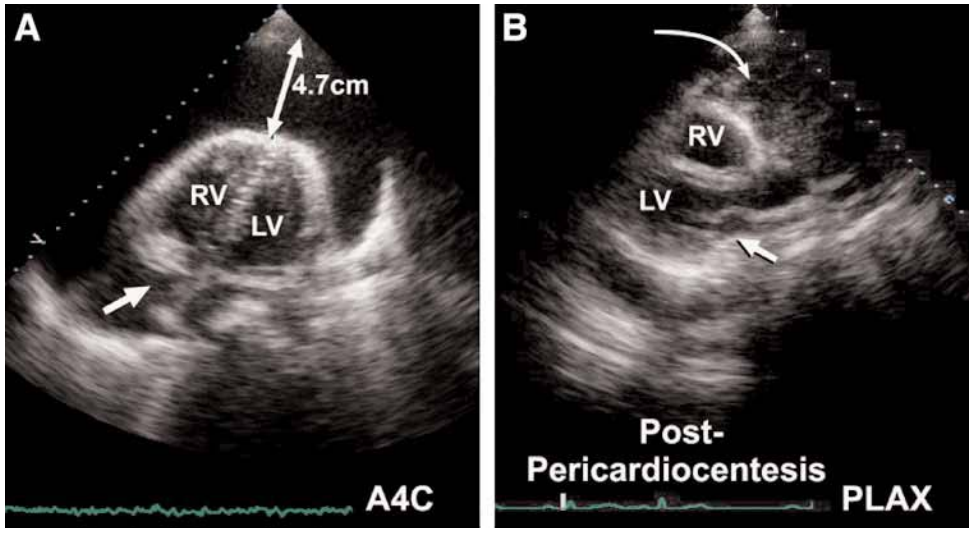

Fig. 20. These transthoracic images are from a 31-yr-old female who presented postpartum with a large pericardial effusion with echocardiographic signs of tamponade. Following removal of almost 1 L of fluid, a large anterior mediastinal mass (curved arrow) that displaced the heart posteriorly, compressing the aorta and left atrium (arrow) was noted on the parasternal long-axis (PLAX, **B**). Computed tomography scans and computed tomography-guided biopsy and histology confirmed a lymphoma.

Valvular Involvement

Valvular involvement by a tumor can cause leaflet prolapse and associated regurgitation (e.g., the mechanisms behind the myxoma "plop" detected by auscultation), as well as a functional stenosis because of obstruction. Atrial fibrillation may be the indirect result. Carcinoid heart disease is a distinctive clinical syndrome associated with malignant carcinoid tumors (particularly APUDomas and bronchial tumors), which secrete serotoninergic substances into the bloodstream. These vasoactive peptides cause episodic symptoms such as flushing and diarrhea. Within the heart, the hormones cause severe thickening and fibrosis of the atrioventricular valves, leading to retraction and fixation of the leaflets in the open position during diastole, and hence severe regurgitation. Typically with tumors involving hepatic metastases, the tricuspid valve and/or pulmonic valves are affected, whereas tumors involving the lungs cause left-sided valvular abnormalities. Figure 19 shows apical and right ventricle inflow views of the tricuspid valve in a patient with carcinoid heart disease; note the immobilized leaflets without closure, and consequent severe tricuspid regurgitation by color Doppler (please *see* companion DVD for corresponding video). Also note the Eustachian valve within the right atrium, which is a normal anatomic structure.

Pericardial Involvement

Pericardial involvement is a common sequelae of cancers that have invaded the pericardial space by direct extension, or else via hematogenous or lymphatic spread. The echolucent space is caused by effusive pericarditis, which can occasionally be hemorraghic (especially when caused by mesotheliomas) and expand rapidly enough to cause tamponade. Areas of solid tumor are usually seen as highly reflective, relatively thick or nodular echodensities adjacent to the visceral or parietal pericardium, which may invade underlying myocardium as well (Fig. 20). If solid tumor encases a significant portion of the pericardial sac, constrictive pericarditis can occur in addition to effusive pericarditis.

Late and/or Indirect Effects

Finally, even when cancers do not directly involve the heart, the treatment may have cardiac effects, despite remission or even cure of the primary malignancy. Chemotherapeutics of the vincristine class (adriamycin, daunorubicin, and others) are notorious for causing dilated cardiomyopathy as a side effect in some patients. The anti-*HER2* monoclonal antibody, herceptin, is often used in combination with anthracyclines, and appears to cause heart failure, particularly in patients who are older or have other cardiac risk factors. Thus, the ejection fraction should be followed serially in these patients. Radiation therapy to the mediastinum can cause radiation pericarditis, which may be eventually evolve into constrictive pericarditis; exposure to such radiation also associated with accelerated coronary artery disease in cancer survivors.

SUGGESTED READING

European Cooperative Study Group. Diagnosis of heart tumours by transoesophageal echocardiography: a multicentre study in 154 patients. European Cooperative Study Group. Eur Heart J 1993;14:1223–1228.

Joffe II, Jacobs LE, Owen AN, Ioli A, Kotler MN. Noninfective valvular masses: review of the literature with emphasis on imaging techniques and management. Am Heart J 1996;131: 1175–1183.

Orsinelli DA, Pearson AC. Usefulness of multiplane transesophageal echocardiography in differentiating left atrial appendage thrombus from pectinate muscles. Am Heart J 1996;131:622, 623.

Reynen K. Cardiac myxomas. New Engl J Med 1995;333: 1610–1617.

Roberts WC. A unique heart disease associated with a unique cancer: carcinoid heart disease. Am J Cardiol 1997;80: 251–256.

Sun JP, Asher CR, Yang XS, et al. Clinical and echocardiographic characteristics of papillary fibroelastomas: a retrospective and prospective study in 162 patients. Circulation 2001; 103:2687–2693.

20 Aortic Dissection and Other Diseases of the Aorta

Laura Benzaquen, MD

Contents

CASE PRESENTATION 1

A 56-yr-old man with a history of hypertension presented to the emergency department after an episode of syncope. Earlier that evening, while attending a business meeting, he experienced dizziness and diaphoresis, followed by a sudden loss of consciousness. He was brought immediately to the emergency department. On arrival, his blood pressure was 80/50 mmHg and his cardiac rhythm was regular at a rate of 75 bpm. Examination of the head and neck revealed no signs of trauma. There was no jugular venous distention or carotid bruits. Heart sounds were normal, and there were no murmurs, rubs, or gallops. The neurological examination was notable for the presence of a rightward gaze and left-sided weakness**.** An electrocardiogram showed significant diffuse ST segment depressions. Emergent surface echocardiography showed a moderately dilated aortic root with mild aortic regurgitation. This study also showed a linear, highly mobile echogenic structure in the aortic root that partially prolapsed into the left ventricle (Fig. 1; please *see* companion DVD for corresponding video). This study prompted the requisition of an emergent transesophageal echocardiogram (TEE) (Fig. 2; please *see* companion DVD for corresponding video).

AORTIC DISSECTION: EPIDEMIOLOGY AND PATHOPHYSIOLOGY

Aortic dissection is frequently a life-threatening condition and it is the most common emergency involving the aorta. In the United States, approx 10–20 cases per million people occur annually. If the condition is left untreated, the mortality rate has been reported to increase by 1–3% per hour after presentation, and is approx 36–72% within 48 h of diagnosis, and 62–91% within 1 wk.

Aortic dissection occurs when a tear in the aortic intima exposes the underlying media to the hydrodynamic forces of blood within the aortic lumen leading to dissection within the media. A false lumen is created by blood

From: *Contemporary Cardiology: Essential Echocardiography: A Practical Handbook With DVD*
Edited by: S. D. Solomon © Humana Press, Totowa, NJ

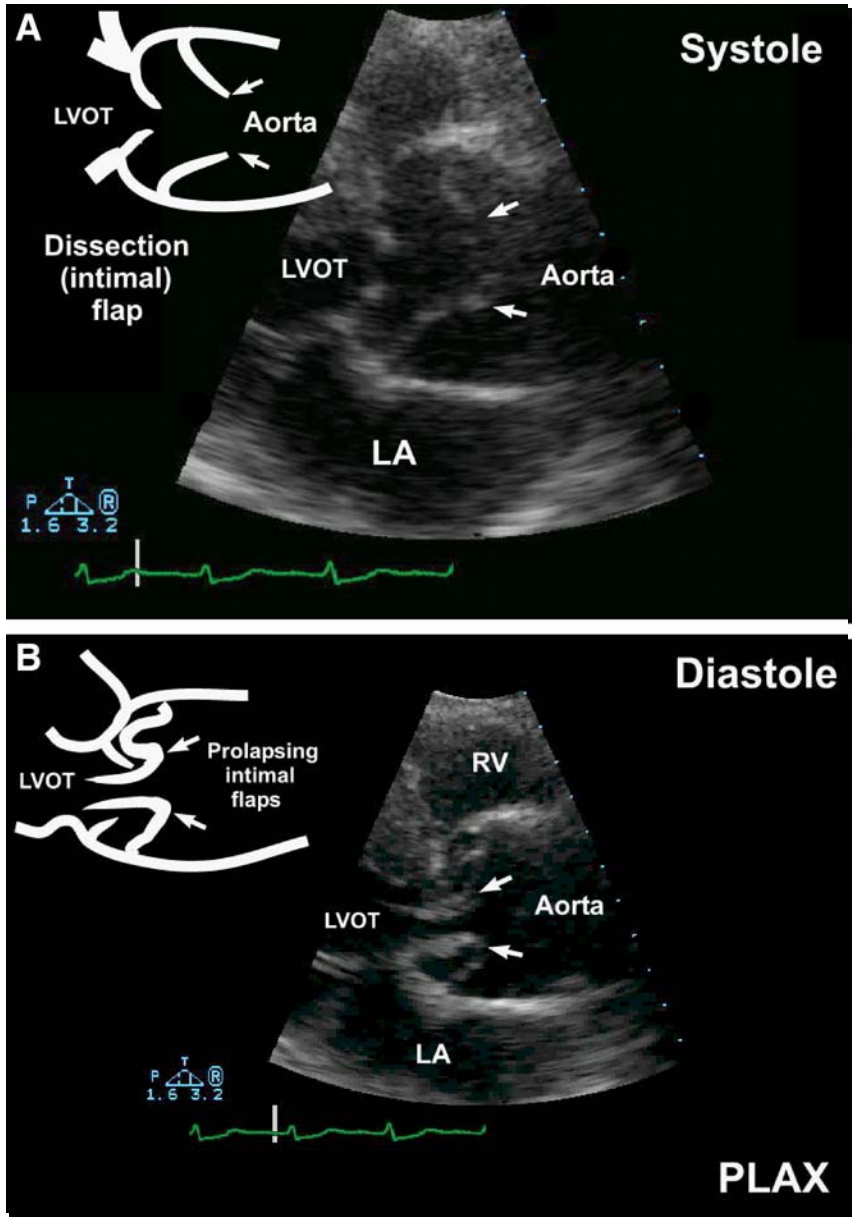

Fig. 1. Parasternal long-axis (PLAX) view showing aortic root dissection flap that prolapses into the left ventricular outflow tract during diastole. It was accompanied by new onset aortic regurgitation. (Please *see* companion DVD for corresponding video.)

filling the space within the media between the intimal flap and the adventitia (Fig. 3). The initiating event is generally felt to be rupture of the intima with the subsequent dissection through the media, although primary hemorrhage within the media with subsequent intimal perforation is a potential alternative mechanism. Shear forces may lead to further tears in the intimal flap, which may function as additional entry sites for blood into and from the false lumen.

Etiology of Aortic Dissection

Acute aortic dissection usually occurs in association with medial degeneration (Table 1). The great majority of patients have a history of hypertension. Several connective tissue disorders are also associated with aortic dissection, such as Marfan and Ehlers-Danlos syndromes. Marfan syndrome is responsible for the majority of aortic dissection in patients under 40 yr old. Bicuspid aortic valve, coarctation, Turner's and Noonan's syndromes, polycystic kidney disease, and family histories of dissection have been associated with a higher risk of dissection. Pregnancy is another condition that increases the risk of dissection, especially during the third trimester or during labor. Direct or indirect trauma such as deceleration owing to a motor vehicle accident may cause aortic dissection; usually this occurs

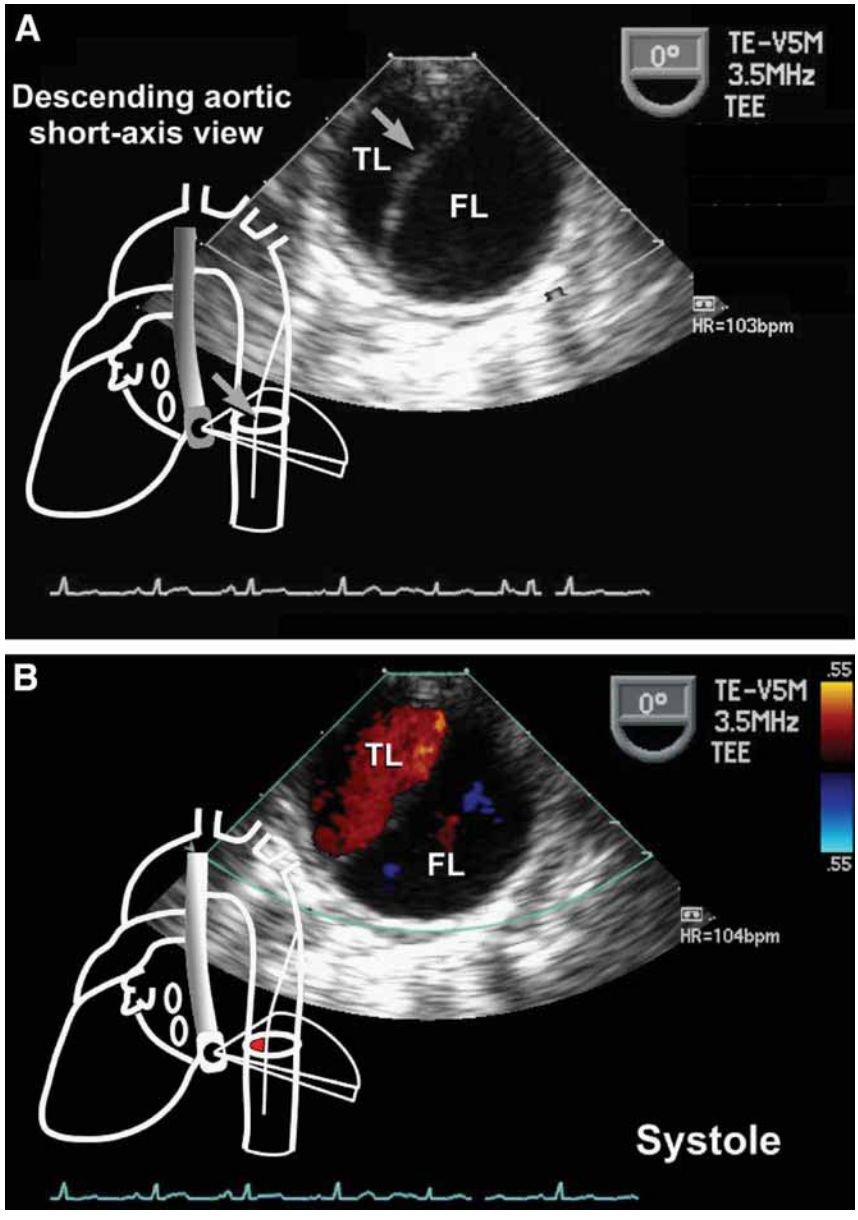

Fig. 2. Transesophageal descending thoracic aorta short-axis in the same patient in Fig. 1A,B. Color flow Doppler shows systolic flow within the true lumen (TL). Compare this to the false lumen (FL). (Please *see* companion DVD for corresponding video.)

in the aortic isthmus distal to the ligamentum arteriosum. Cardiac surgery is also associated with a risk of aortic dissection, in particular bypass surgery and aortic valve replacement. Patients with Takayasu's disease and other inflammatory collagen vascular diseases are also at increased risk. Corticosteroid use has also been associated with increased risk of dissection. Aortic dissection has also been reported to occur in association with cocaine use, particularly crack cocaine, presumably owing to abrupt elevations in systemic blood pressure.

Location of Dissection

It is important to distinguish proximal from distal dissection for prognostic and therapeutic reasons (Fig. 4). Proximal dissections involve the aortic root. Acute proximal dissections are an acute cardiovascular emergency requiring immediate surgical correction. Distal dissections commence after the origin of the left subclavian artery and propagate distally without aortic root involvement. These distal lesions can usually be managed medically.

Associated Findings in Aortic Dissection

The marked increased morbidity and mortality associated with proximal aortic dissection is secondary to the potentially morbid sequelae of dissection. Dissection proximally toward the heart represents one of the most morbid complications of dissection. Dissections that

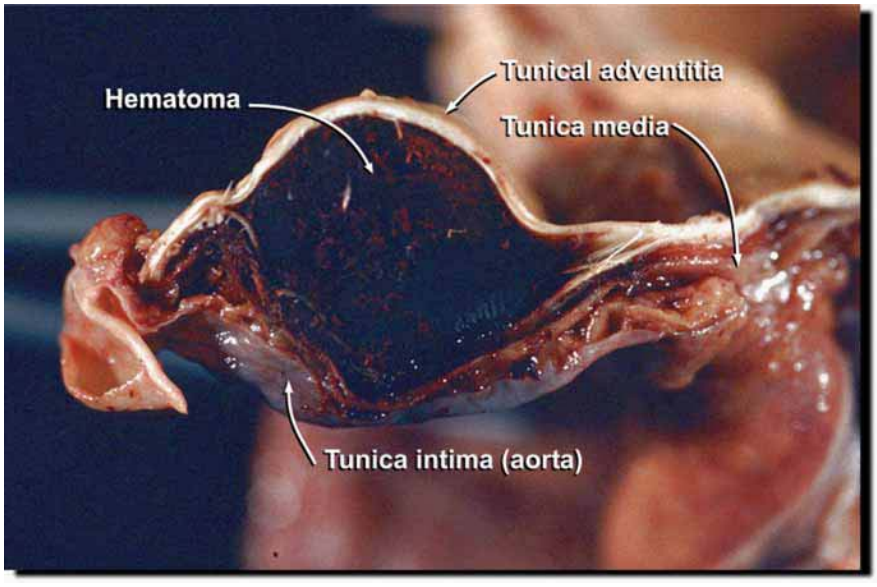

Fig. 3. Pathological specimen showing a large intramural hematoma in a patient with acute aortic dissection. This 54-yr-old male presented to the emergency department with severe neck pains. His had a history of bicuspid aortic valve with aortic stenosis and regurgitation. (Image courtesy of Robert Padera, MD, Brigham and Women's Hospital.)

Table 1
Factors Predisposing to Aortic Dissection

Predisposing factors for AD
• Hypertension (co-exists in 72–80% of AD)
• Bicuspid aortic valve disease (7–14%)
• Cystic medial degeneration (e.g., Marfan syndrome [5–9% of all AD cases], Ehlers-Danlos syndrome)
• Iatrogenic trauma: intra-arterial catheterization and coronary angiography, cardiac surgery (aortic cannulation site), intra-aortic balloon pump cardiopulmonary bypass); before cardiac surgery (up to 18% of all AD)
• Direct trauma
• Pregnancy (third trimester)
• Aging
• Cocaine abuse
• Coarctation of the aorta
• Takayasu's disease
• Polycystic kidney disease
• Family history of AD
• Corticosteriods (prolonged use)
• Turner's and Noonan's syndromes
• Arteritis (e.g., Giant cell arteritis)

involve the aortic root can extend into the coronary arteries causing an acute coronary syndrome; similarly, dissections that involve the aortic arch can extend into the great vessels causing stroke or transient ischemic attack. Dissections extending into the aortic root can also involve the aortic valve itself resulting in acute aortic insufficiency. Dissections extending to the heart can also extend into the pericardial space resulting in pericardial effusion or even acute tamponade. Finally, dissections are associated with marked weakening of the aortic lining and can be associated with catastrophic rupture of the aorta itself.

Transthoracic Imaging

Transthoracic imaging (TTE) has a sensitivity of 59–85% and specificity of 63–96% for the diagnosis of aortic dissection. This low sensitivity is mainly secondary to the suboptimal visualization of the ascending aorta beyond the sinotubular junction and poor visualization of the aortic arch (Fig. 5). However, TTE is a highly valuable tool for identifying complications of dissection. Aortic regurgitation and aortic root dilatation are frequent findings and easily seen by TTE (Fig. 6; please *see* companion DVD for corresponding video). Wall motion abnormalities caused by occlusion of the coronary arteries by the dissecting flap may be occasionally identified. Furthermore, TTE is the preferred modality to assess pericardial effusion and tamponade caused by rupture of the dissected aorta into the pericardial space (Table 2). TTE is also useful in the initial evaluation of suspected aortic dissection involving the proximal abdominal aorta (Fig. 7).

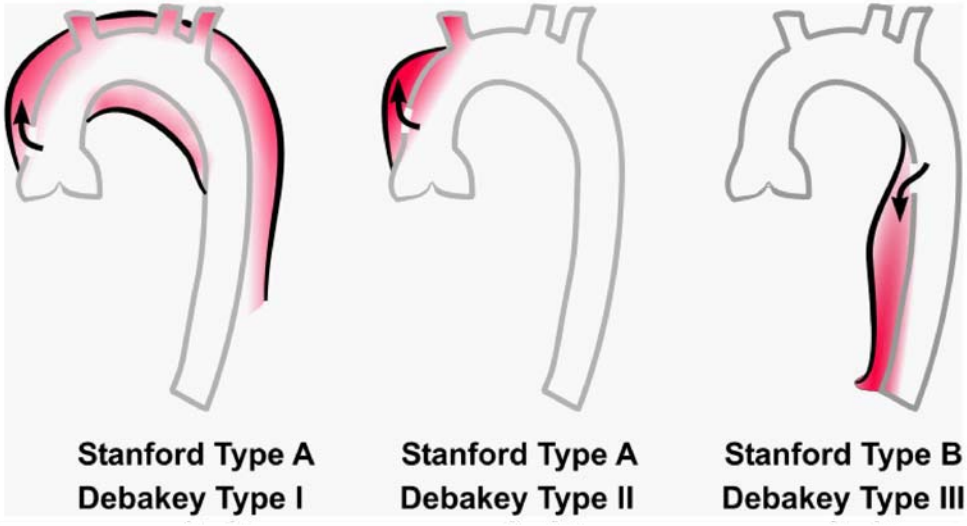

Fig. 4. The Debakey and Stanford classifications of aortic dissection. The Stanford classification is the most commonly used. Type A dissections involve the ascending aorta and aortic arch irrespective of the number or location of entry sites. Type A dissections are generally surgical emergencies. Type B dissections, beginning distal to the subclavian, are most often managed medically.

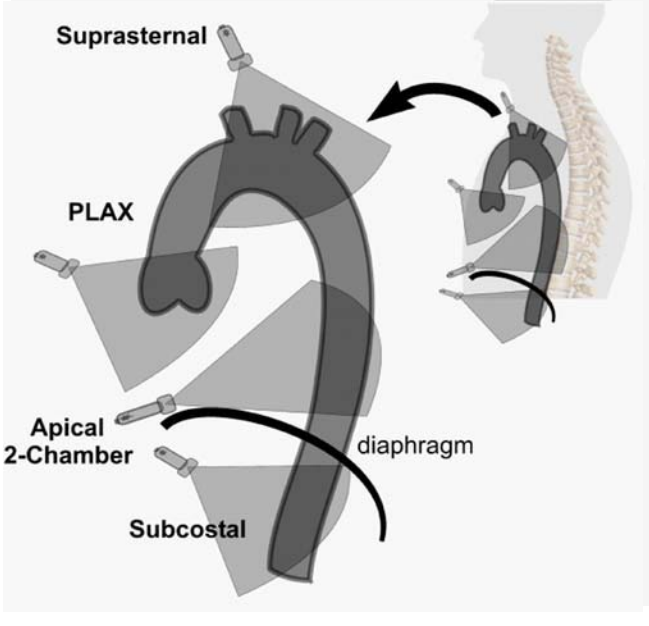

Fig. 5. Visualization of the aorta on transthoracic echocardiography (TTE). Limited acoustic windows leave gaps in the TTE examination of the aorta and renders relatively low sensitivity (59–85%) of TTE in the diagnosis of aortic dissection. TTE is nonetheless valuable in assessing related complications of aortic dissection (e.g., wall motion abnormalities, pericardial effusion, or tamponade, or evaluating other conditions that mimic aortic dissection).

In general, TTE is of limited diagnostic value in the initial assessment of aortic dissection and should be used as an initial screening test among patients in whom the clinical suspicion for aortic dissection is very low. In this group of patients, the absence of direct and indirect signs of dissection makes the diagnosis highly unlikely. On the other hand, TTE is highly specific and the visualization of the typical echocardiographic findings of aortic dissection, particularly in patients with proximal dissections, confirms the diagnosis (Table 3).

One of the most important uses of TTE in the evaluation of a patient with suspected aortic dissection is to rule out other conditions that mimic aortic dissection (Table 4). These include acute coronary syndrome and myocardial infarction (might be associated with a regional wall motion abnormality), acute pulmonary embolism (might be associated with right ventricular dysfunction). In addition, TTE can be very useful in diagnosing associated conditions seen in conjunction with or as complications of aortic dissection. These include acute aortic insufficiency, pericardial effusion or tamponade caused by dissection into the pericardium.

Transesophageal Imaging (*see* Chapter 23, TEE Primer)

Early recognition of aortic dissection is critical because the mortality rate is very high if left untreated. Thus, diagnostic accuracy is of crucial importance when selecting an initial diagnostic test to evaluate a patient with suspected aortic dissection. There are a number of noninvasive approaches to rapid diagnosis of suspected aortic dissection. Although contrast-enhanced computed tomography scanning has become the method of choice in many institutions (Table 5), TEE is a good alternative

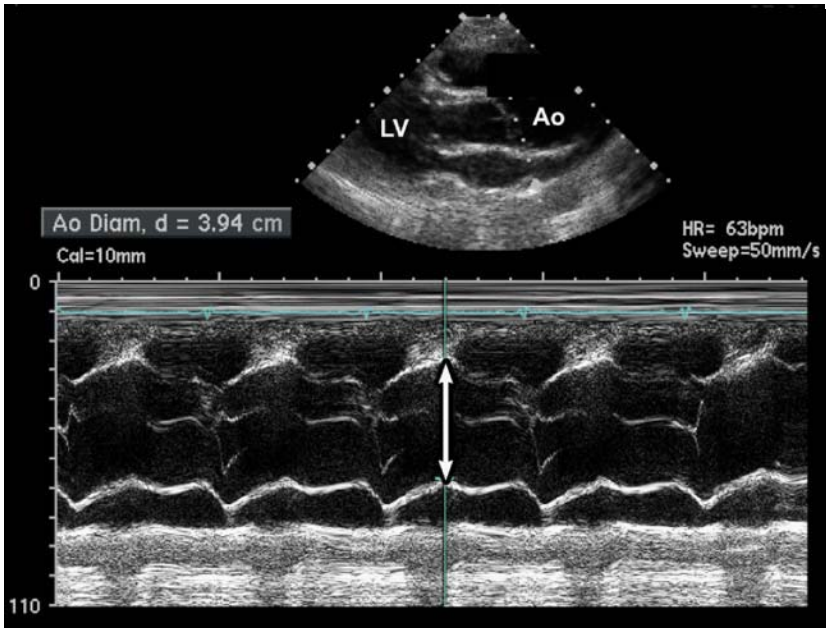

Fig. 6. Two-dimensional guided M-mode showing aortic root dilatation in a 44-yr-old female with Marfan syndrome. (Please *see* companion DVD for corresponding video.)

Table 2
Possible Transthoracic Echocardiography Findings in Aortic Dissection

1. Mobile dissection (intimal) flap within:
   a. Aortic root (PLAX, PSAX)
   b. Sino-tubular junction and ascending aorta (high PLAX)
   c. Aortic arch (SSN)
   d. Descending thoracic aorta (PLAX, A2C)
   e. Proximal abdominal aorta (SC)
2. Flail aortic leaflet(s) (PLAX, PSAX, apicals)
3. Aortic root dilatation
4. Acute aortic insufficiency (PLAX, PSAX, apicals)
5. Wall motion abnormality (left ventricle)
6. Pericardial effusion or tamponade (SC, PLAX, SAX)
7. Differential color Doppler flow patterns within true and false lumen (PLAX, SSN, SC, apicals)
8. Pulse Doppler examination of flow at entry/exit sites and within true and false lumen (SSN, SC, apicals)

Apicals, apical five-chamber and apical (long-axis) five-chamber view, Apical two-Chamber (A2C); PLAX, parasternal long-axis views; PSAX, parasternal short-axis views; SC, subcostal views; SSN, suprasternal notch views. TTE, transthoracic echocardiographic.

choice (Table 6). TEE offers several advantages when compared to other noninvasive methods: it is highly accurate, fast, relatively safe, and inexpensive. Because it can be performed at the bedside, it is often preferred among intubated and critically ill patients. Moreover, TEE is the only diagnostic modality that can be used in the operating room during aortic dissection repair to monitor flow in the thoracic aorta during cardiopulmonary bypass, and to evaluate the need for further surgical interventions such as aortic valve replacement in patients with aortic dissection complicated by significant aortic regurgitation.

The aortic valve, aortic root, proximal ascending, distal aortic arch, descending thoracic, and proximal abdominal aortas are all well visualized with this approach (Figs. 8 and 9). However, the region of the distal ascending aorta and proximal aortic arch (TEE blind areas) is suboptimally visualized by this technique owing to the interposition of the trachea and bronchi between the transducer in the esophagus and the aorta. One potential limitation of the technique because of this "blind spot" is that dissections that begin at the site of aortic cannulation following bypass surgery and travel distally can be missed.

In several studies, the sensitivity and specificity of TEE has consistently been high, ranging from 97 to 100% and 95 to 98%, respectively, for the diagnosis of aortic dissection. The echocardiographic finding considered diagnostic of an aortic dissection is the presence of an undulating linear density (intimal flap) within the aortic lumen separating the true and false channels (Figs. 10–12 [please *see* companion DVD for corresponding video for Figs. 10 and 11]; Table 7). The flap usually has independent motion from that of the

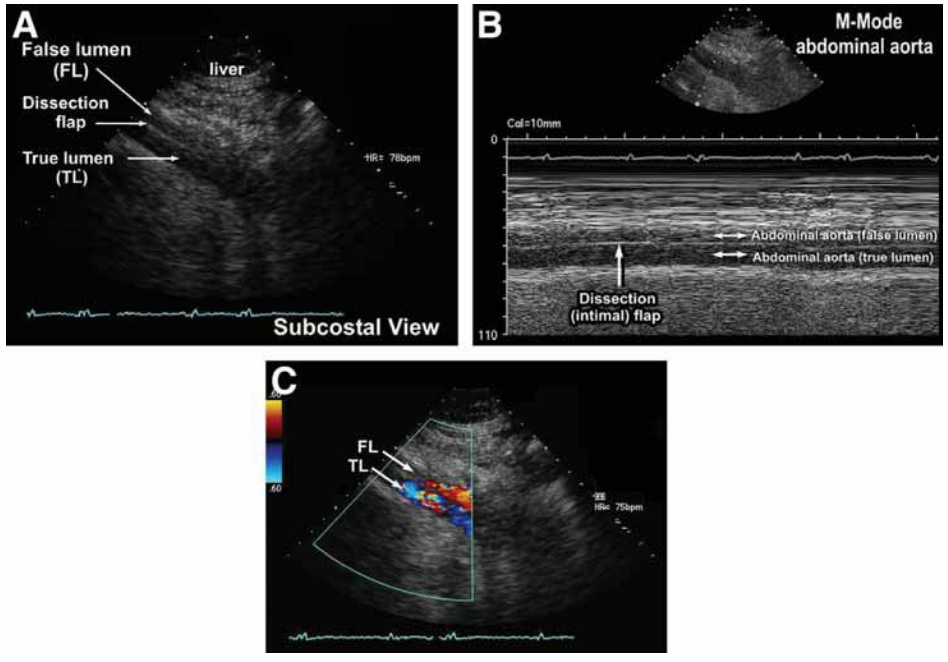

Fig. 7. Transthoracic echoardiography (TTE) can provide information on aortic dissection involving the proximal abdominal aorta. This 54-yr-old female patient presented with a history of back pains. Two-dimensional, M-mode, and Color flow Doppler images of her dissection appear below. Note the differential flow patterns between the true lumen (TL) and the false lumen (FL).

Table 3
Utility of Transthoracic Echocardiography in Aortic Dissection

Advantages/disadvantages of TTE in Aortic Dissection
Advantages
Rapid diagnosis (for sinotubular and abdominal aortic dissection)
Best utility for complications accompanying aortic dissection (e.g., aortic, myocardical, and pericardial involvement)
Portable (bedside or operating room)
Safe
Inexpensive
Requires no sedation or anesthesia
Disadvantages
Suboptimal visualization of thoracic aorta
Limited diagnostic value for initial diagnosis and assessment
Relatively low sensitivity (59–85%) and specifity (63–96%)

TTE, transthoracic echocardiography.

Table 4
Conditions Mimicking Acute Aortic Dissection

Differential diagnosis of acute aortic dissection
1. Acute coronary syndromes and myocardial infarction
2. Acute pulmonary embolism
3. Acute pericarditis
4. Acute pleurisy
5. Esophageal spasm
6. Other causes of acute chest pain syndromes
7. Other causes of the acute abdomen (for abdominal aortic dissection)

heart and aortic walls and its presence should be sought in different planes. Color flow Doppler confirms the presence of two lumina by the demonstration of differential color flow patterns between the true and the false lumen with the true lumen usually displays pulsatile systolic flow. Identification of the entry site of the dissection may also help in the identification of the true lumen from the false one (Figs. 13 and 14; please *see* companion DVD for corresponding video for Fig. 13). TEE can identify the spatial extent of dissection and sites of intimal tears. TEE can also detect and characterize complications of potential prognostic and therapeutic importance such as pericardial effusion, aortic regurgitation, and dissection into the right ventricle or the right atrium creating aorta-to-right ventricle or atrium fistulas. TEE may provide additional information useful to the surgeon such as whether the intimal flap

Table 5
Imaging Modalities and Diagnostic Performance in Suspected Aortic Dissection

Diagnostic performance	*Transesophageal echocardiography*	*Angiography*	*Computed tomography*	*Magnetic resonance imaging*
Sensitivity	+++	++	+++	+++
Specificity	+++	+++	+++	+++
Site of internal tear	++	++	+	+++
Presence of thrombus	+	+++	++	+++
Presence of aortic insufficiency	+++	+++	–	+
Pericardial effusion	+++	–	++	+++
Branch vessel involvement	+	+++	++	++
Coronary artery involvement	++	++	–	–

Modified from Cigarroa JE, Isselbacher EM, DeSantis RW, Eagle KA. Diagnostic imaging in the evaluation of suspected aortic dissection: old standards and new directions. N Engl J Med 1993;328:35.
+++ excellent; ++ good; + fair; – not detected

Table 6
Utility of Transesophageal Echocardiography in Aortic Dissection

Advantages
Accurate (sensitivity 97–100%; specificity 95–98%)
Rapid diagnosis
Portable (bedside or operating room)
Real-time intra-operative monitoring and evaluation
Safe—low complication rate
Inexpensive
Disadvantages
Blind spots in thoracic aorta (distal ascending aorta and aortic arch)
No visualization of abdominal aorta
Intravenous conscious sedation; topical oropharyngeal anesthesia
Relative contraindication in certain cervicofacial and esophageal injuries

involves the ostia and proximal segments of the coronary arteries.

Pitfalls in the Diagnosis of Aortic Dissection

Reverberations and beam-width artifacts can cause false linear echodensities within the aortic lumen that mimic aortic dissection. This is not an uncommon finding in aortas with extensive plaque formation or in dilated ectatic vessels (Fig. 4A; *see* Chapter 1, Fig. 8). TEE-derived M-mode echocardiography can help to identify reverberation artifacts originating from the posterior wall of the aorta or adjacent venous structures, and to differentiate these artifacts from dissection. Artifacts are located at a distance from the source that is predicted by ultrasound physical principles; and they have similar motion patterns with the suspected source. In one study, the use of M-mode echocardiography significantly improved the sensitivity and specificity of TEE from 87–93.5% to 93.5–96.8% and from 85.1–94.1% to 99–100%, respectively, suggesting that M-mode echocardiography should be performed in indeterminate cases of aortic dissection.

On the other hand, small dissections limited to the distal ascending aorta and proximal aortic arch could be missed because of interference from the air-filled trachea. Sometimes, intimal thickening with minor distortion of the aortic wall may be the only sign of a localized dissection when the false lumen is thrombosed and the flap is relatively immobile.

CASE PRESENTATION 2

A 72-yr-old woman was brought to a hospital emergency room with severe chest pain. She had a history of hypertension and hypercholesterolemia. She had no history of chest pain before this episode and had been in her usual state of health. On arrival to the emergency department, her blood pressure was 190/105 mmHg and her cardiac rhythm was regular at a rate of 87 bpm. An emergent transesophageal echocardiogram was obtained (Fig. 15; please *see* companion DVD for corresponding video).

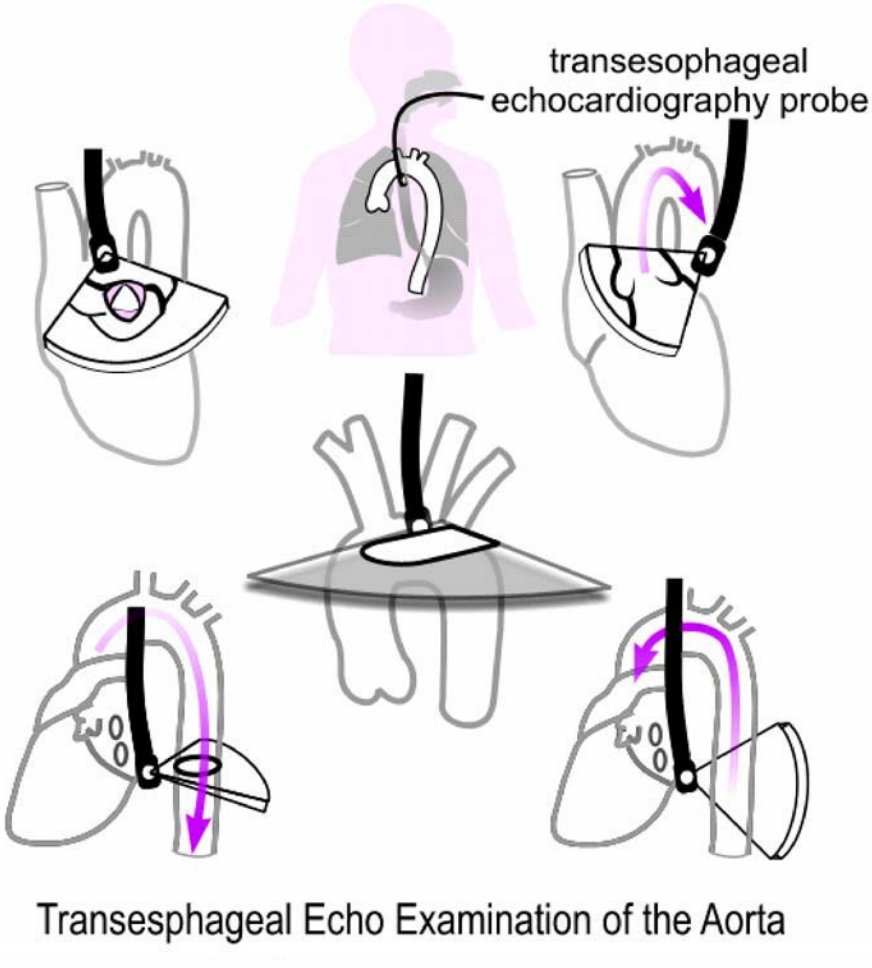

Fig. 8. Transesophageal examination of the aorta (*see* Chapter 23, transesophageal echocardiography primer).

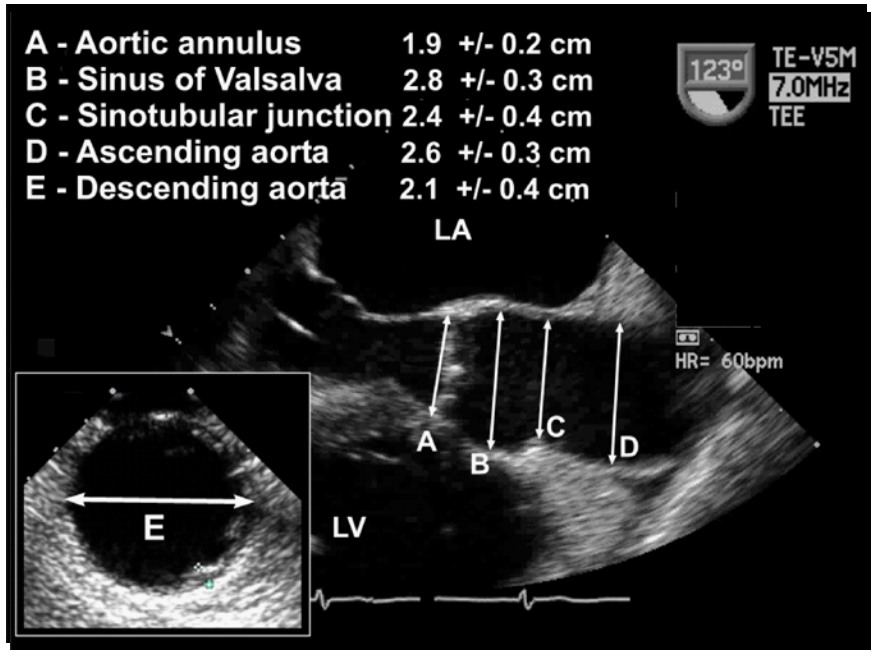

Fig. 9. Aortic measurements by transesophageal echocardiography of mid esophageal aortic valve long-axis and the descending aortic short-axis (insert) still frames. Mild dilatation of the proximal ascending aorta is seen in this study.

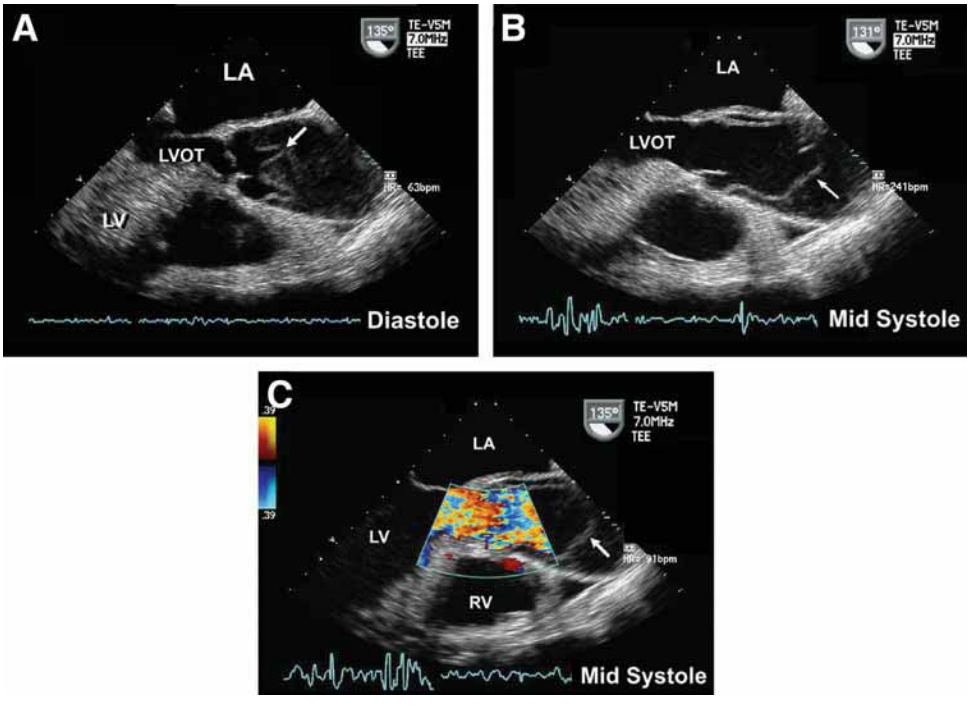

Fig. 10. Midesophageal aortic valve long-axis views of a 69-yr-old male with a history of hypertension and paroxysmal atrial fibrillation. Moderate dilatation of the proximal aorta with a mobile dissection (intimal) flap were seen (arrows). Severe aortic regurgitation was present. He underwent total replacement of his aortic root with coronary artery re-implantation. (Please *see* companion DVD for corresponding video.)

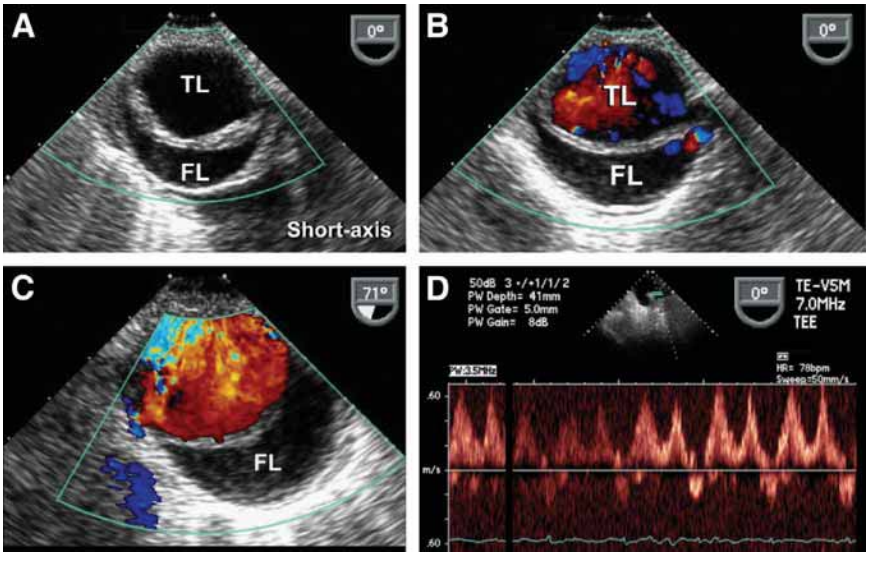

Fig. 11. Further transthoracic echocardiography (TEE) descending aortic short axis views of the patient in Fig.10 revealed involvement of the entire thoracic aorta. This is therefore a Stanford type A or Debakey type I aortic dissection (Fig. 4). Note color flow Doppler pattern within the true lumen (TL) and the false lumen (FL) and pulsed Doppler interrogation revealing pulsatile flow within the true lumen. (Please *see* companion DVD for corresponding video.)

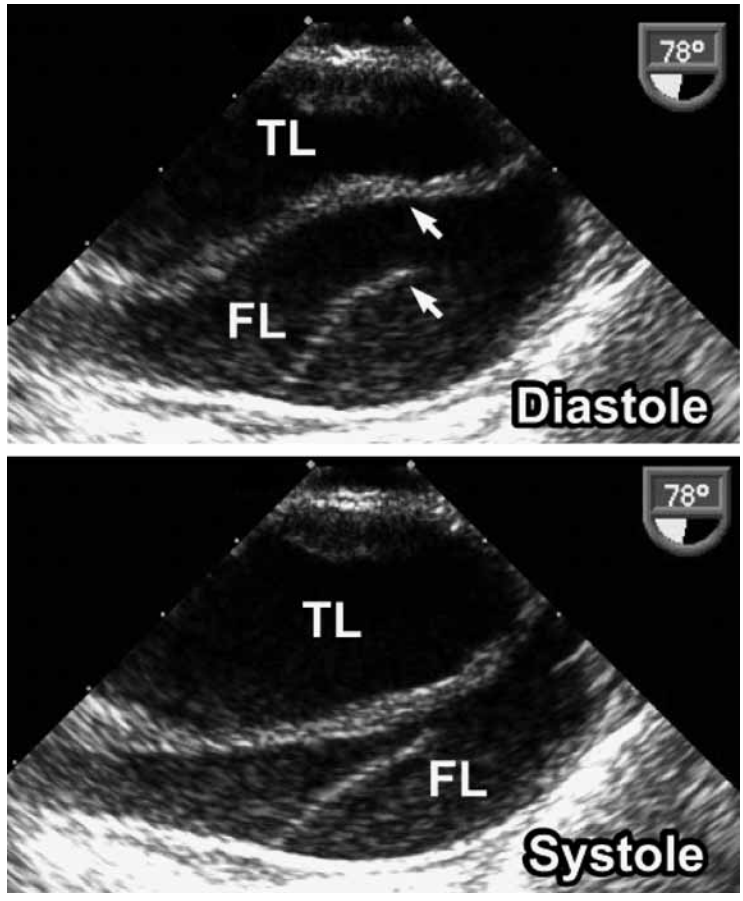

Fig. 12. Transesophageal echocardiographic examination of the aorta in suspected aortic dissection involves careful multiplane examination of the entire thoracic aorta (Fig. 8). Images in this patient (omniplane 78°) revealed undulating intimal flaps that moved independently of the aortic walls. The perfusing lumen can be differentiated from the nonperfusing lumen on Color flow Doppler and pulsed Doppler interrogation. Note the systolic expansion of the true or perfusing lumen (TL) during systole.

INTRAMURAL HEMATOMA

An aortic intramural hematoma (IMH) is a hemorrhage limited to the medial layer of the aortic wall without intimal disruption (Figs. 3 and 15A,B; please *see* companion DVD for corresponding video for Fig. 15). Although the pathogenesis of IMH remains unclear, rupture of the vasa vasorum located within the medial layer of the aorta and rupture of an atherosclerotic plaque are considered to be the initiating events that lead to IMH.

TEE is an important imaging modality for the diagnosis of IMH. The typical TEE finding of IMH is a focal or diffuse thickening of the aortic wall in the absence of an intimal flap or any communication between the aortic lumen and the IMH. IMH should be differentiated from thrombosed aortic aneurysms, dissection with thrombosed false lumen, and complex aortic atherosclerotic plaques.

Table 7
TEE Findings in AD

1. Mobile dissection (intimal) flap within aortic root, aortic arch, ascending and descending aorta
2. True and false lumen separated by intimal flap
3. Intimal tear(s) with communication site(s): entry or exit site(s)
4. Aortic aneurysm
5. Coronary branch artery involvement
6. Aortic branch artery involvement
7. Aortic intramural hematoma
8. Flail aortic leaflet(s)
9. Acute aortic insufficiency
10. Hemopericardium and pericardial tamponade

In some patients, IMH may regress or even completely disappear, whereas it may progress to aortic

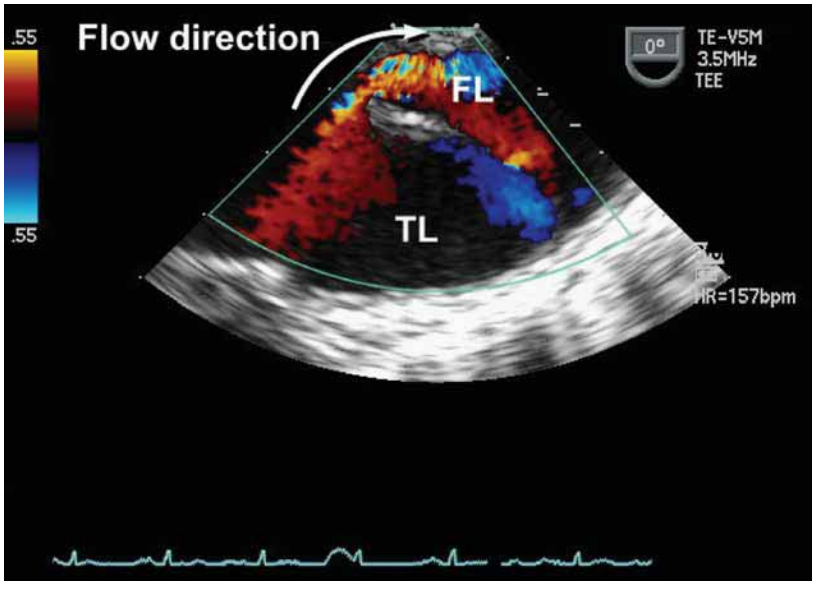

Fig. 13. Midesophageal short-axis view (omniplane 0°). Color flow Doppler examination in this 42-yr-old female patient with acute aortic dissection reveals the entry site and flow from true lumen (TL) to the false lumen (FL). (Please *see* companion DVD for corresponding video.)

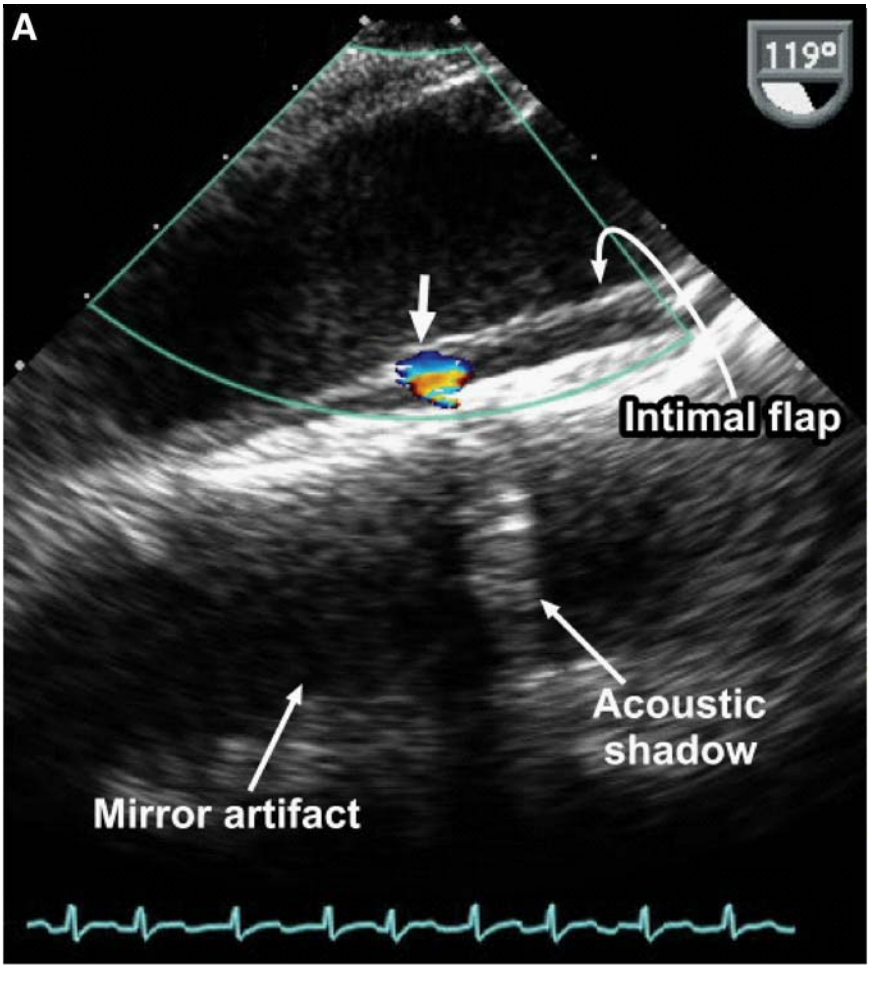

Fig. 14. (*See* legend, facing page)

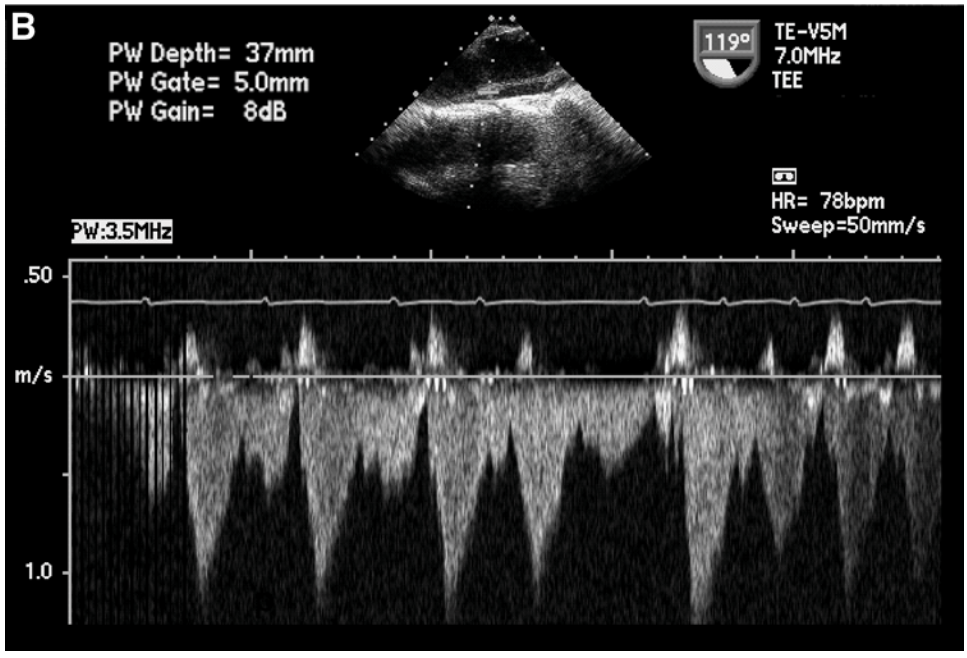

Fig. 14. (**A**) Descending aortic long axis view in a patient with Type B aortic dissection shows intimal tear (arrow) and flow acceleration at entry site. Note acoustic shadowing from calcific atheromatous changes near intimal tear. Mirror artifacts are common on transesophageal echocardiography (*see* Chapter 1, Fig. 8). (**B**) Pulse Doppler interrogation at the site of intimal tear confirms flow from true to false lumen.

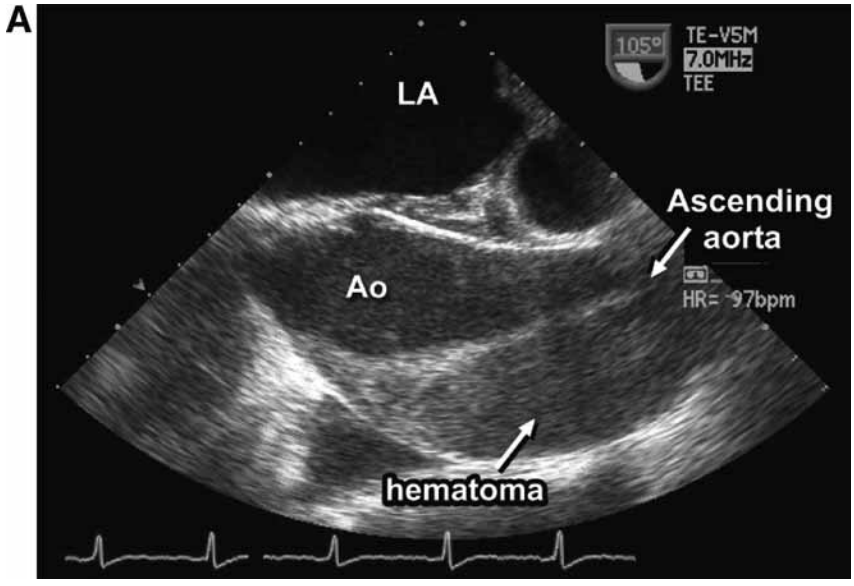

Fig. 15. (**A**) Midesophageal ascending aortic long axis view in 72-yr-old female showing proximal ascending aorta with large echodensisity protruding into aortic lumen, but confined by intima. It proved to be an intramural hematoma that involved the entire ascending aorta. No intimal tear was seen at surgery. (**B**) Color flow Doppler examination of patient (**A**) shows flow confined to the true aortic lumen with no communication visible between both cavities. (**C**) Midesophageal ascending aortic short-axis views of the aora in the same patient showing the intramural hematoma (left panel) and luminal flow confined to the aortic lumen (right panel). (Please *see* companion DVD for corresponding video.)

dissection and aortic rupture in other patients. These vascular complications account for the high acute mortality from IMH (up to 30%). In general, proximal IMH are treated surgically, whereas medical management with serial imaging studies is reserved for patients with distal IMH. Persistence of IMH has been associated with a poor prognosis so close follow-up is recommended.

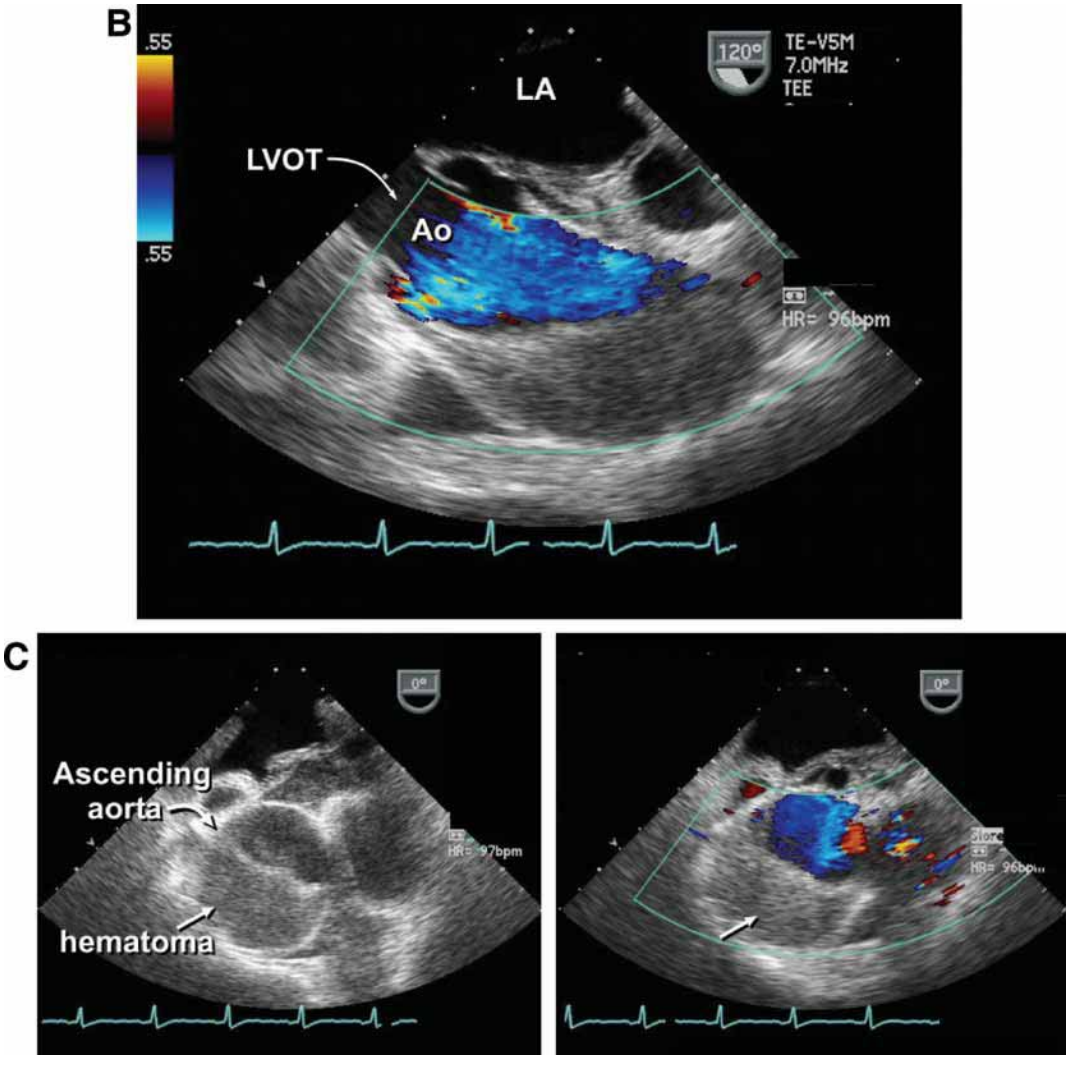

Fig. 15. *(Continued)*

OTHER DISEASES OF THE AORTA: PROXIMAL AORTIC ANEURYSM WITHOUT DISSECTION AND MARFAN SYNDROME

As previously mentioned, patients with Marfan syndrome are at significantly increased risk for aortic dissection. Echocardiographic evaluation of patients with Marfan syndrome should include a careful evaluation of the proximal aorta. The aortic size should be measured in three separate locations (Fig. 9; *see* Chapter 12, Fig. 3) at the root, just below the aortic valve, at the sinotubular junction, and approx 1 cm above the sinotubular junction. In advanced aortic disease secondary to Marfan syndrome, the normal contour of the root and sinotubular junction (which resembles an old-fashioned Coca-Cola® glass, wider at the sinuses and tapering at the sinotubular junction), can become stretched and the sinotubular junction itself can become indistinct. Aortic diameters more than 5 cm or rapidly changing aortic diameter (even at lower absolute diameters) in patients with Marfan syndrome should prompt surgical intervention.

SUGGESTED READING

Ballal RS, Nanda NC, Gatewood R, et al. Usefulness of transesophageal echocardiography in assessment of aortic dissection. Circulation 1991;84:1903–1914.

Borner N, Erbel R, Braun B, Henkel B, Meyer J, Rumpelt J. Diagnosis of aortic dissection by transesophageal echocardiography. Am J Cardiol 1984;54:1157,1158.

Cohen IS. Intimal flap prolapse in aortic dissection. J Am Coll Cardiol 1984;4:1332–1333.

Eisenberg MJ, Rice SA, Paraschos A, Caputo GR, Schiller NB. The clinical spectrum of patients with aneurysms of the ascending aorta. Am Heart J 1993;125:1380–1385.

Erbel R, Engberding R, Daniel W, Roelandt J, Visser C, Rennollet H. Echocardiography in diagnosis of aortic dissection. Lancet 1989;1:457–461.

Evangelista A, Garcia-del-Castillo H, Gonzalez-Alujas T, et al. Diagnosis of ascending aortic dissection by transesophageal echocardiography: utility of M-mode in recognizing artifacts. J Am Coll Cardiol 1996;27:102–107.

Evangelista A, Avegliano G, Elorz C, Gonzalez-Alujas T, Garcia del Castillo H, Soler-Soler J. Transesophageal echocardiography in the diagnosis of acute aortic syndrome. J Card Surg 2002; 17:95–106.

Fox R, Ren JF, Panidis IP, Kotler MN, Mintz GS, Ross J. Anuloaortic ectasia: a clinical and echocardiographic study. Am J Cardiol 1984;54:177–181.

Goldman AP, Kotler MN, Scanlon MH, Ostrum BJ, Parameswaran R, Parry WR. Magnetic resonance imaging and two-dimensional echocardiography. Alternative approach to aortography in diagnosis of aortic dissecting aneurysm. Am J Med 1986;80: 1225–1229.

Goldman AP, Kotler MN, Scanlon MH, Ostrum B, Parameswaran R, Parry WR. The complementary role of magnetic resonance imaging, Doppler echocardiography, and computed tomography in the diagnosis of dissecting thoracic aneurysms. Am Heart J 1986;111:970–981.

Iliceto S, Nanda NC, Rizzon P, et al. Color Doppler evaluation of aortic dissection. Circulation 1987;75:748–755.

Keren A, Kim CB, Hu BS, et al. Accuracy of biplane and multiplane transesophageal echocardiography in diagnosis of typical acute aortic dissection and intramural hematoma. J Am Coll Cardiol 1996;28:627–636.

Mansour M, Berkery W, Kozlowski L, Widell J, Obeid A. *Mild thickening of the aortic wall: subtle intramural hematoma?* Echocardiography 2001;18:519–522.

Mathew T, Nanda NC. Two-dimensional and Doppler echocardiographic evaluation of aortic aneurysm and dissection. Am J Cardiol 1984;54:379–385.

Matsumoto M, Matsuo H, Ohara T, Yoshioka Y, Abe H. A two-dimensional echoaortocardiographic approach to dissecting aneurysms of the aorta to prevent false-positive diagnoses. Radiology 1978;127:491–499.

Mohr-Kahaly S, Erbel R, Steller D, Borner N, Drexler M, Meyer J. Aortic dissection detected by transoesophageal echocardiography. Int J Card Imaging 1986;2:31–35.

Nienaber CA, von Kodolitsch Y, Nicolas V, et al. The diagnosis of thoracic aortic dissection by noninvasive imaging procedures. N Engl J Med 1993;328:1–9.

Nienaber CA, von Kodolitsch Y, Brockhoff CJ, Koschyk DH, Spielmann RP. Comparison of conventional and transesophageal echocardiography with magnetic resonance imaging for anatomical mapping of thoracic aortic dissection. A dual noninvasive imaging study with anatomical and/or angiographic validation. Int J Card Imaging 1994; 10:1–14.

Nienaber CA, von Kodolitsch Y, Petersen B, et al. Intramural hemorrhage of the thoracic aorta. Diagnostic and therapeutic implications. Circulation 1995;92:1465–1472.

Nishigami K, Tsuchiya T, Shono H, Horibata Y, Honda T. Disappearance of aortic intramural hematoma and its significance to the prognosis. Circulation 2000;102:III243–III247.

Oh JK, Seward JB, Khandheria BK, et al., Transesophageal echocardiography in critically ill patients. Am J Cardiol 1990;66: 1492–1495.

Patel S, Alam M, Rosman H. Pitfalls in the echocardiographic diagnosis of aortic dissection. Angiology 1997;48:939–946.

Rizzo RJ, Aranki SF, Aklog L, et al. Rapid noninvasive diagnosis and surgical repair of acute ascending aortic dissection. Improved survival with less angiography. J Thorac Cardiovasc Surg 1994;108:567–574.

Rosenzweig BP, Goldstein S, Sherrid M, Kronzon I. Aortic dissection with flap prolapse into the left ventricle. Am J Cardiol 1996;77:214–216.

Rosenzweig BP, Guarneri E. Transesophageal Echocardiography in the Evaluation of Aortic Trauma. Echocardiography 1996;13: 247–258.

Seward JB, Khandheria BK, Oh JK, et al. Transesophageal echocardiography: technique, anatomic correlations, implementation, and clinical applications. Mayo Clin Proc 1988;63: 649–680.

Simon P, Owen AN, Havel M, et al. Transesophageal echocardiography in the emergency surgical management of patients with aortic dissection. J Thorac Cardiovasc Surg 1992;103: 1113–1117.

Victor MF, Mintz GS, Kotler MN, Wilson AR, Segal BL. Two dimensional echocardiographic diagnosis of aortic dissection. Am J Cardiol 1981;48:1155–1159.

Vignon P, Spencer KT, Rambaud G, et al. Differential transesophageal echocardiographic diagnosis between linear artifacts and intraluminal flap of aortic dissection or disruption. Chest 2001;119:1778–1790.

21 Echocardiography in the Assessment of Atrial Septal Defects

Edmund A. Bermudez, MD, MPH

Contents

INTRODUCTION

Historically, the evaluation of patients with suspected congenital heart disease relied heavily on the results of the physical exam and cardiac catheterization. In the current era, the initial assessment of congenital lesions can now be safely and easily accomplished with cardiac ultrasound, often without the need for further invasive testing. One of the most frequently encountered acyanotic congenital lesions in clinical practice is the atrial septal defect (ASD), of which echocardiography provides invaluable information in the initial assessment, follow-up, and management. The spatial resolution of echocardiography allows for accurate classification of ASDs and a comprehensive evaluation of associated cardiac pathology. A quantification of shunt flow and hemodynamics can be easily accomplished with Doppler, and provide an objective means of follow up for these patients. Finally, echocardiography can be used to guide percutaneous closure of ASDs, providing an important avenue for minimally invasive intervention. Thus, echocardiography is currently the basis for the initial diagnosis, follow-up, and when appropriate, management of ASDs.

ANATOMIC AND ECHOCARDIOGRAPHIC OVERVIEW

During embryological development, the right and left cardiac atria are formed with the growth of the atrial septum. This dividing wall between the atria originates with the growth of two separate septa: septum primum and septum secundum. The first to be formed is the septum primum, which grows from the superior aspect of the atria wall inferiorly, toward the enodcardial cushions between the atria and ventricles (Fig. 1A). In its normal development, the septum primum attaches to the endocardial cushions, with eventual resorption of the superior attachment. Concurrently, a second septum develops slightly to the right of the septum primum, with progressive growth from the superior aspect of the atrium toward the endocardial cushions, but does not reach or attach to this area. Therefore, when developed, the septum primum attaches inferiorly to the floor of the atrial cavity and the septum secundum superiorly to the roof the atria. Together, these two septa overlap to form the basis of the interatrial septum, between which the foramen ovale is formed (Fig. 1B). The foramen ovale is patent during development but normally closes

From: *Contemporary Cardiology: Essential Echocardiography: A Practical Handbook With DVD*
Edited by: S. D. Solomon © Humana Press, Totowa, NJ

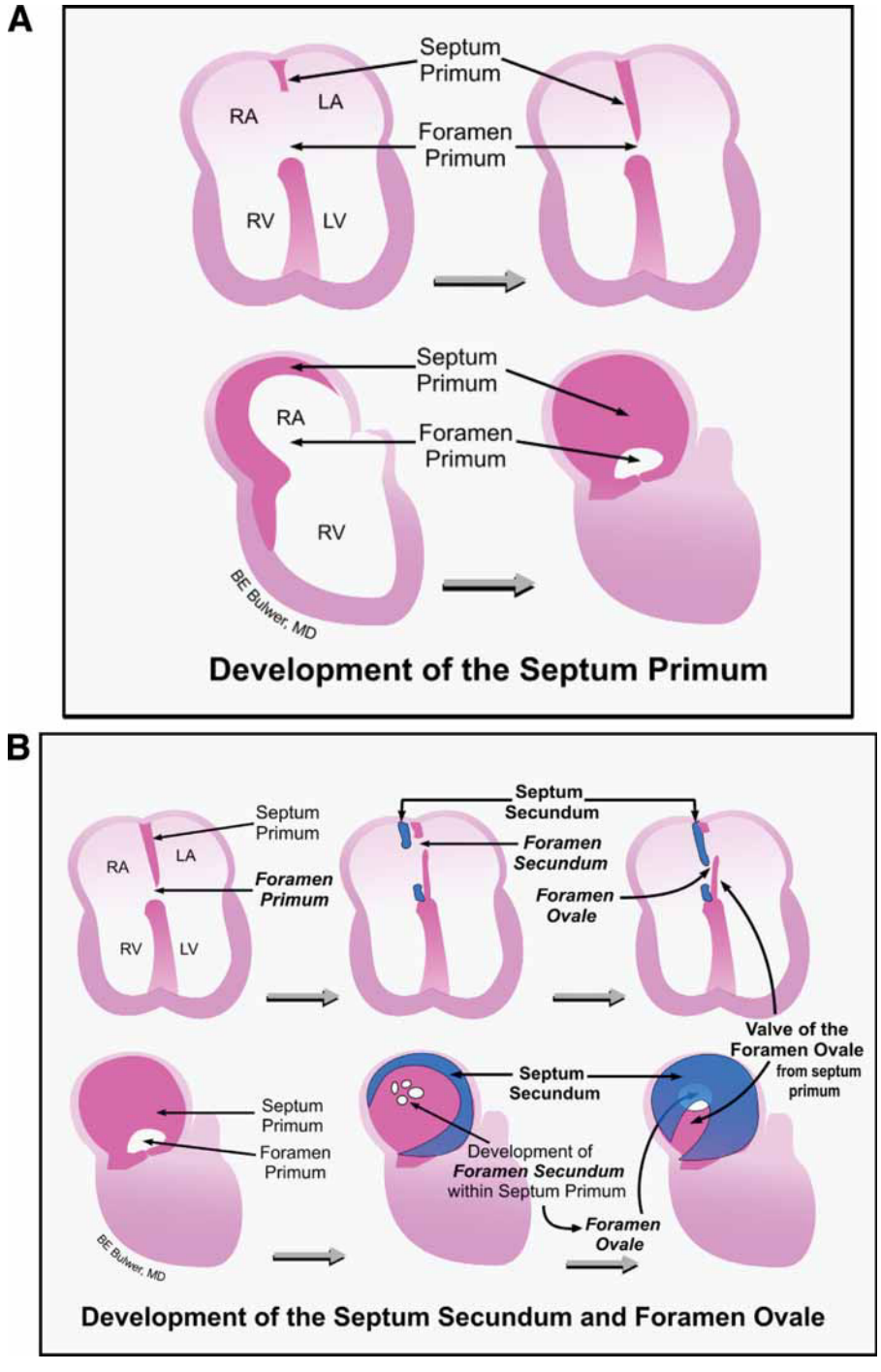

Fig. 1. (**A**) The first step in the formation of the interatrial septum is the growth of the primum septum. (**B**) Partial resorption of the primum septum leaves fenestrations that coalesce in the formation of a second interatrial connection—the ostium secundum. This occurs concurrently with the descent of a second septum—the septum secundum—to the right of the septum primum. Both septae fuse except in the region called the foramen ovale which permits oxygenated blood to bypass the fetal lungs and hence to the fetal systemic circulation.

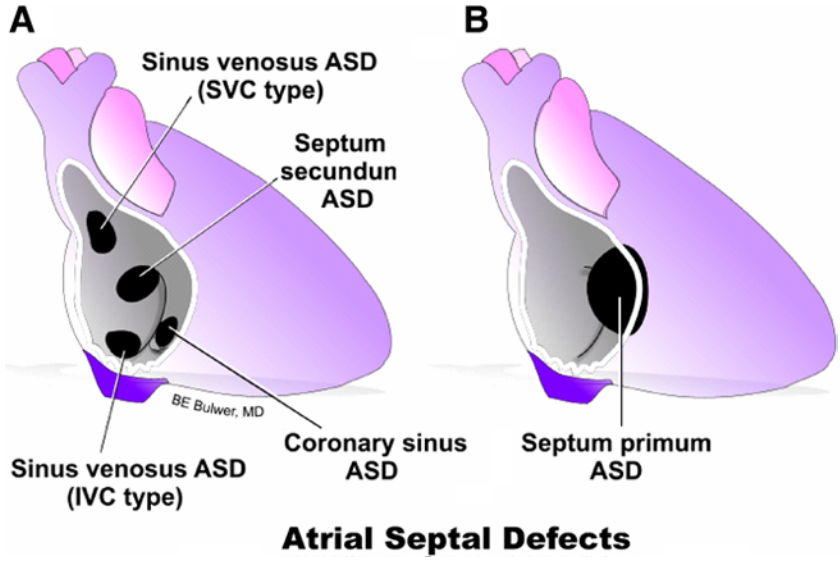

Fig. 2. The anatomic distribution of atrial septal defects. Four major types are described as shown.

shortly after birth when left-sided pressures exceed right and seal the two septa together.

ASDs form when the interplay of septal formation is deranged. Several forms of interatrial communication can therefore result. Four major ASDs can be classified and correspond to the anatomic region where the defect arises: secundum defect, primum defect, sinus venosus defect, and coronary sinus defect (Fig. 2). Occasionally, when the septum primum and secundum do not fuse after birth, a persistent orifice may be present, the so-called patent foramen ovale (PFO). This foramen can be physiologically patent with interatrial shunting in the direction of higher to lower pressure. Each of these congenital lesions of the atrial septum can be easily characterized by echocardiographic measures.

Transthoracic echocardiography is useful in the diagnosis and assessment of ASDs. Three main transthoracic views can be used to assess for ASDs in the majority of cases: (1) parasternal short axis at the level of the aortic valve, (2) apical four-chamber view, and (3) subcostal four-chamber view. In the apical four-chamber view, the atrial septum is a relatively deep structure and susceptible to echo signal dropout. Echolucency of this region should therefore be interpreted with caution without confirmation in other views or with color Doppler. Of these views, the subcostal four-chamber view may be most suited for the two-dimensional assessment of ASDs, as the ultrasound beam is most perpendicular to the septa in these views.

Table 1
ASD Types and Associated Cardiac Anomalies

Type	*Associated anomalies*
Septum secundum	Atrial septal aneurysm
Septum primum	Cleft mitral valve
Sinus venosus	Anomalous pulmonary venous drainage
Coronary sinus	Persistent left superior vena cava

Associated anomalies are not mutually exclusive.

Typically, secundum and primum septal defects can be seen with transthoracic imaging. However, multiplane transesophageal echocardiography may be needed to visualize sinus venosus or coronary sinus defects with certainty. Multiplane transesophageal imaging is highly accurate in visualizing the anatomical relationships and associated anomalies sometimes seen with ASDs (Table 1).

The use of color and spectral Doppler can enhance the detection of these defects. Color flow Doppler can confirm the presence and direction of interatrial shunting across visualized aspects of the atrial septum (Fig. 3; please *see* companion DVD for corresponding video). The color flow signal may also aid in measuring the size and number of defects. For example, should several color flow jets be seen across the area of the septum, a fenestrated defect is implied. Thus, color should be used in different views in order to assess for these flow abnormalities.

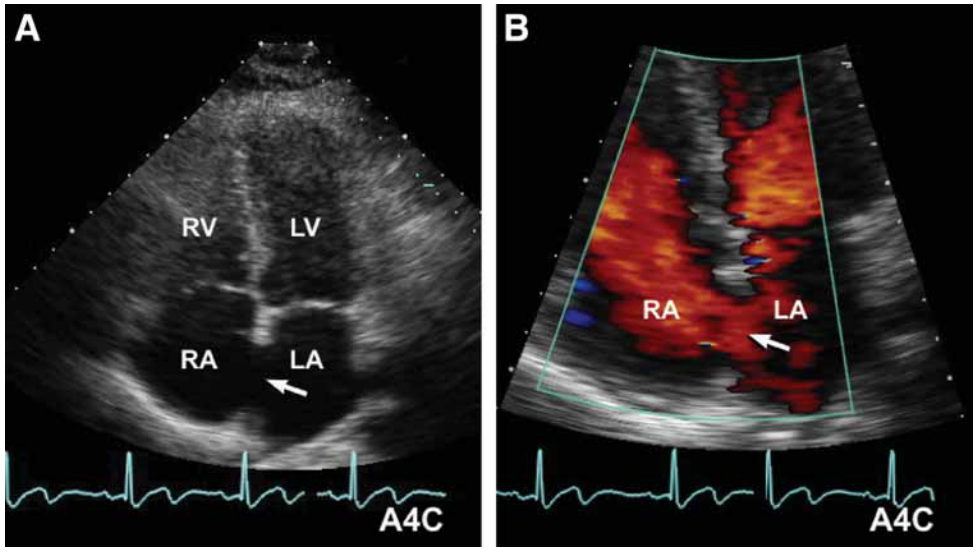

Fig. 3. Atrial four-chamber view showing defect or possible drop out in the interatrial septum (arrow, **A**). Color flow Doppler interrogation showed a typical pattern of predominant left-to-right shunting as seen with secundum atrial septal defects **(B)**. (Please *see* companion DVD for corresponding video.)

Should the result of a color and spectral Doppler exam be equivocal, an intravenous agitated contrast saline injection can be used to detect interatrial shunting. This effect is dependent on the fact that the bubbles created from the agitated saline are filtered in the pulmonary vasculature and do not cross to the left heart. Thus, contrast should only be seen in the right heart chambers in the absence of intracardiac and intrapulmonary shunting. In the typical case of an uncomplicated ASD, left atrial pressures are higher than right atrial pressures and direct predominant left-to-right shunting with occasional early crossing of contrast bubbles to the left heart from right-to-left shunting. Contrast is injected from an upper extremity and enters the right atrium via the superior vena cava (SVC) and tends to be directed more toward the tricuspid valve than the atrial septum, in contrast to blood from the inferior vena cava (IVC), which is usually directed more toward the atrial septum via the eustachian valve. An adequate contrast injection is attained when the bubble contrast is seen to appose the area of the septum. Valsalva maneuver is often used to assess for interatrial shunting with contrast by accentuating right-to-left shunting. The presence of contrast bubbles in the left heart early after injection signifies an interatrial shunt, whereas the appearance of late contrast bubbles (>3–5 cardiac cycles) in the left heart suggests an intrapulmonary shunt (Fig. 4; please *see* companion DVD for corresponding video).

Typically, ASDs confer a volume load on the right heart. Therefore, a pattern of right ventricular overload is often seen. The right ventricle is often dilated with preserved systolic function. The right atrium is often enlarged. Because of the volume load, ventricular septal motion may be abnormal and display paradoxical motion. The pulmonary pressures will vary depending on the hemodynamic impact of the lesion. In the extreme and rare case, Eisenmenger's physiology may result, with pulmonic pressures equal to or higher than systemic blood pressure.

Quantification of shunt flow can be accomplished with a comparison of pulmonary blood flow to systemic blood flow. The Qp/Qs ratio has been used to measure the hemodynamic impact ASDs. This result is found by calculating flow across the pulmonary valve and dividing this by flow across the aortic valve (Figs. 5 and 6). Flow is calculated by multiplying the cross-sectional area of the outflow tract with the time-velocity integral (TVI). Therefore,

$$Q_P/Q_S = \frac{\pi\,(\text{radius of RVOT})^2 \times \text{TVI}_{\text{RVOT}}}{\pi\,(\text{radius of LVOT})^2 \times \text{TVI}_{\text{LVOT}}}$$

Accurate Qp/Qs calculations necessitate precise measurements, particularly pertaining to the size of the valvular annuli, and are valid in the absence of significant regurgitant or stenotic lesions of the semilunar valves.

SECUNDUM ASD

Secundum ASDs are one of the most frequently encountered congenital cardiac defects in clinical practice

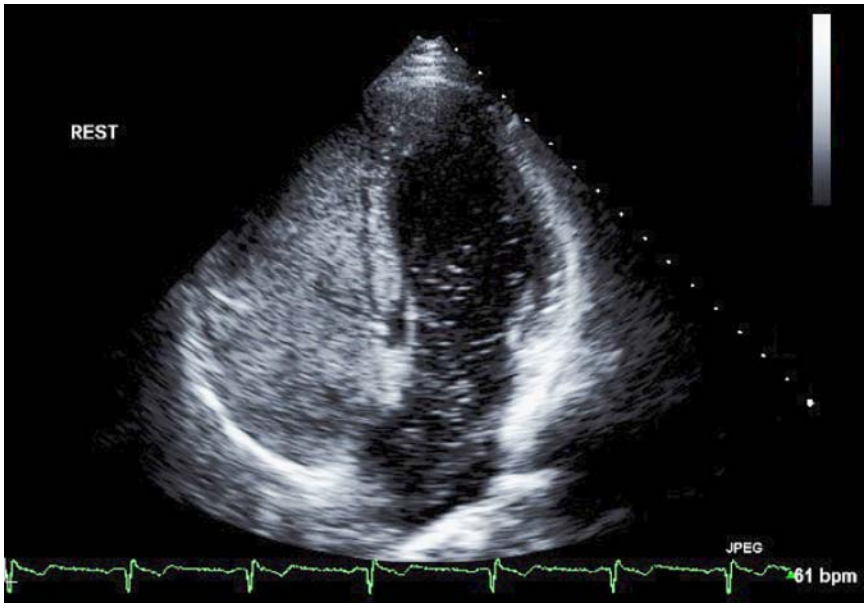

Fig. 4. Agitated saline contrast echocardiography in this 28-yr-old female who complained of migraine headaches shows good opacification of right heart chambers. Clear evidence of right-to-left shunting (appearance of saline bubbles into left heart chambers) occurred early during rest. She was diagnosed with a secundum atrial septal defect. (Please *see* companion DVD for corresponding video.)

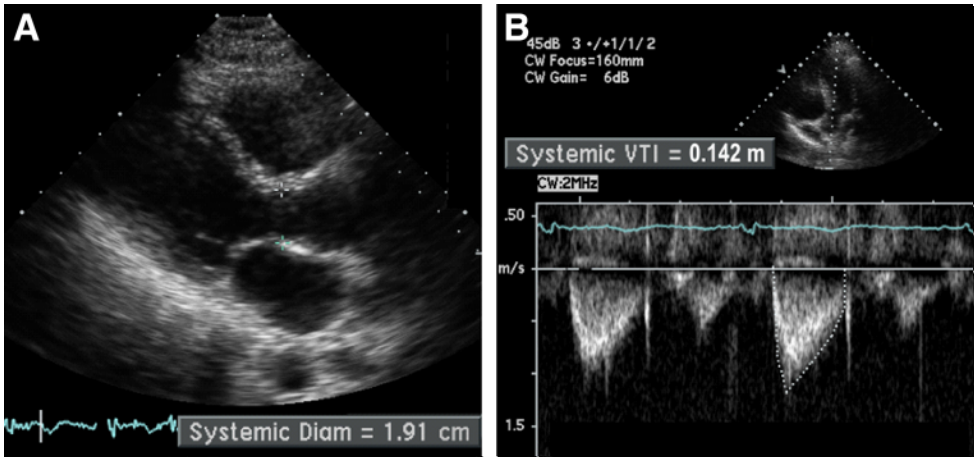

Fig. 5. Quantification of shunt flow (Qp:Qs) requires measurement (*see* Anatomic and Echocardiographic Overview section). Systemic flow calculation requires measurement of left ventricular outflow tract diameter **(A)** and the velocity time integral (VTI) by PW Doppler **(B)**.

along with bicuspid aortic valves. The lesion results from the incomplete development of the septum secundum, leaving a central patency between the right and left atria (Fig. 7; please *see* companion DVD for corresponding video). Occasionally, there may be more than one opening in the septum so that a fenestrated septum results. This is often clearly delineated on transthoracic imaging with the use of color flow Doppler around the area of the central portion of the septum (Fig. 8). Shunt flow can be seen with the use of pulse wave Doppler across the defect. Usually some transient right-to-left shunting can be seen with these defects, typically corresponding with ventricular contraction. Occasionally, with the use of intravenous agitated saline in the right heart, an echolucent silhouette of blood flow may be seen in the right atrium when predominant left-to-right shunting is present, the so-called "negative contrast effect." However, because saline contrast is often injected from an upper extremity, this "negative contrast effect" should be interpreted with caution as this can also be produced by contrast-free caval blood flow emanating

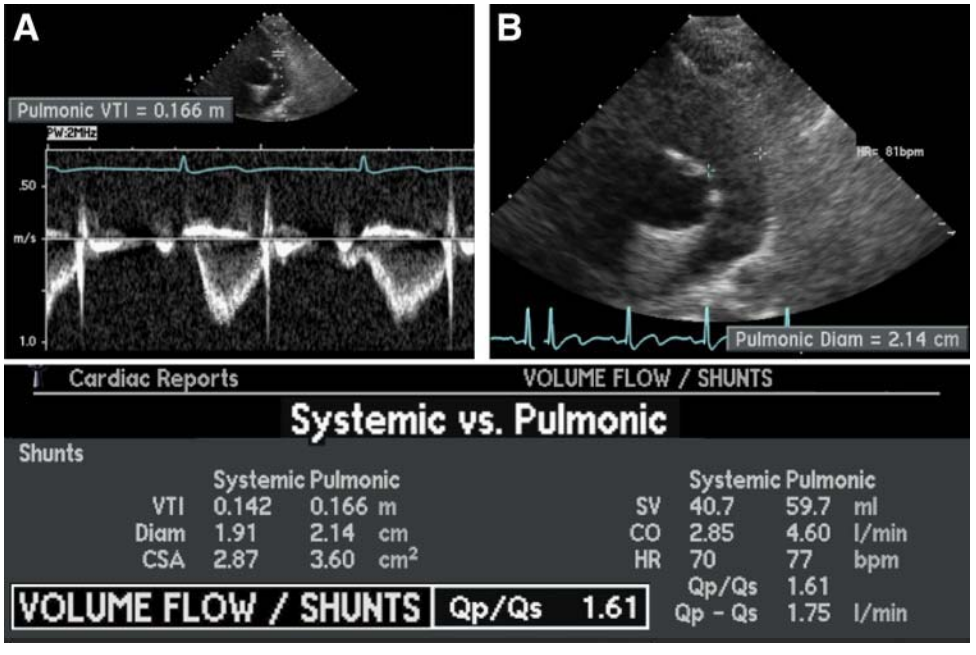

Fig. 6. Pulmonary flow is similarly calculated following measurement of the right ventricular outflow tract at the level of the pulmonary valve **(B)**.

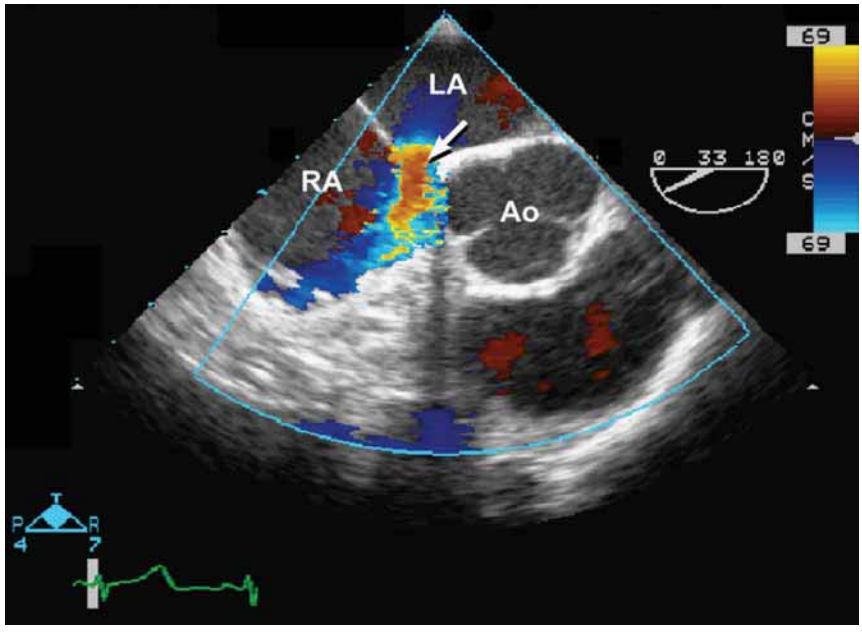

Fig. 7. Midesophageal view of the interatrial septum with color Doppler applied shows left-to-right shunt via a secundum atrial septal defect. (Please *see* companion DVD for corresponding video.)

from the IVC flushing against the area of the fossa ovalis.

Secundum ASDs may be associated with other cardiac anomalies. Occasionally, atrial septal aneurysms may be seen with secundum ASDs. In these cases, the atrial septum is hypermobile and bows into either atrial chamber, varying with respiratory variation. When rheumatic involvement of the mitral valve is concomitantly present with an ASD, Lutembacher's syndrome is said to be present.

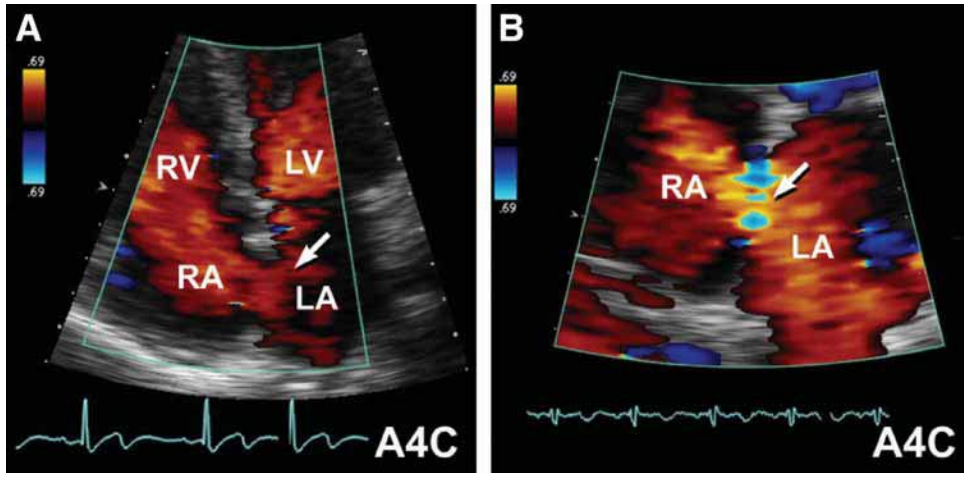

Fig. 8. Transthoracic apical four-chamber view (A4C) with color flow Doppler interrogation of the interatrial septum shows left-to-right shunt via a secundum defect.

PRIMUM ASDs

Primum ASDs result from the incomplete development of the septum primum with the endocardial cushions in the region of the atrioventricular (AV) valves. Also called partial AV canal defects, this lesion results in an atrial communication that is seen inferiorly, in the lower portion of the atrial septum that normally is fused with the AV valvular apparatus. The AV valves are therefore affected, typically involving the mitral valve, where a cleft may be seen in the anterior leaflet. Mitral regurgitation may also be seen. Interventricular shunts are not generally seen with this abnormality.

The features of this defect can usually been seen with transthoracic imaging. In the four-chamber view (apical or subcostal), the AV valves may appear to lie on the same plane, forming a "T," referring to the alignment of the AV valves with the ventricular septum. An echolucent space can be seen above the AV valves, usually with a nonrestrictive shunt seen by color flow Doppler. The "goose neck" deformity seen angiographically on left ventriculography can occasionally be seen echocardiographically as an abnormal appearing left ventricular outflow tract.

SINUS VENOSUS SEPTAL DEFECT

The sinus venosus ASD is an interatrial communication that arises near the junction of the vena cava with the right atrium (Fig. 9; please *see* companion DVD for corresponding video). Therefore, this defect can present in two distinct morphologies. More commonly, the defect is located superiorly at the site of the SVC drainage to the right atrium but can be present inferiorly at the junction of the IVC and right atrium. In either case, these defects may be difficult to define anatomically via transthoracic imaging alone. However, transesophageal echocardiography can easily define the defect and any associated pathology. Imaging the atrial septum in the superior-inferior dimension (bicaval transesophageal view) often may reveal the defect.

Sinus venosus defects can be associated with other cardiac pathology. Commonly, the right upper pulmonary vein is anomalous when the venosus defect is seen at the junction of the SVC and right atrium. The anomalous vessel can connect to the SVC in the more typical case. However, the anomalous connections can be diverse in either morphology of sinus venosus defect, necessitating a meticulous definition of pulmonary venous drainage in these cases as a further cause of left-to-right shunting.

CORONARY SINUS ASD

This rare type of ASD presents an interatrial communication via an unroofed coronary sinus. Therefore, the defect is seen at the site of origin of the coronary sinus. A persistent left SVC is associated with this defect and can often be seen to drain into the coronary sinus or left atrium.

This defect may not be visualized on routine transthoracic echocardiography. However, the defect may be suggested by the constellation of right heart overload, a dilated coronary sinus, and the presence of a persistent left SVC. Multiplane transesophageal echocardiography

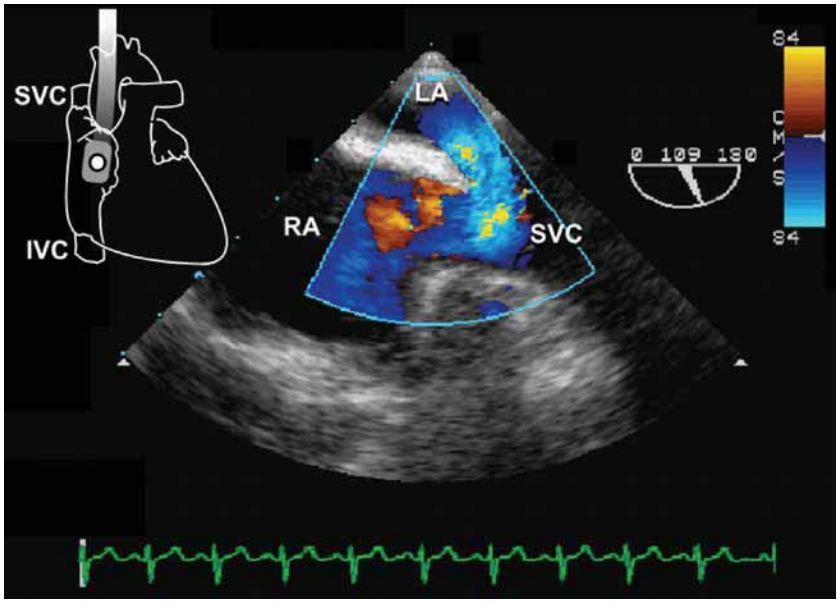

Fig. 9. Mid esophageal bicaval view showing sinus venous defect (superior vena cava [SVC]-type). Note the direction of flow across the defect—from left atrium to right atrium. (Please *see* companion DVD for corresponding video.)

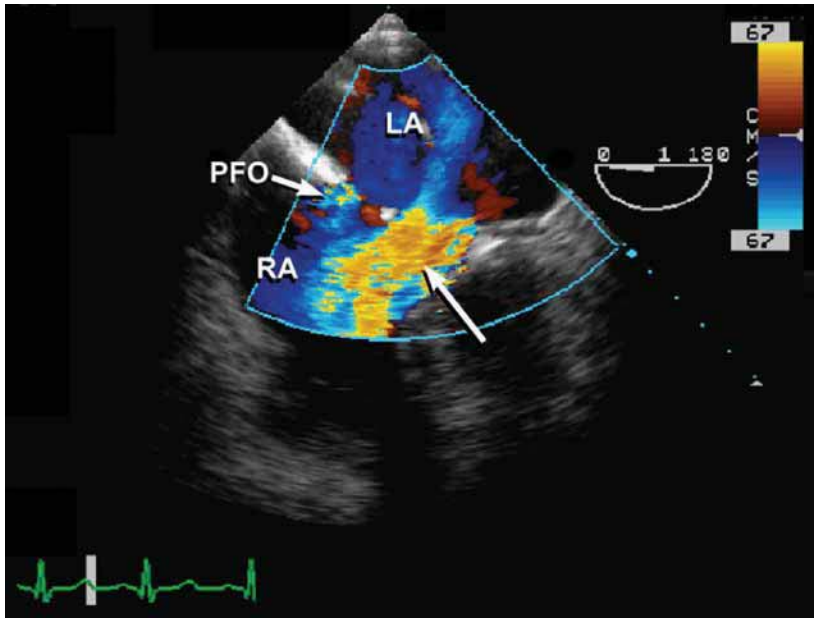

Fig. 10. Color flow Doppler demonstrates the presence of the coronary sinus ASD with left-to-right shunt. Note also the small shunt arising from a patent foramen ovale (PFO).

should be used to confirm the presence of this defect and associated pathology (Fig. 10). Intravenous injection of agitated saline contrast into the left arm can be used to evaluate the site of drainage of the left SVC (Fig. 11).

PATENT FORAMEN OVALE

This defect is not a true defect in embryological development of the either the septum primum or secundum. Rather, this lesion is the result of the failure of permanent fusion of the normally developed atrial septa.

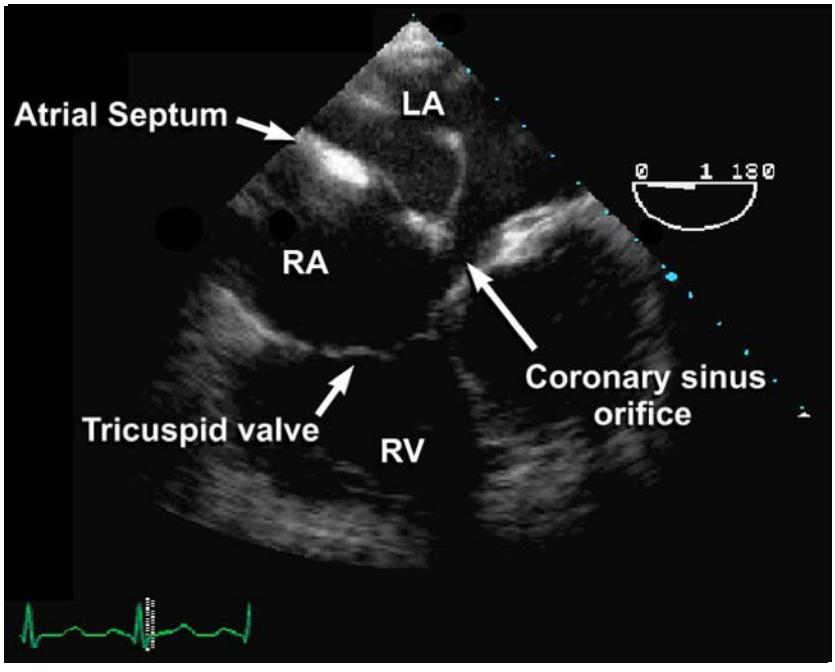

Fig. 11. Midesophageal view showing agitated saline contrast (bubble) study injection into the left arm. Bubbles were seen entering the coronary sinus, then the left atrium (LA), and then into the right atrium (RA).

Therefore, a dynamically patent orifice acting similar to a flap valve is present and may respond to interatrial pressure changes (Fig. 12; please *see* companion DVD for corresponding video; *see als0o* Chapter 17). Thus a right-to-left shunt may be present when right atrial pressures increase higher than left atrial pressures, such as with Valsalva, coughing, and so on. The defect may be functionally sealed when left atrial pressures exceed right, with only occasional right-to-left shunting.

The presence of this defect is easily evaluated with agitated saline contrast injection. Normally, the procedure is performed with and without Valsalva maneuver, as right-to-left shunting may not be seen under baseline conditions. The presence of contrast bubbles early after appearance in the right heart indicates the presence of right-to-left shunting. Color Doppler over the area of the fossa ovalis can often detect this defect. Transthoracic subcostal imaging or multiplane transesophageal echocardiography can usually illustrate the defect.

ECHOCARDIOGRAPHY IN THE MANAGEMENT OF ASDs

An accurate evaluation of the hemodynamic impact of the shunt is necessary following diagnosis. The degree of shunt flow is quantified by indexing pulmonary blood flow to systemic blood flow, the Qp/Qs ratio. Traditionally, when pulmonary blood flow exceeds systemic blood flow by 50% (a Qp/Qs ratio of 1.5:1.0), repair of the defect is recommended. However, in the case of ASDs with smaller shunts (ratios of <1.5:1.0), repair may still be appropriate owing to the risks for other problems including atrial arrhythmias, progressive pulmonary hypertension, congestive failure, or paradoxic emboli. PFOs have been repaired after cryptogenic stroke, especially in young patients.

Percutaneous closure of secundum ASDs and PFOs have been performed using transcatheter devices in experienced centers. Recent clinical data suggests that percutaneous closure techniques are safe and effective, supporting a less invasive alternative to surgical closure. A variety of devices are available for transcatheter closure such as the Amplatzer and CardioSeal closure devices.

The deployment of transcatheter devices for ASD or PFOs are generally guided by echocardiographic techniques (Fig. 12; please *see* companion DVD for corresponding video). Transesophageal echocardiography or intracardiac echocardiography are important tools for the morphological characterization of the lesion. For example, an accurate description of the ASD size and rim measurements is invaluable information in guiding device deployment. During PFO

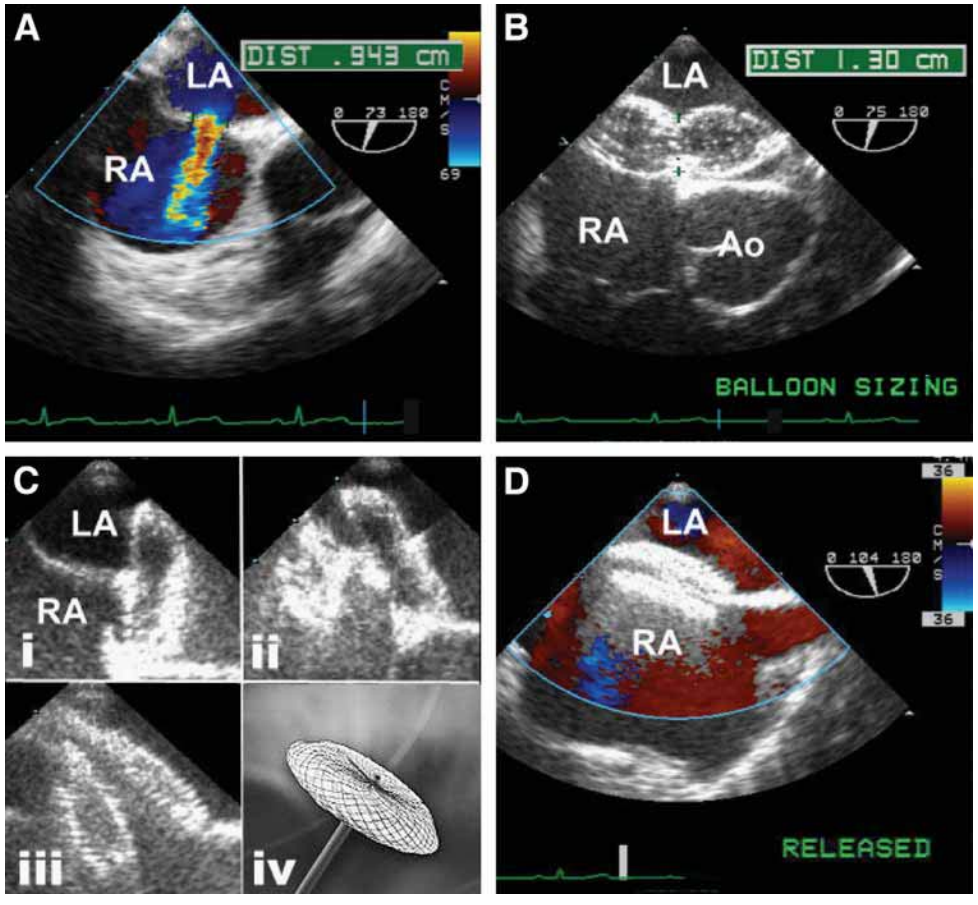

Fig. 12. Stages of percutaneous closure of a secundum atrial septal defect (ASD; **A**) using an Amplatzer device are shown on transesophageal echocardiography guidance. Balloon sizing of the defect **(B)** is followed by sequential deployment of the left atrial and right atrial arms of the device **(C)** (picture insert: AMPLATZER® Septal Occluder ASD). Following release of the device, interrogation of the closure was performed using Color Doppler **(D)** and agitated saline contrast. (Please *see* companion DVD for corresponding video.)

closure, transeptal puncture can be guided as well as an assessment of the PFO tunnel size and septal stiffness. Overall, echocardiography during device deployment is important for device sizing, positioning, and the assessment of residual shunting postdevice deployment (Fig. 12; please *see* companion DVD for corresponding video).

SUMMARY

In the current era, echocardiography provides a comprehensive assessment of ASDs. From initial diagnosis, classification, and assessment of associated lesions, echocardiographic techniques have largely supplanted cardiac catheterization. Further, as the placement of transcatheter devices for shunt closure is becoming an increasingly popular alternative to surgical closure, echocardiography is rapidly expanding as an interventional tool. As cardiac ultrasound expands to intracardiac and three-dimensional technologies, its future role in the assessment of simple and complex congenital cardiac lesions will certainly continue to evolve.

SUGGESTED READING

Bruch L, Parsi A, Grad MO, et al. Transcatheter closure of interatrial communications for secondary prevention of paradoxical embolism: single-center experience. Circulation 2002;105: 2845–2848.

Chessa M, Carminati M, Butera G, et al. Early and late complications associated with transcatheter occlusion of secundum atrial septal defect. J Am Coll Cardiol 2002;39:1061–1065.

Cooke JC, Gelman JS, Harper RW. Echocardiologists' role in the deployment of the Amplatzer atrial septal occluder device in adults. J Am Soc Echocardiogr 2001;14:588–594.

Cowley CG, Lloyd TR, Bove EL, Gaffney D, Dietrich M, Rocchini AP. Comparison of results of closure of secundum atrial septal defect by surgery versus Amplatzer septal occluder. Am J Cardiol 2001;88:589–591.

Dittmann H, Jacksch R, Voelker W, Karsch KR, Seipel L. Accuracy of Doppler echocardiography in quantification of left to right shunts in adult patients with atrial septal defect. J Am Coll Cardiol 1988;11:338–342.

Hausmann D, Daniel WG, Mugge A, Ziemer G, Pearlman AS. Value of transesophageal color Doppler echocardiography for detection of different types of atrial septal defect in adults. J Am Soc Echocardiogr 1992;5:481–488.

Kerber RE, Dippel WF, Abboud FM. Abnormal motion of the interventricular septum in right ventricular volume overload. Experimental and clinical echocardiographic studies. Circulation 1973;48:86–96.

Kitabatake A, Inoue M, Asao M, et al. Noninvasive evaluation of the ratio of pulmonary to systemic flow in atrial septal defect by duplex Doppler echocardiography. Circulation 1984;69:73–79.

Kronzon I, Tunick PA, Freedberg RS, Trehan N, Rosenzweig BP, Schwinger ME. Transesophageal echocardiography is superior to transthoracic echocardiography in the diagnosis of sinus venosus atrial septal defect. J Am Coll Cardiol 1991;17:537–542.

Losay J, Petit J, Lambert V, et al. Percutaneous closure with Amplatzer device is a safe and efficient alternative to surgery in adults with large atrial septal defects. Am Heart J 2001; 142:544–548.

Martin F, Sanchez PL, Doherty E, et al. Percutaneous transcatheter closure of patent foramen ovale in patients with paradoxical embolism. Circulation 2002;106:1121–1126.

Mazic U, Gavora P, Masura J. The role of transesophageal echocardiography in transcatheter closure of secundum atrial septal defects by the Amplatzer septal occluder. Am Heart J 2001; 142:482–488.

O'Rahilly R, Muller F. Human Embryology and Teratology, 3rd ed. New York: Wiley-Liss, 2001.

Shub C, Dimopoulos IN, Seward JB, et al. Sensitivity of two-dimensional echocardiography in the direct visualization of atrial septal defect utilizing the subcostal approach: experience with 154 patients. J Am Coll Cardiol 1983;2:127–135.

Weyman A. Principles and Practice of Echocardiography, 2nd ed. Philadelphia: Lea and Febiger, 1994.

22 Adult Congenital Heart Disease in General Echocardiography Practice

An Introduction

Bernard E. Bulwer, MD, MSc, and Michael J. Landzberg, MD

Contents

ADULT CONGENITAL HEART DISEASE IN GENERAL ECHOCARDIOGRAPHY PRACTICE

The spectrum of adult congenital heart defects seen in echocardiography practice varies according to institutional practice and expertise. Half a century ago, survival with severe congenital heart disease was less common. Today, nearly 80% of such patients in industrialized societies now survive into adulthood. Most are followed up in centers that specialize in adult congenital heart diseases (CHDs), but it is not uncommon for such adults to be seen in general echocardiography practice.

Most CHDs are compatible with survival to adulthood without need for surgical intervention (Table 1). Indeed, some lesions, e.g., mitral valve prolapse, bicuspid aortic valves (BAVs), patent foramen ovale, atrial septal defects, and Marfan syndrome may be completely asymptomatic. More severe or complex defects require interventions early in life (Table 2).

This chapter introduces the fundamentals of echocardiographic assessment in CHD followed by a concise summary of the more common CHD seen in general adult echocardiography practice. All images shown are from adults who were seen in general echocardiography practice.

From: *Contemporary Cardiology: Essential Echocardiography: A Practical Handbook With DVD*
Edited by: S. D. Solomon © Humana Press, Totowa, NJ

Table 1
Congenital Heart Disease in Adults Compatible With Survival to Adulthood With No Prior Surgery or Intervention

Mitral valve prolapse
Bicuspid aortic valve
ASD
Marfan syndrome
Isolated restrictive or moderately restrictive ventricular septal defects
Mild aortic stenosis (valvular, supravalvular, subvalvular)
Mild pulmonary valve stenosis
Small patent ductus arteriosus
Ostium primum ASD (AV septal defect)
Ebstein's malformation
Corrected transposition (transposition of the great arteries) (AV-to-ventriculoatrial discordance)

ASD, atrial septal defect; AV, atrioventricular.

Echocardiography in Adult CHD

Echocardiography, both transthoracic (TTE) and transesphageal (TEE), play central roles in the diagnosis and management of CHD (*see* Chapter 4, Table 15 for Class I indications for echocardiography in adult CHD).

Optimal echocardiographic examination and interpretation requires knowledge and experience in the following:

- Normal cardiac anatomy and physiology.
- The spectrum of adult CHDs.
- The segmental approach to echocardiography examination.
- Palliative and corrective surgical and transcatheter interventions and techniques (past and present).
- Postoperative and postintervention residua and complications.
- Superimposed acquired age-related heart disease, e.g., hypertension, coronary artery disease.

Table 2
Spectrum of Congenital Heart Disease

I. *Chambers and valves in normal sequence and position {S,D,S}*
   - A **Shunting predominant**
     1. Atrial septal defect (Chapter 21)
     2. Atrioventricular septal defects (Chapter 21)
     3. Isolated ventricular septal defect[a]
     4. Patent ductus arteriosus[a]
   - B **Stenosis or obstruction predominant**
     1. Absent AV connections (tricuspid and mitral atresia)
     2. Absent or obstructed ventriculoarterial connections (pulmonary atresia, aortic atresia, subaortic obstruction, aortic stenosis)
     3. Obstructed great arteries (coarctation of the aorta[a], aortic atresia)
     4. Obstructed venous flow (total anomalous pulmonary venous return)
   - C **Anomalous valve position**
     1. Ebstein's malformation (anomaly)[a]

II. *Chambers and valves not in normal sequence or relationship*
   - A **Anomalies of relationships between atria and ventricles**
     1. Double-inlet left or right ventricle (with univentricular heart)
     2. AV discordance (congenitally corrected transposition of great arteries [L-TGA])[a]
   - B **Anomalies of relationships between ventricles and great arteries**
     1. Tetralogy of Fallot[a]
     2. Double-outlet right and left ventricles
     3. Truncus arteriosus
     4. Ventriculoarterial discordance (transposition of the great vessels D-TGA)[a]

[a]Discussed in this chapter.

AV, atrioventricular.

Modified from Kisslo JA, Adams DB, Leech GJ. Essentials of Echocardiography: Congenital Heart Disease. New York: Ceiba-Geigy, 1988.

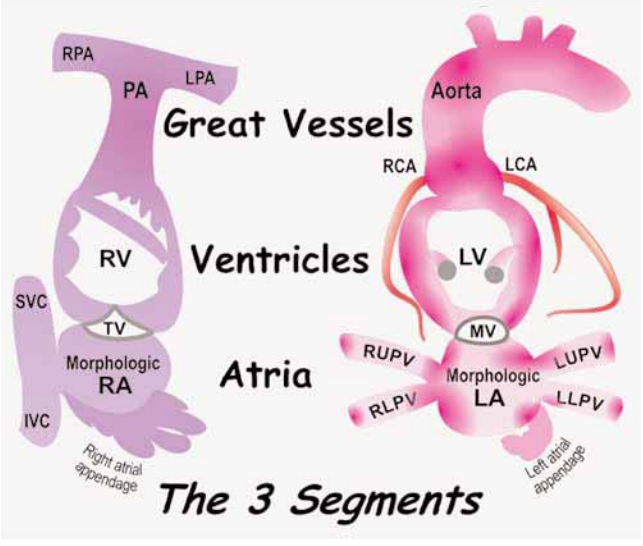

Fig. 1. The distinguishing characteristics of each cardiac segment—atria, ventricles, and great vessels—are used in the segmental approach to describe cardiac anatomical relationships. IVC, Inferior vena cava; LCA, left coronary artery; LLPV, left lower pulmonary vein; LUPV, left upper pulmonary vein; PA, pulmonary artery (right and left); RCA, right coronary artery; RLPV, right lower pulmonary vein; RUPV, right upper pulmonary vein; SVC, superior vena cava.

Segmental Approach to CHD

A good relationship between adult and pediatric sonographers and cardiologists can optimize the quality of the echocardiographic examination in patients with adult CHD.

To simplify and standardize the complicated and confusing embryological descriptions of the past, a logical descriptive method called the segmental approach or sequential segmental analysis has been adopted. This method evaluates the sequence of bloodflow throughout the entire cardiac circuit. It is segmental in that it compartmentalizes the heart into three main segments or building blocks—atria, ventricles, and great arteries—that are analyzed separately (Fig. 1). In pediatric cardiology, these are designated by three letters in curly brackets {X,X,X} that describe the arrangement.

Assigning the Segments

The normal segmental arrangement is {S,D,S}.

The first letter "S" means *solitus*—Latin for normal visceral and atrial position (*situs*). It describes the positions of the major unpaired abdominal organs (liver, stomach, spleen) and atria that are almost always situated on the same side of the body cavity (concordant) (Fig. 2).

The second letter "D" denotes the normal D-looping or rightward (dextro) folding of the heart tube during cardiac embryonic development (Fig. 3A). This results in the normal atrioventricular (AV) relationship or concordance. L-looping occurs when ventricular folding proceeds in the opposite (levo) direction, resulting in AV discordance (Fig. 3B). This terminology is used to differentiate between the two forms of transposition of the great arteries (TGA).

The third letter "S" means that a normal relationship exists between the great arteries—the main pulmonary artery and the aorta. Parasternal short-axis (PSAX) views at the aortic valve level can define this relationship on echocardiography (Fig. 4; *see* Chapter 3, Figs. 23–26). These relationships are summarized in Tables 3–5.

Morphological Characteristics of the Connecting Segments

Defining cardiac chambers is important in identification and assignment of segmental *situs* and describing the connections between the segments. The morphological characteristics of the right and left ventricles (LVs) and the internal cardiac crux can be readily defined on examination (Fig. 5). The major echocardiographic morphological characteristics are summarized in Table 3.

Transthoracic Examination

The standard protocol outlined in Chapter 3 applies to adults with CHD, but pediatric/adult CHD sonographers perform an initial four-step segmental analysis before proceeding with the standard examination (Table 5). Subcostal (subxyphoid) views are used to

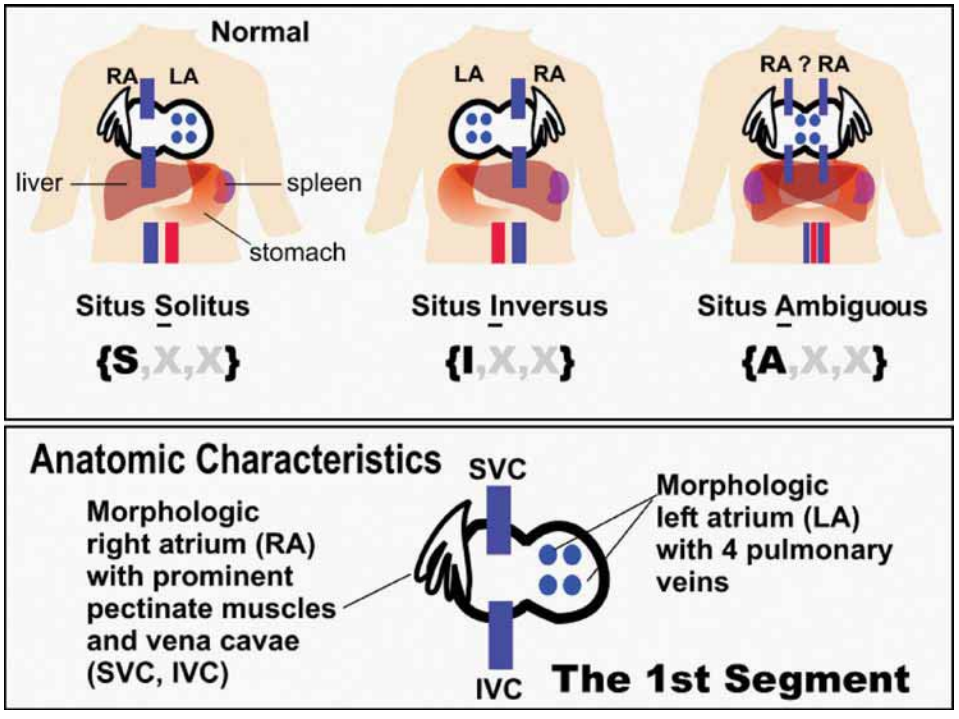

Fig. 2. The first segment. The most distinctive anatomical features that define the first segment—atrial and visceral situs—are depicted. The distinguishing features of right versus left atrium are highlighted in the lower panel. On echocardiography, the atrial chamber into which the pulmonary veins enter is the morphological left atrium. The chamber into which the vena cavae empty is the morphological right atrium. The right atrial appendage is used by cardiac anatomical pathologists to define atrial situs, but this structure is poorly visualized during echocardiography.

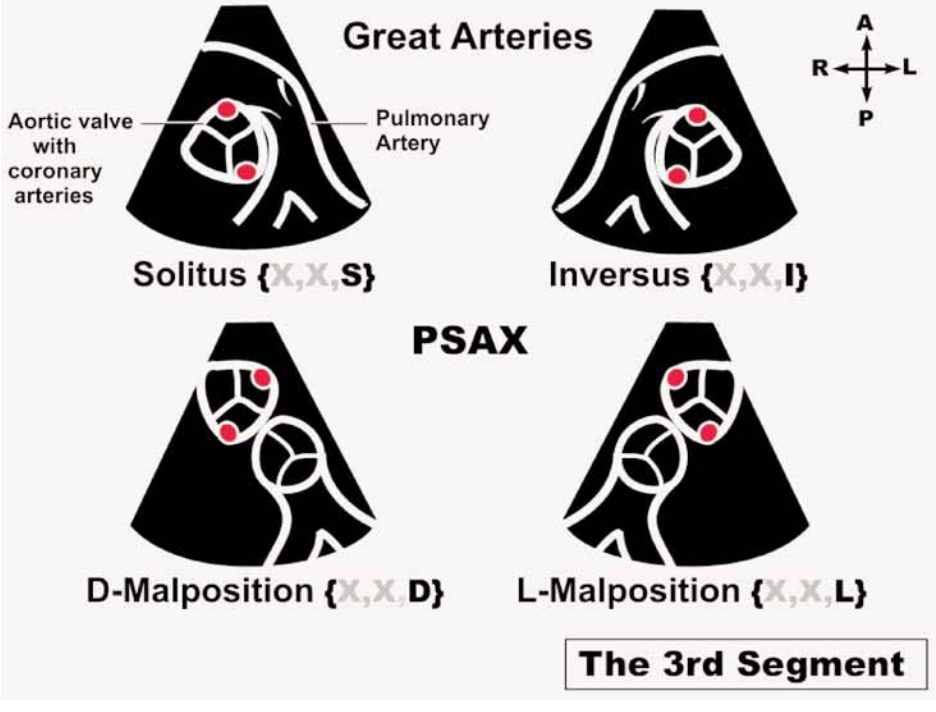

Fig. 4. The third segment: the great arteries. The relative positions of the great arteries on the parasternal short-axis view (PSAX, aortic valve level) provides the echocardiographic basis for naming the third segment. The normal "S" (solitus) position and the "I" (inversus) relationships are shown in the upper panels. When the aortic valve is to the right and anterior to the pulmonary valve, it is called D-transposition. When the aortic valve is to the left and anterior to the to the pulmonary valve, it is called L-transposition (lower panels). Two other relationships (not shown) are: the "A" anterior and the "P" posterior positions. These describe the position of the aortic valve relative to the pulmonary valve.

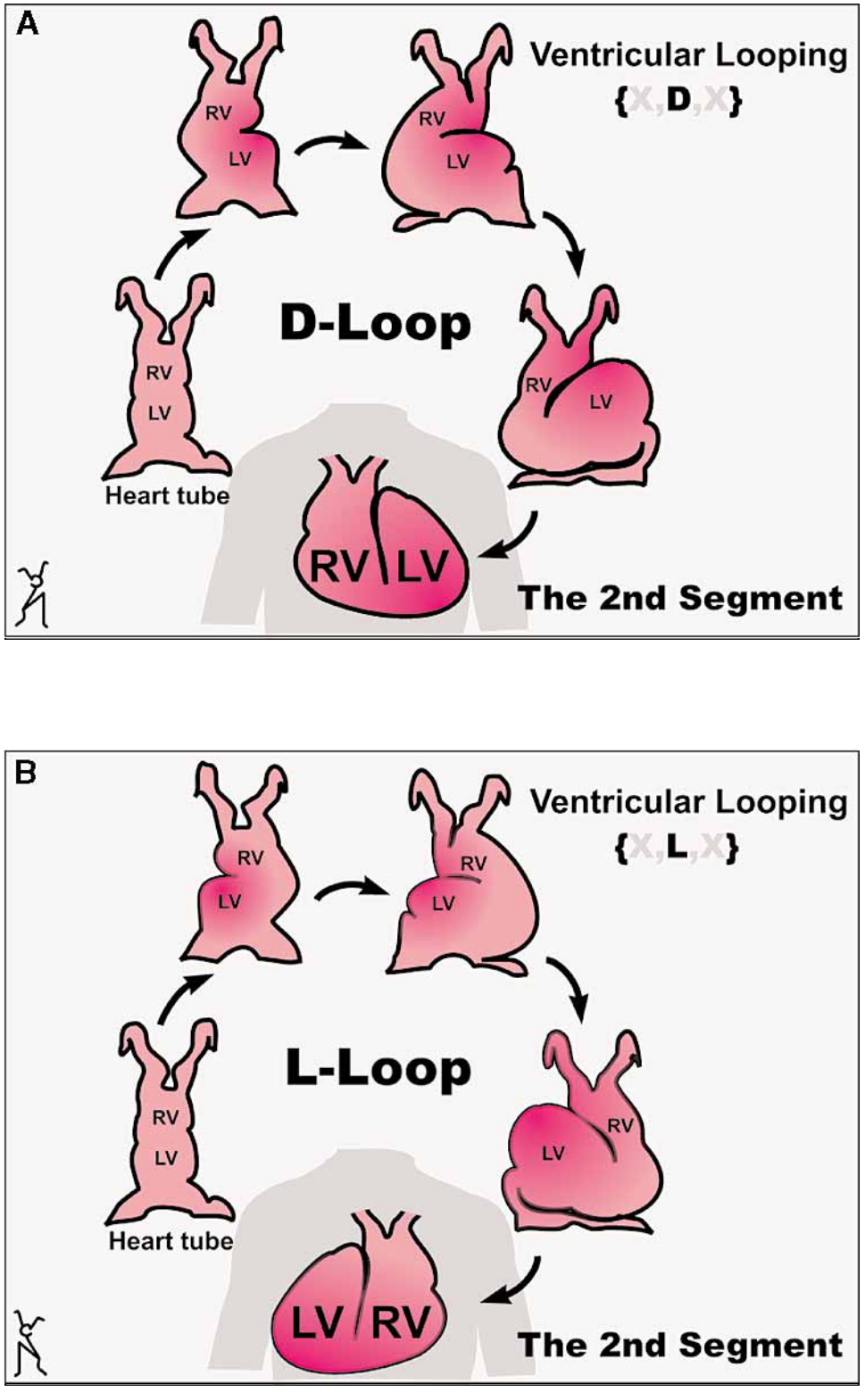

Fig. 3. The second segment. **(A)** The basis of the atrioventricular concordance lies in the folding (ventricular looping) of the tubular embryonic heart to form a folded four-chamber heart. Initially, the cardiac apex is on the right, but final looping of the tube swings the apex to the left and places the right ventricle anterior and rightward to the left ventricle. This is the normal or D-loop pattern. **(B)** Rarely, an L-loop folding pattern lands the right ventricle to the left of the left ventricle. This is seen in "congenitally corrected" transposition of the great arteries.

Table 3
Echocardiographic Features of Cardiac Segments and Connections

Morphological right atrium	**Morphological left atrium**
Receives right-sided inferior vena cava and superior vena cava	Receives four pulmonic veins
Morphological right atrial appendage (triangular, broad-based, with pectinate muscles extending outside appendage lumen)	Attached to left atrial appendage—smaller tubular with pectinate muscles confined to appendage lumen
Tricuspid valve	**Mitral valve**
Trileaflet	Bileaflet
Septal leaflet (attached to ventricular septum)	No septal leaflet or chordae
Septal insertion more apical than mitral valve	
Morphological right ventricle	**Morphological left ventricle**
Coarse trabeculations	Less coarse trabeculations
Moderator (septo-marginal) band	Two clearly defined papillary muscles
Trileaflet (tricuspid) valve	Ellipsoid ventricular cavity
"Triangular" ventricular cavity	Bileaflet (mitral) valve
Septal chordae	
Infundibular muscle band	
Morphological main pulmonary artery	**Morphological aorta**
Branch pattern: main trunk with right and left branches	Coronary arteries (with coronary sinuses)
	Aortic arch with arteries to head and neck

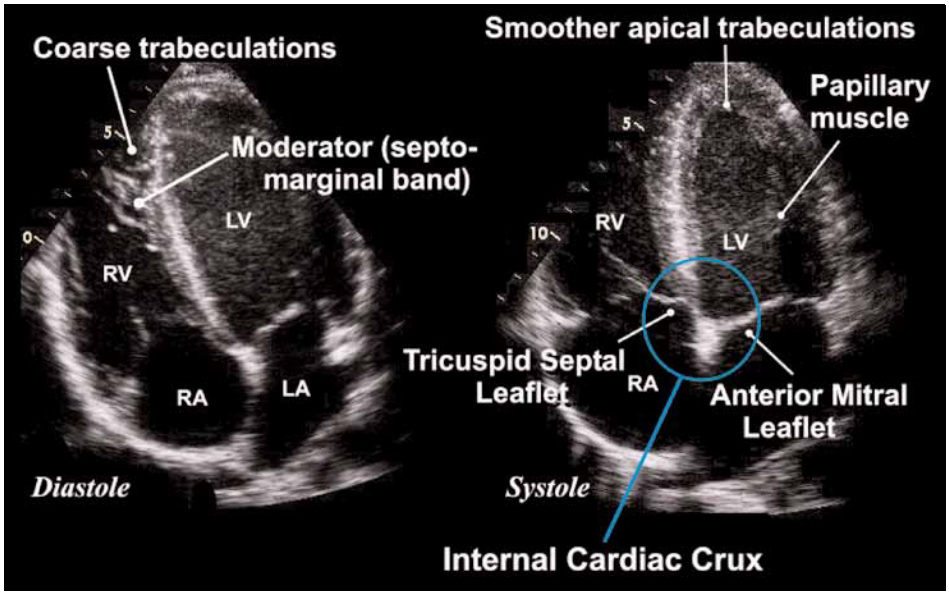

Fig. 5. Morphological left and right ventricle. What defines right vs left ventricle are the morphological characteristics. On echocardiography, the defining features of the right ventricle are the heavy trabeculation and apical-ward septal insertion of the atrioventricular valve leaflet. Smoother apical trabeculations, a more basal septal insertion of the atrioventricular valve leaflet, and a pair of prominent papillary muscles are the most reliable defining characteristics of the left ventricle. The confluence of the septal leaflets to the interatrial and interventricular septal is called the internal cardiac crux (cross). Examination of this relationship is important in congenital heart disease. Loss of the normal pattern (circled) can provide valuable clues in congenital heart disease.

Table 4
The Segmental Set (Pediatric Cardiac Pathology)

Segment	*Relationship variants*	*Letter designation*
First (atrial and visceral *situs*)	*Situs solitus*	S
	Situs inversus	I
	Situs ambiguous (R or L isomerism)	A
Second (ventricular looping)	D-Loop	D
	L-Loop	L
Third (great arteries)	Solitus	S
	Inversus	I
	D-Transposition	D
	L-Transposition	L
	Anterior	A
	Posterior	P

Table 5
The Segmental Approach by Echocardiography

Step 1: Position of the apex
Levocardia
Dextrocardia
Mesocardia
Step 2: *Situs* of the atrium
Situs solitus
Situs inversus
Situs ambiguous (isomerism)
Step 3: AV relationship
AV concordance
AV discordance
Double inlet
Absent connection
Step 4: VA relationship
VA concordance
VA discordance
Double inlet
Solitary (common) arterial trunk

AV, atrioventricular; VA, ventriculoarterial.

Reproduced from Therrien J. Echocardiography. Adult congenital heart disease. In: Gatzoulis MA, Webb GD, Daubeney PEF, eds. Diagnosis and Management of Adult Congenital Heart Disease. London: Churchill Livingstone, 2003:35–49.

define the position of the apex, atrial *situs*, the AV connections, and the ventriculoarterial relationship (Figs. 6–8). Apical and subcostal views are projected in the anatomically correct position (apex down) to permit better interpretation, especially of complex lesions.

Surgical scars and deformities of the thoracic cage may make transthoracic examination difficult, and views from all available windows—including additional or nonstandard views—should be acquired whenever necessary. The transthoracic examination should be comprehensive, with special attention given to the questions that need answers. Sonographers in nonspecialized centers should not hesitate to seek help from those so specialized.

The two-dimensional (2D) examination should assess all four chambers, valves, great vessel relationships, aortic arch anatomy, and pulmonary vein connections. Doppler (color flow, pulsed wave [PW], continuous wave [CW]) examination of flow patterns (including direction and velocities) within cardiac and extracardiac structures including all valves, defects, conduits, and shunts should be performed. Assessment of tricuspid regurgitation velocity is important and provides a measure of pulmonary artery pressures. Ventricular function assessment—both systolic and diastolic—is integral (*see* Chapter 5).

Transesophageal Echocardiography

In adults with CHD, TEE has major advantages over TTE and its role is now indispensable in the management of a broad spectrum of pediatric and adult patients with CHD. Complex lesions require optimal anatomic definition, and the windows provided by TEE greatly aid in their evaluation. Pulmonary venous structures, prosthetic valves, baffles, shunts, conduits, closure devices, residua, and other contiguous mediastinal structures are often best evaluated by TEE. Monitoring percutaneous interventions (e.g., patent foramen ovale [PFO] and atrial septal defect [ASD] closure and intra-operative monitoring) is best performed by TEE.

SPECTRUM OF ADULT CHD

A simplified summary of the major types of the major adult CHD are listed in Table 5.

Mitral valve prolapse, BAVs (and congenital forms of aortic stenosis), patent foramen ovale, atrial septal defects, and Marfan syndrome have been discussed previously, and are not covered in this chapter.

Isolated Ventricular Septal Defect

- Ventricular septal defects (VSDs) are the commonest congenital heart defect in children.

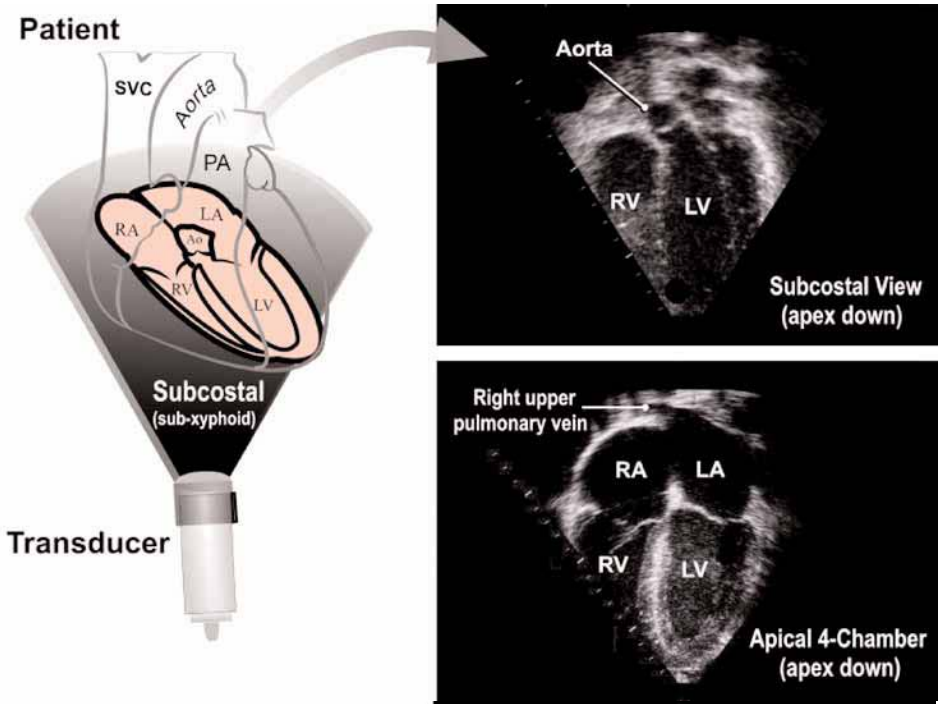

Fig. 6. Subcostal and apical views (apex down orientation) for segmental analysis. The standard echocardiographic examination should be preceded by subcostal and apical (often displayed anatomically correct apex down) views to analyze cardiac *situs* and cardiac segment connections.

- Most smaller defects close spontaneously, but isolated VSDs make up approx 10% of all adult CHD.

Anatomical Sites

Ventricular septal defects occur in a number of anatomic sites, including the membranous septum, inlet septum, outlet septum, and trabecular septum (Figs. 9 and 10). Perimembranous VSDs (~80%) may extend to other areas of the septum, but often close spontaneously (usually located by the septal leaflet of tricuspid valve [TV]). Ventricular septal defects can result in significantly increased flow through the pulmonary artery, with resultant pulmonary hypertension. In cases where pulmonary pressures reach left ventricular systolic pressures, the patient is considered to have "Eisenmenger's" physiology.

Best Echo Windows

- Parasternal long axis, PSAX, apical four chamber, apical five chamber, subcostal 4C (Table 6).
- TEE-midesophageal 4C, right ventricular outflow tract (RVOT) views for infundibular/conal septum.

Table 6
Recommended Echocardiographic Windows for Ventricular Septal Defects

Perimembranous	PLAX, PSAX (10 o'clock), A5C
Inlet/posterior-AV canal-type	A4C PSAX (mitral valve/basal septal level)
Outlet Supracristal Infracristal	PSAX PSAX—aortic valve (2 o'clock) PSAX—aortic valve level (~12 o'clock)
Trabecular (muscular)	PLAX, PSAX (midseptal, apical septal) A4C, A5C, subcostal four-chamber TEE-mid esophageal four-chamber and TEE-RVOT views (*see* Chapter 23).

A4C, apical four-chamber; A5C, apical five-chamber; AV, atrioventricular; PLAX, parasternal long-axis; PSAX, parasternal short-axis; RVOT, right ventricular outflow tract; TEE, transesophageal echocardiography.

Role of Echocardiography in VSDs

- Define anatomical site/type and size (Figs. 11–17; please *see* companion DVD for corresponding video for Figs. 12 and 14); less than 1 cm (small).

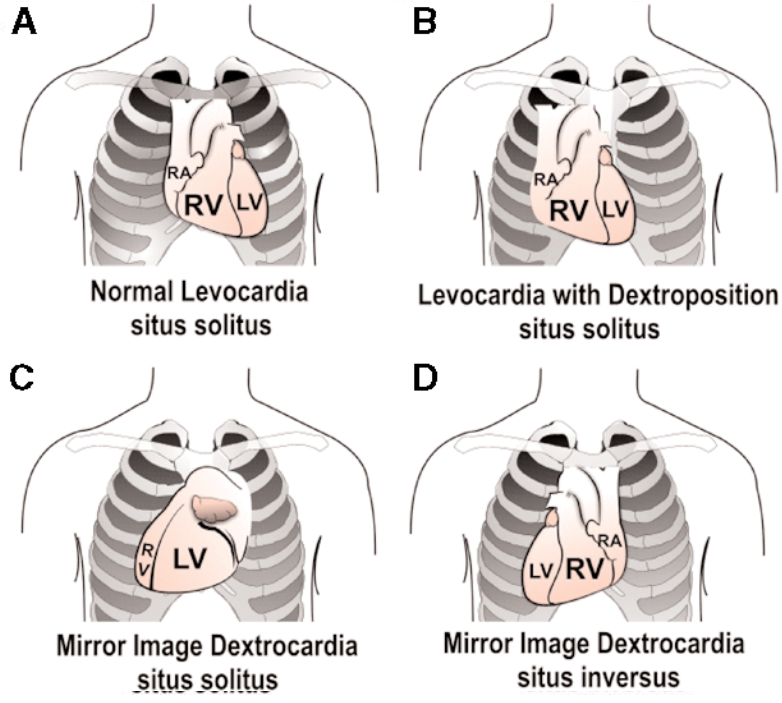

Fig. 7. Position of the cardiac apex. **(A)** Following ventricular looping, the apex normally points toward the left (levocardia). **(B)** Mediastinal shifts can displace the entire heart to the right (dextroposition), but heart chambers are otherwise normal. **(C)** Isolated dextrocardia results from incomplete pivoting, but chambers are *situs solitus* and concordant. **(D)** Mirror image dextrocardia involves both *situs inversus* and discordant cardiac chambers.

- Assess hemodynamic impact on global cardiac indices, especially ventricular function, signs of volume and pressure overload, pulmonary artery pressures, pulmonary vascular resistance (Fig. 11).
- Assess shunt size (restrictive vs nonrestrictive); Qp/Qs measurement by 2D and PW at RVOT and left ventricular outflow tract (*see* Chapter 21).
- Detection and adjunct to management of related conditions, (e.g., aortic valve prolapse with supracristal and paramembraneous VSDs; Fig. 15).
- Detection and adjunct to management of unrelated attendant conditions (e.g., coronary or valvular heart disease).
- Intraprocedural/intraoperative TEE or 2D for transcatheter or surgical closure.
- Follow-up, including postintervention.

Patent Ductus Arteriosus

A patent ductus arteriosus (PDA) is a residual communication between the pulmonary artery and aorta, necessary during gestation. Normally, this communication closes at birth. Most PDAs are diagnosed in infancy and childhood (5–10% of pediatric CHD), but may be incidental finding during echocardiography in the adult (Fig. 18; please *see* companion DVD for corresponding video).

Anatomical Site

- Ductus connects the aorta to the left pulmonary artery (LPA) (Fig. 19).
- A patent ductus arteriosus (PDA) is mainly an isolated defect, usually small and hemodynamically insignificant when seen in the adult.

Physiological Categories

Restrictive or nonrestrictve PDA with or without Eisenmenger's syndrome.

Best Echo Windows

- High PSAX (Fig. 18).
- Suprasternal view—angulate toward the LPA (Fig. 20).
- Color flow Doppler, PW and CW Doppler examining typical anatomic location of PDA with presence of systolic and diastolic flow, but patterns vary (Figs. 21 and 22). Reversal of flow may be seen in the rare Eisenmenger PDA in an adult.

Role of Echocardiography

- Identification of PDA.
- Assessment of size and Qp/Qs ratio.
- Detect changes within the ductus (e.g., aneurysm, atheroma, calcification, infective endocarditis). Aortic dissection involving ductus are rare, but known to occur.

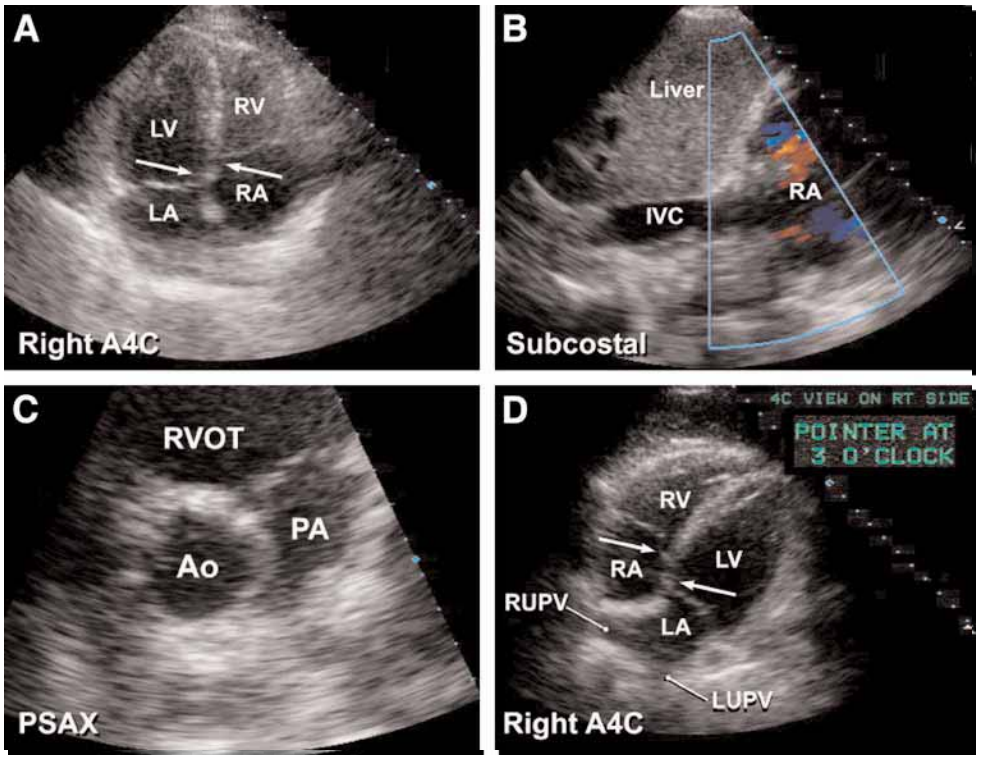

Fig. 8. A 48-yr-old male with a single syncopal episode. Right apical four-chamber (A4C) view shown in **A** was accidentally inverted, with index mark at 9 o'clock instead of the 3 o'clock position (novice sonographer). Note the normal leaflet relationship (arrows) at cardiac crux (**A**; *see* Fig. 5). Subcostal imaging showed the liver and inferior vena cava (IVC) in their normal *situs* **(B)**. Parasternal short axis (PSAX) view showing normal *situs* of the great arteries. Right A4C view by an experienced sonographer **(D)** shows normal atrial *situs* (pulmonary veins—right and left upper pulmonary veins [LUPV, RUPV] flowing into left atrium), atrioventricular concordance, and normal cardiac crux (arrows). This man's segmental nomenclature is therefore dextrocardia (S,D,S).

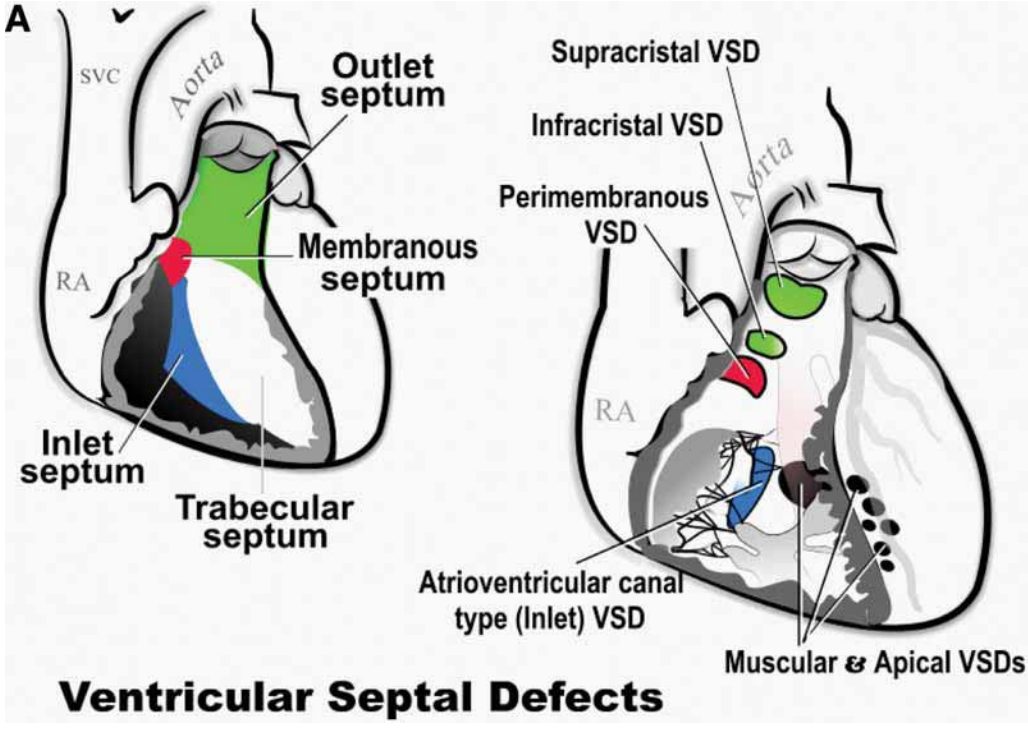

Fig. 9. Ventricular septal defects *(continued).*

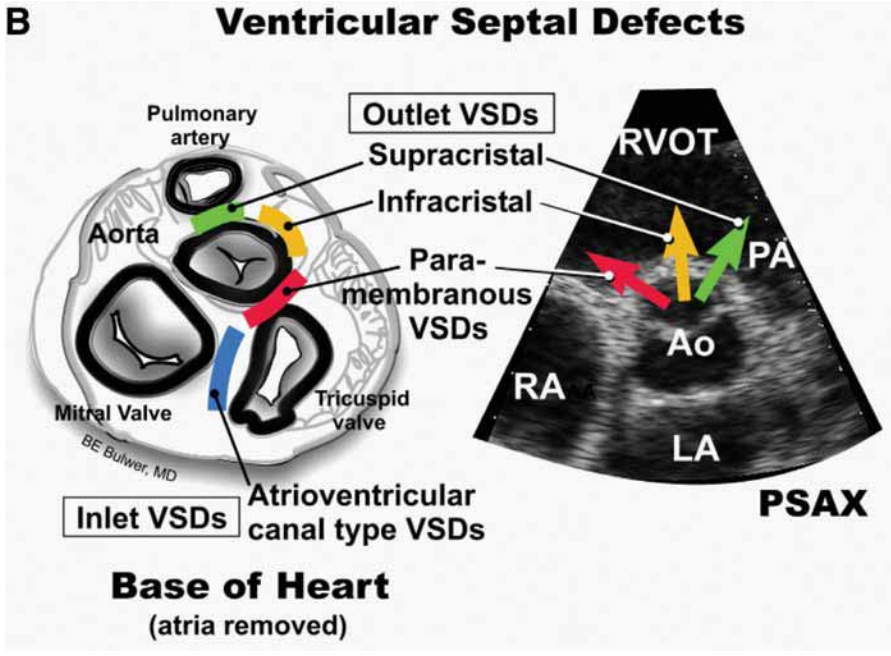

Fig. 9. *(Continued)* Ventricular septal defects.

- TEE role limited because of interposed left bronchus between esophagus and aorta.
- TTE can guide transcatheter closure and establish the diagnosis/differentiate from aortico-pulmonary window (Fig. 23).

Coarctation of the Aorta

Stenotic lesion of the descending thoracic aorta, just distal to the origin of the left subclavian artery.

Anatomical Site

- Narrowing (stenosis) most commonly near the ligamentum arteriosum—preductal and postductal types (Fig. 24).
- Degree of stenosis variable—may be discrete or long and tubular.
- Can be an isolated lesion ("simple" coarctation) or with associated lesions ("complex" coarctation).

Associated Cardiac Lesions

- Aortic stenosis secondary to BAV.
- Collateral circulation involving the internal mammary and intercostal arteries.
- Ventricular septal defect.
- Aortic medial disease with increased risk of aortic dissection.
- VSD.
- Anomalous right subclavian artery.

Best Echo Modalities, Windows

- Suprasternal notch (optimal neck extension).
- Left parasternal (high).
- TEE (aortic arch, descending aortic long and short axes—*see* Chapter 23).

Role of Echocardiography

- Diagnosis of coarctation.
- Assess site and severity (Fig. 25).
- Evaluation for associated lesions.
- Assess ventricular function for hypertensive heart disease (concentric hypertrophy), coronary artery disease (premature), secondary heart failure, aortic rupture/dissection, and infective endocarditis.
- Left ventricular function and the presence (or absence) of left ventricular hypertrophy.
- The presence (or absence) of other extracardiac cardiovascular anomalies such as collateral circulation, involvement of other vessels (subclavian/carotid stenoses) and associated aneurysms.

Doppler Assessment in PDA

Doppler echocardiography is crucial in the assessment of coarctation. The descending aorta should be interrogated with PW and CW Doppler in patients with suspected coarctation to assess velocities and calculate pressures. Color flow Doppler can also be helpful in looking for turbulence in the region of a coarctation, and can often be the first clue of a stenosis.

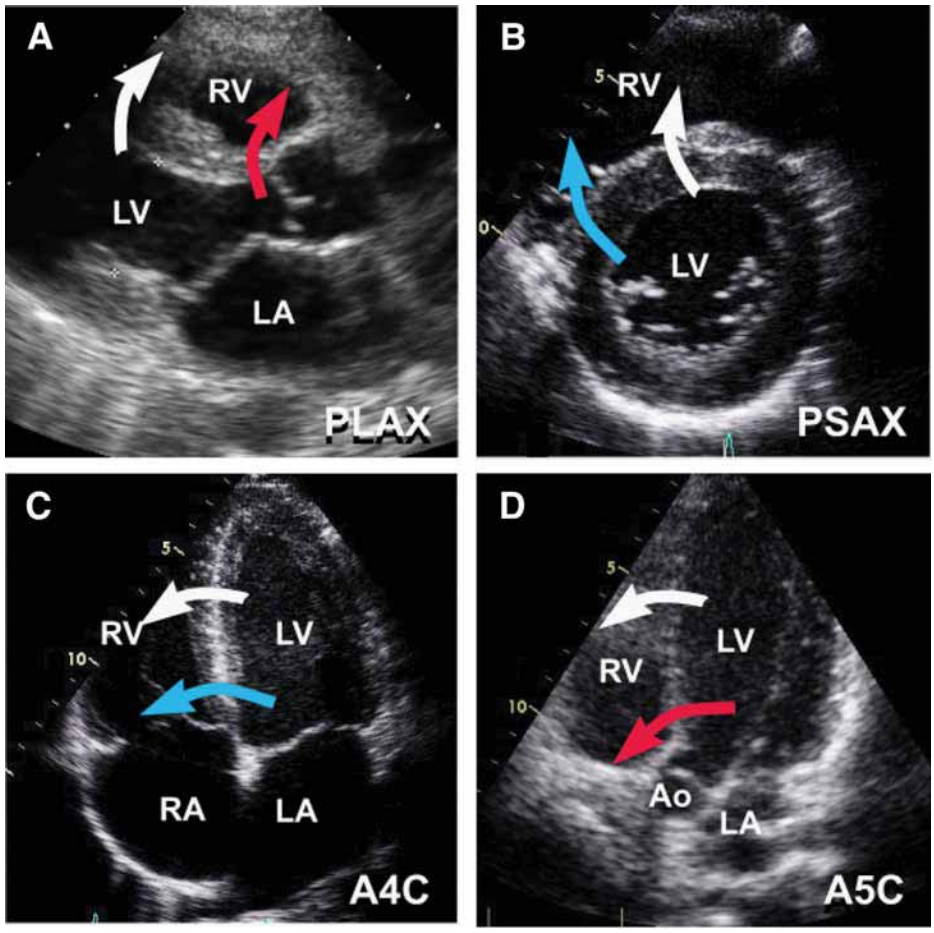

Fig. 10. Recommended echocardiographic windows for visualization of ventricular septal defects. The relative positions of ventricular septal defects on 2D echocardiography using the color scheme used in Figs. 9 and 10.

Tetralogy of Fallot

Category

Cyanotic CHD with RVOT obstruction and shunt.

Anatomy

- One primary defect leads to the tetrad—antero-cephalad displacement of the infundibular septum narrows the pulmonary artery, widens the aorta, and leaves a defect (Fig. 26). Right ventricular hypertrophy is secondary to RVOT obstruction.
- May be accompanied by PFO or ASD.

Pathophysiology

Pulmonary blood flow is obstructed to varying degrees—ranging from mild to severe. Right to left shunting of "blue" blood leading to cyanosis.

Natural History

- Almost all repaired in childhood (industrialized countries).
- Few unoperated patients seen in adulthood (Figs. 27 and 28; please *see* companion DVD for corresponding video for Fig. 27).

Palliative Surgery to Increase Pulmonary Blood Flow

A number of potential repairs have been utilized in patients with Tetralogy of Fallot. These include the Blalock-Taussig shunt (Fig. 29) and a full corrective repair (Fig. 30).

Role of Echocardiography

- Look for residual pulmonary stenosis, pulmonary regurgitation, or residual VSD.
- Assess pulmonary pressures—for signs of pulmonary hypertension.
- Assess aortic root—look for dilatation and aortic regurgitation.
- Assess right and left ventricular size and function (including myocardial performance index).

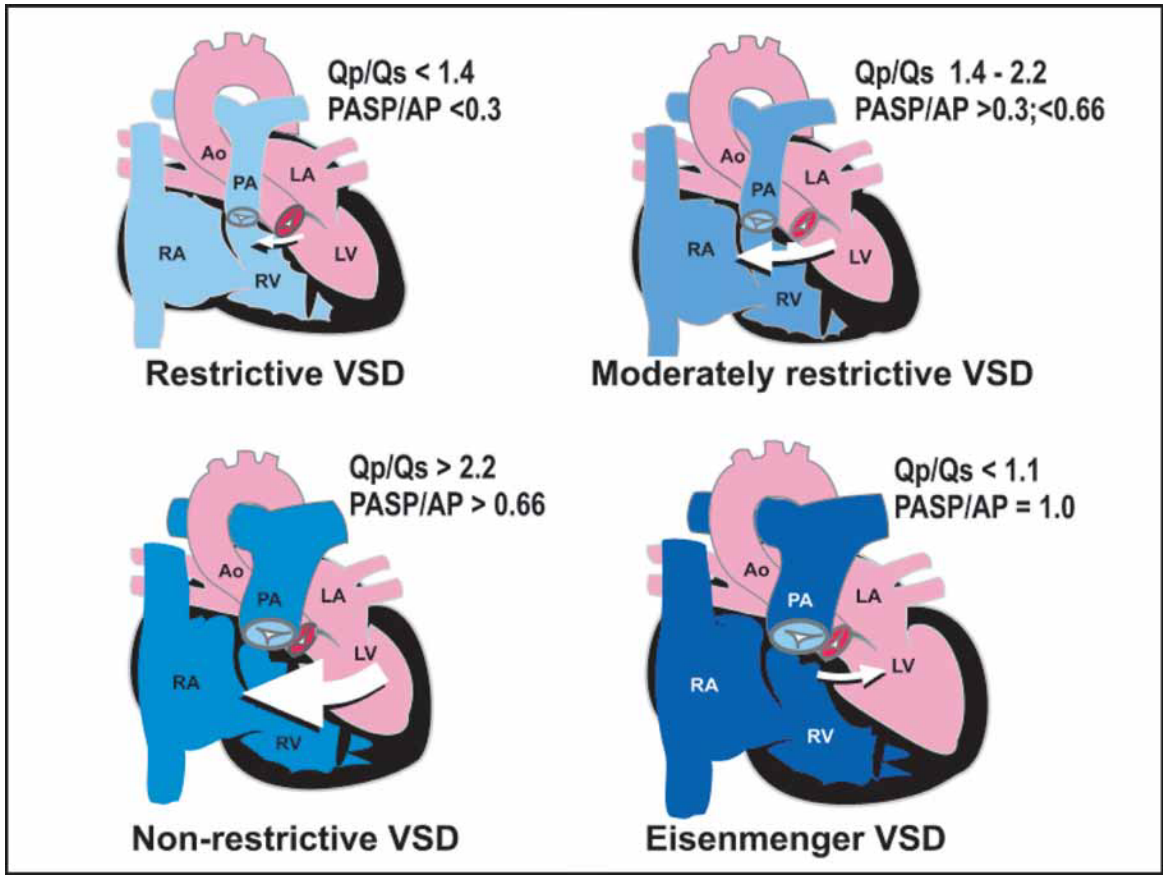

Fig. 11. Ventricular septal defects: physiological categories. Schema illustrating the physiological varieties of ventricular septal defects. Shunt size can be assessed by the pulmonary-to-system flow ratio (Qp/Qs). Smaller shunts (restrictive VSDs) generally have Qp/Qs<1.1, Nonrestrictive or open shunts have Qp/Qs >2.2, indicating significant hemodynamic impact. PASP, pulmonary artery systolic pressure; AP, aortic pressure.

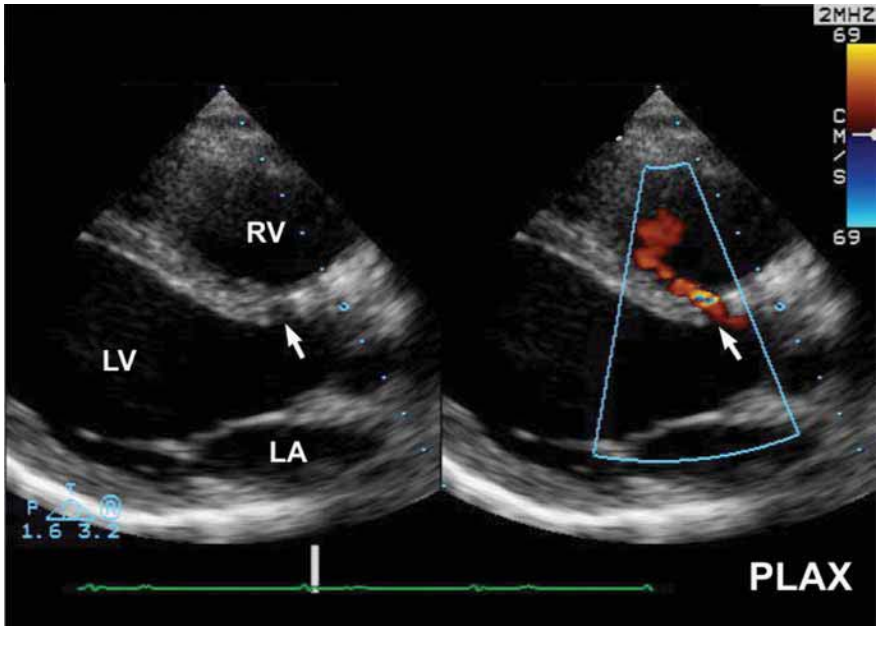

Fig. 12. Ventricular septal defects: small membranous (restrictive). Parasternal long-axis view (PLAX) of a small perimembranous ventricular septal defect in 62-yr-old male. Left ventricular dilation, secondary to ischemic cardiomyopathy, was also present. (Please *see* companion DVD for corresponding video.)

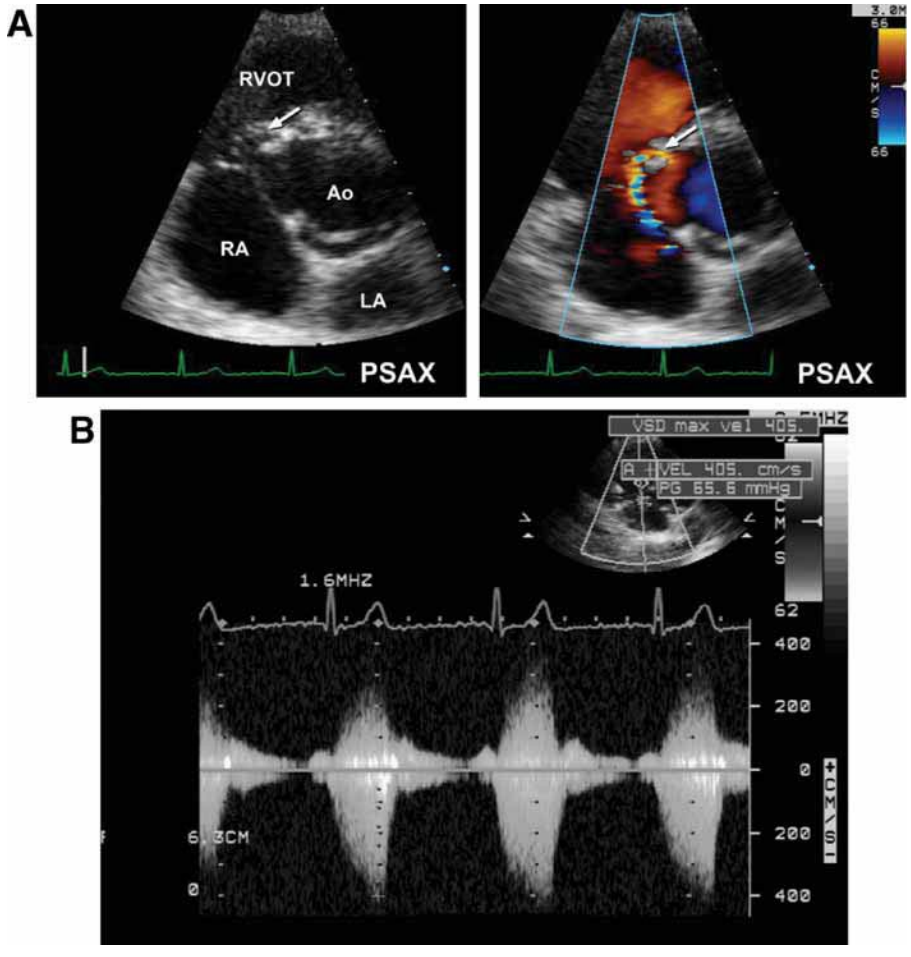

Fig. 13. Ventricular septal defects: small perimembranous (restrictive). **(A)** Classic perimembranous VSD at the 10 o'clock position in parasternal short axis (PSAX) views. **(B)** Peak instantaneous velocity measured 4 m/s (peak instantaneous gradient 65 mmHg), but no increased pulmonary artery pressures or chamber dilatation was present.

- In patients with palliative shunts—assess flow velocities and direction for evidence of shunt stenosis, occlusion, thrombosis, infection, or aneurysm.

Ebstein Malformation

Ebstein's anomaly or malformation is a condition in which the septal leaflet of the tricuspid valve is apically displaced, sometimes dramatically, and the anterior leaflet becomes "sail-like," extending deeply into the RV. Many patients survive into adulthood without surgical intervention (Figs. 31–33; please *see* companion DVD for corresponding video for Fig. 31).

Anatomy/Physiology

- Anatomic and functional anomalies of the TV.
- Apical displacement of the septal and posterior leaflets of the TV.
- "Atrialization" of right ventricular inflow tract (large right atrium) at the expense of the RV.
- Tricuspid regurgitation.
- Atrial level shunts, e.g., ASD frequent.
- Echodiagnosis: apical displacement of septal TV leaflet more than 8 mm/m^2 with elongated "sail-like" TV leaflet.

Associated Cardiac Lesions

PFO, ASD, VSD, pulmonary stenosis.

Role of Echocardiography

- Establish the diagnosis.
- Define anatomic lesion—severity (degree of apical displacement).

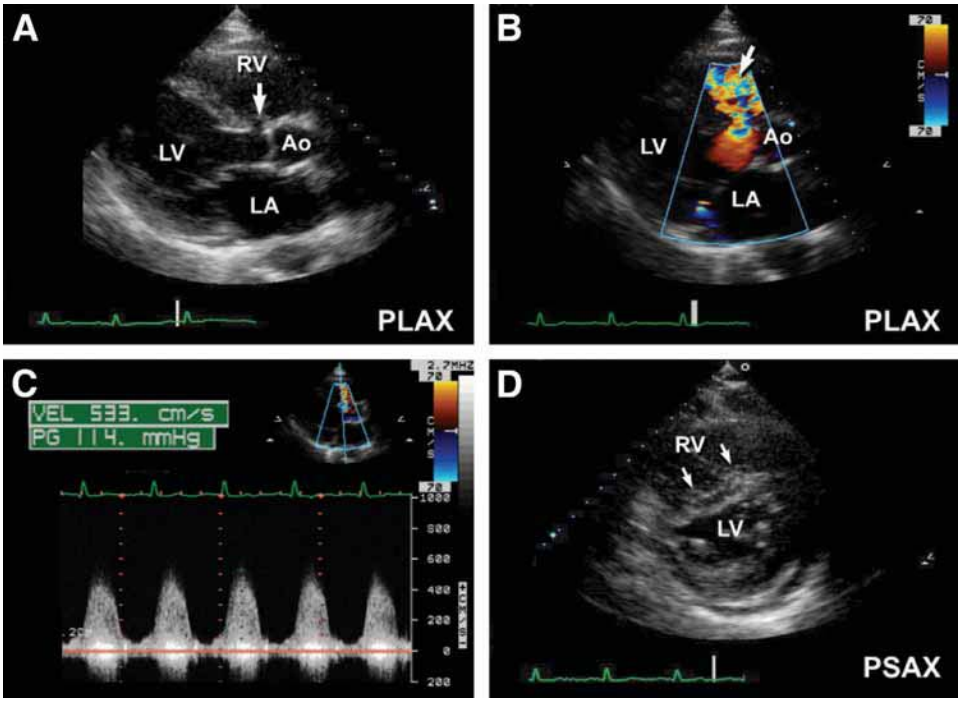

Fig. 14. Ventricular septal defects: moderately restrictive. Parasternal long axis views (PLAX, **A,B**) of 32-yr-old female with a loud systolic murmur and increasing shortness of breath. Note the easily visible perimembraneous VSD with marked shunting (large PISA) on color flow Doppler. Peak instantaneous velocity measured 5.3 m/s (peak gradient 114 mmHg). Her Qp/Qs was 1.4 **(C)**. Note systolic flattening (D-shaped) of the interventricular septum consistent with right ventricular pressure and volume overload. (Please *see* companion DVD for corresponding video.)

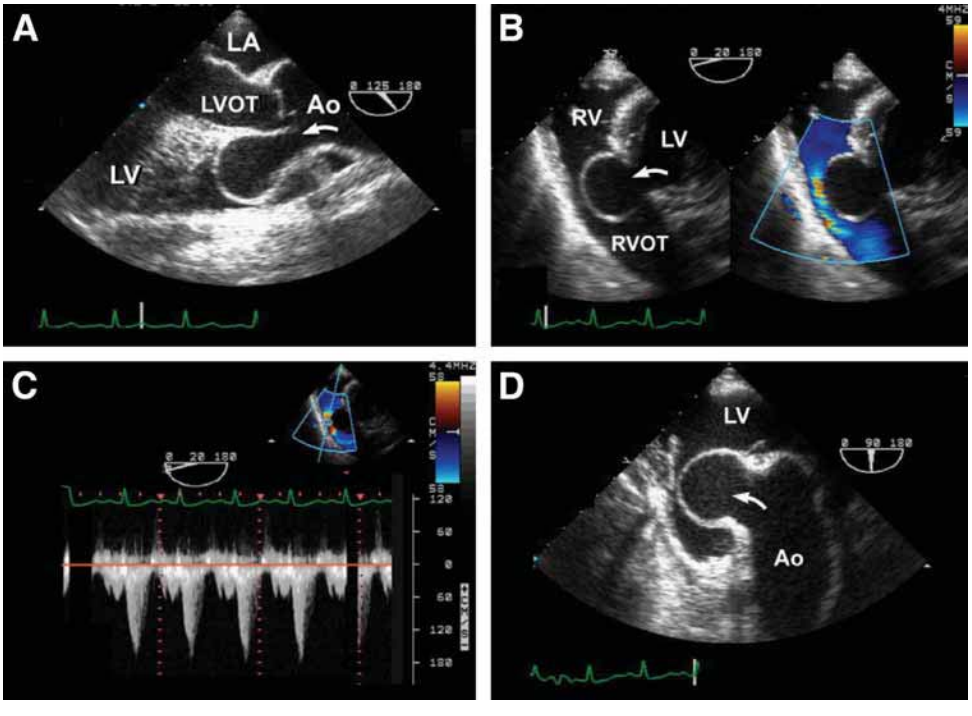

Fig. 15. Transesophageal views of a 58-yr-old male with a ventricular septal defect and worsening aortic regurgitation. Note the marked prolapse of the right cusp in the ME Aortic valve long axis view **(A)**. Flow acceleration was noted on color Doppler and CW Doppler evaluation showed peak velocities exceeding 1.8 m/s **(B,C)**. Transgastric view shows prolapse extending into the ventricular outflow tract.

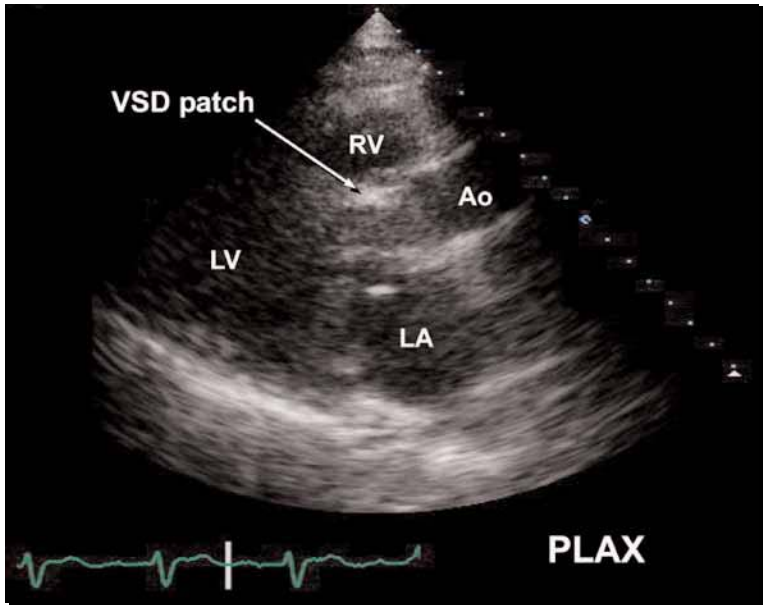

Fig. 16. Ventricular septal defect patch. This patient had a childhood history of a large ventricular septal defect that was patched.

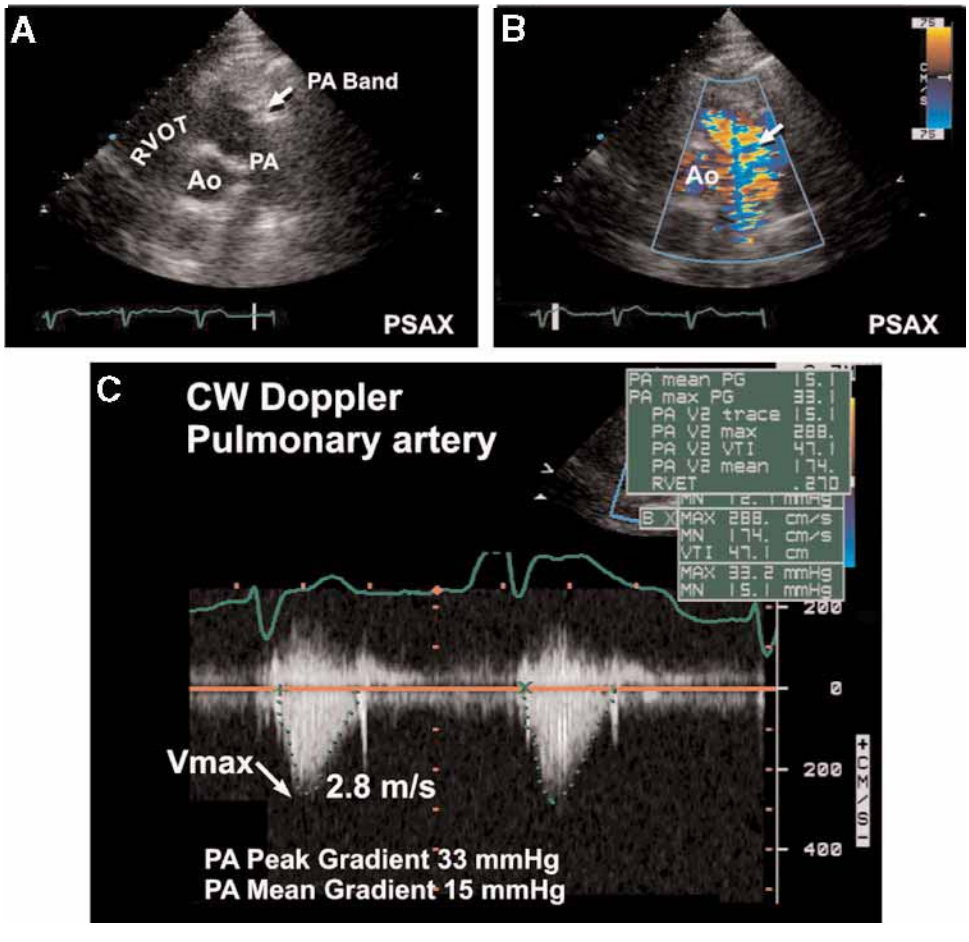

Fig. 17. Pulmonary artery banding was also performed to reduce volume and pressure effects of a previous unrestricted VSD. Note the increased echodensity **(A)**. Flow acceleration indicating band stenosis was noted on color flow Doppler evaluation **(B)**, and stenosis gradient was quantified by CW Doppler **(C)** revealing a peak velocity of 2.8 m/s (peak gradient of = mmHg).

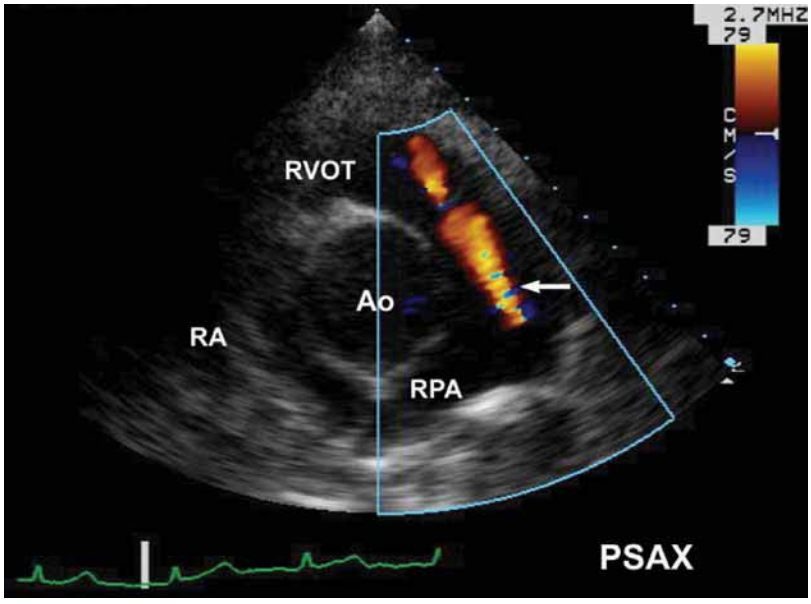

Fig. 18. Patent ductus arteriosus. Parasternal short-axis (PSAX) diastolic frame showing typical jet (arrow) of a patent ductus arteriosus with left-to-right shunt. (Please *see* companion DVD for corresponding video.)

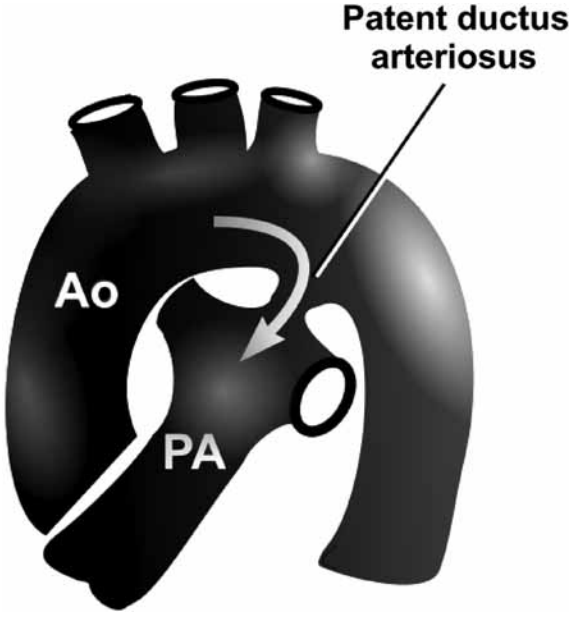

Fig. 19. Patent ductus arteriosus. A patent arterial duct connects the anterior surface of the proximal descending thoracic aorta to the roof of the left pulmonary artery.

- Assess biventricular dimensions and function—often impaired.
- Assess degree of tricuspid regurgitation.
- Pulmonary artery pressures.
- Look for/assess shunts and related lesions (ASDs are commonly associated).
- TEE if inadequate windows on TTE.

Complete Transposition of the Great Arteries (D-TGA)

In transposition of the great arteries, the atrioventricular connections are concordant (correct anatomically), whereas the ventriculo-arterial connections are discordant.

Anatomy

- AV connections concordant.
- Ventriculoarterial connections discordant.
- Most patients have simple TGA, but additional lesions common—"complex" transposition is common, e.g., with VSD and pulmonary/subpulmonic stenosis.

Surgical Correction

Almost all adults have had surgical intervention. A variety of corrective surgical repairs have been used in patients with transposition, the details of which are beyond the scope of this book (Fig. 34).

CHD: MISCELLANEOUS TOPICS

Persistent Left Superior Vena Cava

This is the commonest form of anomalous venous drainage involving the superior vena cava (Fig. 35).

It represents a persistence of the left horn of the embryonic sinus venosus that normally involutes to become the coronary, and therefore, almost always drains into the coronary sinus and manifests as a markedly dilated coronary sinus. This anomaly is of no clinical significance.

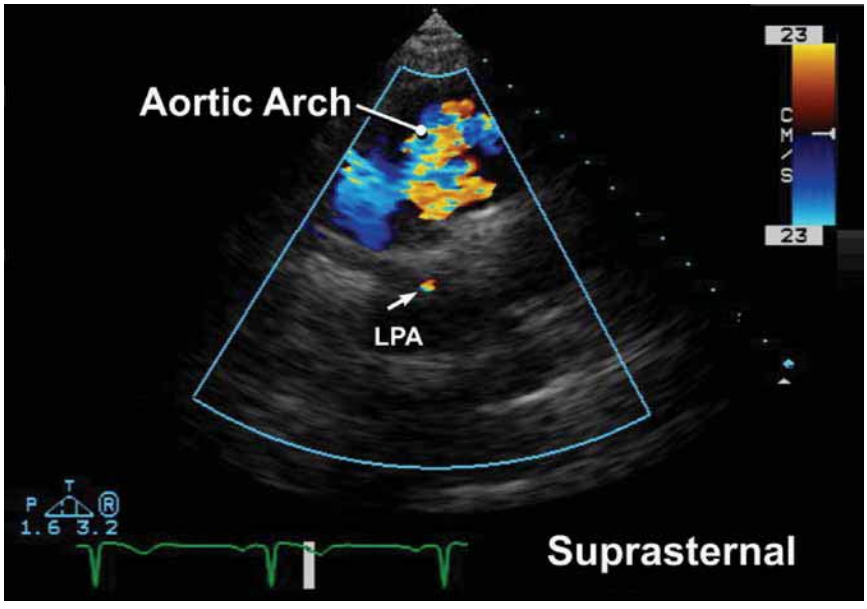

Fig. 20. Patent ductus arteriosus. Tiny jet (arrow) of left-to-right shunt from a small PDA can be seen entering the roof of the left pulmonary artery in relation to the aorta.

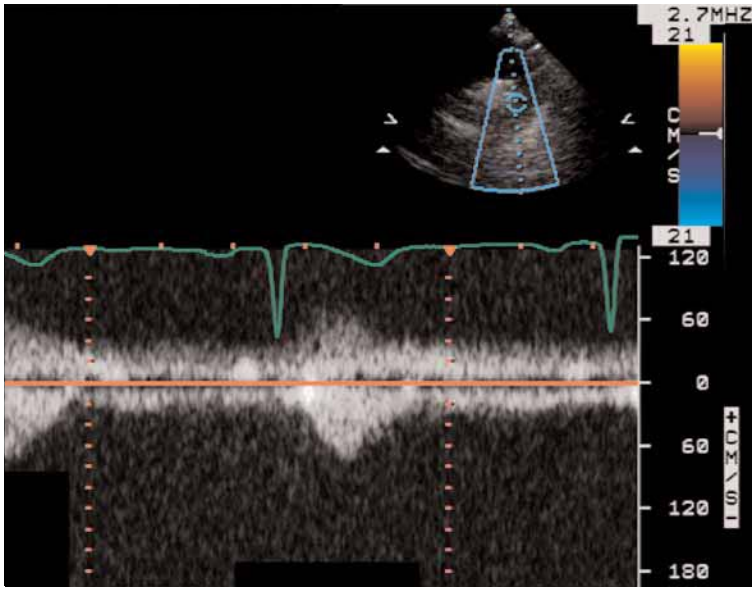

Fig. 21. Patent ductus arteriosus. Pulsed Doppler interrogation at the site (same patient, Fig. 20) shows continuous low velocity flow with systolic accentuation.

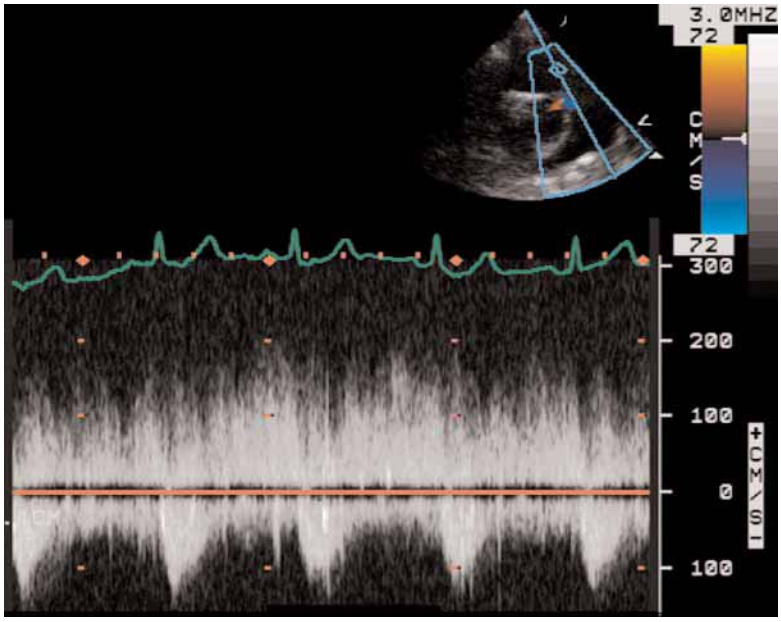

Fig. 22. Patent ductus arteriosus. Continuous-wave Doppler evaluation of PDA flow in the main pulmonary artery of patient (Fig. 18), confirms continuous flow pattern.

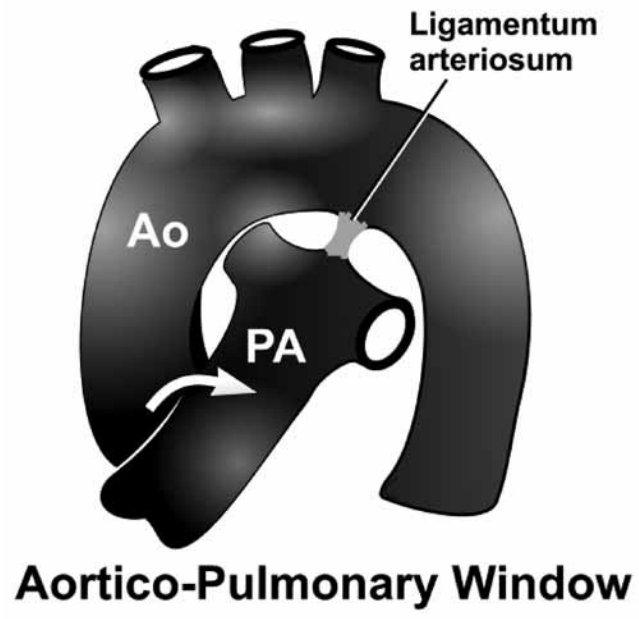

Fig. 23. Another arterio-venous fistula that causes continuous flow is the aortico-pulmonary window—usually an acquired defect that connects walls of the ascending thoracic aorta and the main pulmonary trunk. It can behave similarly to a large PDA with large left-to-right shunt and sequelae may be associated with a PDA, Coarctation, VSD, interrupted aortic arch.

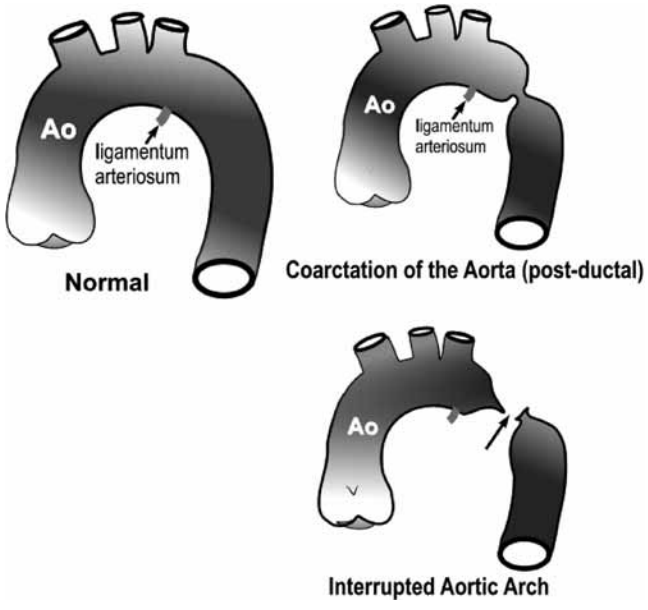

Fig. 24. Coarctation of the aorta (CoA) and interrupted aortic arch (IAA). On echocardiography, CoA can be distinguished from interrupted aortic arch by CW Doppler evaluation: significant CoA shows peak gradient more than 30 mmHg. No significant gradient is seen with IAA. The classic pattern of high peak velocity, delayed upstroke, and antegrade diastolic flow. TEE examination can establish the diagnosis, but CT, MRI, or angiography may be needed for confirmation.

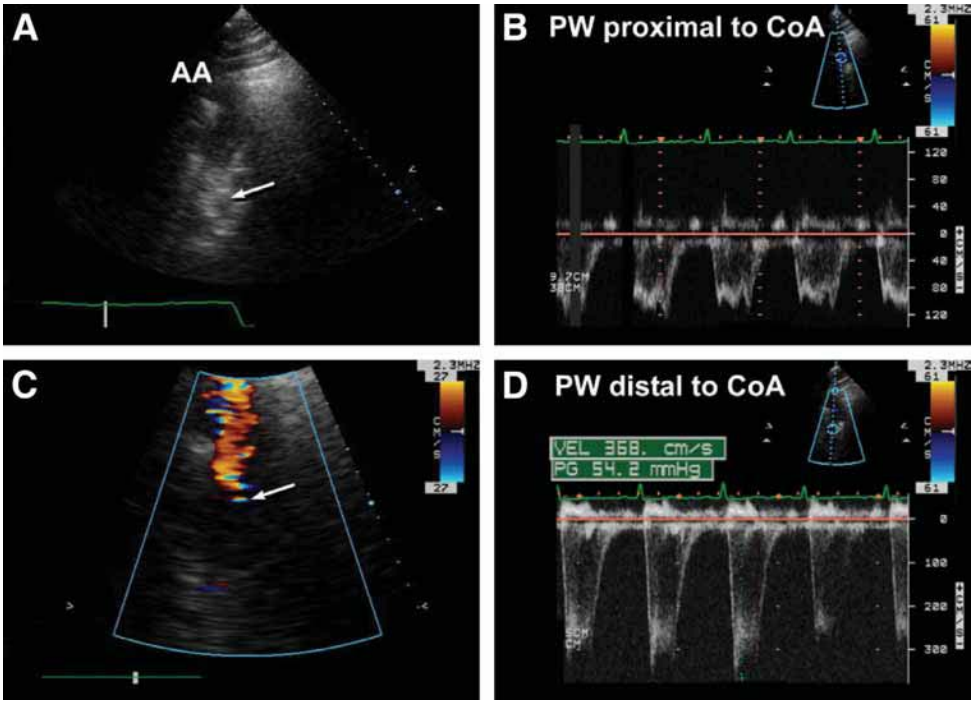

Fig. 25. Coarctation of the aorta. Suprasternal view showing distal aortic arch and descending thoracic aorta shows echodensity (arrow) in the proximal descending thoracic aorta **(A)**. PW Doppler evaluation of flow proximal to the echodensity showed peak instantaneous velocities less than 1.2 m/s **(B)**. Color flow Doppler of the same region shows no diastolic flow distal to the echodense region **(C)**, but peak instantaneous velocities reached 3.7 m/s (peak instantaneous gradient = 54 mmHg) **(D)**.

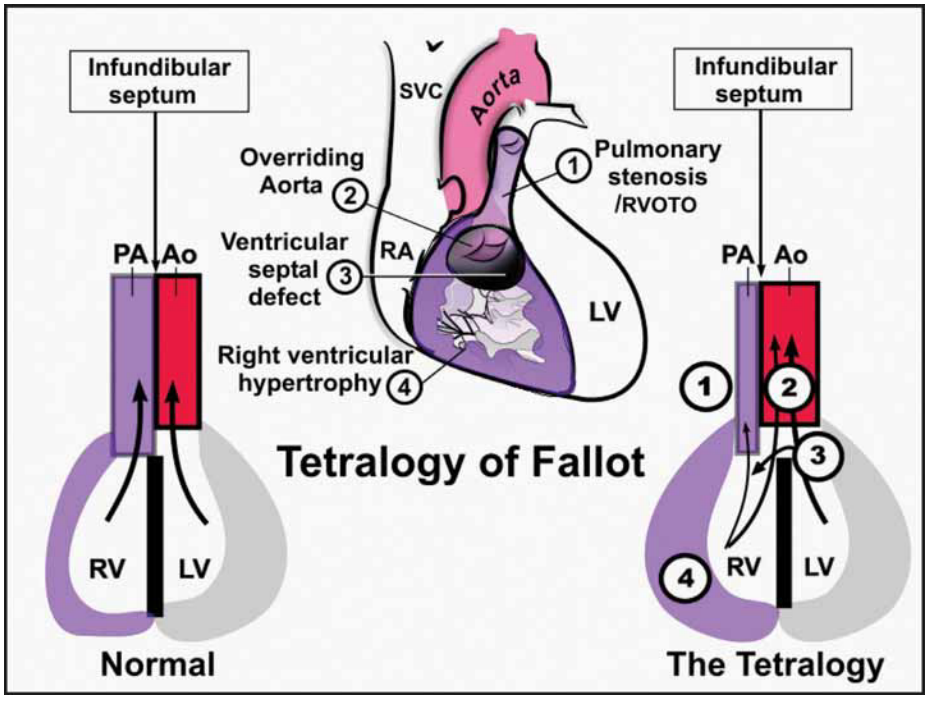

Fig. 26. The basis of the tetralogy of Fallot—one defect—the anterocephalad displacement of the infundibular septum—explains the tetrad.

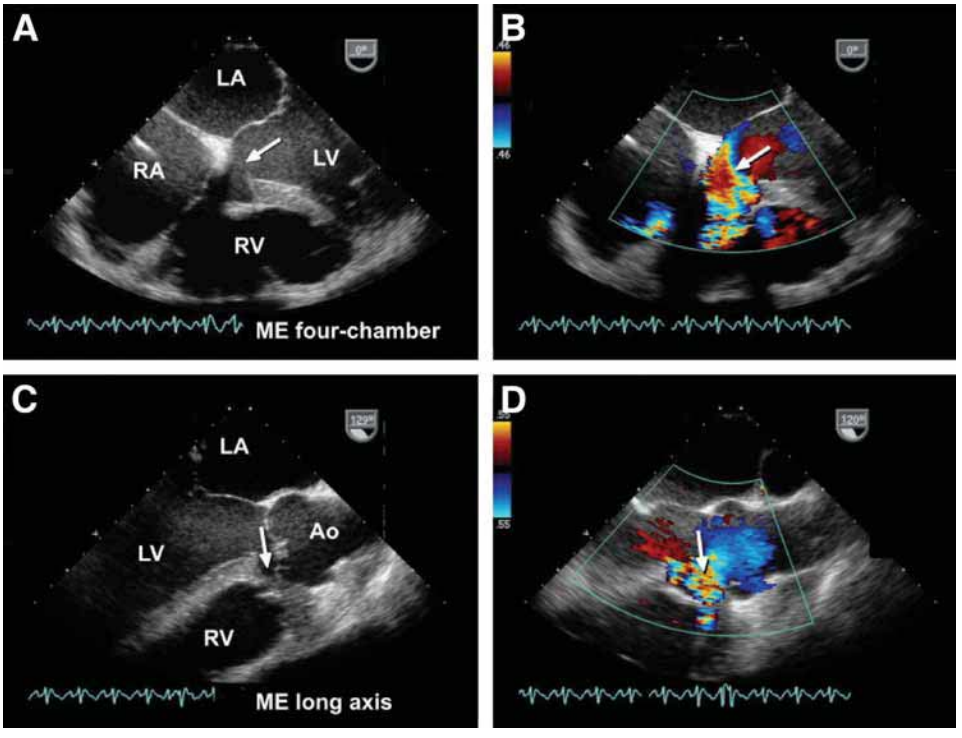

Fig. 27. Tetralogy of fallot. Midesophageal four-chamber views **(A,B)** obtained from a 51-yr-old male with TOF with previous palliative surgery show a significant residual VSD (arrows) with left-to-right shunt. Note the moderate dilation of right cardiac chambers. Midesophageal long-axis views of the same VSD (arrows, **C,D**). (Please *see* companion DVD for corresponding video.)

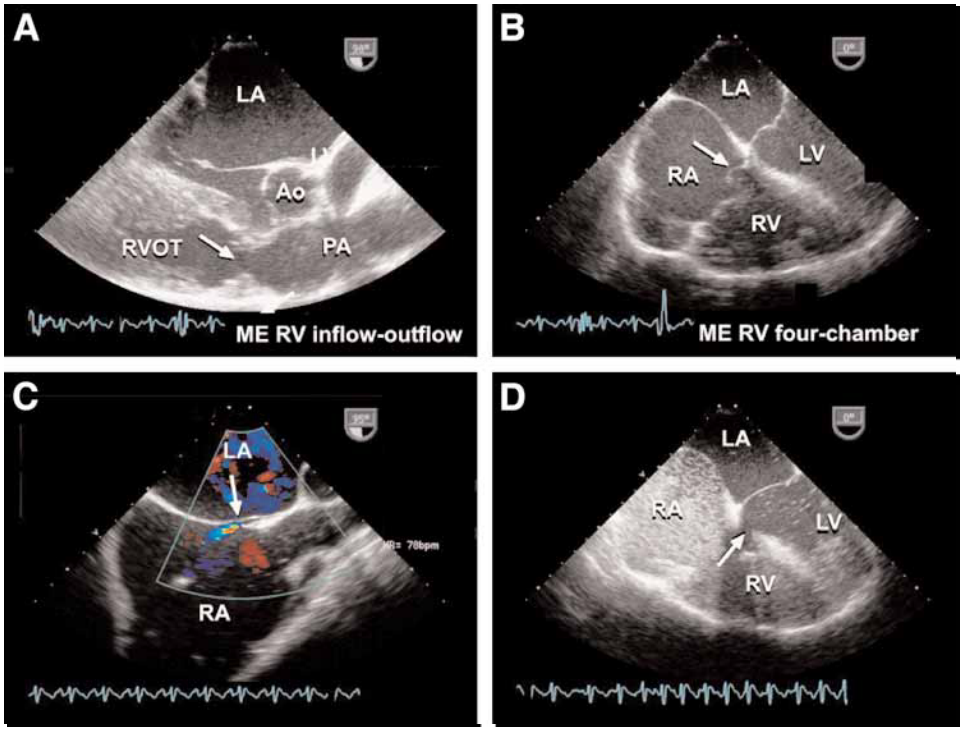

Fig. 28. Tetralogy of fallot. Midesophageal views showing residual stenosis/restenosis (arrow, **A**) of right ventricular outflow tract. Note the dilated right chambers and prolapsed septal leaflet of the tricuspid valve (arrow, **B**). A small jet from a PFO (arrow, **C**) confirmed by agitated saline contrast **(D)** was present. An additional defect, e.g., a PFO or an ASD present in patients with the tetralogy.

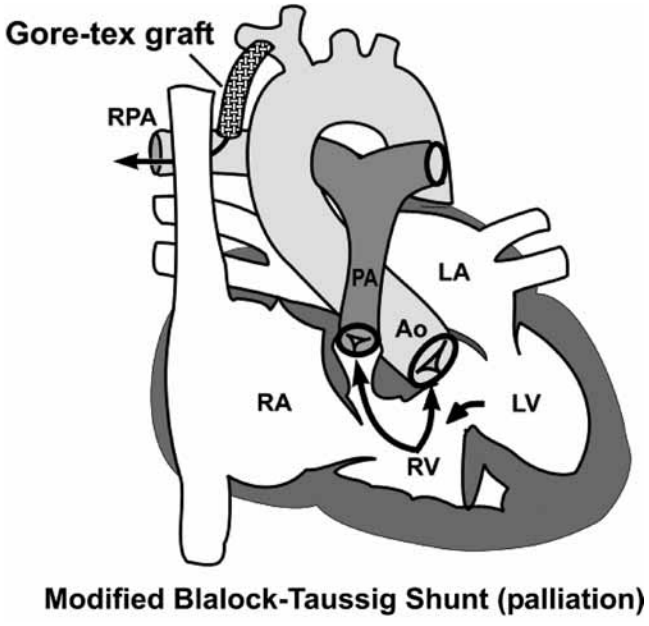

Fig. 29. Palliative surgery to increase pulmonary blood flow: modified Blalock-Taussig (BT) shunt. The modified BT shunt is an aorta-to-right pulmonary artery shunt using a Gore-Tex shunt (the original "classic BT shunt" was a right subclavian-to-right pulmonary artery shunt). These shunts may distort the pulmonary artery; they may stenose, occlude, or develop aneurysms.

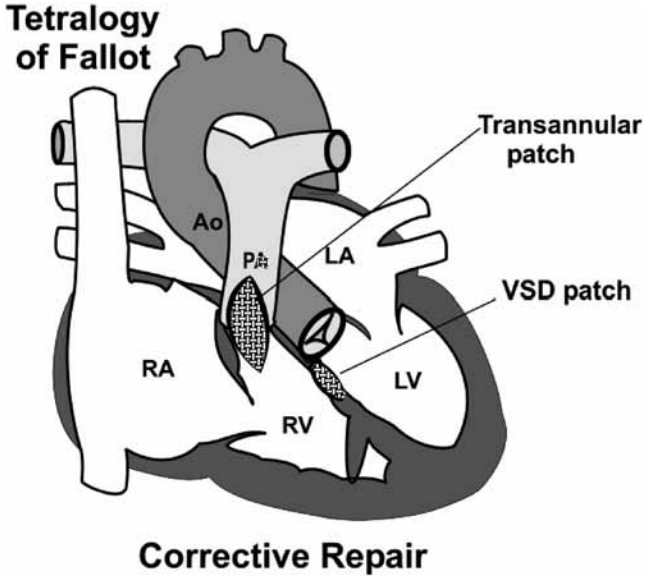

Fig. 30. Tetralogy of fallot: corrective surgery with VSD closure and right ventricular outflow tract (RVOT) surgery.

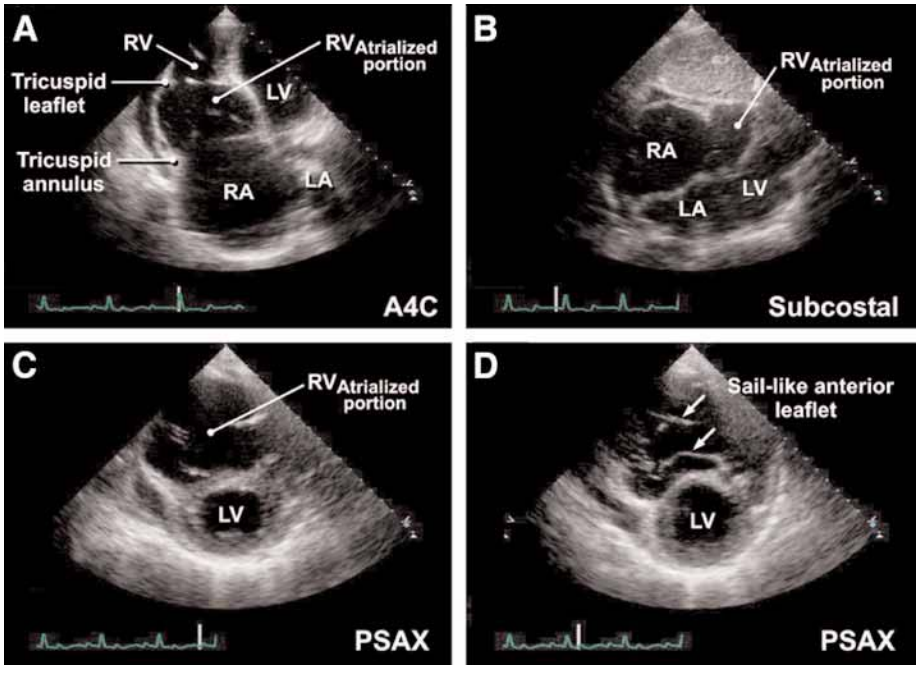

Fig. 31. Ebstein's malformation. Characteristic features of this anomaly are shown the huge right atrium—the apical portion actually an "atrialized" portion of the right ventricle—labeled (ARV) **(A–D)**. Note the "sail-like" anterior tricuspid leaflet in this parasternal short-axis view **(D)**. (Please *see* companion DVD for corresponding video.)

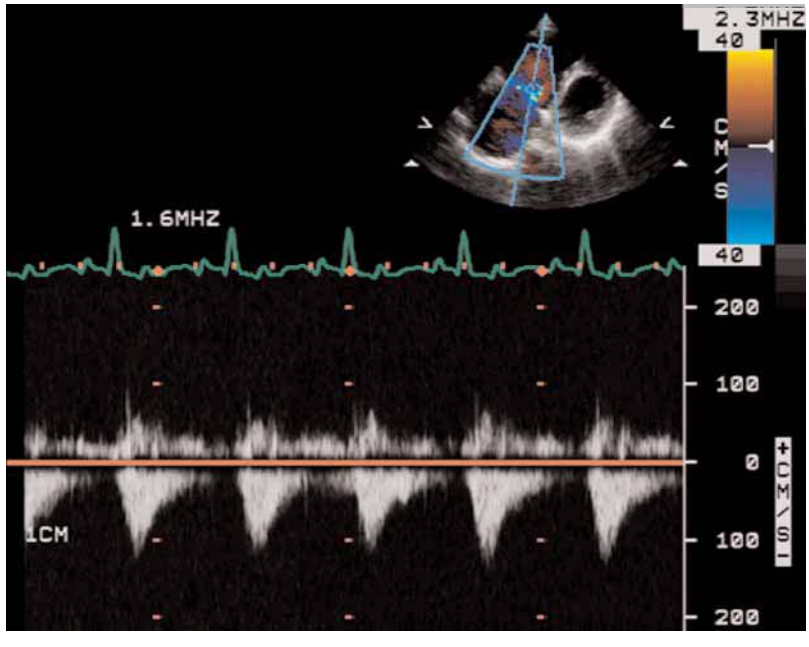

Fig. 32. Ebstein's malformation. The low peak tricuspid regurgitation velocities seen on CW Doppler (<1.2 m/s) in this patient with Ebstein's anomaly are a reflection of right ventricular dysfunction.

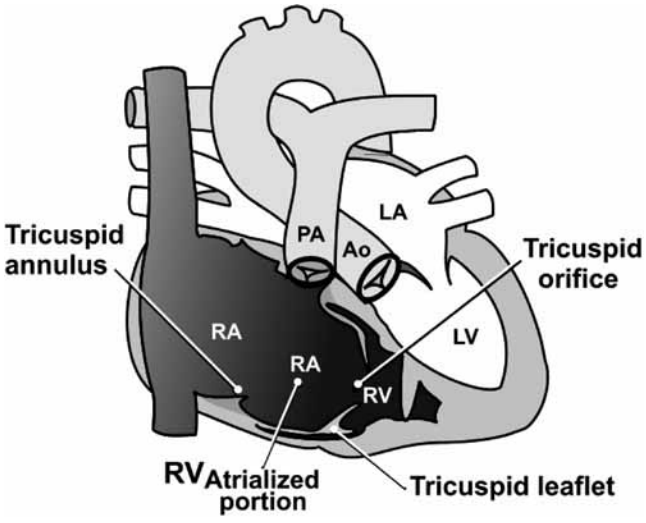

Fig. 33. Ebstein's malformation. Fusion of the tricuspid leaflets to the ventricular wall distally within the RV cavity leads to "atrialization" of the proximal RV segment, diminution in size of the distal RV.

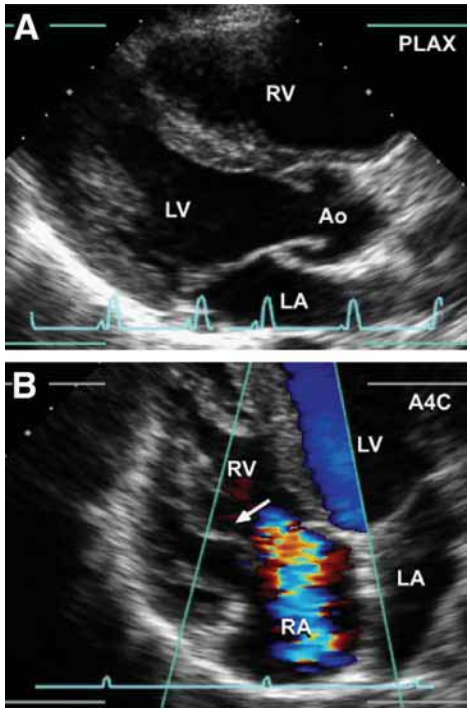

Fig. 34. Corrected D-transposition by arterial switch (Jatene). These exercise stress echocardiography images in this patient with D-TGA shows a rather normal looking parasternal long-axis (PLAX) View. The "Ao" is the neo-aorta is the former pulmonary trunk. This permits the morphologic LV to remain the systemic ventricle. Switch at the arterial level (compared to the switch at the atrial level—Mustard and Senning procedures) results in less long-term ventricular dysfunction. Periodic exercise stress testing to evaluate possible coronary ischemia is recommended, as reimplantation of coronary arteries is an integral part of the arterial switch operation.

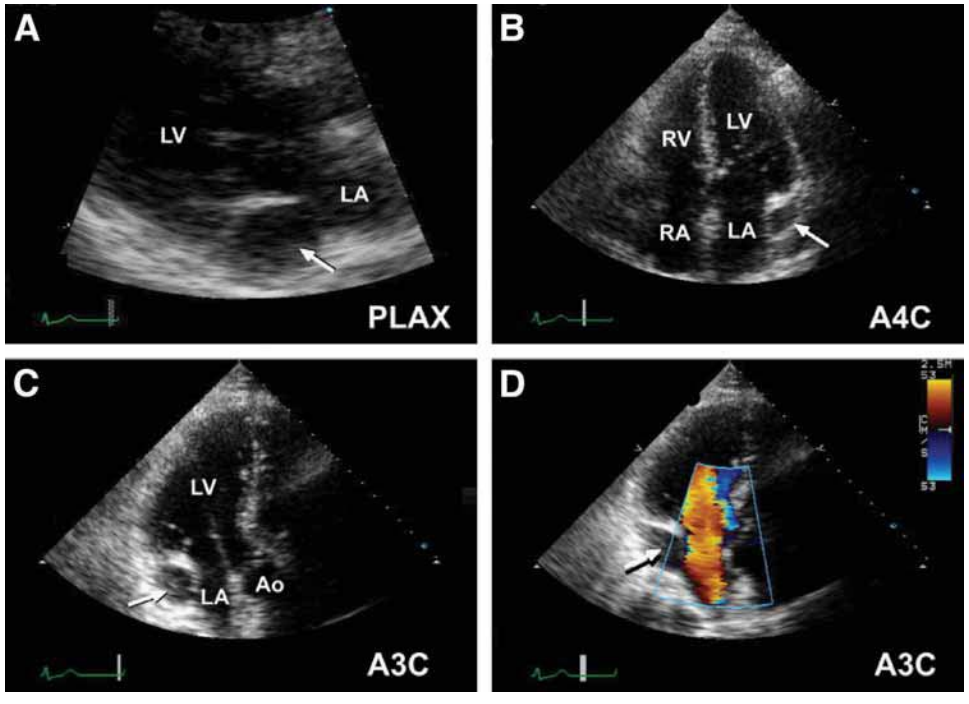

Fig. 35. The presence of a markedly dilated coronary sinus (arrows in all panels) in an otherwise normal heart should trigger consideration of a persistent left superior vena cava that empties directly into the coronary sinus. It has no pathological sequelae. Agitated saline contrast injected into the left arm will opacify the coronary sinus before the right atrium. Injecting contrast into the right arm would opacify the right atrium only.

SUGGESTED READING

Anderson R, Ho SY. Echocardiographic diagnosis and description of congenital heart disease: Anatomic principles and philosophy. In: St. John Sutton MG, Oldershaw PJ, Kotler MN, eds. Textbook of Echocardiography and Doppler in Adults and Children. Cambridge, MA: Blackwell Scientific Publications, 1996;711–743.

Anderson RH, Becker AE, Freedom RM, et al. Sequential segmental analysis of congenital heart disease. Pediatr Cardiol 1984;5:281–287.

Child JS. Echocardiographic evaluation of the adult with postoperative congenital heart disease. In: Otto CM, ed. The Practice of Clinical Echocardiography. Philadelphia: W.B. Saunders, 2002:901–921.

Child JS. Transthoracic and transesophageal echocardiographic imaging: anatomic and hemodynamic assessment. In: Perloff JK, Child JS, eds. Congenital Heart Disease in Adults. Philadelphia: W. B. Saunders, 1998:91–127.

Jurazek AL. Introduction to Pediatric Cardiology. Cardiac Registry. Children's Hospital Boston, June 2004.

Mullins CE, Mayer DC. Congenital Heart Disease. A Diagrammatic Atlas. New York: Wiley-Liss, 1988.

Netter FH. The Heart. CIBA collection of medical illustrations, vol. 5. West Caldwell, NJ: CIBA-Geigy, 1978.

Shinebourne EA, Macartney FJ, Anderson RH. Sequential chamber localization—logical approach to diagnosis in congenital heart disease. Br Heart J 1976;38:327–340.

Therrien J. Echocardiography. In: Gatzoulis MA, Webb GD, Daubeney PEF (eds). Diagnosis and Management of Adult Congenital Heart Disease. London, Churchill Livingstone, 2003:35–49.

Webb GD, Smallhorn JF, Therrien J, Redington AN. Congenital Heart Disease. In: Zipes DP, Libby P, Bonow RO, Braunwald E. eds. Braunwald's Heart Disease—A Textbook of Cardiovascular Medicine. Philadelphia: Elsevier Saunders, 2005:1489–1452.

23 Transesophageal Echocardiography

Multiplane Examination Primer

Bernard E. Bulwer, MD, MSc and Stanton K. Shernan, MD

CONTENTS

This primer is an atlas illustrating basic nomenclature and standard views adopted by the American Society of Echocardiography (ASE) and the Society of Cardiovascular Anesthesiologists (SCA) in the performance of a comprehensive intra-operative multiplane transesophageal echocardiography examination.

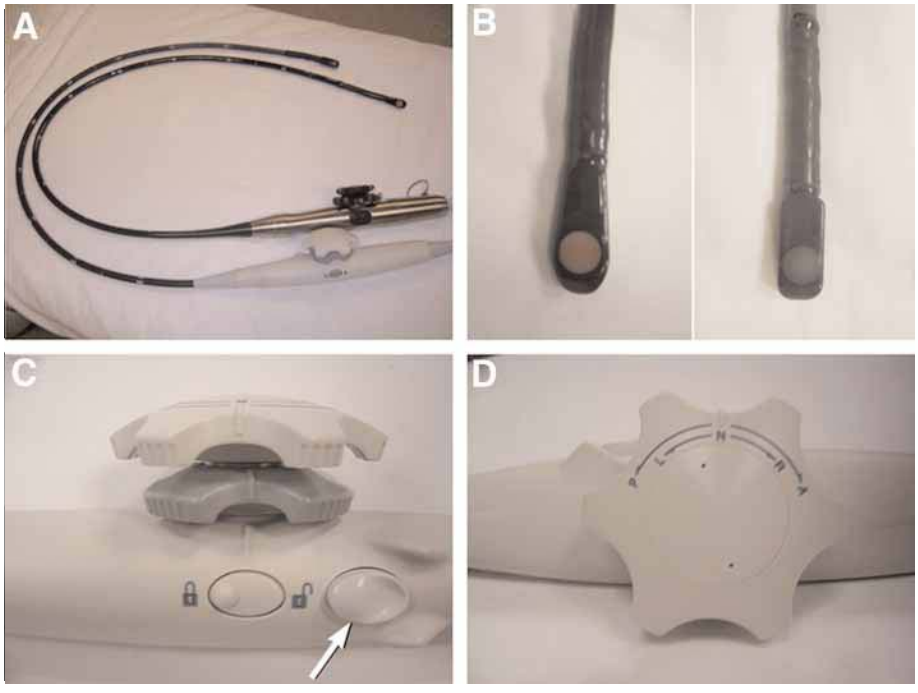

Fig. 1. Instrumentation of transesophageal echocardiography. Two models of transesophageal echocardiography (TEE) probes **(A)**. Miniature multiplanar transducer and housing located at tip of TEE probe **(B)**. Profile of TEE probe controls. Multiplane (Omni) control button is indicated by arrow **(C)**. View from top showing TEE probe control positions as indicated—neutral (N), right (R) and left (L) flexion, anteflex (A), and retroflex (P) **(D)**.

From: *Contemporary Cardiology: Essential Echocardiography: A Practical Handbook With DVD*
Edited by: S. D. Solomon © Humana Press, Totowa, NJ

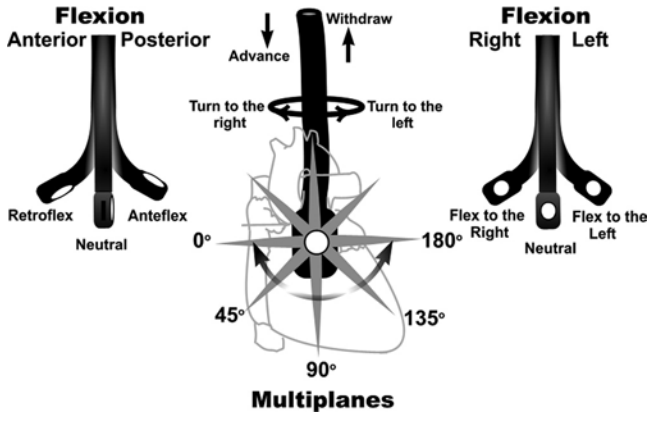

Fig. 2. TEE probe and multiplanar transducer: position basics. Transesophageal echocardiography probe and multiplanar transducer manipulation. Mechnanical movements of the transesophageal probe include anterior and posterior flexion and flexion to the right or left. The entire probe can also be manually rotated to the right or to the left. The first TEE probes permitted only a single, and later two planes of examination. Arrays of crystals in modern miniaturized ultrasound transducers permit visualization along multiple planes—hence, the multiplanar examination.

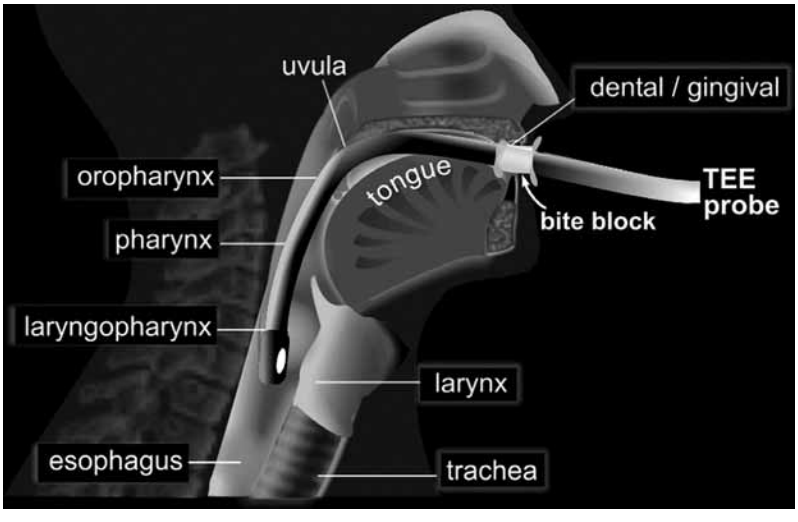

Fig. 3. TEE probe: anatomical relationships. Illustration showing the descent of the probe through the mouth, oropharynx, and pharynx. These are all sites of potential injury during the introduction and manipulation of the probe. Note the use of a bite block to protect the probe.

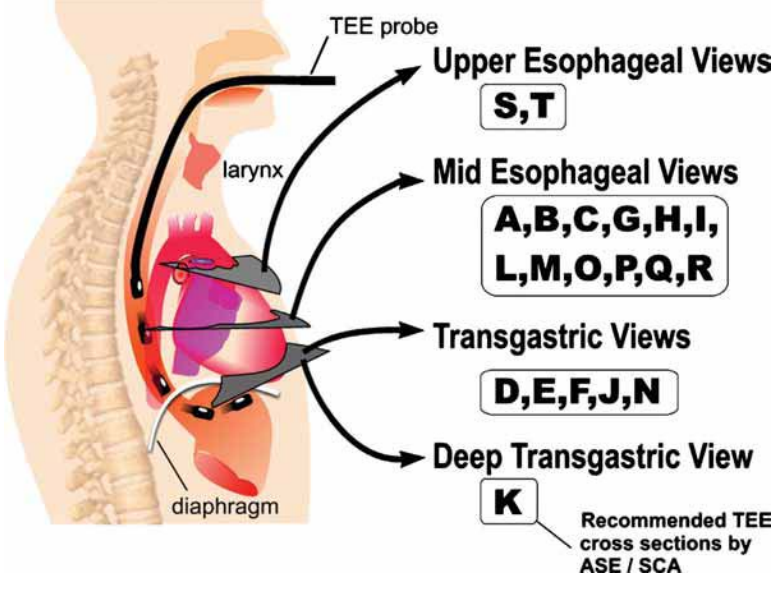

Fig. 4. Anatomic reference scheme and nomenclature adopted by the Society of Echocardiography and the Society of Cardiovascular Anesthesiologists. The fundamental parts of the TEE multiplanar examination are represented by a set of 20 cross-sectional imaging planes represented by letters of the alphabet.

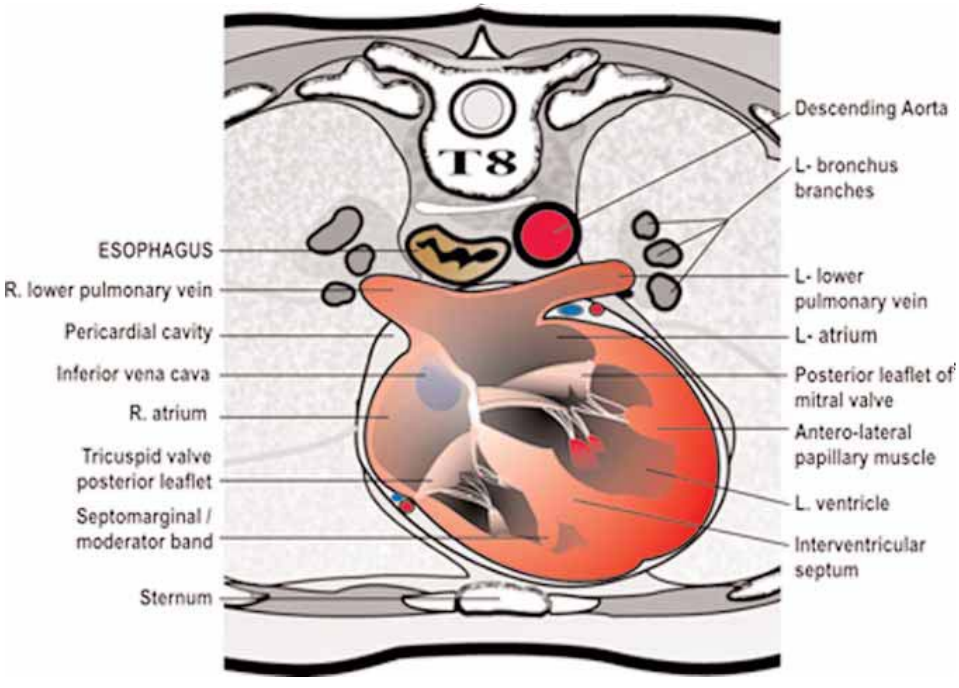

Fig. 5. Anatomical relationships transesophageal echocardiography. Illustration showing the transverse relationships of the major mediastinal structures at the level of the eighth thoracic vertebra. Note the close relationship of the esophagus to the left atrium (LA). As the transducer is confined to the esophagus at this level, this constant relationship orients the operator during the many permutations of images acquired during TEE.

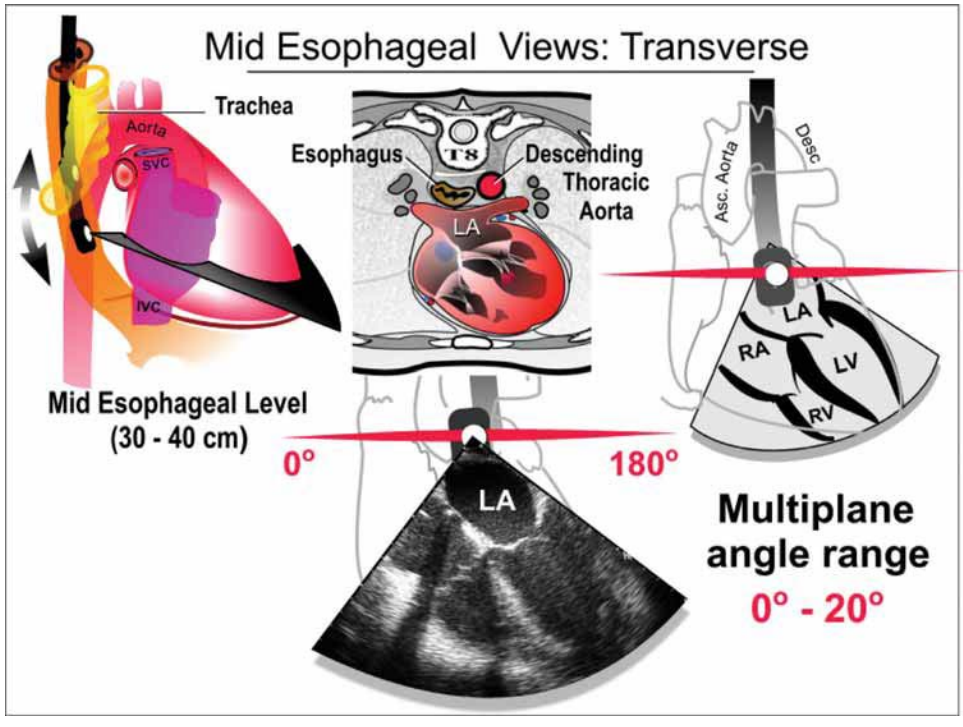

Fig. 6. Spatial relationships of transesophageal echocardiography. Understanding anatomical relationships between the transducer and the major mediastinal structures provide the basis for acquisition and interpretation of TEE images. Spatial relationships at the ME level (approximately at the eighth thoracic vertebra) are shown (*see also* Figs. 5–6). Note the relationship of the transducer within the esophagus to the LA and the descending thoracic aorta. At higher levels, the air filled trachea and bronchi may cause suboptimal visualization of the distal ascending aorta and proximal aortic arch (blind spots).

ORDER OF EXAMINATION: SUMMARY

Stage 1. ME Level: Multiplane from 0 to approx 120°.

- ME four-chamber 15° (A): Figs. 8–10 (please *see* companion DVD for corresponding video for Figs. 8 and 10).
- ME mitral commissural 80° (G): Figs. 11 and 12 (please *see* companion DVD for corresponding video for Fig. 12).
- ME two-chamber 90° (B): Figs. 13 and 14 (please *see* companion DVD for corresponding video for Fig 14).
- ME long axis 120° (C): Figs. 15 and 16 (please *see* companion DVD for corresponding video for Fig. 16).

Stage 2. ME level: with angle approx 90°, sweep R to L.

- ME right ventricular inflow-outflow 80° (M): Figs. 17 and 18 (please *see* companion DVD for corresponding video for Fig. 18).
- ME bicaval 110° (L): Figs. 19 and 20 (please *see* companion DVD for corresponding video for Fig. 20).
- Withdraw: ME ascending aortic long axis 100° (P): Figs. 21 and 22 (please *see* companion DVD for corresponding video for Fig. 22).
- Advance: ME aortic valve long axis 130° (I): Figs. 23 and 24 (please *see* companion DVD for corresponding video for Fig. 24).

Stage 3. Start at 0–20°.

- ME ascending aortic short axis 20° (O): Figs. 25 and 26 (please *see* companion DVD for corresponding video for Fig. 26).
- Withdraw: ME aortic valve (AV) short axis 60° (H): Figs. 27 and 28 (please *see* companion DVD for corresponding video for Fig. 28).
- UE aortic arch long axis 0° (S): Figs. 29 and 30 (please *see* companion DVD for corresponding video for Fig. 30).
- UE aortic arch short axis 90° (T): Fig. 31 (please *see* companion DVD for corresponding video).
- Turn left, advance: descending aortic long axis 90° (R): Figs. 32 and 33 (please *see* companion DVD for corresponding video for Fig. 33).
- Descending aortic short axis 0° (Q): Figs. 34 and 35 (please *see* companion DVD for corresponding video for Fig. 35).

Stage 4. Advance to stomach, anteflex.

- Transgastric mid-short axis 0° (D): Figs. 36 and 37 (please *see* companion DVD for corresponding video for Fig. 37).
- Withdraw slightly: transgastric basal short axis 0° (F): Figs. 38 and 39 (please *see* companion DVD for corresponding video for Fig. 39).
- Transgastric two-chamber 90° (E): Figs. 40 and 41 (please *see* companion DVD for corresponding video for Fig. 41).
- 90–120°: transgastric long axis 120° (J): Figs. 42 and 43.
- Turn right: transgastric right ventricular inflow 120° (N): Figs. 44 and 45 (please *see* companion DVD for corresponding video for Fig. 45).
- Advance, anteflex: deep transgastric long axis 0° (K): Figs. 46 and 47 (please *see* companion DVD for corresponding video for Fig. 46).

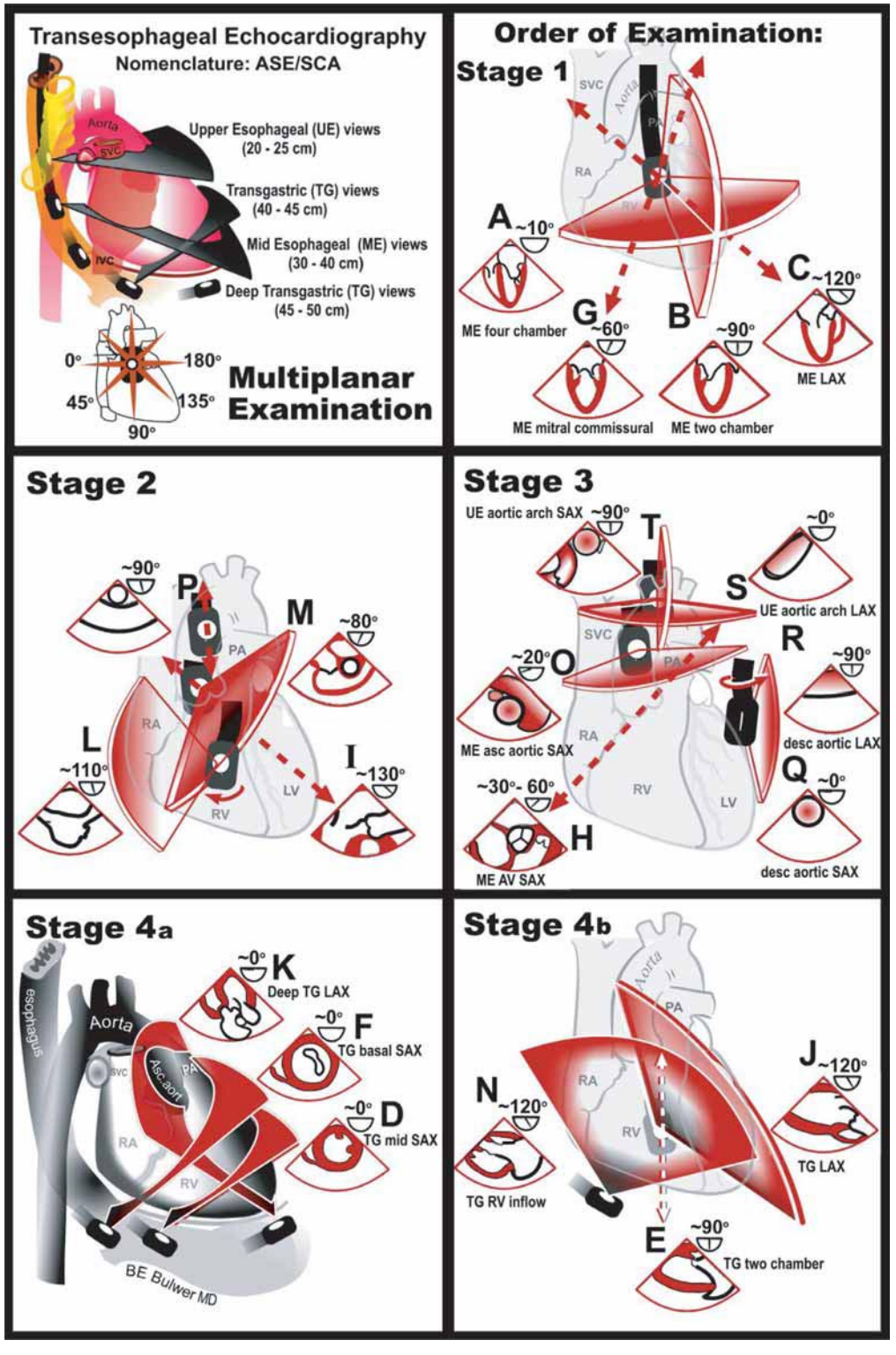

Fig. 7. Anatomic reference scheme and nomenclature adopted by the Society of Echocardiography and the Society of Cardiovascular Anesthesiologists. Variability exists in the precise anatomic relationship between the heart and the esophagus, and the depths at which optimal images are optimally acquired in individual patients, but identifiable anatomic landmarks aid in the reproducibility of images acquired. The terminologies used provide good correlation with images acquired by transthoracic echocardiography, upper esophageal views (20–25 cm), mid-esophageal (ME) views (30–40 cm), transgastric views (40–45 cm), deep transgastric views (45–50 cm).

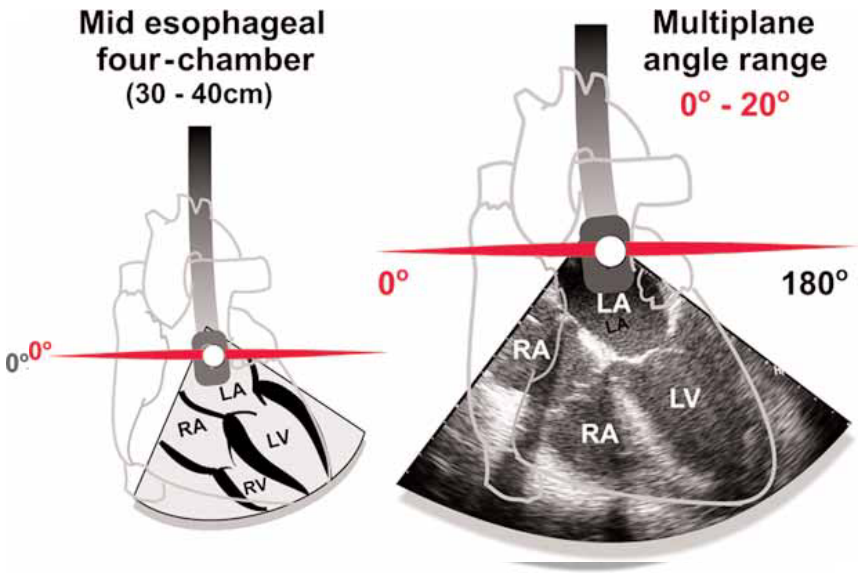

Fig. 8. Midesophageal four-chamber (A). (Please *see* companion DVD for corresponding video.)

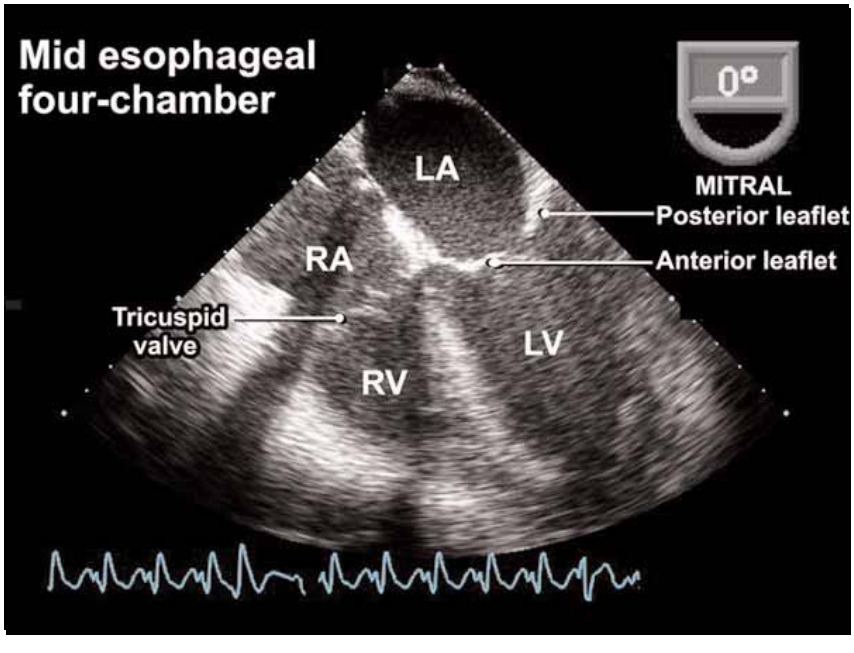

Fig. 9. Midesophageal four-chamber (A).

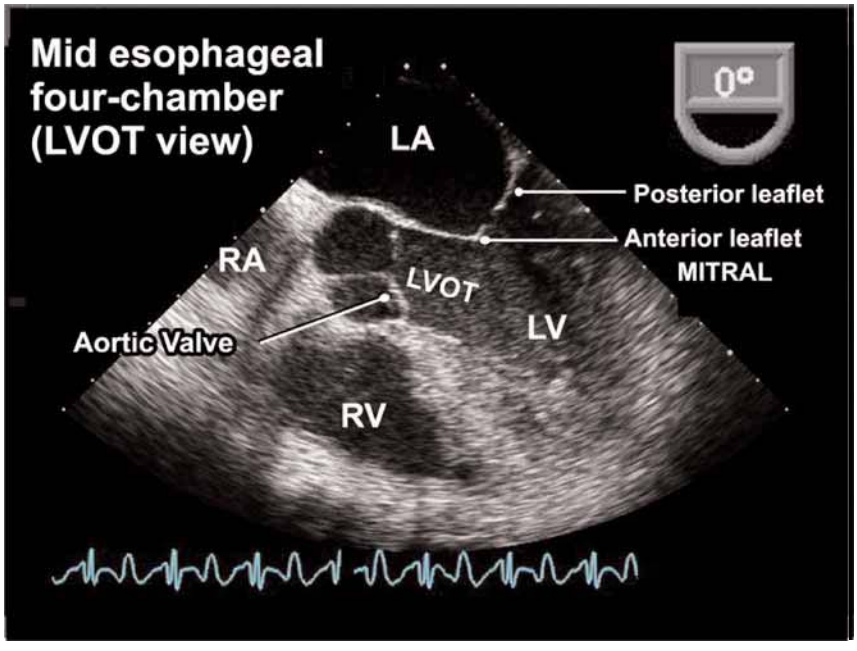

Fig. 10. Midesophageal four-chamber (A). (Please *see* companion DVD for corresponding video.)

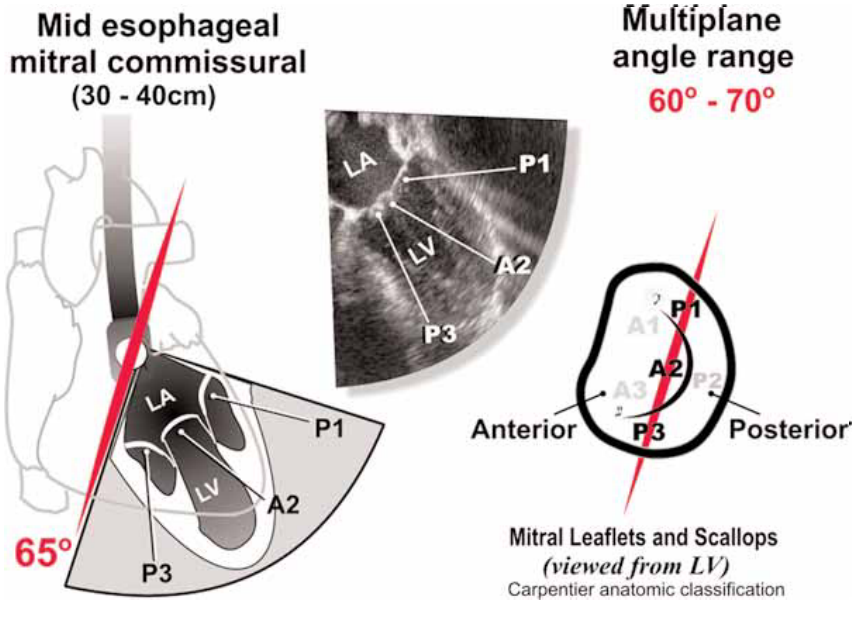

Fig. 11. Midesophageal mitral commissural (G).

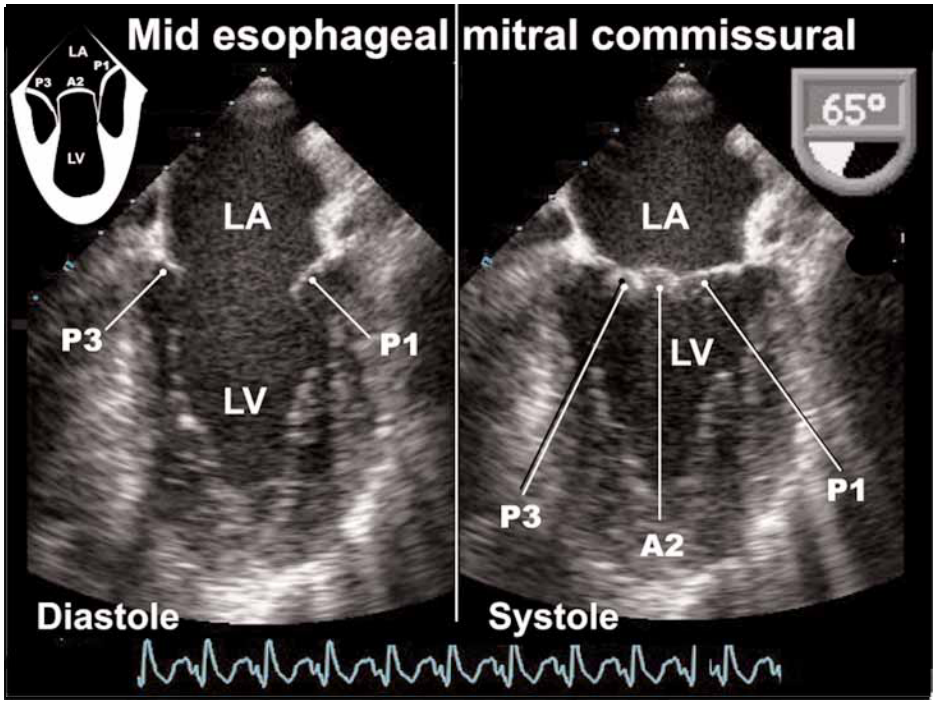

Fig. 12. Midesophageal mitral commissural (G). (Please *see* companion DVD for corresponding video.)

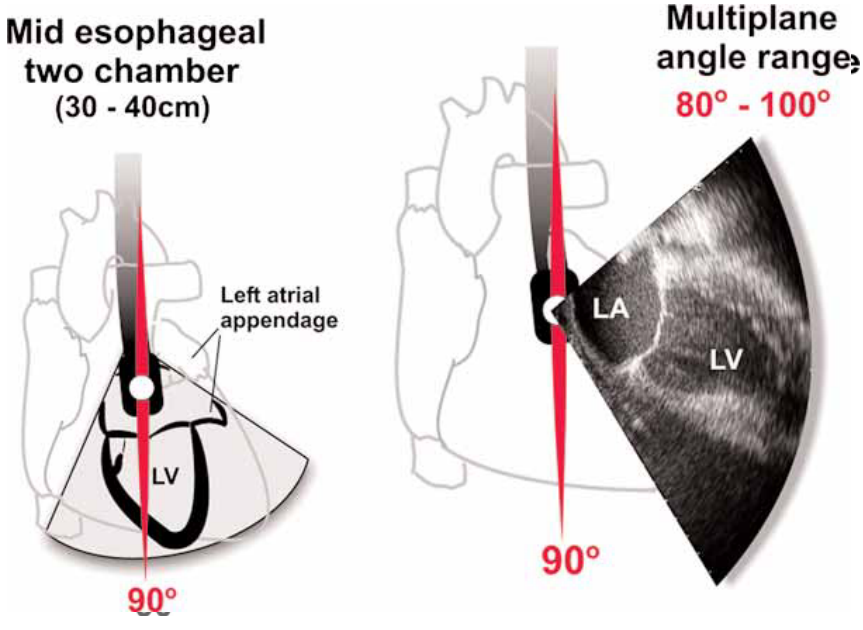

Fig. 13. Midesophageal two-chamber (B).

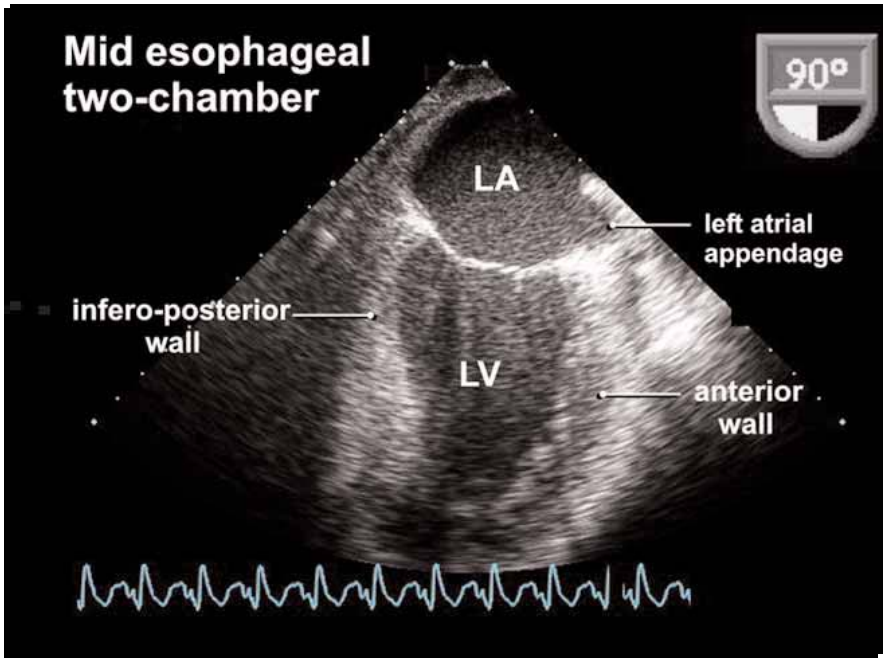

Fig. 14. Midesophageal two-chamber (B). (Please *see* companion DVD for corresponding video.)

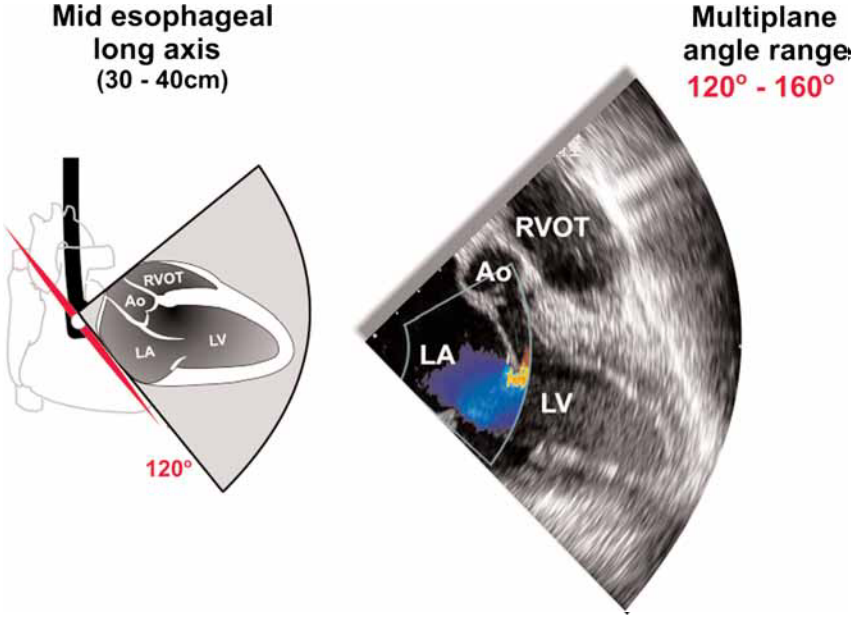

Fig. 15. Midesophageal long axis (C).

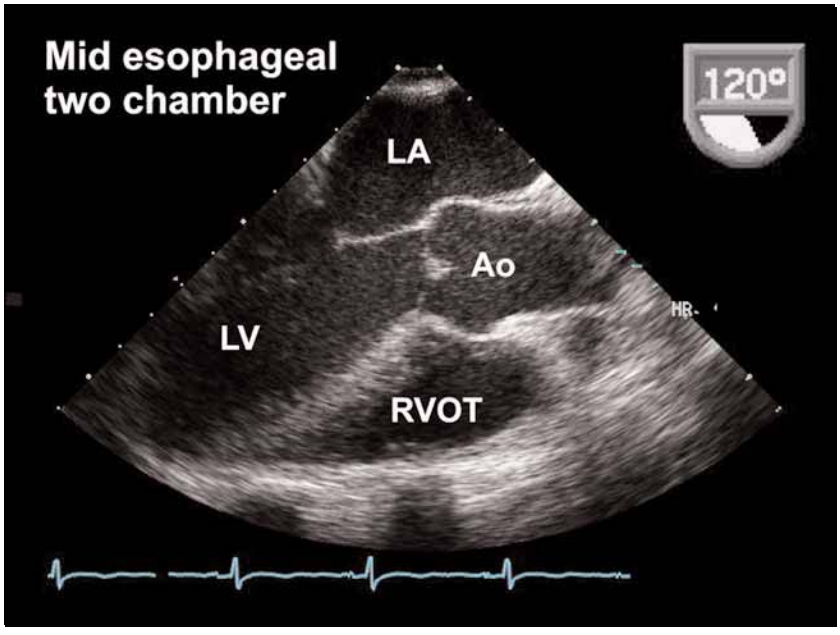

Fig. 16. Midesophageal long axis (C). (Please *see* companion DVD for corresponding video.)

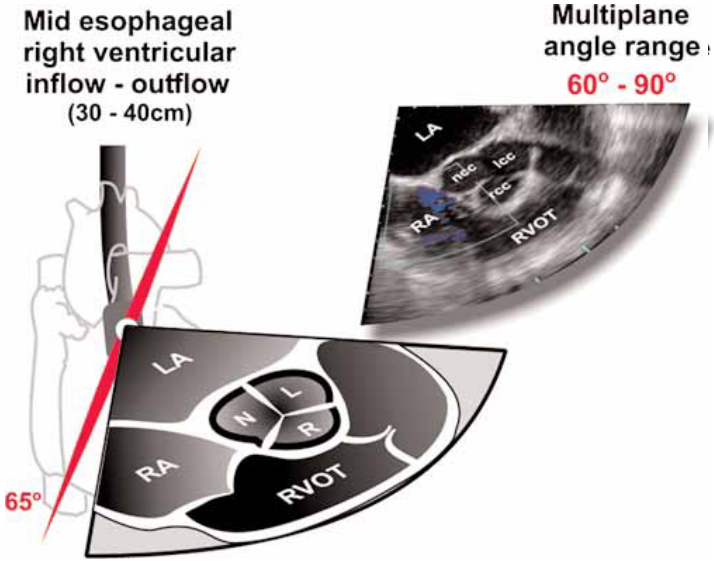

Fig. 17. Midesophageal right ventricular inflow-outflow (M).

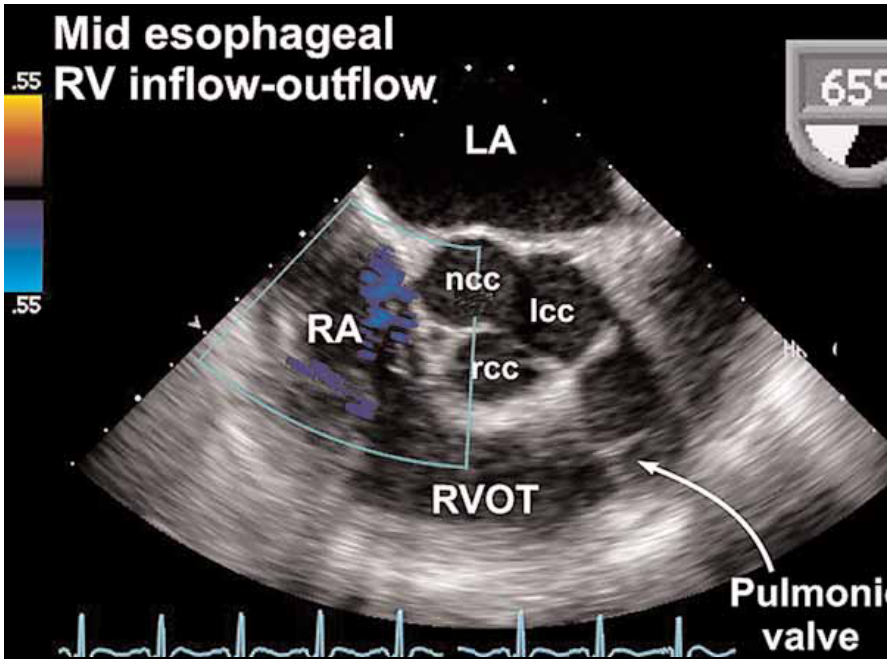

Fig. 18. Midesophageal right ventricular inflow-outflow (M). (Please *see* companion DVD for corresponding video.)

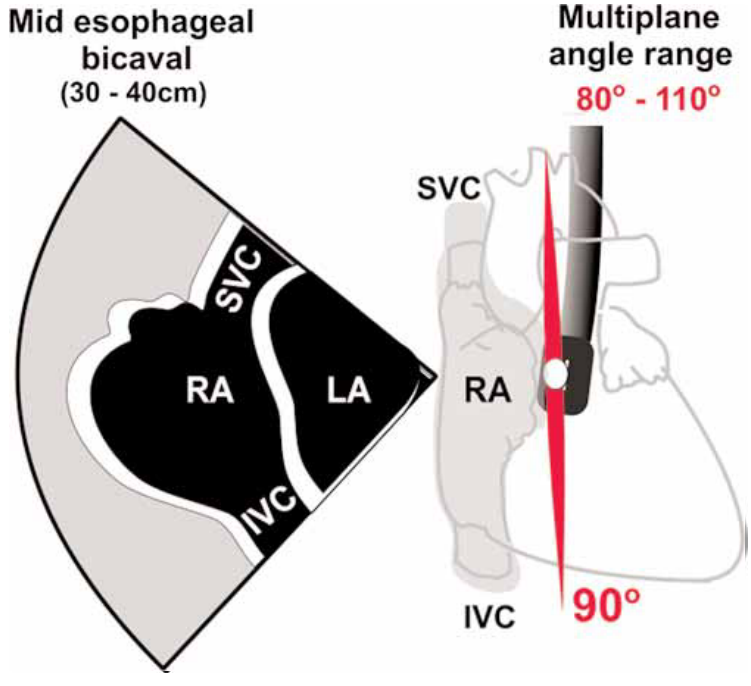

Fig. 19. Midesophageal bicaval (L).

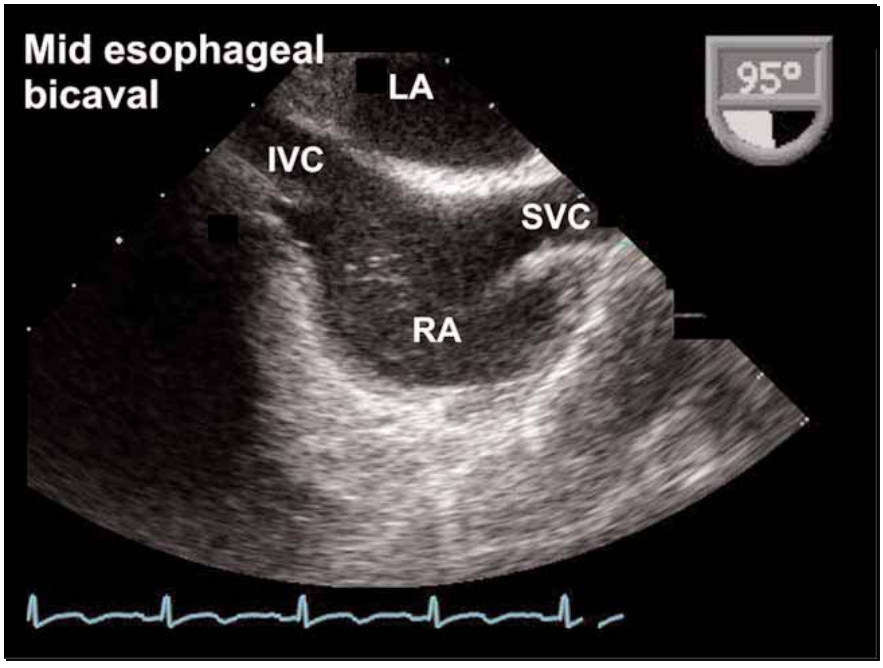

Fig. 20. Midesophageal bicaval (L). (Please *see* companion DVD for corresponding video.)

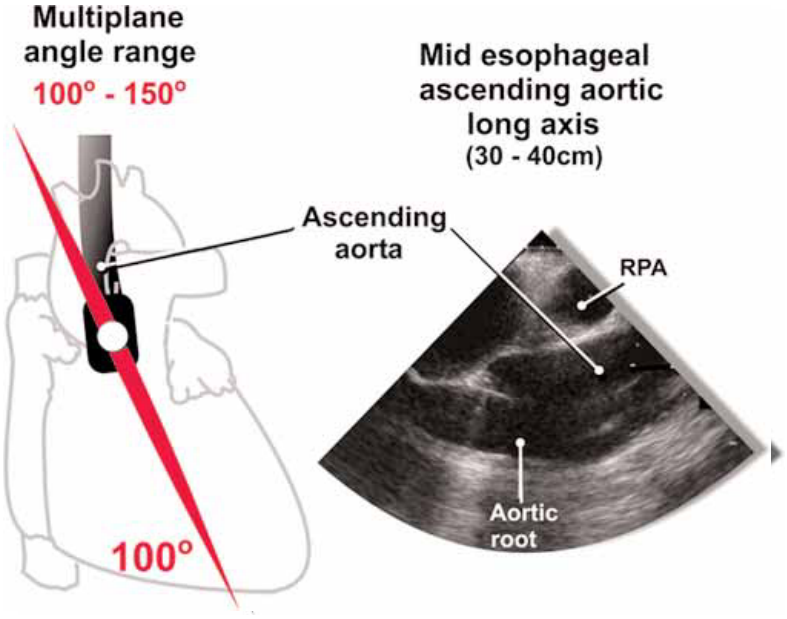

Fig. 21. Midesophageal ascending aortic long axis view (P).

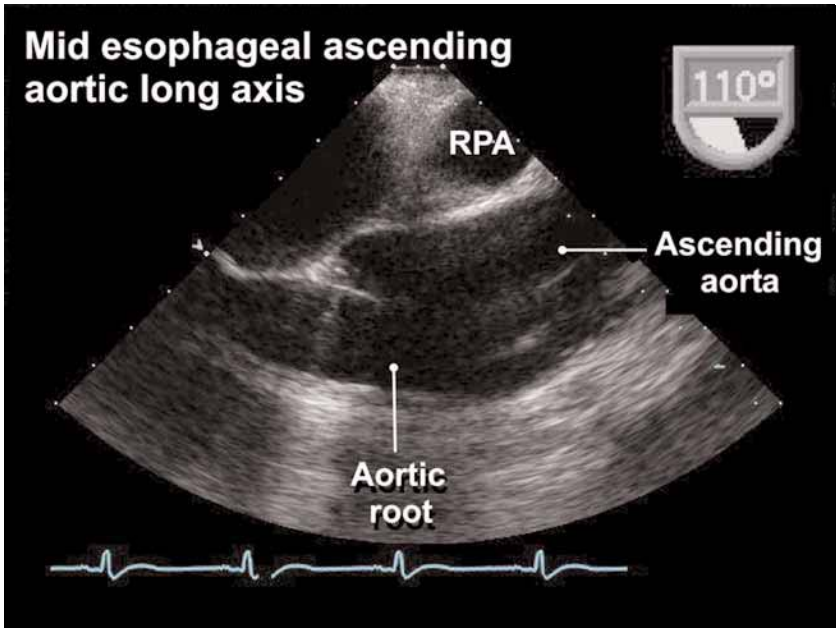

Fig. 22. Midesophageal ascending aortic long axis view (P). (Please *see* companion DVD for corresponding video.)

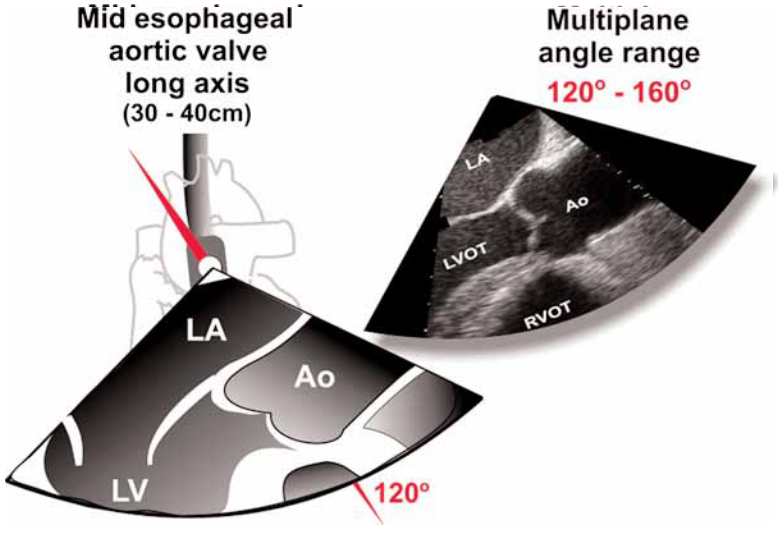

Fig. 23. Midesophageal aortic valve long axis (I).

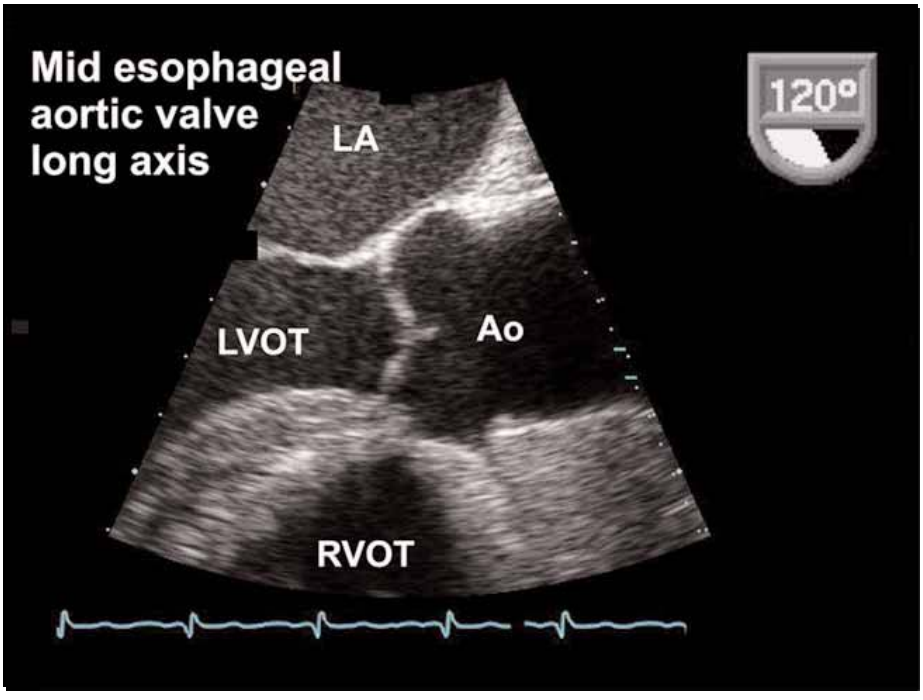

Fig. 24. Midesophageal aortic valve long axis (I). (Please *see* companion DVD for corresponding video.)

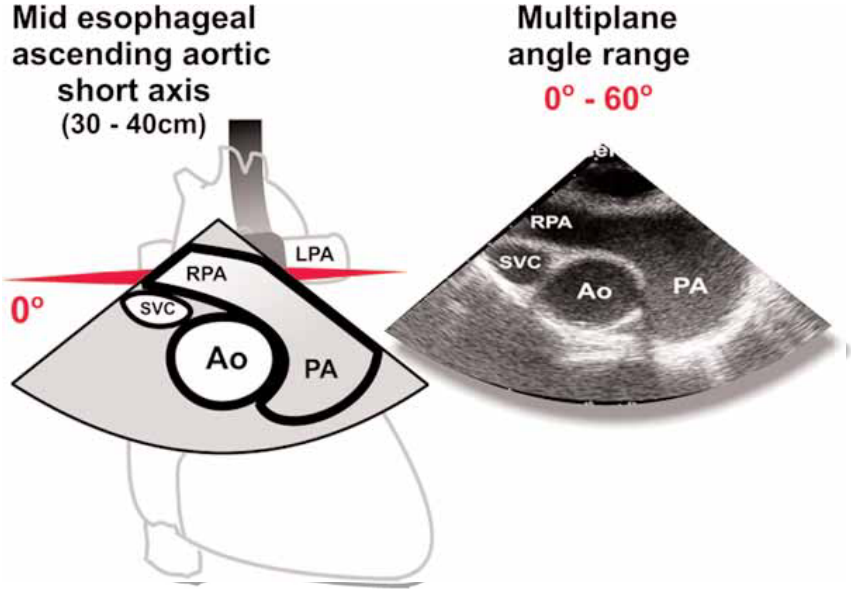

Fig. 25. Midesophageal ascending aortic short axis view (O).

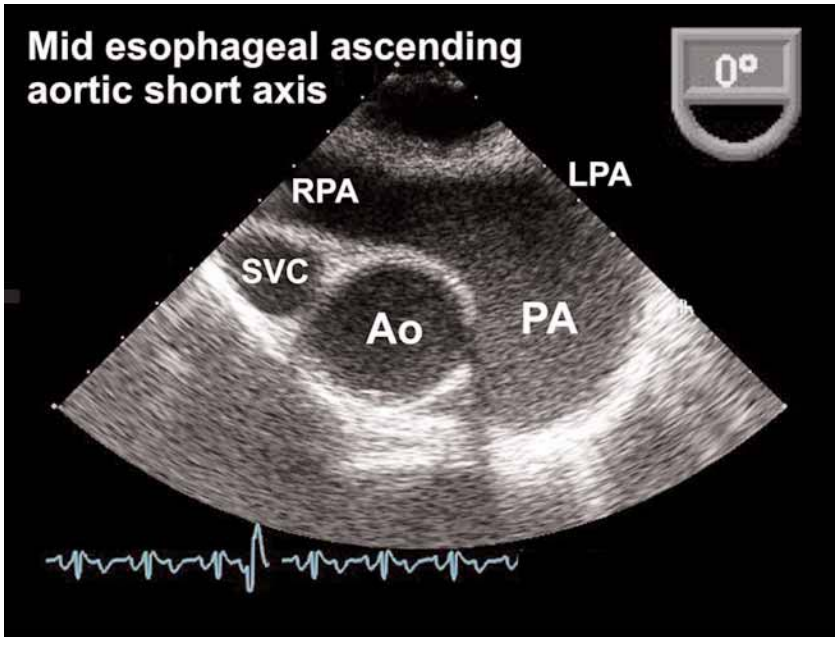

Fig. 26. Midesophageal ascending aortic short axis view (O). (Please *see* companion DVD for corresponding video.)

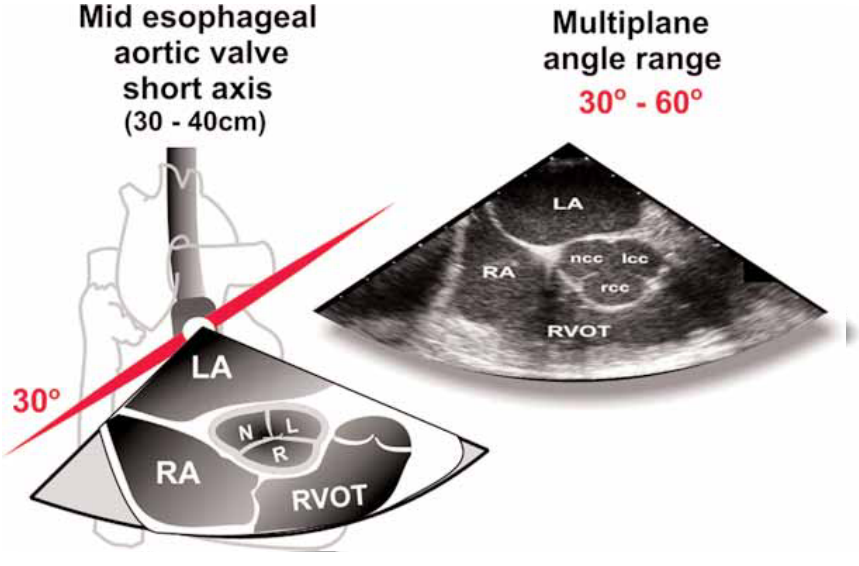

Fig. 27. Midesophageal aortic valve short axis (H).

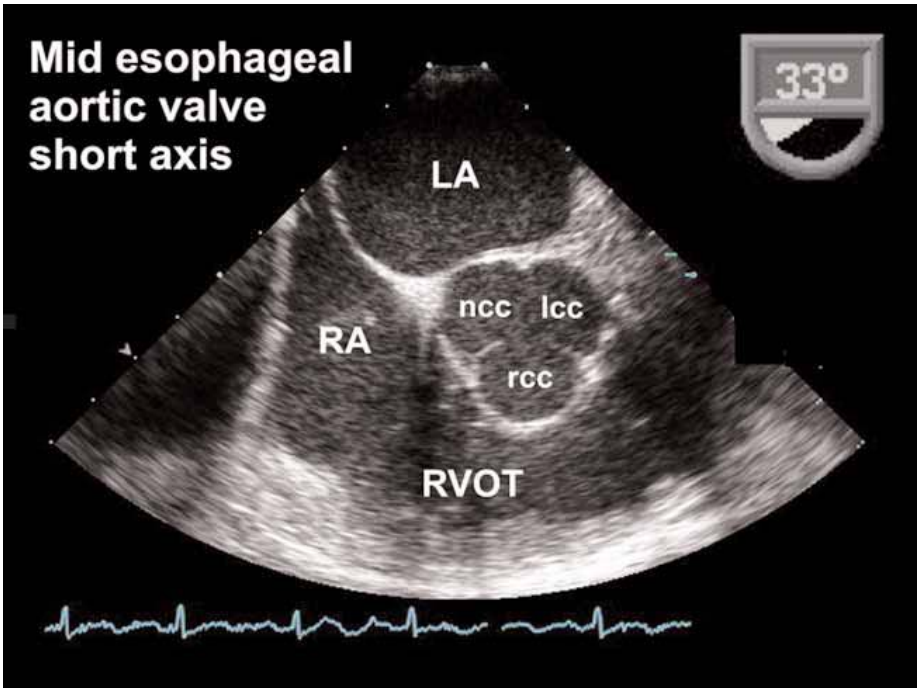

Fig. 28. Midesophageal aortic valve short axis (H). (Please *see* companion DVD for corresponding video.)

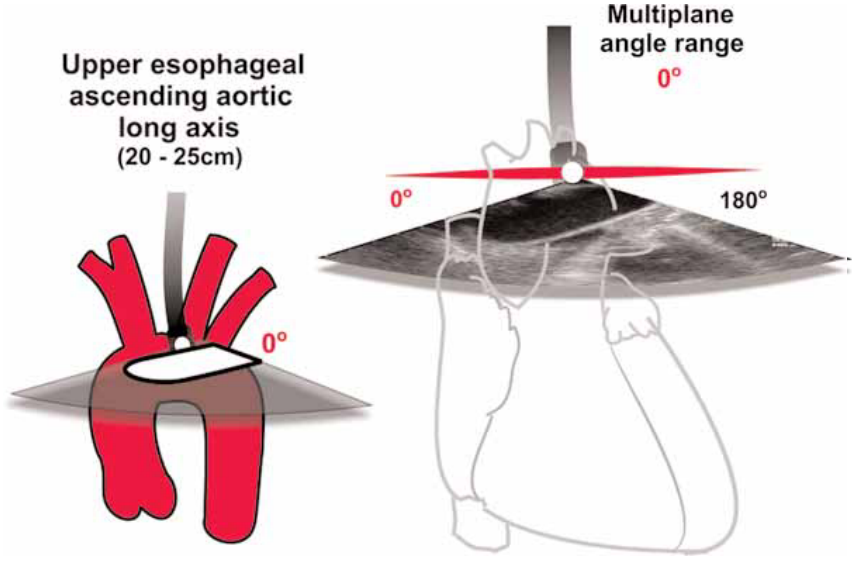

Fig. 29. UE aortic arch long axis (S).

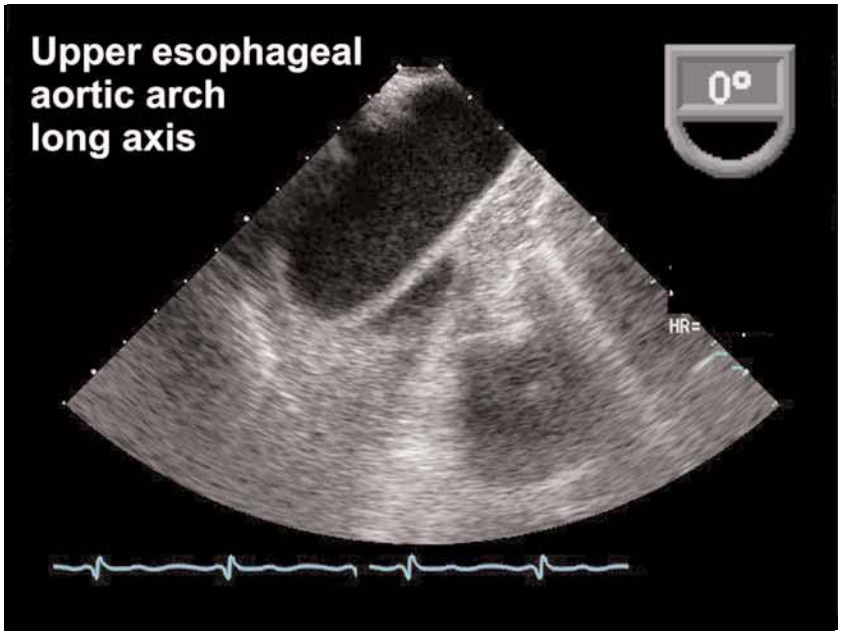

Fig. 30. UE aortic arch long axis (S). (Please *see* companion DVD for corresponding video.)

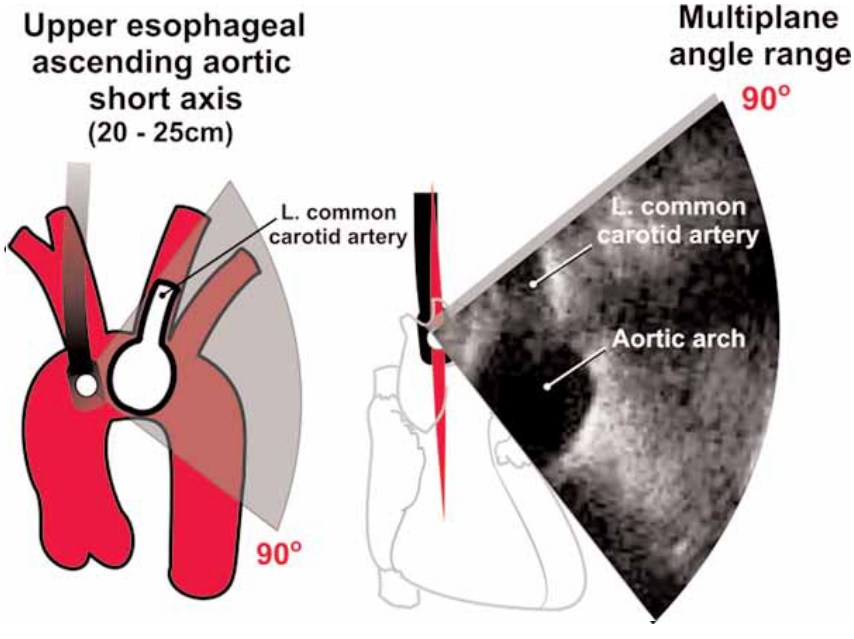

Fig. 31. UE aortic arch short axis (T). (Please *see* companion DVD for corresponding video.)

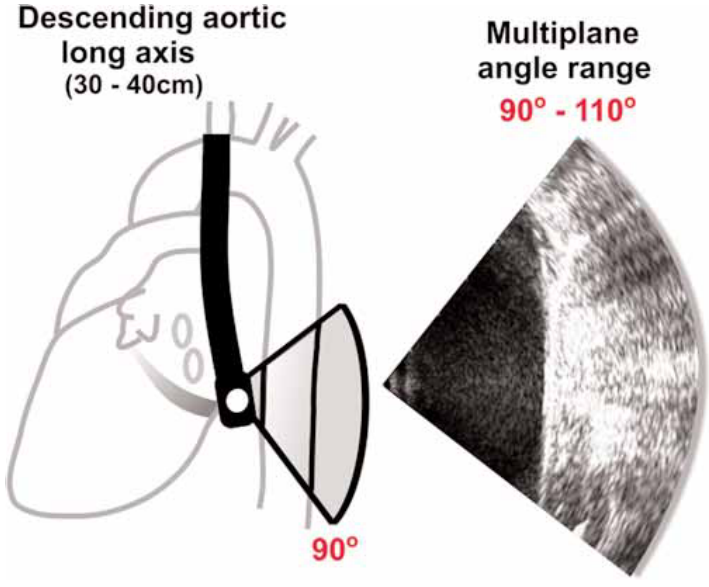

Fig. 32. Descending aortic long axis (R).

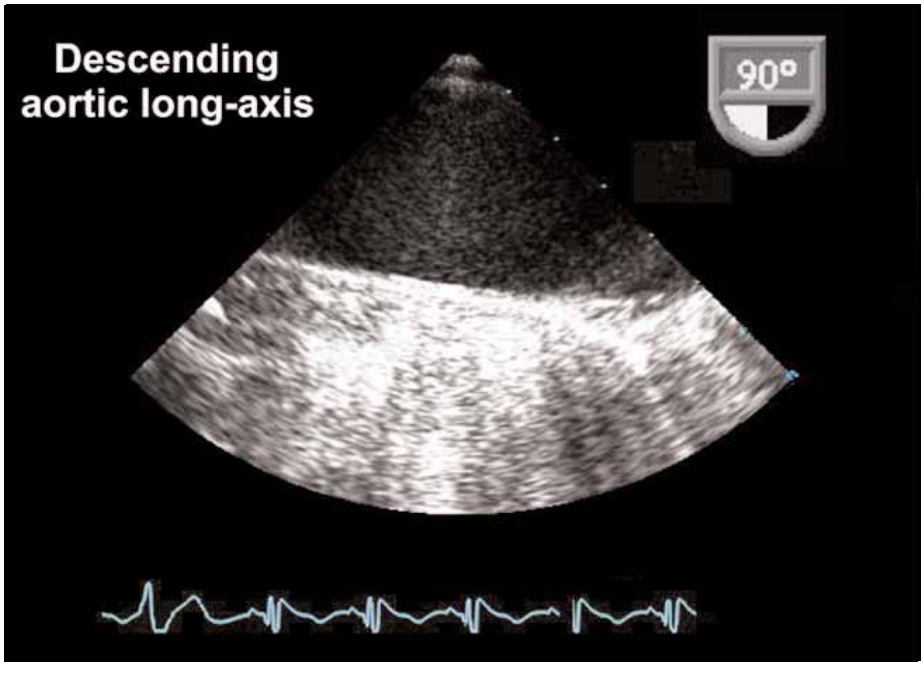

Fig. 33. Descending aortic long axis (R). (Please *see* companion DVD for corresponding video.)

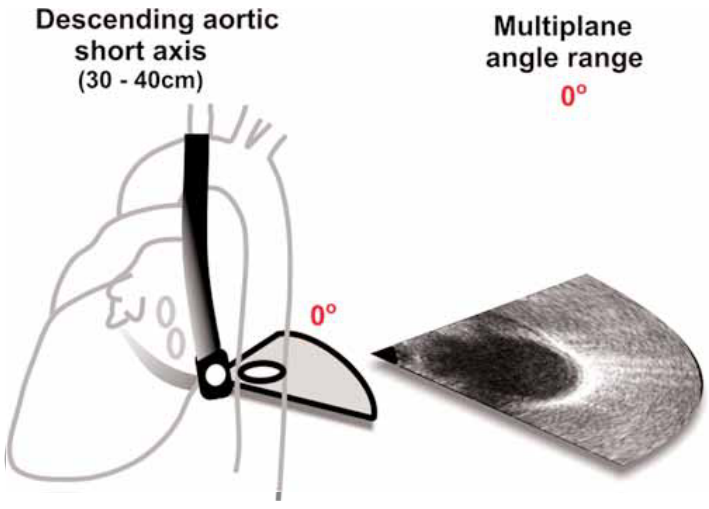

Fig. 34. Descending aortic short axis (Q).

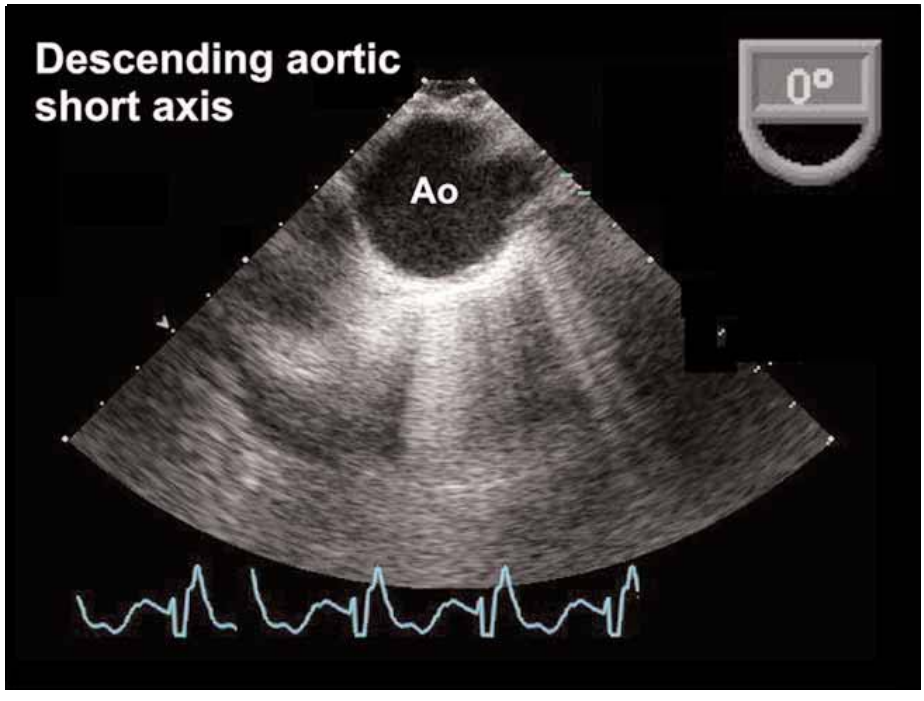

Fig. 35. Descending aortic short axis (Q). (Please *see* companion DVD for corresponding video.)

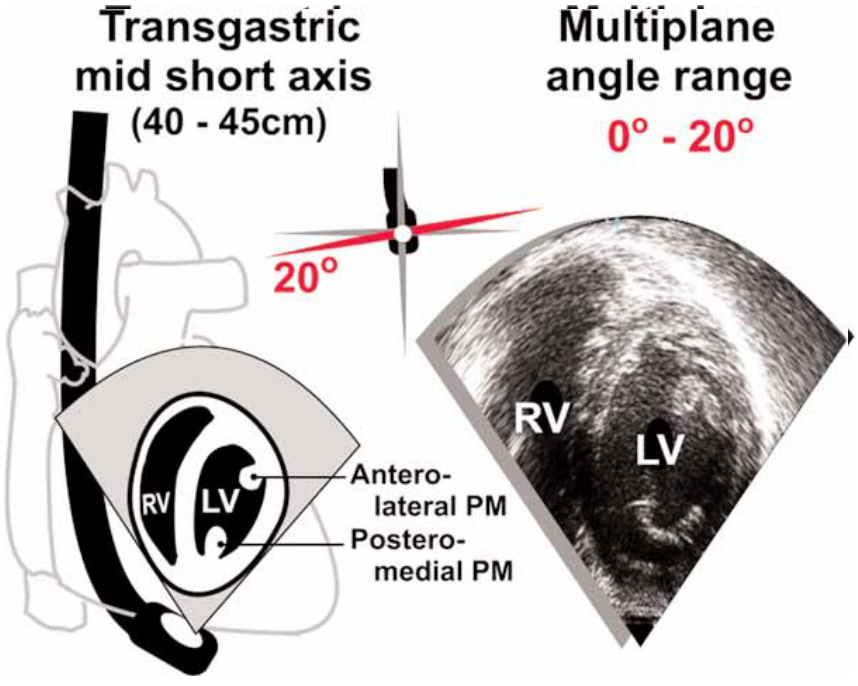

Fig. 36. Transgastric midshort axis (D).

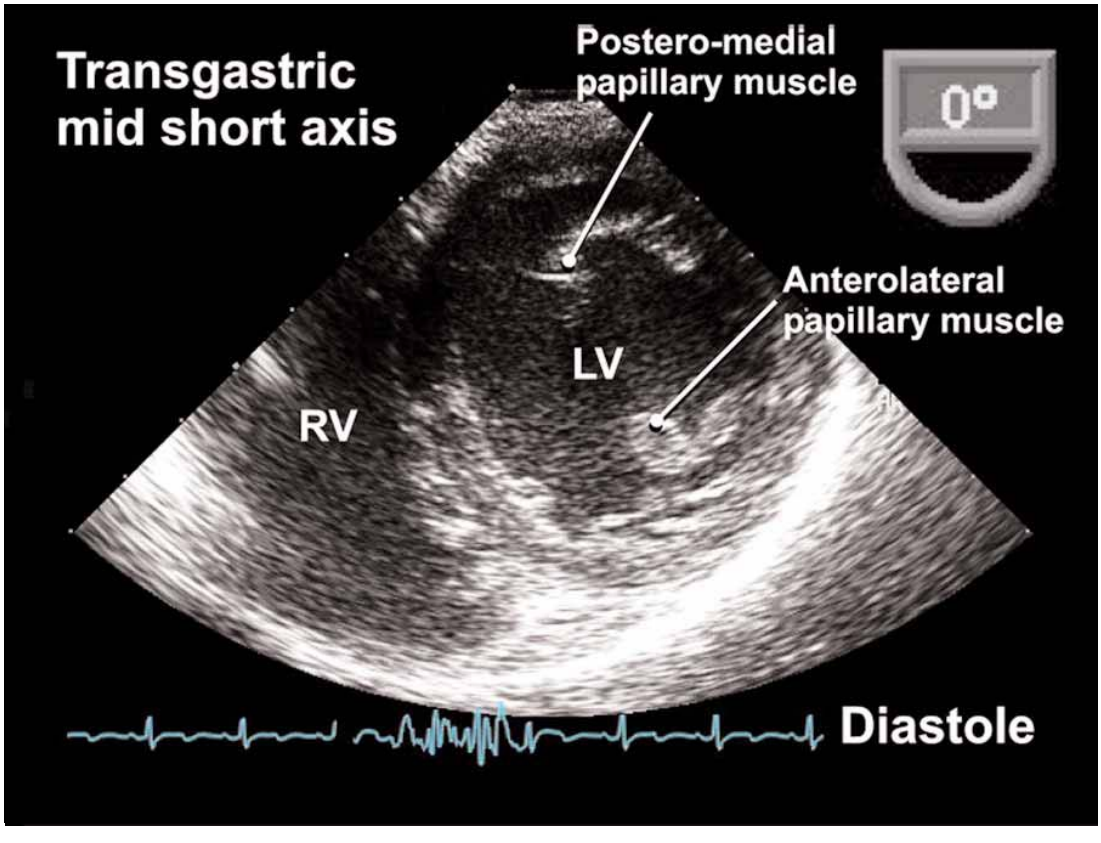

Fig. 37. Transgastric midshort axis (D). (Please *see* companion DVD for corresponding video.)

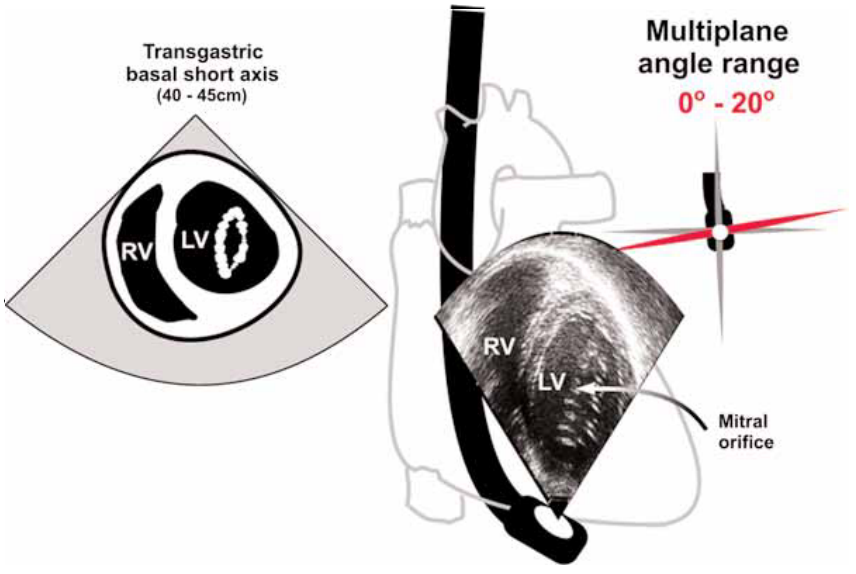

Fig. 38. Transgastric basal short axis (F).

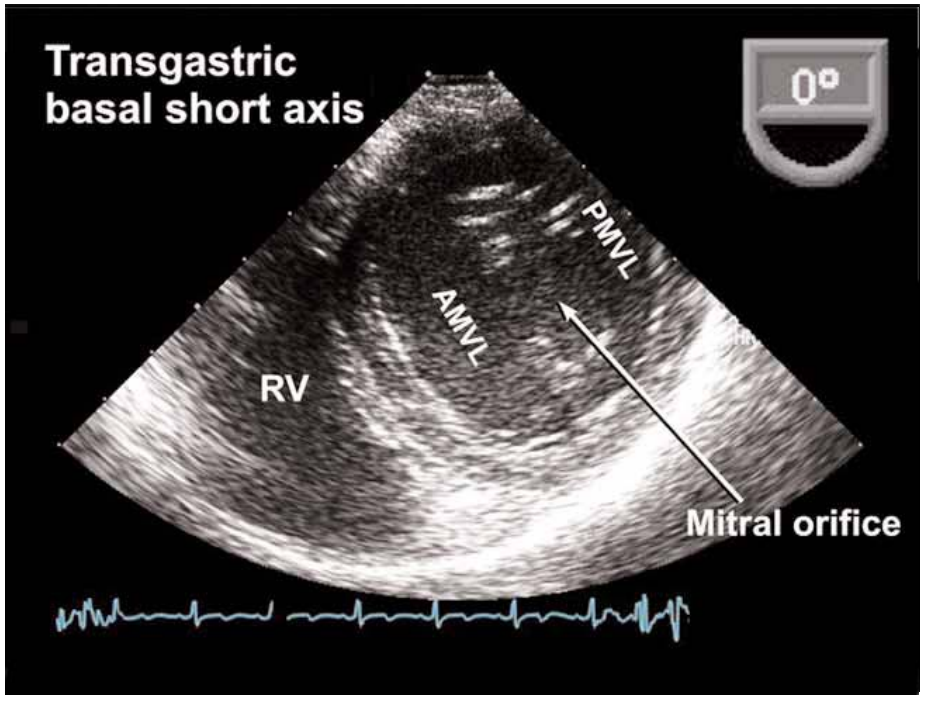

Fig. 39. Transgastric basal short axis (F). (Please *see* companion DVD for corresponding video.)

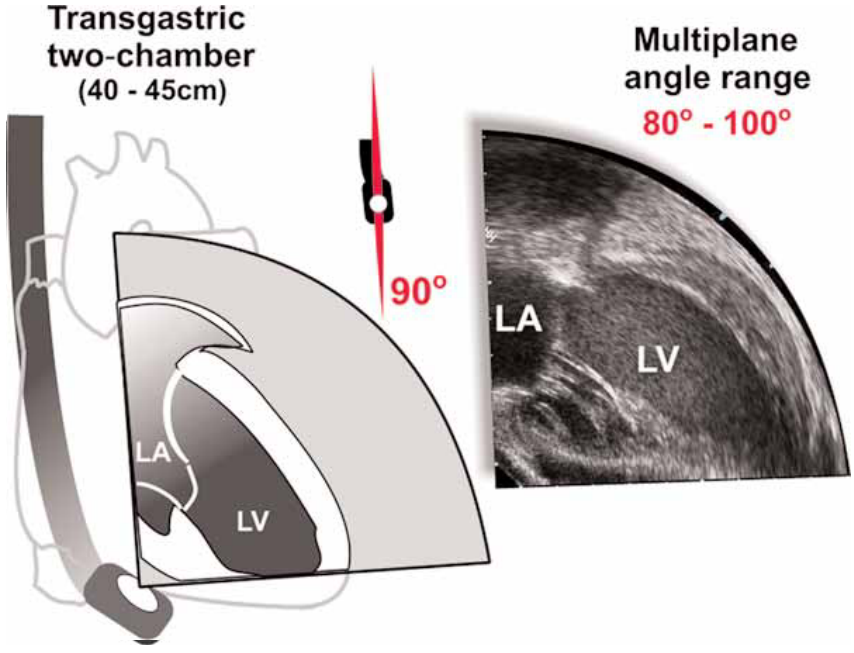

Fig. 40. Transgastric two-chamber (E).

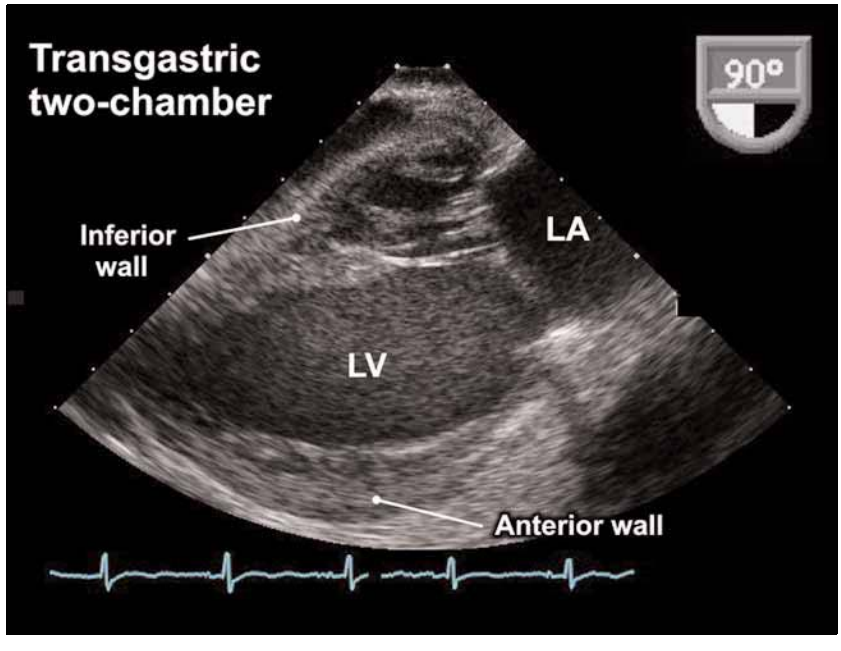

Fig. 41. Transgastric two-chamber (E). (Please *see* companion DVD for corresponding video.)

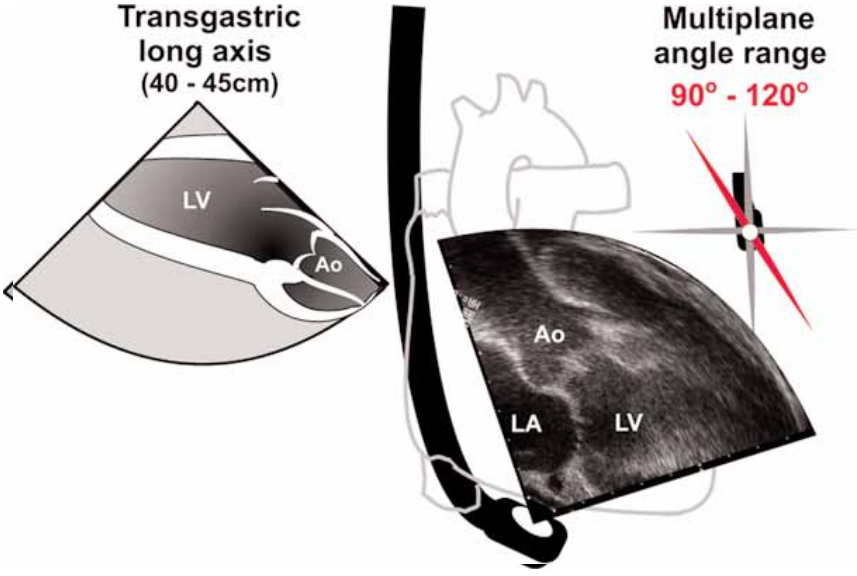

Fig. 42. Transgastric long axis (J).

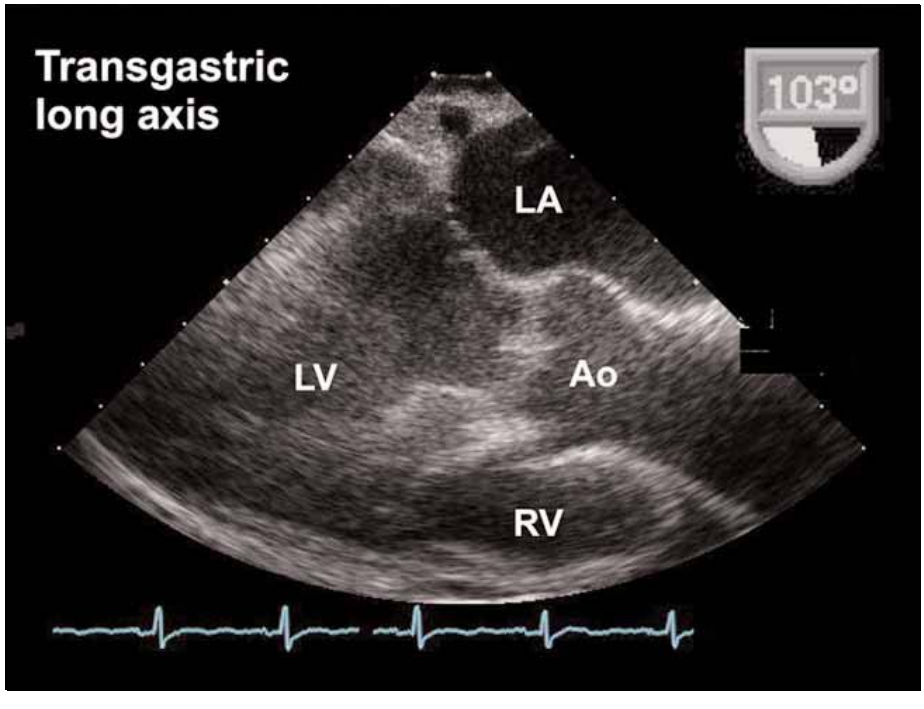

Fig. 43. Transgastric long axis (J).

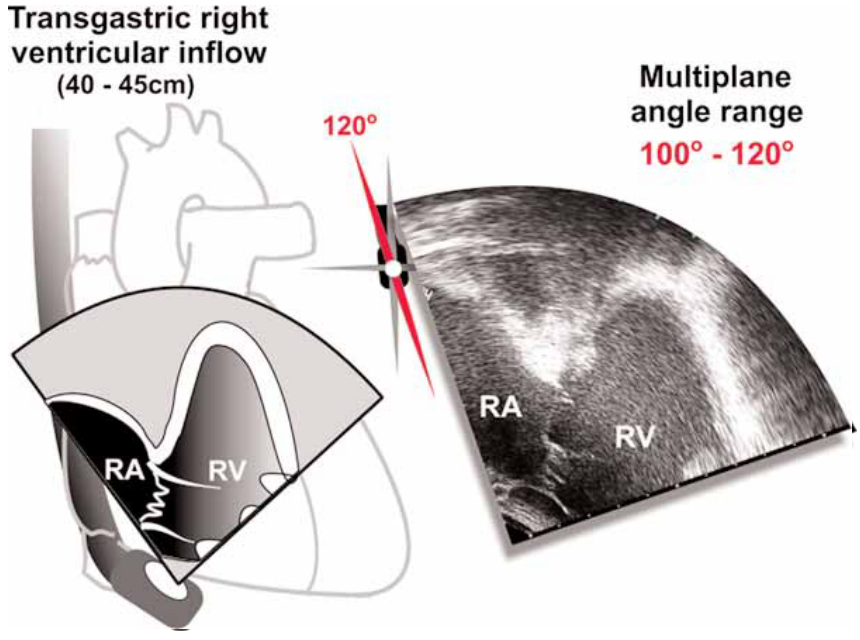

Fig. 44. Transgastric right ventricular inflow (N).

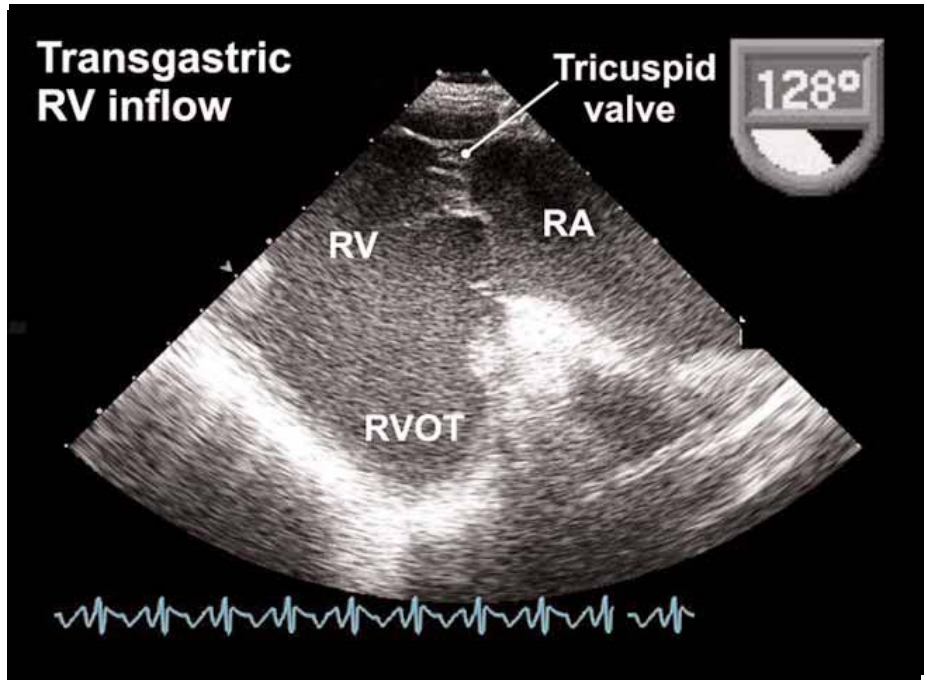

Fig. 45. Transgastric right ventricular inflow (N). (Please *see* companion DVD for corresponding video.)

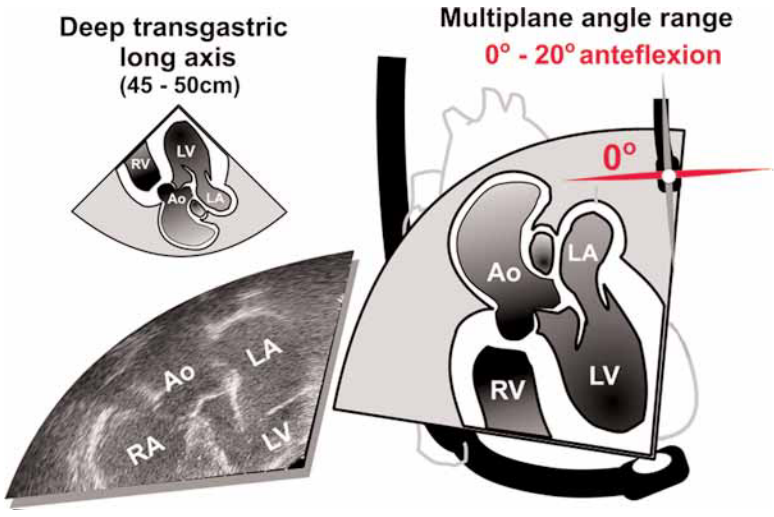

Fig. 46. Deep transgastric long axis (K). (Please *see* companion DVD for corresponding video.)

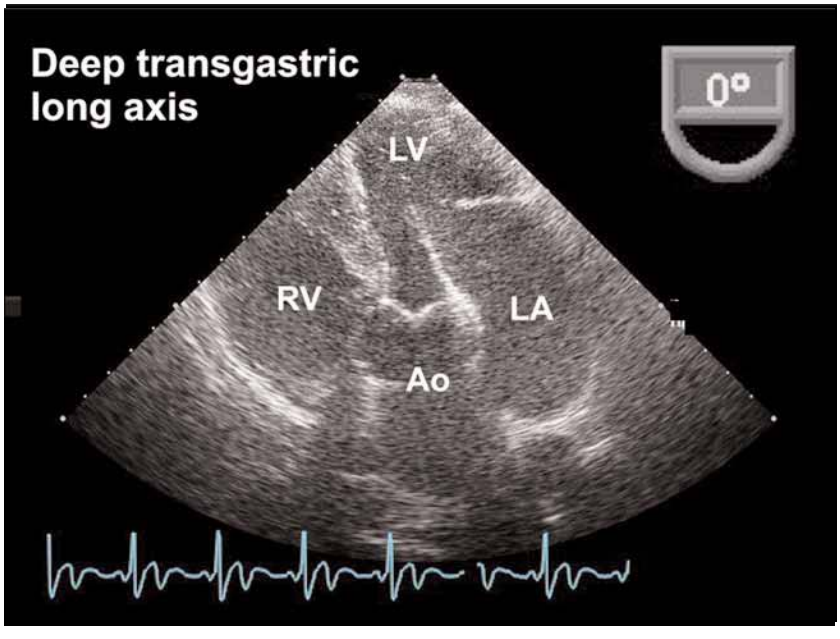

Fig. 47. Deep transgastric long axis (K).

ORDER OF EXAMINATION: STAGE 1

ME level: multiplane from 0 to approx 120°.

- ME four-chamber 15° (A).
- ME mitral commissural 60° (G).
- ME two-chamber 90° (B).
- ME long axis120° (C).

ME four-chamber (A): Figs. 8–10 (please *see* companion DVD for corresponding video for Figs. 8 and 10).

- Multiplane to 15°.
- Inferior septum and lateral wall of left ventricle (LV).
- Right ventricular size and function.
- Atrial size and interatrial septum.
- Withdraw TEE probe "and turn leftward" for visualization of appendage.
- Mitral valve (MV) scallops: A1, P1 (*see* Chapter 14, Figs. 1, 2, 36).
- Color flow Doppler to tricuspid valve.
- Pulsed-wave Doppler to MV to assess LV inflow.

ME mitral commissural 80°(G): Figs. 11 and 12.

- Multiplane 60°.
- MV examination:
- Anterolateral and posteromedial MV commissures.
- Lateral (P1), middle (A2), and medial (P3) scallops of both anterior (A) and posterior (P) leaflets (*see* Chapter 14, Figs. 1, 2, and 36).
- CFD to MV.

ME two-chamber 90° (B): Figs. 13 and 14.

- Multiplane 90°.
- LV function, inferior and anterior walls.
- LA, LAA, and left upper pulmonary vein.
- Color flow Doppler to MV (R to L = A2, P3).
- Continuous-wave (CW) Doppler to LV (A, S, D waves).

ME long axis 120° (C): Figs. 15 and 16.

- Multiplane120°.
- AV and proximal ascending aorta.
- LV anterior septum and posterior wall.
- Color flow Doppler to mitral and AVs.

ORDER OF EXAMINATION: STAGE 2

ME level: with angle approx 90°, sweep R to L.

- ME level: with angle ~90°, sweep R to L.
- ME right ventricular inflow-outflow 80° (M): Figs. 17 and 18 (please *see* companion DVD for corresponding video for Fig. 18).
- ME bicaval 110° (L): Figs. 19 and 20.
- Withdraw: ME ascending aortic long axis 100° (P): Figs. 21 and 22 (please *see* companion DVD for corresponding video for Fig. 22).
- Advance: ME aortic long axis 130° (I): Figs. 23 and 24 (please *see* companion DVD for corresponding video for Fig. 24).

ME Right ventricular inflow-outflow (M): Figs. 17 and 18 (please *see* companion DVD for corresponding video for Fig. 18).

- Multiplane 80°.
- Tricuspid valve, right ventricular outflow, pulmonic valve.
- Color flow Doppler to tricuspid and pulmonic valves.
- CW Doppler for tricuspid regurgitation.

ME bicaval (L): Figs. 19 and 20.

- 110°.
- Turn TEE probe to the right.
- Check for patent foramen ovale using color flow Doppler.
- Check for secundum and sinus venous atrial septal defects.
- Superior vena cava, inferior vena cava, eustachian valve (Chiari) remnants.

ME Ascending aortic long axis view (P): Figs. 21 and 22 (please *see* companion DVD for corresponding video for Fig. 22).

- Multiplane 100°.
- Evaluate for aortic atheroma, dissection, or thrombus.
- Right pulmonary artery as it crosses behind the ascending aorta on its way to the right lung.

ME aortic valve long axis (I): Figs. 23 and 24 (please *see* companion DVD for corresponding video for Fig. 24).

ORDER OF EXAMINATION: STAGE 3

Start at 0–20°.

- ME ascending aortic short axis 20° (O): Figs. 25 and 26 (please *see* companion DVD for corresponding video for Fig. 26).
- Withdraw: ME AV short axis 60° (H): Figs. 27 and 28 (please *see* companion DVD for corresponding video for Fig. 28).

- UE aortic arch long axis 0° (S): Figs. 29 and 30 (please *see* companion DVD for corresponding video for Fig. 30).
- UE aortic arch short axis 90° (T): Fig. 31 (please *see* companion DVD for corresponding video).
- Turn left, advance: descending aortic long axis 90° (R): Figs. 32 and 33 (please *see* companion DVD for corresponding video for Fig. 33).
- Descending aortic short axis 0° (Q): Figs. 34 and 35 (please *see* companion DVD for corresponding video for Fig. 35).

ME ascending aortic short-axis view (O): Figs. 25 and 26 (please *see* companion DVD for corresponding video for Fig. 26).

- Multiplane 20°.
- Evaluate aorta for atheromatous change, aortic dissection, or thrombus.
- Pulmonary artery bifurcation.

ME aortic valve short axis (H): Figs. 27 and 28 (please *see* companion DVD for corresponding video for Fig. 28).

- Multiplane 60°.
- Evaluate AV and aortic cusps.
- Color flow Doppler to AV.
- Evaluate LAA.
- Evaluate coronary arteries and flow: left main and right coronary artery.

UE aortic arch long axis (S): Figs. 29 and 30 (please *see* companion DVD for corresponding video for Fig. 30).

- Multiplane 0°.
- Evaluate aortic arch for atheromatous change, dissection, or thrombus.

UE aortic arch short axis (T): Fig. 31 (please *see* companion DVD for corresponding video).

- Multiplane 90°.
- Evaluate aortic arch atheromatous change, dissection, thrombus.
- Evaluate origin of great vessel(s) for atheroma or dissection.

Descending aortic long axis (R): Figs. 32 and 33 (please *see* companion DVD for corresponding video for Fig. 33).

- Multiplane 90°.
- Evaluate aorta for atheromatous change, dissection, or thrombus.

Descending aortic short axis (Q): Figs. 34 and 35 (please *see* companion DVD for corresponding video for Fig. 35).

- Multiplane 0°.
- Evaluate aorta for atheromatous change, dissection, or thrombus.

ORDER OF EXAMINATION: STAGE 4

Advance to stomach, anteflex.

- Transgastric midshort axis 0° (D): Figs. 36 and 37 (please *see* companion DVD for corresponding video for Fig. 37).
- Withdraw slightly: transgastric basal short axis 0° (F): Figs. 38 and 39 (please *see* companion DVD for corresponding video for Fig. 39).
- Transgastric two-chamber 90° (E): Figs. 40 and 41 (please *see* companion DVD for corresponding video for Fig. 41).
- 90–120°: transgastric long axis 120° (J): Figs. 42 and 43.
- Turn right: transgastric right ventricular inflow 120° (N): Figs. 44 and 45 (please *see* companion DVD for corresponding video for Fig. 45).
- Advance, anteflex: deep transgastric long axis 0° (K): Figs. 46 and 47 (please *see* companion DVD for corresponding video for Fig. 46).

Transgastric mid-short axis (D): Figs. 36 and 37 (please *see* companion DVD for corresponding video for Fig. 37).

- Multiplane 0°.
- Assess wall motion and thickening.
- Assess left and right ventricular size, wall thickness, and function.

Transgastric basal short axis (F): Figs. 38 and 39 (please *see* companion DVD for corresponding video-for Fig. 39).

- Mutiplane 0°.
- Assess MV function and anterior and posterior mitral leaflets.

Transgastric two chamber (E): Figs. 40 and 41 (please *see* companion DVD for corresponding video for Fig. 41).

- Multiplane 90°.

- Color flow Doppler to the MV.
- Assess anterior and inferior LV wall.

Transgastric long axis (J): Figs. 42 and 43.

- Multiplane 120°.
- CW to the AV with velocity time integral.

Transgastric right ventricular inflow (N): Figs. 44 and 45 (please *see* companion DVD for corresponding video for Fig. 45).

- Multipla'ne at 100–120° when indicated.

K. deep transgastric long axis: Figs. 46 and 47 (please *see* companion DVD for corresponding video for Fig. 46).

- Multiplane 0°.
- Aortic flow, including CW Doppler to AV with AV velocity time integral.

ACKNOWLEDGMENT

The anatomic reference scheme and nomenclature used in this chapter was adapted from the Suggested Reading reference.

SUGGESTED READING

Shanewise JS, Cheung AT, Aronson S, et al. ASE/SCA guidelines for performing a comprehensive intraoperative multiplane transesophageal echocardiography examination: recommendations of the American Society of Echocardiography Council for Intraoperative Echocardio- graphy and the Society of Cardiovascular Anesthesiologists Task Force for Certification in Perioperative Transesophageal Echocardiography. J Am Soc Echocardiogr 1999;12: 884–900.

IV Appendix

Reference Values

Recommendations for Chamber Qualification

CONTENTS

From: *Contemporary Cardiology: Essential Echocardiography: A Practical Handbook With DVD*
Edited by: S. D. Solomon © Humana Press, Totowa, NJ

Table A1

Reference Limits and Partition Values of Left Ventricular Mass and Geometry

	Women				*Men*			
	Reference range	*Mildly abnormal*	*Moderately abnormal*	*Severely abnormal*	*Reference range*	*Mildly abnormal*	*Moderately abnormal*	*Severely abnormal*
				Linear method				
LV mass (g)	67–162	163–186	187–210	≥211	88–224	225–258	259–292	≥293
LV mass/BSA(g/m²)	***43–95***	***96–108***	***109–121***	***≥122***	***49–115***	***116–131***	***132–148***	***≥149***
LV mass/height (g/m)	41–99	100–115	116–128	≥129	52–126	127–144	145–162	≥163
LV mass/height (g/m)	18–44	45–51	52–58	≥59	20–48	49–55	56–63	≥64
Relative wall thickness (cm)	0.22–0.42	0.43–0.47	0.48–0.52	≥0.53	0.24–0.42	0.43–0.46	0.47–0.51	≥0.52
Septal Thickness (cm)	***0.6–0.9***	***1.0–1.2***	***1.3–1.5***	***≥1.6***	***0.6–1.0***	***1.1–1.3***	***1.4–1.6***	***≥1.7***
Posterior Wall Thickness (cm)	***0.6–0.9***	***1.0–1.2***	***1.3–1.5***	***≥1.6***	***0.6–1.0***	***1.1–1.3***	***1.4–1.6***	***≥1.7***
				2D Method				
LV mass (g)	66–150	151–171	172–182	≥193	96–200	201–227	228–254	≥255
LV mass/BSA (g/m²)	***44–88***	***89–100***	***101–112***	***≥113***	***50–102***	***103–116***	***117–130***	***≥131***

Bold italic values: recommended and best validated. (Adapted from ref. *1*.)

Table A2

Reference Limits and Partition Values of Left Ventricular Size

	Women				*Men*			
	Reference range	*Mildly abnormal*	*Moderately abnormal*	*Severely abnormal*	*Reference range*	*Mildly abnormal*	*Moderately abnormal*	*Severely abnormal*
				LV dimension				
LV diastolic diameter	3.9–5.3	5.4–5.7	5.8–6.1	≥6.2	4.2–5.9	6.0–6.3	6.4–6.8	≥6.9
LV diastolic diameter/BSA (cm/m²)	2.4–3.2	3.3–3.4	3.5–3.7	≥3.8	2.2–3.1	3.2–3.4	3.5–3.6	≥3.7
LV diastolic diameter/height (cm/m)	2.5–3.2	3.3–3.4	3.5–3.6	≥3.7	2.4–3.3	3.4–3.5	3.6–3.7	≥3.8
				LV volume				
LV diastolic volume (mL)	56–104	105–117	118–130	≥131	67–155	156–178	179–201	≥201
LV diastolic volume/BSA (mL/m²)	***35–75***	***76–86***	***87–96***	***≥97***	***35–75***	***76–86***	***87–96***	***≥97***
LV systolic volume (mL)	19–49	50–59	60–69	≥70	22–58	59–70	71–82	≥83
LV systolic volume/BSA (mL/m²)	***12–30***	***31–36***	***37–42***	***≥43***	***12–30***	***31–36***	***37–42***	***≥43***

Bold italic values: recommended and best validated. (Adapted from ref. *1*.)

Table A3

Reference Limits and Values and Partition Values of Left Ventricular Function

	Women				*Men*			
	Reference range	*Mildly abnormal*	*Moderately abnormal*	*Severely abnormal*	*Reference range*	*Mildly abnormal*	*Moderately abnormal*	*Severely abnormal*
				Linear method				
Endocardial Fractional Shortening (%)	27–45	22–26	17–21	≤16	25–43	20–24	15–19	≤14
Midwall Fractional Shortening (%)	15–23	13–14	11–12	≤10	14–22	12–13	10–11	≤10
				2D method				
Ejection fraction (%)	***≥55***	***45–54***	***30–44***	***<30***	***≥55***	***45–54***	***30–44***	***<30***

Bold italic values: recommended and best validated. (Adapted from ref. *1*.)

Table A4

Reference Limits and Partition Values of Right Ventricular and Pulmonary Artery Size

	Reference range	*Mildly abnormal*	*Moderately abnormal*	*Severely abnormal*
		RV Dimensions (cm)		
Basal RV diameter (RVD no. 1)	2.0–2.8	2.9–3.3	3.4–3.8	≥3.9
Mid RV diameter (RVD no. 2)	2.7–3.3	3.4–3.7	3.8–4.1	≥4.2
Base-to-Apex Length (RVD no. 3)	7.1–7.9	8.0–8.5	8.6 – 9.1	≥9.2
		RVOT diameters (cm)		
Above aortic valve (RVOT no. 1)	2.5–2.9	3.0–3.2	3.3–3.5	≥3.6
Above pulmonic valve (RVOT no. 2)	1.7–2.3	2.4–2.7	2.8–3.1	≥3.2
		PA diameter (cm)		
Below pulmonic valve (PA no. 1)	1.5–2.1	2.2–2.5	2.6–2.9	≥3.0

Adapted from ref. *1*.

Table A5

Reference Limits and Partition Values of Right Ventricular Size and Function as Measured in the Apical Four-Chamber View

	Reference range	*Mildly abnormal*	*Moderately abnormal*	*Severely abnormal*
RV diastolic area (cm^2)	11–28	29–32	33–37	≥38
RV systolic area (cm^2)	7.5–16	17–19	20–22	≥23
RV fractional area change (%)	32–60	25–31	18–24	≥17

Adaptted from ref. *1*.

Table A6

Reference Limits and Partition Values for Left Atrial Dimensions/Volumes

	Women				*Men*			
	Reference range	*Mildly abnormal*	*Moderately abnormal*	*Severely abnormal*	*Reference range*	*Mildly abnormal*	*Moderately abnormal*	*Severely abnormal*
				Atrial dimensions				
LA diameter (cm)	2.7–3.8	3.9–4.2	4.3–4.6	≥4.7	3–4	4.1–4.6	4.7–5.2	≥5.2
LA diameter/BSA (cm/m^2)	1.5–2.3	2.4–2.6	2.7–2.9	≥3.0	1.5–2.3	2.4–2.6	2.7–2.9	≥3
RA minor axis dimension (cm)	2.9–4.5	4.6–4.9	5.0–5.4	≥5.5	2.9–4.5	4.6–4.9	5.0–5.4	≥5.5
RA minor axis dimension/BSA (cm/m^2)	1.7–2.5	2.6–2.8	2.9–3.1	≥3.2	1.7–2.5	2.6–2.8	2.9–3.1	≥3.2
				Atrial area				
LA area (cm^2)	≤20	20–30	30–40	>40	≤20	20–30	30–40	>40
				Atrial volumes				
LA volume (mL)	22–52	53–62	63–72	≥73	18–58	59–68	69–78	≥79
LA volume/BSA (mL/m^2)	***22 ± 6***	***29–33***	***34–39***	***≥40***	***22 ± 6***	***29–33***	***34–39***	***≥40***

Bold italic values: recommended and best validated. (Adapted from ref. *1*.)

REFERENCES

1. Recommendations for Chamber Quantification: A Report from the American Society of Echocardiography's Guidelines and Standards Committee and the Chamber Quantification Writing Group, Developed in Conjunction with the European Association of Echocardiography, a Branch of the European Society of Cardiology. J Am Soc Echocardiogr 2005;18:1440–1463.

INDEX